PROCEEDINGS OF THE INTERNATIONAL SYMPOSIUM

TC 211 IS-GI Brussels 2012

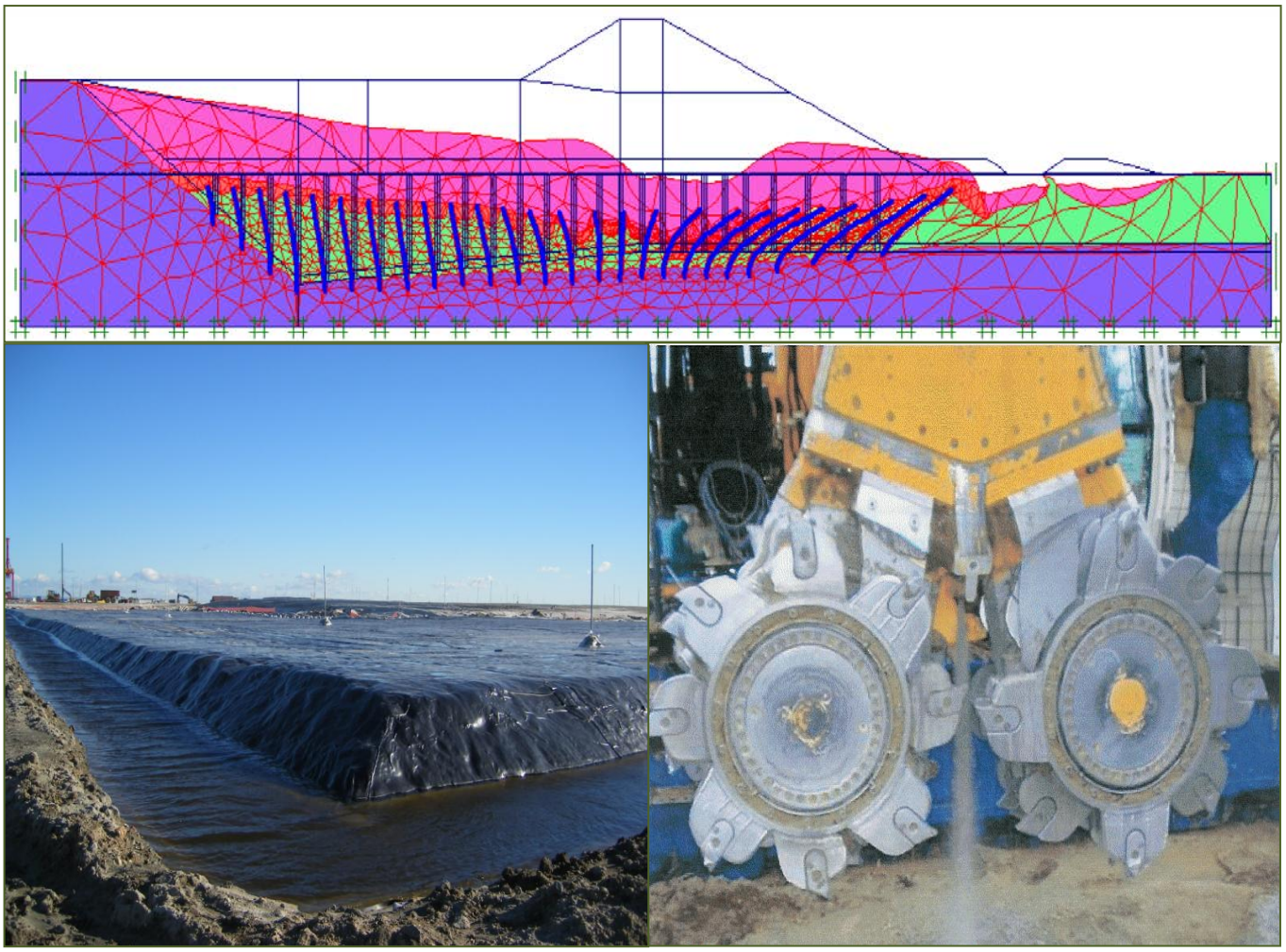

Recent Research, Advances & Execution Aspects of GROUND IMPROVEMENT WORKS

31 May – 1 June 2012, Brussels, BELGIUM

VOLUME III

Organised by:

ISSMGE Technical Committee TC 211 Ground Improvement

Belgische Groepering voor Grondmechanica en Geotechniek
Groupement Belge de Mécanique des Sols et de la Géotechnique

Comité Français de Mécanique des Sols

Edited by:

Nicolas Denies & Noël Huybrechts

SIMSG ISSMGE

GBMS BGGG

CFMS

Recent Research, Advances & Execution Aspects of Ground Improvement Works

Edited by

Dr. Ir. Nicolas Denies
Belgian Building Research Institute (BBRI-CSTC-WTCB), Belgium

Ir. Noël Huybrechts
Belgian Building Research Institute (BBRI-CSTC-WTCB), Belgium

Editorial address

Ground Improvement is a large and important domain in soil mechanics and geotechnical engineering and consists in a wide variety of techniques and methods adapted to a broad range of problems. The amount of contributions to the proceedings of this symposium is certainly a proof of that.

It cannot be denied that during the last decades the importance of the ground improvement market has enormously increased. New methods, tools and procedures have been developed and applied in practice.
In order to support this evolution in a scientific way, research programs have been and are being carried out worldwide, leading to more and better insights and delivering the basis for the establishment of design methods, quality control procedures and standards.

Due to the increasing interest of the construction sector for Ground Improvement techniques, the Belgian Building Research Institute (BBRI) has got more and more involved in projects addressing ground improvement during the last decade, most of them in a fruitful partnership with the Belgian Association of Foundation Contractors (ABEF).
In line with this evolution, the Geotechnical Division of the BBRI supports since 2005 the activities of the ISSMGE TC 211 Ground Improvement, which results today in the organization of an international symposium with more than 1600 pages of publications spread out over 4 Volumes:

- *Volume 1* of the proceedings contains the contributions of the 7 General Reporters, the Louis Ménard lecture held by *Patrick Mengé*, and the specialty lecture of the ISSMGE president *Jean-Louis Briaud*.
- *Volumes 2 to 4* contain more than 140 papers, subdivided in 7 Sessions, each of them dealing with a particular domain of Ground Improvement.

It can be noted that 40% of the papers deal with soil stabilisation and deep mixing, proving the huge interest in these techniques. This is not surprising, as they are outstanding and competitive sustainable construction methods.

We believe that the content of the present proceedings gives a very good overview of recent and on-going research actions and practices with regard to Ground Improvement. Moreover, we are convinced that they will contribute significantly to the further development of quality control procedures and standards.

Finally we would like to thank the Belgian Federal Public Service Economy, the NBN (Belgian standardization organization) and the Flemish Governmental Agency for Innovation by Science and Technology (IWT) for their financial support of the BBRI research programs addressing Ground Improvement techniques.

The Editors,

Nicolas Denies & Noël Huybrechts
Geotechnical Division, Belgian Building Research Institute, Brussels, Belgium

Table of contents of VOLUME III

Session 4 – SOIL MIXING 2 - DEEP MIXING

Partial Factor Design for a Highway Embankment Founded on Lime-cement Columns III-3
M. S. Al-Naqshabandy and S. Larsson

Soil Mix Technology for Integrated Remediation and Ground Improvement: Field Trials III-13
A. Al-Tabbaa, M. Liska, R. McGall and C. Critchlow

Long-term performance of CSM walls in slightly overconsolidated clays III-23
D. Bellato, A. Dalle Coste, F.-W. Gerressen, P. Simonini

Geomix Caissons against liquefaction III-33
L. Benhamou and F. Mathieu

Foundation Soils Improvement by "Cutter Soil Mixing" III-41
J. Bilé Serra and B.F. Mendes

Ground improvement works for an LNG storage tank foundation III-53
G. Chapman, J. Gniel, M. Greenough and A. Bouazza

Lateral displacements due to installation of soil-cement columns III-63
J. Chai and J. Carter

Quality Assurance and Quality Control for Deep Soil Mixing (DSM) in Punggol Waterway Project, Singapore III-73
S.H Chew, C.Y. Tan, T.Y. Yap, K.E Chua, H.M Yim, S.Y Kee, T.K. Khoo and Ja Naw

SOIL MIX WALLS as retaining structures – Belgian practice III-83
N. Denies, N. Huybrechts, F. De Cock, B. Lameire, J. Maertens and A. Vervoort

SOIL MIX WALLS as retaining structures – mechanical characterization III-99
N. Denies, N. Huybrechts, F. De Cock, B. Lameire, A. Vervoort, G. Van Lysebetten and J. Maertens

Mechanical characterization of DEEP SOIL MIX material – procedure description III-117
N. Denies, N. Huybrechts, F. De Cock, B. Lameire, A. Vervoort and J. Maertens

Mechanical characterization of large scale soil mix samples and the analysis of the influence of soil inclusions III-127
A. Vervoort, A. Tavallali, G. Van Lysebetten, J. Maertens, N. Denies, N. Huybrechts, F. De Cock and B. Lameire

Foundations reinforced by soil mixing: Physical and numerical approach III-137
M. Dhaybi, A. Grzyb, R. Trunfio and F. Pellet

Design, Construction and Monitoring of a Test Section for the stabilization of an Active Slide Area utilizing Soil Mixed Shear Keys installed using Cutter Soil Mixing. III-147
S. Gaib, B. Wilson and E. Lapointe

CSM-Cutter Soil Mixing – Worldwide experiences of a young soil mixing method in challenging soil conditions III-159
F.W. Gerressen and Th. Vohs

Deep mixing for reinforcement of railway platforms with a spreadable tool III-169
A. Guimond-Barrett, J.-Fr. Mosser, N. Calon, Ph. Reiffsteck, A. Pantet and A. Le Kouby

Soil-cement columns, an alternative soil improvement method III-179
S. Lambert, F. Rocher-Lacoste and A. Le Kouby

Soil mixing in highly organic materials: the experience of LPV111, New Orleans, Louisiana (USA) III-189
F. M. Leoni and A. Bertero

Stability Analyses of a Floodwall with Deep-Mixed Ground Improvement at Orleans Avenue Canal, New Orleans III-199
M. McGuire, E. Templeton and G. Filz

Assessing the feasibility of a foundation treatment solution based on CSM panels at a river dock in Lisbon III-211
B. Mendes, E. Maranha das Neves, L. Caldeira and J. Bilé Serra

Earth Retaining Structure using Cutter Soil Mixing technology for the "Villa Paradisio" Project at Cannes, France III-223
A. Peixoto, E. Sousa and P. Gomes

Permanent Excavation Support in Urban Area using Cutter Soil Mixing technology at Cannes, France III-233
A. Peixoto, E. Sousa and P. Gomes

Solutions for soil foundation improvement of an industrial building using Cutter Soil Mixing technology at Fréjus, France III-243
A. Peixoto, E. Sousa and P. Gomes

Solution of earth retaining structure using Cutter Soil Mixing technology: "Parking Saint Nicolas" Project at Cannes, France III-251
A. Peixoto, E. Sousa, P. Gomes

The application of Cutter Soil Mixing to an urban excavation at the riverside of Lagos, Portugal III-261
A. Peixoto, M. Matos Fernandes, E. Sousa, P. Gomes

Ground Improvement Solutions using CSM Technology III-271
A. Pinto, R. Tomásio, X. Pita, P. Godinho and A. Peixoto

State of the art in "Dry Soil Mixing" – Basics and case study III-285
P. Quasthoff

Parametric study of embankments founded on soft organic clay using numerical simulations III-299
K. Suganya and P. V. Sivapullaiah

Design of in-situ soil mixing III-309
M. Topolnicki and P. Pandrea

Session 5 - RIGID INCLUSIONS and STONE COLUMNS

Reliability-based design of stone columns for ground improvement considering settlement and bulging as failure *modes* III-319
J. A. Alonso and R. Jimenez

Ordinary and Encased Stone Columns Under Repeated Loading III-329
N. K.S.Al-Saoudi, M. R. Mahmoud, F.H. Rahil and Z. W.S.Abbawi

Assessment of software for the design of columnar reinforced soil III-339
M. Bouassida, L. Hazzar and A. Mejri

Possibilities and limitations of embedded pile elements for lateral loading III-347
R.B.J. Brinkgreve, E. Engin and T. Dao

Full Scale Instrumented Load Test for Support of Oil Tanks on Deep Soft Clay Deposits in Louisiana using Controlled Modulus Columns III-359
Br Buschmeier, Fr. Masse, S. Swift and M. Walker

Theoretical analyses of laboratory tests of kaolin clay improved with stone columns III-373
J. Cañizal, J. Castro, A. Cimentada, A. Da Costa, M. Miranda and C. Sagaseta

Numerical modelling of stone column installation in Bothkennar clay III-383
J. Castro, D. Kamrat-Pietraszewska and M. Karstunen

Settlement reduction and stress concentration factors in rammed aggregate piers determined from full- scale group load tests III-393
A. ÇEVİK ÖZKESKİN, O. EROL and Z. ÇEKİNMEZ

Behavior of a Pile-Supported Embankment using rigid piles with variable inertia III-401
D. Dias, J. Grippon and M. Nunez

Spread foundations on rigid inclusions subjected to complex loading: Comparison of 3D numerical and simplified analytical modelling III-411
D. Dias and B. Simon

Improvement of soft soils using reinforced sand over stone columns III-423
N. A. H. El Mahallawy

Determination of pore size distribution to identify plastic zones around stone columns III-433
J.N.F. Gautray, J. Laue and S. M. Springman

Optimisation of Stone Column Design Using Transparent Soil and Particle Image Velocimetry (PIV) III-443
P. Kelly and J. A. Black

Ground improvement methods for establishment of the federal road B 176 on a new elevated dump in the brown coal area of MIBRAG III-453
J. F. Kirstein, C. Ahner, S. Uhlemann and P. Uhlich

Rigid inclusions in combination with fast wick drain consolidation as soil improvement method in very soft and fat northern German clay III-469
J. Kirstein and N. Wittorf

Critical Height of Column-Supported Embankments from Bench-Scale and Field-Scale Tests III-481
M. McGuire, J. Sloan, J. Collin and G. Filz

Load-settlement responses of columnar foundation reinforcements III-491
G. Modoni, J. Bzówka, A. Juzwa, A. Mandolini and F. Valentino

Axial Capacity of Vibro-Concrete Columns III-503
A. B. Reeb and J. G. Collin

A Study on the Use of Drilled Shafts to Reinforce Stiff Clay with Very Weak Sliding Planes III-509
R. Sancio, O. Safaqah, P. Wong, Ch. Li, P. Sabatini, B. Villet

Behaviour of a shallow foundation on soil reinforced by Mixed Module Columns® – Experimental study III-519
H. Santruckova, P. Foray, S. Grange, A. Cofone, S. Lambert, Ph. Gotteland and J. Wher

A model study on settlement behaviour of granular columns in clay under compression loading III-529
M. Tekin and M. Ufuk Ergun

Basal reinforced piled embankments in the Netherlands, Field studies and laboratory tests III-539
S.J.M. Van Eekelen and A. Bezuijen

Design risks of ground improvement methods including rigid inclusions III-551
J. Wehr, M. Topolnicki and W. Sondermann

CONTRIBUTIONS

SESSION 4
SOIL MIXING 2 – DEEP MIXING

Partial Factor Design for a Highway Embankment Founded on Lime-cement Columns

Mohammed Salim Al-Naqshabandy, KTH Royal Institute of Technology, Sweden, msban@kth.se
Stefan Larsson, KTH Royal Institute of Technology, Sweden, Stefan.larsson@byv.kth.se

ABSTRACT

Stability assessment of highway embankments is a common practice in geotechnical engineering. Rational estimation of soil properties is essential for reliable and safe design. However, previous research has shown that high degree of uncertainty is associated with engineering properties and the behavior of the ground improvement with lime-cement columns. Current design methods for stability of lime-cement column are deterministic and the uncertainties are not treated rationally. A reliable design requires rational treatment of uncertainties. This paper addresses the need for application of partial factor design for safety and reliability assessment of lime-cement columns. The study was carried out on an example highway embankment of 6 m height. Resistance and load parameters were considered random variables. The sensitivity factors for the random variables were evaluated from the first order reliability method (FORM). Partial factors were evaluated for the random variables according to the approximate location of the design values. It was shown that the design by partial factor method fulfills both safety and reliability requirements.

1. INTRODUCTION

High uncertainty is normally associated with strength property of lime-cement columns. The property's uncertainty arises mainly from a variety of sources named inherent variability, measurement errors, statistical and model transformation uncertainties (Al-Naqshabandy and Larsson, 2011; Bergman et al., 2011). However, current design methods applied for the design of lime-cement columns are deterministic, where only the central value of the parameters are considered (i.e. the mean value μ). The uncertainties involved with μ are incorporated into a single value represented by the total factor of safety (FS), which is the ratio of the resisting forces (R) to the loading forces (L). The safety requirement for embankments improved with lime-cement columns should normally fulfils FS>1.5 for an undrained analysis (Broms, 2004). Accordingly, the current design method used for assessing stability of lime-cement columns does not deal with the uncertainty in a rational way. In order to design an embankment with a certain level of confidence, the uncertainties involved should be considered in a rational way. This could be achieved by using reliability-based design (RBD) approaches (Christian et al., 1994; Phoon et al., 2003; El-Ramly et al., 2002; Filz and Navin, 2006; Kitasume et al., 2009).

However, RBD has not been applied in practice for lime-cement columns yet. This is because RBD is based on some assumptions which are rarely all fulfilled in geotechnical systems. The presence of high uncertainty makes the prediction of the strength and deformation properties of the improved soil to be very difficult, and also because application of lime-cement column is relatively young. In this study, RBD presented for the design of lime-cement columns supported embankments. The design was applied on an example embankment of 6 m height. Two RBD methods were applied, the first was according to first order reliability method (FORM), which is relatively sophisticated but provides exact location of the design point. In FORM design, R parameters (i.e. the undrained shear strength of the columns ($c_{u,col}$) and the surrounding soil ($c_{u,soil}$)) and L parameters (i.e. columns' unit weight (γ_{col}), soils' unit weight (γ_{soil}), embankment's unit weight (γ_{emb}) and traffic load (q)) were considered random variables. The random variables were assumed to be uncorrelated and log-normally distributed. The second was according to the partial factor method (PFM) which is practically simpler. PFM is applied on the embankment at different conditions, where the number of the random variables was varying in each condition. The accuracy of the PFM was examined by analysing the embankment by FORM analysis.
In this design procedure, FORM design was performed on the most critical slip failure surface, found by Bishop's model, which is defined as the slip surface with the lowest FS among all trial failure surfaces. Shear failure was assumed to occur along the circular slip surface through the columns and the surrounding soil. The analyses only considered the total stress analysis based on the undrained condition. The uncertainty due to; spatial variability, measurement errors, statistical and model transformation were considered. Spatial variability was evaluated based on the random field theory proposed by Vanmarcke

(1977). In addition to μ and standard deviation (σ), the scale of fluctuation (δ), which is the distance within which soil property reveals strong correlation or dependency, is incorporated in the design for handling the spatial variability. Area replacement ratio ($\overline{a}$), which is the ratio of the area of lime-cement columns to the total area, is assumed to be constant throughout the design and the analysis, since the main aim in the presented design procedure was to find the target value of the most uncertain parameter in lime-cement columns (i.e. $\mu c_{u,col}$).

2. METHODS

The example embankment shown in Fig.(1) was analysed using the deterministic FS to find the location of the most critical slip surface. RBD represented by FORM approach is then performed to find the design value of $\mu c_{u,col}$ that meets the target level of reliability, which is chosen in accordance with the Swedish Transport Administration (2009). According to this design code if the RBD is used, the embankments should meet the requirements of safety class two (SC2) that is to say the target reliability index (β_T) should be at least 3.8. This value has therefore been adopted in this study and considered as reasonable value. The over all in-data used in the design and the analyses are presented in Table 1.

2.1. Deterministic design

Bishop's simplified method of slices with a circular slip surface is normally used to assess the internal stability of lime-cement columns. The FS is evaluated as follows

$$FS = \left(\sum_{i=1}^{i=j} \left(l_i \cos\theta_i c_{u,i} + w_i \tan\phi \right) m_{(\alpha)_i} \right) \Bigg/ \sum_{i=1}^{i=j} w_i \sin\theta_i \tag{1}$$

where i is the slice number, $i=1,2,3,4.....j$; j is the total number of slices; l_i, θ_i, and w_i are the length, the inclination angle, and the weight of slice i respectively; c_u and ϕ are the soil cohesion and friction angle at the base of slice i, and $m_{(\alpha)}$ can be calculated from the expression $m_{(\alpha)} = \left(\cos\theta_i + \left(\sin\theta_i \tan\phi_i / FS \right) \right)^{-1}$.

Including the traffic load (q), Eq.(1) can be modified to fit the system in Fig.(1) according to the following equations

$$FS = \frac{R}{L} = \frac{\sum_{i=1}^{i=j_{soil}} l_{soil} c_{u,soil} + \sum_{i=1}^{i=j_{comp}} l_{comp} c_{u,comp} + \sum_{i=1}^{i=j_{emb}} \left(w_{emb} \tan\phi_{emb} \right) m_{(\alpha)_{emb}} + \sum_{i=1}^{i=j_{emb}} \left(qb_{emb} \tan\phi_{emb} \right) m_{(\alpha)_{emb}}}{\sum_{i=1}^{i=j_{soil}} w_{soil} \sin\theta_{soil} + \sum_{i=1}^{i=j_{comp}} w_{comp} \sin\theta_{comp} + \sum_{i=1}^{i=j_{emb}} w_{emb} \sin\theta_{emb} + \sum_{i=1}^{i=j_q} qb_q \sin\theta_q} \tag{2a}$$

$$c_{u,comp} = \overline{a} c_{u,col} + (1-\overline{a}) c_{u,soil} \tag{2b}$$

$$w_{comp} = \overline{a} w_{col} + (1-\overline{a}) w_{soil} \tag{2c}$$

where the subscripts (*soil*, *comp* and *emb*) denote the material properties and the failure geometry in the soil, the composite material (i.e. the columns and the surrounding soil) and the embankment respectively; q is a traffic load assumed to be uniformly distributed with an intensity of 12 kN/m^2 (Sundquist, 2010); $\overline{a}$ is the area replacement ratio which is assumed to be constant $\overline{a} = 0.5$; w is evaluated from $w=\gamma bh$; γ, b and h are; the unit weight, the width and the central height of a slice respectively.

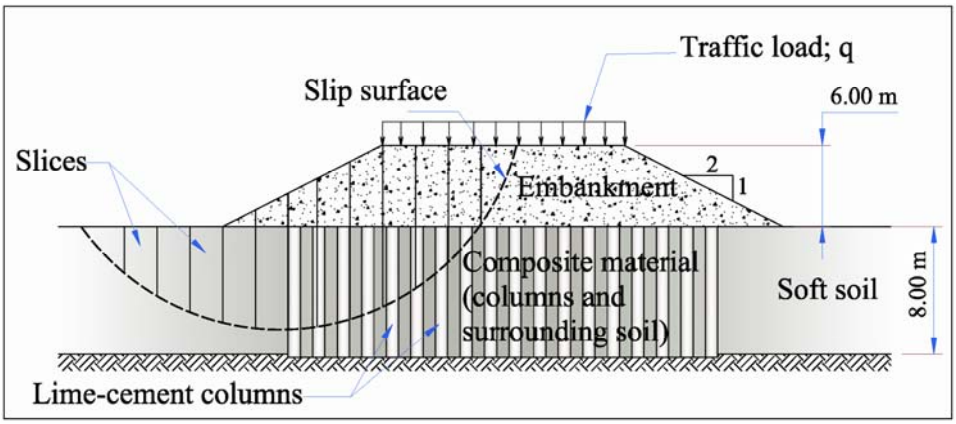

Figure 1: Geometry and the cross-section of the example highway embankment

The parameters that appear in the numerator and denominator in Eq.(2a) represent the resistance R and L parameters respectively. Soil parameters (i.e. $c_{u,col}$, $c_{u,soil}$, γ_{col}, γ_{soil}, γ_{emb} and q) in Eq.(2) were represented by their characteristic values (i.e. the mean values) to determine the most critical failure surface defined as a slip surface.

2.2. Reliability-based design

Reliability analysis requires knowledge about the type of probability distribution function of the random variables (PDF) and the correlation among them. The random variables (i.e. $c_{u,col}$, $c_{u,soil}$, γ_{col}, γ_{soil} and q) were assumed to be uncorrelated following log-normal PDF_s. The latter is a reasonable assumption since it prevents random variables from getting negative values in which negative values of these properties are physically meaningless (Fenton and Griffiths, 2008). The former assumption can also be reasonable due to the size of the examined scale of failure (Fig. 1) in comparison with the full scale of the improved area, where the mixing process has a major influence on the variability with respect to $c_{u,col}$ (Larsson et al., 2005a).

2.2.1. Performance function

The performance function is represented by a linear margin of safety (M). For n-dimensional space of random variables denotes by a victor (**X**), M can be presented as a function, g(**X**), in the multivariate space as follows

$$M=g(X)=R-L \tag{3}$$

The limit state function or the failure criteria is the boundary between the safe and failure regions. The limit state function and the probability of failure (P_f) at the multivariate space can be defined as follows

$$M=g(X)=R-L=0 \tag{4}$$

$$P_f = P[g(X)\leq 0] \tag{5}$$

2.2.2. First-order reliability method

FORM method was performed on the most critical failure surface to calculate the corresponding reliability index (β). This method is characterized by providing a geometrical interpretation of β defined as a measure of numbers of standard deviation in a dimensionless space from the peak of the joint PDF distribution of all random variables and the limit state function g(**X**)=0. The random variables should be transformed to their normalized form (i.e. following standard normal distribution). For the log-normally distributed random variables, the normalized form and the design value (x_{di}), evaluated at the failure surface ($*$), can be determined as follows

$$z_i = \frac{\ln x_{di}^* - \mu_{\ln x_i}}{\sigma_{\ln x_i}} \tag{6}$$

$$x_{d_i}^* = Exp(\mu_{\ln x_i} + z_i \sigma_{\ln x_i}) \tag{7}$$

where z_i is the normalized form of **X** which also identifies the coordinates of the design point in the multivariate space at failure ($z_i=\alpha_i\beta$); α is the sensitivity factor that identifies the significance of the random variables to the performance function, for R and L parameters α takes negative and positive values respectively. $\mu_{\ln x}$ and $\sigma_{\ln x}$ are the distribution parameters of the log-normal distribution defined as follows

$$\mu_{\ln x_i} = \ln \mu_{x_i} - 0.5\sigma^2_{\ln x_i} \tag{8}$$

$$\sigma_{\ln x_i} = \sqrt{\ln\left(1+\left(COV\right)^2\right)} \tag{9}$$

where *COV* is the coefficient of variation which is the ratio of the mean (μ_{xi}) and the standard deviation (σ_{xi}) of the random variable *x*. In order to find the coordinates of the design point at failure, the limit state in Eq.(4) must be satisfied. This kind of solutions is however mathematically complex due to the optimization problem. Several algorithms have been proposed for the solution of this problem (Hasofer and Lind, 1974; Rackwitz and Fiessler, 1978). In this study, the optimisation algorithm proposed by Rackwitz and Fiessler (1978) is used to evaluate β and α. For this purpose, a Microsoft Excel spreadsheet was developed for the iterative calculations.

2.2.3. Partial factor design

The basic principle of the partial factor design is that it replaces the single FS with a set of partial safety factors (or partial coefficients) of the individual parameters of R and L. The partial factors can be evaluated in such a way that they consider different sources of uncertainty associated with the individual parameters as described previously by Al-Naqshabandy et al., 2012. According to the Thoft-Christensen and Baker (1982) the partial factors for R and L components can be found as follows

$$\gamma_{R_i} = \frac{x_{Rsp_i}}{x^*_{Rd_i}} \tag{10}$$

$$\gamma_{L_i} = \frac{x^*_{Ld_i}}{x_{Lsp_i}} \tag{11}$$

where γ_{R_i} and γ_{L_i}, $x^*_{Rd_i}$ and $x^*_{Ld_i}$, x_{Rsp_i} and x_{Lsp_i} are the partial factors, the design value (*d*) and the specified characteristic value (*sp*) for the resistance, R, and the load, L, components. It is obvious from Eqs.(10) and (11) that γ_{R_i} and γ_{L_i} are only dependent on x_{spi} and x_{di} of the random variables, in which some of the parameters are unknown at the design stage. However, in this study x_{spi} were evaluated from μ_i, and x_{di} were evaluated from following equation

$$x^*_{d_i} = \mu_i e^{\alpha_i \beta_T COV_{Total_i}} \tag{12}$$

where β_T is the target reliability index. The total uncertainty COV_{Total_i} associated with the properties (viz., spatial variability (*spt*), statistical (*stat*), measurement errors (*err*) and transformation (*trs*) uncertainties) was evaluated according to the following equation

$$COV_{Total_i} = \sqrt{COV^2_{spt} + COV^2_{stat} + COV^2_{err} + COV^2_{trs}} \tag{13}$$

In order to estimate the design value, the parameters in the Eqs. (12 and 13) must be predefined for the random variables. However, this is not the case with the improved soil properties (i.e. $c_{u,col}$), since they are not defined beforehand the design of lime-cement columns. Also, because RBD has not been established yet for DM methods, and there is lack of knowledge about many parameters e.g. α and β in relation to geotechnical system. Accordingly those parameters are normally chosen in accordance with the design codes, technical specifications and literature studies. According to the Swedish Transport Administration (2009) the embankment should be designed according to SC2, which corresponds to β_T =3.8 (CEN, 2001). Thus, the values of β_T=3.8 was adopted in this study to find the design value of $\mu c_{u,col}$. The design value of $\mu c_{u,col}$ was chosen from different trial values of $\mu c_{u,col}$ (i.e. 100, 110,120, 130, 140,

and 150) kPa. The parameters of COV_{Total} were chosen in accordance with the literatures as shown in *Table 1*. However, with regard to α_i, neither suggestions nor recommendations were found from the above-mentioned design codes that can be adopted in this study. This is due to the fact that evaluation of α_i is very complex because it depends on many other factors such as, number of random variables in **X** and their PDFs, the level of safety (i.e. the value of β_T) and the type of the limit state function. In this study α_i were estimated from FORM method.

Table 1: The In-data used in the analyses

System component	Property (unit)	Statistical parameters						Probability distribution function; PDF	uncertainty					Total uncertain.; COV_{Total}
		Mean; μ	Stand. Dev.;σ	COV; μ/σ	Scale of fluctuation; $\delta^{\dagger}$, (m)				Spatial var.;COV_{spa}	Statistical $COV_{stat}=\frac{COV}{\sqrt{N}}$		Measurement error; COV_{err}	Transform.; COV_{trs}	
					δ_x	δ_y	δ_z			N	COV_{stat}			
Soft soil	$c_{u,soil}$ (kPa)	15	1	0.1†	40	40	0.2	Log-normal	0.008	10	0.031	0.05	0.1	0.11
	γ_{soil} (kN/m^3)	16	1.6	0.1†				Log-normal	0.1	10	0.031	0.02		0.11
Lime-cement columns	$c_{u,col}$ (kPa)	100-150		0.28‡	4	4	0.4	Log-normal	≈0.00	10	0.08	0.05	0.29‡	0.31
	γ_{col} (kN/m^3)	16	1.6	0.1				Log-normal	0.1	10	0.031	0.02		0.11
Embankment	ϕ (°)	35						Deterministic						
	γ_{emb} (kN/m^3)	18	1.8	0.1†				Log-normal	0.1	10	0.031	0.02		0.11
Traffic load	q (kN/m^2)	12††	2.4	0.05††				Log-normal	0.05	>1000	≈0.00			0.05

Notation:

† data collected from Al-Naqshabandy and Larsson (2011)

†† data collected from Sundquist (2010)

‡ data collected form Phoon and Kulhawy (1999)

3. RESULTS AND DISCUSSION

In the following, two design procedures are presented. The first is based on the combination of the traditional deterministic design and the RBD design, while the second is based only on the partial factor design. The key parameter in both methods is to identify the location of the design values at the limit state.

3.1. FORM analysis in combination with deterministic desgin

3.1.1. Search for the critical slip surface

In the RBD design, the prerequisite knowledge is the location of the most critical slip surface. Since the information about $\overline{a}$ and $\mu c_{u,col}$ are unknown at the design stage, the first parameter was assumed to be $\overline{a}=0.5$, and the second parameter was varying from 100-150 kPa throughout this design procedure. The location of the most critical slip surface at different $\mu c_{u,col}$ (i.e. 100, 110, 120, 130, 140 and 150 kPa) for the embankment shown in Fig.1 is searched for and found among many trial failure surfaces. The result of the location of the most critical slip surface is presented in Fig.2. It was observed that the location of the critical slip surface has not been changed during the analyses when $\mu c_{u,col}$ was changed from 100-150 kPa. This unchange in the location of the critical slip surface with $\mu c_{u,col}$ could be due to the adopted values of $\mu c_{u,col}$ were all in the range of low strength columns, and also the embankment was analysed under the effect of the constant loading from the embankment height.

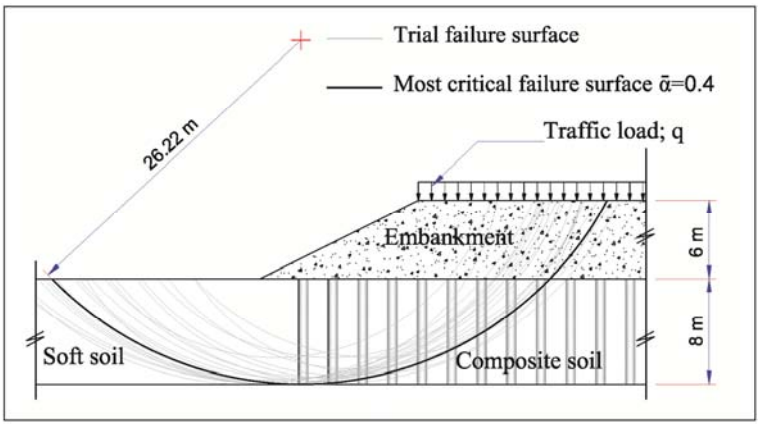

Figure 2: Position of the most critical slip surface for the embankment based on the deterministic analysis

3.1.2. Safety and reliability assessment

The deterministic FS was found for varying $\mu c_{u,col}$, the results are presented in Fig.3. As shown from the figure, the evaluated FS is varying linearly from 1.8-2.4 when $\mu c_{u,col}$ is varying from 100-150 kPa respectively. The results imply that the embankment is theoretically safe according to the deterministic method since the evaluated FS in all cases is satisfactory according to FS>1.5. Accordingly, based on to the deterministic design, if the embankment is designed according to $\mu c_{u,col}$ =100 kPa and $\bar{a} = 0.5$ values, a convenient degree of safety can be achieved.

The embankment was designed by RBD method according to FORM. The design was performed on the same location of the critical slip surface, for comparison purpose, the results of the design procedure are also illustrated in Fig.3. As shown β increases from 3.3 to 4.5 when $\mu c_{u,col}$ increases from100 to 150 kPa, these vales of β correspond to P_f 0.0004 and 0.000004 respectively. This means that reliability of embankment can be substantially improved within this range of $\mu c_{u,col}$. In this case, the required value of $\mu c_{u,col}$ that meets $\beta_T = 3.8$ should not be less than 120 kPa. However, the suggested design value from the deterministic design was $\mu c_{u,col}$ =100 kPa to satisfy the safety requirement, the corresponding β is equal to 3.3 which is far from $\beta_T = 3.8$. Therefore, using deterministic design for assessing stability of lime-cement columns as a single design tool may overestimate the reliability. Reliability-based design should be therefore adopted for the design of lime-cement column.

In order to find the effect of uncertainties on the reliability, the embankment was redesigned at different levels of uncertainties with respect to $\mu c_{u,col}$, where COV_{Total} were varied from 0.2-0.4. The results are depicted in Fig.4. As shown from the figure, in general, the reliability increases with increasing $\mu c_{u,col}$ and decreases with the total uncertainties. The increase in the reliability is significant, e.g. in the case of $\mu c_{u,col}$ =100 kPa, β is increasing from 2.8-4.2 when COV_{Total} decreasing from 0.4-0.2 respectively. This means that the reliability of embankments can be significantly improved by rational evaluation of the engineering property (e.g. $c_{u,col}$). Better understanding and evaluating the sources of uncertainty may improve the reliability. In this case, the reliability of the analysed embankment can reach their target value at $\mu c_{u,col}$ =100 kPa if the total uncertainty is decreased from 0.31to 0.25. For instance, this can be achieved by reducing the variability, or by performing sufficient number of samples and reducing the transformation uncertainty. It is also worth noting that the effect of uncertainties cannot be captured in the traditional deterministic design method, since FS is not changing with COV_{Total}, this behaviour can be clearly shown in Fig.3. It is therefore important that the uncertainty is integrated in the design of lime-cement columns. By performing one single design method for assessing stability of lime-cement columns, the design is not necessarily meeting reliability requirement.

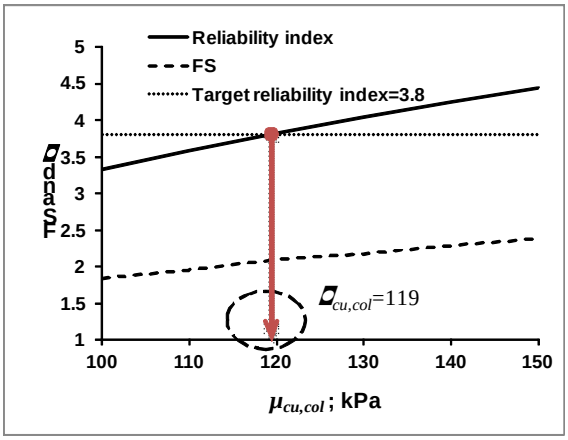

Figure 3: Deterministic and RBD designs for the highway embankment at varying $\mu c_{u,col}$

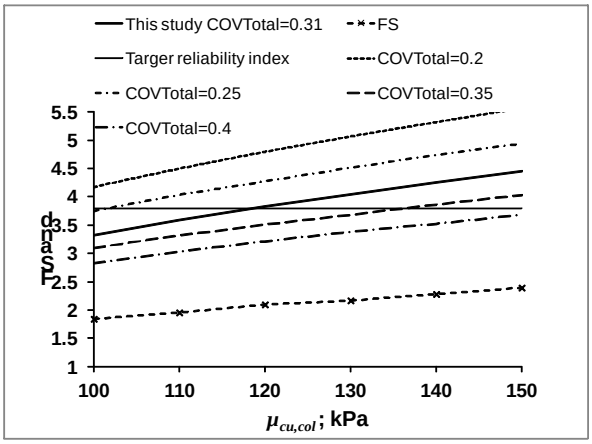

Figure 4: Effect of the total uncertainty in $c_{u,col}$ on the reliability of the embankment

3.2. Design procedure based on partial factors

3.2.1. Evaluation of the design value and the sensitivity factor from FORM

The by-product of FORM analyses is that it provides the exact location of the design point, i.e. α_i, defined at the limit state surface. The design values, $x^*_{Rd_i}$ and $x^*_{Ld_i}$, and the corresponding partial factors, γ_{R_i} and γ_{L_i}, for R and L parameters were respectively evaluated from Eq.(12) and Eqs.(10 and 11). Since the procedure is based on the stochastic process, the results will also be stochastic. The evaluated design values and the partial factors are presented in Fig.5 (a) and (b), respectively. It can be seen from the figure that there are differences between the evaluated mean, the maximum and the minimum values of $x^*_{Rd_i}$, $x^*_{Ld_i}$, γ_{R_i} and γ_{L_i}. In order to find the statistical significance between these differences, the results were tested statistically at 95% level of confidence. The difference between the averages, maximum and minimum values for the parameter X2 to X8 were found to be insignificant. This means that the evaluated design values and the corresponded partial factors by FORM can be applied reasonably at different geotechnical conditions at the same level of uncertainty. On the other hand the difference in the parameter, X1, was found to be statistically significant according to 95% level of confidence. However, this statistical significance does not necessarily reflect the practical significance. This subject will therefore be further investigated in the following section. Furthermore, the parameter with the highest γ has more relative importance to the mechanical system. Thus the most important parameters, found from the analysed embankment, for R and L respectively were $c_{u,col}$ and γ_{emb}.

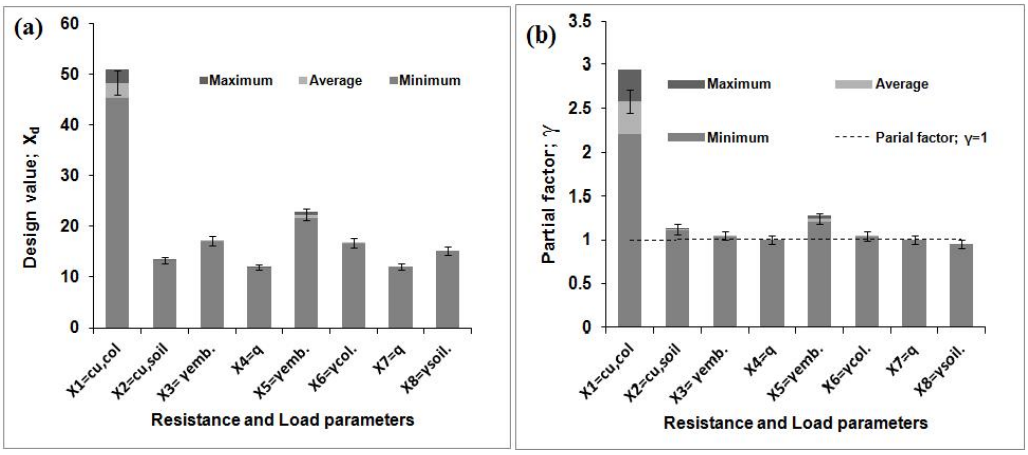

Figure5: a) Design values and b) partial factors evaluated from RBD analysis for the resistance and the load parameters. The resistance parameters rank is varying from (X1 to X 4), while the load parameters rank is varying from(X 5, X 8)

3.2.2. Partial factor design

The evaluated design values for the eight parameters in Fig. 4(a) were used directly in Eq.2(a) to find the target value of $\mu c_{u,col}$ for the embankment that meets $\beta_T = 3.8$. The evaluated $\mu c_{u,col}$ was 120 kPa which is almost identical to $\mu c_{u,col}$ =119 kPa from FORM analyses as shown in Fig.3. This result is reasonable since the design values used in the analysis were infact evaluated from information about the exact location of the design point, i.e. α_i, founded from FORM analyses. However, providing a design based on a large number of random variables, which is in this special case equals to eight, is practically complicated and unreasonable. Thus, a huge advantage can be gained from the statistical analysis carried out on the evaluated partial factors for the eight random variables shown in Fig. 5(b). Accordingly, the variables that are not deviating significantly from the limits γ =1 can be considered as deterministic parameters. Therefore, according to Fig.4(b) the partial factors for five of these parameters (i.e. X3, X4, X6, X7 and X8) are almost within the limits of γ =1. Accordingly the partial factors of these parameters can be discarded practically and replaced by γ =1. Only three parameters were left with their partial factors found to be deviated from γ =1 limits (i.e. X1and X2 from resistance corresponding to $c_{u,col}$ and $c_{u,soil}$, and X5 from load corresponds to γ_{emb}). Accordingly, these parameters can be called the *significant variables*, because they are expected to have significant influence on the performance function. Thus, the design values for only the significant parameters (i.e. $c_{u,col}$, $c_{u,soil}$ and γ_{emb}) were used to find the proper $\mu c_{u,col}$ value for the embankment. The results are presented in Fig.5. The evaluated value of $\mu c_{u,col}$ was 122 kPa. FORM analysis and deterministic analysis were performed to check whether evaluated value of $\mu c_{u,col}$ is meeting $\beta_T = 3.8$ and FS>1.5 or not. The evaluated β and the corresponded FS were 3.92 and 2.2 respectively, which are both greater than the required reliability and safety limits. These results imply the significant advantage of the partial factor design in terms of fulfilling rational assessment of the reliability and the safety of the embankment founded on improved soils with lime-cement columns.

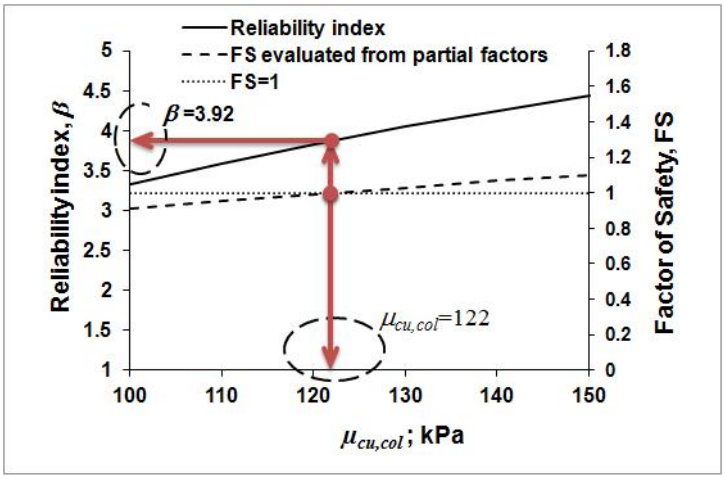

Figure 5: Partial factor design for the design of the embankment, the partial factors for only the important parameters ($c_{u,col}$, $c_{u,soil}$ and γ_{emb}) were considered and evaluated from FORM analysis

4. CONCLUSIONS

The total uncertainty with respect to $c_{u,col}$ was found to have a significant influence on the reliability of the tested embankment. The effect of the total uncertainty (COV_{Total}) on the design of lime-cement columns however failed to be captured by performing deterministic analysis. The study highlights the significant importance of using RBD approaches for the design of lime-cement columns. It is shown that RBD can be applied for lime-cement column in its simplest form presented in this study (i.e. partial factor method). According to FORM analyses conducted on this special case of embankment, the evaluated partial factor for $c_{u,col}$ found to vary from 2.2-2.85 with the average of 2.54.

The evaluated partial factor for $c_{u,col}$ was applied for the design of lime-cement columns, the design showed that the target level of safety can be reached reasonably by performing PFM method, instead of conducting full probabilistic analyses by FORM. Knowledge about the location of the most critical slip surface is not required in order to perform PFM. There is however needs for further studies that can be conducted on other cases and at different conditions in order to further support this conclusion.

REFERENCES

Al-Naqshabandy, M. S., Bergman, N. S., Larsson, S. (2012). Strength variability in lime-cement columns based on cone penetration test data. Ground improvement,165(1), 15-30.

Al-Naqshabandy, M. S., Larsson, S. (2011). Effect of uncertainties of improved soil shear strength on the reliability of embankments. Submitted to J. Geotech. Geoenviro. Engrg. ASCE.

Baecher, G. B., and Christian, J. T. (2003). Reliability and Statistics in Geotechnical Engineering. Wiley and Sons Ltd., England.

Begman, N. S., Al-Naqshabandy, M. S., Larsson, S. (2011). Strength variability in lime-cement columns evaluated using CPT and KPS. Submitted to Georisk.

Broms, B.B. (2004). Lime and lime/cement columns. Ch. 8 in Ground Improvement 2nd edition, edited by M.P. Moseley and K. Kirsch. Spon Press, London and New York.

Broms, B.B. (1999). Progressive failure of lime, lime-cement and cement columns. Proc. int. conf. on dry mix methods for deep soil stabilization, Stockholm, Sweden, 177-184.

CEN. (2001). Eurocode – Basis of structural design. EN 1990. European Committee for Standardization (CEN), Brussels, Belgium.

Christian, J.T., Ladd, C.C., Baecher, B. (1994). Reliability applied to slope stability analysis. J. Geotech. Geoenviro. Engrg. ASCE, 120(12), 2180-2206.

El-Ramly, H., Morgenstern, N.R., Cruden, D.M. (2002). Probabilistic slope stability analysis for practice. Can. Geotech. J., 39 (3), 665-683.

Fenton, G. A., and Griffiths, D. V. (2008). Risk assessment in geotechnical engineering. Wiley and Sons Inc., Hoboken, New Jersey.

Filz, G.M., Navin, M.P. (2006). Stability of column-supported embankments. Report on state project. Report No. VTRC 06-CR13, 73 pp.

Hasofer, A. M., Lind, N. C. (1974). Exact and invariant second moment code format. J. Eng. Mech. Div. 100(1), 111–121.

Kitasume, M., Maruyama, K., Hashizume, H. (2009). Centrifuge model tests on failure mode of deep mixing columns. Proce. deep mixing 2009, Int. symp. on deep mixing and admixture stabilization, Okinawa, 337-342.

Larsson, S., Dahlström, M., Nilsson, B. (2005). A complementary field study on the uniformity of lime-cement columns for deep mixing. Ground improvement, 9(2), 67-77.

Phoon, K.K., Kulhawy, F.H., Grigoriu, M.D. (2003). Development of a reliability-based design framework for transmission line structure foundations. J. Geotech. Geoenviron. Engrg. ASCE, 129 (9), 798-806.

Phoon, K.K., Kulhawy, F.H. (1999). Evaluation of geotechnical property variability. Can. Geotech. J., 36(4), 625-639.

Rackwitz, R., Fiessler, B. (1978). Structural reliability under combined load sequences. Comput. Structures, 9(5), 489-494.

Sundquist, H. (2010). Safety, loads and load distribution on structures. Report108, Structural design and bridges 2007, 3rd edition 2010 ISSN 1103-4289.

Swedish Transport Administration (2009). TK Geo. Geotechnical design guide. Publication 2009:46. Borlänge, 156 pp.

Terashi, M., Kitazume, M. (2011). QA/QC for deep-mixed ground: current practice and future research needs. Ground improvement, 164(G13), 161-177.

Thoft-Christensen, P. and Baker, M. J. (1982) Structural reliability and its application. Springer-Verlag, Berlin, 1982, 267 pp.

Vanmarcke, E. H. (1977). Probabilistic modeling of soil profiles. J. Geotech. Geoenviron. Eng., 103(GT11), 1227-1246.

Soil Mix Technology for Integrated Remediation and Ground Improvement: Field Trials

Abir Al-Tabbaa, University of Cambridge, United Kingdom, aa22@cam.ac.uk
Martin Liska, University of Cambridge, United Kingdom, ml393@cam.ac.uk
Robert McGall, Eco Foundations, United Kingdom, Robert.mcgall@eco-foundations.co.uk
Colin Critchlow, Eco Foundations, United Kingdom, colin.critchlow@eco-foundations.co.uk

ABSTRACT

Soil mix technology applied to the in-situ remediation of contaminated land is relatively new in the UK. It involves the use of mixing tools and additives to construct permeable reactive in-ground barriers and low permeability containment walls and for "hot-spot" soil treatment by stabilisation/solidification. Contaminated land remediation using soil mix technology is a cost effective and versatile approach with numerous environmental advantages. Further commercial advantages can be realised by combining this with ground improvement which is the core objective of project SMiRT (Soil Mix Remediation Technology); being the largest UK government funded R&D project involving academia-industry collaboration. Project SMiRT involved a number of tasks including laboratory treatability studies, field trials, field testing and monitoring, assessment of field trials performance and wide stakeholder consultation and dissemination. This paper presents details of the design and execution of the field trials activities as well as initial sampling and in-situ testing activities which all took place over the summer of 2011in terms of the treatments applied, binders employed and soil mix technology systems used and highlights project and site specific issues that had to be addressed.

1. INTRODUCTION

Soil mix technology (SMT) applied to the in-situ remediation of contaminated land is relatively new in the UK (Al-Tabbaa, 2003). It involves the use of mixing tools and additives to construct permeable reactive in-ground barriers and low-permeability containment walls and for "hot-spot" soil treatment by stabilisation/solidification. Permeable reactive barriers (PRBs) are permeable walls installed in the ground to intersect the flow of contaminated groundwater (Gavaskar et al, 1998). Reactive material placed in the barrier is designed to remove the contaminants by one of more processes including sorption, precipitation, oxidation, biodegradation and encapsulation. Low permeability containment walls are cut-off low permeability walls designed to isolate a contaminated area from the surrounding environment. Stabilisation/ solidification (S/S) treatments include the physical encapsulation and chemical fixation of contaminants in place through a range of processes including sorption, precipitation, lattice incorporation, complexation and encapsulation (LaGrega et al, 2001). Contaminated land remediation using SMT is a cost effective and versatile approach with numerous technical and environmental advantages including the use of simple and well established techniques, speedy implementation, applicability to sites of any size and to multiple contaminants, elimination of off-site disposal as well as low risk and low emissions. SMT has been used in a limited number of contaminated land remediation projects in the UK dating back to 1994 and in ground improvement to the late 1980 (Al-Tabbaa, 2003, Al-Tabbaa et al, 2009a). There is however a lack of competing alternative technologies, that offer the same level of versatility and economic, environmental and social benefits, under the current constraints of UK legislation. In addition, most currently available contaminated land remediation techniques are only partially successful, and are relatively contaminant-specific. This makes SMT a promising and timely contender to lead the market place in offering a cost-effective, efficient and low risk solution to contaminated soil and groundwater remediation. This, combined with recent innovations in SMT equipment, treatments and materials (Al-Tabbaa et al 2009a) was the rationale behind Soil Mix Remediation Technology project SMiRT (Anon, 2008, Gee, 2008, Al-Tabbaa et al, 2009b).

Project SMiRT is the largest (£1.24M) research and development funded project to date by the UK Technology Strategy Board on Contaminated Land Remediation Technologies. It is led by Eco Foundations and involved the collaboration with Cambridge University and 17 industrial partners and is a four year project which commenced in October 2007. Project SMiRT aimed to achieve significant technical advancement and cost-savings by developing innovative SMT systems for integrated remediation and ground improvement, with simultaneous delivery of wet and dry additives, and with advanced quality assurance system. Currently available equipment worldwide generally involves either

wet binder delivery for containment and remediation or dry binder delivery for ground improvement purposes. As a new technology SMT suffers from lack of proven track record and associated stakeholder confidence. SMiRT is taking major steps towards filling this gap, providing the much needed field validation and science-based knowledge of SMT by performing extensive laboratory testing and field trials to increase validation with full involvement of stakeholders. The project was also testing a wide range of additives and binders with emphasis on enhanced sustainability (Jegandan et al, 2010).

The UK brownfield and contaminated land remediation market is valued at £450-700M/year. While until a few years ago most contaminated soils were destined to landfills, with the recent introduction of the EU Landfill Directive most contaminated soils are now retained on site in one form or another. Current typical costs of SMT for contaminated land remediation in the UK are ~£45-65/m^3; being less than most other currently available remediation techniques, and currently accounting for ~5% of the total number of sites remediated in the UK. With increasing pressures to redevelop contaminated land in a sustainable manner, leading to significant reduction in landfilling, the SMT share of the market is expected to increase ten fold over the next 4-7 years, given its economic and environmental benefits, with a reduction in associated treatment costs. In the ground improvement market, worth ~£150M, except for vibro-compaction, which dominates the market, SMT is the most cost-effective technique and is hence likely to see increased exploitation in the UK. Project SMiRT consisted of the following eight tasks: (a) Developing and constructing SMT equipment for delivery of dry and wet additives, (b) Implementing advanced quality assurance software for performance control, (c) Performing laboratory treatability studies for the field trials, (d) Performing large scale field trials, (e) Performing extensive field testing, monitoring and sampling, (f) Performing extensive laboratory testing of field samples, (g) Holding stakeholder consultation meetings and (h) Disseminating the results to the wider community. An overview of project SMiRT activities can be found on the project website at www.smirt.org.uk and in Al-Tabbaa et al 2009a.

Extensive laboratory treatability studies were performed during the first stages of the project using both generic soils and soils from the field trials site in which a wide range of binders and additives, both conventional and novel, were tested for their applications to the three treatments of stabilisation/solidification (S/S), permeable reactive barriers (PRB) and ground improvement (GI). Many variables were considered including binder composition, ratios and dosages and binder delivery (both wet and dry). One objective was to develop further understanding the performance of such materials for those SMT applications and to develop novel materials, but with enhanced performance as well as materials with reduced environmental impacts. Another objective was to design the field trials which were to follow. The binders used for the S/S, GI and low permeability wall applications were divided into groups based on their main binder constituents: namely Portland cement (PC), ground granulated blastfurnace slag (GGBS) in PC-GGBS-based blends, pulverised fuel ash (PFA) in PC-PFA-based blends and reactive magnesia (MgO) either alone or in blends with one or more of the above three materials. For the PRB treatment walls reactive materials namely zeolites and a number of modified bentonites in either granular or slurry form were used. Blends of reactive materials were used and always included a slurry in order to prevent segregation, something which was realised on site. In addition, these reactive materials, in powder form, were also incorporated into the S/S and low permeability wall section binders to enhance their sorptive capacity in particular for organic contamination. Results and findings of various aspects of this treatability study work have been presented elsewhere (Al-Tabbaa et al, 2009 a&b and 2012, Jegandan et al, 2010, Ouellet-Plamondon et al, 2010 a&b and 2011). The aim of this paper is to present details of the design and execution of the field trials which initial field testing which followed and which took place in the summer of 2011 and to highlight site and project specific issues related to the use of Soil Mix Technology for integrated remediation and ground improvement.

2. FIELD TRIALS

The Field trials took place in a previous chemical works site in the north of England. The site consisted of up to 4m of made ground with LL ~30%, PL ~24% and water content of ~25%, overlain by 0-1m of silts and clays with LL ~28%, PL ~23% and water content of ~22%, then by 3-4m of natural sand and gravel deposits with wc of 33-45% which was in turn overlain by bedrock at ~8m bgl. The soils had a high level of contamination consisting of heavy metals: Pb, Zn, As, Cr, Cu and Ni at up to 2200mg/kg and significant organic contamination including VOCs: BTEX up to 160mg/kg, SVOCs: analines, chloroanalines, nitrobenzense and dinitrotoloune up to 1600mg/kg, TPHs up to 7000mg/kg and PAHs up to 20mg/kg. The groundwater table is at ~4mbgl with some perched water table in the madeground. The ground water was also heavily contaminated, mainly with the organics above: VOCs up to 1.5mg/L,

SVOCs up to 6.5mg/L, TPHs up to 70mg/L as well as limited metal contamination. The pH of the groundwater was 6-7.9.

A number of SMT systems were used in the field trials. One was a triple auger system (Figure 1) with three overlapping augers of 0.55mm diameter each and which installs a section of 1.2m long with each installation. The second was the ALLU mass stabilisation system, which consists of a power mix attachment mounted to the dipper arm of an excavator with a pair of mixing drums at the end and a pressure feeder mounted on a powered crawler chassis which delivers dry binder into the ground with the aid of compressed air (ALLU, 2010, Figure 2). The third is a standard single auger system mounted at the end of a CFA pile shaft (Figure 3a). The fourth is a double rotary head auger developed by Eco Foundations (Figure 3b) which consists of two sets of cutting and mixing blades which rotate in opposite directions resulting in a much enhanced mixing process. The larger number of materials employed, namely PC, GGBS, PFA, pre-bagged PC-GGBS CEM III cement, MgO, zeolite (both granular and powder), organoclay (powder and granular) and natural bentonite and chemically modified bentonite slurry chemicals, required the use of different storage and delivery systems including vertical and horizontal silos and hoppers as well as manual mixing, where all materials were delivered to the mixing and batching plant, Figure 4.

Figure 1: The triple auger system used in the field trials to install the PRB walls, low permeability wall sections and individual S/S sections

Figure 2: The ALLU system used in the ground improvement treatment sections

(a) (b)

Figure 3: The two single auger systems used (a) standard single auger and (b) double rotary head auger developed by Eco Foundations.

Figure 4: The batching plant and materials storage on site

The layout of the various field trials activities are shown in Figure 5. The PRB system is the hexagon system shown in Figure 5 and enlarged in Figure 6 and was constructed using the triple auger system. The inner section of the hexagon formed six separate PRB walls in which different reactive materials in slurry form were introduced and mixed with the soil down to a depth of 8m. The outer hexagon wall sections and the short intersections are low permeability sections and were installed down to ~8m keyed into the bedrock layer, and were constructed using cementitious binders. Those walls served a dual function of being a reactive low permeability S/S or wall system as well as hydraulically isolate the individual PRB sections and the whole system from the surrounding environment. Some installation photos and the whole hexagon are shown in Figure 7. The triple auger system was also used to install individual S/S sections, the 24 orange sections in Figure 5 and shown in Figure 8a, in which a wide range of the binders and binder contents were tested as well as a number of different installation variables including speed or rotation, speed of penetration and withdrawal and number of mixing systems.

The ALLU mass stabilisation system was used for the ground improvement sections of the soft made ground soils in the areas of very low or no contamination; the 31 blue rectangular sections in Figure 5 and shown in Figure 8b. In addition to the employment of different binders and binder compositions in the different individual treatment areas (both triple auger and ALLU system), installation variables such as speed of rotation, penetration and withdrawal and mixing cycles were also tested using a given binder in each case. The single auger and double rotary auger were used to install 5 columns each, the yellow and green sections in Figure 5 respectively.

A number of issues had to be addressed on site as they arose. This was partly caused by the fact that the binders and additives used on site were not necessarily those previously tested in the laboratory. This is mainly due to the short time period which was available to source the materials for the field trials. It was also caused by differences in samples preparations in the laboratory and in field applications. Hence a number of the binder and additive mixes had to be revised on site because of associated problems encountered. One of the main revisions performed on site was changing of the water content of the slurries applied as some of the materials had a different water demand from those tested in the laboratory and hence some mixes were too viscous to pump. Another change was related to the PRB section, where

some segregation occurred leading to the clogging up of the mixer. This was resolved by incorporating a modified bentonite slurry in all the PRB sections. For the ALLU mass stabilisation system, some softening of the ground with the addition of water (pre-wetting) had to initially be performed as the ground was too strong for the equipment, before the dry binder was added.

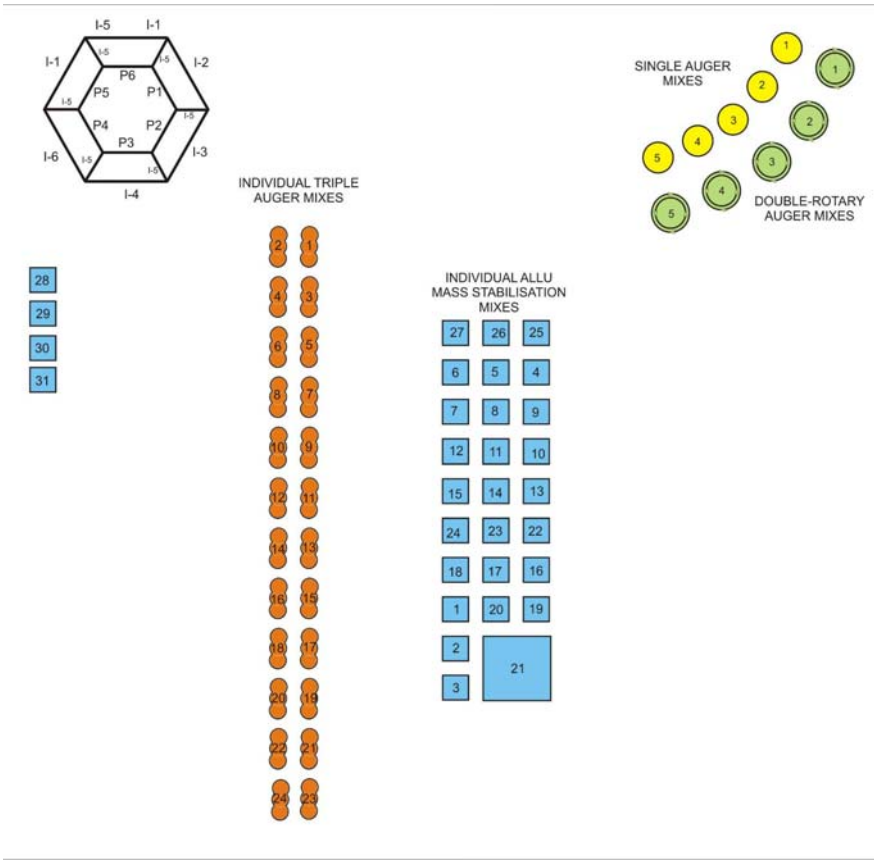

Figure 5: Schematic of the field trials treatments

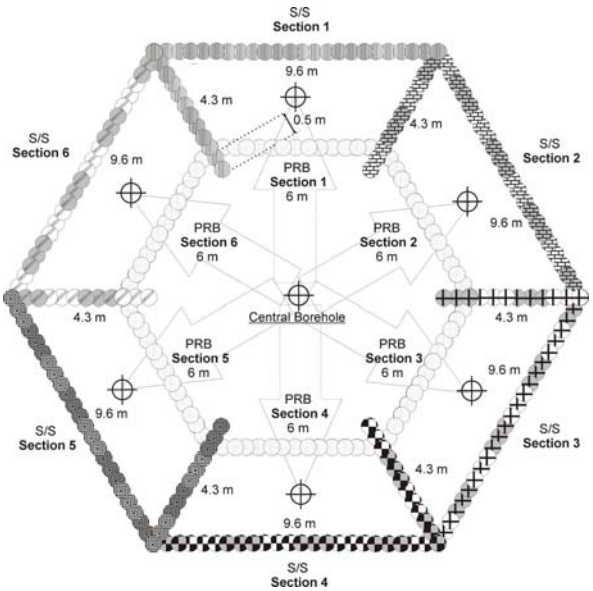

Figure 6: Schematic of the hexagon of inner PRB walls and outer low permeability walls.

Figure 7: The hexagon set up with 6 inner PRB wall sections and 6 outer low permeability walls.

(a) *(b)*

Figure 8: The completed individual sections (a) triple auger S/S sections and (b) the ALLU mass stabilisation sections.

Figure 9: Pumping from one of the PRB walls.

Figure 10: Surface sampling of the various installations during construction and sample preparation.

Figure 11. Window sampling from the individual triple auger S/S sections

A well was installed in the centre of the hexagon and in the middle of each of the six outer sections (as shown schematically in Figure 6) as well as a well around 20m away from the hexagon. The intention is that water will initially be extracted from the wells in each of the outer sections one at a time over a given period of time and the extracted water will be analysed for contaminants concentrations. This will then be followed by pumping water down the central well from elsewhere in the site and forced through the six walls over a long period of time to assess the performance of the walls in the long term. Initial pumping activities, Figure 9, have indicated that the water being pumped out is that from the vicinity of the outer wells and hence no reduction in contaminant concentration has been seen yet. For the low permeability walls, S/S and ground improvement sections, bulk surface samples were taken during the installation of the columns from which samples for testing were prepared, as shown in Figure 10. Window sampling was

then employed around 2 weeks after installation from which samples of up 50-90mm diameter were obtained down to the full depth of construction from the majority of the installations. The quality of the cores varied between mixes and depths, examples of good and poor quality cores are shown in Figure 12. Figure 12a clearly shows the typical good quality intact samples obtained while Figure 12b shows samples with significant fragmentation and fracturing and with missing sections, which dropped out of the base of the sampling tool. The surface samples and the cores (trimmed) are being tested in the laboratory for a range of properties such as density, strength, leachability (batch, flow through and tank), leachate pH and permeability amongst others and a wide range of comparisons are being made including: between the different binder mixes, between the different SMT equipment, between the different installation parameters, between wet and dry binder delivery, between surface samples, core samples and laboratory samples.

Figure 12: Typical window sampling cores: (a) good quality and (b) poor quality.

3. CONCLUSIONS

This paper presented details of a large scale field trials application of soil mix technology to the integrated remediation and ground improvement of a contaminated site with the use of a range of mixing tools. The site with its range of contaminants, both in soil and groundwater, as well as low or no contamination areas was ideal for such an application. A hexagon of permeable reactive barrier walls using different reactive materials was installed using a triple auger. A large number of individual triple auger, ALLU mass stabilisation and two single auger sections were successfully installed with a wide range of different binders, composition and dosage and different installation parameters. Except for some pre-wetting to initially soften some of the ground areas, the SMT equipment successfully installed all the required sections. A number of modifications had to be performed during the field trials to resolve issues which arose from differences between laboratory and field mixing as well as the use of different materials between the two. Window sampling cores have been successfully obtained from the majority of the installations and are being tested and compared. These field trials, which are part of the R&D project SMiRT, have so far demonstrated the versatility and ease of application of SMT in remediation and ground improvement applications. Extensive testing and field validations are still on-going to develop a better understanding of SMT in those applications.

4. ACKNOWLEDGEMENTS

The authors are grateful to the other SMiRT project partners: Amcol Minerals Europe, Arcadis, Arup, Bachy Soletanche, BURA, Civil & Marine Ltd, HBR Ltd, Kelsdale, Kentish Minerals, Merebrook Consulting, Mineral Products Association, NewFields, OWM, Richard Baker Harrison, Site Ops, UK Quality Ash Association and WSP Remediation for their contributions. The funding from the UK Technology Strategy Board for project SMiRT (TP/5/CON/6/I/H0304E) is gratefully acknowledged.

REFERENCES

Al-Tabbaa, A. (2003). "Soil mixing in the UK 1991-2001: state of practice report". ICE Ground Improvement, Thomas Telford, 7(3): 117-126.

Al-Tabbaa, A., Liska, M., Jegandan, S., Barker, P. (2009a). "Overview of project SMiRT for integrated remediation and ground improvement", Proc. Int. Symp. Deep Mixing and Admixture Stabilisation, Okinawa, May.

Al-Tabbaa, A., Barker, P., Evans, C.W. (2009b). "Innovation in soil mix technology for remediation of contaminated land", Keynote lecture, Proc. Int. Symp. Deep Mixing and Admixture Stabilisation, Okinawa, May.

Al-Tabbaa, A., Liska, M., Ouellet-Plamondon, C., Jegandan, S., Shrestha, R., Barker, P., McGall, R. and Critchlow, C. (2012). Soil mix technology for integrated remediation and ground improvement: From laboratory work to field trials. 4th International Conference on Grouting and Deep Mixing, New Orleans, (accepted).

ALLU (2010). "Mass Stabilisation Manual", ALLU Finland Oy.

Anon. (2008). "The good mixer", Ground Engineering, July: 26.

Gavaskar, A., Gupta, N., Sass, B., Janosy, R. and O'Sullivan, D. (1998). Permeable barriers for groundwater remediation, Battelle Press.

Gee, T. (2008). "Dirty Business", The Engineer, February: 11.

Jegandan, S., Liska, M., Osman, A. And Al-Tabbaa, A. (2010). "Sustainable binders for soil stabilisation", ICE Journal of Ground Improvement 163, Issue 1, 53-61.

LaGrega, M. D., Buckingham, P. L. and Evans, J. C. (2001). Chapter 11: Stabilization/ Solidification. In Hazardous Waste Management. London, McGraw-Hill, 641-704.

Ouellet-Plamondon, C. (2011). Charaterisation and performance of novel aluminosilicates for soil mix technology permeable reactive barrier systems. PhD Thesis, University of Cambridge, UK.

Ouellet-Plamondon, C., Lynch, R.J. and Al-Tabbaa, A. (2010a). "Metal retention experiments for the design of soil mix technology permeable reactive barriers". 5th Int. Conf. Environmental Science and Technology, Houston, July.

Ouellet-Plamondon, C., Lynch, R.J. and Al-Tabbaa, A. (2010b). "Sorption behaviour of granular zeolite and organoclay for soil mix technology permeable reactive barriers". ConSoil 2010, Austria, September.

Ouellet-Plamondon, C., Lynch, R.J. and Al-Tabbaa, A. (2011). "Metal retention experiments for the design of soil mix technology permeable reactive barriers." CLEAN – Soil, Air, Water 39(9): 844-852.

Long-term performance of CSM walls in slightly overconsolidated clays

Diego Bellato, University of Padova, Italy, diego.bellato.1@studenti.unipd.it
Alberto Dalle Coste, Bauer Macchine Italia s.r.l, Italy, Alberto.DalleCoste@bauer-italia.it
Franz-Werner Gerressen, Bauer Maschinen GmbH, Germany, Franz-Werner.Gerressen@bauer.de
Paolo Simonini, University of Padova, Italy, paolo.simonini@unipd.it

ABSTRACT

The paper is concerned with the results of a comprehensive laboratory investigation carried out on soil samples drawn up from more than 50000 m^2 panels realized using the Cutter Soil Mixing (CSM) for the construction of the new railway station in Bologna (Italy) where the subsoil is constituted mostly by overconsolidated clays. On the CSM-treated samples, hydraulic and mechanical laboratory tests at different curing time, from 14 days to more than 2 years, were performed, in order to study the influence of curing time on the overall mixture response and to propose a model aimed at describing the increase of mechanical properties along with time. The paper presents and discusses the outcome of the experimental investigation carried out so far, comparing the results obtained from preliminary tests on samples retrieved from trial panels with those obtained directly from the working structure. Furthermore, in order to understand the degree of mixture homogeneity reached by site mixing and the amount of cement effectively bonding the soil matrix, CSM-treated clayey soil was studied at micro-scale using microcomputed tomography.

1. INTRODUCTION

CSM (Cutter Soil Mixing), a suitable system to realize retaining walls, cut-off walls or foundation elements (Fiorotto et al., 2005), can be considered to belong to the category of deep mixing methods, but the homogeneity of the treated soil is more effective than that obtained from traditional mixing techniques, especially in clayey soils. For this reason, CSM technique was selected in 2008 for the construction of around 50000 m^2 of improved-ground walls acting as containment system for the effective retaining structure (composed of traditional diaphragm walls) of the excavations necessary to accommodate the new high-speed railway station in Bologna. This technical solution was designed in order to prevent settlements of the nearby buildings and the old railway station.
To determine the best procedure and bonding slurry to be used, several trial panels were performed on site, from which samples were recovered and subjected (at a predefined curing time) to mechanical tests such as unconfined compression tests. Further mechanical and permeability tests were performed after more than two years of curing time on additional samples obtained from other definitive panels.
To investigate the quality of mixing achieved and to estimate the amount of cement reaction products leading to the strength gain of the stabilized soil, mineralogical and micro-structural analysis on the same samples were also carried out.
In addition, on the basis of the comparison between the panel production data (collected directly on site by the mixing machine during the realization of the CSM panels) and the results of laboratory tests, a new parameter, named the "*mixing quality factor*", that seems to be able to take into account the effect of on-site mixing procedure, was tentatively proposed. This parameter along with other significant factors, affecting strength and permeability of treated soil, have been included in a provisional model which can predict the unconfined compression strength at 28 days of curing time and in longer term conditions.

2. GEOTECHNICAL SITE CHARACTERIZATION

Figure 2.1 sketches the results of the site and laboratory geotechnical investigation carried out on the natural soil deposit, that is mainly composed by inorganic silty clay or clayey silt with local lamination of fine to coarse granular sediments. Fine grained soils are characterized by medium to high plasticity with natural water content approaching plastic limit. The clayey fraction varies from 23% to 47%, while the sand fraction varies from 0% to 28%.
CPTU profiles show a slight increase of cone resistance especially at higher depths. Excess pore pressure generated during undrained penetration oscillates very rapidly but seems always positive confirming the slight degree of overconsolidation. From oedometer tests, it was possible to define the compressibility parameters and to estimate the overconsolidation ratio.

Furthermore, for some specimens it was possible to measure the vertical hydraulic permeability, that ranges from $1.04 \cdot 10^{-10}$ m/s to $7.39 \cdot 10^{-10}$ m/s.
The undrained shear strength has been found to vary with depth from 40 kPa between the ground level and 10 m, to 75 kPa between 10 m to 21 m, and more than 100 kPa at higher depths.

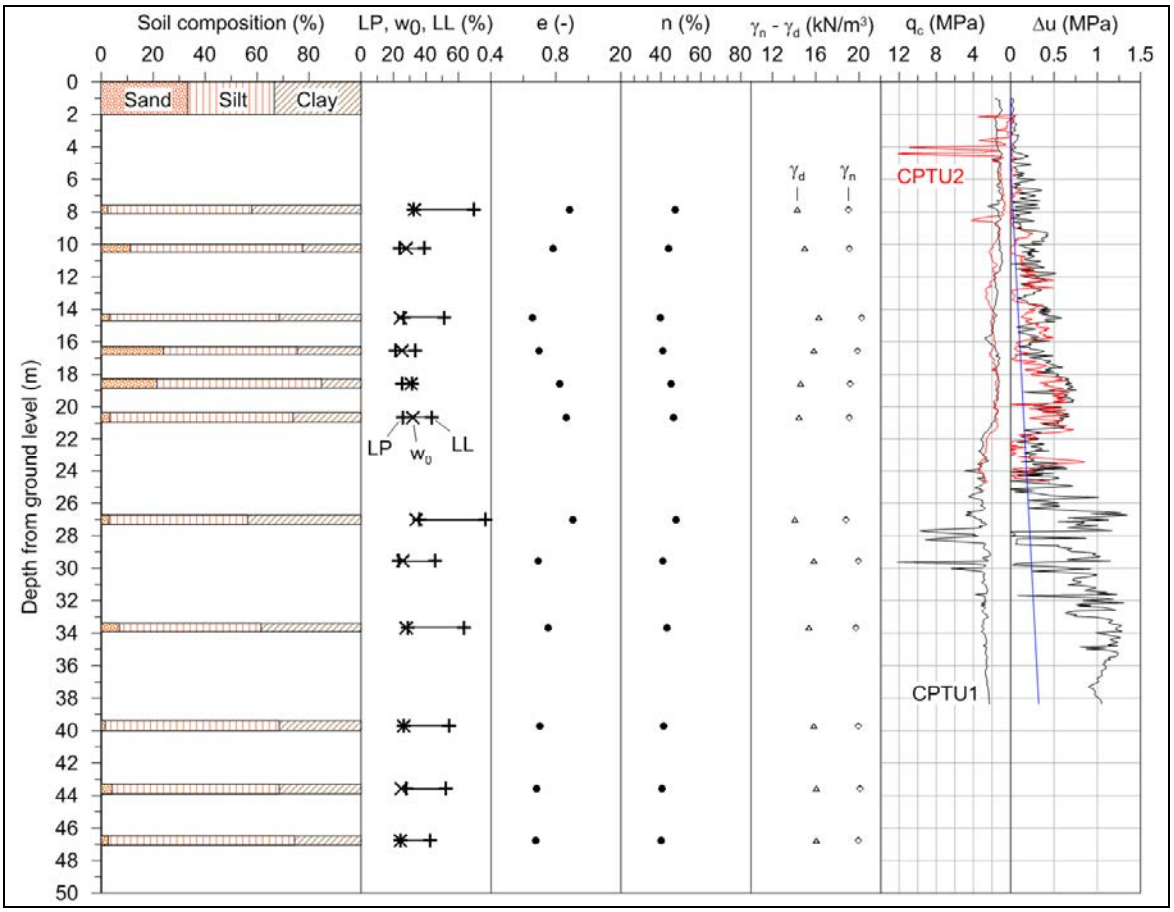

Figure 1: Soil profile and geotechnical properties from geotechnical investigations

3. CONSTRUCTION DETAILS

3.1. Procedure and mix design

Two cutters were used on the jobsite for the construction of the 23 m deep, 2.4 or 2.8 m wide, and 0.8 m thick CSM panels. The selected procedure is referred as the *two phases system*, in which a bentonite suspension was used during cutter penetration to loosen and liquefy the soil. From the maximum depth, the mixing head was retrieved injecting and blending the cement slurry with the soil. The construction sequence was realized according to the "back-step" procedure and the "fresh in hard" method, whereby secondary panels were installed in the soil between two already hardened primary panels with an overcut of 23.5 cm. The cylindrical specimens were obtained by coring trial and working panels with a water/cement ratio (wcr) ranging from 0.6 to 0.7 and a cement content (c_c) of 300÷500 kg_{cem}/m^3 of natural soil. Taking into account the porosity (45%) and the degree of saturation (95%) of the clayey soils, an effective water-cement ratio, wcr_{eff}, was estimated ranging from 1.5 to 1.8. The binder was a pozzolanic cement classified as CEM IV/A 32,5 R, in accordance with EN 197-1, where 65÷89% is composed of clinker and the remaining part of pozzolanas and fly ash.

3.2. In situ mixing parameters

All the most important parameters regarding the CSM treatment are recorded during the construction of each panel. These data can be subsequently elaborated in order to obtain a reliable profile over depth, whose typical layout is provided in Fig. 3.2.
From this information it was possible to define a new parameter, namely the *mixing quality parameter* (μ), which represents an estimate of the homogeneity achieved in the panel and takes into account the

effect of real site mixing conditions, which differ very often from those controlled during preliminary laboratory tests.

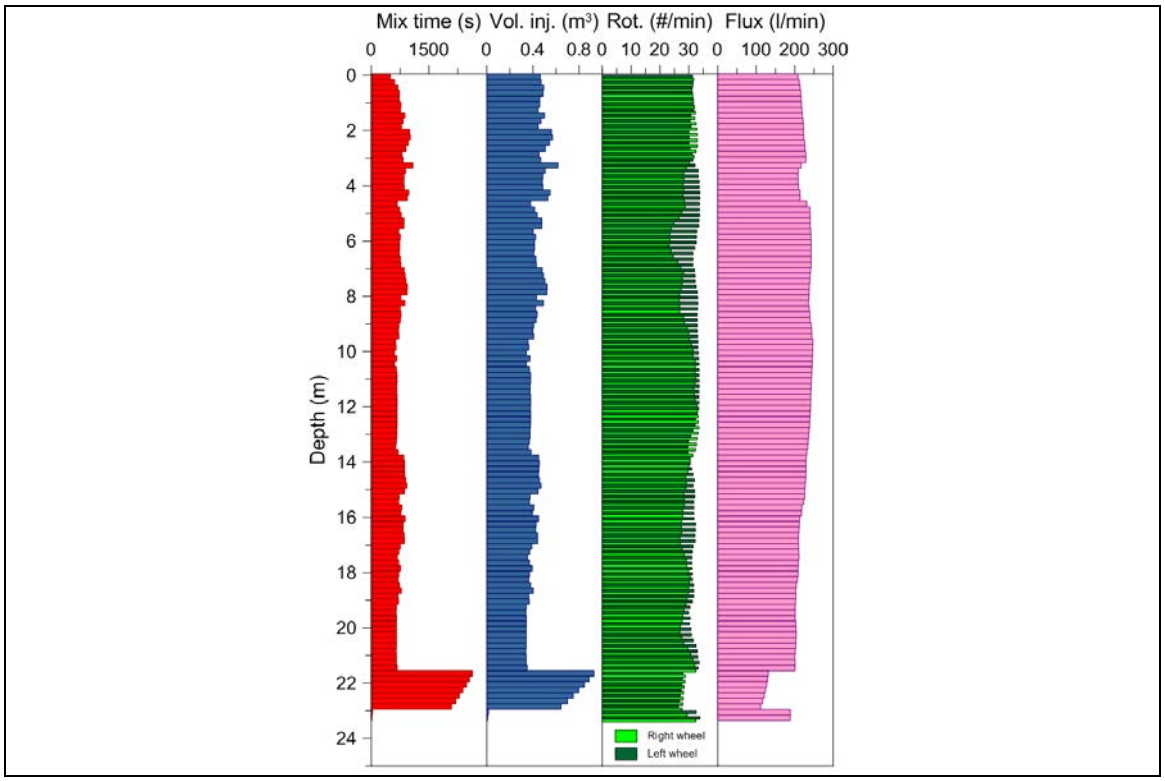

Figure 2: panel 47.S-01 – diagrams over depth of the main mixing parameters

The *mixing quality factor* is given by

$$\mu_i = \left[\left(\varphi_d \cdot R_{d,i} \cdot T_{d,i}\right) + \left(R_{u,i} \cdot T_{u,i}\right)\right] \cdot \frac{N_c \cdot M}{100\, V_c} \quad (1)$$

where $R_{d,i}$ and $R_{u,i}$ are the average rotational speed of the mixing wheels during the penetration and the retrieval phase, respectively, $T_{d,i}$ and $T_{u,i}$ are the total time taken to blend the soil during the downstroke and the upstroke, respectively, N_c is the number of mixing wheels (2), M is the number of mixing element per each wheel (6, in this case) and V_c is the volume occupied by the cutter. All quantities with the subscript "i" are referred to a single i^{th} layer of predefined thickness. φ_d (equal to 0.5 or 1) is called *phase factor* and takes into account the different role played by the executive procedure adopted to realize the panel, i.e. one phase ($\varphi_d = 1$) or two phases system ($\varphi_d = 0.5$).
Several authors (Mitchell, 1981; Terashi et al., 1983; Babasaki et al., 1996; Rathmayer, 1996; Yoshizawa et al., 1996; Usui, 2002; Kitazume, 2005) suggested to take into account, among the other factors, the mixing degree when estimating the effectiveness of the treatment and the unconfined compressive strength usually assumed to measure the improvement effect of the treated soil.

4. LABORATORY INVESTIGATION

To investigate the hydro-mechanical properties of CSM treated clayey soil, a series of unconfined compression (UC) tests, indirect traction tests and permeability tests have been carried out on several specimens cored directly from CSM trial and definitive panels.

4.1. Unconfined compression tests

More than 60 specimens have been tested according to EN 12390-3:2003 at different curing time t_{cur} in order to estimate the UC strength. Three diameters, namely D = 83, 54 and 37 mm, and two aspect ratio, namely h/D = 1 or 2, have been selected and the specimens were driven to failure at rate equal to 0.5 mm/min. Curing time was between 14 days and more than two years from the completion of the soil treatment. Some of the results of the tests carried out so far are summarized in Tab. 1.

Table 1: average unconfined compressive strength obtained from specimens at different curing time

Panel	Curing time t_{cur} (days)	Amount of cement (kg/m^3)	Diameter (mm)	h/ D (-)	$q_{u,av}$ (MPa)
Trial 1 - 4	40	400	83	2	2,04
Trial 1 - 5	40	500	83	2	2,11
Trial 1 - 8	40	500	83	2	2,19
Trial 2 - A	12÷14	300	82	2	1,77
Trial 2 - D	14	350	82	2	2,73
27.V.10	>700	440	54,5	2	6,12
27.V.10	>700	440	37,5	2	9.05

Feature to note are:

- UC strength increases as specimen diameter decreases (30% from D = 37 to D = 54 mm). This may be explained considering the possible presence of more defects or weak inclusions in larger samples. It is assumed, in this context, that the reference strength is that provided by the specimen with D = 100 mm;
- Trial panel D provides higher UC strength if compared to trial panels 4, 5 and 8, even if the former was realized with a lower cement dosage and tested at shorter t_{cur}. This can be attributed to the longer time taken by the mixing process, corresponding to a higher mixing quality factor.
- Similarly to concrete, the h/D influences considerably the UC strength. More particularly, a specimen with h/D = 1 is characterized by an UC strength ($q_{u,cub}$) greater than the one ($q_{u,cyl}$) provided by the specimen with h/D = 2. The ratio ($q_{u,cub}/q_{u,cyl}$) falls in the range between 0.75 to 0.85.
- Specimens with t_{cur} > 2 years gave smaller UC strength if they had been previously subjected to permeability tests. This could be due to an increase of material saturation, that, in turn, reduces the UC strength.
- UC strengths reported in Tab. 1 (especially those at t_{cur} = 40 days) seem to be in agreement with the results reported by Ganne et al. (2010), who measured an average UC strength equal to 1.7 MPa at 28 curing days for CSM treatment of clayey materials.

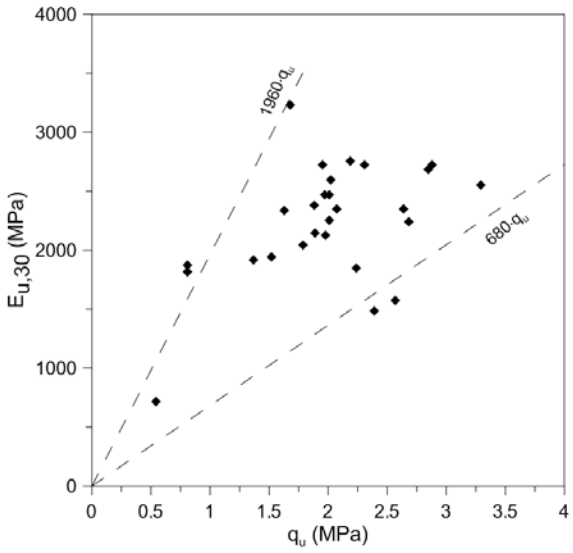

Figure 3: relationship between E_{30} and q_u at 40 curing days

Fig. 3 sketches the secant modulus of elasticity E_{30} (evaluated at 0.30 q_u) as a function of the UC strength obtained from D = 83 mm and h/D = 2 specimens. To notice the almost linear increase of elasticity modulus with the UC strength, being the 5% and 95% fractile of a log-normal distribution characterized by the following equations:

$$E_{30,\min} = 680 \cdot q_u \quad (2)$$

$$E_{30,\max} = 1960 \cdot q_u \quad (3)$$

The previous equations are consistent with those proposed by Ganne et al. (2010), who carried out tests on 100 cores with a diameter between 85 mm and 115 mm and h/D = 2.

4.2. Indirect traction tests

The indirect tensile strength (EN 12390-6:2002) of the treated material was determined on 5 specimens of 37 mm in diameter and aspect ratio of 2, characterized by a curing time of more than two years. The tests were performed with a displacement rate of 0.2 mm/min.
According to Okumura (1996), the indirect tensile strength of the treated clay has been found to range from 0.1 to 0.25 of the UC strength.

4.3. Permeability tests

A flexible wall permeameter was used to measure the hydraulic permeability of 3 specimens (D = 37 mm, h/D = 2 and h/D = 1), drown up from a definitive panel formed by CSM treated silty clay with a fine content greater than 90%.
Different gradients were applied ranging from 30 (ASTM D5084) to 302. The results are summarized in Tab. 2.

Table 2: permeability test results

Specimen	D (mm)	h (mm)	Age (days)	gradient i (-)	q_u (MPa)	k (m/s)
B6s	37.4	77.2	>700	259	-	$2.07 \cdot 10^{-11}$
B11s	37.3	38.2	>700	30 (ASTM D5084)	7.92	$2.61 \cdot 10^{-11}$
B12s	37.9	37.7	>700	302	8.30	$2.75 \cdot 10^{-11}$

It is interesting to note the very low permeability of mixed soil even under very high hydraulic gradients which are unusual in real applications. This feature is of particular relevance when CSM panels are used to prevent seepage of polluted fluids.

4.4. Mineralogical and microstructural tests

To investigate the degree of homogeneity of CMS treated soil and the spatial distribution of cement bonding the soil matrix, different techniques such as scanning electron microscopy, X-rays powder diffraction and X-rays micro-tomography have been extensively used throughout the research. For the sake of brevity, only the typical result of a X-ray micro-tomography carried out on the mixed soil is shown here.
X-ray computed analysis is a non destructive technique to measure variations in material density (e.g. Farber et. al, 2003), thus allowing for a three-dimensional reconstruction of a samples by back-projecting its shadow X-ray projections using a mathematical algorithm. In general, with the most recent systems it is possible to achieve a spatial resolution approaching 1 micron.
This type of analysis is very useful for material sciences as it is suitable to investigate the microstructure of a wide range of substances for the most various purposes and applications. In particular, X-ray micro-tomography can be used as an alternative way to determine both porosity and pore size distribution within an object (Farber et al., 2003).
Micro-tomographic analysis performed on a small cylindrical specimen with D = 8 mm is depicted in Fig. 4. It is worthwhile to note the relative homogeneity of cemented soil matrix, showing the effectiveness of CSM treatment as mixing method. However, because the X-rays generated from the source are absorbed by the specimen according to the element atomic number, some inclusions can be recognized, that basically consist of untreated clay or mineral compounds. From the analysis of the cross sections obtained by elaborating the back-projected images recorded with X-ray scanning, it was possible to estimate a level of diffuse micro-porosity ranging from 5.5% to 6.8% in the mixture and a dominant pore radius of about 22 μm.

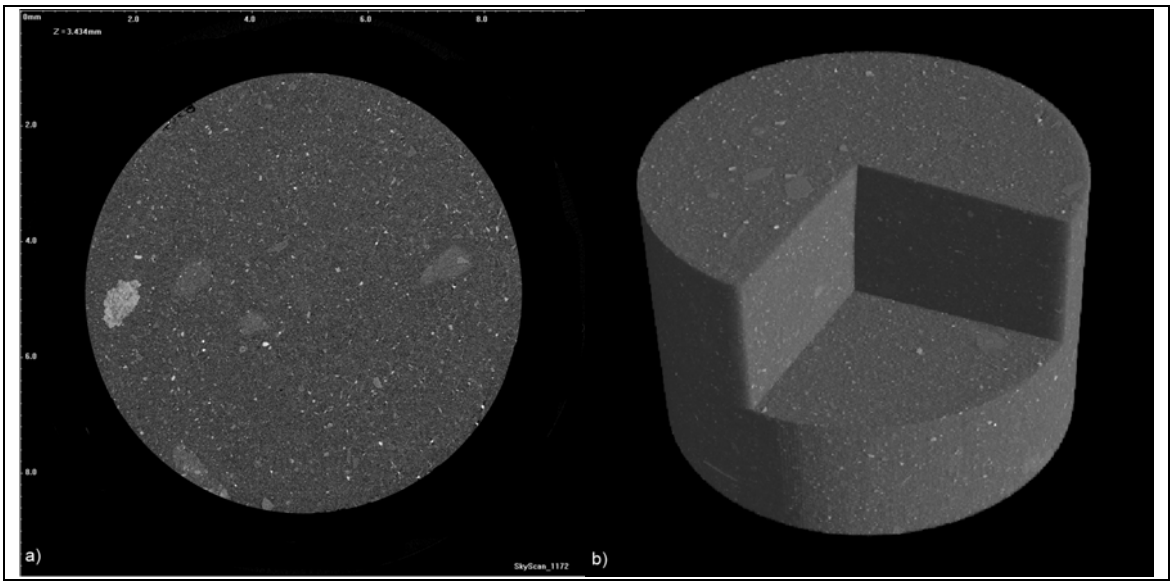

Figure 4: micro-CT analysis of a CSM treated speciment: a) 2D cross section; b) 3D reconstruction.

5. TEST RESULT INTERPRETATION

According to several researchers (e.g. Terashi et al., 1983; Babasaki et al., 1996; Kitazume, 2005), the most important factors affecting the soil improvement due to mechanical deep mixing are the binder characteristics, the soil type and state, the curing condition, and the mixing method; the latter being mostly influenced by the mixing tool (different from one machine to another) and the system used for each specific site.

Simplified approaches to predict the UC strength of stabilized soils have been already proposed, but none of these are characterized by a significant degree of accuracy. As a consequence of that, there is no widely applicable equation to predict the field strength gain, according to the above mentioned relevant factors.

Kitazume (2005) proposed the simplified scheme of Figure 5 valid for mechanical mixing method to relate the UC strength to the amount of binder used. When the soil is mixed in the laboratory under controlled condition, the UC strength increases linearly with the amount of added binder, exceeding necessarily a minimum threshold value ranging from 30 to 50 kg/m^3. This latter limit is somewhat higher in the field, that is around 50 kg/m^3 (5% of soil dry weight is basically necessary), but the linear trend between strength and binder amount is somewhat less sloping and limited by an upper binder amount, above which no further improvement is achieved.

Keeping in mind the scheme shown in Fig. 5, a novel equation was tentatively developed to predict the UC strength of CSM treated soil as a function of the relevant factors listed above, such as binder characteristics, the soil type and state, the mixing**,** and curing conditions.

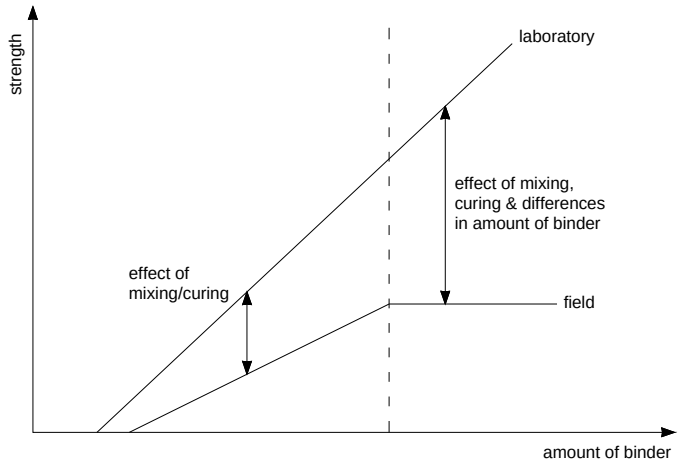

Figure 5: Effect of binder dosage on treated soil strength for mechanical mixing technique (from Kitazume, 2005)

5.1. Prediction of UC strength at 28 curing days

The fundamental factor affecting the UC strength is the amount of cement (c_c) introduced into the ground, that is directly related to the *wcr* of the bonding slurry and to the flow rate at which the slurry is injected. Additional factors considered here are the soil fine content *FC* and the mixing quality factor μ.
The basic equation linking the UC strength of treated soil $q_{u,28}$ at t_{cur} = 28 days to the binder amount may be as follows:

$$q_{u,28} = q_{u,28}^{MAX} \cdot e^{-\left(\frac{\kappa}{1+c_c}\right)^2} \quad (5)$$

where $q_{u,28}^{MAX}$ is the maximum UC strength at t_{cur} = 28 days corresponding to a binder dosage beyond which no further strength increment occurs (here assumed equal to 3 MPa), κ is a reference value for the amount of binder introduced into the ground (200 kg/m^3), and c_c is the amount of cement selected for the treatment.
Equation (5) has to be modified to take into account the influence of the fine content and the mixing quality factor.
Therefore, equation (5) can be rewritten as:

$$\bar{q}_{u,28} = q_{u,28} \cdot \bar{F} = q_{u,28} \cdot F_{\mu} \cdot F_{FC} \quad (6)$$

in which $\bar{q}_{u,28}$ is the corrected UC strength at t_{cur} =28 days, and

$$F_{FC} = \alpha \cdot \left[1 + e^{-\left(\frac{FC}{FC^*}\right)^2}\right] \quad (FC \text{ in } \%) \quad (7)$$

$$F_{\mu} = \alpha \cdot \left[1 + \frac{1}{2} \cdot e^{-\left(\frac{\mu^*}{\mu}\right)^3}\right] \quad (8)$$

where α = 0.9, *FC** is a reference value for the fine content of the original soil to be stabilized (here assumed equal to 60%), μ* is a reference value for the mixing quality factor (assumed equal to 22).
It is noteworthy that Eq. (7) and Eq. (8) have been calibrated for the soils of Bologna, i.e. for FC > 50%.
Clay treated strength at t_{cur} = 28 days predicted by Eq. (5) and (6) is displayed in Fig. 6. The solid line represents the curve defined by Eq. (5), whereas the dotted lines show the effect of the correction factor F_{μ} on the strength increase.

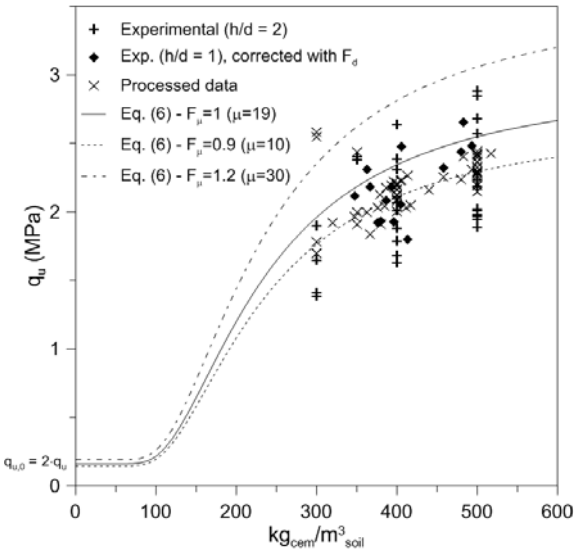

Figure 6: empirical model for the prevision of the unconfined compressive strength at 28 curing days of clayey soils treated with the CSM technology.

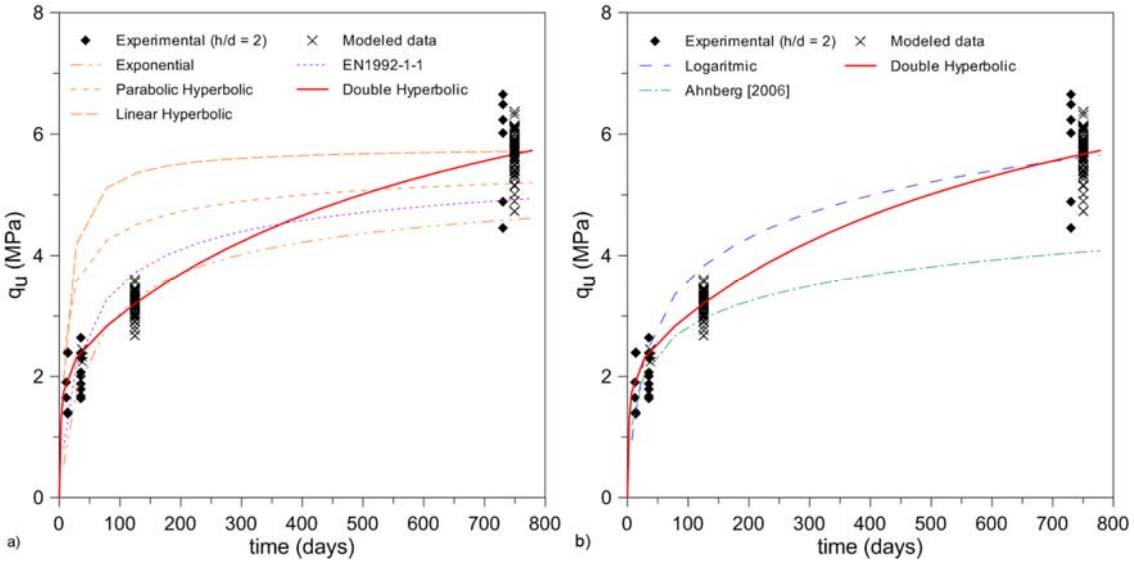

Figure 7: influence of curing time on strength development for treated clayey soil from Bologna: a) comparison between double hyperbolic formulation and classical models proposed for concrete; b) comparison between double hyperbolic formulation and some proposed for DMM.

It is interesting to note from equation (6) that, as long as the binder dosage is not greater than 75 kg/m^3 (approximately 5% of the soil dry weight), the strength gain is almost zero. Overcoming this latter value, the strength increases rapidly and, finally, for binder contents beyond 500 kg/m^3 its effect becomes less important.
Equation (6) can be easily adapted to take into consideration further effects on the UC strength due to the other possible influencing factors, such as *pH*, ignition loss, the humic acid content, etc. For instance, the amount of binder, c_c, to be introduced into equation (5) and (6) can be modified in order to consider the effect of *pH* (e.g. Gotoh, 1996) for alluvial clayey and sandy soils as follows:

$$F = \frac{c_c}{9 - pH} \qquad \text{for } pH < 8 \tag{9}$$

$$F = c_c \qquad \text{for } pH \geq 8 \tag{10}$$

5.2. Influence of curing condition

One of the most accepted approaches taking into consideration curing time and temperature on strength development in self-hardening material such as concrete is the so called “Maturity method” (e.g. Nurse, 1949; Saul, 1951).
Starting with this approach, several relationships were developed in the past to account for the effect of both the curing time and curing temperature on the strength development of concrete, such as those based on linear and double hyperbolic equations, exponential and logarithmic functions.
These empirical relationships have been preliminarily used to fit the experimental data obtained from laboratory test on CSM treated soils (Fig. 7a), but with unsatisfactory results except the case of the formula provided by EN 1992-1-1 (Ganne et al., 2010). This may be due to the fact that stabilized soils show delayed strength development compared to concrete, and showing also a pronounced long-term increase dependent on the type of soil and cement used for stabilization (e.g. Åhnberg, 2006). In our case, a CEM IV A was used, leading thus to slower formation of pozzolanic reaction products.
The applicability of other empirical relationships provided in the literature has been verified, as shown in Fig. 7b. Kitazume (2005) observed that the UC strength of clays increases almost linearly with the logarithm of curing time. Hence, two logarithmic equations have been considered in the following analysis. The most satisfactory fit for $t_{cur} > 3$ days was found with the equation (blue dot line in Fig. 7b):

$$q_u(t_{cur}) = \log(t_{cur}) - 1 \tag{11}$$

To better represent the UC strength increase with curing time observed in Bologna specimens, a new empirical equation, based on a double hyperbolic function, has been proposed. This function is composed of two terms: the former describes the strength increase in the first 28 curing days, whereas the second one defines the development of long-term strength. The relation is given by:

$$q_u(t_{cur}) = \frac{\bar{q}_{u,28} \cdot t_{cur}}{t_{cur} + K_1 \cdot \bar{q}_{u,28}} + \frac{\Delta q_\infty \cdot t_{cur}}{t_{cur} + K_2 \cdot \Delta q_\infty} \quad (12)$$

in which $\bar{q}_{u,28}$ is the corrected UC strength resulting from Eq. (6), Δq_∞ is the strength increment due to long-term reaction products, and K_1 and K_2 are two constants dependent on the type of clay and cement used in the treatment (in this case K_1 =1 and K_2 =100 have been selected).
If the curing temperature is available, it would be possible to take into account the maturity effect introducing in the formula the equivalent age, t_e, at the reference temperature (Carino & Lew, 2001), instead of the curing time, t_{cur}. By means of constants K_1 and K_2 it is, in principle, theoretically possible to consider different site mixing conditions.

6. CONCLUSIONS

In the paper, a comprehensive study on clayey soils treated with the Cutter Soil Mixing technique was presented and discussed.
The experimental programme included soil geotechnical characterization, elaboration of the raw machine data collected during the realization of trial and definitive CSM panels, intensive investigation on structural and hydro-mechanical properties of the treated material, and, finally, the formulation of a predictive equation to estimate the unconfined compressive strength of the stabilized clay.
One of the key factors for the performance of the treatment is the "mixing quality factor", introduced to better describe the site working conditions. This parameter can also be regarded as a practical way to confirm the quality required for the CSM panels.
Permeability tests have shown a surprisingly low permeability, of the order of magnitude of 10^{-11} m/s, a value of particular relevance when CSM is used to prevent leaching of polluted fluids.
From the interpretation of the mechanical test results, an empirical equation has been formulated taking into account the main factors affecting the performance of the treatment, i.e. characteristics of binder, characteristics and conditions of soil, mixing and curing conditions. The applicability of the proposed equation, calibrated for the jobsite of Bologna (Italy), to include further influencing factors has been discussed. Future research has been already planned for its validation in different ground and site conditions.

7. AKNOWLEDGEMENTS

The authors gratefully acknowledge Prof. Stefano Ciufegni (Italferr S.p.A.) and Eng. Stefano Neri (Astaldi S.p.A.), who provided geotechnical and technical information and data about the jobsite in Bologna.

REFERENCES

ASTM D 5084-00: Standard test methods for measurement of hydraulic conductivity of saturated porous materials using a flexible wall permeameter.

Åhnberg, H. (2006). Strength of Stabilised Soils – A laboratory study on clays and organic soils stabilized with different types of binder. Ph.D. Thesis, Swedish Geotechnical Institute, Stockholm, Sweden.

Babasaki, R., Maekawa, H., Terashi, M., Kawamura, M., Suzuki, T., Fukuzawa, E. (1996). JGS TC Report: Factors influencing the strength of improved soil. Proc. 2° Int. Conf. on Ground Improv. Geosyst., Tokio, Vol.1, pp. 913-918.

Carino, N.J., Lew, H.S. (2001). The maturity method: from theory to application. Proceedings of the 2001 Structures Congress & Exposition, Washington, D.C.
EN 12390-3:2003: Trial on hardened concrete – Sample compression strength.
EN 12390-6:2002: Trial on hardened concrete – Sample indirect traction strength.

Farber, L., Tardos, G., Michaels, J.N. (2003). Use of X-ray tomography to study the porosity and morphology of granules. Powder Technology, No. 132, pp. 57-63.

Fiorotto, R., Schöpf, M., and Stötzer,E. (2005). Cutter Soil Mixing(CSM) - An innovation in Soil mixing for creating Cut-off and Retaining walls. Proc. 16th ICSMGE, 15 sept. 2005, Osaka-Japan, pp. 1185-1188.

Ganne, P., Huybrechts, N., De Cock, F., Lameire, B., Maertens, J. (2010). SOIL MIX walls as retaining structures – critical analysis of the material design parameters. International conference on geotechnical challenges in megacities, Moscow, pp. 991-998.

Gotoh, M. (1996). Study on soil properties affecting the strength of cement treated soils. Proc. 2° Int. Conf. on Ground Improvement Geosystems, Tokio, Vol.2, pp. 399-402.

Kitazume, M. (2005). State of Practice Report: Field and laboratory investigation, properties of binders and stabilized soils. Proc. of the Int. Conf. on Deep Mixing Best Practice and Recent Advances, Stockholm, pp. 660-684

Kohata, Y., Maekawa, H., Muramoto, K., Yajima, J., Babasaki, R. (1996). JGS TC Report: Deformation and strength properties of DM cement-treated soils. Proc. 2° Int. Conf. on Ground Improv. Geosyst., Tokio, Vol.1, pp .905-911.

Mitchell, J. K. (1981). Soil Improvement: State-of-the-Art Report, Proc. 10th ICSMGE, Stockholm, pp. 509-565.

Nurse, R.W. (1949). Steam curing of concrete. Magazine of concrete research, Vol. 1, No. 2, pp. 79-88.

Rathmayer, H. (1996). Deep mixing methods for soft subsoil improvement in the Nordic Countries. Proc. 2° Int. Conf. on Ground Improvement Geosystems, Tokio, Vol.1, pp. 869-877.

Saitoh, S., Suzuki, Y., Nishioka, S., Okumura, R. (1996). Required strength of cement improved ground. Proc. 2° Int. Conf. on Ground Improvement Geosystems, Tokio, Vol. 2, pp. 557-562.

Tatsuoka, F., Kohata, Y., Uchida, K., Imai, K. (1996). Deformation and strength characteristics of cement-treated soils in Trans-Tokio Bay Highway Project. Proc. 2° Int. Conf. on Ground Improvement Geosystems, Tokio, Vol.2, pp. 453-459.

Saul, A.G.A. (1951). Principles underlying the steam curing of concrete at atmospheric pressure. Magazine of concrete research, Vol. 2, No. 6, pp. 127-140.

Terashi, M., Tanaka, H., Mitsumoto, T., Honma, S., Ohhashi, T. (1983). Fundamental properties of lime and cement treated soils (3rd Report). Report of the Port and Harbour Research Institute, Vol. 22, No.1, pp. 69-96 (In Japanese).

Terashi, M. (1997). Theme lecture: Deep Mixing Method – Brief State of the Art. Proc. 14th ICSMGE, Vol. 4, pp. 2475-2478.

Yoshizawa, H., Hosoya, Y., Okumura, R., Sumi, M., Yamada, T. (1996). JTS TC Report: Factors affecting the quality of treated soil during execution of DMM. Proc. 2° Int. Conf. on Ground Improvement Geosystems, Tokio, Vol.1, pp. 931-937.

Usui, H. (2005). Quality control of cement deep mixing method – wet mixing method – in Japan. Proc. Int. Conf. on Deep Mixing Best Practice and Recent Advances, Stockholm, pp. 635–638.

Geomix Caissons against liquefaction

Lucie Benhamou, Soletanche Bachy France, France, lucie.benhamou@soletanche-bachy.com
Fabrice Mathieu, Soletanche Bachy, fabrice.mathieu@soletanche-bachy.com

ABSTRACT

The latest earthquake in Martinique (Carribean Islands) occurred in November 2007. It caused a lot of damages on buildings, as some administration offices in Fort-de-France. Therefore, construction of two new buildings was launched in 2010.

Site conditions are very soft (PMT Limit Pressure~0.3 MPa, Menard Modulus~2.2 MPa), silty sandy alluvia over 9 to 18 m depth. Foundations of the new buildings must report both static and seismic loads on the substratum strata.

The concern was to present a solution preventing soils liquefaction as well as post liquefaction injuries caused by soils flow along the substratum slope. Solution consisted in building a new type of foundations based on a Geomix caisson arrangement under buildings surface (circa 36 m x 40 m). The designed arrangement consisted on a grid made by Geomix trenches, 0.50 m thick, and about 4.0 to 4.3 m spacing at centreline.
Due to their strong inertia (compared to rigid inclusions for instance) and geometry, Geomix panels displacements are limited during earthquake episode.
Additionnal shear stress of the soil and horizontal forces coming from the structure are concentrated on Geomix bands and liquefaction on the uncaged ground is avoided. This treatment also resists to the external post-liquefaction soil flow.
Geomix foundations also reduce settlements under the structure for current situation without earthquake.

This type of deep mixing treatment is already used in Japan. Using the Geomix technique, less excavation materials needs to be evacuated and less impact on the environment as noise and vibrations is generated during works. It was indeed chosen by the Client for all those technical reasons.

1. GEOLOGICAL AND GEOTECHNICAL CONDITIONS

1.1. Seismic background of Caribbean Islands

Martinique Island is classified as Zone III, the highest zone, on France seismic map. At this location, Caribbean plate moves compared to North and South American plate by about 2 cm/year. One part of this convergence is absorbed in the subduction area where the Atlantic lithosphere sinks below Caribbean arch, the other part induces deformation of Caribbean plate itself.

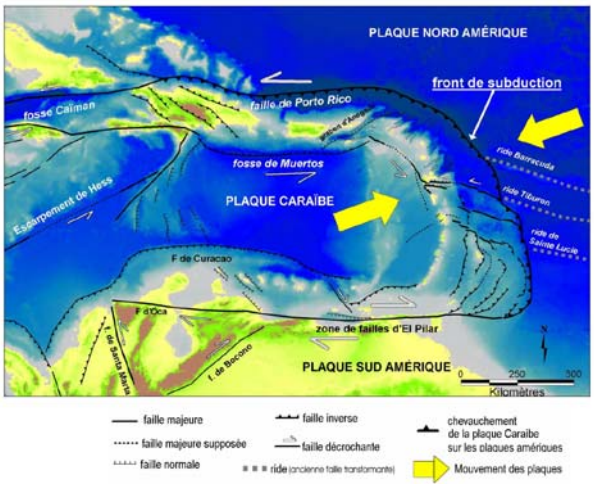

Figure 1: Caribbean seismic arch (Stephan et al, 1985 ; Taboada et al, 1999 ; Feuillet, 2000)

Due to this situation, Caribbean Islands area is particularly exposed to seismic risks.

As an answer to this risk, French government has launched in January 20007 a specific seismic plan on the area. First step of the plan consists in either reinforcing foundations or rebuilding public buildings like schools and administration offices.

Liquefaction remediation works in Fort-de-France described in this article were carried out in this context.

1.2. Geotechnical parameters

A complete site investigation was carried out in 2009 on the whole job-site area, including dynamic penetrometric tests, pressiometer tests and piezometric drillings. Results enhanced previous investigations performed in 2008 on the base of several static penetrometer tests. Fort–de-France geotechnical conditions can be summarized in table 1 below :

Table 1: Geotechnical parameters

	Strata base NGM	g kN/m^3	pl MPa	Em MPa	a	c' kPa	f' (°)
Fill and sandy alluvia	+2.0	18	0.26	2.2	0.50	0	25
Alterated clay	-7.0 to -16.0	19	1.6 to 2.4	20.0 to 30.0	0.67	10	28
Tuffite	-	20	5.0	60.0	0.67	20	30

Water table has been recognized at 1 m depth ~ +1 NGM.

Static and shear deformation moduli are given by equations 1 and 2 :

$$E_{s,stat} = \frac{E_m}{\alpha} \quad (1)$$

$$G_{s,stat} = \frac{E_{s,stat}}{2(1+n)} \quad (2)$$

with n~0.33 for static et ~0.50 for dynamic conditions.

Minimum dynamic deformation modulus has been estimated to be $E_{dyn} \approx 6\ E_{stat}$.

1.3. Liquefaction evaluation

Liquefaction risk was evaluated on base of the National Center for Earthquake Engineering Research (NCEER) procedure " Workshop on evaluation of liquefaction resistance of soils - Report NCEER-97-0022".

In this procedure, two variables are defined for a liquefiable soil layer :
- The seismic demand on this layer, called Cyclic Stress Ratio (CSR);
- The capacity of soil to resist liquefaction, called Cyclic Resistance Ratio (CRR).

According to this procedure, liquefaction risk has to be considered if Cyclic Stress Ratio becomes greater than Cyclic Resistance Ratio with a given safety factor.

Analysis of CPT tests obtained in 2008 shown that alluvium layer can be liquefied under seismic conditions. Factor of safety in this layer between Cyclic Resistance Ratio CRR and Cyclic Shear Resistance CSR is a lot smaller than 1.0.

2. DEEP SOIL MIXING METHODS AGAINST LIQUEFACTION

As shown in figure 2 below, deep soil mixing can be used to construct liquefaction remediation structures. This type of solutions has been applied in Japan for many years.

As an example, Oriental Hotel in Kobe was founded on piles surrounded by a grid-type structure made of deep mixing walls. During 1995 earthquake, the Oriental Hotel structure did not show any damages despite important displacement on surrounding structures under accelerations up to 0.8g.

Method	Soil Type	Effective Depth	Attainable Improvement	Advantages	Limitations	Prior Experience	Potential Future Developments
Explosive Compaction	Sands, silty sands	Unlimited	D_r = 75 % $(N_1)_{60}$ = 20-25 q_{c1} = 10-12 MPa	Inexpensive, Simple technology	Vibrations, Psychological barriers	Extensive use; no EQ yet at improved sites	Quantification of process, Better prediction of improvement level, Optimization of charge size, location and detonation sequence
Vertical Drains	Sands, silty sands	20 m (?)	Reduce pore pressure buildup, Intercept pore pressure plumes	Inexpensive, Does not require treatment of full area	May require very close spacing, Settlement not prevented	Some applications for interception of pore pressure plumes	Use in combination with other methods, More definitive confirmation of effectiveness
Surcharge and Buttress Fills (below and above ground)	All soil types	NA	Site specific, Increased σ_v' reduces liquefaction potential, Barriers against lateral spreading	Lower cost, Protection of existing embankments and large unimproved sites	Liquefaction settlement in retained areas, Space needed for above ground buttresses	Seismic retrofit of embankment dams and retention of liquefiable sites	Development of simplified methods for analysis of stability and deformations
Deep Soil Mixing	Most soil types	20 m	Depends on size, strength and configuration of DSM elements	Positive ground reinforcement, Grid pattern contains liquefiable soil, High strength	Requires special equipment, Brittle elements	Excellent performance in 1995 Kobe EQ	Techniques for ground response analysis, Improvements in materials, equipment and installation technology, Combination with other grouting technologies

Figure 2: Summary of ground improvement methods for remediation of large, open, undeveloped sites

3. GEOMIX CAISSON SOLUTION

3.1. Geomix technique

Geomix® is a Deep Soil Mixing technique on base of Hydrofraise technology combined with Cutter Soil Mixing (CSM) principle. Basics of the process are shown in figure 3.

Figure 3: Construction process in Geomix technique with CSM equipment

When drilling under action of two counter rotative cutting wheels, natural soil is bulked and mixed with a specific injected fluid and then displaced above the cutting head. During withdrawal, rotation of wheels is reversed to displace the mix below the cutting head and final homogenisation is done while completing the slurry incorporation.

Depending on soil conditions and type of construction, the incorporated fluid during drilling and withdrawal can be similar.

Specific instructions for treatment such as injected volumes and mixing factors are adapted according to natural soil characteristics (e.g. type of soil, sieve analysis, permeability, water table level). These instructions are controlled and recorded through a monitoring system installed on the base carrier.

Geomix can be applied for various applications such as retaining walls, cut-off walls or soil improvement.

3.2. Construction schedule

Completion of treatment by Geomix method on Fort-de-France site has been carried out by drilling under bentonite mud down to 19m depth. Section of the drilling tool was 2,800mm x 500mm.

Prior construction of each panel, the platform was prepared by execution of 1.5m deep pre-trench aimed to purge few concrete blocks and canalize the volume of excess materials produced during treatment.

Geomix caisson was constructed through the surface fills, fine compressive sandy alluvia layer and alterated clay layer. Keying of each panel has been done by 1m drilling through compact tuffite layer located below.

Specific quality control of this keying was allowed through real time drilling parameters displayed and recorded on the supervision installed in cabin. Reports processed in office for each panel have shown good correlations with soil investigation reports.

Panels have been executed through a primary/secondary sequence, with a sufficient overlap between consecutive panels to ensure the construction of a continuous structure. Deviations measured in real time in supervision have been post processed in office to build a tri-dimensional view of the constructed structure, as shown on figure 4.

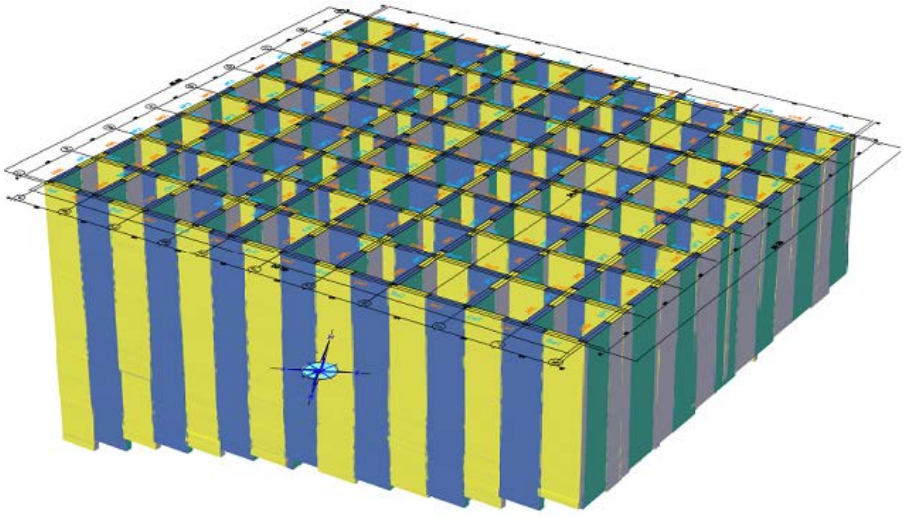

Figure 4: 3D view of Geomix caisson structure.

Due to working sequence, cement slurry has been incorporated in the mix during withdrawal of CSM equipment. A few days delay between execution of primaries and secondaries has been considered to prevent soil mixed material to be washed out by bentonite when drilling an adjacent panel.

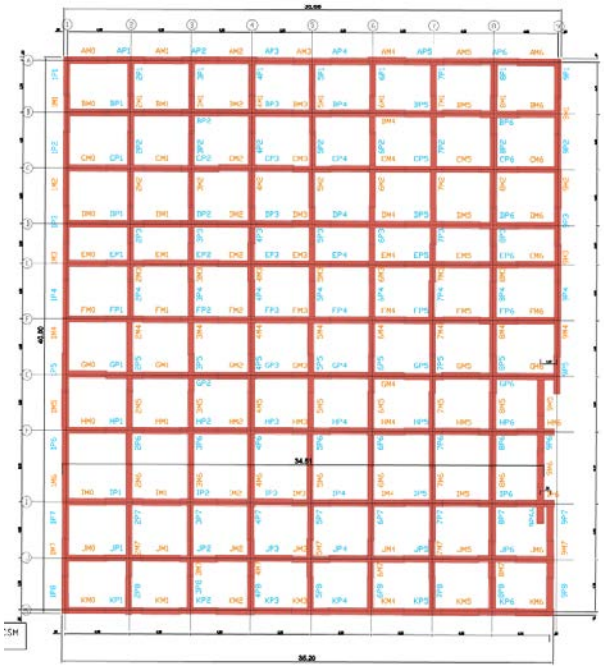

Figure 5: As built cross section at 10m depth.

Specific treatment parameters such as homogeneity factor and water/cement ratio of the final mix were determined taking into account cement type, water table level and properties of natural soil layers to reach 1MPa minimum UCS at 90 days in the anchoring layer.

Works last 3 months, including plant set up. Over 10 people worked on this site, organised in 2 shifts.

Key figures are:

Treated surface	36 m x 40 m = 1440 m²
Geomix® depth	11 to 19 m
Panel width	0.50 m
Panels quantity	279

4. DESIGN ISSUES

4.1. Geomix design properties

Unconfined compressive strength	>1 MPa
Static deformation modulus	Ec,stat ≥ 250*UCS = 250 MPa
Dynamic shear modulus	Gc,dyn = 500 MPa
Wet specific gravity	γ = 18 kN/m3
Internal friction angle	Φ‘ = 30°
Cu_{Geomix} (seismic conditions)	UCS/2
Traction resistance	Min (0.2 MPa ; 0.15*UCS)

4.2. Settlement calculation under static load

Depending on the area, buildings settlement under static loading is between 1.0 to 2.0 cm. Compression stress is given in § 4.4.2.

4.3. Seismic loading: Checking stability and internal forces

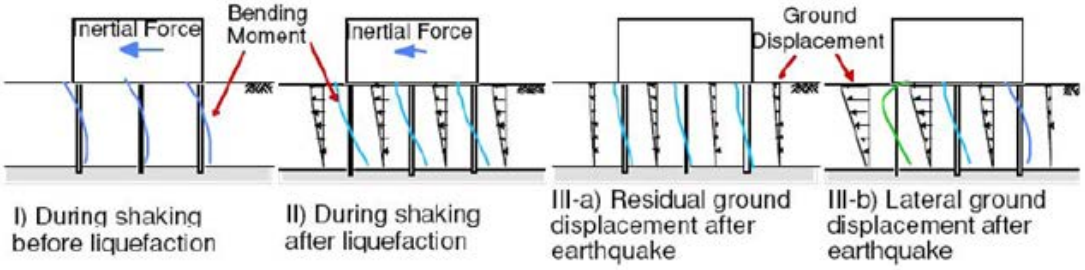

Figure 6: Typical Earthquake steps.

Design consisted in checking that overall stability of Geomix caisson and verifying internal forces into Geomix material were allowable at all earthquake stages.

Stress sharing between soil and Geomix during shaking was based on the results of a numerical model.

After shaking, the liquefied soil acts like a soil flow along the substratum. No more structural loads were considered at this stage but an hydrostatic pressure due to the soil on Geomix caisson barrier.

4.4. Results summary

4.4.1. Stability checks

For each building D1 and D2, safety factors for each earthquake stage are given in table 2.

Table 2: Stability check table

	Sliding // OX	**Sliding // OY**	**Rotation / OX**	**Rotation / OY**
ULS-1	D1/ 7.2 D2/ 17.2	D1/ 1.33 D2/ 2.1	D1/ 1.7 D2/ 1.6	D1/ 18.5 D2/ 30.3
ULS-2	D1/ 61.2 D2/ 66.4	D1/ 7.5 D2/ 8.1	D1/ 9.6 D2/ 6.2	D1/ 157 D2/ 116
ULS-3	--	**D1/ 1.4** **D2/ 1.26**	**D1/ 3.5** **D2/ 2.04**	--

Stability of reinforced soil block has been verified for all cases for both buildings with a minimum factor of 1.26 (> 1.25 required).

4.4.2. Resistance checks

Stress calculation results are summarized on the following table 3.

Table 3: Resistance table

	s_c (MPa)	**t (Mpa)**
SLS	G+Q ; D1 : 0.24 ; D2 : 0.30	--
ULS-1	**$F'z_{max} + g.h$** **D1 : 44222/156.7+(18)(13)=> 0.52** **D2 : 50830/146.4 +(18)(18)=> 0.67**	**D1 : 0.235** **D2 : 0.286**

So unconfined compressive strength of Geomix must verify:
- At the SLS,
$1.35 * s_{els\text{-}max} = UCS_{90days} / 1.4$ e.g. UCS_{90days} = 0.57 MPa

- At the ULS accidental,
$1.00 * s_{ela\text{-}max} = UCS_{90days} / 1.25$ e.g. UCS_{90days} = 0.84 MPa
$1.00 * t_{ela} < UCS_{90days} / (1.25 * 2)$ e.g. UCS_{90days} = 0.72 MPa

To conclude, a 1.0 MPa minimum unconfined compressive strength at 90 days is required.

5. QUALITY ASSESSMENT / QUALITY CONTROL

Construction of Geomix caissons has been closely controlled during works, after hardening of soil mixed material and during partial excavation of one cell of the structure.

These controls included :
- a full analysis of the operating parameters recorded during the process,
- compressive strength measurements on slurry samples and wet grab samples,
- several core-borings inside panels,
- deformation modulus determined in lab,
- visual aspect of the final material after excavation.

UCS and deformation modulus tests were carried out regarding European requirements of NF EN 13286-41 and 13286-43.

The laboratory tests performed on samples confirmed that specified characteristics of the Geomix material were achieved with namely UCS resistance ranging from 1.0 to 2.0 MPa.

Design values for both UCS resistance and deformation modulus were validated.

Recorded data have been summarized in a report created for each panel, where incorporated material volumes, verticality and mixing ratios were displayed according to depth.
Verticality data were post-processed in office to construct the as-built tridimensionnal Geomix caisson structure shown in figures 2 and 3 for final checking of treatment continuity at different depths.

Partial excavation of one cell on the structure was done after completion of works, as shown on Photo 4 in Annex.

6. CONCLUSION

Geomix technique does not induce lateral or vertical stress into the in-situ ground. Underground structures can be constructed without vibration and dust emission and with a low noise production.

Size of the equipment is relatively small, making the construction of panels close to surroundings possible (see Photo. 5 in Annex).

Like other deep soil mixing technique, Geomix limits the production of excess materials to be evacuated to waste. The in-situ soil is used as a construction material, requiring a compact plant, easier to install and requiring no large concrete slab.

This gives to Geomix/CSM some technical, environmental and economical advantages compared to standard techniques such as D-Walls, and makes this technique particularly well adapted to urban site conditions, even more when environment and sustainable development may be a concern.

The successful creation of this caisson structure opens a huge field of application on any other site with a liquefaction hazard.
By its containment of weak soil and its strong inertia geometry, Geomix Caissons remains a ground improvement solution efficient for all earthquake steps.

To conclude, the technical solution applied in Martinique is strong, innovative, and based on a competitive technique than can definitely be applied on other seismic sites.

REFERENCES

C. Quentin, L. Wang, T. Martin (Ecole des ponts Paris Tech) with A. Pecker and P. de Buhan expertise, Analyse élastique d'un procédé de renforcement de sol : le Trenchmix, 2010.

Takahashi et al., 2006, Effect of deep mixing wall spacing on liquefaction mitigation, Physical Modelling in Geotechnics, 6th ICPMG 2006.

The Deep mixing method, Principle, Design and Construction edited by Coastal development institute of technology, Japan, 2002.

European requirements NF EN 13286-41 and NF EN 13286-43 for UCS and deformation modulus tests procedure.

Mathieu et al. ,2006, CSM : an innovative solution for mixed-in-situ retaining walls, cut-off walls and soil improvement, DFI Amsterdam 2006.

ANNEX

Photo 2 :CSM Equipment on LRB155

Photo 3 :Platform after execution of works

Photo 4 :Excavated caisson

Photo 5 :Construction of panels close to existing buildings

Foundation Soils Improvement by "Cutter Soil Mixing"

Bilé Serra João, LNEC, Portugal, biles@lnec.pt
Mendes Bruno Filipe, formerly LNEC, Portugal, bfmendes@sapo.pt

ABSTRACT

The improvement of foundation soils by Cutter Soil Mixing (CSM) aims at creating a reinforced foundation system whose strength and stiffness characteristics are likely to lie between those of DSM columns and concrete pile system. The safety evaluation of this mixed foundation system follows the definition of the serviceability and ultimate limit states criteria.
In this paper a detailed analysis of a CSM reinforced roadway embankment over a soft clay deposit is presented. From serviceability limit state requirements minimum values of panels mass density and Young modulus were first defined. The safety evaluation against serviceability limit states was performed by a detailed 2D plane deformation model with Plaxis software. Both construction sequence and time lagged effects due to the hydromechanical coupled behavior of soil and CSM panels were considered. A comparison between the analytical empirical methods proposed by EBGEO (2011) and the numerical results is presented as far as the stress distribution and arch effect relevance.
The consequences of the existence of weak zones in the panels, due to inadequacy of construction process, are analyzed by 2D numerical models with consideration of two types of zones regarding the reduction of properties, either with significant reduction or with drastic reduction. The position and length of these zones were defined in a deterministic way.

1. INTRODUCTION

The *Cutter Soil Mixing* (CSM) technique is one type of *deep mixing*. The in situ soil is cut and mixed with cement slurry, eventually with some additives such as bentonite, aiming at obtaining artificial panels with improved mechanical properties. It may be used for reducing settlements and improving the overall stability of supported embankments, building retaining walls, impermeabilization curtains or environmental confinement barriers and improving soil seismic resistance. The design of CSM panels requires safety verification against both ultimate and serviceability limit states of the improved ground and the supported structures or embankment. For those purposes, both analytical and numerical methods may be used. In this paper a hypothetical case of a road embankment on an alluvial basin is considered. The adopted geotechnical parameters of the ground and the CSM panels are based in a companion paper to this Conference [Mendes *et al.*, 2012].

2. FOUNDATION REINFORCEMENT WITH DEEP SOIL MIXING PANELS

2.1. Available normative documents

The increasing incidence of infrastructure construction on alluvial areas has led to the development of ground reinforcement techniques based on soil-water-binding mixtures. For safety verification purposes serviceability and ultimate limit states of these foundation systems must be analysed. Three different codes of practice are available for consideration when designing the panels, i.e. the BS 8006 (1995), the EN 14679 (2005) and the recent EBGEO (2011).

In the BS 8006 standard the adoption of partial factors based design is recommended. It contains a chapter on the design of geosynthetic reinforced embankments founded on soft soils. A load transfer model from the embankment to the reinforced foundation elements by arch effect is adopted in this standard.

The EN 14679 standard contains considerations about design and guidance for testing, supervising and monitoring of deep mixing implementation. However, no guidance is given about numerical models of the panels or about geosynthetic reinforcement interaction.

In 2003 a number of recommendations for reinforced earth structures (EBGEO) were published in Germany, aiming at standardizing the design procedures. In chapter 6.9 of this document a calculation procedure for geosynthetic-reinforced embankments is introduced. A revised version was published in 2010,

followed by an English version in the following year. Several authors (Kempfert *et al*., 2004 and Van Eekelen *et al*., 2008) have reported successful designs based on the EBGEO recommendations.
In this paper the design approach based on the analytical models of EBGEO (2011) was adopted for comparison purposes with the numerical modelling results.

2.2. Simplified consideration of three dimensional effects

For the numerical modelling of landfills founded on vertical reinforcement elements, a 3D problem, several types of models may be used, e.g. three-dimensional models, axisymmetric models or plane strain models. Given the substantially higher computational effort associated with three-dimensional models, equivalent plane strain models are usually implemented for analysis (Satibo, 2009). According to Bergado and Long (1994), the three-dimensional model of a network of reinforcing pillars can be well approached by a plane strain model with a geometrical idealization of a solid wall of equivalent thickness (teq). This thickness is calculated based on the improved area ratio, i.e. the ratio between the pillar area (Ac) and the area of the influence zone of the pillar (Ae). Since the pillar is transformed into a solid wall the adoption of a smaller width for the continuous wall preserves that ratio value between both situations. Equation 1 exemplifies the determination of the equivalent width for a column dimensions 0.9mx2.4 m and an influence area of area 2.4 mx3.4 m, which corresponds to the case studied in this paper

$$\frac{A_c}{A_E} = \frac{0.9 \cdot 2.4}{2.4 \cdot 3.4} = 0.265 \Rightarrow 0.265 = \frac{t_{eq} \cdot 3.4}{2.4 \cdot 3.4} \Rightarrow t_{eq} = 0.636m \tag{1}$$

Alternatively, the three dimensional arrangement of vertical elements may be replaced by a plane strain deformation model of a continuous wall with the same width but with a corrected stiffness E_{eq}. The equivalent Young's modulus is calculated based on the homogenization of the moduli of the pillar and of the soil weighted (respectively E_c and E_s) by the areas of the pillar and of the wall (A_c and A_p, respectively), as shown in equation (2).

$$E_{eq} = \frac{E_c \cdot A_c + E_s \cdot \left(A_p - A_c\right)}{A_p} \tag{2}$$

2.2.1. Determination of the load on the soil-cement panels through empirical (EBGEO) analysis

The load transference model in EBGEO (2011) allows calculating the load supported by the panels and by the soil, according with equations 3 to 6. Let's consider the case of an embankment with height *h* and characteristic value of unit weight γ_k with a permanent distributed load at the top with characteristic value p_k . The foundation panel system is characterized by dimensions d_x and d_y (panel width, i.e. in longitudinal direction, and panel length, in the transversal direction, respectively and spacing s_x and s_y between panel axis in x direction and y direction, respectively.
One obtains the following expressions for the vertical stress at the contact plane between the embankment and the ground between the panels $\sigma_{zo,k}$ and at the panels at the contact plane $\sigma_{zs,k}$;

$$\sigma_{zo,k} = \lambda_1{}^{\chi} \cdot \left(\gamma_k + \frac{p_k}{h}\right) \cdot \left\{ h \cdot \left(\lambda_1 + h_g{}^2 \cdot \lambda_2\right)^{-\chi} + h_g \cdot \left[\left(\lambda_1 + \frac{h_g{}^2 \cdot \lambda_2}{4} \right)^{-\chi} - \left(\lambda_1 + h_g{}^2 \cdot \lambda_2\right)^{-\chi} \right] \right\} \tag{3}$$

$$\sigma_{zs,k} = \left[\left(\gamma_k \cdot h + p_k\right) - \sigma_{zo,k} \right] \cdot \frac{A_E}{A_c} + \sigma_{zo,k} \tag{4}$$

$$\chi = \frac{d_x \cdot \left(K_{crit} - 1\right)}{\lambda_2 \cdot s_x} \qquad K_{crit} = tan^2\left[45^o + \frac{\phi'_k}{2}\right] \qquad \lambda_1 = \frac{1}{8} \cdot \left(s_x - d_x\right)^2 \tag{5}$$

$$\lambda_2 = \frac{s_x{}^2 + 2 \cdot d_x \cdot s_x - d_x{}^2}{2 \cdot s_x{}^2} \qquad h_g = \frac{s_x}{2} \qquad A_E = s_x \cdot s_y \_\_\_\_\_ A_c = d_x \cdot d_y \tag{6}$$

where K_{crit} stands for the critical principal stress ratio and $h_g$for the arc height.

3. CASE STUDY OF AN EMBANKMENT ON CSM COLUMNS

3.1. Case description

A hypothetical case study of a road embankment founded on a soft soil improved by CSM columns is here considered (Figure 1). *In situ* conditions are those typical of alluvial basin conditions, i.e., soft clayey organic soils with an average thickness of 19 m, underneath which exists a layer of overconsolidated silty clays thicker than 30 m. The groundwater level is assumed at the ground surface. In order to reduce the likelihood of short term failure of the foundation and the long term settlements due weak properties of the *in situ* soil, the foundation reinforcement by CSM panels is therefore advisable.

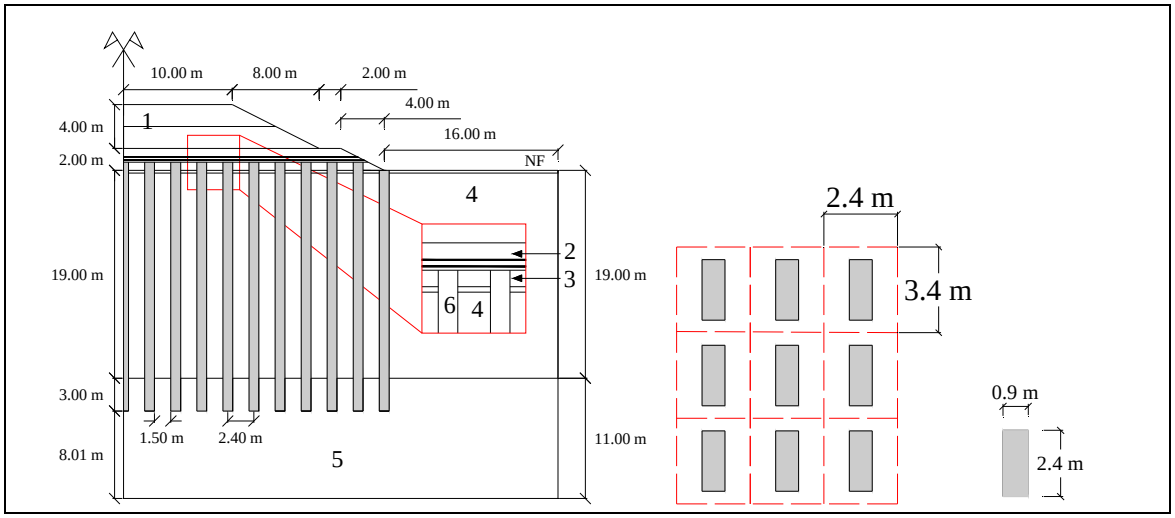

Figure 1: Cross section of the embankment and panels and plan view of the panel setup

As shown in Figure 1, the embankment geometry is the following: crest width (20 m), base width (40 m) and height (5 m). Due to workability requirements a working platform of dense sand one meter thick is to be constructed prior to the landfill placement. The embankment will be constructed in three layers, i.e., consecutively from bottom to top: i) a layer 1 m thick (material # 2), including two sheets of geosynthetic, 15 cm apart from each other, ii) a layer 2 m thick (material # 1) iii) and a third layer 2 m thick (also material # 1).

The embankment will be founded on a grid of CSM vertical panels 22 m long with 0.9 m x 2.4 m cross section. The shorter dimension is aligned with the transversal direction of the embankment. The distance in the longitudinal direction between panel axes is 3.4 m. For comparison purposes two alternative distances between panel axes (in the transversal direction) of 2.4 m (a total of 11 panels) and 2.9 m (9 panels) are considered. These panel arrangements will be identified as SC1 and SC2, respectively.

The analysis was performed both by the algebraic method of EBGEO (2001) and by a plane strain numerical model with Plaxis v8.2.

3.2. Analytical results

The results of the analytical formulation of EBGEO (2011) obtained according with equations 3 to 6 are shown in Table 1, where the variables meaning is the same as described above.

Table 1: Empirical analysis results for panels arrangement SC1 and SC2

Case	h (m)	γ_k (kN/m^3)	p_k (kPa)	s_x (m)	s_y (m)	d_x (m)	d_y (m)	$\sigma_{zo,k}$ (kPa)	$\sigma_{zs,k}$ (kPa)
SC1	5	20	15	2.4	3.4	0.9	2.4	387	17,2
SC2	5	20	15	2.9	3.4	0.9	2.4	425	28,0

In both situations the reinforcement effect is evident. However, the increase from case SC1 and SC2 of the vertical stress at the soil between panels (60%) is larger than that of the stress at the panels (only 10%).

3.3. Numerical results

3.3.1. Numerical model

A plane deformation model of 15 nodes triangular elements was adopted (Figure 2). The geometrical and mechanical symmetry of the problem was used to reduce the model dimension by restricting it to the portion to right of the symmetry axis.
The lower stratum of soil is stiff silty clay, so its contribution to the overall deformations is expected to be negligible. Accordingly, a fixed boundary condition was adopted at the horizontal bottom line. The nodes at both vertical boundaries are fixed against horizontal movement but allowed to slide freely in the vertical direction, either because of symmetry or mesh horizontal size effects considerations. At the symmetry axis and at the bottom boundary (due to extremely low permeability) impermeable boundary conditions are assumed. The same was assumed at the vertical right boundary for simplicity reasons, whereas at the surface free draining boundary conditions are assumed.

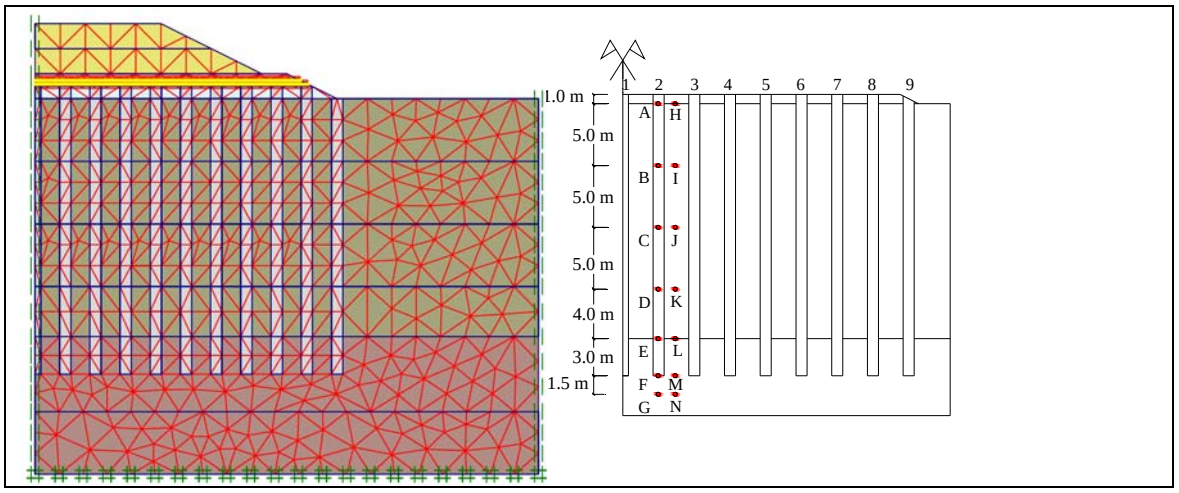

Figure 2: Finite element mesh and nodal points for output results representation

In order to keep the focus on the parametric sensitivity study of the foundation resistance rather than in elaborated modelling details, an elastic perfectly plastic Mohr-Coulomb model was selected for the CSM panels. For the soft clay (material #4) the Soft Soil model was adopted due to the relevance of the primary compression for such slightly consolidated material. The adopted material models and corresponding parameters are shown in Table 2. The calculation steps were defined in correspondence with the assumed construction phases of the embankment, as indicated in Table 3.

Table 2: Material models and parameters

Parameter	Embankement	Fill	Sand	Soft clay	Stiff clay	Soil-cement mixture
Material #	1	2	3	4	5	6
Material model	M-C	M-C	M-C	SS	M-C	M-C
Unsaturated unit weight γ_{unsat} (kN/m^3)	20	20	17	-	-	-
Saturated unit weight γ_{sat} (kN/m^3)	-	-	-	14.5	19.0	15.5
Horizontal and vertical permeability $k_h = k_v$ (m/s)	1	1	6×10^{-6}	1×10^{-9}	1×10^{-11}	1×10^{-10}
Effective Young's modulus E (MPa)	40	45	120	1	10	1000
Equivalent Young's modulus E_{eq} (MPa)	-	-	-	-	-	706
Poisson's ratio ν	0.35	0.35	0.35	0	0	301
Effective cohesion c' (kPa)	0	0	0	0	0	301
Effective friction angle ϕ'(º)	38	39	38	21	35	35

Parameter	Embanke-ment	Fill	Sand	Soft clay	Stiff clay	Soil-cement mixture
Dilatancy angle ψ (º)	0	0	8	0	5	0
Undrained strength s_u (kPa)	-	-	-	20	120	550
Modified compressibility coefficient λ^*	-	-	-	0.15	-	-
Modified unload/reload compressibility coefficient κ^*	-	-	-	0.028	-	-
OCR	-	-	-	1	-	-

Table 3: Calculation phases adopted in Plaxis the numerical model

Calculation phase	Analysis type	Time increment (days)	Total time (days)	Description
1	Elastoplastic	0	0	Model equilibrium
2	Elastoplastic & consolidation	30	30	Placement of the 1st and 2nd layers of fill (1m+2 m)
3	Elastoplastic & consolidation	20	50	Placement of the 2nd layer of fill (2 m)
4	Elastoplastic & consolidation	720	770	Two years consolidation time, necessary for the conclusion of the embankment
5	Elastoplastic	0	770	Roadway surcharge application (15 kPa)
6	Elastoplastic & consolidation	21900	22600	Long term behaviour (60 years)

The three-dimensional nature of the problem was addressed by the correction of the CSM panels Young modulus following equation 2.

3.3.2. Numerical estimative of settlement and vertical stress

The mechanical response of the reinforced system composed by the embankment, geosynthetic layers, panels and the ground between the panels is analyzed in the following. The output results to be analyzed are those obtained at the nodal points shown in the right part of Figure 2.

Settlements

A significant influence of the panels spacing in the predicted settlements may be observed in Figure 3a, where the 9 panels' arrangement (SC2) are systematically larger than those of the 11 panels' case. The reinforcing effect of the panels is evident in both the general decrease of the settlements and the difference between the settlements between the panels and of the panels top. As one would anticipate this difference is more important in the 9 panels arrangement due to the larger gap between panels.
The maximum amplitude of vertical displacements at the contact with the embankment was 19 mm and 65.8 mm, respectively for the SC1 and the SC2 geometries. The difference between the two calculation cases decreases with depth, as may be observed at the position 10 m deep (e.g. Figure 3b).

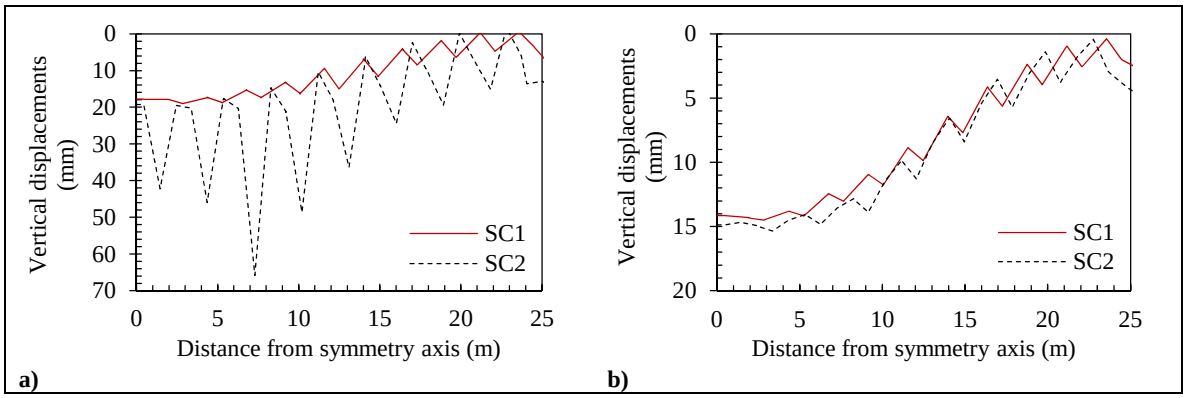

Figure 3: Settlements at the completion of calculation phase #6: a) embankment base, b) at the depth of 10 m

No significant difference is observed in Figures 4a and 4b between cases SC1 and SC2 as far as the panels' displacements are concerned. Differently, due to the larger load at the soil embankment contact, the settlements in the soil top for the 9 panels arrangement almost double the corresponding ones in the 11 panels arrangement (Figures 5a and 5b). The amplitude of the settlements in the soil decreases with depth, e.g. at the depth of 10 m as shown in Figures 5a and 5b, showing a similar trend to that in the panels. The settlement acceleration is more important during the initial 50 days during the construction of the embankment (see Table 1), when the on going consolidation is simultaneous with the embankment rise. A similar situation occurs after 770 days (calculation phase #5) with the road surcharge of 15 kPa. The settlement stabilization occurs after a consolidation period of 25 years. Around 60% of the final settlement is completed during loading, due to the embankment weight and the surcharge.

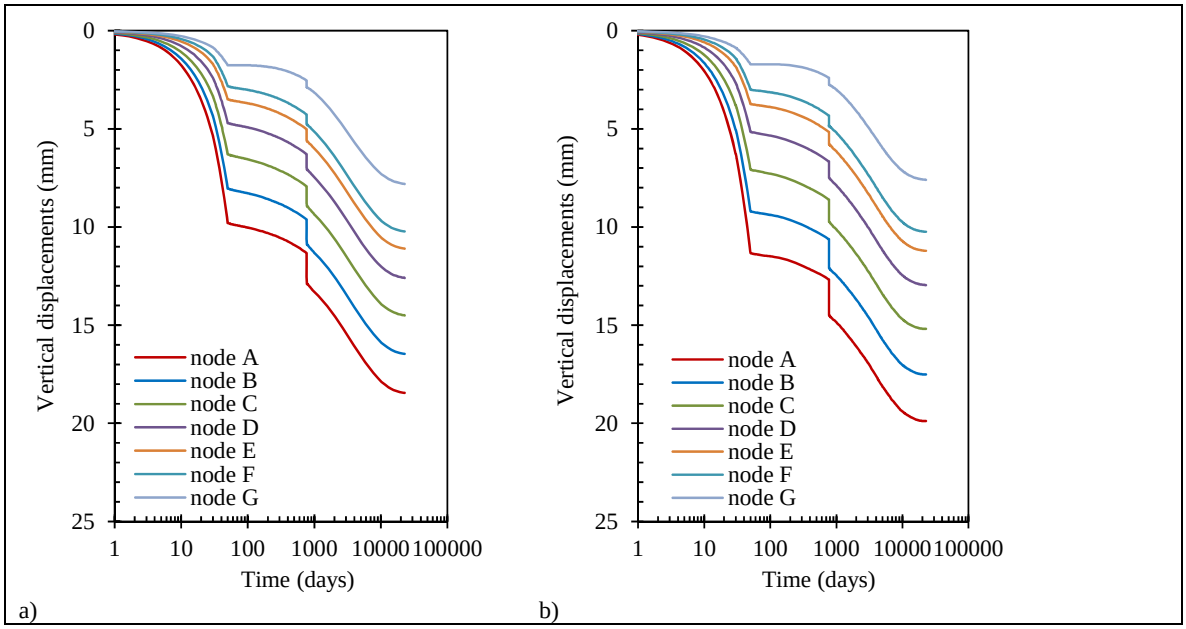

Figure 4: Time history of settlements at output points: a) panel #2, SC1 case; b) panel #2, SC2 case

Vertical stress distribution

The deformation response of the embankment depends on the effectiveness of the load transfer platform. The load transfer arch mechanism was almost fully mobilized as one may observe in Figure 5a. The load stress supported by the panels was 417 kPa and 507 kPa, respectively for cases SC1 and SC2. For both arrangements a larger value of stress than that calculated by the empirical approach for the corresponding arrangement, i.e. respectively 387 kPa and 425 kPa, was obtained. Considering that the stress values at depth 10 m must include the effect of the self weight of the 10 m column length, a significant decrease of stress induced in the panels by the embankment may be inferred: e.g. in panel #2 the maximum stress is, respectively, 406 kPa (SC1 case) and 509 kPa (SC2 case) as may be observed in Figures 6a and 6b.

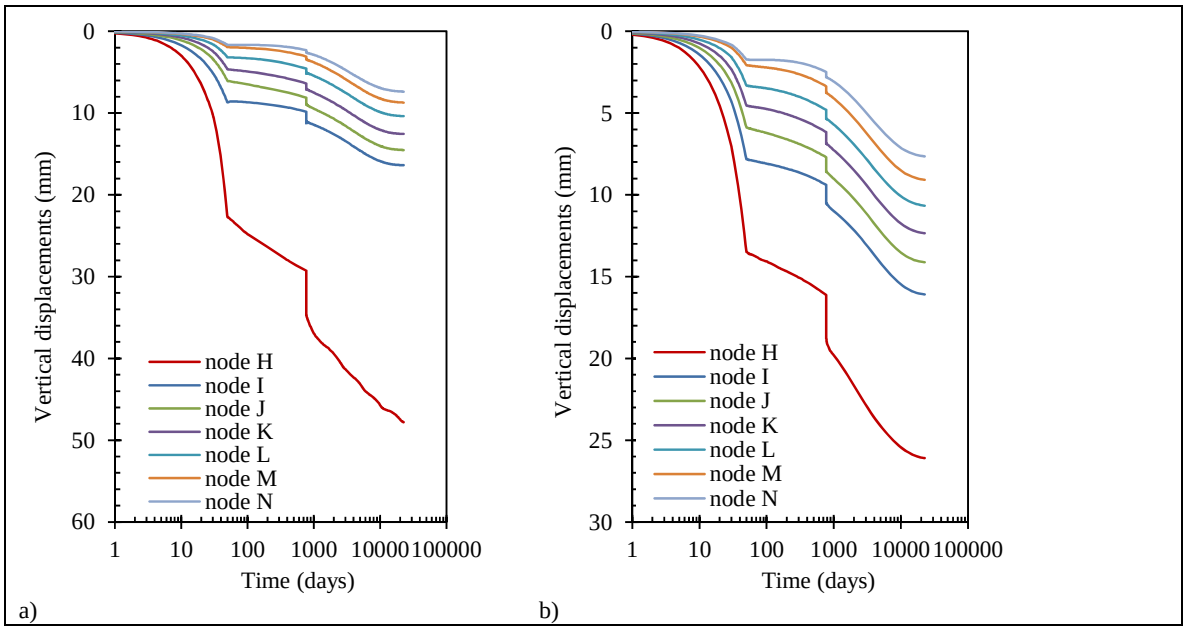

Figure 5: Time history of settlements at output points: a) soft soil, SC1 case; b) soft soil, SC2 case

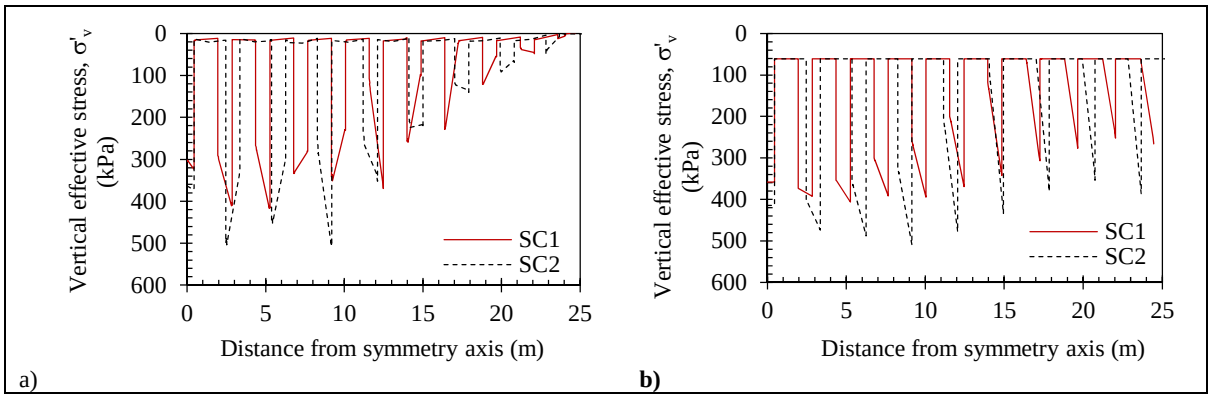

Figure 6: Vertical effective stress after calculation phase #6 completion: a) embankment base; b) at depth 10 m

The evolution of the vertical stress in the panels with time for both cases is shown in Figure 7 The arching effect manifests itself by the settlement increase of the soil points and the consequent load (stress) transfer between the soil and the panels. The most significant increase of the vertical stress is due to the embankment weight application and later to the surcharge after 770 days. The stabilization of the vertical stress at the panels is concomitant with that of the vertical displacement since the ongoing consolidation process in the panels involves both the soil and panels. The vertical stress at points I, J, K and L, i.e. those between panels #2 and #3 does not change significantly during the loading and consolidation processes. The calculated stress there corresponds to the geostatic vertical stress plus the remaining loading in excess to the transmitted to the neighbouring panels.

On the other hand, points M and N in the soil, as well as points F and G in panel #2 show continuous effective stress increase due to the consolidation process, being the stress increment caused by the load transmitted by the panel from the top directly to the lower tip.

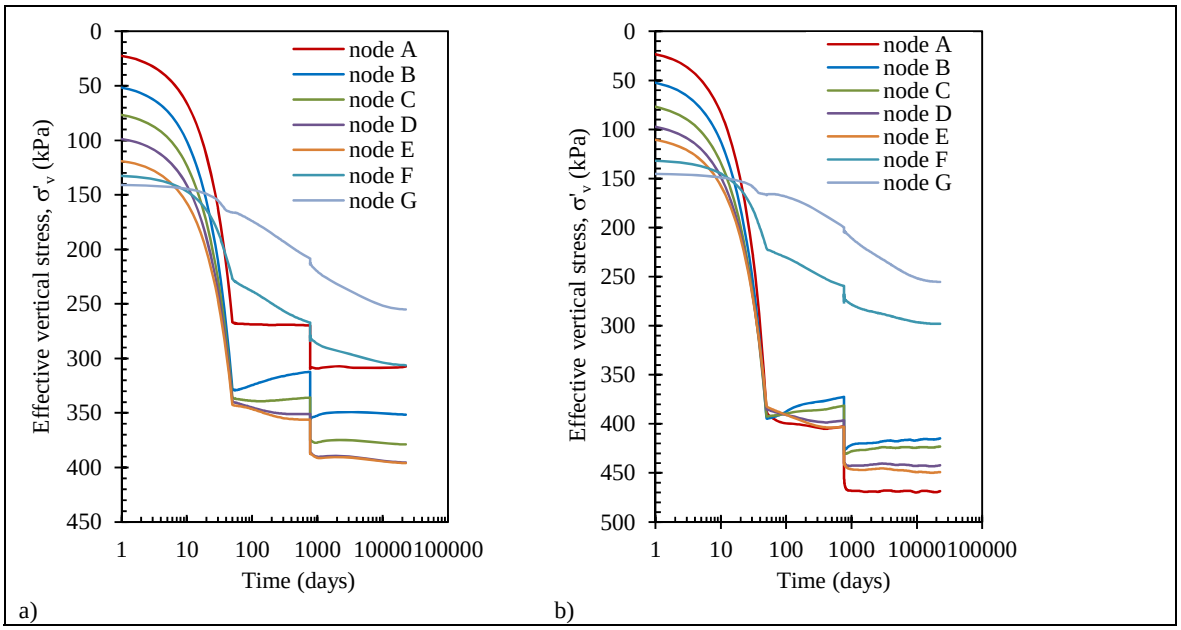

Figure 7: Vertical stress at output points in panel #2: a) SC1 case; b) SC2 case

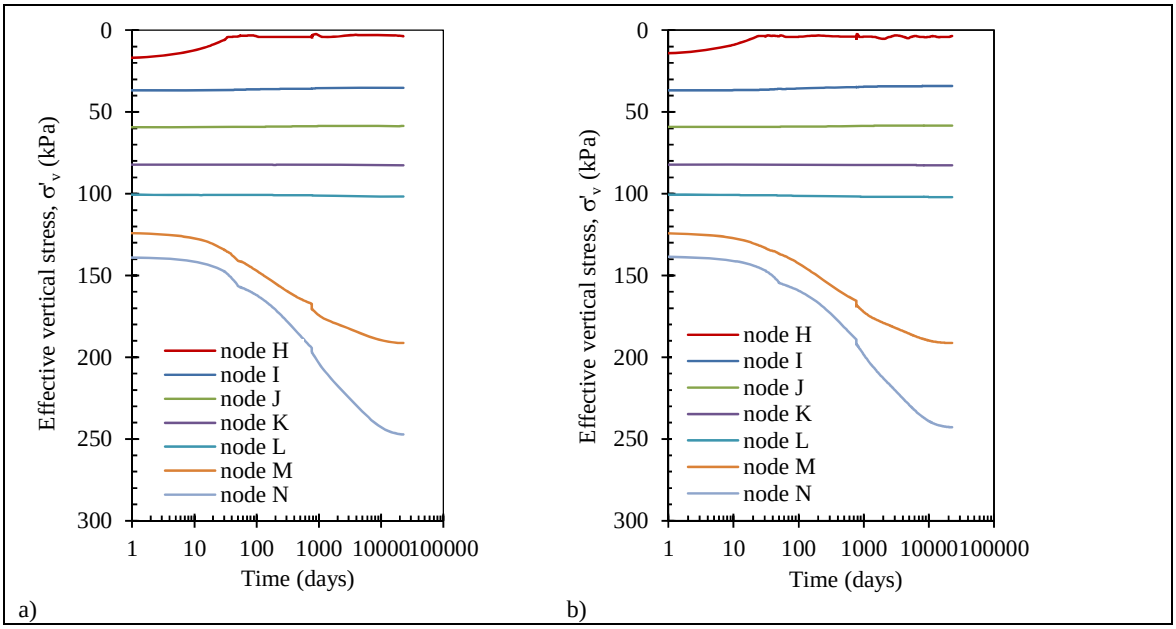

Figure 8: Vertical stress evolution at output points in soft soil: a) SC1 case; b) SC2 case

4. EFFECT OF THE PRESENCE OF WEAK PANELS DUE TO CEMENT CONTENT DEFICIENCY

4.1. Relevance of the cement content heterogeneity

The problem of the quality control of the CSM panels is mentioned in the literature ((Horpibulsuk *et al.*, 2004 and Mendes, 2011). In the later reference a quick, yet indirect, process for cement content determination from calcium carbonate content of the mixture is described. The soil cutting and mixing with cement paste process is prone to heterogeneity. Local deficiency of cement content is likely to reduce significantly the geomechanical properties of the panels. In this paper a preliminary analysis of the effect of cement content deficiency is presented.

Two types of weak panels were considered. A first one with a significant reduction of properties corresponding to a reduction of 40% of the Young's modulus and a second one that corresponds to a severe reduction of properties, namely of the Young's modulus (60%). Two cases are consequently defined. The

case SC3 (corresponding to the 11 panels arrangement) and the case SC4 (9 panels arrangement). In both cases a deterministic distribution of the weak zones of both types was considered, as shown in Figure 9.

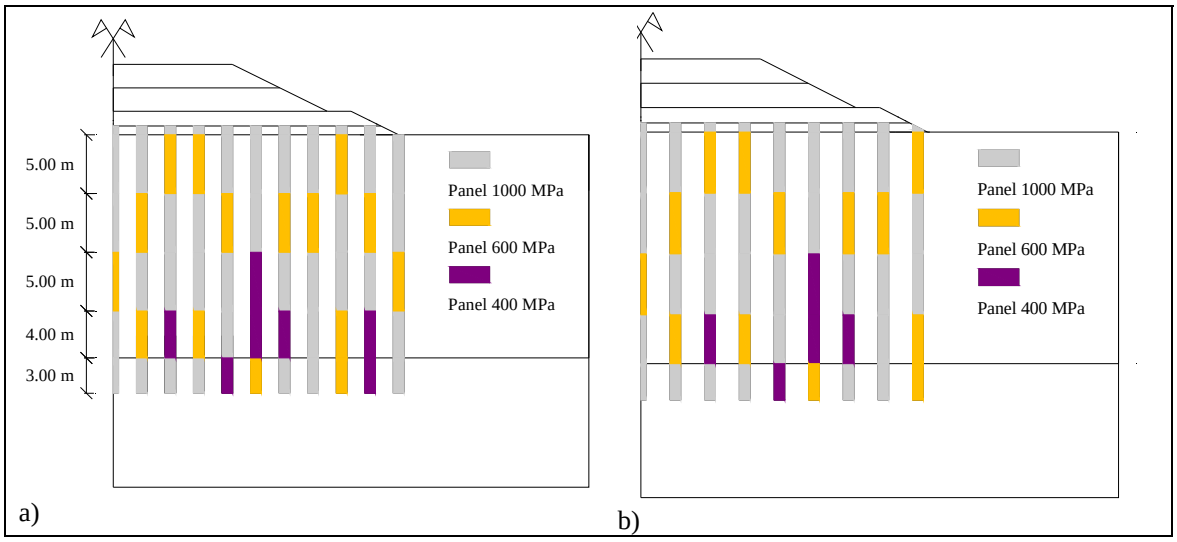

Figure 9: Models with weak zones in soil-cement panels: a) SC3 case; b) SC4 case

(Horpibulsuk *et al*., 2004) reported that the deficiency of cement content effect on reducing the effective cohesion intercept (c') is more noteworthy than that on the effective shearing resistance angle (ϕ'). Accordingly, in this paper it was decided to focus on the effect to the c' value rather than on the effect on ϕ'. Material codes #7 and #8 are adopted for the severe and most severe deficiency, respectively with their properties shown in Table 4, together with their counterparts for the CSM ideal mixture (Material #6). The parameters of materials #7 and #8 not mentioned in Table 4 are equal to the corresponding ones of material #6 in Table 2.

Table 4: Geomechanical parameters of the weak imbedded zones

Material #	6	7	8
E (MPa)	1000	600	400
E_{eq} (MPa)	706	424	283
c' (kPa)	301	155	110
ϕ' (º)	35	35	33
s_u (kPa)	550	300	200

4.2. Discussion of the results

The presence of weak zones in the panels did not change the pattern of structural response comparatively with that presented in section 3.3.2. Regarding the settlements, the overall effect may be described as an increase under the central section of the embankment and only a minor increase in the remaining area. The maximum relative increase occurs for the 11 panels arrangement at the contact of the embankment and the soil, varying between 10% and 35%. At the depth of 10 m, a smaller increase may be observed ranging between 10% and 20%. As a general situation the 9 panels arrangement is less sensitive to the weak zones presence than the 11 panels one.

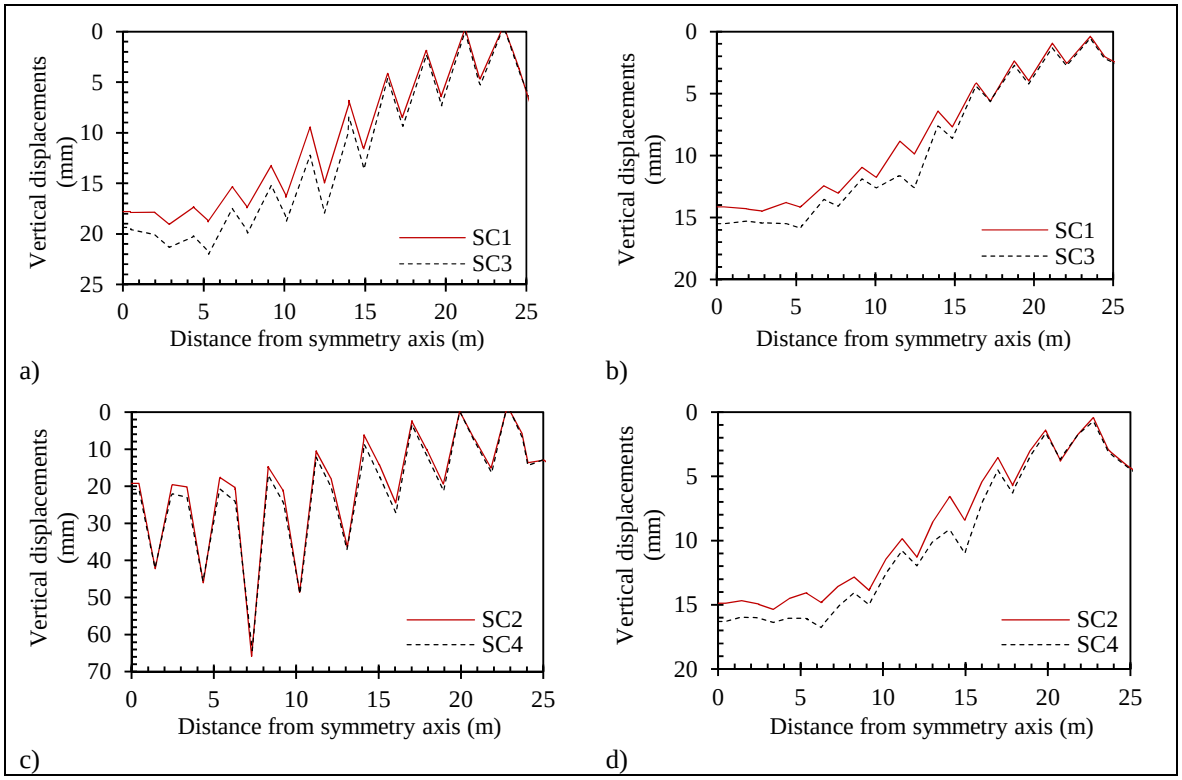

Figure 10: Settlements at the completion of calculation phase #6: a) SC1 and SC3 cases, at the base of embankment; b) SC1 and SC3 cases, at depth of 10 m; c) SC2 and SC4 cases, at the base of embankment; d) SC2 and SC4 cases, at depth of 10 m

A quite different situation may be observed in Figure 11 regarding the stress distribution. Only slight differences were obtained in models SC3 and SC4 as compared with the models SC1 and SC2, respectively. A preliminary conclusion may be drawn from this comparison, i.e. the existence of weak zones distributed over the panels' length is likely to have only minor effect on the overall stress distribution. This is valid both for the panels and the non improved soil. Further studies are necessary, namely involving a random distribution of weak zones and a reduction of both the cohesion intercept and the friction angle. In this study the weak zones are essentially concentrated at deep positions and only minor reduction of the friction angle in the weakest panels (material #8) was considered.

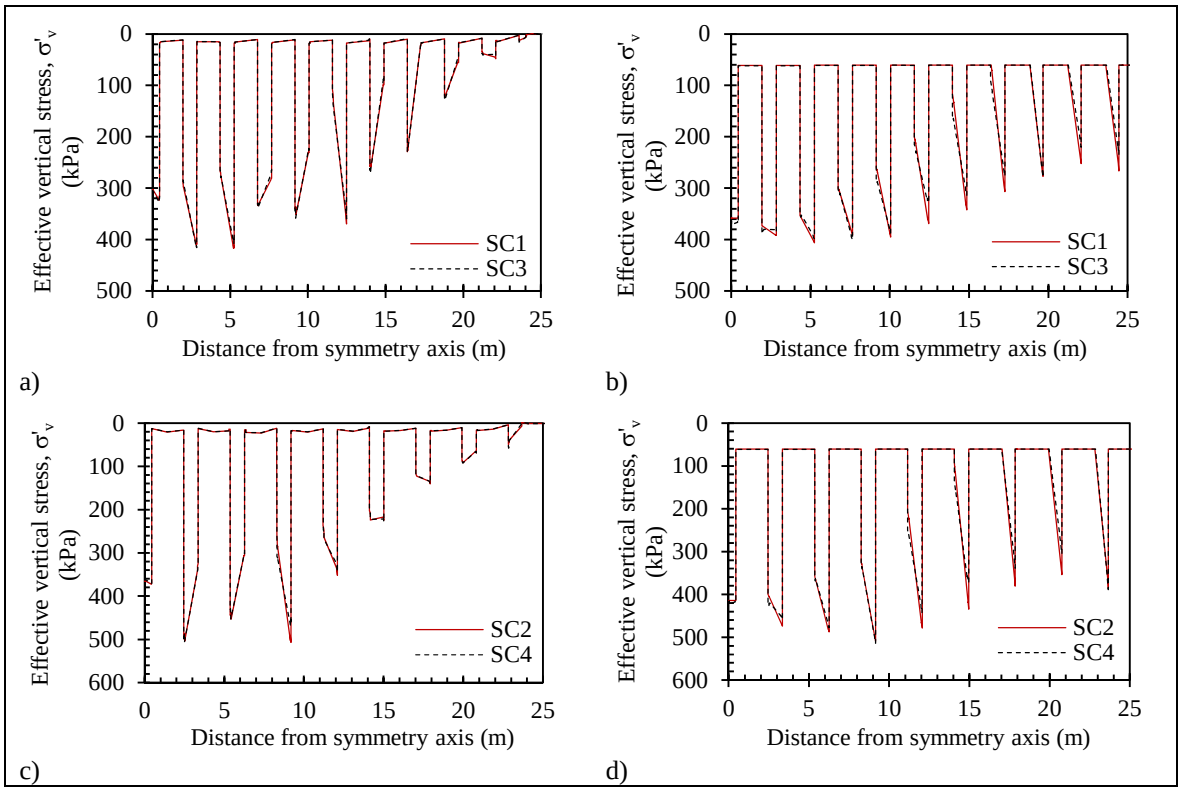

Figure 11: Effective vertical stress distribution at completion of calculation phase #6: a) SC1 and SC3 cases, at the base of embankment; b) SC1 and SC3 cases, at depth of 10 m; c) SC2 and SC4 cases, at the base of embankment; d) SC2 and SC4 cases, at depth of 10 m

5. FINAL REMARKS

The design of Cutter Soil Mixing panels may be developed based on simplified analytical models or numerical models. The three-dimensional nature of the problem is often taken in consideration by 2D models with transformed properties, namely the geometry or the deformation modulus.

A comparative study between those approaches was presented in this paper related with a hypothetical road embankment on an alluvial basin. The mechanical properties of both the in situ soil and of the CSM panels were partly defined from a detailed and through experimental program of a real site presented in a companion paper to this Conference.

A sensitivity analysis was developed regarding the density of panels, i.e. two distinct arrangements of 9 and 11 panels in the half cross section of the embankment were considered. The preliminary design of the panels was based on the analytical approach. The comparison between analytical and numerical results from the standpoint of the imposed vertical stress at the panels and at the foundation soil showed that the former are pessimistic as compared with the numerical model results. This is particularly valid for the 9 panels' arrangement (case SC2).

As the comparison between numerical and analytical results suggests, the EBGEO (2011) analytical model was found to be the most adequate for preliminary design. An adequate safety margin was identified from the serviceability point of view for the 11 panels arrangement. The long term behavior of the embankment-soil-panel system depends on the hydraulic-consolidation coupled behavior of the soil and the panels. A period as large as 25 years was identified as necessary for primary consolidation stabilization of the settlements.

The presence of weak zones in the panels was simulated by a deterministic selection of weak and extremely weak portions of those. From the settlement point of view a maximum of 30% increase was identified at the embankment base for the 11 panels arrangement. Further studies are necessary.

REFERENCES

Bergado, D.T.; Long, P.V. (1994). "Numerical analysis of embankment on subsiding ground improved by vertical drains and granular piles". Proceedings of the XIII International Conference on Soil Mechanics and Foundation Engineering, Morgantown, USA, Vol. 4, pp. 1361-1366. (quoted in Satibi, 2009).

Bilé Serra, J.; Mendes, B. (2009). "Rehabilitation and reinforcement of the dock between Santa Apolónia and Jardim do Tabaco, by CSM technology. Laboratory formulation tests". LNEC, Lisboa, Report 414/2009 – DG/NT. (in Portuguese).

BS 8006 (1995). "Code of practice for strengthened/reinforced soils and other fills". British Standard Institution, London, U.K.

EBGEO (2011). "Recommendations for design and analysis of earth structures using geosynthetic reinforcements – EBGEO. German Geotechnical Society, Ernst & Sohn. (Translation of the 2nd German edition).

EN 14679 (2005). "Execution of special geotechnical works – deep mixing". CEN, English version.EN 1997-1 (2004).

"Eurocode 7 part 1, geotechnical design. General rules".

Horpibulsuk, S.; Miura, N., Bergado, D. (2004). "Undrained shear behavior of cement admixed clay at high water content". Journal of Geotechnical and Geoenvironmental Engineering, ASCE, Vol. 130, No. 10, pp. 1096-1105.

Kempfert, H.G.; Gobel, C.; Alexiew, D.; Heitz, C. (2004). "German recommendations for reinforced embankments on pile-similar elements". Third European Geosynthetic Conference, DGGT (German Geotechnical Society), Vol. 1, pp. 279-284.

Mendes, B.; Maranha das Neves, E.; Caldeira, L.; Bilé Serra, J. (2012). "Assessing the feasibility of a foundation treatment solution based on CSM panels at a river dock in Lisbon". ISSMGE - TC 211 International Symposium on Ground Improvement, IS-GI Brussels 2012, Brussels.

Satibi, S. (2009). "Numerical analysis and design criteria of embankments on floating piles". PhD Thesis, Instituts für Geotechnik, Universität Stuggart, Germany.

Swedish Geotechnical Society (1997). "Lime and lime cement columns". Swedish Geotechnical Society, Linkoping, SGF Report 4:95E.

Van Eekelen, S.J.M. van; Bezuijen, A.; Dimiter, A. (2008). "Piled embankments in the Netherlands, a full-scale test, comparing 2 years of measurements with design calculations". Proceedings of EuroGeo4, Edimburgh, No. 264.

Ground improvement works for an LNG storage tank foundation

Gary Chapman, Golder Associates Pty. Ltd., Australia, gchapman@golder.com.au
Joel Gniel, Golder Associates Pty. Ltd., Australia, jgniel@golder.com.au
Matt Greenough, Golder Associates Pty. Ltd., Australia, mgreenough@golder.com.au
Abdelmalek Bouazza, Monash University, Australia, malek.bouazza@monash.edu

ABSTRACT

Located on the coast of North Queensland is the site of a proposed coal seam gas (CSG) to liquefied natural gas (LNG) process plant. A large LNG storage tank was to be built at the site. This site is located on reclaimed land from the sea and therefore creates an issue of poor ground conditions. Due to the poor ground conditions at the site, a simple shallow foundation system was not possible, requiring alternative foundations to be considered. Due to the large size of the tank, conventional piling techniques would have been highly expensive and time consuming. Ground improvement was considered to be the most viable option. The requirements of this project were a high increase in bearing capacity of the soil and a large reduction in settlement properties. The chosen option was deep soil mixing (DSM) using the recent technological improvement of cutter soil mixing (CSM). To ensure adequate quality assurance of the CSM columns, 20% of the production columns were to be sampled and UCS tested. An analysis of this testing is presented to evaluate the process together with numerical analyses conducted to assess the foundation performance.

1. INTRODUCTION

Australia's first coal seam gas (CSG) to liquefied natural gas (LNG) project was to be developed on the coast of North Queensland. Unfortunately work on thisd project was halted when the tank foundation was 30% complete due to an unsuccessful transfer of ownership of the project. This paper presents the work done up to the day the project stopped. The plant site is located on tidal flats adjacent to a deep water navigation channel. The founding materials at the site are of very poor quality in terms of strength and compressibility and range from very soft clays to loose sands. The proposed LNG tank is 85 m in diameter and 54 m high. Its content will impose a maximum service pressure under hydro-test of 260 kPa over the central portion of the tank floor. The site ground profile imposed geotechnical constraints on the project. The traditional engineering solution for this type of site has been to introduce deep foundation (piles) to transfer loads through the low strength material to deeper more competent layers. However this solution was found to be an expensive alternative. Alternatives strategies of dealing with low strength material have been developed over the past 30 years. Rather than bridge or bypass the poor strength soil materials, these techniques known as soil mixing methods, are predicated on modifying the properties of the in-situ soils by addition of cementitious materials. By use of appropriate techniques, the strength and compressibility of the soil can be improved sufficiently to obviate the need for structural elements. The chosen option for this site was deep soil mixing using the cutter soil mixing (CSM) process. A foundation solution was designed to include CSM columns (CSMCs) and a granular load transfer layer placed over the top of the CSMCs. The design comprised 605 CSMCs installed to depths of between 13 m and 15 m below the underside of the proposed load transfer layer. This paper presents the results of the UCS tests conducted as part of the quality assurance program together with numerical analyses to assess the foundation performance.

2. SITE GEOTECHNICAL PROFILE

The LNG tank was to be founded on tidal mangrove mud flats which have been reclaimed using dredged spoil hydraulically deposited in bunded settlement ponds over a series of dredging campaigns. The materials deposited have come from dredging of the berthing areas of the adjacent industrial wharves. A final dredging campaign used hydraulically placed granular fill to raise the plant site level to final design level. A site investigation was carried out in stages as access across the upper very soft hydraulic fill in the top of the settlement ponds became available. Boreholes and electric friction cone penetrometer tests (CPTs), some with pore pressure measurement, were carried out across the site to depths of up to 50 m. A simplified layering of the soil inferred from the CPT testing and the borehole logs is shown in Figure 1. The site generally consists of four soil layers, which overlie the mudstone bedrock. The soil layers consist of the dredged fill, a soft to firm clay layer inferred to comprise natural mangrove mud, a stiff to very stiff

clay layer, and a hard clay layer. Ground water was present 2 m below the ground surface. Typical soil properties are presented in Table 1.

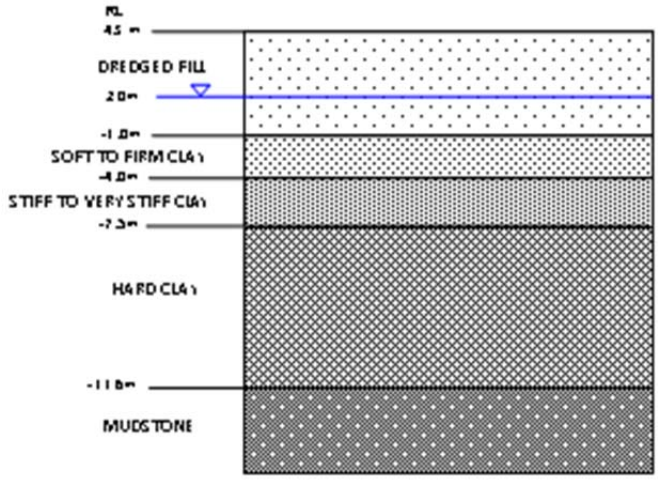

Figure 1 Simplified soil layering below the LNG tank

Table 1: Soil properties at the site.

Soil Layer	Dredged Fill	Soft to Firm Clay	Stiff to Very Stiff Clay	Hard Clay
nit Weight	18 kN/m^3	18 kN/m^3	19 kN/m^3	19 kN/m^3
Cohesion c_u, c'	0	5 kPa	2 kPa	20 kPa
Friction Angle φ'	32°	25°	27°	26°
Young' Modulus	10 MPa	5 MPa	12 MPa	60 MPa

3. CSM COLUMNS FOUNDATION DESIGN

The geotechnical design of the CSMC foundation for the LNG tank considered both tank settlement and bearing capacity. The BS 7777 (1993) recommended limits for differential settlement were adopted for the project. Differential settlements along a radial line from the tank centre to periphery were limited to 1:300 and 1:500 around the tank perimeter walls. Total settlements were controlled to facilitate connection between the tank and adjacent pipe work. The CSM column foundation design was based on installing a regular pattern of CSMCs with enlarged heads beneath the tank base slab. The enlarged heads were then to be covered by a layer of compacted granular fill to act as a load transfer layer. The load transfer layer included a basal layer of geogrid with an in-place biaxial working strength of 60 kN/m. The geogrid was to assist with load transfer from the CSMC heads to the underside of the tank base. The design CSMC layout is presented in Figure 2. The CSMCs were laid out to provide an area replacement ratio (defined as the net cross sectional area of CSMC divided by the gross plan area in which the columns are installed) of 13.4% over the central tank area (radius 35 m). Under the more heavily loaded edge of the tank base slab, two concentric rings, 3 m and 5 m wide respectively, were installed with increased CSMC area replacement ratios. The two outer rings of columns with area replacement ratios of 13.5% and 15% were also founded deeper to increase the stiffness of the outer tank area to help smooth out the tank settlement profile. Each column has plan dimensions of 3.6 m by 1.75 at the surface, tapering to 2.4 m by 0.55 m, 1.0 m below the surface and remaining at these dimensions for the remaining length of the column.

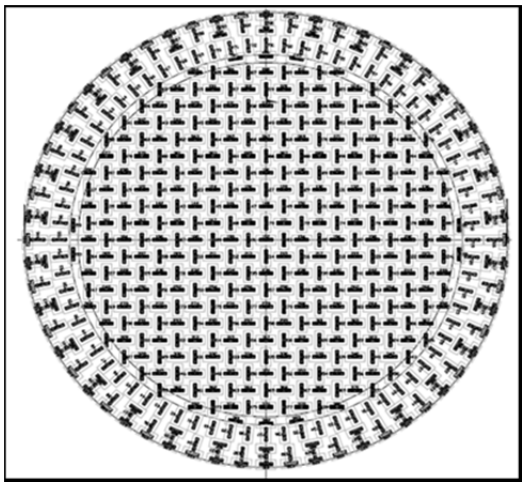

Figure 2: CSM Column layout

Each CSMC was designed to carry a maximum vertical working load of about 2.55 MN, imposing a column compressive stress of about 2 MPa. A target column Youngs Modulus (E) of 1000 MPa or 300 times the unconfined compressive strength (UCS) of the column material was adopted for preliminary design. The CSMCs were designed to penetrate from the underside of the load transfer layer at RL +5.3 m through the full thickness of the loose sands and soft clay layers to found in the underlying firm to stiff to hard clays. Target CSMC toe levels are shown in table 2.

Table 2: CSM column depth

	Radius	**Depth (RL)**
Inner column	0 to 35m	-8.0m
Inner ring	35 to 38m	-9.0m
Outer ring	38 to 43m	-10.0m

4. DESIGN OF CSM COLUMNS

For the CSMC foundation to perform as designed, it was imperative that the columns were constructed with strength and stiffness properties similar to those adopted for the geotechnical design of the tank foundation. The optimisation of the mix for the CSMCs was conducted through laboratory and trial column tests carried out between December 2009 and February 2010. The final binder mix selected was: 25% fly ash and 75% GP cement with the addition of a retarder. Based on an assessment of the trial column test results, single phase mixing (injection of grout on penetration and extraction of the CSM cutter rather than two phase mixing using injection of bentonite fluid on penetration and grout on extraction) with a target cement content of 800 kg/m^3 using grout with a water cement ratio of 0.85 was selected for the production columns. During CSMC production, testing of samples from CSMCs was to be carried out at a rate of 20% of the columns installed in any shift or a minimum of two CSMCs per shift, whichever was the greater. The stiffness properties of the CSMCs were also to be confirmed using the results of a static load test carried out on a trial CSMC considered to be representative of the production columns. Recognising the difficulties in testing of CSMC materials and the likely variation in test results that may be obtained, the specification called for a target UCS strength of CSMC material of 4 MPa and a minimum UCS of 2 MPa at the base of the CSMC columns founded in the firm to stiff clay. A target CSMC Young's modulus of 1000 MPa was also specified.

4.1. UCS Testing and Plate Load Test

The testing performed on production columns was primarily UCS testing. This process involved the loading of a sample until failure. Local displacement transducers were used to measure local displacement of the specimen to account for end effects (local stiffness) or middle third modulus. Wet grab samples were recovered from selected CSMCs during the production stage by plunging a rectangular steel section fitted with a flap valve into a wet CSMC. The CSMC material sampled by the plunger was transferred into a barrel from which samples were hand moulded into smooth walled PVC tubes filled in layers with tamping and vibration and cured for various amount of time.

Figure 2 presents the results obtained from the UCS testing undertaken at approximately 7, 14, 28 day and 90 days intervals on wet grab samples. This represented 20% of the columns installed. The trend line indicates that the strength increases steadily for an initial period of time, and gradually smoothes to a slower increase. It can be seen that all the wet grab samples have clearly met the required strength of 4 MPa after 28 days. The average elastic modulus was 822 MPa at 28 days but increased to around 2500 MPa at 90 days. A summary of the range and averages of the UCS and elastic modulus values are presented in Table3. The middle third modulus typically ranged from 1000 MPa to greater than 3000 MPa. The plate load test verified that the CSMC could support 1.3 to 1.4 times the design load.

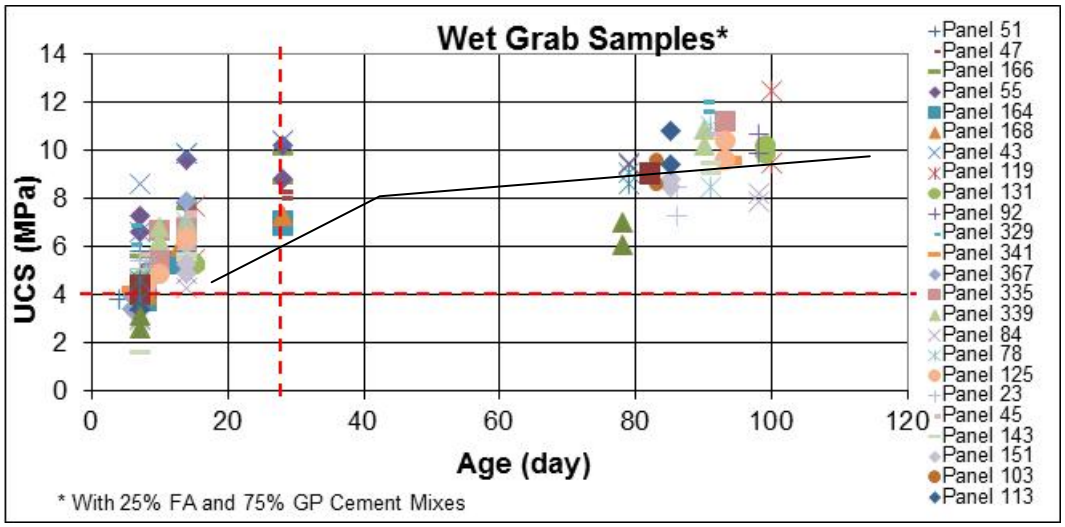

Figure 2: Results obtained from the UCS tests on wet grab samples from production columns

Table 3: Summary of UCS and Young's modulus values from production stage columns

Age	UCS_{min} (MPa)	UCS_{max} (MPa)	UCS_{ave} (MPa)	E_{min} (MPa)	E_{max} (MPa)	E_{ave} (MPa)
7 days	1.6	8.6	4.6	310	580	424
14 days	4.3	>10.0	6.6	414	687	562
28 days	6.9	>10.4	8.6	635	1429	822
~90 days	5.9	12.5	9.3	1667	3429	2524

5. NUMERICAL ANALYSES

2D plane strain and an axisymmetric-2D analyses of the CSMC tank foundation were carried out, respectively, using the commercially available geotechnical finite element package PLAXIS 2D. The CSMCs were modelled as a series of radial zones of stiffer foundation material. The soil between the stiffer rings was modelled as unimproved ground. The analyses were carried out to estimate the long term settlement of the tank foundation as well as the variation of the normal stresses and coefficients of subgrade reaction. These were conducted for Serviceability Limit State (SLS) conditions including operating basis earthquake (OBE) conditions and Ultimate Limit State (ULS) conditions including safe shutdown earthquake (SSE) conditions. The soil materials were modelled as hardening soil materials and the bedrock as a linear elastic material. The CSM reinforced zones were assumed to behave as elastic-perfectly plastic (Mohr-Coulomb) materials. The density of the columns is greater beneath the tank wall (zone B) than the interior zone or outside the tank footprint (Zone A) (Figure 3). It was therefore assumed that all the tank loading was carried by the CSM reinforcement.

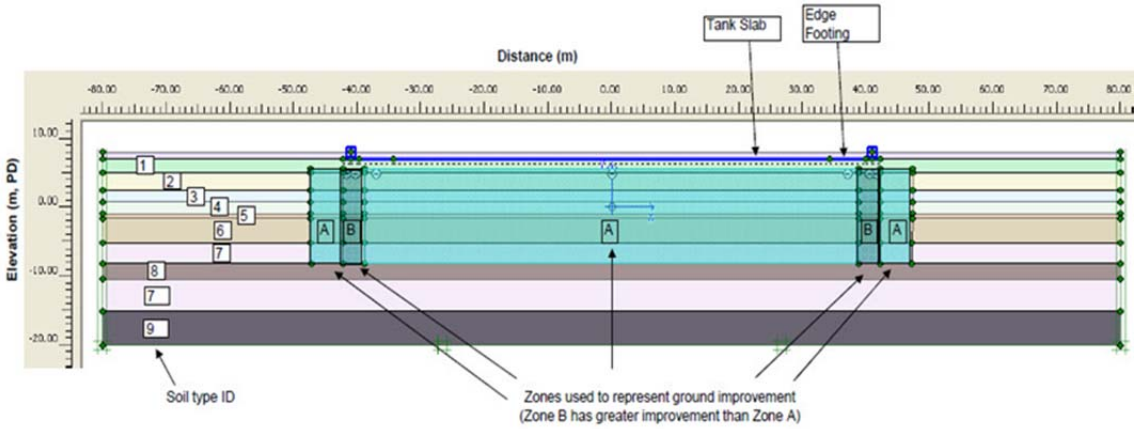

Figure 3 Plaxis plain strain model

To analyse the consolidation of the tank, a loading sequence was used to simulate the construction and lifecycle of the tank. This included 1) soil model including improved ground; 2) empty tank; 3) hydro-testing; 4) empty tank; 5) empty tank normal operating conditions; 6) normal operating conditions. The analysis was carried out initially on the basis of 10% replacement ratio at the interior of the tank and 30% at its perimeter.

Further analyses were also performed with a two-dimensional axisymmetric model. The purpose of these analyses was to obtain tank base load-deflection information with which to develop coefficient of subgrade reaction values that were used in structural analysis of the tank. Obtaining this information from the 2D software is significantly more straightforward, and therefore less time consuming, than with the 3D model.

5.1. Results and Discussion

5.1.1. Tank on unimproved ground

Before considering ground improvement, an initial 2D analysis was performed with the tank on the existing ground conditions as represented by Figure 1. This analysis considered ULS values for: Hydrotest loading, consolidation under hydro test loading, normal operating conditions with minimum pressure with and without safe shutdown earthquake (SSE). The results of this analysis are summarised in Table 3.

Table 3: Results for unimproved ground

Condition	Maximum Cumulative base displacement (m)	Maximum angular rotation along base	Safety factor
Hydrotest loading	0.29	1 in 70	1.6
Consolidation under hydrotest loading	1.51	1 in 20	2.5
Normal operating conditions with minimum pressure	1.13	1 in 20	2.1
Normal operating conditions with minimum pressure and SSE loading	1.18	1 in 20	1.7

The maximum base displacement occurs at the edge of the tank base. The maximum angular rotation occurs at a distance of about 75% of the tank radius from the centre. The absence of a failure condition demonstrates that the kinematic constraint on the relatively thin layer of weak soil (about 10% of the tank diameter) over much stronger soils produced significantly greater bearing capacity than would be the case for a relatively thick layer of the same weak soil. However, foundation displacements are unacceptably large, including substantial consolidation settlement, warranting improvement of the ground below the tank.

5.1.2. Tank on improved ground

Settlements of the base slab for SLS cases at the end of Hydro testing, minimum normal operating pressure with and without earthquake loading and maximum normal operating pressure with and without OBE earthquake are shown in Figure 4.

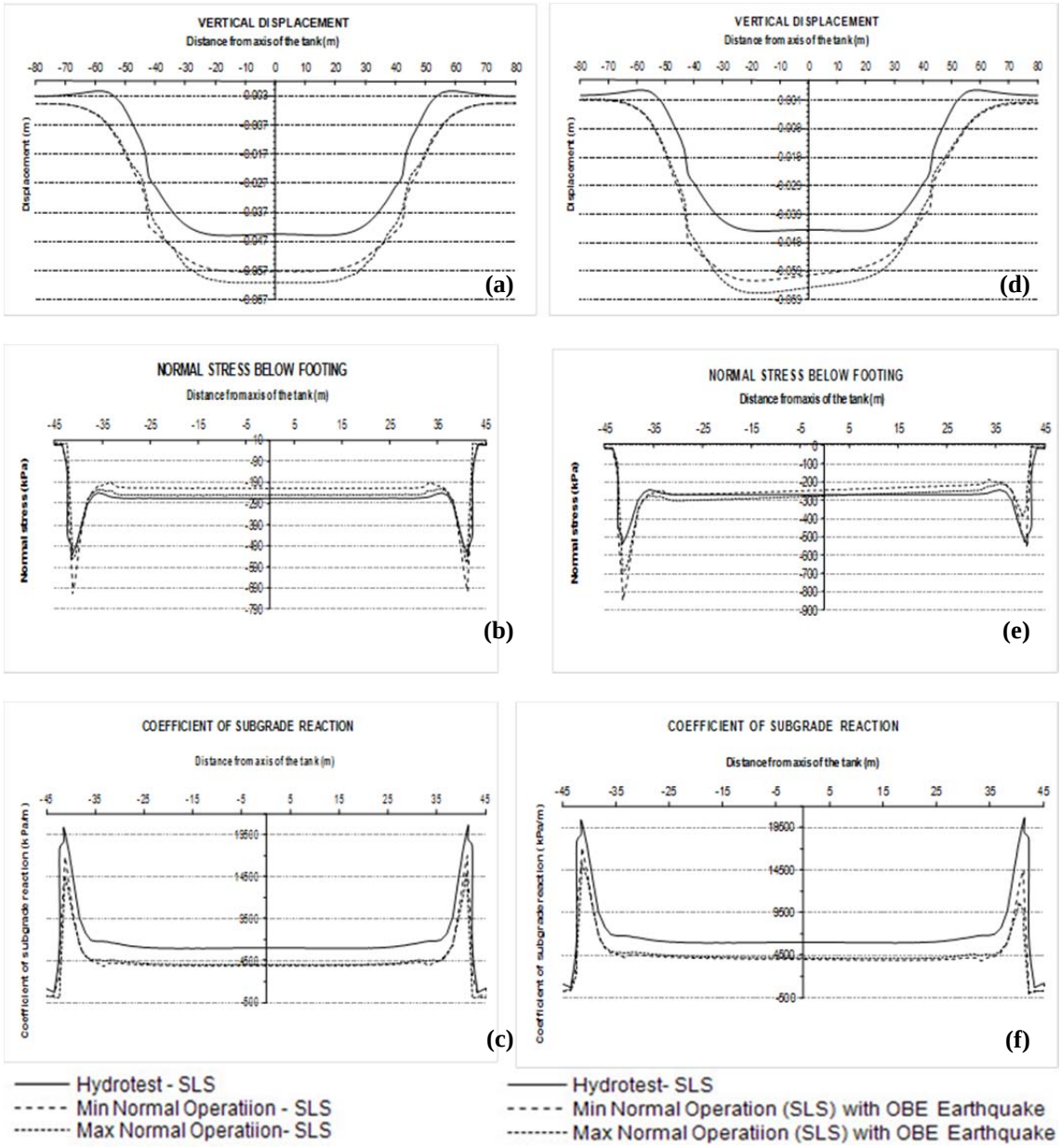

Figure 4: Settlement, normal stress and coefficient of subgrade reaction variations of the base slab for SLS cases at the end of Hydro-Testing, normal operation conditions with minimum pressures and maximum pressures without earthquake loading (a,b, c) and with OBE earthquake loading (d,e,f)

Settlements of the base slab for ULS cases at the end of Hydro testing, minimum normal operating pressure with and without earthquake loading and maximum normal operating pressure with and without earthquake are shown in Figure 5

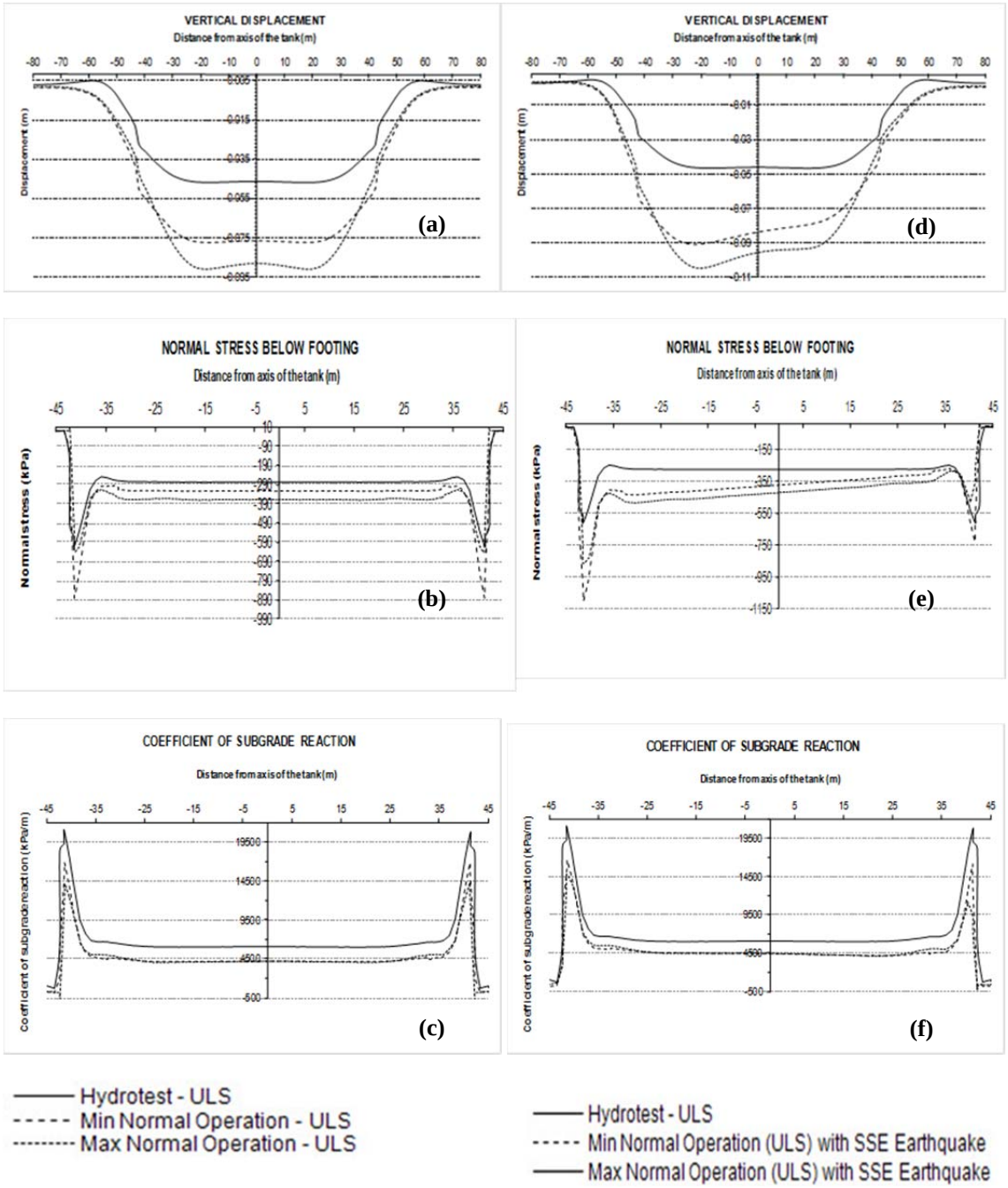

Figure 5: Settlement, normal stress and coefficient of subgrade reaction variations of the base slab for ULS cases at the end of Hydro-Testing, normal operation conditions with minimum pressures and maximum pressures without earthquake loading (a,b, c) and with SSE earthquake loading (d,e,f)

Comparison of the results shown in Figures 4 and 5 indicate that earthquake loading has a minor effect on the displacement of the tank base and on the subgrade bearing stresses. The coefficient of subgrade reaction magnitude distributions are essentially the same for all the normal operating and earthquake conditions and limit states considered. Computed vertical displacement of the tank base is in the order of 50 to 100 mm. Tank perimeter settlement is about 0.5 to 0.67 of the maximum interior values. The associated maximum interior to perimeter angular distortion values are about 1/400. Thus satisfying design requirements.

5.1.3. Axisymmetric analysis

Figure 6 shows the axisymmetric model which has the tank wall at its actual height and the domed tank roof. The CSM reinforcement is the initial assumption, with 30% replacement at the perimeter and a 5 m wide zone beyond the tank edge. The loading is the ULS normal operating condition with minimum pressure. The edge and interior displacement are 19 mm and 68 mm, respectively (Figure 6a). Reducing the perimeter replacement ratio to 20% and eliminating the CSM zone outside the tank resulted in edge and interior base displacements of 36 mm and 67 mm, respectively, Figure 6b, thus meeting design requirements.

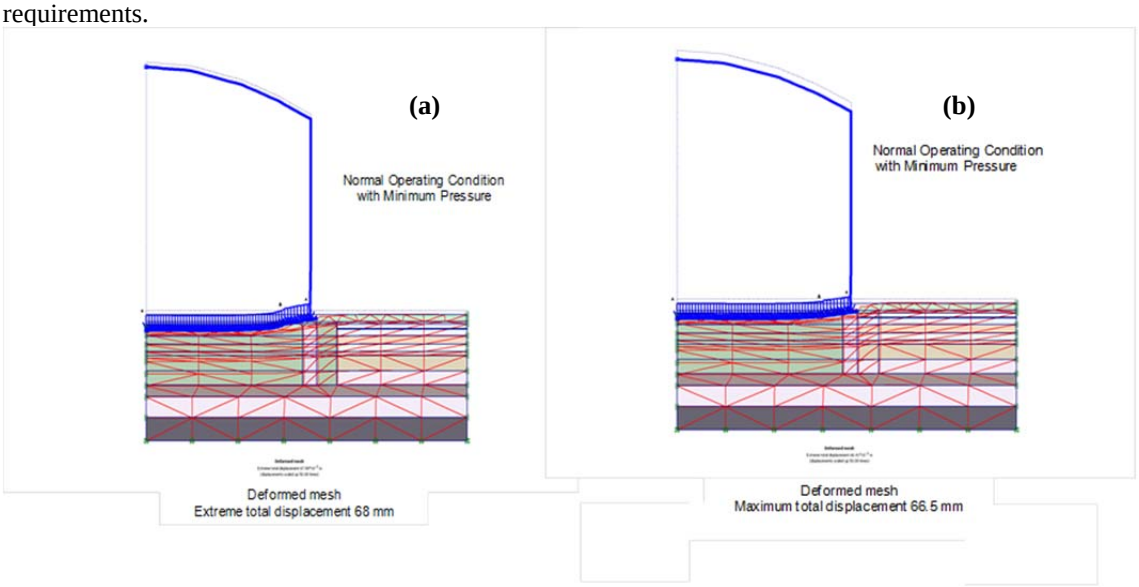

Figure 6: Base slab deflection, ULS conditions (a) replacement ratio 30% below tank wall; (b) replacement ratio 20% below tank wall.

The coefficient of subgrade reaction resulting from changing the perimeter replacement ratio to 20% is shown in Figure 7 for ULS conditions. The results obtained with the 2D plain strain model (Figs. 4 and 5) indicated the coefficient of subgrade reaction magnitude distribution are insensitive to the variations in applied loading conditions considered herein. Therefore, the distribution obtained from axisymmetric analysis of the tank with the ULS minimum pressure normal operating condition could be used in structural tank design with other loading conditions. Refinement of the design using the axisymmetric analysis allowed the change of the replacement ratio for both the interior and the perimeter of the tank. Furthermore it eliminated the need to reinforce the outside of the tank. Further refinement in the column design led to an increase in the numbers of columns in the interior and perimeter of the tank and further reduction of the replacement ratio to 15% at the perimeter and an increase of the replacement ratio to 13% at the interior of the tank. This led to a slightly larger total number of columns than initially proposed with no major impact on the geotechnical aspects of the ground improvement design.

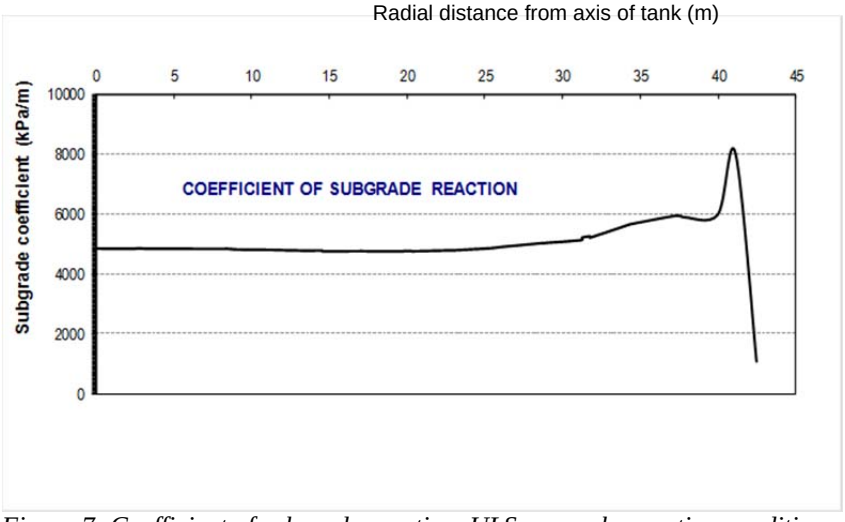

Figure 7: Coefficient of subgrade reaction, ULS, normal operating condition, minimum pressure

6. CONCLUSION

Ground improvement of the site using Cutter Soil Mixing columns has been shown to provide an adequate solution to the poor ground conditions. Analysis of the UCS undertaken on samples from production columns indicated that the project requirements were achieved in terms of strength and Young modulus. Numerical analyses allowed the refinement of the ground improvement design leading to a more economical solution to be provided.

7. ACKNOWLDGEMENTS

The authors wish to acknowledge BG&E Pty. Ltd., Laing O'Rourke and Wagstaff Piling for their assistance in this project and for providing permission to publish this paper

8. REFERENCES

BS 7777 (1993). Specifications for the design of flat bottomed, vertical, cylindrical storage tanks for low temperature service. British Standards Institute, London.

Lateral displacements due to installation of soil-cement columns

Jinchun Chai, Department of Civil Engineering and Architecture, Saga University, Japan, chai@cc.saga-u.ac.jp

John Carter, Faculty of Engineering and Built Environment, University of Newcastle, Australia, John.Carter@newcastle.edu.au

ABSTRACT

A method for predicting the lateral displacement of the ground induced by the installation of soil-cement columns is briefly summarized and then applied to two field tests conducted in Japan in the 1990s. The prediction method was developed by Chai et al. in 2009 using cavity expansion theory. This method can consider explicitly the effect of the amount of injected admixture and the stiffness and strength of the deposit as well as empirically account for the construction method. The two field tests were conducted at two different sites where, in each case, sandy layers exist at the ground surface underlain by a clayey layer, which in turn is underlain by another sandy layer. A comparison of the predicted and measured lateral displacement profiles indicates that the calculation method under-estimated the lateral displacement of the clayey layers but generally over-estimated the displacements of the sandy layers in cases where the volumetric strain (Δ) of the soil was assumed to be zero. When it was assumed that Δ = 2% in the sandy layers, the calculated values of lateral displacement provide a good match to the measured data for the sandy surface layer, which indicates that during the column installation process, the soil may deform under conditions of partial drainage.

1. INTRODUCTION

Deep mixing of cement, normally forming soil-cement columns in the ground, is a widely used and effective soft ground improvement method. It has been used to increase the bearing capacity and reduce the compressibility of soft clayey deposits; to form retaining walls for excavation in clayey ground (Bergado et al. 1994); and to increase the liquefaction resistance of saturated loose sandy ground (Sato et al. 2007). During field construction, either cement slurry (wet mixing) or cement powder (dry mixing) is injected into the ground under pressure. Based on the injection pressure and the physical conditions of the admixtures injected, the construction methods can be classified into three groups, namely, the cement slurry deep mixing (CDM) method, the dry jet mixing (DJM) method, and the wet jet mixing (WJM) method (Chai et al. 2009).

Injecting admixtures into the ground under pressure will cause deformation of the surrounding subsoil. In cases where there are existing structures or buildings adjacent to the construction site, the consequential lateral displacement may be significant because of the effects it may have on these structures. Therefore, predicting the lateral displacements induced by soil-cement column installation and ultimately controlling them are important design considerations. During the installation of columns in a clayey deposit, the ground will deform in a manner of close to undrained, while in a sandy deposit partial drainage may occur. When predicting lateral displacements induced by the column installation, possible soil drainage has to be considered.

In this paper, a prediction method based on cavity expansion theory is summarized. Two field tests conducted in Japan, using the CDM method are presented subsequently and comparisons between the calculated and measured lateral displacement profiles are made. The volumetric strain that may occur in sandy layers during soil-cement column installation is also discussed.

2. PREDICTION METHOD

Chai et al. (2009) proposed a method for predicting the lateral displacements in a soil deposit caused by the installation of multiple rows of soil-cement columns. It is believed to be the only method currently available for the analysis of this particular case. A brief summary of this method is provided as follows.

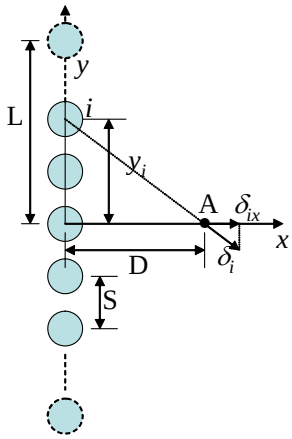

Figure 1: Plan section illustrating the lateral displacement in the x direction caused by installation of a single row of soil-cement columns (after Chai et al. 2005)

2.1. Lateral displacement due to a single row of infinitely long columns

As shown in Fig. 1, for point A the lateral displacement in the *x*-direction (δ_{xA}) caused by installing a row of infinitely long columns can be calculated by the equations presented in Table 1. These equations were derived using cylindrical cavity expansion theory. It can be seen that in addition to the geometric conditions, the significant parameters controlling the lateral displacement are R_p and δ_p.

Table 1: Equations for lateral displacement caused by installation of a single row of columns

Eq. No.	Condition	Lateral displacement
Eq. (1)	For $D < R_p$ and $D^2 + L^2 > R_p^2$	$\delta_{xA} = \frac{2D(2R_p + \delta_p)\delta_p}{S\sqrt{4D^2 + 2R_p\delta_p}} \cdot \tan^{-1}\sqrt{\frac{2(R_p^2 - D^2)}{2D^2 + R_p\delta_p}} + \frac{2R_p}{S}\delta_p\left(\tan^{-1}\frac{L}{D} - \tan^{-1}\sqrt{\frac{R_p^2}{D^2} - 1}\right)$
Eq. (2)	$D < R_p$ and $D^2 + L^2 \le R_p^2$	$\delta_{xA} = \frac{2D(2R_p + \delta_p)\delta_p}{S\sqrt{4D^2 + 2R_p\delta_p}} \tan^{-1}\sqrt{\frac{2L^2}{2D^2 + R_p\delta_p}}$
Eq. (3)	For $D \ge R_p$	$\delta_{xA} = \frac{2R_p}{S}\delta_p(\tan^{-1}\frac{L}{D})$

D = the offset distance from the centre of a row of columns to the point of interest; S = the spacing between two adjacent columns in a row; R_p = the radius of plastic zone around a cylindrical cavity; δ_p = the displacement at $r=R_p$; L = the half length of a row.

The equations in Table 1 assume that the point of interest is on the perpendicular bisector of a row of columns. If the point of interest is not on the bisector of the row, two calculations are needed, i.e., using two different values of L and then combining the results.

According to Vesic (1972), the parameter R_p can be calculated as:

$$\frac{R_p}{R_u} = \sqrt{I_{rr}\sec\phi'} \tag{4}$$

where ϕ' = the effective internal friction angle (for a clayey deposit, assuming $\phi' = 0$), R_u = the diameter of the cavity, and I_{rr} = the reduced rigidity index. I_{rr} is calculated from the rigidity index (I_r) as follows (Vesic 1972):

$$I_{rr} = \frac{I_r}{1 + I_r\Delta\sec\phi'} \tag{5}$$

$$I_r = \frac{E}{2(1+\nu)S_u} = \frac{G}{S_u} \tag{6}$$

where: E = Young's modulus, G = shear modulus, ν = Poisson's ratio, Δ = volumetric strain, and

s_u = undrained shear strength. For a clayey deposit, $\Delta = 0$ ($I_{rr} = I_r$) can be assumed, and s_u can be determined by field vane shear tests or laboratory unconfined compression tests using undisturbed samples, or else it can be estimated using Ladd's (1991) empirical equation:

$$s_u = S \cdot \sigma_v^{'} \cdot (OCR)^m \tag{7}$$

where σ'_v = vertical effective stress, OCR = over-consolidation ratio, and S and m = constants. Ladd (1991) proposed that the range of values for S is typically 0.162 to 0.25 and for m it is 0.75 to 1.0. We propose using S = 0.2 to 0.25 and m = 1.0. For a sandy deposit, s_u can be calculated as follows:

$$s_u = c' + p_0 \tan\phi' \tag{8}$$

where c' = effective cohesion, and p_0 = initial effective mean stress, and for calculating the value of p_0, a value of the at-rest earth pressure coefficient (K_0) of 0.5 can be assumed.

R_u is a crucial parameter controlling the amount of lateral displacement that will occur. Several factors will affect the selection of an appropriate value of R_u. The first of these is the injection pressure (p) of the admixture and the second is the effective volume of the admixture injected into the subsoil per unit length of column (Δvol). The effective volume means the net volume of admixture injected into the ground (subtracting the volume of returned spoil from the total volume injected). The third and fourth factors affecting the value of R_u are the undrained shear strength (s_u) and the Young's modulus (E) of the subsoil. At present, there are insufficient data available to derive a meaningful theoretical expression for R_u in terms of all these factors. Instead, empirical equations were proposed to evaluate R_u (Chai *et al*., 2005).

The effect of the injection pressure p is incorporated indirectly in the back-fitted radius of the cavity, R_{u0}, which also depends on the amount of injected admixture and the soil conditions (specifically the modulus E_0). An empirical equation has been proposed to consider the effects of s_u and E on R_u. Since for most soft clayey deposits, E can be estimated as a linear function of s_u, only the value of E is required in this empirical expression, and consequently the following simple power function was selected:

$$R_u = R_{u0}\left(\frac{E_0}{E}\right)^{1/3} \tag{9}$$

where R_{u0} = the radius of the cavity corresponding to a soil modulus E_0.

By back-fitting the field measured data from three sites in Saga, Japan, for three different construction methods, namely the CDM method, DJM method, and WJM method, Chai *et al*. (2005) proposed values of R_{u0} for these three methods, as listed in Table 2, together with the corresponding values of p, Δvol and E_0.

Table 2: Back estimated empirical parameters

Mixing method	Injection pressure p (MPa)	Injected volume Δvol (m^3/m)	Radius, R_{u0} (m) (E_0 = 2250 kPa)
CDM	0.1 – 0.2	0.146	0.21
DJM	0.5 – 0.7	0.036	0.46
WJM	~20	0.146	0.58

For a given installation method, the effect of varying Δvol on R_{u0} can be estimated under equivalent volume conditions. Suppose the value of R_{u0} corresponding to Δvol_1 is R_{u01}, then for Δvol_2, the corresponding value R_{u02} can be approximated as:

$$R_{u02} = R_{u01} - \frac{\Delta vol_1 - \Delta vol_2}{2\pi R_{u01}} \tag{10}$$

The value of δ_p, for a clayey deposit can be calculated as (Chai et al. 2005; 2007):

$$\delta_p = \frac{1+\nu}{E} R_p S_u \tag{11}$$

and for a sandy deposit (Chai et al. 2009):

$$\delta_p = \frac{1+\nu}{E} R_p (c' \cdot \cot\phi' + p_0) \sin\phi' \tag{12}$$

2.2 Limited column length

In engineering practice, the length of the columns is necessarily limited. A correction function is used to consider the effect of the limited length of the columns. The correction function was developed by comparing the solution based on the theory for a spherical cavity expansion with that for a cylindrical cavity expansion corresponding to a single column installation. Simulation of the installation of a single column was achieved by a series of spherical cavity expansions with a nominated spacing. By comparing the lateral displacement corresponding to a series of spherical cavity expansions over a limited length with that for a single cylindrical capacity expansion, the correction function required for a limited length of column was derived as follows (Chai et al. 2009):

$$RLD = \frac{1}{2}\left(\frac{H_1}{\sqrt{D_r^2 + H_1^2}} + \frac{H_2}{\sqrt{D_r^2 + H_2^2}} + \frac{2Z_0 + H_2 + H}{\sqrt{D_r^2 + (2Z_0 + H_2 + H)^2}} - \frac{2Z_0 + H_2}{\sqrt{D_r^2 + (2Z_0 + H_2)^2}} \right) \tag{13}$$

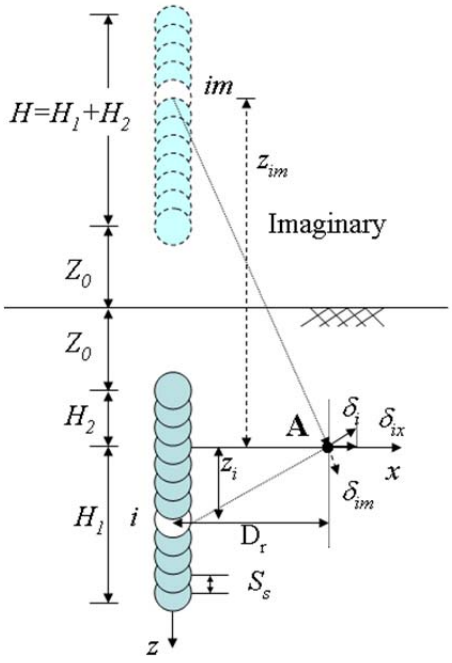

Figure 2: Vertical section illustrating the lateral displacement in the x direction caused by installation of a single soil-cement column (after Chai et al. 2009)

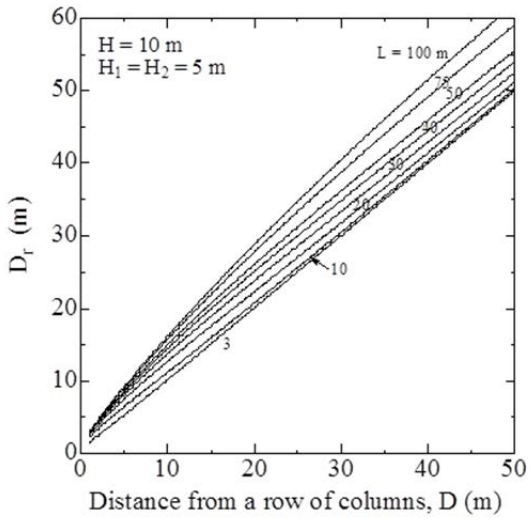

Figure 3: -Radial distance D_r as a function of D and L

The meanings of the symbols H, H_1, H_2 and Z_0 and D_r are illustrated in Fig. 2. Equation (13) provides a correction function for a single column applies. In order to apply this correction to the equations presented in Table 1 (for one-row of columns) a representative value of D_r has to be determined, which involves a complicated integration. The value of D_r is mainly influenced by the offset distance, D and the parameter L and some numerical results are plotted in Fig. 3. The combination of Eqs (1) to (6), (9) to (13) and the results in Fig. 3 forms the basis of the prediction method for estimating the effects of a row of soil-cement columns.

2.3 Effect of multiple rows

When a column or a row of columns is installed in a soil deposit, the strength and stiffness of the soil layer containing the columns will be different from the original soil. Therefore, the installed columns will subsequently influence the lateral displacement caused by the newly installed column(s). However, in the method proposed by Chai et al. (2009), this kind of the effect has not been considered. Instead, the multi-row effect can be dealt with for two extreme conditions, i.e., (1) superposition of the effect of all rows, which is likely to result in an overestimate of the lateral displacement; and (2) considering the effect of only a single row of columns adjacent to the point interested, which should under-predict the overall lateral displacement.

3. FIELD TEST RESULTS AND COMPARISONS WITH CALCULATED VALUES

Hiraide and Baba (1996) reported field tests conducted at two different sites in Japan which were used to investigate soil-cement column installation and the induced lateral displacements of the soil deposits. The results obtained for the CDM method are analyzed and discussed here.

3.1. Tests site-1

At site-1, the soil deposit consists of a sandy surface layer about 4 m thick underlain by a sandy layer to about 9.0 m depth. Below the sandy layer were soft to stiff clayey layers to about 30 m depth followed another sandy layer. The standard penetration test N-values in the ground from 0 to 9 m depth were less than 10 (Hiraide and Bala 1996). Based on the data reported by Hiraide and Baba (1996) and Kakihara and Hiraide (1997), the estimated values of the unit weight (γ_t), voids ratio (e), over-consolidation ratio (OCR), the ratio between Young's modulus (E) and undrained shear strength (s_u) of all soil layers, and the effective stress strength parameters, c' and ϕ' of the sandy layers, and the value of S adopted in Eq. (7) for the clayey layers are listed in Table 3. With the E/s_u ratios shown in Table 3 and assuming $\nu = 0.5$, the rigidity index (I_r) will be about 67 to 100. The groundwater level was assumed to be 1.0 m below the ground surface.

Table 3: Estimated and assumed soil properties for site-1

Depth (m)	Soil	γ_t (kN/m^3)	e	OCR	c' (kPa)	ϕ' (°)	S (Eq. 7)	E/s_u
0-4	Surface	17.6	1.1	-	20	30	-	200
4-9	Sand	17.6	1.1	-	10	30	-	200
9-12	Clay 1	15.2	2.1	1.0	-	-	0.25	200
12-20		15.2	2.1	1.0	-	-	0.2	200
20-25	Clay 2	15.7	1.8	1.2	-	-	0.25	200
25-30	Clay 3	15.7	1.8	1.5	-	-	0.25	200
30-35	Sand	18.0	1.0	-	20	35	-	300

The layout of the columns and the plan position at which lateral displacements were measured at site-1 are shown in Fig. 4. The diameter of each column was 1.0 m, and the columns were arranged in a square pattern immediately adjacent to each other, which resulted in an area replacement ratio of about 78.5%. The columns were constructed in the order from row-1 to row-3. The length of each column was approximately 27.3 m and the amount of cement used varied with depth as indicated in Fig. 5. The water/cement ratio (w/c) was 1.0.

With the conditions described above, the volumes injected in the ground were 0.157 m^3/m and 0.105 m^3/m and the amount of cement used was 1.47 kN/m^3 and 0.98 kN/m^3, respectively. Thus from Eq. (10), the radii (R_{u0}) of the cavities corresponding to a Young's modulus (E_0) of 2250 kPa are 0.218 m and

0.179 m, respectively. A comparison of the measured and calculated lateral displacements is given in Fig. 6 (a) for the case where $\Delta = 0$ and $\nu = 0.5$ were assumed. The zigzags apparent in the calculated curves are due to one of the limitations of the method, which does not consider the interaction between different soil layers. It can be seen that the calculation has over-predicted the lateral displacement in the sandy layers and under-predicted the measured values in clayey layers. For the clayey layers, further refinement cannot be made because of the lack of detailed information related to the strength and the stiffness of the soil layers. As for the sandy layers, there is a possibility that during the soil-cement column installation finite volumetric strain may have occurred. Figure 6 (b) shows the results obtained if it is assumed that $\Delta = 2\%$ in the sandy layers. In the surface sandy layer, the calculated values almost matched the measured displacements. A value of $\Delta = 2\%$ is less than the value of $\Delta = 4.5\%$ back-calculated for a loose sandy deposit, as reported by Chai et al. (2009). It is considered that the appropriate value of Δ may be related to the permeability and density of the soil deposit. For the sandy layers from 0 to 9 m depth, Kakihara and Hiraide (1997) reported that the values of permeability of the layers are 10^{-6} to 10^{-7} m/s.

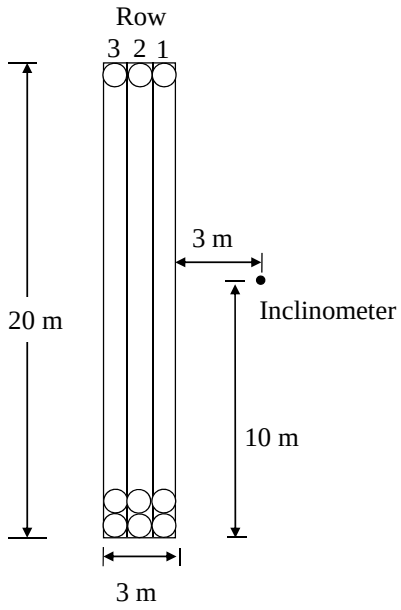

Figure 4: Plan view of the test arrangement

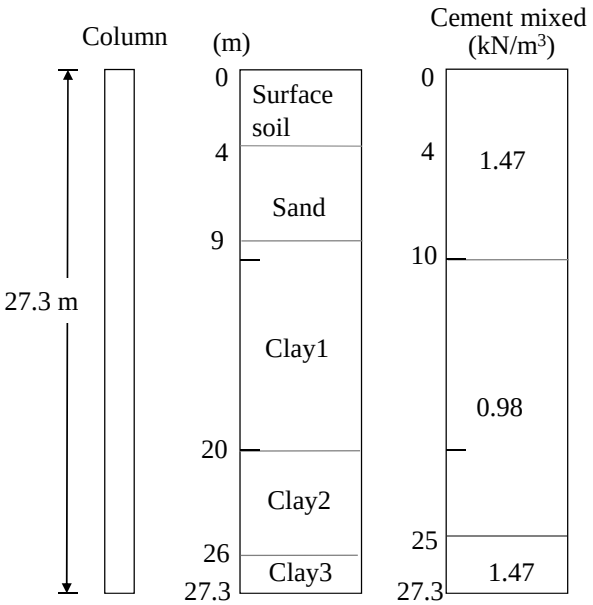

Figure 5: Amount of cement used

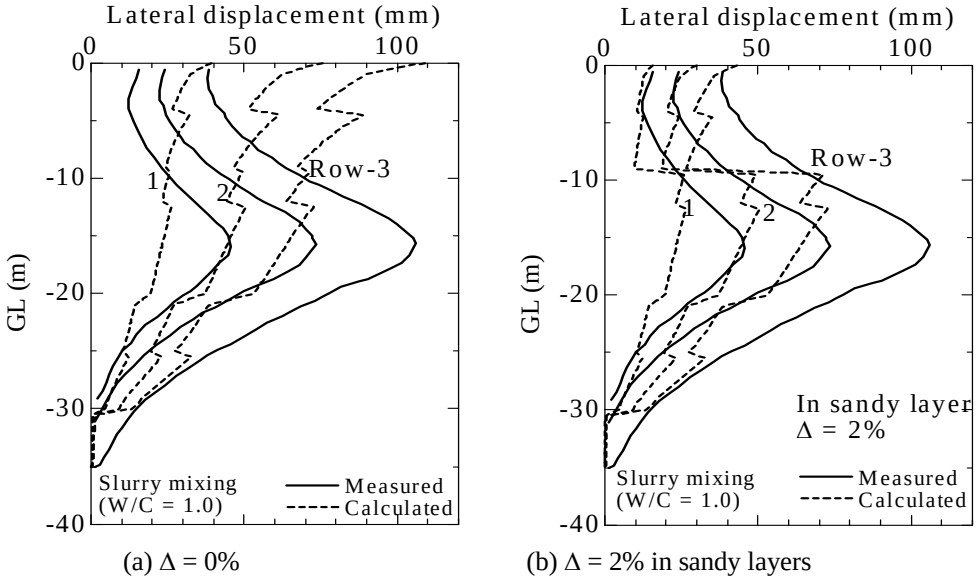

Figure 6: Comparison of measured and calculated lateral displacement profiles at site-1

3.2 Test site-2

Site-2 had a soil profile similar to that at site-1, but the sandy surface layer and the sandy layer below it were thicker than that at site-1. The estimated or assumed values of the parameters used to calculate the lateral displacements are listed in Table 4. The groundwater level was assumed to be 1.0 m below the ground surface.

The layout of the columns and the plan position at which the lateral displacements were measured at site-2 are shown in Fig. 7. The diameter of the column was also 1.0 m, and the area replacement ratio was about 78.5%. The length of the columns was about 44.3 m and the amount of cement used was varied with depth according to the two patterns shown in Fig. 8. The pattern with w/c ratio of 1.0 was applied in the rows designated as ① and ③, as indicated in Fig. 7, and the pattern with w/c of 1.2 was applied to the rows designated as ②. For cases where w/c = 1.0, the estimated values of R_{u0} are 0.187 to 0.202 m, and for w/c = 1.2, the corresponding values are 0.20 to 0.236 m. The construction sequence is also indicated in Fig. 7.

Table 4: Estimated or assumed soil properties of site-2

Depth (m)	Soil	γ_t (kN/m^3)	E	OCR	c' (kPa)	ϕ' (°)	S (Eq. 7)	E/s_u
0-8	Surface	17.6	1.1	-	20	30	-	200
8-17	Sand	17.6	1.1	-	10	30	-	200
17-20	Clay 1	15.2	2.1	1.0	-	-	0.25	200
20-30		15.2	2.1	1.0	-	-	0.2	200
30-35	Clay 2	15.7	1.8	1.2	-	-	0.2	200
35-42		15.7	1.8	1.5	-	-	0.25	200
42-50	Clayey sand	18.0	1.0	-	20	35	-	300

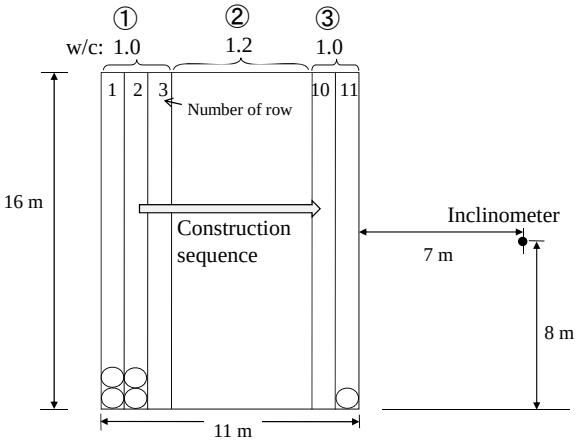

Figure 7: Plan view of the layout of columns and construction sequence

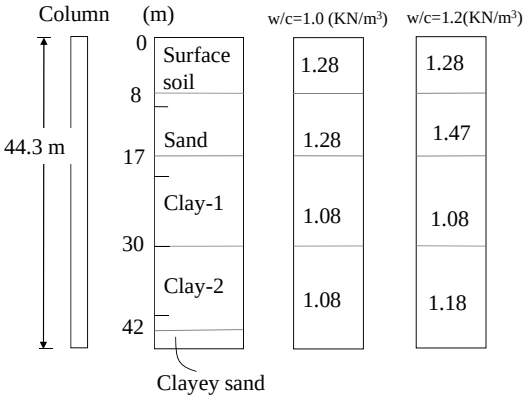

Figure 8: Amount of cement used and w/c ratio

Figures 9(a) and (b) show a comparison of the measured and calculated lateral displacement profiles. As for site-1, in the clayey layers the calculated values of displacement are generally less than the measured ones. When assuming $\Delta = 0$, the calculated values over-predicted the lateral displacement of the surface layers, and when using $\Delta = 2\%$ for the sandy layers, the calculation generally results in good predictions for the layer from the ground surface to about 5 m depth.

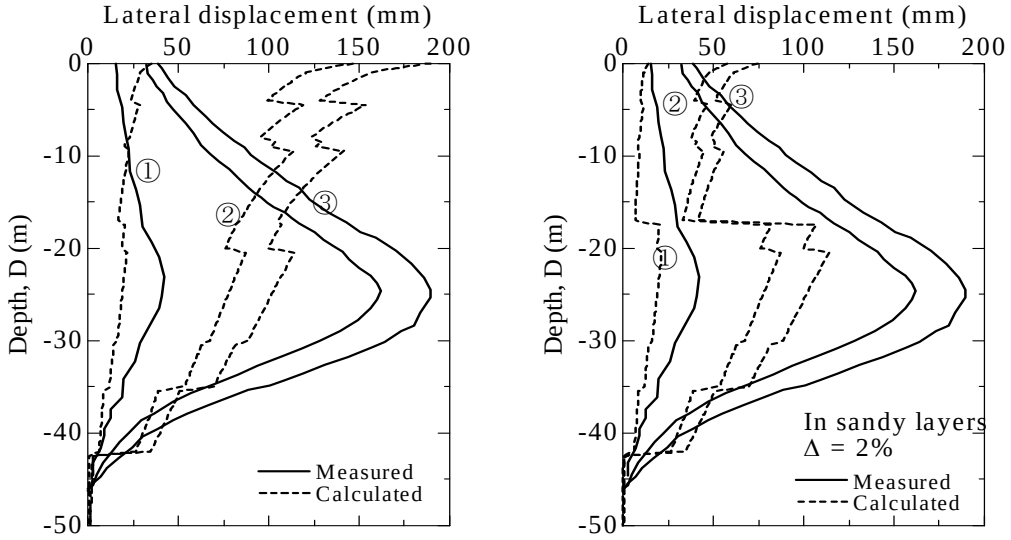

(a) Δ = 0% (b) Δ = 2% in sandy layers

Figure 9: Comparison of measured and calculated lateral displacement profiles at site-2

4. Summary

A method for predicting lateral soil displacements due to the installation of soil-cement columns has been summarized briefly and then applied to two field tests conducted in Japan in the 1990s.

The prediction method was developed by Chai et al. (2009) using cavity expansion theory. It can explicitly consider the effect of the amount of admixture injected into the soil and its stiffness and strength, as well as accounting for the construction method empirically. For the case of multi-column installation, the method is considered to be the only semi-theoretical method currently available.

Two field tests were conducted at two quite similar but separate sites in Japan using the cement slurry mixing method (CDM). These deposits consist of sandy layers at the ground surface underlain by clays. Underlying the clayey layers were further sandy layers. Comparing the predicted and measured lateral displacement profiles indicates that the semi-theoretical method generally under-estimates the lateral displacement of the clayey layers but over-estimates the values of the sandy layers when assuming zero volumetric strain (Δ). Assuming Δ = 2% in the sandy layers, the calculated lateral displacements provide a good match to the measured data for the surface layer, indicating that for a sandy layer the soil may deform in a partially drained manner.

REFERENCES

Bergado, D. T., Chai, J.-C., Alfaro, M. C. and Balasubramaniam, A. S. (1994). Improvement techniques of soft ground in subsiding and lowland environment. Balkema, Rotterdam, p. 222.

Chai, J.-C., Miura, N, and Koga, H. (2005). "Lateral displacement of ground caused by soil-cementμ column installation." Journal of Geotechnical and Geoenvironmental Engineering, ASCE, Vol. 131, No. 5, pp. 623-632.

Chai, J.-C., Miura, N, and Koga, H. (2007). Closure to "Lateral displacement of ground caused by soil-cement column installation." by J.-C. Chai, N. Miura, and H. Koga, Journal of Geotechnical and Geoenvironmental Engineering (JGGE), ASCE, 131(5), 623-632, JGGE, ASCE, Vol. 133, No. 1, pp. 124-126.

Chai, J.-C., Carter, J. P., Miura, N. and Zhu, H.-H. (2009). Improved prediction of lateral deformations due to installation of soil-cement columns. Journal of Geotechnical and Geoenvironmental Engineering, ASCE, Vol. 135, No. 12, pp. 1836-1845.

Hiraide, A. and Baba, K. (1996). Displacements of nearby soil made by soil improvement with cement deep mixing method – part I. Proc. of 31th Annual Meeting of Japanese Geotechnical Society, Kitami, Hokaido, Japan, pp. 151-152 (in Japanese).

Kakihara, Y. and Hiraide, A. (1997). Study on cause of ground displacement by deep mixing soil stabilization. Proc. of 32th Annual Meeting of Japanese Geotechnical Society, Kumamoto, Japan, pp. 2371-2372 (in Japanese).

Ladd, C. C. (1991). "Stability evaluation during staged construction." Journal of Geotechnical Engineering, ASCE, 117(4), 541-615.

Sato, E., Minami, T., Namikawa, T., Aoki, M. (2007). Evaluation of ground deformation during construction of deep mixing method – part II: effect of deformation control method. Proceedings of the 42th Annual Meeting of Japanese Geotechnical Society, pp. 907-908 (In Japanese).

Vesic, A. S. (1972). Expansion of cavities in infinite soil mass. Journal of Soil Mechanics and Foundation Engineering, ASCE, Vol. 98, No. SM3, pp. 265-290.

Quality Assurance and Quality Control for Deep Soil Mixing (DSM) in Punggol Waterway Project, Singapore

S.H Chew and C.Y. Tan, National University of Singapore (NUS), Singapore, ceecsh@nus.edu.sg, cyheaw@gmail.com

T.Y Yap, K.E Chua, H.M Yim and S.Y Kee
Housing Development Board, Singapore

T.K Khoo and Ja Naw
Surbana International Consultant Pte Ltd, Singapore

ABSTRACT

Construction of Punggol Waterway in Singapore has to be carried out over difficult soil conditions, which poses slope stability concern. Deep Soil Mixing method (DSM) was selected as one of the ground improvement schemes for this construction. Due to the non-uniformity of the mixing, the strength of the DSM columns is often highly variable and thus, the quality control and assessment of the DSM columns is always a concern in practical project. As massive amount of DSM is to be constructed in this project, it is thus very important to ascertain its quality and consistency. As such, a rationale, comprehensive and representative quality assurance and quality control (QA/QC) plan with clear acceptance criteria was developed taking into account the average value within the sub-zone, overall average value across all zones, as well as each and every individual tested data. Both strength (using UCS strength) and Total Core Recovery (TCR) from the cored samples were evaluated based on the above concept. This is a holistic and yet statistically sounds method. This proposed revised quality assurance and quality control plan for Deep Soil Mixing was applied for Punggol Waterway Singapore Project. It successfully covered the long stretch of Punggol Waterway in good detail, yielding "accurate" representation of the quality of the DSM columns installed, thereby, ensuring the quality of the soil improvement works. The required rectification measure, if needed, also found to be adequate and cost effective.

1. INTRODUCTION

The Housing & Development Board in Singapore (HDB) is implementing the Punggol Waterway project as part of its initiative of "Remaking of the Heartlands Plan" for the development of Punggol 21+. Punggol Town is situated at the northeastern part of Singapore (Figure 1) and the proposed Punggol waterway is a 4.2-kilometre long, 20-30 meter wide man-made waterway which runs through the housing estate and linking two rivers. An overview of the project area is given in Figure 2 and the cross section view of the waterway is shown in Figure 3. The geological history indicates that some branches of ancient streams and rivers run through part of the site. As such, this project is to be constructed on difficult soil conditions like thick layers of soft marine clay and soft peaty clay, inter-bedded with some loose sandy silty soil, which poses slope stability concern. Deep Soil Mixing method (DSM), which has gained popularity for the past 10 years in Singapore, was selected as one of the ground improvement scheme for the construction of Punggol Waterway Part I.

The technique of deep cement mixing has been well developed in the 70s to 80s (Kawasaki, et al., 1981; Ingles and Metcalf, 1972). In particular, the techniques of jet grouting and deep cement mixing have been widely used in Singapore for the treatment of soft marine clay for deep excavation and subway construction (Chew et al., 1997; Kamruzzaman et al., 2001). Significant study on the strength development of the DSM on Singapore marine clay was also conducted (Tan et al., 2002). Due to the non-uniformity of the mixing, the strength of the DSM columns is often highly variable and this has been a problem in practice (Chen et al, 2011). The quality control and assessment of the DSM Columns is always a concern in practical project.

As massive amount of DSM is to be constructed in this project, it is thus very important to ascertain its quality and consistency. Furthermore, as deep excavation of about 13 m was required for the construction of the waterway, good and consistent results from DSM soil improvement works are required to ensure adequate slope stability. As such, a rationale, comprehensive and representative quality assurance and quality control (QA/QC) plan with clear acceptance criteria stated were required for this project. This

paper highlights the quality assurance and quality control plan proposed and implemented successfully for this project. It provides an effective and consistent way of evaluating the overall quality of the DSM works in similar projects.

2. SOIL CONDITIONS & DEEP SOIL MIXING DESIGN

A total of 42 boreholes & 66 numbers of CPTs were carried out for the soil investigation for the project. Generally, the top ground consists of filled material overlaying a layer of either soft marine CLAY or Peaty CLAY, which was further underlined by the Old Alluvium which is a dense sand formation. A typical soil profile that is encountered in that area is shown in Figure 4.

The design of Deep Soil Mixing (DSM) is based on column diameter of 850mm at spacing of 750mm center to center. Grid patterns of DSM columns are used (Figure 5) instead of full blocks of DSM for cost effectiveness. The DSM columns are being implemented on both sides of the waterway, as seen in the cross-section view given in Figure 6. Based on the equivalent area ratio of the DSM and the required strength for the slope stability, the minimum design strength and stiffness of the individual DSM columns is:

- Unconfined Compression Strength, q_u = 1000 kPa
- Undrained shear Strength, Cu = 500 kPa
- Undrained Young's Modulus, E_u = 200,000 kPa

3. ORIGINAL ACCEPTANCE CRITERIA FOR CORE SAMPLES AND TEST RESULTS

As part of the Quality Assurance (QA) and Quality Control (QC) plans for this project, core samples are required to be taken from the completed columns at specified interval. The Deep Soil Mixing (DSM) treated area was divided into blocks of 25m chainage along waterway on each bank. Sampling was carried out with two coring points per block. Each sets of coring points consist of three samples (i.e top, middle, and bottom) from the selected DSM columns and the unconfined compressive strength tests of the cored samples were carried out. The acceptance criteria for each DSM cored sample were originally defined as:-

1. Total core recovery (TCR) shall be at least 85%
2. Unconfined compressive strength (UCS) shall be at least 1000 kPa
3. Modulus of Elasticity (E) shall be at least 200 MPa .

As long as one sample failed one of the above criteria, the whole block of 25 m length of DSM works has to be considered as FAILED section, and replacement or repairing was needed, according to this contract. However, first few series of test results revealed that this practice may not be fair as a single failed sample may just only be an outlier of the limited number of sampling data point and the DSM columns may still be reasonably well constructed. On the other hand, it may encounter cases where all of the above criteria were met, and yet the visual observation of the cored sample has shown that the DSM column was indeed not consistently or uniformly mixed with cement.

Thus, it is difficult to evaluate the quality and performance of DSM columns based on the above original criteria. One such outcome of the cored results is provided in Figure 7 of which a single DSM column was cored four times and producing very different results based on the above criteria. Photos of the cored samples indicating inconsistent or ununiformed mixing of DSM are shown in Figure 8.

4. REVISED QUALITY ASSURANCE AND QUALITY CONTROL METHOD FOR DSM COLUMNS

The quality assurance and quality control plan was revised with the aim to establish a more holistic methodology for checking the quality of resulted DSM columns consistently and fairly. This is very critical in ensuring the performance of the DSM columns is satisfying the requirement. The outlines of the revised QA/QC plan and its acceptance criteria are as follow:

4.1. Number of Coring Points

The quality of Deep Soil Mixing columns should be inspected by coring the completed column. The total length of the DSM column, from the toe to the top, shall be cored. The whole stretch of the project site that required DSM treatment is divided into many "panels" of 25 m each. Two (2) coring points shall be done in each "Panel", on each bank.

4.2. Cored samples for testing

Each cored point is subdivided into three (3) zones, i.e. Upper Zone, Middle Zone and Bottom Zone. At each zone, three (3) cored samples shall be randomly selected and sent for laboratory Unconfined Compression Test to obtain the UCS and modulus parameter. There should be some clear distance between each of these cored samples. To ensure a better representation, this clear distance shall be more than 1.0 m and less than 2.0 m for this project site in views that the expected length of the DSM columns is about 12 to 15 m.

4.3. Acceptance Criteria for cored samples of DSM Column

After the UCS testing, the acceptances of the samples are based on a newly established revised "acceptance criteria". There are two components in the acceptance criteria – one is Unconfined Compressive Strength (UCS), and the second one is Total Cored Recovery (TCR).

4.3.1 Based on UCS – the following acceptance criteria (assuming the intended target UCS strength is 1.0 MPa as in this project site) shall be satisfied:

i. For each zone, the average UCS value (i.e. average of 3 cored samples) must be > 90% of targeted UCS value, i.e. 0.9 MPa;
ii. UCS for each individual sample must be > 75% of the Targeted UCS value, i.e. 0.75 MPa; and
iii. Overall Average UCS for the whole column (i.e. the average of all three zones 9 individual samples UCS values) must be > targeted UCS value, i.e. 1.0 MPa

4.3.2 Based on TCR - The acceptance criteria for total core recovery (TCR) area as follows:

i. For each zone, the average TCR value (i.e. average of all length in this zone) must be > 75% ;
ii. TCR value for each individual sample of 1 m length must be > 25%
iii. Overall Average TCR for the whole column (i.e. the average of all three zones TCR values) must be > 85%.

The cored point is considered as "Passed" if all the above mentioned criteria were met. Vice versa, the cored point cannot be accepted if any one of the criteria has not been met. This process is illustrated in graphical form in Figure 9.

5. ACTUAL CONSTRUCTION WORK AND QA/QC CONTROL

The actual QA/QC plan was implemented for the actual construction work at Punggol Waterway. Coring samples were extracted from the completed DSM column using wet boring method. Coring samples were taken only after at least 21 days from date of completion of the columns. Total of 9 test samples were tested for each cored column or sampling point.

For illustration purposes, two sets of results were discussed below. One set being taken from a satisfactory panel, while the other being taken from a not so well constructed panel. The test results for unconfined compressive strength and the TCR for the two coring points are summarized in Table 1.

For the well-constructed panel, a sample point, labeled as N92-06, the average UCS test results for the top, middle and bottom zone were found to be 1.23 MPa, 1.07 MPa and 0.97 MPa respectively. All individual cored samples were having the UCS strength higher than 0.75 MPa, with the overall average of all 9 cored sample of 1.09 MPa. It was clearly indicated that it passed all requirement with respect to the UCS component. Similarly, with respect to TCR, it also satisfied all three requirements. Thus, it can be concluded that this panel was well constructed and uniform results were obtained, and it has well met the acceptance criteria and this column has been considered passed. The cored pictures of the typical DSM piles in this panel showing very consistent and well treated soil were shown in Figure 10.

For the second illustrated panel, the sample point is labeled as N99-01. The average UCS test results for the top, middle and bottom zone were found to be 0.99 MPa, 0.66 MPa and 1.65 MPa respectively. While the overall average of all 9 cored samples was higher than 1.00 MPa, some of the individual cored samples were having the UCS strength as low as 0.55 MPa, 0.66 MPa, which is lower than the acceptable individual value of 0.75 MPa. It indicated that it did not pass all requirements with respect to the UCS component. Although, with respect to TCR, it satisfied all three requirements, it was concluded that this panel was not so consistently constructed and some sections were clearly not well mixed during the operation process. It was concluded that these results have NOT met the acceptance criteria and this panel (of 25 m length) was considered as "Fail". So, rectification works have been considered and additional columns have been installed for the entire 25 m panel. The picture of cored sample which shows a non-uniformly constructed panel is shown in Figure 11. Several weak spots can be seen in the cored sample.

Table 1: Summary of Two Coring Points

Ref: No.	Zone	UCS (MPa)	Avg UCS (MPa)	TCR (%)	**Avg UCS for whole coring point**	Pass/Fail
N92-06	TOP	1.06	1.23	90%	1.09	Pass
		1.15				
		1.48				
	MID	1.18	1.07	100%		
		1.14				
		0.88				
	BOT	0.81	0.97	95%		
		1.3				
		0.8				
N99-01	TOP	1.00	0.99	80%	1.10	Fail
		1.02				
		0.96				
	MID	0.76	0.66	90%		
		0.55				
		0.66				
	BOT	1.84	1.65	85%		
		1.34				
		1.76				

6. RECTIFICATION WORKS

In the event that the DSM treatment work for certain panels was deemed to be not satisfactory based on the above mentioned acceptance criteria, rectification work is required to compensate for the ground treatment work within this whole panel of 25 m length. This additional treatment work is needed to ensure that the whole "unit cell" will have an adequate overall strength as what was designed based on achieving the targeted strength. The short fall of the TCR and UCS strength from the designed targeted values has to be compensated from the additional columns of DSM within the "unit cell". Thus, the relationship of the DSM columns area and their strength values can be written as follow:

$$A_{Design} \cdot S_{Targeted} = A_1 \cdot S_1 + A_c \cdot S_c \quad (1)$$

where:
A_{Design} and $S_{Targeted}$ are the area and UCS targeted strength of the designed DSM columns area;
A_1 and S_1 are the area and UCS strength of the previously installed DSM columns area (which is the achieved strength and lower than the targeted strength);
A_c and S_c are the area and UCS strength of the additional compensation DSM columns and its strength.

In general, if the evaluation is done only at the completion of the treatment of the whole panel, thus $A_1 = A_{Design}$, and taking $S_c = S_{Targeted}$; the additional compensation DSM columns can be computed from:

$$A_c = A_{Design}\left(1 - \frac{S_1}{S_{Targeted}}\right) \quad (2)$$

In this situation, S_1 is computed based on the achieved TCR and UCS strength as obtained from,

$$S_1 = \alpha \cdot \beta \cdot S_{Targeted} \quad (3)$$

where:
α is the coefficient corresponding to the TCR value, which is equal to the ratio of overall average TCR achieved to the value of 85%, with maximum value of 1.0;
β is the coefficient corresponding to the UCS strength, which is equal to the ratio of the overall average UCS strength achieved to the targeted strength value, with maximum value of 1.0.

The above mentioned methodology provides a rationale way to design for the required compensation DSM columns based on the actual TCR and strength achieved in the case where they are fall short of the design targeted values. It ensures adequate safety and stability, and yet is cost effective.

7. CONCLUSION

For a major project involving large volume of DSM treatment works, a properly designed and executable QA/QC plan with clear and balanced acceptable criteria is very important for a successful project. The ultimate aim is to achieve an adequate and uniform treated area. The evaluation of the "pass or fail" should be consistent and should reflect the actual quality of the treated area fairly and adequately. One such methodology is proposed here by taking into account the average value within the zone (can be divided by depth), overall average value across all zones, as well as each and every individual tested data. Both strength (using UCS strength) and Total Core Recovery (TCR) from the cored samples were evaluated based on the above concept. This is a holistic and yet statistically sounds method.
This proposed revised quality assurance and quality control plan for Deep Soil Mixing was applied for Punggol Waterway Singapore Project. It was found to be effective and consistent. It successfully covered the long stretch of Punggol Waterway in good detail, yielding "accurate" representation of the quality of the DSM columns installed, thereby, ensuring the quality of the soil improvement works. The required rectification measure, if needed, also found to be adequate and cost effective.

8. ACKNOWLEDGMENTS

Special thanks to the main contractor of Punggol Waterway project - Koh Brothers Building & Civil Engineering Contractor (Pte.) Ltd, and the geotechnical specialist contractor – Ryobi Kiso (S) Pte Ltd for the successful conduct of this DSM works.

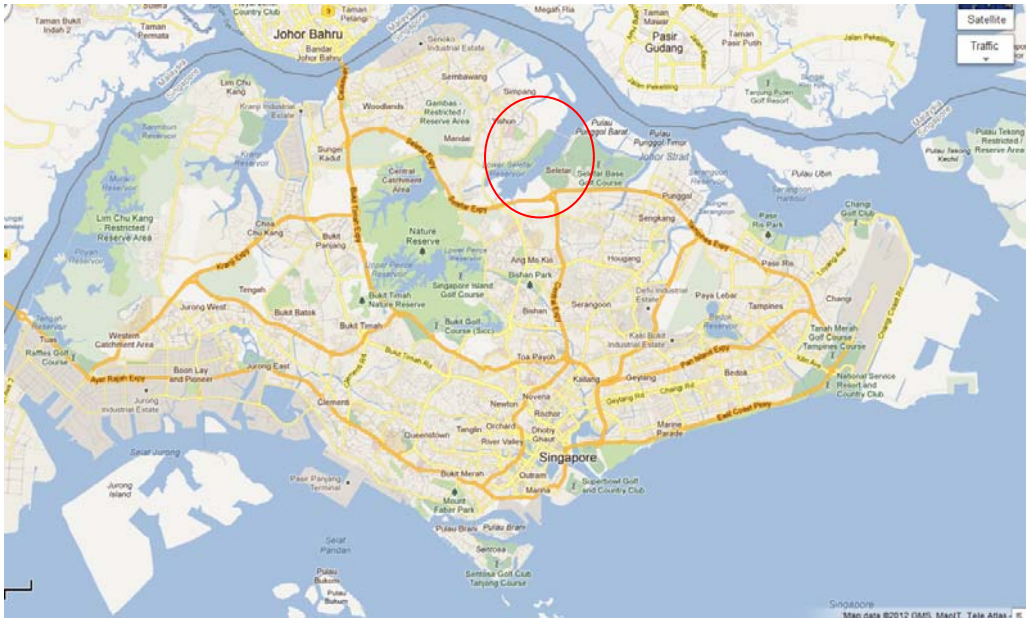

Figure 1: Location of Punggol Town in Singapore (Source: Google Map)

Figure 2: Overview of Punggol Waterway project, Singapore.

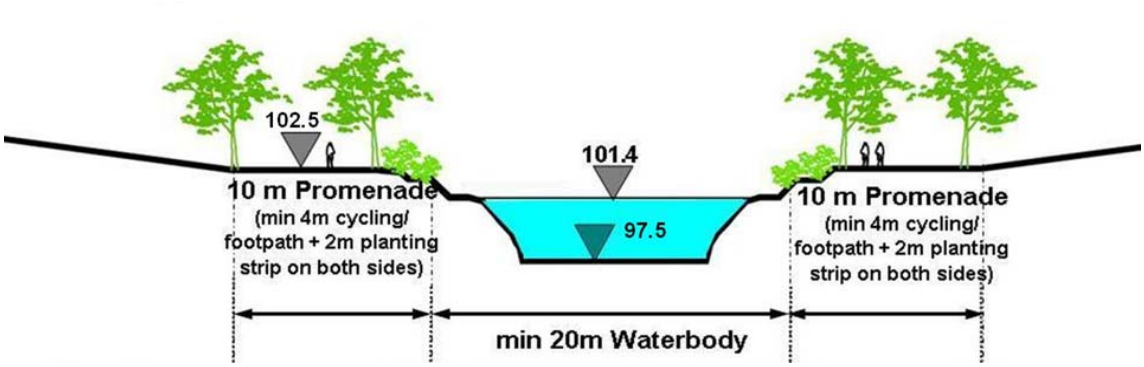

Figure 3: Cross-sectional View of the Punggol Waterway

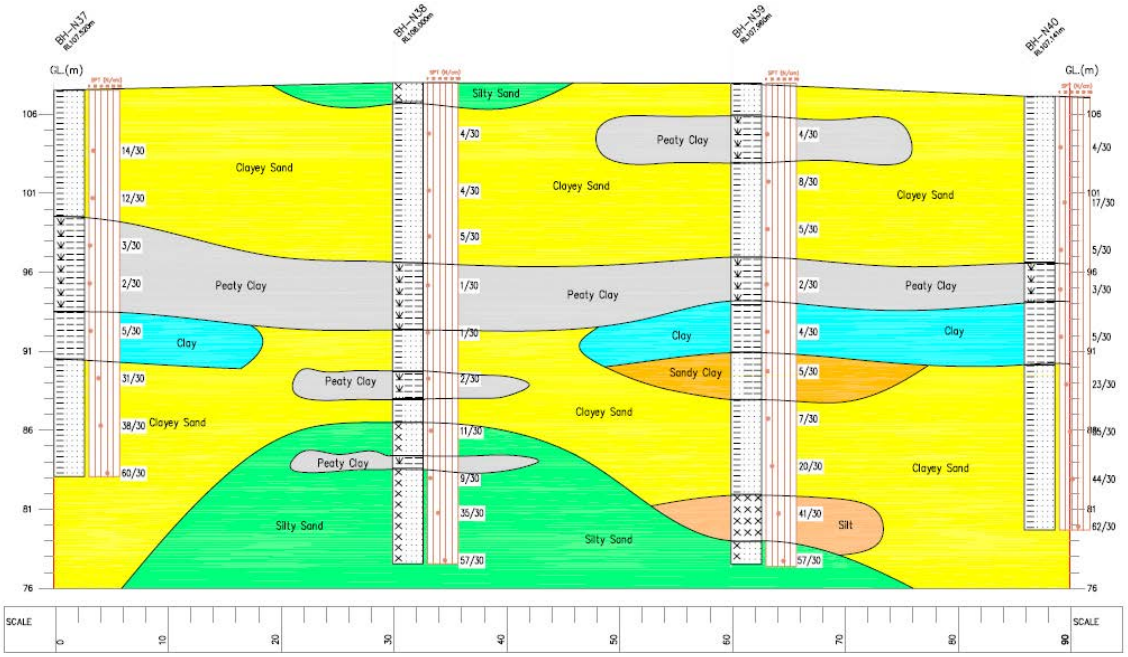

Figure 4: Typical Soil Profile in this project.

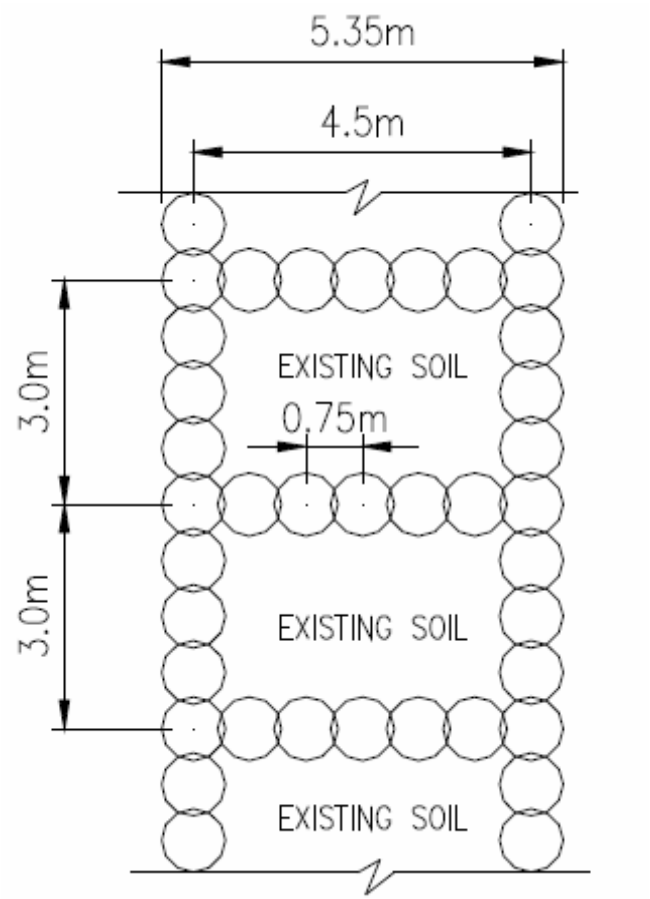

Figure 5: Typical Grid Pattern of Deep Soil Mixing (DSM) Columns.

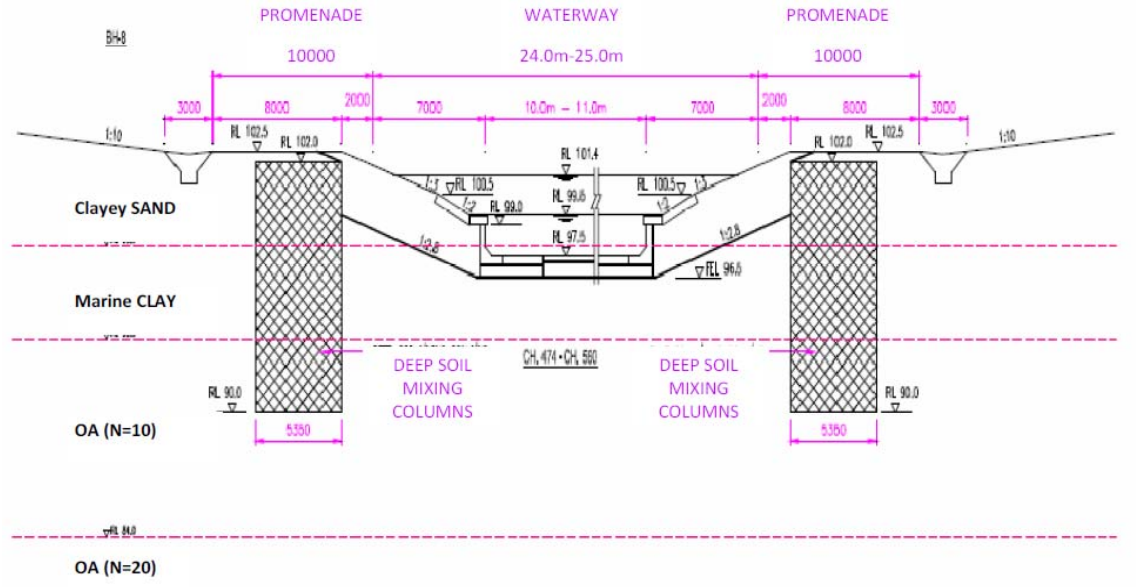

Figure 6: Typical Scheme of DSM for enhancing the slope stability of Punggol Waterway

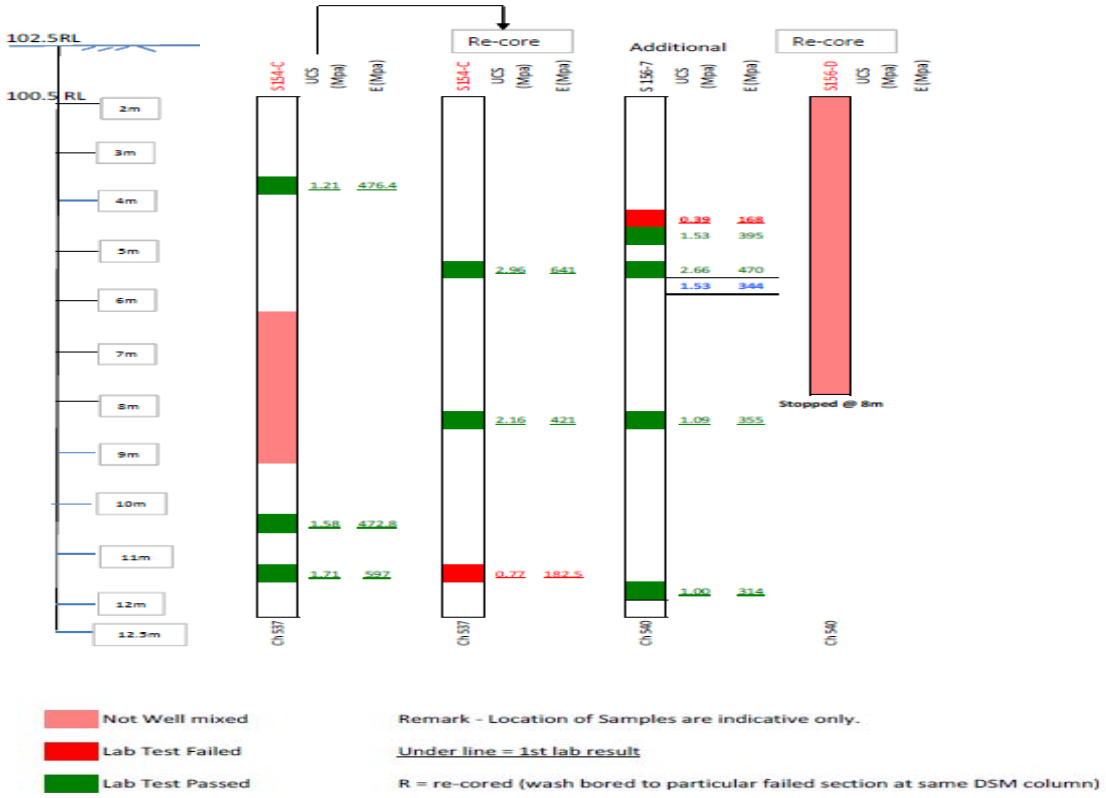

Figure 7: Test Results of the DSM Column showing the inconsistence of the original method

Figure 8: Coring Samples Photo showing some inconsistent results

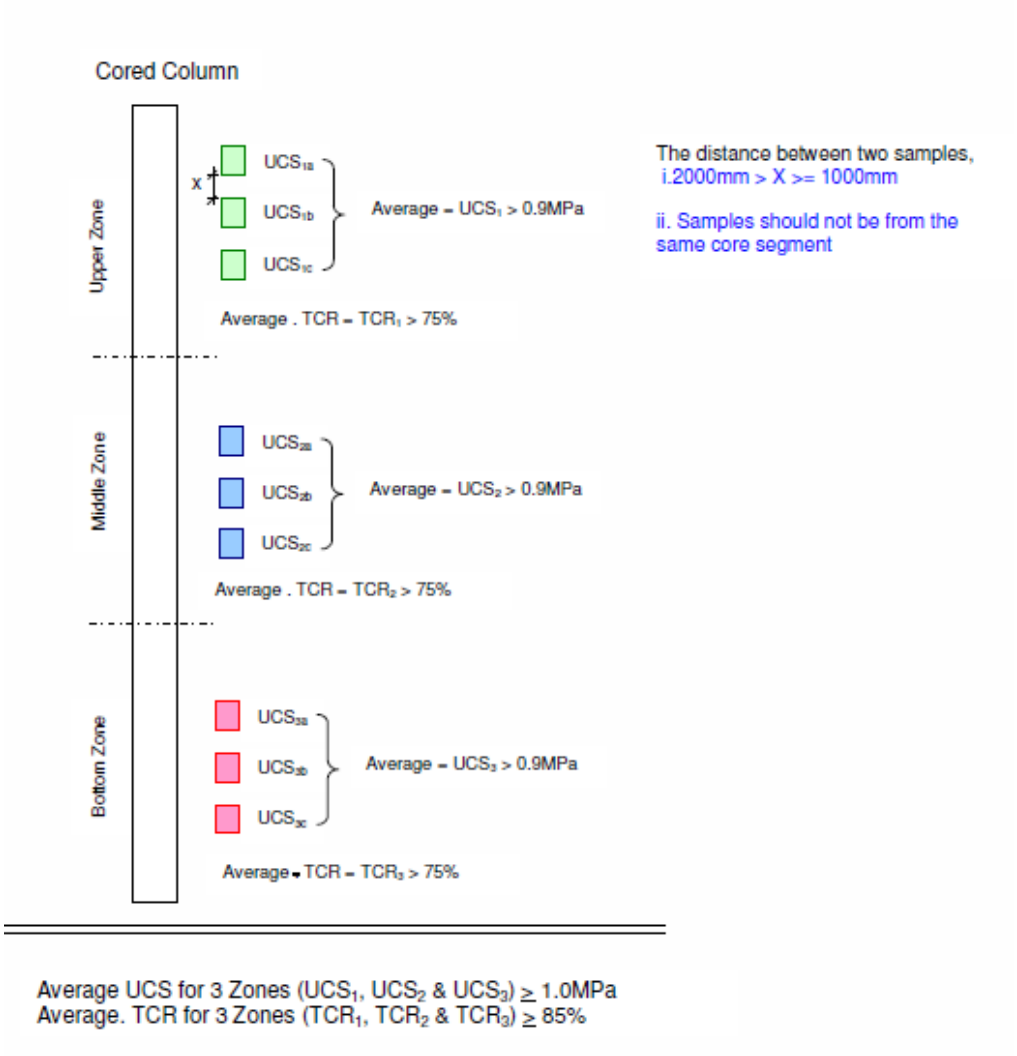

Figure 9: Revised Acceptance Criteria for DSM Column

Figure 10: Cored Sample of a well-constructed and uniformly treated DSM column

Figure 11: Cored Sample of a poorly constructed and non-uniform DSM column

REFERENCES

Chen, J., Lee, F.H., and Ng, C.C. (2011). "Statistical Analysis for Strength Variation of Deep Mixing Columns in Singapore." Proceedings, ASCE Conf. Proc. Geo-Frontiers 2011: Advances in Geotechnical Engineering ,

Chew, S.H., Lee, F.H. and Lee, Y. (1997). "Jet Grouting in Singapore Marine Clay". Proceedings of the Third Asian Young Geotechnical Engineers Conference, Singapore, 14-16 May, Tan et al.(eds)., pp.231-238.

Ingles, O.G. and Metcalf, J.B. (1972). Soil Stabilization Principle and Practice, Butterworths, Melbourne, Australia.

Kamruzzaman, A.H.M., Chew, S.H., and Lee, F.H. (2001). "Behavior of Soft Singapore Marine Clay Treated with Cement", Foundations and Ground Improvement, ASCE Geotechnical Special Publication No 113, Edited by T L Brandon, pp 472-485.

Kawasaki, T., Niina, A., Saitoh, S., Suzuki, Y. and Honjyo, Y. (1981). "Deep Mixing Method Using Cement Hardening Agent", Proceedings of the Tenth International Conference on Soil Mechanics andFoundation Engineering, Vol. 1, pp. 721-724.

Tan, T.S., Goh, T. L., and Yong, K. Y. (2002). "Properties of Singapore Marine Clays Improved by Cement Mixing." Geotechnical Testing Journal, ASTM, Dec. 2002, Vol. 25, No. 4.

SOIL MIX WALLS as retaining structures – Belgian practice

N. Denies, N. Huybrechts, Belgian Building Research Institute, Geotechnical division, Belgium, nde@bbri.be, nh@bbri.be
F. De Cock, Geotechnical Expert Office Geo.be, Belgium, fdc.geobe@skynet.be
B. Lameire, Belgian Association of Foundation Contractors ABEF, Belgium, bart@lameireft.be
J. Maertens, Jan Maertens bvba & KU Leuven, Belgium, jan.maertens.bvba@skynet.be
A. Vervoort, KU Leuven, Belgium, andre.vervoort@bwk.kuleuven.be

ABSTRACT

Since several decennia, the deep soil mix (DSM) technique has been used for ground improvement (GI) applications. In recent years, soil mix walls (SMW) have become an economical alternative to traditional excavation support systems.
The present paper concentrates on the application of SMW technology in Belgium. It focuses on the three main types of DSM systems currently used in Belgium: the Cutter Soil Mix (CSM), the Tubular Soil Mix (TSM) and the CVR C-mix® techniques.
In a second step, BBRI information sheets (BBRI, 2012a and b), developed within the framework of the Flemish regional research project IWT 080736, are presented. BBRI info sheets have been established for the purpose of helping contractors to improve the quality control (QC) of their finished product. They consist of guidelines for the execution phases and give some requirements with regard to the material quality, the characteristic dimensions, the bearing capacity and the lateral SMW displacement.
The BBRI info sheets define QA (Quality Assurance)/QC requirements in function of the DSM application – retaining wall, water barrier or foundation – and with regard to the permanent or temporary use of the construction. The acceptance criteria are proposed in terms of the number of unconfined compressive strength (UCS) tests, the limitation of soil inclusion percentage into the mix, the determination of the elastic modulus and the execution tolerances. Finally, the BBRI info sheets are discussed from an international view point regarding QA/QC procedures for deep mixing.

1. INTRODUCTION

1.1. DSM technique as excavation support

The DSM process was introduced in the 70's in Japan and in the Scandinavian countries. Since several decennia, DSM has been known as a GI technique, as reported in Porbaha et al. (1998 and 2000). Porbaha has notably proposed a terminology for the DSM technology, as given in Table 1.
According to the classification of GI methods adopted by the TC 17 (Chu et al. 2009), DSM can be classified as ground improvement with grouting type admixtures, as illustrated in Table 2.
A lot of reviews describing various Deep Mixing Methods (DMM) are available in Terashi (2003), Topolnicki (2004), Larsson (2005), Essler and Kitazume (2008) and Arulrajah et al. (2009). In parallel, the results of national and European research programs have been published in multiple interesting reports (such as Eurosoilstab, 2002), while also the European standard for the execution of deep mixing "Execution of special geotechnical works – Deep Mixing" (EN 14679) was published in 2005. Most of these research projects focused on the global stabilisation of soft cohesive soils such as peat, clay, gyttja and silt.
More recently, DSM has still increasingly been used for the retaining of soil and water in the case of excavations, as illustrated in Fig. 1. As a matter of fact, SMW represent a more economical alternative to concrete secant pile walls and even in several cases for king post walls (i.e. soldier pile walls).
Rutherford et al. (2005) have proposed a historical background of excavation support using SMW. Table 3 and 4 respectively compare the usual types of excavation support and the GI techniques used for retaining wall construction.

Table 1: Terminology of the deep mixing family, after Porbaha (1998)

CCP: chemical churning pile	DeMIC: deep mixing improvement by cement stabilizer
CDM: cement deep mixing	*In situ* soil mixing
CMC: clay mixing consolidation method	JACSMAN: jet and churning system management
DCCM: deep cement continuous method	Lime-cement columns
DCM: deep chemical mixing	Mixed-in-place piles
DJM: dry jet mixing	RM: rectangular mixing method
DLM: deep lime mixing	Soil-cement columns
DMM: deep mixing method	SMW : soil mix wall
DSM: deep soil mixing	SWING: spreadable WING method

Table 2: Classification of GI methods adopted by TC17 (after Chu et al., 2009)

D. Ground improvement with grouting type admixtures	D1. Particulate grouting	Grout granular soil or cavities or fissures in soil or rock by injecting cement or other particulate grouts to either increase the strength or reduce the permeability of soil or ground.
	D2. Chemical grouting	Solutions of two or more chemicals react in soil pores to form a gel or a solid precipitate to either increase the strength or reduce the permeability of soil or ground.
	D3. Mixing methods (including premixing or deep mixing)	**Treat the weak soil by mixing it with cement, lime, or other binders in-situ using a mixing machine or before placement**
	D4. Jet grouting	High speed jets at depth erode the soil and inject grout to form columns or panels
	D5. Compaction grouting	Very stiff, mortar-like grout is injected into discrete soil zones and remains in a homogeneous mass so as to densify loose soil or lift settled ground.
	D6. Compensation grouting	Medium to high viscosity particulate suspension is injected into the ground between a subsurface excavation and a structure in order to negate or reduce settlement of the structure due to ongoing excavation.

Figure 1: SMW with ground and water retaining functions

Table 3: Comparison of usual types of excavation support, after Rutherford et al. (2005)

Excavation support system	**Advantages**	**Limitations**
Structural diaphragm (slurry) wall	Constructed before excavation and below ground-water, good water seal, can be used as permanent wall and can be used in most soils. Relatively high stiffness. Can become part of the permanent wall.	Large volume of spoils generated and disposal of slurry required. Costly compared to other methods. Must be used with caution or special techniques must be used when adjacent to shallow spread footing.
Sheetpile wall	Constructed before excavation and below ground-water. Can be used only in soft to medium stiff soils. Quickly constructed and easily removed. Low initial cost.	Cannot be driven through complex fills, boulders or other obstructions. Vibration and noise with installation. Possible problems with joints. Limited depth and stiffness. Can undergo relatively large lateral movements.
Soldier pile and lagging wall	Low initial cost. Easy to handle and construct.	Lagging cannot be practically installed below groundwater. Cannot be used in soils that do not have arching or that exhibit base instability. Lagging only to bottom of excavation and pervious.
Secant wall/Tangent pile wall (similar to DSM walls)	**Constructed before excavation and below ground-water. Low vibration and noise. Can use wide flange beams for reinforcement.**	**Equipment cannot penetrate boulders, requires pre–drilling. Continuity can be a problem if piles drilled one at a time.**
Micro–pile wall	Constructed before excavation and below ground-water. Useful when limited right of way.	Large number required. Continuity a problem, low bending resistance.

Table 4: Comparison of excavation support using GI techniques, after Rutherford et al. (2005)

Excavation support using GI	**Advantages**	**Limitations**
DSM method	**Constructed before excavation and below ground-water. Low vibration and noise levels. Fast construction. Reduced excavated spoils compared to slurry (diaphram) walls. Improved continuity with multi-drill tool.**	**Difficult with boulders and utilities, spoil generated.**
Permeation grouting	Constructed before excavation and below ground-water.	Pre–grouting to control flow of grout through cobbles, does not penetrate soil with more than 15% fines.
Soil nailing	Rapid construction, boulders could be drilled through. Can be used in stiff soils.	Cannot install below groundwater, easements required, cannot be used in soft soils or soils that exhibit base instability. Excavation must have a stable face prior to installation.
Jet grouting	Constructed before excavation and below ground-water.	Difficult with boulders, large volume of spoils generated. Obstructions can obstruct lateral spread of mixing
Soil freezing	Constructed before excavation and below ground-water.	Difficult to install with flowing groundwater and around boulders. Very costly for large area and/or prolonged time. Temporary. Ground heave during freezing and settlement during thaw.

In a more general perspective, Bruce et al. (1998) provided a chronology of the major events related to the DMM and proposed a classification of the DSM systems largely used to date.
In the DSM process, the ground is in situ mechanically mixed while a binder, based on cement, is injected. The DSM cylindrical columns or rectangular panels can be placed next to each other, in a secant way. By overlapping the different DSM elements, a continuous SMW is realised, as illustrated in Fig. 2. Steel H or I-beams are inserted into the fresh DSM material to resist the shear forces and bending moments. The maximum installation depth of the SMW lies – so far – in the order of 20 m. The main structural difference between SMW and the more traditional secant pile walls is the constitutive material which consists of a mixture of soil and cement instead of traditional concrete.

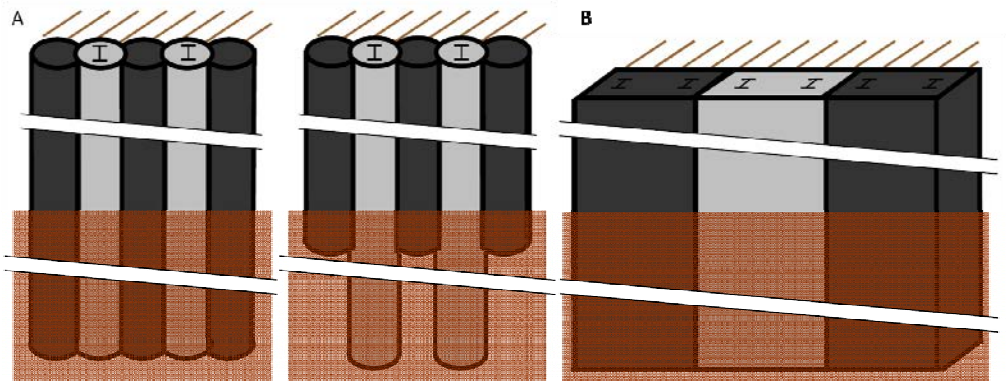

Figure 2: Schematic plan view of the secant execution of (A) cylindrical DSM columns and (B) rectangular DSM panels

1.2. Deep Soil Mix (DSM) material

Several parameters have an influence on the produced DSM material. Terashi (1997) highlighted the factors affecting the strength of the DSM material, as illustrated in Table 5. The DSM material quality depends on the cement type and content, on the in situ soil and on the execution process.
The hardening agent is usually a mixture of cement, water, and in several cases bentonite. The water/binder mixture (w/b weight ratio) is also a governing parameter which plays a major role in the mechanical/durability characteristics of the material.
Moreover, the nature of the ground has a huge impact on the strength and uniformity of the material. For example, stiff cohesive soil does not allow an effective mix of the components and can lead to the presence of unmixed material in the DSM element.
Finally, the final product will be the result of a given DSM system available on the local market. There are a lot of differences between the various systems – especially with regard to the drilling/mixing tools – and the execution process influences the quality of the DSM material in terms of strength, uniformity and continuity. The following paragraphs present the three main DSM systems available on the Belgian market.

Table 5: Factors affecting the strength of the DSM material, after Terashi (1997)

I. Characteristics of hardening agent	1. Type of hardening agent 2. Quality 3. Mixing water and additives
II. Characteristics and conditions of soil	1. Physical chemical and mineralogical properties of soil 2. Organic content 3. pH of pore water 4. Water content
III. Mixing conditions	1. Degree of mixing (Mixing energy) 2. Timing of mixing/re–mixing 3. Quantity of hardening agent
IV. Curing conditions	1. Temperature 2. Curing time 3. Humidity 4. Wetting and drying/freezing and thawing, etc.

2. DEEP SOIL MIX SYSTEMS IN BELGIUM

The CVR C-mix®, the TSM and the CSM are the three most widely used DSM systems in Belgium. All three are wet soil mixing systems.

2.1. CVR C-mix®

The CVR C-mix® is performed with an adapted bored pile rig and a specific designed shaft and mixing tool. This tool rotates around a vertical axis at about 100 rpm and cuts the soil mechanically. Simultaneously, the water\binder mixture (w\b weight ratio between 0.6 and 0.8), is injected at low pressure (< 5 bar). The injected quantity of binder amounts mostly to 350 and 450 kg binder/m³, depending on the soil conditions and specifications. The binder partly (between 0% and 30%) returns to the surface. This is called 'spoil return'.
The resulting DSM elements are cylindrical columns with diameter corresponding to the mixing tool diameter, varying between 0.43 and 1.03 m. For retaining structures, the production rate is about 160 m² of SMW per day (single 8 hrs shift).
In order to increase the production rate, a CVR Twinmix® and a CVR Triple C-MIX® have been designed. A twinmix has two mixing tools, mixing two overlapping cylindrical columns (wall element length of 0.8 to 1.2 m) at the same time. The daily production increases till 210 m²/day. A CVR Triple C-mix® has three mixing tools in line, with a wall element length of 1.5 to 1.8 m. The production rate increases to 300 m²/day. Figure 3 illustrates the CVR C-mix® machine and its Triple version.

Figure 3: CVR C-mix® machine and its Triple version

2.2. Tubular Soil Mix (TSM)

As represented in Fig. 4, the TSM technique uses a mechanical and a hydraulic way of mixing. Apart from the rotating (around the vertical axis) mixing tool, the soil is cut by the high pressure injection (till 500 bars) of the water\binder mixture with w\b chosen between 0.6 and 1.2. The injected quantity of binder mixture amounts mostly to 200 and 450 kg binder/m³. Part of the binder (between 0% and 30%) returns to the surface as spoil return.
The resulting DSM elements are cylindrical columns with a diameter between 0.38 and 0.73 m. The production rate is about 80 m² of SMW per day.

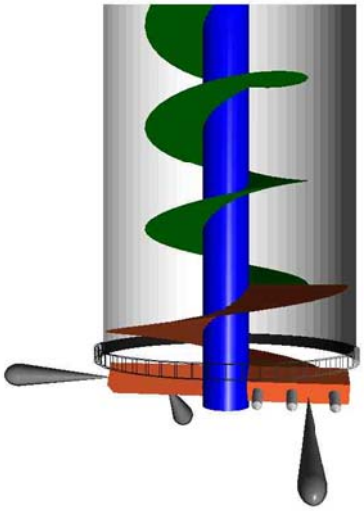

Figure 4: Scheme of the TSM mixing tool (Smet-F&C)

Again, a twin and a triple version exist, leading to wall element lengths respectively varying between 0.8 and 1.4 m or 1.2 and 2.1 m. The production rate is increased till about 180 (twin) and 250 m² (triple) of SMW per day. Figure 5 illustrates a retaining structure executed with the help of the triple version of TSM.

Figure 5: SMW performed with the help of the triple version of TSM (SMET-F&C)

2.3. Cutter Soil Mix (CSM)

A CSM device is commercially available. Two cutting wheels rotate independently around a horizontal axis and cut the soil. At the same time, the water\binder mixture is injected at low pressure (< 5 bar) with w\b ratio chosen between 0.6 and 1.2. The injected quantity of binder amounts mostly to 200 and 400 kg binder/m³. Again, spoil return ranges between 0% and 30%.
The resulting DSM elements are rectangular panels. In Belgium, these panels have usually a length of 2.4 m and a thickness of 0.55 m, though cutter devices with other dimensions are internationally available. The production rate is about 100 m² to 250 m² of SMW per day. Figure 6 illustrates the CSM cutting wheels and the resulting DSM panel. Figure 7 gives an example of a CSM wall.

Figure 6: The cutting wheels of the CSM machine and the resulting CSM panel (Soetaert - Soiltech)

Figure 7: SMW performed with the CSM technique (Lameire Funderingstechnieken n. v.)

3. BBRI INFORMATION SHEETS: FIRST STEPS FOR BELGIAN GUIDELINES

Unfortunately, up to now, guidance rules and recommendations concerning the realization of SMW with soil and/or water retaining functions are lacking. In view of QA/QC development and in the context of European standardization, basic rules are required with regard to design, execution and control of the different DSM processes.

For the purpose of investigating this question, the Belgian Building Research Institute (BBRI) initiated the "Soil Mix" project (IWT 080736) in 2009 in collaboration with the KU Leuven and the Belgian Association of Foundation Contractors (ABEF). Financial support has been obtained from IWT, the Flemish government agency for Innovation by Science and Technology (http://www.iwt.be/). Numerous tests on in situ DSM material have been performed. A good insight has been acquired with regard to strength and stiffness characteristics that can be obtained with the CVR C-mix®, the TSM and the CSM systems in several Belgian soils (Denies et al., 2012a). In addition, info sheets have been developed within the framework of the project (BBRI, 2012a and b). They consist in guidelines for execution phases and give some requirements with regard to the quality of the DSM material, the characteristic dimensions, the bearing capacity and the lateral SMW displacement. The BBRI info sheets are structured as follows:

a. Types of DSM systems
b. Execution: general remarks
c. Materials
d. Dimensions of the SMW elements
e. Bearing capacity
f. Horizontal deflection
g. Domain of use
h. Special attention points
i. Variants (if existing)
j. Quality Control (QC) aspects

The following paragraphs concentrate on the execution sequence, the domain of use, the QC aspects and the execution tolerances detailed in these info sheets.

3.1. Execution of the DSM elements

Figure 8 illustrates the usual execution sequence for DSM columns and panels. In both cases, a guidance device can be used in such a way to control the positioning of the DSM elements during the down grade of the mixing tool into the soil.

As illustrated in Fig. 8a, only the secondary columns are reinforced with the help of steel beams. For the use of reinforcement cage, additional investigation is required. The excavation is performed until the depth of the first horizontal support or until its final depth. Potential horizontal support (anchors, struts, tension piles) can be applied. Anchors and tension piles must be installed at the intersection between primary and secondary columns. After their installation, the excavation is carried on until the next level of horizontal support or until its final depth, usually limited to 20 m. The minimum overlap between the primary and secondary columns is 6 cm. If the SMW is used as a silo structure or in case of water retaining application, the minimum overlap becomes D/8 where D is the column diameter.

As illustrated in Fig. 8b, the primary and secondary panels are reinforced using steel beams. The overlap between the primary and secondary panels must be larger than 10 cm.

3.2. Domain of application

SMW can be used for temporary soil and/or water retaining application. The effects of potential deviations in the positioning of the DSM columns/panels during installation on the SMW sealing should be assessed prior to the execution. The resulting leaks must immediately be treated. Bearing capacity is related to the soil mechanical characteristics, the cement content, the execution parameters and the reinforcement. In view of permanent use, additional testing must be planned.

Little vibration occurs during execution. Underground obstacles are critical for the design and should be considered prior to the execution. If previous dewatering is not required, eventual washing of DSM material should be examined in presence of groundwater flows.

The applicability of DMM also depends on the in situ ground, as illustrated in Table 6. Special attention should be awarded to coarse gravel layers and peaty soils.

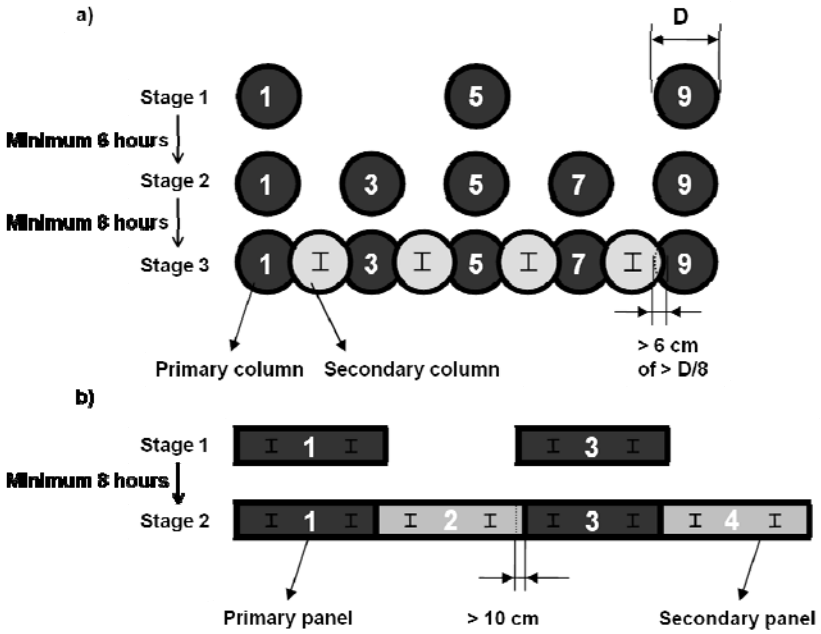

Figure 8: Scheme of the execution sequence for DSM columns (a) and panels (b) according to the BBRI info sheets

Table 6: Applicability of DMM in function of the in situ ground

Sand	Loam	Soft clay	Firm clay
VVV‡	VV†	VV†	V*

VVV‡: always applicable;
VV†: almost always applicable;
V*: applicable in certain circumstances.

3.3. Quality Control (QC) aspects

QC of DSM material depends on the function of the SMW.

3.3.1. Temporary SMW with earth retaining function

If the role of the DSM material only coexists in transmitting the earth pressure to the steel reinforcement, the SMW stiffness is related to the stiffness of the steel reinforcement. The following tests and acceptance criteria are required:

- 1 sample for 150 m³ of DSM material (with a minimum of 6 samples) must be cored;
- the UCS must be determined;
- the amount of unmixed soil inclusions in the DSM material must remain less than 20%;
- and the method of sampling shall be defined in the project specifications.

These requirements become optional if the contractor has gathered experience in terms of test results for minimum two construction sites with the same DSM system and in similar circumstances (including soil conditions).
Additionally, the determination of the modulus of elasticity of DSM material is required if this parameter is integrated into the calculation of the SMW stiffness.

3.3.2. Temporary or permanent SMW with water retaining and/or bearing functions

The requirements are adapted as follows:

- 1 sample for 75 m³ of DSM material (with a minimum of 12 samples);
- determination of the UCS and the modulus of elasticity;
- amount of soil inclusions again less than 20%;
- and the method of sampling shall be defined in the project specifications.

The test programme can be limited to 1 sample for 200 m³ (with minimum 6 samples) if the contractor has gathered test results for minimum two construction sites with the same DSM system and in similar circumstances. In case of soil inclusions larger than 1/3 of the SMW thickness, the designer must specify if immediate remediation of the SMW should be applied.

3.3.3. Execution tolerances

Execution tolerances are illustrated in Fig. 9. The tolerance on the inclination is limited to 1.3 %. In the presence of cavities or large hard stones or in weak layers, large enlargements are unavoidable. Hence, local enlargements of 100 mm are tolerated. The project specifications shall take into account the effect of these tolerances on the implantation of the underground constructions and the possible related additional costs.
Other QC procedure and tolerances can be required in function of the owner's specifications. For example, for SMW used as a silo structure and for water retaining function, the inclination is often limited to 0.5 %.

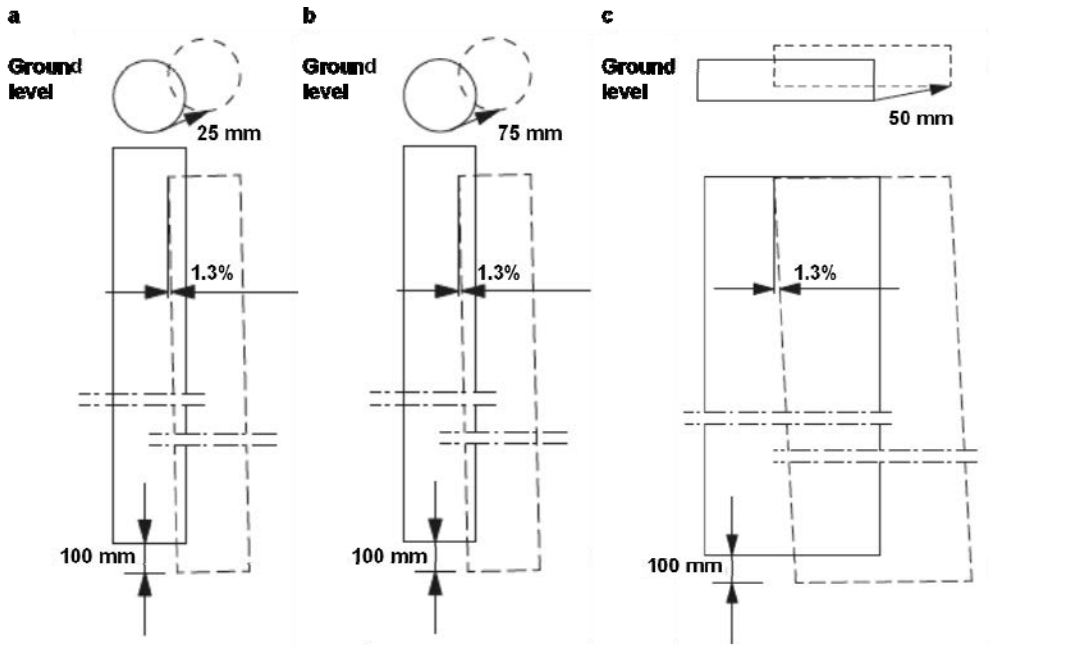

Figure 9: Scheme of the execution tolerances for SMW with regard to the positioning of the (a) DSM columns performed with the help of a guidance device (b) DSM columns performed without guidance device (c) DSM panels

4. BELGIAN VS. INTERNATIONAL QA/QC PROCEDURES

4.1. Workflow of DSM project according to Terashi and Kitazume (2011)

BBRI info sheets adhere to the international workflow of deep-mixing project, developed by Terashi and Kitazume (2011). This workflow is represented in Fig. 10, where q_{uf} means UCS of core samples and q_{ul} UCS of laboratory mix samples. These authors discussed the similarities and differences in the QA/QC procedures followed in different countries (Finland, Japan, Sweden, UK, USA and more generally in Europe), and proposed future research needs with this regard.
As a conclusion of their study, conducted in collaboration with experts of 45 organisations from seven countries, the current QA/QC activities are commonly related to laboratory mix tests, field tests, monitoring and control of the execution parameters and verification of the final products by measuring the mechanical characteristics of the DSM material by tests on core samples (usually UCS tests) or by sounding.

4.2. QA/QC activities of DSM project according to Maswoswe (2001)

In 2001, Maswoswe described the development and the implementation of QA/QC procedures for installation of 410 000 m³ of DSM material with the help of triple-auger DSM rigs, in the framework of the Central Artery/Tunnel (CA/T) project, in Boston. At the beginning of the 90's, it was the largest land-based DSM installation in the USA, and perhaps in the world. Maswoswe (2001) related the **QC activities** to:

- the choice of the **suitable DSM equipment**,
- the determination of the **process parameters** ensuring acceptable performances: the grout mix composition, the auger rotation (or withdrawal) rate and the grout (and drilling water) flow rate,
- and the selection of **procedures** allowing auger penetration and verticality.

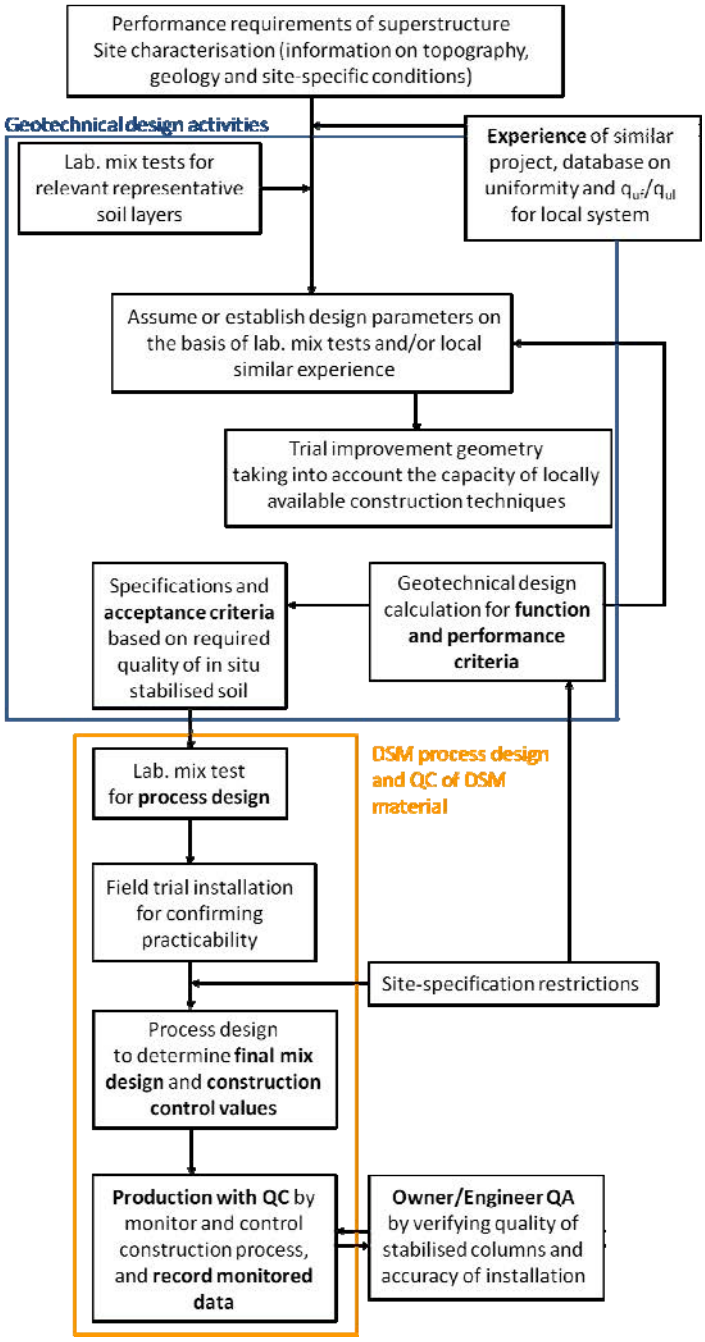

Figure 10: Workflow of deep-mixing project, after Terashi and Kitazume (2011)

If the choice of the DSM equipments, the installation parameters and the procedure were left up to the contractors, specifications would require the DSM material to meet the following **acceptance criteria for QA** related to:

- the minimum and maximum values of **UCS** on wet samples, after a determined number of days,
- the control of the **homogeneity and uniformity**,
- the minimum **unit weight** of core samples,
- the **vertical tolerance** with a limitation of the horizontal deviation with depth in any direction,
- the control of the auger penetration and the **final depth**.

It is to be noted that cores can be considered more representative than fluid samples.

If BBRI info sheets support all the QA/QC activities, reported by Maswoswe (2001), they specify the QA/QC aspects in function of the DSM application (retaining wall, water barrier or foundation) and take the temporary or permanent character of the construction into account. Indeed, as underlined by Terashi and Kitazume (2011), the acceptance criteria and verification procedures should depend on the DSM function.

As explained in Holm (2001), uniformity and homogeneity of DSM material can be controlled computing the coefficient of variation of UCS test results on core samples or comparing field and laboratory UCS test results (calculation of q_{uf}/q_{ul}). Nevertheless, in the framework of the BBRI 'Soil Mix' project, a methodology taking into account the amount of unmixed soil inclusions into the mix was developed and illustrated with case studies of DSM material executed in several Belgian soils (Denies, 2012b). BBRI info sheets refer to this methodology with an acceptance criterion in terms of a limit on the percentage of soil inclusions.

4.3. QC by monitoring

According to Maswoswe (2001), the critical factor in the execution of SMW is to maintain an auger withdrawal rate consistent with the grout flow rate. One way to control the success of the procedure and its efficiency is to estimate the cement factor or cement content (the cement mass per cubic meter of DSM material) at different locations. The cement factor can be estimated considering the grout flow rate, the auger withdrawal rate and the assumed percentage of grout loss during the process.
Beyond the mechanical characterization, the continuity and the overlapping of the SMW components (columns/panels) must be verified with regard to the execution tolerances. Locations and verticality of the DSM elements should be controlled during execution.
The best way to ensure QC during execution is by monitoring. Current technology allows not only to record execution data but also to visualize the parameters during the production process, as illustrated in Fig. 11 and 12.

Figure 11: QC monitoring of grout flow rates, injection volume and pressure and penetration rate during execution of CSM wall (photo with courtesy of Malcolm Drilling Company)

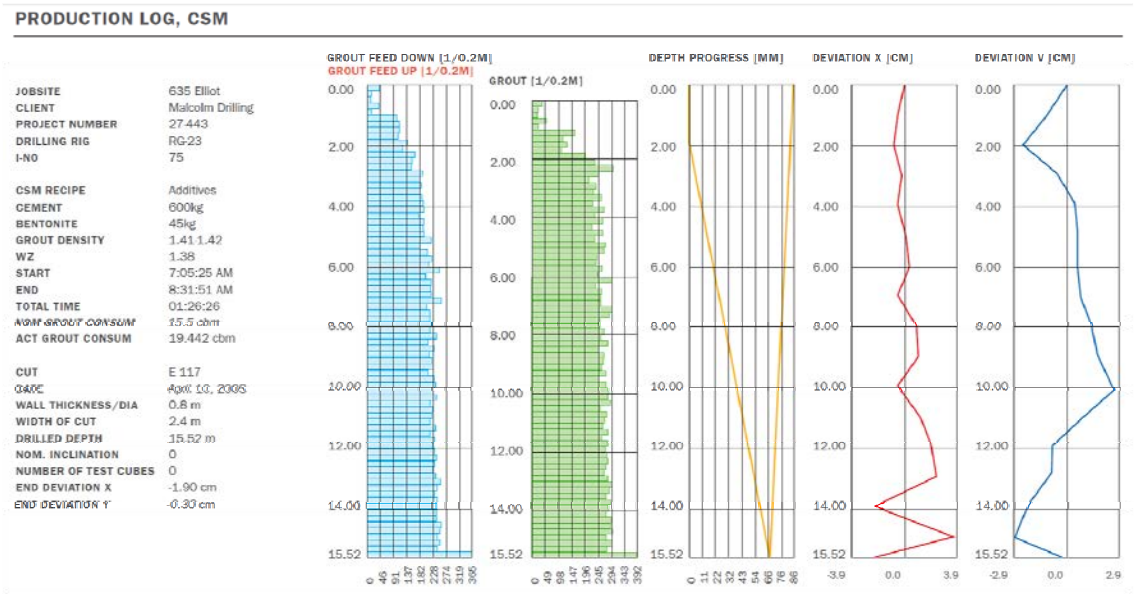

Figure 12: Typical production log (photo with courtesy of Malcolm Drilling Company)

For wet mixing, EN 14679 (2005) puts the emphasis on the continuous monitoring (or at least at a depth interval of 0.5m) of the following construction parameters and information during execution:

- slurry pressure; air pressure (if any),
- penetration and retrieval rate,
- rotation speed (revs/min. during penetration and retrieval),
- quantity of slurry per meter of depth during penetration and retrieval.

4.4. Laboratory mix vs. field tests

Concerning the laboratory test results, Terashi and Kitazume (2011) highlight the influence of the test procedure, especially the method of preparation and the curing of the specimens. Methods differ from one country to another and even in the same region. These differences must be taken into account when comparisons are made. The sample preparation (mixing time/energy, time between mixing and moulding, moulding procedure) and the curing conditions (temperature, humidity, potential application of surcharge) differ from one procedure to another.

Moreover, the quality of DSM material, in terms of strength, stiffness, continuity and uniformity depends on the execution process. Indeed, the way the soil is mixed during the process varies from one system to another. The result will be different if the soil stratification is preserved after the mix or if the soil is transported from depth to the surface during the process. Hence, field tests are essential in comparison with laboratory mix tests which can not entirely simulate the field conditions.

4.5. Belgian deep mixing experience and database

According to the BBRI info sheets, in the case of temporary SMW with an earth retaining function, preliminary laboratory mix tests (for QC stage) can be considered as facultative if the deep-mixing contractor can demonstrate that its deep-mixing experience is large enough (for a DSM system in a given soil type). Indeed, the test campaign on in situ DSM material, performed within the framework of the BBRI 'Soil Mix' project, coupled with the experience accumulated by each contractor in several types of Belgian soils, provides a useful database in order to assume or establish the design parameters, as well as the performance and the acceptance criteria. In Belgium, the decision on the mix composition is therefore left to the deep-mixing contractors who determine this latter in function of the soil/cement characteristics and the equipment/installation devices in such a way to reach the design requirements.

In practice, the DSM material quality is often controlled with the help of UCS tests regardless of the DSM application. Within the framework of the BBRI 'Soil Mix' project, various tests were performed to determine characteristics of DSM material such as porosity, permeability, UCS, creep and tensile strength, as well as the modulus of elasticity, the ultrasonic pulse velocity and the adherence between DSM material and steel reinforcement (Denies et al., 2012a).

5. CONCLUSIONS

The present paper concentrates on the application of SMW technology and focuses on the three main types of DSM systems currently used in Belgium: the Cutter Soil Mix (CSM), the Tubular Soil Mix (TSM) and the CVR C-mix®.
BBRI information sheets, developed within the framework of the Flemish regional research project IWT 080736, are then presented. They adhere to the international QA/QC activities, as reported in Maswoswe (2001) and Terashi and Kitazume (2011), and are specially adapted to the SMW applications in Belgium. BBRI information sheets complete the information available in EN 14679 (2005) with regard to the QA/QC requirements. They provide for the owner/contractor/engineer practical criteria in terms of the execution sequence and tolerances and give some requirements with regard to the quality of the DSM material.
Generally, QA/QC procedures should be defined as soon as possible at the beginning of the project according to the BBRI info sheets or with a logic similar to the QC workflow (presented in Fig. 10) and deep soil mix should be discussed using the international terminology proposed in Table 1.
As for all engineering projects, a precise and preliminary definition of the responsibilities and acceptance criteria is a significant point to make sure the DSM process goes smoothly. In several cases, test procedures can even be proposed or imposed for the QA/QC of the final DSM product. In function of these requirements, the deep-mixing contractors will choose the most adapted mixing tool alternative and the best execution process.

REFERENCES

Arulrajah, A., Abdullah, A, Bo, M.W. & Bouazza, A. 2009. Ground improvement techniques for railway embankments, Ground Improvement, Vol. 162, issue 1, pp. 3-14.

BBRI. 2012a. Uitvoeringsfiche. Soil mix wanden. Type 1: wanden opgebouwd uit kolommen. BBRI information sheet 50.5, www.bbri.be (in Dutch and French).

BBRI. 2012b. Uitvoeringsfiche. Soil mix wanden. Type 2: wanden opgebouwd uit panelen. BBRI information sheet 50.6, www.bbri.be (in Dutch and French).

Bruce, D. A., Bruce, M. E. C. and DiMillio, A. F. 1998. Deep mixing method: a global perspective. ASCE, Geotechnical special publication, n°81, pp. 1-26.

Chu, J., Varaskin, S., Klotz, U. and Mengé, P. 2009. Construction Processes, Proceedings of the 17th International Conference on Soil Mechanics and Geotechnical Engineering, 5-9 October 2009, Alexandria, Egypt, M. Hamza et al. (Eds.), IOS Press, Amsterdam, Vol. 4, pp. 3006-3135.

Denies, N., Huybrechts, N., De Cock, F., Lameire, B., Vervoort, A., Van Lysebetten, G. and Maertens, J. 2012a. Soil Mix walls as retaining structures – mechanical characterization. International symposium & short courses of TC211. Recent research, advances & execution aspects of ground improvement works. 30 May-1 June 2012, Brussels, Belgium.

Denies, N., Huybrechts, N., De Cock, F., Lameire, B., Vervoort, A. and Maertens, J. 2012b. Mechanical characterization of deep soil mix material – procedure description. International symposium & short courses of TC211. Recent research, advances & execution aspects of ground improvement works. 30 May-1 June 2012, Brussels, Belgium.

Essler, R. and Kitazume, M. 2008. Application of Ground Improvement: Deep Mixing. TC17 website: www.bbri.be/go/tc17.

Eurosoilstab. 2002. Development of design and construction methods to stabilise soft organic soils. Design Guide Soft Soil Stabilisation. EC project BE 96-3177.

Holm, G. 2000. Deep Mixing. ASCE, Geotechnical special publication, N°112, pp. 105-122.

Larsson, S.M. 2005. State of practice report - Execution, monitoring and quality control, International Conference on Deep Mixing, pp. 732-785.

Maswoswe, J. J. G. 2001. QA/QC for CA/T Deep Soil-Cement. ASCE, Geotechnical special publication, N°113, pp. 610-624.

Porbaha, A. 1998. State of the art in deep mixing technology: part I. Basic concepts and overview. Ground Improvement, Vol. 2, pp. 81-92.

Porbaha, A., Tanaka H. and Kobayashi M. 1998. State of the art in deep mixing technology, part II. Applications. Ground Improvement Journal, Vol. 3, pp. 125-139.

Porbaha, A. Shibuya, S. and Kishida, T. 2000. State of the art in deep mixing technology. Part III: geomaterial characterization. Ground Improvement, Vol. 3, pp. 91-110.

Porbaha, A. 2000. State of the art in deep mixing technology. Part IV: design considerations. Ground improvement. Vol. 3, pp. 111-125.

Rutherford, C., Biscontin, G. and Briaud, J.-L. 2005. Design manual for excavation support using deep mixing technology. Texas A&M University. March 31, 2005.

Terashi M. 1997. Theme lecture: Deep mixing method – Brief state of the art. Proceedings of the 14th International Conference of Soil Mechanics and Foundation Engineering, Hambourg, 6-12 september 1997. A. A. Balkema/Rotterdam/Brookfield/1999. Vol. 4, pp. 2475-2478.

Terashi, M. 2003. The State of Practice in Deep Mixing Methods. Grouting and Ground Treatment (GSP 120), 3rd International Specialty Conference on Grouting and Ground Treatment New Orleans, Louisiana, USA, pp. 25-49.

Terashi, M. and Kitazume, M. 2011. QA/QC for deep-mixing ground: current practice and future research needs. Ground improvement, Vol. 164, Issue GI3, pp. 161-177.

Topolnicki, M. 2004. In situ soil mixing. In M. P. Moseley & K. Kirsch (Eds.), Ground improvement, 2nd ed., Spon Press.

SOIL MIX WALLS as retaining structures – mechanical characterization

N. Denies, N. Huybrechts, Belgian Building Research Institute, Geotechnical division, Belgium, nde@bbri.be, nh@bbri.be
F. De Cock, Geotechnical Expert Office Geo.be, Belgium, fdc.geobe@skynet.be
B. Lameire, Belgian Association of Foundation Contractors ABEF, Belgium, bart@lameireft.be
A. Vervoort, G. Van Lysebetten, KU Leuven, Belgium, andre.vervoort@bwk.kuleuven.be, gust.vanLysebetten@bwk.kuleuven.be
J. Maertens, Jan Maertens bvba & KU Leuven, Belgium, jan.maertens.bvba@skynet.be

ABSTRACT

Since several decennia, the deep soil mix (DSM) technique has been used for ground improvement (GI) applications. In recent years, soil mix walls (SMW) have become an economical alternative to traditional excavation support systems. The Belgian building market has also witnessed such development with the growing use of the Cutter Soil Mix (CSM), the Tubular Soil Mix (TSM) and the CVR C-mix® systems.
Unfortunately, standardized guidelines for SMW are not currently available. For the purpose of developing such guidelines, mechanical characteristics of DSM material must be investigated. Within the framework of a Flemish regional research program (IWT 080736), DSM material from 38 Belgian construction sites, with various soil conditions and for different execution processes, has been tested.
In the present paper, results of various tests, performed to determine characteristics of DSM material are firstly described. Porosity, permeability, Unconfined Compressive Strength (UCS) and tensile strength, as well as the modulus of elasticity, the ultrasonic pulse velocity and the adherence between DSM material and steel reinforcement are investigated. In addition, results of petrographic analysis performed using thin section technology are also presented in order to obtain a microscopic view of the material.
On the basis of UCS tests performed on core samples, the determination of the 5% quantile characteristic UCS value of the DSM material is then discussed with regard to the influence of unmixed soil inclusions in the material and considering the scale effect.

1. INTRODUCTION

Since several decennia, the deep soil mix method (DMM) has been used for GI applications. In recent years, SMW have increasingly been used – in Belgium and in several other countries – for the retaining of soil and water in the case of excavations. Indeed, SMW represent a more economical alternative to concrete secant pile walls and even in several cases to king post walls.
In the DSM process, the ground is in situ mechanically mixed, while a binder, based on cement, is injected. For SMW applications, the DSM cylindrical columns or the rectangular panels are placed next to each other, in a secant way. By overlapping the different soil mix elements, a continuous SMW is realized. Steel profiles are inserted into the DSM fresh material to resist the shear forces and bending moments. The main structural difference between SMW and the more traditional secant pile walls is the constitutive DSM material which consists of a soil – cement mixture instead of concrete.
Unfortunately, up to now, guidance rules and recommendations concerning the realization of SMW with a soil and/or water retaining function are lacking while various DSM systems are active on the Belgian market such as the CVR C-mix®, the Tubular Soil Mix (TSM) and the Cutter Soil Mixing (CSM). Moreover, the number of applications is fast increasing. For QA/QC development and in the context of the European standardization, basic rules are required with regard to design, execution and control of these different DSM execution processes.
These issues have encouraged the Belgian Building Research Institute (BBRI) to initiate research actions that address the execution, design and testing of DSM systems in Belgium. For the purpose of investigating the DSM technology and its applicability in the various Belgian soils, the 'Soil Mix' project was initiated in 2009 in collaboration with the KU Leuven and the Belgian Association of Foundation Contractors (ABEF). Financial support has been obtained from IWT, the Flemish government agency for Innovation by Science and Technology (http://www.iwt.be/).
If DSM technique is currently used for retaining structures with a temporary character, permanent and bearing applications are fast increasing in spite of the lack of knowledge concerning the strength, the stiffness, the permeability, the durability of DSM material and its adherence with steel. Hence, within the framework of the BBRI 'Soil Mix' project, numerous tests on in situ DSM material have been performed.

A good insight has been acquired with regard to mechanical characteristics that can be obtained with the CVR C-mix®, the TSM and the CSM systems in several Belgian soils. This article gives an overview of the test results. The CVR C-mix®, the TSM and the CSM systems are presented in Denies et al. (2012a).

2. MECHANICAL CHARACTERIZATION OF DSM MATERIAL

During the first part of the experimental campaign, cores of DSM material have been drilled at 38 Belgian construction sites, with different soil conditions and for various DSM systems. The cylindrical core samples have a diameter ranging between 85 mm and 115 mm. The measurement accuracy of the core diameter is 0.3 mm. Before testing, they are preserved in an acclimatized chamber with a relative humidity larger than 95% and a temperature equal to 20 ± 2°C.
The following paragraphs illustrate the mechanical characterization of the DSM material with the help of UCS and tensile splitting strength tests, as well as tests to determine its modulus of elasticity and its ultrasonic pulse velocity.

2.1. Unconfined Compressive Strength (UCS)

2.1.1. UCS tests on core samples

UCS tests are performed by a MFL 250 kN loading machine according to NBN EN 12390-3. The loading rate amounts to 2.5 kN/s. The height to diameter ratio is 1. This choice was based on the necessity to collect a maximum of cores and was made in order to compare the UCS test results on cylindrical cores with cube strength (NBN EN 12504-1). It can be noted that the height to diameter ratio will have an influence on the failure pattern and on the UCS test results. In such a way to investigate this question, a laboratory study is currently performed in collaboration with KU Leuven.
Figures 1 to 6 give the histograms of the UCS test results in function of the soil type and with regard to the execution technique. The age of the samples ranges between 7 and 200 days. Currently, no correction regarding to the influence of the sample age on the UCS results has been applied. Based on on-going laboratory experiments, this parameter will be introduced in the near future in order to generate more precise information, notably on the average UCS value and on the standard deviations for the different DSM systems in typical Belgian soils. Table 1 gives the minimal and maximal UCS values in function of the soil type and with regard to the execution technique.
On the basis of the previous results, several tendencies can be drawn:
- the UCS values in sandy soils are larger than UCS values in silty and clayey soils;
- the UCS values of CSM systems are generally smaller than UCS values of DSM columns;
- the variability of the UCS results is smaller for the CSM systems than for DSM columns.

The density of samples, measured according to NBN EN 12390-7, varies between 1372 and 2176 kg/m³. No specific correlation was observed between the density and the UCS. The depth of coring is always larger than 1 m. Indeed, Ganne et al. (2010) have observed on different sites that the strength of the DSM material over the first meter is strongly influenced by the execution process (e.g. infiltration of rinsing water), as illustrated in Fig. 7 for a CSM panel in quaternary sand. Hence, the top of the SMW is not representative for the deeper part with regard to its strength.

2.1.2. UCS tests on wet grab samples

At two construction sites (for CSM technique in sandy soils), wet grab sampling was conducted in the first half hour after execution. For wet grab sampling a cylindrical sampler is pushed in the fresh DSM material. It stays closed until the sampling depth is reached (about 2 m in the present case). At this moment, the sampler opens with a 0.2 m gap. After filling, it is locked and pulled up. The DSM material is preserved in a cylindrical mould – 113 mm diameter and 220 mm height – in the acclimatized chamber. Two weeks later, DSM material is in situ cored at the same location and similar depth. The cores and the wet grab samples are tested on the same day (age = 14 days). For all the UCS tests, the height to diameter ratio is 1. Table 2 illustrates the UCS test results.

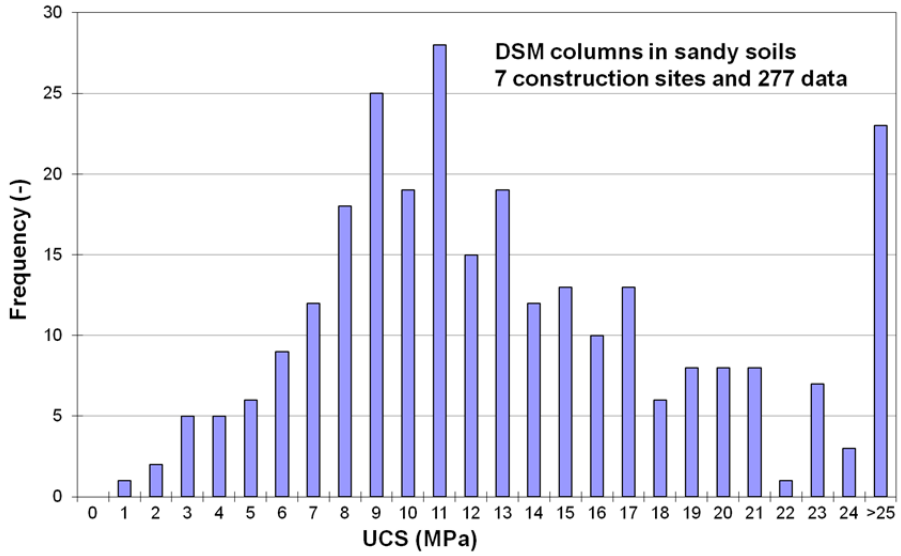

Figure 1: Histogram of the UCS test results for DSM column systems in sandy soils

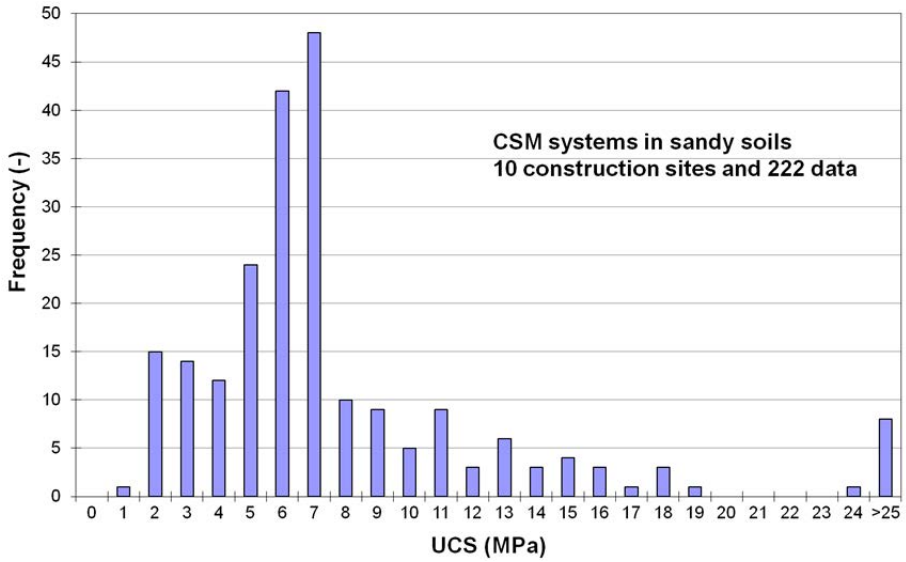

Figure 2: Histogram of the UCS test results for CSM systems in sandy soils

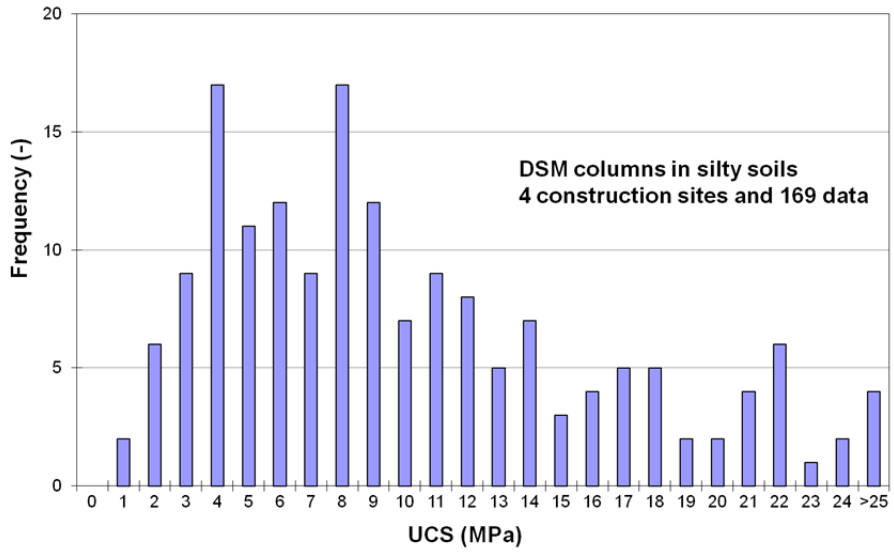

Figure 3: Histogram of the UCS test results for DSM column systems in silty soils

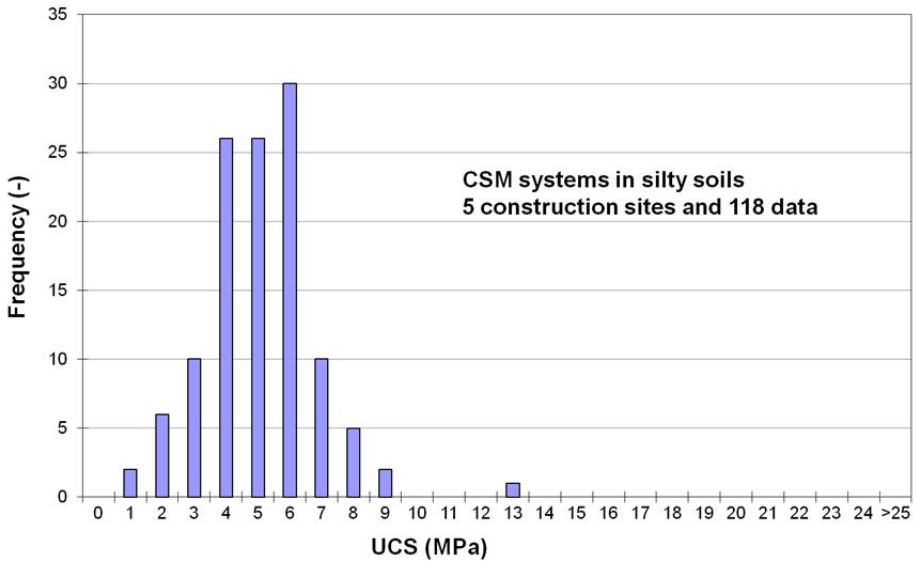

Figure 4: Histogram of the UCS test results for CSM systems in silty soils

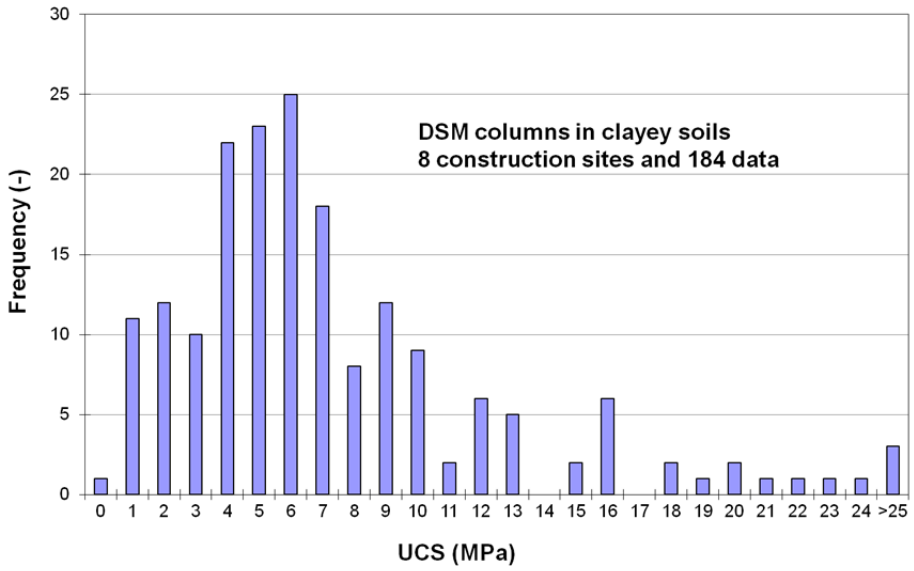

Figure 5: Histogram of the UCS test results for DSM column systems in clayey soils

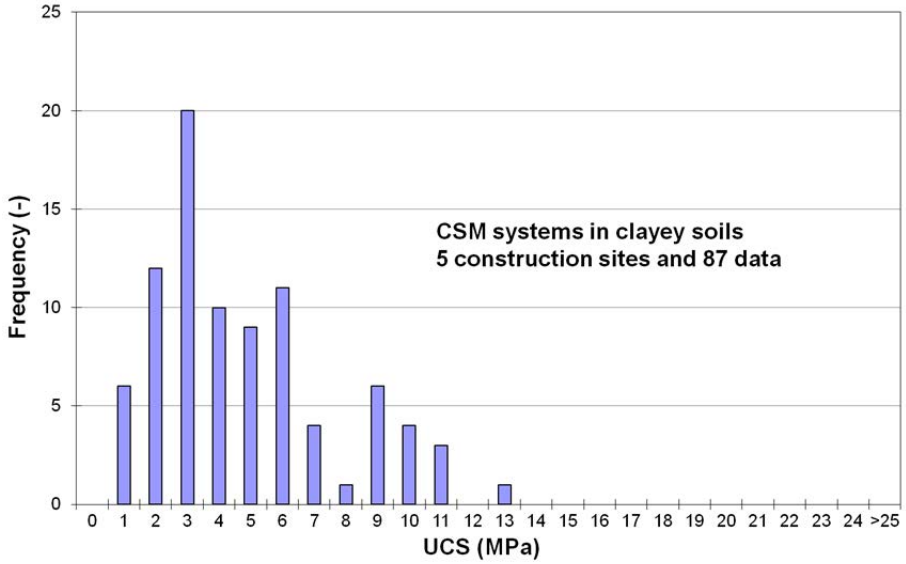

Figure 6: Histogram of the UCS test results for CSM systems in clayey soils

Table 1: Minimal and maximal UCS values in function of the soil type and with regard to the execution technique

	Sandy soils		Silty soils		Clayey soils	
	DSM columns	**CSM systems**	**DSM columns**	**CSM systems**	**DSM columns**	**CSM systems**
Minimal UCS values	1.32 MPa	1.28 MPa	0.93 MPa	0.66 MPa	0.44 MPa	0.65 MPa
Maximal UCS values	39.90 MPa	32.07 MPa	31.17 MPa	12.63 MPa	33.23 MPa	12.69 MPa

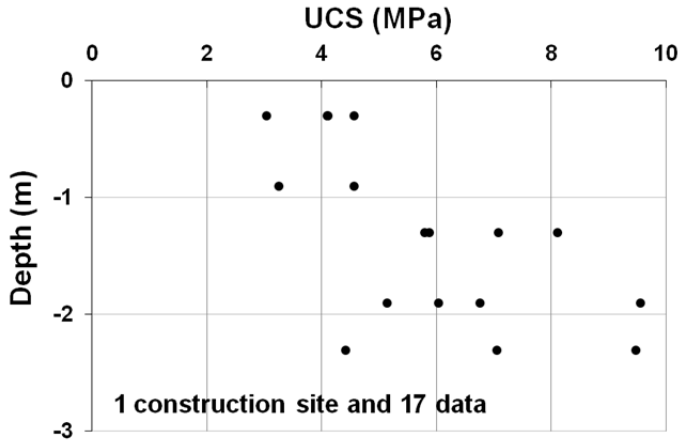

Figure 7: UCS test results of samples, cored at different depths (CSM panel in quaternary sand), after Ganne et al. (2010)

Table 2: UCS results of tests on core and wet grab samples (μ is the average UCS value), after Ganne et al. (2010)

	Core samples		**Wet grab samples**	
Site I – CSM element 1	UCS_1=2.33	UCS_2=2.04	UCS_1=2.94	UCS_2=2.46
	UCS_3=2.27	UCS_4=2.85	UCS_3=2.44	UCS_4=2.59
	UCS_5=2.85			
	μ = 2.47 (MPa)		**μ = 2.61 (MPa)**	
Site I – CSM element 2	UCS_1=1.62	UCS_2=1.63	UCS_1=1.82	UCS_2=2.00
	UCS_3=1.28	UCS_4=1.88	UCS_3=1.78	UCS_4=1.80
	UCS_5=1.90			
	μ = 1.66 (MPa)		**μ = 1.85 (MPa)**	
Site II – CSM element 3	UCS_1=2.95	UCS_2=4.53	UCS_1=3.80	UCS_2=3.40
	UCS_3=4.64	UCS_4=3.79	UCS_3=3.66	UCS_4=3.89
	μ = 3.98 (MPa)		**μ = 3.68 (MPa)**	
Site II – CSM element 4	UCS_1=5.27	UCS_2=5.03	UCS_1=4.18	UCS_2=3.07
	UCS_3=4.12	UCS_4=5.54	UCS_3=3.64	UCS_4=3.69
	μ = 4.99 (MPa)		**μ = 3.64 (MPa)**	

The differences between drilled cores and wet grab samples can be explained by the limited number of samples and the lack of uniformity of the samples on the one hand and by the different curing conditions on the other hand. In the following, only tests on core samples are discussed.

2.2. Modulus of elasticity (E)

The laboratory test to determine the modulus of elasticity (E) is performed in an unconfined way with the help of a MFL 250 kN loading machine according to NBN B 15-203.
The loading rate amounts once again to 2.5 kN/s. The height to diameter ratio is 2, according to NBN B 15-203. A selection is made of cores that are visually of a better quality in order to preserve the uniaxial behavior of the tested samples. E is determined in a tangent way varying the applied load between 10% ($\sigma_{10\%UCS}$) and 30% ($\sigma_{30\%UCS}$) of the estimated UCS. The sample deformations (ε) are measured along

three axes using DEMEC mechanical strain gauges. Once the difference between two cycles is smaller than 10 µstrains, E is calculated as the ratio:

$$E = \frac{\sigma_{30\%UCS} - \sigma_{10\%UCS}}{\varepsilon_{30\%UCS} - \varepsilon_{10\%UCS}} \quad (1)$$

The loading is then continued to determine the UCS.
Figure 8 presents the correlation between E and the density of the core samples without distinction of the soil type. Figure 9 illustrates the relationship between E and the determined UCS of the core samples regardless of the soil type. The age of the samples varies between 30 and 200 days. Since the aim is to determine the correlation between E and the UCS, the test results are not corrected for the age of the samples.

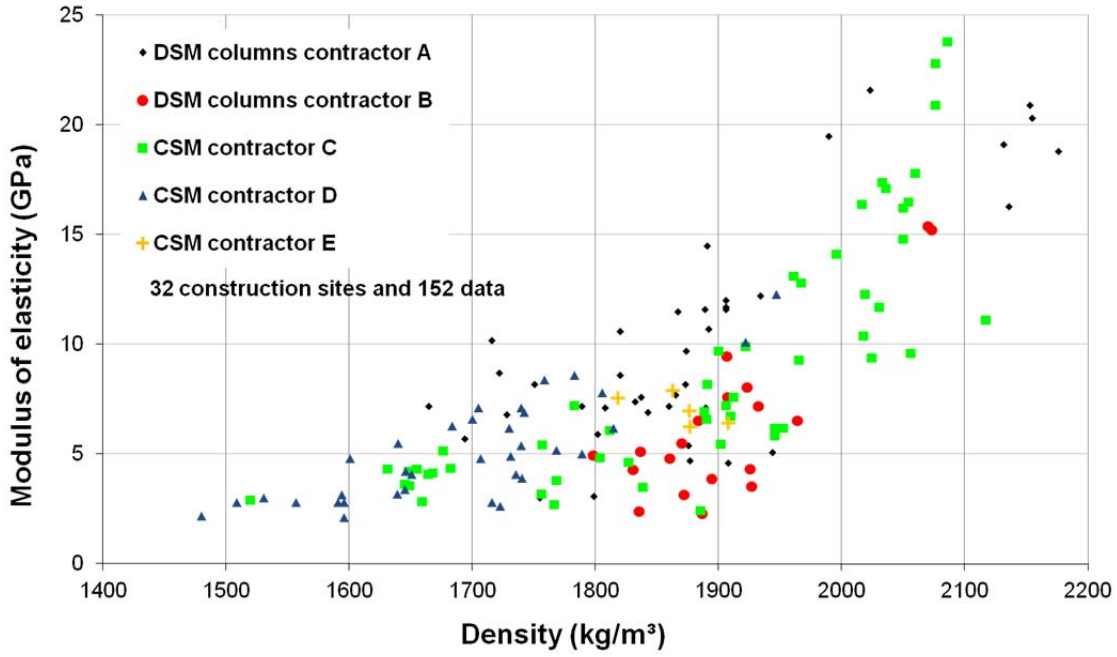

Figure 8: Relationship between the modulus of elasticity and the density of DSM material

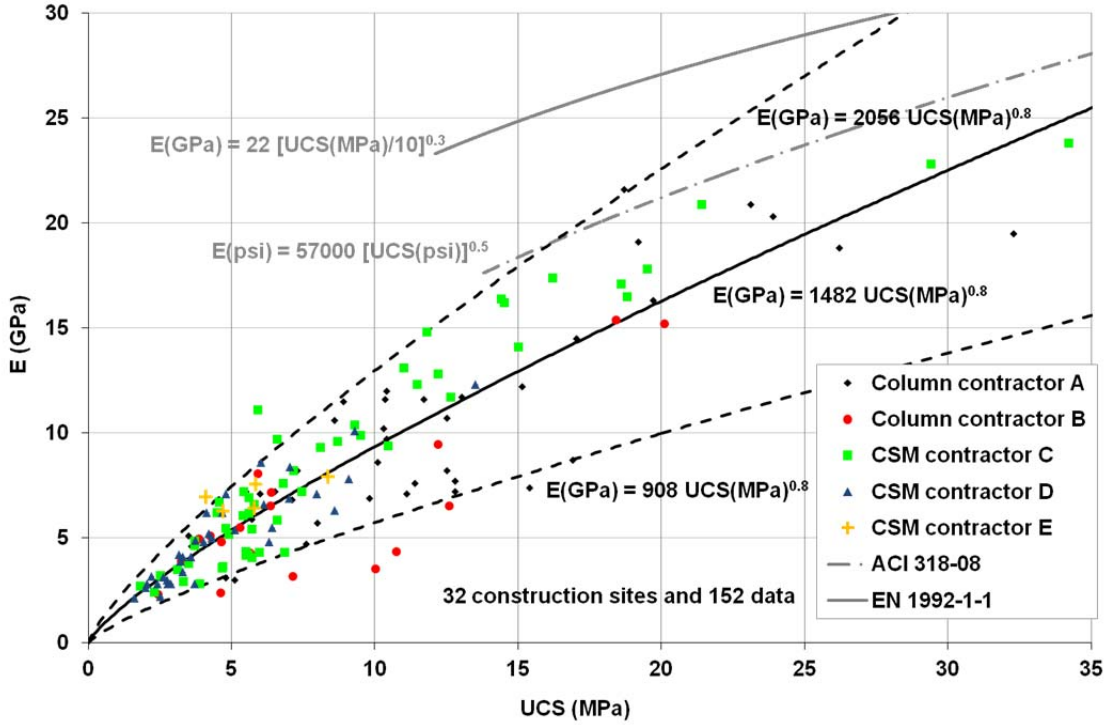

Figure 9: Relationship between the modulus of elasticity and the UCS of DSM material

The best fit corresponds to:

$$E = 1482\,UCS^{0.8} \quad (2)$$

with a coefficient of determination close to 0.80 (-). Lower and higher 5% quantile estimations of E respectively correspond with:

$$E = 908\,UCS^{0.8} \quad (3)$$

and

$$E = 2056\,UCS^{0.8} \quad (4)$$

These estimations are only valid for the range 1.5 MPa < UCS < 35 MPa.
In Fig. 9, relationships for normal concrete, from ACI 318-08 and EN 1992-1-1, are given for comparisons. According to ACI 318-08, the modulus of elasticity for normalweight concrete can be defined with regard to the UCS with the help of the following equation:

$$E\,(psi) = 57000\sqrt{UCS\,(psi)} \quad (5)$$

where E is defined as the secant modulus of elasticity between 0 and 45% ($\sigma_{40\%UCS}$) of the UCS. Based on previous research of Pauw (1960), equation (5) is valid for UCS values larger than 2000 psi (or 13.8MPa).
Eurocode 2 (EN 1992-1-1) provides the following relationship for concrete:

$$E(GPa) = 22\left[UCS(MPa)/10\right]^{0.3} \quad (6)$$

where E is the secant modulus of elasticity between 0 and 40% ($\sigma_{40\%UCS}$) of the UCS. Equation (6) is only valid for concrete samples containing quartzite aggregates and for a range of UCS varying between 12 and 90 MPa.

2.3. Tensile splitting strength (T)

For the determination of the tensile splitting strength (T), sometimes called Brazilian tensile strength, samples with H/D close to 1 have been tested with the help of a MFL 250 kN loading machine (2.5 kN/s of loading rate), according to NBN EN 12390-6. Figure 10 gives the relationship between T and the UCS, without distinction of the soil type. The samples were tested after a period varying between 32 and 200 days. Test results are not corrected for the age of the sample. In Fig. 10, experimental results for DSM cores are compared with well-established empirical relationships for concrete.

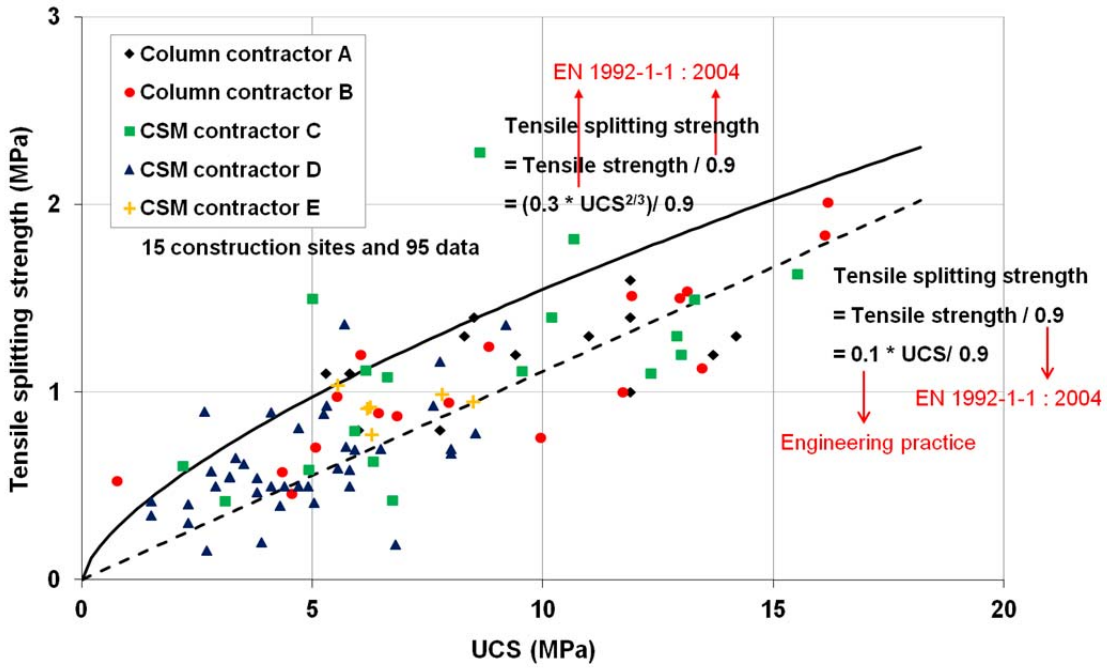

Figure 10: Relationship between the tensile splitting strength and the UCS of DSM material

According to Eurocode 2 (EN 1992-1-1), when the tensile strength is determined as the splitting tensile strength, an approximate value of the axial tensile strength, T_a, may be determined as:

$$T_a = 0.9T \tag{7}$$

Eurocode 2 also provides a correlation with the UCS:

$$T_a = 0.30UCS^{2/3} \tag{8}$$

which is only valid for concrete with UCS values less than the UCS of the C50/60 concrete type.
It is to note that in the engineering practice, the axial tensile strength of concrete is often related to the UCS by the following relationship:

$$T_a = 0.1UCS \tag{9}$$

2.4. Ultrasonic pulse velocity

The ultrasonic pulse velocity, V_p, of longitudinal stress waves in DSM cores was measured according to ASTM C597-09. Theoretically, V_p can be related to the elastic properties and density with the help of the following relationship:

$$V_p = \sqrt{\frac{E(1-\nu)}{\rho(1+\nu)(1-2\nu)}} \tag{10}$$

where E is the dynamic modulus of elasticity, ν the Poisson's ratio and ρ the density. Nevertheless, as illustrated in Fig. 11a, most of the measured values of V_p are less than their theoretical values assuming ν = 0.35 (-). This could be due to the non-homogeneous and discontinuous character of the DSM material. Figure 11b presents the relationship between V_p and the UCS for DSM cores of 6 different construction sites, regardless of the soil conditions. For one particular site, the measurement of the ultrasonic pulse velocity, as well as the UCS test results, can be considered as an indicator of the homogeneity of the DSM material. Indeed, ultrasonic tests performed on laboratory mix homogeneous samples with the same age present limited variability (Hird and Chan, 2005).

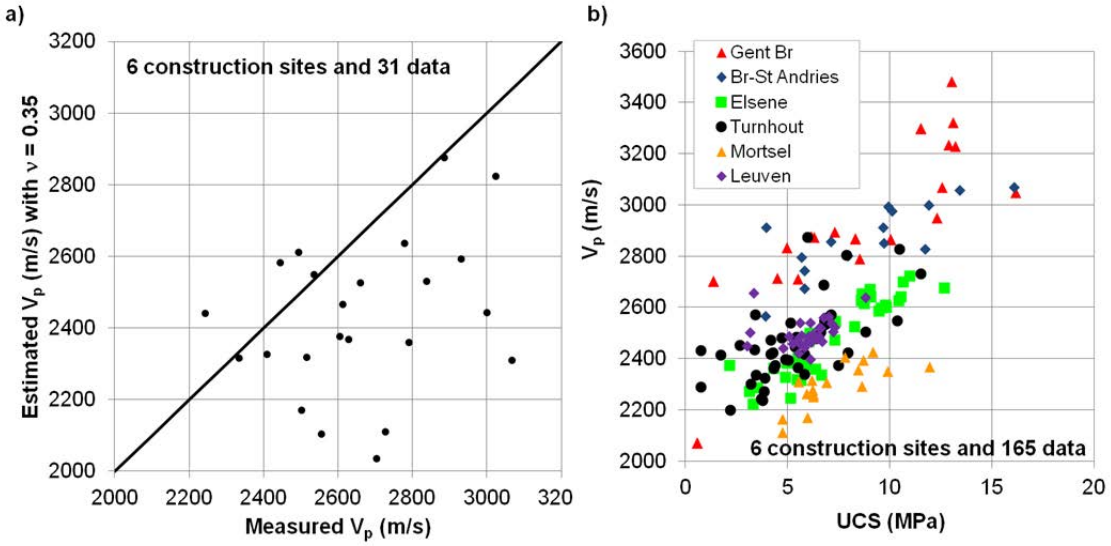

Figure 11: Correlation between the ultrasonic pulse velocity and a) the elastic properties and density of the DSM material; b) the UCS of DSM material.

3. POROSITY OF DSM MATERIAL AND PETROGRAPHIC ANALYSIS

In parallel to mechanical investigations, the porosity of DSM cores is determined according to NBN B15-215. As illustrated in Fig. 12, porosity varies between 25 and 65% for all soil types. In order to explain these high values, a petrographic analysis is conducted on samples from two construction sites (in silty and sandy soils) with the help of image processing techniques (IPT) and thin section technology.

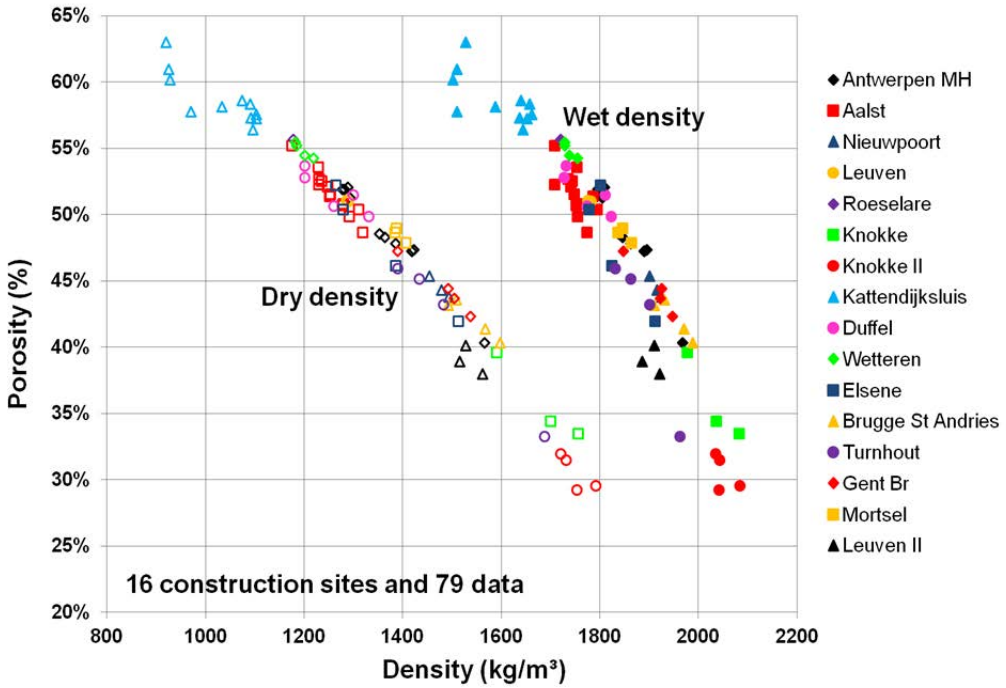

Figure 12: Relationship between dry and wet density and porosity for DSM cores

Figure 13 gives an example of microscopic analysis of a thin section cut from a DSM core, where P represents the pores, S the sand grains and C the cement stone. If open cracks, without specific orientation, are observed, they have a limited width varying between 10 and 200 µm.
The pores in the DSM sample are coloured by the resin used in the production of the thin section. All the pores with a surface area higher than 10 µm² are indicated as macropores. They represent around 2.4% of the total surface area. As a result, high porosity values, illustrated in Fig. 12, can only be related to the high and homogeneous capillary porosity. The high capillary porosity could result from the high water/cement ratio, W/C, used for the execution of the SMW. The high hydration level and the presence of portlandite $Ca(OH)_2$ in the DSM samples consolidate this assumption.

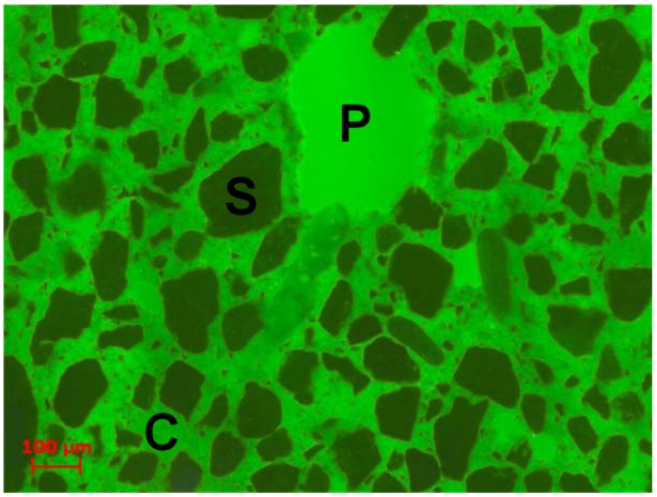

Figure 13: Microscopic analysis of DSM thin section with fluorescent light

4. HYDRAULIC CONDUCTIVITY OF DSM MATERIAL

Permeability tests are performed on DSM samples according to DIN 18130-1. As presented in Fig. 14, the coefficient of hydraulic conductivity of DSM material varies between 10^{-8} and 10^{-12} m/s, regardless of the soil conditions. No correlation is observed between porosity and permeability. Hence, assuming adequate positioning of the DSM columns/panels, the DSM material ensures the sealing of the SMW with water retaining function.

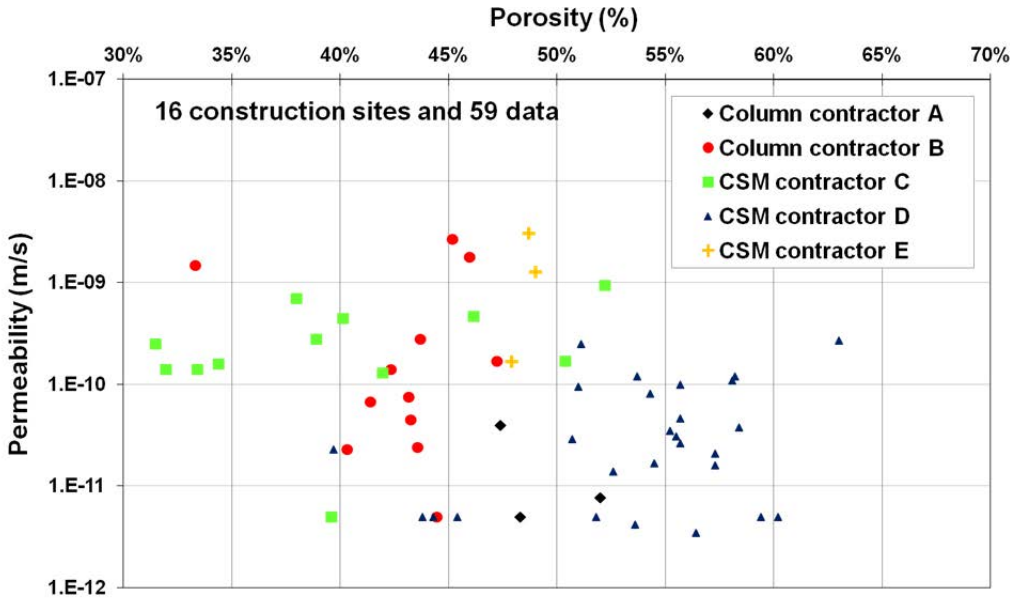

Figure 14: Relationship between permeability and porosity for DSM cores

5. 'STEEL – SOIL MIX' ADHERENCE

To investigate the adhesion between DSM material and various steel profiles, in situ pull-out tests were conducted on the basis of NBN EN 12504-3. Figure 15a presents the test setup. After the execution of the DSM element, steel reinforcement was suspended from the guidance device and vertically installed into the soil mix. As illustrated in Fig. 15b, the top part of the steel profile (over 1 m) is made frictionless using a flexible protection tube in order to eliminate the influence of the first non-representative meter on the results.

Figure 16 presents the peak extraction resistance in function of the UCS of DSM cores, for different types of steel reinforcements.

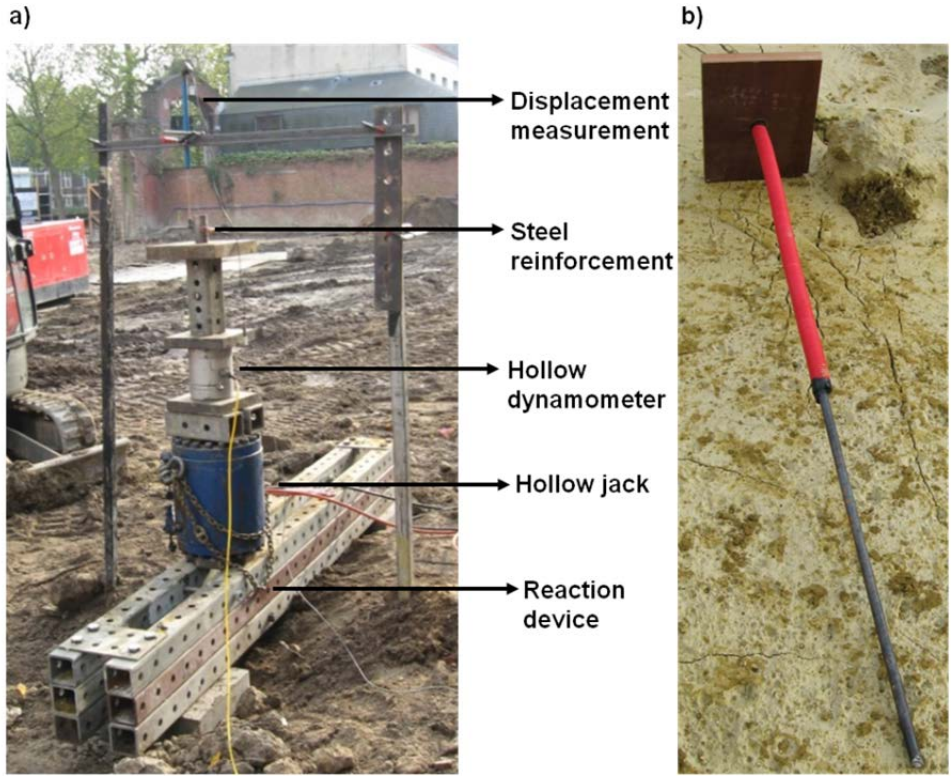

Figure 15: a) Pull-out test set-up and b) steel profile with protecting tube

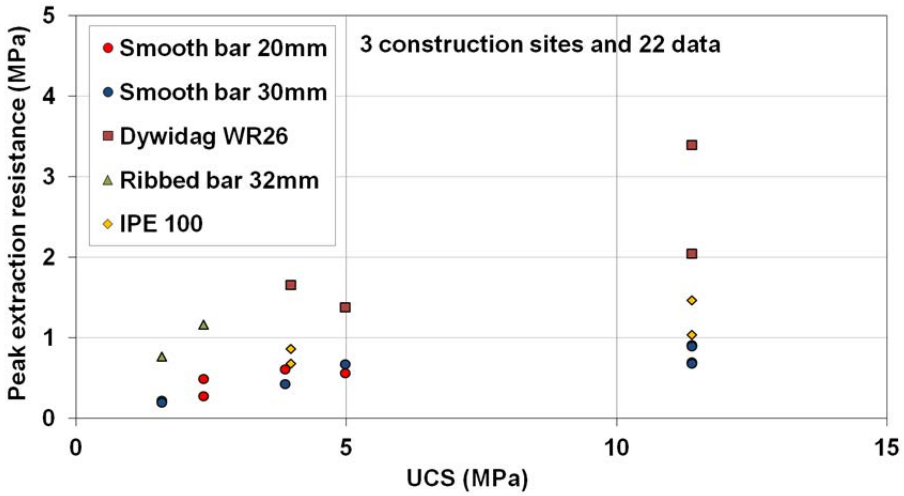

Figure 16: Peak pull-out resistance in function of the UCS of cored DSM material

6. UCS CHARACTERISTIC VALUE OF DSM MATERIAL

For engineering purposes and in particular with regard to the semi-probabilistic design approach in Eurocode 7, it is important to define a 'characteristic value' of the UCS that can be taken into account in the design of DSM structures. The definition of this value still remains a subject of discussion and further research is needed. In general terms, the determination of the characteristic value can be divided into two categories. The first category uses the average value of the population combined with a safety factor (methodology A), while the second category defines the characteristic value as a lower limit, e.g. 5% quantile (methodologies B and C). The (dis)advantages of both categories are discussed below.

6.1. Methodology A: average value with safety factor

If the definition of the characteristic value is based on the average value of a population combined with a safety factor, one should note that the determination of the average is not straightforward. First, one can argue which definition is most suitable (arithmetic mean, median, geometric mean, etc.). Second, problems may arise when estimating these values. For a Gaussian distribution, everything is relatively straightforward and the main problem is linked to a limited number of samples. However, when a population is composed of different subpopulations or when the population is skewed, the complexity increases and there is no single methodology for the different types of dataset. For example, when the original dataset is skewed, the value of the arithmetic mean is affected by the way it is estimated (i.e. applying e.g. the lognormal theory or not, and which method is considered). For example, for a lognormal distribution the geometric mean is considered to be a more efficient (with a larger reliability) estimator than the arithmetic mean (Rendu, 1981).

6.2. Methodology B: X% lower limit on the basis of a distribution function

As already mentioned before, a characteristic value can also be a reasonable choice of a minimum value (with or without considering an additional safety factor). This can be done by fitting one of the standard distribution functions to the dataset and working further with this theoretical function. In this way, an X% lower limit value can be determined (i.e. any percentage that is considered appropriate). This way of working takes (apart from the mean) also the spread of the dataset into account. Note that the easiest definition of the spread is the minimum and maximum value recorded. The advantage of this method is that it overcomes problems such as the fact that the minimum and maximum values of a dataset are normally not the proper extreme values (if one increases the number of data points, there is always the chance that an additional data point is situated outside the first recorded range). Besides, by assuming a theoretical distribution function one avoids to base the limit value on the information of one single data point.

Nevertheless, it is not always easy to fit a standard distribution to a given dataset. The most appropriate distribution should be determined, followed by the estimation of its properties. This distribution function can be different for each site and it is even not guaranteed that a suitable standard distribution exists. Apart from these remarks, it should also be noted that the properties of the theoretical distribution face similar problems as discussed for the average, i.e. the effect of the limited number of data points, but additional uncertainties introduced by the assumed statistical theory are also possible.

This is illustrated for the lognormal theory applied on a dataset of 41 UCS values with an arithmetic mean, μ, of 8.63 MPa and a standard deviation, σ, of 6.99 MPa (see Figure 17a for its distribution). This distribution is clearly not Gaussian; the red curve in Figure 17a is the theoretical Gaussian curve for μ and σ calculated. If a dataset is lognormally distributed, then the logarithm of the dataset is normally distributed. Possibly, a factor β has to be added to the values to obtain an optimal fit with a normal distribution after transformation (see Figure 17b, where β = 0.6).
Based on these logarithmic values, a confidence limit is then determined by the theory for Gaussian distributions, as illustrated in Figure 17b by the vertical red line for a 5% lower limit. The actual characteristic value is then obtained by back-transformation, resulting, in a value of 1.46 MPa.
Problems of this approach are the choice of a correct value for β, the fact if the distribution is really lognormal or not and the effect of the limited number of data points.

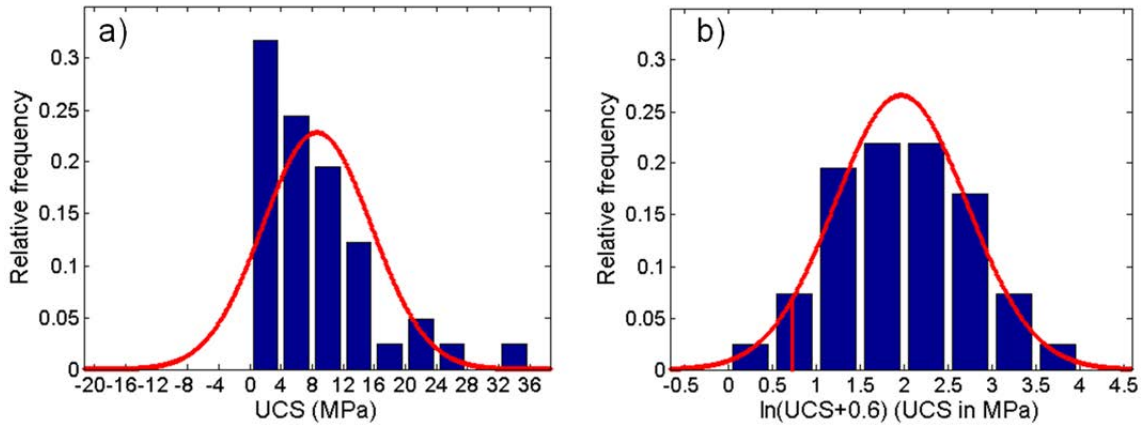

Figure 17: a) Distribution of the UCS values of 41 cores of DSM material from a site in Gent and the corresponding theoretical Gaussian curve. b) Distribution of the logarithm of the UCS values of the same site but increased with β = 0.6 and the corresponding Gaussian curve. The vertical red line indicates the 5% lower limit value

6.3. Methodology C: X% lower limit on the basis of the cumulative curve

Therefore, one should maybe consider determining the X% quantile directly on the original experimental dataset and independent of any distribution function. For the mentioned dataset this results in a 5% quantile UCS value of 1.36 MPa.
Of course, when one disposes of less than 20 data points, this method (i.e. direct estimation on the cumulative curve) cannot be applied. However, any other method probably results in a large uncertainty.

6.4. Determination of the percentage X

Note that for both approaches X needs to be defined. In Eurocode 7 design X is often stated at 5%, but in the case of the UCS of DSM material a more detailed analysis of all the experimental test data is necessary in order to determine if a 5% lower limit is a representative characteristic value, in particular with regard to the treatment (elimination rule or not) of the samples with large inclusions (see Section 7).

It is clear that more extensive investigation is necessary in order to formulate clear directives. Some points to be further investigated are the statistical methodology, the scale effect, the effect of the execution method and the difference between soil types. However, it is recommended to (i) plot the distribution, (ii) look at the range (minimum and maximum) and (iii) compare mode, median and mean before applying any statistical approach.

Table 3 presents an overview of some of these statistical values for DSM cores originating from several Belgian sites.

Table 3: Some important statistical values for DSM cores originating from several Belgian sites

Site	Soil type	Age (days)	N[†] (-)	Min. (MPa)	Max. (MPa)	Median (MPa)	μ[†] (MPa)	σ[‡] (MPa)
Alsemberg	Clayey loam	120	15	1.49	3.54	2.75	2.72	0.52
Brugge	Sand	55	51	2.33	9.56	5.80	5.65	1.88
Zeebrugge	Sand	86	40	4.14	7.79	6.65	6.44	0.9
Gent I	Alluvial clay	60	41	0.96	33.23	6.44	8.63	6.99
Borgloon	Soft clay	130	26	0.53	15.44	5.36	5.65	3.1
Antwerpen J	Sand	30	29	2.30	18.74	11.76	11.00	3.72
Antwerpen K	Sandy clay	30	12	2.20	24.80	10.80	12.79	6.75
Knokke I	Peaty clay	30	25	0.44	30.81	5.45	7.33	7.19
St-Lievens Houtem	Loam	30	31	3.56	23.03	9.34	10.78	4.93
Limelette	Loam	150	45	3.76	31.04	13.57	14.05	6.2
Antwerpen MH	Sand	30	50	4.88	23.77	10.91	11.93	4.09
Duffel	Alluvial clay	85	6	0.65	1.52	1.27	1.18	0.36
Gent II	Remolded and sandy soil	14	18	1.28	2.94	2.02	2.14	0.48
Knokke II	Sand	91	16	5.05	13.60	10.95	10.71	2.15
		523	17	11.78	19.98	13.61	14.16	2.14
Wetteren	Remolded and loamy/sandy soil	49	25	0.66	6.80	4.27	4.03	1.33
		91	24	2.07	8.84	4.63	4.72	1.61
Elsene	Clay	117	10	2.19	12.69	9.71	9.38	2.77
Turnhout	Sand with bricks	57	11	3.40	11.54	6.79	6.74	2.75

[†]N is the number of UCS test data
[†]μ is the arithmetic mean of the UCS data
[‡]σ is the standard deviation of the UCS data

7. PRELIMINARY CONCLUSIONS ABOUT THE INFLUENCE OF SOIL INCLUSIONS

Within the framework of the BBRI 'Soil Mix' research, all inclusions in DSM material are considered as unmixed soft soil inclusions. A methodology taking into account these inclusions was developed and illustrated with case studies of DSM material executed in several Belgian soils (Ganne et al., 2011 and 2012). Figure 18 gives an overview of the results for 27 Belgian construction sites.

The amount of soil inclusions in DSM material mainly depends on the nature of the soil:

- in quaternary or tertiary sands, it is less than 3.5%,
- in silty (or loamy) soils and alluvial clays, it ranges between 3 and 10%,
- in clayey soils with high organic content (such as peat) or in tertiary (overconsolidated) stiff clays, it can amount up to 35% and higher.

One major issue concerns the representativeness of the core samples with regard to the in situ executed DSM material. On the one hand, there is the question of the scale effect and on the other hand, the question of the influence of soil inclusions. Both have an influence on the UCS test results. To investigate these topics, an experimental, as well as a numerical simulation research programme has been initiated at KU Leuven (Vervoort et al., 2012). This research programme studies the behaviour before and after failure of the DSM material.

The experimental part focuses on laboratory experiments with the study of the scale effect. The behaviour in laboratory is certainly affected by the scale and the dimensions of the test samples. Apart from traditional cores (with a diameter around 10 cm), large scale tests are conducted on rectangular blocks with approximately a square section, with a width corresponding to the width of the in situ SMW (about half a meter) and with a height approximately twice the width.

In parallel, numerical simulations (2D) were performed to quantify the effect of soil inclusions on the strength and stiffness of the DSM material. The following parameters are being considered: size, number, relative position and percentage of soil inclusions. Three approaches were followed with the help of:

- an elastic model only focusing on the DSM stiffness,
- an elasto-plastic model whereby, apart from the stiffness, the strength is analysed,
- a discontinuous model concentrating on the initiation and growth of individual fractures.

That research programme should quantify the maximum acceptable limits of volume percentages of inclusions and optimize the test procedure with regard to the tests on samples with soil inclusions larger than 1/6 of the specimen diameter. In engineering practice test specimens with inclusions/particles larger than one sixth of the specimen diameter must be cautiously regarded, as highlighted in the following standards.

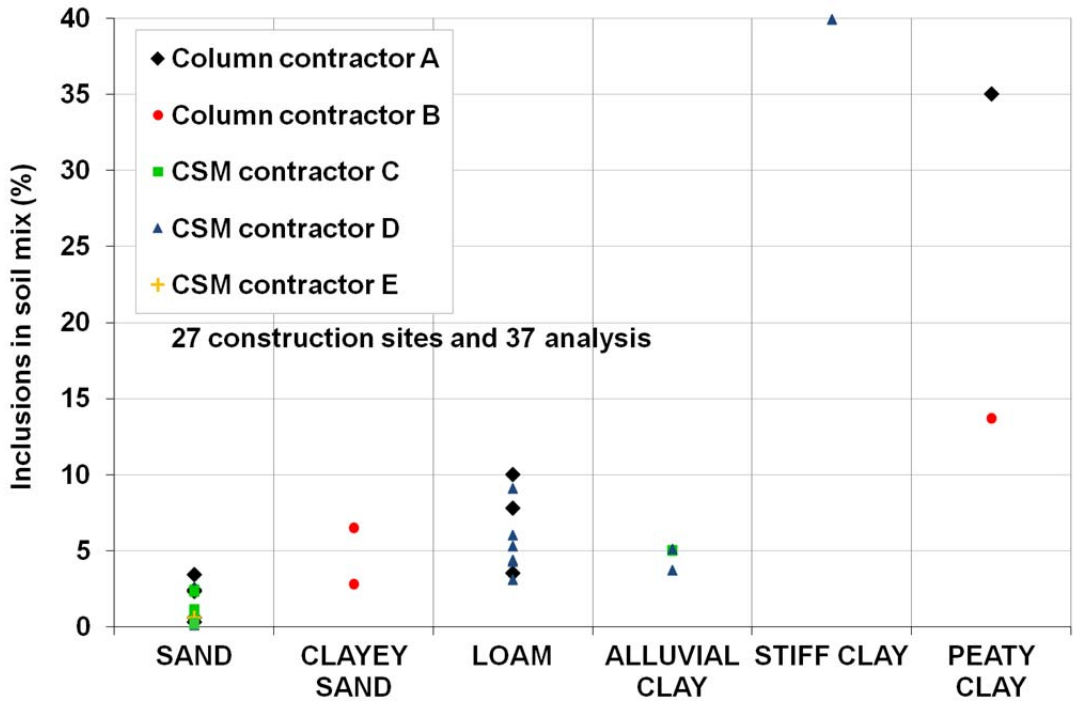

Figure 18: Percentage of soil inclusions in DSM material

As reported in ASTM D 2166-91, describing the standard test method for **UCS of cohesive soil**: *"For specimens having a diameter of 72 mm (2.8 in.) or larger, the largest particle size shall be smaller than one sixth of the specimen diameter. If, after completion of a test on an undisturbed specimen, it is found, based on a visual observation, that larger particles than permitted are present, indicate this information in the remarks section of the report of test data"*.
The procedure for **UCS tests on fine grained soils** is described in NBN CEN ISO/TS 17892-7: 2005, which specifies that: *"The largest particle in the specimen should not exceed 1/6 of the specimen diameter for cylindrical specimens and not exceed 1/6 of the side length for square specimens"*.
ATSM D 5102-90, dedicated to **UCS tests of compacted soil-lime mixtures**, reports that: *"For specimens having a diameter of 72 mm (2.8in.) or larger, the largest particle size shall be smaller than 1/6 of the specimen diameter"*.
For **testing hardened concrete** samples, the requirements concerning the dimensions of the specimens intended for UCS tests are described in NBN EN 12390-1. According to this standard: *"for each shape of test specimen, cube, cylinder and prism, the basic dimension should be chosen to be at least three and a half times the nominal size of the aggregate in the concrete"*.
The philosophy behind these standards is that samples with inclusions or particles larger than 1/6 of the sample dimension are not representative for the material as such. The practical question is what to do when in the core material with a fixed diameter such inclusions or particles are observed. The theoretical answer to this question is that one should drill again, but now with a larger diameter. For various reasons, this is not necessary feasible: often the wall is not easily accessible anymore, one cannot drill too many boreholes and certainly with large diameter without weakening the wall, etc. In other applications for concrete or rock masses, one has often a good idea beforehand of the size of inclusions or particles. This is for soil mix material not really the case. The BBRI 'Soil Mix' project aims to quantify the effect of such large inclusions on the behaviour of core samples, of large blocks and on in situ walls (Vervoort et al., 2012). For example, for a core sample with a diameter of 90 mm, an inclusion larger than 15 mm affects the strength in most cases significantly; however such an inclusion of 15 mm diameter within an in-situ wall is most likely acceptable. This is the main reason why Ganne et al. (2010) proposed to reject all test samples with soil inclusions larger than 1/6 of the specimen diameter, on the condition that no more than 15% of the test samples from one particular site are rejected. If more than 15% of the test samples are rejected, it is obvious that the problem is not a local one and that further investigation and evaluation are needed, combined with a good engineering judgement. For the calculation of the values of Table 3 this elimination rule was not applied.
In Fig. 19, two examples are given for the distribution of UCS values whereby the samples with inclusion(s) larger than 1/6 of the diameter are indicated. For the first site (Fig. 19a), these samples (6 on a total of 51 samples) have a UCS value less than 3.95 MPa and are clearly situated in the left part of the distribution, as one would normally expect. For the second site (Fig. 19b), some of these samples are situated in the left part of the distribution (6 of the 9 samples with inclusion(s) larger than 1/6 of the diameter on a total of 26 samples), but the other 3 samples have a UCS value of more than 7.37 MPa. The reason why such samples still result in a relatively large strength value is probably linked to the number and relative position of the inclusion(s) (among themselves and within the sample). This forms also part of the BBRI 'Soil Mix' project, where numerical simulations are conducted to quantify the effect of various positions, sizes, shapes, number, etc. of inclusions and this for different scales (Vervoort et al., 2012). These examples show that the way how is dealt with samples containing large inclusions, can have a considerable influence on the deduction of engineering parameters (cfr. Section 6)

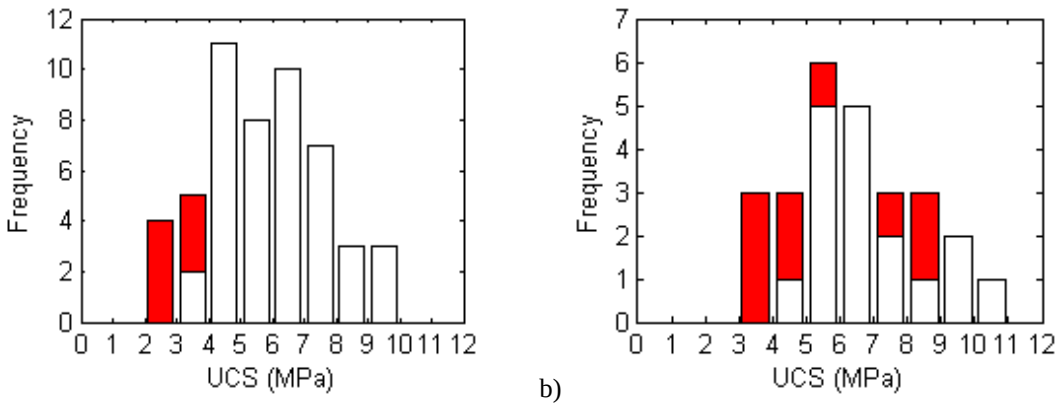

a) b)

Figure 19: Distribution of the UCS values from 2 different sites. The samples with inclusions larger than 1/6 of the specimen diameter are indicated in red: a) 6 on a total of 51 samples; b) 9 on a total of 26 samples

8. CONCLUSIONS AND PERSPECTIVES

Within the framework of a Flemish regional research program "Soil Mix" (IWT 080736), DSM materials from 38 Belgian construction sites, with various soil conditions and for different execution processes, have been tested. The present paper describes results of mechanical tests performed on DSM material executed with the Cutter Soil Mix (CSM), the Tubular Soil Mix (TSM) and the CVR C-mix® systems (Denies et al., 2012a). The UCS, the modulus of elasticity and the tensile strength are determined, as well as the porosity, the permeability and the ultrasonic pulse velocity of core samples. As illustrated in Fig. 9 and 10, UCS, modulus of Elasticity and tensile strength are correlated with the help of equations (2) to (4) and (7) to (9). They correspond to previous correlations proposed by Topolnicki and Trunk (2006), as presented in Table 4.

Table 4: Correlations between the UCS, the modulus of elasticity, the shear and tensile strengths, after Topolnicki and Trunk (2006)

Parameter	**Empirical relationships**	
Age of the specimen (days)	$UCS_{28\ days}$	$= 2.0\ UCS_{4\ days}$
		$= 1.4 – 1.5\ UCS_{7\ days}$ (silt and clay)
		$= 1.5 – 2.0\ UCS_{7\ days}$ (sand)
	$UCS_{56\ days}$	$= 1.4 – 1.5\ UCS_{28\ days}$ (silt and clay)
Coefficient of variation (%)	COV	= 20 – 60
		= 30 – 50 (usually)
Shear strength (MPa)	τ	= 0.40 – 0.50 UCS for UCS < 1 MPa
		= 0.30 – 0.35 UCS for 1< UCS < 4 MPa
		= 0.20 UCS for UCS > 4 MPa
Tensile strength (MPa)	T_a	= 0.08 – 0.15 UCS with a maximal value of 0.2 MPa
Secant modulus of elasticity (50% UCS) (MPa)	E_{50}	= 50 – 300 UCS for UCS < 2 MPa
		= 300 – 1000 UCS for UCS > 2 MPa
Elongation at maximal force (%)	ε_u	= 0.5 – 1.0 for UCS > 1 MPa
		= 1.0 – 3.0 for UCS < 1 MPa
Poisson ratio (-)	ν	= 0.25 – 0.45
		= 0.30 – 0.40 (usually)

Some of the findings so far are:

- As a result of the petrographic analysis, high porosity values of the DSM material can be related to the high and homogeneous capillary porosity of cement stone resulting from high W/C ratio used for the execution of the SMW. From permeability tests, the coefficient of hydraulic conductivity of DSM material varies between 10^{-8} and 10^{-12} m/s.
- The sampling, the transportation, the storage, the handling and the preparation of the test specimens are detailed in Denies et al. (2012b).
- In situ pull-out test results are also described in order to verify the adherence between DSM material and various steel profiles ensuring the SMW stiffness.
- On the basis of UCS tests performed on core samples, the determination of the 5% quantile characteristic UCS value is then discussed.
- Finally, the results of a methodology quantifying unmixed soil inclusion in the material are presented for various Belgian soils. The representativeness of the core samples is questioned with regard to the influence of unmixed soil inclusions in the material and considering the scale effect.For the purpose of investigating this engineering issue, reference is made to the experimental and numerical research program performed in KU Leuven with the help of large scale tests and numerical developments (Vervoort et al., 2012).

While SMW was previously used only for temporary excavation support, permanent retaining and foundation applications with DMM are increasingly applied in Belgium. Hence, the durability aspects of the DSM material have to be considered. In the second period of the BBRI 'Soil Mix' project, the DSM material shall be investigated in terms of its alkalinity properties, with the help of pH long term measurements, in order to control its level of corrosion protection. The viability of the process in the presence of polluted soils shall also be considered.
Based on the results of the BBRI 'Soil Mix' project, a design method for DSM structures, accounting for the presence of the heterogeneities and unmixed soil inclusions, the scale effects and the time effects such as curing time and creep shall be developed.

9. ACKNOWLEDGEMENTS

The authors wish to thank members of the BBRI for their technical assistance and experience, especially, Bernard André, Rosario Bonsangue, Christian Mertens and Christian Verbeke. This research program is financially supported by the Agency for Innovation by Science and Technology of the Flemish Region IWT (BBRI, 2009-2013).

REFERENCES

Denies, N., Huybrechts, N., De Cock, F., Lameire, B., Maertens, J. and Vervoort, A. 2012a. Soil Mix walls as retaining structures – Belgian practice. International symposium & short courses of TC211. Recent research, advances & execution aspects of ground improvement works. 30 May-1 June 2012, Brussels, Belgium.

Denies, N., Huybrechts, N., De Cock, F., Lameire, B., Vervoort, A. and Maertens, J. 2012b. Mechanical characterization of deep soil mix material – procedure description. International symposium & short courses of TC211. Recent research, advances & execution aspects of ground improvement works. 30 May-1 June 2012, Brussels, Belgium.

Ganne, P., Huybrechts, N., De Cock, F., Lameire, B. and Maertens, J. 2010. Soil mix walls as retaining structures – critical analysis of the material design parameters, International conference on geotechnical challenges in megacities, June 07-10, 2010, Moscow, Russia, pp. 991-998.

Ganne, P., Denies, N., Huybrechts, N., Vervoort, A., Tavallali, A., Maertens, J, Lameire, B. and De Cock, F. 2011. Soil mix: influence of soil inclusions on structural behaviour. Proceedings of the XV European conference on soil mechanics and geotechnical engineering, Sept. 12-15, 2011, Athens, Greece, pp. 977-982.

Ganne, P., Denies, N., Huybrechts, N., Vervoort, A., Tavallali, A., Maertens, J, Lameire, B. and De Cock F. 2012. Deep Soil Mix technology in Belgium: Effect of inclusions on design properties. Proceedings of the 4th International conference on grouting and deep mixing, Feb. 15-18, 2012, New Orleans, Louisiana, USA.

Hird, C. C. and Chan, C. M. 2005. Correlation of shear wave velocity with unconfined compressive strength of cement-stabilised clay. Proceedings of the International Conference on Deep Mixing: Best Practice and Recent Advances, May 23-25, 2005, Stockholm, Sweden, pp. 79-85.

Pauw, A. 1960. Static modulus of elasticity of concrete as affected by density. Journal of the American Concrete Institute, Vol. 32, N°6, pp. 679-687.

Rendu, J.-M, 1981. An Introduction to Geostatistical Methods of Mineral Evaluation, Geostatistics 2. South African Institute of Mining and Metallurgy.

Topolnicki, M. and Trunk, U. 2006. Tiefreichende bodenstabilisierung. Einsatz im Verkehrswegebau für Baugrundverbesserung und Gründungen. Tiefbau, Vol. 118, N°6, pp. 319 – 330 (in German).

Vervoort, A., Tavallali, A., Van Lysebetten, G., Maertens, J., Denies, N., Huybrechts, N., De Cock, F. and Lameire, B. 2012. Mechanical characterization of large scale soil mix samples and the analysis of the influence of soil inclusions. International symposium & short courses of TC211. Recent research, advances & execution aspects of ground improvement works. 30 May-1 June 2012, Brussels, Belgium.

Mechanical characterization of DEEP SOIL MIX material – procedure description

N. Denies, N. Huybrechts, Belgian Building Research Institute, Geotechnical division, Belgium, nde@bbri.be, nh@bbri.be
F. De Cock, Geotechnical Expert Office Geo.be, Belgium, fdc.geobe@skynet.be
B. Lameire, Belgian Association of Foundation Contractors ABEF, Belgium, bart@lameireft.be
A. Vervoort, KU Leuven, Belgium, andre.vervoort@bwk.kuleuven.be
J. Maertens, Jan Maertens bvba & KU Leuven, Belgium, jan.maertens.bvba@skynet.be

ABSTRACT

Since several decennia, the deep soil mix (DSM) technique has been used for ground improvement (GI) applications. In recent years, soil mix walls (SMW) have become an economical alternative to traditional excavation support systems. The Belgian building market has also witnessed such development with the growing use of the Cutter Soil Mix (CSM), the Tubular Soil Mix (TSM) and the CVR C-mix® systems (Denies et al., 2012a). Unfortunately, standardized guidelines for SMW design are not currently available. For the purpose of developing such standard, mechanical characteristics of DSM material must be investigated. Within the framework of a Flemish regional research program (IWT 080736), DSM materials from 38 Belgian construction sites, with various soil conditions and for different execution processes, have been tested. Test results are detailed in Denies et al. (2012b).
Beyond the site conditions and the execution technique, the preparation of the test specimens is an important issue and can have an influence on the test results. For that reason, the present paper focuses on the sampling, the transport, the storage, the handling and the preparation of the DSM test specimens. In addition, two methods to quantify the volume of unmixed soil inclusions in the mix are presented.

1. INTRODUCTION

Since several decennia, the deep soil mix method (DMM) has been used for GI applications. In recent years, SMW have increasingly been used – in Belgium and in several other countries – for the retaining of soil and water in the case of excavations. Indeed, SMW represent a more economical alternative to concrete secant pile walls and even in several cases to king post walls.
The main structural difference between SMW and the more traditional secant pile walls is the constitutive DSM material which consists of a soil – cement mixture instead of traditional concrete.
Unfortunately, up to now, guidance rules and recommendations concerning the realization of SMW with a soil and/or water retaining function have been lacking while various DSM systems are active on the Belgian market such as the CVR C-mix®, the Tubular Soil Mix (TSM) and the Cutter Soil Mixing (CSM). However, the number of applications is fast increasing (Denies et al. 2012a). As part of QA/QC development and of the European standardization, basic rules are required with regard to design, execution and control of these different DSM execution processes.
These issues encouraged the Belgian Building Research Institute (BBRI) to initiate research actions that address the execution, design and testing of DSM systems in Belgium. For the purpose of investigating the DSM technology and its applicability in the various Belgian soils, a “Soil Mix” project was initiated in 2009 in collaboration with the KU Leuven and the Belgian Association of Foundation Contractors (ABEF). Financial support has been obtained from IWT, the Flemish government agency for Innovation by Science and Technology (http://www.iwt.be/).
Within the framework of the BBRI ‘Soil Mix’ project, numerous tests on in situ DSM material have been performed. A good insight has been acquired with regard to mechanical characteristics that can be obtained with the different DSM systems in several Belgian soils (Denies et al., 2012b).
If the design and the QC of the execution are generally based on laboratory tests performed on cored material, each sample is characterized by its own history influencing the test result and its interpretation. Beyond the question of the representativeness of the core samples with regard to the in situ executed material, discussed in Denies et al. (2012b), the present paper concentrates on the sampling, the transport, the storage, the handling and the preparation of the test specimen which constitute the main preliminary stages to the mechanical characterization.
For the geotechnical survey, these topics are addressed, in a general view, in the European and American standards, respectively EN ISO 22475-1 and ASTM D 420 - 93. For DSM material, the Annex B of EN 14679 (2005) – the European standard for the execution of deep mixing – gives some indications with

regard to the laboratory testing on core samples but the preparation of the test specimen is not detailed. In order to take into account the specific nature of the mixing of the DSM material, the test procedures, developed within the framework of the BBRI 'Soil Mix' project, have been based on various soil, rock and concrete standards. Special attention has been given to the presence of soft soil inclusion in the DSM material. Two methodologies to quantify the volume of soft soil inclusions have been developed. In addition, a handling procedure for the preparation of the DSM test specimens has been established. Table 1 illustrates the timeline of the DSM sample life with regard to the standards or test methodologies supporting its several stages.

2. SAMPLING

For geotechnical investigation, it is imperative to obtain samples adequately representing each subsurface material significant to the project design, construction and control. The size, the type and the amount of samples required depend on the tests to be performed, the relative amount of coarse particles present, and the limitations of the test equipment to be used.
In the case of DSM material, the sampling also depends on the amount of unmixed soil inclusions in the mix. The heterogeneous character of the DSM material must be taken into account.
Each sample must be accurately identified with a waterproof tag that refers to its construction site, its borehole and its depth. Each borehole shall be located (in horizontal and vertical directions) with reference to some established and permanent coordinate system. The coring date and all indications useful for the test and its interpretation should be indicated in the sampling report such as the climatic conditions and the groundwater level observed during coring operations. The coring direction (horizontal or vertical) must also be specified. In case of subdivided samples, reference must be made to the original sample.
In addition, colour photographs of cleaned samples, filled sample boxes and accessible soil strata may be directly performed after coring.
For additional information on the sampling methods, the reader can consult EN 12504-1 or ASTM D 2113 - 83 especially for diamond core drilling.
In the case of DSM structures, the sampling is generally performed with a water based drilling technique; hence, it is not possible to determine the water content of the samples.

3. TRANSPORTATION

In the case of DSM material, drying/freezing of samples may affect the mechanical properties. Hence, samples must be protected in order to minimize moisture loss. For that reason, samples shall be transported in sealed containers equipped with padding material preventing any moisture loss and sample cracks due to shocks or vibrations. These containers should be designed in such a way to withstand rough transportation conditions and must be clearly marked. If necessary, special shipping and/or laboratory handling instructions are associated with the sample box.
Specific information concerning transportation is given in:
- ASTM D 4220 - 89 for soil samples,
- and ASTM D 5079 – 90 for rock core samples.

4. PRESERVING/STORAGE

During the whole period between delivery and testing of DSM samples, they are stored in an acclimatized chamber with a relative humidity larger than 95% and a temperature equal to 20 ± 2°C, as indicated in EN 12390-2: 2009.

Table 1: Timeline of the DSM samples: procedures followed within the framework of the BBRI 'Soil Mix' project

Sampling	**Transportation**	**Preserving/Storage**	**Handling/Preparation of test specimens/Test and report**	
In situ	In situ	In laboratory	In laboratory	
EN ISO 22475-1: 2007 Geotechnical investigation and testing - Sampling methods and groundwater measurements - Part 1: Technical principles for execution **EN 14679: 2005** Execution of special geotechnical works – Deep mixing **ASTM D 420 – 93** Standard Guide to Site characterization for Engineering, Design, and Construction Purposes				
EN 12504-1: 2009 Testing concrete in structures - Part 1: Cored specimens - Taking, examining and testing in compression **ASTM D 2113 - 83** Diamond Core Drilling for Site Investigation	**ASTM D 4220 - 89** Standard Practices for Preserving and Transporting Soil Samples **ASTM D 5079 - 90** Standard Practices for Preserving and Transporting Rock Core Samples	**EN 12390-2: 2009** Testing hardened concrete - Part 2: Making and curing specimens for strength tests **ASTM D 1632 - 87** Standard Practice for Making and Curing Soil-Cement Compression and Flexure Test Specimens in the Laboratory	Visual analysis and quantification of soft soil inclusions	**Section 5.2** of the present paper, after **Ganne et al. (2011 and 2012)**
			Handling procedure for the preparation of DSM test specimens	**Section 5.3** of the present paper
			Density	**EN 12390-7: 2009** Testing hardened concrete - Part 7: Density of hardened concrete
			Unconfined compressive strength, UCS	**EN 12390-3: 2009** Testing hardened concrete - Part 3: Compressive strength of test specimens
			Modulus of elasticity, E	**NBN B 15-203: 1990** Concrete testing - Statical module of elasticity with compression **ISO/FDIS 1920-10: 2010** Testing of concrete - Part 10: Determination of static modulus of elasticity in compression
			Tensile splitting strength, T	**EN 12390-6: 2010** Testing hardened concrete - Part 6: Tensile splitting strength of test specimens
			Ultrasonic pulse velocity, V_p	**ASTM C 597 - 09** Standard Test Method for Pulse Velocity Through Concrete **EN 12504-4: 2004** Testing concrete in structures - Part 4: Determination of ultrasonic pulse velocity
			Porosity	**NBN B 15-215: 1989** Concrete testing - Absorption of water by immersion
			Hydraulic conductivity	**DIN 18130-1: 1998** Laboratory tests for determining the coefficient of permeability of soil

5. HANDLING/PREPARATION OF TEST SPECIMENS

5.1. Identification

Once a technically qualified person receives the sample boxes, the cataloging and specimen identification operations start. First, a catalogsheet is established with the following information: the construction site, the contractor's name, the material type and the number of boxes and samples. The type of test may already be mentioned with the required sample age for the test realization. A reference should be made to the sampling report associated with the sample boxes.
The samples are then removed from their box for a first visual analysis and in order to determine the type of test(s). Each sample is identified with a unique identification mark allowing traceability to its original coring and depth. A colour photograph that includes the name of the construction site, the sample identification and a reference scale is performed (see Fig. 1).

Figure 1: Identification of core sample

5.2. Visual analysis and consideration of soil inclusions

Due to the specific procedure of deep mixing, soft soil inclusions in the DSM material are inevitable. Nevertheless, the volume of soil inclusions in DSM structure is an important factor to quantify as it has an influence on the material strength, its stiffness and its permeability. Hence, within the framework of the BBRI 'Soil Mix' project, two methodologies to quantify soil inclusions have been developed (Ganne et al., 2011 and 2012).

5.2.1. Description of the methodologies

In the present test procedure, the inclusions are considered as soft soil inclusions. In order to quantify the volume of soil inclusions, DSM material from in situ executed DSM columns and panels have been observed.
Soil inclusions can be described based:
- on drilled cores, as illustrated in Fig. 1,
- on entire sections of DSM columns/panels, as illustrated in Fig. 2.

The two methodologies quantifying the amount of soil inclusions are the surface percentage (A) and a simplified procedure: the line percentage (B).

Methodology (A):
The calculation of the surface percentage of soil inclusions involves six successive steps:
1. DSM columns or panels are executed in situ by standard DSM procedure
2. The test columns/panels are (partly) excavated, as illustrated in Fig. 3
3. The column/panel is then sawed to create a statistically representative 'fresh' saw-cut section (see Fig. 4).
4. The saw-cut surface, as presented in Fig. 2a, is photographically digitized to recompose one digital mosaic photo. The pixel resolution is about 0.3 mm.
5. Using commercially available image processing techniques (IPT), soft soil inclusions, as highlighted in Fig. 2b, are assigned in black on the digital mosaic photo. As the soft soil inclusions are not always observable, manual verifications are performed on the saw-cut surface.
6. The determination of the surface percentage of soil inclusions consists in the calculation of the amount of assigned (black) inclusions and the total surface of the saw-cut using IPT.

Alternatively, the saw-cut section of a core sample can also be used.

Figure 2: a) Saw-cut section of a CSM panel, b) enlargement of a soft soil inclusion

Figure 3: Excavation of an in situ executed CSM panel (Lameire Funderingstechnieken n. v.)

Figure 4: Sawing of a CSM panel

Methodology (B):
The line percentage methodology is a simplified procedure that is fairly easy to apply for drilled cores. As illustrated in Fig. 5a, four lines are drawn, distributed equidistantly around the core diameter and the cumulative length of soil inclusions along the lines is manually measured (see Fig. 5b). The line percentage is calculated as the proportion of this cumulative length to the total lines length.
This methodology is applied to complete core lengths as they are received and before sawing, in order to avoid loss of information with regard to soft soil inclusion due to further treatment of the samples.
Methodology (B) can also be applied to an entire section of DSM columns/panels considering parallel lines drawn on the saw-cut surface. Then, line and surface percentages of soft soil inclusions can be compared.

a) **b)**

Figure 5: Application of the methodology (B) for a drilled core

Both methodologies are based on the Delesse principle (after Weibel, 1980): the observed line and surface percentages of inclusions in a representative volume of material can be considered as unbiased estimations of the volume percentage of inclusions in the material, assuming a chaotic distribution of the inclusions into the block. Figure 6 illustrates the Delesse principle for inclusions in a cubic block of side l. In Fig. 6b, η(y) is the percentage of inclusion in the *y* direction. Each column corresponds to the percentage of inclusion for a slice of material with a width dy. $\overline{\eta}$ is the average percentage in the *y* direction.

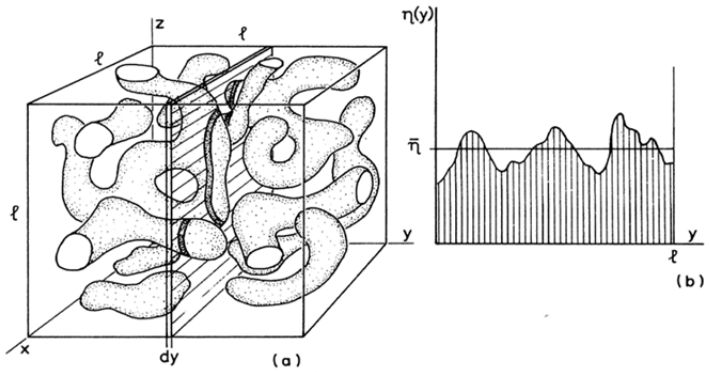

Figure 6: The principle of Delesse, after Weibel (1980)

After completion of the mechanical test, the surface or line percentage can be correlated to the test result (UCS, T and E). Nevertheless, if it is found after testing, based on a visual observation, that large soft soil inclusions become only visibly after testing, as there are not visible on the outer surface. The operator should indicate this information in the remarks section of the test report.

5.3. Handling/Preparation of the test specimens – procedure description

5.3.1. Size of the test specimens

After visual analysis, each core sample must be sawed and treated to comply with its test type. Table 2 describes requirements for the size of the test specimen.

Table 2: Requirements for the specimen size for the tests performed within the framework of the BBRI 'Soil Mix' project

Density	According to **EN 12390-7: 2009**, "*The minimum volume of a specimen shall be 0.785 l*". This condition is encountered with 100 mm diameter samples with height to diameter ratio, H/D, close to 1.
UCS	The height to diameter ratio is 1. This choice was based on the necessity to collect a maximum of cores and was made in order to compare the UCS test results on cylindrical cores with cube strength, as indicated in **EN 12390-3: 2009** and especially in **EN 12504-1:2009**.
Modulus of elasticity	According to **NBN B 15-203: 1990**, the height to diameter ratio is 2, which is in line with the indications of the **ISO/FDIS 1920-10: 2010**: "*The length to diameter ratio of the test specimens shall be between L/d = 2 to 4 and 2 is recommended*".
Tensile splitting strength	Samples with height to diameter ratio close to 1 have been tested in order to use similar size ratio as for UCS test. As reported in **NBN EN 12390-6: 2010** for concrete samples: "*the effect of cylinder size on measured tensile strength was not found to be significant, possibly due to the variability of the data*". Such variability is also observed for DSM material.
Ultrasonic pulse velocity	As indicated in **ASTM C597-09**: "*The least dimension of the test object must exceed the wavelength of the ultrasonic vibrations*". Considering the natural frequency of the transducers used for the test, 160 kHz, and the range of pulse velocities recorded for DSM material, varying between 2000 and 3600 m/s, the specimen size was always comfortably larger than the wavelength: H/λ is close to 6.
Porosity	In accordance with the **NBN B 15-215: 1989**, the volume of the tested specimens, with H/D close to 1, was larger than 800 cm^3.
Hydraulic conductivity	The permeability of the DSM specimens was determined with the help of the **DIN 18130-1: 1998**. This latter gives requirement for cohesive and coarse-grained soils: "*The cross-sectional area of the specimen, A, shall be not less than 10 cm^2 for cohesive soil, and not less than 20 cm^2 for coarse-grained soil, unless the test equipment requires the use of larger specimens*". In the present study, the test specimens had cross-sectional area close to 80 cm^2.

5.3.2. Handling procedure description

At this stage of the test process, the way the operator handles the core sample is significant for the test result. Within the framework of the BBRI 'Soil Mix' project, the same handling procedure was followed for every DSM sample. Figures 7 to 9 describe the handling and the marking of test specimens by the operator for different situations.

First, the operator determines the usable part of the DSM sample. In most cases, the sample edges are particularly damaged (due to the drilling operations) and are not representative for the DSM material. The center of the workable part is indicated on the core (see Fig. 7a).

Afterwards, the operator defines the dimensions of the test specimen(s) in the usable area in such a way to use a maximal part of the DSM sample and to avoid subjective positioning of the test specimen(s) due to the presence of local soft soil inclusion(s) at the extremities of the core. To ensure this objective selection, the same quantity of DSM material is rejected at both extremities of the usable part of the core. In Fig. 7b and 7c, the sawing lines are drawn on the DSM core. Figure 7d illustrates the full marking of the core.

Each test specimen, defined according to this procedure, must be once again identified and recorded.

After the marking, the test specimens are generally sawed or possibly ground. The intended load-bearing surfaces could be prepared by grinding or by capping, as indicated in the Annex A of EN 12390-3.

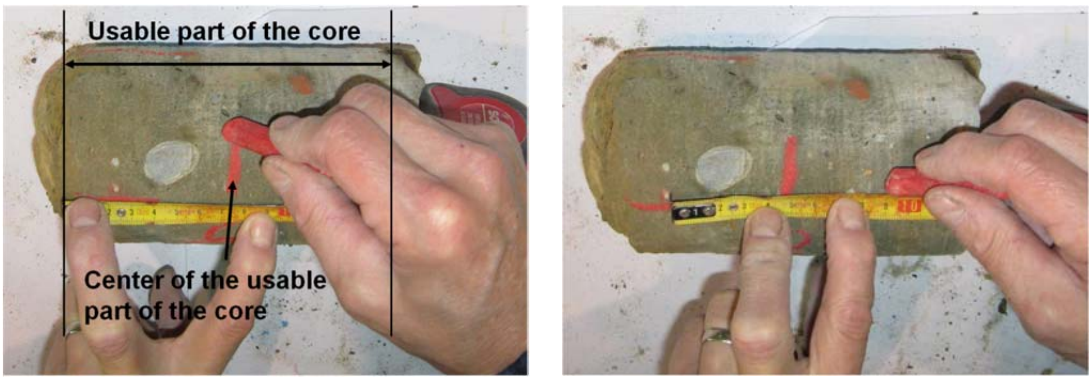

a) Definition of the usable part of the sample
b) Drawing of the first sawing line
c) Drawing of the second sawing line
d) Full marking of the DSM core

Figure 7: Preparation of a DSM test specimen intended for UCS test (H/D ratio close to 1)

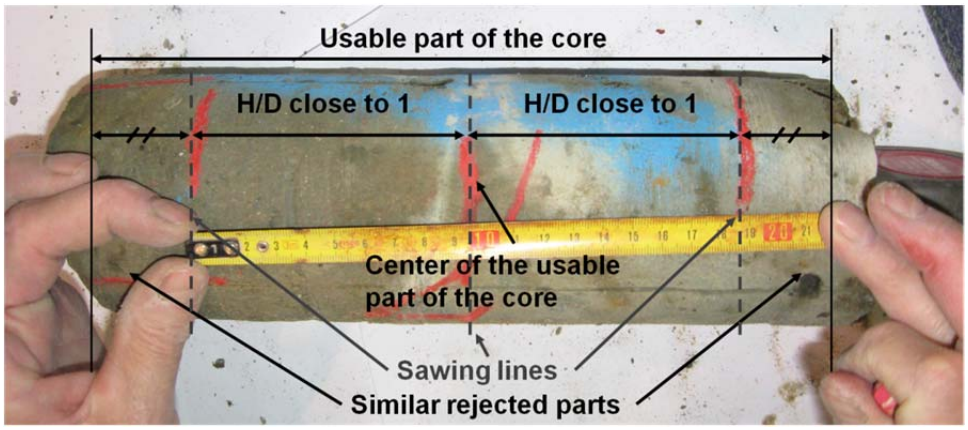

Figure 8: Preparation of two DSM test specimens, both intended for UCS tests

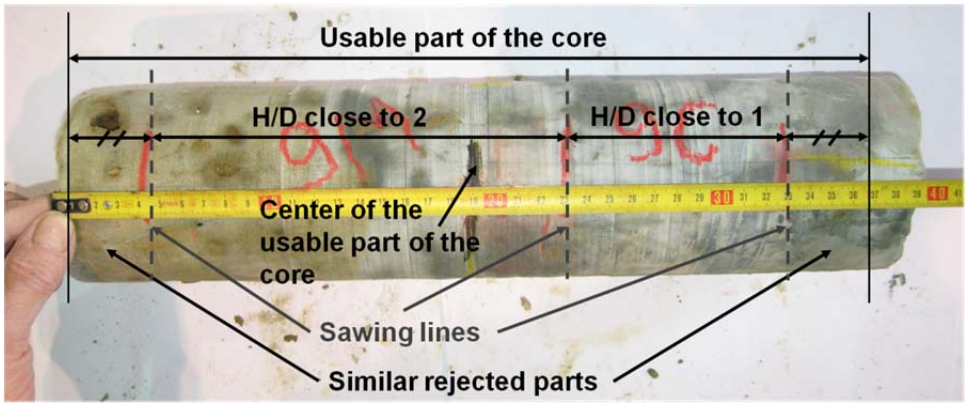

Figure 9: Preparation of two DSM test specimens for the determination of the modulus of elasticity (sample 9M) and the UCS (9C)

6. TEST AND REPORT

6.1. Test procedures

Within the framework of the BBRI 'Soil Mix' project, several tests have been conducted to characterize the DSM material:

- unconfined compressive strength,
- tensile splitting strength,
- modulus of elasticity,
- ultrasonic pulse velocity,
- adherence with steel reinforcement.

These tests have been performed on the basis of the standards for concrete and soils referred in Table 1. Nevertheless, there are specificities related to the nature of the DSM material. The details of the test procedures are defined in Denies et al. (2012b).

6.2. Test report

The content of the test report depends on the type of tests. Nevertheless, several elements should always be included:

- date and time of the test;
- identification of the test specimen;
- percentage of soft soil inclusions measured with methodology (A) and/or (B);
- conditions of the specimen on receipt and the date of delivery;
- storage conditions since receipt;
- age of the specimen at the time of the test;
- dimensions of the test specimen (height, diameter and H/D ratio);
- specimen mass;
- density of the specimen;
- surface condition of the specimen at the time of the test,
- indications on adjustment by grinding and/or capping (if it has been applied to the specimen);
- maximum load at failure (kN) – in case of UCS and tensile splitting strength tests and for the determination of the modulus of elasticity;
- strength based on the maximum load (MPa).

If it is the purpose to obtain more detailed information with regard to the failure pattern, the loading of the DSM sample must be performed with a constant rate of deformation and not with a constant rate of load as usually recommended in the standards to determine the UCS value of concrete. In that case, the test report shall also be documented with pictures of the failure pattern of the sample, as illustrated in Fig. 10. It is to note that the failure pattern also depends on the specimen size and on the ratio H/D.

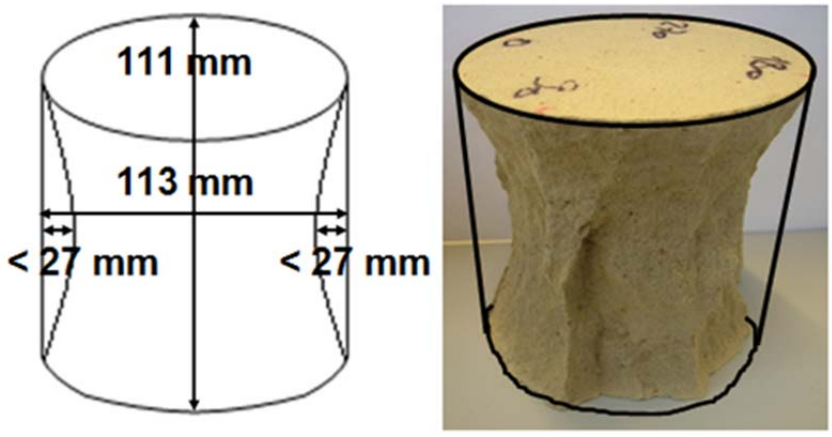

Figure 10: Schematic drawing of the inner zone without macro-fractures in the DSM samples (L/D ratio close to 1)

The final purpose of the laboratory tests on core samples is to characterize the in situ executed DSM material. Hence, whatever the considered stage in the timeline of the sample, **traceability is the key to a successful test campaign**. Indeed, in the test report, the results associated with a particular sample should be correlated to its original borehole location and depth and hence, to the parameters and date of execution of a specific SMW element.

7. CONCLUSIONS

In recent years, SMW have increasingly been used – in Belgium and in several other countries – for the retaining of soil and water in the case of excavations. Unfortunately, up till now, guidance rules and recommendations concerning the realization of SMW with a soil and/or water retaining function have been lacking in spite of the fast increasing number of applications (Denies et al., 2012a). As part of QA/QC development and European standardization, basic rules are required with regard to design, execution and control of these different DSM execution processes. For the purpose of developing such standard, several tests to characterize DSM material, executed in situ by standard DSM procedure, have been performed (Denies et al., 2012b).

The European standard for the execution of deep mixing (EN 14679: 2005) gives some indications with regard to the laboratory testing on DSM core samples, but no specific requirements are provided for the preparation of the test specimens and the details of the different test procedures (for the determination of the UCS, the modulus of elasticity and the permeability) are not described. For that reason, within the framework of the BBRI 'Soil Mix' project, procedures for the sampling, the transportation, the storage, the handling and the preparation of the DSM test specimens have been proposed on the basis of several standards for soil and concrete materials (see Table 1).

With the present paper the authors hope to contribute to the development and the establishment of test procedures in the continuity of the content of the European standard EN 14679 (2005) for deep mixing. In addition, for the purpose of controlling the uniformity and homogeneity of DSM material, two methodologies to quantify the volume of soft soil inclusions have also been developed.

8. ACKNOWLEDGEMENTS

The authors wish to thank members of the BBRI for their technical assistance and experience in the development of the handling and test procedures, especially, Bernard André, Rosario Bonsangue, Christian Mertens and Christian Verbeke. This research program is financially supported by the Agency for Innovation by Science and Technology of the Flemish Region IWT (BBRI, 2009-2013).

REFERENCES

Denies, N., Huybrechts, N., De Cock, F., Lameire, Maertens, J. and Vervoort, A. 2012a. Soil Mix walls as retaining structures – Belgian practice. International symposium & short courses of TC211. Recent research, advances & execution aspects of ground improvement works. 30 May-1 June 2012, Brussels, Belgium.

Denies, N., Huybrechts, N., De Cock, F., Lameire, B., Vervoort, A., Van Lysebetten, G. and Maertens, J. 2012b. Soil Mix walls as retaining structures – mechanical characterization. International symposium & short courses of TC211. Recent research, advances & execution aspects of ground improvement works. 30 May-1 June 2012, Brussels, Belgium.

Ganne, P., Denies, N., Huybrechts, N., Vervoort, A., Tavallali, A., Maertens, J, Lameire, B. and De Cock, F. 2011. Soil mix: influence of soil inclusions on structural behaviour. Proceedings of the XV European conference on soil mechanics and geotechnical engineering, Sept. 12-15, 2011, Athens, Greece, pp. 977-982.

Ganne, P., Denies, N., Huybrechts, N., Vervoort, A., Tavallali, A., Maertens, J, Lameire, B. and De Cock F. 2012. Deep Soil Mix technology in Belgium: Effect of inclusions on design properties. Proceedings of the 4th International conference on grouting and deep mixing, Feb. 15-18, 2012, New Orleans, Louisiana, USA.

Weibel, E. R. 1980. Stereological methods. Vol. 2. Theoretical foundations, Academic Press, New York.

Mechanical characterization of large scale soil mix samples and the analysis of the influence of soil inclusions

A. Vervoort, A. Tavallali, G. Van Lysebetten
KU Leuven, Belgium, andre.vervoort@bwk.kuleuven.be, and Gust.VanLysebetten@bwk.kuleuven.be

J. Maertens
Jan Maertens bvba & KU Leuven, Belgium, jan.maertens.bvba@skynet.be

N. Denies, N. Huybrechts
Belgian Building Research Institute, Geotechnical division, Belgium, nde@bbri.be and nh@bbri.be

F. De Cock
Geotechnical Expert Office Geo.be, Belgium, fdc.geobe@skynet.be

B. Lameire
Belgian Association of Foundation Contractors ABEF, Belgium, bart@lameireft.be

ABSTRACT

Since several decennia, the deep soil mix technique is used for ground improvement applications and for the realisation of retaining walls. In recent years, soil mix walls have become an economical alternative to traditional excavation support systems. However, as a natural material (i.e. soil) is being mixed, it is to be expected that the entire wall is not perfectly mixed and homogeneous. In other words, inclusions of poorly mixed or even unmixed (i.e. soil) material are present. The amount of such inclusions can be less than 1% of the total volume at some sites, but 10% or more is also observed. Some of these inclusions are very small, while in other cases they can have dimensions of several centimetres. It is generally assumed that below a certain volume percentage and/or for small dimensions of the individual inclusions, these inclusions have no negative impact on the behaviour and on the strength of the soil mix material. To quantify the maximum acceptable volume percentages of inclusions, an experimental, as well as a numerical simulation research programme has been initiated in the framework of a Flemish regional research project (IWT 080736) that is carried out in collaboration with the BBRI, the Belgian federation of foundation contractors (ABEF) and KU Leuven. This research aims also to better understand the behaviour of this material and the failure of it.

The experimental part of this research focuses on laboratory experiments. The behaviour in laboratory is certainly affected by the scale and the dimensions of the test samples. Apart from traditional cores (e.g. with a diameter of about 10 cm), large scale tests are being conducted. The large samples tested are rectangular blocks with approximately a square section (about half a meter) and with a height of approximately two times the width. The stress-strain behaviour of the blocks tested so far shows a significant stress drop after reaching its peak strength. The failure is a combination of extension type of fractures and shear failure.

By conducting complementary numerical simulations (2D), one tries to better understand the effect of the inclusions of unmixed material, i.e. the effect of their size, the total surface percentage, the number of inclusions, the relative position, etc. By numerical models, it is relatively easy to consider numerous cases, while experimentally (e.g. by artificial samples) it is much more difficult and time consuming. Three approaches have been used: (i) elastic models are applied, whereby the focus is on the stiffness of the material, (ii) elasto-plastic models, whereby apart from the stiffness the strength is analysed and (iii) a discontinuous approach, whereby individual fracture initiation and growth can be modelled, apart from the stiffness and strength. The most prominent conclusion is that even a small percentage of inclusions has a significant effect on the strength of the material and to a lesser extent on the stiffness. For 1% of unmixed material, the strength is reduced on average by 20%, while for 10% of unmixed material about half of the strength disappears. Another consistent result is that other characteristics than the total surface percentage of unmixed material can have a significant effect, e.g. large sharp-ended individual inclusions have a negative effect on the strength and stiffness.

1. INTRODUCTION

The application of deep soil mix technology in Belgium is sharply increasing. Next to soil improvement applications, deep soil mix walls are extensively used for excavation support. The CVR C-mix®, the TSM and the CSM are the three most used types of deep soil mix systems in Belgium. All three are wet deep mixing systems. More details of the execution procedures are given in (Denies et al., 2012). Due to the specific procedure of deep mixing and as a natural material is being mixed, it is to be expected that the entire wall is not perfectly mixed and homogeneous. Hence, soil inclusions are inevitable. In this paper, all inclusions in soil mix material are considered as soft soil inclusions. In other words, inclusions of poorly mixed or even unmixed (i.e. soil) material are present. The amount of such inclusions can be less than 1% of the total volume at some sites, but 10% or even 35% have also been observed. The amount of soil inclusions depends on the nature of the soil wherein the deep mix is performed (Ganne et al., 2012): e.g. in tertiary or quaternary sands, the amount of soil inclusions is less than 3.5 vol%, in silty soils or alluvial clays, it varies between 3 and 10 vol%, and in clayey soils with organic material (such as peat) or in tertiary (overconsolidated) clays, it can amount up to 35 vol% and higher. Some of these inclusions are very small, while in other cases they can have dimensions of several centimetres. It is generally assumed that below a certain volume percentage and/or for small dimensions of the individual inclusions, these inclusions have no negative impact on the strength and on the behaviour of the soil mix wall. To quantify the maximum acceptable limits of volume percentages and inclusions, an experimental, as well as a numerical simulation research programme has been initiated. This research aims also to better understand the behaviour of this material and the failure of it.

The experimental part of this research focuses on laboratory experiments (see paragraph 2). The behaviour in laboratory is certainly affected by the scale and the dimensions of the test samples. Apart from traditional cores (e.g. with a diameter of about 10 cm), large scale tests are being conducted. The large samples tested are rectangular blocks with approximately a square section, with a width corresponding to the width of the in situ wall (about half a meter) and with a height approximately two times the width.

By conducting complementary numerical simulations in 2D (see paragraph 3), one tries to better understand the effect of the presence of the inclusions of unmixed material, i.e. the effect of their size, the total surface percentage, the number of inclusions, the relative position, etc. By numerical models, it is relatively easy to consider numerous cases, while experimentally (e.g. by artificial samples) it is much more difficult and time consuming. Three approaches are being taken: (i) elastic models are applied, whereby the focus is on the stiffness of the material, (ii) elasto-plastic models, whereby apart from the stiffness the strength is analysed and (iii) in comparison to both continuum models, a discontinuous approach, whereby individual fracture initiation and growth can be modelled, apart from the stiffness and strength.

2. LABORATORY EXPERIMENTS

2.1. Large scale tests on rectangular blocks

The main aim of testing large blocks is to get a better idea about the in situ behaviour and characteristics of real soil mix material. In particular, if the material is more heterogeneous the scale effect should be more important. For example, if a soil inclusion with a diameter of about 5 cm is present or not in a core sample with a diameter of 10 cm, this will affect the strength and the stress-strain behaviour of the core significantly, in comparison to the presence or absence of such a single inclusion in a block with a width of half a meter.

So far, soil mix panels from three construction sites (A, B and C) with different soil types have been tested. For each site an additional soil mix panel has been installed for test purposes only. After being excavated, several types of tests are conducted. One of them is loading a large block cut out from the panel. One horizontal dimension corresponds to the width of the in situ panel, the other horizontal dimension is about the same and the height is approximately two times the width (see Table 1). At sites A and C the soil can be considered as homogeneous (i.e. tertiary and quaternary sand), while at site B the soil is very heterogeneous. Apart from natural loam and sand material, it also contains small particles of construction waste.

The blocks are vertically loaded. The loading is displacement controlled. The loading rate is 0.5 mm/min in order to detail the occurrence and growth of the various fractures. The loading is only stopped after a large vertical displacement has occurred beyond the peak strength, enabling to quantify the post peak behaviour (see Figure 1). The vertical deformation is recorded by four LVDT's with a measurement base of about one fourth of the height, around the centre of each vertical side.

Table 1: Overview of large scale tests and cored samples for the three different sites studied

Site	A: Quaternary sand	B: Mixed soil and construction waste	C: Tertiary sand
Dimensions blocks	61 × 53 × 124 cm	55 × 48 × 90 cm	58 × 53 × 120 cm
Characteristics blocks Uniaxial strength: Young's modulus (tan):	 8.3 MPa 13.6 GPa	 2.1 MPa 2.9 GPa	 4.2 MPa 5.5 GPa
Dimensions cores Diameter: Height:	 113 mm 230 mm	 113 mm 230 mm	 94 mm 200 mm
Characteristics cores UCS: Young's modulus (tan):	 11.1-12.4 MPa 12.5-13.2 GPa	 3.4-4.9 MPa 1.3-2.7 GPa	 5.0-7.6 MPa 5.6-6.9 GPa

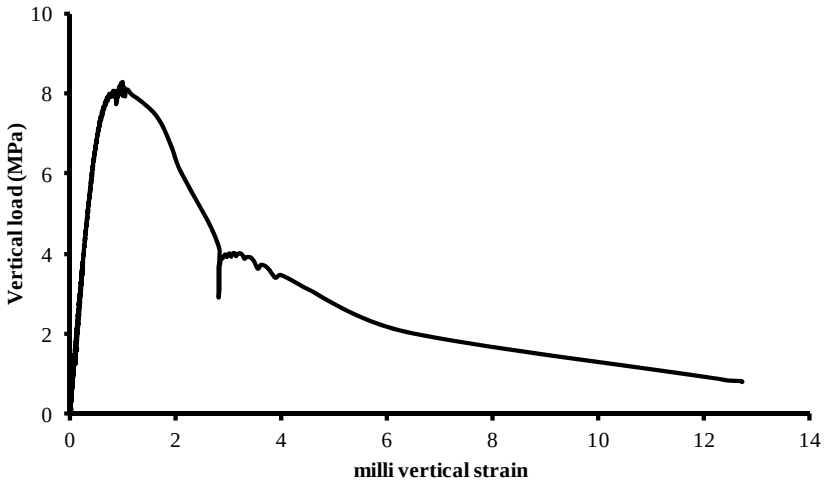

Figure 1: Full stress-strain curve of a large rectangular block from site A

The peak uniaxial strength of the three sites is significantly different, 2.1 MPa for site B, 4.2 MPa for site C and 8.3 MPa for site A. The Young's or elastic modulus varies accordingly. The tangent modulus at 50% of the UCS peak value is respectively 2.9 GPa for site B, 5.5 GPa for site C and 13.6 GPa for site A. The fractures occurring during loading are in one way similar for the three blocks, but also different (see different pictures in Photo 1). All induced macro-fractures have a strike which is roughly parallel to the original soil-wall contact. Further investigation has to clarify if this is related to the mixing procedure. For all three blocks the first macro-fracture is only observed very close to the peak. Most of the final macro-fracture pattern is induced during the post-peak behaviour. For the block from site A, first a vertical fracture is observed (close to the maximum strength; photo a). It is probably due to the splitting of the block (extension type of fracture). When the load reaches about half the maximum load after the peak, the part delineated by the vertical fracture buckles (photo b). The test is continued and a new vertical macro-fracture is induced, again parallel to the wall of the soil mix panel. This fracture is combined with some inclined fractures at the bottom and top part of the block (photo c and d), probably due to the non-central loading of the remaining part of the block. For the block of site B, the failure pattern is mainly characterised by two macro-fractures, which are inclined at the bottom and are more vertical towards the top. Probably, the main mode is shear rather than extension or splitting. Apart from these two fractures, parallel fractures are also observed. For the block from site C, the first visible fracture is a vertically orientated fracture which inclination decreases slightly toward the bottom of the block (photo a). After the peak strength is reached, the inclination of the new induced fractures is about 60° to 80°. Two large (probably shear) fractures are observed (photos b, c and d). It is remarkable that at the top of the block all fractures are (sub)vertically orientated.

a. b. c. d.

Site A

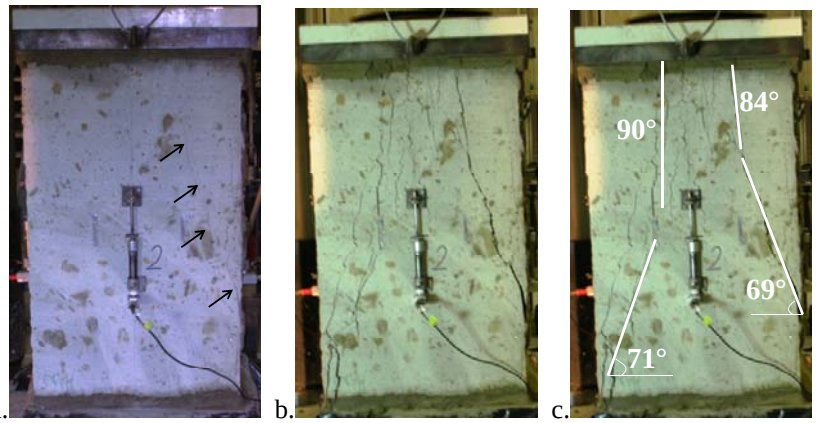

a. b. c.

Site B

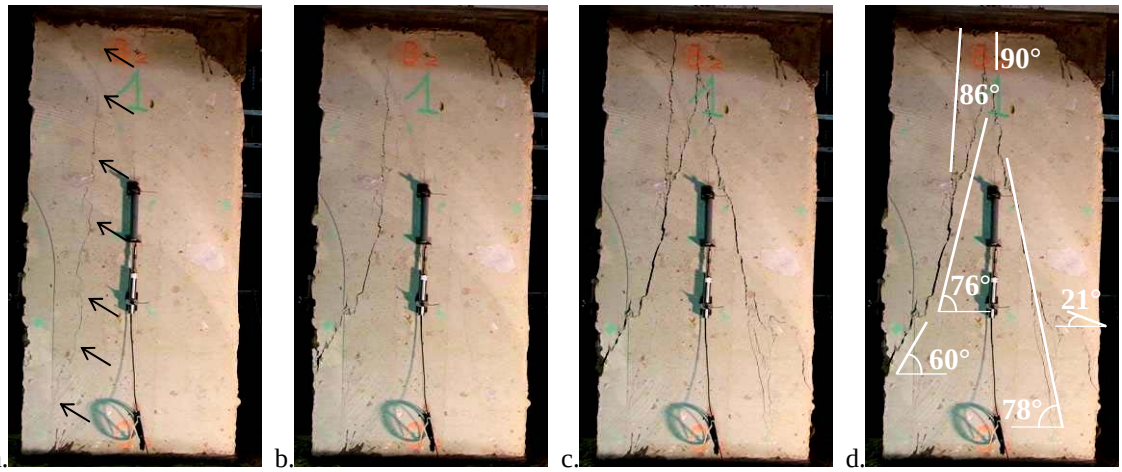

a. b. c. d.

Site C

Photo 1: Pictures taken from the loaded block from the three sites, illustrating the occurrence of fractures during loading

2.2. UCS tests on core samples

As in the long term it is not possible to test each time a block of such dimensions, conventional cores have also been tested. The cores have a diameter of 94 to 113 mm and a height of 2 to 2.5 times the diameter. The vertical deformation is measured by strain gauges with a length of about one fourth of the total height (i.e. the same measurement base as for the large blocks). For site A, the tests result in a UCS value between 11.1 and 12.4 MPa (in comparison to the block strength of 8.3 MPa). For site C, the difference between the cores and the block is similar: 5.0 to 7.6 MPa for the cores in comparison to 4.2 MPa for the block. For site B, with much more heterogeneous material, the difference is on average about

a factor 2: UCS values of 3.4 to 4.9 MPa, while the block has a strength of 2.1 MPa. For typical rock material, one would expect a reduction by a factor 2 or 3 for a block which is about 5 times larger (Bell, 1992). The reason why this is not observed at site A and C is probably the fact that the soil mix material is relatively more homogeneous than most rocks.

3. NUMERICAL SIMULATIONS

3.1. Description of 2D model

Soil inclusions or volumetric parts which are not well mixed are an integral part of soil mix material. Various observations allow deriving certain conclusions on how the number of inclusions, their sizes, their shapes and their relative positions influence the soil mix material behaviour. However, it is not possible to analyse in detail this influence by observations only. That is the reason why laboratory tests and numerical simulations have to complement each other. Sensitivity analyses can be conducted more easily in numerical modelling.

The starting point for the model is a real 2D section with dimensions of 120 × 240 mm, in which 11 inclusions are observed, corresponding to about 11% surface area (see Figure 2.a). From this, 69 different models were generated. The % surface area of inclusions was changed by varying the number and size of the inclusions resulting in 1, 5, 10 and 20% inclusions. The basic model representing 10% inclusions is presented in Figure 2.b. Apart from changing the number and the size, also the shape of the inclusion was varied. Hence, some of these models contain inclusions with a more rounded shape or inclusions with sharper corners.

Three approaches with increasing complexity are conducted. First, a linear elastic continuum model is used (paragraph 3.2), followed by a perfect elasto-plastic behaviour for the same continuum model (paragraph 3.3). Both approaches are based on FLAC simulations. Finally, a discontinuum UDEC model is used to simulate the fracturing process in detail (paragraph 3.4).

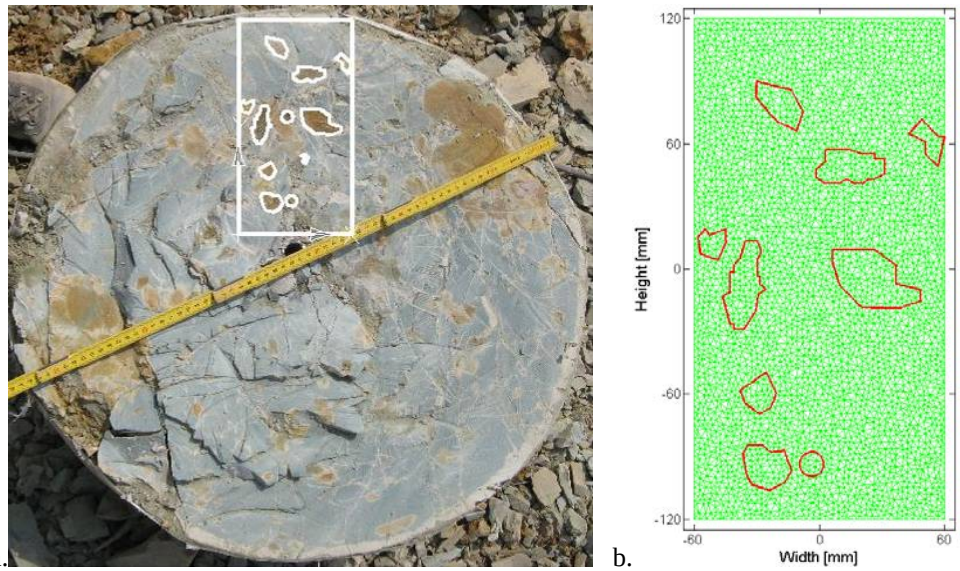

Figure 2: a. Section through a soil mix column; in this section a rectangular sample with dimensions of 120×240 mm is selected; b. Mesh generated for the discontinuous simulations (red lines indicate the soil inclusions)

3.2. Linear elastic simulations

The mixed part in each model corresponds to a material with a Young's modulus, E, and a Poisson's ratio of respectively 11.6 GPa and 0.3, while for the soil inclusions (unmixed material) these values are 0.165 GPa and 0.4. The resulting Young's moduli for the complete set of models are presented in Figure 3.a, as a function of the % surface area of soil inclusions. The presence of 1% of weak inclusions results in an average reduction of about 3% of the stiffness, while 10% of inclusions results in a 30% reduction (on average) of the stiffness. It can also be observed that for a certain percentage the variation in Young's moduli is relatively large, but there is no real overlap between the four percentages considered. For example, for 10% inclusions, the E-modulus varies between 7.3 and 8.9 GPa, while the smallest value for 5% is 9.4 GPa and the largest value for 20% is 6.5 GPa.

For a given percentage, the variation of the Young's modulus is mainly related to the shape of the inclusions. Sharp corners strongly reduce the Young's modulus, while rounded shapes (e.g. circle) are less harmful to the stiffness of the material. Figure 3.b illustrates the influence of the shape for 30 different models corresponding to 10% of inclusions. Of course, size and number of the inclusions play also a role.

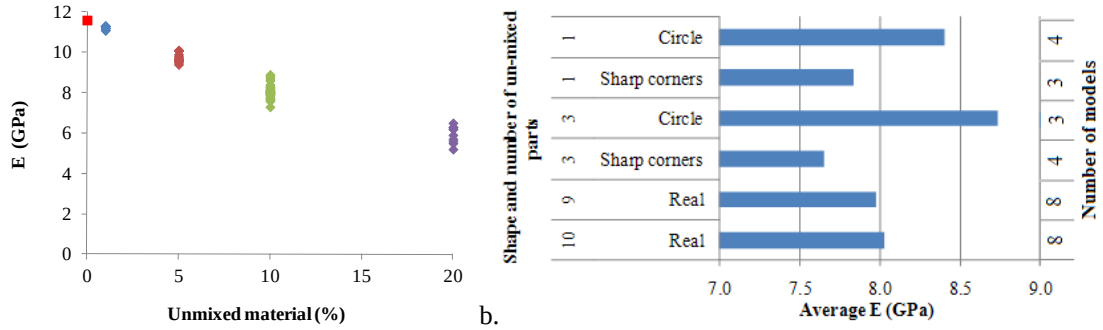

Figure 3: a. Variation of Young's modulus as a function of the percentage of unmixed material (surface area); b. Effect of the number of inclusions and their shape on the average Young's modulus for 30 numerical models (10% unmixed material)

3.3. Elasto-plastic simulations

A strain-softening model is applied, based on the Mohr-Coulomb criteria. The cohesion and tension cut-off fall back to zero after the onset of plastic yield. The elasto-plastic model is calibrated, based on UCS, Young's modulus and failure behaviour. After calibration, the Young's modulus of the basic model equals 7.8 GPa (this is very close to the Young's modulus of the basic model in elastic simulations, which is equal to 8 GPa). The UCS value for the basic case corresponds to 5.3 MPa.

Figure 4.a illustrates the large effect of the unmixed percentage on the UCS of the simulated models. For 1% of unmixed material the strength is reduced on average by about 20%. For 10% of inclusions the UCS is reduced on average by about 50% and for 20% even by about 70%. As for the Young's modulus, one observes also a significant variation for a given percentage of soft inclusions. For example, for the models with 10% inclusions, the UCS value varies between 4.5 and 6.3 MPa, while the smallest value for 5% is 5.5 MPa. In other words, other parameters than the surface percentage of weak material are also important. This is illustrated in Figure 4.b for the models with 10% unmixed material. This figure shows that sharp-ended heterogeneities generally cause smaller UCS values than rounded inclusions, at least for the same number of inclusions or the same size of inclusions. An increase in the size of the inclusions, for the same percentage of weak areas, reduces the UCS significantly. For example, models with only one, sharp-ended heterogeneity present the lowest average UCS value (4.6 MPa), while the highest average UCS (6 MPa) is found in models with three rounded inclusions, representing 10% of the sample surface.

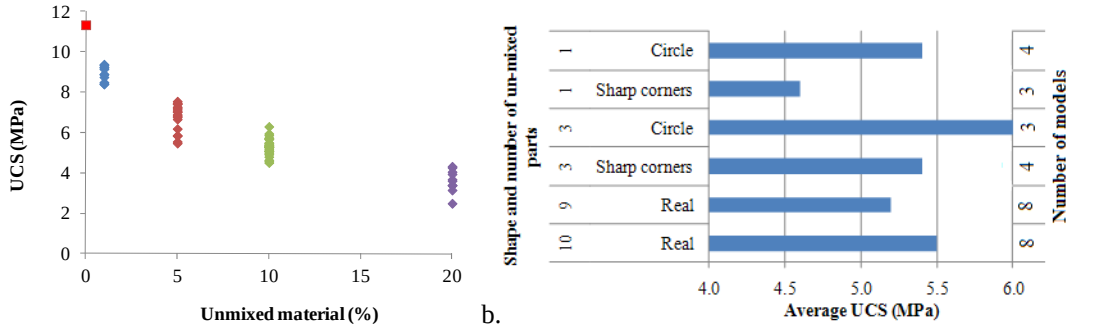

Figure 4: a. Variation of UCS values as a function of the percentage of unmixed material (surface area); b. Effect of the number of inclusions and their shape on the average UCS value for 30 numerical models (10% unmixed material)

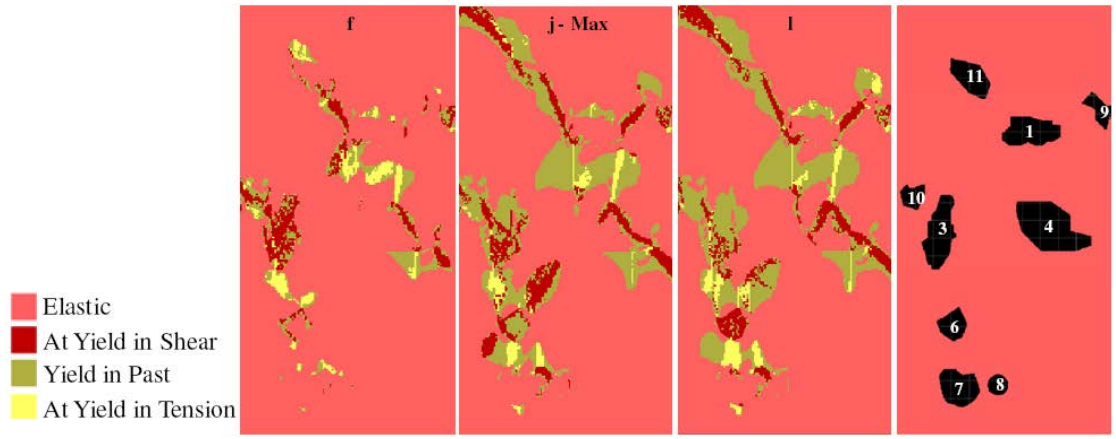

Figure 5: Occurrence of plastic deformation at the moment just prior to reaching the UCS value (left), at the peak value (middle) and just after the peak (right). The extreme right picture illustrates the position and size of the soft inclusions (in black)

The occurrence of plastic deformation during the elasto-plastic simulations for some of the loading steps around the maximum UCS peak value is presented in Figure 5. On this figure, a V-shape failure is visible corresponding to shear, but also some vertical tensile fractures can be observed.

3.4. Simulations of fracturing

The discontinuous simulations are done in UDEC, a 2D numerical program that is based on the discrete element method (Van Lysebetten, 2011). The studied medium is divided into a network of discrete blocks which are tightly bounded together by contacts. In the concept of this study, the blocks only deform elastically, while the contacts are assigned a Mohr-Coulomb shear criterion. Initially, the sample is considered as intact material in which the contacts act as potential fracture paths. Once the failure criterion of a contact is reached, it is considered as a physical crack. The behaviour of the entire model is determined by the material and contact properties. Of course, different properties are assigned to mixed and unmixed material. Note that the contact properties are determined by calibration, since they cannot be measured physically. Though simulations in UDEC and FLAC are based on different concepts, the discontinuous and elasto-plastic simulations provide rather comparable results (especially in relative terms). The surface area percentage of unmixed material affects the strength and stiffness of a sample in a very similar way for both simulations. Similar conclusions can be drawn with regard to the effect of the shape and the number of inclusions on the stiffness for models with 10% unmixed material.

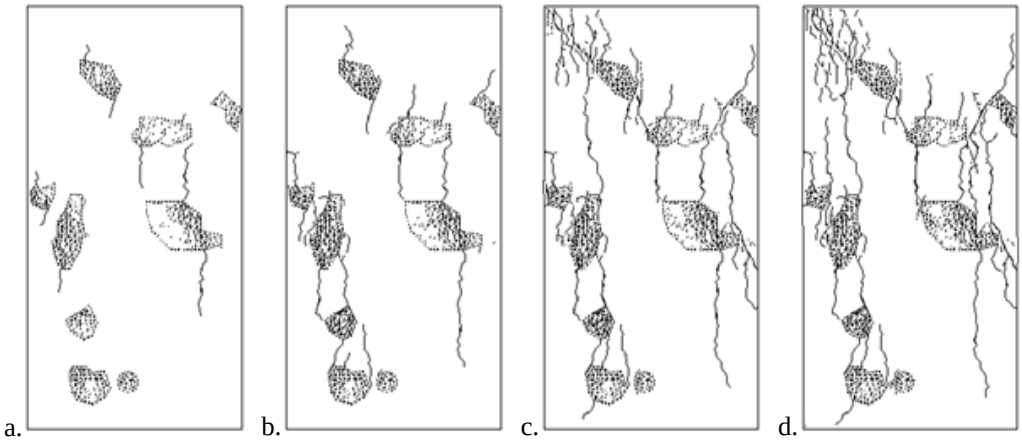

Figure 6: Evolution of the fracture pattern of the basic model during the simulated UCS test in UDEC. a. Fracture pattern before the peak strength is reached; b. At a stress level corresponding to the peak strength; c and d. At lower stress levels after peak strength is reached.

a.  b.  c. 

Photo 2: Details of induced fracture patterns in uniaxially loaded samples, cored from the rectangular block originating of site B (see Table 1), the width of the photos is about 2 cm

The evolution of the fracture pattern of the basic model during a UCS test is shown in Figure 6. Generally, the resulting fracture pattern is very similar to the results of the elasto-plastic simulations (see Figure 5). The shear zone that extends from the upper left corner of the sample to the lower right part is clearly visible for both methods, as well as the vertical fractures at the top and bottom of the inclusions. Nevertheless, some important differences can be observed. For example, failure occurs more locally along discrete fractures in the discontinuous simulations while the elasto-plastic simulations show larger zones of plastically deformed elements. Moreover, shear failure seems to occur earlier in the elasto-plastic simulations, at the moment that UDEC still simulates exclusively tensile fracturing.
In general, one can say that the discontinuous character of the UDEC simulations approaches better reality and, hence, are more suitable, if one wants to study the fracture initiation and growth in detail. Photo 2 shows some details of fracture patterns of uniaxially loaded samples cored from the rectangular block that originates from site B (Table 1). In these samples relatively large inclusions (unmixed soil) are visible. Very similar failure patterns as simulated in UDEC (Figure 6) are observed in the vicinity of inclusions, especially the vertical fractures at the top and bottom of the inclusions.

4. DISCUSSION OF EXPERIMENTAL AND NUMERICAL RESULTS

The experiments on large blocks and cores, as well as the three types of numerical simulations indicate some important trends. The influence of weak soil inclusions on the strength and stiffness of the soil mix material is significant. The reduction of the stiffness and strength is much more than what one would expect from a weighted average of the material properties (mixed and unmixed material) based on the percentage of both material types. Apart from the percentage of unmixed material, the shape, the number, the size and relative position of the inclusions are important parameters too. Hence, they have to be taken into account when conducting a detailed study. For both the continuous and discontinuous simulations, similar trends are observed for the effect on the stiffness and strength. However, the discontinuous simulations better distinguish between tensile and shear fracturing, and indicates more accurately the onset of fracturing. This means that they will be better suited to extrapolate a calibrated model, e.g. for the study of the scale effect or for other loading configurations (e.g. bending instead of uniaxial compression loading). Within this framework, the simultaneous testing of the conventional core material and the large rectangular blocks helps to better understand the possible failure of soil mix material and are really necessary as input for further numerical simulations.
In the future, more experiments are planned, so that as many soil types as possible can be investigated, resulting in a better understanding of the scale effect and the influence of heterogeneities on the mechanical behaviour of the soil mix material.

5. ACKNOWLEDGEMENTS

This research program is financially supported by the Agency for Innovation by Science and Technology of the Flemish Region IWT (BBRI, 2009-2013). The results of the discontinuous simulations are part of the thesis by Gust Van Lysebetten to obtain a M.Sc. in Geotechnical and Mining Engineering at the KU Leuven (2010-2011).

REFERENCES

Bell, F.G. 1992. Engineering rock masses. Butterworth-Heinemann Ltd, 580 pg.

Denies, N., Huybrechts, N., De Cock, F., Lameire, Maertens, J. and Vervoort, A. 2012. Soil Mix walls as retaining structures – Belgian practice. International symposium & short courses of TC211. Recent research, advances & execution aspects of ground improvement works. 30 May-1 June 2012, Brussels, Belgium.

Ganne, P., Denies, N., Huybrechts, N., Vervoort, A., Tavallali, A., Maertens, J., Lameire, B. and De Cock, F. 2012. Deep mixing technology in Belgium: execution of retaining walls and design properties of deep mixed material. 4th International Conference on Grouting and Deep Mixing, New Orleans, USA, 15-18 February 2012.

Van Lysebetten, G. 2011. SOIL MIX for construction purposes: quality control. M.Sc. thesis (Geotechnical and Mining Engineering). KU Leuven.

Foundations reinforced by soil mixing: Physical and numerical approach

Mahmoud DHAYBI, INSA de Lyon, France, mahmoud.dhaybi@insa-lyon.fr
Anna GRZYB, INSA de Lyon, France, anna.grzyb@insa-lyon.fr
Romain TRUNFIO, INSA de Lyon, France, romain.trunfio@insa-lyon.fr
Frédéric PELLET, INSA de Lyon, France, frederic.pellet@insa-lyon.fr

ABSTRACT

The aim of this on-going research project is to identify the influence of Soil Mixing (SM) and analyze the consequences on the structure's behavior. The present study is divided into two parts. First, in order to show the influence of SM reinforcement on shallow foundations, a reduced scale model was developed. It consisted of a rectangular foundation, vertically loaded, and laying on the top of a 2m^3 tank filled with Hostun sand. The composition of SM columns, their installation procedure in soil and the type of reinforcement were parameters we changed in our study in order to see their effects. After the reinforcement, load was partially transferred from foundation to SM columns so that we could reduce the foundation stress on soil and the settlements range.
Second, the work was focused on an axisymmetric FEM numerical modeling in ABAQUS. It concerned the behavior of composite foundation (footing strengthened by the SM column). The behavior of the homogenous soil and SM column were modeled with elastic-perfectly plastic law using Mohr-Coulomb failure criterion. Steel Footing was characterized by elastic constitutive law.

1. INTRODUCTION

With the increase of construction in urban areas, ground reinforcement as well as existing foundation support becomes one of the most important geotechnical issues. In order to increase bearing capacity of foundations or to reduce their settlements, different techniques could be applied. Some of the most common methods are: geosynthetics, light-weight fill, jet-grouting, rigid inclusions, sand columns etc. Soil-Mixing method consists in reinforcing soil by mixing it with cementitious material in order to create composite stiff columns. The most commonly used material is Portland cement which it is has been replaced with other kind of binder such as lime, fly ash or combination of them. The original concept of soil-mixing method has been developed in '60 in United States. However contemporary technology reflects Japanese and Scandinavian modifications. The mainly applications of this method are ground treatment for transportation (roads, railways) and harbor facilities. Recently, due to technology advancement, soil-mixing can be form in different shapes. Selection of element shapes bases on its function.
The behaviour of cemented soil has been investigated in different studies. The addition of few cement percentages was able to increase significantly the drying rate of soil. It leads to change soil properties like plasticity index, optimum water content, unconfined compressive strength and young modulus. Soil treated with high percentage of cement exhibits brittle behaviour compared to non treated soil.

2. PHYSICAL MODEL

2.1. Soil mixing characterization

With the aim to characterize soil mixing behavior under axial loading, some laboratory tests are performed on small cylindrical specimens of 45 mm diameter and 90 mm height.
The soil used is Hostun dry sand HN 31 (fig 1) and cement CEM III/C 32.5N is used as a binder. Sand, cement and water are mixed together during 10 minutes under a rotation velocity of 62.5 RPM.
The preparation of specimens should be performed immediately after the mixing operation. The mixture is placed in cylindrical molds in three layers and the material is vibrated manually to allow the evacuation of trapped air. The blending and the casting must be completed in less than 40 minutes.
Produced specimens were sealed with PVC lids and stored vertically in dry bags with paper towel soaked in water. The temperature must be maintained at about 20 ° C.

Three different mixes are prepared with different cement content (table1). Unconfined compression tests were carried out on these SM specimens at 7, 14, 21 and 28 days in order to show the effect of curing time on specimen's behavior.

Figure 1: Particle size distribution curve for Hostun sand

Table 1: Mix composition (S: Sand, C: Cement, W: Water)

Mix	Cement content	Ratio C/S	Ratio C/W	Ratio W/(S+C)
Mix 1	320 Kg/m^3	0.2	0.69	0.2
Mix 2	240 Kg/m^3	0.15	0.53	0.19
Mix 3	160 Kg/m^3	0.1	0.39	0.18

Some characterization tests are done on the mix to show its consistency. Slump test (2 to 4 cm slump) and flow tests (27 to 32 cm spread) prove that our mix is very consistent, cured sample's density is about 2000Kg/m^3.

In every test, three specimens of the same mix are tested at the same day. Results show that specimens with the highest cement content have higher resistance which can achieve 7 MPa. However, specimens of mix 3 have the lowest resistance. It's even hard to unmold them at day 7 and they can barely achieve unconfined compressive strength of 1.2 MPa at day 28.

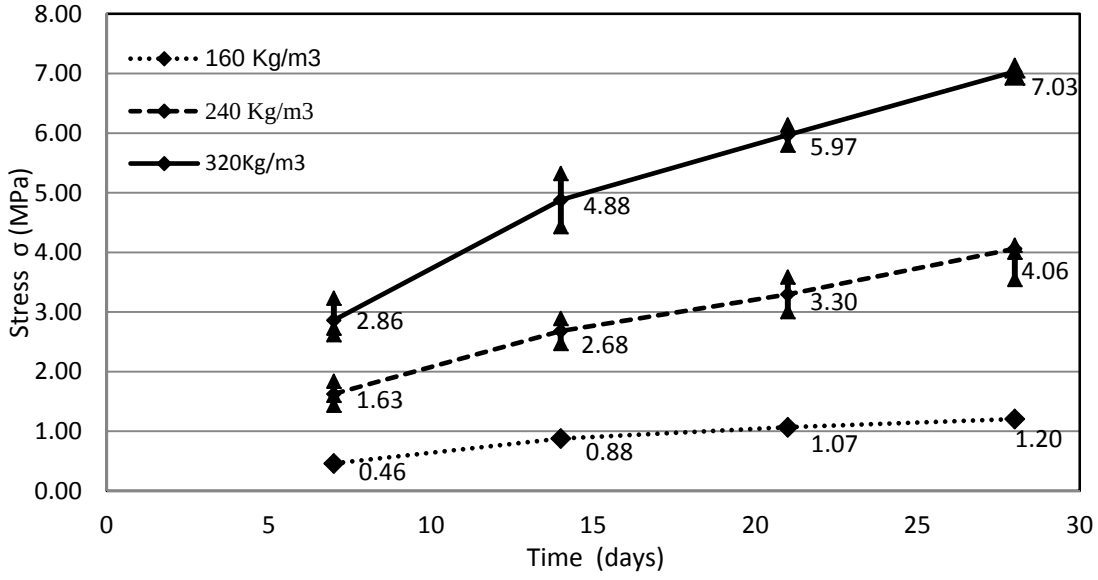

Figure 2: Evolution of unconfined compressive strength of specimens of soil mixing depending on curing time (for different cement contents).

2.2. Description of the experimental model

In order to analyze the behavior of shallow foundations reinforced by SM columns and mechanisms of composite interface, an experimental setup was constructed (fig 3). It consists of a tank 2m long, 1m wide

and 1m high, where a model scale of 1/10 is placed. The tank is built using the HEB 120 profiles and metal sheets of 5mm thick, and it is divided into two parts, 1 m^3 each.
Filling the tank is achieved by layers of 10 cm thick of Hostun dry sand to ensure an appropriate homogeneity and an accurate degree of compactness of the soil mass.
A rectangular metal plate 25 cm x 20 cm in dimensions is installed at the top surface of the fill. The plate is vertically loaded using a servo- hydraulic jack. A special metal frame based on a guidance system on rails allows the jack to move easily in the horizontal plane, covering the entire upper surface of the tank.
Guidance on rails is a system of Linear Ball compact rigidity and high load capacity. These guides can support forces from all directions and moments about all axes which provide suitable instrument for applications with high demands of guiding and positioning.

Figure 3: Photo of the constructed tank

Setting up SM column is done by sinking a steel tube in soil. Sand found in the tube is removed using vacuum. Then the mixture prepared in the laboratory is poured into the tube and the mixture cure is completed in the soil mass. The SM column is remained in sand for the curing time (7 days, 14 days). Then the rigid steel plate is installed on the top of the column in order to apply the load.

2.3. Loading test

The loading tests consist in loading footing (steel plate) lying on reinforced and unreinforced soil mass. Three different tests were conducted in order to highlight the effect of different parameters on the bearing capacity, settlements and failure. In all the tests, tank is filled in the way described before, the density of soil is around 1500kg/m^3 and the loading velocity is 0.027 mm/s. The first test consists in loading the footing lying on sand to characterize the behavior of soil without any reinforcement. Second and third tests are carried on with reinforcement. In both tests, footing is reinforced by a SM column (fig 4) and loading is carried out until failure.

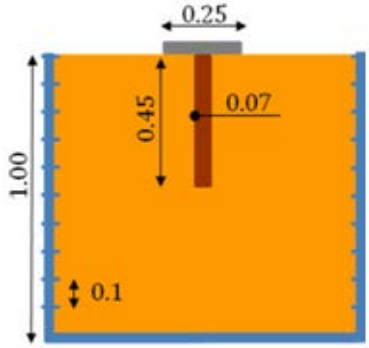

Figure 4: Physical model sketch

Table 2: description of three type of tests

Test	Reinforcement	Age of column	Soil density (Kg/m^3)	Loading velocity
Test 1	No	-	1500	0.027 mm/s
Test 2	Yes	7 days	1500	0.027 mm/s
Test 3	Yes	14 days	1500	0.027 mm/s

In terms of bearing capacity, loading tests curves show that footing reinforced with SM column loaded at day 14 has the highest bearing capacity. It's 12.5 % higher than the one loaded at day 7. In the reinforced cases, three stages corresponding to elastic, plastic behavior as well as failure can be noticed. On the contrary, unreinforced footing exhibits a plastic ductile behavior and the failure was not reached. Actually, the failure in test 2 and in test 3 is due to columns damage which explains the sharp decreasing of the axial force.
In term of displacement, the more the column ages the less foundation vertical displacement is. With aging, SM columns become stiffer due to cement curing, but this makes brittle failure appears for lower displacement.

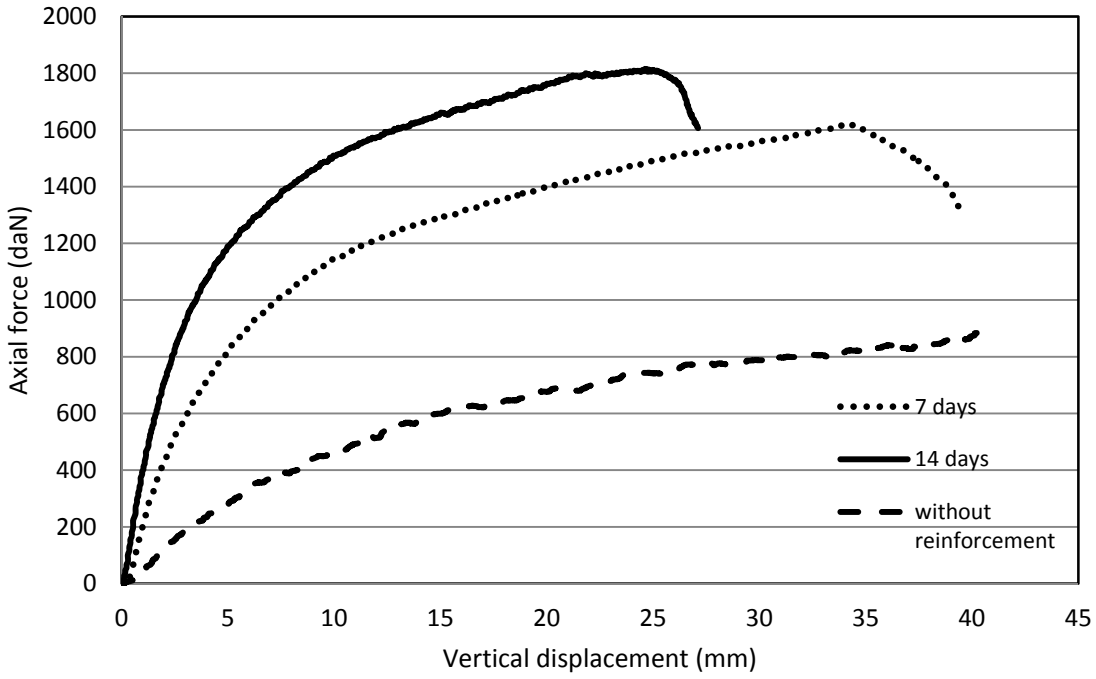

Figure 5: Evolution of the bearing capacity of foundation in terms of vertical displacement.

After testing, columns are taken out of sand to examine the failure mode and failure location. In both tests failure starts 16-19 cm from the head of columns.
In test 2, column is split in three parts. The first part from head to failure zone with 18 cm long and ends with a conic shape, the second part is from tip to failure area and it is 14 cm long and the third which is the damaged part is 13 cm long.
After the failure in test three, column is damaged into two parts. The upper part, from head to failure is 19 cm long and the rest of column collapsed into pieces.
UCS tests are performed on parts of columns in tests two and three. For 7 days column, specimens have 1.55 MPa resistance and 2.57 MPa for 14 days. As we are working in dry sand, water content test is carried out in order to show how much water remains in columns after curing period. Starting with 19.5% of water content, we reach 12% after 7 days and 2.7% after 14 days.
As a result and due to the dryness of our soil, we can predict that later tests on 21and 28 days will not bring a lot of resistance to our footing. SM column doesn't contain enough water to ensure the curing of unhydrated left cement.

Figures 6a-6b-6c: on the left, unloaded column and damaged column from test 2 - in the middle, failure of SM specimen taken from test 2 after a UCS test- On the right, failure of SM specimen taken from test 3 after a UCS test.

3. NUMERICAL MODEL

The SM column behavior was simulated by an axisymmetric model in ABAQUS. Both cases; with and without reinforcement were taken under consideration.
Numerical model dimensions are the tank dimensions (Figure 8a). The footing requires to be modeled as a circular plate.

The equivalent radius, r_{eq} =130 mm, was calculated according to equation:

$$r_{eq} = 0.5\sqrt{\frac{4S_m}{\pi}} \quad (1)$$

where S_m is the foundation section.
Figure 8a shows the FE mesh used in the analysis. It consists of 6-node modified quadratic axisymmetric triangle elements (CAX6M). In order to simulate contact between soil-mixing column and soil, interface elements with zero initial thickness with Mohr-Coulomb failure criterion were used. Friction coefficient is taken as tangent of 2/3 of soil friction angle. Interaction between foundation and soil is modeled by rigid constraints. It means footing and soil surface displacements are equal (Figure 8b).The boundary conditions are no horizontal displacement at the two lateral vertical sides. In the bottom boundary, displacements are restricted in both vertical and horizontal directions. Footing is loaded by imposing displacement until model collapses.

3.1. Parameters and constitutive law

The behavior of foundation was modeled by a linear elastic law whereas soil and both types of soil-mixing columns (after 7 and 14 days) were modeled using an elasto-plastic law with Mohr-Coulomb criterion. Parameters used in calculations are provided by experimental tests (Table 3).

Table 3: Material parameters

Parameters	Units	Footing	Sand	Soil-mixing column	
				7 days	14 days
Density	[kg/m^3]	7500	1500	1800	1800
Young's modulus	[MPa]	200000	80	220	300
Poisson ratio	[-]	0.3	0.3	0.2	0.2
Friction angle	[°]	-	39	40	46
Cohesion	[kPa]	-	1	700	700

3.2. Analysis of results

The ability of the numerical model to describe the response of reinforced soil is shown in Figure 7. It is observed that numerical predictions obtained from ABAQUS simulations show a good agreement with physical modeling. Numerical analysis provides larger elastic displacements (Table 4). The Figure 10 shows the ability of the numerical model to predict the failure. Displacements, stresses and plastic zones for soil reinforced by column 14 days after its installation are presented with more details in Figure 8. The maximum values obtained from calculations are 25.2 mm for footing displacements, 7996 kPa for maximum stress in the column.

Loading applied to the footing is distributed only on soil, in case without reinforcement, or both on soil and column in case of reinforced models. The repartition of axial stress under the steel plate is presented in Figure 9. Curves show that the concentration of stresses appears in the column zone and decreases sharply in the soil-column contact. It is because the most part of loading is bore by much stiffer column. Axial stress seems to be constant until the edge of the footing where it slightly decreases. The relation between average axial stress value in column and soil is presented by two parameters n_1 and n_2 defined as:

$$n_1 = \frac{\sigma^r_{yy}(soil)}{\sigma^{wr}_{yy}}, \tag{2}$$

$$n_2 = \frac{\sigma^r_{yy}(column)}{\sigma^r_{yy}(soil)} \tag{3}$$

Where:
σ^{wr}_{yy} – average of axial stress in soil without reinforcement (depth z=0mm – under foundation)
σ^{r}_{yy}(soil) – average of axial stress in soil with reinforcement (depth z=0mm – under foundation)
σ^{r}_{yy}(column) – average of axial stress in column (depth z=0mm – under foundation)

Table 4: Elastic displacements

Case	Experimental	Numerical
Without reinforcement	5 mm	7 mm
With reinforcement 7 days	4 mm	9 mm
With reinforcement 14 days	4 mm	10 m

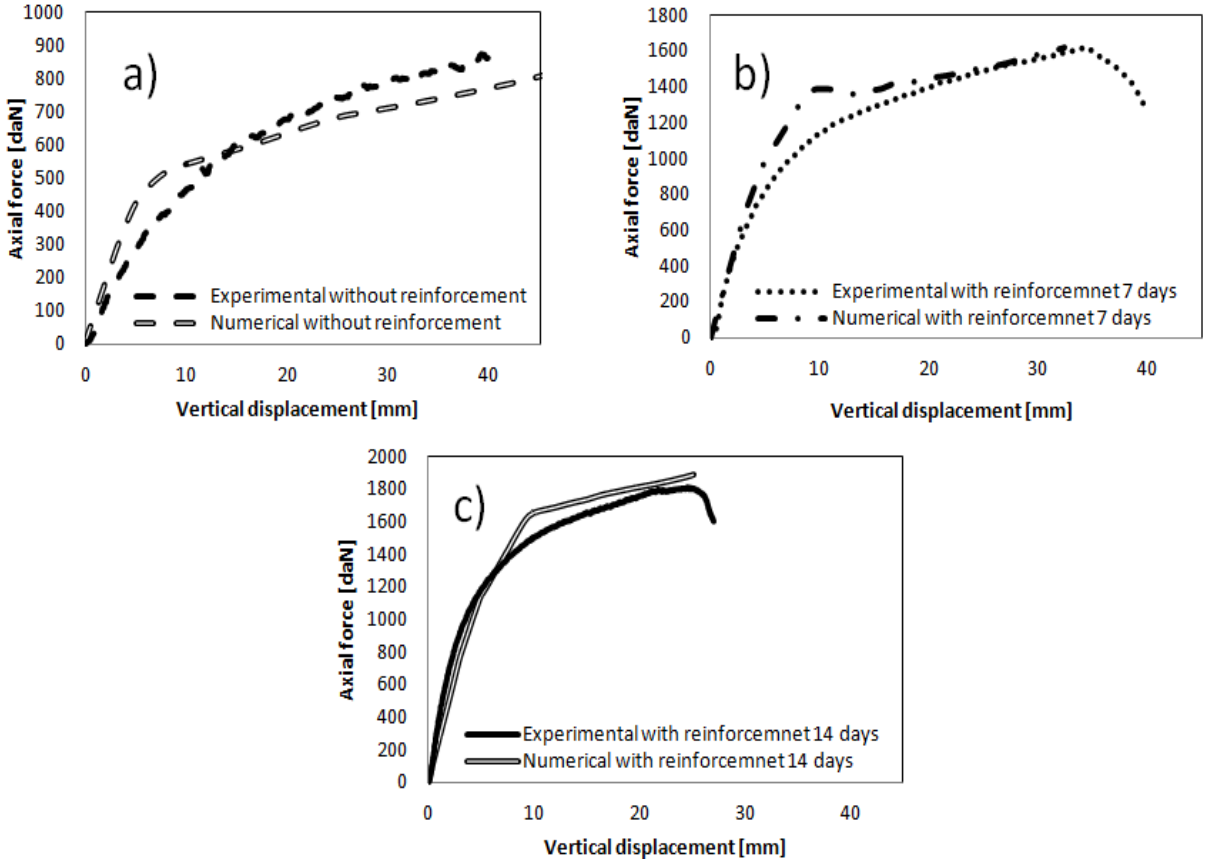

Figure 7: Experimental observations and numerical predictions of soil behavior: a- without reinforcement, b- reinforced by column after 7days, c- reinforced by column after 14days

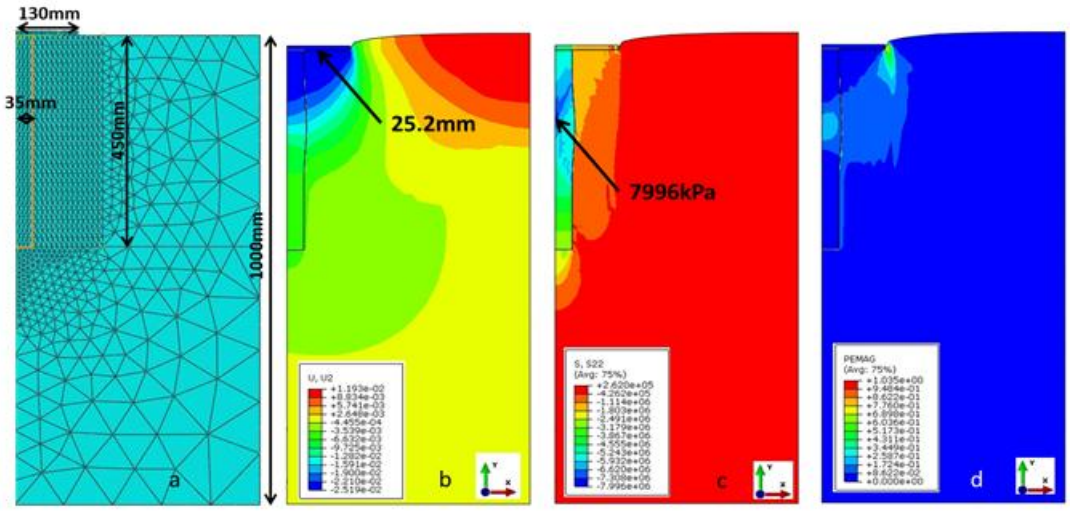

Figure 8: Numerical modeling results for reinforced soil (14 days after column installation): a- mesh and model dimensions, b- map of vertical displacement U_y, c- map of axial stress σ_{yy}, D) plastic zones

Table 5: Influence of reinforcement on axial stress distribution

Case	Average of axial stress [kPa]		n_1	n_2
	Soil	Column		
Without reinforcement	2209	0	1	0
With reinforcement 7 days	1089	4240	0.49	3.89
With reinforcement 14 days	1140	5025	0.52	4.41

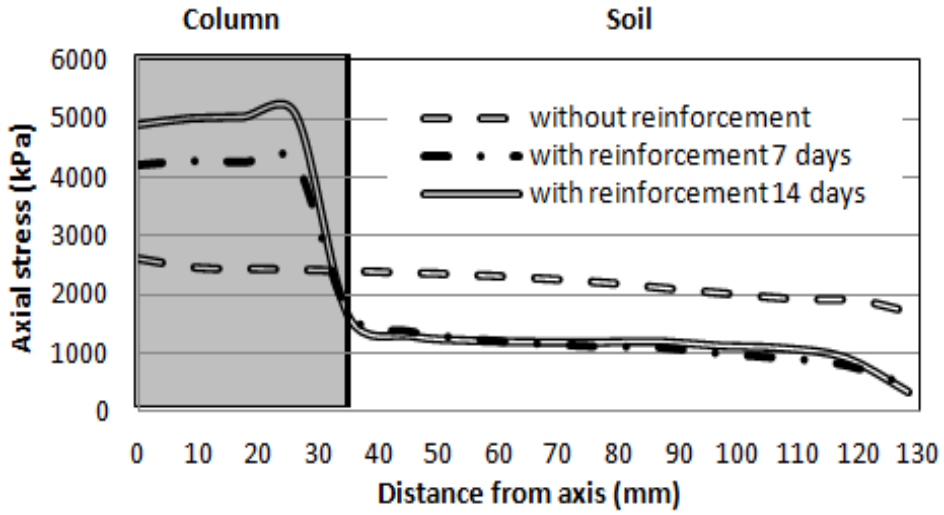

Figure 9: Axial stress distribution under foundation

The analysis was carried out until column failure. Location of axial stress concentration (P and Q presented at Figure 10b and 10c) as well as the conic shape (Figure 10b and 10c dotted line) obtained from calculations reveal good agreement between the numerical and experimental test (Figure 6a). FEM simulation predicted column's damage locus at depth 176mm for 7days case and 156mm for 14days case whereas measured values are about 180mm and 190mm respectively.

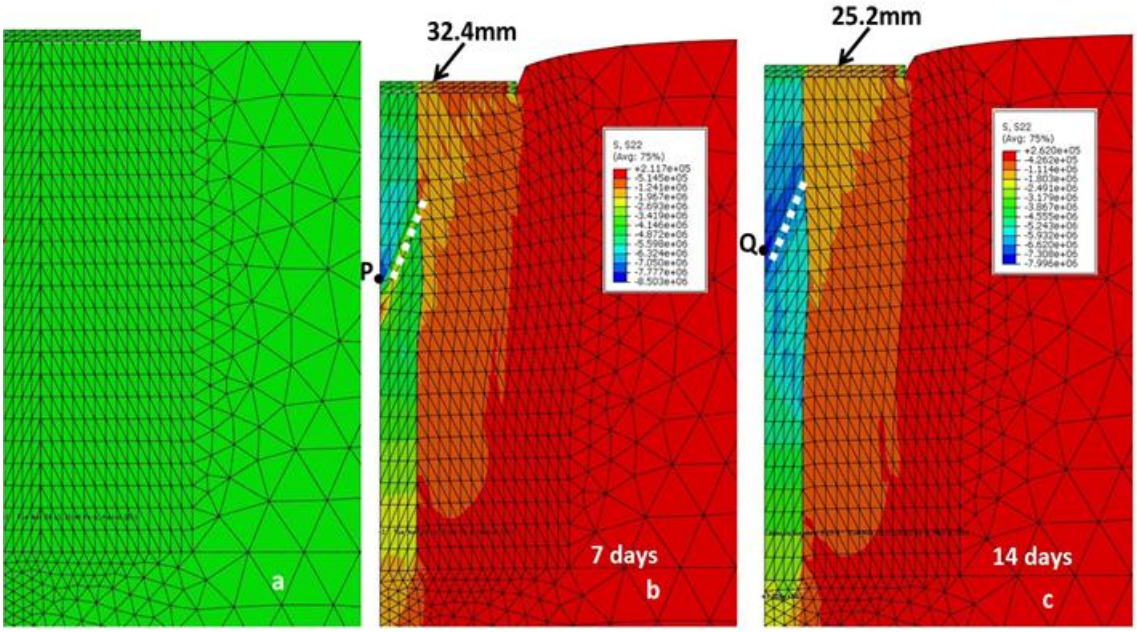

Figure 10: Column's damage location. a- undeformed mesh, b- deformed mesh and axial stress for the moment of column destruction in point P - 7 days, c- deformed mesh and axial stress for the moment of column destruction in point Q - 14 days

4. CONCLUSION

The physical model in this study highlight the differences between reinforced an unreinforced foundation and their behaviour under axial load. The effect of SM columns was investigated in this paper. The study included tests on cemented sand specimens. Some conclusions could be drawn:

- Cement dosage of 240 kg/m^3 gives a good resistance at 28 days that reaches 4MPa. This content could the best according to ratio resistance/ economy.
- Soil reinforced with SM columns has larger elastic behaviour than unreinforced soil which is in its majority plastic.
- With reinforcement, bearing capacity will be higher but foundation will stand smaller settlements.

- Numerical results obtained from simulations show a good agreement with physical modeling in cases of axial stresses and displacements.
- SM column failure location obtained from numerical analysis corresponds well with physical test observation.

After this study, a lot of future tests are foreseeable. The instrumentation of our model is primordial in order to show the contribution of SM columns and soil in the foundation resistance. In addition, other reinforcement models have to be tested, especially to emphasis the role of an interposed granular layer on the foundation behaviour. Heterogeneous soil case will studied also.

REFERENCES

Sariosseiri F., Balasingam M., 2009, Effect of cement treatment on geotechnical properties of some Washington state soils, Engineering Geology.

Fioravante V., 2011, Load transfer from a raft to a pile with an interposed layer, Geotechnique.

Ajorloo A., 2010, Characterization of the mechanical behavior of improved loose sand for application in soil-cement deep mixing, PhD thesis, Lille University.

Wang X., ZHENG J-J, Yin J-J.,2010, On composite foundation with different vertical reinforcing elements under vertical loading: physical model testing study, journal of Zhejian university/China.

Guimond-Barrett A., 2010, Protocole de référence pour la réalisation des mélanges sol-ciment en laboratoire, IFSTTAR.

Lee J.H., Salgado R., 1999, journal of geotechnical and geoenvironmental engineering, Determination of pile base resistance in sand.

Boulon M., 2006, Studia geotechnical et mechanica, Amélioration du frottement latéral dans les sols fin.
Spécifications générales du projet RUFEX, 2011, Renforcement er réutilisation des plateformes ferroviaires et des fondations existantes.

Design, Construction and Monitoring of a Test Section for the stabilization of an Active Slide Area utilizing Soil Mixed Shear Keys installed using Cutter Soil Mixing.

Sarah Gaib P. Eng., British Colombia Ministry of Transportation and Infrastructure, Canada, Sarah.Gaib@gov.bc.ca
Brian Wilson, P.Eng. Golder Construction Inc., Canada, BWWilson@golder.com
Emilie Lapointe, EIT, Golder Construction Inc., Canada, ELapointe@golder.com

ABSTRACT

The Fountain Slide is located on Highway 99 approximately 17km east of Lillooet, British Colombia, Canada. The slide, which is part of an ancient earthflow, has been active for decades, and is some 205m wide at the highway, extending from just below rail tracks, located 55m above the highway, down to the Fraser River which is approximately 85m below the highway, incorporating about 750,000m^3 of material.

In 2007, as a result of extensive slide movement at the highway, the British Colombia Ministry of Transportation and Infrastructure converted approximately 300m of the paved road surface to gravel so that it could be better maintained. A comparison of aerial mapping from 2006 to 2009 indicates that some areas of horizontal movement above the highway have exceeded 4m in three years. The sliding mass has continued to deform requiring frequent monitoring and additional maintenance to keep the highway operational.

Review of the monitoring data indicates that the active Fountain Slide moves constantly throughout the year. Rates of movement at the surface and along the failure plane have increased in the past year to in the order of 10mm/day, initiating the requirement to investigate and evaluate stabilization options.

Following an internal assessment of the engineering parameters of the slide and a review of potential stabilization options, the Ministry elected to design and install a test stabilization section comprising a series of soil-cement shear keys installed using Cutter Soil Mixing. This paper presents the background data to the slide evaluation, an overview of the conceptual design and rationale for the test section, the challenges and experiences gained during installation of the test shear keys, as well as the results of both the on-going monitoring of the slope and the in-situ strengths achieved in the soil-cement shear keys.

1. SITE LOCATION AND GEOLOGY

The site is located along Highway 99 in south-western British Columbia, Canada, about 17km east of the town of Lillooet, and approximately 300km northeast of Vancouver *(Figure 1)*.

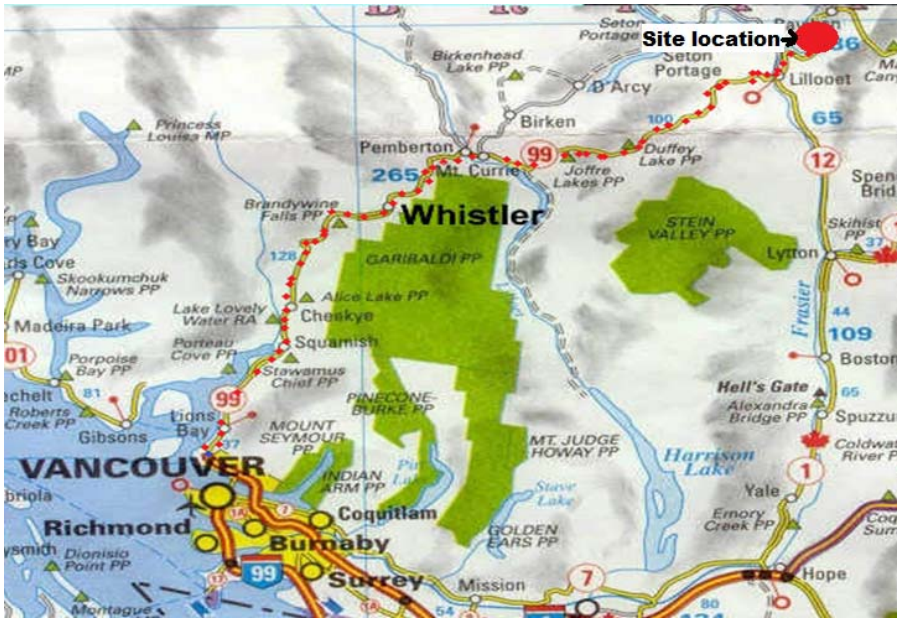

Figure 1: Site location

The active slide is part of a massive postglacial earthflow known as the Tunnel Earthflow as seen in an overview of the site in Figure 2.
The Interior Plateau region of BC is an arid area of the province. Thirty years of weather data from Environment Canada for Lillooet Seton recorded at an elevation of 200m, indicates that temperatures vary from extreme highs of 40˚C in the summer to extreme lows of around -30˚C in the winter. Average annual precipitation is 330mm. Local data for the slide area is unavailable but conditions are similar.

Most earthflows in the BC interior are post-Pleistocene and have developed in areas of poorly lithified Tertiary sediments dominated by shale, mudstone, or clay, or in areas underlain by volcaniclastic rocks which have suffered prolonged subaerial weathering or hydrothermal alteration *(Bovis, 1985)*. Locally the sedimentary rocks are interlayered with volcanic deposits.

1.1. Site history

The highway in this area was built prior to 1950 likely using cut and fill techniques common during that time. In 1970 the highway was widened. Fountain Slide first appeared as a small slide below the highway, with tension cracks initially appearing along the outside edge of the highway. A major realignment was completed in 1989 to address the ongoing deterioration of the road surface with a second realignment in 1995 to address accelerated movement. The slide volume has increased with time and the upper boundary now extends above the highway as far as the CN Rail track some 55m upslope.

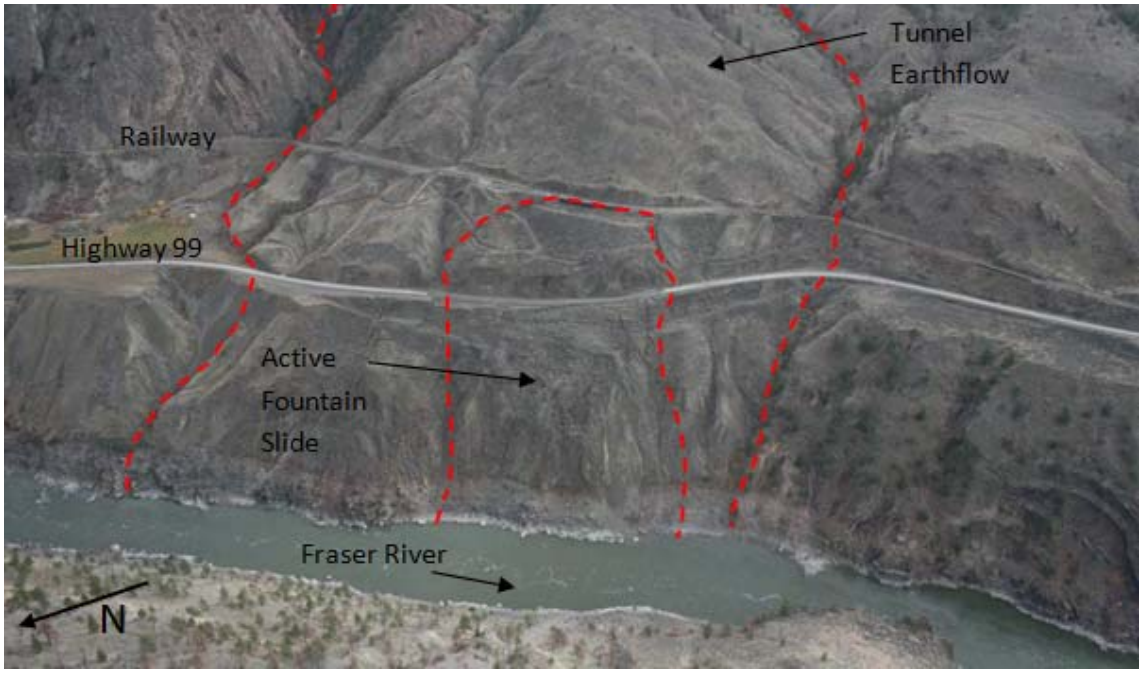

Figure 2: Aerial view of Tunnel Earthflow and Fountain Slide

Currently the Fountain Slide is bordered by the CN Rail tracks to the southeast and the Fraser River to the northwest. The highway elevation averages about 305m, with the CN Rail tracks at elevation 359m and the Fraser River at elevation 220m. The slide currently extends from the rail tracks to approximately 20m above the Fraser River, elevation 240m. The width of the failure is defined by tension cracks approximately 205m apart at the highway elevation and the average slope length between the slide toe and the railway is approximately 300m. The estimated landslide volume is 750,000m^3.

Prior to 2006 average movement rates were recorded at 1mm/day using surface survey monitors. Aerial LiDAR was completed in 2006 and again in 2009, the data indicates movement during that period predominately occurred in the section of the slide between the highway and railway. During that time period, movement below the railway was determined to be in the order of 3-5m vertically down, with lateral movement of the cut slopes at the highway of in the order of 3m out of the slope. A number of large tension cracks opened up on the slide surface above the highway as shown in Figure 3. The open cracks were 2-3m wide and roughly 10m deep based on the LiDAR.

Figure 3: Aerial view of slide - October 2009:[1]

Since 2009 movement rates have averaged 5mm/day, with observations of up to 10mm/day during periods of increased activity. Standard 70mm slope indicators installed in both 2009 and 2010 were sheared within 2 weeks of installation. It is theorized that initially movement may have occurred on a number of individual slide planes, but as time went on and movement increased, the failure surfaces appear to have aligned or become connected resulting in increased movement rates. As a result there has been a requirement for significant ongoing maintenance of the highway.

Since 1989 twenty-two drill holes have been completed at the site. Review of these boring logs indicates a very heterogeneous profile with little to no consistency in soil stratigraphy across the site. For the most part, the matrix is composed of predominantly fined grained soils, equal parts clay and silt, with sand and gravels, and to a lesser extent, occasional boulders of volcanic origin. Seventeen slope inclinometers have been installed within the slide area since 1989 allowing a reasonable definition of the sliding plane(s). A number of piezometers have been installed, and these do not indicate excessive piezometric pressures at the slide plane. Review of monitoring results indicates that, in general, the slide area does not seem to move as a single body, instead different segments of the slide appear to move at different rates and to some extent at different times. Some signs of seasonal seepage appear on the slide slopes, and as expected, increased movement is seen during wetter times of the year. More recently the mass above the highway appears to be moving faster than the mass below the highway.

2. ANALYSIS

Based on slope indicator data the failure appears to occur within a distinct layer, which is thought to be more or less continuous across the slide. The plane of failure is inferred to be inclined at approximately 22˚ based on projecting the failure plane from instrumentation and surface cracks. Analysis of the slide was carried out using the limit equilibrium slope stability program SLIDE 5.0, with the groundwater located just above the failure plane as recorded by piezometers, and soil parameters generalized across the site as follows:

Soil Parameter	**Compact to dense Silty, Sandy GRAVEL**	**Loose/soft Gravelly, Sandy SILT (Residual)**	**Very Dense Sandy, Silty GRAVEL with cobbles**	**Hard Gravelly, Sandy SILT**	**Solid BEDROCK**
Unit Weight γ'(kN/m^3)	20	20	21	20	24
Cohesion C' (kPa)	0	0	0	100	1000
Friction Angle φ' (°)	31	-	35	30	40
Residual Friction Angle φr (°)	-	20	-	-	-

Results of the analysis indicate a calculated factor of safety of 0.92 for a shallow failure surface below the highway, consistent with the originally noted movement, and with a factor of safety of 1.25 for a shallow failure surface above the highway, *i.e.* one daylighting at the road surface. Modelling the active slide surface inferred from the site investigation data, and extending from above the Fraser River to the railway elevation, produces a factor of safety of 1.05 using the residual friction angle of 20° in the soft silt, hence there is reasonable agreement between the stability model, observations and instrumentation data. A deep seated failure surface yields a factor of safety of 2.26. There is no evidence of this type of movement.

2.1. REVIEW OF OPTIONS

Standard approaches for remediation of the slide have been considered. These included improving drainage conditions, changing the slope geometry and adding passive or active measures. While costs and impacts to traffic were factors, the ongoing movement, and associated safety concerns were the most important considerations in assessing the likely effectiveness of proposed remedial options. Further realignment outside the active zone was not an option since it would require over 3km of highway relocation.

Drainage works within the slide were not considered feasible given the rates of ongoing movement. Instead a 5m deep trench drain was installed upslope at an elevation of 560m to limit water flows in the slide area. This work was not expected to stabilize the slide, but rather to reduce the infiltration of groundwater which would hopefully slow further movement.

General resloping of the slide area was not pursued due to space limitations and the concern that any redistribution of material may cause the failure plane to retrogress further up the hillside. However in the fall of 2010, a localized area of the slope between the highway and railway was graded to close open tension cracks. No material was removed from the site during this work.

Active measures evaluated, with the objective of enhancing the factor of safety to a value of about 1.2, included a retaining wall with soil anchors, and a piled wall. For both these structural solutions, estimated costs were prohibitive irrespective of the fact that the observed ongoing movements of the slide would significantly complicate the work, particularly with respect to short-term loads on anchors during the construction sequence.

The last option considered for stabilization was the use of Cutter Soil Mixing (CSM), a form of Deep Mixing (DM) to develop in-situ shear keys across the slide area. While initially not considered an ideal application of the technology due to the relative density of the soils, this option was pursued as a test section based on experience gained on a similar project on the Alaska Highway and because of the low comparative cost compared to other options. In addition the method could allow for single lane traffic to be accommodated during
construction, and, most importantly no excavation would be required to complete the work.

3. DEEP MIXING/CUTTER SOIL MIXING

Deep mixing (DM) is a technique that involves the addition of binders (most commonly combinations of cement, lime, gypsum, and slag) to in-situ soils to create a chemical reaction product which bonds the soil particles together and results in improved soil mass consistency, strength, and deformation characteristics. The improved soil strength and stiffness within the DM zone can be utilized to limit both vertical deformations from fill and building loads as well as horizontal deformation due to slope instability. Deep mixing has been used successfully in many environments around the world for the support of structures on weak foundation soils, for the stabilization of highway embankments and remediation of slope instability, for the support of vertical

excavations, and for the containment of groundwater and stabilization of contaminants in-situ. While the performance of the improved soils are largely a function of the nature and quantity of binder added to the soil, the nature of the original soil can have significant impact on the engineering properties of the final product, particularly with respect to strength and stiffness.

DM methods rely on the physical mixing of in-situ soils with binders using mixing shafts or other means to form in-situ columns or panels of strengthened soil. While there is a growing variety of equipment available to complete this type of work, the methods typically fall into one of three main categories – vertical axis rotation, horizontal axis cutting wheels, and vertical continuous trenching. The former of these can employ wet or dry binder additions whereas the other methods are typically restricted to the use of wet binder.

Traditional vertical axis DM machines, such as those developed in Japan and Scandinavian countries, are constructed with mixing shafts consisting of auger cutting heads, discontinuous auger flights, and mixing paddles. They can vary from single to 8-shaft configurations depending on the purpose of the DM. The machines install augers from the surface into the existing ground, the augers are turned, and binders are added to the soil in-situ, forming a strengthened column of ground. The shape of the column is a function of the configuration of the mixing head and can vary from a single circular column to a short wall of interlinked circular columns. By virtue of the technique, these methods tend to be used in areas with soft to medium consistency soils. The columns have a higher proportion of overlap than other methods and hence have a greater consumption of binder (cement) for the same effective area. Furthermore, the cross section is not structurally efficient.

Cutter Soil Mixing (CSM) utilizes horizontal axis cutting wheels, which allows for the installation of rectangular-shaped panels resulting in a more efficient use of cement, and creation of a more structurally efficient and relatively homogeneous section, particularly where the design is required to resist bending and large shear forces. The method is also better suited to penetration through stiffer or denser soil deposits such as those at the Lillooet site.

As indicated below, CSM uses two cutting wheels rotating about horizontal axes (*Figure 4*). These are supported on a Kelly bar, typically mounted on a large drill. By rotating the cutter wheels with sufficient torque, and applying downward crowd force via the Kelly Bar, the CSM is able to cut a vertical slot into the ground, thoroughly breaking up and mixing the soil, while injecting suspension fluids such as cement slurry to create a liquefied panel of soil. The suspension is pumped through a port located between the wheels for optimum delivery and ease of mixing. Due to the rotation of the cutting wheels about a horizontal axis, and the novel tooth and cutting wheel design, the cutting head is able to penetrate dense layers of soils and thoroughly blend and mix the in-situ soils with the added suspension. In the case of a cement slurry suspension, hydration of the cement results in strength gain of the liquefied column producing the desired stabilized soil reinforcing element. A summary of the sequence involved in CSM panel/column construction is depicted in Figure 5.

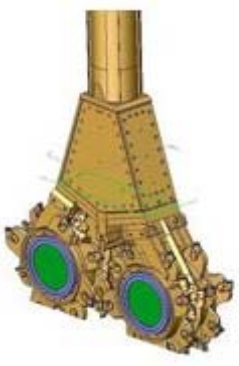

Figure 4: CSM Cutter Head

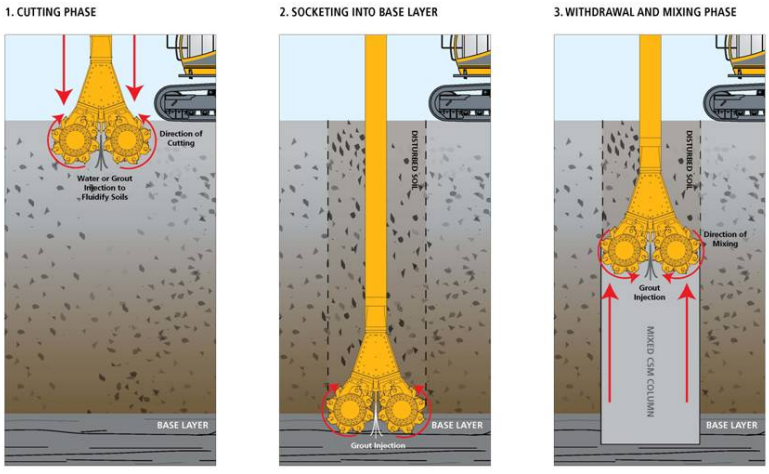

Figure 5: Schematic of CSM Panel Construction

Due to the nature of the equipment, a wall is constructed in a series of interconnected panels or columns which form a larger continuous wall. A series of primary panels are installed initially and allowed to achieve initial set of the mix, allowing the panels to remain intact as the area adjacent to them is mixed. Secondary panels are then installed to overlap with and link the primary panels. The secondary panels cut into the primaries to ensure an

intimate connection. Timing of the delay between primaries and secondaries is often selected to complete the connection while the curing process of the cement in the primary panel is ongoing. This avoids the development of "cold joints" and helps make sure that the wall functions as designed. Control of the overlap is achieved by careful monitoring of the on-board computer system which is able to identify the position of the cutter head to within about 25mm in any direction. Data from the system is recorded to electronic files which are then available to the engineer for review to check that the minimum design overlap has been achieved. These data files also allow the engineer to review items such as suspension volume, mixing time, cutting resistance, and other parameters that provide a record of the wall construction including total depth, penetration into the key material, suspension volume and degree of mixing, and of course, overlap of adjacent panels.
One of the major differences between the CSM approach and that of other DM techniques is that the cutting head design generates sufficient torque to allow walls to extend relatively deep into competent soil and/or relatively soft rock strata, thereby providing a mechanism to construct walls through stiff zones, or in the case of slope stability or load transfer applications, allow provision of the all important key into competent strata at depth with a high level of quality control. By moving the cutter vertically through the soil, the technique also allows vertical blending of layered soils to provide a relatively homogenous mix in the vertical panel.

The following illustrations show the differences in section between a CSM wall and a secant (auger mixed) column wall. The number of joints in a secant column wall is a function of the number of augers in the DM system. At each joint there is significant overlap required to provide a wide effective section hence there can be significant waste.

Several sized cutter heads are available for deployment with the CSM depending on the application, geotechnical conditions and the specifications. Each have different torque ratings and hence ability to penetrate dense strata. For the Lillooet project a BCM 10 cutter head was used producing panels of treated soil 1m thick by 2.8m long, extending to the design depth. To achieve a similar cross section using multiple auger systems would require the use of a four auger system with 1.22m diameter augers which would result in an effective wasteage of about 15 to 20% of the volume.

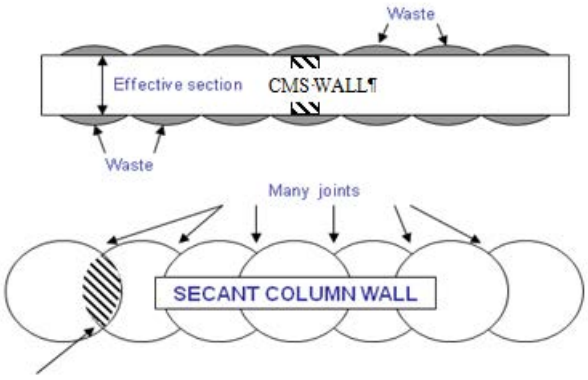

Figure 6: Comparison of CSM Construction with traditional DM methods

4. DESIGN OF TRIAL SECTION AND SELECTION OF TARGET STRENGTH

Based on the information derived from the slope stability analyses, a review of the site access constraints, and the findings of the research by Filz and Navan (2006) regarding the efficiency of shear walls relative to that of individual columns, it was proposed to construct a trial section consisting of a number of subsurface shear walls, or barrettes, across the eastern end of the active slide area to allow evaluation of the approach. A total of 20 barrettes, each approximately 8.0 m long and made up of 60 individual panels of cement-treated soil would be constructed with an orientation perpendicular to the slide. The barrettes were distributed along the affected highway alignment, with barrettes spaced at centre to centre distances of 3.0 and 5.0m in an effort to provide different levels of resistance against sliding across the test section. A layout of the works is presented in Figure 7.

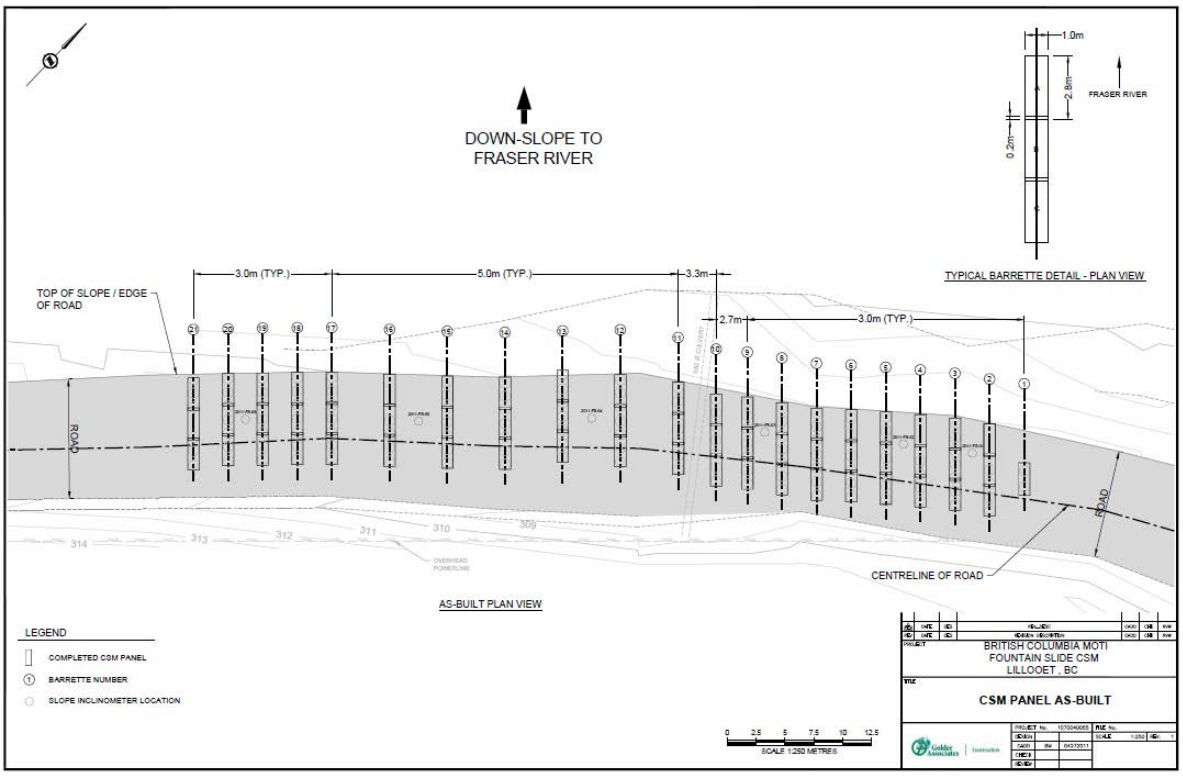

Figure 7: CSM Barrette Layout Plan

Utilizing the results of both the previous long-term monitoring, and the slope stability analysis the barrettes were constructed such that they extended beyond the estimated depth to the slip surface and were embedded at least 1m into the underlying competent till layer. To gain the required level of shearing resistance required by the analysis, soil strengths within each of the barrettes was specified at a minimum Unconfined Compressive Strength [UCS] of 2MPa to yield a shear strength of about 1MPa. For contractual purposes the time to achieve this strength was initially set at 14 days, however it was recognized that substantial strength increase was likely to occur beyond the 14 day period. Based on experience, and the characteristics of the in-situ soils, it was estimated that a cement content of in the order of 350 kg/m^3 would be required to achieve the specified strength at the 14 day time period.

The location of the test area within the slide was chosen to take advantage of the relatively consistent road grades at the eastern end of the site, and to avoid, as far as was practical, interference of equipment with the overhead utilities. This location also allowed for the best management of traffic on the highway, which had to be fully accommodated throughout the construction period with temporary road shut-downs of only 20 minutes allowed.

5. FIELD IMPLEMENTATION

Golder Construction Inc. (formerly GAIA Contractors) was selected to construct the trial section following submission of a tender to the BC Ministry of Transportation and Infrastructure. A BCM 10 CSM cutter head mounted on an RG19T drill rig was deployed to the site on March 3, 2011. In addition, and in expectation that the soils at this site would be sufficiently dense to result in poor productivity of even the BCM 10 cutter head, a BG18 drill rig was also deployed to assist with possible pre-drilling and hence loosening of the upper portion of the in-situ soils. Initial barrettes were installed without the benefit of pre-drilling however, as expected productivities were such that the economics of the project would be unacceptable based purely on the progress of the CSM rig on its own, and hence pre-drilling to about 2.0 m above the postulated shear plane was incorporated into the program.

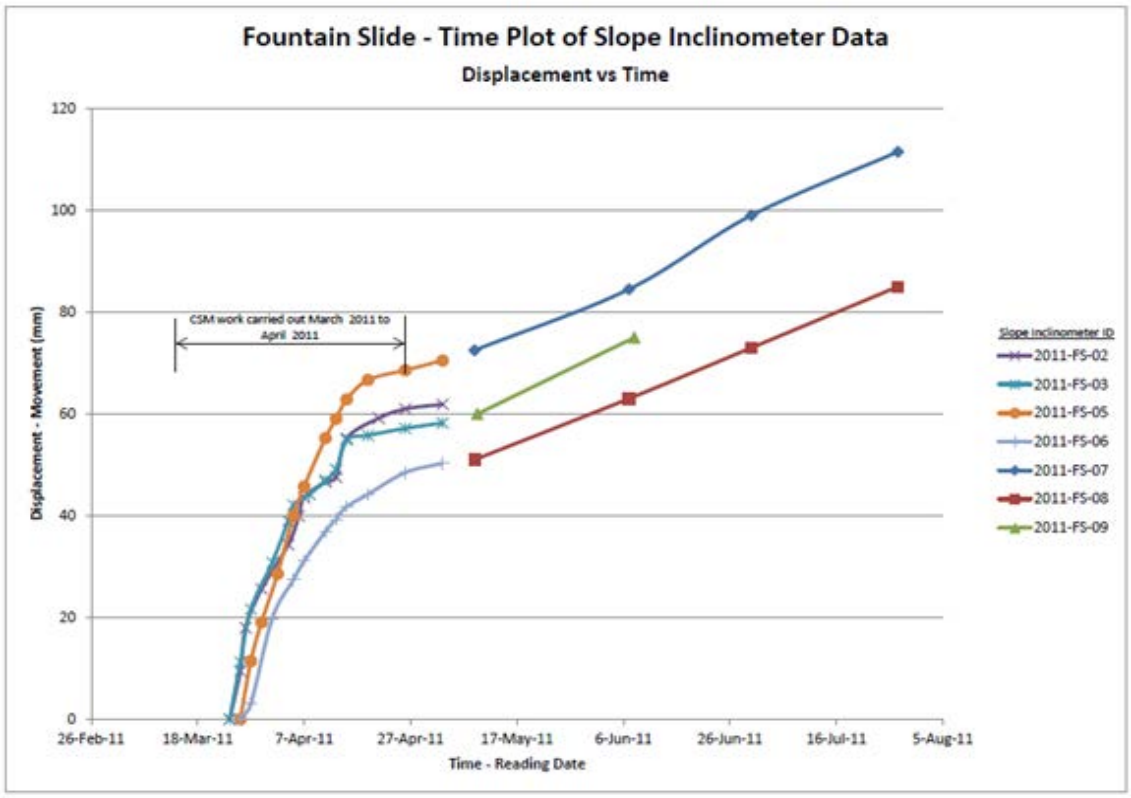

Figure 8: Slope Inclinometer Data

Due to the site geology, and the fact that Lillooet is located in a relatively arid region, in-situ moisture contents of the native soils were low and it was found that a large volume of grout and or cutting water was required to both advance the individual panels and to maintain the column in a liquefied state so as to permit withdrawal of the cutting tool. A small quantity of bentonite was therefore added to the mix during the second week of panel installation in an effort to develop a filter cake on the sides of the cut slot, and maintain the fluidity of the panel during construction. This process was generally successful, however previous experience of bentonite in soil improvement mixes indicated that the addition of bentonite even at the cutting stage can impact the final panel strength, hence this aspect was carefully controlled.

The strategy of using bentonite was generally successful, but not completely. Since the work was being completed on an active slide, with movements at the start of construction of in the order of 10mm/day, it became apparent that in portions of the site, tension cracks were either already present or opening up, and that in occasional panels we suffered rapid loss of fluid and/or movement of the surrounding soil. From a general operational perspective this required that the CSM cutter head be regularly cycled vertically through the column to ensure adequate moisture and mixing, as well as clear access for withdrawal. A loss of fluid above the cutting head would result in a localized decrease in the water-cement ratio potentially leading to an early set of the mix and subsequent difficulties in withdrawal. Regular cycling of the head typically avoided such occurrences however one such incident did occur during cutting of the key-in portion of a very deep panel. Manipulation of the cutter head and expansion of the panel in the longitudinal direction by rotating both cutting wheels in the same direction was ultimately necessary to free the cutter head from what could have been a very cementitious grave.

Even with pre-drilling of the upper portion of the panels, the maximum productivity achieved on site was four panels in one 12 hour shift, the total of 60 panels being installed over a period of 30 working days. At least one panel was sampled during each day of operation with wet grab samples of the mixed soil taken at two depths within the panel. Samples were taken using a bailer fitted to the cutter head, the head being replunged to the selected sampling depth following completion of the panel. Cylinders were cast and stored on site, with subsequent testing at 14 days in the field laboratory. As a check on the reliability of the wet grab samples, six of the barrettes were cored when the panels had achieved at least 21 day strength to allow corroboratory testing and provide a visual indication of the quality of the soil-cement mix over the entire depth of the panel.

Panel installation across the site was sequenced to avoid a concentration of effort in one specific area due to concerns that the addition of fluid for cutting may in fact accelerate movements on a local basis. The drawback of this approach was that it was not possible to develop full barrettes in any portion of the site until quite late in the process and hence individual panels were exposed to on-going shearing from slope movement throughout the process. Nonetheless, daily monitoring of both surface survey monitors and slope inclinometers installed early in the construction process indicated that the progressive installation of barrettes appeared to reduce the magnitude of slope movement throughout the construction period, and more noticeably, after about 10 to 15 days when the first panels had achieved in-situ strengths close to the target design strength. Plots of a select number of slope indicators are included as Figure 9 which clearly shows the effect of test section construction on the overall slope movement. Unfortunately, road reconstruction work following completion of the CSM barrettes damaged a number of slope indicators requiring that additional slope indication be installed to facilitate long-term monitoring.

6. QUALITY CONTROL (QC)/QUALITY ASSURANCE (QA)

As indicated above, the quality control program on site included the recovery of wet grab samples from at least one panel on each day of operation, and typically from at least two depths within the panel. Each grab sample was used to cast 6 cylinders to allow testing at 7, 14 and 28 days. The seven day tests were used to provide an indication of any suspect columns, the fourteen day tests to allow comparison to the specification, and the 28 day to provide assurance that the target strength would be met, if there was concern regarding a 14 day result. In addition to the sampling of the panels the quality control process involved regular monitoring of the specific gravity of the cement slurry and review of the automated batch plant records to verify the water-cement ratio of the injected slurry, as well as review of the CSM computerized reports which record the quantity of slurry injected over each 200 mm vertical increment and the total volume injected over the entire depth of the column.

Wet grab samples were also used for quality assurance, however coring of panels was viewed as the best means of verifying actual strengths in-situ with core samples typically tested at 56 days to verify strength. The computerized reports from the CSM were used to provide evidence of consistency of construction process and slurry addition. Results of UCS testing from a number of panels, including several that were subsequently cored are shown in Figure 9.

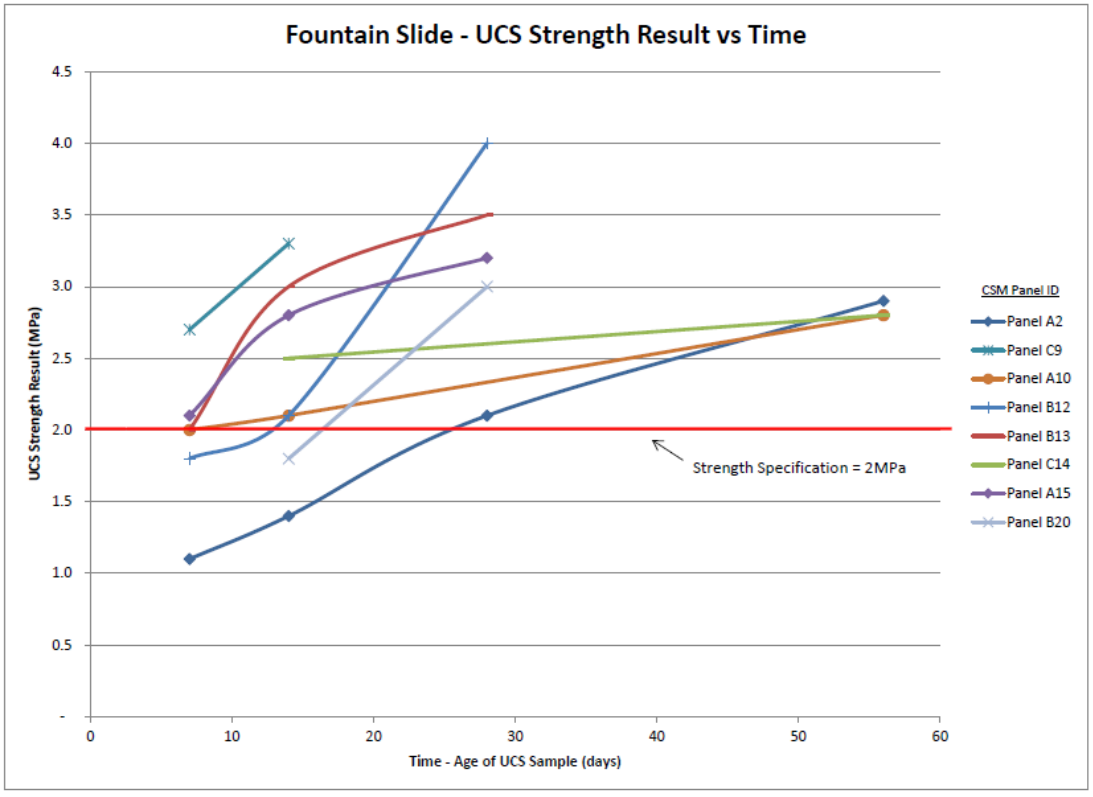

Figure 9: UCS Test Data

Several issues came to the fore throughout both the QC and the QA processes. The sampling technique adopted for recovery of wet grab samples at this site had been used very successfully on previous projects, but gave rise

to a number of issues on this site due to the nature of the in-situ soils, the low water-cement ratio used to try to achieve relatively high early strength, and the mechanics of the sampler itself. The system used was akin to a traditional borehole water bailer in that, as the cutter head was advanced through the soils, the material would flow up through the sampler, and only upon retrieval, would the bottom flap of the sampler close recovering sample from the target elevation. This process has typically been very successful in soft deposits with little or no gravel and cobble sized fraction, and where the water-cement ratio of the mix is high and the column of treated soil remains in a generally liquefied state during the construction process. As discussed above, the nature of the in-situ soils and the loss of fluid in several panels meant that in some instances the consistency of the soils in the upper portion of the panel, where the cement content was not as high, by design, would be such that the soils would clog the bailer and effectively act as a plug as it was lowered through the column of treated soil. This plug would then be trapped during withdrawal with the consequence that the recovered sample would be unrepresentative of the material at depth. Use of a sampler that allows activation of the sample port at the target depth is likely to resolve this issue.

Coring of panels also presented challenges. While in general core recovery was good, experience on previous projects had indicated that an exceptionally good driller is required to obtain core from such weak materials. The difficulty in this process is influenced by a number of factors however one of the most significant is the presence of gravel size fractions in the in-situ soil. Where gravel was present and coring was advanced at even moderate speed there was significant lack of recovery. Where the coring was completed very cautiously full core was recovered but, the outer surface of the core showed significant signs of damage from gravel particles grinding at the face of the core barrel. It does not take much to understand that with higher rotational speeds these gravel particles would all but destroy the relatively weak soil cement matrix. Coring at the site typically resulted in core recovery of about 75% of the total drilled length.
Results of UCS testing of cored and wet grab samples are presented in Figure 9 and show significant scatter. This is attributed to the variation of the effective in-situ water:cement ratio and the heterogeneity of the soils at the site.

7. MONITORING/OBSERVATIONS

A total of 11 slope indicators were installed within the area treated using CSM. Two of the initial installations were sheared (as they were installed before the work was completed) and several others have been damaged by traffic and/or road regrading activities. The remainder show a marked decrease in the rate of movement across the slope (Figure 8). The slowing of movement occurred gradually as the number of installed panels increased and the soil-cement gained strength, however monitoring results six months after completion of the works still indicate movement albeit at a slow rate. It is unknown how much movement will take place before the soil is fully constricted or if the soil will continue to move slowly perhaps because the barrettes are spaced too far apart, are of insufficient length to provide the shearing resistance required to fully halt movement, or are operating at residual strength levels due to the shearing that occurred during the early part of construction and hence are of insufficient capacity. Data collected at the site has indicated a reduction in movement from in the order of 10 mm/day to between about 0.3 and 1mm/day six months after work completion. There appears to be little difference in the movement rates between the 3m and 5m spaced panels. It is anticipated that monitoring will continue at least until the summer of 2012.

Aerial LIDAR has been completed bi-monthly since the completion of work. Only small localized slopes movements have been noted. It is unclear how much load the test section will take, or can tolerate, from the slide mass upslope of it, and it is too early to determine how wide of an influence shadow the test section has.

8. CONCLUSIONS

The test section has been a success. It has demonstrated that the installation of Deep Mixed shear keys through the failure horizon is technically feasible and effective, and that the use of CSM provides an economically viable construction method for this type of work. Completion of the trial section has shown that such work on an active sliding area is possible but not without its' challenges. Provision of additional redundancy in the installation to allow for shearing of the installations while strength is gained in the system needs to be factored in. Furthermore it may be prudent to design future installations using residual strengths for the soil cement panels.

The test section has slowed down the relatively rapid movements that had been observed in recent years and has reduced the level of maintenance required along this section of highway. The treated area will attract additional load but the residual strength is still much greater than the original in-situ strength. The Ministry of Transportation and Infrastructure will continue to monitor and observe the slope, particularly through the spring melt, traditionally a time of increased movement at this site, and will assess the next steps.

REFERENCES

Bovis, M., 1985, Earthflows in the Interior Plateau, Southwest British Columbia, Canadian Geotechnical Journal, Volume 22, Number 3, August 1985. P. 313-334.

Filz, GM and Navan, MP (2006. Stability of Column-Supported Embankments, Virginia Transportation Research Council, Charlottesville, Virginia.

CSM-Cutter Soil Mixing – Worldwide experiences of a young soil mixing method in challenging soil conditions

Franz-Werner Gerressen, BAUER Maschinen GmbH, Germany, franz-werner.gerressen@bauer.de
Thomas Vohs, BAUER Maschinen GmbH, Germany, thomas.vohs@bauer.de

ABSTRACT

The CSM -Cutter Soil Mixing- developed by BAUER Maschinen GmbH, is a new and effective method of deep soil mixing, based on the principle of trench cutter technique. It is mainly used for the construction of cut-off walls, earth retaining structures, and ground improvement. As it is derived from BAUER Cutter technology, the system extends the applicability of the soil mixing into much harder strata; as the self-hardening slurry is being introduced, soil formations can be easily penetrated, broken down, and mixed with the slurry, using the cutter wheels as cutting and mixing tool. Hence a very intensive intermixing of loosened soil and self-hardened slurry can be achieved. The system has been in operation since 2003, it has been used all over the world and has proven to be effective in various soil conditions ranging from soft to hard cohesive soils, loose to very dense granular material, and socketing into rock. It has achieved excellent results both technical and economical. Its use has been extended to replace many Jet Grouting and other conventional deep soil mixing projects as well as plastic diaphragm walls, sheet piles and other cut-off walls on prestigious projects.

1. INTRODUCTION

BAUER Maschinen GmbH developed the CSM technique in 2003 by drawing on the experience gained in the production and deployment of diaphragm wall cutters in the construction of cut-off and diaphragm retaining walls in the early stage the development was done in a Joint Venture with Bachy-Soletanche. Since 2003 more than 160 CSM jobsites were documented by BAUER.

2. CONSTRUCTION PRINCIPLE

The CSM System differs essentially from traditional techniques in that the in situ mixing of the existing soil with self-hardening slurry is performed by mixing tools rotating about horizontal axis rather than the traditional vertical axis. The in-situ soil mixed with self-hardening slurry produces a wall construction material that takes on the role of a cut-off and/or structural retaining wall.
The cement and bentonite content and the water/cement ratios of the mixing slurry are determined by the strength and/or permeability requirements of the project and the properties of the soil being mixed. In general, for a stronger wall, cement content is increased and water/cement ratio is lowered. Typically, sandy soils will require a larger amount of bentonite in the slurry than clays. At some clay sites where enhanced resistance to permeability is not required, acceptable liquefaction of the soil can be achieved without the use of bentonite.
A typical construction sequence is as follows:

a) Construction of a open guide trench for retaining excess slurry.
b) Liquefaction of the soil mass during penetration to the final depth as an appropriate slurry is simultaneously introduced. Depending on the prevailing conditions, either bentonite slurry is added to the mixing and liquefaction process or cement slurry is introduced into the soil during penetration. The volume of slurry injected is determined by the rate of cutter penetration.
c) During upstroke, the precise volume of slurry required for producing the final wall construction material is injected.
d) A continuous wall is formed by the construction of individual panels in an alternating sequence of overlapping primary and secondary panels. Secondary panels can be constructed immediately after completion of primary panels, i.e. „wet-into-wet“. The cutter technology does, however, also enable cutting into panels that have already hardened, i.e. “hard-into-hard".
e) To utilize the wall as a structural retaining wall, steel beams (IPB sections) are inserted into the freshly mixed wall panels.

In mixing applications less than 15m deep in relatively soft ground, a one phase mixing procedure may be used. In the one phase procedure, the final slurry product consists of cement and water or a cement, bentonite and water mixture, which is injected on both the down stroke and the upstroke of the machine. Advantages of this procedure include the additional mixing of the cement and the soil and the simplicity of only having one slurry mix.
When mixing deeper panels or penetrating difficult (slow) to mix soils or rock, a two phase system is used. Instead of using self-hardening slurry from the beginning onward as in a one-phase system, just bentonite slurry is used on the down stroke. Once the final depth is achieved, the cement slurry is introduced and mixed on the upstroke. This method prevents the mixing tool from being trapped in the panel if the panel construction time exceeds the initial set time for the cement slurry.
The size of individual panels is determined by the type and size of equipment being deployed. Panels can be constructed in lengths ranging from 2.4 m to 2.8 m and wall thicknesses of 0.55 m to 1.2 m.

3. EQUIPMENT

The most important elements of the CSM unit are the cutter gear drives. They are driven by hydraulic motors which are located in a water-tight housing. The slurry is introduced into the soil directly between the mixing wheels. During construction, the counter-rotating mixing wheels and vertically mounted plates are effectively acting like a forced action mixer. For loosening and mixing the soil different types of mixing wheels were developed.

Photo 1: Mixing wheels and housing for hydraulic gear drives

Photo 2: Kelly-guided CSM unit, China

The mixing unit (Photo 1) is either mounted on a guided Kelly bar or on a wire rope-suspended cutter frame equipped with special steering devices. The standard set-up is the "Kelly-guided" variant capable of reaching depths up to 43 m (Photo 2).
"Rope-suspended" systems are particularly suited for construction of deep soil mix walls. The greatest depth at which a wire rope-suspended unit has successfully installed a soil mix wall to date is 60 m, using a compact unit called QuattroCutter (Photo 3).

Photo 3: Wire rope-suspended CSM unit, QuattroCutter, Germany

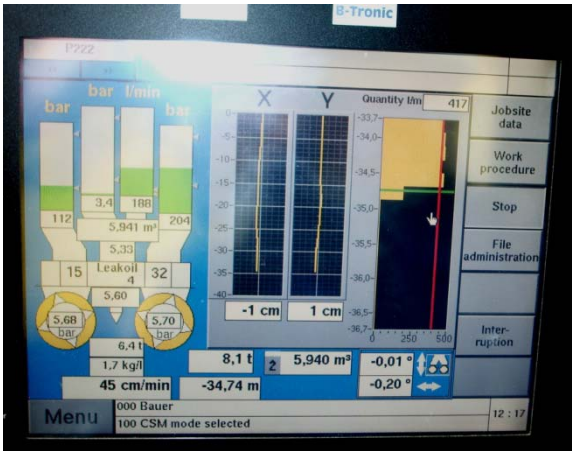

Photo 4: Rig operator's on-board computer screen

Both systems must be accompanied by an intensive quality assurance program. All process-specific production and plant-specific operating data are visualized throughout the construction phase and stored for subsequent documentation and evaluation. Information presented includes penetration rates, alignment, and slurry injection rates and volumes (photo 4).

4. COMPARISON WITH OTHER TECHNIQUES

The CSM process has significant advantages over conventional techniques like e.g. secant pile walls or sheet piling walls. These are:

- The existing soil is utilized as construction material.
- Very little spoil material is generated. Therefore the technique is particularly suited for work on contaminated sites.
- CSM is an ideal alternative to the traditional "Berlin wall" system, which is better known as soldier beam wall with timber lagging, for the use in high groundwater conditions, or to sheet pile walls in soil formations unsuitable for pile driving or in close proximity to vibration-sensitive buildings.
- CSM is a vibration free method.
- No delivery of ready mixed concrete is necessary.

In comparison to traditional deep mixing methods, CSM has the following advantages:

- A high degree of verticality of wall panels is achieved by the counter-rotating cutter wheels.
- The cutter principle ensures construction of clean and trouble-free joints even between wall panels of different construction age e.g. after weekend breaks or prolonged stoppages on site.
- Harder soil formations can be easily penetrated, broken down and mixed by using the cutter wheels as cutting and mixing tool.
- Homogenize the cohesive soils and self-harden slurry through horizontal mixing.
- In relation to small base units, high daily output and high panel depth may be achieved.

5. POSSIBLE APPLICATIONS

There are many possible applications for the CSM method. The mean applications are:

- Cut-off walls
- Retaining walls (often with cut-off wall function)
- Foundations
- Slope stabilization
- Soil improvement / soil stabilization

6. JOBSITE EXAMPLES

6.1. Retaining wall with cut-off wall function

6.1.1. General project information

The use of CSM as a retaining wall for excavation pits is the most often used application. The chance to use the system as a kind of watertight soldier beam system allows a lot of projects to substitute e.g. secant pile walling or, sheet piling, which can be difficult adjacent to sensitive buildings inner-city.
An example for an excavated pit shows a jobsite executed in Sydney, Australia. For the new construction of some residential buildings a retaining wall was executed with CSM method. The first project stage consists of a 13-storey building with one additional underground car park floor; see figure 1 and figure 2.

Figure 1: Overview complete project with marked position of in the first stage executed building

Figure 2: Computer simulated building of first stage

The soil mix wall will be used as retaining wall during construction of the building as well as permanent external wall for the car park floors.
The mixing depth was between 10 and 16 m and the wall thickness 55 cm. The total wall area for this building was about 4000 m². After finishing the soil mixing wall the pit was excavated incremental to a depth of about 6 m. To a depth of 10.5 m, the wall acts as a retaining wall, below 10.5 m as a cut-off wall. The required 28-day unconfined compressive strength (UCS) was 5 MPa for the retaining wall function

and 3 MPa for the cut-off wall function. The requirements on the water tightness of the wall were relatively high. The principal of our customers insisted that no leaks are visible on the wall after excavation. The permeability of the wall was allowed to be maximum 10^{-8} m/s after 28 days.
One main reason for the decision to use the CSM method on this site was that it is possible to produce soil mixing walls with a relatively smooth surface. Hence it is possible to use the produced walls as permanent face concrete walls without costly wall surface cutting.

6.1.2. Soil conditions

The subsoil investigation indicated a subsurface profile generally comprising filling to depths of 0.6 m to 1.4 m over Quaternary alluvial deposits, which typically comprise fine to medium grained "marine" sands with podsols natural sand, clayey sand, sandy clay. The permeability of the natural sands was between $2 \cdot 10^{-4}$ and $5 \cdot 10^{-5}$ m/s. These sediments overlie the Hawkesbury Sandstone, which surface was found in depth between 10 and 19 m. The rock surface was quite uneven. The determined rock strength vacillate between extremely low (UCS < 0.6 MPa) and medium (UCS 6 < 20 MPa).
For sealing the excavation pit it was necessary to sock minimum 1 m into the sandstone or 2 m into the clay layer.

The Hawkesbury Sandstone which is also known as Sydney sandstone or Yellowblock forms the bedrock for the most areas of the region of Sydney. This sandstone is well-known for its durability, which caused by a high to very high quartz content. The quartz content varies depending on the rock layer and can be up to 95 percent.

Two example borehole logs are shown in figure 3.

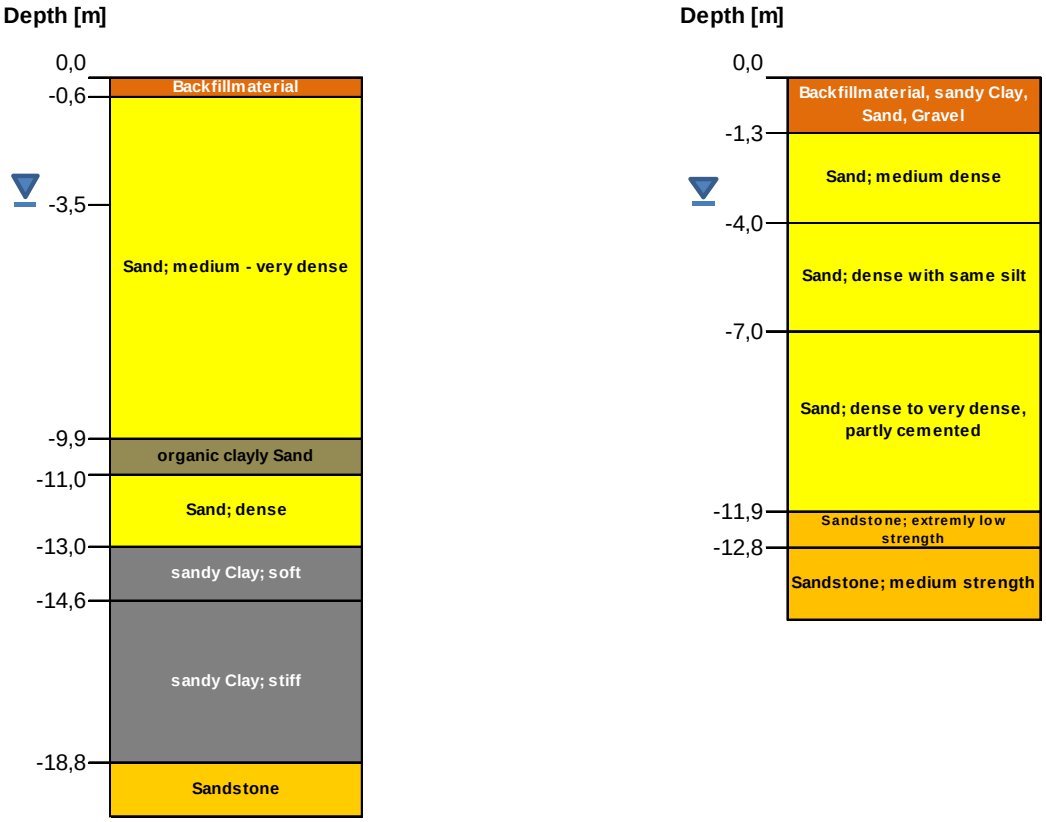

Figure 3: Example borehole logs; left for socketing into clay (2 m); right socketing into Sandstone (1 m)

6.1.3. Soil mix wall construction

During the first stage of this project about 4000 m² were constructed. Because of for the CSM method relatively low mixing depth and resulting from this relative short mixing time per panel; the 1-Phase method was used. The soil mix wall was executed by using the “hard-into-hard” sequence with an overcut of minimum 20 cm.

The CSM wall was installed using a BCM 5 mixing head mounted on a RTG RG 19 T base rig via a round Kelly bar, see photo 5.

Photo 5: RTG RG 19 T and excavator for pre-excavation and backflow handling

For the slurry supply a MAT SCC-20 colloidal batch mixer with a maximum mixing capacity of 20 m³ per hour were used. The mixer was assembled with a water tank and a cement silo. The cement slurry was delivered to the CSM by an eccentric screw pump. This pump was remote controlled by the rig operator. For the pre-excavation and backflow handling an excavator was used.
The pre-excavation was about one meter deep and also one meter wide. After finishing the pre excavation the soil mixing process was started. Course of producing the first panel it turned out that the used teeth at the mixing wheels were not perfect suitable for socket into the sandstone. The penetration speed into the sandstone was about 3 cm per minute. The reason was that the sandstone had a much higher resistance than expected. Therefore it was decided to change to new by BAUER developed tooth named BAUER SB 38 HR DC, shown in photo 6. This tooth has carbide cutting edges on both sides. It can cut the sandstone much more aggressive and make it also possible to change the direction of mixing wheel rotation without raised tooth wear. By using the BAUER SB 38 HR DC tooth the penetration speed in the sand could be improved by about 28 % and the penetration speed into the sandstone by about 143 %.
Figure 4 shows an exemplary depth-time diagram for a panel with 1 m socketing into the Sandstone after changing the tooth to BAUER SB 38 HR DC.
The achieved average penetration speed for panels with socketing into clay was about 23 cm/min. The average extraction speed was about 65 cm/min and the mixing depth 16 m. An exemplary time-depth diagram is shown in figure 5. Up to 6 panels per working day (10 hours) were executed.
The injected cement amounted was about 450 kg/m³ mixed soil. Immediately after finishing the mixing process 2 steel beams were installed per panel.

For quality control cores were drilled out of the CSM wall. The laboratory tests showed unconfined compressive strengths between 5 and 10 MPa (depending on the different soil layers). The results for the permeability were between $1.5 \cdot 10^{-9}$ m/s and $7.7 \cdot 10^{-10}$ m/s. No leaks could be seen when the pit was excavated. Furthermore the wall surface was as smooth as expected so that no further treatment of the wall surface was required.

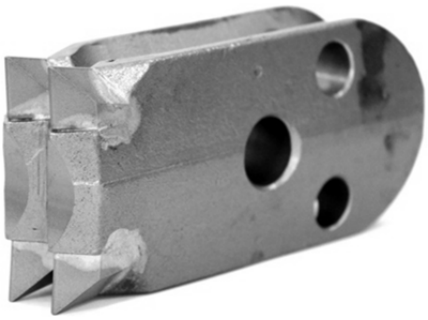

Photo 6: New developed cutting tooth BAUER SB 38 HR DC

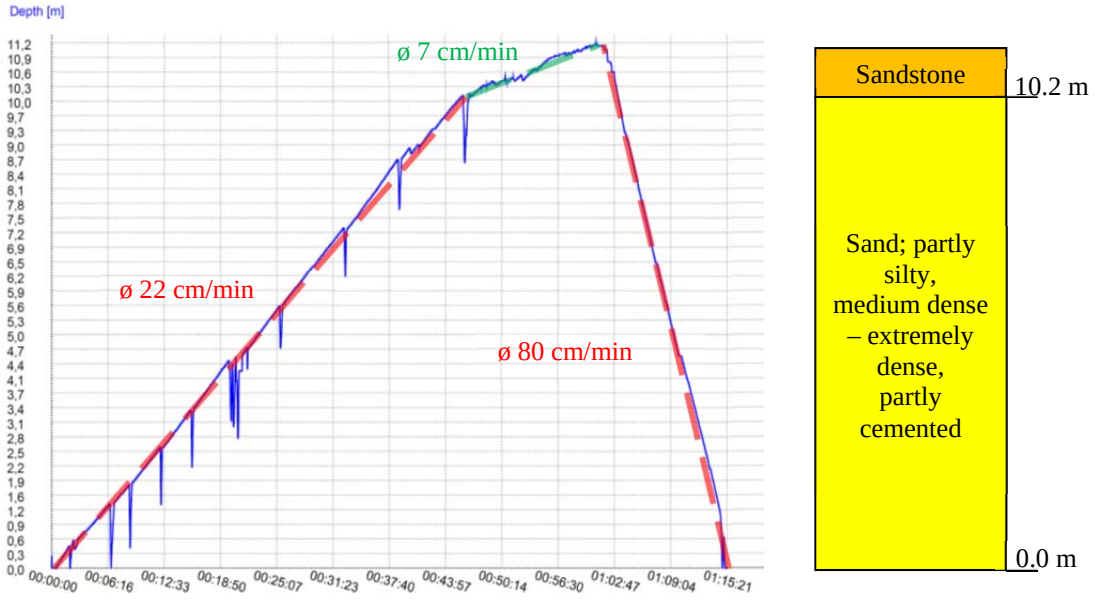

Figure 4: Exemplary depth-time-diagram with average mixing speeds and the associated soil profile for a panel with 1 m socketing into rock

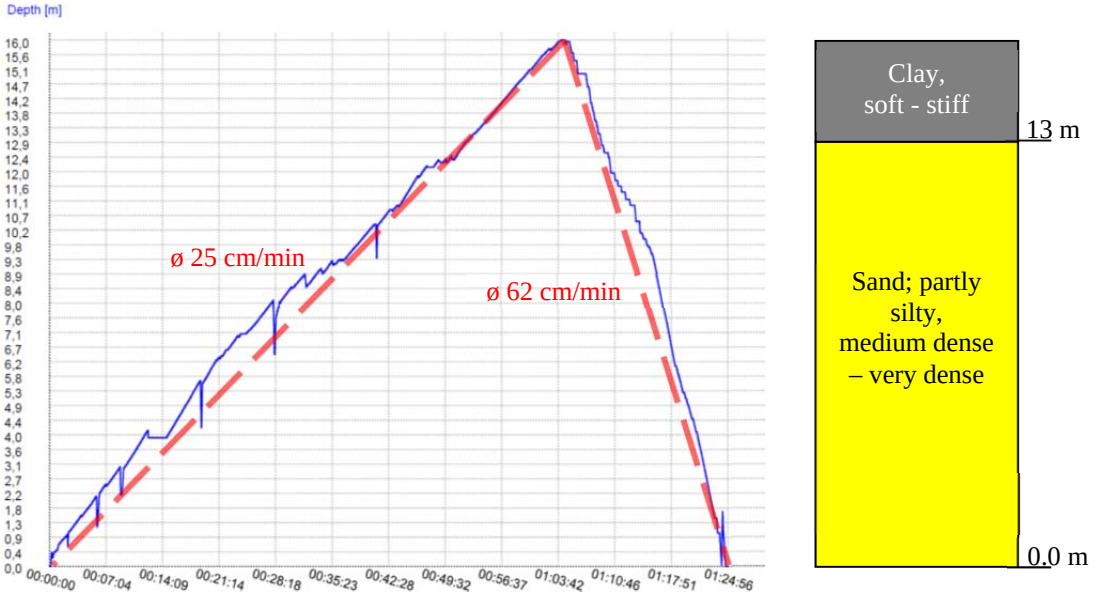

Figure 5: Exemplary depth-time-diagram with average mixing speeds and associated soil profile for a panel with socketing into clay

6.2. Shafts

6.2.1. General project information

An example project for shaft execution with the CSM method in difficult soil conditions was executed in Portland, USA. This project is part of Portland's 20 year program to control combined sewer and storm water overflows to the Willamette River. It includes the construction of 5 shafts for jacking and receiving of two micro tunneling boring machine and future maintenance access. The diameters of the tunneling machines were about 163 cm and 201 cm.
5 shafts were produced by using the CSM method between fall 2009 and summer 2010. The required mixing depths for the shafts were between 16.8 m and 26.9 m. In addition, soil improvement in two further sites up to depths of 10 respectively 12.3 m was carried out by using the CSM method, see figure 6.
The difficult soil conditions made this project very challenging, especially for shaft "L" and "C".

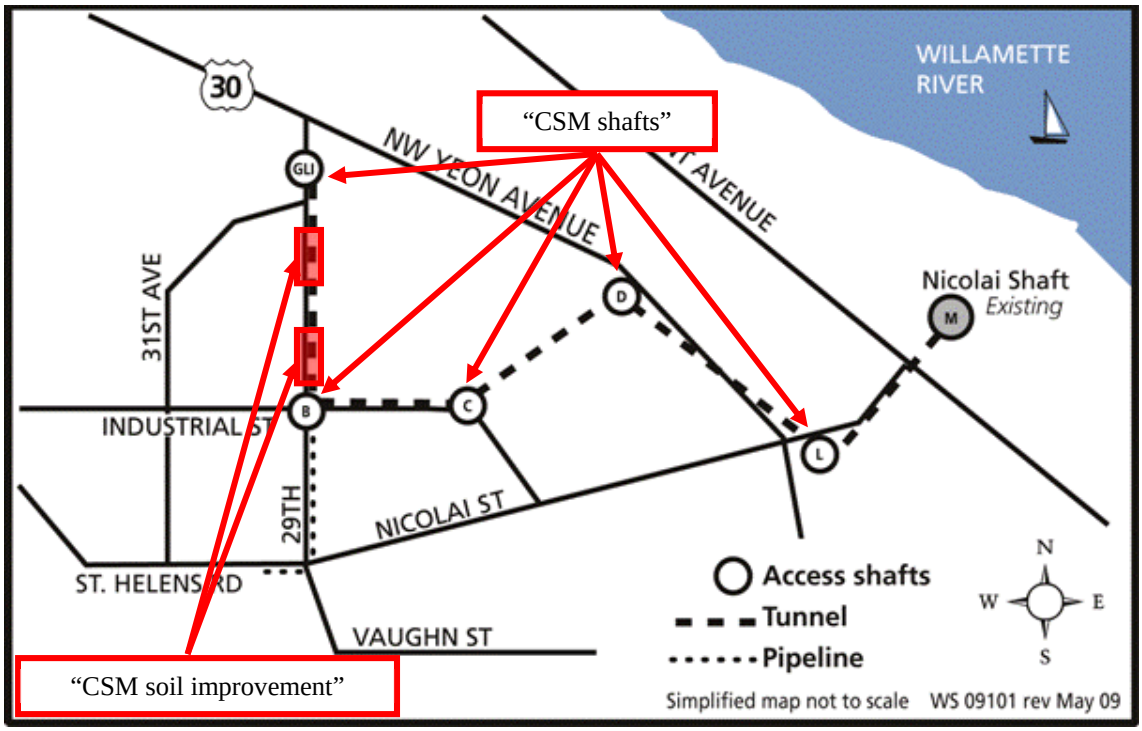

Figure 6: Overview sketch CSM project in Portland, USA

6.2.2. Soil conditions

The subsurface material in the vicinity of shaft L consisted of approximately about 1 m of miscellaneous fill material followed by stratified sand and silt alluvial to approximately 8 m below ground level. There under, gravel alluvium with cobbles and boulders were encountered which extend to approximately 26.5 m. The gravel alluvium was underlain by sand with gravel extending to the test boring bottom depth at 27.5 m below the surface. The soil report describes the sand/silt alluvium as medium dense with a running behavior below the water table. The dense gravel alluvium is open graded and will exhibit running behavior below the water table. The gravel alluvium contains a large number of cobbles (stones: about 8 cm < Ø < 30 cm) and can contain boulders. These are composed of basalt and andesite. The strength of the cobbles and boulders ranges from 70 MPa to 270 MPa.

6.2.3. Shaft construction

Point 7.2.2 shows soil conditions that are absolutely not typical for a soil mixing application. However, the CSM method was used because other methods would be less suitable in these soil conditions. E.g. there would be very high risk of losing a high volume of bentonite slurry in the open porous soil layers. In addition, the stabilization of these soil layers would be probably impossible. By using the CSM method the slurry-soil mix has normally a less liquid consistence. So it is possible to seal and stabilize open graded soil layers more effectively.
By using a secant bored pile wall boulders (strength up to 270 MPa) would be a massive problem.

The CSM work was executed with a BG 40 V and a BCM 10. The backflow was partly recycled by using a MAT mobile sieve unit ES 250-W and a MAT desanding unit BE-100-60.

Shaft L had a cylindrical shape (compression ring) with a total of 16 CSM panels (8 Primary and 8 secondary). The shaft inter diameter was 9.45 m. The panels were 2.8 x 1.0 m and the mixing depth 27m. As reinforcement 14 bars (44.45 mm diameter bar) to a depth of 12.19 m below ground level were installed. Due to the soil conditions and mixing depth the 2-phase method and the hard-in-hard panel sequence were used.

During construction the first panels of shaft L the open graded alluvial gravel couldn't be stabilized by the soil-slurry mix. This increased the risk of the mixing head getting stuck in the panel. Hence the required mixing depth couldn't be reached. Also a relative high volume of the bentonite slurry was drained away into the big pores of the gravel layer. For this reason the alluvial gravel layer was stabilized by cement slurry injections. After these injections the alluvial gravel layer was stable enough to getting penetrated without bigger risk of panel collapses. However the cement injections couldn't close the big pores in the gravel layer. So the bentonite slurry loss was still relative high.
Figure 7 shows an exemplary depth-time-diagram with associated soil profile of shaft L after the cement slurry injections were carried out.

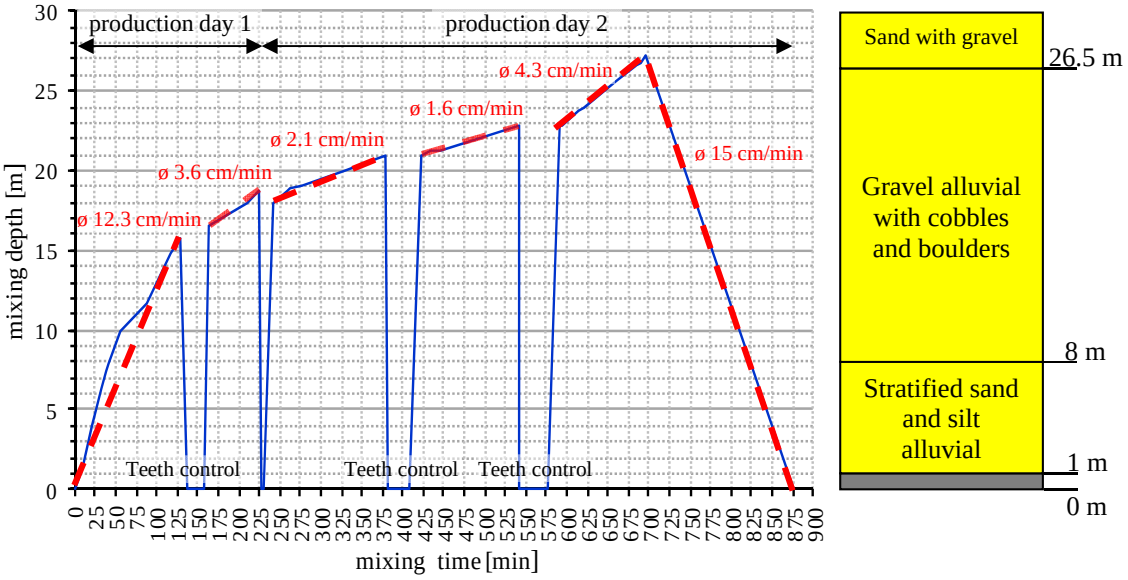

Figure 7: Exemplary depth-time-diagram with average mixing speeds and associated soil profile for a panel of shaft L

The required UCS strength for shaft L was about 11 MPa. The injected amount of cement content per cubic meter of treated soil was 650 kg (2-Phase method - cement slurry was only pumped during the upstroke). A wet sample was obtained from every panel from a depth of approximately 15 m below ground level for QA/QC purpose. The samples showed UCS strengths of about 4 MPa after 3 days and 11.7 MPa after 14 days.
The excavation depth of shaft L was about 22 m.

Photo 7 shows the ready excavated shaft L as an example of quality which could be achieved in this extremely difficult soil conditions.

After finishing the CSM work on this project, the project owner - City of Portland - was surprised about the good quality of the produced CSM shafts and was very satisfied with the job.

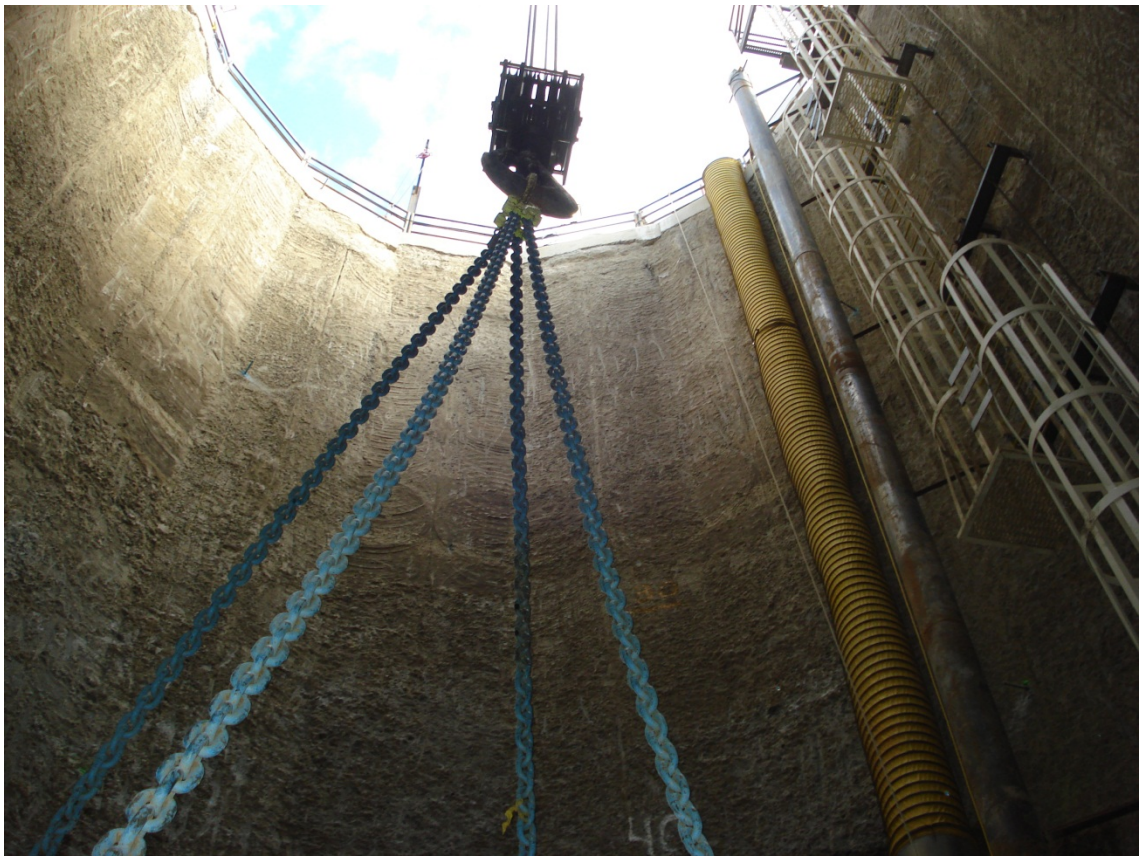

Photo 7: Excavated shaft L, excavation depth about 22 m

7. SUMMARY

The described examples have demonstrated that this young construction technique, which combines the advantages of the cutter and the soil mixing technique, can be used in soil conditions common mixing methods can't cope with. Even in these soil conditions the CSM elements showed a very high quality Thus, the CSM method is a useful supplement to traditional soil mixing methods.

REFERENCES

E.Stötzer, W. Brunner, R.Fiorotto, F.-W. Gerressen, M.Schöpf, "CSM Cutter Soil Mixing - A New Technique for the Construction of subterranean walls - Initial experiences Gained on completed projects", 2006, 10th international Conference on Piling an Deep Foundations, (534), 7 p.

Fiorotto, R., Stötzer, E., Schöpf, M., Brunner, W., " CSM Cutter Soil Mixing - An innovation in Soil Mixing for creating cut-off and retaining walls", 2005, International Conference on Deep Mixing

F.-W. Gerressen, M.Schöpf, E.Stötzer, „Venedig macht dicht -Das CSM Verfahren Cutter Soil Mixing als Teil des Hochwasserschutzkonzeptes MOSE", 2008, 6. Kolloquium Bauen in Boden und Fels, (591), 6p. (German)

F.-W. Gerressen, M.Schöpf, E.Stötzer, „CSM-Cutter Soil Mixing - Worldwide experiences of a young soil mixing method", 2009, Deep Mixing 2009 Okinawa Symposium

Deep mixing for reinforcement of railway platforms with a spreadable tool

Antoine Guimond-Barrett, IFSTTAR-LCPC / Université du Havre, France, antoine.guimond-barrett@ifsttar.fr
Jean-Francois Mosser, Soletanche Bachy, France, jean-francois.mosser@soletanche-bachy.com
Nicolas Calon, SNCF, France, CALON Nicolas nicolas.calon@sncf.fr
Philippe Reiffsteck, IFSTTAR-LCPC, France, philippe.reiffsteck@ifsttar.fr
Anne Pantet, Université du Havre, France, anne.pantet@univ-lehavre.fr
Alain Le Kouby, IFSTTAR-LCPC, France, alain.lekouby@ifsttar.fr

ABSTRACT

Many old railway lines in Europe need to be reinforced as they no longer meet the requirements of modern traffic. This paper presents the results of field tests carried out, as part of the French RUFEX research project (Reinforcement and re-Use of railway tracks and existing foundations), to study the installation of vertical soil-mix columns of 400 mm and 600 mm diameters under existing railway lines without removing the tracks or cementing the ballast.
The test site is a marshalling yard located near the river Seine in Vernouillet (78), France. The ground conditions consist of clayey silt overlaying gravelly sand.
Soil-cement columns were installed under and beside an existing track, down to the gravelly sand, using a spreadable mixing tool named Springsol. Mixing with the Springsol tool is performed by the wet method: the binder is added as slurry into the soil and mixed with two foldable blades. The tool has two positions: initially it is lodged inside a casing and once it reaches the end of the casing and penetrates the underlying soil, the blades spread out under the action of springs. Such casing is installed through the ballast, between the track's sleepers. This enables the recovery of the spoil without polluting the track with cement.
Some columns were excavated in order to control their geometry and several soil-mix samples were taken for laboratory testing.
In this paper, the tool and its uses in the field are explained. The quality assessment and quality control systems carried out to control the properties of the soil-mixed material on site and in the laboratory are also discussed.

1. INTRODUCTION

The foundations of many old railway lines in Europe need to be reinforced as they do not meet the requirements of modern traffic. Degradation of the platform is often related to insufficient drainage causing a reduction in the mechanical properties of the subgrade. Railway structures lying on degraded platforms can experience problems such as reduced stability, increase of settlements, and extensive vibrations (Eurosoilstab, 2002). In all those cases, remediation works generally involve increasing the stiffness of the subsoil.
Classic platform reinforcement works are very time consuming as they require a temporary removal of the tracks entailing significant traffic interruptions. These types of works are also expensive and the production rates are low. Optimizing track maintenance operations and reducing their impact on traffic is an important issue in railway network management.
Different ground improvement techniques such as jet grouting and injections, carried out while keeping the tracks and sleepers in place, have been tested. These methods were interesting in terms of platform stiffness increase but proved to be unsuitable because of the generation of significant amounts of spoil which polluted the ballast with cement.
Currently, there is still no platform foundation reinforcement method compatible with the requirements of maintaining traffic (working under low catenaries without removing the tracks and with minimal impact on the ballast).
Deep soil mixing is a ground improvement method used in various marine and on-land applications mainly for the stabilization and reinforcement of soft soils, construction of retaining walls, mitigation of liquefaction, environmental remediation and installation of cut-off barriers (Topolniki, 2004). In this method, soils are mechanically mixed in situ with a hydraulic binder. The most frequently used binders are lime and cement. The soil can be mixed with the binder either in dry powder form (dry mixing method) or in slurry form (wet method) (Porbaha, 1998).

The objective is to produce a stabilized soil that has a higher strength, lower permeability and lower compressibility than the original soil.
The dry soil mixing method has been tested on many new railway construction projects in soft soils in Scandinavia (Baker, 2000; Holm et al., 2002; Alen et al., 2005; Olsson et al., 2008)). In the UK, the wet method has been tested on an existing railway line (Konstantelias et al., 2002).
In France, the first field trial to evaluate the effects of vertical soil-cement columns constructed using the wet soil mixing method to reinforce an existing railway platform was undertaken in the European research project Innotrack (INNOvative TRACK systems) (Rocher-Lacoste et al., 2008). This project was established with the objective of reducing the life cycle cost of railway infrastructures. Field tests were conducted on an existing LGV railway using a spreadable mixing tool named Springsol. Preliminary results from these tests were promising as they showed that the wet mixing method could meet the requirements for traffic maintenance.
Following Innotrack, the RUFEX research project, which started in 2010, focuses on the Reinforcement and re-Use of existing railway track and building foundations by deep soil mixing. Its main objectives are to increase knowledge and understanding of the behaviour of such structures by working on both technological (tools and compositions of binders used) and design aspects of wet deep soil mixing.
This paper presents the results of field tests carried out as part of the RUFEX research project, to study the installation of vertical soil-mix columns of 400 mm and 600 mm diameters constructed under existing railway lines without removing the tracks and to determine the properties of the soil-mix material produced by the addition of a cement slurry.

2. VERNOUILLET TEST SITE

2.1. Site location

The test site is located in Vernouillet (Yvelines), France, approximately 35 km North-West of Paris (Figure 1). The test site is occupied by a marshalling yard and is located near the river Seine (roughly 500m).

Figure 1: Site location maps (www.geoportail.fr).

2.2. Site investigation

A preliminary site investigation was carried out to determine the ground conditions at the test site. The ground investigation consisted of 2 trial pits (dug down to approximately 2 m), 15 dynamic penetration tests and 3 boreholes drilled down to depths of 6 and 9 m. Three pressuremeter tests were performed at different depths in each borehole. Soils sampled from the trial pits were identified in the laboratory by moisture content measurements, grain size distribution analyses and methylene blue value tests.

2.3. Ground conditions

The ground investigation revealed that the site was covered by a 0,5 m thick layer of fill consisting of dark greyish brown sandy gravel, overlaying a 3 m thick layer of brownish beige clayey silt. An average penetration resistance of 4MPa and pressuremeter limit pressures between 0.70 and 1.70 MPa were measured in this silt layer. Underlaying the clayey silt are old alluvium deposits of the river Seine which may be described as dense brownish orange gravelly sand. This sand is present down to a depth of at least 9 m below ground level. The average penetration resistance in this layer is much higher with 16 MPa. Pressuremeter limit pressures greater than 2.40 MPa were measured. No groundwater was encountered

during the site investigation. The geotechnical properties of the different soils from the Vernouillet test site are summarized in Table 1.

Table 1: Summary of soil characteristics.

Strata	Fill	Clayey Silt	Gravelly sand
Thickness (m)	0.5	3	>5.5
Moisture content (%)	7.6	11.9 to 19.7	5 to 7.6
% passing 80 µm	/	72.5	17.9
VBS	/	1.38	0.71
Dynamic penetration resistance qd (MPa)	7	4	16
Limit pressure pl* (MPa)	/	0.70 to 1.70	>2.40

3. FIELD TRIAL – OUTLINE OF COLUMN INSTALLATION WORKS

3.1. Soil mixing equipment and column installation procedure

Soil-cement columns were installed in Vernouillet using a Casagrande C4 drilling rig. Soil mixing was performed by the Springsol mixing tool (Photo 1). This tool is equipped with two mixing blades that spread out under the action of springs. In its folded configuration, the tool diameter is 160 mm enabling its insertion into a temporary casing. By increasing the length of the mixing blades, two different diameters were tested for the open configuration: 400 and 600 mm. The binder is delivered through outlet holes in the drag bit located at the bottom end of the tool.

Photo 1: Springsol mixing tools (400 mm (left) and 600 mm (right) diameters).

Soil mixing using the Springsol tool is carried out by the wet method: the binder is mixed with water forming a slurry before it is added into the soil. The slurry is injected during the penetration (downward) phase. Depending on the column, the penetration speeds used in Vernouillet varied between 10 and 25 in metres per hour (m/hr) and the tool rotation speed was between 70 and 160 revolutions per minute (rpm). The blade rotation number is defined by (EN 14679, 2005):

$$T = M \times \frac{N}{V} \quad (1)$$

Where T is the blade rotation number per metre, M is the total number of mixing blades, N is the rotational speed of the blades (rpm) and V is the penetration rate in metres per minute (m/min).
The blade rotation number for the columns in Vernouillet was between 700 and 1500 rotations/m. The binder used was a slag cement containing 85% of granulated ground blastfurnace slag (CEM III/C 32.5 PMES). Bentonite was added to stabilise the cement grouts. The cement factors (mass of dry binder per cubic meter of soil) tested varied between 200 and 400 kg/m^3. It is important to note that these cement contents represent the amount of binder injected into the columns. The actual binder contents are

probably slightly lower as approximately 30% of spoil returns to the surface during mixing operations. This spoil is immediately pumped and evacuated as the column installation process continues.

3.2. Outline of column installation works

A total of 25 soil-mix columns of 400 and 600 mm diameters were executed under and beside an existing track. All columns were drilled down to the gravelly sand layer approximately 5 m below ground level. The columns were installed in 4 different areas (Figure 2).

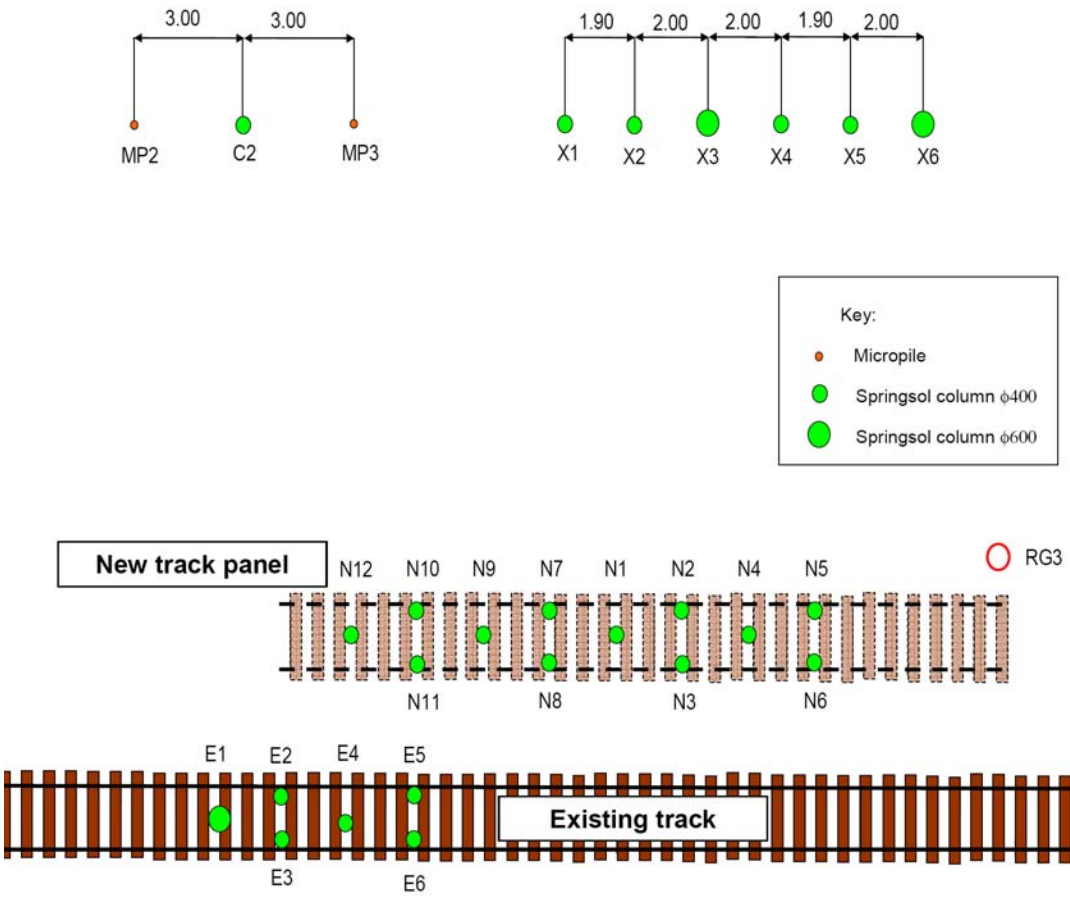

Figure 2: Location of soil-cement columns installed at Vernouillet.

3.2.1. Columns under the existing track

Six soil-cement columns were executed under an existing railway track to verify the feasibility of platform reinforcement by soil-mix columns (columns E1 to E6, Figure 2). Column E1 was executed with the 600 mm diameter Springsol tool whereas the other five columns were installed using the 400 mm diameter tool (columns E2 to E6).

The installation procedure for columns under existing tracks is as follows (Photo 2):

- a steel casing placed between the sleepers is driven through the ballast to the desired depth (Photo 2 n°1),
- the Springsol tool is lodged inside the casing (Photo 2 n°2). Once it reaches the end of the casing and penetrates the underlying soil, the blades spread out under the action of springs,
- the column is installed to the desired depth by mixing the soil with cement grout (Photo 2 n°3),
- finally, the steel casing is withdrawn (Photo 2 n°4).

These columns (E) were installed in a triangular configuration with one column in the centre of the track and two near the rail.

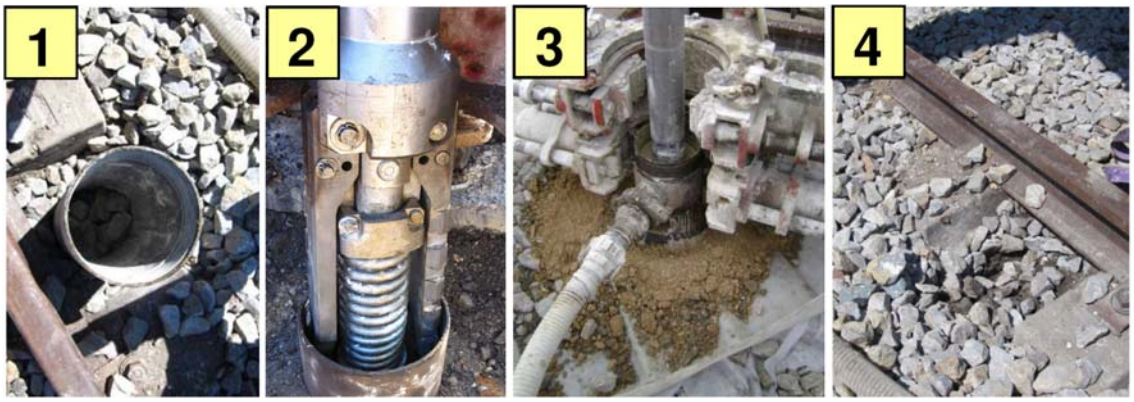

Photo 2: installation procedure for columns under existing tracks.

A portancemeter (bearingmeter), which is a rolling falling-weight deflectometer adapted to railway tracks (INNOTRACK, 2008) will be used to study the impact of these columns on the stiffness of the platform.

3.2.2. Columns under the new track panel

To investigate the potential benefits of installing soil-cement columns under a load distribution mattress consisting of ballast overlying a geosynthetic for new railway line projects, 12 columns (N1 to N12) were installed beside the existing track (Figure 2). They were drilled directly with the 400 mm diameter tool open down to 5 m below ground level. They are installed following the same triangular configuration as those under the existing track. An 18 m long new track panel will be built over these columns and their effect on the platform stiffness will also be investigated with the railway portancemeter developed during the INNOTRACK research project.

3.2.3. Columns designed to be excavated

Six columns (X1 to X6) were designed to be excavated after different curing times for laboratory testing to determine the characteristics of the stabilised soil. Four columns are of 400 mm in diameter (X1, X2, X4 and X5). Columns X3 and X6 were built using the 600 mm Springsol tool. Columns X4, X5 and X6 were excavated 28 days after construction. Columns X1, X2 and X3 will be extracted after 180 days.

3.2.4. Column for static load test

Column C2 was installed to be subjected to a static loading test according to NF 94-150-1 (1999) approximately 90 days after installation. The mixing was carried out with the 400 mm diameter tool open down to 5 m below ground level. The head of column C2 is confined in a metal collar to ensure that the load is correctly transmitted to the column.

4. QUALITY CONTROL

4.1. Quality control during construction

Quality control on site during construction included monitoring and recording the execution parameters and grout density measurements. The density of the spoil produced during mixing was also determined.
The mixing process was monitored with the Enpamix system (developed by Soletanche Bachy). The parameters recorded during the installation of the columns were the volume of grout injected, the mixing torque, the vertical thrust on the mixing tool, the penetration/withdrawal rates and the tool rotation speed.
The grout density was controlled using a Baroid mud balance. The measured densities confirmed that the slurries were prepared with the appropriate water / cement ratios.
The spoil produced during mixing of the columns was light yellowish brown to beige, visually homogeneous, liquid to pasty and composed of a mixture of silt and grout. Density measurements of the spoil were also carried out using a mud balance. The spoil density varied between 1.73 and 1.99. These values, higher than those of the slurry, confirm the presence of significant amounts of soil in the spoil and hence the blending of the slurry with the soil produced by the mixing process.

4.2. Column excavation

Three columns (X4, X5 and X6) were excavated with a 20-ton mechanical excavator approximately 1 month after construction (Photo 3 n°1 and 2). The aim was to verify the geometry of the columns and to examine the homogeneity of the soil-mix material.
The three columns had a length of 5 m. Column X6 was installed through a steel casing using the 600mm diameter tool. The head of column X6 was cone-shaped marking the spreading of the mixing blades as the tool enters the soil (Photo 3 n°1 and 3). The columns were found to be well mixed with few inhomogeneities visible.
The first 3 meters of the columns generally consisted of treated silt. Centimetric inclusions of beige/brown unmixed soil were visible in a matrix of well mixed soil-cement (Photo 3 n°5). The central/axial part of the column section appeared to be more homogeneous and concentrated in slurry. The diameter of the columns in the silt layer was close to the diameter of the tool used. Centimetric striations were visible on the outer surface of the columns (Photo 3 n°4). These striations were drawn by the rotation of the tool during the installation of the column. They probably have a significant effect on the skin friction mobilized in cohesive soils.
The lower part of the columns consisted of stabilised sand down to 5 m. The mixture produced was visually homogeneous with no unmixed soil inclusion (Photo 3 n°6) pointing to the fact that it is easier to obtain well mixed soil-cement columns in coarse grained soils than in fine grained soils.
The diameter of the lower part of the columns was slightly larger than that of the tool (about 70 cm for column X6) due to the migration of slurry in the permeable sand strata.

4.3. Laboratory testing - Unconfined compressive strength

Block samples were taken from the three excavated columns for laboratory testing to determine the mechanical properties of the soil-mix material. Specimens of 100 x 50 mm (height to diameter ratio of 2) were cored from these blocks (Photo 4).
The unit weight of the specimens cored from the treated silt blocks varied between 1700 and 1900 kg/m^3 whereas the unit weight of the stabilised sand specimens ranged between 1870 and 2200 kg/m^3.
The strength of the cored specimens was measured by unconfined compression tests carried out according to standard EN 13286-41 (2003) with a constant deformation rate of 1.5 % / minute. The results of these tests are presented in Figure 3.

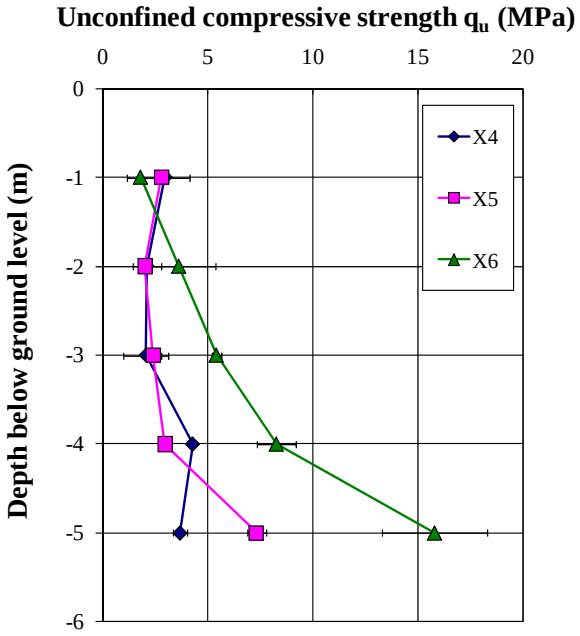

Figure 3: Unconfined compressive strength q_u versus depth for columns X4, X5 and X6.

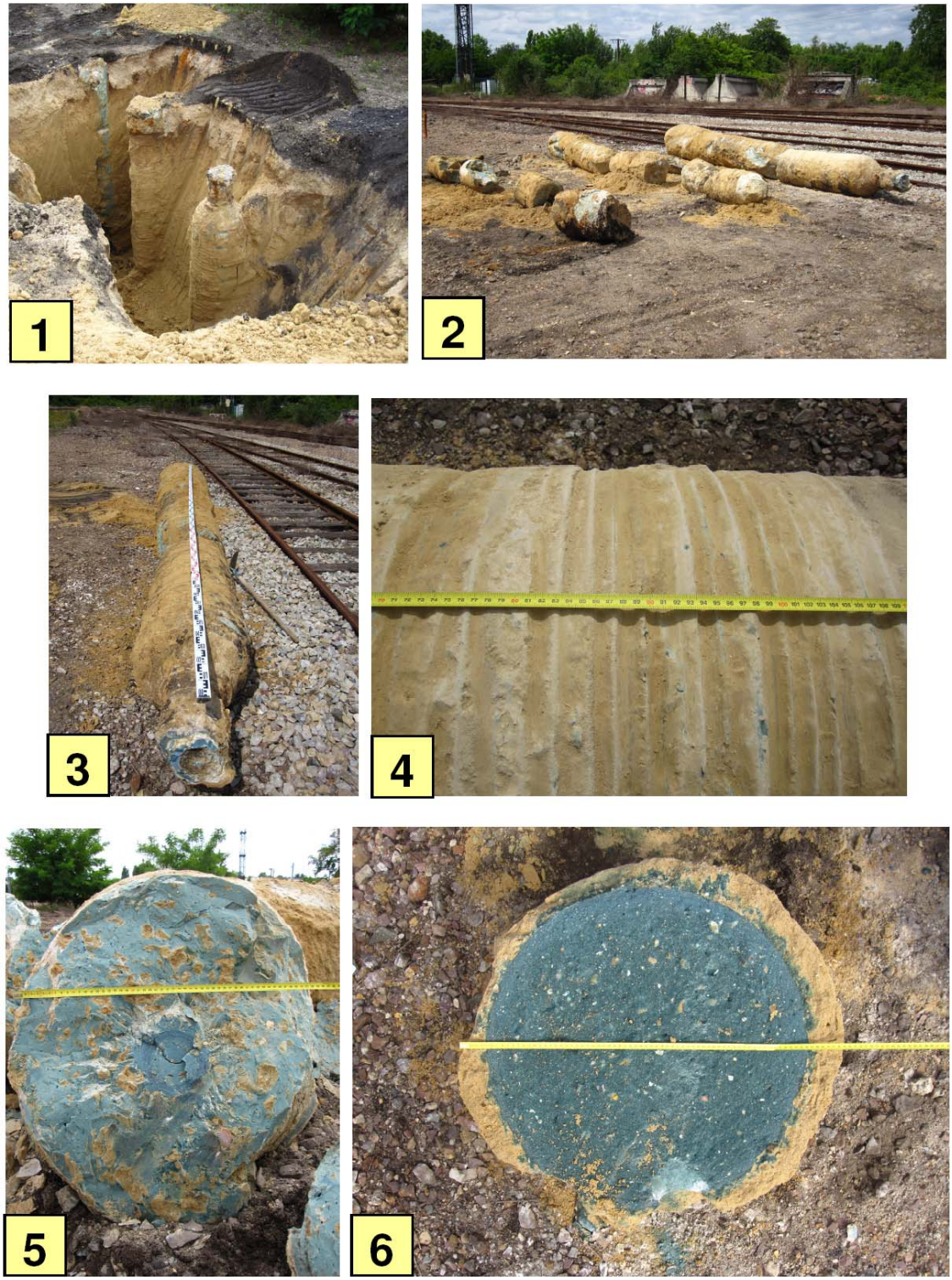

Photo 3: Excavation of columns X4 – X5 and X6 after 1 month.

Photo 4: Specimens cored from block samples of columns X4 – X5 and X6.

The average unconfined compressive strength measured in the stabilised silt for all three excavated columns was close to 2.5 MPa after 28 days. A coefficient of variation of 39% was determined for the 23 samples tested. This value can be related to the heterogeneity of the initial soil, variations in binder distribution, variations in the execution parameters (different sets of parameters were tested) and to the presence of some unmixed soil inclusions.
The strengths measured in the sand layer are much higher than those in the silt and more variable between the different columns with a coefficient of variation close to 60%. These variations can largely be attributed to the heterogeneity of the initial alluvial sand layer which contains lenses of gravel. These heterogeneities in the soil were observed during the coring of the block samples.
The coefficients of variation evaluated from the compression tests on specimens from Vernouillet are in the range of those compiled by Larsson (2005) from a number of reported studies.

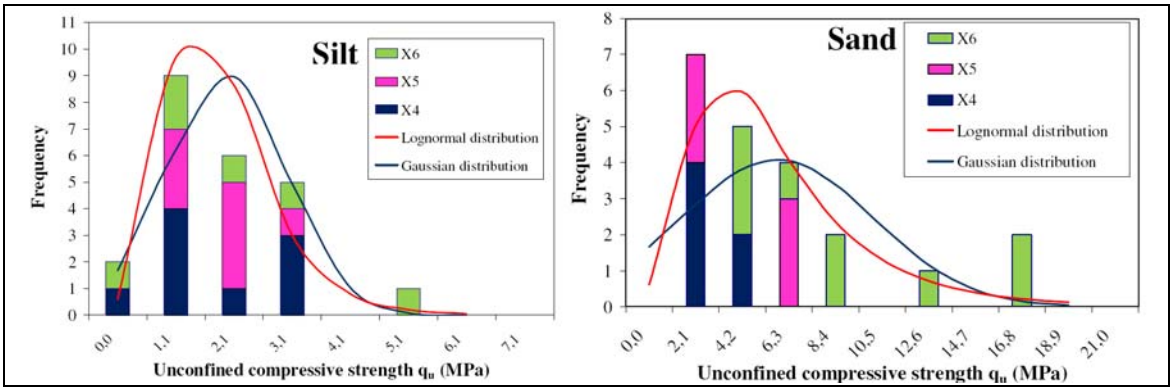

Figure 4: Histograms of q_u obtained on cored samples from columns X4, X5 and X6.

The distribution of unconfined compressive strengths measured in the treated silt and sand is shown in Figure 4 and compared with normal (Gaussian) and log normal distributions.
The characteristic strength value $q_{u5\%}$ considered in design is defined as the 5% fractile value of the unconfined compressive strength (Eurocode, 2006).
This characteristic strength was determined for each column for the silt and the sand by calculating the 5% fractile (Table 2):
- lowest strength value from the measured test results;
- assuming a Gaussian distribution of q_u;
- assuming a lognormal distribution of q_u.

The characteristic strength values calculated assuming a normal distribution are quite pessimistic, generally much lower than the 5% fractile lowest strength obtained from the actual compressive strength test results. Because of the asymmetry of the strength distributions, which is particularly visible here in Figure 3, the use of the lognormal distribution seems more appropriate for the determination of $q_{u5\%}$. The values calculated with this distribution are in line with the 5% fractile lowest values obtained from the strength test results. Similar results were reported by Ganne et al. (2010) on soil-mix materials in Belgium.

Table 2: Results of unconfined compression tests: characteristic strength values.

	Column	Average q_u (MPa)	$q_{u5\%}$ (MPa) (test population)	$q_{u5\%}$ (MPa) (Gaussian distribution)	$q_{u5\%}$ (MPa) (Lognormal distribution)
Silt	X4	2.38	1.20	0.81	1.08
	X5	2.41	1.99	1.72	1.79
	X6	2.72	1.32	0.19	0.98
	Total	2.48	1.12	0.88	1.23
	Column	Average q_u (MPa)	$q_{u5\%}$ (MPa) (test population)	$q_{u5\%}$ (MPa) (Gaussian distribution)	$q_{u5\%}$ (MPa) (Lognormal distribution)
Sand	X4	3.99	3.43	3.33	3.35
	X5	5.15	2.88	1.18	2.05
	X6	9.83	5.28	1.88	4.06
	Total	6.82	2.9	-0.18	2.41

The characteristic values were obtained by testing a limited number of samples of 100 mm in length and 50 mm in diameter. Additional tests are to be performed on samples taken in following excavations in Vernouillet to confirm these tendencies. The effect of specimen size will be analysed by unconfined compressive strength tests on 200 x 100 mm cored specimens.

5. CONCLUSIONS

This paper presents an overview of field tests carried out, as part of the RUFEX research project (Reinforcement and re-Use of railway tracks and existing foundations), to study the installation of vertical soil-mix columns of 400 mm and 600 mm diameters under existing railway lines without removing the tracks or cementing the ballast. Soil-cement columns were installed by the wet deep mixing method under and beside an existing track, down to a gravely sand layer using a spreadable mixing tool named Springsol. Some columns were excavated after 28 days in order to control their geometry and several soil-mix samples were taken for laboratory testing. The columns were found to be well mixed with few inhomogeneities visible. Further examination of the excavated columns showed that the first 3 meters were composed of treated silt whereas the last two meters of the columns were made of treated sand. Results of unconfined compressive strength tests showed significant differences within a single column between the upper treated silt and the treated sand. It was found that the lognormal distribution seems more appropriate for the determination of characteristic strength values as reported in the literature. The field trial confirmed that it was possible to build soil-cement columns under an existing track in soils stiffer than those in which deep soil mixing is normally used. The field tests in Vernouillet are ongoing as subsequent column excavations are planned, a static load test will be performed on one of the columns and the increase in stiffness produced by the columns will be investigated by a portancemeter. The results of these tests will serve as a basis for numerical analyses of the effects of soil-mix columns in railway platform reinforcement.

REFERENCES

AFNOR, NF P 94-150-1, 1999, Soil - Investigation and testing - Static test on single pile - Part 1 : in compression.

AFNOR, EN 13286-41, 2003, Unbound and hydraulically bound mixtures - Part 41 : test method for the determination of the compressive strength of hydraulically bound mixtures

AFNOR, EN 14679, 2005, Execution of special geotechnical works - Deep mixing. CEN TC 288.

Alen, C., S. Baker, J. Ekström, A. Hallingberg, V. Svanand G. Sällfors, 2005, Test Embankments on Lime/Cement Stabilized Clay, Deep mixing, Stockholm, Sweden, Balkema.

Eurocode, 2006, Basis for Design.

Baker, S., 2000, Deformation Behaviour of Lime/Cement Column Stabilized Clay, Svensk Djupstabilisering (Swedish Deep Stabilization Research Centre). Chalmers University of technology, Report 7.

Eurosoilstab, 2002, Development of design and construction methods to stabilise soft organic soils. Design guide soft soil stabilisation. European project BE 96-3177. Report CT97- 0351.

Ganne, P., Huybrechts, N., De Cock, F., Lameire, B., Maertens, J., 2010, Soil Mix walls as retaining structures - critical analysis of the material design parameters, Geotechnical challenges in Megacities, Moscow, Russia.

Holm, G., Andréasson, B., Bengtsson, P. E., Bodare, A., Eriksson, H., 2002, Mitigation of track and ground vibrations by high speed trains at Ledsgard, Swedish Deep Stabilization Research Centre Report 10.

INNOTRACK, 2008, "Portancemetre" for track structure stiffness measurement on existing tracks TIP5-CT-2006-031415.

Konstantelias, S., Ghataora, G. Brough, M. Stirlingand, A. Madelin, K, 2002, Soil/Grout mixing auger trial at Leominster Herefordshire - A case study,. Proceedings of the international conference on Railway engineering, 2002, London, UK.

Larsson, S., 2005, State of Practise Report - Execution, monitoring and quality control. In International Conference on Deep Mixing. Best Practise and Recent Advances; Proceedings of the International Conference on Deep Mixing (Deep mixing '05), Stockholm, Sweden, Swedish Deep Stabilization Research Centre.

Olsson, M., Edstamand, T., Alén, C., 2008, Some experiences from full scale test embankments on floating lime-cement columns. Proceedings of the Second International workshop on Geotechnics of soft soils, AMGISS Glasgow, Scotland. Taylor & Francis Group.

Porbaha, A., 1998, State of the art in deep mixing technology: part I. Basic concepts and overview. Ground Improvement, Vol. 2.

Rocher-Lacoste, F.and Le Kouby, A., 2008, Subgrade improvement method : vertical soil-cement columns drilled through existing track; field test. INNOTRACK project. 37.

Topolnicki, M., 2004, Chapter 9 In situ soil mixing, Ground Improvement, M. P. M. K. Kirsch. Abingdon, Oxon, Spon Press.

Soil-cement columns, an alternative soil improvement method

S. Lambert, KELLER Fondations Spéciales, Entzheim, France, serge.lambert@keller-france.com
F. Rocher-Lacoste, SETRA, Sourdun, France, frederic.rocher-lacoste@developpement-durable.gouv.fr
A. Le Kouby, Université Paris Est, IFSTTAR, Paris, France, alain.lekouby@ifsttar.fr

ABSTRACT

Within the European Research project INNOTRACK (2006-2009), SNCF, Keller Foundations and IFSTTAR tested the feasibility of an alternative soil reinforcement technique the FLAPWINGS, based on vertical soil-cement mixed columns with variable diameter. Field load tests have been carried out on two columns built in a silty soil. The columns have been instrumented, using the French extensometer technique, in order to estimate the distribution of load along the column. The results show the strong mechanical response of the column. Moreover, from the excavated columns, samples were collected to perform laboratory tests. They show some heterogeneity of the new mixture and consequently on the distribution of unconfined compression strength and stiffness modulus. Nevertheless it was acceptable to justify the technique. Another interesting observation is that the mechanical behaviour of the soil-cement column might be assimilated to jet grouting inclusions in terms of UCS resistance for similar soils and similar cement contents. A new tool has been developed by Keller that shows interesting results.

1. INTRODUCTION

In order to reduce the Life Cycle Cost of railway infrastructure, many research works are performed concerning of track support structure. Development and implementation of several subgrade improvement methods allowing limited traffic interruption and privileged recourse to local material are the keynote of the work of the research European project INNOTRACK (INNOvative TRACK system) (2006-2009). The technique proposed by the SNCF/KELLER/IFSTTAR was a ground reinforcement with vertical soil-cement columns. Research based upon field and laboratory tests were carried out aiming at:

- studying the feasibility of soil-cement columns in some soils as an alternative soil reinforcement technique.
- assessing the load distribution along the column, in order to obtain a shaft friction and a tip resistance.
- carrying out mechanical laboratory testing to measure unconfined resistance R_c and elastic modulus E_c from the samples extracted from excavated columns.

An experimental site has been selected and the tests were performed in an area close to the TGV station Haute Picardie in 2006. A research report was provided [1].
The technique used in the research work represents the wet soil-mixing method as the soil is mixed with a cement grout characterized by a Water/Cement (W/C) ratio. Many publications linked to research works exist on this technique as it is widely used in Sweden and Japan (SGF Report 4:95 E [2] and CDIT [6]).

In the paper, we consider static field load tests performed on two 600 mm soil-cement columns; characterized by two different W/C ratios respectively 1 and 0.83. Their bearing capacity as well as the local response in terms of shaft friction and tip resistance has been analysed.
A comparison is made between the response of a soil cement columns and jet grouting columns through UCS resistance of soil-cement mixtures samples got from both techniques.
Besides, design rules [3] are available to calculate the bearing capacity of jet grouting columns from local design rules (shaft friction and tip resistance).
An interesting issue is to compare the available design rules with the results of the soil-cement columns pile tests even if the mixing mechanisms can be considered as different.
The cement content determined at the end of the building of columns by the two techniques. In addition, in both cases, soil inclusions are located within the mixed material.

Moreover, the Keller soil mixing tool (FLAPWINGS) has technically evolved. A new version has been proposed. In this paper, a description of the experimental test site and of the built columns is made as well as the presentation of results of UCS tests from test sites soil-cement samples.

2. EVOLUTION AND SPECIFICITIES OF THE MIXING TOOL

In the railway environment (soil improvement between the tracks), the technique can be used as follows:
- a steel tube was jacked vertically through the railway structure layers (ballast, sub-ballast, treated soils) down to the natural soil ; i.e. about 1-1.50 m deep; in order to make the tool reach the layers that were to be improved;
- the folded device was inserted through the steel tube. At the base of the tube, it began to rotate and as it moves away from the tube, it opened up in order to perform the mixing phase of existing soil and cement grout and achieved 600mm reinforcement columns.

Other applications are also possible (Figure 1):
- soil improvement of a paving and foundation raft and building up of secant columns,
- subgrade reinforcement of railway and highway embankments.

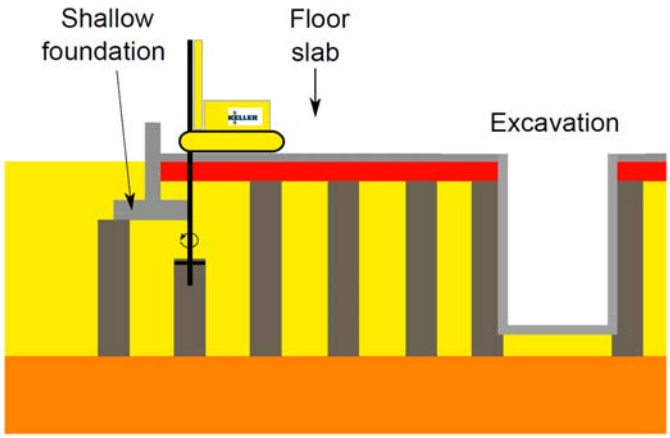

Figure 1: Soil improvement applications

The first tool developed by Keller Foundations [1] had an opening system that was simple with stems that were operated with an external jack located at the top pole of the drilling machine. The external diameter of the closed tool was 300 mm core retractable tool that was too big for classic tubing or for preboring with usual diameters.

Keller Foundations has designed a new patented device [9] (FLAPWINGS) (Figure 2) to achieve soil-cement columns following execution requirements in a railway environment. It consisted in a 150 mm core retractable tool able to open up in order to perform the soil mixing phase on a 600 mm column. The new designed tool also allows us to open and close the retrieval blades but it is controlled by a two way hydraulic jack located in the mixing tool.

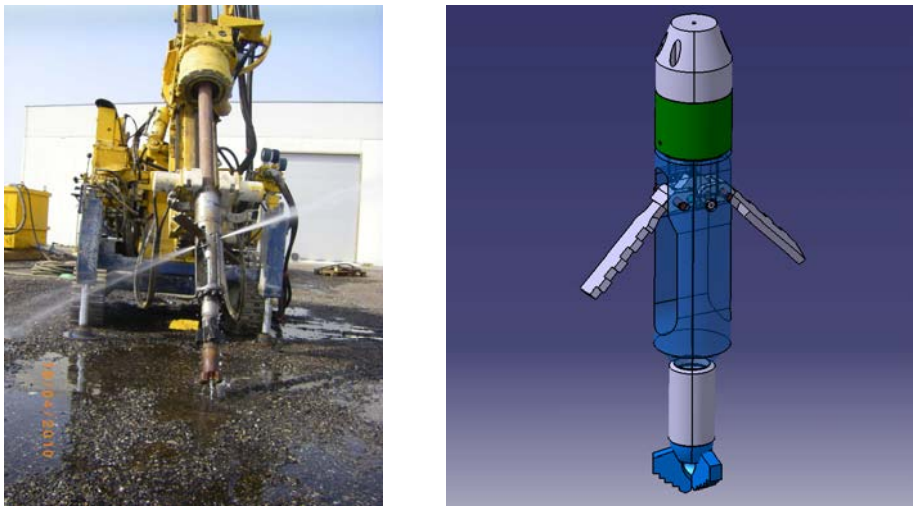

Figure 2: New soil-mixing folding tool FLAPWINGS

The main advantages of the new tool FLAPWINGS are :
- Small boring machine is required to achieve this kind of field works. Then, it is useful for field areas difficult to access like for example within a building and with limited heights for field works,
- 150 mm drilling with possible tubing (closed tool)
- Possibility of protecting the drilling with steel tubes in order to avoid pollution with grout of the top layers like ballast for example,
- Column diameter of the mixed column : 600 mm,
- Possibility to reach compact top layers in order to reinforce soft soil layers underneath.

3. TESTS ON THE 300 MM CORE RETRACTABLE MIXING TOOL

3.1. Soil investigation

The experimental site [1] was investigated with in situ tests (pressiometer test) and laboratory tests. We only consider the pressiometer test in the paper.
A 12 m long borehole was done to achieve pressiometer tests. No water table was found. The borehole pointed out:
- from 0 and 1.20 m: dark silt layer characterised by a limit pressure pl around 0.54 MPa (1 value)
- from 1.20 m to 5 m: clayey sandy silt with chalk particles ; with a limit pressure pl encompassed between 0.27 MPa ≤ pl ≤ 1.31 MPa
- from 5 m to 6.5m : a silty chalk layer with a limit pressure pl ≥ 2.94 MPa (1 value),
- from 6.5 m to 12m : a chalk layer with a limit pressure pl ≥ 2.44 MPa ,
- water contents were about 20%.

3.2. Characteristics of columns

The soil-cement column technique was considered as an alternative to rigid inclusions and stone columns. Indeed, the latter was generally assumed to be too soft in terms of stiffness and bearing capacity whereas the rigid inclusions appeared to be rather too stiff. The intermediate case represented by soil-cement columns would provide a better homogeneity of the distribution of load on the sub-grade layer as well as a homogeneous settlement profile.
As for stabilization or reinforcement purposes, there was a great need for homogeneous admixture in (soil-cement) columns [2], we analysed this aspect in the paper.
The set up of columns was done with wet soil mixing method i.e. the soil was mixed with cement grout. A specific device has been used in order to achieve an homogeneous soil-cement mixing. The cement used was a CEM III/C 32.5 N PM-ES.
The built up procedure of columns can be described as follows:
- the Ø 600mm diameter rotating mixing tool is jacked and sheared the soil by mixing it with cement. One top-down phase:
- from top to base: rotation and injection and from base to top: rotation and injection.
- soil-cement columns were instrumented using the French extensometer technique. Indeed, a close ended steel tube was installed in each column on the day the construction of the column occurred. Consequently, the cement set with the enclosed steel tube and both elements were tied up.
- after a few days, a specific pile head was built with steel reinforcement to ensure a good connection between the head of the column so that the LCPC load cell could be positioned and the load could be applied vertically.
- the soil-cement column with the enclosed steel tube was loaded as a whole.

The soil-cement column was built in about one hour. The columns P1 and P2 have been built respectively on the 30th and 31st October 2006 by Keller. The anchors required for the reaction frame were built on 31st October 2006. Samples 160mm in diameter and 320mm long were collected at the head of the test column to perform unconfined compression tests. The length of the columns located the column bases at an intermediate level between the silt and the good chalk layer. The physical properties of the columns are described in table 1.

Table 1. Characteristics of the columns

Column n°	Diameter (mm)	Length (m)	W/C	Density* kg/m^3
P1	600	5,30	1	338
P2	600	5,30	0.83	397

* estimate mass of cement in one m^3 of soil-cement column

3.3. Excavation of the columns and Laboratory tests (INNOTRACK project)

Two columns are considered in this paper: column P1, column P2 and a test column similar to P1 in terms of density and W/C ratio (but not loaded). The test column and column P2 were excavated (Figure 3). The shape was regular and looked like a cylinder. The measured diameter of the test column was about 640 mm (more than the 600 mm diameter expected).
From the head of a excavated test column, (different from P2), lumps at the top 2-3 m of the soil-cement columns were collected to achieve laboratory tests and to get mechanical parameters.

For design, the assessment of the shear strength of soil-cement from the results of field load tests presupposes that the stabiliser is mixed uniformly over the whole cross section and that the column can be considered as homogeneous. Such was not the case. Indeed, the sampling of the side part of the column (Figure 3) showed different materials within the soil-cement column sample. Soil areas, cement-areas as well as soil-cement areas could be clearly identified in the ∅80 mm sample. It illustrated the significance of the heterogeneity of soil-cement column in this sample. The samples 7 and 8 were collected at the column head by KELLER during the building of the columns and tested. During the installation of the column, the grout backflow seemed mostly composed of cement. The values of R_c (unconfined compression test) and E (elastic modulus) (Table 2) were expected to be larger than the values obtained from the samples collected at a bigger depth when the column was completed. For the collected samples (after the setting of cement), the ranges of R_c were 4.98 – 8.95 MPa (we did not consider sample 1) in comparison with 3.2-4.6 MPa.
A sample of the side part of the column shows some heterogeneities with soil parts, cement parts and mixed parts (figure 4).
On Table 3, as a comparison, an abacus is given of the UCS results for jet grouting samples for different soils and different cement contents.

Figure 3: Excavation of column P2

Figure 4: Sample of the side part of the test column

Table 2: Test results on soil-cement columns samples (silt)

Sample number	∅ (mm)	Length(mm)	R_c (MPa)	E (GPa)
Sample 1	37.8	77.2	0.62	-
Sample 2	38.97	73.84	8.95	4.9711
Sample 3	38	73.3	6.41	-
Sample 4	37.80	68.20	7.26	2.431
Sample 5	37.95	80.92	4.98	4.086
Samples collected at the head of the column (P2) - 7	160	320	3.2	-
Samples collected at the head of the column (P2) - 8	160	320	4.6	-

Table 3: Abacus UCS as a function of Cement content C and of the type of soil for jet grouting [10]

Soil	Cement content kg/m^3	Unconfined Compression Strength (MPa)
Silt	250	2
	300	3 à 4
	350	5 à 7

The results of the laboratory tests carried out on samples that come from the silt – cement mixing (cement content encompassed between 338 and 397 kg/m^3) and the jet grouting samples are compared. In the latter, from table 3, for 350 kg/m^3, the UCS values are between 5 and 7 MPa; values that are quite close to values obtained on table 2 from soil mixing columns. Then, it might be interesting as a first step to consider them as materials that have the same strength. It also justifies the fact that we could compare the column response under pile load test.

3.4. Instrumentation of the columns for pile load tests

The columns were instrumented using the French removable extensometer [4, 5]. A ∅ 52/60 mm diameter and 5.30 m long closed ended steel tube was used. It was installed in the middle of the column just after the soil-cement column had been set up. A column head was built for each soil-cement column on the same day as the column; 60 cm squared concrete block and 25 cm thick. During the loading test, the load was applied on the column head. The top of the steel tube reached the top of the column head. When the soil-cement column load test was performed, several segments of packers and steel ribbons [4, 5] (with strain gauges stuck on it) (Figure 5) were installed in the steel tube to perform the strain measures.

3.5. Measurement devices and tests

Reaction frame and loading system used during the field test consisted in :
- a steel beam laying on wood beams and linked to four bars DYWIDAG ∅ 22mm and consequently to four reaction piles ∅ 200mm (Figure 6). They work in tension when the column was tested in compression.
- four displacement gauges with a 1/100th accuracy at the pile head
- five extensometer segments with deformation Δl/l (Figure 5)
- data acquisition system and a computer.

The soil-cement columns have been loaded following the LPC (Laboratoire des Ponts et Chaussées) method and the standard method [7]. The load applied increased through constant load increments (each load was applied during one hour) until failure load. After the load test, two columns were excavated; in particular the load tested column P2.

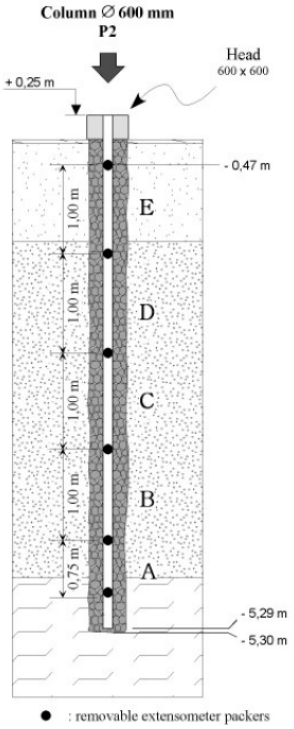

Figure 5: Removable extensometer in soil-cement

3.6. Load tests and analyses

Two W/C ratio were tested, 1 and 0.83 respectively. In figure 7, we show the plot of the pile-head load Q_0 – pile head displacement S_0 (mm) curve for the two column tests. For column P1, seven load steps had been achieved whereas for column P2, 10 load steps were performed. In both cases, the maximum reached settlement were respectively 5.8 mm (maximum load 300 kN) and 7.2 mm (maximum load 450 kN) as the columns showed a bearing capacity greater than expected.
In the paper, we add an interpolation made from the Chin method [8] to evaluate the bearing capacity as well as the distribution of the resistance along the column i.e. shaft friction and tip resistance.

Figure 6: View of the load test system

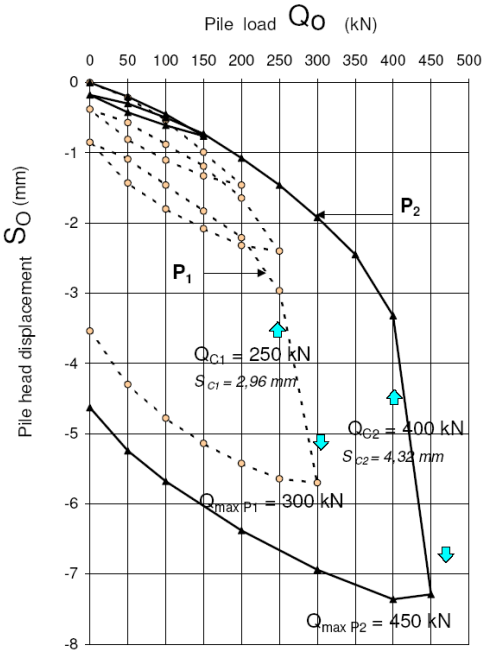

Figure 7: Load-settlement curve for column P1 and P2.

3.6.1. Column P1

The load test was performed after 36 setting days. The maximum load applied was 300 kN for a settlement of 5.8 mm (about 1% of the pile diameter). The creep load reached Q_c = 250 kN.
The load distribution along the pile and its mobilisation were determined from the unit strains ε. Young moduli were estimated from the results of R_c laboratory tests (table 2) in order to draw the mobilisation curves of the shaft friction q_s for different soil layers and different depths. On figure 8, we noticed that the biggest part of the load is mobilized on the segment A which would transfer it to the underneath levels. The limit load Q_u = 300 kN was composed with 86% by shaft friction (Q_s = 258 kN) and 14% by the tip (Q_p = 42 kN). Chin method [8] was used to estimate the bearing capacity of the soil cement column. From Chin method, the bearing capacity was estimated at 417 kN with a shaft friction of 266 kN (64%) and a tip resistance of 151 kN (36 % of the total load). Therefore, as expected, the shaft friction had been fully mobilized for a settlement of 5.8 mm whereas the tip mobilization required more settlement to be fully mobilized.
The tip resistance stress reached about 0.5 MPa (151 kN/(πx0.3^2)) which is rather small in comparison with the pressumeter results (0.97 MPa at 4.8m and > 2.94 MPa at 5.8m) if we analysed the results in the same way as for a pile. However, in terms of soil reinforcement, the mechanical properties of the soil were actually improved.

3.6.2. Column P2

The load test was performed after 38 setting days. The maximum load reached for column P2 was 450 kN with a settlement of 7.2 mm (about 1% of the pile diameter). The creep load Q_c reached Q_c = 400 kN.
The load distribution along the pile and its mobilisation were determined from the strains ε. On the figure 9, we noticed that again, the biggest part of the load was transferred to the level A. The limit load Q_u = 450 kN was composed with 62% by shaft friction (Q_s = 279 kN) and 38% by the tip (Q_p = 171 kN). From Chin method, the bearing capacity was estimated at 811 kN with a shaft friction of 570 kN (70%) and a tip resistance of 241 kN (30 % of the total load). In this case, the shaft friction had not been mobilized for a settlement of 7.2 mm contrary to column P1. Again, the tip mobilization required more settlement to be fully mobilized.
On figure 9, at the load step 9 (400 kN), the steel tube and the column slid on each other as the shaft friction reached its maximum. Therefore, from this load, we were not able any more to measure the distribution of load along the column. The evaluated shaft friction and tip resistance were made from the load of 400 kN. Therefore, we were only able to analyse data from the extensometer until the load step at 350 kN.
As far as the shaft friction was concerned, the mobilisation curves of the unit load ; for the different depths along the sleeve: A – B – C – D – E, are represented on figure 9. The plots show that the load carried at the levels B and A are much bigger than the other levels as at those depths, we were reaching a strong soil resistance area. As a comparison to the column P1, the q_s values, for P2 at the load step 300 kN, were equal to: level E : $q_S \approx$ 5 kPa, level D : $q_S \approx$ 20 kPa, level C : $q_S \approx$ 18 kPa, level B : $q_S \approx$ 45 kPa, level A, $q_S \approx$ 47 kPa
For the two columns, the distribution of load looked similar with about 70 % taken from the shaft and 30 % from the tip. However, the difference in terms of bearing capacity could not only be explained by the W/C ratio and the cement contents of 338 and 397 kg/m^3. The actual distribution of cement along the column would need to be considered.
Besides, for both columns, the shaft friction was fully mobilized at the levels E, D, C and B with measured values greater in the case of the column P2. At level A, the skin friction was not completely mobilized in both cases as it went on increasing with the applied load.

As far as the shaft friction is concerned, the mobilisation curves of the load; for the different depths along the sleeve : A – B – C – D – E, are represented on figure 10. The plots show that the load carried at the levels B and A were much bigger than the other levels due to the vicinity of the good soil layer. At these levels, the q_s values are equal to: levels D et E (D and E gathered together due to experimental reasons) : $q_S \approx$ 13 kPa, level C : $q_S \approx$ 13 kPa, level B : $q_S \approx$ 37 kPa, level A, $q_S \approx$ 72 kPa (Figure 11).

A general remark is that none of the two pile tests have been conducted until failure. The maximum loads reached were 450 kN.

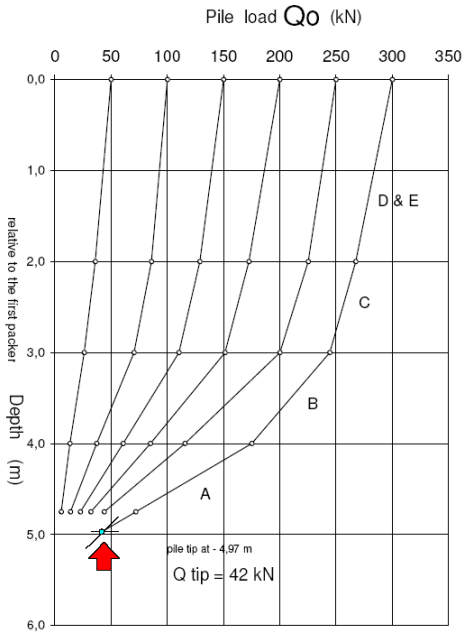

Figure 8: Load distribution along the column P1

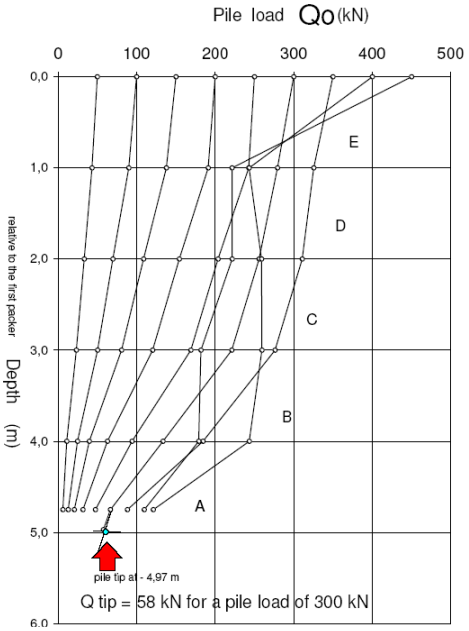

Figure 9: Load distribution along the column P2

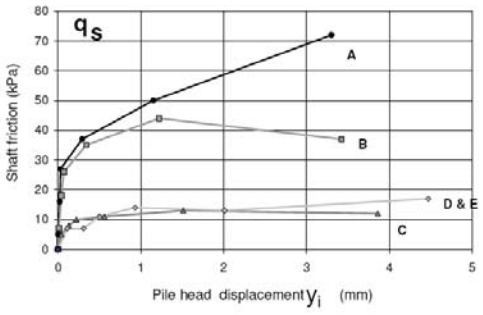

Figure 10: Load distribution along column P1

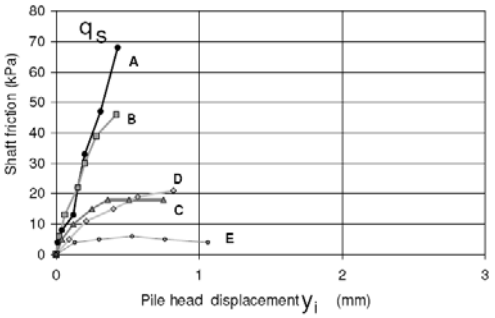

Figure 11: Load distribution along the column P2

On Figure 12, we have tried to plot the p_l-q_s points from tests P1 and P2 in a proposed abacus for jet grouting [3].

As far as shaft friction is concerned, the following values of q_s were chosen : for pile segments A and B :
- the p_l considered are respectively 1.34 and 1.14 MPa,
- the shaft friction taken as the average of the maximum values obtained during pile tests P1 and P2 i.e. respectively 70 kPa and 43 kPa.

The following values of q_s have been chosen : for pile segments C and D :
- the p_l considered are respectively 1.05 and 0,58 MPa,
- the shaft friction taken as the average of the maximum values obtained during pile tests P1 and P2 can be taken as one value i.e. respectively 15 and 20 kPa.

In all the cases, the points are lower than the silt line probably due to the fact that the piles could not be been loaded until failure as the two techniques enter the non-displacement pile category.

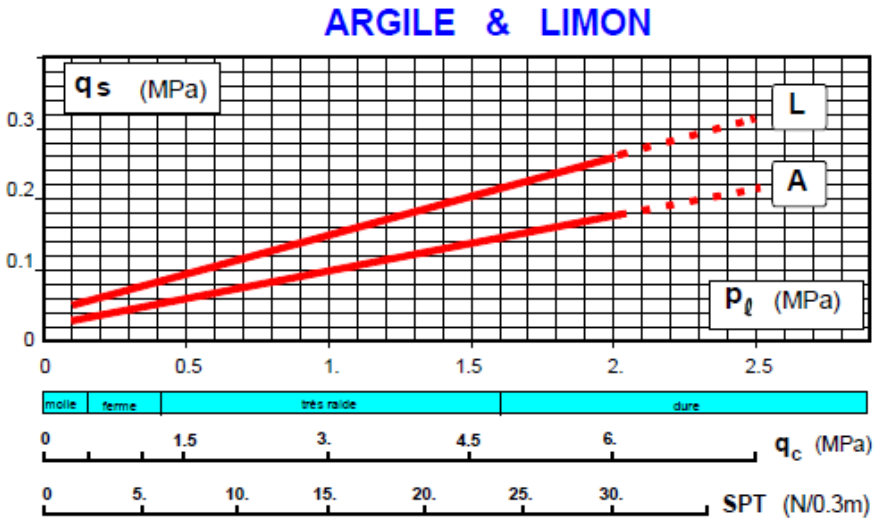

Figure 12: Abacus for the calculation of shaft friction qs in jet grouting columns for silt and clay [3]

4. FEASABILITY TESTS ON THE NEW DEVICE

On 2009, an experimental site has been chosen in Woerth (67), France on an EHPAD field work. The chosen cement content was about 280 kg/m^3.

The built up procedure of columns is the same as the procedure described in paragraph 3 ; i.e. two top-down phases were performed in order to get the best soil-cement mixture and the most homogeneous material. Some results of UCS tests on samples from soil-cement columns are given on Table 4. If we compare from Table 3, the values obtained are comparable to silt –cement mixtures.

Table 4 Test results on soil-cement columns samples (silty clay)

Depth (m)	Soil	L/d ratio	Dates		Raw results		Density
			Building up	Age	Rc	Young Modulus	
				j	MPa	MPa	
1.50	Silty Clay	2.0	23-nov.-09	66.00	2.66	NC	1.58
2.50	Silty Clay	2.0	23-nov.-09	66.00	3.40	NC	1.65

Figure 13: Photos of soil-cement samples before and after UCS tests

Some pictures of the samples are shown on Figure 13. Some inclusions are observed within the soil cement mixed material but it can be considered as acceptable for this technique used in a clayey soil.

5. CONCLUSIONS

The planned objectives regarding the feasibility of the soil-cement columns have been reached.
From the first test sites, it can be assumed that the mechanical behaviour of the soil-cement column might be assimilated to jet grouting inclusions in terms of UCS resistance for similar soils and similar cement contents.
The pile load tests showed bearing capacities for the two columns 417 kN and 811 kN respectively extrapolated from the Chin Method. The difference between the two columns, beyond the influence of the W/C ratio and the density of cement, illustrated the better distribution of cement in the column P2 in comparison to the column P1.
Using the extensometer technique, it was possible to achieve the distribution of load along the column. Indeed, the distribution of load along the columns seemed constant regarding the Chin method calculations with 70% of load taken by the shaft and 30% taken by the tip. The distribution of cement and soil in the soil-cement column needs to be checked to avoid heterogeneity issues.
A new 150 mm core retractable tool has been developed and also showed good results in terms of homogeneity of the mixture and soil-cement material resistance.
Other pile load tests should be carried out to validate our hypothesis relative to the similarities in the DSM and jet grouting columns mechanical response (bearing capacity, shaft friction and tip resistance).

REFERENCES

[1] Rocher-Lacoste, F. and Le Kouby A., 2007. Plots d'essais réalisés sur le site de la gare TGV Haute Picardie (80). Essais de chargement et instrumentation d'ouvrages. Essais LCPC/KELLER. INNOTRACK (27 pages).

[2] Swedish Geotechnical Institute Report 4:95E. 1997. Lime and Lime cement columns.

[3] Bustamante, M. 2002. Les colonnes de Jet Grouting : dimensionnement et contrôle. Séminaire Franco – Tunisien : Pathologie des sols et des fondations, Hammamet, 7-8 février 2012.

[4] Rocher-Lacoste,R., Dudouyt, F., Le Kouby, A., 2011. Méthode d'essai n°68 – Essai statique de pieu isolé instrumenté avec la technique de l'extensomètre amovible , sous charge axiale. Laboratoire Central des Ponts et Chaussées / IFSTTAR, Paris, 40 pages.

[5] Bustamante, M and Doix, B.1991. A new model of LPC removable extensometer. Proceedings of the 4th International on Deep Foundation (DFI), pp. 475-480.

[6] CDIT (Coastal Development institute of Technology). The Deep Mixing method, principle, design and construction. Balkema publishers, Tokyo, Japan.

[7] Norme Française NF P 94-150. 1991. Essai statique de pieu isolé sous compression axiale.

[8] Tomlinson, M. J. 1995. Pile design and construction practice. Fourth edition, E&FN SPON.

[9] Keller. 2005. European patent. Verfahren zur Fundmentsicherung sowie Bohr – und Mischwerkzeug. EP1 630 299 A1

[10] Chambosse, G. & Kirsch, K. 1995. State of the Art of Jet Grouting method in Germany. 4th Pacific Rim International Conference on Water jet technology, Shimizu, Japan

Soil mixing in highly organic materials: the experience of LPV111, New Orleans, Louisiana (USA)

Filippo Maria LEONI, TREVIICOS Corp., USA, fleoni@treviicos.com
Alessandro BERTERO, TREVI SpA, Italy, abertero@trevispa.com

ABSTRACT

The LPV111 project involved raising the existing 8.5 kilometer levee, which rests on a foundation of soft organic clay, approximately 10 feet in a period of about 1.5 years. Due to several constraints (time, environment, real estate) the Deep Mixing Method (DMM) was selected to improve the adverse geotechnical properties of the foundation soils and consequently stabilize and support the burden of the new levee. DMM entails the in-situ mixing of soil with an established amount of cement binder. One of the technologies chosen to perform the 1.3 million cubic meters of treatment was the Trevi Turbo Mix (TTM). A preliminary laboratory program (Bench-Scale Test, 4 phases) and a field test program (Validation Tests, 5+ phases) were conducted to estimate the appropriate binder type and dosage, and equipment configuration capable to efficiently meet the technical requirements of the project. Acceptance criteria were based on continuity, uniformity and unconfined compressive strength of the treatment. The extensive presence of highly organic layers (peats) in the geological sequence was given special considerations. Typically, due the very poor geotechnical properties, considerable amount of binder and mixing time are required to stabilize these materials. By comparing and interpreting the significant quantity of results from the various stages of the project, it was possible to fine-tune the construction parameters and effectively reduce the potential impact of the presence of such materials on production time and consumption of materials. Ultimately, a high-quality end product was provided ahead of schedule, under budget and without remedial work. This document presents the results achieved by the soil mixing operations at LPV111, the largest land DMM project ever accomplished outside of Japan. Particular mention is made to the development of the construction procedures implemented to successfully address the difficulties that the presence of organic materials initially presented.

1. INTRODUCTION

Reach LPV111 is part of the New Orleans East Back Levee, which is an essential component of the New Orleans Hurricane Protection System in Orleans Parish (*Figure 1*).

Figure 1: location of LPV111

The existing levee sections and concrete T-wall suffered extensive damage from Hurricane Katrina, such that the US Army Corps of Engineers (USACE) elected to provide earth stabilization and rebuild the 8.5 kilometer levee section as part of the Greater New Orleans Hurricane Storm Damage Risk Reduction System (HSDRRS). Due to the adverse geotechnical properties of the foundation soil, which included soft clays and thick organic layers, ground improvement was deemed necessary to stabilize the footprint of the new levee and allow the placement of fill to the required elevation. The Hurricane Protection Office (HPO) of the USACE and URS Corporation (URS) designed the Deep Mixing Method (DMM) as the most suitable technology to accomplish the ground improvement (*Figure 2*) and awarded the joint venture of Archer-Western and Alberici Constructors in alliance with Treviicos South (TIS) the contract for its construction.

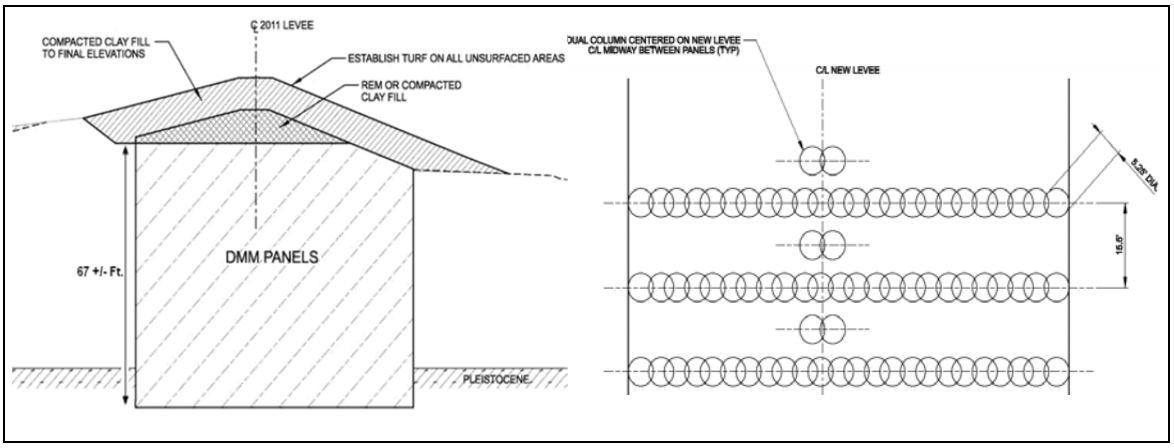

Figure 2: typical design of DMM stabilization at LPV111 (cross section & plan view)

In order to estimate the operative parameters and the technical procedures for the DMM work, a laboratory mixing program was conceived and named Bench-Scale Test program (BST) to differentiate it from the field-scale Validation Test program (VT). As many as four BST phases and five VT stages (plus additional tests) were accomplished prior to and during the construction period. The outcomes of the various phases of the laboratory tests (BST-I through IV) and field tests (VT-1 through 5), as well as testing during the production mixing, consisting primarily of Unconfined Compressive Strength (UCS) results, were recorded, analyzed, interpreted, and used to fine-tune the production parameters in a continuous process that enabled TIS to ultimately provide the highest standard of quality end product.

2. TECHNOLOGIES

At LPV111 two different technologies were applied to treat over 1.3 million cubic meters of foundation soil: 1) Trevi Turbo Mix (TTM), single and double, and 2) Contrivance Innovation Cement Mixing Columns (CI-CMC). Both technologies are considered “wet systems”. These innovative and distinct DMM systems were able to produce large (1.6 m diameter), uniform, and continuous improved elements in a faster and more consistent fashion than the traditional deep soil mixing methods.
In the DMM, the combination of vertical penetration/withdrawal rates, rotational speed, and tool configuration, along with the injection parameters and the properties of the grout, is fundamental for the success of the soil treatment. Nonetheless, the effectiveness of these parameters depends largely on the physical and mechanical properties of the soil to be treated. Therefore, well designed laboratory and field test programs, aimed to disclose the interaction between the site-specific soils and the mixing parameters, are critical to achieve the desired end product.

3. LOCAL GEOLOGY

Geological and geotechnical information was obtained through soil investigation and classification performed prior to and during construction.
In general, most of the present landmass of the southeast Louisiana was formed by deltaic processes of the Mississippi River over the past several centuries. The deltaic to marine deposits consist of interbedded and interfingered clays, silts and sands, with a typical presence of organic layers.
In particular, the soils underlying the LPV111 levee were typically characterized by the following sequence from the ground surface downwards: existing levee fill, soft clay, marsh/peat deposits, fat clay, and Pleistocene soils (*Table 1*). The challenge was to properly and uniformly treat both, soils with very poor geotechnical properties (peat) and soils typically difficult to mix (stiff clay).

Table 1: typical soil sequence at LPV111

ID	Soil Type	Avg. Elev. Range (m)	Description
S1	Levee fill	From +6.0 to +0.5	Stiff to hard Fat Clay (CH), Sandy Clay (CL) and very loose to loose Sandy Silt (ML), Silty Sand (SM) with occasional organics and wood
S3*	Soft Clay	From +2.5 to -4.0	Very soft to hard Fat Clay (CH) and Lean Clay (CL) with occasional sand and silt layers, sand pockets, peat pockets, wood and organics
S4	Peat	From -1.0 to -5.5	Organic Clay (OH) to Peat (P) with roots, fibers and occasional wood
S5	Fat Clay	From -1.0 to -16.0	Very soft to stiff Fat Clay (CH) with sand seams and occasional sand and silt layers
S6	Pleistocene	From -14.0	Firm to hard Fat Clay (CH), Lean Clay (CL), and loose to very dense fine sand (SP)

*with ID S2 was labeled the imported material used to build the working platform

Index property testing including natural water content, Atterberg limits, particle size, unit weight, organic content, specific gravity of solids, pH, sodium content, and sulphate content were performed on selected soil samples. Resulting plots are presented in *Figure 3*.

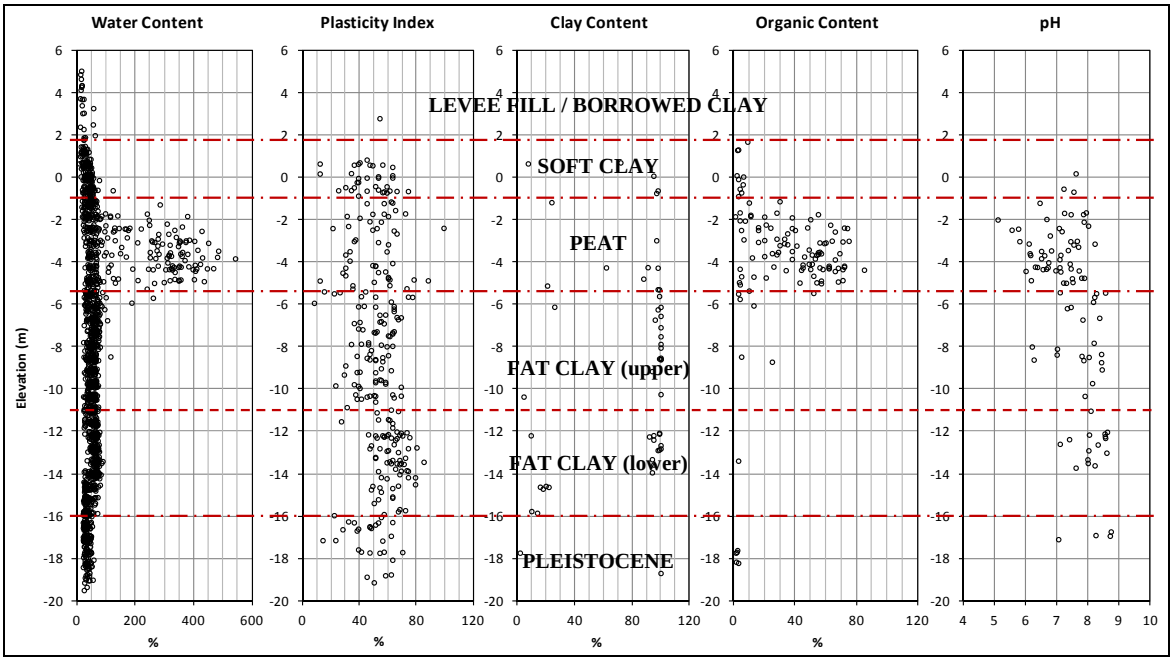

Figure 3: Soil properties plots and interpolation

The further distinction between upper and lower region applied to the Fat Clay layer was introduced at a later stage based on field results. The upper layer was separately tested in the fourth phase of the Bench Scale Test program.

4. BENCH SCALE TEST PROGRAM

The main objective of the Bench Scale Test program (BST) was to investigate the impacts of binder type, binder amount, and water-to-binder ratio on the unconfined compressive strength of mixtures from the various types of soil that would be treated during production mixing.

The BST program included four phases. Phases I, II, and III used soils from reaches 12B, 12A, and 11B, respectively, progressing from west to east and then north along the project alignment. A smaller Phase IV was undertaken to supplement previous investigations of binder type mainly targeting the organic layers.

Mixing, curing, testing, and data reduction and presentation were performed in general conformance with the procedures described by Hodges et al. (2008). Some of the clay soils at this site are stiff and/or high plasticity, which made them relatively difficult to mix, compared to soft, low-plasticity clays and to soils

with low clay content. Consequently, special care was given to mixing and casting the mixtures for curing.
During much of the BST, the construction specification for production DMM elements called for 90% of tested specimens to have an unconfined compressive strength at least 827 kPa (120 psi) after 28 days of curing time. To account for differences between laboratory and field mixing, as well as variability in subsurface conditions, target 28-day strength of 1654 kPa (240 psi) was established for laboratory mixed specimens.
Two binder types were incorporated in the BST program: ordinary Portland cement (PC), and Portland blast furnace slag cement (PBFC). Four different compositions of binder, combining OPC and PBFC with different percentages, were tested. Binder factors ranging from 180 to 550 kg/m3 were employed in the test program, where the binder factor is the dry weight of binder divided by the volume of soil to be treated. Water-to-binder ratios varied from 0.8 to 1.25. In addition, some of the relatively stiff and plastic clay samples were pre-treated by mixing with water to determine whether such pre-treatment could increase the mixture strength by softening the soil and promoting more thorough mixing with the binder slurry after pre-treatment. Not all combinations of variables were tested for all soil types. For example, binder factors near the high end of the range mentioned above were applied to the marsh/peat deposits based on prior experience with similar soils.
The general pattern for each batch was to prepare enough 50-mm-diameter by 100-mm-tall specimens that two specimens could be tested at each of 7, 14, 28, and 56 days, and also allow some extra specimens to account for damage during handling and for additional testing in case of anomalies. Altogether, 86 batches were prepared and 688 unconfined compression tests were performed. For each batch, the unconfined compression test results were plotted versus curing time. Additional insights into the influences of mixture components on mixture strength were obtained by plotting the results for each soil type and binder type versus binder factor (defined above), binder factor in-place (weight of dry binder divided by the volume of treated soil plus volume of grout), and total water-to-cement ratio of the mixture (dry weight of binder divided by the weight of soil water plus the slurry water). These terms are defined and their use is illustrated by Filz et al. (2005).
Although all the soils underwent extensive tests and analyses during the different phases of the BST, the following paragraphs will focus on the interpretation of the results obtained for the peat layer that presented, at least at first, the toughest challenge for the deep mixing design.

4.1. Phase I

For Phase I of the BST, seven different batches were prepared using soil samples retrieved in the peat layer (*Table 2*); the average natural water content of the samples before mixing was 287%.
The results of Phase I testing on the organic material indicated the following:

a. The peat material is relatively easy to mix, based on visual observations of the mixing process. Nevertheless, there was considerable scatter in the Phase 1 test results for the peat.
b. Adding water prior to adding the binder grout had adverse effects on the compressive strength.
c. Adding slag to the binder considerably enhanced the strength values and the trend of the strength gain with time. It is noted that the peat material treated with pure OPC showed very little to no strength gain with time (*Figure 4a*).
d. The peat material achieved the target strength with a minimum binder factor of 350 kg/m^3 using the PBFC binder without added water (*Figure 4b*).

4.2. Phase II

For Phase II of the BST, four different batches were prepared using soil samples retrieved from the peat layer of hydraulic reach 12A (*Table 3*); the average natural water content of the samples before mixing was 272%. For this phase, the evidence and observations of the previous phase, although performed on peat sampled in a different stretch of the LPV111 levee, were utilized to narrow down the parameter range and improve the thoroughness of the mixtures. One of the measures adopted, for instance, was to use a supposedly more effective mixing device.
The results of Phase II testing indicated the following:

a. The peat is fairly easy to mix.
b. The data scatter in was much less than in Phase I.
c. The target strength was achieved for all binder factors evaluated.
d. Adding fluid to the mix while maintaining the total water/cement ratio (B23) had a slight adverse effect on the strength (*Figure 5a*)
e. Increasing the binder factor above 350 kg/m3 had relatively little effect on the mixture strength (*Figure 5b*).

4.3. Phase III

For Phase III of the BST, the experience acquired through the two previous phases and through some field validation tests, that in the mean time had started, led to the selection of only the high PBFC binder blend for the mixing operations. Moreover, project schedule constraints necessitated the construction be initiated before all the planned phases of BST and VT were completed, therefore requiring the application of somehow conservative parameters for the installation of the DMM.
Nevertheless, four different batches were prepared in this phase using peat samples (*Table 4*) collected in hydraulic reach 11B; the average water content for the soil samples used to prepare the batches was 320%.
The results of Phase III testing indicated the following:

a. The peat is fairly easy to mix.
b. The data scatter was largely reduced.
c. The target strength was attained with all tested batches and all the binder factors (*Figure 6a*).
d. The high PBFC binder blend appeared to provide the most consistent results (*Figure 6b*).

4.4. Phase IV

This phase was undertaken to investigate more in detail the influence of the proportions of cement and slag on the strength of the soil-binder mixtures. For Phases II and III, as well as for the field mixing, a binder composed by low percentage of OPC and high percentage of PBFC was used in light of the results of Phase I, which proved this blend overall more effective than the sole OPC.
Due to concerns about availability and cost of the Slag, Phase IV tests were performed to investigate whether the portion of slag in the binder could be reduced, while still producing high quality mixtures.
Three different batches were prepared using samples of peat material from reach 11B (*Table 5*).
The test results of Phase IV showed the following:

a. The peat responded much better to the high PBFC blend than to the 50%OPC-50%PBFC blend, which in turn produced better results than the low-slag blend.
b. The high PBFC binder was the only one capable of meeting the strength criterion for the project when mixing the organic material (*Figure 7a*).
c. The combination of a binder factor of 320 kg/m3, a blend of with high PBFC content, and a water-to-cement ratio of 1.0, showed the values of 28-day unconfined compressive strength were essentially equal to the target strength of 1380 kPa (200 psi - reduced with respect to the previous phases due to changes in the project specifications explained in Par. 6.) for laboratory mixed and cured specimens (*Figure 7b*).

5. FIELD-SCALE PROGRAM (VALIDATION TEST)

It is known that many factors influence the results of the DMM, including: soil composition, groundwater chemistry, types of dissolved salts, concentration of organic material, characteristics of the binders utilized, equipment configuration, etc. DMM results cannot be accurately predicted based only on past experience. In addition to a well targeted laboratory test program, a field test program should usually be performed prior to actual production mixing. The field tests should follow a comprehensive but flexible approach, allowing adjustments and modifications to the parameters initially foreseen as the operations proceed and new or more detailed information is acquired.
At the LPV111 project, the field test program was conceived to achieve the following objectives: 1) verify and refine the binder type and content, preliminarily determined through the bench scale testing, to attain the target mechanical characteristics of the treated soil; 2) determine the most appropriate DMM operating parameters and equipment configuration; and 3) develop QC/QA procedures for the DMM production stages.
Five field campaigns, called Validation Tests (VT), were planned at five different locations along the levee, characterized by diverse underground conditions, to verify the responses of the soils to various ranges of installation parameters.
At each VT location, both technologies were tested and verified for compliance with the project specifications and the desired quality of the product. The installation of the elements was accomplished by applying different combinations of binder content, water-cement ratio (W/C), and construction parameters, such as: penetration and retrieval speeds; rotational speed; grout delivery rates; grout pressure; air pressure and flow rate (only for CI-CMC); grout and cement quantities; and mixing tool configuration. This approach allowed the development of relationships between the construction parameters and the final result in terms of continuity, homogeneity, and mechanical characteristics of the improved soil. Overall, 75 elements (TTM single, TTM double, and CI-CMC double) were installed.

Table 2: batches prepared for the BST-Phase I on peat samples

Batch ID	Water Content of Molded Soil (%)	Binder Type	Binder Factor (kg/m3)	Binder W/C Ratio	Total W/C Ratio	Add Water (y/n)
S4-B9	208.0	PBFC	250	0.8	3.96	n
S4-B10	152.1	PBFC	350	0.8	2.82	n
S4-B11	208.0	PBFC	350	0.8	3.86	y
S4-B12	152.1	PBFC	550	0.8	2.08	n
S4-B13	234.6	OPC	250	0.8	4.11	n
S4-B14	234.6	OPC	350	0.8	3.16	n
S4-B15	234.6	OPC	550	0.8	2.30	n

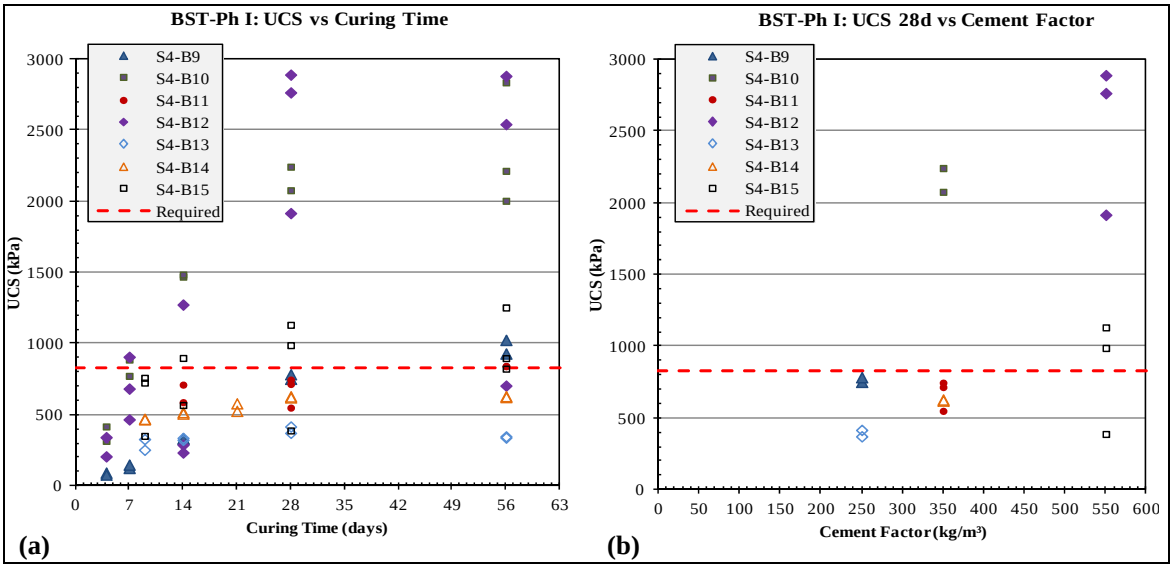

Figure 4: BST - Phase I results (a) UCS vs Curing time; (b) 28 days UCS vs Binder Factor

Table 3: batches prepared for the BST-Phase II on peat samples

Batch ID	Water Content of Molded Soil (%)	Binder Type	Binder Factor (kg/m3)	Binder W/C Ratio	Total W/C Ratio
S4-B20	268.6	PBFC	350	0.8	3.19
S4-B21	251.2	PBFC	400	0.8	2.85
S4-B22	240.1	PBFC	500	0.8	2.42
S4-B23	267.1	PBFC	441	1.0	2.89

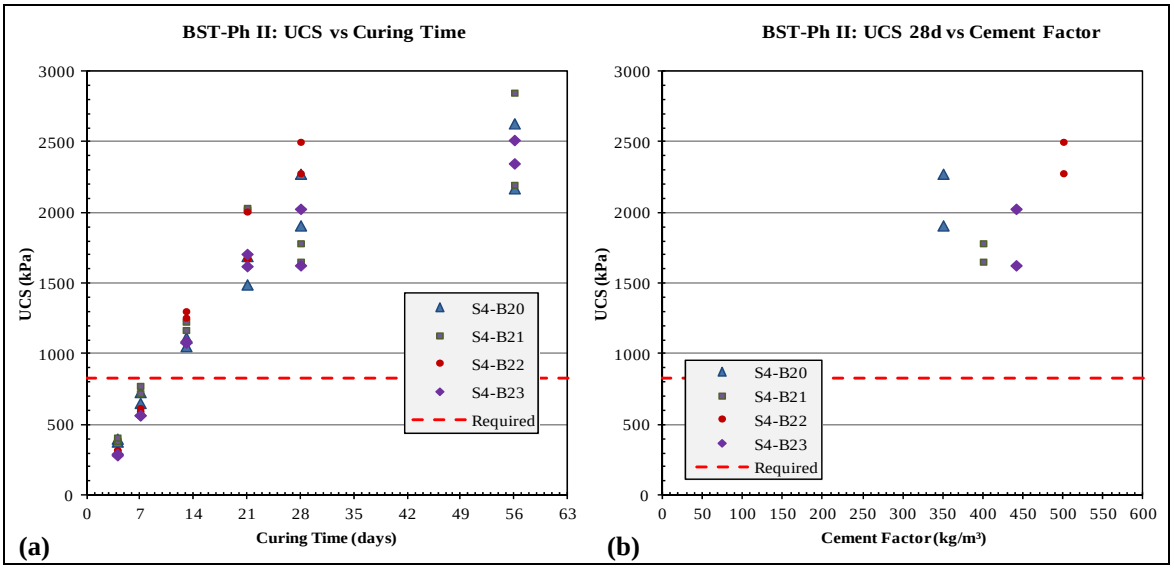

Figure 5: BST - Phase II results (a) UCS vs Curing time; (b) 28 days UCS vs Binder Factor

Table 4: batches prepared for the BST-Phase III on peat samples

Batch ID	Water Content of Molded Soil (%)	Binder Type	Binder Factor (kg/m3)	Binder W/C Ratio	Total W/C Ratio
S4-B36	323.3	PBFC	350	0.8	3.26
S4-B37	327.4	PBFC	450	0.8	2.72
S4-B38	314.8	PBFC	400	1.25	3.39
S4-B39	319.9	PBFC	193	1.0	2.97

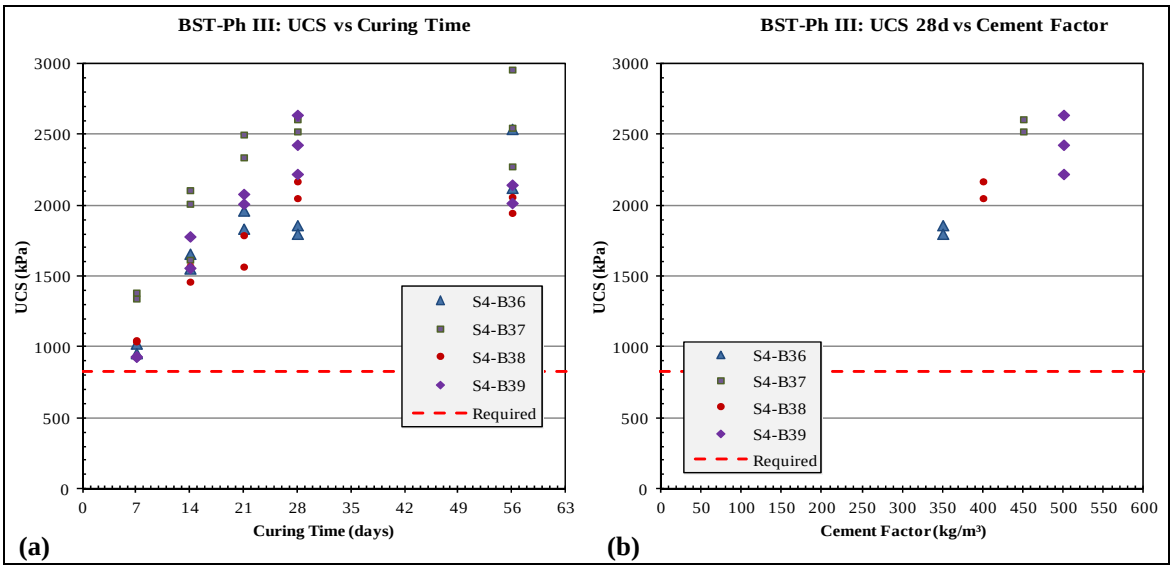

Figure 6: BST - Phase III results (a) UCS vs Curing time; (b) 28 days UCS vs Binder Factor

Table 5: batches prepared for the BST-Phase IV on peat samples

Batch ID	Water Content of Molded Soil (%)	Binder Type	Binder Factor (kg/m3)	Binder W/C Ratio
S4-B90	242	Low Slag	320	1.0
S4-B91	242	50% Slag	320	1.0
S4-B92	253	High Slag	320	1.0

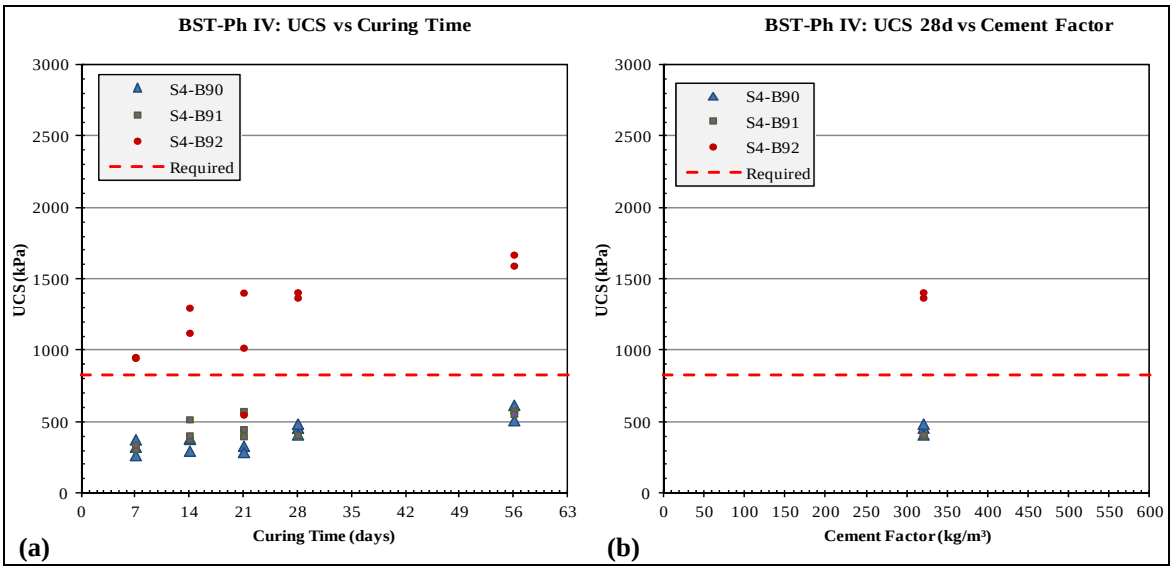

Figure 7: BST - Phase IV results (a) UCS vs Curing time; (b) 28 days UCS vs Binder Factor

Each test element was cored for its entire length. Samples were measured, observed, and moved to the test lab. Unconfined compressive strength, unit weight, and water content tests were then conducted on selected specimens from each test element at different depths and at various ages. Over 1,000 specimens

were UCS tested; the results were analyzed and plotted in different fashions to provide the necessary interpretations. For instance, since the DMM technology is based on the combination of blade rotation number, which controls the consistency and homogeneity of the mixing process, and the binder factor, which governs the final amount of cement in the treated soil, these factors were weighed against the UCS results for each type of soil treated to select the most effective combination of parameters to achieve the required treatment quality.
The BST and VT testing provided an opportunity to investigate the correlation between strength results for materials mixed in the lab and in the field. As previously mentioned, considering the more ideal conditions in the lab (more energy, mixing time, and accuracy are used to mix and cast specimens), the target strengths of the lab trials are typically set two times higher than the required field strengths.
In reality, the VT results showed that, for the peat layer, the field strength test results are generally up to 15% higher than the laboratory results.
These results confirmed the preliminary BST indications that the peat material was relatively easy to mix, as opposed to the original expectation, but that still required a larger amount of binder to meet the specified criteria (*Figure 8*).

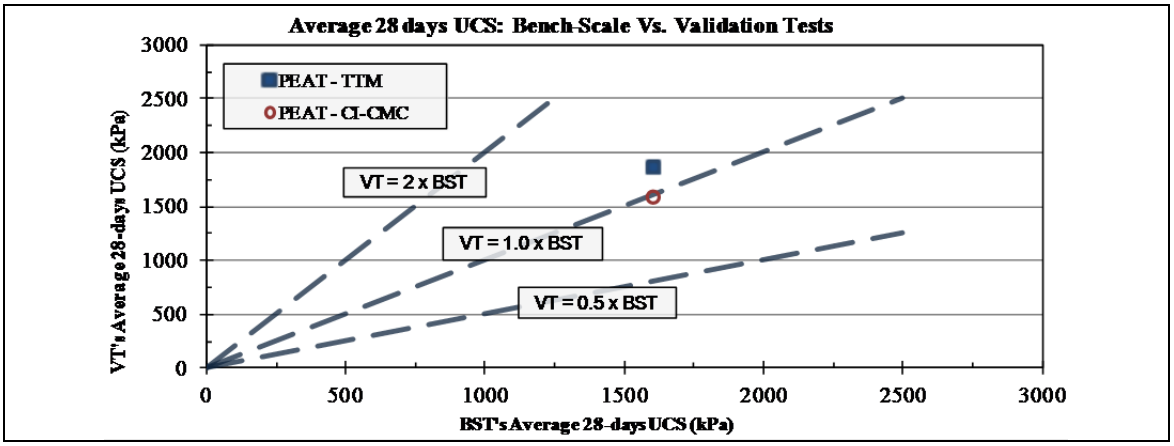

Figure 8: BST/VT Comparison of 28 days UCS for the peat layer

6. QC/QA TESTING, RESULTS AND INTERPRETATION

During the production stage of LPV111 project, over 500 corings were performed through the entire length of the treatment (approximately 20.5 m) per contract requirements, and each 1.5 m core run was accurately measured, logged, and photographed. Over 5,000 cored specimens were selected to and tested for UCS assessment. All the results were tracked, analyzed, and combined with the other available data from the BST and VT programs on a day-by-day basis to fine tune the production parameters and the QC/QA procedures, and to determine whether corrective actions had to be taken.
It is to be noted that the specifications initially required the UCS results from nine of the ten specimens from each cored element must equal or exceed 827 kPa (value that was used for the BST and some VT phases). This requirement was based on a statistical analysis (Filz and Navin 2010) using an assumed coefficient of variation of 0.6 for DMM strength. When the actual data from cored elements showed that the coefficient of variation was much smaller, the same type of statistical analysis showed that the strength requirement could be reduced, and the USACE and URS determined that the strength requirement could be reduced from 827 to 689 kPa (100 psi), with 10% of the strengths that could fall below this value. Additional requirements involved the core recovery (80% required each run); the overall average core recovery resulted around 98%.
Mixing quality involving the organic material was tested 956 times and the results were beyond satisfactory (*Table 6 and Figure 9*).

Table 6: tests performed on prodcution specimens in the peat layer

Layer	Tested Specimens	Avg. UCS	UCS below required strength (689 kPa)		Std. Dev.	Coeff. Of Variation	Median
	N	kPa	N	%	kPa		kPa
Peat	956	2,089	4	0.42%	846	0.405	1,965

To verify effectiveness of the DMM parameter selection for each type of soil condition, the UCS results were divided into target cement factor groups, and then individually analyzed (*Figure 10*).

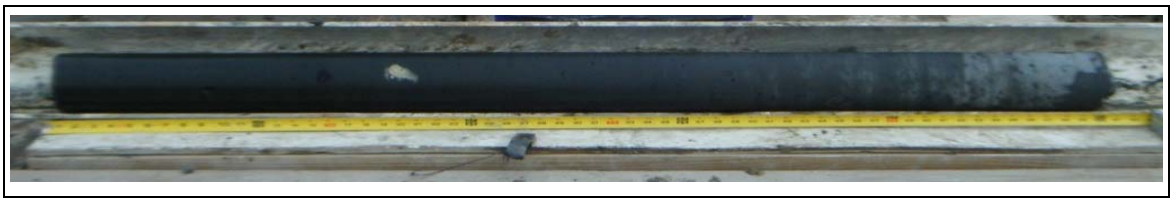

Figure 9: Typical example of core samples retrieved from treated organic soils

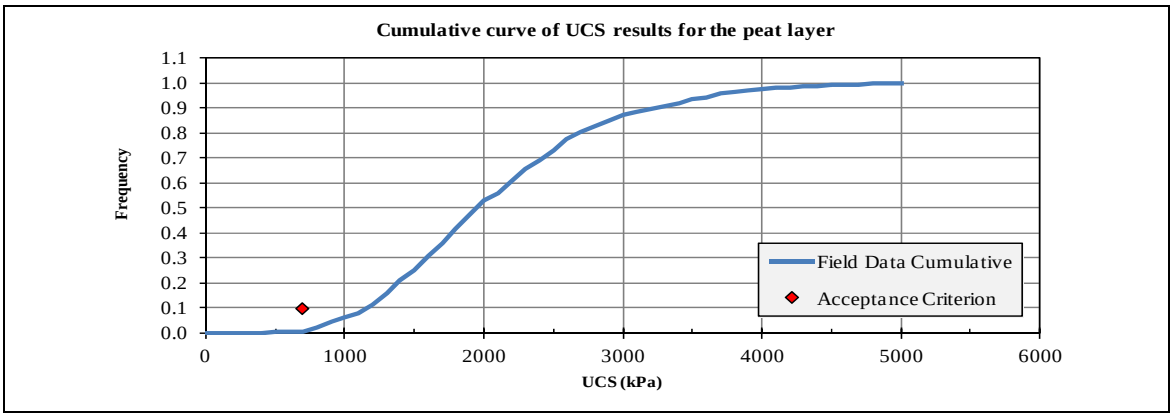

Figure 10: Statistical distribution of 28 days UCS for the peat layer (CF between 330 and 480 kg/m³)

Although not shown in this document, the same analysis was performed on all the specimens and the outcomes demonstrated the mixing performed at LPV111 produced strengths that consistently exceeded the specification requirements for all soil types encountered.

The massive amount of data obtained through the QC/QA program at LPV 111 allowed pin-pointing of construction features to optimize the installation time and cement consumption. Generally the adjustments were the result of observations carried out in the field and through the QC/QA testing during the production stages. Nonetheless, all the changes, especially if entailing a reduction of the cement dosage, were validated before they could be implemented for the production elements, as per the project requirements. This iteration gave an opportunity for a better design of the BST and VT stages as the project progressed.

The most significant consequence of this process was primarily related to the cement consumption. The dosage of the binder was, in fact, reduced without affecting the overall quality of the ground improvement *Figure 11* shows that, while the average cement dosage, expressed as cement used per volume of soil treated during injection, was reduced by about 18% of the initial value, the 28-day UCS increased. This valuable achievement is the fruit of the implementation of more appropriate installation parameters as well as more effective configurations of mixing blades and slurry jets, derived from careful and constructive analysis of the accumulated QC/QA observations and test results.

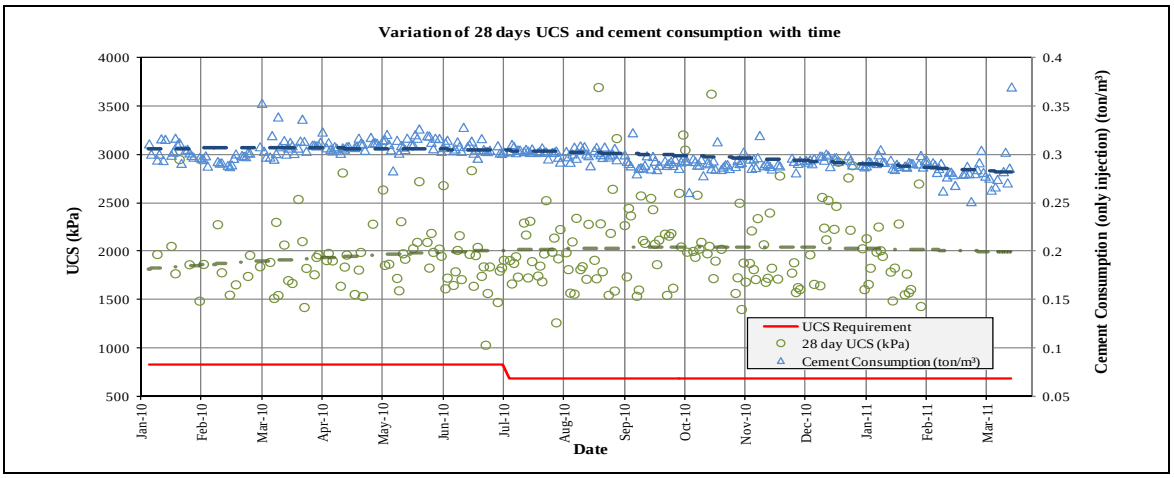

Figure 11: Statistical distribution of 28 days UCS for the peat layer (CF between 330 and 480 kg/m³)

7. CONCLUSIONS

Extensive laboratory and field tests, combined with ongoing QC/QA test during production, allowed the determination of the most appropriate installation parameters for the mixing of over 1.3 million cubic meter of soil at LPV111, the largest deep mixing project ever accomplished outside of Japan. This is especially impressive when the poor geotechnical properties of the soils to be treated are considered, in particular the organic material.
In the specific, the four phases of the Bench Scale Testing program allowed to draw the following conclusions with regards to the peat deposits:

1. The binder with high percentage of slag performed dramatically better than any of the other blinder ratios tested for the marsh/peat deposits. This is related to the enhanced binding process of binders containing relatively higher percentages of chemical components such as: sulphur trioxide (SO3), aluminium oxide (Al2O3) and calcium oxide (CaO) used to treat organic materials (Hayashi and Nishimoto 2005).
2. The mixture strength increased with curing time, and a typical rate of strength gain is for the 56 day strength to be about 1.25 times the 28-day strength.
3. The mixture strength increased with increasing binder factor up to a point, after which diminishing benefit was observed.
4. Pre-mixing with water generally did not produce any benefit; actually it reduced mixture strengths for the thoroughly mixed specimens in the BST program, the reason being that the additional water increased the total water-to-cement ratio, and this lowered the mixture strength.

The Validation Test program, on the other side, permitted the conveying of the lab experience into the field and vice versa. The main conclusions can be summarized as follows:

5. Although mixing in the field is typically more difficult than in the lab, applying well designed mixing procedures, parameters, and equipment configuration the gap can be reduced if not overturned.
6. The peat deposits encountered at the site were relatively easy to mix and blend with the binder, although still required larger amounts of cement to meet the design criteria.

The QC/QA confirmed the outcomes of the test stages and, in turn, produced such a massive amount of data that allowed the continuous fine tuning of the construction aspects to the point that none of the over 18000 DMM elements necessitated remedial work associated to non compliance with the quality criteria. The final conclusions that can be draw are:

7. Consistent laboratory procedures that include thorough mixing and preparation of specimens without voids were necessary to produce useful results
8. The coefficient of variation of UCS values recorded on cored specimens at the peat layer depths was lower than typically reported for DMM projects, which indicates high quality construction operations.
9. Specification requirements were consistently met and exceeded throughout the project duration
10. Integration of BST, VT, and QC/QA programs permitted perfecting the mixing parameters and equipment configuration to continuously improve economy and effectiveness as the project progressed.

REFERENCES

Filz, G.M., Hodges, D.E., Weatherby, D.E., and Marr, W.A., 2005, "Standardized Definitions and Laboratory Procedures for Soil-Cement Specimens Applicable to the Wet Method of Deep Mixing", Innovations in Grouting and Soil Improvement, GSP 136 (on CD-ROM), ASCE, Reston, Virginia, 13 p.

Filz, G.M., and Navin, M.P., 2010, "A Practical Method to Account for Strength Variability of Deep-Mixed Ground", GeoFlorida 2010: Advances in Analysis, Modeling & Design, (GSP 199), ASCE, Reston, 8 p.

Hodges, D.K., Filz, G.M., and Weatherby, D.E., 2008, "Laboratory Mixing, Curing, and Strength Testing of Soil-Cement Specimens Applicable to the Wet Method of Deep Mixing", CGPR Report #48, Virginia Tech Center for Geotechnical Practice and Research, Blacksburg, 60 p. plus appendices.

Hayashi, H. and Nishimoto, S., 2005, "Strength Characteristic of Stabilized Peat using Different Types of Binders", International Conference on Deep Mixing May 23-25, 2005, Stockholm, Sweden. Proceedings pp. 55-62.

Stability Analyses of a Floodwall with Deep-Mixed Ground Improvement at Orleans Avenue Canal, New Orleans

Michael McGuire, Virginia Tech, U.S.A., mcguirem@vt.edu
Eddie Templeton, Burns Cooley Dennis, Inc., U.S.A, etempleton@bcdgeo.com
George Filz, Virginia Tech, U.S.A., filz@vt.edu

ABSTRACT

The dry method of deep mixing was used to improve the stability of a section of the levee and floodwall along Orleans Avenue Canal in New Orleans. Numerical analyses and limit equilibrium analyses of stability of the stabilized levee and floodwall system were performed, and the results were consistent for comparable cases. The numerical analyses were performed using the finite difference method with strength reduction approach applied to a linear elastic perfectly plastic constitutive model. The limit equilibrium analyses were performed using Spencer's Method. The numerical analyses permitted investigating the influence of vertical joints in the deep-mixed zone and the influence of a water-filled gap on the flood side of the cantilevered floodwall. The limit equilibrium analyses permitted evaluating the influence of water-filled tension cracks in the ground on the flood side of the floodwall. The results show that: (1) vertical joints in the deep-mixed zone did not have an appreciable influence on stability, (2) a water-filled gap on the flood side of the floodwall decreased stability, and (3) water-filled tension cracks in the ground on the flood-side of the floodwall decreased stability. The lowest calculated factor of safety was equal to 1.51, and this occurred for water-filled tension cracks in the ground on the flood-side of the floodwall when analyzed using the limit equilibrium method.

1. INTRODUCTION

The deep mixing method has been used to stabilize many levees and floodwalls, including several recent projects in Louisiana (Bruce 2012). This paper describes stability analyses of an existing floodwall at Orleans Avenue Canal in New Orleans with ground improvement on the protected side. The deep-mixed zone was designed using the simplified method described by Filz and Templeton (2011) and Filz et al. (2012). The design analyses were performed assuming that the ground improvement would be done by the deep mixing method, and the project specifications were established to require that either deep mixing or jet grouting meet the same end result in terms of strength, area replacement ratio, column overlap, and clear spacing between adjacent buttresses. Ultimately, the project was constructed using the dry method of deep mixing. In addition to the limit equilibrium analyses, numerical analyses of stability were performed to further investigate the behaviour of the system, in particular the potential impact of a water-filled gap forming on the flood side of the floodwall. The following sections of the paper present the project background, the analysis cross-section and material property values, numerical analyses with comparison to limit equilibrium analyses, and conclusions.

2. BACKGROUND INFORMATION

The Orleans Avenue Outfall Canal is one of several canals that collect and transmit surface drainage from the northern portions of New Orleans. The canal begins just south of Interstate 610 and empties into Lake Pontchartrain approximately 2.4 miles to the north. The canal was initially excavated in the mid 1800's and has been subsequently modified and enlarged. The earthen levees/floodwalls that flank the east and west banks of the canal were designed to provide parallel protection from tidal intrusion from Lake Pontchartrain. Intermittent improvements to the canal have included levee enlargements and the addition of pump stations and floodwalls. As a result of the staggered construction sequence and variable foundation conditions, the floodwalls and levees over the length of the canal vary in terms of cross-section, floodwall type, floodwall dimensions, and sheet pile embedment depths.

The City of New Orleans was flooded during hurricane Katrina, in part due to failures along the 17th Street and the London Avenue Outfall Canals. No failures occurred along the Orleans Avenue Canal, although a low section of earthen levee was overtopped during the hurricane. In response to the observed failures, new design methodologies and criteria were adopted by the U. S. Army Corps of Engineers (USACE), and the entire New Orleans hurricane protection system was evaluated in terms of these new

criteria. Remedial designs were then prepared and constructed within those portions of the system found to be deficient.

Stability berms are the preferred remedial method for floodwalls identified as deficient in terms of stability. A stability berm was deemed impractical in two deficient floodwall reaches along the Orleans Avenue Canal due to right-of-way constraints and environmental concerns. Ground improvement by the deep mixing method was selected for use in these two reaches.

The deep-mixed zone consisted of continuous shear panels oriented perpendicular to the levee/floodwall centerline. This configuration is more efficient for stability than isolated columns because shear panels are not subject to the same type of bending failure that isolated columns can experience. Even when continuous shear panels are used, stability analyses must consider multiple modes of failure, such as composite shearing, rotation of the deep-mixed zone, shearing on vertical planes along column overlaps, extrusion between shear panels, crushing of the deep-mixed ground at the toe of the deep-mixed zone, and global instability. These potential failure modes were evaluated using the simplified method described by Filz and Templeton (2011) and Filz et al. (2012). In addition to the limit equilibrium analyses, numerical analyses of stability were performed to further investigate the behaviour of the system, in particular the potential impact of a water-filled gap forming on the flood side of the floodwall. Due to space limitations, only the stability analyses results (both numerical and limit equilibrium) are presented here for one of the design reaches, which is designated Reach 17.

The stratification and engineering properties of the soils underlying the Orleans Avenue Canal and adjacent flood protection were evaluated using historical soil borings made during the period from 1970 through 1985 for design of previous improvements to the flood wall system, as well as post-Katrina borings, cone penetration tests, and vane shear tests made to support re-evaluation of the flood wall system.

3. ANALYSIS CROSS-SECTION AND MATERIAL PROPERTY VALUES

3.1. Geometry and Stratigraphy

The existing levee, I-Wall, and foundation soil profile considered in the analysis section for Reach 17 are shown in Figure 1. Strata 1 through 5 and Stratum 7 are represented as clays in undrained loading during the flood event, while Stratum 6 is represented as cohesionless material in drained loading. The horizontal distance axis shown in Figure 1 was established during design of the remediation measures for Reach 17, and all elevations are measured in feet. The centerline of the levee is at x = 200.0 ft, corresponding to the horizontal position of the sheetpiles. The existing concrete I-Wall above the sheetpiles has a top elevation of +14.0, which is 7.7 ft above the protected-side top of the levee (El. +6.3), and the sheetpiles have a tip elevation of -9.8. In the analysis section for Reach 17, the flood-side edge of the DMM zone is at x = 204.0 ft. The DMM zone has a top elevation of -2, a base elevation of -22, and a width of 8 ft. In plan view, the panels of overlapping DMM columns comprising the DMM zone have a center-to-center spacing of 13 ft parallel to the levee alignment. The minimum required diameter of the individual columns is 31.5 inches, with a minimum horizontal overlap distance of 9.8 inches between adjacent columns. The area replacement ratio of the shear panels equals the average panel width divided by the panel spacing and is important for determining resistance to shearing on non-vertical planes through the DMM zone. The minimum panel width equals the length of the only chord shared by two adjacent overlapping columns and is important for determining shearing resistance along vertical planes. Using the values of minimum column diameter, column overlap, and panel spacing for the DMM zone along Reach 17 and the geometric relationships provided in Filz and Templeton (2011), the average panel width equals 28.7 inches, the minimum panel width equals 22.8 inches, and the area replacement ratio equals 18.4%.

The canal levels used in the numerical analyses are El. +0.0 for normal conditions and El. +8.0 for flood conditions. The piezometric surface for the sand layer crosses El. -6.2 at a distance x = 0 ft and El. -6.5 at x = 350 ft for normal conditions. During flood stage, the piezometric surface changes slightly, crossing El. -5.8 at x = 0 ft and x = 130 ft, while remaining at El. -6.5 at x = 350 ft.

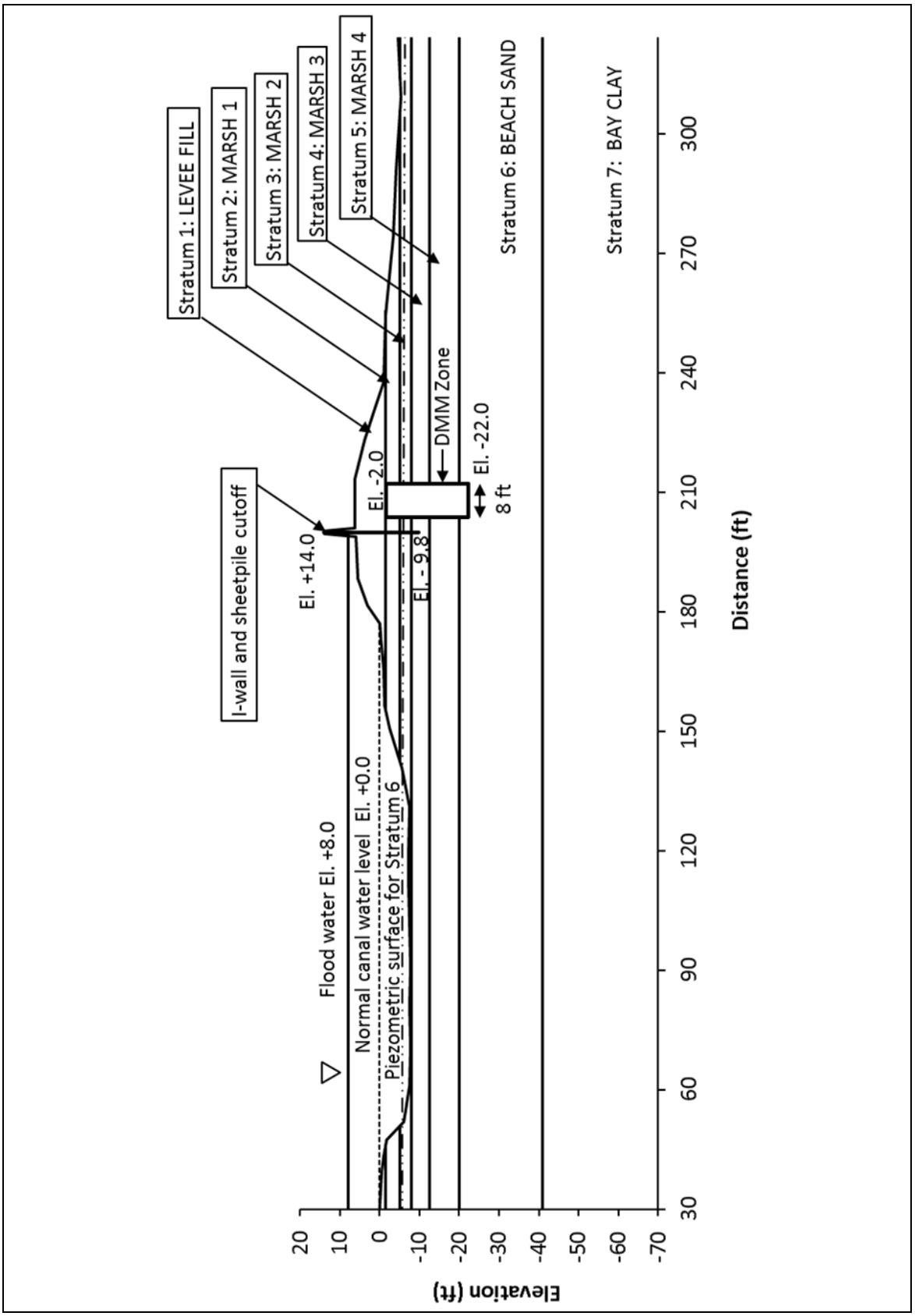

Figure 1: Analysis cross section for Reach 17

3.2. Material Property Values

The material properties of the levee fill and foundation soils in the analysis cross section are provided in Table 1. The undrained strength of clay soils is defined for the analysis section along three vertical profiles located at the centerline of the levee (x = 200.0 ft), the flood side of the levee (x = 164.1 ft), and the protected side of the levee (x = 241.6 ft). For Stratum 7 clay, the undrained strength at each profile location is also defined at the top of the stratum (El. -41.0) and at the bottom of the numerical model (El. -70.0). The undrained strength of clay soils other than Stratum 7 is assumed to be constant over the layer thickness. The undrained strength of soils located between the profile locations (164.1 < x < 241.6 ft) and the top and bottom of Stratum 7 was assigned assuming linear variation. The undrained strength for soils located outside the profile locations (x < 164.1 ft, x > 241.6 ft) was assigned assuming no variation from the closest profile location.

Table 1: Material properties used in numerical analysis of Reach 17

	Top elevation (ft)	Total unit weight, γ (pcf)	Undrained strength, S_u (psf)		Stiffness ratios, E/S_u
Stratum	All x	All x	x = 164.1 ft x = 241.6 ft	x = 200.0 ft	All x
(1) Levee Fill	varies	116	N/A	700	540
(2) Marsh 1	-1.5	97	200	275	390
(3) Marsh 2	-5.0	97	350	400	390
(4) Marsh 3	-8.0	73	180	250	390
(5) Marsh 4	-12.5	111	180	250	390
(6) Beach Sand	-20.0	122	Drained friction angle, $\phi = 33^o$		E = 230 ksf
(7) Bay Clay[2]	-41.0	105	t 580, b 855	t 610, b 885	480

Notes:
1. x equals the horizontal position of profiles in Figure 1 defining material properties.
2. S_u defined at t = top of stratum, El. -41.0, and b = bottom of model, El. -71.0.

Clay soils are modeled as being nearly incompressible, with an assigned Poisson's ratio of 0.49. This value of Poisson's ratio is reduced from the theoretical value of 0.5 for undrained response of saturated clays to avoid numerical instability in the analyses. The value of Poisson's ratio, ν, for the sand layer (Stratum 6) was estimated to be 0.31, based on an effective stress friction angle of 33 degrees and the relationship $\nu = (1-\sin\varphi')/(2-\sin\varphi')$.

The steel sheetpiles beneath the concrete portion of the existing I-Walls along Reach 17 consist of PZ-22 sections. In the numerical models, the I-Wall and sheetpiles are both represented using beam elements with the sheetpile properties extending to the top of the I-Wall. The beam elements were assigned a unit weight of 491 pcf, Young's modulus of 29 x 10^6 psi, moment of inertia of 4.1×10^{-3} ft^4/ft, and a cross-sectional area of 4.6×10^{-2} ft^2/ft.

The design shear strength of the panels was 31.2 psi. As described by Adams and Filz (2010), the composite undrained strength of the DMM zone was estimated by neglecting the strength of the native soil between the DMM panels. This approach accounts for the fact that, relative to the native soils, the stiffer DMM panels develop peak strength at strains that are much smaller than required to fully mobilize the strength of the untreated soil. If the native soil strength is ignored, the composite DMM strength is equal to the design shear strength of the DMM panels multiplied by the area replacement ratio, which equals 827 psf for the current case.

Based on information in a publication by CDIT (2002), a ratio of 300 is considered between the unconfined compressive strength of the deep-mixed ground and Young's modulus, which translates to a stiffness ratio, E/S_u, of 600. This ratio agrees reasonably well with the guidance provided by Navin (2005) and Filz and Navin (2006). For the composite stiffness of the DMM zone, the stiffness ratio is applied to the composite design shear strength of the DMM zone, which yields a modulus value equal to 496,200 psf. A value of Poisson's ratio equal to 0.45 was used for the DMM zone, based on information described by Navin (2005) and Filz and Navin (2006).

The numerical model incorporates four vertical joints in the DMM zone in order to represent the potential for shearing along vertical planes at column overlaps. Various sources (CDIT 2002, Broms 2003, Sehn 2005) cite the potential for weak vertical joints developing at column overlaps. The factors leading to

weak vertical joints, including reduced panel width at column overlaps due to column misalignment, are discussed by Adams and Filz (2010). The design strength along the vertical joints between overlapping columns can range from the full design mixture strength applied to the full design column overlap (100% efficiency) to the case where there is no overlap between columns and the joint strength is equal to the native soil strength (0% efficiency).

For the full design column overlap distance, the ratio of the minimum panel width (22.8 in.) to the average panel width (28.7 in.) serves as a reduction factor that should be applied to the design composite strength of the DMM zone (827 psf) to obtain the shear strength along vertical planes at column overlaps corresponding to 100% efficiency (657 psf). The joint strength corresponding to 0% efficiency was estimated to equal 294 psf by taking the weighted average of the native soil strengths along the flood- and protected-side boundaries of the DMM zone. For the sand layer in each cross section, an equivalent undrained shear strength was estimated based on the average vertical effective stress in the portion of sand occupied by the DMM zone, the effective friction angle, and assuming at-rest lateral earth pressure conditions. Using the approach described by Adams and Filz (2010), the vertical joint strengths for intermediate efficiencies can be obtained by interpolating between the values for 0% and 100% efficiencies.

4. NUMERICAL ANALYSES

4.1. Analysis Methods

The numerical model was developed using the two-dimensional finite difference code FLAC2D (Itasca, 2005), based on previous modeling work by Adams and Filz (2010) that was done to evaluate the stability of levees and floodwalls supported by deep-mixed shear walls in the New Orleans area. Separate analyses showed that extrusion between DMM buttresses along Reach 17 was not an issue, thereby justifying the 2D representation.

The mesh developed for Reach 17 cross section extends 179 ft beyond the I-Wall in the flood-side direction, 124 ft beyond the I-Wall in the protected-side direction, and 48 ft below the base of the DMM zone (El. -70). The bottom elevation of the mesh is consistent with the boundary used in the limit equilibrium analyses of the Reach 17 cross section. The lateral extents of the meshes were secured with roller supports that prevent horizontal displacement, and the bottom of the meshes were fixed with pin supports that prevent vertical and lateral movement. Using guidance from refinement studies performed by Adams and Filz (2010), the mesh was refined near the floodwall and DMM zone. In total, 3,573 soil elements were used in the model.

The existing levee, foundation soils, and DMM zone were modeled in FLAC using the built-in implementation of the Mohr-Coulomb constitutive model. The four equally spaced vertical joints in the DMM zone were modeled by assigning FLAC's "Ubiquitous Joint" model to the mesh zones along each joint and specifying a vertical orientation for the reduced strength. The reduced strength, which is only applied along the vertical joint direction, depends on the specified joint efficiency. The full composite DMM zone shear strength applies to all other planes of potential shearing. The DMM improved material between vertical joints was modeled using the full composite DMM zone strength in all directions. The influence of joint efficiency on the potential for shearing along vertical joints was investigated by performing FLAC analyses over a range of specified joint efficiencies. Since the Ubiquitous Joint model does not allow for assignment of a different modulus on the joint plane, the modulus of the joint material was not reduced for shearing along the vertical plane. According to the FLAC manual and Adams and Filz (2010), modulus values typically have an insignificant influence on the factor of safety calculations.

The I-Wall and sheetpiles were modeled using FLAC's built-in beam elements. A column of dummy zones, shown above the top of the levee in Figure 2, having insignificant mass, stiffness, and strength were defined on the protected side of the beam elements located above the top of the levee in order to associate these elements with the rest of the mesh.

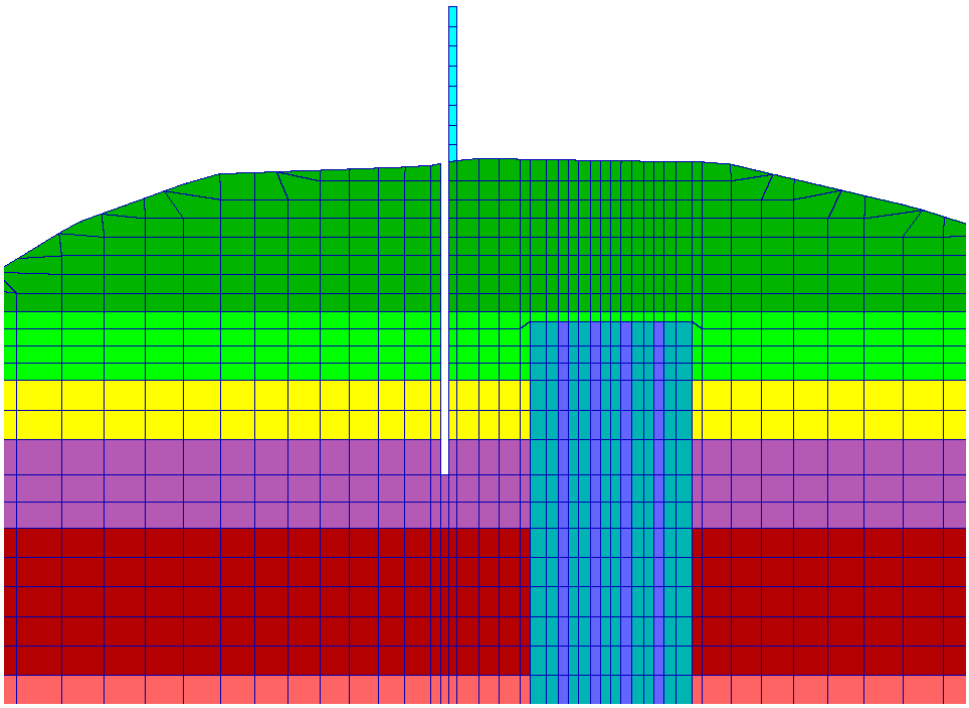

Figure 2: Consideration of water-filled gap in FLAC model

For the stratigraphy considered in the analysis section, there is potential for formation of a water-filled gap on the flood side of the sheetpiles. The water-filled gap was modeled in FLAC to a particular depth by removing the soil to the depth of the gap along a narrow column of mesh zones adjacent to the sheetpiles as shown in Figure 2. Hydrostatic pressures were applied to both sides of the gap as well as the base of the gap. The zones immediately adjacent to the flood side and base of the gap were assigned a high value of cohesion to prevent local failure of these zones from controlling the overall factor of safety calculations in FLAC. The influence of the gap depth on stability was evaluated by incrementally increasing the gap depth from zero (El. +6.1) to the full depth of the sheetpiles (El -9.8).

FLAC's automatic factor of safety routine was used to calculate the factors of safety. This procedure reduces the shear strength of all of the materials in the model by a uniform reduction factor until the program is not able to satisfy convergence criteria in a limited number of iterations. The final factor of safety for the analysis is the largest strength reduction factor at which convergence is still achieved within the limited number of iterations. The factor of safety routine in FLAC calculates the factor of safety to a precision of 0.01.

The tensile strength of the soil and DMM zone were set to zero for all analyses to allow for the possibility of tensile failure.

4.2. Analysis Results

Stability analyses were performed for a range of joint efficiencies without a water-filled gap on the flood side of the sheetpiles. The calculated factors of safety equal 1.68 for the case of 100% joint efficiency and 1.67 for the case of 0% joint efficiency. The shear strain contours at failure indicate that the critical failure mode consists of global failure characterized by rotation and translation of the levee, I-Wall, sheetpiles, and DMM zone along the top of the beach sand. At 100% joint efficiency, the shearing passes through the DMM zone, while at 0% efficiency, the shear contours also show some movement along the vertical joints, indicating the beginning of an internal "racking" type failure at the column overlaps in the shear walls, as described by Adams and Filz (2010). The shear strain contours at failure for the case of 0% joint efficiency are shown in Figure 3. The contours indicate that high strains in the joints for 0% joint efficiency do not extend all the way to the top and bottom of the DMM zone, and the reduction in factor of safety from the case with 100% efficient vertical joints is within the precision of the factor of safety calculations of 0.01.

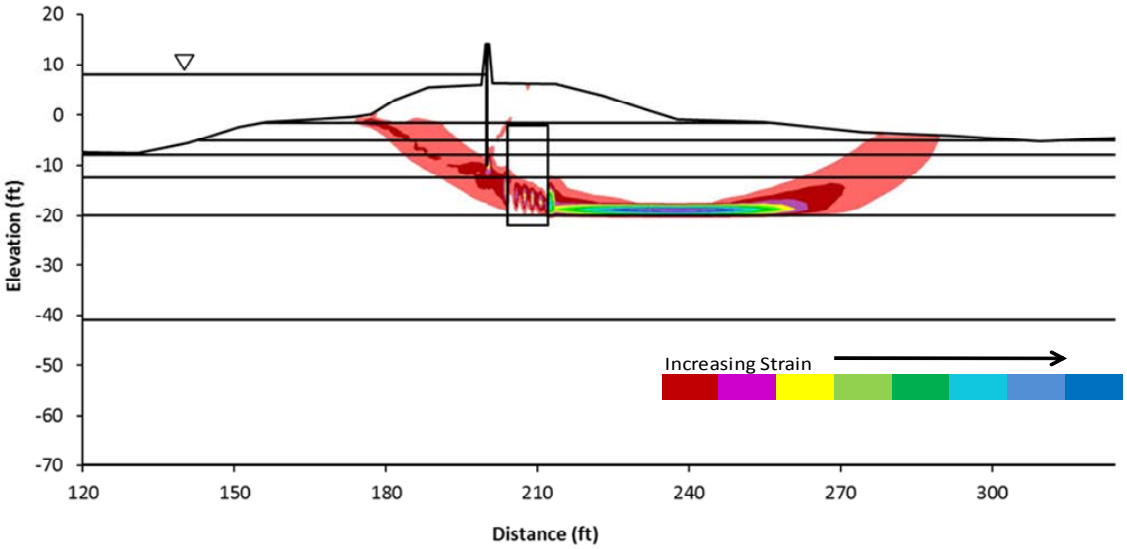

Figure 3: An example of shear strain contours from the numerical stability analyses without a water-filled gap and 0% joint efficiency.

The relationship between the calculated factor of safety and vertical joint strength, along with joint efficiency, is shown in Figure 4. The results include cases for vertical joint strengths less than the joint strength at 0% efficiency to demonstrate the physical response of these systems, including reductions in the factor of safety as the strength of the vertical joints decreases. This outcome is consistent with the findings described by Adams and Filz (2010). However, it is worth reiterating that, for the conditions analyzed at Reach 17 of Orleans Avenue Canal, the decrease in factor of safety associated with decreasing the vertical joint efficiency from 100% to 0% is very small (within 0.01).

Stability analyses were also performed for the case where a water-filled gap develops on the flood side of the sheetpiles. The depth of the gap was varied from zero to the full depth of the sheetpiles, corresponding to an elevation of -9.8. The analyses were performed for joint efficiencies of 100% and 0%. Figure 5 shows the resulting calculated factors of safety plotted against gap depth. The lowest factor of safety, equal to 1.64, occurs for the case where a full-depth gap is present. Like the analyses performed without a water-filled gap, the calculated factors of safety including a gap are not significantly sensitive to joint efficiency (within 0.01). The shear strain contours at failure for analyses including a gap are similar to those shown in Figure 3 and thus indicate a global failure mode.

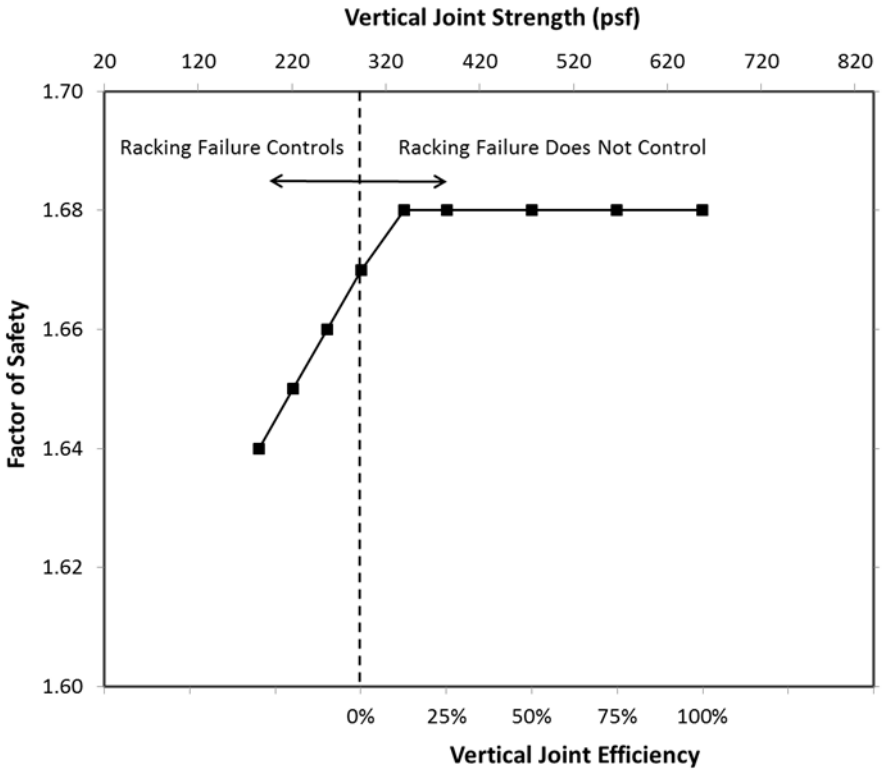

Figure 4: Factor of safety versus efficiency of vertical joints for Reach 17

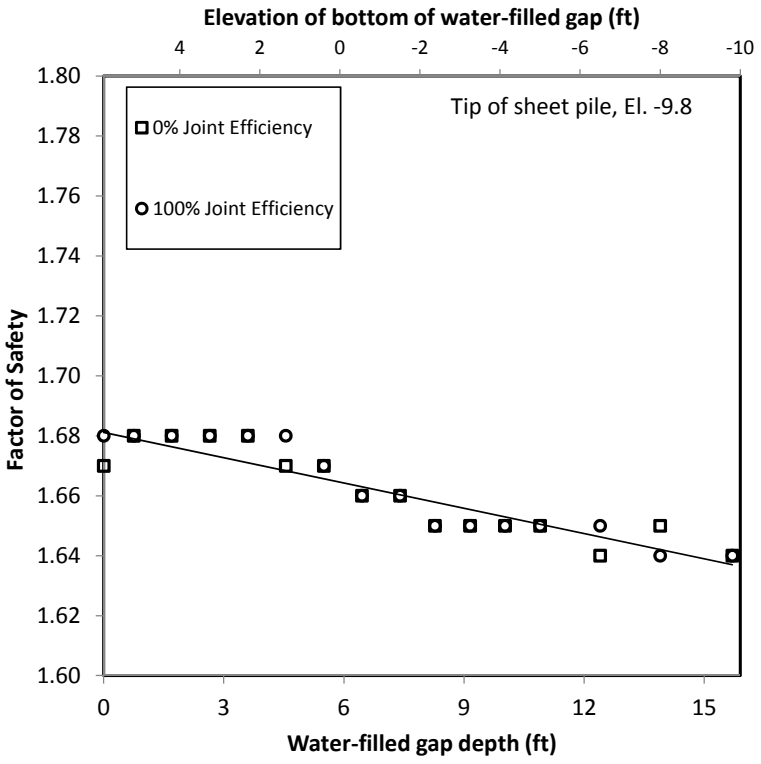

Figure 5: Factor of safety versus depth of gap on flood side of sheetpiles for Reach 17

4.3. Comparisons with Limit Equilibrium Results

As part of the overall design process, limit equilibrium analyses were performed for the analysis cross section for Reach 17 of the Orleans Avenue Canal using Slope/W 2007 (Geo-Slope, 2007). Table 2 summarizes the factors of safety calculated from the limit equilibrium analyses and the numerical analyses performed using FLAC2D. Limit equilibrium analyses were performed for cases with and without a water-filled gap at the flood side of the sheetpiles extending from the ground surface at El. +6.1 to the tip elevation of the sheetpiles at El. -9.8. The limit equilibrium analyses also considered the presence of a water-filled tension crack forming in the cohesive soils at the ground surface. Results are reported for analyses using Spencer's Method and allowing for development of non-circular slip surfaces.

Table 2: Summary of factors of safety determined for the analysis section using FLAC2D and Slope/W

	Factor of Safety	
Analysis	No Gap	Gap
FLAC2D, 100% Joint Efficiency	1.68	1.64
FLAC2D, 0% Joint Efficiency	1.67	1.64
Slope/W Spencer's Method without a tension crack[1]	1.64	1.56[3]
Slope/W Spencer's Method with tension crack[1,2]	1.51	--

[1]Optimized results presented for Spencer's Method using entry-exit and block methods to search for the critical slip surface

[2]The depth of the tension crack was varied until no negative forces act on the sides and base of slices on the flood side.

[3]These analyses were performed using the method proposed by Brandon et al. (2008)

According to the results shown in Table 2, the factors of safety calculated using FLAC and Spencer's Method without a tension crack are within 5% for all comparable cases. The primary mode of failure in the FLAC analyses of Reach 17 is global rotation and translation of the levee and I-Wall with shearing through the DMM zone. This mode of failure is also captured by the limit equilibrium analyses, so it is not surprising that the factors of safety determined for these methods of analysis are similar for this case. When comparing factors of safety determined using different limit equilibrium methods that satisfy all conditions of equilibrium, variations of ±6% are typically considered to be acceptable (Duncan, 1996).

The presence of a water-filled gap adjacent to the sheetpiles produces a decrease of about 2 to 5% in the calculated factor of safety, depending on the analysis method.

The FLAC analyses did not consider the influences of pre-existing tension cracks or formation of tension cracks in the mesh during flood loading. Since the tensile strength of the soil and DMM zone were set to zero, zones in the mesh were allowed to fail in tension, but the FLAC analyses did not permit the development of water-filled tension cracks in the mesh. Compared to the case without a water-filled gap adjacent to the sheetpiles, the limit equilibrium analyses show an 8% reduction in the calculated factor of safety due to the presence of water-filled tension cracks in the soil. This result suggests that, for the analysis section for Reach 17, the reduction in the factor of safety due to presence of a tension crack is slightly larger than the reduction in the factor of safety due to the presence of a gap on the flood side of the sheetpiles.

5. CONCLUSIONS

Based on the numerical and limit equilibrium analyses described above, the following conclusions can be drawn regarding stability of the I-Wall and levee along Reach 17 of the Orleans Avenue Canal after construction of the DMM shear walls and when the canal water level is at El. +8:

- According to the numerical analyses, the calculated factor of safety without the presence of a water-filled gap on the flood side of the sheetpiles and with 100% efficient vertical joints is 1.68. At 0% vertical joint efficiency, the factor of safety is 1.67. For other configurations of DMM support, vertical joint efficiency can be more important, e.g., Adams et al. (2009) and Adams and Filz (2010).

- The presence of cohesive materials near the ground surface where overburden stresses are low creates the potential for formation of a water-filled gap on the flood side of the sheetpiles. When the water-filled gap extends to the bottom of the sheetpiles (El. -9.8), the calculated factor of safety equals 1.64, regardless of joint efficiency, according to the numerical analyses.

- The influence of vertical joint efficiency on the factor of safety is very small for numerical analyses with and without the formation of a gap. The influence of a gap on the factor of safety is more significant than the influence of vertical joints. The overall critical factor of safety from the numerical analyses is 1.64 for a water-filled gap extending to the bottom of the sheetpile, regardless of vertical joint efficiency.

- For cases with and without a water-filled gap, the critical failure mode from the numerical analyses involves shearing across the DMM zone, regardless of joint efficiency.

- The calculated factors of safety using numerical methods are within 5% of the values calculated using Spencer's Method of limit equilibrium analysis. The similarity in the factors of safety determined using these methods is attributed to the fact that the primary mode of failure in the numerical analyses is global rotation and translation of the levee and I-Wall with shearing through the DMM zone, which is a mode of failure that is also captured in the limit equilibrium analyses.

- The numerical analyses and limit equilibrium analyses both indicate that the presence of a water-filled gap adjacent to the sheetpiles decreases the calculated factor of safety between 2 and 5% of the equivalent case without a gap.

REFERENCES

Adams, T.E. and Filz, G.M. (2010). Stability of Levees and Floodwalls Supported by Deep-Mixed Shear Walls: Five Case Studies in the New Orleans Area, prepared for the New Orleans District, US Army Corps of Engineers, Virginia Polytechnic Institute and State University, Blacksburg, Virginia.

Adams, T., Filz, G., and Navin, M. (2009). "Stability of Embankments and Levees on Deep-Mixed Foundations," Proc. Int. Symp. Deep Mixing & Admixture Stabilization, Japanese Port and Airport Research Institution, Tokyo, 8 p.

Brandon, T.L., Wright, S.G., and Duncan, J.M. (2008). "Analysis of the stability of I-Walls with gaps between the I-Wall and the levee fill", ASCE Journal of Geotechnical and Geoenvironmental Engineering, Vol. 134, No. 5, pp. 692-700.

Broms, B.B. (2003). Deep Soil Stabilization: Design and Construction of Lime and Lime/Cement Columns, Royal Institute of Technology, Stockholm, Sweden.

Bruce, D.A. (2012). "The History of Deep Mixing in New Orleans," Proc. Grouting and Deep Mixing 2012, Deep Foundations Institute, Hawthorne, NJ, in press.

CDIT, Coastal Development Institute of Technology. (2002). The Deep Mixing Method: Principle, Design, and Constructions, A.A. Balkema, The Netherlands.

Duncan, J.M. (1996). "State of the art: Limit equilibrium and finite-element analyses of slopes", ASCE Journal of Geotechnical Engineering, Vol. 122, No. 7, pp. 577-596.

Filz, G., Adams, T., Navin, M., and Templeton, A. (2012). "Design of Deep Mixing for Support of Levees and Floodwalls," Proc. Grouting and Deep Mixing 2012, Deep Foundations Institute, Hawthorne, NJ, in press.

Filz, G.M. and Templeton, E. (2011). Design Guide for Levee and Floodwall Stability Using Deep-Mixed Shear Walls, Report prepared by Burns Cooley Dennis for the New Orleans District and the Hurricane Protection Office of the US Army Corps of Engineers.

Filz, G.M. and Navin, M.P. (2006). Stability of Column-Supported Embankments, Virginia Transportation Research Council Report No. 06-CR13, Charlottesville, Virginia.

GEO-SLOPE International, Ltd. (2007). Slope/W 2007, GEO-SLOPE International, Ltd., Calgary, Alberta, Canada.

ITASCA Consulting Group, Inc. (2005). FLAC2D: Fast Lagrangian Analysis of Continua, ITASCA Consulting Group, Minneapolis, Minnesota.

Navin, M.P. (2005). Stability of Embankments Founded on Soft Soil Improved with Deep-Mixing-Method Columns, Ph.D. dissertation, Virginia Polytechnic Institute and State University, Blacksburg, Virginia.

Sehn, A.L. (2005). Personal communication.

Assessing the feasibility of a foundation treatment solution based on CSM panels at a river dock in Lisbon

Mendes, Bruno, formerly Laboratório Nacional de Engenharia Civil, Portugal, bfmendes@sapo.pt
Maranha das Neves, E. Instituto Superior Técnico, Portugal, emanuelmaranhadasneves@gmail.com
Caldeira, L. , Laboratório Nacional de Engenharia Civil, Portugal (laurac@lnec.pt)
Bilé Serra, J., Laboratório Nacional de Engenharia Civil, Portugal (biles@lnec.pt)

ABSTRACT

In an alternative design for the soil reinforcement of a reclamation area at Tejo River front in Lisbon it was proposed to construct an embankment on Cutter Soil Mixing (CSM) columns. A detailed in situ and laboratory characterization program was conducted to evaluate the technical effectiveness and economical feasibility of the solution. Fresh paste and core samples from the CSM test panels and formulation cement-soil mixture specimens, with 35% cement content, were tested. The program aimed at characterizing the mechanical and hydraulic properties of the mixture. In situ characterization tests were also conducted.

In this paper only the tests results on formulation mixture specimens are presented. The tests intended to determine the physical parameters of the mixtures such as the cement, organic matter and sulfates contents. From the engineering point of view, the following characteristics of the mixture specimens were analyzed: water content, small strain stiffness (P wave velocity propagation tests), unconfined compression strength and secant stiffness (with local measurements), tensile strength (Brazilian test) and shear strength (consolidated undrained triaxial tests). A comparative analysis of the test results on samples cured for 14, 28, 54 and 91 days is presented allowing the characterization of the material properties evolution with curing process. A quality index was introduced to help the sample selection for testing.

1. INTRODUCTION

The design of several engineering structures usually involves consideration of excessive deformation and stability issues. Ground improvement techniques are available to tackle such problems, namely those making use of column type elements of soil-binder mixtures. Partly because of the soil confinement, relatively stiff columns, in comparison with the in situ soft soil, may be obtained.

At the dock between Santa Apolónia and Jardim do Tabaco of the river Tejo in Lisboa an alternative solution for the foundation of buildings on a landfill has been considered. The proposed solution relied on land filling the dock through the treatment of the soft soil by execution of CSM panels (cf. Photo 1a). On the top of the soil-cement panels a load transfer platform composed by geosynthetics and a landfill was planned for a better vertical load distribution to the CSM panels. In this project, the construction consortium leaded by Somague Engenharia decided to undertake a detailed laboratory and in situ characterization program in order to evaluate the technical effectiveness and economic feasibility of the solution. The program aimed at characterizing the mechanical and hydraulic properties of the mixture, through the use of fresh paste and core specimens from the CSM test panels and formulation cement-soil mixture specimens. Despite the use of several tentative cement content values in the panels, the unconfined compression strength of both the fresh cubic molded and core samples was below 2 MPa, the threshold value for ultimate limit state safety verification for the pre-designed panel dimensions. This was particularity observed in some core specimens due to poor final quality of the panels and of the coring procedure, as shown in Photo 1b.

Based on this observation, a new expeditious, yet sufficiently rigorous, method based on X-ray fluorescence (XRF) was implemented at LNEC to determine the weight fraction of calcium and indirectly, based on a calibrated correlation, the cement content of soil-cement mixtures (Jorge *et al.*, 2009). This method was applied to determine the real cement content of the CSM test panels. The results obtained in the CSM panels executed in the dock of Jardim do Tabaco, showed the existence of panels with cement content higher than the design (nominal) value, but also panels were the opposite happened, such as panels with a nominal cement content of 300 and 350 kg/m^3 with a real cement content from 250

to 290 kg/m^3 (cf. Figure 1). The low values of unconfined compression strength of the specimens from the CSM panels were partly due to a deficient mixture of the cement with the soil.

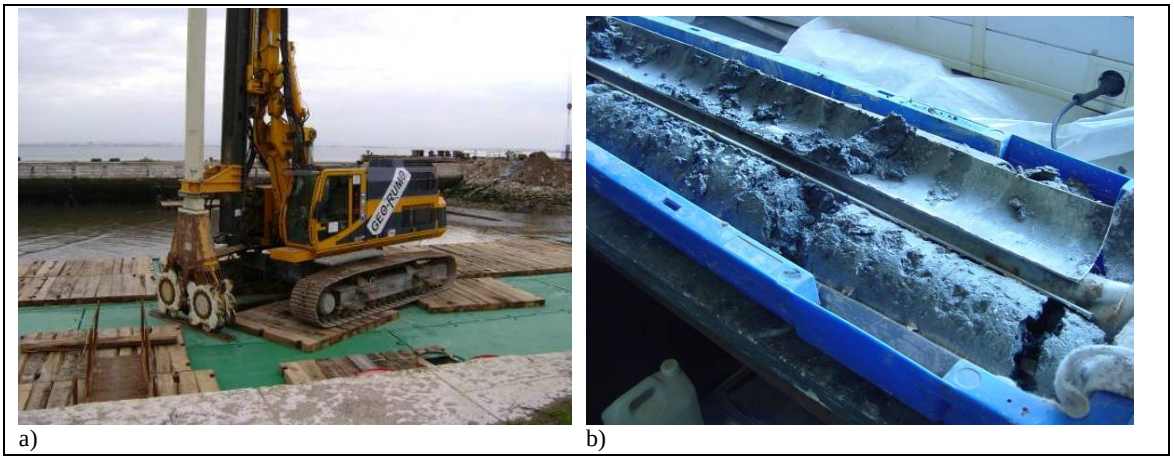

Photo 1: a) CSM RG 19 rig; b) core samples from test panels

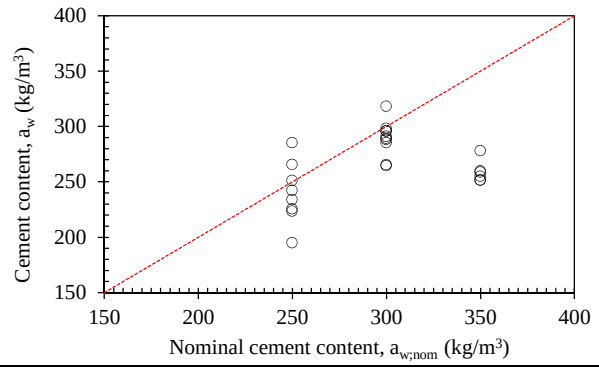

Figure 1: Cement content versus nominal cement content in the CSM panels

2. GEOTECHNICAL CONDITIONS AT THE SITE

2.1. Physical characterization of the natural soil

Four disturbed samples of the soft fluvial soil were collected at different depths, being sample #1, (an organic clay) the most contrasting one in the group. Samples #2, #3 and #4 were organic silts with a unit activity and significant organic content. The clayey-silty fraction of the soil was quite similar in all samples, with only small differences between samples #2, #3 and #4. The physical properties are summarized in Table 1.

Table 1: Geotechnical properties of natural soil

	Sample 1	Sample 2	Sample 3	Sample 4
Liquid limit, w_L (%)	56.8	56.6	54.4	56.1
Plastic limit, w_P (%)	22.4	30.5	29.5	30.3
Plasticity index, PI (%)	34.4	26.2	24.9	25.8
Liquidity index, LI (%)	208	242	259	246
Water content (%)	90.5	98.5	92.5	92.9
Activity	1.40	1.04	0.97	0.99
Specific gravity, Gs	2.62	2.75	2.72	2.74
Organic content (%)	3.3	3.3	3.2	3.2
Sulfate content (%)	0.33	0.33	0.24	0.37
Grain size distribution (%)				
Clay fraction (<2 μm)	22	22	22	22
Silt fraction (< 60 μm)	71	66	65	64

	Sample 1	Sample 2	Sample 3	Sample 4
Sand fraction (< 2 mm)	7	8	9	9
Unified Soil Classification (ASTM D2487-06)	OH	OH	OH	OH

It was therefore decided to merge the samples to reproduce the in situ diversity of the ground. A total mass of 28 kg was so obtained. No information was gathered about the in situ water content and bulk unit weight due to the disturbance introduced during soil collection. The position in the plasticity chart is illustrated in Figure 2.

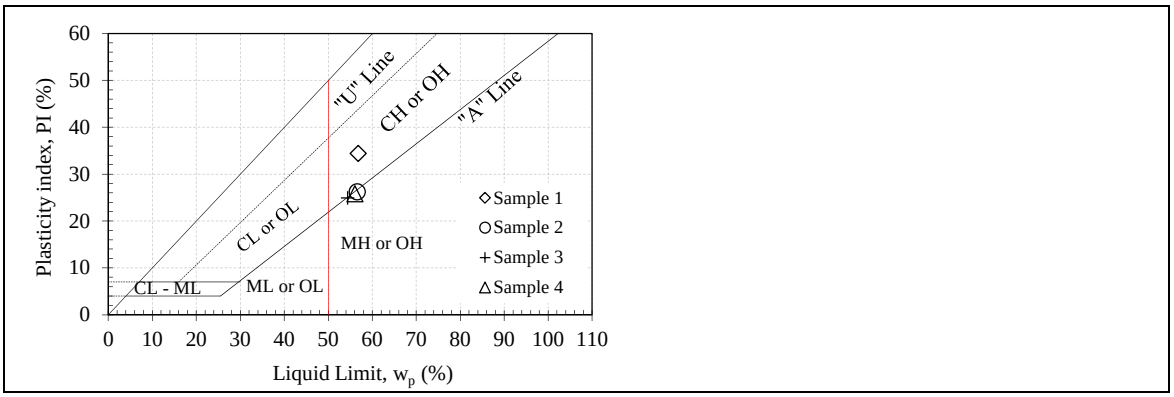

Figure 2: In situ soil samples position in plasticity chart

2.2. Organic and sulfates contents

As discussed in Janz and Johansson (2002), the presence of a significant amount of organic matter in the mixture makes the hydration of cement difficult, thus restraining the improvement of the mechanical properties of the soil-cement mixture. Consequently, it is important to determine the content of organic matter in the soil as an indicator of the potential quality of the final mixture. Pozzolanic cement was used in the mixtures to reduce, yet not avoiding, the sulfates attack. The determined sulfate and organic contents of the in situ soil are shown in Table 5.

Table 5: Sulfate and organic content of natural soil samples

Description	Sulfates (SO_3) (%)	Organic content (%)
Sample 1	0.33	3.3
Sample 2	0.33	3.3
Sample 3	0.24	3.2
Sample 4	0.27	3.2
Mixture	0.66	3.0

According to the classification proposed by the Swedish Geotechnical Society (Hansbo, 1994), the in situ soil is classified as slightly organic (organic content between 2% and 6%). Nevertheless, as observed by Xu *et al.* (2008), the organic matter content (about 3.3%) is expected to influence the mechanical behavior of the soil cement panels.

On what concerns the sulfate content, according to the proposal by the American Concrete Institute (ACI 318M-08, 2008), the soil can be classified as severe (sulfate content between 0.2% and 2%). Despite pozzolanic cement properties retard/inhibit attack by sulfates, it is expected that the sulfate in the soil influence the mechanical behavior of soil cement panels in the long term, especially because it is a fluvial structure. Therefore, to reproduce the in situ conditions, it was decided to use water from the dock of Jardim do Tabaco as mixing water.

3. LABORATORY CHARACTERIZATION OF THE SOIL-CEMENT MIXTURE

3.1. Specimens Preparation

Soil cement specimens were prepared from the in situ soil sample and a cement slurry of Type IV/B (V) 32.5 pozzolanic cement produced by Cimpor. The cement slurry was prepared with a water content of 26.3% and a water-cement ratio (w/c) of 0.75 and mixed during 20 minutes. Then, at a speed of 40 rpm the cement slurry was added to the soil sample (w_{nat}=93.9%), as illustrated in Photo 2a, and, given the soil cohesive nature, mixed during 30 minutes, to ensure a uniform mixing. The mixture was then poured and slightly pressed into PVC cylindrical opaque cases with diameter of 72 mm and height of 140 mm. The samples shown in Photo 2b were used for unconfined compression, Brazilian and consolidated undrained triaxial compression tests. The partial masses of the components are listed in Table 2.

a) b)

Photo 2: Preparation of soil-cement specimens: a) soil (dark) mixed with the cement slurry; b) soil-cement specimens in a container with water from the Jardim do Tabaco dock

Table 2: Soil-cement mixture composition

Soil-cement mixture				
Soil		Cement slurry – w/c=0.75		Total mass (kg)
Dry soil mass (kg)	Water (kg)	Cement dry mass (kg)	Water (kg)	
13.5	12.7	7.3	5.5	39.0

3.2. Visual Quality Index of the Specimens

The reproducibility of the specimens' initial conditions is a prerequisite for the repeatability of results in similar tests and also for the homogeneity of the specimen set. Unfortunately, the procedure adopted in the specimen preparation did not universally assure the desired sample homogeneity, so there was a need for sample discrimination. A quality visual index (ranging from 0 to 5) based on the defects frequency and voids volume of the visible surface was adopted for sample pre-selection, allowing a first evaluation of specimens' quality. A total of 32 specimens were prepared, but only 21 of those were used, i.e. those with non-null index values. The index values of the pre-selected samples are listed in Table 3, with a classification between 1 (lowest quality) to 5 (highest quality). The density, water content and cement content values of the pre-selected samples were statistically characterized for homogeneity's sake.

Table 3: Visual quality index of the laboratory specimens

Quality index	Sample reference	Quality index	Sample reference
5	5, 7, 8, 14, 19, 25	2	12, 24, 29
4	3, 17, 20, 21, 26, 30, 31	1	10. 13
3	6, 18, 23		

Photo 3a and Photo 3b show two rejected specimens due to excessive voids (index 0). Otherwise, specimen # 26 (quality index 4), tested in unconfined compression, is shown in Photo 3c.

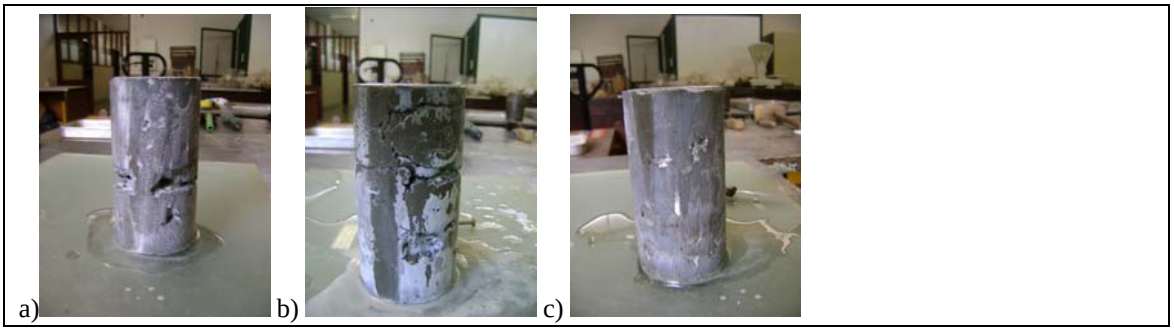

Photo 3 : Soil-cements specimens prepared in laboratory: a) specimen # 28, rejected; b) specimen # 9, rejected; c) specimen # 26, tested under unconfined compression

3.3. Tests Results and Discussion

The test program aimed at characterizing of the soil-cement mixture for four different curing times (14, 28, 56 and 91 days) from the standpoints of physical and chemical characteristics and of strength and deformability. In the following sections the tests results are presented and discussed.

3.3.1. Specimen water content and density

The water content of each specimen at test setup was determined from the central core material immediately after test completion, assuming that during unconfined compression and Brazilian tests no outward water migration (cf. Photo 4) occurred. Table 4 shows the so determined water content values illustrating the low dispersion achieved for all the curing durations, since the coefficient of variation ranged between 1.2% and 3.6%. A slight water intake during the curing process is also shown by the evolution of the average value of the water content, although due to hydration and pozzolanic reactions the water content is supposed to decrease (Chew *et al*. 2004; Kamruzzaman *et al*. 2009).That may be explained by the adopted procedure of submerging the specimens in a dock water filled container in order to reproduce the in situ conditions. Therefore, the soil-water-binder physical-chemical interactions occurred without significant change in water content. The symbols listed in Table 4 are, respectively: μ – average; σ – standard deviation; cov – coefficient of variation.

Photo 4: Water content determination of cylindrical specimen preparation after unconfined compression test

Table 4: Statistical data of the water content (soil-cement specimens)

Curing time (days)	μ (%)	σ (%)	cov (%)
15 to 16	70.5	1.0	1.5
28 to 32	72.0	1.2	1.6
56	71.1	0.9	1.2
91 to 93	72.0	2.6	3.6

Figure 3a and Figure 3b show, respectively, the evolution of wet and dry density with curing time. The physicochemical interactions of soil-water-binder tend to increase the density, due to the deposition of primary and secondary reaction products. In Figure 3a and Figure 3b only a small increase in the density with curing time may be observed, since the solid component of the mixture did not change significantly, in spite of the cementitious products formation.

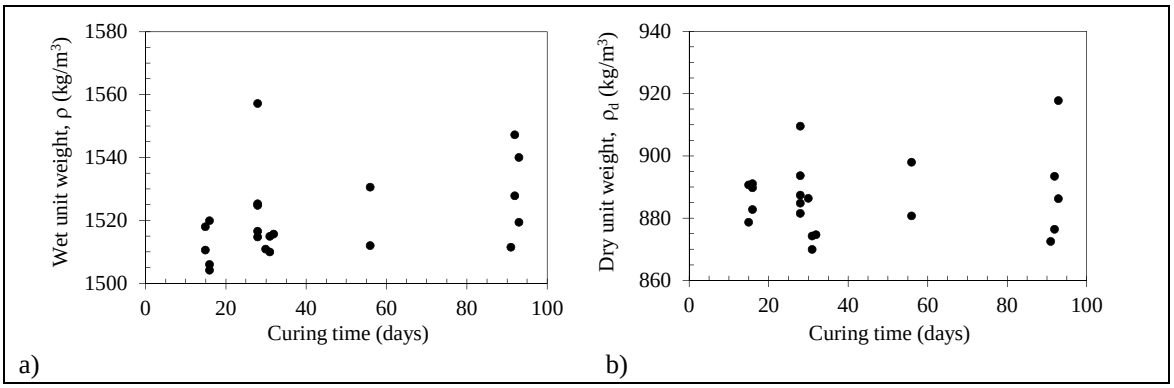

Figure 3: Evolution of (total and dry) density with curing time

3.3.2. Cement content by X-Ray fluorescence

An opportunity to assess the reliability of the X-Ray fluorescence test (cf. Photo 5) to measure the cement content of the in situ CSM panels was identified during this experimental program. A very accurate correlation was found between the (known) cement content of specimens (35%) and that inferred from the FRX test: an average value of 35.5% for 15 days curing time. No significant evolution of the cement content with curing time was identified, as shown in Table 6.

Photo 5: Preparation of the XRF samples for cement content determination, with the equipment NITON series XLI 700 Analyser (Jorge et al., 2009)

Table 6: Cement content of formulation mixtures

Curing duration (days)	μ (%)	σ (%)	cov (%)
15 or 16	35.5	0.3	0.8
28 to 30	35.3	0.5	1.4
56 to 59	35.3	0.8	2.2
91 to 100	35.2	0.5	1.5

3.3.3. P wave propagation speed

The results of P wave propagation speed (V_P) in specimens cured during 14, 28, 56 and 91 days are presented in Figure 4. The values at 14 days may mainly correspond to propagation through interstitial

water, given the proximity of the values obtained with the speed of propagation of P waves in the water (i.e., 1450 m/s). In the remaining curing durations, the values correspond to the propagation through the solid matrix as a result of the solid matrix hardening.

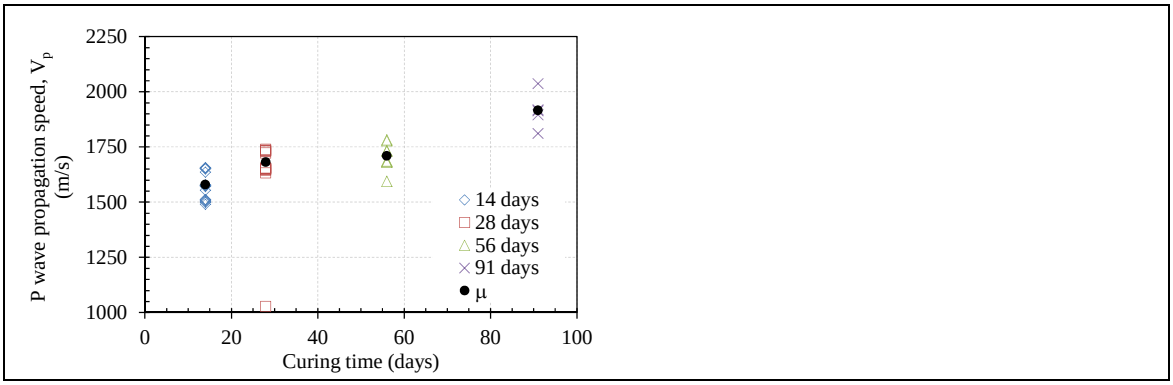

Figure 4: P wave propagation speed in soil-cement specimens with different curing duration

3.3.4. Unconfined compression tests

Cement hydration and pozzolanic reactions cause the increase of the unconfined compression strength ($q_{u;max}$) with cement content. For the same reason, the progression of these processes may be also observed in the $q_{u;max}$ increase with time. The unconfined compression strength of samples cured for14, 28, 56 and 93 days are presented in Table 7. An approximately linear increase (cf. Figure 5) of $q_{u;max}$ with the curing time may be observed, although its validity for curing time greater than 28 days may be questionable, given the scarcity of specimens cured for 56 and 93 days. The symbols listed in Table 4 are ε_{max} – axial strain at peak strength $q_{u;max}$, $\varepsilon_{50;sec}$ – axial strain for $q_{u;max}/2$, $q_{u;max}$ – maximum unconfined compressive strength , $E_{50;sec}$ – secant young modulus for $q_{u;max}/2$, ρ – density; ρ_d – dry density. All but one sample showed a brittle failure, at local axial strains below 1%.

Table 7: Unconfined compression test results

Sample number	Curing duration (days)	ε_{max}	$\varepsilon_{50;sec}$	Strength type	$q_{u;max}$ (kPa)	$E_{50;sec}$ (MPa)	ρ (kg/m^3)	ρ_d (kg/m^3)
20	15	9.3E-03	2.4E-04	Brittle	793	1648	1518	891
6	16	3.6E-03	2.6E-04	Brittle	783	1486	1520	890
29	16	1.7E-02	4.7E-04	Ductile	919	975	1506	891
10	28	5.0E-03	4.5E-04	Brittle	917	1023	1516	885
13	28	5.6E-03	5.4E-04	Brittle	1098	1027	1515	881
23	28	5.4E-03	5.3E-04	Brittle	1113	1057	1525	887
26	30	6.6E-03	7.8E-04	Brittle	1211	775	1511	886
14	56	3.2E-03	4.5E-04	Brittle	1427	1031	1530	898
31	93	5.1E-03	1.0E-03	Brittle	2128	1045	1519	886

The results of sample #14, with a quality index of 5, indicate that a slower evolution of the hydration process may have occurred around the 56 days curing time. However, as only one sample has been tested at this curing duration, this conclusion is questionable from the statistical point of view.

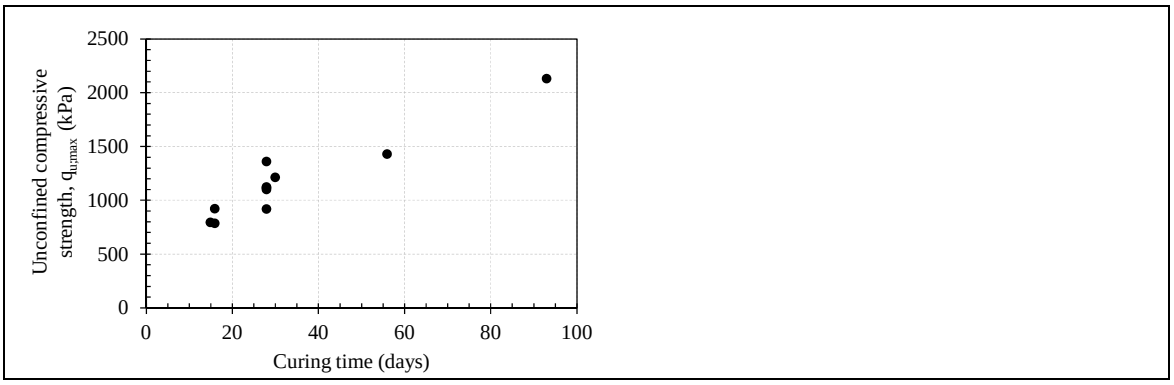

Figure 5: Evolution of maximum unconfined compression strength with curing time

3.3.5. Brazilian tests

The tensile strength is a key property for the bending behavior of the CSM panels under horizontal loads, such as caused by an earthquake. The determination of the tensile strength of the soil-cement specimens was done using the Brazilian test, also known as diametral compression test (cf. Photo 6). Similar to the unconfined compression test trend, an increase in the tensile strength with curing time may be observed in Figure 6.

It should be noted the small increase of tensile strength of the specimen tested at 56 days of curing. Since it was a single test, no rebuttal was possible. Nevertheless the result can be explained by the lower quality of this specimen (specimen # 24, quality index 2), with small voids on the surface. The ratio between determined unconfined compression and tensile strengths at a given curing time is between 5 and 6.5.

Photo 6: Execution of the Brazilian test

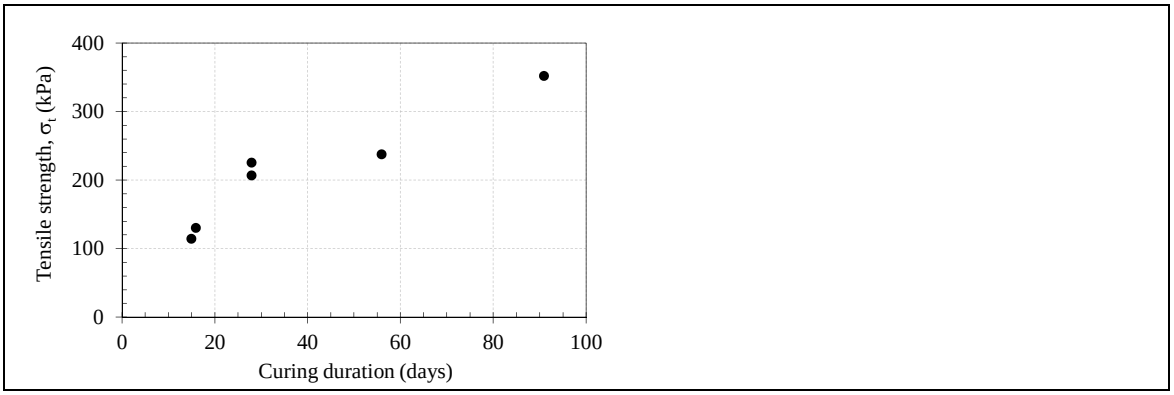

Figure 6: Evolution of tensile strength with curing duration

3.3.6. Consolidated undrained triaxial compression test

The consolidated undrained triaxial compression tests of six specimens have been performed, for two different curing times through isotropic consolidation under effective confining pressure (p'_c) values of

70, 120, 180 and 280 kPa, all in the range of the expected in situ confining stresses. The dependence of the peak deviator stress upon the preshear effective confining pressure is not evident. The same situation has been reported by Horpibulsuk *et al*. (2004). Unlike the deviator stress, the peak pore pressure grows with the effective confinement pressure increase in both curing times. The peak pore pressure was attained almost simultaneously with the peak mobilized deviator stress at relatively small axial strain values, confirming the brittleness of the mixture. After this compressive tendency, all the samples exhibited a dilatant behaviour. In both curing times it was observed an increase of dilatancy effects with both the initial effective confining pressure and the shearing. The same tendency was observed regarding the curing time effect on the samples with initial confining effective pressure of 70 and 120 kPa.

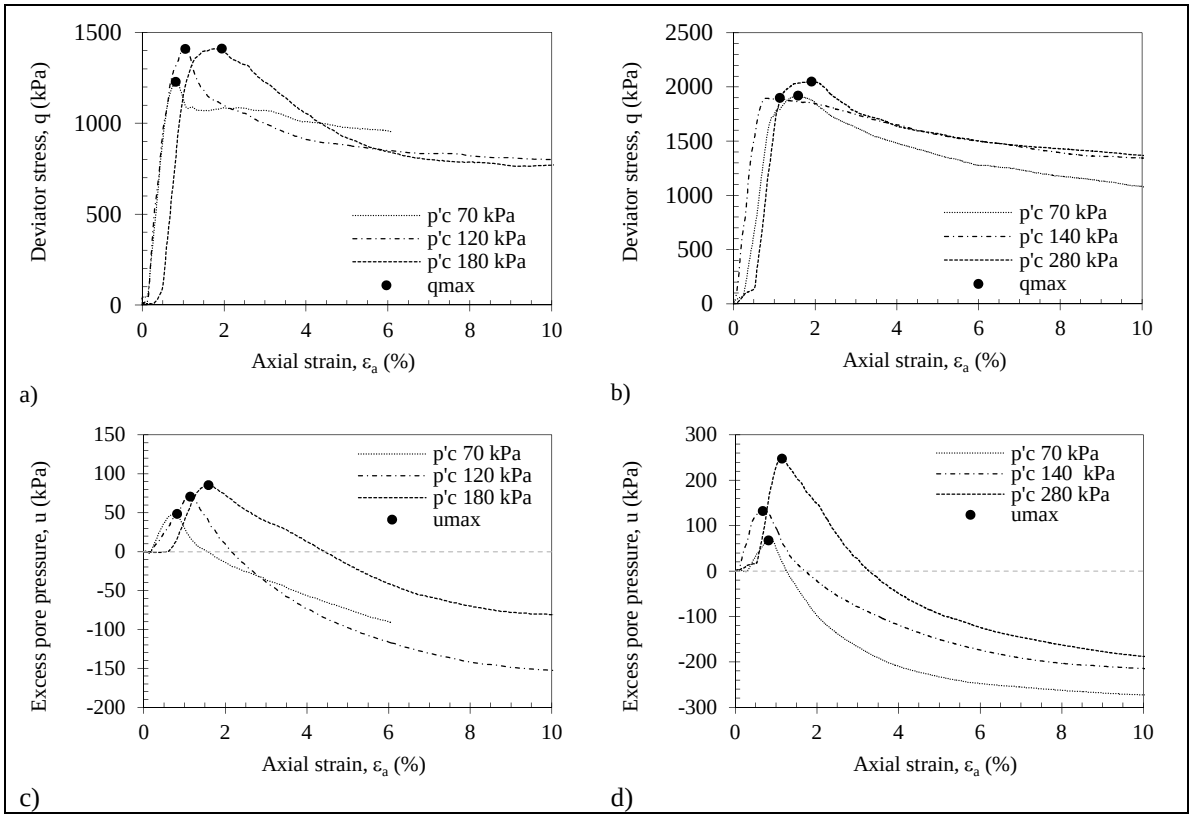

Figure 7: Stress-strain response in confined triaxial compression: a) q-ε_a plot for 31/32 curing days; b) q-ε_a plot for 92/93 curing days; c) u-ε_a plot for 31/32 curing days; d) u-ε_a plot for 92/93 curing days

Based on the test results (Mendes, 2011), the effective Mohr-Coulomb peak shear strength parameters, ϕ' and c', have been determined according to equations 1 and 2, where M is the critical state line slope in the (p', q) plane represented by the red lines in Figure 8, q_0 is the ordinate at the origin. According to Figure 8, the effective shear strength parameters are: i) 31/32 days – ϕ'=34.8º and c'=301 kPa; ii) 92/93 days – ϕ'=43.3º and c'=371 kPa.

$$sen(\phi') = \frac{3 \cdot M}{6 + M} \tag{1}$$

$$c' = \frac{3 - sen(\phi')}{6 \cdot cos(\phi')} \cdot q_0 \tag{2}$$

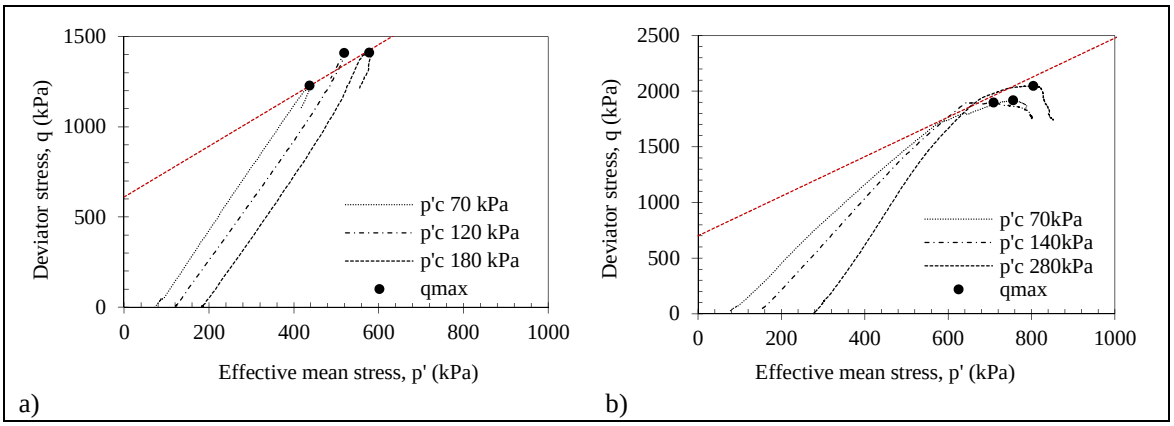

Figure 8: (p',q) stress paths during undrained triaxial compression: a) 31/32 curing days; b) 92/93 curing days

4. CONCLUSIONS

The results obtained in the tests of formulation mixture specimens demonstrated the potential benefits of the in situ soft soil improvement in Jardim do Tabaco dock by CSM panels. The thorough experimental program on formulation mixtures demonstrated the ability of the cement admixed soil regarding the compressibility, the uniaxial and undrained triaxial compression strength as well as the tensile strength.

A significant improvement of the ground properties may be expected from the adoption of such panels, once an effective quality control procedure is adopted for the panels production. The methodology here reported for quality control of cement content of the CSM mixture seems very promising since it provides a quick way to assess the quality of the construction process, through collection of core samples or fresh paste specimens from the panels.

5. ACKNOWLEDGMENTS

The permission of the project owner, the APL - Administração do Porto de Lisboa, S.A., for the publication of this paper is gratefully acknowledged.

REFERENCES

ACI 318 M-08 (2008). "Building code requirements for structural concrete (ACI 318M-08) and commentary". ACI Standard, American Concrete Institute.

Bilé Serra, J.; Mendes, B. (2009b). "Rehabilitation and reinforcement of the dock between Santa Apolónia and Jardim do Tabaco, by CSM technology. Laboratory formulation tests". LNEC, Lisboa, Report 414/2009 – DG/NT. (in Portuguese).

Chew, S.H.; Kamruzzaman, A.H.M.; Lee, F.H. (2004). "Physicochemical and engineering behavior of cement treated clays". Journal of Geotechnical and Geoenvironmental Engineering, ASCE, Vol. 130, No. 7, pp. 696-706.

Hansbo, S. (1994). "Foundation engineering". Developments in Geotechnical Engineering: 75, Elsevier, pp. 519.

Horpibulsuk, S.; Miura, N., Bergado, D. (2004). "Undrained shear behaviour of cement admixed clay at high water content". Journal of Geotechnical and Geoenvironmental Engineering, ASCE, Vol. 130, No. 10, pp. 1096-1105.

Janz, M.; Johansson, S.E. (2002). "The function of different binding agents in deep stabilization". Swedish Deep Stabilization Research Centre, Report 9, Linköping, Sweden, pp. 47.

Jorge, C.; Sousa, F.; Mendes, B. (2009). "Validation of a method for determining the content of soil cement mixtures ¬ cement". LNEC, Lisbon, Report 287/2009 – DG/NGEA. (in Portuguese).

Kamruzzaman, A.H.M.; Chew, S.H.; Lee, F.H. (2009). "Structuration and destructuration behavior of cement-treated Singapore marine clay". Journal of Geotechnical and Geoenvironmental Engineering, ASCE, Vol. 135, No. 4, pp. 573-589.

Mendes, B. (2011). "Soil foundation improvement through Cutter Soil Mixing". MsC Thesis, Science and Technology Faculty of New Lisbon University, Lisbon. (in Portuguese).

Xu, R.; Guo, Y.; Liu, Z. (2008). "Mechanical properties of stabilized artificial organic soil". Frontiers of Architecture and Civil Engineering in China, SpringerLink, Vol. 2, No. 2, pp. 161-165.

Earth Retaining Structure using Cutter Soil Mixing technology for the "Villa Paradisio" Project at Cannes, France

Peixoto Artur, Geo-Rumo,Tecnologia de Fundações, S.A., Portugal, artur.peixoto@georumo.pt
Sousa Estela, Geo-Rumo, Tecnologia de Fundações, S.A., Portugal, estela.sousa@georumo.pt
Gomes Pedro, Geo-Rumo, Tecnologia de Fundações, S.A., Portugal, pedro.gomes@georumo.pt

ABSTRACT

This paper presents the most relevant design and execution aspects of a retaining wall for the construction of the underground floors of "Villa Paradisio" residential building, at Cannes, France. The geology of the site is characterized by the presence of a clayey fill overlying a fractured dolomitic substrate for the analysed depths. Taking into account the existing constraints, mainly the geological and geotechnical conditions and the urban area conditions, the adopted solution was a retaining wall executed by soil-cement panels, through the application of deep soil mixing technology, particularly the Cutter Soil Mixing (CSM) technology. The retaining wall was reinforced with vertical steel piles and temporarily supported by one level of horizontal steel pipe struts. The particularities of this work are the maximum depth of excavation, which is about 12 m, with a single level of struts, in addition to the geotechnical characteristics of the formations overlying the bedrock and the location of the water level, nearby halfway up the excavation. The main aspects of execution process, the numerical modelling and the quality control of the work are also presented in this paper.

1. INTRODUCTION

In this paper is presented the case of the peripheral retaining structure to the excavation of the underground floors of the residential building "Villa Paradisio", at Cannes, France.
The building is developed in four underground floors for car parking and seven floors high to the distribution of the 81 residential apartments (Figure 1). The excavation site presents in plan an area of about 840 m^2 with a maximum excavation depth of 12 m.

Figure 1: Representation of an external view of the building (www.cannes-paradisio.fr).

In urban excavations, one of the main constrains during the execution process is the minimization of interferences in the neighbouring structures.
The building is located in a densely built-up area and is bounded by streets and neighbouring buildings. Additionally, an old concrete pipeline is located near of the north alignment of the work and its integrity must be assured during the excavation. This urban excavation presents a maximum depth of 12 m, in the presence of water nearby halfway up the excavation, but the presence of the dolomitic bedrock detected above the bottom of the excavation constituted a good support of the bottom of the retaining wall, allowing to design of a safe solution with only one level of horizontal steel pipe struts.

The retaining wall consisted of a continuous CSM wall formed by soil-cement panels with only one level of struts. This solution, besides allowing the vertical excavation, was conceived with a second objective of limitation of the water inflow to the interior of the excavation.

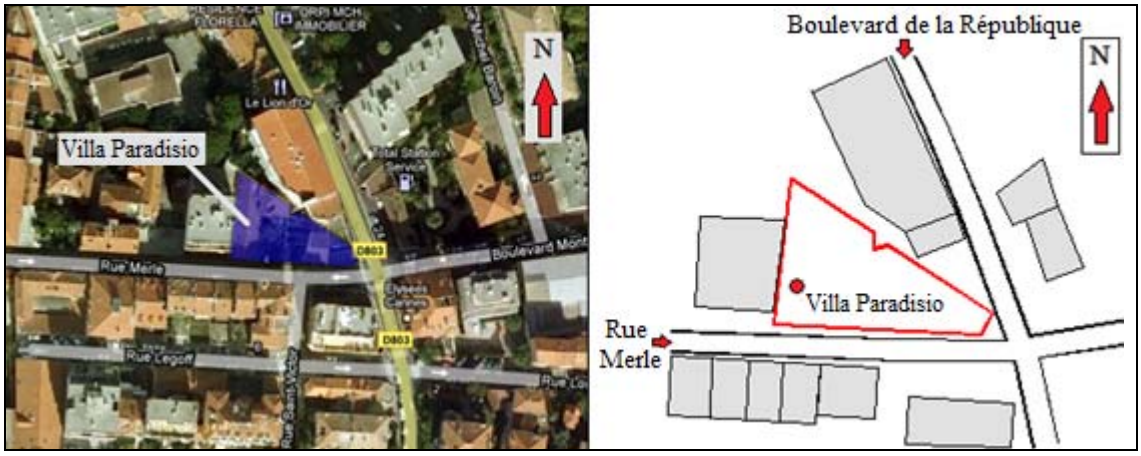

Figure 2: Site plan.

2. MAIN CONTRAINTS

2.1. Geological and Geotechnical conditions

The geological and geotechnical characterization of the ground was carried out in a first phase by an initial study including the execution of a borehole and laboratory tests on intact samples from the work site. In this first study the objective was the evaluation of the nature of the soils. It was identified a clayey fill superficial layer resting over a dolomitic rock fractured at the top and successively less fractured in depth.

To specify the interfaces of the layers, the water table conditions and the geomechanical characteristics of the soils, it was performed a second study including the installation of three piezometers, the execution of three Ménard Pressiometer Tests (PMT) and laboratory tests in intact samples.

In Figure 3 are represented the defined geotechnical zones and the respective main geotechnical parameters.

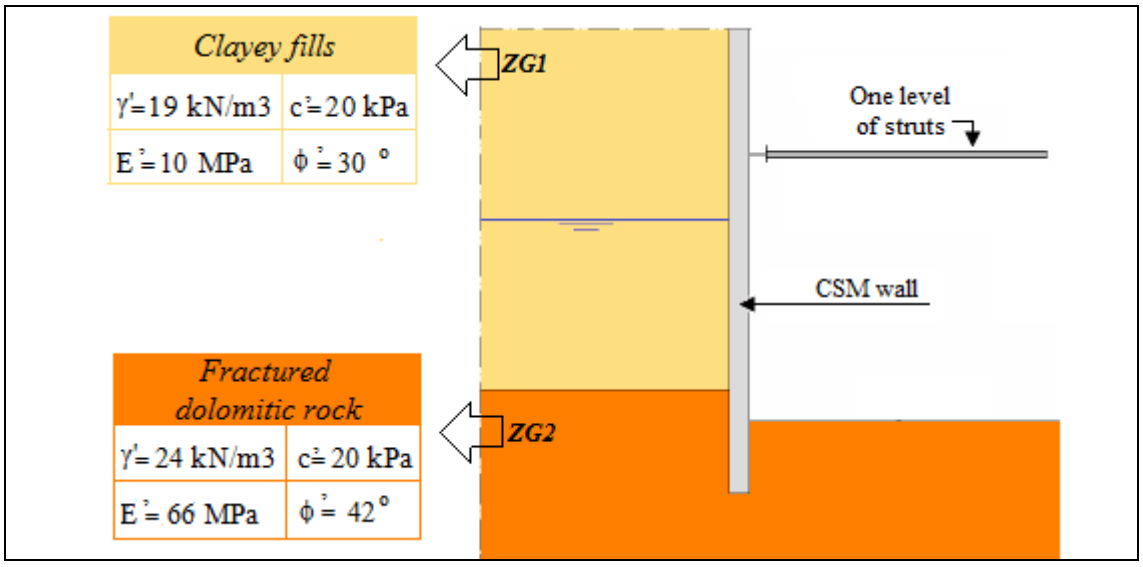

Figure 3: Main geotechnical parameters and cross-section of the excavation.

As it was presented in Figure 3, the interpretation of the results obtained allows to the definition of the following geotechnical zones:

- Clayey fills detected from the surface to a depth between 4.2 m and 9.6 m (Geotechnical Zone 1 – ZG1);

- Fractured dolomitic rock (Geotechnical Zone 2 – ZG2).

The water table was detected approximately 6 m below the surface.

2.2. Neighbouring constraints

The work is located in an urban area and is bounded to the north by a concrete old pipeline and an existing building with three underground floors and seven floors high, to the south by a street (*Rue Merle*), to the west by a building with three underground floors and five floors high and to the east by a street (*Boulevard de la République*).
In the design and execution of the retaining wall one of the main concerns was the minimization of the impact in the surrounding area.
In the following figure are presented the two neighbouring buildings of the excavation.

Figure 4: Neighbouring buildings of the excavation.

As showed in Figure 5, a concrete old pipeline is located near of the north alignment of the work and its integrity must be assured during the excavation.

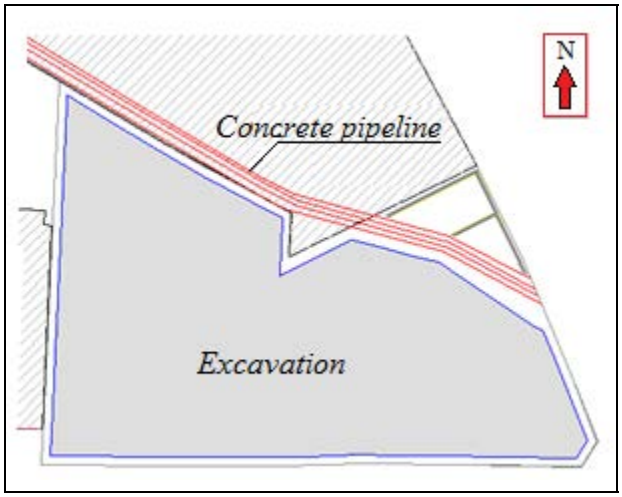

Figure 5: Location of the concrete pipeline.

3. CSM RETAINING WALL

The performed solution to the retaining wall was a continuous wall, formed by soil-cement panels with a rectangular cross-section, executed through the CSM technology. The CSM panels were executed with a minimum length of 15 m to assure a minimum penetration of 3 m below the bottom of the excavation, into the bedrock.

The CSM retaining wall, 0.55 m thick, was reinforced by vertical steel piles (IPE 450 piles) placed at 1.10 m intervals, to additional resistance to the bending moments resulting from the earth pressure, the hydrostatic pressure and the overloads on the surface.
At the top of the retaining wall was executed a concrete beam to connect the vertical steel piles.
To the 12 m depth of excavation was defined only one level of steel pipe struts (Figures 6 and 7) connected to steel waler beams.

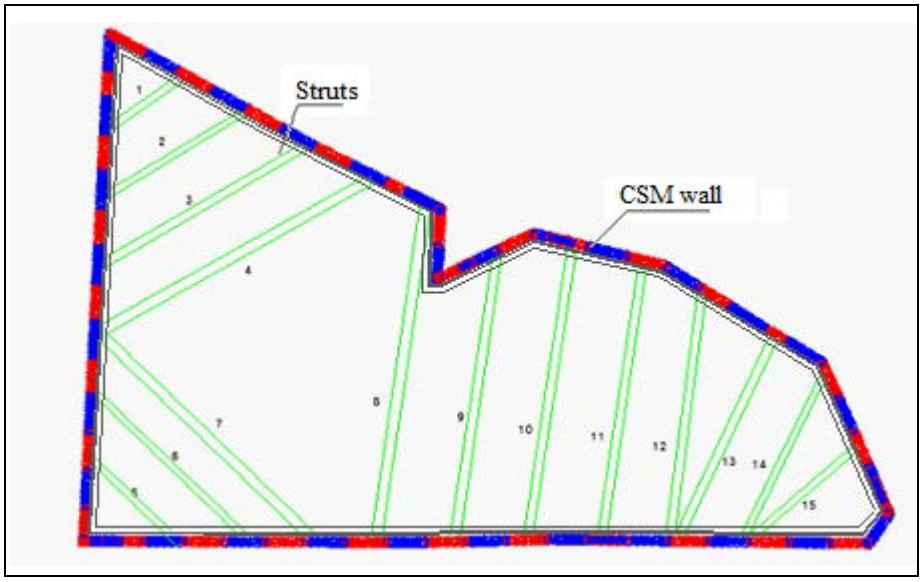

Figure 6: Representation of the CSM retaining structure in a plan view.

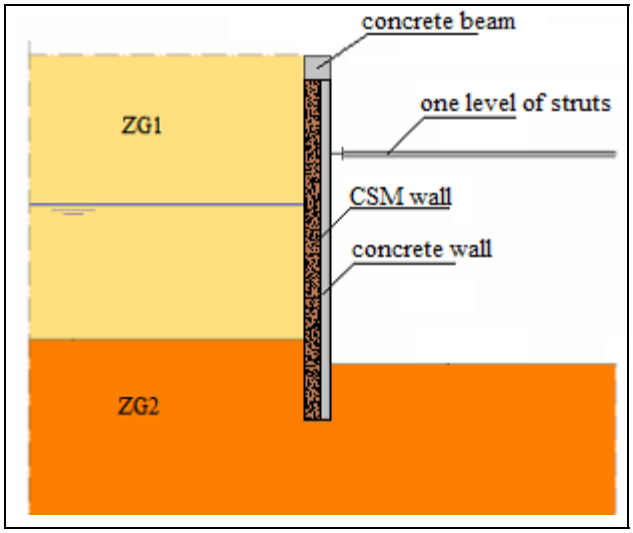

Figure 7: Cross-section of the retaining wall.

The continuous CSM wall was formed by overlapping primary and secondary panels, with an overlap length of 0.20 m to assure an effective connection of the panels in depth.
It was performed a concrete wall, 0.15 m thick, executed after each level of excavation, against the CSM wall.
In the following figure is presented a partial view of the retaining wall with the steel waler beams, the internal struts and the concrete wall.

Figure 8: Partial view of the retaining wall with the steel waler beams, the internal struts and the concrete wall.

The CSM technology was developed from the Deep Soil Mixing (DSM) and the main difference between the two technologies is related to the use, in CSM technology, of a cutter tool that integrates two sets of cutting wheels that rotate about horizontal axes to produce soil-cement panels with a rectangular cross-section contrarily to DSM technology that uses cutting tools that rotate about vertical axis to produce soil-cement columns (Stoetzer et al., 2006).

Figure 9: View of the CSM equipment and a CSM panel (on the left) and the equipment used in DSM technology (on the right).

The rectangular geometry of the CSM panels is advantageous when compared to the circular column sections, the most significant of which are the coast, the reduction of the number joints in the wall and the freedom to use different types of reinforcements (Fiorotto et al., 2005).
The use of panels with a rectangular cross-section to create continuous walls offers some advantages when compared to the use of circular columns, particularly the need of significantly lower volume of treatment to obtain the same effect and the possibility to optimize the distribution of the vertical steel piles of the reinforcement (Figure 10).
The application of CSM technology allows the use of the existing soil as a construction material, resulting a little generation of spoil, which constitutes an environmental advantage when compared to traditional technologies as concrete pile walls or diaphragm walls.
The possibility of control the execution parameters in real time is another advantage of CSM technology. The process of mixture of the cement slurry in the disaggregated soil by the cutting wheels may be influenced by a lot of variables and, to obtain the required characteristics of the CSM panels and a reproducibility in its execution, is essentially the control of execution parameters as the speed of the mixing tool, the pumped volume in depth, the inclination of the mixing tool, among others (Bringiotti et al., 2009).

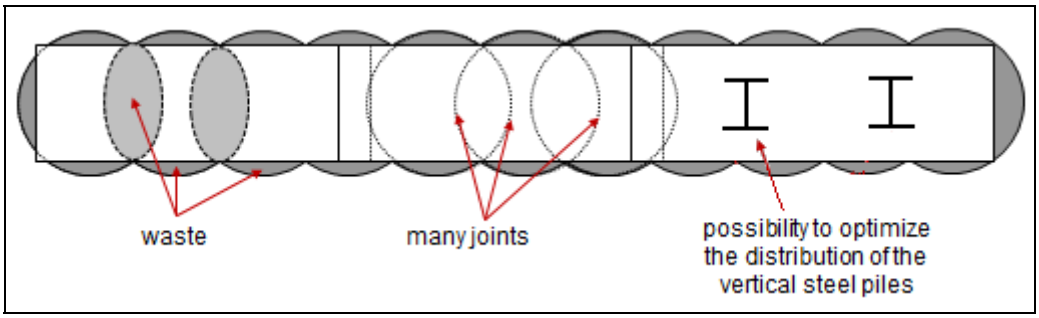

Figure 10: Comparison between rectangular soil-cement panels (CSM technology) and circular soil-cement columns (DSM technology).

4. ANALYSIS MODEL OF THE RETAINING WALL

A numerical analysis was carried out in the design phase using the finite element program PLAXIS®.
The ground was modelled in depth with the geomechanical parameters presented in section 2.1., with the Mohr-Coulomb model.
The most representative sections of the work were selected to the numerical analyses. The most unfavourable sections were selected to assure the security in design process and other least unfavourable sections are also selected to avoid the overdesign of the solution.
Figure 11 presents a plan view of the work with the indication of the six analysed cross-sections.
In the analysis of the different sections, was carried out the evaluation of the efforts in the retaining wall due to the earth pressures, the hydrostatic pressures and the surrounding conditions, specially the existing high buildings. The design was based on the limitation of the horizontal displacements of the retaining wall and the settlements of the surface.
The execution process was simulated in four main phases. The initial phase consisted of the simulation of the retaining wall execution. In a second phase, the first level of excavation was simulated. The third stage was the simulation of the installation of the first level of struts. The final phase consisted of the excavation to the maximum depth.
According the surrounding conditions, the following limits to the horizontal displacements to the retaining wall were defined: 15 mm on the top of the wall and 25 mm along the depth of the retaining wall.
In Table 1 are presented the values of the maximum horizontal displacements obtained in the numerical analysis.

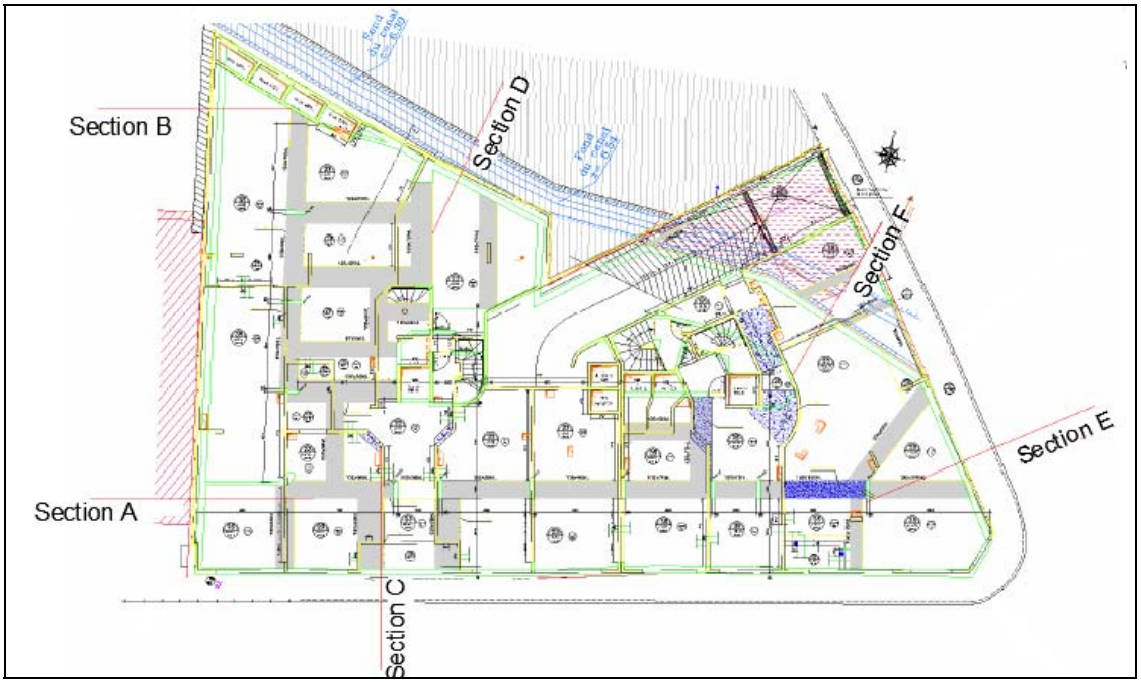

Figure 11: Plan view of the work with the indication of the six analysed cross-sections.

Table 1: Values of the maximum horizontal displacements obtained in the numerical analysis.

	Maximum horizontal displacements (mm)
At the top of the retaining wall	10.3
Along the height of the retaining wall	21.2

The results obtained by the numerical analyses were lower than the acceptable values defined.
The real displacements recorded during the excavation through the instrumentation implemented (surveying targets and inclinometers defined in a monitoring plan of the work) were slightly lower than the expected values.

5. EXECUTION PROCESS

The execution process included some of the characteristic stages of the CSM execution process that are summarized in this section.
Before the execution of the panels of the CSM retaining wall, a panel test was executed to obtain samples to laboratory tests (unconfined compressive strength tests) and to the calibration of the equipment. After the calibration of the equipment, the execution of the CSM wall was started with the sequential execution of primary and secondary soil-cement panels with a minimum overlap of 0.20 m between adjacent panels. During the execution of the CSM panels, the rig operator controls the values of the deviations of the mixing tool and other execution parameters in each instant, being able to correct the positioning of the cutter and the other parameters. After the execution of each CSM panel the vertical steel piles (IPE 450 piles) were installed to additional resistance to bending moments. The quality control of the soil-cement panels was carried out by laboratory tests (unconfined compressive strength tests) on samples from the panels of the retaining wall to the validation of the design parameters of strength and deformability.
The succeeding phase consisted of the execution of a small excavation to the execution of the concrete beam in the top of the retaining wall to connect the vertical steel piles.
The subsequent level of excavation was carried out to a maximum depth of 0.5 m below the level of struts with the succeeding installation of the steel pipe struts (Figure 12).

Figure 12: Partial views of the steel pipe struts.

The solution included a 0.15 m thick concrete wall, executed against the CSM wall during the progress of the excavation (Figure 13).

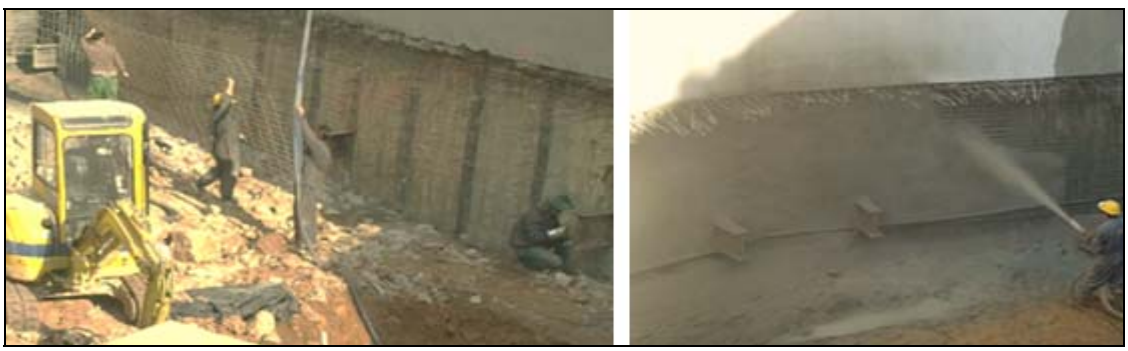

Figure 13: Execution of the concrete wall.

The final phase was the excavation to the maximum depth. In Figure 14 are presented different views of the work and a detail of a pipe strut.

Figure 14: Different views of the work and a detail of a pipe strut.

The following figure shows the cutting head used to the CSM panels execution and an example of a rocky block collected during the excavation that represents the type of materials overtaken by the equipment.

Figure 15: Cutting head used to the execution of the CSM panels (on the left) and example of a rocky block collected during the excavation (on the right).

6. CONCLUSIONS

The application of Cutter Soil Mixing technology in the retaining wall to the urban excavation presented in this paper allowed a satisfactory performance with only a level of steel pipe struts to horizontal support.

As it was pointed out in the paper, CSM technology allows the execution of rectangular shaped soil-cement panels with some advantages when compared to the circular shaped soil-cement columns obtained

with the traditional Deep Soil Mixing method. Some of these advantages are the need of significantly lower volume of treatment to obtain the same effect and the possibility to optimize the distribution of the vertical steel piles of the reinforcement. The possibility of the control of the execution parameters in real time is a very important advantage of CSM technology to obtain the required characteristics of the soil-cement panels and a reproducibility in its execution.
The CSM technology has been applied with a satisfactory performance in different kinds of works, mainly to the execution of retaining structures in urban areas as well as in the improvement of foundation soil and constitutes an interesting innovative solution with great potential to develop.

REFERENCES

Bringiotti, M., Dossi, M., Nicastro D. (2009), Miscelazione profonda dei terreni: metodi classici e tecnologie innovative – CSM by BAUER. Geofluid 2009.

Fiorotto, R., Schöpf, M. and Stötzer, E. (2005), Cutter Soil Mixing(CSM) An innovation in Soil mixing for creating Cut-off and Retaining walls, In:16 ICSMGE: International Conference on soil mechanics and geotechnical engineering, Osaka-Japan.

Stoetzer, E., Brunner, W., Fiorotto, R., Gerressen, F.W. and Schoepf, M. (2006), CSM Cutter Soil Mixing – A New Technique for the Construction of Subterranean Walls Initial Experiences Gained on Completed. In: Proceedings DFI/EFFC 10th International Conference on Piling and Deep Foundations, Amsterdam.

Permanent Excavation Support in Urban Area using Cutter Soil Mixing technology at Cannes, France

Peixoto Artur, Geo-Rumo,Tecnologia de Fundações, S.A., Portugal, artur.peixoto@georumo.pt
Sousa Estela, Geo-Rumo, Tecnologia de Fundações, S.A., Portugal, estela.sousa@georumo.pt
Gomes Pedro, Geo-Rumo, Tecnologia de Fundações, S.A., Portugal, pedro.gomes@georumo.fr

ABSTRACT

This paper describes the general design and execution aspects of a peripheral retaining wall to the construction of the underground floors of "Hotel Montaigne" building, located at Cannes, France. Considering the geological and geotechnical constraints, the presence of high water table and the surrounding conditions near existing buildings, it was performed a retaining wall of soil-cement panels executed using the deep soil mixing technology, in particular the Cutter Soil Mixing (CSM) technology. The soil-cement panels were reinforced with vertical steel piles and temporarily supported by two levels of steel pipe struts. Besides allowing a safe vertical excavation and limiting the water inflow to the interior of the excavation, the retaining structure was designed as a secondary foundation element of the final structure together with a concrete wall executed against the CSM wall and the principal foundation elements constituted by micropiles. The main results of modelling and quality control of the work are also presented.

1. INTRODUCTION

This paper refers to the retaining structure executed to the refurbishment of the building "Hotel Montaigne", located in the city of Cannes, France. The existing hotel was remodelled and expanded, with the construction of an additional high floor in the existing building and a new building block with seven floors high and three underground floors (Figure 1).
The retaining wall was designed to allow the excavation of the underground floors of the new building block.

Figure 1: Representation of "Hotel Montaigne" surrounding.

The excavation site plan, with a trapezoidal geometry, presents an area of about 300 m^2 and is bounded by streets and existing buildings (Figure 2).
The main challenge of this project consisted in the execution of an urban excavation with an average depth of 9 m under demanding ground and water table conditions.
The main concerns in the design of the retaining wall were the guarantee of minimum interference in the surrounding area, assuring the security during and after the works and, simultaneously, the reduction of the water inflow to the interior of the excavation. In this context was defined a retaining wall formed by

soil-cement panels executed using the Cutter Soil Mixing (CSM) technology. The CSM wall was reinforced by vertical steel piles and horizontally supported by two levels of horizontal struts.

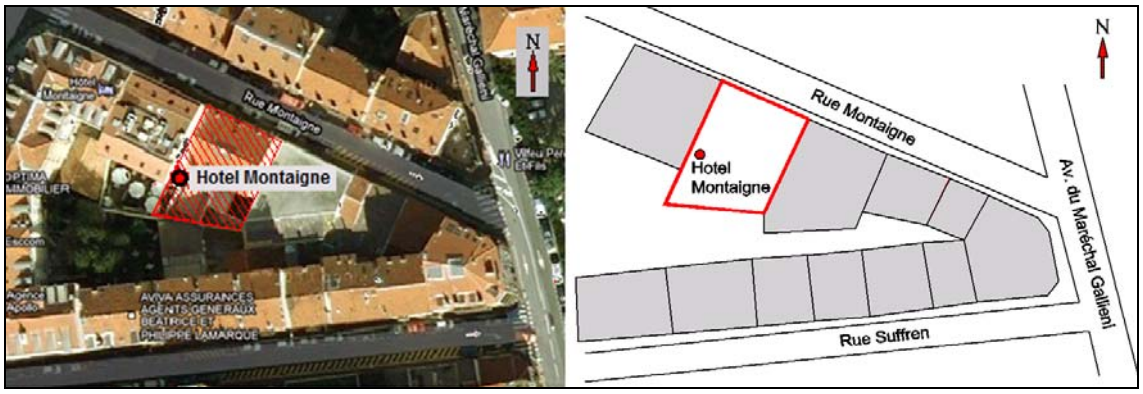

Figure 2: Site plan.

CSM was developed from Deep Soil Mixing (DSM) and is based on the mechanical mixing of the existing soil with cement slurry to form soil-cement panels in depth with a rectangular cross-section (Fiorotto et al., 2005; Gerressen et al., 2009).
The execution of CSM panels doesn't require the removal of the soil unlike other techniques, for example, concrete pile walls or diaphragm walls. There is no soil decompression during the execution of CSM panels which allows the minimization of the interference with the surrounding area.
The continuous wall formed by CSM panels was reinforced with vertical steel piles to satisfy simultaneously the following main objectives:

- allow a safe vertical excavation with the minimum interference in the surrounding area;
- foundation element of the internal structure;
- reduce the water inflow to the interior of the excavation.

2. MAIN CONSTRAINTS

2.1. Geological and Geotechnical conditions

The soil characterization was based in two geotechnical studies, performed in different phases.
In an initial phase, with a restricted access to the work site, a preliminary study was carried out, including the installation of a piezometer to the measure of the water table, the execution of a drill boring test and the execution of a Ménard Pressiometer Test (PMT).
In another phase a second geotechnical study was carried out to complement the initial study. This second study included the installation of a piezometer, the execution of two drill boring tests, two PMT tests and laboratory tests in intact samples, particularly Triaxial tests.
The laboratory tests were carried out to identify the type of soils in depth and its geomechanical characteristics. Through the analysis of the in-situ and laboratory tests results, three distinct layers were identified (Figure 3):

- Heterogeneous clayey and silty fill detected from the surface to an average depth of 5 m (Geotechnical Zone 1 – ZG1);
- Sandy Clays under the heterogeneous fill until a depth of about 9 m (Geotechnical Zone 2 – ZG2);
- Sandstone Bedrock under the previous layer (Geotechnical Zone 3 – ZG3).

The water table was detected approximately 3.5 m below the surface.

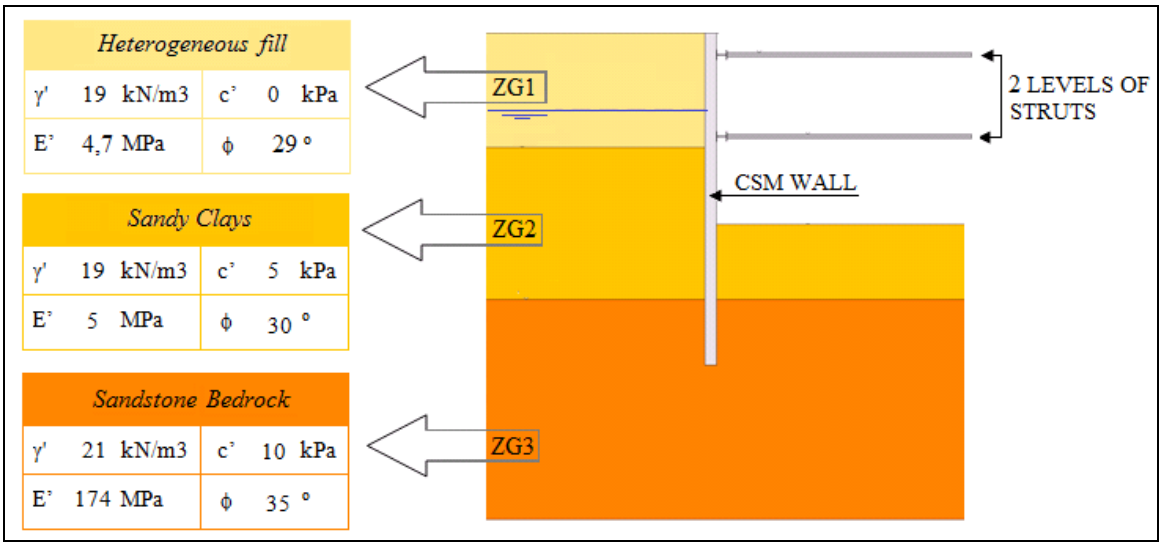

Figure 3: Main Geotechnical parameters and representation of a cross-section of the excavation.

2.2. Neighboring constraints

The work is located in an urban area with high neighbouring buildings and, because of that, one of the main concerns during the design of the retaining structure and the execution of the works was the guarantee of safety of neighbouring buildings and streets.
The excavation is bounded to the north by a street (*Rue Montaigne*), to the south by a building with three floors high, to the west by the building of the existing hotel with three underground floors and seven floors high and to the east by a small building to demolish before the start of the excavation.
At the time of the equipment installation in the work site, the demolition of the small neighbouring building hadn't been started and the space to the equipment installation was very conditioned (Figure 4).

Figure 4: Installation of the equipment.

2.3. Seismic conditions

The work is located in the city of Cannes, France, and the seismic risk was classified with the Standard Norms of the country.
According the Decree "nº 2010-1255" of 22th October 2010, in the French territory are distinguish five zones with different degrees of seismic intensity (Figure 5): very low (1), low (2), moderate (3), medium (4) and high (5).

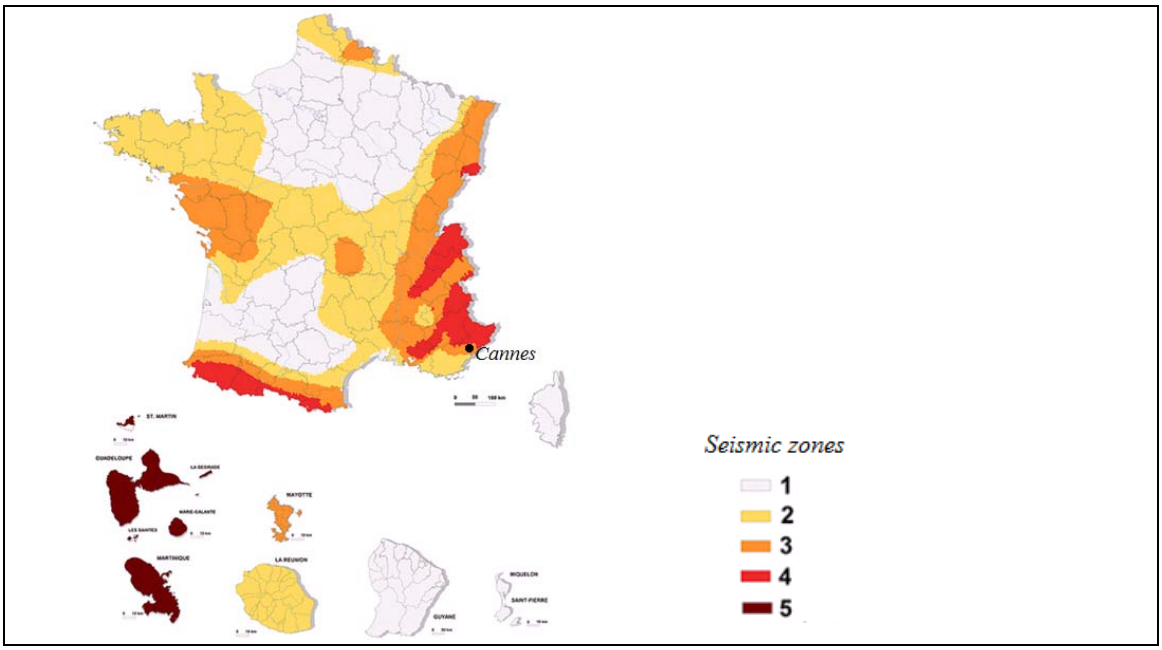

Figure 5: Zones of seismic intensity of the French territory (Decree "n° 2010-1255" of 22th October 2010).

The city of Cannes is located in a zone of moderate seismic intensity.
According to the same Decree, four Categories of Importance to the buildings are defined, by an increasing order of importance: Categories I, II, III and IV. The new building block of the "Hotel Montaigne" is inserted in the Category of Importance II (collective housing building with height up to 28 m).

3. CSM RETAINING WALL

The performed solution to the support of the excavation consisted in a peripheral CSM retaining wall with two horizontal levels of temporary steel pipe struts. In Figure 6 is represented a plan of the CSM retaining wall and the horizontal struts.

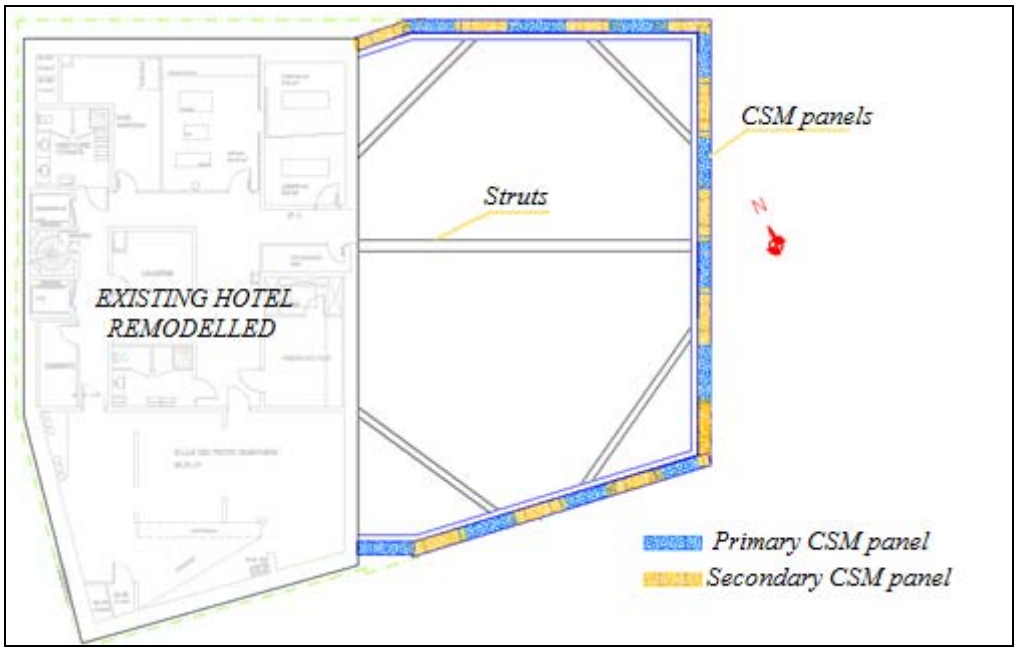

Figure 6: Plan of the CSM retaining wall and the horizontal steel pipe struts.

The continuous CSM wall was executed by overlapping primary and secondary soil-cement panels, with a rectangular cross-section with dimensions of 2.40 m x 0.55 m, considering a minimum overlapping between adjacent panels of 0.20 m to assure an effective connection throughout the height of the panels.
The reduction of the water inflow to the interior of the excavation was one of the main concerns during the conception of the retaining structure and, with this aim, was defined to the CSM panels a minimum penetration length of 3 m below the bottom of the excavation, into the sandstone substrate (ZG3).
The CSM panels were reinforced by vertical steel piles (IPE 450 piles), installed at 1.10 m intervals (two piles in each panel). The placement of the steel piles in CSM panels allows the protection of these elements against buckling problems, minimizing simultaneously possible corrosion problems.
The solution included also a 0.15 m thick concrete wall, executed from the bottom of the excavation, against the CSM wall.
The retaining wall was designed to support, together with the concrete wall and the micropiles performed as the principal foundation elements, the total vertical efforts transmitted from the permanent structure of the building.
The execution of a CSM panel comprises essentially two main phases:

- Cutting phase: the cutting head is vertically driven through the ground until it reaches the designed depth. The existing soil is desegregated by the movement of rotation of the cutting wheels while cement slurry is added simultaneously;
- Extraction and mixing phase: the cutting head is extracted while cement slurry is added to the homogenization of the mixture.

During the cutting phase, the soil matrix is broken up and cement soil is blended to fluidify the soil. The penetration rate of the cutting head and the cement slurry volume added to the soil must be adjusted by the rig operator to create homogeneous soil-cement panels. Depending on the characteristics of the existing soil, during this phase may be necessary the use of bentonite instead of the cement slurry.
When the design depth is reached, the extraction of the cutting head begins and the rotation direction of the cutting wheels is inverted. During this phase, the remaining quantity of cement slurry is added to homogenize the mixture.
In Figure 7 is presented the CSM execution process.

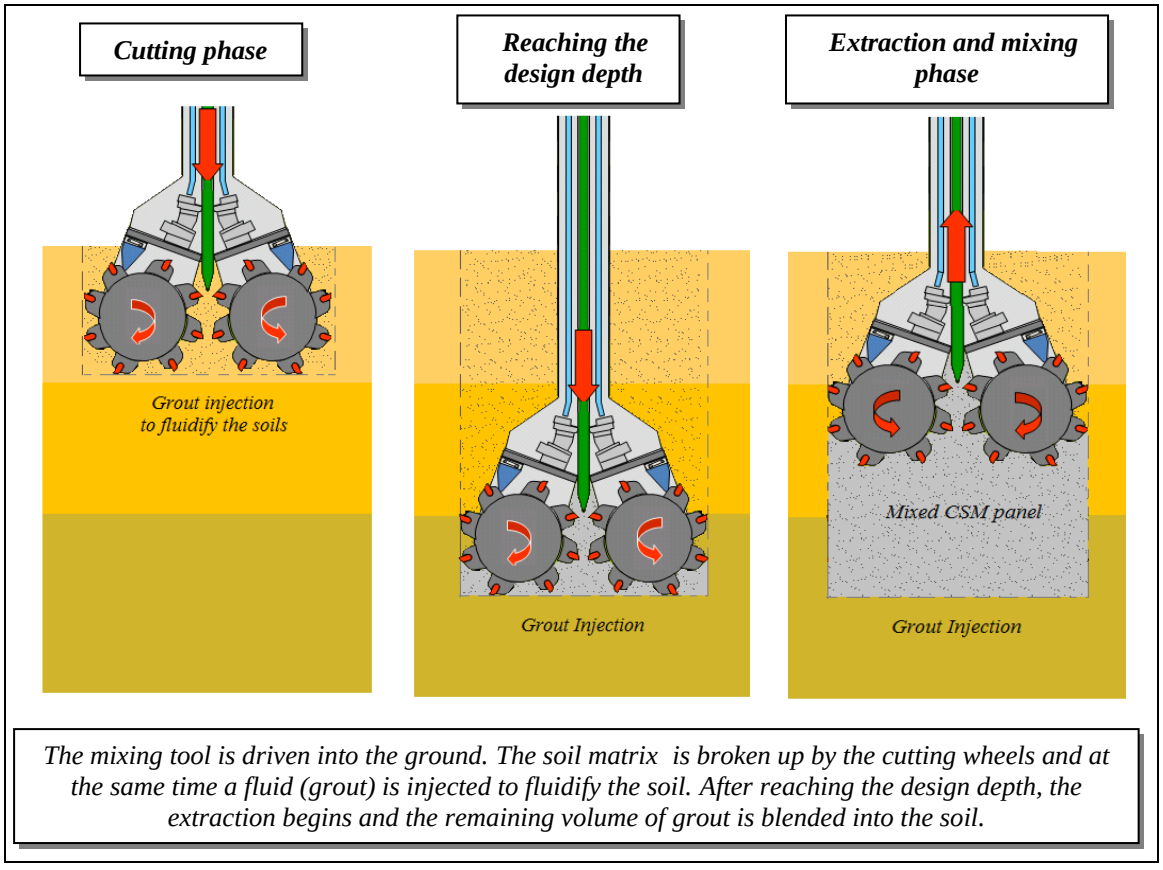

Figure 7: Illustration of the main phases of the CSM execution process.

4. ANALYSIS MODEL OF THE RETAINING WALL

The analysis of the retaining wall was carried out using a numerical model developed with the finite element program PLAXIS®.
The soil was simulated using the Hardening-Soil model with the geomechanical parameters already presented in section 2.1. The retaining structure was simulated with a one-dimensional linear beam element.
The numerical analysis was carried out in plane strain. The representative sections of the four elevations of the retaining structure were studied.
Figure 8 presents an example of one of the analysed sections (Section A), representing a cross-section of the north alignment, near a street (*Rue Montaigne*).

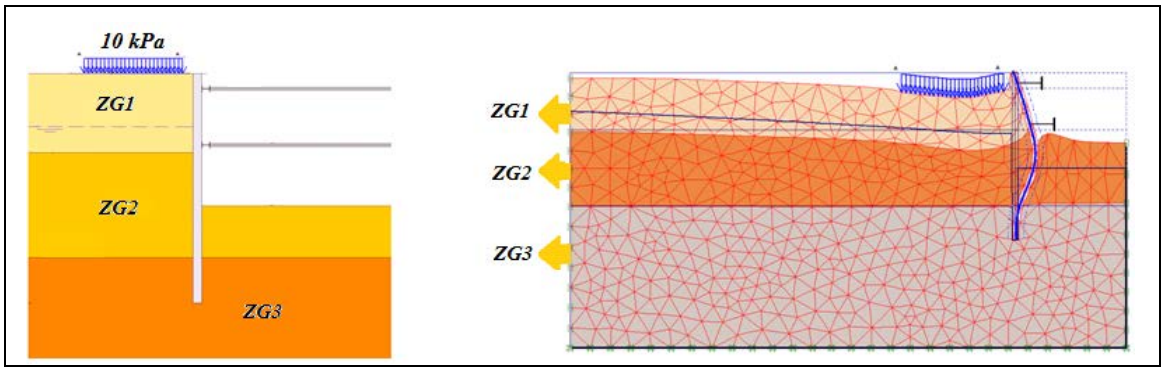

Figure 8: Section A: cross-section (on the left) and analysis model representing the deformation at the maximum excavation depth (on the right).

In the following table are presented the maximum values of the horizontal displacements of the retaining structure obtained in the numerical analysis of the Section A.

Table 1: Maximum values of the horizontal displacements obtained in the numerical analysis of the Section A.

	Maximum horizontal displacements (mm)
At the top of the retaining wall	2.0
Along the height of the retaining wall	18.5

According to the surrounding conditions and the characteristics of the excavation, the following acceptable limits to the horizontal displacements of the retaining wall were defined: 5 mm at the top of the retaining wall and 20 mm along the height of the retaining wall.
In the numerical analyses of all studied sections were obtained lower values than the defined limits and, during the excavation, the horizontal displacements obtained were slightly lower than the expected values.
CSM panels were designed considering a compressive strength of 2 MPa (with a safety factor of 2) and an elasticity modulus of 1 GPa. These values were confirmed by laboratory tests (unconfined compressive strength tests), carried out on samples from the panels of the CSM retaining wall. The minimum acceptable result of the unconfined compressive strength tests was 4 MPa, to allow the use of a safety factor of 2. The results of the laboratory tests carried out are detailed in the section 6 of this paper.

5. EXECUTION PROCESS

The execution process started with the execution of the CSM panels before the excavation (Figure 9).
The equipment to the execution of CSM is constituted by a crane with a vertical tower (RTG RG19T) with a total height of about 23 m, associated to a kelly bar system with a height of about 20 m. The cutting head used (BCM 5 - Bauer Machinen) is held and guided by the kelly bar system.
To the reinforcement of the CSM panels, vertical steel piles were installed immediately after its execution as close as possible to the excavation face to allow the connection of the steel waler beams and the steel pipe struts (Figures 10 e 11).

Figure 9: Components of the equipment: cutter head and kelly bar.

Figure 10: View of the execution of a CSM panel (on the left) and installation of the IPE piles (on the right).

Figure 11: Detail of the steel waler beams connected to the pipe struts.

The continuous wall was formed by overlapping primary and secondary CSM panels, with an overlap length of 0.20 m. The secondary panels can be executed immediately after the construction of the primary panels, process known as “soft-into-soft” or after the hardening of the primary panels, process known as “soft-into-hard”. These two hypotheses are possible due to the versatility of the CSM cutting tool allowing the application of the technology to all soil types, although not all kinds of soils are equally suitable.
The next stage consisted in a small excavation to allow the execution of the concrete beam at the top of the retaining wall. After the construction of the concrete beam, an excavation to a maximum depth of 0.5 m below to the first level of struts was carried out. In this stage were executed the steel waler beams to the connection of the horizontal steel pipe struts.
The second level of excavation and the execution of the second level of struts were carried out by a similar process to that described to the first level.

After reaching the maximum depth of excavation, a concrete wall is constructed against the CSM wall. The temporary levels of struts are deactivated with the execution of the concrete slabs of the building structure.

Figure 12: View of the work after the execution of the second level of struts.

6. QUALITY CONTROL

The application of CSM technology allows the control, in real time, of the execution parameters by the rig operator through the monitor of the equipment (Larsson, 2005).

The variability of strength and deformability parameters of the soil-cement obtained using CSM technology is directly related with the degree of homogeneity of the mixture that is influenced by a lot of variables as the type of the existing soil, the water table presence, the distribution of the cement slurry in the desegregated soil, the chemical reactions during the process, among others. There are a lot of variables that can influence the quality of the final result obtained and, because of that, the effective control of the execution parameters is essential. During the execution of a CSM panel, the rig operator control and adjusts, in real time, the execution parameters as the speed of the mixing tool, the cement slurry volume added, the cement slurry pressure in hoses, the inclination of the mixing tool, among others (Figure 13).

The control of the execution parameters must be complemented with the execution of laboratory tests to the evaluation of strength and deformability parameters of the soil-cement obtained for the validation of the design hypotheses. Before the execution of the panels of the CSM retaining wall, test panels are executed to obtain samples to laboratory tests. This allows the calibration of the equipment. In a subsequent phase, the quality control is provided by laboratory tests on samples from the panels of the CSM retaining wall.

In the Table 2 are presented the values obtained in the unconfined compressive strength tests carried out on samples from the panels of the CSM retaining wall (average values).

To verify the evolution of the compressive strength of the samples along the time, laboratory tests were carried out on samples after 7, 14 and 28 days.

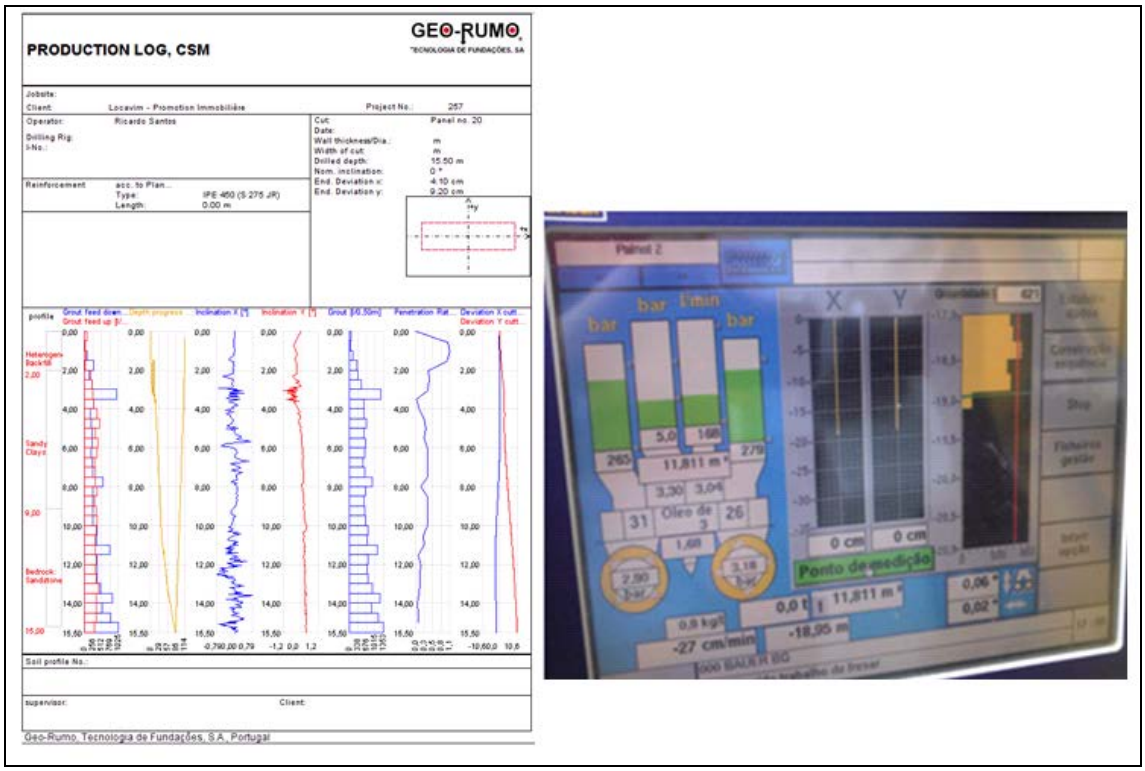

Figure 13: Production report (on the left) and rig operator's monitor for the control of the production process (on the right).

Table 2: Values obtained in the unconfined compressive strength tests (average values to 7, 14 and 28 days)

	7 days	14 days	28 days
Unconfined compressive strength (MPa)	5.0	7.0	7.8

The samples tested after 7 days presented a value of unconfined compressive strength of 5 MPa (average value), a higher value than the required value of 4 MPa. This allows to the validation of the design hypotheses.
The control was also carried out through the monitoring plan implemented, including surveying targets placed in the retaining wall, inclinometers placed behind the retaining wall and extensometers placed in the pipe struts. Throughout the different excavation phases the recorded values of the displacements of the retaining wall were slightly lower than the expected values and the defined alert limits.

7. CONCLUSIONS

The execution of the Cutter Soil Mixing retaining wall for the excavation of the new building block of "Hotel Montaigne" constituted an appropriate option with technical, economic and environmental advantages, as demonstrated in this paper.
The main objective of ensuring the minimization of interferences in the surrounding area was achieved with the CSM retaining wall. During the excavation, the CSM panels allowed also the reduction of the water inflow to the interior of the excavation. The low displacements of the retaining wall during the excavation demonstrate the excellent performance of the adopted solution.
CSM technology has a wide-ranging application field and it can be applied to all soil types.
As it was referred in the paper, the quality and the homogeneity of the soil-cement panels depends on several factors that affect the execution process and, because of that, the control and monitoring of the work is essential, especially in urban excavations.
Regarding the experience of the company Geo-Rumo in the application of this technology, it has been sucessfully applied in Portugal and France in different types of works, especially the execution of retaining structures and the improvement of foundation soil.

REFERENCES

Fiorotto, R., Schöpf, M. and Stötzer, E. (2005), Cutter Soil Mixing(CSM) An innovation in Soil mixing for creating Cut-off and Retaining walls, 16 ICSMGE: International Conference on soil mechanics and geotechnical engineering, Osaka-Japan.

Gerressen, F. W., Schopf, M. and Stotzer, E. (2009), CSM – Cutter Soil Mixing – Wordwide experiences of a young soil mixing method, International Symposium on Deep Mixing & Admixture Stabilization, Okinawa, Japan.

Larsson, S. (2005), State of Practice Report – Execution, Monitoring, and Quality Control, International Conference on Deep Mixing. Best Practice and Recent Advances. Deep Mixing ´05, Stockholm, Sweden.

Solutions for soil foundation improvement of an industrial building using Cutter Soil Mixing technology at Fréjus, France

Peixoto Artur, Geo-Rumo,Tecnologia de Fundações, S.A., Portugal, artur.peixoto@georumo.pt
Sousa Estela, Geo-Rumo, Tecnologia de Fundações, S.A., Portugal, estela.sousa@georumo.pt
Gomes Pedro, Geo-Rumo, Tecnologia de Fundações, S.A., Portugal, pedro.gomes@georumo.pt

ABSTRACT

This paper describes the most relevant design and execution aspects of foundation soil treatment to the construction of an industrial building at Fréjus, France. The time constraints related to the execution period of the work associated with the geological and geotechnical conditions, led to the adoption of a non-conventional solution of foundation soil treatment. The solution consisted of soil-cement panels, performed through the deep soil mixing technology, particularly using the Cutter Soil Mixing technology. Geological and geotechnical analyses indicated that the soil at the work site is formed by a one meter thick layer of predominantly gravelly fills, superjacent to a 2-6 meter thick layer of colluvial soils with low strength and deformability, over a marl-sandstone substrate. This paper presents some of the aspects with greater interest related to the execution process and the main results of quality control of the work.

1. INTRODUCTION

The increasing need of occupation of alluvial soils to new constructions has allowed to the challenge of create new suitable solutions of soil improvement that optimize the work execution time and the economic questions. In the described context, is presented in this paper the application of CSM technology to the improvement of the foundation soil to the construction of an industrial building at Fréjus, France.
The building, with an approximately rectangular geometry in plan, has an implantation area of about 3800 m^2. In the following figure is presented the location of the work.

Figure 1: Location of the work.

The new industrial building presents only one high floor (Figure 2) and the respective surrounding is characterized by the absence of adjacent constructions.

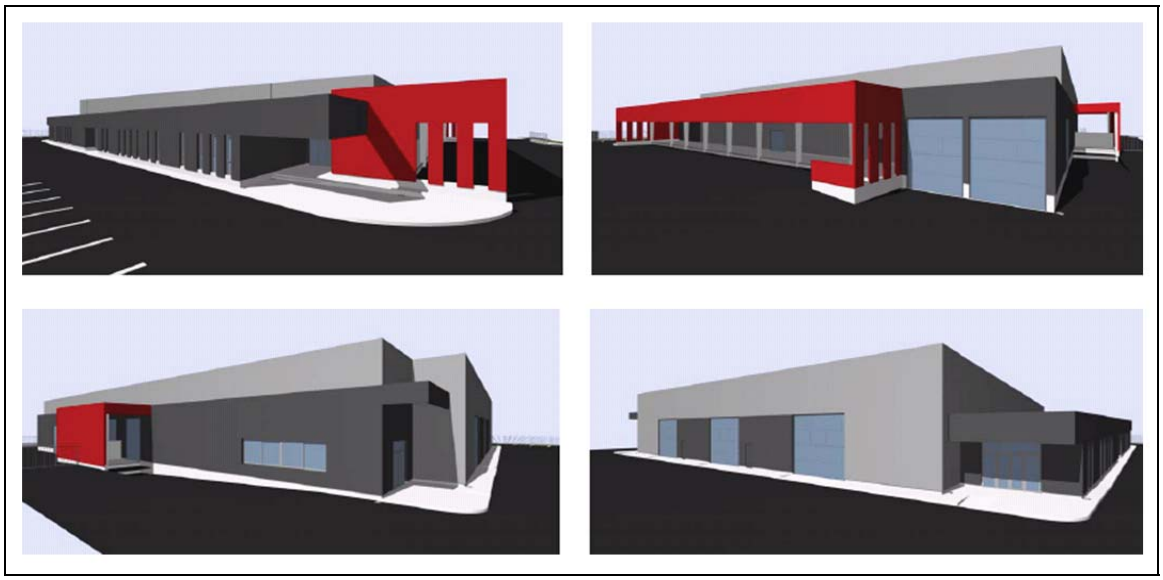

Figure 2: Representation of the final aspect of the new industrial building.

The main concern during the design of the presented solution was the minimization of the total and differential settlements of the building structure.
According to the geotechnical conditions of the ground, it was necessary to transmit the efforts to the substrate with appropriated characteristics (marl-sandstone substrate), detected at variable depths between 3 m and 7 m. The performed solution to the efforts transmission consisted, generally, in soil-cement panels executed by the CSM technology. Above the CSM panels was executed a load transfer layer, 0.60 m thick, made of granular material, upon which was placed the concrete bottom slab of the building.
The CSM technology constitutes an interesting alternative to the traditional solutions, with some technical, economic and environmental advantages and it has been successfully applied in other cases of ground improvement (Ameratunga et al., 2009).

2. MAIN CONSTRAINTS

2.1. Geological and Geotechnical conditions

The design of the presented solution was based in a geotechnical study of the ground at the site, including the execution of Cone Penetration Tests (CPT) and laboratory tests. The analysis of the obtained results allowed the identification of a superficial gravelly fill layer (Geotechnical Zone 1 – ZG1) detected to a maximum depth of 1 m, over colluvial soils (Geotechnical Zone 2 – ZG2) with high compressibility and low strength and a marl-sandstone substrate (Geotechnical Zone 3 – ZG3) detected in variable depths between 3 m and 7 m (Figure 3).

		ZG1 Gravelly fills	ZG2 Colluvial Soils	ZG3 Marl-Sandstone Substrate
γ'	[kN/m³]	19	17	21
c'	[kPa]	0	5	10
ϕ'	[°]	25	22	35
E	[kPa]	10000	5000	170000

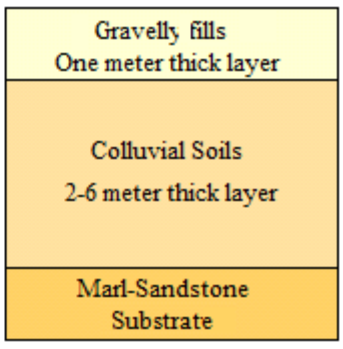

Figure 3: Geotechnical zones and respective main geomechanical parameters.

2.2. Execution time constraint

The contractor has imposed a maximum limit time of four weeks to the execution of the soil improvement. The proposed solution was conceived with the concern of achieving this objective.

3. PERFORMED SOLUTION

In the described context, the solution performed to assure the correct transmission of the efforts to the marl-sandstone substrate with appropriated characteristics of strength to foundation, consisted of the execution of 118 CSM panels, with a rectangular cross-section with dimensions of 0.6 m x 2.4 m, disposed on a rectangular mesh, as illustrated in Figure 4.
The CSM panels were executed to variable depths between 3.5 m and 7.5 m to assure a minimum penetration of 0.5 m in the marl-sandstone substrate.

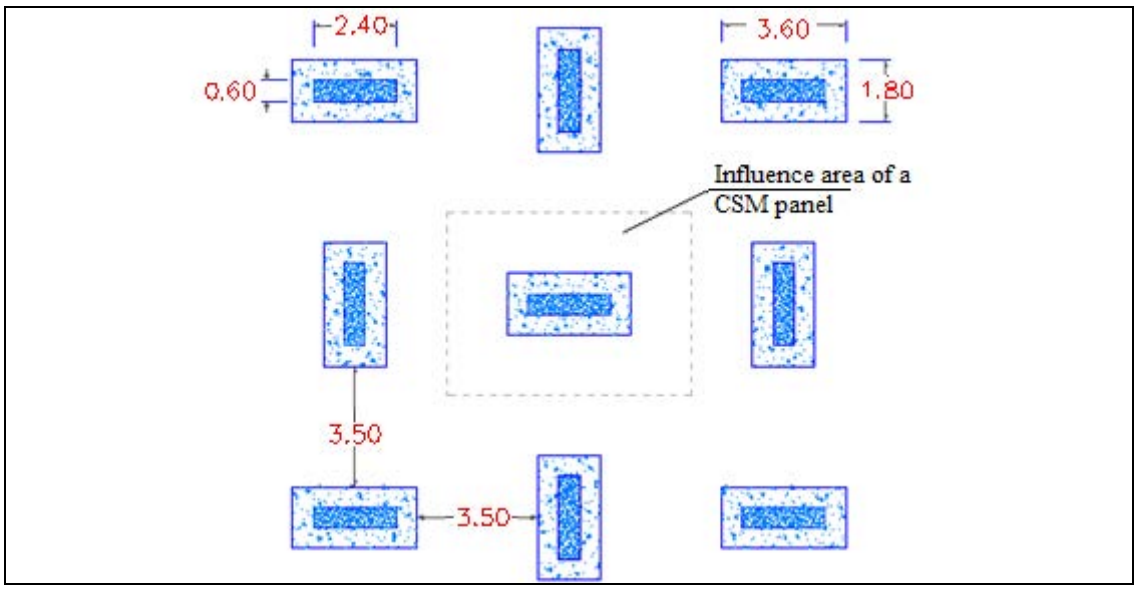

Figure 4: Rectangular mesh of the CSM panels.

To allow a more efficient loading transfer to the soil-cement panels it was performed the execution of an enlargement on the top of the panels, forming panel caps of larger dimensions than the panels in depth. The panel caps with dimensions in plan of 3.6 m x 1.8 m and 1 m height were executed through a small pre-excavation of 1.0 m depth with the geometry of the panel caps, subsequently filled by the overflow slurry resulting from the execution of the CSM panels.
The solution included also a load transfer layer, 0.60 m thick, made of granular material, upon which was placed the concrete bottom slab of the building.
The following figure presents a view of some CSM panel caps.

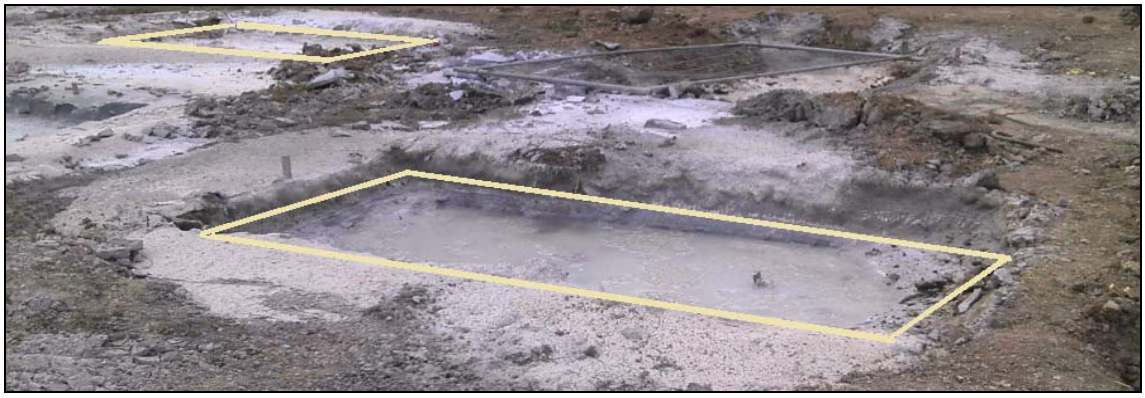

Figure 5: View of some panel caps..

In figures 6 and 7 are presented, respectively, a cross-section and a plan view of the performed solution.

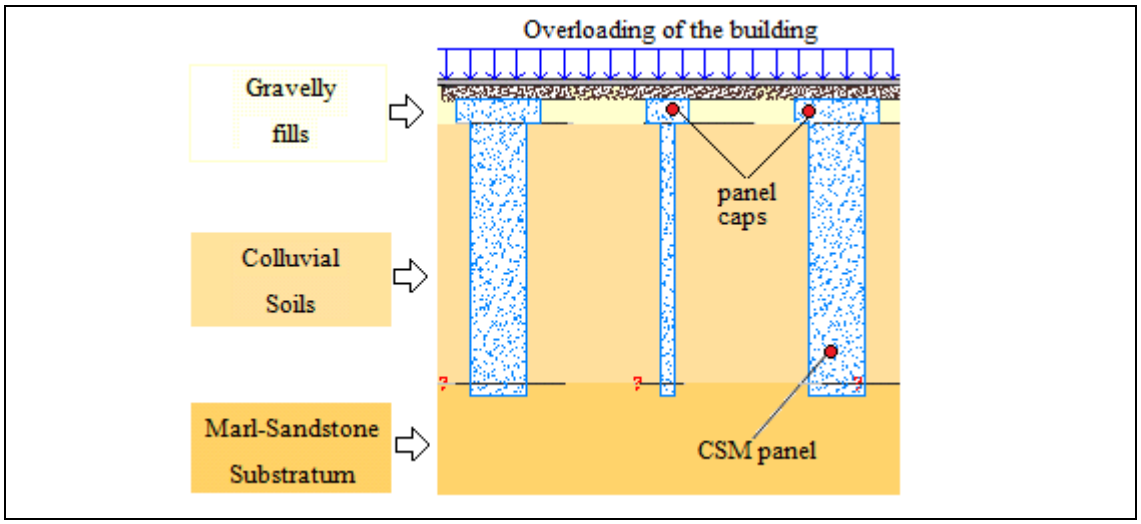

Figure 6: Cross-section of the performed solution.

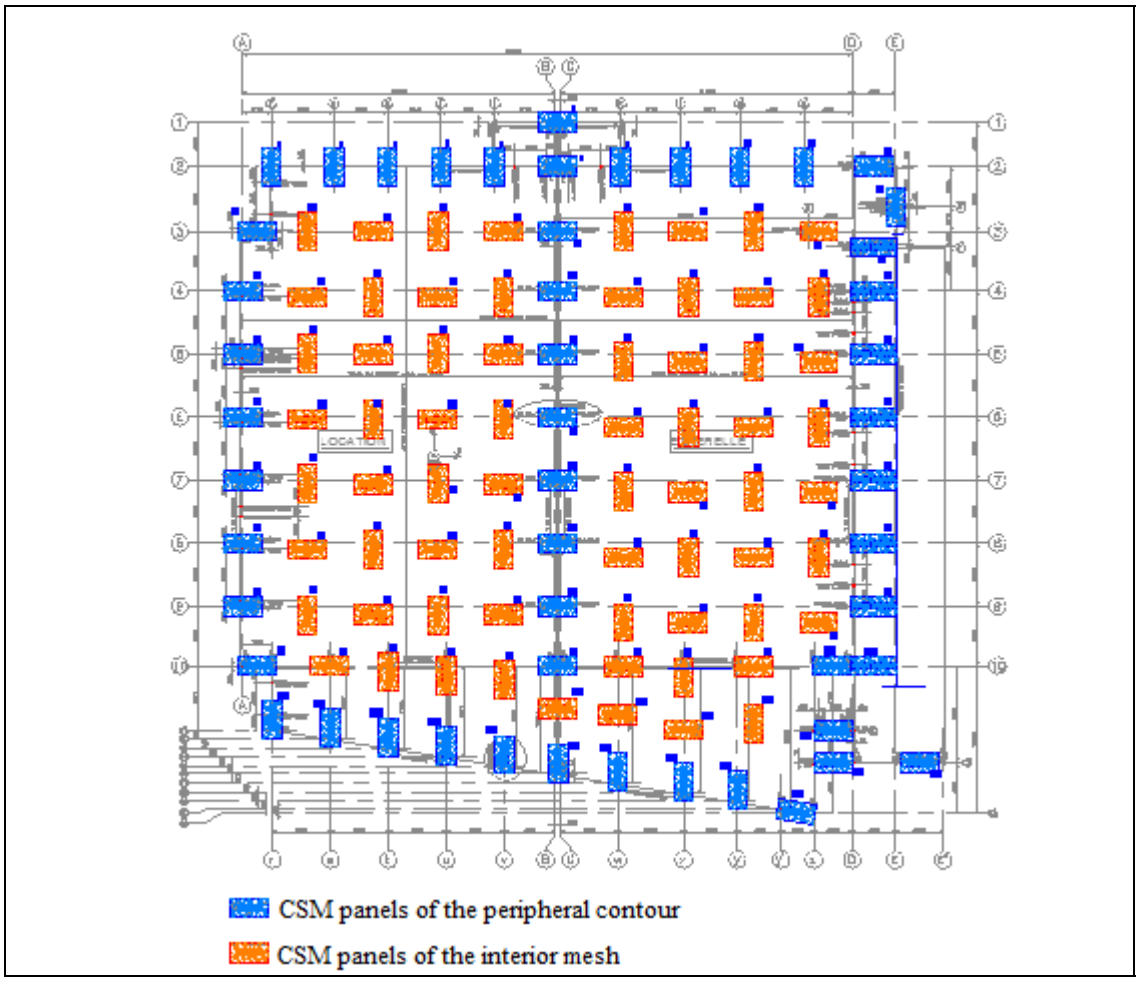

Figure 7: Plan view of CSM panels distribution.

With the application of this solution it was possible the exectution of the soil improvement in the maximum limit time of four weeks, with an average daily execution rhythm of 6 CSM panels.
The CSM technology consists in the mechanical mixture of the in-situ soil with cement slurry to obtain soil-cement panels with improved resistance and deformability characteristics to allow its application, for example, in the execution of retaining walls, cut-off walls or foundation soil improvements (Gerressen et al., 2009).
The equipment consists of a hydromill with two sets of cutting wheels that rotate about horizontal axis (Figures 8 and 9).

Figure 8: Equipment to the application of CSM technology.

Figure 9: Execution of a CSM panel.

In this case study, the use of the overflow slurry to fill the panel caps avoided the removal of excess cementitious material from the execution process.
The CSM equipment presents the versatility to allow the execution on all types of soils with the advantages of use the existing soil as a construction material, the minimization of the generation of spoil, the possibility of knowing the exact geometry of the panel in depth, the reduced vibrations during construction, among others.

4. ANALYSIS MODEL

In an initial phase, the initial estimative of the CSM panels mesh was based in the limitation of the compressive strength on the CSM panels to a maximum value of 1,5 MPa, to service loads, admitting that the total load is transmitted to the panels.
Based on the initial defined mesh, the analysis of the solution in terms of long-term settlements was carried out using the finite element program PLAXIS®.
To the modellation of the existing ground conditions, the Mohr-Coulomb model was used, considering the geomechanical parameters indicated in section 2.1. To the modellation of the load transfer granular layer it was also used the Mohr-Coulomb model, with an elasticity modulus of 20 MPa and this parameter was afterwards submitted to validation in-situ tests.
The concrete slab of the building was simulated with a linear elastic model, considering an appropriated elasticity modulus to take into account fluency effects.
In Figure 10 are presented the simplified geometry, the finite elements mesh and the boundary conditions of the numerical model.

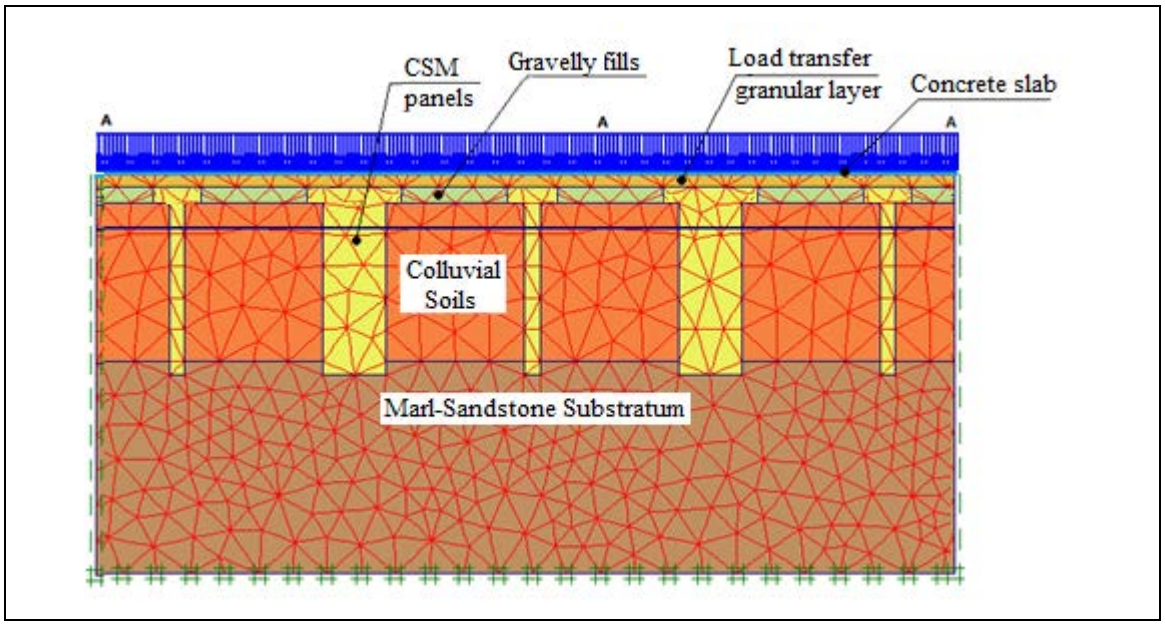

Figure 10: Simplified geometry, finite elements mesh and boundary conditions of the numerical model.

For the evaluation of the effects of the parameters variations, were carried out sensitivity analyses.
The results of the numerical analyses were evaluated in terms of angular distortions (β) that represents the measure of differential movement between two adjacent points separated by the distance. The angular distortion was in every studied cases lower than 1/800, with acceptable values of total and differential settlements. The maximum value of the long-term settlement obtained in analysis was 11 mm, which is within the settlement criterion.
In the following figure is presented the deformed mesh obtained in one of the numerical analysis.

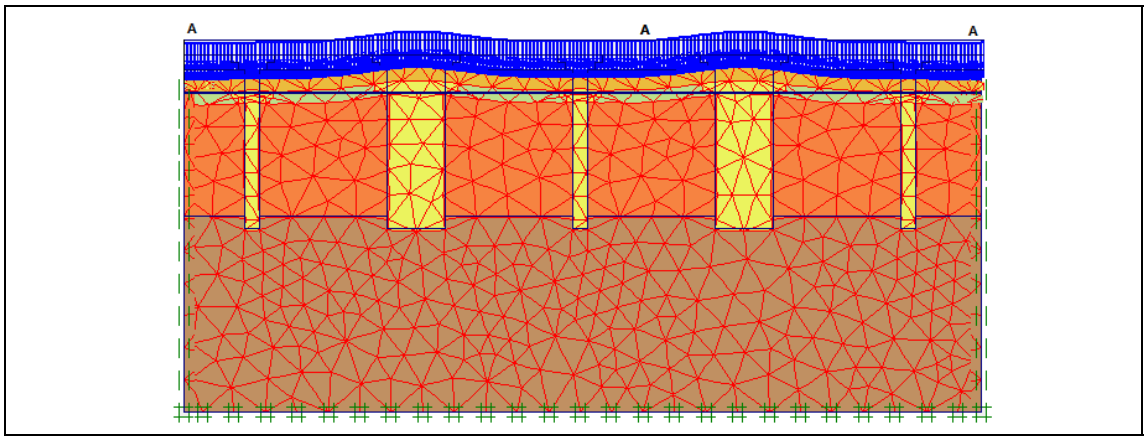

Figure 11: Deformed mesh obtained in one of the numerical analysis.

5. QUALITY CONTROL

Due to the particularities associated to the CSM execution process and, specially, due to the use of existing soil as a construction material, the quality control becomes essential to obtain the required characteristics and reproducibility on the panels executed.
The control was carried out, in an initial phase, during the execution of CSM panels by the rig operator that have the possibility to control and adjust the execution parameters in real time (Bringiotti et al., 2009).
In the following figure is presented the monitor of the rig operator to the control of the execution parameters

Figure 12: Rig operator's monitor to control of the execution parameters.

The quality control is also carried out through the execution of unconfined compressive strength tests on samples from the CSM panels, to adjust the execution parameters and obtain the required characteristics to the soil-cement panels.
In Table 1 are summarized the values of the compressive strength obtained in the two series of tests carried out on samples of the CSM panels.

Table 1: Values of the compressive strength obtained in the two series of tests carried out on samples from the CSM panels (tests after 7 days).

	Series I	Series II
Unconfined compressive strength (MPa)	7.0	6.5

The design value of the compressive strength of the soil-cement panels was 1,5 MPa, with a safety factor of 2 and, because of that, the minimum value defined to the compressive strength of the samples collected to laboratory tests was 3 MPa.
The results of the tests carried out after 7 days, presented in Table 1, evidenced that the compressive strength is highly superior to the required values. Because of that, the validation of the results was done without the tests after 14 and 28 days.

6. CONCLUSIONS

The Cutter Soil Mixing technology allows the use of the in-situ soil as a construction material and constitutes an alternative to the traditional solutions, with some technical, economic and environmental advantages. The panel caps executed at the top of the CSM panels ensured a more efficient transference of loads and with the use of the overflow slurry to fill the panel caps, the removal of excess cementitious material from the execution process wasn't necessary.
It should be point out the excellent performance of this innovative solution to the improvement of the foundation soil in the presented case, executed in the required execution time.

Figure 13: Views of the building after construction.

REFERENCES

Ameratunga, J., Brown, D., Ramachadran, R. and Denny, R. (2009), Ground improvement for a large above ground storage tank using cutter soil mixing columns. Proceedings of the 17th ICSMGE, pages 2280-2283.

Bringiotti, M., Dossi, M. and Nicastro, D. (2009), Miscelazione profonda dei terreni: metodi classici e tecnologie innovative – CSM by BAUER. Geofluid 2009.

Gerressen, F. W., Schopf, M. and Stotzer, E (2009), CSM – Cutter Soil Mixing – Wordwide experiences of a young soil mixing method. Proceedings of International Symposium on Deep Mixing & Admixture Stabilization, Okinawa, Japan.

Solution of earth retaining structure using Cutter Soil Mixing technology: "Parking Saint Nicolas" Project at Cannes, France

Peixoto Artur, Geo-Rumo,Tecnologia de Fundações, S.A., Portugal, artur.peixoto@georumo.pt
Sousa Estela, Geo-Rumo, Tecnologia de Fundações, S.A., Portugal, estela.sousa@georumo.pt
Gomes Pedro, Geo-Rumo, Tecnologia de Fundações, S.A., Portugal, pedro.gomes@georumo.pt

ABSTRACT

This paper presents the most relevant design and execution aspects of a peripheral retaining structure for the construction of "Parking Saint Nicolas", an underground parking lot located at Cannes, France. The retaining wall to the construction of the four underground floors was executed through soil-cement panels by the application of deep soil mixing technology, particularly the Cutter Soil Mixing (CSM) technology, reinforced with vertical steel piles. Taking in account the constrains related to the urban surrounding, including the proximity of buildings and streets, were implemented two levels of reinforced concrete slab bands at the levels of floors "0" and "-2", creating a rigid support system of the four elevations. The slab bands were incorporated on the final structure of the building and with this solution was dispensed the execution of ground-anchors with big lengths that would lead to the occupation of the neighbour underground. This solution brought some economic benefits, especially due to the incorporation of elements used in the final structure at the preliminary stage of the work. The main objectives of the retaining wall solution were allow the vertical excavation assuring simultaneously the stability of nearby structures and infrastructures, and also reduce the inflow of water into the interior of the excavation during the construction phase. The main results of modelling, instrumentation, monitoring and quality control of the work are also presented.

1. INTRODUCTION

This paper is intended to present the case of the retaining structure for the excavation of "Parking Saint Nicolas", an underground parking lot at Cannes, France. To the construction of this underground parking, with a capacity for 420 cars, developed in four underground floors, was carried out an excavation with a maximum depth of 14 m. The excavation plan presents a rectangular geometry with dimensions of about 48 m x 55 m and is bounded by existing buildings and streets (Figure 1).

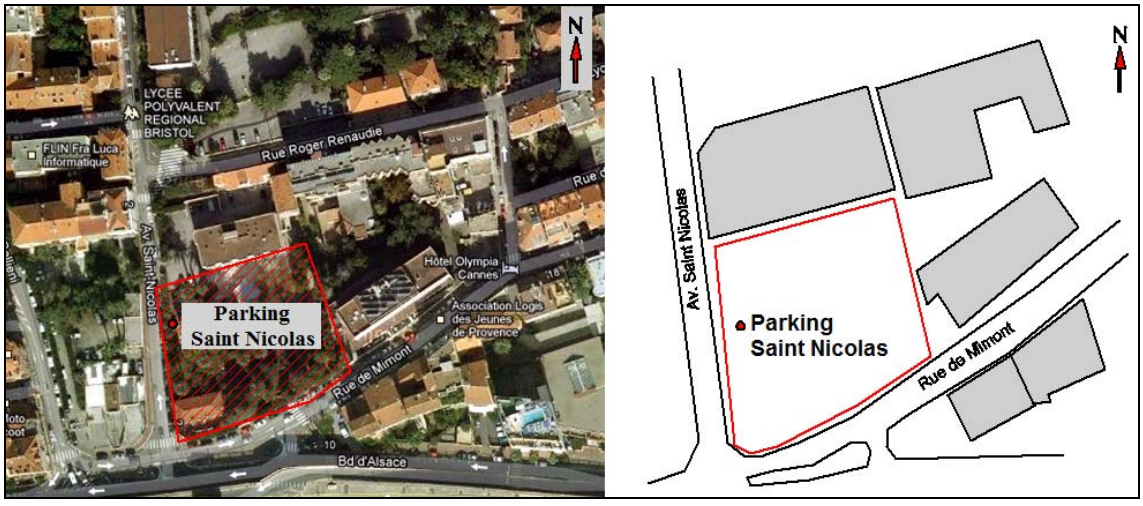

Figure 1: Location of the work.

In Figure 2 are represented two views of the exterior of the underground parking.

Figure 2: Representation of two views of the exterior of the underground parking.

To the excavation of the underground parking was performed a retaining structure formed by soil-cement panels executed through the Cutter Soil Mixing (CSM) technology, with a rectangular cross-section and a geometry similar to the panels of diaphragm walls. The retaining wall was horizontally supported by two levels of reinforced concrete slab bands, executed along the perimeter of the work, creating a rigid support system of the four elevations. Temporary foundation micropiles were executed to, together with the retaining structure, allow the vertical support of the slab bands.
CSM was developed from Deep Soil Mixing (DSM) technology and is based on the mixture of the in-situ soil with cement-slurry to create continuous walls formed by soil-cement panels of improved characteristics of strength and deformability, executed by a hydromill.
The CSM panels are produced by the mechanical action of the cutting wheels (Figure 3), rotating around horizontal axis, by desegregating the soil and mixing it with the cement slurry added simultaneously. (Fiorotto et al., 2005).

Figure 3: Detail of the cutting wheels (on the left) and general aspect of the hidromill (on the right).

During the conception of the solution and the execution of the work, one of the main concerns was assuring the minimization of the impact in the surrounding area.

2. MAIN CONSTRAINTS

2.1. Geological and Geotechnical conditions

The evaluation of the ground conditions was based, in an initial phase, on the preliminary geotechnical study and in a second phase, in a second geotechnical study carried out to complement the first one.
The preliminary geotechnical study included the execution of three drill boring tests, three Ménard Pressiometer Tests (PMT) and a pumping test as well as the installation of five piezometers and the execution of laboratory tests.

The second geotechnical study, carried out to complement the information obtained through the first study, included the execution of six PMT tests, the installation of three piezometers to measurements of the water table and the execution of laboratory tests.
The results of the in-situ tests together with the laboratory analysis allowed to the identification of a heterogeneous geological context of the ground in the work site. The local soil is composed by a sandy clay layer detected from the surface to variable depths between 5 and 10 meters, overlying the substratum of marls.
Table 1 presents the main geotechnical parameters, obtained by the interpretation of the in-situ and laboratory tests.
The water table was detected approximately 5 m below the surface.
To the evaluation of the permeability, was carried out a hydrological study, which led to the values of the permeability coefficients ($\mathbf{k_h}$ – horizontal permeability coefficient; $\mathbf{k_v}$ – vertical permeability coefficient) also presented in Table 1. The hydrological study also enabled to define the minimum length of the panels below the bottom of the excavation to obtain the minimization of the water inflow to the interior of the excavation. With this aim, was defined to the CSM panels a minimum penetration length of 4 m below the bottom of the excavation, into the marls substrate.

Table 1: Main geotechnical parameters.

		Sandy Clays (upstream)	Sandy Clays (downstream)	Altered Marls	Hard Marls
γ'	[kN/m³]	19	19	19	22
c'	[kPa]	10	10	25	70
ϕ'	[°]	25	25	25	30
E	[kPa]	15 000	6 000	6 000	225 000
K_h	[m/s]	1×10^{-4}	1×10^{-4}	1×10^{-5} to $2{,}5\times10^{-6}$	1×10^{-5} to $2{,}5\times10^{-6}$
K_v	[m/s]	5×10^{-5}	5×10^{-5}	1×10^{-5} to $2{,}5\times10^{-6}$	1×10^{-5} to $2{,}5\times10^{-6}$

2.2. Neighbouring constraints

The work is located at an urban zone and it is bounded by neighbouring streets and buildings. To ensure the minimization of the impact in the surrounding area, a rigorous accompaniment of the movements of the retaining structure throughout the different phases of the work is essentially.
The work site is bounded to the north by an existing building with four floors high and an underground floor, to the south by streets (*Boulevard d'Alsace / Rue de Mimont*) to the west by an avenue (*Avenue Saint Nicolas*) and to the east by an existing building with four floors high and three underground floors.

3. CSM RETAINING WALL

The retaining wall performed to the excavation of the underground parking lot consists of a continuous CSM retaining wall, reinforced by vertical steel piles (IPE piles) along the panels in depth.
Each panel of the retaining wall was reinforced by two vertical steel piles (IPE 450), installed at 1.1 m intervals. The CSM mixing tool used, allows the execution of soil-cement panels with a rectangular cross-section, with dimensions of 2.4 m x 0.6 m. The continuous wall was obtained by overlapping primary and secondary panels, with a minimum overlap length of 0.2 m to assure an efficient connection between panels in depth (Figure 4).
At the top of the retaining wall a concrete beam was executed to connect all steel soldier piles.
The horizontal support of the CSM wall was performed by two levels of concrete slab bands, creating a rigid support system of the four elevations that were afterwards incorporated in the structure of the building. The two slab bands were executed at the "0" and "-2" floors. The horizontal support in small slab holes was guaranteed by small steel struts.
The temporary support of the slab bands was performed by foundation micropiles (N80 ϕ177,8 x 10 mm – API5A) with a Gewi bar (ϕ50 mm) in the interior.

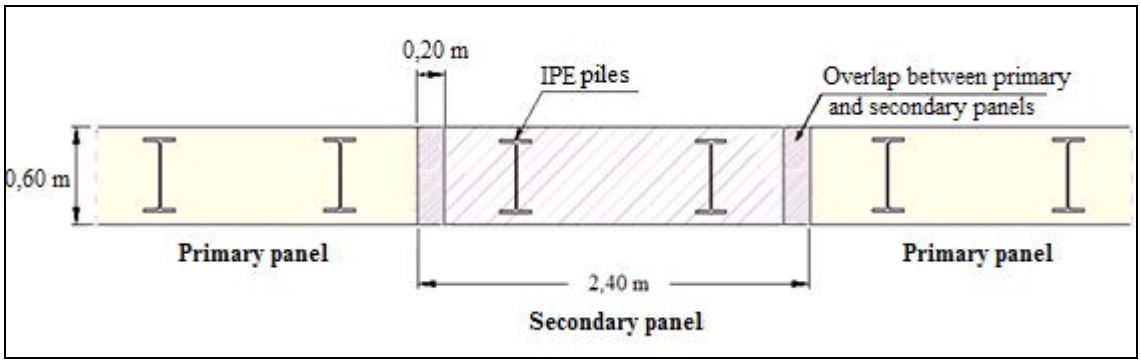

Figure 4: Representation of the overlapping of primary and secondary panels of the CSM retaining wall.

The solution included a 0.2 m thick concrete wall, executed against the CSM wall during the progress of the excavation.
In the case of this excavation with the presented dimensions, an alternative solution using steel pipe struts would require the use of large diameter and big length steel struts and, due to the surrounding conditions, the execution of ground anchors wouldn't be viable. The use of slab bands to the horizontal support of the CSM retaining structure was considered technical and economical advantageous, presenting the main advantage of the incorporation of elements used in the final structure at a preliminary stage of the work.
Figure 5 presents a partial view of the work with the slab bands and the temporary foundation micropiles and a cross-section of the retaining wall structure.

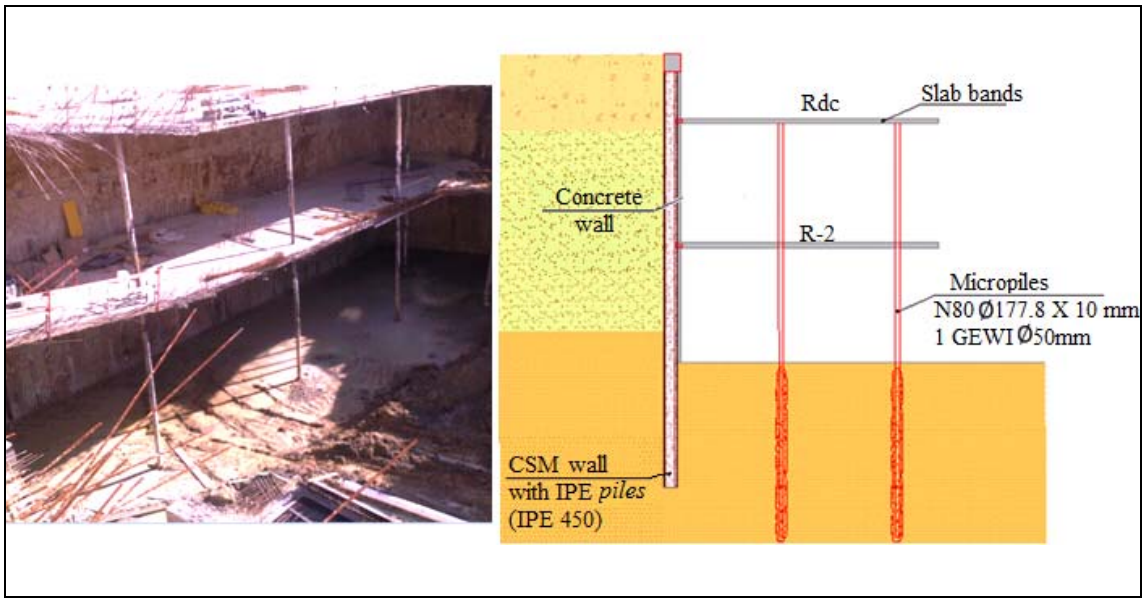

Figure 5: Partial view of the work (on the left) and cross-section of the retaining wall (on the right).

The slab bands are connected to the CSM wall through horizontal rolled steel profiles (HEA profiles) incorporated into the slabs and directly connected to the vertical steel piles of the CSM wall.
Figure 6 presents a plan view of the general configuration of the retaining wall structure. The peripheral CSM wall was composed of a total of 95 CSM panels. To the temporary support of the slab bands were executed 28 foundation micropiles.

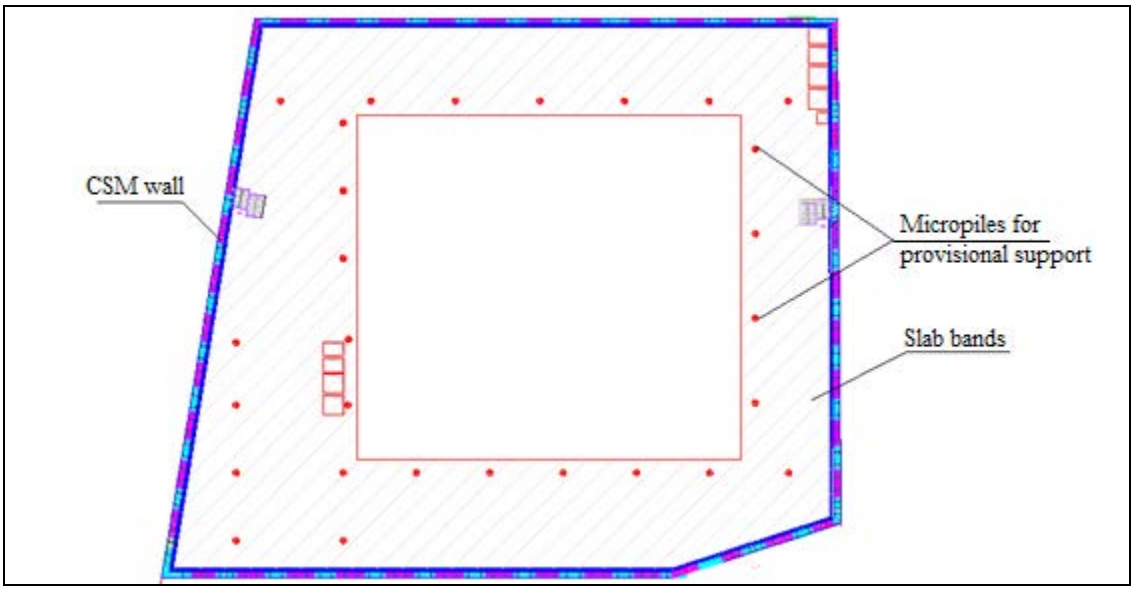

Figure 6: Plan view of the general configuration of the retaining wall structure.

4. ANALYSIS MODEL OF THE RETAINING WALL

In the analysis of the retaining wall were defined four cross-sections to represent the four elevations of the retaining wall.

The performance of the retaining wall was evaluated using the finite element program PLAXIS®. Through the referred program, all the phases of the execution process were modelled to obtain numerical simulations as close as possible to the real situations. The ground was modelled using the Hardening-Soil model with the geomechanical parameters presented in section 2.1.

The analysis included the determination of the maximum values of the efforts and displacements of the retaining wall.

In figures 7 and 8 are presented two sections of the model studied: Section A, representing a cross-section of the west alignment of the retaining wall and Section B representing a cross-section of the east alignment.

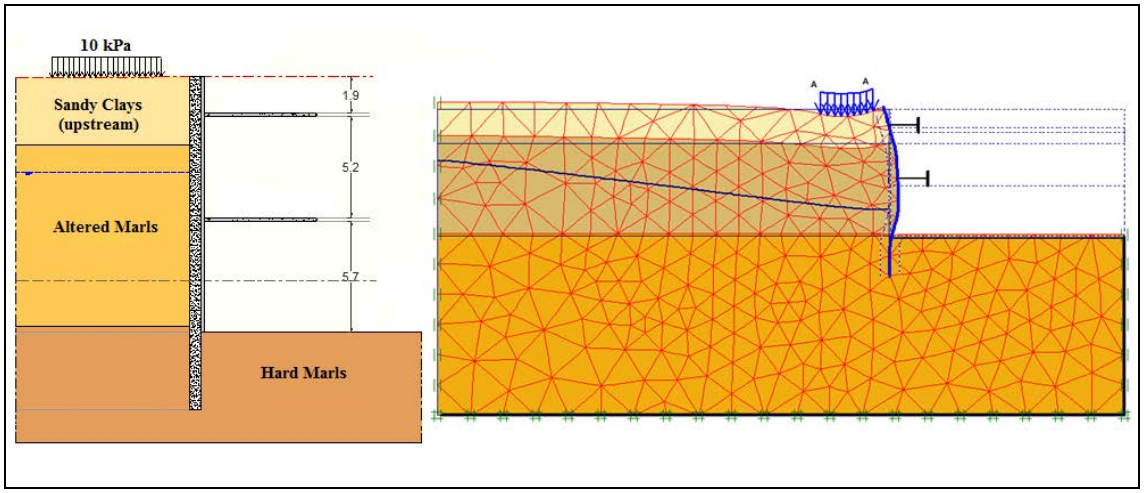

Figure 7: Section A: cross-section (on the left) and analysis model representing the deformation at the maximum excavation depth (on the right).

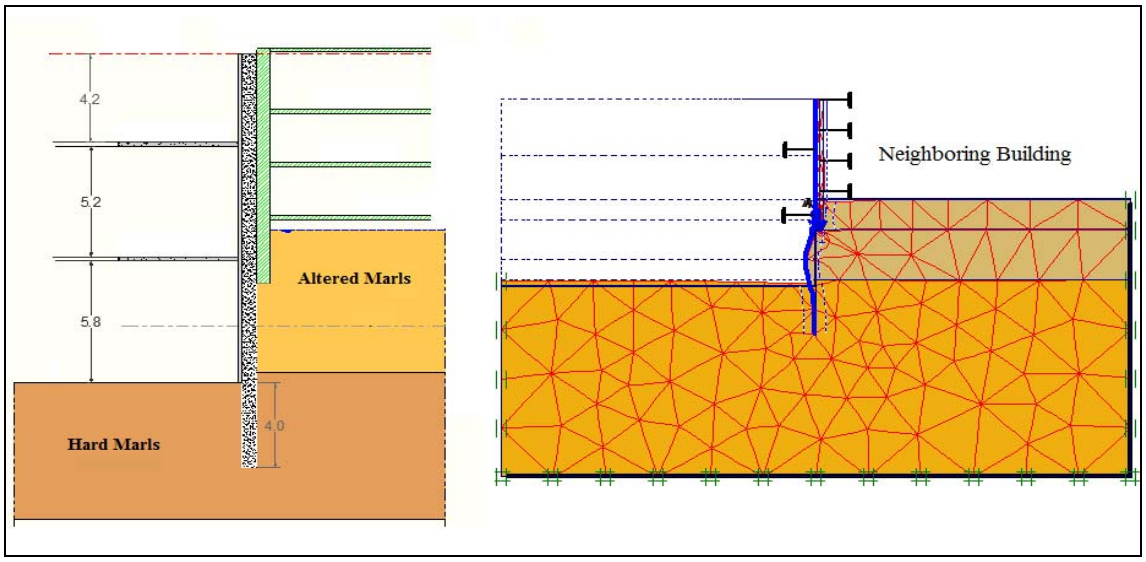

Figure 8: Section B: cross-section (on the left) and analysis model representing the deformation at the maximum excavation depth (on the right).

The simulation of the execution process started with the CSM wall construction. In another phase was simulated the first level of excavation, to a maximum depth of 0.5 m below the first level of the slab bands and the third phase consisted in the simulation of the execution of the first level of slab bands. In a subsequent phase was modelled the excavation to a maximum depth of 0.5 m below the second level of the slab bands. The fifth phase consisted in the simulation of the execution of the second level of slab bands and, in a final phase was modelled the excavation to the maximum depth.
Table 2 presents the maximum horizontal displacements of the retaining structure obtained in the numerical analyses of sections A and B.

Table 2: Maximum horizontal displacements of the retaining structure obtained in the numerical analyses of sections A and B.

	Section A	Section B
Displacements at the top of the retaining wall (mm)	-8.0	0.2
Displacements along the height of the retaining wall (mm)	15.0	5.0

The results obtained in the numerical analyses of all studied sections are in the range of values considered acceptable to the characteristics of this excavation.
Regarding the results obtained to Section B it should be pointed out that the retaining wall is bounded in this alignment by a building with three underground floors. Until the excavation reaches the corresponding depth of the bottom slab of the neighbouring building, practically no efforts and displacements were introduced in the retaining structure. For deep excavation phases were obtained horizontal displacements and efforts in the retaining wall with low values, due to the small depth of excavation below the foundations of the neighbouring building.
The design of the reinforcements to the slab bands to its correct performance during the temporary phase was based on the maximum efforts obtained in the numerical simulations.

5. EXECUTION PROCESS

The execution principle of the CSM technology consists in desegregation and mixture of the existing soil with cement slurry, to obtain rectangular soil-cement panels with strength and deformability values defined in the design phase (Arnold et al. 2011).
The execution process started with the execution of a CSM test panel to obtain samples for laboratory tests and to allow the calibration of the execution parameters.

The equipment used to realize the CSM panels allows to the rig operator control in real-time the execution parameters (Bringiotti et al., 2009).

After the initial phase of the equipment calibration, the panels of the retaining wall were executed.
Immediately after the execution of each panel and before the hardening of soil-cement, were installed two vertical steel piles (IPE 450) in each soil-cement panel.
In this stage were also installed the inclinometers behind the retaining wall to the control of the horizontal movements.
The succeeding phase consisted in the execution of the foundation micropiles to the temporary support of the slab bands (Figure 9).

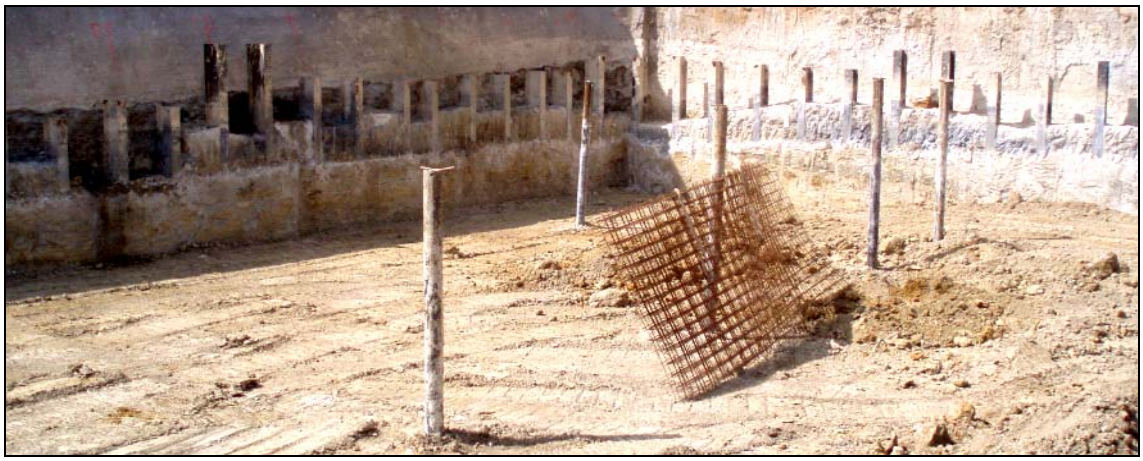

Figure 9: Foundation micropiles to the temporary support of the slab bands.

The solution included the execution of a concrete beam in the top of the retaining wall, connecting all vertical steel piles.
The first level of excavation was carried out to a maximum depth of 0.5 m below to the first level of slab bands. After the execution of the first level of excavation, horizontal rolled steel profiles (HEA profiles) with a length of about 0.50 m were connected to the vertical steel piles of the retaining wall to allow the connection between the retaining wall and the concrete slab bands. In this phase, the first level of slab bands was executed at the level of floor "0". To monitoring the movements, surveying targets were installed in the slab bands at this stage.
The subsequent phase consisted in the excavation to a maximum depth of 0.5 m below the second level of slab bands. Figure 10 presents two views of the work during this phase. After the execution of the second level of the slab bands at the level of floor "-2", was carried out the excavation to the maximum depth (Figure 11).
The CSM panels were executed to a depth that allowed the minimization of the water inflow to the interior of the excavation, to make more efficient the excavation process.

Figure 10: Views of the work during the execution of the second level of excavation.

Figure 11: View of the work during the second level of excavation (on the left) and after the execution of the second level of slab bands (on the right).

Once the maximum depth of excavation is reached, the bottom concrete slab and the internal structure of the underground parking were executed and the temporary foundation micropiles were deactivated.
Figure 2 presents the general aspect in the final phase of the work.

Figure 12: General aspect in the final phase of the work.

6. QUALITY CONTROL AND MONITORING PLAN

The quality control of the work was carried out at different levels. In an initial phase, during the execution of the CSM panels, was performed the control, in real time, of the execution parameters by the rig operator. A second level of control was carried out by laboratory tests (unconfined compressive strength tests) on samples from a CSM test panel and from the panels of the CSM retaining wall. During the excavation, the control of the work was performed by the implementation of a monitoring plan, including the installation of surveying targets and inclinometers. The temporary foundation elements were also subject to control through the execution of Load Tests.
The results obtained in the unconfined compressive strength tests on samples from the panels of the CSM retaining wall are presented in Table 3.

Table 3: Results obtained in the unconfined compressive strength tests on samples from the panels of the CSM retaining wall.

Tests Series	Number of tested samples	Unconfined compressive strength (MPa)			
		3 days	7 days	14 days	28 days
Series I	**6**	4.4	6.5	8.4	-
Series II	**6**	-	2.5	4.5	8.0
Series III	**4**	-	2.5	4.5	-
Series IV	**4**	-	2.5	6.0	-

The compressive strength of the samples tested after 14 days are higher than the required design strength (4 MPa) in every performed series of tests.
Figure 13 presents the location of the 19 surveying targets and the 3 inclinometers installed according to the monitoring plan of the work. The surveying targets were installed at the first level of the concrete slab bands. The installation of inclinometers and the surveying targets allowed the measurement of lateral movement and deformation of the retaining wall as the excavation progressed. The inclinometer and the surveying targets were read manually during the excavation.

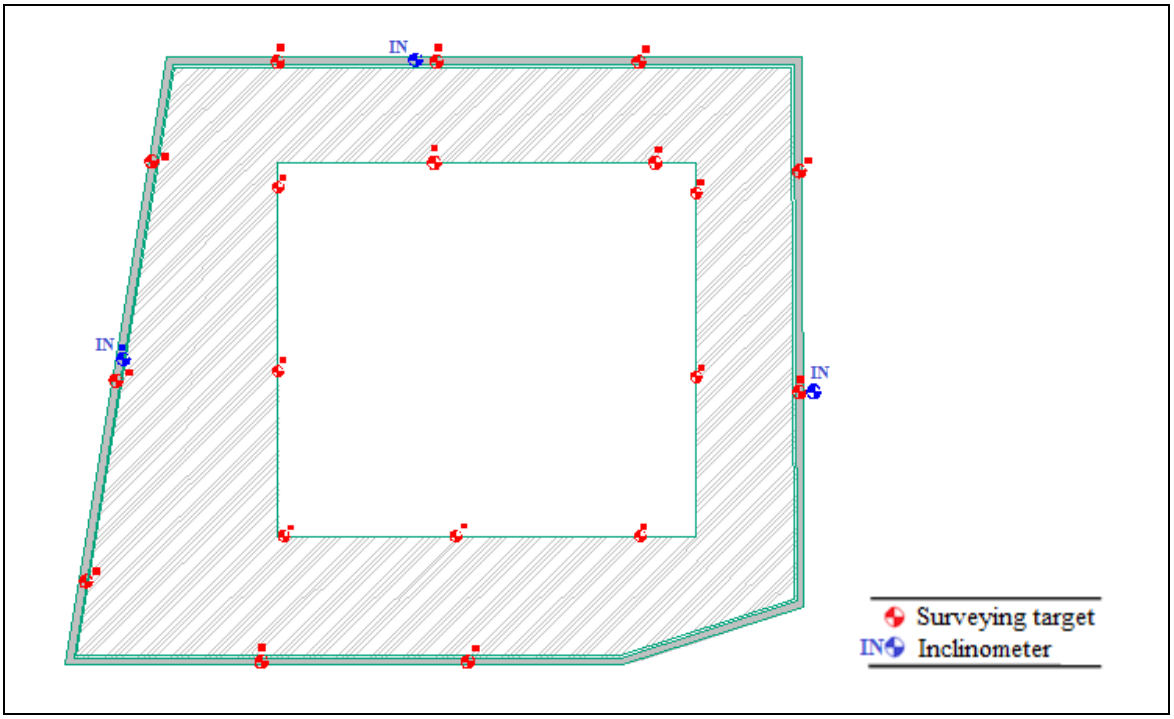

Figure 13: Surveying targets and inclinometers installed according to the monitoring plan of the work.

The results obtained in the monitoring of the work presented lower values than the alert limits defined. As it would be expected, in the parallel direction of the retaining wall practically no displacements of the retaining wall were observed and in the perpendicular direction, were observed the main displacements of the retaining wall.
It should be pointed out the importance of the control and monitoring of the work as an essential tool to the reduction of the risk to the work site and to the surrounding constructions, especially in urban excavations, allowing in advance the prevention of problems in the execution process.

7. CONCLUSIONS

The paper has pointed out the good performance of the application of the Cutter Soil Mixing technology to the execution of the retaining wall to allow the excavation of "Parking Saint Nicolas", an underground parking lot located at Cannes, France.
The main objectives of the work were achieved. The CSM wall allowed the execution of a vertical excavation with a maximum depth of 14 m and the reduction of the water inflow to the interior of the excavation.

The horizontal support of the retaining structure using concrete slab bands was one of the most significant advantages of the presented solution, allowing the integration of elements of the final structure at a preliminary stage of the work to avoid temporary elements to the horizontal support as grouting anchors or steel struts.
The use of slab bands as horizontal supports of the retaining structure has some advantages when compared with ground anchors because of the non-occupation of the neighboring ground and the elimination of problems related to its execution below the water table (problems of internal erosion).
The presented work constitutes a good example of a technical, economical and environmentally interesting solution.

REFERENCES

Arnold, M., Beckhaus, K. and Wiedenmann, U. (2011), Cut-off wall construction using Cutter Soil Mixing: a case study. Geotechnik, volume 34: pages 11-21.

Bringiotti, M., Dossi, M. and Nicastro, D. (2009), Miscelazione profonda dei terreni: metodi classici e tecnologie innovative – CSM by BAUER. Geofluid 2009.

Fiorotto, R.,Schöpf, M. and Stötzer, E. (2005), Cutter Soil Mixing(CSM) An innovation in Soil mixing for creating Cut-off and Retaining walls, In:16 ICSMGE: International Conference on soil mechanics and geotechnical engineering, Osaka-Japan.

The application of Cutter Soil Mixing to an urban excavation at the riverside of Lagos, Portugal

Peixoto Artur, Geo-Rumo,Tecnologia de Fundações, S.A., Portugal, artur.peixoto@georumo.pt
Matos Fernandes Manuel, Faculty of Engeneering of the University of Oporto – FEUP, Portugal, mfern@fe.up.pt
Sousa Estela, Geo-Rumo, Tecnologia de Fundações, S.A., Portugal, estela.sousa@georumo.pt
Gomes Pedro, Geo-Rumo, Tecnologia de Fundações, S.A., Portugal, pedro.gomes@georumo.pt

ABSTRACT

The Cutter Soil Mixing (CSM) technology consists of the execution of soil-cement panels through the soil disaggregation by mechanical action of two sets of cutting wheels that rotate around a horizontal axis while providing a cement slurry injection simultaneously. The CSM technology is a development of Deep Soil Mixing technique, using a hydromill to create soil-cement panels with a rectangular cross-section. Some advantages of this technology are the possibility to know the exact geometry of the soil-cement panels in depth, the effective connection between the panels and the possibility of the mixing quality control in real time. This paper describes the application of CSM to the construction of a temporary retaining wall for an urban excavation at the riverside of Lagos, Portugal. The paper describes the general aspects of the execution process and the main results of the instrumentation and monitoring work, which confirm the excellent performance of the adopted solution.

1. INTRODUCTION

Underground parking is a need in many cities and one of the advantages of the subsoil use is the possibility of the surface occupation with leisure areas. The work presented in this paper is a good example of the recognition of this necessity in the city of Lagos, Portugal, and it concerns the execution of a temporary retaining wall for the construction of the underground parking FUTURLAGOS, inserted in the Strategic Regeneration Plan of the riverside of the city (Figure 1).

Figure 1: Site plan.

In this paper is discussed the application of Cutter Soil Mixing (CSM) technology to the construction of the temporary retaining wall for the excavation of the underground parking lot. The solution consists of a continuous wall formed by CSM panels reinforced with vertical steel piles (IPE piles) with a level of ground anchors in the top.
This solution was presented as an alternative to the initial solution consisting of a concrete pile wall formed by piles of diameter 800 mm placed at 1.0 m intervals, with soil treatment by jet grouting columns in the pile ranges, also with a level of ground anchors in the top.
In Geotechnical Engineering and, particularly, in the context of soil improvement techniques one of the main concerns is the development of new solutions, technical and economically more attractive, with lower environmental impact. The use of the existing soil as a construction material through its mixture

with cement slurry has been intensified and diversified over the time and new versatile and innovative techniques have been developed to achieve more sustainable solutions. In this context has been developed the CSM technology which is based on the use of the in-situ soil as a construction material to create soil-cement panels with a rectangular cross-section by the use of a hydromill. This technology is a new and effective method for the construction of cut-off walls, earth retaining structures, soil improvement and foundation elements.

2. THE PRINCIPLE OF THE CSM TECHNOLOGY

2.1. General description

The application of CSM technology consists of the disaggregation of the in-situ soil through the action of two sets of mixing wheels that rotate about horizontal axis while the cement slurry is simultaneously mixed into the existing soil. This creates soil-cement panels with the soil particles becoming the aggregates (Arnold et al., 2011).

CSM had a development based in some principles of Deep Soil Mixing (DSM), using also some implementation principles of diaphragm walls, in particular the hydrofraise.

Recent successful projects confirm that this is an interesting solution, with technical and economic advantages, already implemented in several countries (Gerressen et al., 2009).

Some advantages that make this technology competitive, particularly when compared with jet grouting and some traditional solutions of retaining structures are:

- the possibility of knowing the exact geometry of the panel in depth;
- the reduced vibrations during construction;
- the disaggregation of in-situ soil allowing to optimize the mixing process;
- the effective connection between panels even with different ages of construction;
- the very little generation of spoil;
- the possibility of execution in the presence of water table;
- the use of in-situ soil as a construction material;
- the possibility of application to all soil types, although not all kinds of soils are equally suitable.

This technology presents a better performance in soils like sand and gravel, but in soils like clay or silt the strength obtained with the same cement content is lower.

2.2. Execution Process

The application of this technology involves a construction process that must be adapted to the ground conditions and to the specific requirements of each project.

After the correct positioning of the equipment and the cutting head at the specified panel location, the cutting wheels are driven through the ground at a continuous rate until it reached the design depth.

During the cutting phase, the soil matrix is broken up and the cement slurry is added to fluidify the soil. The penetration speed of the mixing tool during this phase can be adjusted at any time to optimize the use of energy, according to the soil characteristics.

In difficult soil conditions or in the execution of deep panels, it may be necessary the use of bentonite during this phase and, in this case, the cement slurry is added just in the extraction phase. The second phase of the process consists of the extraction of the cutting head. The rotation direction of the cutting wheels is inverted in this stage and cement slurry is added to the homogenization of the mixture. The cement slurry added in this phase must be only the difference between the total quantity and the quantity already mixed in the cutting phase.

The CSM panels can be reinforced with vertical steel piles inserted into the freshly mixed soil-cement. The steel piles are inserted into panels of soil-cement by gravity or using vibration hammers.

A continuous CSM wall is formed by the execution of individual panels in an alternating sequence, overlapping primary and secondary panels. The distinction between primary and secondary panels is only related with the execution sequence. Figure 2 illustrates the main phases of the CSM execution process.

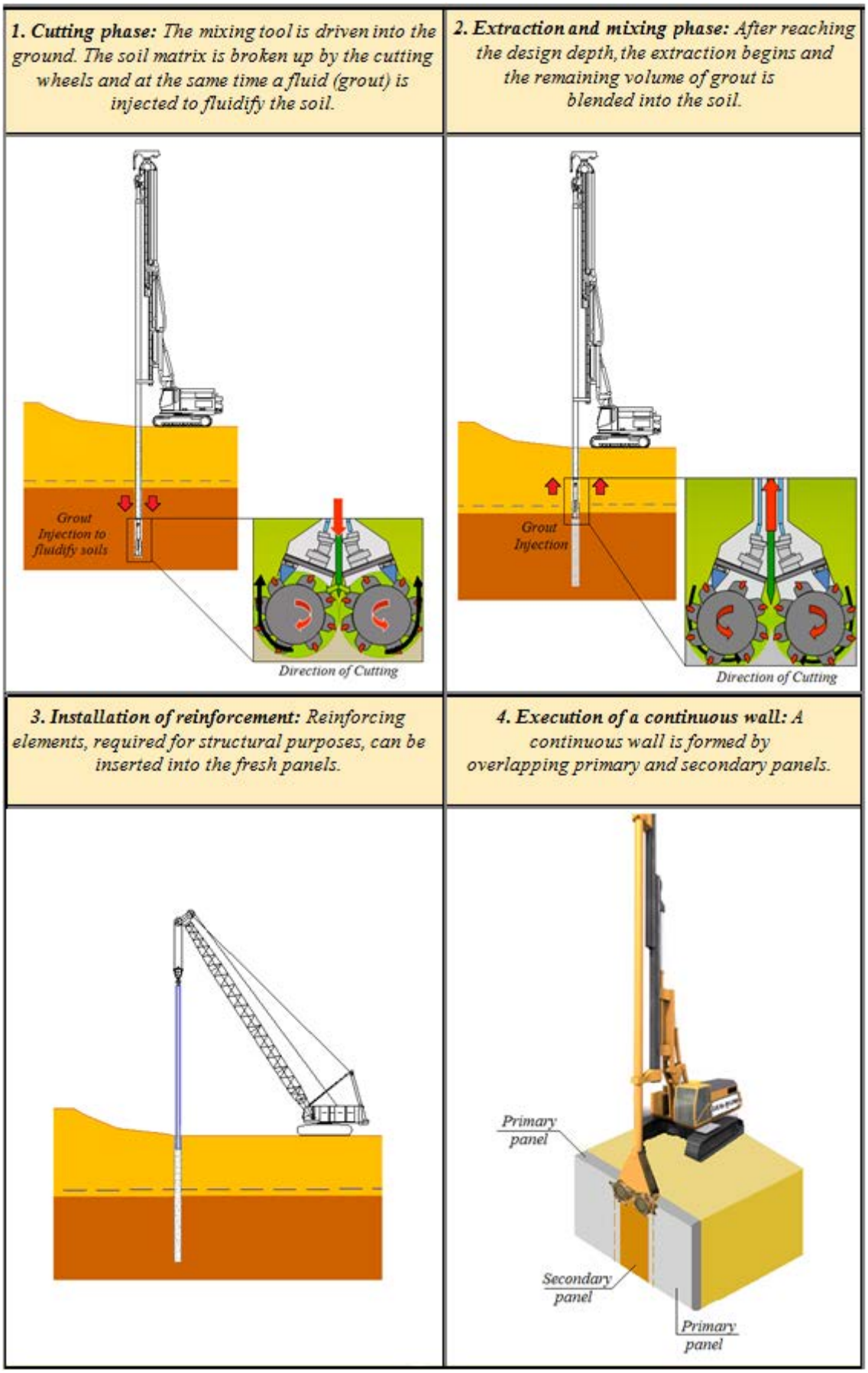

Figure 2: Illustration of the main phases of CSM execution process.

The main objective of this procedure is the improvement of the soil characteristics, through the increase of the resistance as well as the reduction of the permeability. The properties of the mixture obtained are

reflected not only by the characteristics of the existing soil but also by the properties of the cement slurry added.

2.3. Equipment

The soil-cement panel dimensions depend only on the dimensions of the mixing head used. Figure 3 presents the characteristics of two models of mixing heads. Different types of cutting wheels and different types of cutting teeth allow the adaptation of the method to the different types of soils.

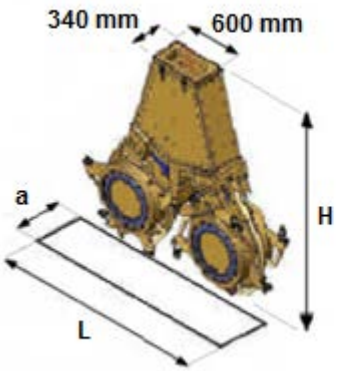

	BCM 5	BCM 10
Torque	0 - 57 kN.m	0 - 100 kN.m
Rotation speed	0 - 40 r.p.m.	0 - 35 r.p.m.
Weight	5100 kg (wheels 500 mm)	7400 kg (wheels 640 mm)
Heigh (H)	2.35 m	2.80 m
Panel length (L)	2.40 m	2.80 m
Panel width (a)	500 - 1000 mm	640 - 1200 mm

Figure 3: Characteristics of the Cutter Heads BCM 5 and BCM 10 (Bauer Maschinen).

The equipment enables the control of the following main parameters during the production (Lopez et al., 2005):

- cement slurry volume added;
- cement slurry pressure in hoses;
- slurry-soil pressure in trench;
- pumped volume in depth;
- pumped volume in time;
- inclination;
- speed of the mixing tool.

The documentation of the production process with respect to quality control is stored for subsequent evaluation. Figure 4 presents the monitor of the rig operator.

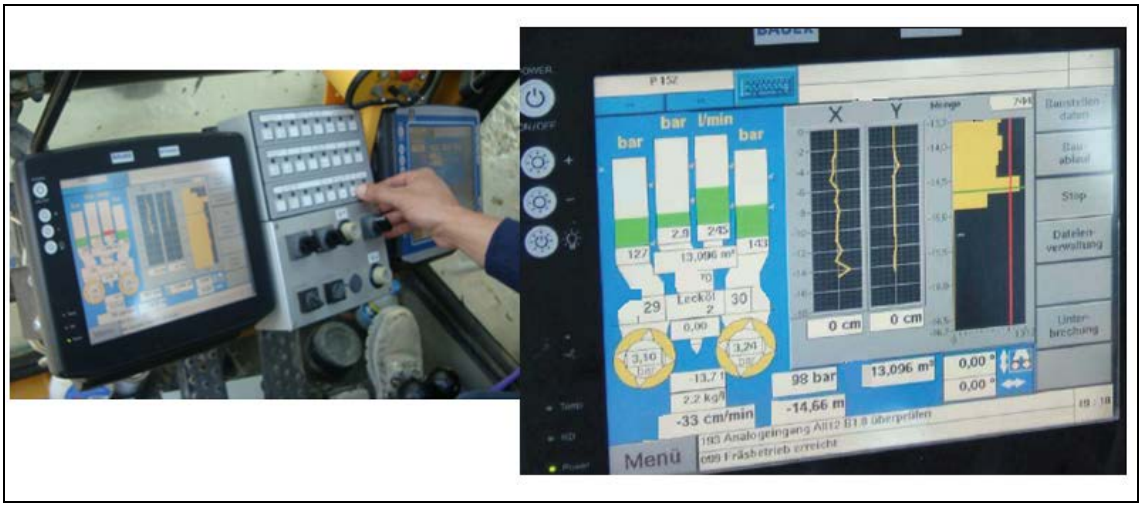

Figure 4: Rig operator's monitor to the control of execution parameters.

3. CASE STUDY

3.1. General description and Geotechnical conditions

The presented case study consists of the execution of a temporary retaining wall for the excavation of an underground parking lot at the riverside of Lagos, Portugal. The plan area of the excavation is about 6335 m^2, with a perimeter of 531 m (Figure 5) and a maximum depth of 6.0 m.
This parking, with two underground floors, has a construction area of about 12 670 m^2 and a capacity for 480 cars. The retaining wall consisted of a continuous CSM wall reinforced with vertical steel piles and a level of ground anchors in the top.
The work site is located near the marina of Lagos and is bounded to the northeast by an avenue, to the northwest by the building of the city's court and to the southwest by the ancient monumental fortress of the city.
The evaluation of the ground conditions was based on 12 geotechnical borings (Figure 5) to allow the execution of Standard Penetration Tests (SPT – S1 to S12), the installation of piezometers (Pz) and the execution of pumping tests (Pump) complemented with laboratory tests.

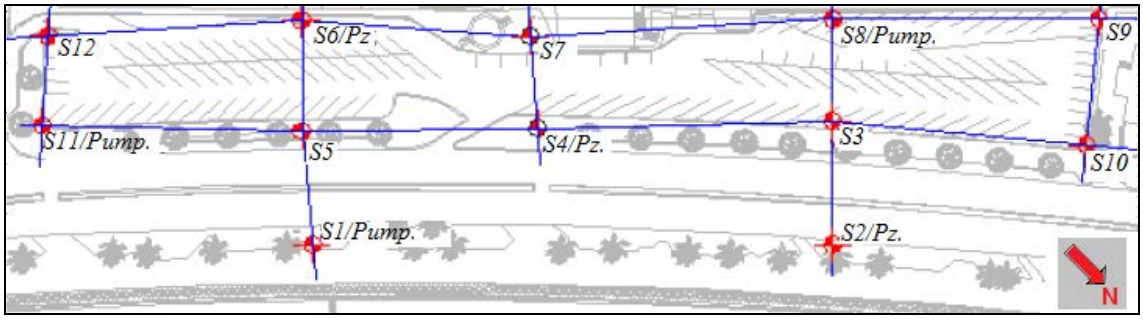

Figure 5: Location of the geotechnical borings executed to the evaluation of the ground conditions.

The ground at the site is composed by a sandy fill layer detected from the surface to a maximum depth of 6 m (N_{SPT} between 6 and 60, with global average value of 13), resting over the calcarenite substrate of the Miocene period (N_{SPT} between 7 and 60, with global value of 40). The tests carried out revealed a high heterogeneity of the soil in depth. The water table was detected near the surface with variations related to the tides. In Figure 6 is represented a geological-geotechnical profile with the SPT results of two of the boreholes executed (S11 and S12).

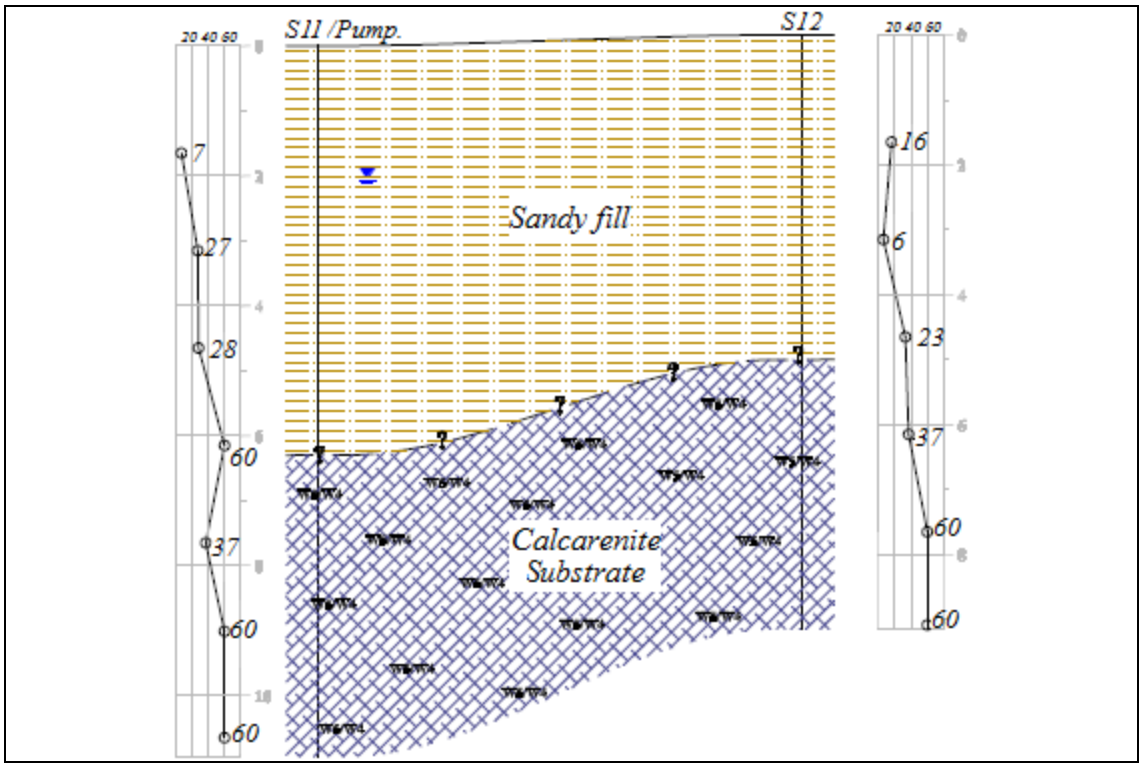

Figure 6: Geological-geotechnical profile (S11 and S12).

Table 1 presents the main geotechnical parameters, obtained by the interpretation of the in-situ and laboratory tests.

Table 1: Main geotechnical parameters.

	γ (kN/m3)	c' (kPa)	ϕ' (º)	E (MPa)
Sandy Fill	19	0	28	14
Calcarenite Substrate	20	10	30	42

3.2. CSM Retaining Wall

The adopted solution consisted of a peripheral CSM retaining structure executed to allow the vertical excavation, while ensuring the stability of nearby structures and infrastructures and reducing the inflow of water into the excavation during the construction phase.
The CSM panels were reinforced by vertical steel piles (IPE 330) and it was defined one level of ground anchors in the top. The retaining wall, 0.60 m thick, was composed of 262 CSM panels, in an alternating sequence of overlapping primary and secondary panels. The overlapping between them was 0.20 m. The vertical steel piles were installed at 0.70 m intervals, as close as possible to the excavation face.
In the crown of the CSM panels was executed a concrete beam to allow the application of the prestressing in ground anchors. Along the perimeter of the retaining structure were executed 196 ground anchors, with an inclination of 35º and a horizontal spacing of 2.5 m, with a design load of 600 kN. For the definitive stage was performed a concrete wall placed against the CSM wall.
Figures 7 and 8 present the structural solution defined to the retaining wall.

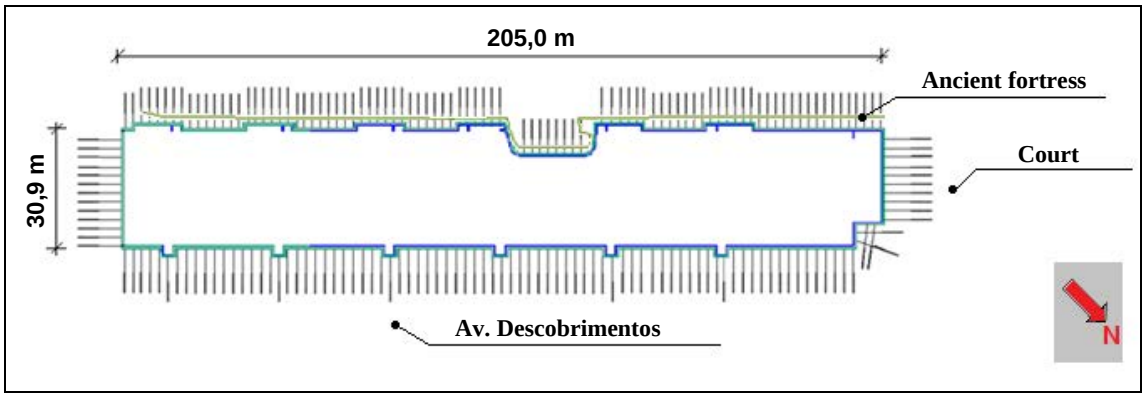

Figure 7: Plan of the excavation and surrounding conditions.

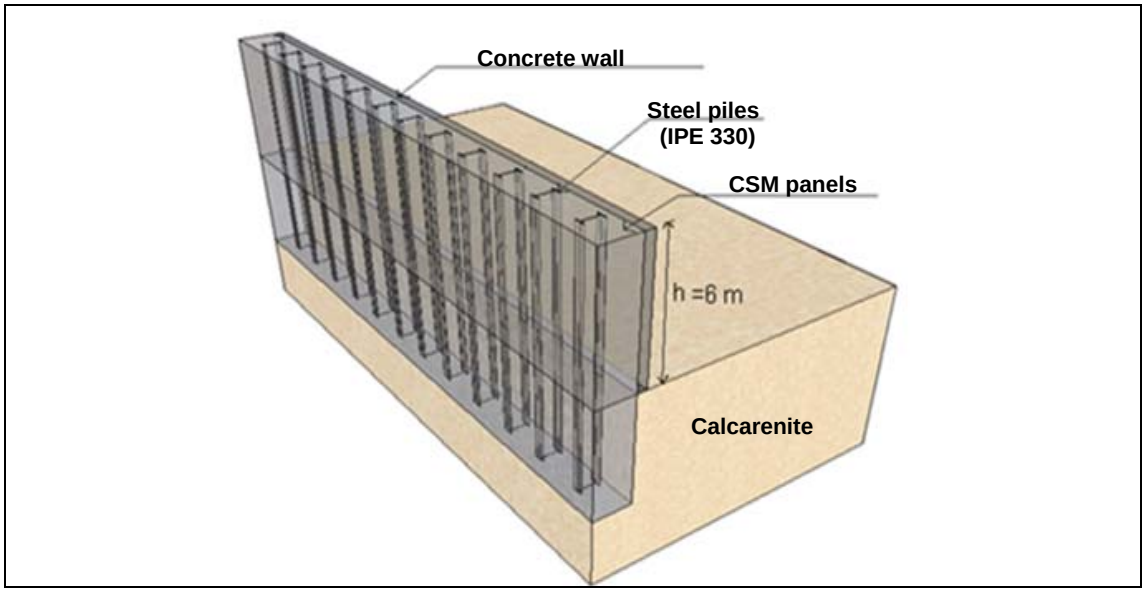

Figure 8: Structural solution: 3D view of the retaining wall.

3.3. Construction monitoring and observation of the work

3.3.1. Excavation and drainage system

Throughout the different excavation stages, no water inflow from the outside to the inside of the excavation through the CSM panels was observed. However, with the progress of excavation, the inflow of water occurred from the bottom of the excavation, trough the calcarenites, and it was controlled by a temporary drainage system. With this aim, were executed 14 pumping wells, interconnected by a mesh of drains distributed along the excavation area. The pumping wells were installed gradually as the avancement of the excavation, according to the water volume to draw. This system was desactivated after the excavation works with the implementation of the definitive drainage system.
Figure 9 presents some views of the work during the excavation.

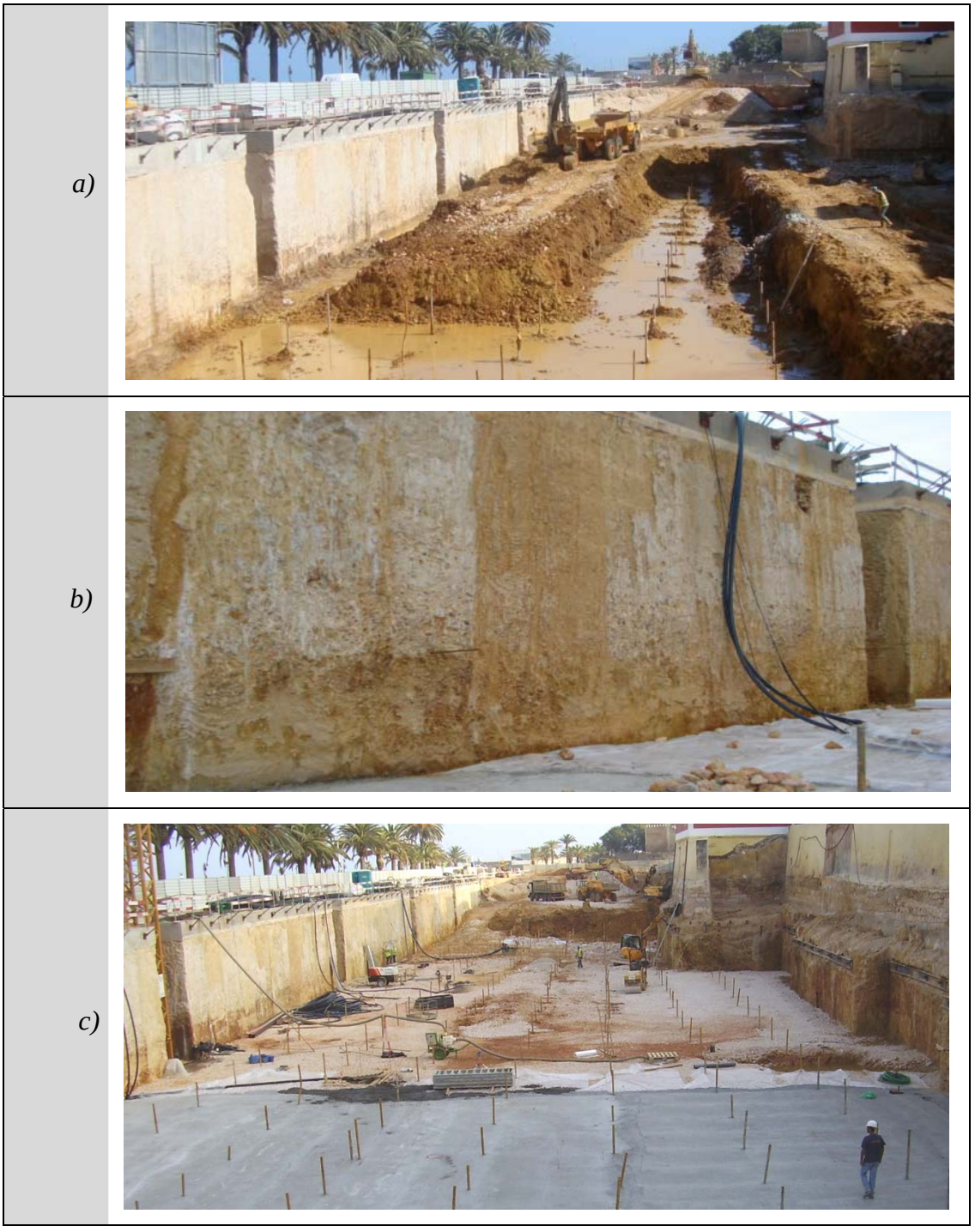

Figure 9: Views of the work during the excavation: a) excavation of 6 m depth; b) detail of the CSM wall; c) regularization of the bottom of the excavation.

3.3.2. *Quality control*

In the aim of the quality control, some CSM test panels were executed in advance, to obtain samples for laboratory tests. This procedure allows the calibration of the equipment before starting the execution of the retaining wall panels. Once the execution of the retaining wall started, quality control was provided by laboratory tests on samples from the panels of the CSM retaining wall.
The laboratory tests performed were:
- unconfined compressive strength tests;
- Brazilian tests.

A total of 36 samples were submitted to laboratory tests. The results obtained were a compressive strength of 3.1 MPa, a tensile strength of 0.3 MPa and an elasticity modulus of 2.9 GPa (average values). Figure 10 presents some of the samples during the laboratory tests.

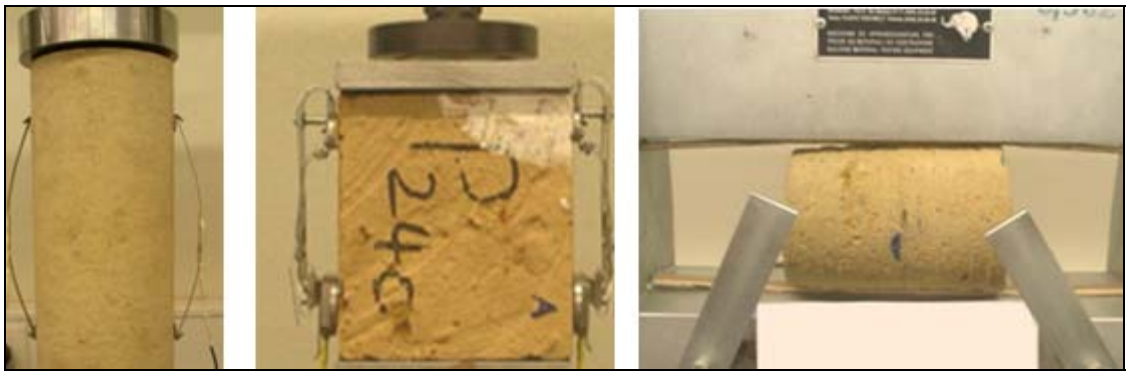

Figure 10: Laboratory tests.

3.3.3. *Monitoring Plan*

The monitoring plan was established to allow the control of horizontal and vertical movements of the wall and the load variation on the ground anchors through the construction process.
The location of monitoring instruments was defined according to the Figure 11.
The implemented monitoring instruments were:
- 5 inclinometers installed behind the retaining wall;
- 5 load cells installed in the head of the ground anchors;
- 17 surveying targets installed in the concrete beam in the top of the retaining wall.

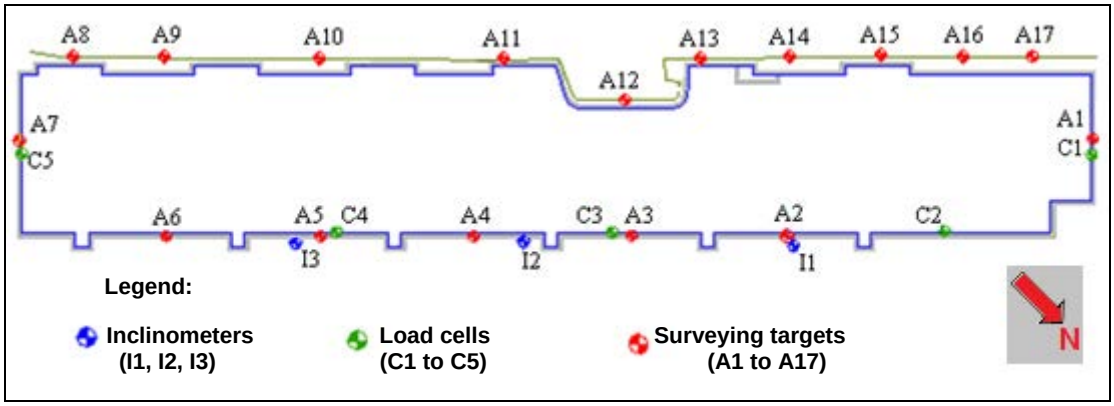

Figure 11: Location of the monitoring instruments.

There were performed five measurements of the inclinometers during the excavation. In Figure 12 are represented the envelope of the horizontal displacements obtained in the inclinometers I1, I2 and I3. The movements of the wall towards the excavation are represented by the positive values.

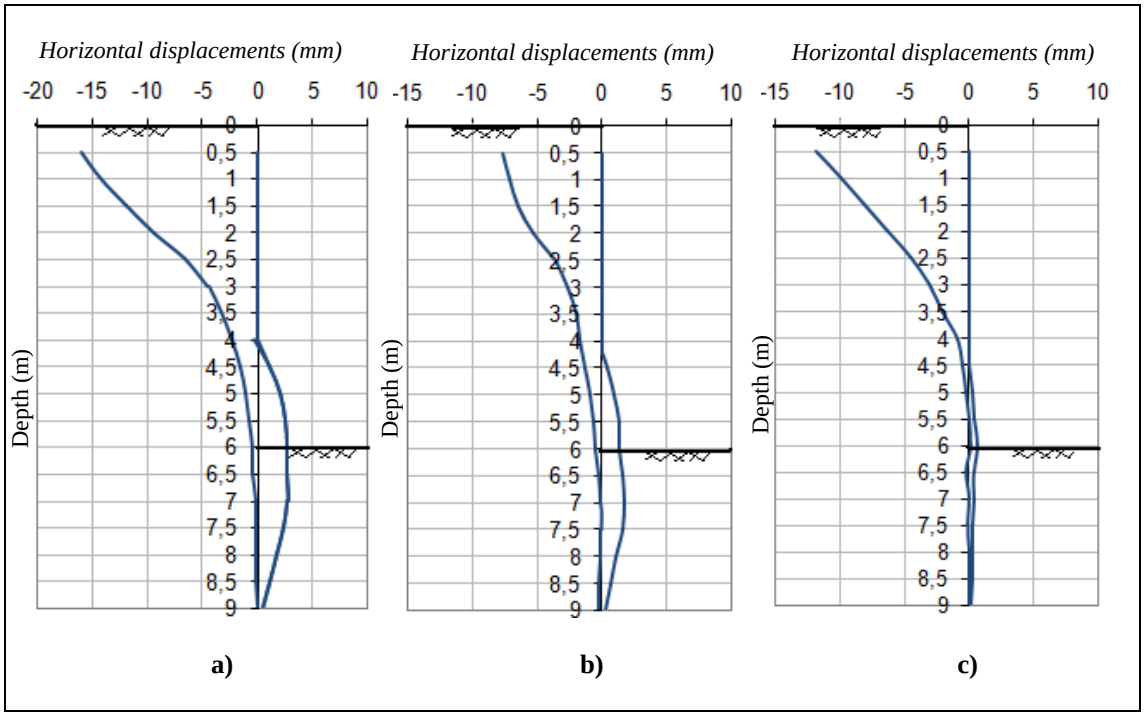

Figure 12: Envelope of the horizontal displacements: a) inclinometer I1; b) inclinometer I2; c) inclinometer I3.

The horizontal displacements globally present low values in every phases of the execution process. The recorded values were lower than the alert limits. The maximum values occurred in the last phase of the excavation, for a depth of excavation of 6.0 m (H).
The horizontal maximum displacement (δH_{max}) towards the excavation was about 3 mm and the maximum horizontal displacement in the opposite sense was about 16 mm.
Considering the movement of the wall in the opposite sense of the excavation, ($\delta H_{max}/H$) is about 0.27 % and considering the movement of the wall towards the excavation, ($\delta H_{max}/H$) is about 0.05 %. These values are in accordance with those observed in similar conditions in excavations with satisfactory performance (Clough and O'Rourke, 1990).
The measurements of the load cells were done in the following phases:
- Measure 1: after the prestressing of the ground anchors;
- Measure 2: after reaching an excavation depth of 3 m;
- Measure 3: after reaching an excavation depth of 6 m;
- Measure 4: before the execution of the permanent underground parking structure.

In the following table are compiled the results obtained through the measurements of the load cells.

Table 2: Results obtained through the measurements of the load cells.

Load in the ground anchor (kN)					Variation of load on ground anchor	
Load cell	Measure 1	Measure 2	Measure 3	Measure 4		
C1	640	590	590	590	- 50 kN	(7.8 %)
C2	640	545	545	540	- 100 kN	(15.6 %)
C3	550	510	510	500	- 50 kN	(9.1 %)
C4	620	580	580	580	- 40 kN	(6.5 %)

After the prestressing of the ground anchors, the installed load presented the minimum value and, with the advancement of the excavation, there was a slight increase of the load until its stabilization for an excavation depth between 3 m and 6 m.
The results are consistent with the variation of the horizontal displacements of the retaining wall because, after the prestressing of the ground anchors, there was a movement of the top of the wall in the opposite sense of the excavation and a subsequent decrease of the load on the ground anchors. The load tends to stabilize over the time.
The observation of the surveying targets led to satisfactory values of vertical displacements (settlements) of the retaining wall, presenting a maximum value of 9 mm.

4. CONCLUSIONS

This paper demonstrates that the application of Cutter Soil Mixing in the construction of a large underground parking in Lagos, Portugal, allowed a quite satisfactory behaviour in terms of stability and deformations, as well as the reduction of the water inflow to the interior of the excavation.
It should be pointed out the good performance even under demanding ground and water table conditions.
The horizontal and vertical displacements of the CSM wall during the excavation process presented low values. The maximum horizontal displacement towards the excavation was about 3 mm and the maximum horizontal displacement in the opposite sense was about 16 mm. The movements of the CSM wall were always lower than the alert limits defined.
The good results using CSM technology depending on several factors such as geological and geotechnical conditions, the specific requirements of each project, the experience of the engineers, the availability of appropriate equipment and qualified staff, among others. The control and monitoring of the works is particularly important, especially in the application of CSM technology in urban areas because there are a lot of factors which may influence the construction process. The implementation of an efficient monitoring plan and control allows to the application of preventive measures, reducing the risk for the neighbouring buildings and structures.

REFERENCES

Arnold, M., Beckhaus, K. and Wiedenmann, U. (2011), Cut-off wall construction using Cutter Soil Mixing: a case study. Geotechnik, volume 34: pages 11-21.

Clough, G. W. and O'Rourke, T. D. (1990), Construction induced movements of insitu walls. ASCE Geotechnical Special Publication No. 25, Design and Performance of Earth Retaining Structures, Cornell University, Ithaca, pages 439-445.

Gerressen, F. W., Schopf, M. and Stotzer, E (2009), CSM – Cutter Soil Mixing – Wordwide experiences of a young soil mixing method. Proceedings of International Symposium on Deep Mixing & Admixture Stabilization, Okinawa, Japan.

Lopez, R. A., Majewski, A. and Harvey, T. (2009), Permanent excavation support in urban areas using Cutter Soil Mixing technology: Elliott Avenue case history. Proceedings of International Foundation Congress and Equipment Expo, Contemporary Topics in Ground Modification, Problem Soils, and Geo-Support, Geotechnical Special Publication No. 187, ASCE, Orlando, Florida, pages 185-192.

Ground Improvement Solutions using CSM Technology

Alexandre Pinto, JetSJ Geotecnia Lda, Portugal, geral@jetsj.pt
Rui Tomásio, JetSJ Geotecnia Lda, Portugal
Xavier Pita, JetSJ Geotecnia Lda, Portugal
Pedro Godinho, JetSJ Geotecnia Lda, Portugal
Artur Peixoto, Geo Rumo, Tecnologia de Fundações S.A, Portugal, artur.peixoto@georumo.pt

ABSTRACT

The new Cutter Soil Mixing (CSM) technology, inspired on the cutter technology allowing the execution of rectangular panels with resistance and chemical features specially fitted to the ground characteristics was been applied since the last three years in various geotechnical scenarios. The aim of this paper is to present some case histories where the CSM technology was successfully used, emphasizing the main design and execution criteria, mainly for foundations, slope stabilization and earth retaining applications, above and below ground water table. It is also pointed out the importance of the quality control and quality assurance on site, before and during the construction of the final soil – binder panels. Finally, the technical, economic and environmental advantages of the CSM technique, comparing with some more conventional solutions, are pointed out.

1. INTRODUCTION

The CSM technique consists on mixing the ground with a binder (cement, gravel, lime, etc.), using two sets of cutting wheels – inspired on cutter technology, to produce rectangular panels with resistance and chemical features specially fitted to the ground characteristics. Cutter wheels break up the soil matrix and mix it with cement slurry in order to obtain a homogeneous soil - binder mixture. The heart of the system is a mixing unit comprising two cutter gear drives, each driving a standard cutter wheel, able to rotate in both directions. The technology is applicable in various ground conditions, even in hard or layered strata, which is very important in sites with very heterogeneous geological conditions. Highly developed equipment and methods allow mixing cementitious materials with natural ground in order to build very economic high quality vertical underground structures, varying from cut-off and retaining walls to soil stabilizing, foundation and slope stability elements.
During cutting the natural ground is mixed with cementitious slurry which is introduced through the nozzle located between the cutting - mixing wheels. The rectangular CSM elements can be produced in coarse, clayey and rocky soils with a thickness up to 1,5m and depths up to 60m. For execution control the following data are permanently displayed in the operator cabin: production data - depth, speed and rotational direction of cutter wheels, hydraulic pressure on cutter wheels, pressure at cutter head, rate of pumping, total volume of slurry pumped, etc. (Figure 1).

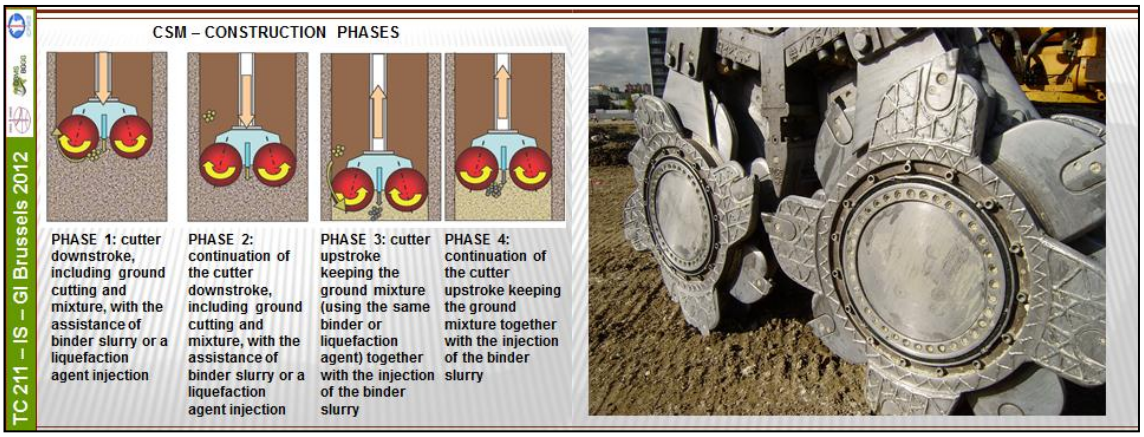

Figure 1: Main execution sequence of the CSM technology and view of the cutter wheels.

2. CSM USED AS FOUNDATION SOLUTION

As example of the CSM technique applied as foundation solution is presented the case of the "Pedro Arrupe Scholl", built in Lisbon, at Tagus river right bank. The school was built close to the "Beirolas Sanitary Landfill", where previously to the Expo 98 Exhibition, was located an industrial complex (Figure 10).

Figure 2: Pedro Arrupe Scholl location and perspective.

The geological conditions were very complex, with the ground water table located near to the surface on the transition between the surficial landfills, partial filled with the previous industrial complex demolishing waste, and the alluvial soft soils (undrained shear resistance lesser than 20KPa). Due to the Trancão and Tagus rivers proximity the depth of the alluvial soils ranged from about 5 to 25m, resting over the Miocene bed rock, formed by weathered sandstones and limestone (W5 and W4).
For the foundations of the "Pedro Arrupe School" buildings, with a maximum of four stories, soil - cement panels with a maximum depth of about 25m and a cross section of 2,4 x 0,5m^2, were built using the CSM technology. The panels were reinforced with vertical HEB steel profiles (Euronorm 19-57) in order to resist to the compression and tension loads. The profiles were capped by reinforced concrete caps, braced by a grillage of beams. Due to the geological conditions the buildings ground floor slabs were design as structural elements and supported by the foundation beams. The soil - cement panels were designed in order to transmit to the Miocene bed rock the overall building loads, including the seismic ones. For this purpose, an unconfined compression resistance of at least 2,0MPa was achieved. Due to the tension seismic loads, some panels were designed with about 7m of embedment at the Miocene bed rock. Due to the soil chemical properties, pozolanic cement was adopted, allowing also a better protection and confinement of the steel profiles (Figure 3).

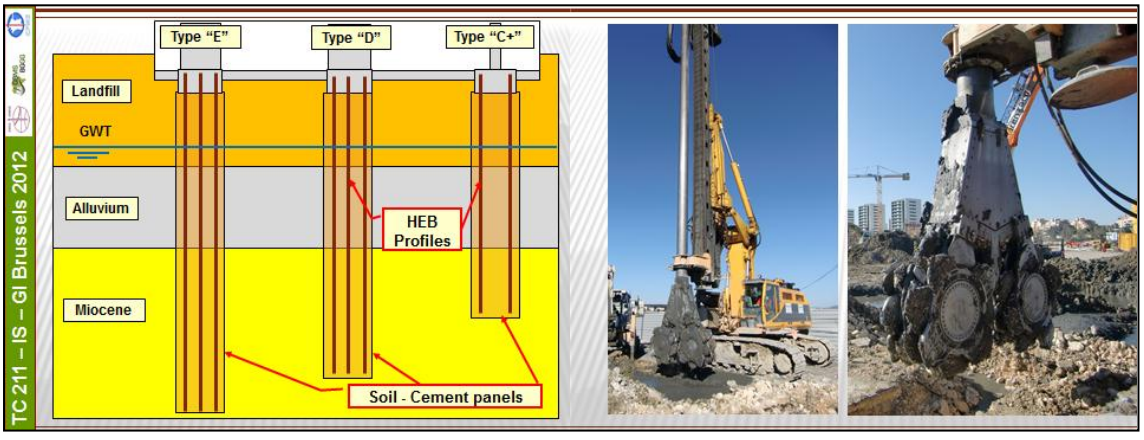

Figure 3: Cross section of the adopted solutions and view of the soil – cement panels execution using CSM technology.

As already described by Ameratunga J. et al. (2009) the adopted solution allowed the fulfilment of the following main objectives: technical (capability to excavate various types of ground materials, ranging from heterogeneous landfills, soft soils to Miocene bed rock), and control of both costs and construction schedule, with an average productivity of 85m per day (Figure 4). It should also be pointed out the tight

execution and quality control and quality assurance of the soil – cement panels, which included the permanent monitoring of all the execution parameters, the collection of soil - cement samples and cores for UCS laboratorial tests, with assessment of the Young Modulus, as well as the monitoring of the buildings behaviour during and after construction

Figure 4: View of the previous industrial complex located on the site and example of the demolished waste found inside the heterogeneous landfill.

3. CSM USED AS EARTH RETAING SOLUTION

3.1. Temporary Circular Shaft for excavation below ground water table level

As example of the CSM technique applied for earth retaining solution below ground water table level is presented the case of two shafts built at the River Lima banks, at Ponte de Lima, Portugal. Those shafts with about 18m depth and 15m diameter were built in order to allow the installation of a water supply pipe, ∅2400mm with reinforced concrete structure, under the river using micro tunneling technology (Figure 5).

Figure 5: Site location and geological conditions.

The geological conditions were very heterogeneous, with the ground water table located near the surface. The excavation works intersected, from the surface, heterogeneous landfills, sandy and gravel soils and weathered schist.

In order to allow the excavation works, soil - cement panels with an overall depth of 24m and a cross section of 2,4 x 0,8m^2, including 0,30m of overlapping, were built using the CSM technology. The panels were reinforced with vertical IPE300 steel profiles (Euronorm 19-57), in order to resist to the earth and water pressures. The profiles were braced, at the top, by a reinforced concrete capping beam and by three lower levels of steel ring beams (Figure 6). The soil - cement panels were designed in order to transmit horizontally the earth and water pressures to the vertical profiles. For this purpose, a minimum unconfined compression resistance of 4,0MPa was achieved. Due to the soil chemical properties, pozolanic cement was adopted.

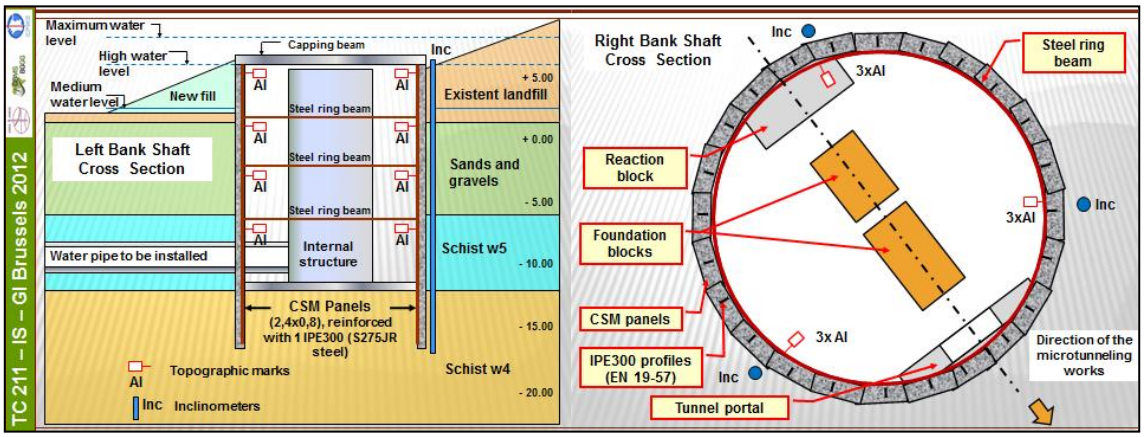

Figure 6: Cross section and plan of the adopted solutions.

For the design of the adopted solution a 2D FEM axisymmetric model was adopted, using Plaxis software. The maximum estimated deformation was about 10mm, very similar to the one obtained through the inclinometer readings (figure 7).

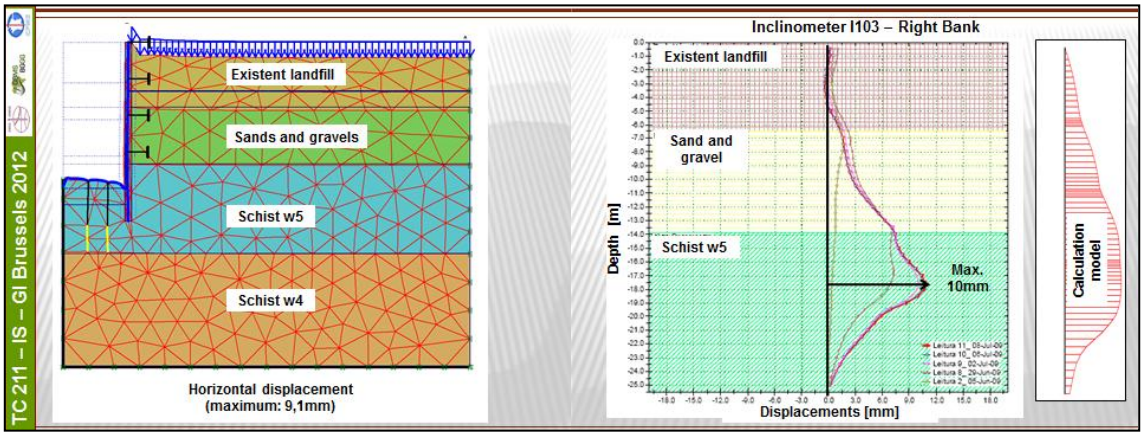

Figure 7: View of the adopted FEM model and horizontal displacements.

The adopted solution allowed the fulfilment of the following main objectives: technical (low deformations and high water tightness) and control of both costs and construction schedule (Figure 8).

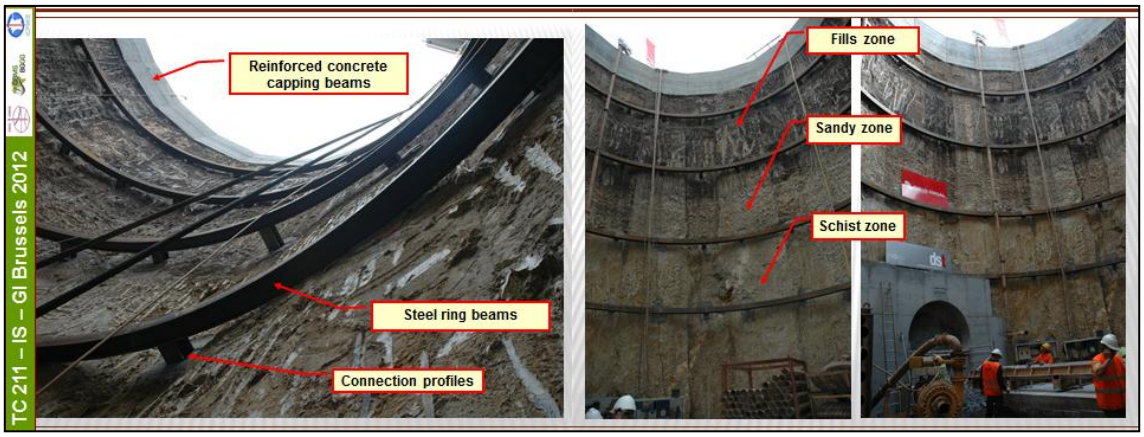

Figure 8: Views from the inside of the right bank shaft after excavation.

It should also be pointed out the quality control and quality assurance during the execution of the soil – cement panels, including the permanent monitoring of all the execution parameters, the collection of soil - cement samples and cores for UCS and Young modulus laboratorial tests, as well as the monitoring of the pit behaviour.

3.2. Permanent Retaining Wall for excavation above ground water table level

As example of the CSM technique applied for earth retaining solution above water table level is presented the case of the enlargement of a railway platform, in order to accommodate the new infrastructures of High Speed train in Lisbon. For the enlargement of the railway platform it was necessary to perform several excavations with 13m of maximum depth. Due to neighbourhood conditions, three retaining structures (M1, M2 and M3) were built using the CSM technology. In this paper the case of the M3 wall is presented, with 13m height and about 66m wide (Figure 9).

Figure 9: Site location and execution of the CSM panels at wall M2.

The local geological conditions were heterogeneous. The excavation works intersected, from the surface, heterogeneous landfills and Miocene medium dense to dense sands and sandstones. The ground water table was located about 5m above the final excavation level (Figure 10).

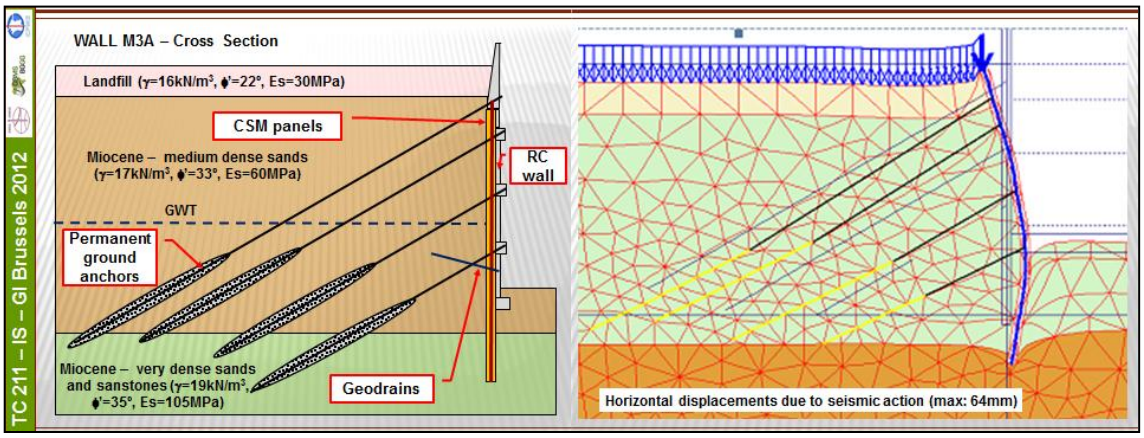

Figure 10: Cross section of the adopted solution, with geological conditions, and FEM analysis.

In order to allow the excavation works minimizing the ground loss of confinement effect, soil - cement panels with an maximum depth of about 18m and a cross section of 2.4 x 0.5m^2, including 0.20m of overlapping, were built using the CSM technology. The panels were reinforced with vertical IPE240 hot rolled steel profiles (Euronorm 19-57), spaced in average 1,1m, in order to resist to the earth and water pressures, as well as to assure a better control of deformations. The soil - cement panels were design in order to be integrated on the final earth retaining solution, including the lining reinforced concrete (RC) wall and beams, and also to minimize the water inflow to the excavation platform.

The steel profiles were placed inside the panels, before the cement started the curing process, and were braced by four or three levels of permanent ground anchors, applied at the reinforced concrete capping beam as well as at the distribution beams (Figures 11, 12, 13, 14 and 15).

All the soil cement panels were design in order to achieve an unconfined compression resistance of at least 4,0MPa and a Young Modulus of 1GPa. Due to the soil and water chemical properties, pozolanic cement was adopted. For the design of the adopted solution FEM analysis was carried out, using Plaxis software. The maximum estimated horizontal displacement was about 64mm due to the seismic action (Figure 10).

At the figures 11, 12 and 13, the main construction phases are described. It should be pointed out the big advantage of the full width excavation, only possible due to the soil – cement panels ground improvement effect, leading to the optimization of the construction overall schedule.

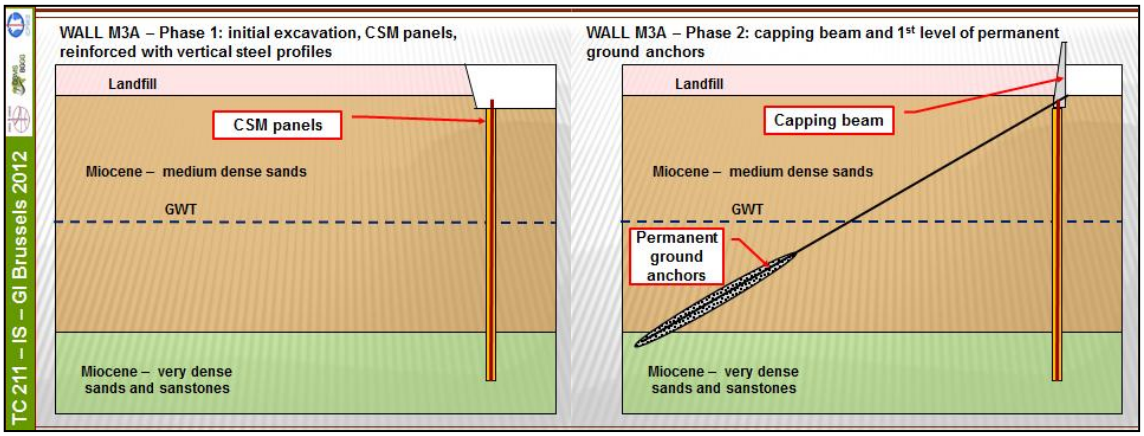

Figure 11: Construction phases 1 and 2.

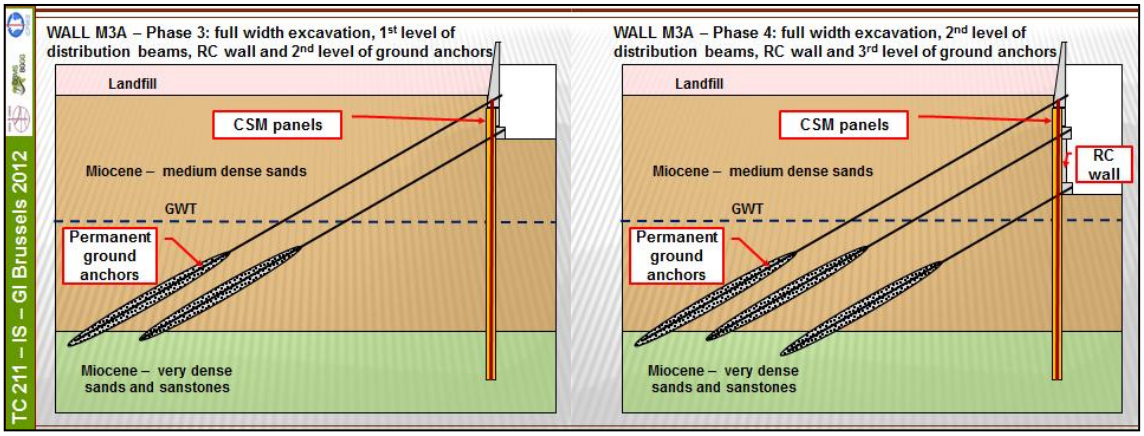

Figure 12: Construction phases 3 and 4.

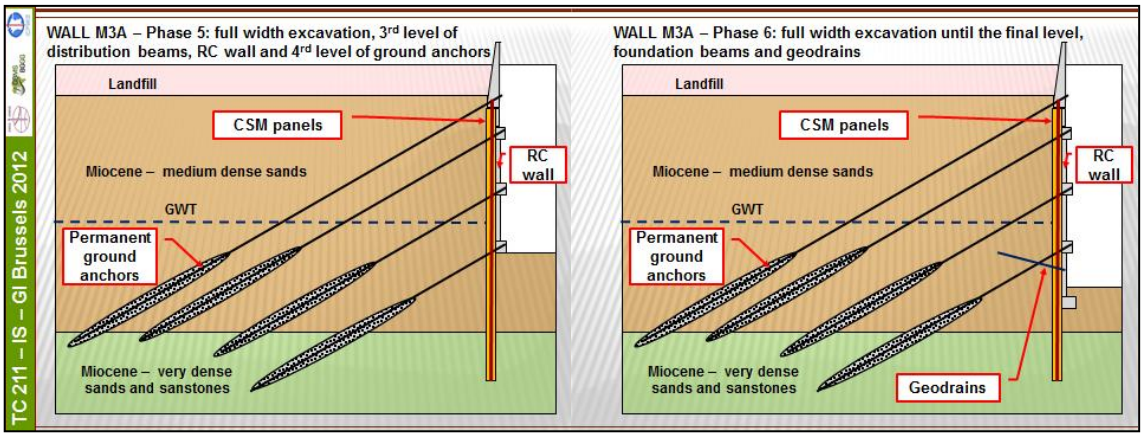

Figure 13: Construction phases 5 and 6.

The excavation works started in April 2011 and was performed by levels, including, at each excavation level, the full wall width at the same time. It is expected that the adopted solution will allow the fulfilment of all the main objectives, specially the following technical issues:

- Good confinement of the excavated soils, due to the ground improvement effect, allowing a very high construction rate, comparing, for instance with Berlin reinforced concrete king post walls solution;
- Low deformations until now, as confirmed by the instrumentation readings;
- Good concrete final surface and high water tightness, as shown at Figures 14 and 15.

Also very important was the control of both costs and construction schedule, has no major deviations have been noticed.

Figure 14: Views of the excavation works.

It should also be pointed out the tight quality control (vertical deviation lesser than 1%) and quality assurance during the execution of the soil – cement panels, which included the permanent monitoring of all the execution parameters, the collection of soil cement samples and cores for UCS laboratorial tests, as well as the monitoring and survey plan (inclinometers and topographic marks).

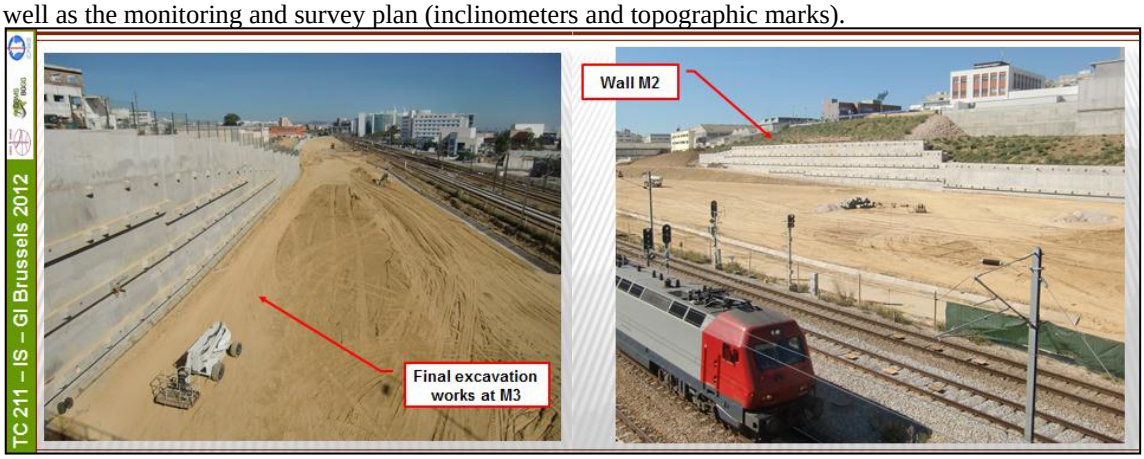

Figure 15: Views of the walls after the conclusion of the excavation works.

3.3. Permanent Retaining Wall for excavation below water table level

As example of the CSM technique applied for both earth retaining and foundations solution is presented the case of the "Agências" Pumping Station, located at the Tagus river right bank, in Lisbon. For the construction of the Pumping Station it was necessary to perform an excavation with 12m depth on a 30x12m^2 rectangular shape area. The geological conditions were complex, with ground water table located near the surface. The excavation works intersected, from the surface, heterogeneous landfills and alluvial muddy soils, located over the Miocene very stiff clays (Figure 16).
In order to allow excavation works in dry conditions, soil - cement panels with an overall depth of about 24m and a cross section of 2.4 x 0.6m^2, including 0.20m of overlapping, were built using the CSM technology. The panels were reinforced with vertical IPE300 hot rolled steel profiles (Euronorm 19-57), spaced in average 1m, in order to resist to all the structural loads, earth and water pressures, as well as to assure a better control of deformations. Buttress panels were also built in order to increase the earth retaining structure overall stiffness.

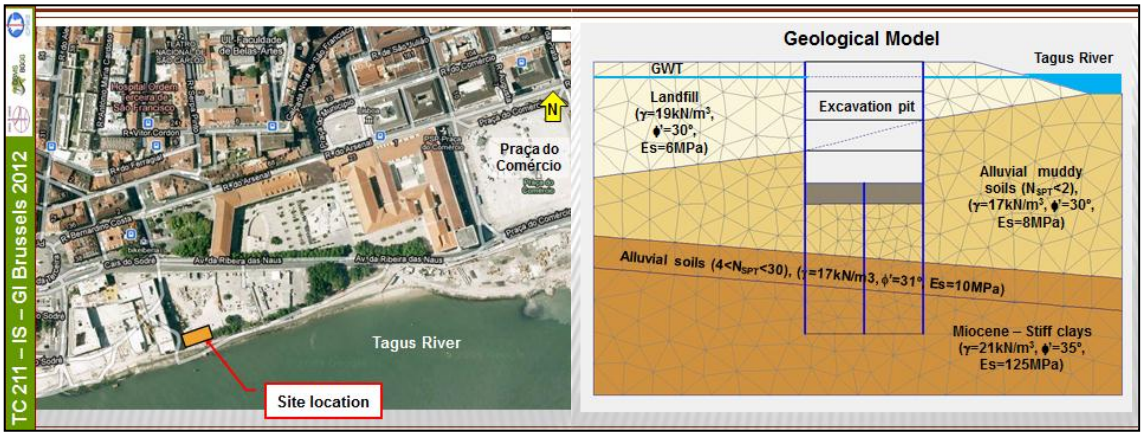

Figure 16: Site location and geological model.

The soil - cement panels were design in order to be integrated on the final foundations and earth retaining solution, including the internal reinforced concrete lining mat and peripheral walls, and also to assure an overall cofferdam effect, minimizing the water inflow to the excavation pit. The steel profiles were placed inside the peripheral panels, before the cement started curing, and were braced by four or three levels of steel struts, as well as by a grid of soil – cement panels with 3m height, located just below the final excavation level. All the soil - cement panels were design in order to achieve an unconfined compression resistance of 3MPa and a Young Modulus not lesser than 1GPa. Due to the soil and water chemical properties, pozolanic cement was adopted (Figure 17).

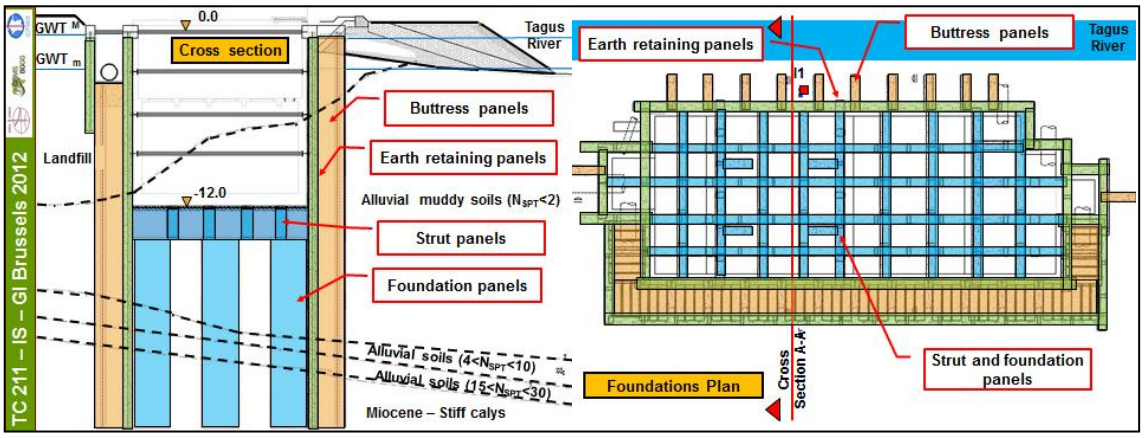

Figure 17: Cross section and plan of the adopted solution.

For the design of the adopted solution 2D FEM analysis were carried out, using Plaxis software. The maximum estimated horizontal displacement was about 7mm, very similar to the one obtained through the inclinometer readings (Figure 18).

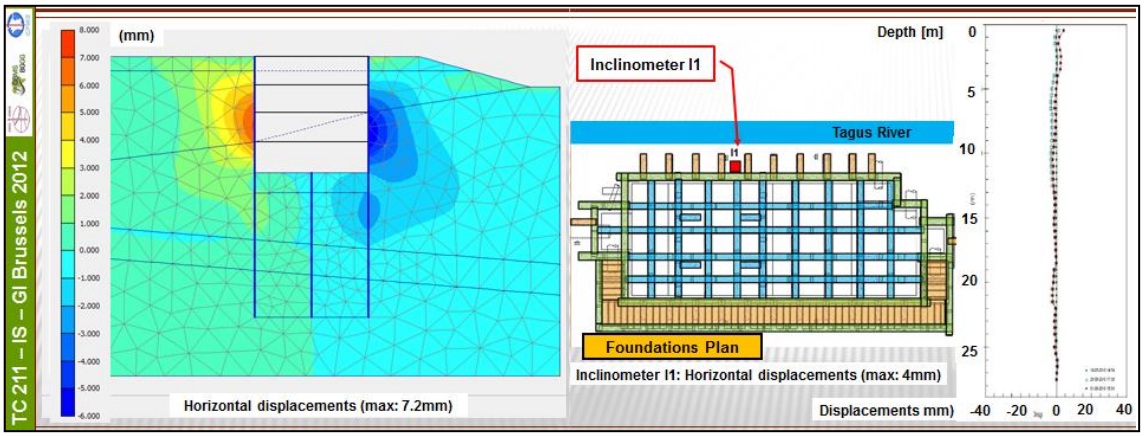

Figure 18: Main deformations obtained through FEM analysis and measured at the inclinometer I1.

The adopted solution allowed the fulfilment of all the main objectives, specially the following technical issues:

- Low deformations, as shown by the inclinometers readings (Figure 18);
- Total compatibility with the internal reinforced concrete structure (Figure 19);
- High water tightness, as shown during the excavation works, as no water inflow was observed (Figure 19 and 20).

Also very important was the control of both costs and construction schedule, as no deviations were noticed at the end of the construction.

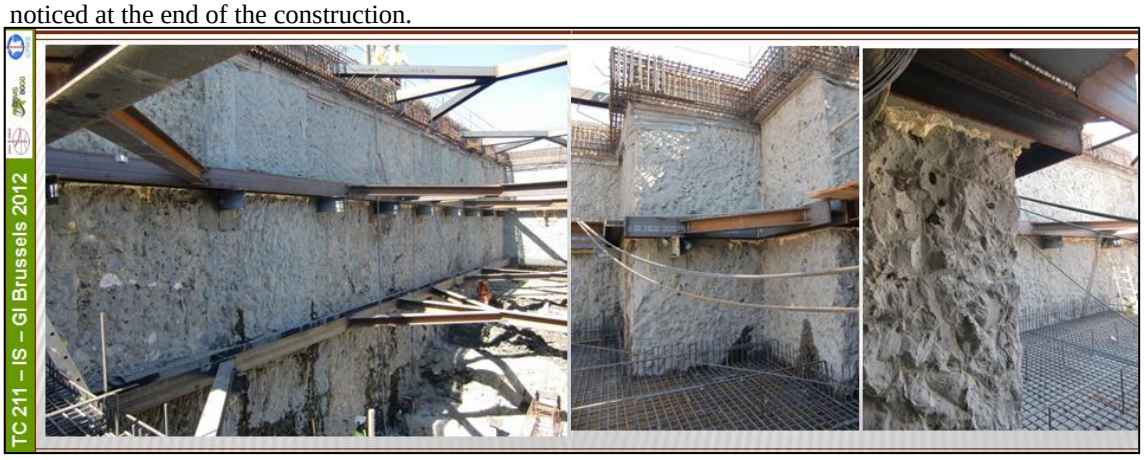

Figure 19: Views of the excavation works, with no water inflow, and details of the compatibility of the CSM panels with the internal structures.

It should also be pointed out the tight quality control (vertical deviation lesser than 1%) and quality assurance during the execution of the soil – cement panels, which included the permanent monitoring of all the execution parameters, the collection of soil cement samples and cores for UCS laboratorial tests, as well as the monitoring and survey plan (inclinometers and topographic marks).

Figure 20: Views of the internal structure construction.

4. CSM USED AS SLOPE STABILIZATION SOLUTION

As example of the CSM technique applied as foundation and slope stability solution is presented the case of two mechanically stabilized earth walls, M4A and M4B, built at the "Marão" Mountain Motorway, at the city of Amarante, Portugal. Those walls with a maximum height of about 20m were built in order to allow the widening of the existing road platform (IP4), for the construction of the new "Marão" Motorway (Figure 21). The walls included precast facing panels and a back granular fill, reinforced with polyester high tenacity strips, protected, by durability reasons, by a polyethylene sheet.

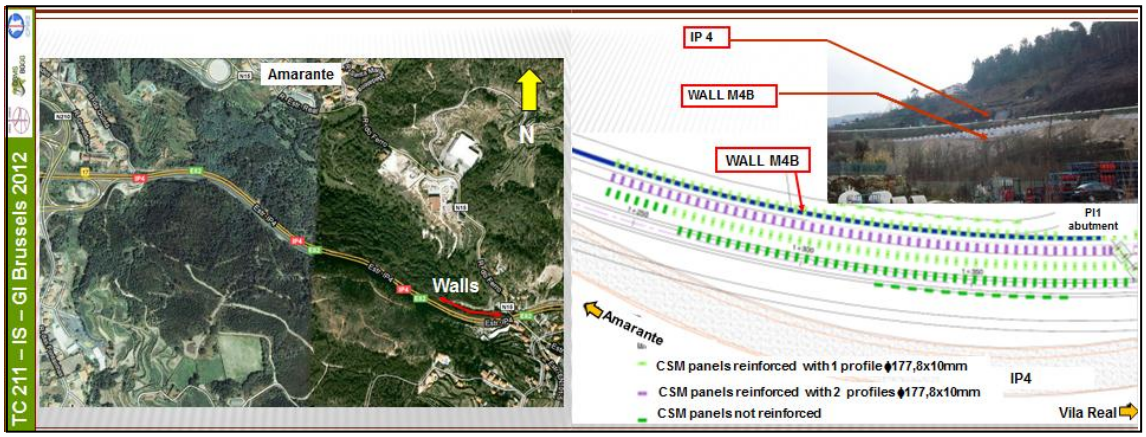

Figure 21: Location and plan of the walls.

The walls intersected heterogeneous landfills, used for the construction of the existing road platform (IP4), about 25 years ago, and located over weathered granite. Soil – cement panels under a LTP (load transfer platform), using CSM technology, as both slope stability and walls foundation, was adopted. This solution allowed the optimization of the walls overall height and cost, comparing with other alternatives, as for example a viaduct or the integral replacement of the existent fills (Figures 22 and 23).

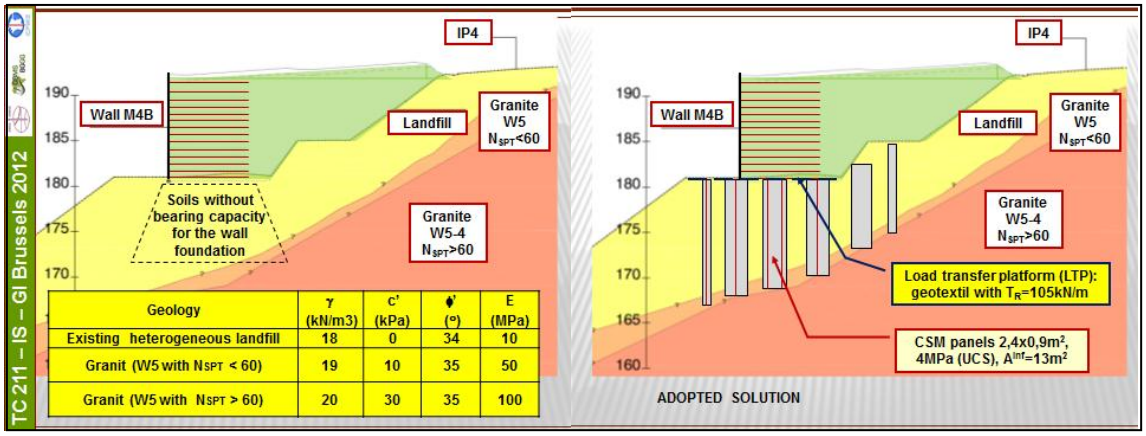

Figure 22: Cross section geological conditions and adopted solution.

To achieve the main design requirements, soil - cement panels with a cross section of 2,4x0,9m^2 and a maximum depth of about 15m were built in order to assure a minimum embedment length of 1m on the granite bed rock. The majority of the panels were reinforced with tubular steel profiles ∅177,8x10mm (API – 5A), in order to increase the overall shear resistance. The adopted panels mesh was 4,4x2,9m^2.The LTP was built over the panels head with one layer of high resistance polypropylene geotextile (tension resistance of 105kN/m), including ultraviolet stabilizers. The soil - cement panels were designed in order to transmit to the granite bed rock the loads due to both the motorway traffic and the walls self - weight. For this purpose an unconfined compression resistance of at least 4,0MPa was achieved. Due to the soil and water chemical properties, pozolanic cement was adopted for the soil cement panels, allowing also a better protection and confinement of the steel profiles (Figure 24).

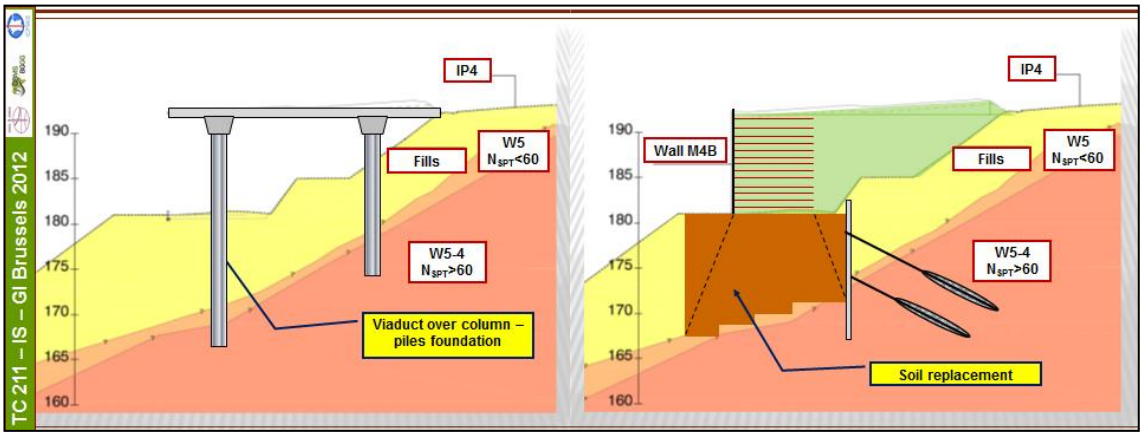

Figure 23: Cross section of the non-adopted solutions.

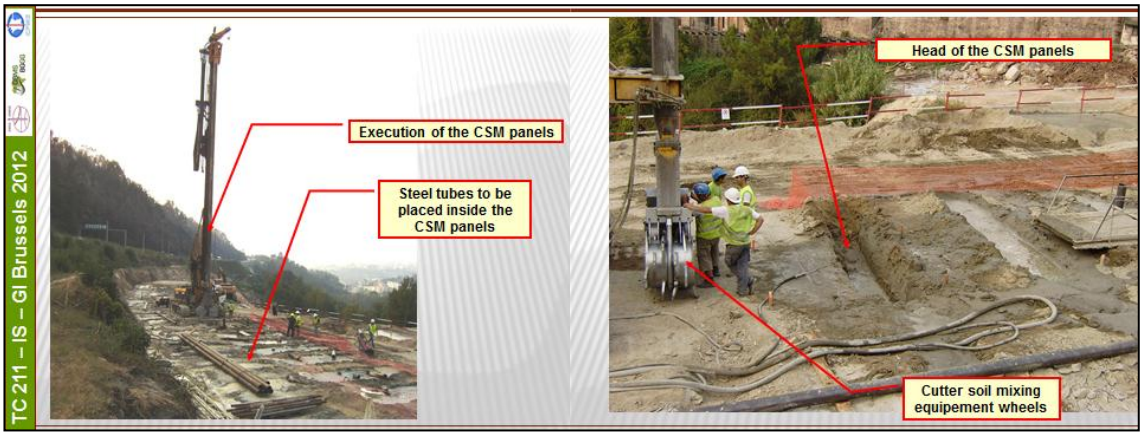

Figure 24: View of the soil – cement panels execution using CSM technology.

For the design of the adopted solution equilibrium limit (overall stability for static and seismic loads) and 2D FEM (deformations) analysis were carried out, using Slide and Plaxis software. The maximum estimated horizontal displacements at the IP4 after the conclusion of the earth retaining works were about 5mm, very similar to the ones obtained through the instrumentation readings (Figure 25).

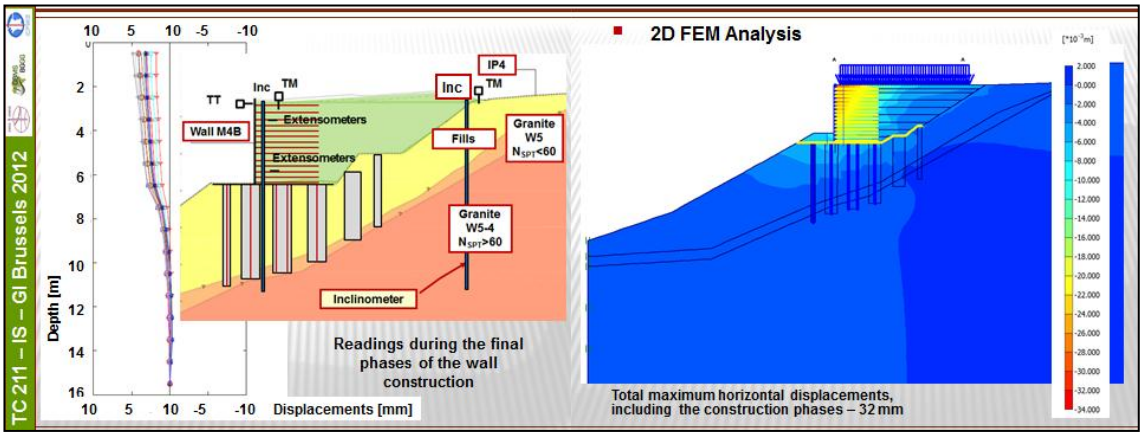

Figure 25: Horizontal displacements: measured and obtained through 2D FEM analysis.

The adopted solution allowed the fulfilment of the following main objectives: technical (low deformations) and control of both costs and construction schedule (Figures 25 and 26). It should also be pointed out the tight quality control and quality assurance of the soil – cement panels, which included the permanent monitoring of all the execution parameters, the collection of soil - cement samples and cores for UCS and Young Modulus laboratorial tests, the execution of CPT tests, as well as the monitoring of the walls overall behaviour.

Figure 26: Views of the wall at the end of the works.

5. QUALITY CONTROL AND QUALITY ASSURANCE

One of the major issues of the CSM technology is the high quality control and quality assurance, allowing the monitoring and correction of important parameters, such as: depth, inclination, speed of mixing tools, pressure (ground and binder slurry) on cutter wheels, rate and total volume of pumped slurry (Figure 27).

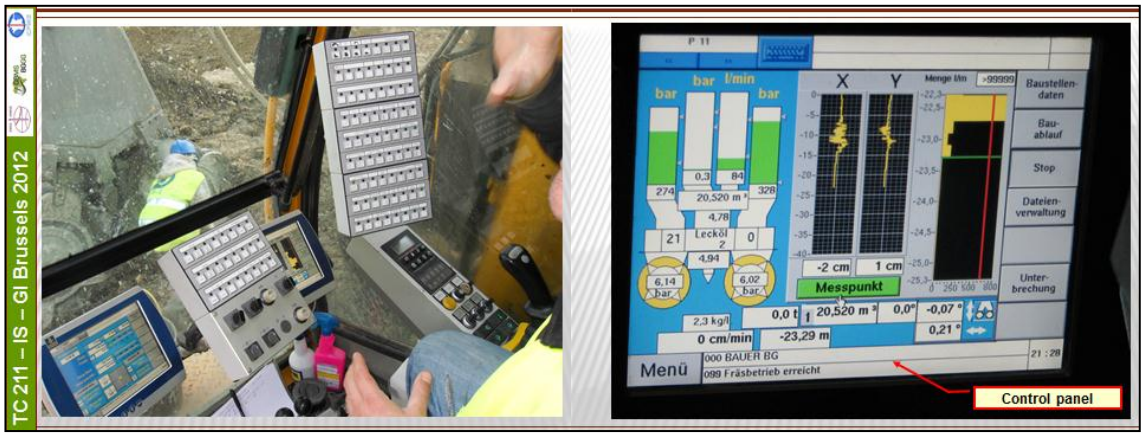

Figure 27: Execution control of the CSM technology.

The execution control is complemented by a tight quality control and quality assurance, allowing on real time the confirmation of both the main resistance, homogeneity and deformability of the soil – binder parameters. For this purpose, samples from fresh material and cores should be collected, from test and final panels, in order to access the material homogeneity, as well as to perform laboratorial tests with different ages, mainly UCS and Young Modulus (Figure 28).

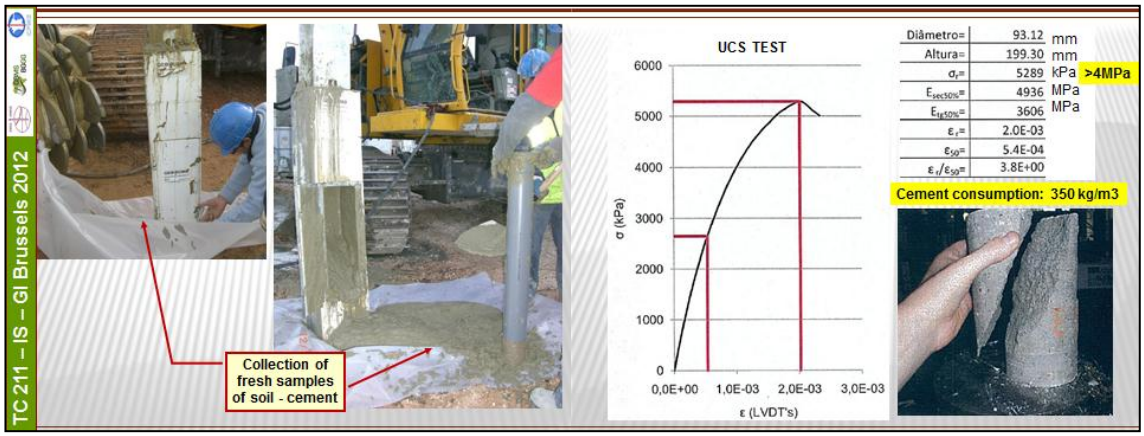

Figure 28: Quality control and quality assurance of the panels performed using the CSM technology.

Figure 29: CPT tests at the "Marão" Motorway M4B wall base.

When necessary, as for instance the case of the LTP foundations adopted at the "Marão" Highway, the execution control could include also in situ CPT tests, inside and outside the panels, in order to access the panel's resistance, as well as the confinement effect on the soil located between the panels (Figure 29).
Finally it should be stated, as a complement of the quality control and quality assurance, the importance of full scale load tests, as well of a complete monitoring of the solutions, which should include a wide number and type of devices allowing the confirmation in real time of both the main design and execution criteria (Figure 30).

Figure 30: Devices adopted for monitoring the "Marão" Motorway M4B wall.

6. MAIN CONCLUSIONS

In spite of the recent development and applications of the CSM technology it is possible to point out some advantages, taking into account the presented examples and comparing with some more traditional ones, as for instance (Pinto et al, 2011 a) and 2011b)):

- Possibility to be applied to almost every kind of soils and weathered rocks, with low vibration, low-noise and small spoil, as well as minimum ground perturbation;
- The ground is improved with a binder addition, using a mechanical process, in order to be integrated on the final engineering solution with both economic and environmental advantages;
- The water tightness efficiency for earth retaining and cut off solutions, due to the very low permeability as well as to the absence of joints, due to the overlapping length between two panels assuring the solution efficient continuity
- Possibility to reinforce the panels with steel profiles in any position on the cross section, in order to better resist to shear and tension efforts due to bending moments and tension loads, as well as to facilitate the connection to the capping elements and other structural elements, as for instance basement slabs or distribution beams;
- Very complete execution control due to the sophisticated equipment, allowing in real time the assessment and correction of the execution parameters.

As main restrictions of the CSM technology the following ones could be point out:
- Big dimension and overall height of the CSM equipment, leading to the lack of versatility, which could be overtaken using Quattro or Side Cutters;
- Depth limitation to about 60m;
- Very demanding quality control and quality assurance, as applied to the majority of the ground improvement techniques, stated by Simon, B. (2009).

The CSM technology is being used in Portugal in other applications on wide geological and geotechnical scenarios, proving its technical and economic advantages, mainly on retaining, foundations and slope stabilization solutions (Figure 31).

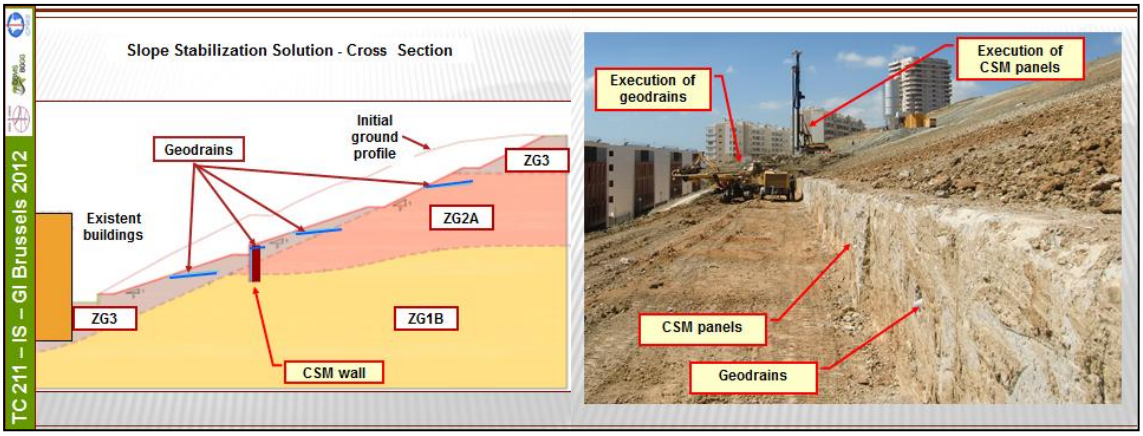

Figure 31: Slope stabilization solution in Lisbon, where the CSM solution was used to increase the slope stability (global and local) and allow the future use of the ground without any restrictions.

7. ACKNOWLEDGMENTS

The authors thank to the owners of the described case histories their permission for the presentation of this paper.

REFERENCES

Ameratunga J.; Brown D.; Ramachadran R.; Denny R. (2009). "Ground improvement for a large above ground storage tank using cutter soil mixing columns." Proceedings of the 17th ICSMGE, pp. 2280-2283.

Pinto, A.; Tomásio, R.; Pita, X.; Godinho, P.; Peixoto, A. (2011 a)) "Ground Improvement Solutions using Cutter Soil Mixing Technology" – International Conference on Advances in Geotechnical Engineering, Perth, Australia, November 2011, ISBN: 978-0-646-55142-5, Ground improvement and soil stabilization. pp. 511 – 518.

Pinto, A.; Tomásio, R.; Pita, X.; Pereira, A.; Peixoto, A. (2011 b)) "Cutter Soil Mixing Solutions in Portugal on Hard Soils and Weak Rocks" - 15th European Conference on Soil Mechanics and Geotechnical Engineering, September 2011, Athens, Greece, Part 2 – 3.3 – Ground Reinforcement, pp. 1037 – 1042.

Simon, B. (2009). "Projet national de recherche et développement. Amélioration des sols par inclusions verticales rigides." Travaux nº862, pp. 65-72.

State of the art in "Dry Soil Mixing" – Basics and case study

Peter QUASTHOFF, Liebherr-Werk Nenzing GmbH, Austria, peter.quasthoff@liebherr.com

ABSTRACT

Soil mixing in the dry version is a method for improving building ground consisting of unsustainable soils or soils with insufficient load-bearing capacity by adding a binding agent. Unlike the wet version, which is applied much more frequently, the binding agent is added to the soil in dry form. The method of dry soil mixing is applied in soft, plastic soils.
The binding agents used are mainly cement and lime, but also ashes, gypsum and mixtures of the mentioned products. They react with the prevailing soil and the contained water and form a soil mortar, which then provides low permeability, greater strength and increased shear strength.
For the production of the soil mortar a hollow drilling rod fitted with mixing blades is drilled into the ground. Once the final depth has been reached, the binding agent is added in powder form. The powder is injected into the mixed soil with the help of compressed air delivered through nozzles situated at the lower end of the mixing tool. By constantly rotating and extracting under simultaneous addition of binding agent a column-shaped element of soil mortar is produced.
The mortar columns can be installed next to each other, thus creating grid-type, block-type or area-wide stabilizing elements.
The method of dry soil mixing is used for various building tasks, e.g. traffic route construction, foundation pit linings, cut-off walls in embankments, slope stabilisations and shallow foundations.
This article describes the method of dry soil mixing with its fields of application, explains the required and currently available machinery and finally discusses the production and quality assurance of lime cement columns to be used as shallow foundation elements in traffic route construction in Sweden.

1. BASICS PRINCIPLES

1.1. General

The method of deep mixing is used for the most varied building tasks e.g. improvement of soft cohesive soils for instance in traffic route construction, foundation pit linings, cut-off walls in embankments, slope stabilisation and shallow foundations.
Dry soil mixing is a method used for soil improvement and/or soil stabilization by adding a binding agent with the help of compressed air in dry form.
As early as the beginning of the 1970s soil mixing in dry form was developed in Sweden by adding (unslaked) lime in powder form in order to improve the settlement properties of soft plastic soils.
Dry soil mixing is treated in the DIN standard EN 14679 [German Institute for Standardization / Deutsches Institut für Normung e.V.] "Execution of special geotechnical works – Deep mixing" [Ausführung von besonderen geotechnischen Arbeiten (Spezieltiefbau) – Tiefreichende Bodenstabilisierung] with its applications and mainly serves to produce column-type or wall-type soil improvement elements as stabilization columns.

1.2. Principle of the method

The method of dry mixing is based on the mechanical breakdown of the soil with mainly vertical movements of the mixing tools. During extraction the binding agent is injected into the soil (at a continuous flow rate). Thereby the mixing blades rotate at a constant speed and mix the soil and the binding agent to form a homogeneous soil mortar.
The binding agents used are mainly cement and lime, but also fly ashes, other types of ashes, gypsum and mixtures of the mentioned products. The binding agent reacts with the prevailing soil and/or the ground water to form a soil mortar. For the dry mixing process the binding agent is usually injected into the soil in dry powder form with the help of compressed air delivered through nozzles situated at the lower end of the mixing tool. This is especially advantageous for work carried out under severe freezing temperatures, e.g. during long periods of frost in Scandinavia. The method is also frequently named the "Nordic method". In contrast, there is also the Japanese mixing technique which is not discussed here.

1.3. Production steps in dry soil mixing

The production of a dry soil mixing element includes the following steps as shown in figure 1:

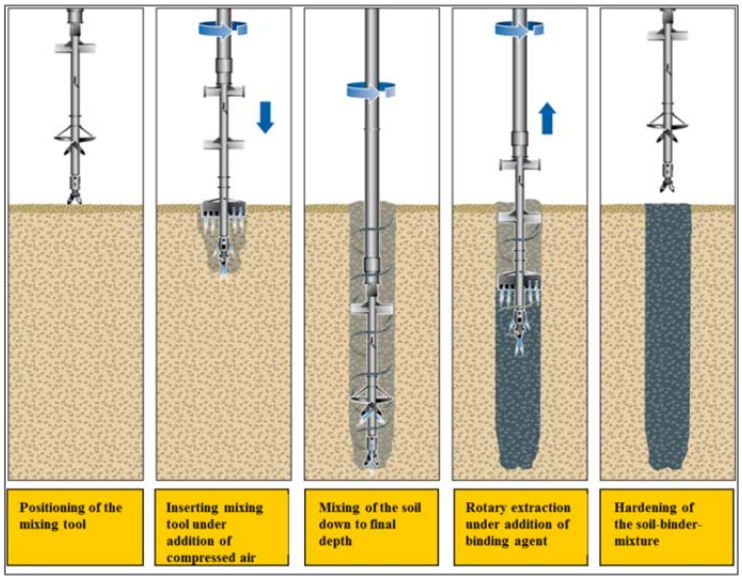

Figure 1: Schematic production steps [Liebherr - BVV 2010];

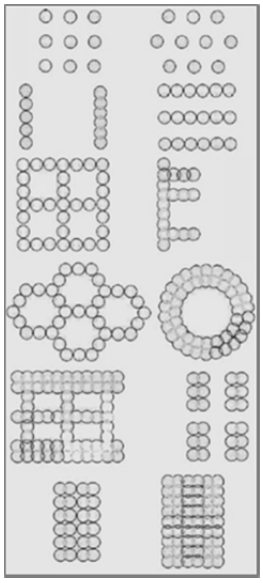

Figure 2: Design of the soil mixing columns [Topolnicki, 2006]

1) The mixing tool is correctly positioned at the relevant drilling point;
2) Then the mixing tool is inserted in the soil under the addition of compressed air in sections.
3) The mixing tool is rotated down to the projected depth so mixing the soil for the first time.
4) After the final depth has been reached the mixing tool is extracted under simultaneous rotation; thereby the binding agent is injected into the soil in dry powder form with the help of compressed air. The mixing tool rotates on a horizontal plane and so mixes soil and binding agent.
5) The column is completed. Then the dry soil mixing element is left to harden. After hardening the dry soil mixing element forms the basis for further construction work.

With the dry soil mixing method column-type soil improvement elements or soil mixing elements, so-called mortar columns, are produced. These can vary not only in depth but also in pattern: they can either be produced as single columns or as tangent or secant rows, grids or blocks. Some examples of execution with various arrangements of soil mixing elements are shown in figure 2.

2. FIELDS OF APPLICATION

2.1. Applications of deep mixing

The method is predominantly used for improving the properties of mainly cohesive soils with insufficient load-bearing capacity. The treated soil usually offers increased shear strength, lower permeability and ductility and thus greater stiffness than the untreated soil.
Suitable soils are silt, clay and peat, but also loose and non-cohesive soils. The moisture content of the soil must be ≥ 0.20.

The most common fields of application of deep mixing are:

- Increasing the load-bearing capacity of the soil for shallow foundations in traffic route construction
- Stabilizing soils susceptible to settlement
- Stabilizing slopes and embankments
- Reducing the active soil pressure on retaining walls resulting from adjacent construction
- Land reclamation
- Containment of contaminated material on jobsite (e.g. heavy metals)

3. MACHINERY

3.1. Basic machine and mixing drive

The equipment required for dry mixing consists of a basic machine, a mixing drive, the corresponding drilling rod with mixing tool and a lime cement station. The carrier machine is a LIEBHERR piling and drilling rig LRB 125 XL with 450 kW engine power. It has a 15.5 m long leader which can be adjusted hydraulically. Thanks to a vertical leader adjustment of max. 5.0 m above ground level drilling depths of max. 17.0 m can be achieved. The carrier machine offers special features such as:

- High hydraulic power
- Robust and rigid leader design
- High push and pull forces
- High torque
- Automatic leader adjustment
- Quality assurance using process data recording

The LRB 125 XL is a multi-functional machine which can be used for all common deep foundation methods such as vibrating, impact pile driving and drilling, when adapted accordingly.

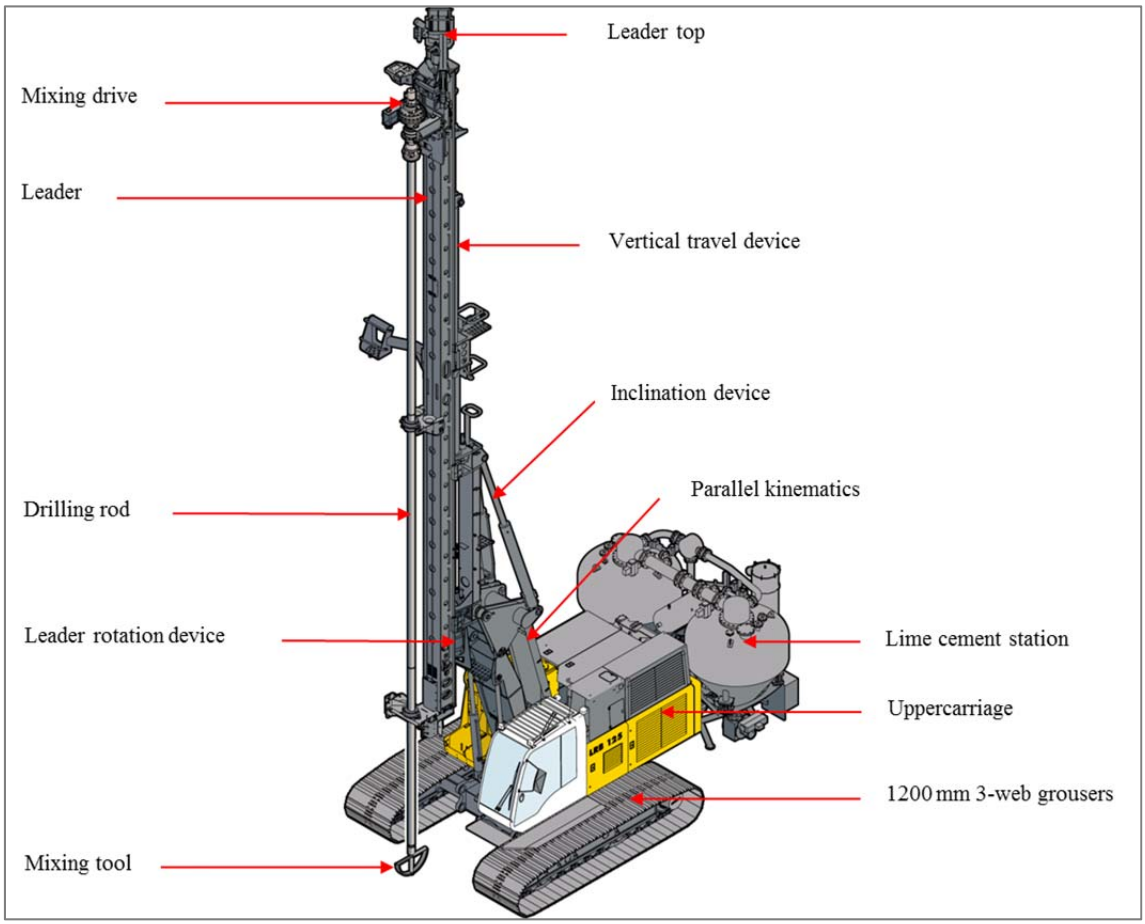

Figure 3: carrier unit LRB 125 XL for dry soil mixing [Liebherr – BVV 2010]

The MA 35 Turbo mixing drive is a special rotary drive for the soil mixing method. It is connected to the drilling rod with a flange and mounted on the leader with a slide. The leader is equipped with a crowd system offering a crowd force of 15 t for push and 20 t for pull. The rotating extraction of the mixing drive with the drilling rod is carried out using the crowd system in a fully automated working process. The extended 1200 mm 3-web grousers were specially designed for dry mixing in order to better distribute the ground pressure of the machine weighing approx. 55 t (net weight). This reduces the pressure on the working surface so causing less settlement and the machine is prevented from sinking into the ground. The machine designed for dry mixing is shown in figure 3.

3.2. Lime cement station

3.2.1. Basic concept

On the one hand, the design of the lime cement station was based on special technical specifications in terms of the process. On the other hand, it was important to comply with the requirements of the technologies already in use on the Scandinavian market. For this purpose a concept was developed which projected to equip the lime cement station with two silos. The use of two silos made it possible to carry out the filling during the working process. The aim was to prevent interruption of the ongoing working process during dry mixing. It was absolutely necessary to avoid any standstill. Another consideration was to mount the lime cement station on the back of the machine so the complete equipment forms a single unit. Thus, the complete unit is much more flexible both during repositioning of the machine and in the complete working process. Delivery of materials is carried out exclusively by an external off-road truck so there is no need for the carrier machine to travel long distances to the lime cement depot.

3.2.2. Description of the method and components

The lime cement station was designed for the pneumatic introduction of a lime cement mixture into the building ground for soil stabilization. Basically the system consists of two identical silos with a weighing

system. With these load cells the consumption of binding agent from the silos during column production can be exactly measured. An independent compressor provides the station with compressed air. The compressed air is cooled in the refrigeration dryer (after cooler) and prepared in the membrane filter (membrane dryer). The compressed air can be supplied via an external connector, if required. Each silo is fitted with a filling level sensor so the filling level can reliably be monitored using the load cells. The exhaust air from the silos is collected and discharged to the atmosphere through a filter. The dosing unit installed under the silos consists of two rotary valves (with a flow rate from 60 – 210 kg/min) and the compressed air supply. It is followed by the conveyor pipe and the conveyor hose. In order to improve the discharge of the lime cement mixture the silos are equipped with a fluidisation. The lime cement station with all its components is designed for temperatures ranging from – 25° C to + 50° C. The setup of the lime cement station is shown in figure 4.

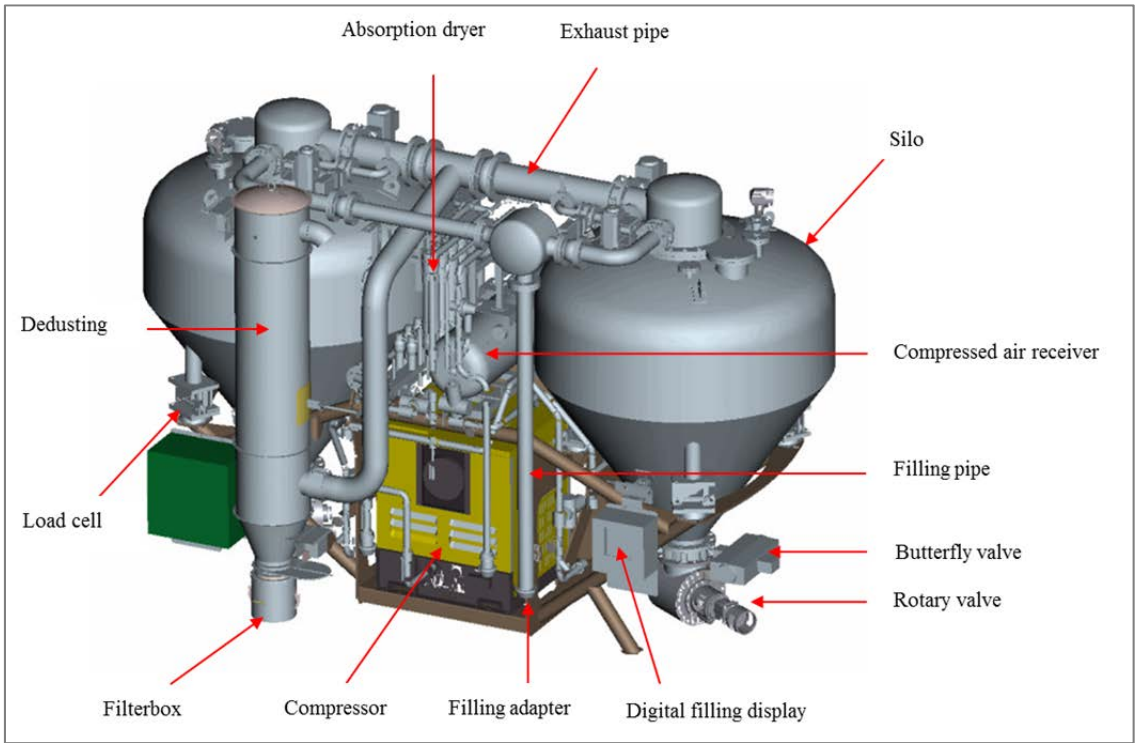

Figure 4: Lime cement station [Liebherr – BVV 2010]

3.2.3. Rotary valve

The rotary valve as dosing unit is the core of the lime cement station. The complete flow of binding agent is controlled via the rotary valve. It mainly consists of the star feeder, a hydraulic motor, a gearbox and a coupling. Through a compressed air line leading into the valve the compressed air is injected into the conveyor pipe together with the lime cement mixture. The rotary valve with its components is shown in photos 1 and 2.

Photo 1: Star feeder with butterfly valve and silo; Photo 2: Rotary valve with hydraulic motor, gear box and coupling

A decisive criterion during column production is to transport a continuous amount of binding agent per time unit through the rotary valve into the conveyor pipe. Another important criterion during dry mixing is the exact dosing of the lime cement mixture into the conveyor pipe. This is guaranteed by an electronic control system developed by LIEBHERR. The LITRONIC control system ensures that the values for dosing [kg/m] previously entered in the operator´s cab are precisely maintained and that a continuous conveying with a constant flow of binding agent is achieved.
Moreover, additional important control elements are implemented in the LITRONIC control system. It is, for instance, possible to adjust the amount of binding agent supplied during column production from the operator´s cab: on the one hand the rotation speed of the rotary valve can be varied, on the other hand, it is possible to increase the conveying pressure during column production.
This results from the following finding:
In practice it was detected that neighbouring columns produced with the same production parameters displayed various strengths when quality controlled. It was found that this was due to varying amounts of binding agent introduced.
The reason for this is, amongst others, to be found in the different compression ratio in the soil. These are caused by the various lengths of the columns and by changing and strongly inhomogeneous layers of soil. This means that the conveying pressure and thus the flow rate have to be adapted to the compression ratio in the soil during column production in order to achieve a uniform homogeneous mortar column.
Remark: If the conveying pressure is too low the binding agent may not be distributed over the full cross section of the column. If the conveying pressure is too high this may lead to explosive air and soil emersions and thus to undesired soil movements.
The control functions described so offer the possibility to guarantee the constant binder dosage during column production as required.

4. CASE STUDY JOBSITE STOCKHOLM

4.1. Project description

Near Stockholm a large of chain DIY stores has built a new subsidiary. The complete site covers 31,000 m² and is situated directly next to the E 18 motorway as ideal transport link. The DIY store covers an area of 17,200 m², 5,800 m² of which are parking and traffic area. Due to the geological conditions the northern area had to be stabilized with lime cement columns for better load transfer.

4.2. Soil conditions

The geological conditions in the area were as follows: whereas in the southern section compact rock was encountered after only a few metres, the soil below the working surface in the northern section was composed of thin layers of banded clay with enclosures of sand. Beneath, there were mainly silts and partly clayey layers with small enclosures of sand in parts. With a water content of approx. 0.40 to 0.60 and a liquid limit of $w_l \leq 0.50$ the silts were predominantly soft and medium-plastic. The shear strength of the undisturbed soil samples was between 12 kPa and 20 kPa.

4.3. Planning and design principles

For dry mixing suitability tests are carried out before starting work on the jobsite. Thereby the properties of the prevailing soil are tested with regard to the desired homogeneity and stiffness. This is necessary to correctly select the binding agent, to determine the amount of binding agent and the mixing ratio. By analysing the test results in the laboratory the required production parameters can be determined. The most important parameters are the column diameter, the mixing ratio, the amount of binding agent [kg/m], the rotational speed of the mixing tool [rpm], the pitch [mm/r] and the extraction speed [m/min]. These parameters are specified before starting construction work and must be recorded accordingly during production of the columns.
For this construction task various mixing ratios were tested in the laboratory with regard to their load-bearing capacity and the best ductility behaviour. Then the number and arrangement of the columns was determined accordingly. In the design phase it was decided to produce a larger number of columns for lower loads rather than only a few columns for higher loads. Overloading due to excessive load concentration would lead to breaking and/or buckling of the columns.
For load transfer in the traffic and parking section approx. 3,500 stabilization columns were planned. The columns were specified to be arranged in grids, rows and partly in blocks.

4.4. Specified design parameters

The design parameters were assessed by the geotechnical office on the basis of the suitability test results and are displayed in table 1:

Table 1: Design parameters for the lime cement columns

Column diameter	Ø 800 mm
Mixing ratio lime / cement	KC 25 / 75 %
Top edge column / lower edge column	1.0 m below working level down to the rock
Column length	7.0 m – 16.0 m
Binder dosage	50 kg/m column
Rotation speed mixing tool	150 – 200 rpm
Pitch	15 – 20 mm/revolution
Inclination	+/- 2.0 cm/m

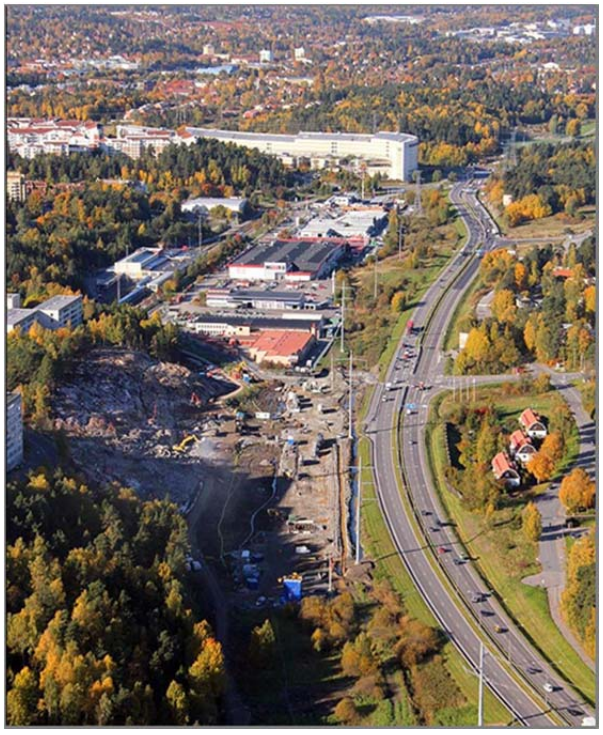

Photo 3: Jobsite Stockholm for the lime cement columns

4.5. Process steps during column production

After the drilling tool was positioned on the drilling point, the silo was charged with compressed air. First, drilling rod and mixing tool were drilled down to final depth under slight rotation thus mixing the soil for the first time. Drilling was carried out under occasional injection of compressed air between 4 and

5 bar to prevent blockage of the nozzle. Afterwards, the rotary valve and the automated extraction process were started simultaneously. Under a silo pressure of approx. 4.5 to 5.5 bar the binding agent was permanently injected from the silo through the rotary valve and the conveyor line into the drilling rod. At the lower end of the drill string, to which the mixing tool was fixed, the lime cement mixture was injected into the soil through the nozzle. During rotary extraction of the tool the lime cement mixture was introduced, the soil was uniformly mixed and thus a homogeneous mortar column was produced.
After completion of the column the drilling rod with the mixing tool was extracted from the borehole and positioned on the new drilling point by swinging the leader to the side or by repositioning the machine.

Photo 4 and 5: LRB 125 XL during column production

The silos were filled with the lime cement mixture on site using an off-road truck that was able to drive directly to the carrier machine. From the operator´s cab the silo to be filled had first to be unlocked by the operator. Then the mixture was injected through a filling hose and the filling pipe into the empty and depressurized silo under a pressure of approx. 1 to 2 bar. It was possible to carry out the filling process during operation as material was added only to the empty silo. The filling process lasted approx. 5 to 10 minutes. The respective filling level in the individual silos was measured with the load cells and could be read on the digital filling display on the back of the machine. The maximum filling capacity was limited to 3.0 t per silo. Photo 6 shows the filling procedure and photo 7 the filling display during filling.

Photo 6: Filling procedure using a dumper

Photo 7: Digital filling display

A very decisive criterion during column production was the exact adjustment of the specified pitch and the rotational speed of the mixing tool, i.e. of the extraction speed and the addition of binding agent. This was monitored by the LITRONIC control system. For this reason extraction using the crowd system and control of the rotary valve had to be done with utmost precision in order to exactly adhere to the required parameters.
Remark: If the pitch was too high the cross section of the column would be reduced; if the pitch was too slow this would lead to significant excesses and so loss of material.

A special feature was the reutilization of the material remaining in the conveyor pipes and hoses after the working process through another implemented control function called “blow-down function”. This made it possible to optimize the consumption of binding agent using a special control technique, not to waste any material and thus to contribute to improved cost-effectiveness regarding material consumption.
Furthermore, the LITRONIC control system allowed to switch the supply of the binding agent from one silo (when it was nearly empty) to the other silo (which was still full) during column production. Thus the complete binding agent material from both silos could be used without any residue.

4.6. Execution of the construction work and performance specifications

For the production of approx. 3,500 lime cement columns a LRB 125 XL unit with lime cement station was used. The columns were continuously installed from a gravelled working surface which was also used as construction road. Due to the excellent performance of the unit and the fully automated control process during column production the average production time was between 5 and 12 minutes, depending on the depth of the column.
Thanks to the robust and rigid leader design and the high crowd forces high penetration speeds of the mixing tool were achieved during the drilling process. The automatic leader alignment significantly facilitates positioning and aligning at the new drilling point. The process of repositioning between the individual drilling points was also optimized due to the carrier machine´s high flexibility. The filling cycle was carried out during the working process so no interruptions occurred during column production.
All process-related control functions were performed by the operator from the cab. Consequently, the only personnel required for this construction task were the operator and an assistant for filling. As a result high daily production rates of between 900 and 1200 running meters of lime cement columns were achieved. The lime cement columns were installed in compliance with the specified production tolerances. The soil stabilization project was completed within approx. 4-5 months and thus within the scheduled period of time. Photos 8 and 9 show the LRB 125 XL during column production.

Photos 8 and 9: LRB 125 XL during execution of the construction work

5. QUALITY ASSURANCE AND QUALITY CONTROL

5.1. Litronic control system

Thanks to modern CAN-Bus technology the dry mixing process is controlled entirely from the operator´s cab via comfortable electro-hydraulic proportional control. An extensive sensor system monitors and visualises all relevant process data. All information, warnings and failure indications required for the current machine operation are clearly displayed on the monitor in the operator´s cab and stored.

5.2. PDE® process data recording system

For documentation of the work carried out a PDE® process data recording system is incorporated. The PDE® process data recording system serves to electronically record and visualize the process data. Operation and display is carried out via the PDE colour touchscreen in the operator´s cab. On the PDE monitor important information can be displayed during production of the columns. The column diameter depending on the depth, for instance, is visualized on a large colour display. Thus the operator has the opportunity to visually monitor the column and to carry out corrections, if required, during the production process. Thereby, all relevant process data are stored on a PC-MCIA card and can be either printed as

graphic directly in the operator´s cab or further processed via database on the PC. Photo 10 shows the monitor display in the cabin, photo 11 the visualisation during column production on the PDE screen.

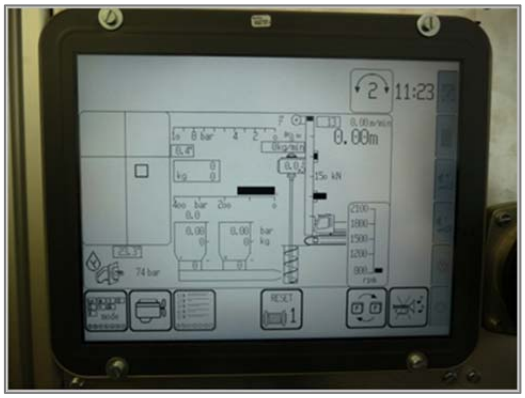

Photo 10: Monitor display in the cabin;

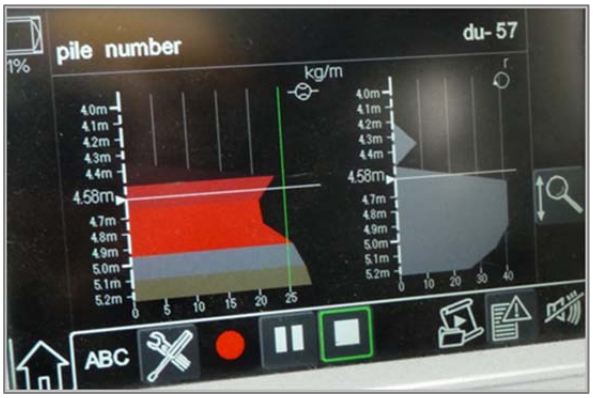

Photo11: PDE screen, visualisation of the column production

5.3. PDR process data reporting

PDR, the process data reporting software, enables comprehensive data evaluation and report generation on a PC. The recordings generated by the PDE® process data recording system can be imported and managed in PDR. Data are imported directly from the compact Flash memory card. The data can be displayed tabularly or as diagrams. An extensive data analysis (e.g. total consumption of binding agent, average production time) is possible. Using the report generator detailed jobsite descriptions can be generated. These reports are displayed in the form of depth-dependent and time-dependent diagrams and are individually configurable as required. They can either be printed directly or saved as PDF files. Figure 5 shows an example of a jobsite report after the column production.

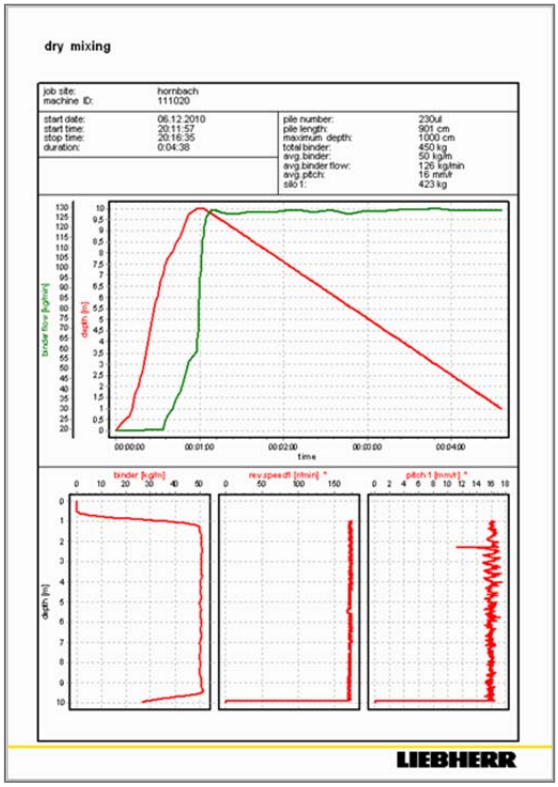

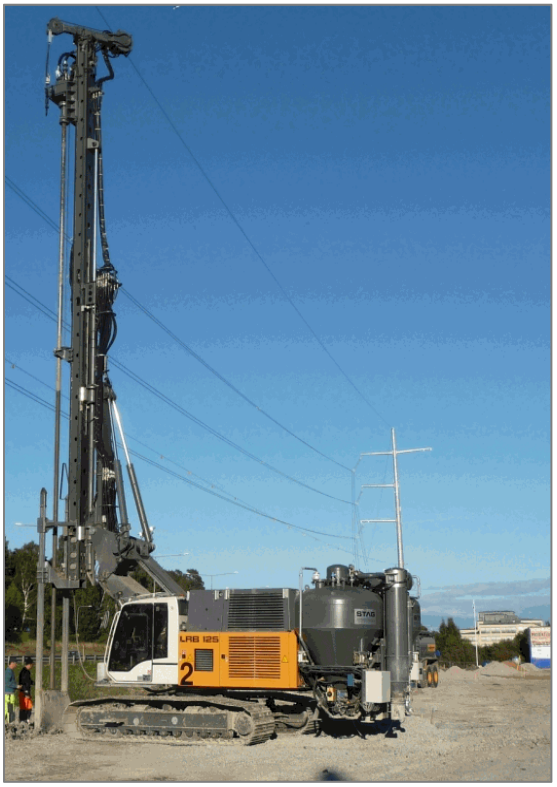

Figure 5: Jobsite report from the column no. 230 ul; Photo 12: Column production at the jobsite

5.4. Column penetration test jobsite Stockholm

In consideration of the specified design parameters a control plan was established to determine the quantity of columns to be tested in order to check the columns 'strength and ductility properties and their homogeneity. Therefore several columns were tested in the construction phase using the column penetration test. The column penetration test (KPS) is the most widely spread testing method for lime cement columns in Sweden. For this method a test probe with two wings is pressed into the lime cement column. The probe has a diameter of 36 mm and is pressed into the centre of the column with a continuous speed of approx. 20 mm/s. Thereby, the penetration resistance of the probe is measured and allows to determine the shear strength of the column. This method can be applied down to a column depth of approx. 8 m and an expected shear strength of < 150 kPa. The probe´s wings are 400 mm to 600 mm wide and must be 100 mm smaller than the column diameter. For longer or firmer columns there is a danger that the winged probe will deflect out of the lime cement column into the adjacent soil. With the help of a vertical borehole as a guide in the centre of these columns it is possible, however, to test longer columns with higher shear strengths. In this case the wings must be smaller (200 mm to 400 mm). Figure 6 shows the standard winged probe for the column penetration test according to the DIN standard EN 14679.

According to the equation (1) the undrained shear strength is calculated as follows:

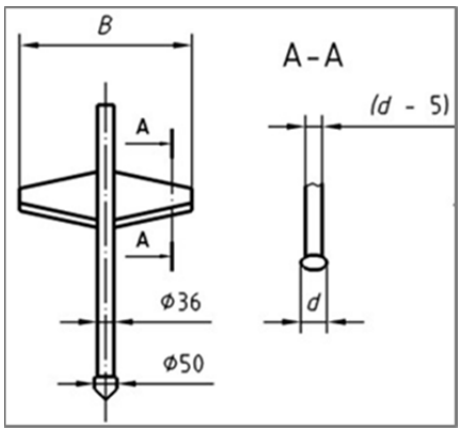

Figure 6: Test probe for column penetration test [DIN EN 14679]

$$C_{fu} = \frac{F}{Nc * A} \qquad (1)$$

With C_{fu} = undrained shear strength [kPa]
F = penetration resistance of the probe [kN]
N_c = empirical correction value [-]
A = surface of the winged probe [m²]

The column tests carried out on the jobsite were standard column penetration tests (KPS tests). The tested columns had a diameter of 800 mm and lengths between 12 m and 17 m. As vertical guides boreholes with a diameter of 57 mm were drilled into the centre of the columns. The winged probe featured a wing width of 250 mm. On the basis of the measured penetration resistances the corresponding undrained shear strengths were estimated. The test results are specified in figures 7 and 8.

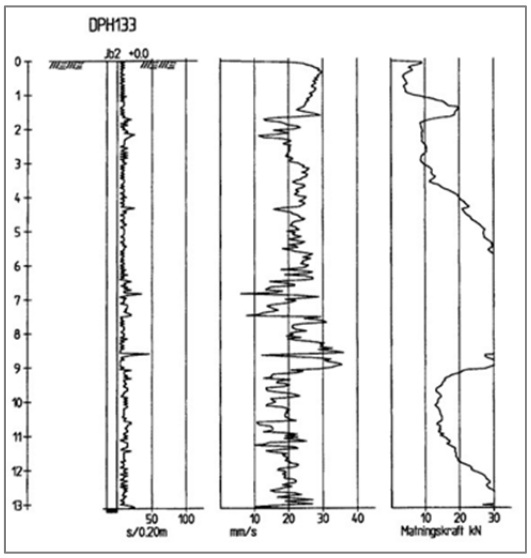

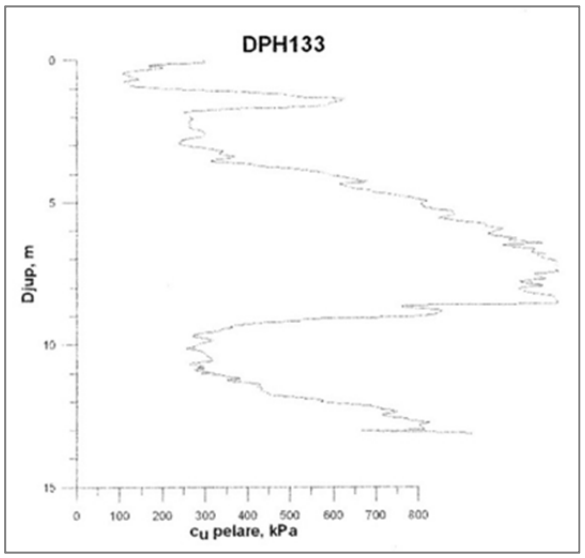

Figures 7 and 8: Test results for column no. DPH 133 [Fa. Bjerking 2010]

6. SUMMARY AND OUTLOOK

Due to growing practical experience over the last decades and increasing environmental awareness the method of deep mixing has continuously developed. Today this quiet and vibration-free process represents a very cost-effective and efficient method for stabilizing soils susceptible to settling.

With the LRB 125 XL carrier machine and the lime cement station a new equipment combination for the dry mixing method was developed offering a series of technical advantages related to execution.

The LRB 125 XL carrier machine is known as a reliable piling and drilling rig for leader-mounted work. Due to its high hydraulic power, the transfer of high push and pull forces and its high torque it has proved its worth in the most various fields of application such as vibrating, impact pile driving and drilling. Thus, this multi-functional machine is not only suitable for dry mixing but also for a large number of common deep foundation applications.

Thanks to the robust and rigid leader design high crowd forces can be applied and thus high penetration speeds with the mixing tool are achieved. Moreover, the hydraulically adjustable leader system with automatic leader alignment facilitates positioning and alignment on the new drilling point.

Further advantages result from the equipment design of fitting the lime cement station with two silos and mounting it on the back of the machine in order to form a compact machine unit. Thus, the filling process can be carried out during column production and no interruptions of work are caused. Furthermore, a compact machine unit is much more flexible during the production process, especially with numerous repositioning operations. Likewise, delivery of materials is carried out by an off-road truck so there is no need for the carrier machine to travel long distances to the binder depot.

The LITRONIC control system developed and manufactured by LIEBHERR includes all control and monitoring functions and is operated entirely from the cab. Thanks to the electronic control system most of the working processes are fully automated. Moreover, several additional process-related control elements optimizing the quality of the production process are implemented in the LITRONIC control system. In addition, high quality production is guaranteed through quality assurance using the PDE® process data recording system. This system records and visualizes all process data. The process data reporting software PDR allows the generation of individual and detailed protocols of every single column using a report generator.

The target to develop an economic and efficient machine and to fulfil the procedural requirements in comparison with the technologies already applied in Scandinavia was achieved. Thanks to a powerful and compact machine combined with a high level of automation very high daily production rates were attained. The LRB 125 XL with lime cement station excels above all in its high flexibility and ease of operation.

Technological developments such as a leader extension in order to install columns down to greater depths are planned for the future. This is to meet with the requests to produce columns down to 22 m depth using this equipment combination and applying the “Nordic method”. Moreover, further developments of the LITRONIC control system are projected in order to achieve even better quality assurance and user-friendliness.

REFERENCES

Deutsches Institut für Normung e.V. (2005): DIN EN 14679 Ausführung von besonderen geotechnischen Arbeiten (Spezialtiefbau) – Tiefreichende Bodenstabilisierung; Deutsche Fassung EN 14679:2005, Beuth Verlag, Berlin

LIEBHERR – BVV (2010): Soil Mixing Verfahren/ Firmenprospekt, Nenzing

Topolnicki, M.; Trunk U. (2006): Tiefreichende Bodenstabilisierung – Einsatz im Verkehrswegebau für Baugrundverbesserungen und Gründungen; Vortrag auf dem Geotechnik Tag an der TU München, Fachaufsatz 32 – 56 D; Keller Grundbau GmbH

Massarsch, K.R.; Topolnicki, M.: Regional Report: European Practice of Soil Mixing Technology

Fransson, J. (2011): A study of the correlation between soil-rock sounding and column penetration test data; KTH Architecture and the Built Environment

Andersson, M. et al (2009): Djupstabilisering i sulfidjord – laboratorie – och fältstudie; Swedish Geotechnical Institute, Linköping
Author, Year, Title, Journal/ Place of issue/Editor

Parametric study of embankments founded on soft organic clay using numerical simulations

K. Suganya, Indian Institute of Science, Bangalore, India, suganyak@civil.iisc.ernet.in
P. V. Sivapullaiah, Indian Institute of Science, Bangalore, India, siva@civil.iisc.ernet.in

ABSTRACT

Embankments founded on deep mixed soil-cement (DMC) column reinforced soft organic clay ground results in enhanced bearing capacity and reduced settlements. The extent of improvement in stability and settlement characteristics of embankments founded on deep mixed column improved ground mainly depend up on the properties of DMC columns, column spacing and column diameter. Laboratory studies revealed that the water cement ratio plays a significant role in determining the engineering behaviour of the DMC columns. The paper investigates through two dimensional finite difference method (FLAC 2D) with advanced constitutive models, the performance of embankments founded on organic clay stratum reinforced with deep mixed columns. Settlement, excess pore pressures and factor of safety got from numerical simulations are used in the study for analyzing the predicted responses for various cases. Initially embankments with out the columnar inclusions were analyzed. Then the effect of parametric variations such as properties of the DMC columns, column spacing, column diameter and inclusion of mass stabilized zone has been analysed.

1. INRODUCTION

Structures founded on soft organic clays have high probability of foundation failures such as bearing capacity failure and excessive settlement. With growing need for infrastructural developments it is necessary to construct various structures on soft grounds also. Hence various techniques are used to improve the soft ground and safely construct over it. Most widely used techniques for improving soft soil deposits are preloading, stone columns, deep mixing, mass stabilization and rigid piling. Deep mixed soil-cement columns are used for improving soft organic clay extending to great depths especially when the construction has to be speeded up and when differential settlements with respect to the adjacent structure are to be restricted. DMC columns are widely used for supporting embankments on soft soils in countries like Japan, Sweden, and the United Kingdom. Several case histories are reported in literature regarding the successful use of DMC columns for improving soft ground [1] & [2].

The soft organic clay considered in this study is Kuttanad clay in Kerala, India. Kuttanad clay has a very low shear strength and high compressibility. The in situ water content of the clay ranges from 100 to 200 %, almost equal to or more than its liquid limit. Ramanatha Ayyar [3] has reported failure of embankments of even 2 m height when founded on Kuttanad clay. So it is mandatory to improve the ground before going in for any kind of infrastructural development. The effect of techniques such as preloading and stone columns in improving Kuttanad clay have been investigated by researchers in recent past [4-6]. Ground improvement with in situ deep mixed cement columns has advantages of accelerated construction and reduced settlements and is a promising technique that can be used for improving Kuttanad clay. In the present study a numerical analysis is conducted to evaluate the performance of the deep mixed soil cement column technique for supporting a typical highway embankment using two dimensional Finite difference program, Fast Lagrangian Analysis of Continua (FLAC). FLAC2D was chosen for carrying out the numerical simulations because it is widely used by many researchers to effectively model column-supported embankments [7-9].

Its well established [10] that the water cement ratio (WC) is the critical factor which governs the shear strength characteristics of the soil cement columns. The shear strength parameters of cement mixed Kuttanad clay at different water cement ratios got through detailed laboratory investigation was used in the analysis to simulate the effect of column properties on the embankment performance. Sodium silicate(NaSi) was used with cement and was found to be effective in improving the shear strength of the soil cement column to a great extent and hence the performance of the soil cement column with sodium silicate additive was also investigated.

Parametric study was conducted in terms of embankment settlement and lateral displacement by varying the important design factors such as column diameter, column spacing and depth of mass stabilized zone

beneath the embankment. Researchers[9] have worked on the effect of the constitutive models used for analysis of the embankment and reported that material properties chosen based on the model used to simulate the foundation can have effect on the predicted responses. Hence in the present study two series of FLAC analysis were performed to compare the behaviour Modified Cam Clay(MCC) modeled DMC columns to the behaviour of Mohr Coulomb modeled columns for different columns properties. The model parameters were obtained from the results of an extensive laboratory test program performed which included Unconfined Compressive Strength tests, triaxial compression and 1-D consolidation.

2. NUMERICAL MODEL

The finite-difference code FLAC 2D [11] was used in simulating the performance of the embankments constructed on the Kuttanad clay, reinforced with deep mixed cement columns. The foundation soil is assumed to have 10 m thick Kuttanad clay overlying 5 m thick sand and the embankment height chosen was 3 m. Due to the symmetry of the model only half of the cross-section was analyzed using the FLAC software. Rows of DMC columns were modeled as continuous strips running parallel to the centerline of the embankment as shown in the schematic sketch, Fig.1. The dimensions and spacing of DMC columns and the overall embankment and foundation dimensions were selected based on a common practice in the field.

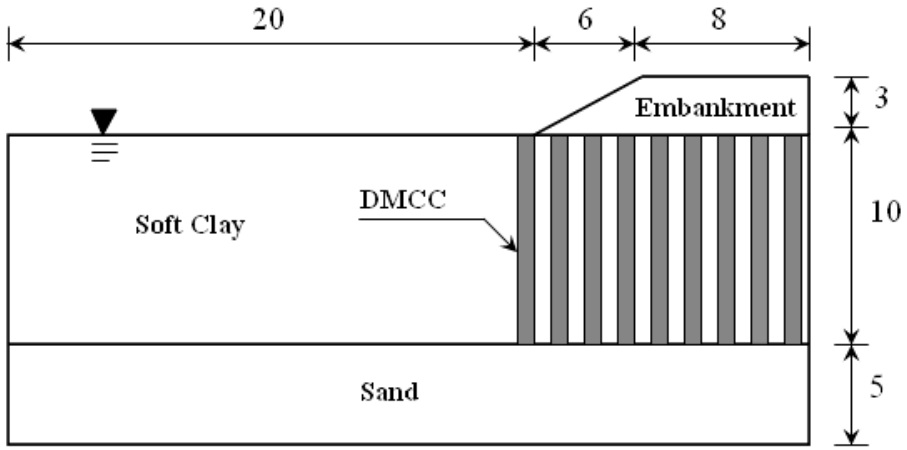

Figure 1: *Half section view of embankment on DMC columns (all dimensions in m)*

The model geometry was discretized in to 8400 zones. The minimum mesh width used was 0.2 m in regions of high stress and strain gradients. One of the vertical boundaries was fixed at 20 m away from the toe of the embankment to have minimal boundary effects [8]. The horizontal boundary underlying the sand layer was fixed for displacements in both x and y directions. The vertical boundaries were fixed for horizontal displacements but vertical displacements were allowed.

The embankment, the foundation soft soil, and the DMC columns were modeled as linearly elastic-perfectly plastic materials with Mohr – Coulomb failure criteria. Initially the foundation without embankment was analysed. Then the staged construction of embankment was modeled in the current analysis by increasing the height with 1 m lifts until it reached the final height of 3 m. After placing each lift, the model was run to equilibrium with no drainage allowed and the bulk modulus of water set to 200 MPa. The vertical settlements were measured at the embankment base and the horizontal displacement profile was monitored at the toe of the embankment. The embankment over unimproved ground was analysed as reference case. The parameters used for modeling the embankment, soft clay and the under lying sand layer are listed in Table 1. In addition to it the DMC column properties varied in the model corresponding to two different water cement ratios and one with Sodium Silicate additive is also listed.

Table 1: Properties of Foundation soil, Embankment and DMC columns

Material Properties	Soft Clay	Sand layer	Embankment	DMC columns, Initial water content (IW) = 165 %		
				WC 6.5	WC 3.33	WC 3.33 (10 % NaSi)
Dry density (kg/m3)	617	2100	1800	629	707	732
Bulk Modulus (MPa)	3.6	26.7	26.7	12.0	24.9	28.4
Shear Modulus (MPa)	1.3	16.0	16.0	4.6	9.6	10.9
Cohesion (kPa)	7	0	1	32	125	295
Friction angle (degrees)	0	35	35	0	0	0
Poisson's ratio	0.33	0.25	0.25	0.33	0.33	0.33
Porosity	0.76	0.31	0.45	0.75	0.73	0.71
Permeability (cm/s)	1.59×10^{-8}	2×10^{-4}	1×10^{-5}	3.97×10^{-8}	6.2×10^{-8}	4.9×10^{-8}

In the first case DMC columns were located on a 1.6 m by 1.6 m rectangular spacing beneath the embankment materials. The columns were added in the numerical model by changing zones representing columns from clay properties to the column properties. Initially strip width of 1 m representing an area improvement ratio (AIR) of 39 % was used in the analysis where AIR [12] is given by,

$$AIR = \frac{A_c}{A} \tag{1}$$

A_c= Cross sectional area of the column

A = Total cross sectional area improved by column

Rows of columns in the present model were represented with nine strips in the foundation running parallel to the centre line of the embambant. For the same DMC column spacing and cross section a series of analysis was carried out with different column strengths corresponding to varying water cement ratios as listed in Table 1.

Table 2: Modified Cam Clay Material properties

	DMCC , IW = 165 %	
Material	WC 6.5	WC 3.33
Dry density (kg/m3)	629	707
Bulk Modulus K_{max} (MPa)	14.3	44.5
Kappa(κ)	0.020	0.006
Lambda(λ)	0.52	0.42
Frictional constant, M	1.37	1.64
Preconsolidation Pressure (kPa)	85	320
Reference Presure (kPa)	1	1
Specific Volume (V_Γ)	6.15	5.84
Poisson's ratio	0.33	0.33
Porosity	0.75	0.73
Permeability (cm/s)	3.97×10^{-8}	6.2×10^{-8}

As a part of the parametric study, centre to centre column spacing was reduced to 1.4 m and analysis was carried out with the same strip width of 1 m. Then the clear spacing between the strips was kept as 0.6 m as in the first case and the strip width was increased to 1.4 m and the simulations were carried out in order to understand the effect of increased column diameter on the settlement and lateral displacement response. In addition to this another series of numerical analysis was carried out with the DMC columns

being modeled as Modified Cam Clay (MCC) material with the properties listed in Table 2. The MCC properties for modeling the DMC columns were obtained by conducting a series Triaxial compression tests and 1 dimensional consolidation tests. For the MCC model, K_{max}, which is an upper bound for the soil bulk modulus was used as an input parameter [9].

3. PARAMETRIC STUDY

3.1 Influence of column properties

The displacement vectors of the unimproved ground under the embankment are shown in Fig.2. It can be observed that the failure has occurred along the circular slip surface. It is also clearly seen that the slip surface is restricted by the firm layer of sand beneath the soft clay.

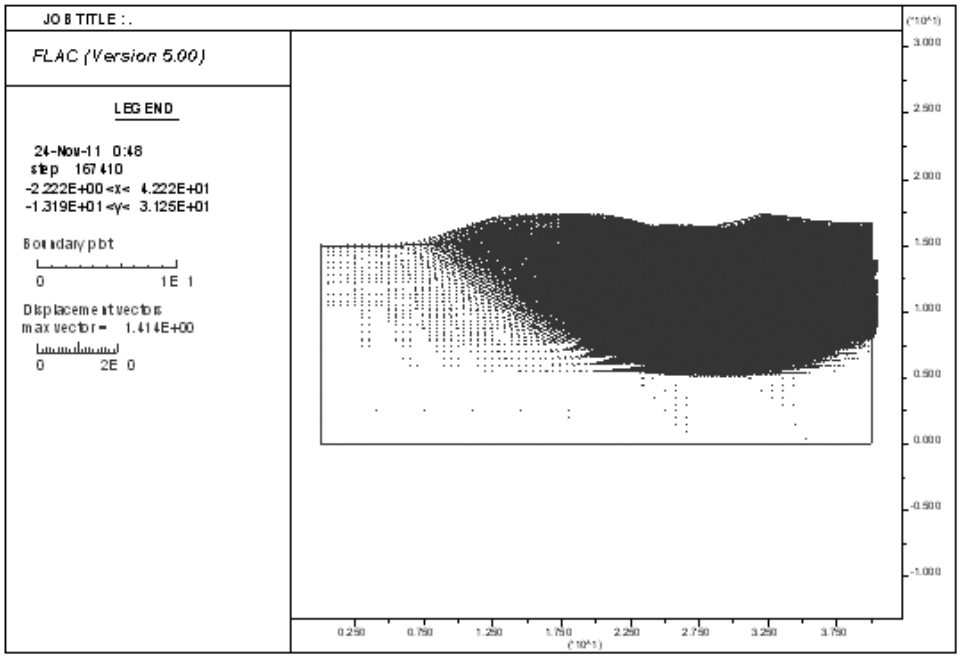

Figure 2: Displacement vector of the unimproved ground

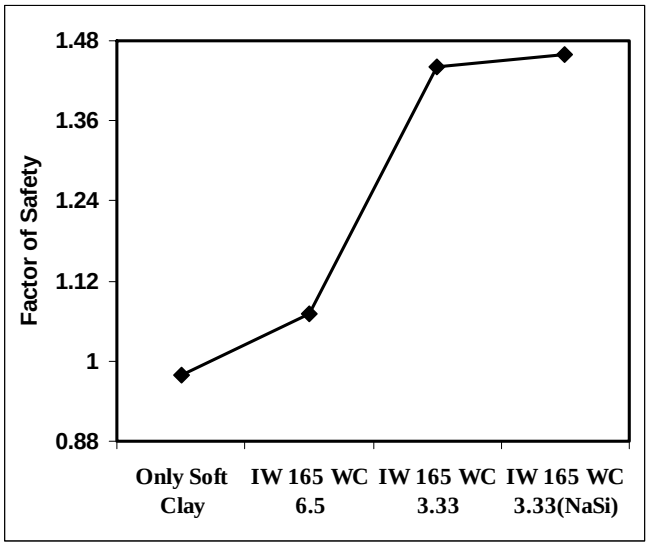

Figure3: Influence of column properties on Factor of Safety

The influence of column properties on the factor of safety (FOS) of the embankment over DMC columns is shown in Fig. 3. FLAC has an automated procedure to evaluate the FOS by reducing strength values to determine the point of impending failure, at which the model is no longer in equilibrium. The FOS of the embankment founded on the in situ soil without DMC columns was 0.98. With inclusion of DMC

columns having a higher water cement ratio of 6.5, the FOS increased to 1.07. When the analysis was again carried out with properties of DMC columns corresponding to a lower WC ratio say 3.33, FOS further increased to 1.44. Sodium Silicate additive with cement at WC of 3.33 significantly improves the column cohesion and modulus. But when the columns were modeled with the corresponding properties the enhancement in the FOS value was very less.

The predicted surface settlements beneath the embankment for different column properties are shown in the Fig. 4. The numerically simulated settlement responses beneath the embankment show a reduction of maximum settlement of the foundation soil with provision of DMC columns. And the settlements observed reduce with reducing water cement ratio of the DMC columns. The effect of Sodium Silicate additive along with cement (WC 3.33) and subsequent increment in column strength does not have a major influence on the settlement reduction. For DMC columns with W/C ratio 3.33 the settlement decreased from 139 cm to 4 cm. DMC reinforcement also causes reduced differential settlement between the column and the soft foundation soil.

The heave outside the embankment toe decreased (Fig. 4) with reinforcement of the foundation soil with DMC columns. The reduction of heave is more as the columns get stiffer. The predicted heave reduced from 63 cm for the unreinforced case to 1.35 cm for the soil cement column having WC 3.33 with sodium silicate additive.

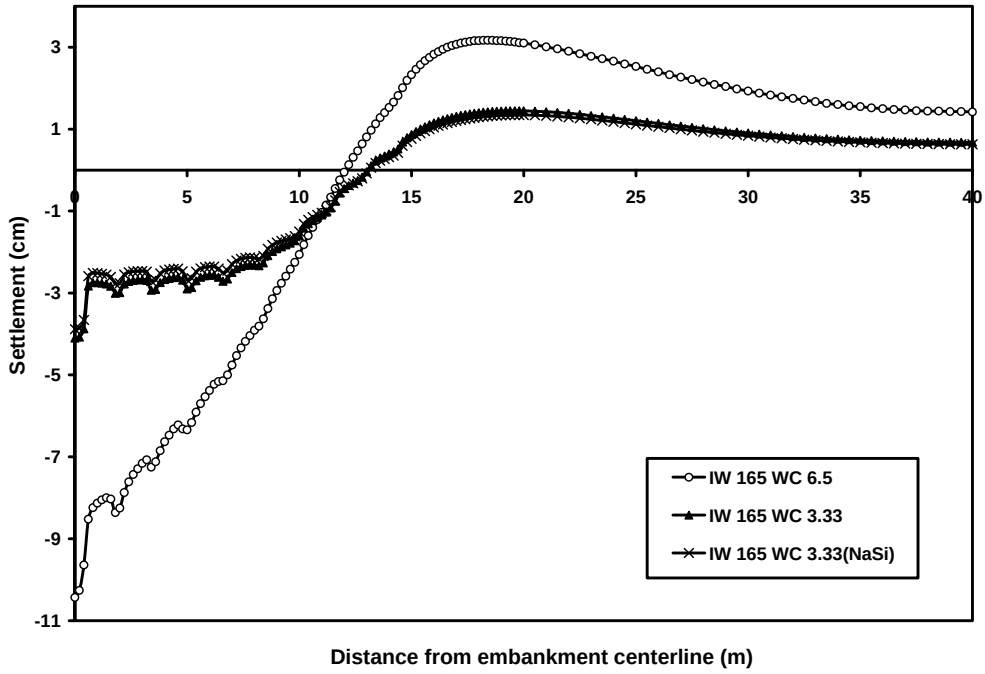

Figure 4: Vertical Displacement along base of the embankment supported on DMC columns

The numerical analysis results of horizontal displacement trends at the embankment toe are shown in Fig. 5. The maximum horizontal displacement with out reinforcement was as high as 100 cm near the toe and with introduction of DMC columns(W/C 3.33) it got reduced to a great extent as low as 3.2 cm. The variation of the predicted pore pressures with depth along the centre line of the embankment is shown in Fig. 6. The pore pressure variation plots indicate that the development of excess pore pressure in the soft soil due to embankment loading reduces with introduction of DMC columns. With reducing water cement ratio of the columns the pore pressure development further reduces.

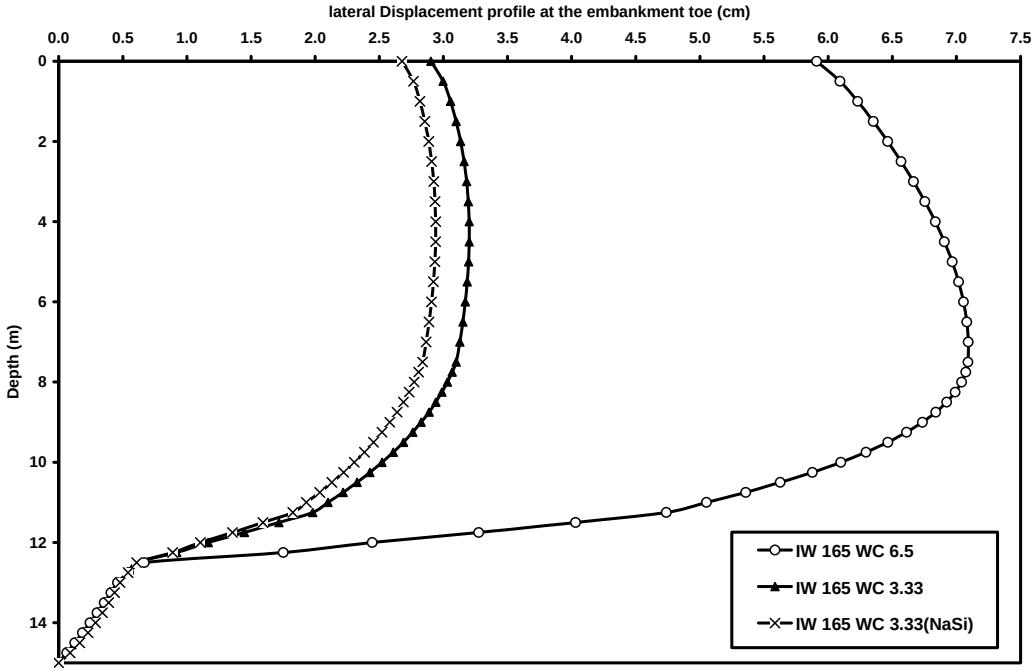

Figure 5: Horizontal Displacement profile at the toe of the embankment supported on DMCC columns

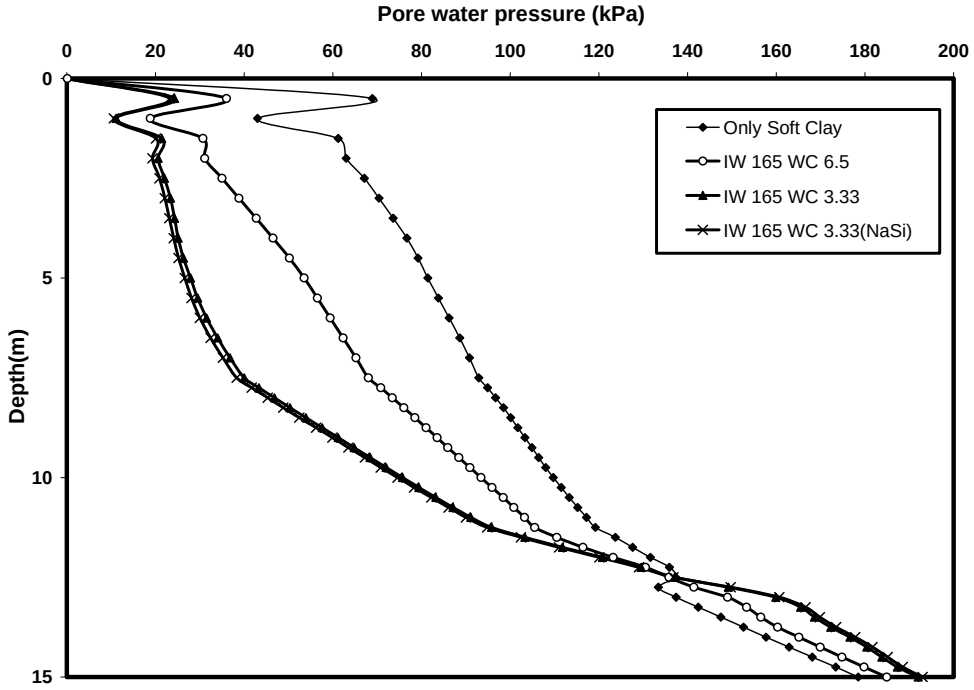

Figure 6: Pore Pressures distribution beneath center of embankment

3.2 Influence of column spacing, column area and introduction of mass stabilized zone

For the DMC column (WC 3.33) supported embankment system the strip width was kept constant and the centre to centre column spacing was reduced to 1.4 m from 1.6 m which resulted in an equivalent increase of area improvement ratio from 39 % to 51 %. As can be seen from the Fig. 7 & 8 the maximum settlement and horizontal displacement reduced by 7 % and 12 % respectively owing to the reduction in spacing of the columns.

In order to study the effect of column area on the settlement characteristics, the strip width used in the analysis was increased to 1.4 m instead of 1m. The corresponding area improvement ratio for such an arrangement increases to 49 %. Now from the simulation results (Fig. 7 & 8) we can see that the maximum settlement reduced by 17 % and horizontal displacements reduced by 15 % with increase in column area.

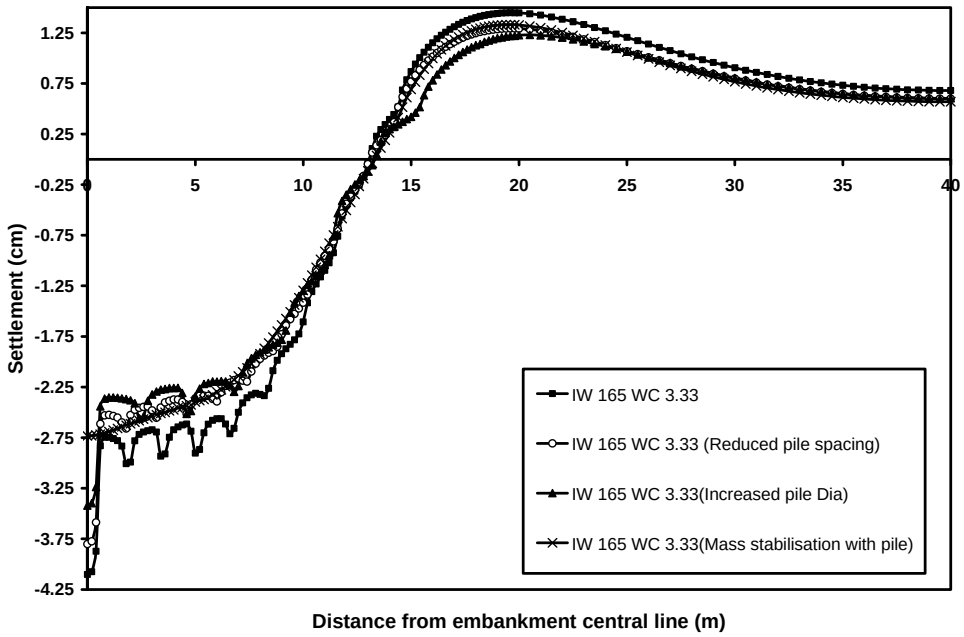

Figure7: Vertical Displacement profile along base of the embankment supported on DMCC columns

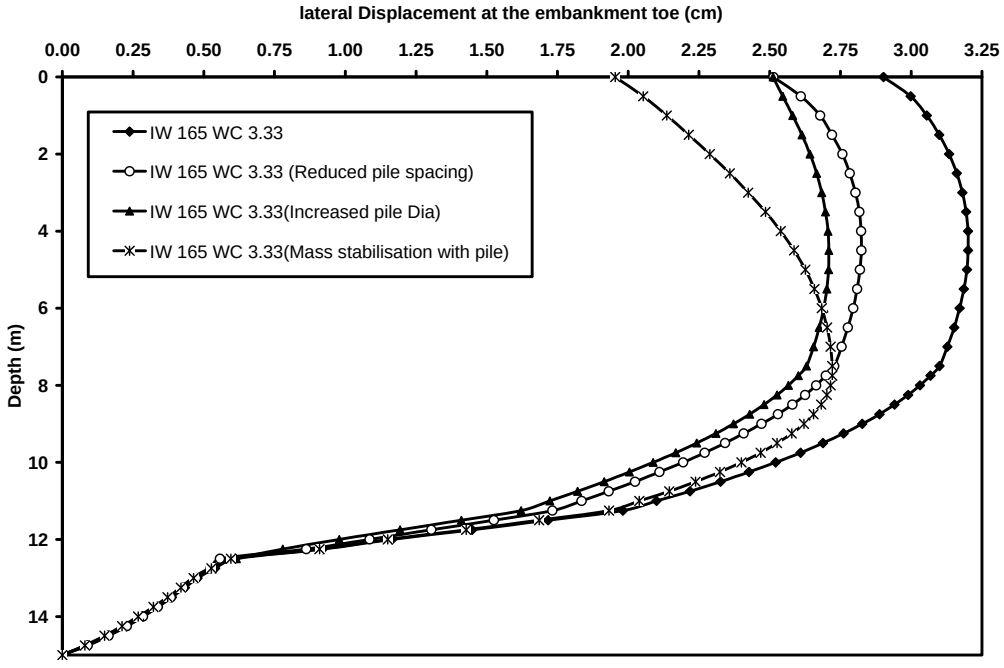

Figure 8: Horizontal Displacement profile at the toe of the embankment supported on DMCC columns

Another analysis was carried out with a mass stabilized zone of 2 m depth between the embankment and the columns. Mass stabilized zone had the same properties as that of columns (WC 3.33). The simulation results (Fig. 7 & 8) show that the mass stabilized zone is capable of reducing the maximum settlement of the foundation soil by 33 % as compared to the column only case. From the numerically simulated results the provision of mass stabilized zone above the columns seems to be more effective in reducing the settlements as compared to column area increase or the column spacing reduction techniques. The

magnitude of reduction of horizontal displacement was 15 % which was found to be same as that of the previous case where the column area was increased.

3.3 Influence of pile material modelling

In the previous cases the pile material was modeled as linearly elastic, perfectly plastic with the Mohr-Coulomb failure criteria. Previous studies [13] report that Modified Cam Clay model (MCC) has a good ability to predict the behaviour of soil. Hence the analysis was repeated by simulating the DMC columns (WC 6.5 and 3.33) with MCC model. The studies revealed (Fig. 9) that when the columns were modeled as MCC material the settlements predicted was higher compared to columns modeled with Mohr-Coulomb failure criteria. The percentage increase in maximum settlement was about 18 % when MCC properties were used in modelling DMC columns. Hence it can be understood that Mohr- Coulomb model when used for simulating the columns underestimates the settlements. Settlement analysis with MCC modeled columns predicts the material behavior better and hence expected to give more realistic predictions of settlement.

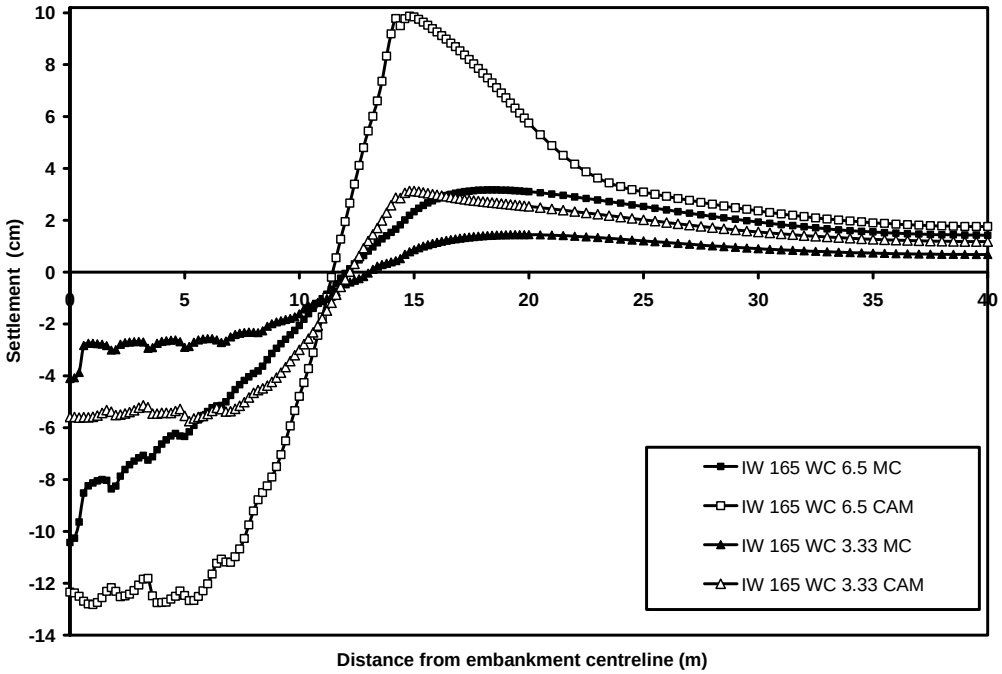

Figure 9: Vertical Displacement profile along base of the embankment

4. CONCLUSION

In this work the factor of safety, settlement and horizontal displacement of embankments on soft soil with and without DMC columns has been analysed using FLAC modeling. The following are the main conclusions:

1. The provision of DMC columns is found to be effective in improving the overall performance of the foundation for embankment construction in terms of settlement, horizontal displacement and Factor of safety.
2. With reduction in water cement ratio of the DMC columnar inclusions it was found that the stability and settlement characteristics of the embankment foundation system improved, for a given column spacing and area.
3. Though Sodium silicate additive along with cement for WC of 3.33 has considerably improved column strength characteristics its effect on FOS and settlements calculated using FLAC was less significant.
4. With WC of 3.33, as the column spacing reduces, settlement and horizontal displacement of foundation soil reduces. There is a further decrease in settlement and horizontal displacement of foundation soil with increase in column area.
5. Mass stabilized clay beneath the embankment along with columns is found to be effective in reducing the settlement and the horizontal displacement of the soft clay foundation.
6. DMC columns simulated with MCC model predict more settlement when compared to the Mohr-Coulomb model.

REFERENCES

[1] *Bergado, D. T., Ruenkrairergsa, T., Taesiri, Y., and Balasubramaniam, A.S. (1999), Deep soil mixing to reduce embankment settlement. Ground Improvement J., 3(3), 145–162.*

[2] *Lin, K.Q. and Wong, I.H. (1999), Use of deep cement mixing to reduce settlements at bridge approaches. Journal of Geotechnical and Geoenvironmental Engineering, ASCE, 125(4): 309-320.*

[3] *Ramanatha Ayyar, T.S. (1966), Strength Characteristics of Kuttanad Clays, Ph.D. Thesis, University of Roorkee, Roorkee, India.*

[4] *Bindu, J. and Vinod, P. (2008), Mini-plate load test on preloaded Kuttanad clay, Proceedings of Indian geotechnical Conference (IGC 2008), 2: 90-91.*

[5] *Bindu, J. and Vinod, P. (2010), Design of preload for reducing the compressibility of kuttanad clays, Proceedings of International Conference on Materials, Mechanics and Management (IMMM-2010), 1:424-428.*

[6] *Isaac, D.S. and Girish M.S, (2009), Suitability of Different Materials for Stone Column Construction, Electronic Journal of Geotechnical Engineering, 14: 1-12.*

[7] *Han, J., Chai, J.C., Leshchinsky, D., and Shen, S.L. (2004), Evaluation of deep-seated slope stability of embankments over deep mixed foundations. Geotechnical Special Publication No. 124, J.P. Turner and P.W. Mayne (eds), GeoSupport 2004, ASCE Geo-Institute and ADSC, Jan. 29-31, Orlando, 945-954.*

[8] *Abusharar, S.W. and Han, J. (2011), Two-dimensional deep-seated slope stability analysis of embankments over stone column-improved soft clay, Engineering Geology, 120: 103-110.*

[9] *Navin, M.P. (2005), Stability of Embankments Founded on Soft Soil Improved with Deep-Mixing-Method Columns, Ph.D. Thesis, Virginia Polytechnic Institute and State University, Blacksburg, VA.*

[10] *Miura, N., Horpibulsok, S., and Nagaraj, T. S. (2001), Engineering behavior of cement stabilized clay at high water content, Soils Found., 41(5): 33–45.*

[11] *ITASCA (2002), Fast Lagrangian Analysis of Continua, FLAC2D, Itasca Consulting Group,Ltd.*

[12] *Chai, J. and Carter, J.P. (2011), Deformation Analysis in Soft Ground Improvement, Springer Verlag, New York.*

[13] *Oliveira, P.J. V., Pinheiro, J.L.P., and Correiaa, A.A.S. (2011), Numerical analysis of an embankment built on soft soil reinforced with deep mixing columns: Parametric study, Computers and Geotechnics, 38(4):566-576.*

Design of in-situ soil mixing

Michal Topolnicki, Keller Polska Sp. z o. o., Poland, mtopolnicki@keller.com.pl
Paul Pandrea, Keller Holding GmbH, Germany, p.pandrea@kellerholding.com

ABSTRACT

In-situ soil mixing has become a widely and successfully used technique to improve soil properties, treat or encapsulate contaminated soil and to form elements and bodies with static effect. The design procedure for this method however is very different from that of other elements comprising only standardized and fully controllable components like piles, diaphragm walls and others due to the use of the existing soil as an essential component of the final product. Its physical and chemical properties govern the achievable strength, stiffness and permeability.
Therefore the design process is done in several steps. First a suitable mixing process has to be selected in compliance with the scope of work and the existing soil, then the possible strength and stiffness has to be assessed and finally the geometry and its coverage by the single elements has to be fixed.
The first step depends mainly on the available machinery and mixing tools of which innumerable types and variants exist. As long as a sufficient mixing of soil and binder is granted (e.g. expressed as a blade rotation number) the selection is an objective of the economic optimization. The last step is subject to conventional geotechnical design. Although it might be very complex it is well covered by the rules fixed in the known standard codes for design.
The second of the above mentioned steps is the most difficult and requires a lot of engineering experience and appropriate statistical models. The same amount and type of binder in two different types of soil can result in very different strength and available laboratory tests for that usually cannot be fully transferred to field conditions. The necessity of a comprehensive continuous quality control to check the assumptions in reality in every project is obvious. The authors will present the current state of the art for the design of in-situ soil mixing in geotechnical practice and its representation in latest standardization attempts.

1. THE PROCESS OF IN-SITU SOIL MXING

Photo 1: DSM Mixing tool with three mixing shafts (property of Keller Grundbau GmbH)

Today a wide variety of different machines and tools are offered on the market for in-situ soil mixing. Although the jet-grouting method using pure hydraulic energy to mix the soil with binder can be seen as one (extreme) form of the method, mechanical mixing with and without support by hydraulic energy has proven to be the most effective mixing technique. The mixing technology applied has to make sure that the soil is mixed with the binder sufficiently to achieve a homogeneous product with a low coefficient of variation for its strength. As a simple index or parameter to quantify the used mixing energy the so called blade rotation number has been introduced first in Japan (e.g. [2]) as a parameter indicating the amount of energy used to mix the soil with binder. Indicator in this sense means that it is not a physically correct value.

The blade rotation number gives the number of passes of mixing blades through 1 m of (single shaft) movement through the soil. For the case that the binder is injected during penetration through an outlet located below the blades the formula to calculate is given in [1] as

$$T = \sum M \cdot \left(\frac{R_p}{V_p} + \frac{R_w}{V_w}\right) \quad (1)$$

T = Blade Rotation Number [R/m]
$\sum M$ = Total number of mixing blades
R_p = Rotational speed during penetration [R/min]
V_p = Penetration Velocity [m/min]
R_w = Rotational speed during withdrawal [R/min]
V_p = Penetration Velocity [m/min]

One full diameter blade mounted on a shaft increases $\sum M$ by 2. As an example for the tool in the left picture below the total $\sum M$ is 8.

Photo 2: DSM Mixing tool with one shaft and four blades (left) and rig with single shaft mixing tool (right) (property of Keller Grundbau GmbH)

The minimum required blade rotation number depends on the soil type. For cohesive and fine grained soils (loose sands and clays) about 400 R/m should be achieved to keep the coefficient of variation for the strength within acceptable limits. In non-cohesive and coarse soils slightly lower values can be sufficient.

2. UNCONFINED COMPRESSIVE STRENGTH

While the coefficient of variation for the unconfined compressive strength depends on the used mixing energy described by the blade rotation number the absolute value depends on the amount of binder and the soil type which contributes to the strength as the aggregate. So far there is no theoretical (chemical) or numerical model to predict that value with available input values. The only reliable source for predictions is experiences from the field. Some values are given in [1].

Table 1: Typical field strength and permeability for ranges of cement factors and soil types (Table 9.5 from [1])

Soil type	Cement factor α [kg/m³]	U.C.S. 28-days q_{uf} [MPa]	Permeability k [m/s]
Sludge	250 – 400	0.1 - 0.4	1×10-8
Peat, organic silts/clays	150 – 350	0.2 - 1.2	5×10-9
Soft clays	150 – 300	0.5 - 1.7	5×10-9
Medium/hard clays	120 – 300	0.7 - 2.5	5×10-9
Silts and silty sands	120 – 300	1.0 - 3.0	1×10-8
Fine-medium sands	120 – 300	1.5 - 5.0	5×10-8
Coarse sands and gravels	120 – 250	3.0 - 7.0	1×10-7

As one can see the unconfined compressive strength especially in cohesive and fine grained soils is lower than in non-cohesive and coarse grained soils. Almost all authors assume that the results of unconfined compressive strength tests fit into a normal distribution.

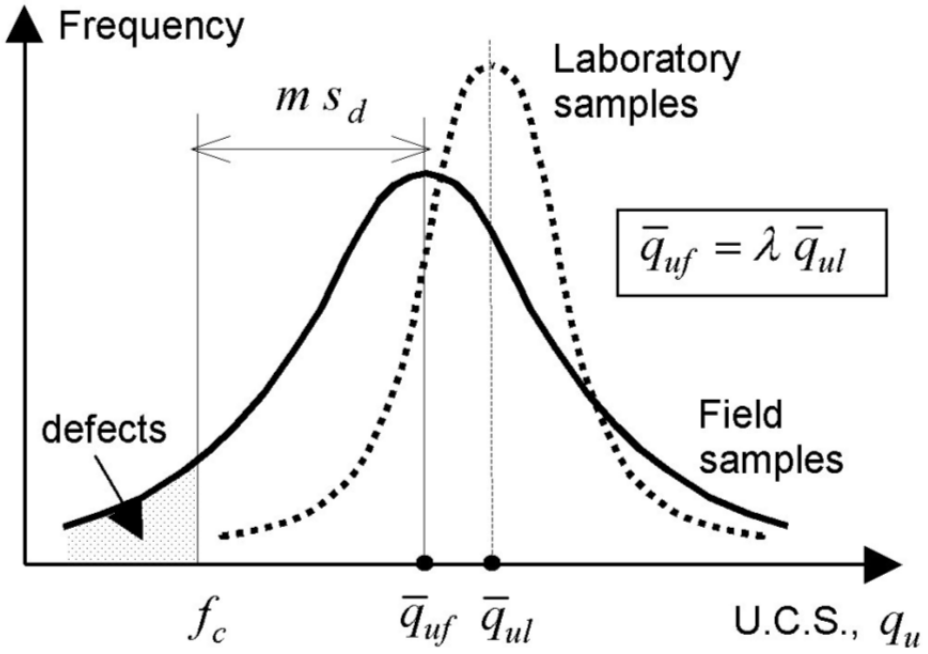

Figure 1: Normal distribution curves for field and laboratory strength data and assessment of the design strength f_c from [1, figure 9.38]

Based on this the strength used for design calculations f_c (in the nomenclature of the Eurocode this is the characteristic value) according to [1] theoretically could be defined as

$$f_c = \bar{q}_{uf} - m \cdot s_d \qquad (2)$$

f_c = Design strength or better characteristic strength from unconfined compressive strength tests
$\overline{q_{uf}}$ = Mean value for the unconfined compressive strength from field tests
m = A factor representing a certain confidence value (e.g. 95%)
s_d = Standard deviation

The unmodified application of the common normal distribution however can lead to strange results as the following example from [3] shows. On a real (jet-grouting) site the following values for the unconfined compressive strength were obtained:

Table 2: UCS [MN/m²] of a series of test samples from a real site from [3]

UCS [MN/m²]	**2,6**	**3,1**	**12,0**	**2,7**	**19,0**	**4,30**

The mean value of theses samples is 7.2833 MN/m² and the standard deviation is 6.7656 MN/m². The 5%-quantile, a commonly used value to determine the characteristic strength for materials, is -3.85 MN/m² in this case, a completely useless value.

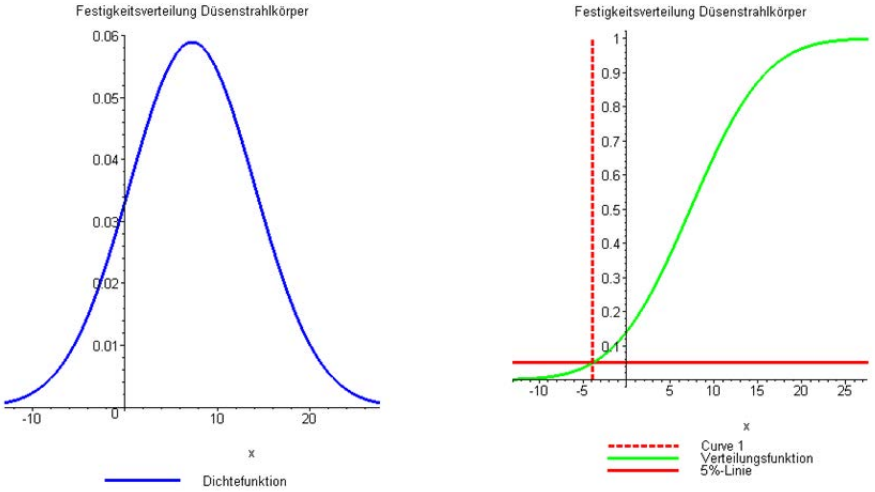

Figure 2: Normal distribution and 5%-quantile for the values from table 1 from [3]

The mathematically correct solution to overcome this problem would be the application of the logarithmic normal distribution which delivers a more realistic image as can be seen from the following figure showing the difference between the normal distribution and the logarithmic normal distribution for case histories with 32 test samples from [3].

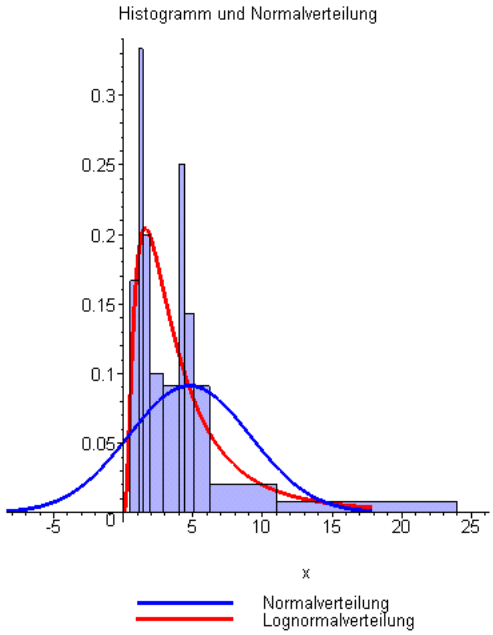

Figure 3: Normal distribution and logarithmic normal distribution for a total of 32 samples from [3]

In practice not the complex logarithmic normal distribution is used. To overcome the problem described above and for the sake of simplicity equation (2) is modified as follows:

$f_c = \alpha \cdot \bar{q}_{uf}$ (3)

f_c = Design strength
$\overline{q_{uf}}$ = Mean value for the unconfined compressive strength from field tests
α = A factor representing a certain confidence and safety level ($\alpha < 1$)

This mathematical formulation avoids negative values for f_c. For the calculation of α different methods have been developed in Japan and in Europe.

3. FORMALIZED DESIGN APPROACHES

3.1. Japan

Based on a large database of 26 case histories from [4] in [5] and [6] it was suggested to use equation (3) with the following algorithm to calculate α:

$f_c = \alpha \cdot \bar{q}_{uf}$ and $\alpha = \alpha_1 \cdot \alpha_2 \cdot \alpha_3$ (4)

α_1 = Factor taking into account the coefficient of variation (0.5 to 0.6)
α_2 = Factor considering the reliability of overlapping of columns (0.8 to 0.9)
α_3 = Factor considering the untreated soil inbetween the columns (typically 0.7 to 0.9)

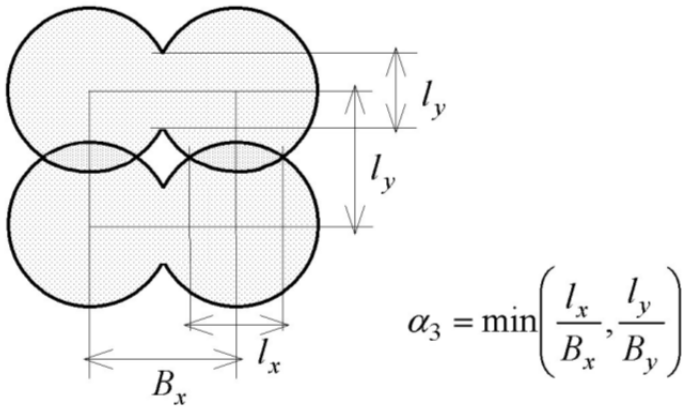

Figure 4: Normal distribution and logarithmic normal distribution for a total of 32 samples from [1] and [6]

For standalone columns α_2 and α_3 can be set to 1.0. If laboratory tests are used instead of field data a correction is introduced assuming that strength in the field is lower and varies more than strength for laboratory samples. Then equation (4) is modified according to [1] as follows:

$f_c = \alpha \cdot \lambda \cdot \bar{q}_{ul}$ (5)

λ = Factor taking into account the difference between field and laboratory data (usually 0.5 to 1.0)
$\bar{q}_{ul}$ = UCS of laboritory mixed samples

From the characteristic strength obtained with the equations (4) or (5) another step has to be made to come to allowed or better design values for the unconfined compressive strength:

$f_{ca} = f_{cd} = \frac{f_c}{F_s}$ (6)

f_{ca} = Allowable compressive strength
f_{cd} = Design value of the compressive strength
F_s = Safety factor (global or partial)

Under an appropriate quality management program, which is necessary for every project, this design value calculated in advance as a prediction to find an arrangement pattern for the columns has to be compared with the real results obtained from field. At this point it has to be stated that proper and state of the art sampling is essential and that in many cases insufficient strength values do not indicate a real lack of strength but rather poor sampling on site.

In Japan also for the evaluation of the field results a statistical approach is used. Based on the number of samples tested a minimum mean value to be achieved in the field is calculated according to [7]:

$$\bar{q}_{uN} \geq \frac{f_{cd} \cdot F_S}{1 - k_a \cdot v_d} \; with \; \bar{q}_{uN} = \frac{\sum_{i=1}^{N} q_{ui}}{N} \; and \; q_{ui} = \frac{q_{u1}^i + q_{u2}^i + q_{u3}^i}{3} \; for \; i = 1 \; to \; N \quad (6)$$

$\bar{q}_{uN}$ = Mean value of field UCS
q_{ui} = Average UCS of a series of 3 tests conducted for one sampling
f_{cd} = Design value of the compressive strength
F_s = Safety factor (typically 3 as a global safety factor)
K_a = Coefficient of acceptance depending on the number of samples (see table 3)
v_d = Design value of the coefficient of variation for a specific mixing method (0.35 for wet mixing)

Table 3: Number of sampling points N and coefficient of acceptance used in Japan from [1] and [7]

N =	**1**	**2**	**3**	**4 to 6**	**7 to 8**	**≥ 9**
K_a =	1.8	1.7	1.6	1.5	1.4	1.3

Using these values and formulas result in a global factor between field UCS and design strength from 5.5 to 8.1. A more detailed design calculation including a 3D-stress-analysis has no effect on the safety factors to be applied.

3.2. DIN 4093:2011 (Draft)

In Germany a new standard code is under development for the design of soils treated with jet-grouting, deep soil mixing and conventional grouting. The exact translation of its title is "Design of cemented soil – Installation with jet-grouting, deep-mixing or grouting". This new standard shall replace the old DIN 4093 from 1987 which described the process and the design of conventional grouting. This standard is necessary because neither in the Eurocode 7 nor in the European standards for grouting, jet-grouting or deep-mixing specifications for the internal bearing capacity of elements made with one of these three techniques are given.

The algorithm developed for this new standard formally is identical for all three methods, only the numerical values of the factors vary.

What was called f_c in chapter 3.1 is $f_{m,k}$ in the nomenclature of DIN 4093.

$$f_{m,k} = min \begin{bmatrix} f_{m,min} \\ \alpha \cdot f_{m,mittel} \\ 12 \; {}^{N}/_{mm^2} \end{bmatrix} \quad (7)$$

$f_{m,k}$ = Characteristic value of the unconfined compressive strength (cylindric sample with h = 2 x Ø)
$f_{m,min}$ = Minimum value found for UCS
$f_{m,mittel}$ = Mean value for the UCS from a series of at least 4 samples
α = Factor for the coefficient of variation to achieve a sufficient level of confidence
= 0.6 for $f_{m,k} \leq 4$ N/mm² and 0.75 for $f_{m,k} = 12$ N/mm² (linear interpolation for interim values)

In case of $f_{m,k} < 4$ N/mm² additional creep tests for material samples have to be performed with a load of 0.5 x $f_{m,k}$ according to annex A of the code. The allowed creep deformation in that case is 0.02 %. The design strength for calculations with the concept of partial safety factors is:

$$f_{m,d} = 0.85 \cdot \frac{f_{m,k}}{\gamma_m} \quad (8)$$

$f_{m,d}$ = Design value for the unconfined compressive strength
0.85 = Factor to consider long term loads (permanent loading)
γ_m = Partial Safety Factor for the material (1.5 for load case BS-P and BS-T and 1.3 for BS-A)

If independent and separate design calculations for compressive and shear stresses are made the maximum allowed compressive stress is 0.7 x $f_{m,d}$ and the maximum allowed shear stress is 0.2 x $f_{m,d}$.

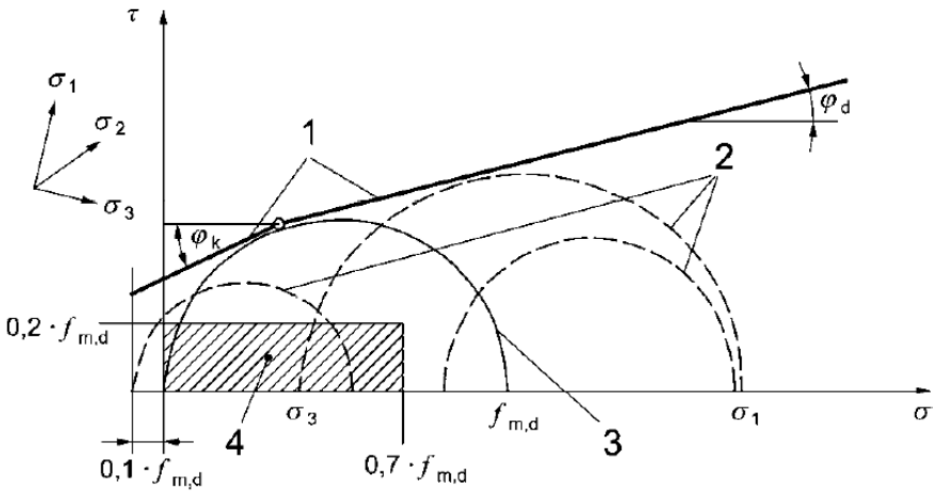

Figure 5: Allowed stresses inside a deep mixing bodey according to [8, Picture 1] © DIN

If a complete 3D-stress-analysis is performed for the design the above described reduction for the allowed stresses is not necessary. Even tensile stresses of 0.1 x $f_{m,d}$ are allowed in certain cases for parts of the cemented body (e.g. as a result of bending moments).

For 3D-stress calculations this results in a total safety factor on the material side between 2.94 and 2.35 for BS-P (permanent load). According to the EC 7 permanent loads for this load case are increased by a partial safety factor of 1.35 and live loads by 1.5 so that the global safety level is between 4.41 and 3.17. In case of simple calculations with the above described reduction we end up with a global safety factor of 6.3 to 4.53. An increase in the number of samples tested has no effect on the safety factors to be applied.

REFERENCES

[1] Michal Topolnicki, 2004, In-situ Soil Mixing, Chapter 9 of the "Ground improvement" book, 2nd edition, Spon Press, www.sponpress.com

[2] Coastal Development Institute of Technology (CDIT), Japan (2002) The Deep Mixing Method, A.A. Balkema Publishers.

[3] Paul Pandrea, Georg Breitsprecher, 2005, Statistische Betrachtungen zur Festigkeit von Verfestigungskörpern im Baugrund und die Ermittlung ihres charakteristischen Wertes, Geotechnik-Tag Munich, Technical University Munich

[4] Building Center of Japan (BCJ), 1997, Design and Quality Control Guideline for Buildings

[5] O. Taki, 2003, Strength Properties of Soil Cement produced by Deep Mixing, Proc. III Int. Conf. Grouting and Ground Treatment, ASCE Geotechnical Special Publ. No 120, 646-657

[6] Coastal Development Institute of Technology (CDIT), 2002, The Deep Mixing Method, A.A., Balkema Publishers

[7] Futaki, M. and Tamura, M., 2002, The quality control in deep mixing method for the building foundation ground in Japan, Proc. Deep Mixing Workshop in Tokyo, Port and Airport Research Institute & Coastal Development Institute of Technology

[8] Deutsches Institut für Normung, 2011, E DIN 4093 Entwurf und Bemessung von Bodenverfestigungen — Herstellung mit Düsenstrahl-, Deep-Mixing- oder Injektions-Verfahren, Beuth Verlag

[9] EN 12715:2000-10 Execution of special geotechnical work – Grouting

[10] EN 12716:2001-12 Execution of special geotechnical works - Jet grouting

[11] EN 14679: 2005-07 Execution of special geotechnical works - Deep mixing

[12] EN 1997-1: 2009-09 Geotechnical design - Part 1: General rules

SESSION 5
RIGID INCLUSIONS & STONE COLUMNS

Reliability-based design of stone columns for ground improvement considering settlement and bulging as failure modes

José A. Alonso, Technical University of Madrid; Spain, jaalonsop@dragados.com
Rafael Jimenez, Technical University of Madrid; Spain, rafael.jimenez@upm.es

ABSTRACT

Stone columns are commonly employed for ground improvement in geotechnical projects. This paper studies the problem of stone column design in the following aspects: (i) settlement (amount and velocity), and (ii) bearing capacity of the stone columns due to bulging. An improved theoretical solution to the coupled column compression/consolidation problem that considers the influence of the radial deformation and yielding of the column on the (radial only) consolidation analysis is employed. In addition, reliability methods are used to consider the effects that uncertainty and variability have on computed estimates of settlement and of bearing capacity due to bulging and, hence, on the probability of failure under such failure modes. Uncertainties and variabilities considered include those related to column "as-built" properties and also those related to soil properties, as well as model uncertainties. Reliability is estimated using First Order Reliability Methods (FORM), and simulation methods (Monte Carlo, MC) are employed to double-check the validity of the results. Results indicate, as expected, that the failure mode due to settlement is clearly determinant in the probability of failure of the system, while the failure mode due to bulging has, in the case studied, an almost irrelevant role.

1. INTRODUCTION

Stone columns are commonly employed for ground improvement in geotechnical projects. Their main purposes are (i) to increase the shear resistance of cohesive and non-cohesive soils (hence increasing bearing capacity); (ii) to increase their stiffness (hence reducing settlements); and (iii) to increase the permeability of the soil mass, therefore speeding up consolidation of cohesive soils or reducing the liquefaction susceptibility of granular soils (see e.g., Hughes et al., 1975; Priebe, 1995, 1998; Phear and Harris, 2008; Kirsch and Kirsch, 2010)

In this paper, we study the problem of stone columns design, under uncertain conditions, in the following aspects: (i) settlement (amount and velocity), and (ii) bearing capacity of the stone columns due to bulging. This is a typical geotechnical problem in which, given uncertain parameters and for a given target probability, we aim to obtain the probability of failure of the system.

The settlement problem has been discussed in detail elsewhere (Alonso y Jiménez, 2011). The aim here is to consider the settlement that will affect a structure to be constructed after a specified waiting (pre-loading) time, and, simultaneously, to compare the reliability of such stone column design with other failure modes related to column instability. In particular, this paper focuses, on the bulging failure mechanism of stone columns under the vertical load acting on them.

Routinely in column´s stability analyses, three different configurations are considered: (a)-Isolated stone columns, (b)-Column groups with rigid concrete foundations, and (c)-Infinite grids of stone columns, used typically for the foundation of storage tanks and embankments. This study only analyzes the behavior of stone columns for the foundation of widespread loading (c), adopting the well-known concept of unit-cell that assumes that the behavior of all column-soil units is the same and, thus, it is only necessary to study one unit (see eg, Barksdale and Bachus, 1983). This concept applies except for the edges of the loaded area (ie., to the columns at the periphery of the group) whose analysis is beyond the scope of this work.

Castro and Sagaseta (2009) have recently presented an improved analytical model to to the coupled problem of column compression/consolidation that considers the influence of the vertical and horizontal deformation of the column on settlements associated to the (radial only) consolidation of the soil mass, in which they consider that the soil behaves elastically and that the stone column has an elasto-plastic behavior (with friction angles ϕs and ϕc, and plastic dilatancy ψc). (In the following, subscript *c* indicates column and subscript s indicates soil.) Consolidation is computed using "equivalent consolidation coefficients" (elastic and plastic), and the evolution of surface settlement versus time is obtained analytically by integration of the equation of radial consolidation. They also show that their model produces values of the stress concentration factor (i.e., SCF = ratio of stress on the stone column and

stress on the soil) that agree well with empirical observations. Further details of the analytical model, as well as solved examples of application, can be found in the original paper (Castro and Sagaseta, 2009).
In addition, reliability methods are used to consider the effects that uncertainties - as well as variabilities - have on our computed estimates of settlement and of bearing capacity due to bulging and, hence, on the probability of failure. That is, we compute the probability of failure of the ground improved with stone columns.
Uncertainties and variabilities considered include those related to column "as-built" properties, such as diameter, strength and stiffness; and also to soil's properties, such as permeability, strength and stiffness (which are themselves modified by the column during installation and/or by the preloading), as well as model uncertainties. The effects of uncertainties on the reliability of the design are quantified by means of First Order Reliability Methods (FORM), and simulation methods (Monte Carlo, MC) are employed to double-check the validity of the results.

2. BEARING CAPACITY. BULGING

Due to the increased stiffness of the stone columns, there is a stress concentration in the column so that only part of the applied external load is shared by the surrounding soil. During consolidation the stress on the column increases, whereas the stress on the soil decreases. In the final (drained) situation, the distribution of stresses between column and soil is as shown in Figure 1, and a constant stress concentration factor (SCF) is achieved. Following standard practice (Castro, 2008) we study the bulging of the column in this final situation. Note, however, that intermediate situations could be more critical since soil's strength increases with time and the SCF does not change much after column yielding (Castro & Sagaseta, 2011). Research is currently underway to develop a methodology to identify the "critical" conditions for bulging from a reliability perspective; results will be presented elsewhere.

The situation studied is, therefore, comparable to an isolated stone column but considering the favorable effect of the surcharge provided by the external load taken by the soil. The possible failure mechanisms of isolated columns are (see e.g., Kirsch and Kirsch, 2010): (i) bulging at the top zone of the column (to a depth of approximately four diameters), (ii) shearing at the surface (short columns), (iii) fail in end bearing (floating columns) and (iv) bulging in soft deeper layers.

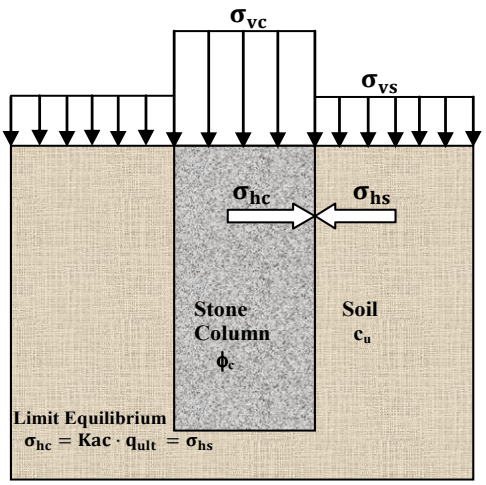

Figure 1: Distribution of stresses in the unit cell

For normal design conditions, bulging is usually the controlling instability mechanism and, hence, is the one studied in the present work. There are numerous methods for calculating the bearing capacity by bulging (see e.g., Gibson y Anderson, 1961; Vesic, 1972; Hughes and Withers, 1974; Hughes et al, 1975; Greenwood y Kirsch, 1983; Van Impe and De Beer, 1983; Barksdale and Bachus, 1983; Ambily et al., 2007; Murugesan et al, 2010; etc). We have chosen to analyze the bulging by the classical method of cylindrical cavity expansion (Vesic, 1972), although in its application the existing dispersion in the results of laboratory and field trials has been taken into account.
The problem of bulging analysis lies in determining the maximum radial stress that the soil can support (soil passive resistance), as a reaction to the horizontal pressure transmitted by the column in its active state. This limit equilibrium condition is expressed as (Barksdale and Bachus, 1983):

$$q_{ult} = Kpc \cdot \quad _{hs} \tag{1}$$

where q_{ult} = ultimate load capacity of stone column; Kpc = passive earth pressure coefficient of stone column; σ_{hs}= passive soil resistance. The passive soil resistance is expressed as:

$$_{hs} = c_u \cdot N_k + \quad _{vs} \tag{2}$$

where c_u = undrained shear strength of soil after consolidation; σ_{vs} = stress on the soil in the final drained situation; N_k = factor that can take a value of around 6 to 8 (Sagaseta, 2006; Castro, 2008). For typical parameters based on Nahrgang's laboratory studies (Greenwood and Kirsch, 1983) its value is 6.16.

Figure 2 presents our comparison of some of the existing calculation methods as well as data from available laboratory and field tests. It can be observed that there is a significant dispersion in the laboratory and field data and, therefore, N_k is taken here as a random variable to represent the existing uncertainty. The mean and standard deviation estimated from the results of laboratory and field trials are included in Table 1.

To estimate the soil´s undrained shear strength, the soft soil has been considered as normally consolidated. Similarly, in its initial state (ie., before loading and subsequent consolidation), and due to the proximity to the surface in the region where bulging would be expected to occur, its undrained shear strength has been (conservatively) adopted as null. After consolidation, it is considered that there is an increase in undrained shear strength given by (Ladd, 1991):

$$c_u = k \cdot \quad _{vs} \tag{3}$$

Where k is a factor that takes a typical (average) value of 0.22, but due to its variability, it will also be modeled as a random variable whose parameters are given in Table 1.

3. UNCERTAINTY CHARACTERIZATION

Table 1 lists the parameters of the statistical distributions employed to characterize uncertainties in this work. E_s and E_c are the Young´s Modulus of soil and column; C_r is the coefficient of radial consolidation of the soil; d_c is the diameter of the stone column; ϕ's and ϕ'c are the friction angles of soil and column; and ψc is the angle of plastic dilation of stone columns. Similarly, as explained above, we have employed two additional random variables for the bulging problem, related to the increase in shear strength of the N.C. soil due to effective stress increases associated to the preloading (k); and related to the computation of the passive soil´s resistance (Nk).

As an initial simplification, we have considered that random variables are uncorrelated and normally distributed, although the computational methods employed in the reliability analysis below can also handle more general cases (see e.g., Jimenez-Rodriguez et al, 2006; Jimenez-Rodriguez & Sitar, 2007; Low, 2007). Ranges of variability are defined (as expressed by their coefficients of variation, or cov's) following the suggestions of the Spanish Recommendations for the Design of Maritime and Harbour Works (Puertos del Estado, 2005). Note, however, that ranges of variability of geotechnical properties (Table 1(a)) are actually *site dependent*, so that values presented herein can only be considered as reasonable estimates. (For additional discussion of cov´s reported in other consolidation analyses, see Alonso & Jimenez (2011); additional suggestions for characterization of geotechnical variability have been published elsewhere, see e.g., Phoon and Kulhawy (1999); Uzielli *et al.* (2007)).

The uncertainty characterization of stone column properties (and, in particular, of stone column diameters, dc), however, has not been studied in such detail in the literature. Magnan et al. (2005) presents empirical evidence that suggests that column diameter depends on several factors such as strength of the soil, type of construction (e.g., dry vs. wet methods), energy transmitted to the soil by the vibrator, sequence of construction, etc. Similarly, the construction method (*e.g.,* top-feed vs. bottom-feed) and the quality of workmanship have a significant influence on the quality of the column and, in particular, in ensuring that the required column diameter is being achieved Slocombe *et al.* (2000).

To analyze the variability of stone column diameters in real projects, we analyzed the distribution of 9370 stone columns constructed (by the dry method, bottom feed) in a stone column project executed by a prestigious specialized contractor in Spain. (See Figure 3). Based on such analysis, we found that a coefficient of variation of approximately 8-10% could be employed to characterize columns executed by specialized contractor in a well-controlled environment. Building on that observation, and to illustrate the importance of variability in the diameter of stone columns, we consider two values of the coefficient of variation of column diameter dc (δdc = 0.1 to represent "good" conditions and δdc = 0.2 to represent "bad" conditions; see Table 1(b)).

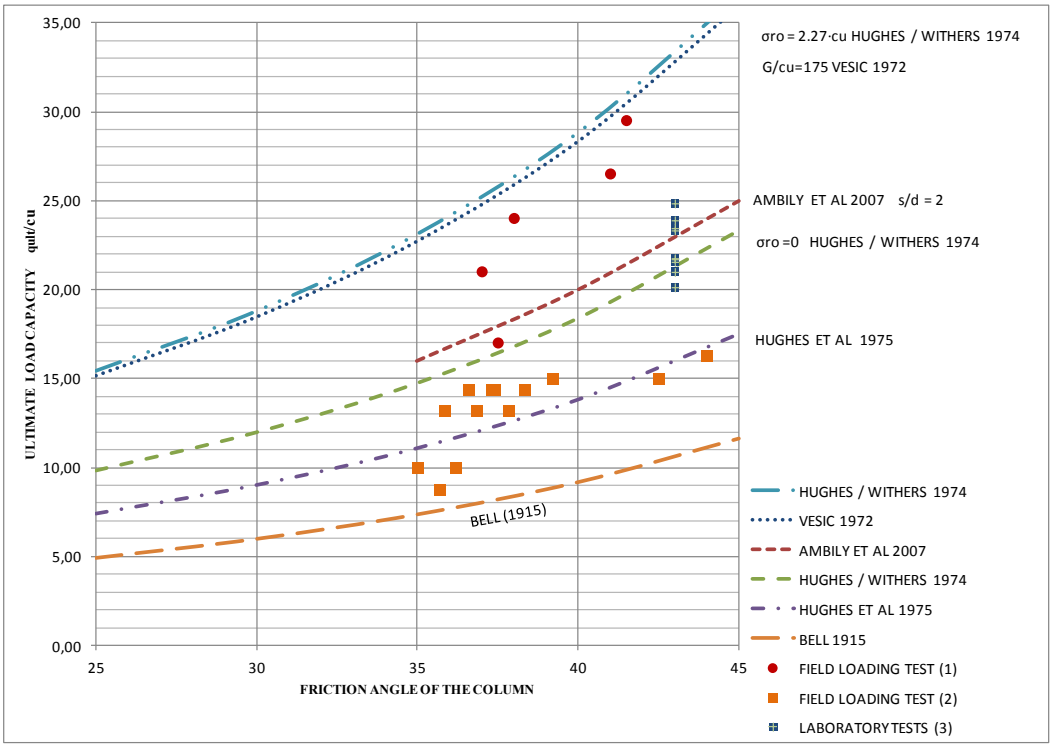

Figure 2: Isolated stone column. Ultimate load capacity.(1), (2), (3) see References

Table 1: Parameters of statistical distributions employed for uncertainty characterization

(a) Geotechnical properties				(b) Stone column properties			
Property	Mean	Coef Var	Std Dev	Property	Mean	Coef Var	Std Dev
Es [kPa]	2000	0.3	600	dc [m]	0.7	0.1 & 0.2	0.07&0.14
Cr[m²/day]	8.64E-03	0.5	4.32E-03	Ec [kPa]	30000	0.3	9000
tan ϕ'_s	0.44	0.07	0.03	tan $\phi'c$	0.84	0.07	0.06
K	0.22	0.15	0.033	tan ψc	0.18	0.07	0.01
(c) Calculation model							
Property	Mean	Coef Var	Std Dev				
N_k	3.91	0.24	0.95				

4. RELIABILITY ANALYSIS

4.1. Methods of analysis

Reliability methods are used to quantify the influence that uncertainties characterized above have on the probability of failure. The problem is to compute the probability of failure Pf (or, alternatively, the reliability index $\beta = -\Phi^{-1}(\mathrm{Pf})$) of a limit state function (LSF) that defines a "success" or "failure" state. Limit states are usually defined by a function g(x) of the *vector* of random variables involved, in a way such that g(x) < 0 indicates "failure". (Note that "failure" does not necessarily represents a mechanical collapse and, for instance, it can also be associated to serviceability limit states as in our settlement analysis below.) The probability of failure can then be computed by solving the following integral:

$$\mathrm{Pf} = \int_{g(x)<0} f(x)\,d(x) \qquad (4)$$

in which f(x) is the joint probability density function for the basic random variables, and the integration is performed over the failure region, that is, g(x) < 0.

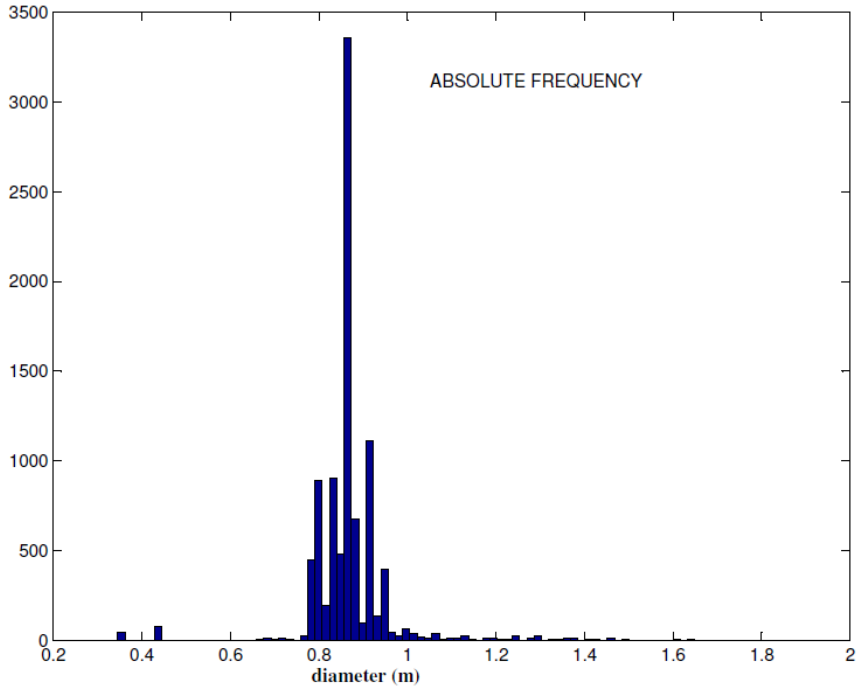

Figure 3: Histogram of the diameter of stone columns. Dry method (bottom feed)

The direct integration of Eq (4) is often an insurmountable challenge and, for that reason, reliability methods have been developed. One of the most common is the First Order Reliability Method (FORM), in which the probability of failure is *approximated* using a linear tangent to g(x) at a properly selected "design" point. In this work, we use the simple ellipsoid approach proposed by Low (1997) to compute FORM estimates of Pf. Such method is based on the solution of the following constrained optimization problem:

$$\textit{Minimizing} \quad = \sqrt{\sum_i (x_i^* - \ _i)^2 / \ _i^2} \qquad \textit{subjected} \text{ to the condition that } g(x) \le 0 \tag{5}$$

where $\sum i$ indicates summation over all random variables considered; x_i^* are the values of such random variables at the solution (ie., at the "design point");μ_i and σ_i^2 are the means and variances of each random variable. FORM methods can also be used to compute sensitivity coefficients, α_i, as:

$$_i = -(x_i^* - \ _i)/(\ \cdot \ _i) \tag{6}$$

Such sensitivity coefficients are useful for practical engineering, as they allow the designer to identify which random variables have a stronger influence on the reliability results, so that they should concentrate the characterization efforts (see eg., Jimenez et al., 2006; Jimenez and Sitar, 2007).
The Monte Carlo simulation method, on the other hand, approximates the probability of failure as:

$$\text{Pf} = \frac{1}{\text{Ns}} \sum_{i=0}^{\text{Ns}} \text{I}(x_i) \tag{7}$$

where Ns is the number of simulations and $I(x_i)$ is a Boolean function indicating whether the vector of randomly generated input parameters x_i produces (or not) failure of the system. (I = 1 indicates failure.)

4.2. Settlement

We define a limit state function (LSF) to express the condition that the remaining settlement after a specified time (t) is less than a specified threshold ($\Delta s,adm$ = 10 cm in this case). That is, we have:

$$g(\cdot) = \Delta s_{adm} - (s \ - s_t) \tag{8}$$

where s_t is the settlement at time t and s is the final settlement once consolidation is completed ($t = t_\infty$). In this case, we have that s is a function of soil's and column's random properties:

$$s \equiv s\ (Es, \tan\phi\ s, dc, Ec, \tan\phi\ c, \tan\psi c) \quad (9)$$

and that s_t is a function of the same variables in addition to the radial coefficient of consolidation, C_r. (See Castro & Sagaseta (2009) for the actual formulas to compute s_t and s settlements depending on the state of the column (elastic, partially plastic, or completely plastic)).

Figure 4 shows an example of our computed reliability results. Figure 4(a) shows the probability of failure for different design times; it is observed that, as expected, it decreases with time or, in other words, as consolidation proceeds. (The difference between FORM and MC results is probably due to the errors introduced when the non-linear LSF is linearized to compute FORM reliability estimates). Also, note that (everything else being equal) Pf tends to be higher for cases in which the variability of column diameters is higher. Similarly, Figure 4(b) shows the relative importance of random variables (as given by the squares of the corresponding components of the sensitivity vector, α_i^2) on the computed reliability results for the case of $\delta dc = 0.1$. (Results for $\delta dc = 0.2$ show a similar trend and, for the sake of space, they have not been reproduced herein.)

Results show that the coefficient of radial consolidation has the highest influence on the reliability results—therefore agreeing with the conclusions of previous research on reliability of wick drain design (see e.g., Hong and Shang, 1998)—, and that column diameter and soil deformability are also important parameters. In addition, they suggest that the relative importance of the random variables considered change with time, so that the relative importance of Cr increases with time while the relative importance of dc and Es decrease with time.

4.3. Bulging

The bulging limit state function is defined as:

$$g(\cdot) = q_{ult} - \sigma_{vc} \quad (10)$$

where q_{ult} is the ultimate load capacity of stone column and σ_{vc} is the stress on the column in the final drained situation. The ultimate load capacity of the column is a function of the following random variables:

$$q_{ult} = q_{ult}(N_k, k, \sigma_{vs}, \tan\phi\ c) \quad (11)$$

where the variable σ_{vs} in Eq. (11), itself depends on all the random variables considered:

$$\sigma_{vs} \equiv \sigma_{vs}(Es, \tan\phi\ s, dc, Ec, \tan\phi\ c, \tan\psi c) \quad (12)$$

Therefore, the reliability analysis of the bearing capacity of the column depends on eigth random variables. The probability of failure Pf is obtained using the reliability techniques of FORM and MC.

To solve the FORM minimization problem in this case, we found it useful to impose limitations on some of the random variables to avoid that the coordinates of the design point represent physically imposible situations. Two conditions are judged critical in this case: (i) N_k should not be less than 2.0, which represents a relationship $q_{ult}/c_u \geq 5$; (ii) The undrained shear strength after consolidation can not take a null value. Since it is difficult to establish a lower bound, we chose to impose $c_u \geq 1.60$ kPa which corresponds to the undrained shear strength of remolded clay with a moisture content equal to the liquid limit (see e.g., Mitchell and Soga, 2005).

Table 2 shows the results of reliability analysis and, in Figure 5, we show the relative importance of random variables on the probability of failure.

Table 2: Bulging probability of failure (Pf)

FORM		MONTE CARLO MC	
CASE	Pf	CASE	Pf
$\delta dc = 0.1$	7.0E-28	$\delta dc = 0.1$	0 (six million trials)
$\delta dc = 0.2$	2.0E-15	$\delta dc = 0.2$	0 (six million trials)

As it can be observed, the computed values of the probability of failure are practically zero. This result is consistent with existing experimental and theoretical considerations (see e.g., Greenwood and Kirsch, 1983; Barksdale and Bachus, 1983; Ambily et al, 2007; Kirsch and Kirsch, 2010).

For both cases considered ($\delta dc = 0.1$ and $\delta dc = 0.2$), the two variables that have the highest influence on the bulging reliability results are the diameter of the column and the undrained shear strength factor (k). The friction angle of the column is also important (mainly for the case $\delta dc = 0.1$) and, to a lesser extent, the angle of dilatancy and the N_k factor of Vesic. For the case of $\delta dc = 0.2$ the relative importance of N_k is

slightly greater than the importance of the friction angle, and the influence of the angle of dilatancy is practically null.

5. CONCLUSIONS

We present an example of application of reliability methods for stone column design, considering failure modes related to the problems of settlement and of bearing capacity due to bulging. Two aspects have been studied in detail: (i) the remaining settlement after a specified waiting period, so that it is below a given threshold; and (ii) the bulging failure due to stresses on the columns that exceed its ultimate load capacity.

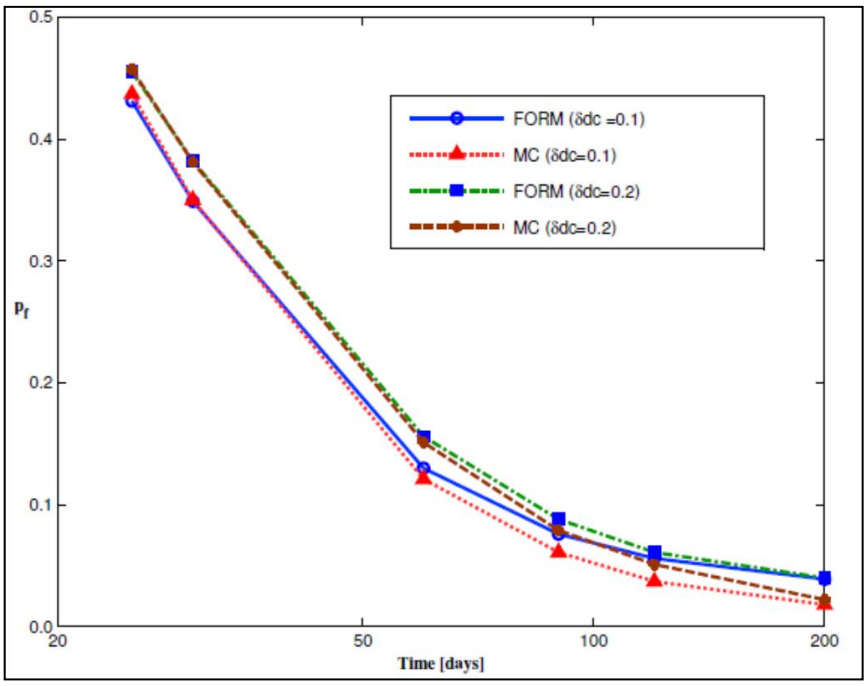

(a) Probability of failure vs time

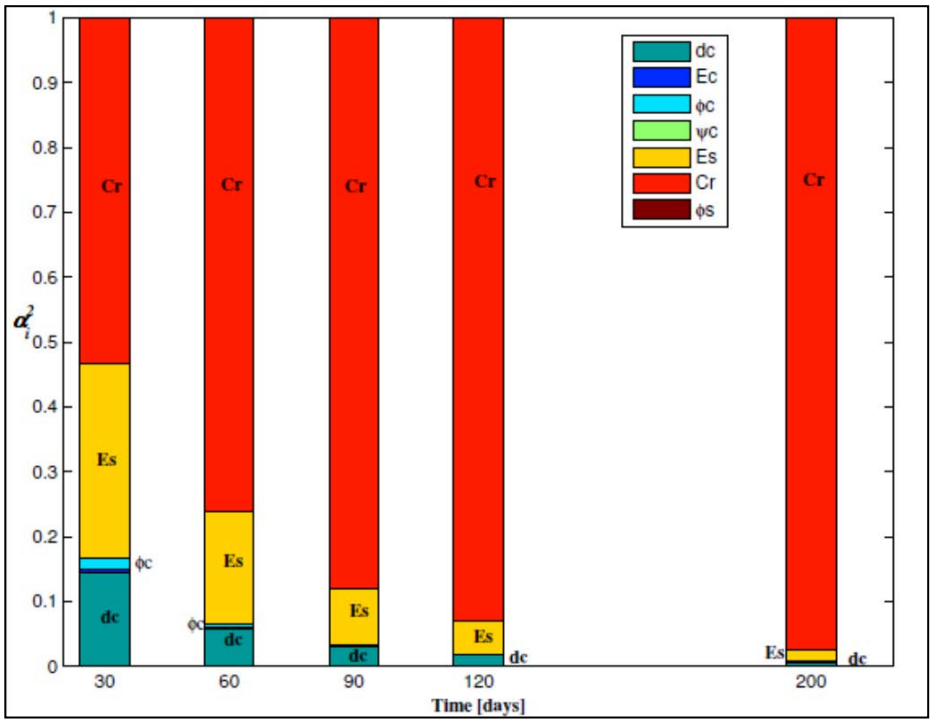

(b) Relative importance of random variables (δdc = 0.1 case)

Figure 4: Settlement. Evolution of computed reliability results as a function of time

Settlements and stresses are computed using an advanced analytical model that considers the coupling between column compression and consolidation, and FORM estimates are computed using a simple spreadsheet implementation of the ellipsoid reliability approach. We also compute the sensitivity results to illustrate the relative importance of the random variables considered. In addition Monte Carlo simulation is employed to double-check the validity of the results.

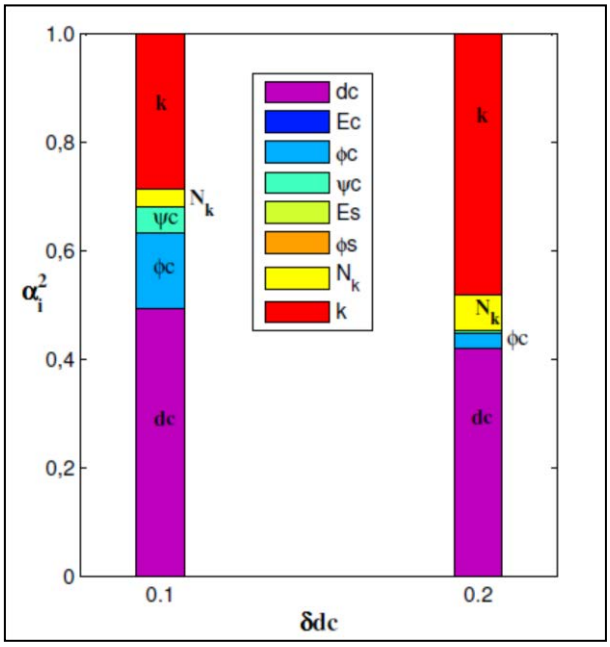

Figure 5: Bulging. Relative importance of random variables

In the case of settlements, results indicate that, as expected (since remaining settlements decrease with time), the reliability of the design increases as consolidation proceeds. Similarly, the probability of failure due to bulging is practically zero in the case studied, a result which is consistent with existing experimental and theoretical considerations. In other words, results show that in this case the failure mode due to settlement is clearly dominant in the probability of failure of the system, while the failure mode due to bulging has, in the case studied, an almost irrelevant role.

Also, we show that reliability methods allow us to quantify the influence of uncertainties in practical design cases; such analysis is not possible with deterministic methods. For instance, in this case, the coefficient of consolidation has the highest influence on the reliability results, since it is the most influent parameter in the failure mode (settlement) that clearly dominates the probability of the system. Similarly, column diameter (for both settlement and bulging), as well as soil deformability (for settlement) and soil and column strength (for bulging), are also very important parameters.

The high importance of column diameter variability (which, incidentally, is the only human-influenced factor among the random variables considered) highlights the importance of the construction method, of quality control, and also of worker´s experience and quality of workmanship.

Furthermore, for the settlement case, results show that the influence of variables depends on the time of construction considered. For instance, it is observed that probabilities of failure tend to increase when the variability of stone column diameters is higher, and also that $^2_{dc}$ is relatively more important for "short" times. This suggests that control of column diameter can be more crucial when time is "expensive" and it is important to construct "early". It is observed that the importance of the radial coefficient of consolidation increases as time increases, hence suggesting that stone column construction method and quality of workmanship are probably less important if time is "cheap" and we can wait for consolidation to occur. In that case, uncertainties associated to the coefficient of consolidation would be more important that those associated to the distribution of column diameters.

REFERENCES

Alonso, J.A., Jimenez, R. (2011). Reliability analysis of stone columns for ground improvement. In JuangC.H. et al (eds) In: Proceedings of Georisk 2011: Geotechnical Risk Assessment and Management (GSP-224). ASCE, Reston (VA). 493-500.

Ambily A.P., Shailesh R, Gandhi, (2007). "Behavior of stone columns based on experimental and FEM analysis". Journal of Geotechnical and Geoenvironmental Engineering, Vol 133(4): 405-415.

Barksdale, R.D. and Bachus, R.C. (1983). "Design and construction of Stone Columns". Federal Highway Administration Office of Engineering and Highway Operations Research and Development, Washington, D.C. . Rep. No. FHWA/RD-83/026.

Castro, J. (2008). "Análisis teórico de la consolidación y deformación alrededor de columnas de grava". Doctoral Thesis. University of Cantabria, Spain (in Spanish).

Castro, J., Sagaseta, C. (2009). "Consolidation around stone columns. influence of column deformation". International Journal for Numerical and Analytical Methods in Geomechanics, Vol. 33: 851-877.

Castro, J., Sagaseta, C. (2011). "Consolidation and deformation around stone columns: Numerical evaluation of analytical solutions". Computer and Geotechnics 38 (2011): 354-362

Gibson, R.D. and Anderson, W.F. (1961). "In-Situ measurements of soil properties with pressuremeter".Civil Engineering and Public Works Review, Vol. 56, No. 658.

Greenwood, D.A.,(1991). "Load test on stone columns". Deep Foundation Improvements: Design, Construction and Testing. ASTM STP 1089, Melvin I. Esrig and Robert C. Bachus, Eds. American Society for Testing and Materials, Philadelphia, 1991.

Greenwood, D.A. and Kirsch, K., (1983). "Specialist Ground Treatment by Vibratory and Dynamic Methods". Advances in pinling and ground treatments for foundations. Thomas Telford Ltd., London, 1983.Technical paper 11-53E.

Hong, H. P., Shang, J. Q. (1998). "Probabilistic analysis of consolidation with prefabricated vertical drains for soil improvement". Canadian Geotechnical Journal, Vol. 35: 666-677.

Hughes, J. M. O., Withers, N. J., Greenwood, D. A. (1975). "A field trial of the reinforcing effect a stone column in soil". Geotechnique, Vol 25 (1): 31-44.

Hughes, J.M.O. and Withers,N.J. (1974). "Reinforcinf of soft cohesive soils with stone columns".Ground Eng., 7(3), 42-49.

Jimenez-Rodriguez, R., Sitar, N., Chacón, J. (2006). "System reliability approach to rock slope stability". International Journal of Rock Mechanics and Mining Sciences, Vol 43(6): 847-859.

Jiménez-Rodriguez, R., Sitar, N. (2007) Rock wedge stability analysis using system reliability methods. Rock Mechanics and Rock Engineering. Vol 40(4):419-427

Kempfert H., and Gebreselassie, B. (2006). "Excavations and Foundations in Soft Soils". Springer

Kirsch, K. and Kirsch,F. (2010). "Ground improvement by deep vibratory methods". Spon Press.

Low, B. K. (1997). "Reliability analysis of rock wedges". Journal of Geotechnical and Geoenvironmental Engineering, Vol 123(6): 498-505.

Low, B. K. (2007). "Reliability analysis of rock slopes involving correlated nonnormals". International Journal of Rock Mechanics and Mining Sciences, Vol 44: 922-935.

Magnan, J. P., Droniuc, N., Canepa, Y., Dhouib, A. (2005). "Réflexions sur la conception des colonnes ballastées". In: Proceedings of 16th International Conference of Soils Mechanics and Foundation Engineering. Osaka, vol. 3, 1377-1380.

Mitchell,K., (1981). "Soil improvement - State-of-the-art Report". X-ICSMFE, Stocolmo,1981.

Mitchell, K.J. and Soga, K. (2005). "Fundamentals of soil behavior". Third Edition. John Wiley and Sons, Inc.

Munfakh, G.A., Lee, W., Abramson, M., Barksdale, R.D., and Juran, I. (1987). "In-situ ground reinforcement". Soil Improvement. A ten year update. Geotechnical Special Publication 12 ASCE.

Murugesan S., Rajagopal, K., (2010). "Studies on the behavior of single and group of geosynthetic encased stone columns". Journal of Geotechnical and Geoenvironmental Engineering, Vol 136(1): 129-139.

Phear, A. G., Harris, S. J. (2008). "Contributions to Géotechnique 1948-2008: Ground improvement". Geotechnique, Vol 58(5): 399-404.

Phoon, K. K., Kulhawy, F. H. (1999). "Characterization of geotechnical variability." Canadian Geotechnical Journal, Vol 36: 612-624.

Priebe, H. J. (1995). "The design of vibro replacement". Ground Engineering, (GT 07-13 E).

Priebe, H. J. (1998). "Vibro replacement to prevent earthquake induced liquefaction". Ground Engineering, 30-33.

Puertos del Estado (ed.) (2005). "ROM 0.5-05. Geotechnical recommendations for the Design of Maritime and Harbour works". Ministerio de Fomento, Madrid.

Sagaseta, C. (2006). "Avances en el diseño de las técnicas de mejora del terreno". Technical Seminars SEMSIG-AETESS 6ª. Técnicas de Meroja del Terreno.(in Spanish)

Slocombe, B. C., Bell, A. L., Baez, J. I. (2000). "The densification of granular soils using vibro methods". Geotechnique, Vol 50 (6): 715-725.

Sondermann W. and Wehr, W. (2004). "Deep vibro techniques". Groun improvement 2nd edition. Edited by Moseley, M.P. and Kirsch, K.Spon Press

Uzielli, M., Lacasse, S., Nadim, F., Phoon, K. K. (2007). "Soil variability analysis for geotechnical practice". In: Tan, T. S., Phoon, K. K., Hight, D. W., Leroueil, S. (eds.), Characterisation and Engineering Properties of Natural Soils. Taylor & Francis Group, London, 1653-1752.

Vesic, A.S. (1972). "Expansion of cavities in infinite soil mass". Journal of the Soil Mechanics and Foundation Engineering Division, ASCE, Vol. 98, No. SM3: 265-290.

Zhou, W., Hong, H. P., Shang, J. Q. (1999). "Probabilistic design method of prefabricated vertical drains for soil improvement". Journal of Geotechnical and Geoenvironmental Engineering, Vol 125: 659-664.

(1) Brauns trials included in Greenwood and Kirsch (1983)

(2) Bernardo&Lam trials included in Castro (2008)

(3) Ambily et al 2007

Ordinary and Encased Stone Columns Under Repeated Loading

Namir K.S.Al-Saoudi , University of Technology,Baghdad,Iraq,namirks@yahoo.com
Mahmoud R. Mahmoud, University of Technology, Baghdad, Iraq, mahmoudal_qaissy@yahoo.com
Falah H. Rahil, University of Technology, Baghdad, Iraq, ffhhhzmr@yahoo.com
Zeena W.S.Abbawi, University of Technology, Baghdad, Iraq, zinawaleed2004@yahoo.com

ABSTRACT

Stone columns become one of the most widely used techniques for improving the load carrying capacity and reducing the settlements of soft soils. Stone columns have been used successfully underneath isolated footings, raft foundations for storage tanks as well as under embankments. Recently attempts have been made to increase the stiffness of the backfill material by adding additives like cement and /or lime. Most recently geotextile materials are used to encase the stone columns to provide extra stiffness and reduce the tendency of lateral deformation.

The available literature demonstrates design requirements and behaviour of stone columns under static vertical loads, as the most common case in many structures. However attention must be paid to investigate the behaviour of stone columns under repeated vertical loads, since in many cases like railway embankment and highway abutment soft soils reinforced with stone columns experience repeated as well as static loading.

*The paper focuses on the behaviour of ordinary and geogrid encased stone columns under repeated loadings. Model tests were performed on beds of soft saturated soil, prepared at undrained shear strength 9 kPa, inside containers of 1000mm*400mm*700mm in dimensions. The beds were reinforced by eight ordinary or geogrid encased stone columns, 50mm in diameter and 300mm long, with 100mm center to center spacing. A a layer of geogrid was placed over the bed of soil covering all stone columns, then crushed stone was spread carefully on the geogrid forming a model embankment of height 100mm and crest 300mm. A model footing, 200mm wide and 400mm long, was placed on the crest of the embankment. Repeated stress increments of 0.4,0.6 and 0.8 of the failure stress obtained from the corresponding monotonic tests were applied and the generated settlements versus number of cycles up to failure were recorded. Results revealed significant improvement in terms of loading carrying capacity and safety against failure achieved by the encased stone columns as compared to ordinary ones.*

1. INTRODUCTION

During the last two decades, encased stone columns were introduced as an improved technique over ordinary stone columns. Several researchers investigated the efficiency of geogrid encased stone columns under vertical static load. Analytical studies performed by Wu and Shen (1997), revealed remarkable increase in rigidity and bearing capacity of soft clay reinforced with geosynthetics – encapsulated stone columns. The results of model tests reported by Zakaria (2001) on encased stone columns stabilized with 5% lime and / or cement demonstrated sufficient residual bearing improvements at large deformations. Malarvizhi and IIamparuthi (2002) investigated the length to diameter ratio of encased stone columns, an increase in the carrying capacity of encased stone columns was observed, irrespective of whether the column is end bearing or floating, their findings were supported and extended by the outcomes of the finite element (PLAXIS) software. The results of the analysis shed the light on the development of hoop stresses generated in the geogrid that restrain the lateral deformation and cause the increase in load carrying capacity of the encased stone columns. Ginel and Bouazza (2008 a), (2008 b) and (2008 c) had thoroughly investigated the performance of encased stone columns through laboratory model tests, finite element modelling using PLAXIS software and field tests. The laboratory model tests exhibited significant reduction in column vertical and radial strains, with increasing length of encased stone columns, this conclusion was in good agreement with the outputs of the numerical analysis. The field study revealed that the vertical strain was effectively reduced by increasing column stiffness, geogrid stiffness and displacement method of column installation. Majed(2008) concluded from the analysis of encased stone columns using CRISP2D program that the effective encasement length ratio was about 0.6 and the failure mode changed into punching failure when encased stone column was used.Yoo (2010) concluded from the analysis of geosynthetic encased stone columns in soft ground underneath an earth embankment that additional confinement provided by the geosynthetic encasement increases the stiffness of the stone columns and reduces the degree of embankment load transferred to the soft ground, thereby decreasing the overall settlement.

In terms of repeated or dynamic loading, Ashford S.A. etal (2000) investigated the use of stone columns to mitigate the liquefaction potential due to earthquake. Jinchi Lu etal (2004) presented a pilot three-dimensional finite element study of stone columns in liquefied silty soils; reasonable agreement was achieved between the computed and recorded responses from simulated centrifuge model
There is limited work concerning the behavior of ordinary or encased stone columns subjected to vertical repeated loading. It is important to have a thorough investigate and better understanding of the performance of stone columns under different patterns of dynamic loading. The present paper summarizes some preliminary outcomes of model tests performed on ordinary and encased stone columns under repeated vertical loading.

2. EXPERIMENTAL WORK

2.1 Properties of materials used

Three types of materials were used; the first was a brown clayey consists of 3.3 % sand, 31.7 % silt and 65% clay. The plasticity index is 16.5, revealing a material classified as CL according to the Unified Soil Classification System.
The crushed stone is produced by crushing big stones brought from Penjewen city located north of Iraq. The crushed stone is poorly graded with D_{10} = 4.66 mm , D_{30} = 5.0 mm and D_{60} = 5.12 mm. The coefficient of uniformity and coefficient of curvature are 1.02 and 1.05 respectively. The angle of internal friction is 42 at relative density 71 % corresponding to dry unit weight 15 kN/m^3 used in preparing the stone columns.
The geogrid used has an aperture size 6*6 mm and mass per unit area 363 g/m2. The strength characteristics tested according to ISO 10319 revealed tensile strength 4.3 kN/m^2 and 7.7 kN/m^2 at 2% and 3% strain respectively. Peak tensile strength and yield point elongation are 13.5 kN/m^2 and 20.0 % respectively.

2.2 Model Preparation and Testing

Beds of fully saturated soil were prepared at undrained shear strengths 9kPa, the soil was placed in ten layers inside a steel container of 1000mm*400mm*700mm in dimensions. Table 1 illustrates the strength and compressibility characteristics of the soil. Eight stone columns were constructed following the same procedure used by Rahil (2007). All stone columns have a diameter of 50mm, length to diameter ratio (L/D = 6) with spacing of 2 times the diameter. A steel template was used to fix the location of the eight stone columns and control their vertical alignment. A hollow plastic PVC pipe with external diameter of 50mm was pushed down in the bed to the predetermined depth and the inside soil was carefully removed by a hand auger.

Table 1: Strength and Compressibility Characteristics of Soil Used

Undrained shear strength (kPa)	9
Initial water content (W_{ci})%	26.8
Initial void ratio (e_o)	0.72
Compression index (C_c)	0.232
Swelling index (C_r)	0.033
Avg. coefficient of volume change m_v (m^2/kN)	7.8*10^{-4}
Coefficient of consolidation (C_v) (m^2/year)	2.004
Coefficient of permeability (k) (cm/min)	2.8*10^{-6}
Dry unit weight (γ_{dry}) (kN/m^3)	15.6

The crushed stone was poured into the hole in layers and compacted gently to attain a dry unit weight of 15 kN/m^3, photo 1 illustrates the process of construction of ordinary stone columns.
The construction of encased stone columns was carried out following the same procedure of the ordinary stone columns, once the excavation of the hole was completed, the geogrid tube was inserted and the same procedure of backfilling of crushed stone was followed. Photo 2 illustrates the process of construction of the encased stone column. At this stage a layer of geogrid was placed over the bed of soil covering all stone columns, then crushed stone was spread carefully on the geogrid in the form of layers each 25 mm thick. .Each layer was compacted gently to end up with final thickness of 100 mm ballast layer taking the form of an embankment with crest width 300mm. The placement unit weight of 15 kN/m^3 was attained for the ballast embankment corresponding to relative density 71 %.
The whole assembly was moved and fixed in position inside a loading rig so that the center of the model footing, 200 mm in width and 400 mm in length, coincides with the center of the bed of soil. The footing

was then lowered and brought in contact with the crest of the ballast embankment; LPTDs were then fixed in position and monotonic or repeated stress was applied. Settlement versus applied stress was recorded for monotonic loading and settlement versus number of stress cycles were recorded continuously for repeated model tests up to failure.

Photo1: Construction of encased stone columns

Photo 2: Construction of encased stone columns

3. PRESENTATION AND DISCUSSION OF MODEL TEST RESULTS

3.1 Model Test Results Monotonic Loading

Three model tests were performed, the first on untreated soil, the second on soil treated with eight ordinary stone columns and the third on soil treated with eight encased stone columns. Figure 1 demonstrates the bearing ratio versus settlement ratio for the three model tests. The figure clearly indicates that the mode of failure for the untreated soil is close to the local pattern. The presence of eight ordinary stone columns demonstrated a significant increase in bearing ratio, exhibiting a mode of failure close to the general shear pattern. The presence of geogrid encasement around the stone particles provided extra stiffness and exhibited further increase in bearing ratio.

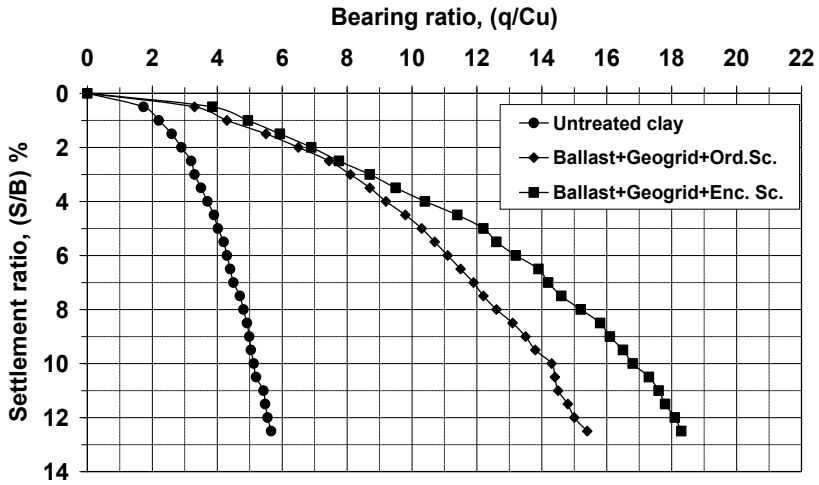

Figure 1: Model test Results- Monotonic loading-

Failure is defined as the bearing ratio corresponding to settlement equal to 10% of the footing width. Table 2 summarizes the bearing ratios for the three model tests. . The influence of the geogride encasement becomes significant when the bearing ratio exceeds about 50 % of the bearing ratio at failure. Full mobilization is achieved at bearing ratios close to failure

Table 2: Summary of Bearing Ratios at Failure Monotonic Loading

Soil Condition	Bearing ratio, q/c_u at failure	Bearing stress at failure q_u kPa
Untreated Clay	5.13	46
Ballast+ Geogrid + Ordinary Stone Col..	14.3	129
Ballast + Geogrid + Encased Stone Col.	16.8	151

3.2 Model Test Results on Untreated soil – Repeated Loading-

Following the monotonic tests, three model tests were performed with applied stresses of 0.4 q_u, 0.6 q_u and 0.8 q_u respectively. The applied stress represents ratio of the bearing stress at failure, q_u=46 kPa. Figure 2 implies the relationship between the settlement ratio S/B and the logarithm of the number stress cycles N for different applied stresses. The figure demonstrates that the first cycle is the most effective in generating the largest settlement followed by gradual cumulative settlement with increasing number of stress cycles N. Other points drawn from the figure that the number of stress cycles N to reach a specific settlement ratio decreases with increasing applied stress. Also the rate of generation of the settlement ratio versus number of cycles N increases with increasing applied stress. The overall behaviour of the bed of soil under different levels of repeated stress cycles can be explained in terms of the rate of build up of excess pore water pressure. At low stress level, $0.4q_u$, the rate of build up of excess pore water is low and hence the accumulated excess pore water requires larger number of stress cycles to build up. On the contrary, at higher repeated stress, $0.8q_u$, a rapid build up of excess pore water pressure is expected and hence less number of stress cycles is needed to reach failure.

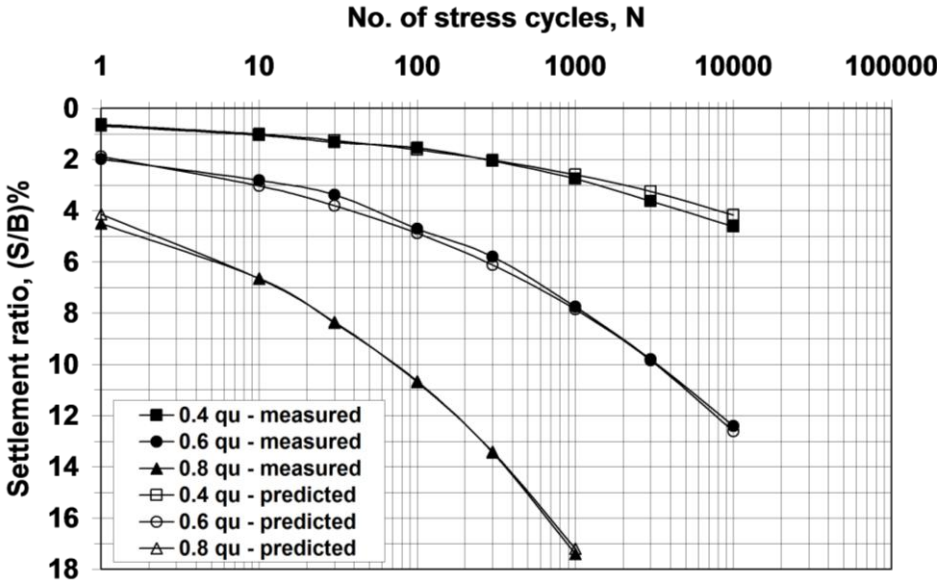

Figure 2: Number of stress cycles & settlement ratio of untreated soil

The test data were also analyzed using **Data Fit Software**, and the following equation was obtained.

$$S/B = 4.344662E\text{-}04(\alpha . q_u)^{2.73} * N^{0.206} \quad (1)$$

Where: S/B: settlement ratio, N: number of stress cycles, α: stress ratio (0.4,0.6 and 0.8), q_u: the ultimate monotonic stress at failure in (kPa). Figure 2 demonstrates that the results obtained from equation 1 are in excellent agreement with experimental results and the coefficient of correlation R^2 is 0.998. The definition of failure in repeated tests is considered as the number of stress cycles required to generate a settlement equal to 10% of the footing width, S/B =10%.

Table 3 demonstrates the number of stress cycles required to reach failure for the three model tests. To correlate the generated settlement ratio after a specific number of stress cycles to the stress ratio, the term factor of safety is introduced denoted by SF. The factor of safety is determined by dividing the bearing ratio at failure from the monotonic test i.e q_u/c_u = 5.13 kN/m^2 by the monotonic bearing ratio that

corresponds to a settlement ratio generated after a specific number of repeated stress cycles for a particular stress ratio.

Table 3: Number of stress cycles at failure for untreated soil at different applied stresses

Applied stress, $\alpha\ q_u$ (kPa)	No. of stress cycles, N	
	Measured	Predicted
0.4 q_u	713090	>10000
0.6 q_u	3307	3400
0.8 q_u	73	75

The variation of safety factor FS versus logarithm number of stress cycles, N, for applied stresses of $0.4q_u$, $0.6q_u$ and $0.8\ q_u$ are shown in Figure 3. The results imply that the factor of safety decreases with increasing both number of stress cycles and applied stress ratio, maximum values occur after the first cycle followed by a gradual decrease with increasing number of stress cycles

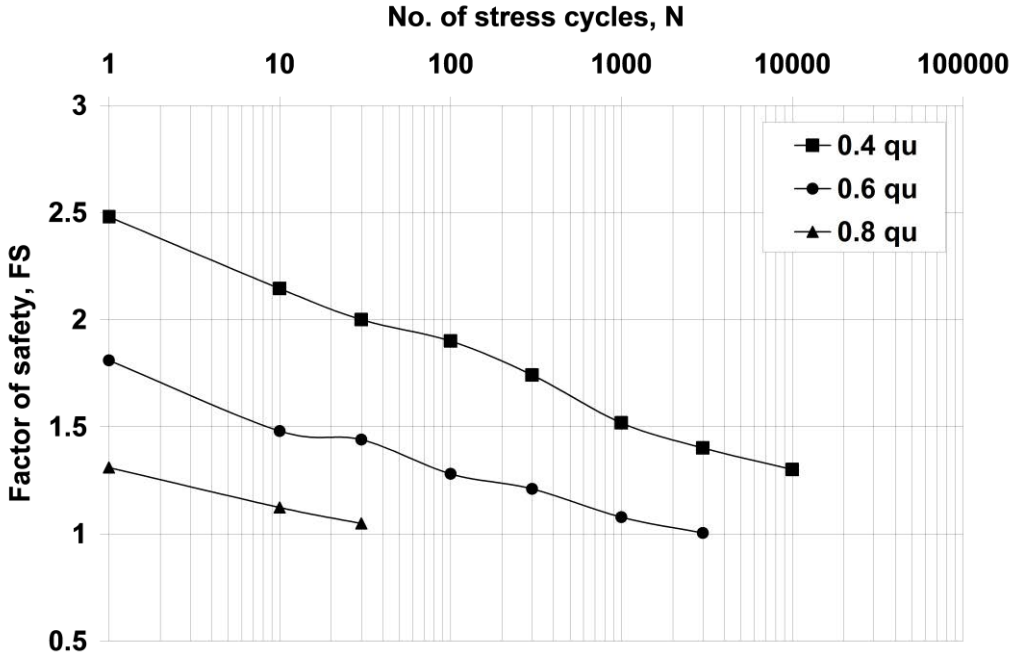

Figure 3: Factor of safety versus number of stress cycles for untreated soil

3.3 Model Test Results of Soil Treated with Reinforced Ballast Embankment and Ordinary Stone Columns

This series consists of three model tests performed on soft clay treated with ballast reinforced by a single geogrid layer placed along the interface between ballast and the bed of clay incorporated with eight ordinary stone columns. Repeated cycles of stress ratio $0.4q_u$, $0.6q_u$ and $0.8q_u$ applied where $q_{u=}$ 129 kPa is the stress at failure. Figure 4 shows the relationship between the settlement ratio S/B and the logarithm of the number stress cycles, N. The figure demonstrates similar behaviour to the untreated soil where the settlement ratio S/B increases with increasing both number of stress cycles N and applied stresses. It appears that at lower number of repeated loading, the tensile strength of the geogrid is mobilized and thereby reducing the lateral movement of the granular particles. However, as the repetition of the load increases, the granular particles were able to interlock and move laterally within the relatively thick layer above the geogrid. Extra resistance to the applied repeated stresses is also provided by the incorporation of ordinary stone columns with the geogrid layer. The test data were analyzed using **Data Fit Software**, and the following equation was obtained

$$S/B = 1.205E\text{-}03(\alpha.\ q_u)^{1.83} * (N)^{0.193} \quad (2)$$

Figure 4 shows that the predicted results obtained from equations 2 are in excellent agreement with experimental results with R^2=0.993. At low stress ratio, 0.4qu, there is marginal difference in the generated settlements up to 1000 stress cycle. This may be attributed that under this low stress the combined effect of reinforced ballast and ordinary stone columns has not yet become effective. As the repeated stress ratio increases to $0.6q_u$ and $0.8q_u$, the combined effect of ballast reinforcement and ordinary stone columns on the generated settlement becomes significant. In other words mobilization of the resisting stresses gradually becomes effective with increasing number of cycles and stress ratio. Table 4 presents measured and predicted number of cycles required to reach failure for applied stresses of $0.4q_u$, $0.6\ q_u$ and $0.8q_u$.

Table 4: Number of stress cycles at failure for soil treated with reinforced ballast incorporated with ordinary stone columns at different applied stresses

Applied stress, $\alpha\ q_u$ (kPa)	No. of stress cycles, N	
	Measured	Predicted
$0.4\ q_u$	>10000	432351
$0.6\ q_u$	7025	9250
$0.8\ q_u$	700	605

Similar to the untreated model tests, the factor of safety was calculated in the same manner for each repeated stress ratio and plotted versus number of cycles in figure 5. The figure indicates a gradual decrease in the factor of safety with increasing number of cycles, the three repeated stress ratios exhibited a consistent trend bounded by the upper limit representing the lower stress level, $0.4\ q_u$ and the lower limit representing the upper stress level, $0.8\ q_u$. The figure provides guide lines for the designer to determine the number of repeated stress cycles before maintenance is needed based on the selected factor of safety and the level of repeated applied stress.

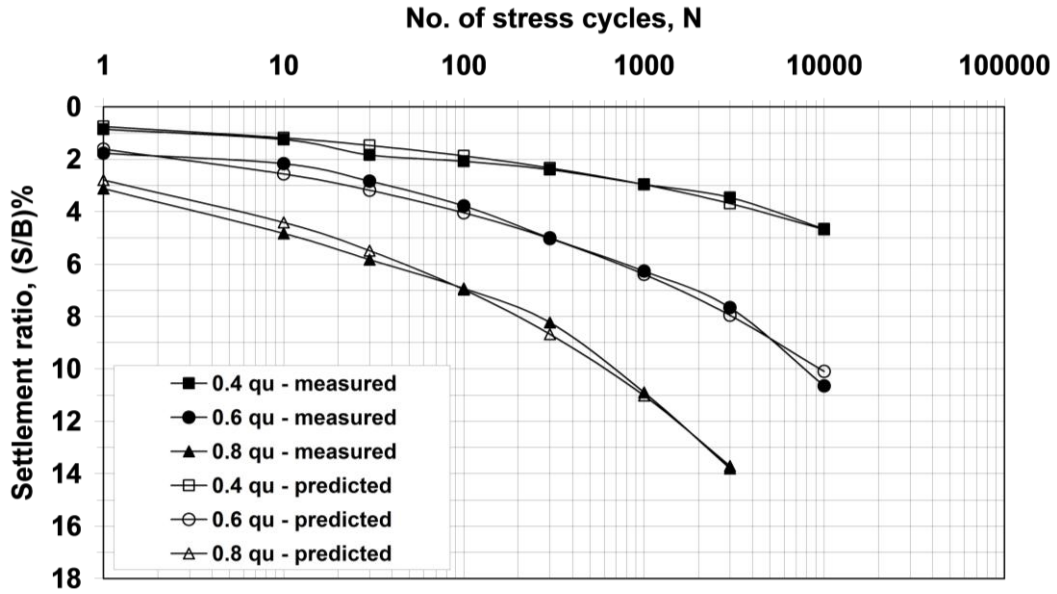

Figure 4: Number of stress cycles & settlement ratio for model tests with reinforced ballast incorporated with ordinary stone columns

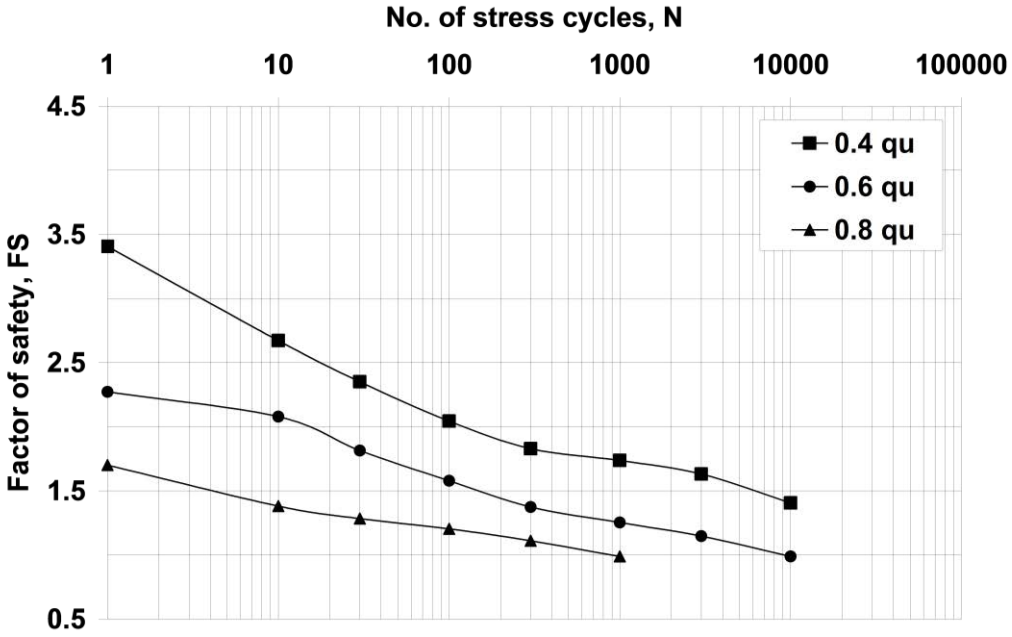

Figure5: Factor of safety versus logarithm number of stress cycles for model tests with reinforced ballast incorporated with ordinary stone columns

3.4 Model Test Results of Soil Treated with Reinforced Ballast Embankment and Encased Stone Columns

Similar to the previous section, three model tests were performed with ballast embankment reinforced with a single geogrid layer along the interface surface overlaying a bed of soft soil reinforced with eight encased stone columns. Repeated stress ratios of 0.4 q_u , 0.6 q_u , and 0.8 q_u were applied for each model respectively, where q_u = 151 kPa is stress at failure obtained from the monotonic test. Figure 6 shows the variation of the number of cycles versus settlement ratio for the three repeated stress ratios. The curve corresponding to repeated stress 0.4q_u demonstrated marginal increase in settlement ratio within the first 10 cycles then gradual increase was observed with increasing number of cycles. The other models tested at applied stress 0.6q_u and 0.8q_u demonstrated a significant increase in settlement ratio from the beginning of the test and increases rapidly with increasing number of cycles. The presence of the geogrid along the base of the embankment and the encasement around the stone particles in the columns provided extra resistance to the applied stress. Data Fit Software was used in the analyses and revealed the following equation

$$S/B = 3.1728E\text{-}04(\alpha.\ q_u)^{1.894} * (N)^{0.199} \quad (3)$$

Predicted results of settlement ratio from equation 3 showed excellent agreement with the measured data, the coefficient of correlation R^2 = 0.993. Table 5 indicates the number of repeated stress cycles required to reach failure for the three stress ratios

Table 5: Number of stress cycles at failure for soil treated with reinforced ballast incorporated with encased stone columns at different applied stress ratios

Applied stress, α q_u (kPa)	No. of stress cycles, N	
	measured	Predicted
0.4 q_u	>10000	445832
0.6 q_u	7800	9402
0.8 q_u	700	608

Figure 7 demonstrates the variation of factor of safety with the logarithm of the number of cycles for the three stress ratios. The figure demonstrated the same trend of relationship between the factor of safety and number of repeated stress cycles. Again if such technique of soil improvement is used to account for a specific type of loading or in case of upgrading an existing railway line, then this figure can provide satisfactory indication about the safety and maintenance requirements.

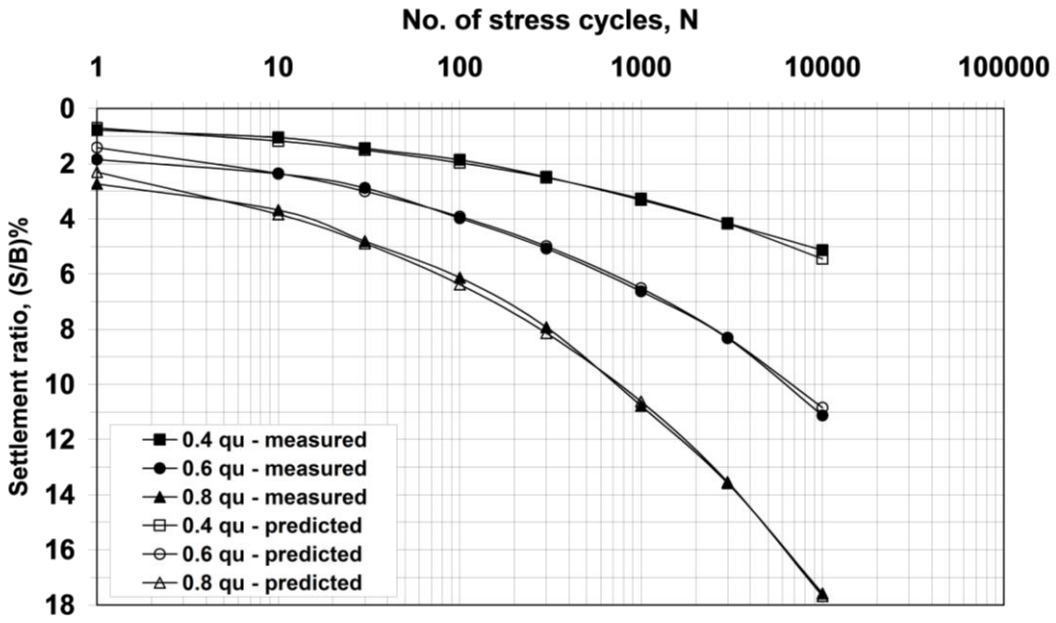

Figure 6: Number of stress cycles & settlement ratio for model tests with reinforced ballast incorporated with encased stone columns

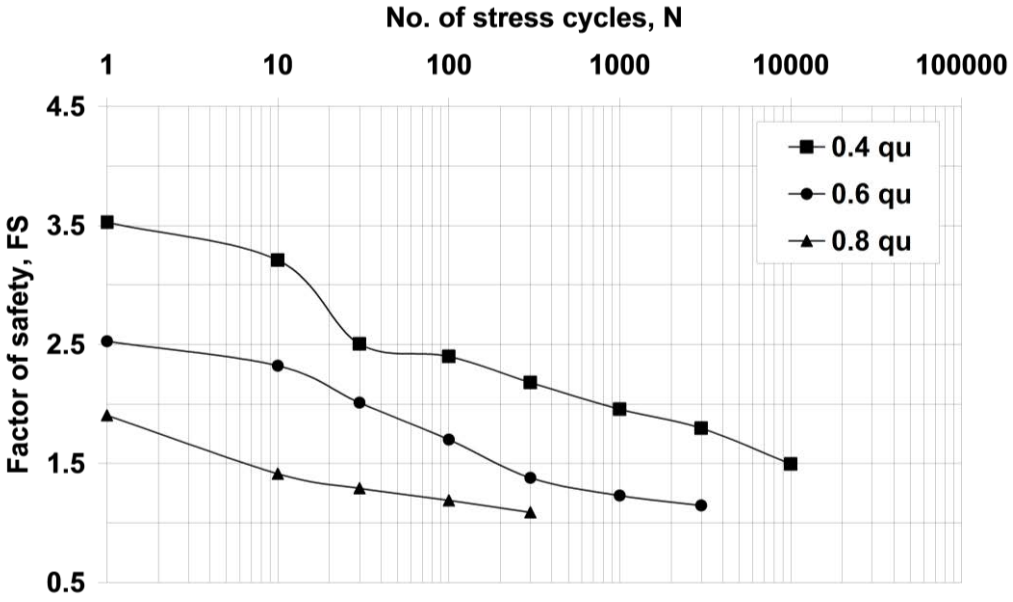

Figure 7: Factor of safety versus number of stress cycles for model tests with reinforced ballast incorporated with encased stone columns

3.5 Comparison at Constant Applied Stress

The previous sections demonstrate the behaviour of both treated and untreated model tests at different stress ratios, in other words $0.4q_u$ of the untreated soil does not equal to $0.4q_u$ of the treated soil because q_u is the stress at failure obtained from the monotonic test for each type of treatment. To clarify this point comparison is made at constant repeated stress. The selected value represents $0.6q_u$ of the untreated soil equivalent to 27.7 kPa. Figure 8 represents the relationship between the number of cycles versus settlement ratio for the untreated soil, soil treated with reinforced ballast embankment incorporated with ordinary stone columns and soil treated with reinforced ballast embankment incorporated with encased stone columns. The figure clarifies that within the range of stress cycles, $\leq$ 10000, both types of treatments generated close settlement ratios increasing at very slow rate with logarithm of cycles. The untreated soil demonstrated a rapid development of settlement and reached failure after 3400 cycle. Thus

it can be stated that both treatments can provide a prolonged period of operation before any maintenance is required.

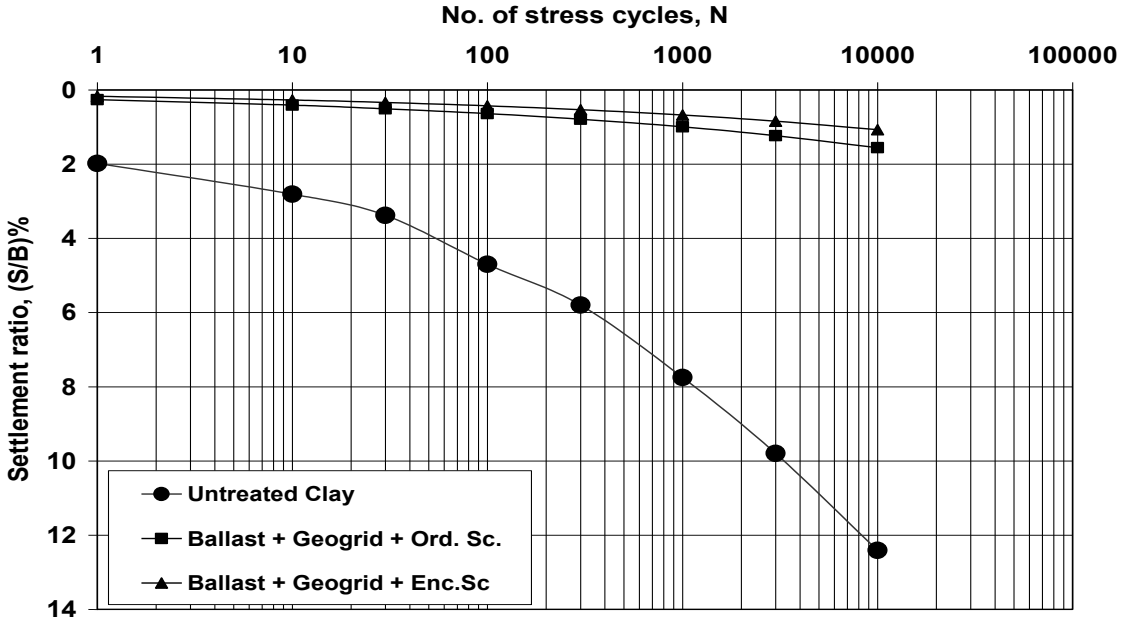

Figure 8: Number of stress cycles versus settlement ratio for different model tests at constant stress

4. CONCLUSIONS

Within the limited number of tests performed, the following points are drawn

1- The model tests performed under monotonic conditions revealed bearing ratio at failure of 5.13, 14.3, and 16.8 for untreated soil, soil treated with reinforced ballast embankment incorporated with ordinary stone columns and soil treated with reinforced ballast embankment incorporated with encased stone columns respectively. These outcomes indicate bearing improvement ratios of 2.8 and 3.3 over the untreated conditions.

2- The overall behaviour observed form all model tests demonstrated an increase in settlement ratio with increasing both applied stress ratio and number of stress cycles.

3- The predicted settlement ratio using equations 1, 2, and 3 exhibited excellent agreements with measured values from model tests.

4- The factor of safety versus number of cycles for each pattern of improvement can provide satisfactory guideline of the life time of the ballast according to the applied stress ratio and the selected failure criteria.

5- The model test performed at constant repeated stress demonstrated the effectiveness of the two improvement patterns in terms of the generated settlement with increasing number of cycles as compared to the untreated soil.

REFERENCES

Wu, C.S. and Shen, C.Y., 1997, Improvement of soft soil by geosynthetic-encapsulated granular column, Proceedings of the 3rd International Conference on Ground Improvement Geosystems, 3-5 June, pp.212-217

Zakariya, W.A.S., 2001, Soil improvement using stabilized and non- stabilized stone columns with different reinforcement configuration , Ph.D. Thesis, University of Technology / Iraq.

Malarvizhi, S.N. and IIamaparuthi, k., 2002, Load versus settlement of clay bed stabilized with stone columns and reinforced stone columns , Proceedings of the 3rd Asian Regional Conference on Geosynthetics, GEOASIA pp.322-329 / Seoul, Korea,.

Ginel, J. and Bouazza, A., 2008a , Model tests on geogrid encased stone columns , Proceedings of the 4th Eourpean Geosynthetics Conferences ,Paper No.150 / Edinburgh.

Ginel, J. and Bouazza, A., 2008b, Numerical modelling of small-scale geogrid encased stone columns , Proceedings of the 2nd International Workshop on Geotechnics of soft soils , pp.143-149 / Glasgow, Scotland.

Ginel, J. and Bouazza, A., 2008c, Predicted site behavior of geogrid encased stone columns, Proceedings of the 5th Eourpean Geosynthetics Conferences, Paper No.120 / Edinburgh

Majeed, K.G., 2008, Assessment of load capacity of reinforced stone column configurations, M.Sc. Thesis / University of Technology / Iraq.

Yoo, C., 2010, Performance of geosynthetic - encased stone columns in embankment construction: numerical investigation, Journal of geosynthetic and geoeniveronmental Engineering, Volume 136, Issue Number 8 / Publisher: American Society of Civil Engineering.

Ashford,S.A., Rollins,K.M., Bradford S.C, Wearer,T.J. and Baez, J.I., 2000, Liquefaction mitigation using stone columns around deep foundation : Full scale test results, TRR No. 1736/ Soil mechanics

Jinchi Lu, Zhaohui Yang, Korhan Adalier, and Ahmad Elgamal .2004, Numerical Analysis of stone column reinforced silty clay, Proceeding of 15th Southeast Asian Geotechnical Conference (15SEAGC), Vol.1 / Bangkok, Thailand, Nov. 23-26.

Rahil, F.H., 2007, Improvement of soft clay underneath a railway track Model using stone columns technique, Ph.D. Thesis, University of Technology / Iraq.

Assessment of software for the design of columnar reinforced soil

Mounir Bouassida, Simpro Geotechnical Consulting Office, Tunisia, contact@simpro-tn.com
Lassaad Hazzar, Simpro Geotechnical Consulting Office, Tunisia, Lassaed.Hazzar@usherbrooke.ca
Abir Mejri, Simpro Geotechnical Consulting Office, Tunisia, mejri.abiir@gmail.com

ABSTRACT

Recently, Columns software has been elaborated for the design foundations on reinforced soil by columns (Bouassida & Hazzar, 2012). Columns software incorporates a methodology of design that is based on two verifications: bearing capacity then settlement to determine the optimized improvement area ratio. In such manner the quantity of column material cannot be overestimated. The group of columns and unit cell models are both programmed to predict the bearing capacity and settlement by of reinforced soil by columns. Reinforcement by stone or sand columns and deep mixing techniques can be considered for different types of foundations: rigid footings, embankments and storage halls. When columns are made up of drained material the evolution of settlement of reinforced soil is predicted by a poro elastic model. The suggested paper aims to a brief presentation of Columns software and the validation of predictions made by this novel tool of design. For this purpose, data provided from different case histories and scaled (or full scale) test models with recorded measurements are considered to carry out the design of foundation on reinforced soil by columns. The comparison between predictions given by Columns software and results obtained by existing methods of design and/or standards is discussed. It is then concluded about the confidence of predictions made by Columns software and its capability to conduct a comprehensive design for all columnar reinforcement techniques.

1. INTRODUCTION

Columns 1.01 is software dedicated to the design of rigid or flexible foundation on a soil reinforced by columns (stone columns, sand columns, Deep Mixing). It has been recently developed by the geotechnical consulting office Simpro, (Bouassida & Hazzar, 2012). The software provides predictions of bearing capacity, settlement (before and after reinforcement), and primary consolidation of columnar reinforced soil, by using various methods and approaches. Also, Columns 1.01 software, proceeds to a rational design that enables an optimized improvement area ratio, which controls the cost of reinforcement. The results obtained by columns.1.0 software have been assessed through analysis several cases histories, scaled test models and full scale experiments, (Bouassida & Hazzar, 2009).

The present paper investigates, the model adopted by Saadeldin et al. [4], in which the performance of road embankment founded on cement stabilized soft clay (CSC), and a compacted sand founded on fill formation are compared. Numerical results have obtained by using Plaxis-2D-V8 in plane strain condition. These finite element results are discussed, then, they are verified by using Columns 1.01 software from which a new solution of reinforcement is suggested and interpreted.

2. GEOMETRY OF THE PROBLEM

A road embankment of 2m thickness and 16m width base is founded on a soft clay layer which extends to 15m depth beneath the ground surface. The underneath soil profile is composed of two layers, the first layer was either CSC or compacted sand fill ,ranging from 1 to 5 m depth under the embankment, while the second one was soft clay extending to 15m depth. In order to simulate different levels of loading on the road embankment, additional surcharge load (q), varying from 10 to 50 kPa, was added on the top of the embankment.

The stability of the embankment has been analyzed for the performances provided by two ground improvement techniques suggested by Saadeldin et al (2011). The first reinforcement technique consisted in the treatment of the soft clay by cement stabilization, and by the second technique, it was proposed the substitution of the upper portion of the soft clay by a compacted sand fill.

3. SOIL MODELING

Saadeldin et al. (2011) carried out their numerical calculation by using Plaxis-2D-V8 software. The hardening soil model (HSM) and Mohr Coulomb (MC) model were respectively adopted to simulate the behavior of the soft clay layer and the improved layer (either by CSC or sand compaction methods) subjected to the load induced by the embankment. Figure 1 presents the numerical model considered by Saadeldin et al. (2011). Tables 1 and 2 summarize the geotechnical parameters of the soft clay, the CSC and the sand fill material adopted for the numerical computation.

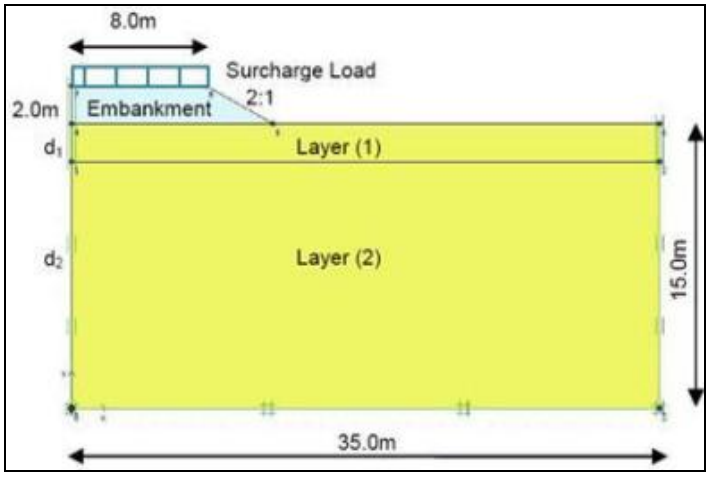

Figure 1: Numerical model (Plaxis-2D-V8) [4]

Table1: Input parameters for the behavior of soft clay layer (HSM) [4]

Parameter	Undrained	Drained
Saturated unit weight (kN/m^3)	15.8	15.8
Cohesion (kPa)	12	1
Friction angle (Degree)	0	25.6
Angle of dilatancy	0	0
Stiffness (kPa)	430	430
Tangent stiffness (kPa)	500	500
Power (m)	1	1
Horizontal permeability (cm/sec)	$1x10^{-6}$	$1x10^{-6}$
Vertical permeability (cm/sec)	$1x10^{-6}$	$1x10^{-6}$
Initial void ratio	1.81	1.81
Unloading / Reloading stiffness (kPa)	1300	1300
Poisson's ratio	0.45	0.2
Reference stress for stiffness's (kPa)	62	0.62
Coefficient of lateral stress in NC	1	0.568
Failure ratio	0.9	0.9

Table 2: Soil parameters used for CSC material and compacted sand fill (MC) [4]

Parameter	CSC (Undrained)	Compacted Sand Fill (Drained)
Saturated Unit weight (kN/m^3)	18.5	20
Cohesion (kPa)	121	1
Dilatancy (degree)	0	41
Friction angle (degree)	0	14
Stiffness (kPa)	5000	37000
Initial void ratio	0.9	1
Poisson's ratio	0.2	0.3

4. PREDICTION OF THE BEARING CAPACITY OF UNREINFORCED GROUND

The ultimate bearing capacity of the initial soil has been estimated by considering Terzaghi's formula for a strip footing:

$$q_u = \frac{1}{2} S_\gamma \gamma B N_\gamma + S_q \gamma D N_q + S_c c N_c \quad (1)$$

S_γ, S_q, S_c : coefficients that depend on the shape of the footing ;

N_γ, N_q, N_c: bearing capacity factors only depending of the angle of internal friction φ;

γ : saturated unit weight (kN/m^3).

The embankment loading has been assumed as uniform surcharge q', applied on the surface of the soil, then the embedment depth is D = 0. In undrained condition, the angle of internal friction is zero and N_γ = 0 and N_c = 5.14, then the ultimate bearing capacity is:

$q_{ult} = 5.14 \times 12 = 61.7kPa$ (2)

The total applied vertical stress at ground surface is:

$q' = \gamma H + q = 20 \times 2 + q = 40 + q$; (3)

H denotes the embankment height, γ is the saturated unit weight of embankment material and q is a uniform surcharge applied to the crest of embankment (Figure 1).

The stability of initial soil is fulfilled under the condition: $q_u > F\, q'$, F denotes the factor of safety against punching the foundation layer of the embankment.

$q_u > F\,(40 + q)$, then: $(q_u/F) - 40 > q$. (4)

When assuming the minimum factor of safety (F = 1) one obtains: $21.7 > q$. It is then concluded that the stability of initial soil is affected, when the surcharge q exceeds 21.7 kPa. Consequently the soil of foundation should be reinforced in order to increase its bearing capacity when subjected to the load induced by a 2 m height of embankment, regardless the verification of settlement.

5. ESTIMATION OF SETTLEMENT OF THE UNREINFORCED SOFT CLAY

The long term settlement, at ground surface, has been predicted, by Saadeldin et al (2011), for different surcharge load cases: q = 10 to 50 kPa. Referring to the previous computation of bearing capacity, for $q > 21.7\ kPa$, the security factor of safety is $FS < 1$, then the prediction of settlement does not makes sense as sketched in Figure 2.

Once the geometrical and mechanical characteristics of the foundation, the applied load and the initial soil are introduced, Columns software can estimate the settlement on unreinforced soil by using the theory of linear elasticity. The obtained results are summarized in Figure 3.

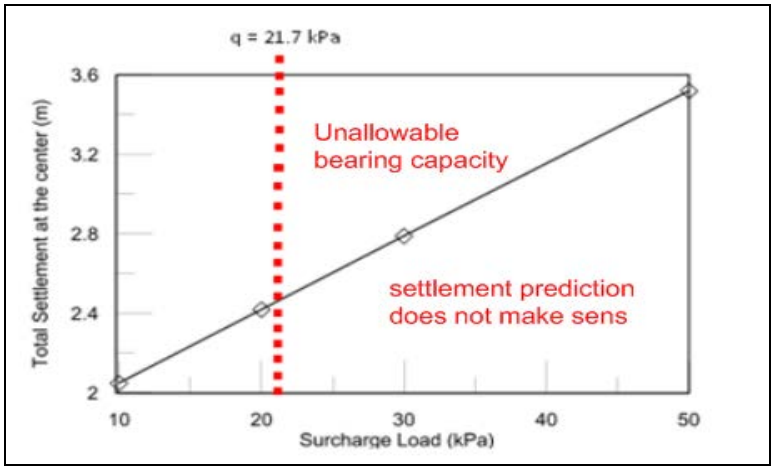

Figure 2: Consolidation settlement versus load intensity (Plaxis) at centre line of embankment [4]

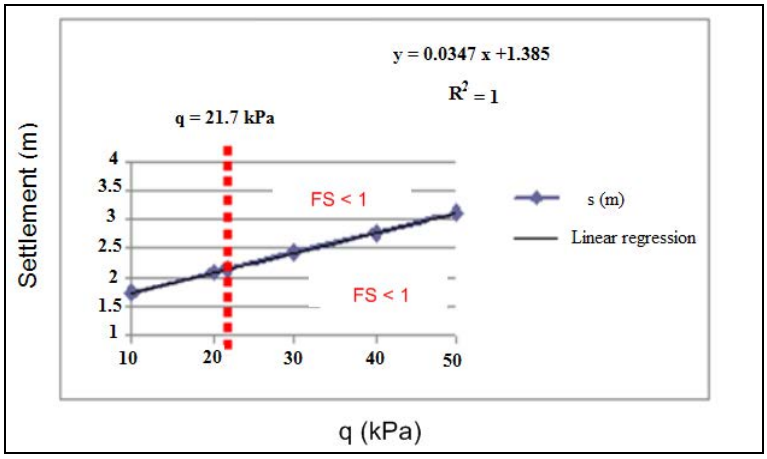

Figure 3: Settlement prediction vs load intensity by Columns software

The variation of total settlement versus the load intensity predicted either by Plaxis software or by Columns software, is almost the same. Indeed, predicted slopes of the linear fits are respectively, 3.7 % and 3.5% (Figures 2 and 3). Otherwise, settlements predicted by Plaxis are more pronounced compared to those estimated by columns software. In fact, results provided by Plaxis (Figure 2) are estimated for the short term behavior, whereas, settlement of the initial soil, by columns software is estimated by using the variational method in linear elasticity (Bouassida et al, 2003) is estimated for the short term behavior especially for clayey soils.

6. COMPARISION BETWEEN CEMENT STABILIZATION AND SOIL REPLACEMENT TECHNIQUES

6.1. Settlement of reinforced soil

To improve the behavior of the embankment, Saadeldin et al (2011) have proposed to substitute the first soil layer, by CSC or by compacted sand material, of depth varying from 1 to 5 m. The normalized settlement (ratio of settlement reinforced ground to that of unreinforced ground) at ground surface versus the depth of reinforcement is shown in Figure 4 for different load levels.

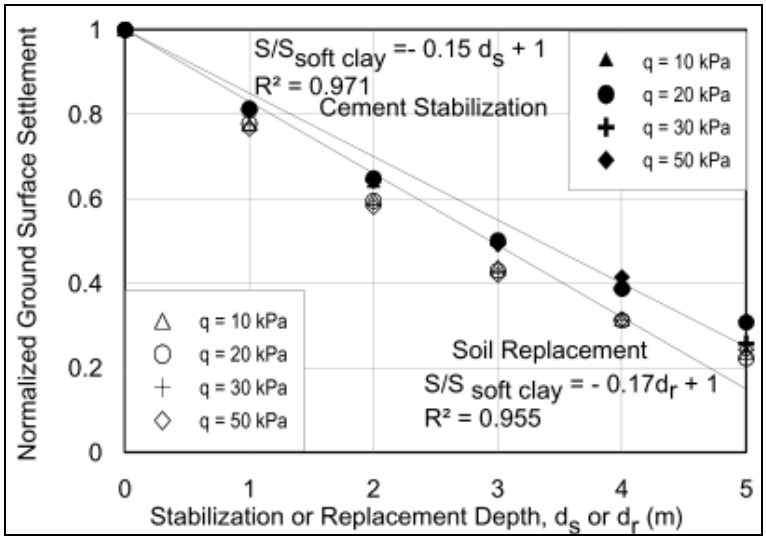

Figure 4: Normalized settlement (Plaxis) at ground surface for cement stabilization & soil replacement vs depth of replacement (Saadeldin et al, 2011)

As first approach, it has been proposed to compare the predicted displacements, by Plaxis (Saadeldin et al, 2011), to settlements estimated by Columns software for an improvement area ratio equals to 100 % (corresponding to total replacement of initial soil) and a depth reinforcement ranging from 1 to 5 m. Results are shown in Figures 5 and 6.

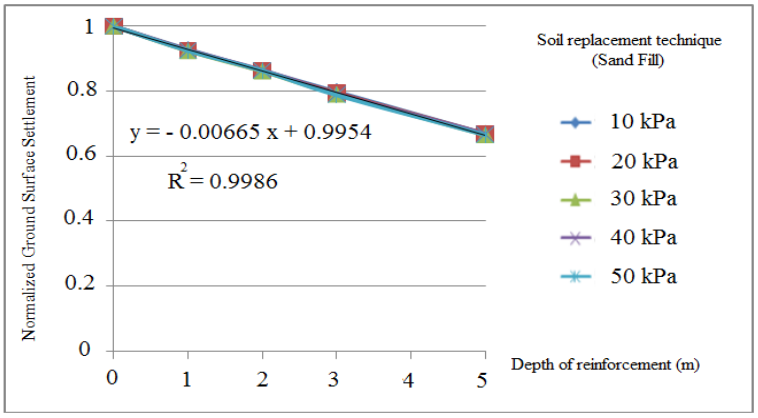

Figure 5: Normalized settlement (Columns) at ground surface for sand fill technique vs depth of replacement

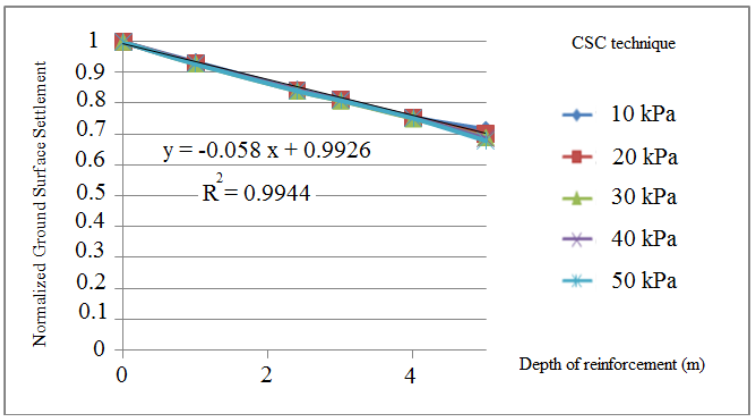

Figure 6: Normalized settlement (Columns) at ground surface for cement stabilization technique vs depth of replacement

Predictions of the reduction of settlement at ground surface are basically similar by Plaxis and Columns software's. Both Plaxis and Columns assessments show that there is no significant difference between the effect of cement stabilization and soil replacement, on the reduction of ground surface settlement. For each additional meter of cement stabilization depth, Plaxis predicts a decrease of normalized settlement by approximately 15 %. While Columns software predicts the normalized settlement is decreased by 5.8 %. For soil replacement technique, the normalized settlement, predicted by Plaxis, decreased by 17 %, and is estimated by 6.6 % by Columns software (Figure 7). It follows that the short term settlement predicted by Columns software is lower than that predicted by Plaxis software that is the long term settlement.

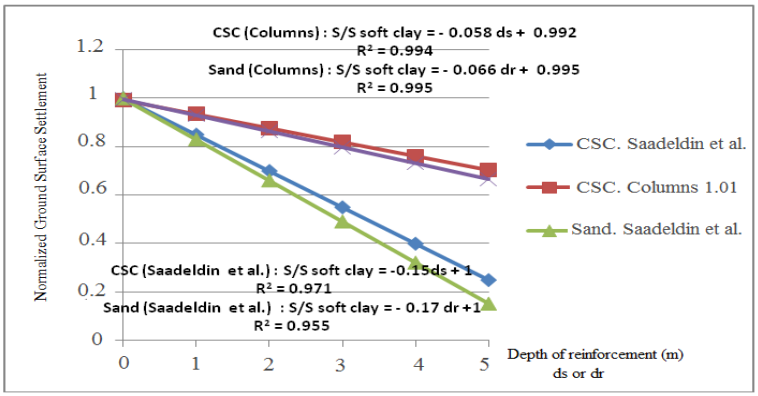

Figure 7: Comparison between normalized settlements by Plaxis & Columns software's for soil substitution of two improvement techniques

6.2. Columnar Reinforcement Technique

Instead of substituting the foundation layer of the embankment along 5m depth, by CSC or by replacement technique, as investigated by Saadeldin et al (2011), it is herein proposed to reinforce the weak soil by CSC or sand columns. The design of the foundation built on columnar reinforced soil was carried out by using Columns 1.01 software. The design procedure consists in estimating the optimized improvement area ratio η_{opt} which complies with the verifications of allowable bearing capacity and settlement.

The optimized substitution factor depends on the allowable settlement, on the applied surcharge and the depth of reinforcement. It was supposed that the allowable settlement is by 10 cm over long term behavior. Once the optimized substitution factor was predicted, Columns is computes, for different diameters, and the number of columns associated. Also, it can predict the volume of the needed material for reinforcement. Then, it is easy to compare the volume of substitution material (η=100%) used by Saadeldin et al (2011) to the one predicted by Columns. Tables 3 and 4 present the optimized substitution factor, the percentage of reduced material, for sand and CSC columns respectively.

Table 3: Optimized improvement area ratio and percentages of saving of Sand Fill substitution

Applied surcharge (kPa)	Column's depth(m)	Optimized improvement area ratio η_{opt} (%)	(%) of saving over 100 m^3 of substitution material
10	7	32	55
20	7.5	17	75
30	7.5	31	54
40	7.5	44.5	33
50	7.5	58	12.5

It can be concluded that the reinforcement by columnar reinforcement is much more economical, than the first technique which consisted in total substitution of weak soil along 5m depth suggested by Saadeldin et al (2011). Indeed, even if the length of columns exceeds 5m, the optimized substitution factor definitely is less than total substitution (η=100 %).

Table 4: Optimized improvement area ratio and percentages of saving of CSC substitution

Applied Load (kPa)	Column's depth(m)	Optimized improvement area ratio η_{opt} (%)	(%) of saving over 100 m^3 of substitution material
10	7.5	47	29
20	7.5	56	15.5
30	7.5	60	10
40	8	31	53
50	8	31	50

7. CONCLUSIONS

This paper has investigated the stability of a 2m height embankment subjected to uniform vertical load founded on soft clay layer reinforced by two improvement techniques: sand compaction and cement stabilization.

The first improvement option was the substitution of weak soil layer along varied depth from 1 m to 5 m. Numerical results of settlement estimations by Plaxis software (plane strain condition by adopting HSM and Coulomb behaviors) have compared to those predicted by Columns 1.0 software based on the linear elastic behavior. It was concluded a similar trend, in very small margin of error, has been obtained for the settlement reduction in function of the increase of treatment depth. The discrepancies between settlements predictions by Plaxis and Columns software's are essentially attributed to the difference between the used constitutive laws.

Second, a reinforcement by columns of the soft clay layer by cement stabilization and sand compacted materials by Columns software that provides an optimized improved ration has revealed much more efficient that a total initial soil substitution even if the length of columns exceeds the treatment of 5 m. Indeed significant savings of column material is noticed in comparison with a total substitution of soft clay layer which is indeed not cost effective and time consuming.

This comparative study has also confirmed that Columns software which based on a novel methodology of design is a useful tool for the study of stability of foundation on reinforced soil by columns.

REFERENCES

[1]. *M. Bouassida, L. Hazzar (2012). Novel tool for optimised design of reinforced soils by columns. In press, Ground Improvement ICE, London.*

[2]. *M. Bouassida, & L. Hazzar (2009). « Columns 1.0 » Software for the design of foundation on reinforced soils by columns. Internal report, Geotechnical Consulting Office SIMPRO, Tunisia.*

[3]. *M. Bouassida, Z. Guetif, P. de Buhan, & L. Dormieux, (2003). Estimation par une approche variationnelle du tassement d'un sol renforcé par colonnes. Revue Française de Géotechnique. 102, 21-29.*

[4]. *R. Saadeldin, M. A. Salem & H.A. Lotfi (2011). Performance of road embankment on cement stabilized soft clay. Proc. 14th Pan-American and 64th Canadian Geotechnical Conf. October 2-6 2011, Toronto, Ontario, Canada.*

Possibilities and limitations of embedded pile elements for lateral loading

Ronald B.J. Brinkgreve, Delft University of Technology, The Netherlands, r.brinkgreve@plaxis.nl
Erjona Engin, Plaxis bv, The Netherlands, e.engin@plaxis.nl
Thao Dao, Delft University of Technology, The Netherlands, daothao.85@gmail.com

ABSTRACT

The embedded pile element, based on original work by Sadek & Shahrour (2004), was further developed in the PLAXIS finite element software for axial loading of foundation piles (Septanika, 2005). In previous publications, the embedded pile has been verified and validated for axial compression, extension and bearing capacity (Engin et al., 2007). Improvements were suggested by Tschuchnigg (2009), which have meanwhile been implemented in the latest PLAXIS 3D version.
In a recent study at Delft University of Technology the embedded pile was evaluated for lateral loading due to external force and soil movement (Dao, 2011). Although the embedded pile formulation was not aimed to be used under lateral loading conditions, it was assumed that it could have good capabilities under such loading conditions due to the region around the pile in which soil behaviour is forced to remain elastic. This paper demonstrates the behaviour of embedded piles under lateral loading conditions by evaluating stress and displacement patterns around the pile and by comparing results with conventional volume pile modelling. Three situations are considered: A simple disk model, a full pile subjected to a lateral force at the top and a pile subjected to lateral soil movement as a result of embankment construction. The paper will conclude on the possibilities and limitations of embedded piles for lateral loading.

1. INTRODUCTION

The numerical modelling of laterally loaded piles in the finite element method and the interaction with the surrounding soil has been subject of several studies. In early years, when three-dimensional finite element calculations were not common practice, researchers modelled the pile as a beam and the surrounding soil as non-linear springs following so-called p-y curves (e.g. Poulos, 1971). Other researchers have modelled the pile-soil interaction with coupled horizontal finite element slices (e.g. Kooijman, 1989). All methods have their possibilities and limitations. In this paper the use of the embedded pile element, which was initially developed for three-dimensional finite element analysis of axially loaded piles, is evaluated for lateral loading conditions.
The embedded pile, based on the embedded beam element developed by Sadek & Shahrour (2004) for the modelling of reinforcement and micro piles, was further developed in the PLAXIS finite element program for axial loading of foundation piles (Septanika, 2005). In the embedded beam concept, a beam element (line element with zero thickness) is placed arbitrarily inside a volume element, using a special line-to-volume interface element to connect the beam to the volume. The properties of the interface are based on the interaction properties of the pile (e.g. shaft friction). In addition to the shaft friction, end bearing properties can be included by adding a point-to-volume interface at the pile tip. The properties of this interface are based on the end bearing capacity of a foundation pile. At the moment, both interfaces include only axial bearing capacity, whereas the response to lateral loading is fully elastic.
In order for a pile with given shaft friction and end bearing to obtain the required axial bearing capacity from the surrounding soil in the numerical model, an *elastic zone* with radius equal to the real pile is assumed around the beam and below the tip. Within this elastic zone, where standard soil properties apply, plastic strains are ignored to enforce irreversible soil behaviour and failure to occur only outside the pile zone. In this way the axial bearing capacity of the embedded pile is indeed governed by the behaviour in the interfaces. This enhancement makes the embedded pile almost behave as a volume pile.
The embedded pile was validated for situations of axial loading by Engin et al. (2007) and Tchuchnigg (2009). An improvement of the elastic interface stiffness was implemented based on suggestions by Tchuchnigg (2009) resulting in a more realistic distribution of the interaction forces.
Meanwhile, some users of the PLAXIS software started to use the embedded pile for lateral loading situations, even though it was mentioned that the embedded pile was not developed nor validated for such loading conditions. Considering the aforementioned observation that the embedded pile almost behaves as a volume pile, it was assumed that it might have lateral loading capabilities as well. A research project

was started at Delft University of Technology to evaluate the capabilities under such loading conditions. The results of that study form the basis of this paper. Since the lateral interaction between the embedded pile and the soil is fully elastic with a high artificial stiffness, the lateral resistance is entirely based on the behaviour of the surrounding soil. It is realised that this can only be valid for rough piles.
The next Section starts with a simple disk subjected to lateral prescribed displacement, representing a cross section with unit thickness across the pile at a particular depth. The subsequent Section considers a full pile embedded in the ground, subjected to a lateral force at the top. The last Section considers a pile next to an embankment, where the pile is subjected to lateral soil movement as a result of the embankment construction. The paper ends with conclusions on the possibilities and limitations of the current embedded pile for lateral loading conditions.

2. SIMPLIFIED DISK MODEL

This Section considers a horizontal slice with dimensions 8m x8m and unit thickness across the pile at a certain depth in the soil. The slice is fixed in vertical direction at the top and bottom, where it is free in horizontal direction. The model boundaries are fixed in horizontal direction. A 'disk' with diameter of 0.7m, representing a section across the laterally loaded circular pile, is included in the centre of the model. The disk is given a horizontal prescribed displacement at the top and bottom with the purpose to evaluate its load-displacement behaviour and the stress and displacement pattern around the pile. Different disk models are considered:

1. Volume pile model without interface elements (rough pile); the disk is composed of volume elements with pile properties (Fig. 1)
2. Volume pile model with inactive interface elements at the disk circumference (rough pile)
3. Volume pile model with active interface elements without strength reduction (rough pile)
4. Embedded pile model with disk, in which the embedded pile has the pile properties and the disk has elastic soil properties
5. Embedded pile model with disk and inactive interface elements
6. Embedded pile model with disk and active interface elements without strength reduction
7. Embedded pile model without disk. This is the 'normal' way embedded piles are used.

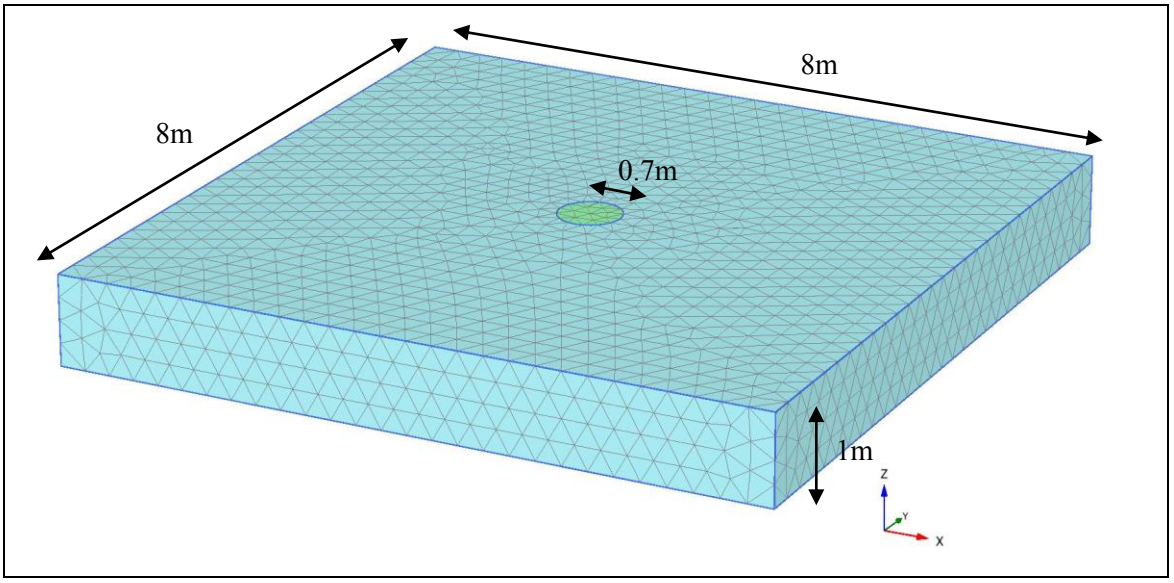

Figure 1: Volume pile model without interface elements – medium mesh density

Although the embedded pile is generally used without surrounding disk, models 4, 5 and 6 still consider a disk in order to make the finite element mesh similar to the corresponding model with volume pile. The size of the disk corresponds to the size of the elastic zone around the embedded pile.
The soil is modelled by means of the linear-elastic perfectly-plastic Tresca model and the pile is considered to be linear elastic. Weight is not relevant in this model. All model parameters are shown in Table 1.
Different finite element meshes are considered for each model, indicated as very coarse (~4000 10-node tetrahedral elements), coarse (~8000 el.), medium (~20000 el.), fine (~50000 el.) and very fine (~120000 el.), to evaluate the influence of the mesh density.

During the calculation, the prescribed displacement is applied to a maximum of 0.2m. The results of the calculations with different models are shown in the figures below.

Table 1: Model parameters

Parameter	**Symbol**	**Value**	**Unit**
Soil			
Model		Tresca	
Drainage type		Drained	
Young's modulus	E	10000	kN/m^2
Poisson's ratio	ν	0.3	-
Cohesion	c	10	kN/m^2
Tension cut-off		Not used	
Rel. interface strength (model 3 and 6)	R_{inter}	1.0	-
Volume pile			
Model		Linear elastic	
Drainage type		Non-porous	
Young's modulus	E	$3 \cdot 10^7$	kN/m^2
Poisson's ratio	ν	0.0	-
Embedded pile			
Equivalent diameter	D	0.7	m
Young's modulus	E	$3 \cdot 10^7$	kN/m^2
Poisson's ratio	ν	0.0	-
Vert. skin resistance at top and bottom	$T_{top,max}$, $T_{bot,max}$	500	kN/m

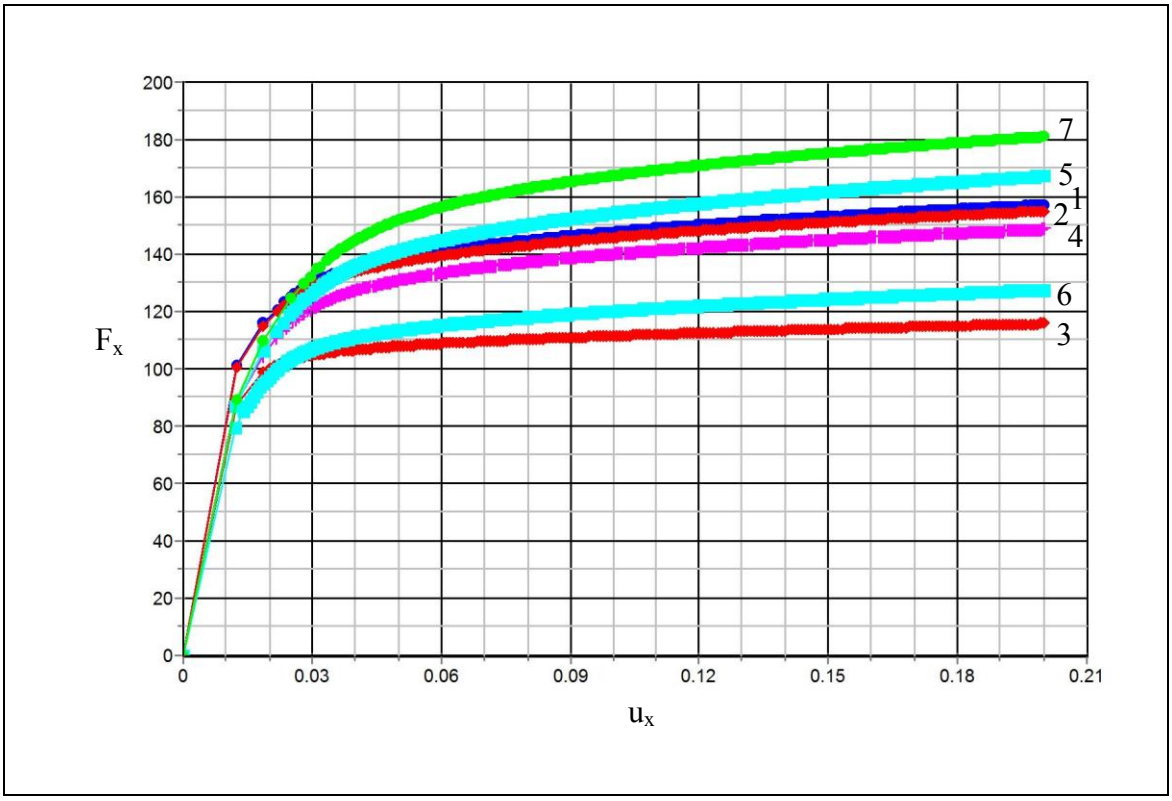

Figure 2: Load-displacement curves of different pile models – medium mesh density

Figure 2 shows the load-displacement curves of the different models for the medium mesh density. Considering the initial part of the curve it can be concluded that the stiffness response at relatively small displacements is very similar. At larger displacements the results become different, both in stiffness response as well as in failure load. The embedded pile seems to over-estimate the failure load compared to the volume pile, depending on the way it is modelled. In the case of a disk around the embedded pile

(corresponding with the elastic zone) the over-estimation is less than in the 'normal' case without disk. Typical is the role of interface elements. Although interface elements are 'logical' to be used to model the pile-soil interaction around the volume pile, it is not logical to use them in the case of the embedded pile, since the line-to-volume and point-to-volume interfaces of the embedded pile itself are supposed to dominate the behaviour. In both cases, the interface elements seem to influence the results significantly. As expected (at least for the volume pile), active interfaces give a less stiff response and smaller failure loads than inactive interfaces, whereas no interfaces gives the stiffest response and highest failure load. Similar conclusions can be made for the other mesh densities (not shown here), with the remark that coarser meshes give a stiffer response and higher failure loads than finer meshes, as expected.
Fig. 3 shows the displacement pattern around the pile at failure for the volume pile model (1; left) and for the embedded pile model (4; right), both without interface for the medium mesh density. The pattern of both models is very similar. Although the embedded pile has a zero thickness and the disk around the embedded pile has soil properties, the elastic zone around the embedded pile (inside the disk) moves as a relatively stiff volume with the pile. As a result, the embedded pile almost behaves as a volume pile.

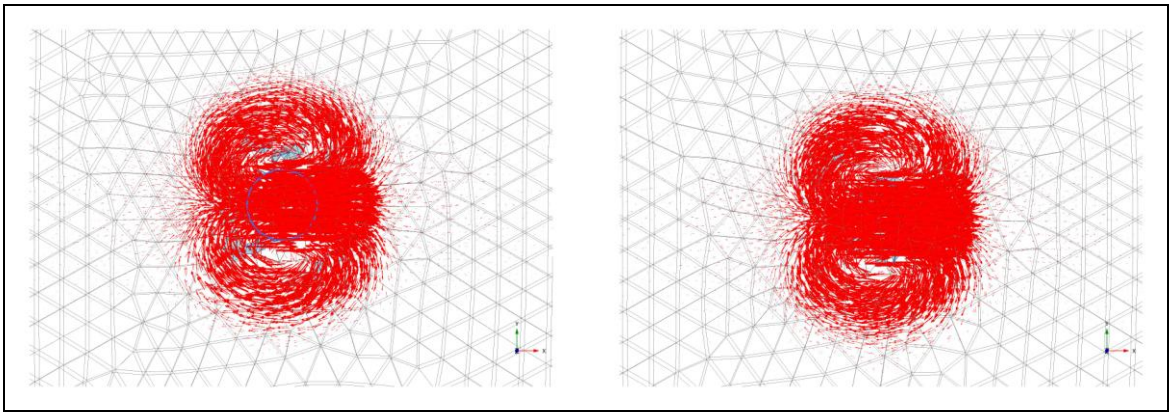

Figure 3: Displacement pattern around the pile at failure. Left: Volume pile; Right: Embedded pile

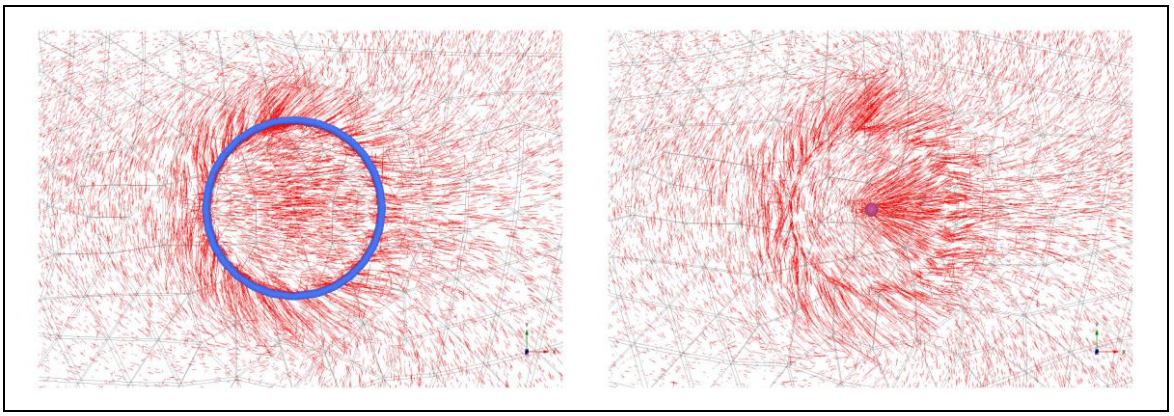

Figure 4:Major principal stresses around the pile at failure. Left: Volume pile; Right: Embedded pile

Fig. 4 shows the major principal stresses around the pile at failure for the volume pile model (1; left) and for the embedded pile model (4; right). The pattern around the pile circumference is again very similar. In front of the pile the major principal stresses are in the direction of the pile movement, whereas behind the pile the principal stresses are perpendicular to the pile movement. The latter is due to the reduction of stresses in the direction of the pile movement. The opposite can be said about the minor principal stresses. At the sides of the pile the principal stresses are rotated due to shearing. All is in accordance with expectation. It should be noted that in the embedded pile model the stresses inside the elastic zone are not realistic; neither as soil stresses, nor as pile stresses. Outside the elastic zone the stresses can be considered realistic, as discussed above.
In the 'normal' embedded pile model without disk (7), the observed diameter of the pile (based on the displacement and stress pattern; not shown here) is slightly larger than in the models with disk. This explains the over-estimation of the failure load. The over-estimation is less for a very fine mesh. This leads to the recommendation that a refined mesh is still needed around embedded piles.

From the results of the simplified disk model it is concluded that the displacement and stress pattern around the embedded pile under lateral loading is realistic for a rough pile, but that the failure load is over-estimated.

3. FULL PILE SUBJECTED TO LATERAL FORCE AT THE TOP

This Section considers a full pile with a length of 15m and a diameter of 0.5m, embedded in a soft soil layer. The pile is loaded by a horizontal force at the top. The full model has dimensions of 20x20x20m^3. Different pile models are used to simulate the pile behaviour with the purpose to compare the performance of the embedded pile with a 'classical' 3D finite element modelling using volume elements in the case of a laterally loaded pile under serviceability states. In addition to the load-displacement behaviour, the pile's deflection curve and bending moment distribution are compared.
The following pile models are considered (medium mesh density, ~10000 elements):

1. Volume pile model without interface around the pile (rough pile)
2. Volume pile model with interface around the pile without strength reduction (rough pile)
3. 'Normal' embedded pile model (without surrounding cylinder or local refinement) (Fig. 5)

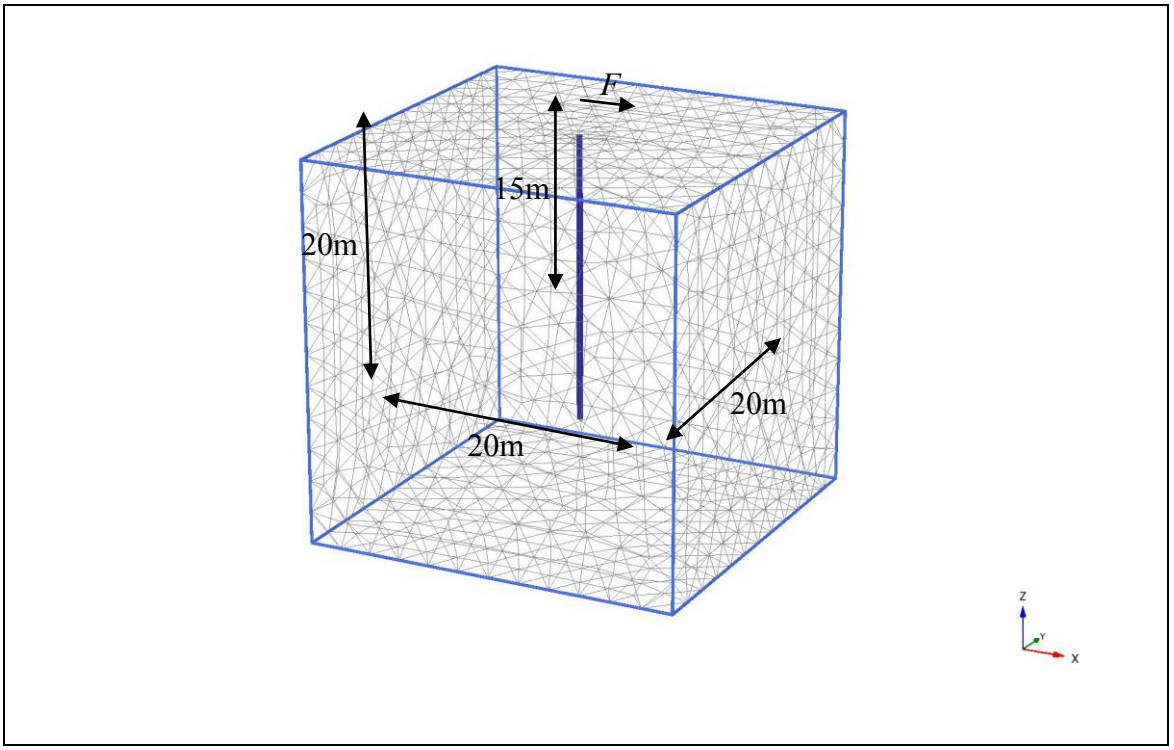

Figure 5: Embedded pile model of laterally loaded pile

The soil is modelled by means of the Soft Soil model and the pile is considered to be linear elastic. A slow loading rate is considered, resulting in a fully drained soil response. Table 2 shows all model parameters. The volume pile has similar properties as listed in Table 1.

Table 2: Model parameters

Parameter	Symbol	Value	Unit
Soil			
Model		Soft Soil model	
Drainage type		Drained	
Unit weight	γ	16.2	kN/m^3
Modified compression index	λ^*	0.085	-
Modified swelling index	κ^*	0.022	-
Poisson's ratio	ν	0.2	-
Cohesion	c	0.5	kN/m^2
Friction angle	φ	22	°
K0 in primary compression	K_0^{nc}	0.64	-
Tensile strength	T	0.0	kN/m^2
Permeability	k_x, k_y	0.004	m/day
Rel. interface strength (model 3 and 6)	R_{inter}	1.0	-
Embedded pile			
Equivalent diameter	D	0.5	M
Young's modulus	E	$3 \cdot 10^7$	kN/m^2
Poisson's ratio	ν	0.0	-
Moment of inertia	I	$3.07 \cdot 10^{-3}$	m^4
Vert. skin resistance at top	$T_{top,max}$	200	kN/m
Vert. skin resistance at bottom	$T_{bot,max}$	500	kN/m
Vert. base resistance	$F_{bot,max}$	10000	kN

The phreatic level is below the model, so pore pressures are zero. The soil is near-normally consolidated with a small pre-overburden pressure POP = 10 kN/m^2. The initial stresses (without pile) are generated using the K0-procedure with default K_0-value. After installation of the pile, displacements are reset to zero and a lateral force F = 500 kN is applied at the top of the pile.

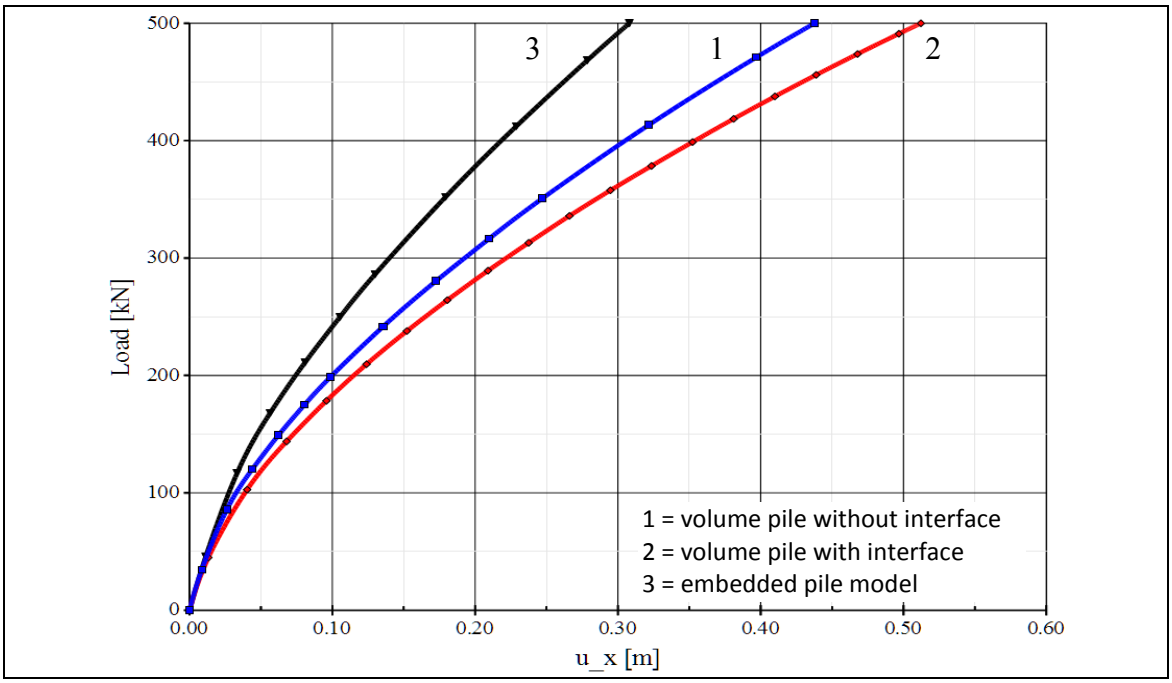

Figure 6: Load-displacement curves of pile top for different pile models

At the end of the test, a significant differential displacement between the (top of the) pile and the soil is observed (not shown here). Fig. 6 shows the load-displacement curves of the top of the pile for the three pile models. Although the load-displacement curve is highly non-linear, it can be concluded that the pile is still far from failure when the maximum force is reached.

At small displacements all models show a similar stiffness response, but at larger displacements there is a clear difference. Considering the volume pile models, the interface makes the response softer, whereas the embedded pile is stiffer than both volume pile models. This is consistent with the findings in the previous Section. The embedded pile response comes closer to volume pile response with a mesh refinement around the embedded pile (not shown here).

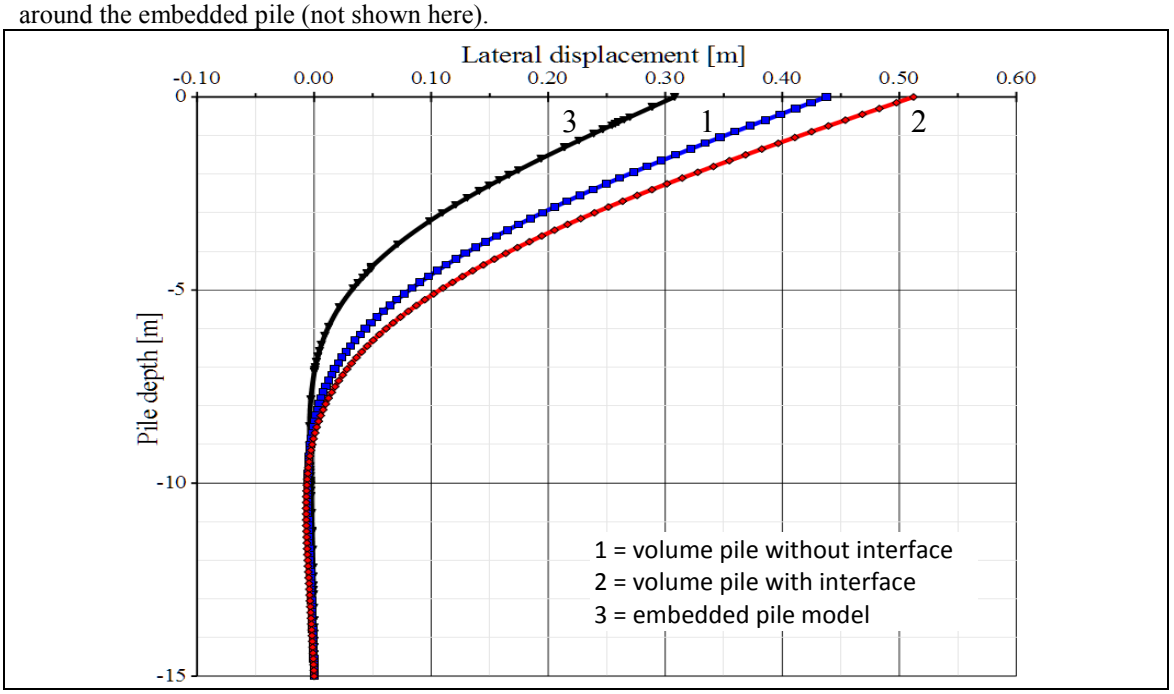

Figure 7 : Pile deflection curve for different pile models

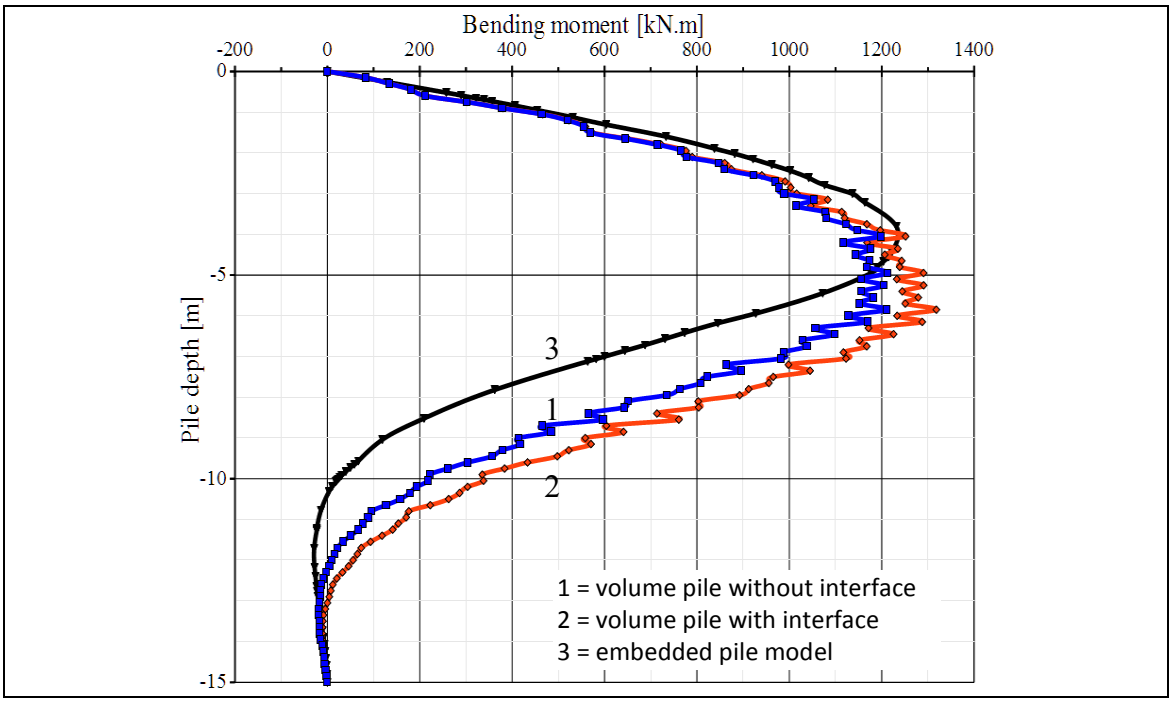

Figure 8: Pile bending moment distribution for different pile models

Fig. 7 and Fig. 8 show a comparison of pile deflection curves and bending moment distributions, respectively, for the situation where the full force is applied. Regarding the pile deflection, it can again be seen that the embedded pile shows a stiffer response than the volume pile models. As a result of this, the bending point is at a lower depth for the embedded pile than for the volume pile. This is confirmed by the plot with the bending moment distributions. However, the maximum value of bending moments is very similar (~1200 kNm) for all models.

It should be noted here that the deflection curves and bending moment distributions for the volume pile models have been obtained by inserting a 'soft beam' inside the volume pile (stiffness 10^{-6} times the real stiffness; bending moments multiplied by 10^{6}). Although this 'trick' is generally accepted, it does not give very smooth bending moments in this case, but the overall behaviour is still supposed to be representative. On the other hand, the embedded pile does give smooth results.
From the results of the calculations with the pile subjected to a lateral force at the top it is concluded that the embedded pile behaves stiffer than the volume pile, at least in a 'standard' mesh without refinement around the pile. This stiffer behaviour also affects the bending moment distribution, but the maximum value of bending moments is still very similar and realistic for rough piles.
In this case the pile has not been brought to failure. Based on the conclusions in the previous Section it can be expected that the embedded pile will over-estimate the lateral bearing capacity.

4. PILE SUBJECTED TO LATERAL SOIL MOVEMENT

In this Section a 15m long pile with a diameter of 0.5m is subjected to lateral soil movement. The lateral soil movement is caused by the construction of an embankment. The model considers one symmetric half of the embankment width, and a cross section length of 10m. The sub-soil has dimensions of $45x10x20m^3$. The embankment is 5m high; the base is 15m wide and the top is 5m wide; the embankment slope has an inclination 1:2. The centre of the pile is 1.0m away from the embankment toe and is placed in the middle of the model.
For this situation a comparison is made between the volume pile and the embedded pile considering a medium mesh density with ~5000 elements. The following pile models are considered:

1. Volume pile model with interface around the pile without strength reduction (rough pile)
2. 'Normal' embedded pile model (without surrounding cylinder or local refinement) (Fig. 9)

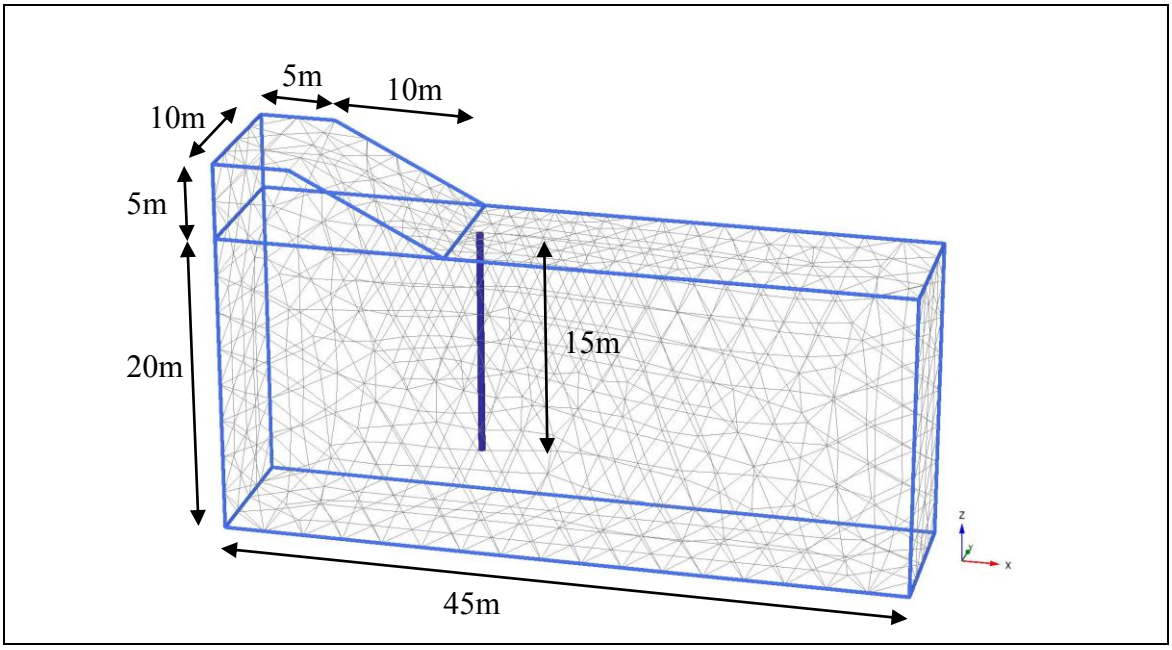

Figure 9: Embedded pile model for situation of lateral soil movement

The subsoil consists of soft soil. In this case the phreatic level is located at 1.0m below the ground surface. A slow embankment construction rate is considered; nevertheless, pore pressures are expected to increase; therefore the embankment construction is simulated by means of a consolidation analysis. The permeability of the soft soil layer is 0.004 m/day. The properties of the soft soil and the pile are similar as described in Section 3. The parameters of the embankment are listed in Table 3.

Table 3: Model parameters of embankment (for soft soil and pile properties see Table 2)

Parameter	**Symbol**	**Value**	**Unit**
Soil			
Model		Mohr-Coulomb	
Drainage type		Drained	
Unit weight	γ	20	kN/m^3
Young's modulus	E	10000	kN/m^2
Poisson's ratio	ν	0.3	-
Cohesion	c	1.0	kN/m^2
Friction angle	φ	30	°
Tensile strength	T	0.0	kN/m^2
Permeability	k_x, k_y	1.0	m/day
Rel. interface strength	R_{inter}	1.0	-

The soft soil is near-normally consolidated with a pre-overburden pressure POP = 10 kN/m^2. The initial stresses (without pile and embankment) are generated using the K0-procedure with a default K_0-value. After installation of the pile, displacements are reset to zero and the embankment is constructed in time in a Biot coupled consolidation analysis with a time interval of 200 days. All model boundaries, except for the top boundary, are 'closed'. Hence, the soil behaves partially undrained; excess pore pressures are generated, which can only dissipate at the ground surface.

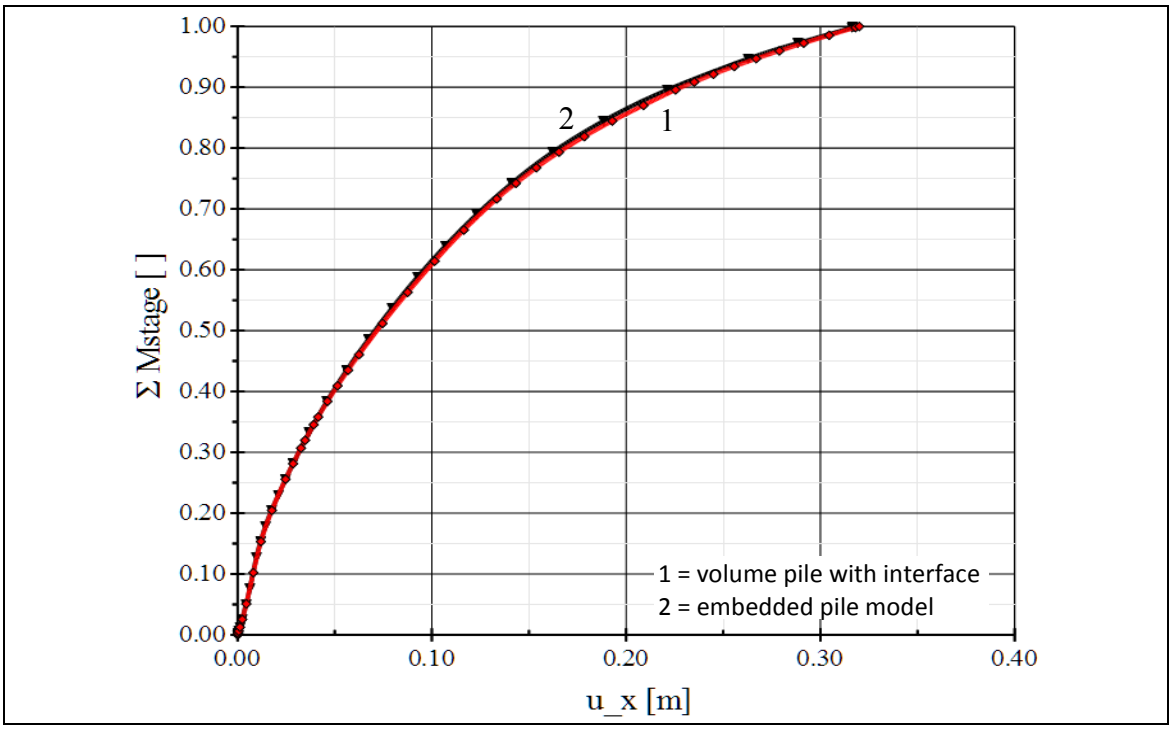

Figure 10: Load-displacement curves of pile top for different pile models (medium mesh)

Fig. 10 shows the load-displacement curves of the top of the pile for the embedded pile and volume pile models. In this situation the curves for both models are very similar.
Although the load-displacement curves are highly non-linear, there is little differential displacement between the pile and the surrounding soil. In fact, in the upper part of the soil, the pile just 'moves along' with the soil. However, the displacement gradient of the soil wedge does not match with the movement of the pile and causes bending of the pile, while the bending stiffness of the pile tries to resist this bending. As a result, the pile pushes against the moving soil in the upper part, leading to small differential displacements (i.e. the soil moves more than the pile), whereas it pushes in the other direction in the lower half of the pile (i.e. the pile moves more than the soil). This effect is more pronounced for stiffer and longer piles (not shown here) and less for less stiff and shorter piles.

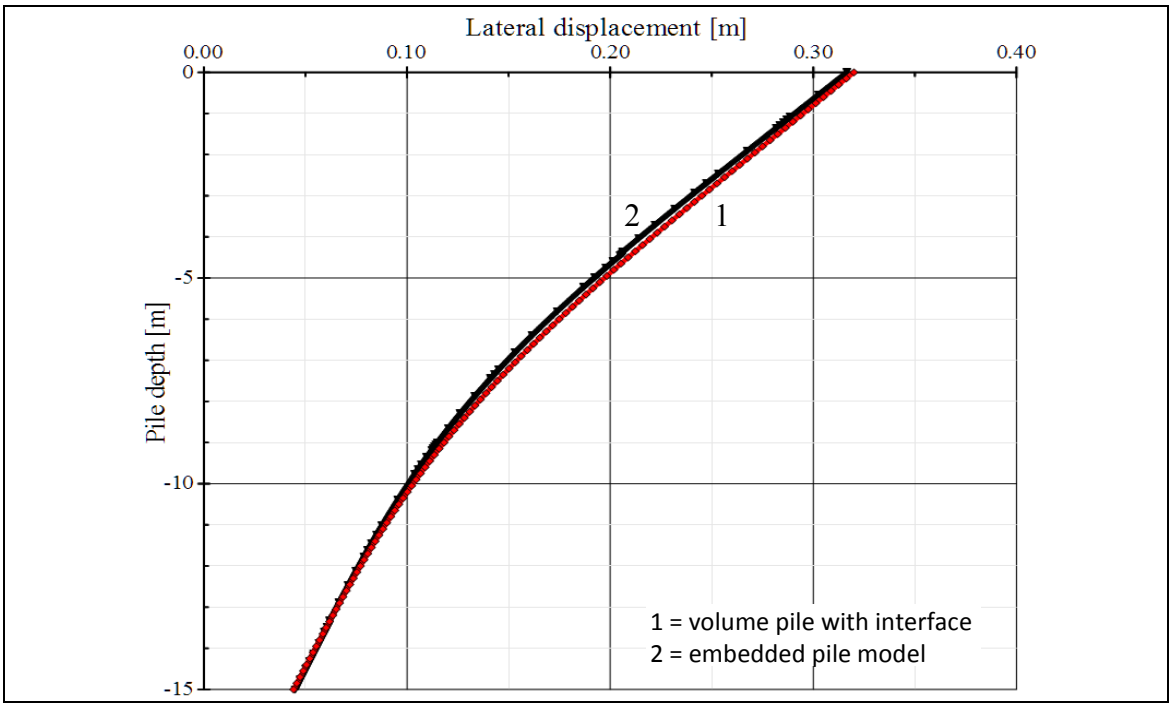

Figure 11: Pile deflection curves for different pile models

Fig. 11 and Fig. 12 show a comparison of pile deflection curves and bending moment distributions, respectively, between the volume pile and the embedded pile model for the situation where the full embankment is constructed. The deflection curves are very similar. The bending moment distributions show some differences. The strange 'wiggles' for the volume pile model are caused by the use of a 'soft beam' inside the volume pile, and are not considered realistic. Nevertheless, the overall behaviour as well as the maximum value of bending moment can still be regarded as similar.

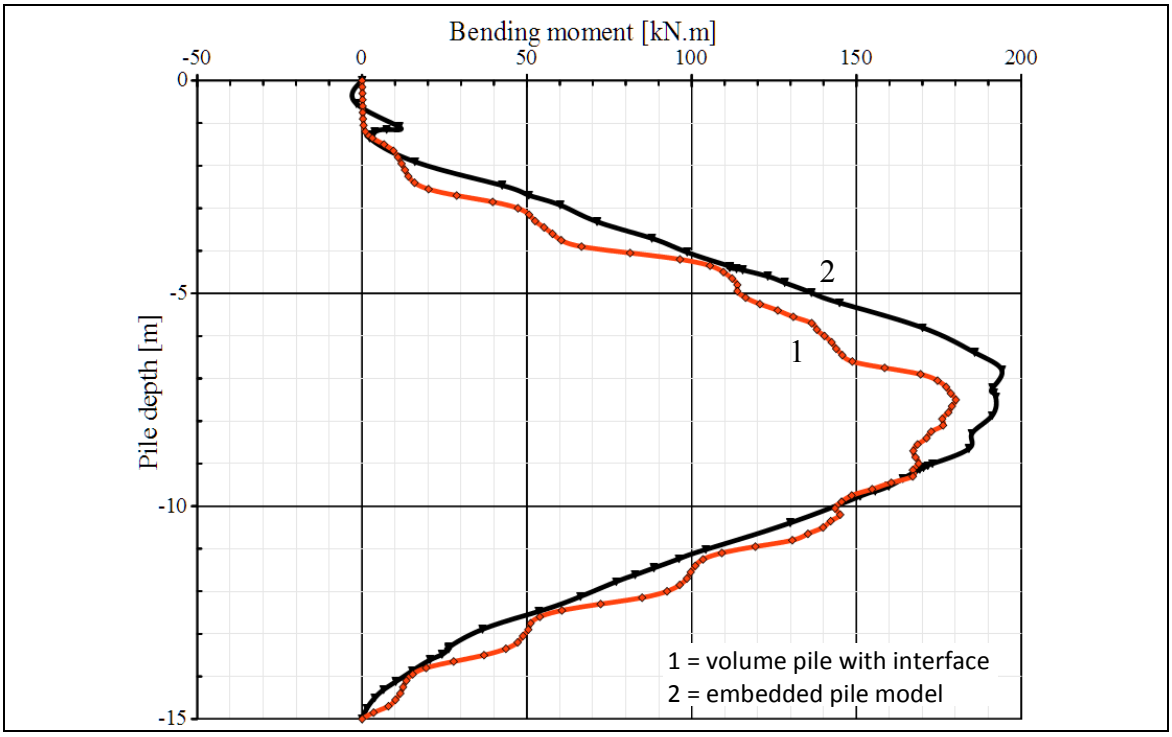

Figure 12: Pile bending moment distribution for different pile models

From the results of the pile subjected to lateral soil movement it is concluded that the embedded pile behaves very similar as the volume pile, at least for situations with small displacement differences between the pile and the soil. Effects such as pushing against the moving soil in the upper part with large

soil movements and pushing in the other direction at larger depth can be simulated quite well using the embedded pile model. The prediction of the pile deflection curve and bending moment distribution is quite realistic in such situations.

5. CONCLUSIONS

This paper describes the results of an evaluation of the PLAXIS embedded pile element with respect to its lateral loading capabilities for rough piles. Although the embedded pile was primarily developed to describe the axial loading behaviour of foundation piles, the results of this research show that it has lateral loading capabilities as well. Distinction should be made between serviceability states (relatively small differential displacements between the pile and the soil) and ultimate limit states (large differential displacements and failure).

Considering serviceability states it can be concluded that the embedded pile behaves quite realistic and similar to a 'classical' finite element model in which the pile is modelled using volume elements with or without surrounding interfaces. Displacements and bending moments of the embedded pile are similar to those observed for the volume pile model. This conclusion applies to piles subjected to a lateral force at the top, as well as piles subjected to lateral soil movement.

Considering ultimate limit states it can be concluded that the embedded pile generally over-estimates the lateral loading capacity, at least when it is used in a 'normal' way, i.e. without defining a cylinder equal to the elastic zone around the embedded beam. In order for users to improve the behaviour of the embedded pile for ultimate limit states, a local refinement around the embedded pile could be applied. Moreover, the developers could consider improving the embedded pile element by extending the line-to-volume and point-to-volume interface elements (as part of the embedded pile formulation) with elastoplastic springs in lateral direction.

Despite the positive outcome of this research, care should be taken in general when using embedded piles in lateral loading situations.

REFERENCES

Dao T. (2011).Validation of PLAXIS embedded piles for lateral loading. MSc thesis. Delft University of Technology.

Engin H.K., Septanika E.G., Brinkgreve R.B.J. (2007). Improved embedded beam elements for the modeling of piles. In: G.N. Pande, S. Pietruszczak (eds.) NUMOG X, Rhodes.

Kooijman A.P. (1989). Numerical model for laterally loaded piles and pile groups. Dissertation. Delft University of Technology.

Poulos, H.G. (1971). Behaviour of laterally loaded piles. I: single piles. Journal of the Soil Mechanics and Foundations Division, ASCE, 97(5), 711-731.

Sadek M., Shahrour I. (2004). A three-dimensional embedded beam element for reinforced geomaterials. Int. J. Num. Anal. Meth. Geomech. 28, 931-946.

Septanika E.G. (2005). A finite element description of the embedded pile model. Plaxis internal report.

Tchuchnigg F. (2009). Embedded piles – 1st report. CGG _IR021_2009. Technical University of Graz.

Full Scale Instrumented Load Test for Support of Oil Tanks on Deep Soft Clay Deposits in Louisiana using Controlled Modulus Columns

Brandon Buschmeier, E.I.T., Menard., USA, bbuschmeier@menardusa.com
Frederic Masse, Menard, USA, fmasse@menardusa.com
Sonia Swift, P.E., GEI Consultants, USA, sswift@geiconsultants.com
Mike Walker, P.E., GEI Consultants, USA, mwalker@geiconsultants.com

ABSTRACT

Controlled Modulus Columns™ (CMC) are pressure grouted auger displacement elements that are installed using a specially designed tool at the working end of a high torque, high down-pressure drilling machine. The tool is hollow so that flowable cementitious grout can be placed from the bottom up once the tool is advanced to the desired depth. The patented CMC system fits in the generic category of inclusions. There are a number of other types of inclusion that are currently designed and constructed using stone, grout, and concrete. The design technology and experience with CMC makes them uniquely efficient for the immediate support of large liquid or bulk solid storage tanks, as well as MSE walls and embankments for public transportation, other infrastructure facilities, buildings, and other structures.

Large-diameter, above-ground storage tanks impart heavy loads, deep into the ground, extending over a wide area. In many locations, the ground is stiff enough to safely support tanks without excessive settlement. However, many terminals, refineries and storage facilities are located along waterways and coastal plains in areas with soft compressible ground, or on uncontrolled fill that cannot safely support tanks. The support options in these areas have traditionally included: removing and replacing the existing soft ground; or installing deep foundation systems, such as piles with a concrete mat to support the tank.
CMCs are an ideal solution for the immediate support of large storage tanks. Using specialized drilling rigs, control of bearing layer penetration is provided in a consistent fashion, and electronic monitoring and recordation of drilling and grouting parameters is routinely used for quality control. The load is distributed to the CMC elements using a compacted granular load transfer platform that serves as an efficient and cost effective foundation. Other features such as leak detection and cathodic protection are detailed into the load transfer platform.

Five large diameter tanks were scheduled to be constructed along the Mississippi river in Southern Louisiana on a site with up to 120 ft of recent soft clay deposits above the pleistocene deposits. A support system using a combination of cmcs of varying diameters installed to two different depths was designed for the project. In order to demonstrate the validity of the design performed using 3D finite element analysis, an instrumented full scale load test was constructed and monitored. The test itself was modelled using the same assumptions as the design to validate the parameters and methodology. This paper will present the proposed design for the project as well as the results of the instrumentation program and the conclusions drawn from this test program.

1. INTRODUCTION

Foundation subgrade is typically evaluated for both strength (bearing capacity) and service (settlement). Traditional approaches use piles to control settlement at sites with poor quality soils. The piles became the supporting elements for the foundation and were designed to resist lateral and vertical loads applied to the foundation. However, the pile capacity required to control settlement may be significantly lower than that required to support the foundations. Therefore, the service goal may require an inefficient system because the pile system ignores the strength of the soil surrounding the piles to support the load of the structure. Ground improvement is typically more efficient because its' design utilizes the strength of the soil while providing additional strength, if required, and meeting service requirements. With widespread acceptance in the market place, many engineers are choosing ground improvement techniques to provide suitable foundation subgrade at sites that would have traditionally required deep foundations. This article discusses the Controlled Modulus Columns (CMC) ground improvement technique and how this technique was innovatevely used on a challenging site in Southern Louisiana for the support of five large

diameter oil tanks. An extensive full scale load test was performed prior to the construction phase to validate and calibrate the innovative design of the solution.

2. OVERVIEW OF THE TECHNOLOGY

CMC are a sustainable and cost-effective ground improvement technology that transmit load from the foundation to a lower bearing stratum through a composite CMC/soil matrix. CMCs have been installed in a variety of soils including; uncontrolled fill, organics, peat, soft to stiff clay, silt, municipal solid waste, and loose sands. Typically, the CMC is installed through the soft or compressible soils and into dense sand, stiff clay, glacial till, or other competent material that serves as the bearing stratum.

2.1. Installation Methodology

CMCs are constructed by use of a displacement auger which laterally compresses the soil mass while generating virtually no spoils. The CMC displacement auger is hollow, which allows placement of the specially-designed grout column, as the auger is withdrawn. The grout is injected under moderate pressure, typically less than 10 bars (150 psi). The unconfined compressive strength of the grout is adapted to the requirements of the design and varies between 1,000 and 3,000 psi for typical applications. CMCs are installed without generating spoils or creating vibrations. The grout for the CMC element is placed with enough back pressure to avoid collapse of the displaced soils during auger withdrawal. The installation process allows for the creation of a column with the diameter that is at least as large as that of the auger. CMCs are installed with drilling equipment that has large torque capacity and high static down thrust to efficiently displace and compress the surrounding soil laterally.

The auger is advanced while turning and displaces the soil. Upon reaching the desired depth, grout is pumped through the end of the auger and into the soil cavity as the auger is withdrawn. Column diameters typically range from 11 to 18 inches and are selected based on the loading conditions, and the site geotechnical conditions.

With a conventional continuous flight auger, “negative displacement”, stress relief, or even lateral mining around the auger is inevitable. This creates a movement of the surrounding soils which are loosened by the augering process toward an active (Ka) condition. This condition creates a risk of necking. On the contrary, with the CMC displacement auger, the effect is opposite: the soil adjacent to the auger is displaced laterally by the displacement stem portion of the auger and brought to a denser passive (Kp) state of stresses. Stress relief does not occur and the risks of necking the CMC are nonexistent, except in a case of operator error. Quality control of the CMC and monitoring to catch any operator error is done with real time monitoring of the following installation parameters:

- Speed of rotation
- Rate of advancement and withdrawal of the auger
- Torque, down-thrust (crowd) during the drilling phase
- Depth of element
- Time of installation
- Grout pressure in the line at the top of the drill string
- Volume of grout as a function of depth from which a profile can be generated.

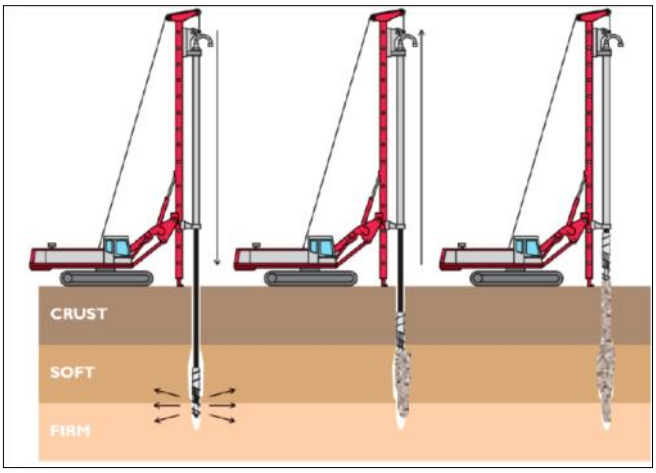

Figure 1: Typical CMC Installation Procedure

The grout pressure is monitored by a sensor located at the top of the concrete line above the swivel attached to the mast drilling head. The CMCs are usually installed using a target overbreak of 5 to 10% of the volume of grout. During the grout phase, pressure readings are kept to a moderate positive pressure. Any loss in pressure can reveal a soft or loose soil zone that may not have been detected during the geotechnical investigation.

A significant benefit of the recordation of installation parameters is that changes in subsurface conditions can be detected in the field, and more importantly, column depths can be adjusted based on the encountered conditions as detected by the response of the drilling equipment. The recorded drilling parameters of down pressure, speed and torque are readily interpreted in the field during drilling and changes in stratigraphy can be sensed based on ease or difficulty of drilling. This ability to adjust column lengths in the field offers a significant advantage over most other forms of column installation.

Other forms of QC include monitoring fluid grout properties for consistency with the expectations of the design mix, and sampling, curing and testing of samples for grout strength. Load testing (ASTM D1143) is routinely completed when there is little previous experience with CMC capacities in the subject strata. Other in-situ testing such as PIT (Pile Integrity Tests) and dynamic loads tests (e.g. Statnamic) have also been used.

2.2. CMC Design Methodology

The behavior of an individual inclusion is predicated on reaching equilibrium under loads (Combarieu, 1988) as shown on Figure 3. While the inclusion is being compressed by the load, negative skin friction is acting in its upper part and positive skin friction in its lower part. When the equilibrium is reached, the stresses acting on the inclusion can be divided into four components:

- The vertical load, Q at the top of the inclusion
- The negative skin friction acting on the upper portion of the inclusion
- The positive skin friction acting at the lower portion
- The vertical reaction at the tip

The load of the structure is usually distributed to a network of inclusions by the Load Transfer Platform (LTP). The LTP is usually made of well-graded granular backfill and is designed to allow arching of the load of the slab / footings onto the CMCs. The thickness, quality and adequacy of the LTP is one of the key factors in the design of CMCs. While high-tensile strength high-modulus geotextile can be used in some cases, the deformations calculated within the LTP are usually too small to allow for the full development of the geotextile tensile strength which renders in many cases the geotextile reinforcement under-utilized. A typical bi-axial high strength geotextile develops its full tensile strength at around 5% elongation. For the typical application under buildings where settlements on the order of ½ to 1 inch are predicted, it is not possible to reach the level of deformation required to fully develop the tensile strength of the geotextile. High strength geotextiles are therefore rarely used and designed within the LTP for CMC applications under buildings.

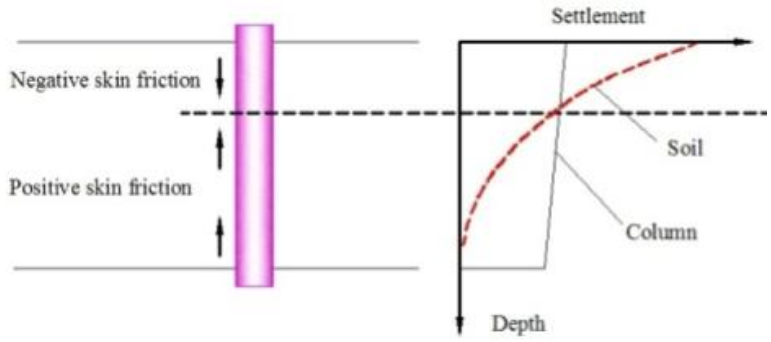

Figure 2: Settlement distribution between soil and an isolated inclusion.

Figure 3 shows how the load is distributed from the structure to the bearing layer. The load distribution between CMCs and surrounding soil is based on reaching an equilibrium between deformations of the CMCs and the surrounding soils. The design of a network of inclusions is thus based on a good knowledge of the distribution of stresses and deformations in the soil and the inclusions.

While calculation methods have been proposed by various authors (see Combarieu), with the development of more powerful computers, finite element method (FEM) analysis has quickly become the method of choice when designing a network of CMCs.

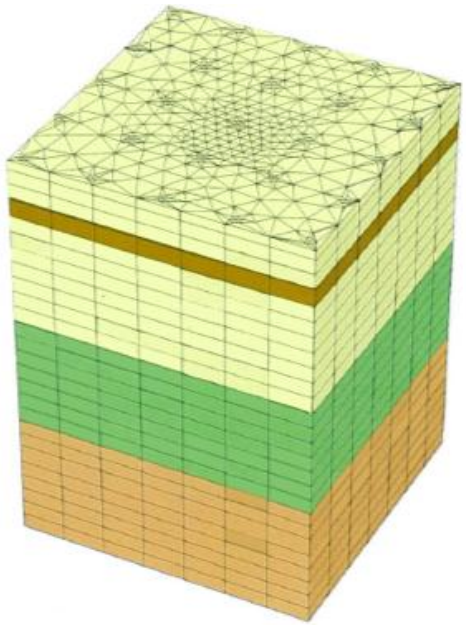

Figure 3: Example of 3D FEM model for support of slab and footings on CMCs

While CMCs can be used with various types of soils and structures, this ground improvement approach is generally limited to light to medium loads (4 to 8 kips per square foot (ksf) bearing pressure under footings and 3 to 4 ksf under tank loads) and the depth of installation is currently limited to 115 feet maximum. In very dense soils overlaying softer compressible layers, because of the lateral displacement created by the drilling method, pre-drilling is sometimes necessary prior to installation of the elements which may have a negative impact on the overall economics of the solution.

While we discuss the use of CMCs to support oil tanks in this paper, CMCs also have been used for a variety of other applications including foundations for buildings, mechanically stabilized earth (MSE) walls, and embankments.

3. CASE HISTORY : SUPPORT OF LARGE DIAMETER OIL TANKS IN NEW ORLEANS, LOUISIANA

3.1. Geological and Geotechnical characterization of the site

The site is located on the banks of the Mississippi river, in Southern Louisiana. The site is generally characterized by Holocene Deposits that overlie Pleistocene Age soils. The Holocene unit consists of Natural levee and interdistributary / nearshore Gulf deposits. The initial soil investigation consisted of borings with undisturbed sampling at various depths up to 150 ft and Cone Penetration Tests (CPT) to a depth of 120 ft below the existing surface. Cohesionless soil samples were obtained during the performance of Standard Penetration tests (SPT) with a 2-in diameter splitspoon sampler. Soil Laboratory tests (Atterberg limits, Consolidation, and Triaxial tests...) were also performed on the samples to evaluate the geotechnical properties of the various soil layers.

Below a surficial layer of 0.5 to 4 ft of fill (clayey silt, silty sands and gravel), natural levee deposits extended to a depth of 13 to 20 ft. These deposits consist of soft to medium stiff silty clays with some trace of organic matter and localized sand pockets.

Underlying these deposits, to a depth ranging between 65 and 80 feet below the existing ground surface are interdistributary deposits of very soft clay with silt and sand. A thin sand layer was constantly observed around 70 ft below ground surface. Below these interdistributary deposits, to depths of up to 105 ft, nearshore guld deposits consist of medium stiff to stiff clay with fine sand pockets and shell fragments. These deposits are fairly recent from the Holocene geological era. Older deposits from the Pleistocene are found below the more recent deposits and consist of stiff to very stiff silty to sandy clays over a very dense layer of silty sands at depth of 115 to 120 ft. Due to the close proximity to the Mississippi river, the water table while fluctuating with the river levels was observed 2 to 3 ft below the ground surface

3.2. Description of the Project

For the extension of the existing oil terminal, five new 42-ft high oil storage tanks are constructed, two with diameters of 150 ft and three 130-ft diameter tanks. Specific gravity of the stored product varies between 0.95 to 1.1. These tanks are built with a steel shell, steel floor, and a peripheral gravel ring wall to support the tank shell and provide a stable platform for the erection of the tank. The tanks will be tested through hydrotest. Because of the presence of very compressible subsurface conditions, the hydrotest program allows for stage loading with monitoring periods at each stage.

3.3. Geotechnical Challenge and Ground Improvement Design

The tanks at full load will impose a maximum service load of up to 3,100 psf consisting of 2,750 psf for the product load plus an additional 350 psf for a 2.5 to 3 ft thick platform to support the tanks. The initial settlement analysis predicted several feet of long term settlements. In addition to that, because of the very low shear strength of the subsoils, the factor of safety against global bearing failure was not sufficient to allow construction of the tanks without ground improvement or deep foundations. As the initial solution of deep foundations (steel piles or timber-composite driven piles) supporting a structural concrete slab or mat was deemed too expensive, a ground improvement approach was proposed.

Because the depth to the Pleistocene was in some locations over 110 ft, and in order to control the total and differential settlement to the serviceability levels required by the terminal owner and recommended by the tank manufacturer (see Table 1), the designers of the ground improvement solution were faced with several challenges:

- Limitation in the depth of treatment due to equipment limitations : maximum achievable depth of 113 ft
- Due to the very soft nature of the holocene deposits, limiting the long term deformations to allowable levels
- Limit the lateral deformation under the gravel ringwall due to the large horizontal forces from the tank load

- Designing an efficient load transfer platform between the tank floor and the top of the ground improvement system to efficiently transfer the spread loads from the product to the ground improvement system and limit the level of additional stress in the soft deposit

Table 1: Tank Performance Criteria (Monitoring Period = 3 years after hydrotest)

Tank	**Center Deflection**	**Tank bottom settlement**	**Uniform Settlement**
Steel bottom	4 inches	50% of API 653 Standard	8 inches

The soil investigation indicated a change in compressibility of the holocene deposits at a depth of around 70 ft with the presence of a thin sand layer at this elevation. The upper part of the deposit displayed high compressibility while the lower part presented better characteristics and was slightly overconsolidated. It was therefore decided to design the project with two different densities of improvement for each holocene deposit layer, a dense treatment for the upper part and a lighter treatment for the lower part. The total depth of treatment was selected to reach the Pleistocene deposit which did not seem to present a risk in terms of long term consolidation.

The proposed design solution used a ground improvement scheme consisting of Controlled Modulus Columns associated with a thick load transfer platform to support the tank. The gravel ring wall was substituted with a Mechanically Stabilized Wall "ring corset" around the edge of the tank. This MSE Ring wall was designed to sustain the large horizontal forces from the tank load with a limited amount of outward movement.

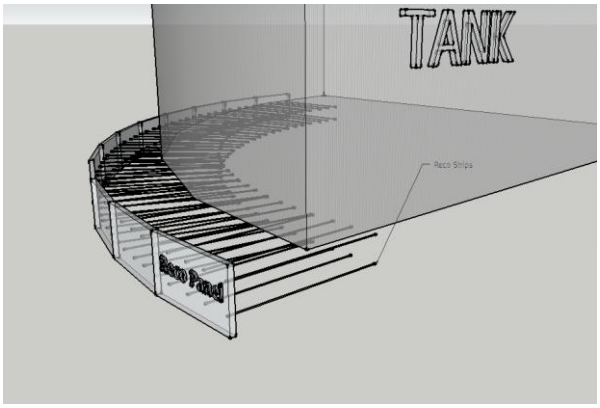

Figure 4: Conceptual view of the MSE Ring Wall

In order to achieve these varying densities of improvement for each layer, two different diameters of columns and two different depths of installation were selected:

- 12.5 inch diameter CMCs installed to a depth of roughly 70 ft
- 18.5 inch diameter CMCs installed to the top of the pleistocene layer (up to 113 ft depth)

The depth of installation of the elements varied for each tank due to the variations in soil profiles under each tank. It was therefore necessary to perform a specific design for each tank. On the first tank, three different types of calculations were conducted in a parametric study in order to compare each method and select the most efficient design methodology:

- A 3D finite element analysis modeling a quarter of the tank
- A 3D thin slice model of the tank
- A hand calculation using Terzaghi's analysis method for rafts on floating piles

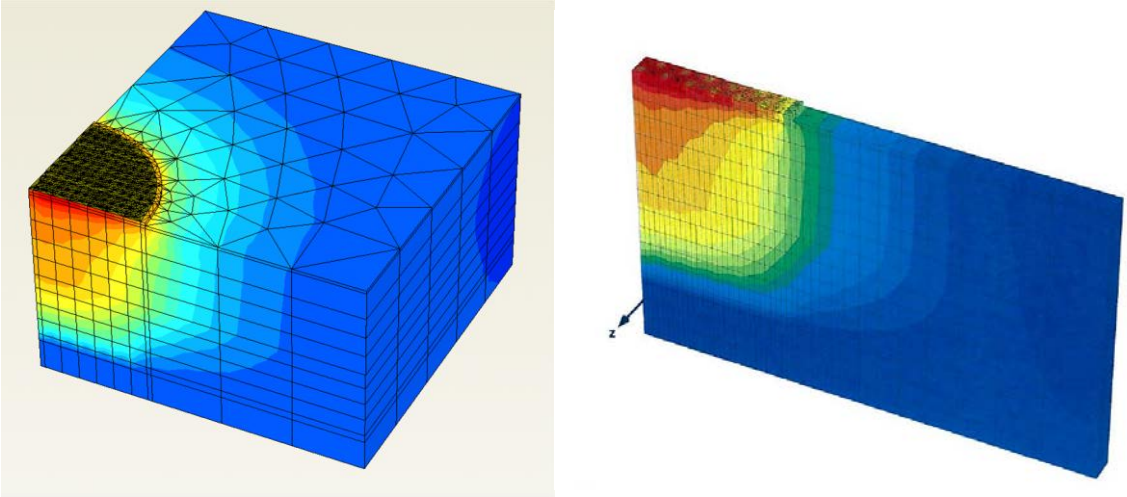

Figure 5: Results of 3D FEM analysis for quarter of tank model (left) and thin slice model (right)

While the deformation results of these three methods were very similar, the main advantage of the finite analysis method over the hand calculation is the ability to calculate differential settlement across the diameter of the tank, examine border effects particularly at the edges of the tank, and obtain directly the stresses and loads in the soils and in the ground improvement elements. Because of the amount of modeling and computation time associated with the 3D quarter tank model and given the relative homogeneity of all the methods in terms of deformation, it was decided to design the ground improvement scheme on all the remaining tanks using a 3D thin slice model.

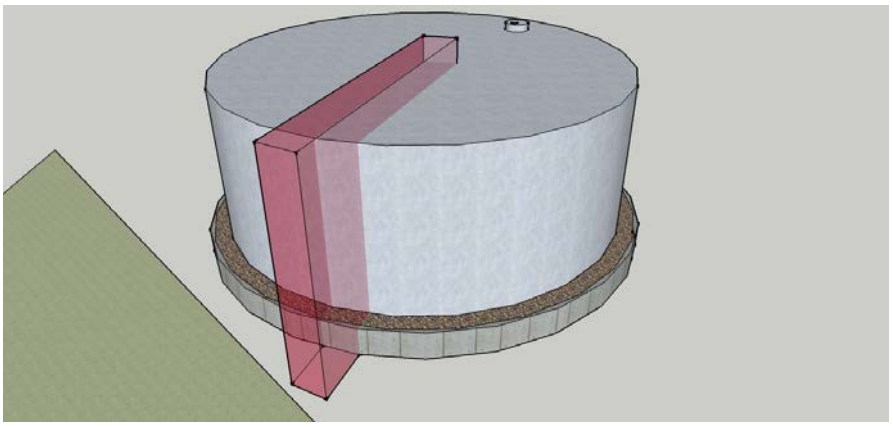

Figure 6: 3D thin slice model concept for the design of all the tanks.

All the calculations were performed using a consolidation type analysis in order to evaluate the expected settlement during the contractual warranty period of three years after the water test. The design of the Load Transfer Platform is an intricate part of the FEM analysis and the model gives a good visualization of the soil-structure interaction and of the arching effect that are taking place above the CMC elements. The results of the design calculations for each tank are shown below for different depth of installation of the larger deep CMCs. The depth of installation was selected to meet the long term settlement criterion of the contract.

Table 2: Results of settlement calculations for various depths of CMCs

Tank	Depth of 18.5" CMC (ft)	Settlement (3 years)	
		Center Tank (inch)	Edge Tank (inch)
A	105	6.6	4.2
	100	8.8	5.6
B	110	8.7	5.6
C	95	7.9	5.1
D	110	5.7	3.6
	105	5.8	3.7
E	90	12.8	8.2
	95	9.1	5.8

The final scheme and CMC pattern are show below. The FEM calculations confirmed that the concept of a variable density of elements with depth was viable: the load of the tank is gradually transferred from the elements with a much denser spacing in the upper Holocene to the more widely spaced elements in the lower Holocene layer. This concept proved to be the most cost-effective solution while maintaining the level of performance of the ground improvement system within the allowable tolerances of the service requirements of the tanks.

3.4. Full Scale Load Test Program

3.4.1. Layout of the test and instrumentation

Before implementing this solution, it was decided to perform a full scale load test program in order to verify and calibrate the assumptions of the design and the validity of the modeling technique.

The usual single element load test was not sufficient to give the contractor and the client the level of comfort necessary to proceed with the installation of the ground improvement elements under the five tanks. It was therefore decided to build a test area with an area of 45 ft x 45 ft and to install CMCs in accordance with the design in this area. A total of 30 CMCs were installed in this zone:

- Fifteen (15) CMCs with 12.5” diameter to a depth of 70 ft
- Fifteen (15) CMCs with 18.5” diameter to a depth of 110 ft.

On one side of the test area, an MSE wall was constructed to mimic the conditions occurring at the edge of the tank under the MSE ring wall. The MSE Wall panels were 5 ft x 10 ft in size with geosynthetic straps (Geomega system) 15 ft long installed into the load transfer platform. One of the challenges was to find a way to replicate the load of the tank (3,000 psf) within this limited area. The solution that was selected was the use of concrete forms to create a rectangular box 20 ft x 20 ft x 32 ft high that was subsequently filled with sand.

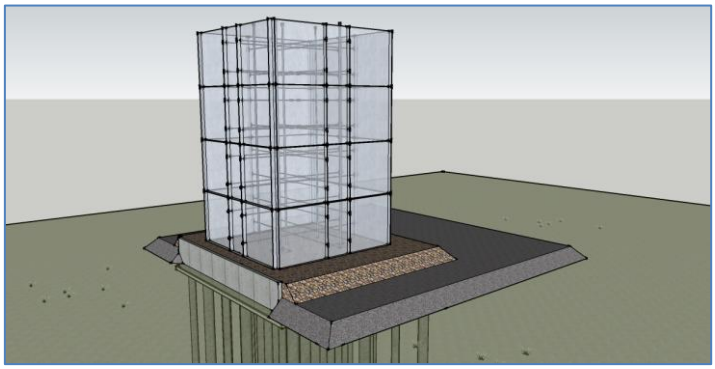

Figure 7: Schematic of the load test area

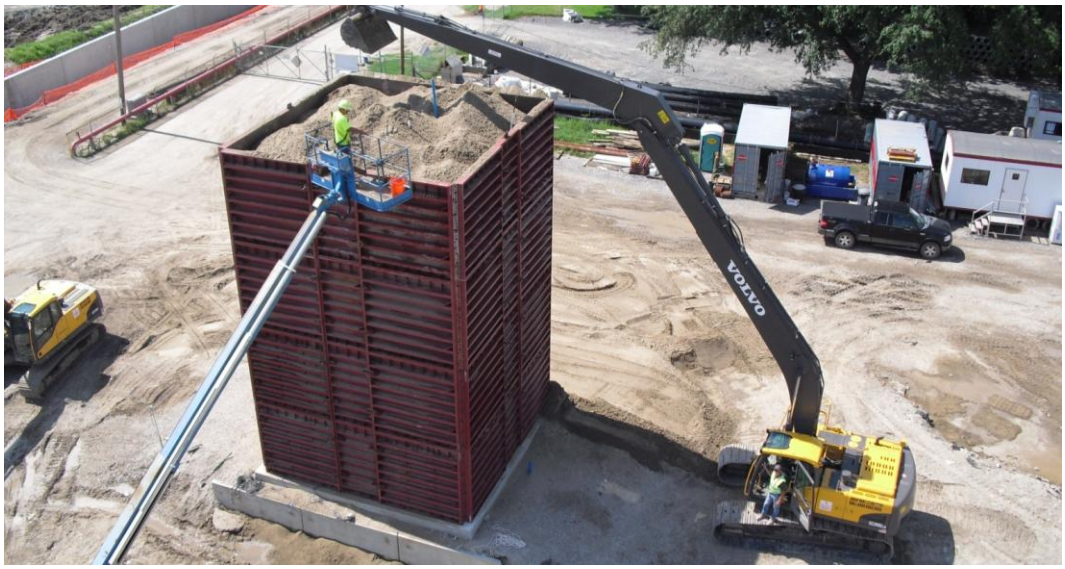

Figure 8: Picture of the construction of the Load Test Area (Form Work)

Instruments were installed to monitor several parameters :

- Ten (10) vibrating wire (VW) piezometers to record the pore-water pressure between CMCs at various depths
- Nine (9) VW rebar strain gages installed inside select CMCs to measure the stresses in the elements at various depths
- Five (5) Multi-depth settlement gages to monitor the strain in different layers
- One (1) Measurand ShapeAccelAray (SAA) – 40 ft long to measure the longitudinal settlement profile across several CMCs (horizontal extensometer)
- Three (3) inclinometers located outside and inside the test area to monitor the lateral deformations
- In addition, the settlement was monitored using:
  - Four (4) settlement plates located at different positions (above and between CMCs) and different elevations (top and bottom of LTP)
  - Six (6) survey points located on top of the MSE Ring Wall to verify vertical deformation of the wall
  - Twelve (12) survey points to measure the horizontal movements of the MSE Ring Wall
  - One (1) survey point at each corner (4 Total) of the form to establish the time-settlement curve at the location corresponding to the edge of the tank

Figure 9: Installation of the Instruments

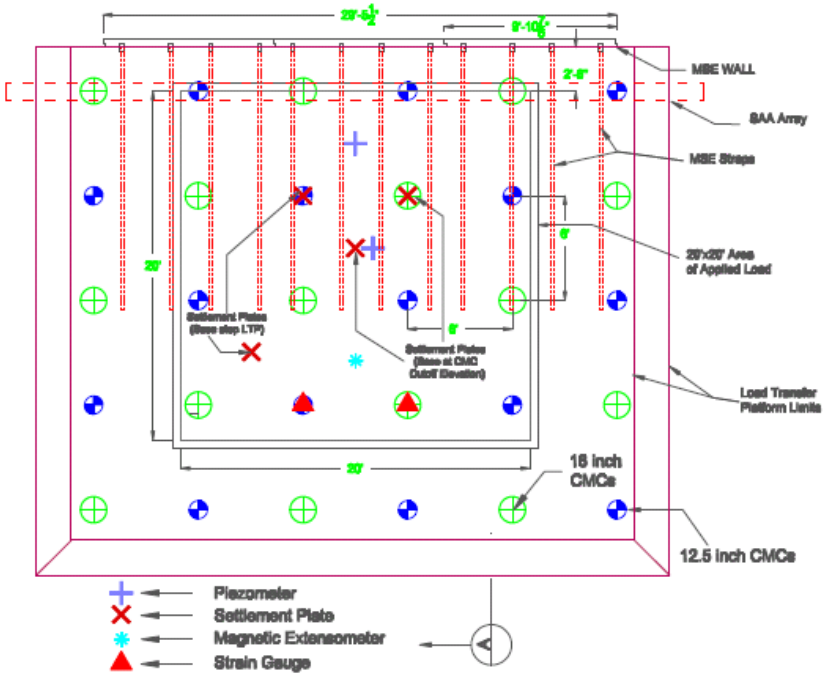

Figure 10: Layout of the test area and location of instruments

Figure 11: Installation of the MSE Ring Wall (Reinforced Earth Omega System)

3.4.2. Monitoring Results - Modeling of the Test Program and back-analysis of the results

After installation of the CMCs, the test was monitored for a period of roughly 3 months.

Because the area of the test was rather limited as compared to the tank, in order to verify the adequacy of the design, it was decided to model the test area into the FEM analysis software using the same geotechnical parameters and assumptions as the design.

Because performing time-dependent 3D FEM analysis is a CPU and time consuming, prior to the development of the 3D test program model, we conducted a 3D single CMC simplified unit cell analysis and ran a time-dependent consolidation calculation using the parameters of the design. This smaller model allowed us to establish the degree of consolidation that was achieved during the monitoring period and therefore extrapolate the results of the test program to the three-year warranty period.

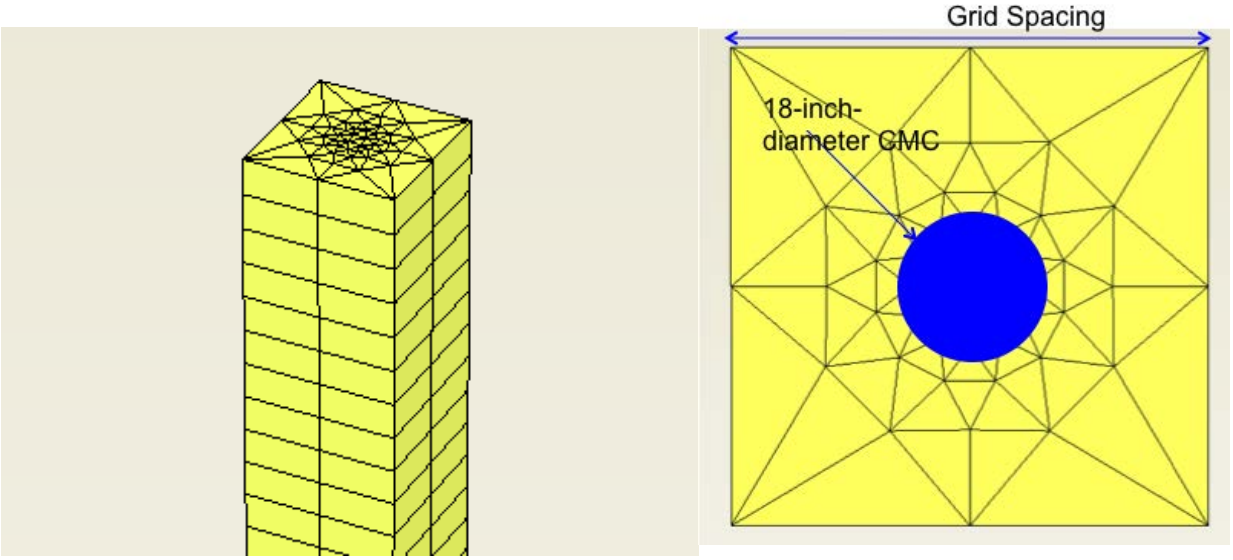

Figure 12: Time-Dependent Unit Cell Simplified Model

A 3D FEM analysis was subsequently built to accurately model the field conditions. Initially, the geotechnical input parameters were the same as the initial design parameters. A fully consolidated model was performed and the results were adjusted to take into account the time-dependent consolidation effect for a period of three months (test monitoring period).

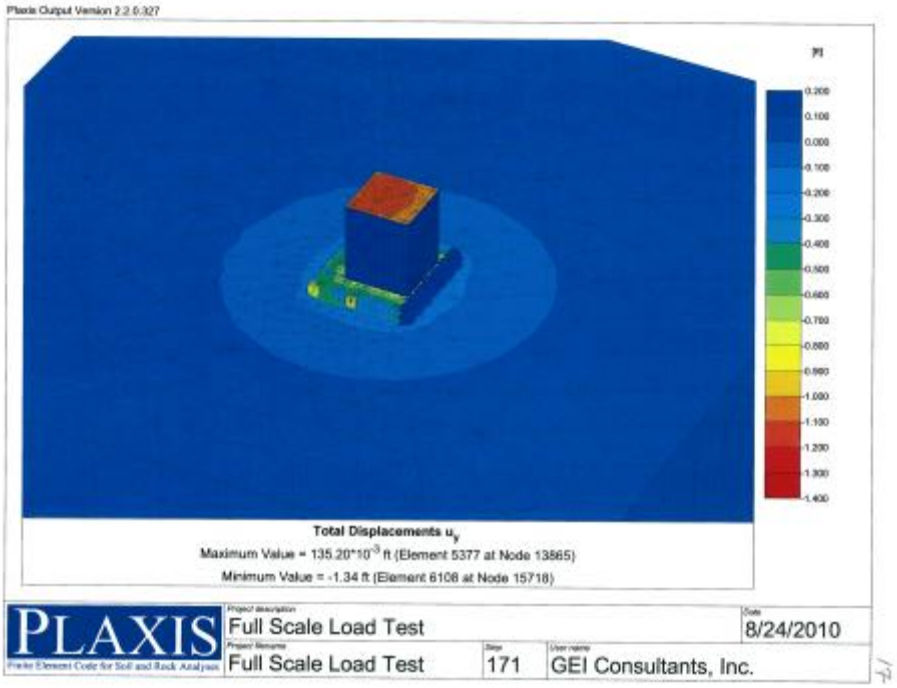

Figure 13: Displacement Plot – 3D FEM analysis of the Test Area

The results of the calculation showed a fairly good agreement with the initial design calculation in terms of settlement of the overall area and deformations within the LTP. The maximum settlement recorded at the top of the LTP was 4.2 inches for a settlement plate located in-between two CMCs. The minimum recorded settlement for the settlement plates was 2.5 inches for a settlement plate directly located atop a CMC at the bottom of LTP elevation. The 3D model predicted a total of 17 inches of settlement at infinite time (100% drained). Taking into account the fact that the test was left in place slightly less than 3 months and using the results of the 3D unit cell simplified model, it was calculated that the model predicted a maximum settlement of 3.8 inches at the top of the LTP.

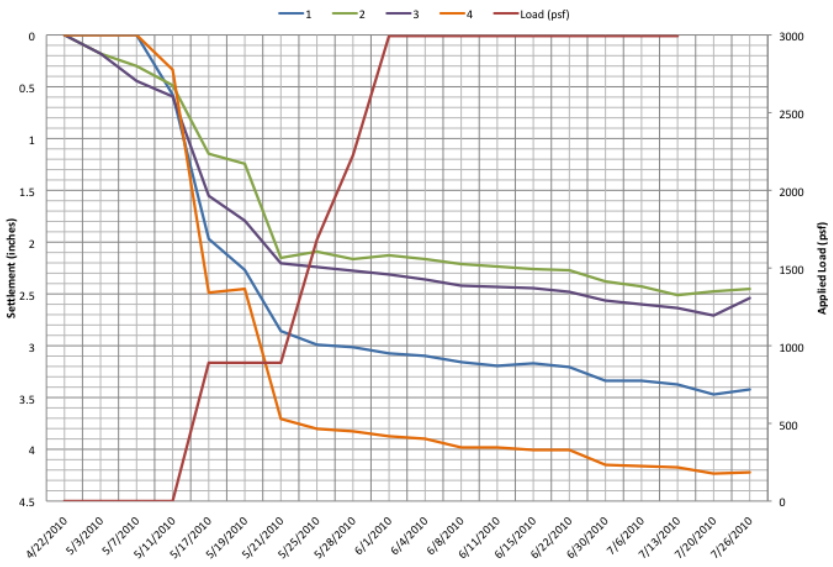

Figure 14: Displacement plot – 3D FEM analysis of the Test Area

As far as the strain gage and the load profile in the CMCs were concerned, the instruments confirmed the following trends:

- There is a load transfer mechanism between the denser treatment zone in the upper Holocene layer and the lower Holocene – The load is gradually shifted from the smaller 12.5 inch short elements to the bigger 18.5 inch elements.
- The arching in the load transfer platform is better than expected and more load reached the top of the CMC in the load transfer platform than what the model shows, particularly on the smaller 12.5 inch elements. It should be noted that the load transfer platform was made of dense-graded aggregates compacted in lifts to 95% of the optimum modified proctor. No geogrid was installed within the LTP.
- The total load being transferred to the CMC elements is higher than predicted by the model. (170 kips actual vs. 100 kips in model).
- The profile of the load in the system is consistent with our understanding of the load transfer mechanism with a neutral point (point of maximum load in the CMC elements) located roughly at the transition between the upper and lower Holocene layer
- Confirmation that given the relatively low level of strains within the LTP, multiple layers of geogrid is not necessary and that the load transfer mechanism is efficient without the need for geogrid layers

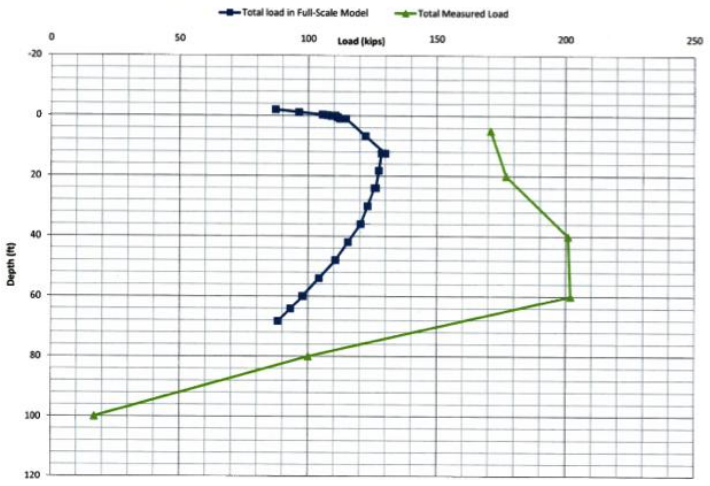

Figure 15: Load profile in CMCs – Actual vs. Model

As more load reaches the rigid CMC elements, it would follow that the level of incremental vertical stress in the soft clay layer is smaller, and less settlement would occur in the field than in the model. The fact that there is nevertheless a good agreement between settlements in the field and in the model can, in our

opinion, be explained by the fact that the movement of the CMCs themselves is greater in the field than in the model due to the observed additional load in the CMCs.

The horizontal extensometer (ShapeAccelArray) confirmed the deformation profile at the lower LTP level. We recorded a maximum deferential settlement between top of CMC and center of grid of roughly 1.5 to 1.7 inches while the model predicted a maximum settlement between CMCs of 2 inches.
The three inclinometers (one inside the test area and two outside) showed a good agreement with the model with an outward maximum movement of roughly 1.0 inch at the surface. They also confirmed the stability of the system as no deeply seated failure plane with large lateral movements was recorded. The maximum horizontal outward movements of the MSE ring wall were slightly higher with 1.5 inch of movement at the top of the wall and 1.2 inch at the bottom showing a slight tilt top-bottom of 0.3 inch, well within the acceptable limits and within the range of the calculated values (0.2 to 0.4 inches).
The differential settlement between the edge of the form work and the top of the MSE wall located 2.5 ft away was also a good indication of the overall performance of the system. Less than 0.2 inch of differential deformation was recorded between these two edges.
Because of the very good agreement in terms of deformations between calculations (maximum settlement of 3.8 inches) and measurements (maximum settlement of 4.2 inches), the initial design was validated and it was decided that it was not necessary to back-calculate adjusted geotechnical parameters and recalibrate the initial design to the actual site conditions.

3.4.3. Results of the Water Tests

Unfortunately, the results of the water test and subsequent readings of the deformation after the water tests have not been made available to the author by the client at the time of this article.

4. CONCLUSION

Five large diameter tanks were constructed along the Mississippi river in southern Louisiana on a site with up to 120 ft of recent soft clay deposits (holocene) above the pleistocene deposits. A support system using a combination of CMCs of varying diameters installed to two different depths was designed for the project. In order to demonstrate the validity of the design performed using 3D finite element analysis, an instrumented full-scale load test was constructed and monitored. The test itself was modelled using the same assumptions as the design to validate the parameters and methodology. The result of the monitoring showed a very good agreement between calculated deformations and actual deformations. It also showed that the load transfer mechanism in the LTP is probably more efficient than the model predicts leading to higher load in the CMCs than calculated. The results of the Test Program validated the initial design parameters and results without the need to back-calculate adjusted geotechnical parameters and re-run the FEM calculations with these adjusted parameters.

REFERENCES

Collin, J.G. & al (2004) – FHWA - NHI Ground improvement manual – Technical summary #10: Columns supported embankment – FHWA – 2004

Combarieu, O. (1988) – Amelioration des sols par inclusions rigides verticals – application a l'edification de remblais sur sols mediocres-Revue Francaise de geotechnique n 44, pp. 57-59

Combarieu, O. (1988)-Calcul d'une foundation mixte-Note d'information technique LCPC

Masse, F., Pearlman, S., Bloomfield, R.A. "Support of MSE walls and reinforced embankments using ground improvement" New Horizons in Earth Reinforcement – Otani, Miyata & Munkunoki (eds) 2008 Taylor and Francis Group, London, ISBN 978-0-415-45775-0

Plaxis finite element code for soil and rock analysis user's manual – Plaxis V8 – 2007 9.

Plomteux, C. & al (2003) – "Controlled Modulus Columns (CMC): Foundation system for Embankment support: a case history" – Geosupport 2004, Orlando, USA, pp 980-992

Rogbeck, Y. & al. (1998) "Two and three dimensional numberical analysis of the performance of piled embankment" 6th International Conference on Geosynthetics, Atlanta

Sanglerat, G. (199?) The Penetrometer and soil exploration Interpretation of penetration diagrams – theory and practice, Part 3 – Page 285

Terzaghi, K. and Peck, R.B. 1987. Soil mechanics in engineering practice, 2nd ed., McGraw Hill, New York, NY, USA.

Theoretical analyses of laboratory tests of kaolin clay improved with stone columns

Cañizal, J., University of Cantabria, Santander, Spain, canizalj@unican.es
Castro, J., University of Cantabria, Santander, Spain, castrogj@unican.es
Cimentada, A., TRIAX S.A. (formerly UC), Santander, Spain, ana.cimentada@triax.es
Da Costa, A., University of Cantabria, Santander, Spain, dacostaa@unican.es
Miranda, M., University of Cantabria, Santander, Spain, mirandam@unican.es
Sagaseta, C., University of Cantabria, Santander, Spain, sagasetac@unican.es

ABSTRACT

Small scale tests were performed in the laboratory to study the deformation and radial consolidation around end-bearing (fully penetrating) stone columns under distributed loads. For this purpose, the behaviour of a horizontal slice of a unit cell representative of a column and the surrounding soil was analysed. Gravel was used for the central column and kaolin clay for the natural soil. The results of the small scale tests are compared with theoretical analyses to assess their accuracy and to validate their hypotheses. Special emphasis is paid to an analytical solution recently developed by the authors that considers plastic strains in the column and the consolidation process of the surrounding soil. A better prediction of the settlement reduction, stress concentration on the column and settlement rate is found with this solution than with previous solutions.

1. INTRODUCTION

In recent years, an increasing number of embankments and structures have to be founded on soft soil. A cost effective solution usually requires a ground improvement technique. One of the most popular techniques are stone columns, which were developed in the 1970's as an extension of vibrocompaction for soft soils. As happens in many fields, construction of stone columns, either by the vibro-replacement or vibro-displacement methods, was further developed than their design methods. Stone columns act mainly as rigid inclusions with a higher stiffness, shear strength and permeability than the natural soil and the effects or improvements caused by these three properties were independently studied by different solutions. So, there were analytical solutions studying separately the radial consolidation (Barron 1948), the settlement reduction (Priebe 1995) or the bearing capacity and the stability of embankments or foundations (Hughes & Withers 1974; Vesic 1972; Bergado et al. 1996). However, the above aspects are inter-related, and an unified approach was desirable.

Stone columns shorten the drainage path in a similar way as vertical drains do. Therefore, the same methods (Barron 1948; Hansbo 1981) are often used to study their radial consolidation. However, columns are much stiffer than vertical drains and support an important part of the applied load. This stiffness of the column leads to a reduction of the final settlement. The most popular method to study this final settlement reduction is probably Priebe's method (1995), which is based on semi-empirical considerations (Dhouib et al. 2004). Only in the last decade there appeared more advanced solutions to study the radial consolidation (Han & Ye 2001) and the settlement reduction (Pulko & Majes 2005; Pulko et al. 2011). Therefore, the authors decided to perform a study of the consolidation and deformation around stone columns that could help to understand their behaviour and to improve the design methods. The study included the development of an analytical solution (Castro & Sagaseta 2009a), numerical analyses (Castro & Sagaseta 2011), small scale tests (Cimentada et al. 2011) and a field instrumentation of a real case (Castro & Sagaseta 2009b).

A considerable number of stone columns are usually involved in a soil treatment, which implies a complex modelling process. Five main approaches to the modelling exist:

- Unit cell approach: Only a “unit cell”, i.e. one column and its surrounding soil, is modelled in axial symmetry (Balaam & Booker 1981).
- Plane strain method: The cylindrical columns are converted to gravel trenches (Van Impe & De Beer 1983). It is commonly used under long loads, such as embankments.
- Axial symmetry technique: The cylindrical columns are converted to gravel rings when columns are used under circular loads, such as tanks (Elshazly et al. 2008).
- Homogenization technique: The soil and columns are modelled as a homogeneous soil with improved properties (Schweiger 1989).
- Full 3D model: Complex numerical models are used to model the system in 3D (Weber et al. 2008).

The study was focused on the consolidation and deformation around end-bearing (fully penetrating) columns under distributed loads and hence, the "unit cell" concept was used for modelling purposes (Figure 1).
In this paper, the results of the small scale tests (Cimentada et al. 2011) are compared with the analytical solutions to assess their accuracy and to validate their hypotheses. Initially, an overview of the analytical solutions and the small scale tests is presented. The main soil responses, such as the stress concentration factor and the settlement reduction factor, are compared using both approaches. The comparison highlights the main features of the stone column behaviour and the capability of the analytical solutions to predict them.

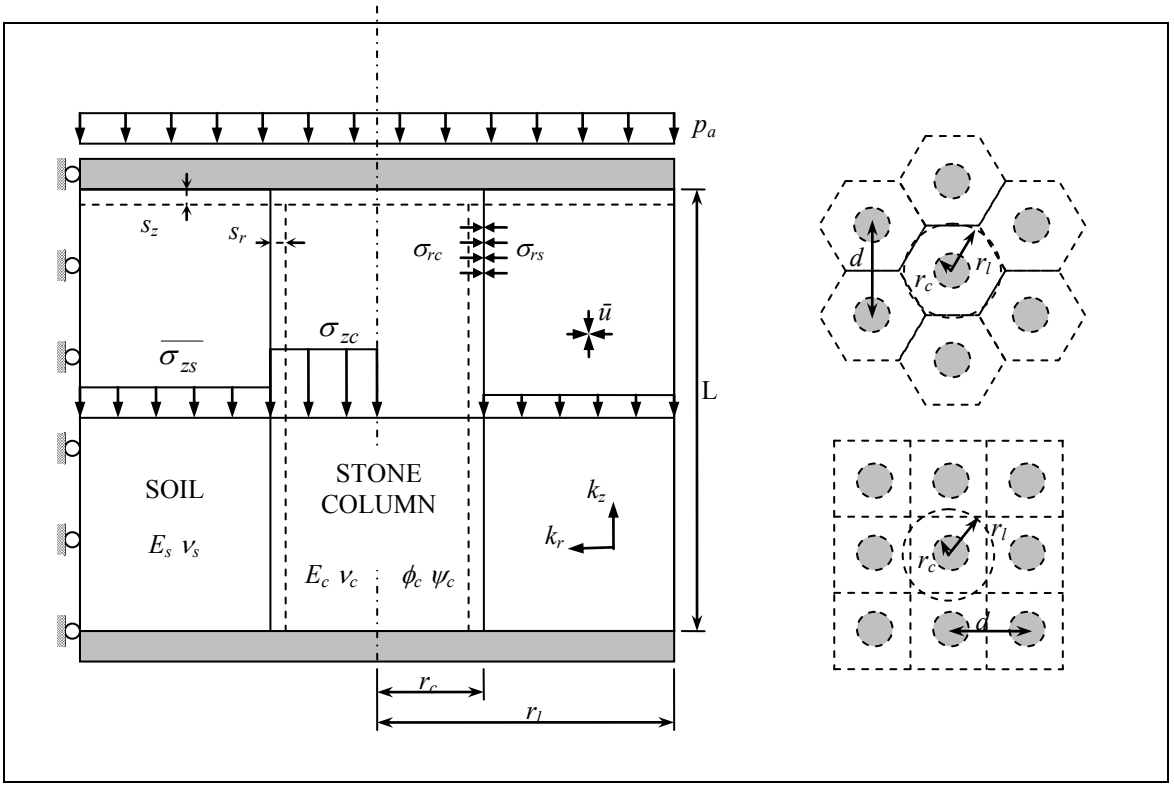

Figure 1: Unit cell.

2. REVIEW OF ANALYTICAL SOLUTIONS

A detailed review of the analytical solutions that study the consolidation and deformation around stone columns is not the scope of this section, which presents only the main features of the analytical solution developed by the authors (Castro & Sagaseta 2009a) and of some solutions that are relevant for comparison purposes.

2.1. Final settlement

The simplest approach to study the final settlement reduction is assuming the soil and the column in elastic and laterally confined (oedometric) conditions. Then, the vertical strains are related to the vertical effective stresses through the respective oedometric (constrained) moduli and the stress concentration factor (the ratio between the vertical stress on the column and on the soil, $SCF=\Delta\sigma_{zc}/=\Delta\sigma_{zs}$) is equal to the oedometric modular ratio, $SCF=E_{mc}/E_{ms}$. This is in contradiction with experience; the modular ratio is usually in the range 10-50, whilst the *SCF* measured in actual cases is much lower, in the range 3-10 (Barksdale & Bachus 1983), as it will be shown later for the small scale tests analysed in this paper. This discrepancy is commonly attributed to the influence of the column lateral deformation, and furthermore, to column yielding.
Balaam & Booker (1981) included the lateral deformation of soil and column and solved the elastic problem. However, the *SCF*, and consequently the settlement reduction, is still overestimated due to the elastic behaviour assumed for the column.
Pulko & Majes (2005) considered the column material as linear elastic-perfectly plastic using the Mohr-Coulomb yield criterion and a non-associated plastic flow rule, with a constant dilatancy angle. While Pulko & Majes (2005) studied the problem in drained conditions, Castro & Sagaseta (2009a) considered

the loading history (undrained loading and consolidation process). Pulko et al. (2011) extended their solution to encased stone columns and included the elastic strains of the column during its plastic deformation, which are relevant when the column is encased and also for drained analyses when it is not encased. If elastic strains of the column during its plastic deformation are included in the drained analysis (Pulko et al. 2011), the differences between drained and consolidation analyses are negligible.
On the other hand, the semi-empirical method by Priebe (1995) is probably the most successful and popular. The column is considered as rigid-plastic, yield limit at the active state and plastic deformation at constant volume (zero dilatancy). Some assumptions of semi-empirical nature are made along the analysis and the influence of the column elastic modulus and of the initial stresses are included as later corrections.

2.2. Radial consolidation

As already introduced, stone columns accelerate the consolidation rate providing a shorter drainage path in a similar way as vertical drains. Hence, the classical solutions of Barron (1948) and Hansbo (1981), available for radial flow around vertical drains, were taken and applied also for stone columns. However, stone columns have a much higher stiffness and replacement area than vertical drains. So, stone columns carry a substantial part of the applied load and the radial consolidation is faster as already shown by Balaam & Booker (1981) through finite element analyses.
Han & Ye (2001) developed an analytical solution for radial consolidation that includes the influence of the column stiffness, i.e. of the applied load carried by the column. They assumed the column and the soil in elastic and laterally confined (oedometric) conditions and obtained the same partial differential equation of consolidation as the solutions for vertical drains but with a modified consolidation coefficient (c_{vr}^{ze}) that includes the influence of the column stiffness:

$$c_{vr}^{ze} = c_{vr}\left(1+\frac{E_{mc}}{E_{ms}}\frac{a_r}{1-a_r}\right) \tag{1}$$

where the superscript "*ze*" refers to the influence of elastic column vertical deformation. It is always $c_{vr}^{ze} > c_{vr}$, so this implies a faster consolidation than for constant load.
The same approach was used by the authors (Castro & Sagaseta 2009a) to obtain the solution for an elastic column including its lateral deformation (c_{vr}^{zre}):

$$c_{vr}^{zre} = c_{vr}\cdot\frac{E_{mm}\left[H-(\lambda_c-\lambda_s)\right]-(1-a_r)(\lambda_c-\lambda_s)^2}{(\lambda_s+2G_s)\left[H-(1-3a_r)(G_c-G_s)\right]} \tag{2}$$

with:

$$H = \frac{1}{a_r}(\lambda_c+G_c+G_s)-(G_c-G_s) \tag{3}$$

$$E_{mm} = a_r(\lambda_c+2G_c)+(1-a_r)(\lambda_s+2G_s) \tag{4}$$

and G and λ are the Lamé's constants.
The superscript "*zre*" refers to the influence of vertical and radial elastic deformation of the column. The quotient (c_{vr}^{zre}/c_{vr}) depends only on the Poisson's ratios of the soil and of the column (v_s, v_c), the modular ratio (E_c/E_s) and the area replacement ratio ($a_r = r_c^2 / r_l^2$, the percentage of soft soil area replaced by columns).
For a plastic column with a constant dilatancy angle (ψ_c), the same approach is also applicable:

$$c_{vr}^{zrp} = c_{vr}\cdot\frac{(1-a_r)+\frac{a_r}{(\lambda_s+2G_s)}\left(\frac{\lambda_s}{k_{\psi c}}+\frac{J}{k_{ac}}\right)}{\left[1+\frac{a_r}{(1-a_r)k_{\psi c}}\right]\left(1-a_r+\frac{a_r}{k_{ac}}\right)} \tag{5}$$

with:

$$J = \lambda_s + \frac{G_s + a_r(\lambda_s+G_s)}{(1-a_r)k_{\psi c}} \tag{6}$$

$$k_{ac} = \frac{1-\sin\phi_c}{1+\sin\phi_c}\ ;\ k_{\psi c} = \frac{1-\sin\psi_c}{1+\sin\psi_c} \tag{7}$$

So, the same classical solutions for vertical drains may be used but including the influence of the stone column through a modified consolidation coefficient.

3. SMALL SCALE TESTS

To compare with analytical solutions, a horizontal slice of the unit cell (Figure 1) was modelled in the laboratory using a scale factor of about 1/10. Two different stone column diameters were investigated ($N=r_c/r_l=$ 4 and 3, which correspond to area replacement ratios of a_r=0.0625 and 0.11, respectively). Heavily compacted gravel (4/5 mm) was used for the central column and kaolin clay for the natural soil. The column was installed when the kaolin clay was consolidated to 100 kPa (Figure 2). Then, five load steps of 100 kPa each were applied. Settlement, pore pressures and vertical and horizontal stresses at different locations were recorded. Further details of the equipment, testing procedure and results are given in Cimentada et al. (2011). Here, the main focus is on the interpretation of the results and their comparison with closed-form solutions.

The relevant kaolin clay and gravel properties for comparison purposes are summarized in Table 1 and Table 2. The gravel friction and dilatancy angles were obtained from drained triaxial tests, showing some decrease with confining pressure. Constant average values of ϕ=46º and ψ=10º were used for the analytical solutions. Other important parameters to select for the analytical solutions are the gravel and kaolin clay moduli. The gravel constrained (oedometric) modulus was obtained from stress path-controlled drained triaxial tests (Figure 3). A value of E_{mc}=39.2 MPa was obtained. Additionally, K_{0c}=0.3 was also obtained from these tests. On the other hand, the kaolin clay modulus varies clearly with the confining pressure, while the analytical solutions assume a linear elastic behaviour. Therefore, the average oedometric modulus of the kaolin clay for each load step, shown in Table 3, is obtained for the range of the mean stresses estimated from vertical and horizontal stresses measured in the kaolin clay during each loading step of the tests. The measurements of horizontal stresses during an oedometer test of the kaolin clay gave K_{0s}=0.52, and from this value a Poisson's ratio of ν_s=0.34 is estimated.

The kaolin clay is initially consolidated at 100 kPa and it is then unloaded to install the column. After column installation, a vertical load of 100 kPa is again applied. However, some of this applied load is now supported by the column, such that the stress on the kaolin clay at the beginning of the test is lower than 100 kPa, as recorded by total stress transducers (TST). Hence, the kaolin clay has some degree of overconsolidation during the start of the first load step (100-200 kPa) and this load step is not an appropriate benchmark for comparison. Furthermore, there are complex processes during column installation that cannot be modelled by the analytical approaches and affect mainly the first load step. Therefore, the second loading step (from 200 to 300 kPa) is chosen for comparison.

Currently, similar small scale tests are being carried out with the gravel in a looser state or with higher column diameters. Those tests will provide further results for analysis.

Table 1: Properties of kaolin clay.

Liquid limit, %	73
Plastic limit, %	38
Plasticity index	35
c_v, cm^2/s	$2.5 \cdot 10^{-3}$
C_c	0.53
C_s	0.10
s_u / σ'_v (C-U triaxial tests)	0.30
ϕ, º (C-U triaxial tests)	26.5

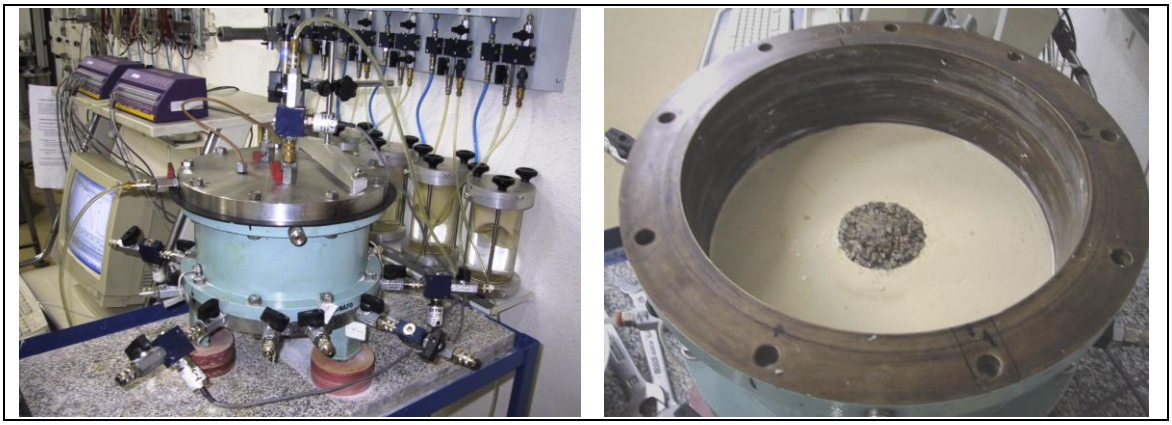

Figure 2: General view of the test and of a column-soil sample.

Table 2: Triaxial tests on gravel.

p'_0 (kPa)	50	100	200	300	400
ϕ (°)	53	48	46	43	41
ψ (°)	19	13	9	4	2
E_{50} (MPa)	21	18	34	29	38
v	0.24	0.17	0.13	0.13	0.16

Table 3: Column-soil stiffness ratio.

	N=4				*N=3*			
Load step (kPa)	p_s' (kPa)	K (MPa)	E_{ms} (MPa)	E_{mc}/E_{ms}	p_s' (kPa)	K (MPa)	E_{ms} (MPa)	E_{mc}/E_{ms}
100-200	60-125	2.2	3.2	12	55-110	3.0	4.4	9
200-300	125-185	1.6	2.3	17	110-160	1.4	2.0	19
300-400	185-245	2.1	3.1	12	160-210	1.8	2.7	14
400-500	245-310	2.7	3.9	10	210-260	2.3	3.4	12
500-600	310-375	3.2	4.7	8	260-315	2.8	4.1	10

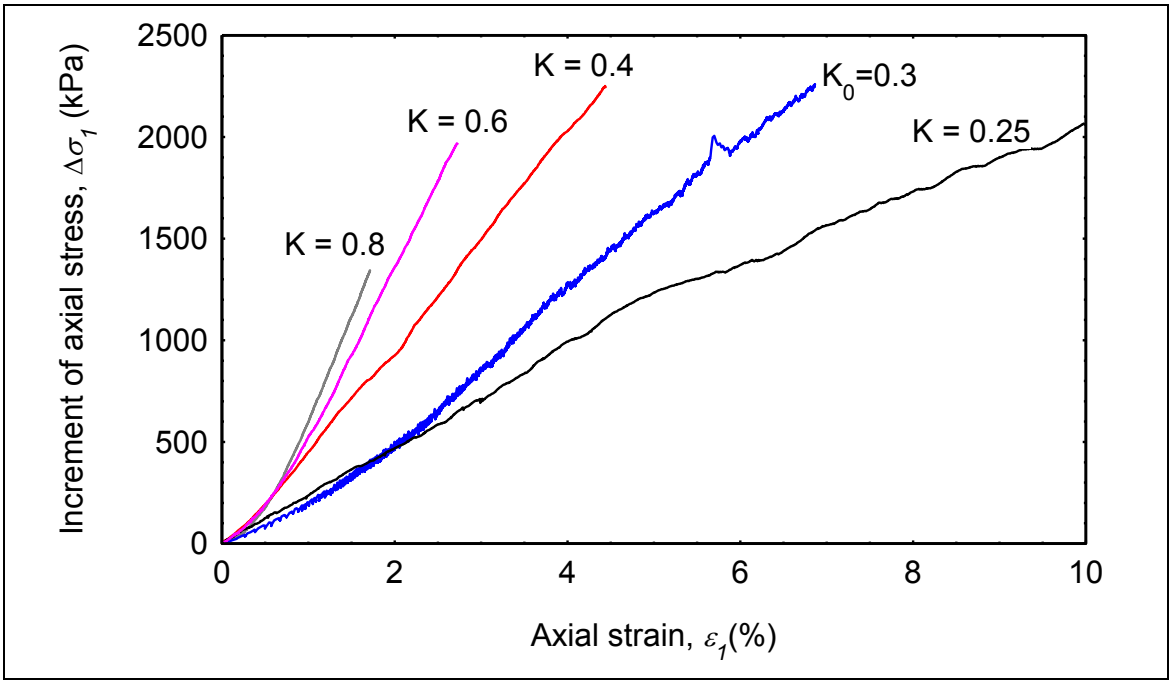

Figure 3: Results of the stress path-controlled drained triaxial tests on gravel samples.

4. COMPARISON AND DISCUSSION

4.1. Stress concentration factor

Stone columns act as rigid inclusions because they have a higher stiffness than the natural soil. Hence, one of the key features of the improvement is the applied load supported by the columns and released from the soil, which is usually quantified by means of the stress concentration factor (*SCF*), the ratio between the vertical stress on the column and on the soil. To analyse each load step independently, the incremental *SCF* is here used ($SCF = \Delta\sigma_{zc}/\Delta\sigma_{zs}$).

The solution by Castro & Sagaseta (2009a) gives the evolution of the *SCF* with time (Figure 4). The results of the small scale tests confirm that the *SCF* increases from an initial value that could be even lower than 1 until the column reaches its active state, and then, the value keeps roughly constant. On the contrary, the solutions that assume an elastic behaviour for the column (Han & Ye 2001) predict a continuous increment of the *SCF* value. In the laboratory tests, the column yields gradually and not for a specific moment as obtained with the analytical solution due to the "ideal" conditions assumed (e.g. absence of shear stresses and side friction). Nevertheless, that difference is not particularly important and the main divergence between the closed-form solutions and the laboratory measurements is the time when the *SCF* starts to increase. In the laboratory results, after roughly 5 minutes, the *SCF* has already reached the value of *SCF*=5, while that time for the theoretical solutions is between 10 and 40 times higher, depending on the geometry and the load level. That behaviour seems to be related to the high small-strain stiffness of the gravel column, which is not modelled by the theoretical solutions but is not important for practical purporses either.

The scatter in the *SCF* obtained from the laboratory measurements is mainly caused by the vertical stress on the column (typical of stress measurements in coarse granular materials). The final value of the *SCF* after each load step is in the common range of 3-10 (Barksdale & Bachus 1983). The analytical solutions that assume an elastic and confined (oedometric) behaviour for the column (Han & Ye 2001) predict a *SCF* equal to the ratio of the oedometric moduli (E_{mc}/E_{ms}), which is usually much higher (10-40) than the values of the *SCF* measured in the field and in the laboratory (3-10). Some analytical solutions (e.g. Balaam & Booker 1981) include the radial deformation of the column, which gives a slightly lower value of the *SCF* but still high because the column yielding is not considered.

Those solutions that account for the yielding of the column (Castro & Sagaseta 2009a; Pulko et al. 2011) predict more realistic values of the *SCF*. Although the solutions by Castro & Sagaseta (2009a) and Pulko et al. (2011) differ in their hypotheses because the first one considers the consolidation process while the second one assumes drained conditions and include the elastic strains of the column during its plastic deformation, both solutions give nearly coincident values for the presented case, and in general, for the final values of non-encased stone columns.

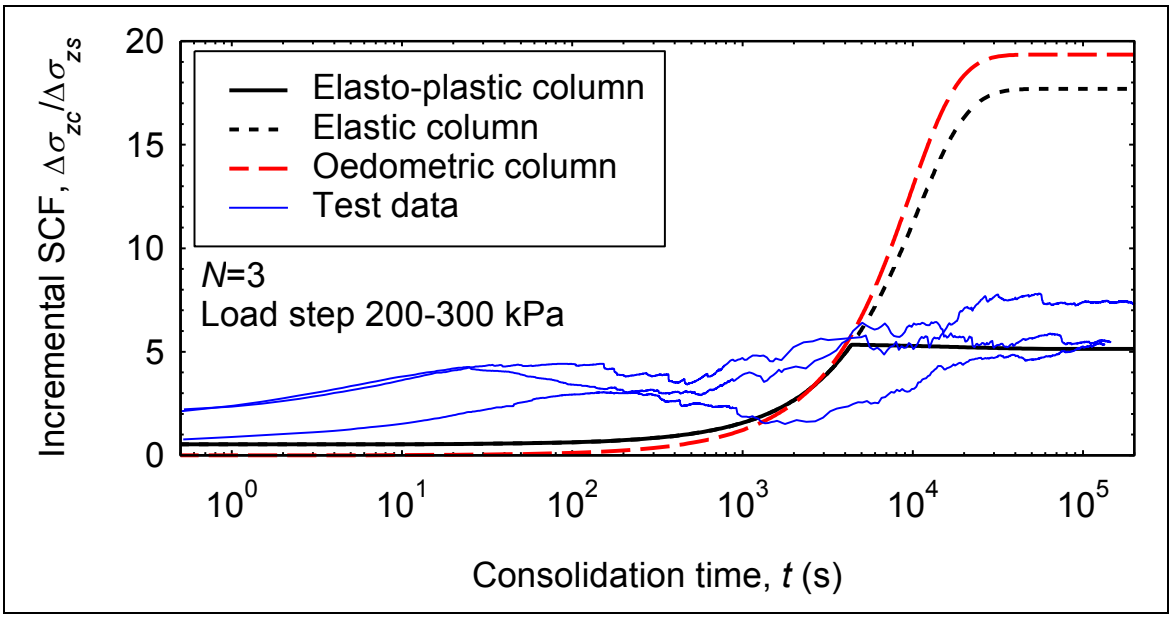

Figure 4: Incremental stress concentration factor (SCF) with time.

4.2. Settlement reduction

The stress concentration on the columns leads to a decrease of the vertical stress on the natural soil, and therefore, the reduction of the settlement proportionally. The settlement reduction caused by the stone columns is a very important issue for their design and is usually expressed by means of the settlement reduction factor (the ratio between the settlement with columns and without columns, $\beta = s_z / s_{z0}$) or its inverse, the improvement factor (n).

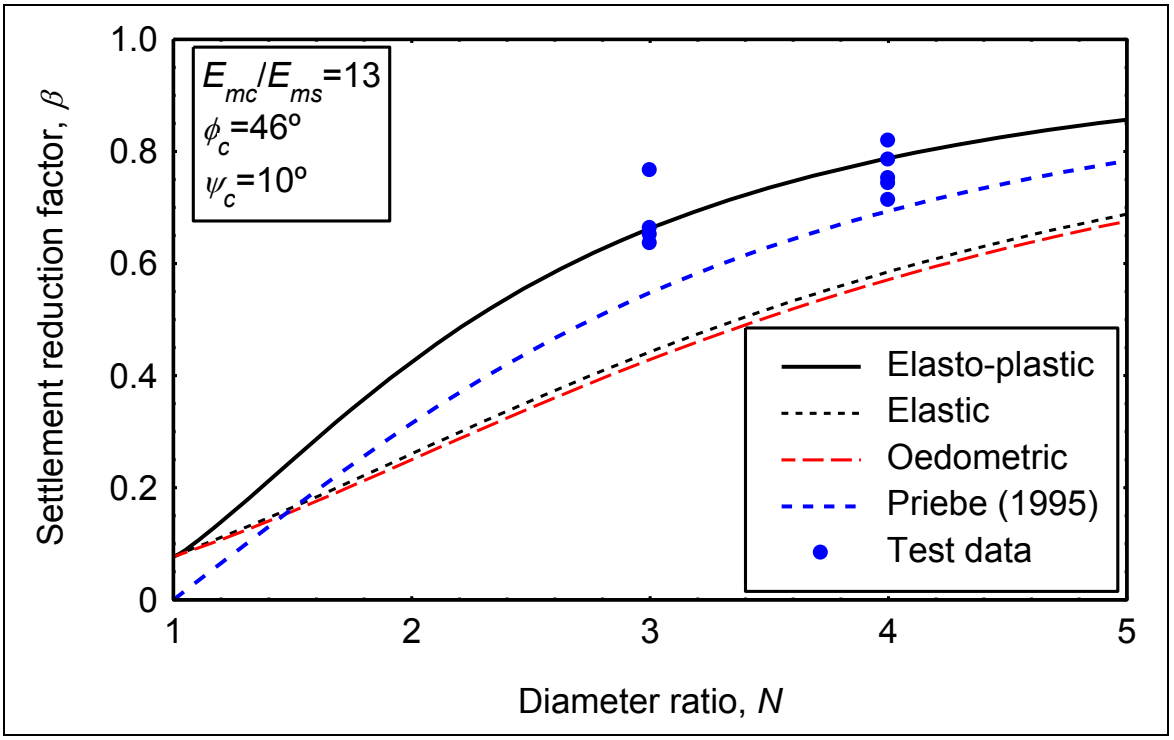

Figure 5: Comparison of the settlement reduction factor.

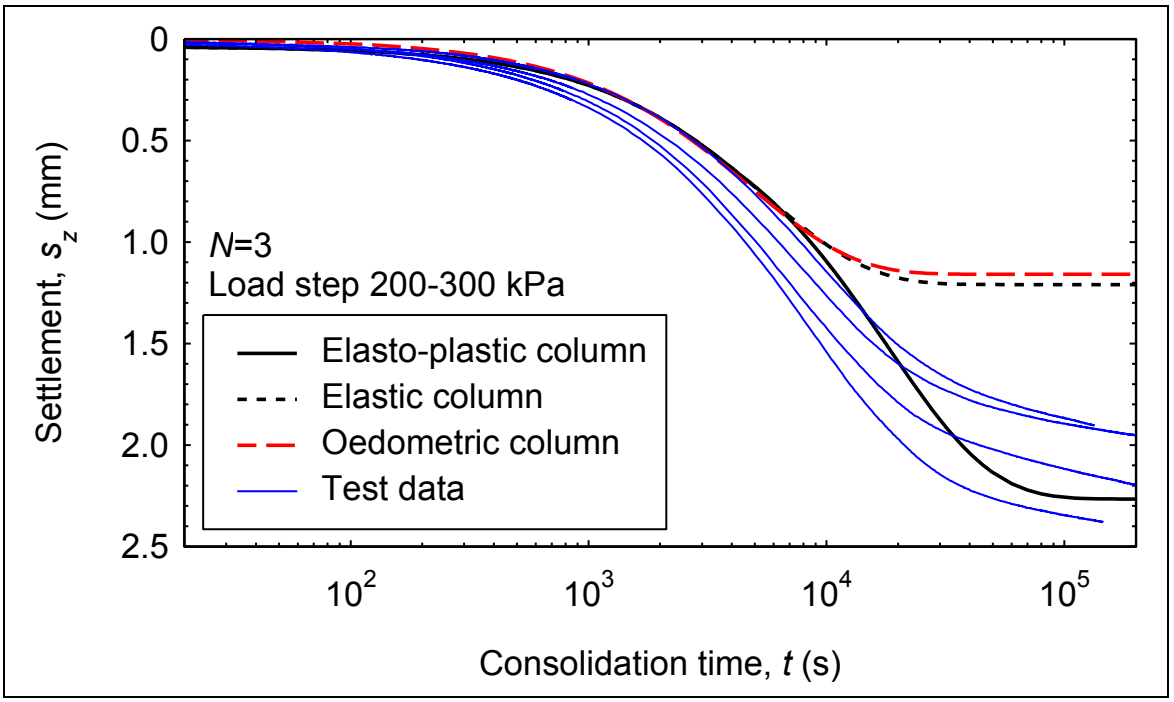

Figure 6: Analysis of the settlement rate.

The results of the small scale tests are a good benchmark to make a detailed comparison of the settlement reduction factor predicted by the analytical solutions (Figure 5). The settlement reduction factor of each

of the small scale tests was obtained dividing the vertical strain of the test with column (from 100 to 600 kPa) by the vertical strain of a reference test of the kaolin clay without column for the same applied load. The analytical solutions that consider an elasto-plastic behaviour of the column (Castro & Sagaseta 2009a; Pulko et al. 2011) agree very well with the tests. Furthermore, they allow for a direct control of most of the soil and column characteristics. An average ratio of the oedometric moduli (E_{mc}/E_{ms} =13) for all the loading steps (Table 3) is used. However, its value has a small influence in the analytical solutions that consider column yielding.

As previously mentioned, the elastic solutions overestimate the settlement reduction, especially if realistic values are used. Priebe's solution without corrections slightly overestimates the settlement reduction. However, conservative values of the column friction angle are assumed for routine design and, contrary to the presented small scale tests where there are minimal installation effects, Priebe's method implicitly assumes an increase of the horizontal stress (K_0=1) after column installation.

Beyond the settlement reduction, the settlement-time curves are necessary for an accurate design. The results of the different approaches are compared in Figure 6. The analytical solution of the authors (Castro & Sagaseta 2009a) agrees very well with the small scale tests. Nevertheless, final settlement values using the analytical solution obviously depend on the soil average stiffness and consequently on the stress range estimated for the soil to obtain the stiffness modulus. In this case, a careful analysis was done (Table 3) but this may not be practical for routine design. Therefore, it may not be convenient to calculate the final settlement directly, but instead it is recommended to do it through the settlement reduction factor and the final settlement without improvement. Furthermore, for routine design column stiffness is not usually available but fortunately, settlement values predicted by the approaches that consider column yielding do not strongly depend on that parameter, and a reasonable value is usually enough to achieve a good prediction.

5. CONCLUSIONS

The results of small scale tests of kaolin clay improved with stone columns are compared with closed-form solutions. The comparison shows the good predictions of the *SCF* and the settlement rate by the authors' solution (Castro & Sagaseta 2009a). There are only slight differences caused by the high small-strain stiffness of the gravel column and the secondary compression of the kaolin clay. However, they are not important for practical purposes.

The final values of the *SCF* and the settlement reduction are well predicted only by the solutions that allow for plastic strains in the column, such as Castro & Sagaseta (2009a) and Pulko et al. (2011). Although Pulko et al. (2011) assumes drained conditions for soil and column, both solutions give the same final values for non-encased stone columns. The column stiffness, which is usually unknown, has a small influence in the results of these solutions.

Solutions that assume an elastic behaviour for the column tend to overpredict the improvement caused by the columns. Therefore, conservative values of the column stiffness are chosen when these solutions are used.

6. ACKNOWLEDGEMENTS

The work presented is part of a research project on "An integrated calculation procedure for stone columns, considering the influence of the method of installation", for the Spanish Ministry of Science and Innovation (Ref.: BIA2009-13602).

REFERENCES

Balaam, N.P. & Booker, J.R. 1981. Analysis of rigid rafts supported by granular piles. Int. Journal for Numerical and Analytical Methods in Geomechanics 5: 379-403.

Barksdale, R.T. & Bachus, R.C. 1983. Design and construction of stone columns. Report FHWA/RD-83/026. Springfield: Nat. Tech. Information Service.

Barron, R.A. 1948. Consolidation of fine-grained soils by drain wells. Transactions ASCE 113: 718-742.

Bergado, D.T., Anderson, L.R., Miura, N. & Balasubramaniam, A.S. 1996. Soft ground improvement in lowland and other environments. New York: ASCE.

Castro, J. & Sagaseta, C. 2009a. Consolidation around stone columns. Influence of column deformation. Int. Journal for Numerical and Analytical Methods in Geomechanics 33: 851-877

Castro, J. & Sagaseta, C. 2009b. Field instrumentation of an embankment on stone columns. 17th International Conference on Soil Mechanics and Geotechnical Engineering, Alexandria, 3, 1865-1868.

Castro, J. & Sagaseta, C. 2011. Consolidation and deformation around stone columns: Numerical evaluation of analytical solutions. Computers and Geotechnics 38(3): 354-362.

Cimentada, A., da Costa, A., Cañizal, J. & Sagaseta, C. 2011. Laboratory study on radial consolidation and deformation in clay reinforced with stone columns. Canadian Geotechnical Journal 48(1): 36-52.

Dhouib, A., Wehr, J., Soyez, B. & Priebe, H.J. 2004. Méthode de Priebe: origine, développement et applications. Symposium International sur l'Amélioration des Sols en Place 2004; Paris, Presses de l'ENPC et LCPC, 131-146.

Elshazly, H. Elkasabgy, M. & Elleboudy, A. 2008. Effect of inter-column spacing on soil stresses due to vibro-installed stone columns: interesting findings. Geotechnical and Geological Engineering 26: 225-236.

Han, J. & Ye, S.L. 2001. A simplified solution for the consolidation rate of stone column reinforced foundations. Journal of Geotechnical and Geoenvironmental Engineering 127(7): 597-603.

Hansbo S. 1981. Consolidation of fine-grained soils by prefabricated drains. 10th International Conference on Soil Mechanics and Foundation Engineering, Stockholm, 3: 677–682.

Hughes, J.M.O. & Withers, N.J. 1974. Reinforcing of soft cohesive soils with stone columns. Ground Engineering 7 (3): 42-49.

Priebe, H.J. 1995. Design of vibro replacement. Ground Engineering 28 (10): 31-37.

Pulko, B. & Majes, B. 2005. Simple and accurate prediction of settlements of stone column reinforced soil. 16th Int. Conf. on Soil Mechanics and Foundation Eng.: 1401-1404. Rotterdam: Millpress.

Pulko, B., Majes, B. & Logar, J. 2011. Geosynthetic-encased stone columns: Analytical calculation model. Geotextiles and Geomembranes 29(1): 29-39.

Schweiger, H.F. 1989. Finite element analysis of stone column reinforced foundations. PhD Thesis, University of Wales, Swansea.

Van Impe, W.F. & De Beer, E. 1983. Improvement of settlement behaviour of soft layers by means of stone columns. 8th Int. Conf. on Soil Mechanics and Foundation Eng.: 309-312. Rotterdam: Balkema.

Vesic, A.S. 1972. Expansion of cavities in infinite soil mass. Journal of the Soil Mechanics and Foundation Division, ASCE 98(SM3): 265–290.

Weber, T.M. Springman, S.M. Gäb, M. Racansky, V. & Schweiger, H.F. 2008. Numerical modelling of stone columns in soft clay under an embankment. In Karstunen & Leoni (eds), Geotechnics of Soft Soils-Focus on Ground Improvement: 305-311. London: Taylor & Francis.

Numerical modelling of stone column installation in Bothkennar clay

Castro, J., University of Cantabria, Santander, Spain, castrogj@unican.es
Kamrat-Pietraszewska, D., University of Strathclyde, Glasgow, UK,
daniela.kamrat-pietraszewska@strath.ac.uk
Karstunen, M., University of Strathclyde, Glasgow, UK, minna.karstunen@strath.ac.uk

ABSTRACT

The paper presents the results of numerical simulations studying the installation effects of stone columns in a natural soft clay. The geometry of the problem is simplified to two-dimensional axial symmetry, considering the installation of one end-bearing column only. Stone column installation is modelled as an undrained expansion of a cylindrical cavity. The excess pore pressures generated in this process are subsequently assumed to dissipate towards the permeable column. The process is simulated using a finite element PLAXIS code that allows for large displacements. The properties of the soft clay correspond to Bothkennar clay, a soft (Carse) clay from Scotland (UK). The complexity of this material is simulated via three advanced recently developed constitutive formulations able to account for anisotropy, destructuration and viscosity, namely S-CLAY1S, EVP-SCLAY1S and ACM-S. The presented boundary value problem is also used as a benchmark for preliminary analysis of the performance of those constitutive models. Stone column installation alters the surrounding soil and the research studies the change in soil anisotropy and degradation of bonding as a result of the undrained cavity expansion. Based on the results, some practical advice is given.

1. INTRODUCTION

Stone columns are a ground improvement technique, which not only increases the overall strength, permeability and stiffness of the foundation system, but also modifies the properties of the soil surrounding the columns. Design of stone columns is usually based on their performance as rigid inclusions (Balaam & Booker 1981; Barksdale & Bachus 1983; Priebe 1995; Castro & Sagaseta 2009) and the alteration caused in the surrounding soil by column installation is commonly not considered. However, the installation effects, whether they are positive, negative or negligible, are currently one of the major concerns for an accurate design (Egan et al. 2008). Field measurements (Watts et al. 2000; Watts et al. 2001; Kirsch 2004; Gäb et al. 2007; Castro 2008, McCabe et al. 2009) have shown some of the effects of column installation, like the increase of pore pressures and horizontal stresses, and the remoulding of the surrounding soil caused by the vibrator penetration. However, based on these measurements it is difficult to achieve conclusions that can be used in stone column design, because they relate to a specific case and hence cannot be generalised in a straightforward manner. There have also been attempts to investigate these effects through physical modelling of the process by means of centrifuge testing (Lee et al. 2004; Weber et al. 2010), but the soils used are reconstituted and hence not representative of natural clays.

Numerical modelling is a useful tool that may well help to derive some conclusions or recommendations of how to account for installation effects for column design, if the assumptions made in the model are validated by experimental measurements. However, there were few attempts (Kirsch 2006; Guetif et al. 2007) in this field and in both cases, the soil model used was very simplistic, and not representative of real soil behaviour: elastic-perfectly plastic with a non-associate Mohr-Coulomb failure criterion. Hence, for example, it was not possible to account for any hardening of the soil due to installation which is a key phenomenon. Therefore, Castro & Karstunen (2010) carried out numerical simulations of installation effects of stone columns using two advanced constitutive models: S-CLAY1 (Wheeler et al. 2003) and S-CLAY1S (Karstunen et al. 2005), which have been especially developed to represent natural structured soft soils, a common type of soils to be treated with stone columns. Those models account for soil anisotropy and the latter also for the effects of structure. In this paper, further numerical simulations are presented using soil models that account additionally for soil viscosity, namely EVP-SCLAY1S (Karstunen & Yin 2010) and ACM-S (Kamrat-Pietraszewska 2011). Firstly, the numerical model is described, followed by an overview of the constitutive models and the values of the model parameters chosen. Finally, the results are discussed in the view of practical design.

2. NUMERICAL MODEL

The finite element code Plaxis v9 (Brinkgreve 2008) was used to develop a numerical model of a reference problem to study installation effects of stone columns. The installation of only one stone column was considered to simplify the problem to an axisymmetric two dimensional geometry. In order to consider a realistic situation, properties of Bothkennar clay were used for the soft soil. The Bothkennar soft clay test site has been the subject of a number of comprehensive studies (Géotechnique Symposium in print 1992). The soil at Bothkennar consists of a firm to stiff silty clay crust about 1.0 m thick, which is underlain by about 19 m of soft clay. The ground water level is 1.0 m below the ground surface. Typically to a structured soil the in situ water content is close to the liquid limit.
Stone columns have been applied in Bothkennar clay (Watts et al. 2001; Serridge & Sarsby 2008) or other Carse clays (Egan et al. 2008). For the numerical model in this paper, a column length of 10 m is assumed. The untreated clay underneath is not modelled, because the installation effects in this part of the soil are not particularly significant and furthermore, modelling the tip of the column may lead to some numerical instabilities. The numerical model is 10 m high and 15 m wide (see Figure 1).

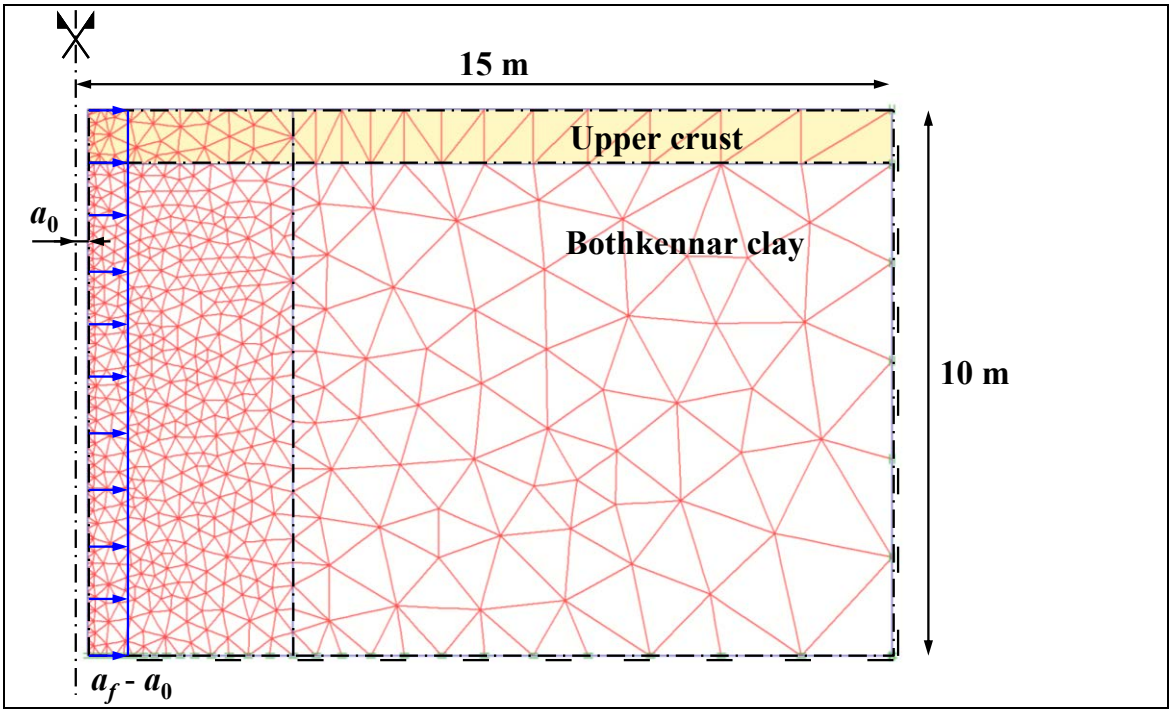

Figure 1: Numerical model.

Parametric studies were carried out to check how wide the model should be to have a negligible influence of the outer boundary. Based on these a width of 15 m was considered sufficient. Roller boundaries were assumed on all sides to enable the soil to move freely due cavity expansion. The finite element mesh is extra fine close to the column cavity, where the installation effects are expected to be noticeable and mesh sensitivity studies were performed to confirm the accuracy of the mesh.
The numerical model accounts only for pure cavity expansion effects of installation, and ignores e.g. the shearing and soil disturbance due to the penetration of the poker, the vibration of the poker, etc. It is, however, thought that the main effect is the cavity expansion. So, column installation is modelled as the expansion of a cylindrical cavity in undrained conditions, because columns are usually installed in a short period of time. The expansion of the cavity is modelled as a prescribed displacement from an initial radius, a_0, to a final one, a_f. Further details on the numerical model are given in Castro & Karstunen (2010).
In summary, two calculation phases are performed after the generation of initial stresses: the expansion of a cavity in undrained conditions followed by consolidation process. The cavity expansion generates large strains, making necessary to account for large displacements in the calculation. The "updated mesh" option in Plaxis software allows for this kind of calculation. Despite the name, a large displacement calculation implies considerably more than simply updating nodal coordinates (Brinkgreve 2008). This updated Lagrangian formulation is described by McMeeking & Rice (1975). The co-rotational rate of Kirchhoff stress (or known as Hill stress rate) is adopted. The details on the implementation can be found in Van Langen (1991). In addition, the value of the pore pressures was also updated in each step, even

though it is not particularly important for this problem. In terms of controlling the solution of the non-linear problem with PLAXIS, the arc-length control was deactivated, the over-relaxation was set to 1.0 and the explicit implementation of the S-CLAY1 model (Wiltafsky 2003) was used, with a step size parameter of -0.5 to avoid numerical instabilities with the User-defined soil model.

3. SOIL CONSTITUTIVE MODELS

In this study, three advanced constitutive models are used, namely S-CLAY1S (Karstunen et al. 2005), EVP-SCLAY1S (Karstunen & Yin 2010) and ACM-S (Kamrat-Pietraszewska 2011). The first is an elasto-plastic formulation accounting for plastic anisotropy and degradation of interparticle bonds of the soft soil, whereas latter two have also ability of accounting for viscous effects in the soft soil material. Additionally, for the sake of comparison, well known isotropic Modified Cam Clay (MCC) model is also applied in some of the simulations, for details on this model please refer to Roscoe & Burland (1968).

The S-CLAY1S model (Karstunen et al. 2005) considers anisotropic behaviour by introducing a rotated natural yield surface and a rotational hardening rule, and the effects of destructuration by incorporation of an inclined intrinsic yield surface and a destructuration rule. The intrinsic yield surface, following the idea by Gens & Nova (1993), allows for the description of the equivalent unbonded material with the same void ratio and fabric as the natural soil. It is of the same shape and orientation as the natural yield surface, but has a smaller size, see Figure 2.a. The size of the intrinsic yield surface p'_{mi} is related to the size of the natural yield surface p'_m by the so-called bonding parameter,χ, which defines the current amount of bonding:

$$p'_m = (1+\chi)p'_{mi} \tag{1}$$

The S-CLAY1S model incorporates three hardening laws. The first and second of these relate to the rotation (orientation) of the yield surface and link the change in size of the intrinsic yield surface to the plastic volumetric strain increment. The third hardening law used in this model describes the degradation of bonding with plastic straining, where the bonding parameter χ is reduced towards a target value of zero by the plastic volumetric strains and plastic deviatoric strains:

$$d\chi = \xi\left[(0-\chi)\left|d\varepsilon_v^p\right| + \xi_d(0-\chi)\left|d\varepsilon_d^p\right|\right] = -\xi\chi\left[\left|d\varepsilon_v^p\right| + \xi_d\left|d\varepsilon_d^p\right|\right] \tag{2}$$

where ε_v^p and ε_d^p are the plastic volumetric and deviatoric strains and ξ and ξ_d are two parameters of the destructuration hardening law. Parameter ξ controls the absolute rate of destructuration and parameter ξ_d controls the relative effectiveness of plastic deviatoric strains and plastic volumetric strains in destroying the bonding.

The EVP-SCLAY1S (Karstunen & Yin 2010) is an over-stress model that is able to account for the viscosity, anisotropy and degradation of the interparticle bonds. The static yield surface acts as a bounding surface between recoverable and irrecoverable strains. Within the static yield surface there is an intrinsic yield surface, used to describe the effects of apparent bonding and destructuration as a function of irrecoverable strains, see Figure 2b. Analogous to the S-CLAY1S model, the evolution of anisotropy and the effect of bonding in EVP-SCLAY1S is accounted by the function of visco-plastic strains (both volumetric and deviatoric), and the difference between the sizes of the static and intrinsic yield surfaces, respectively. The rate of visco-plastic strains in the EVP-SCLAY1S model greatly depends on the fluidity parameter μ and the strain-rate coefficient N, which relate to the strain rate effect on shear strength and preconsolidation pressure. The EVP-SCLAY1S model assumes a Drucker-Prager failure criterion and predicts, similarly to the classical critical state models and S-CLAY1S, strain softening at the "dry side" of critical state.

The ACM-S model (Kamrat-Pietraszewska 2011) is a time-dependent model capable of taking account of anisotropy and degradation of the interparticle bonds of the soft soil. It is based on the Anisotropic Creep Model (Leoni et al. 2008) and incorporates destructuration law similarly to the S-CLAY1S and EVP-SCLAY1 models. The Normal Consolidation Surface (NCS), see Figure 2c, expands and rotates as a function of creep strains. NCS is also a bounding surface between small (but irrecoverable) creep strains, and large irrecoverable creep strains. So, if a stress point in taken outside the NCS by an increment of effective stress, the ACM-S model predicts large irrecoverable time-dependent strains. The second yield surface, so-called Current Stress Surface (CSS), is defined by the current stress point, and the distance between CSS and NCS is treated as a generalized overconsolidation ratio $OCR^*=p'_p/p'_{eq}$, which also relates the creep volumetric strains to the intrinsic modified creep and compression indices and the modified swelling index. The intrinsic yield surface, similarly to the S-CLAY1S and EVP-SCLAY1S models, describes the equivalent unbonded material and the degradation of the interparticle bonds towards zero is attributed to the volumetric and deviatoric creep strains, analogously to the other models

used in the study. The ACM-S, in contrast to EVP-SCLAY1S and S-CLAY1S, assumes Argyris failure criterion (Argyris et al. 1974), which is analogous to Matsuoka-Nakai failure envelope (Matsuoka & Nakai 1982) but is simpler in the mathematical form.
Input parameters used for the numerical simulations with those soil constitutive models are presented in Tables 1-4. Authors would like to emphasise that fluidity parameter μ^* used for the EVP-SCLAY1S model is not comparable and cannot be directly linked to the intrinsic modified creep index μ_i^* applied for simulations with the ACM-S model. All soil constitutive models used for simulations presented in this paper were implemented as User-defined soil models in the two-dimensional version of PLAXIS.

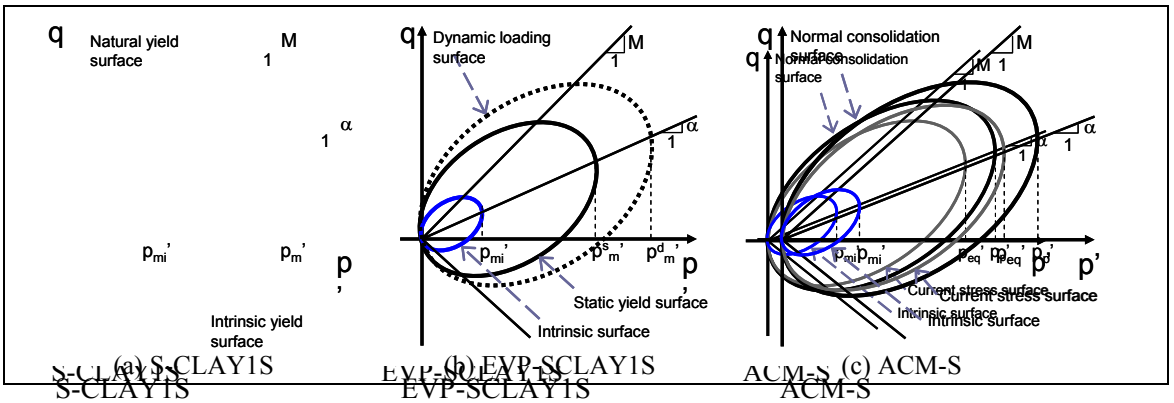

(a) S-CLAY1S (b) EVP-SCLAY1S (c) ACM-S

S-CLAY1S EVP-SCLAY1S ACM-S

Figure 2: Soil constitutive models.

Table 1: Soil constitutive models: parameters for Bothkennar clay.

Depth (m)	γ (kN/m^3)	k_h (m/s)	k_v (m/s)	κ	ν'	λ	M	ω	ω_d
0-1	18.0	2.8×10^{-9}	1.4×10^{-9}	0.02	0.2	0.48	1.4	30	0.94
1-10	16.5	1.4×10^{-9}	0.7×10^{-9}	0.02	0.2	0.48	1.4	30	0.94

Table 2: Soil constitutive models: initial state variables.

Depth (m)	e_0	α_0	OCR	POP (kPa)	K_0
0-1	1.1	0.539	-	30	1.35
1-10	2	0.539	1.5	-	0.544

Table 3: Soil constitutive models: destructuration parameters.

Depth (m)	λ_i	χ_0	ξ	ξ_d
0-10	0.18	5	11	0.2

Table 4: Soil constitutive models: time-dependency parameters.

	EVP-SCLAY1S		ACM-S	
Depth (m)	N^*	μ^* (day^{-1})	μ_i^*	τ (day)
0-1	9	4×10^{-5}	0.0034	1
1-10	9	4×10^{-5}	0.0024	1

4. RESULTS AND DISCUSSION

4.1. Pore pressures

Field measurements (Gäb et al. 2007; Castro 2008; McCabe et al. 2009) clearly show that pore pressures immediately increase during vibrator penetration. The pore pressures reach a peak during column construction and are later dissipated. The value of these peak pore pressures are the first installation effect to be analysed.

The excess pore pressures generated by column construction, Δu, are shown in Figure 3. Following common practice, the distance to column axis, r, is normalised by the column radius, r_c. The MCC, S-CLAY1S and ACM-S models give results in the same range and predict a radius of influence around 12 ($R/r_c = \sqrt{I_r}$ =12.2) and a maximum value at the cavity wall of 5 c_u ($u_{max}/c_u = \ln I_r$). However, it is not possible to normalise by the undrained shear strength of the soil because it is rate dependent for models that account for viscosity. Results show that considering creep does not necessary lead to higher excess pore pressures. The overstress model (EVP) predicts higher values close to the column and lower values far from the column than the other models. That could be explained by the fact that strain rates are higher close to the column and lower far from it. The excess pore pressures generated near the column during the undrained expansion of the cavity are quickly dissipated towards the column, i.e. towards the internal permeable boundary in the numerical model.

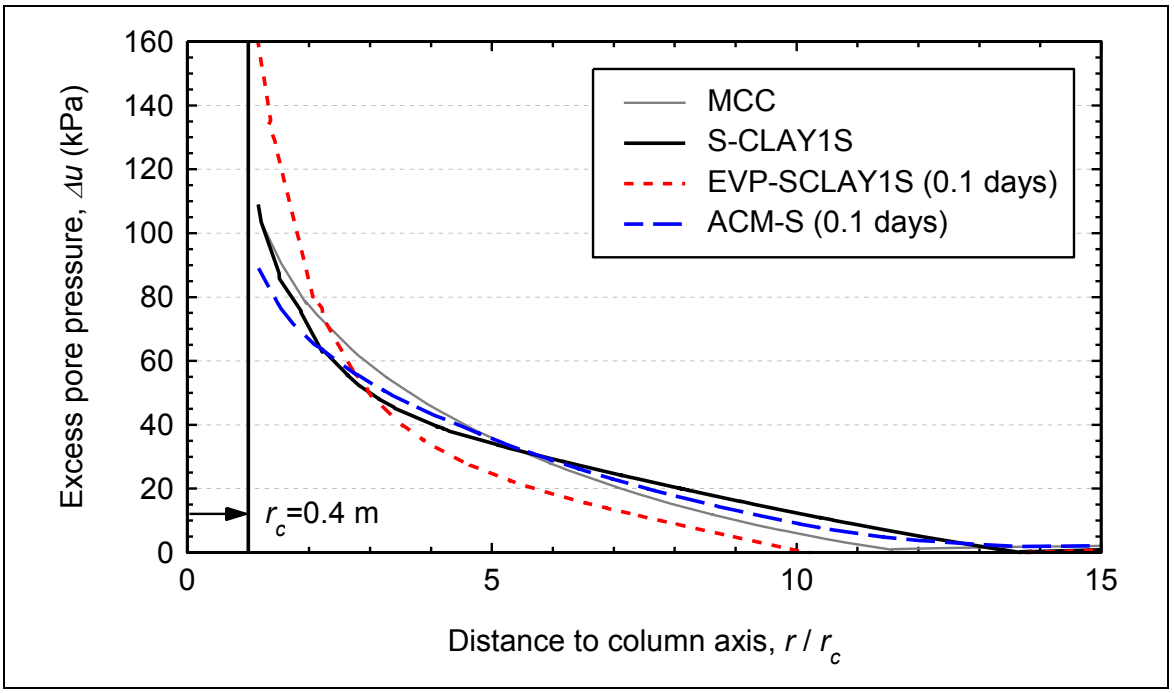

Figure 3: Excess pore pressures after undrained expansion of the cavity at a depth of 5 m.

4.2. Lateral earth pressure

Column installation evidently generates an increase in the horizontal stresses of the surrounding soil. In fact, the positive effects of column installation in soft soils are due to the increase of effective horizontal stresses after the consolidation process that follows the expansion of the cavity. For example, Priebe (1995) already assumed in his analysis a value of the soil lateral earth pressure coefficient of 1, which is higher that the initial value at rest for most soils. The lateral earth pressures clearly influence the improvement factor achieved with a stone column treatment since it gives the lateral support for the column and influences its yielding. The *K* value is therefore an important state parameter in stone column design.

The predicted changes in the lateral earth pressure coefficient after consolidation are shown in Figure 4. That change is nearly constant with depth. Between 4 and 8 column radiuses from the column axis, the curves show a plateau with a nearly constant value of the lateral earth pressure coefficient. This will be the value that should be used for the stone column design, as long as the pore pressures generated during column construction have been dissipated. As shown by Castro & Karstunen (2010), with S-CLAY1 the post installation lateral earth pressure coefficient is nearly 1 while this value is clearly lower using S-CLAY1S, which illustrates that the destructuration caused by column installation has a negative effect not only in the undrained shear strength, but also in the increase of the lateral confinement of the column. That is also valid for the EVP and ACM-S models. Anisotropy has also a major effect, as the isotropic MCC model predicts much higher values of K than the anisotropic models, which dissipate energy in having to change the orientation of the fabric during the cavity expansion. EVP-SCLAY1S predicts similar values to S-CLAY1S after consolidation (around 900 days after column installation). EVP model is an overstress model and, therefore, it cannot reproduce horizontal stress relaxation with time. On the

other hand, ACM-S gives very low values, even lower than the initial one in the far field because the self-weight causes a considerable secondary compression in the soil, and consequently, soil overconsolidation is erased and the lateral earth pressure coefficient changes to its normally consolidated value. This of course is unrealistic.

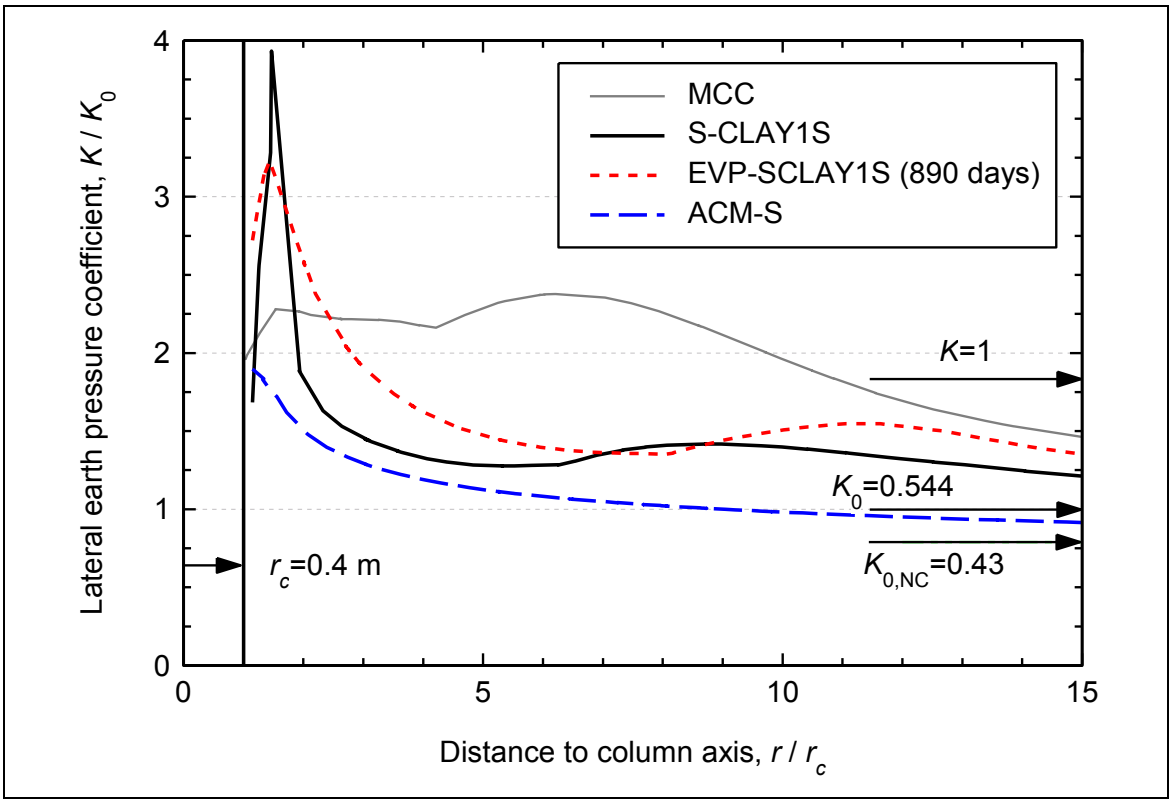

Figure 4: Change in lateral earth pressure for different soil models.

4.3. Destructuration

One of the main goals of using advanced constitutive models such as S-CLAY1S was to study the installation effects of stone columns in the amount of bonding of the surrounding soil. Some field measurements (Watts et al. 2000; Serridge & Sarsby 2008; Castro 2008) alert on the reduction of the undrained shear strength caused by the installation of vibro displacement columns in sensitive soft soils. Therefore, it would be very desirable to be able to account for this effect in the column design. However, undrained shear strength is not a soil constant and nor is it state variable, and furthermore, with rate-dependent models its apparent value is also strain-rate dependent. The predicted apparent value of undrained shear strength relates to the bonding parameter χ. Figure 5 shows the predicted decrease of χ, as a result of column installation, which is directly linked to the sensitivity of the soil. The reduction in the values suggests strain softening, from a peak value of the undrained strength to the respective remoulded value when χ is equal to zero. Additional numerical studies demonstrated that the initial value of the bonding parameter has no influence on the process, and therefore the bonding parameter is normalized by its initial value in Figure 5. The major changes are limited to the area near the column, and for example, beyond 4 column radiuses, the reduction is less than 10 per cent. The results suggest that the main part of the destructuration is caused by the undrained expansion of the cavity and the consolidation process has little influence. S-CLAY1S and EVP-SCLAY1S give the same results in undrained conditions, not only for destructuration but also for change in anisotropy, because the displacement field is exactly the same after undrained expansion of the cavity, independently of the model. Therefore, the strains are the same and as the hardening laws of destructuration and anisotropy are the same, the results are the same.

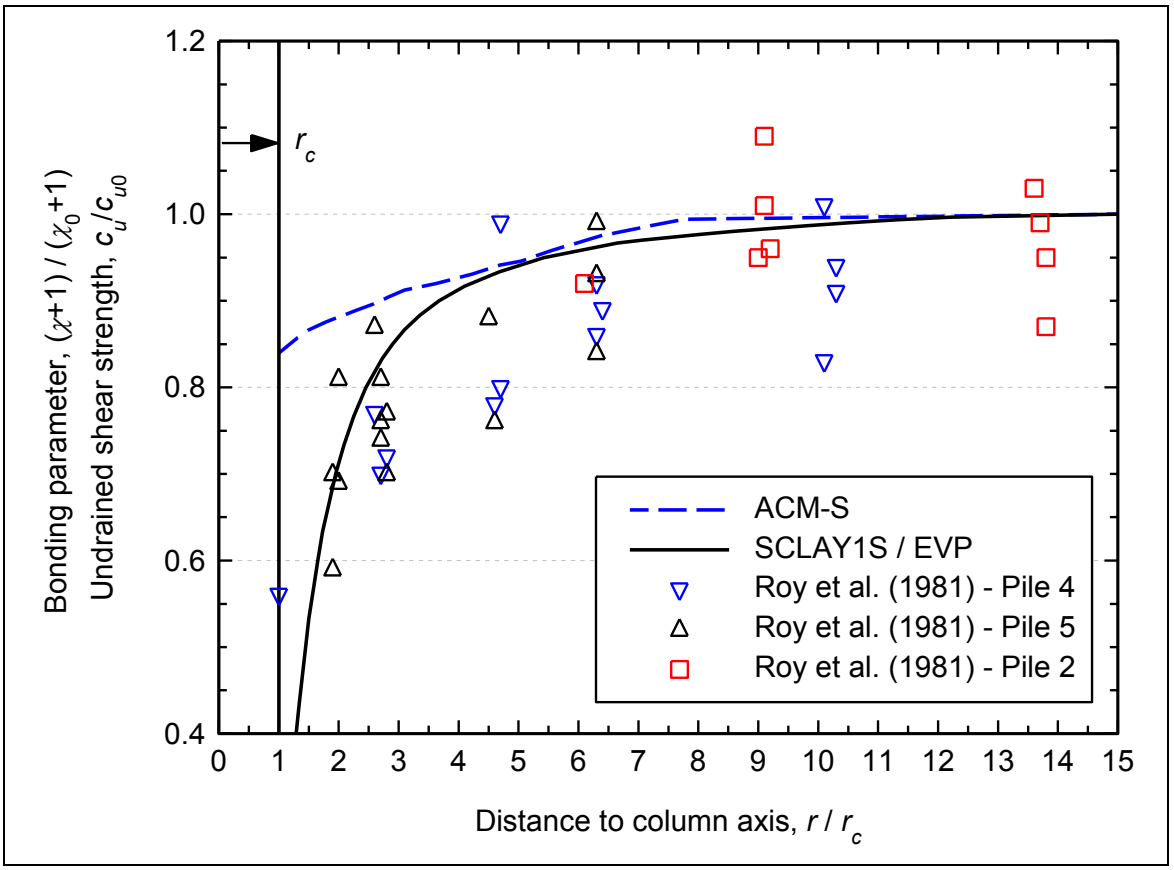

Figure 5: Comparison of destructuration predicted by numerical models with field measurements after undrained expansion of the cavity.

Although it is difficult to have extensive and reliable field data on the destructuration or reduction in undrained shear strength, Roy et al. (1981) measured a good set of values immediately after pile driving in soft sensitive marine clay, namely Saint-Alban clay, and report the variation of the normalized in situ vane strength with the radial distance. The decrease of the undrained shear strength measured in the field is compared with the decrease of the bonding parameter in Figure 5. Despite the scatter of the field measurements, the agreement is very good. Contrary to pile driving, where the main interest is on the soil at the pile wall, in the case of stone columns, the average value between columns is most important. For practical purposes in stone column design, a reduction of 15-20% of the initial value can be used for normal stone column spacings.

5. CONCLUSIONS

Finite element analyses using advanced soil constitutive models show the main effects of stone column installation in a natural soft clay. Stone column installation, which was modelled as the expansion of a cavity in undrained conditions, generates excess pore pressures in the surrounding soil that are later dissipated towards the column. These pore pressures do not seem to be very sensitive to the features of soil modelled (see Figure 3). After consolidation, the lateral earth pressure coefficient K is higher than initially, increasing the lateral constraint of the column. The results demonstrate that the anisotropy has a significant effect on the process: the increase in K value predicted by the rate-dependent (ACM-S and EVP-SCLAY1S) anisotropic models and the anisotropic S-CLAY1S model are notable lower than predicted by the isotropic MCC model. Furthermore, the destructuration caused by column installation reduces the undrained shear strength after installation, as well as the predicted value of lateral earth pressure and hence cannot be ignored. Overall, the values of K predicted (see Figure 4) are notably less than assumed in the Priebe (1995) method, questioning the applicability of the method on structured natural clays. Overall, S-CLAY1S and EVP-SCLAY1S were able to predict the strain softening (i.e. reduction in apparent value of undrained shear strength, in line with field measurements related to pile driving in soft sensitive clay by Roy at al. (1981), see Figure 5.
The ACM-S and EVP-SCLAY1S models account for the effects of soil viscosity, and consequently, the predicted response depends on the strain rates. The comparison were made with a single cavity expansion rate. The comparisons between S-CLAY1S and EVP-SCLAY1S demonstrate that the strain-rate effects

are not particularly significant when the installation alone is considered. The same is unlikely to apply in the case of subsequent loading. Of the two rate-dependent models considered, the results by the ACM-S model do not appear to be realistic, given due to self-weight consolidation triggered by the model, the predicted K value is close to the normally consolidated value (see Figure 4). This is a common, but largely unpublished negative side-effect of the creep models, such as the Leoni et al. (2008) model, which predict creep strains also in the over-consolidated range.

6. ACKNOWLEDGEMENTS

The work presented was carried out as part of a Marie Curie Industry-Academia Partnerships and Pathways project on "Modelling Installation Effects in Geotechnical Engineering (GEO-INSTALL)" (PIAP-GA-2009-230638).

REFERENCES

Argyris, J.H., Faust, G., Szimmat, J., Warnke, E.P. & Willam, K.J. 1974. Recent Development n the Finite Element Analysis of Pressure Container Reactor Vessel. Nucl. Eng. Des. 28: 42-75.

Balaam, N.P. & Booker, J.R. 1981. Analysis of rigid rafts supported by granular piles. Int. Journal for Numerical and Analytical Methods in Geomechanics 5: 379-403.

Barksdale, R.T. & Bachus, R.C. 1983. Design and construction of stone columns. Report FHWA/RD-83/026. Springfield: Nat. Tech. Information Service.

Brinkgreve, R.B.J. 2008. Plaxis finite element code for soil and rock analysis, 2D version 9. Balkema, Rotterdam.

Castro, J. & Sagaseta, C. 2009. Consolidation around stone columns. Influence of column deformation. Int. Journal for Numerical and Analytical Methods in Geomechanics 33: 851-877.

Castro J. & Karstunen, M. 2010. Numerical simulations of stone column installation. Canadian Geotechnical Journal 47(10): 1127-1138.

Egan, D., Scott, W. & McCabe, B. 2008. Installation effects of vibro replacement stone columns in soft clay. In Geotechnics of Soft Soils – Focus on Ground Improvement, Glasgow, 3-5 September 2008. Taylor and Francis, London, pp. 23-29.

Gäb, M., Schweiger, H.F., Thurner, R. & Adam, D. 2007. Field trial to investigate the performance of a floating stone column foundation. In Proc. 14th European Conference on Soil Mechanics and Geotechnical Eng., Madrid, 24-27 September 2007. Millpress, Amsterdam, pp. 1311-1316.

Gens, A. & Nova, R. 1993. Conceptual bases for a constitutive model for bonded soils and weak rocks. Proc. Int. Symp. Hard Soils-Soft Rocks, Athens, pp. 485-494.

Géotechnique Symposium in print. 1992. Bothkennar soft clay test site: characterisation and lessons learned. Géotechnique 42(2).

Guetif, Z., Bouassida, M. & Debats, J.M. 2007. Improved soft clay characteristics due to stone column installation. Computers and Geotechnics 34(2): 104-111.

Kamrat-Pietraszewska, D. 2011. Numerical modelling of soft sopils improved with stone columns. PhD thesis. Department of Civil Engineering, University of Strathclyde.

Karstunen, M., Krenn, H., Wheeler, S.J., Koskinen, M. & Zentar, R. 2005. Effect of anisotropy and destructuration on the behavior of Murro test embankment. ASCE International Journal of Geomechanics 5(2): 87-97.

Karstunen, M. & Yin, Z.Y. 2010. Modelling time-dependent behaviour of Murro test embankment. Géotechnique 60(10): 735-749.

Kirsch, F. 2004. Experimentelle und numerische Untersuchungen zum Tragverthalten von Rüttelstopfsäulengruppen. Dissertation, Technische Universität Braunschweig.

Kirsch, F. 2006. Vibro stone column installation and its effect on ground improvement. In Proceedings of Numerical Modelling of Construction Processes in Geotechnical Engineering for Urban Environment, Bochum, Germany, 23-24 March 2006. Taylor and Francis, London, pp. 115-124

.

Lee, F.H., Juneja, A. & Tan, T.S. 2004. Stress and pore pressure changes due to sand compaction pile installation in soft clay. Géotechnique 54(1): 1-16.

Leoni, M., Karstunen, M. & Vermeer, P.A. 2008. Anisotropic creep model for soft soils. Géotechnique 58(3): 215-226.

Matsuoka, H. & Nakai, T. 1982. A new failure condition for soils in three dimensional stresses. Proc. IUTAM Sym. Deform. Failure Granular Mat., Vermeer P.A. & Luger H.J. (eds), Delft, pp. 253-263.

McCabe, B.A., Nimmons, G.J. & Egan, D. 2009. A review of field performance of stone columns in soft soils. Proc. ICE: Geotechnical Eng. 162 (6): 323-334.

McGinty, K. 2006. The stress–strain behaviour of Bothkennar clay. PhD thesis, University of Glasgow.

McMeeking, R.M. & Rice, J.R. 1975. Finite-element formulations for problems of large elastic-plastic deformation. International Journal of Solids and Structures 11: 606-616.

Priebe, H.J. 1995. Design of vibro replacement. Ground Engineering 28 (10): 31-37.

Roscoe, K.H. & Burland, J.B. 1968. On the generalised stress-strain behaviour of 'wet' clay. Engng. Plasticity, Cambridge University Press, 553-609.

Roy, M., Blanchet, R., Tavenas, F. & La Rochelle, P. 1981. Behaviour of a sensitive clay during pile driving. Canadian Geotechnical Journal 18(2): 67-85.

Serridge, C.J. & Sarsby, R.W. 2008. A review of field trials investigating the performance of partial depth vibro stone columns in a deep soft clay deposit. In Geotechnics of Soft Soils – Focus on Ground Improvement, Glasgow, 3-5 September 2008. Taylor and Francis, London, pp. 293-298.

Van Langen, H. 1991. Numerical analysis of soil-structure interaction. PhD thesis, Delft University of Technology.

Wiltafsky, C. 2003. S-CLAY1S as User Defined Soil Model for Plaxis. University of Glasgow.

Watts, K.S., Chown, R.C. & Serridge, C.J. 2001. Vibro stone columns in soft clay: A trial to study the influence of column installation on foundation performance. In Proceedings of the 15th International Conference on Soil Mechanics and Geotechnical Engineering, Istanbul, 28-31 August 2001. Taylor and Francis, London, pp. 1867-1870.

Watts, K.S., Johnson, D., Wood, L.A. & Saadi, A. 2000. An instrumented trial of vibro ground treatment supporting strip foundations in a variable fill. Géotechnique 50(6): 699-708.

Weber, T.M., Plötze, M., Laue, J., Peschke, G. & Springman, S.M. 2010. Smear zone identification and soil properties around stone columns constructed in-flight in centrifuge model tests. Géotechnique 60(3): 197-206.

Wheeler, S.J., Naatanen, A., Karstunen, K. & Lojander, M. 2003. An anisotropic elastoplastic model for soft clays. Canadian Geotechnical Journal 40(2): 403-418.

Settlement reduction and stress concentration factors in rammed aggregate piers determined from full- scale group load tests

ÇEVİK ÖZKESKİN Aslı, Sonar Drilling and Geological Research Center, Turkey, asli@sonarsondaj.com
EROL Orhan, Middle East Technical University, Turkey, orer@metu.edu.tr
ÇEKİNMEZ Zeynep, Middle East Technical University, Turkey, cekinmez@metu.edu.tr

ABSTRACT

A full-scale field study was performed to investigate the floating aggregate pier behavior in a soft clayey soil. The soil profile consisted of 8 m thick compressible clay overlying weathered rock. Three large plate load test stations were prepared. A rigid steel footing having plan dimensions of 3.0 m by 3.5 m were used for loading. First test comprised of loading the untreated soil up to failure with increments, and monitoring the surface settlements and distribution of settlements with depth. Other two tests were conducted on clay soil improved by rammed aggregate piers. In each station, seven stone columns were installed, having a diameter of 65cm, area ratio of 0.25. The length of the columns was 3 m in one of the station resembling floating columns, and 8 m in the other station to simulate end bearing columns. Field instrumentations included surface and deep settlement gages, and load cell placed on an aggregate pier to determine distribution of the applied vertical stress between the column and the natural soil. It has been found that, the presence of floating aggregate piers reduce settlements, revealing that major improvement in the settlements takes place at relatively short column lengths. It has been also found that the stress concentration factor is not constant, but varies depending on the magnitude of the applied stress. The magnitude of stress concentration factor varies over a range from 2.1 to 5.6 showing a decreasing trend with increasing vertical stress.

1. INTRODUCTION

Although some designers assume conservatively that all the applied foundation loads are carried by the stone columns the stresses are shared between the columns and the surrounding soft ground in the proportion that the relative stiffness of the two materials, the cross section of the columns and their spacing. The stress concentration ratio, n, may be defined as the ratio of the vertical stress in the compacted column to that in the soft ground. This ratio is a key parameter for the design of bearing capacity, stability and settlement soils improved by stone columns. Available information indicates that "n" falls in the range of 2 to 6, with values of 3 to 4 usual (Mitchell 1982).

There are both theoretical and experimental studies reporting the value of stress concentration ratio:

Greenwood 1991measured the stress in the columns and the surrounding clay under a footing of 1.22 m by 2.75 m plan dimensions. The footing was supported by two 1.22 m diameter stone columns. The measurements indicated that at low stresses the stress concentration ratio was about 4, and n value was gradually reduced to 2.5 with increasing loads.

White et al 2007 reported the results of measurement of stresses on both rammed aggregate piers as well as surrounding soft clays soils, and concluded that the stress concentration ratio increases from 3.8 to 5.5 as the compressive load increases. This increasing trend of n as the load increase, contradicts with the trend observed by Greenwood 1991.

Kitazume 2005 summarizes the Japanese experience based on experimental research findings for stress concentration factor, n, on sand compaction piles as follows. He suggested that the results are applicable for stone columns constructed by different methods.

i. The value of "n" decreases with increasing surcharge loads.

ii. Triaxial tests results on composite soils indicate that the value of n is in the range from 4 to 7, increases with increasing degree of consolidation.

iii. The value of "n" reaches the maximum value at the ground surface, and decreases with depth

The current knowledge on the stress concentration factor is rather uncertain, and further research is required to establish a sound stone column design criteria. In the present work load tests on large scale footings, situated on cohesive soils, improved by stone columns are conducted with measurement of settlement profiles as well as stresses on stone columns. The results are presented with special emphasis on the mesured values of the stress concentration ratio.

2. EXPERIMENTAL WORK

2.1. Site Conditions

Site investigations included five boreholes with SPT, sampling with laboratory testing and four CPT soundings.

Soil profile consists of 8 m thick compressible cohesive soil layer underlying an incompressible layer. The SPT-N values are in the range of 6 to 12 with an average of 10 in the first 8 m. Fine and coarse contents of the compressible layer change in the range of 25% to 40% and 10% to 25%, respectively. Liquid limit of the compressible layer changes predominantly in the range of 27% to 43% with and average of 30%, the plastic limit varies over a range of 14% to 20% with an average of 15%.

Based on the laboratory test results, the compressible layer is classified as CL and SC according to United Soil Classification System (USCS). The average of the tip and friction resistance of the compressible soil strata can be taken as 1.1 MN/m^2 and 53 kN/m^2, respectively. Groundwater is located nearly at the ground surface.

2.2. Experimental Set-up

In the study, aggregate piers were constructed by using bored piling equipment. Thus the constructed piers are those known as rammed aggregate piers. An open-ended casing with a diameter of 65 cm was driven as augering was performed. The backfill material was poured into the cased borehole inconsecutive stages and compacted by dropping a weight of 1.5 tons from height of 1.0 m for 10 times. After filling, casing was withdrawn partially and backfill was rammed to the specified set. It was ensured that bottom of the casing was at least 0.3 m below the top of the rammed fill.

Three large plate load tests were conducted. First load test was on untreated soil. Second load test was group loading on improved ground with floating aggregate piers of 3.0 m length and third load test was group loading on improved ground with end-bearing aggregate piers of 8.0 m length. Each group consists of 7 piles. During these tests, the settlement of the large loading plate, 3 m by 3.5 m in plan dimension, and the settlements of 1.5m, 3.0m, 5.0m and 8.0m depths of soil profile were measured by means of deep settlement gages. In addition, stress on the center pier was measured using pressure cell. Location of pier groups together with site investigation works is given in Figure 1.

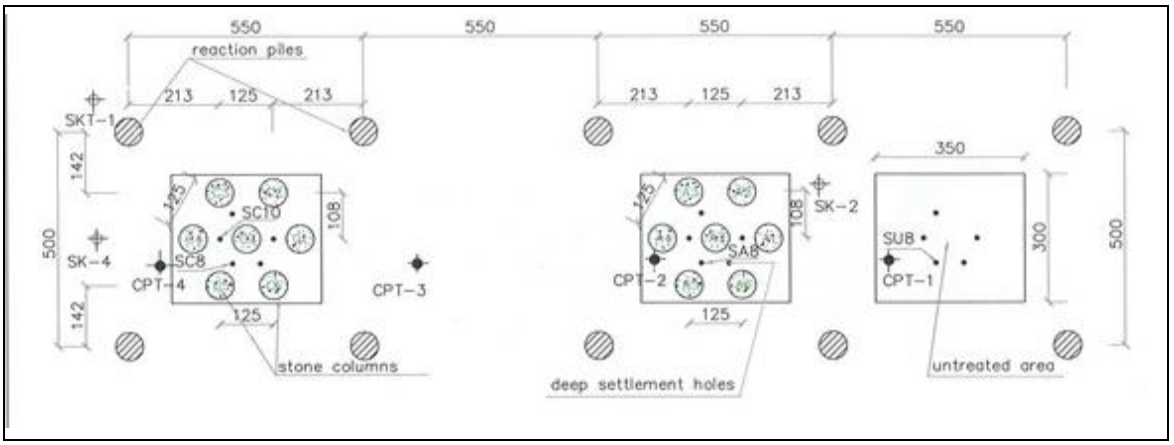

Figure 1: Location of aggregate piers together with site investigation works

3. LOAD – SETTLEMENT DATA

The surface-settlement relationships of the untreated soil and aggregate pier group loadings are given in Figure 2 and Figure 3, respectively. It is observed that at small magnitude of vertical stress the measured

settlements are close to each other at different pier length. The effect of pier length in reducing the settlements becomes effective at relatively higher vertical stress range.

It is also observed that the rate of settlements with respect to applied vertical stress increases significantly for the stresses exceeding 200 kPa. This behavior indicates that the ultimate bearing capacity of the untreated soil reached at about 200 kPa normal stress.

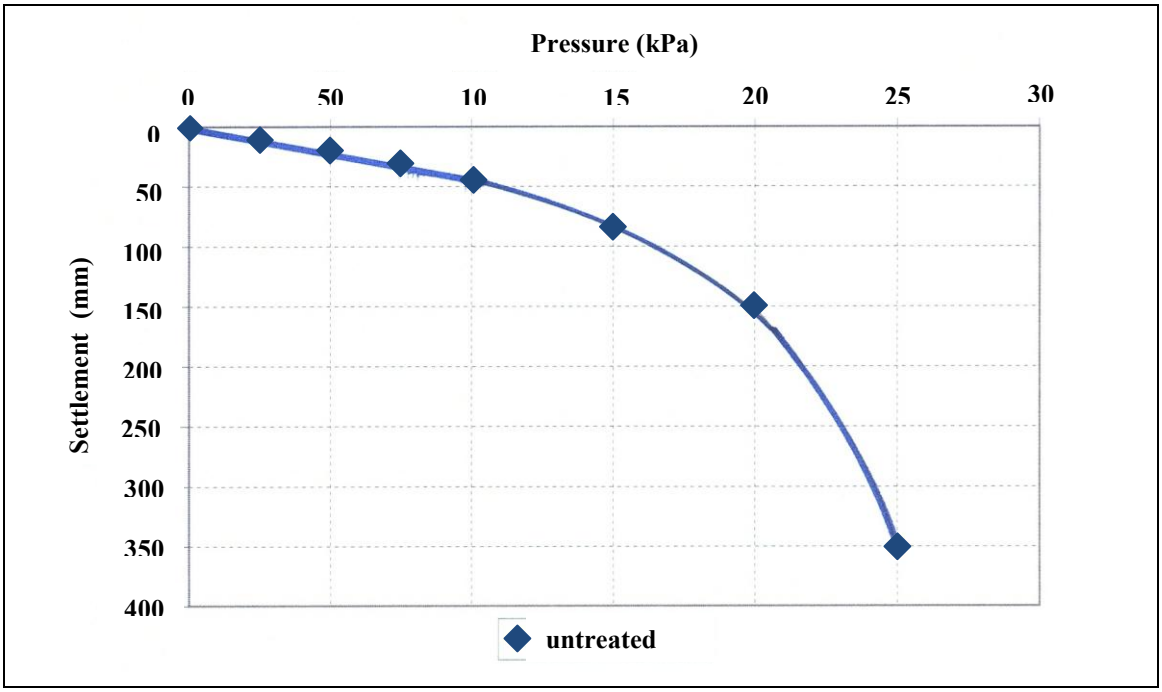

Figure 2: Surface settlement- pressure relationships for untreated soil

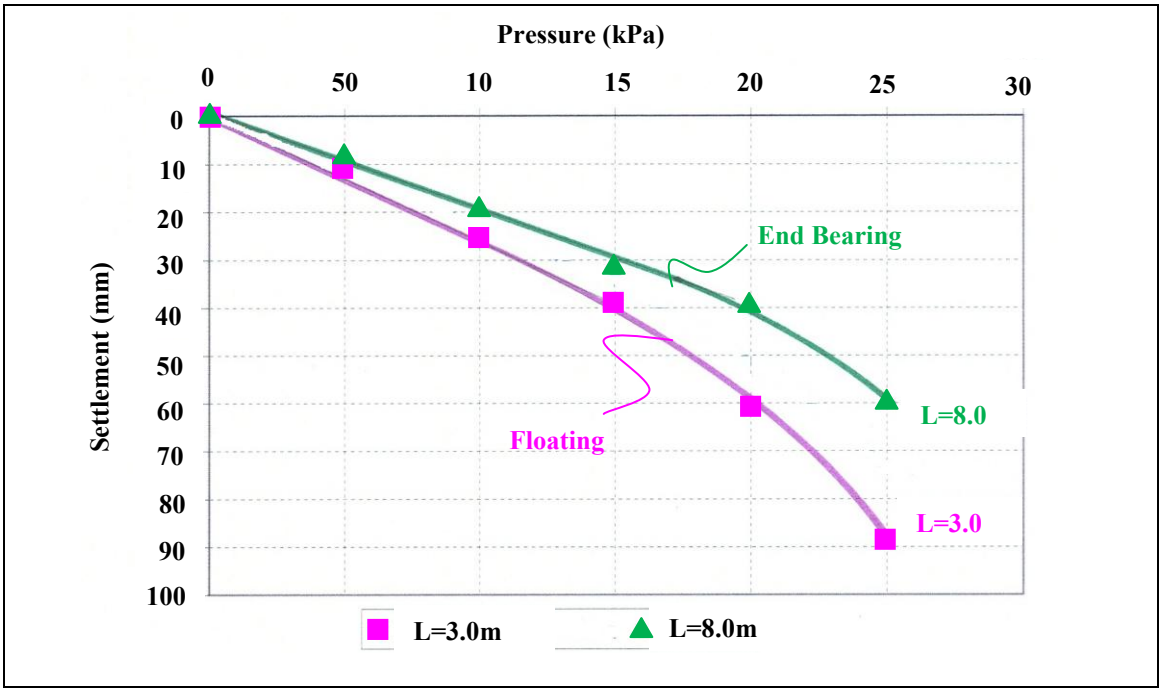

Figure 3: Surface settlement- pressure relationships for aggregate pier groups

4. SETTLEMENT IMPROVEMENT

The settlement factor β is defined as the ratio surface settlements of the footing resting on the improved ground to the surface settlement of the footing on untreated soil. The variation of β factor with applied pressure is shown in Figure 4.

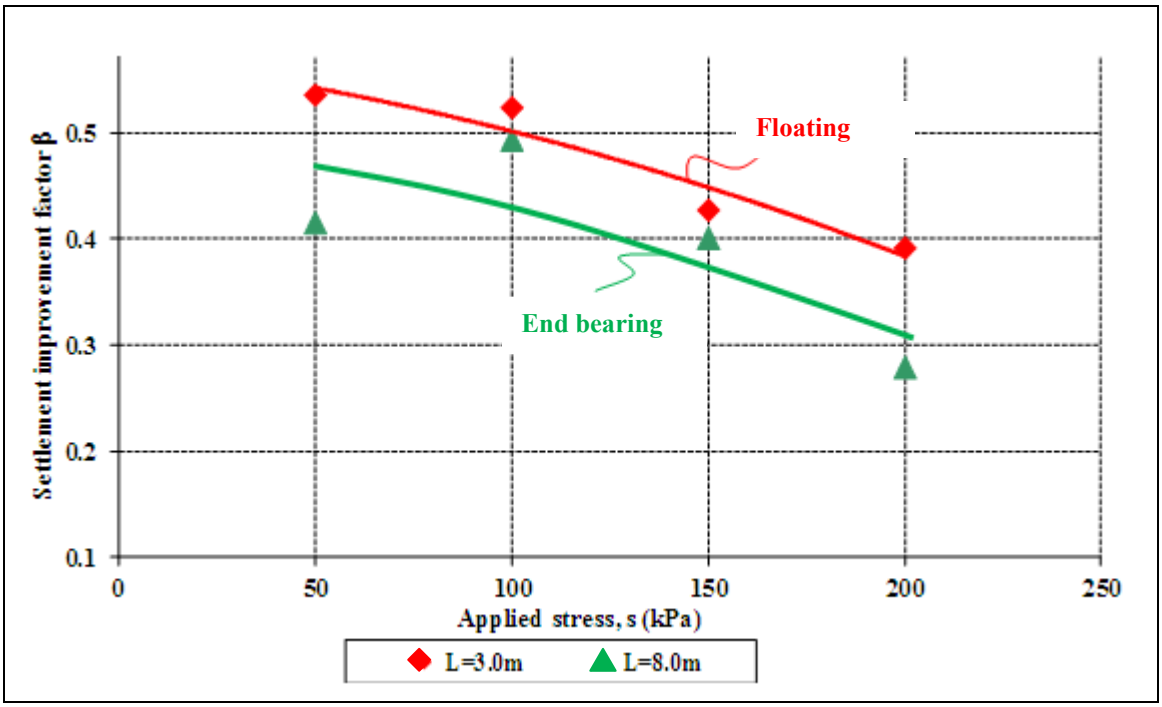

Figure 4: Variation of β ratio with applied pressure

The settlement improvement ratio calculated from the surface settlements shows a decreasing trend with increasing vertical stress. The average value of the improvement ratio, β, is in the order of 0.5 at 50 kPa and is reduced to an average value of 0.3 at 200 kPa of vertical stress. This means that the efficiency of the piers in reducing the settlements becomes more effective at relatively higher vertical stress range. The settlement reduction factor in the group with 3 m long floating piers is in the range from 0.40 to 0.55; whereas it is in the range from 0.30 to 0.45, revealing that increasing the column length from 3 m to 8 m (i.e. end bearing) improves the settlements about thirty percent and the significant improvement in the settlements takes place with floating columns as well.

It has also been observed that, the settlements measured in the compressible layer below piers are consistently smaller as compared to untreated soil settlements. This improvement in the settlements below the piers is illustrated in Figure 5. In this figure, s_1 corresponds to settlement of the untreated loading and s_2 is the settlement of the treated loading below the treated zone. The difference in settlements is defined as Δs. Then a settlement reduction ratio beneath the treated zone is defined as $\beta_{Lz} = s_2/s_1$.

The comparison of β and β_{Lz} values in group loading with 3 m long floating piers, shown in Figure 6, indicates that the improvement in the untreated zone of reinforced soil is more than the cumulative surface settlement improvements.

The results clearly indicate that, there is a net reduction in settlements in the untreated zone of the reinforced soil as compared to untreated soil profile. Since the compressibility of the clay remains the same in both reinforced and unreinforced soil (i.e. below the piers), this improvement should be due to the difference in the transmitted magnitude of vertical stress in the two cases.

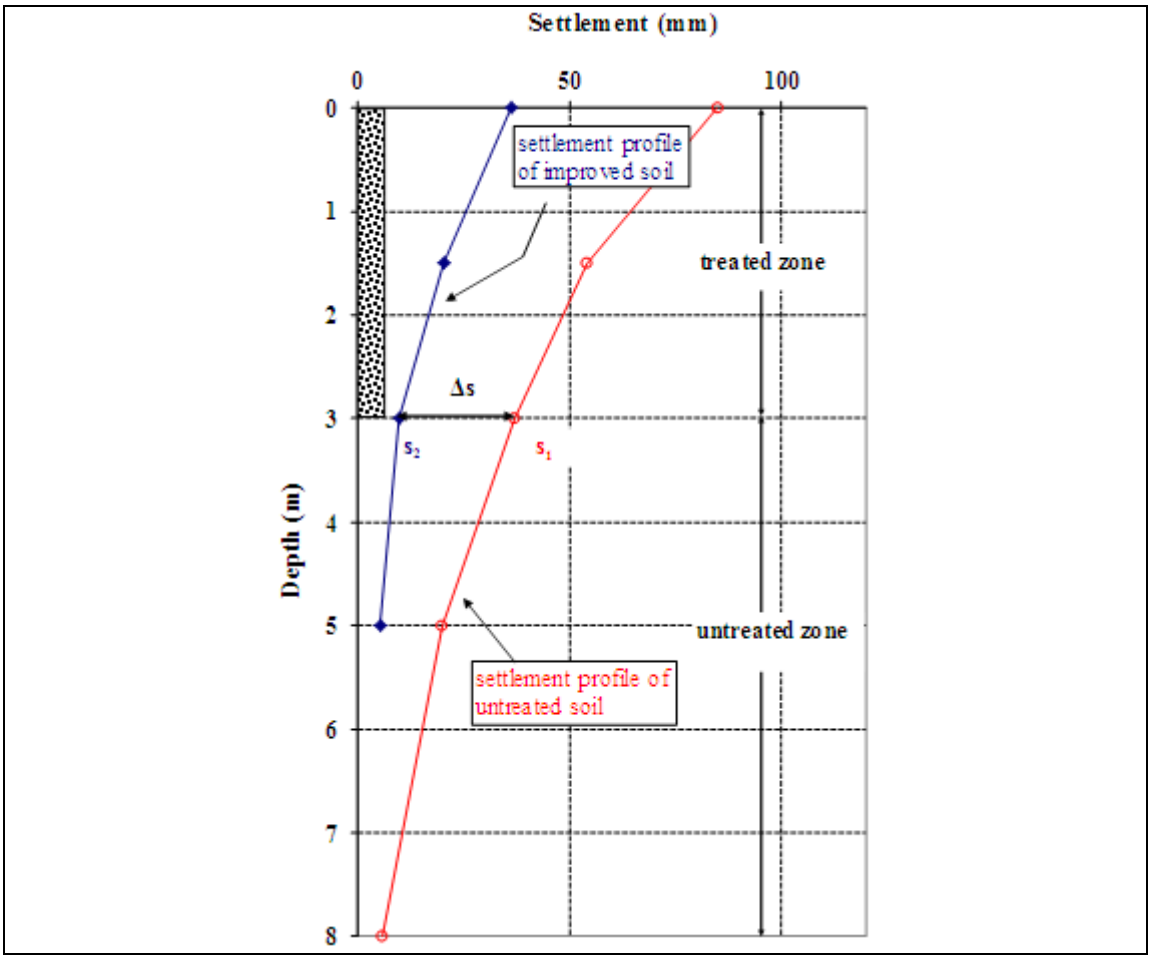

Figure 5: Descriptive sketch showing the improvement in settlements beneath the treated zone (data taken from pier group of L = 3 m, loading under σ = 150 kPa)

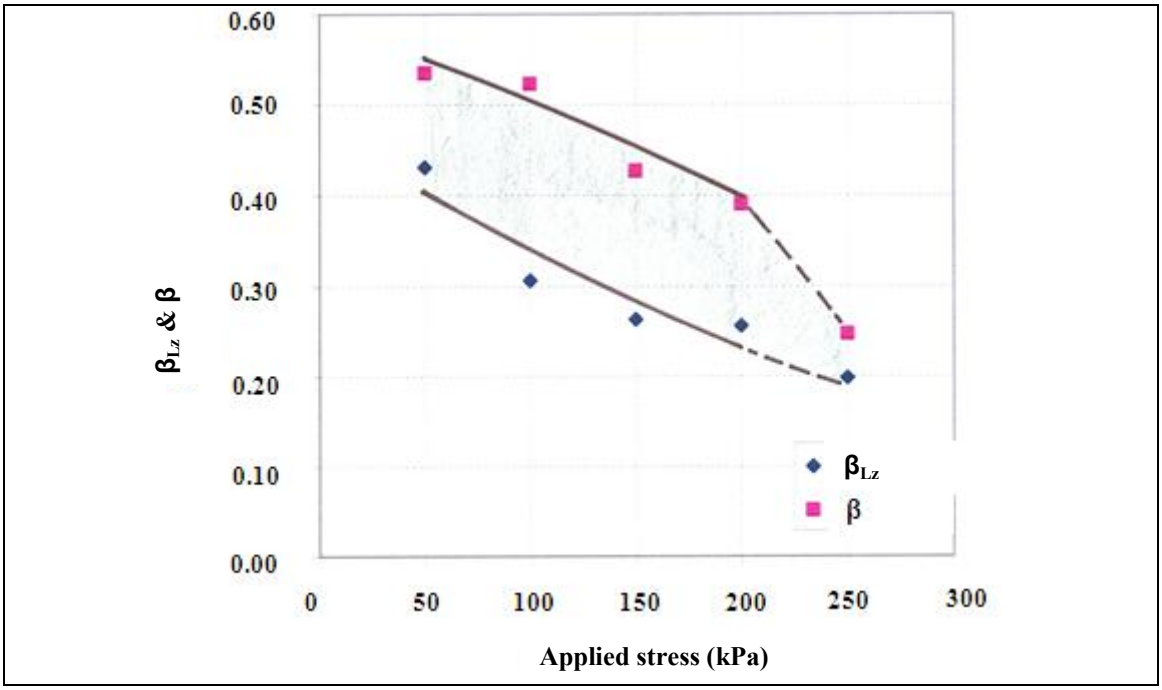

Figure 6: Variation of β_{Lz} with applied pressure on floating pier group of L = 3 m

5. STRESS CONCENTRATION FACTOR

The stress concentration factor n required calculating σ_c, magnitude of the stress in the clay, is usually preferred to estimate from the results of stress measurements made in full-scale load tests instead of driving from the elastic theory. In the present investigation the pressure on the central column was measured with a pressure cell. Then it was possible to estimate the vertical stress on the soil by assuming the stress measured in the central column is the same the other columns as well. The variation of stress concentration factor, n with applied surface pressure is given in Figure 7.

As a general trend the n factor has a tendency to decrease with increasing vertical stress. In this study, values of stress concentration factor, n have been over a range from 2.4 to 5.6, which are comparable with the previously reported values of n.

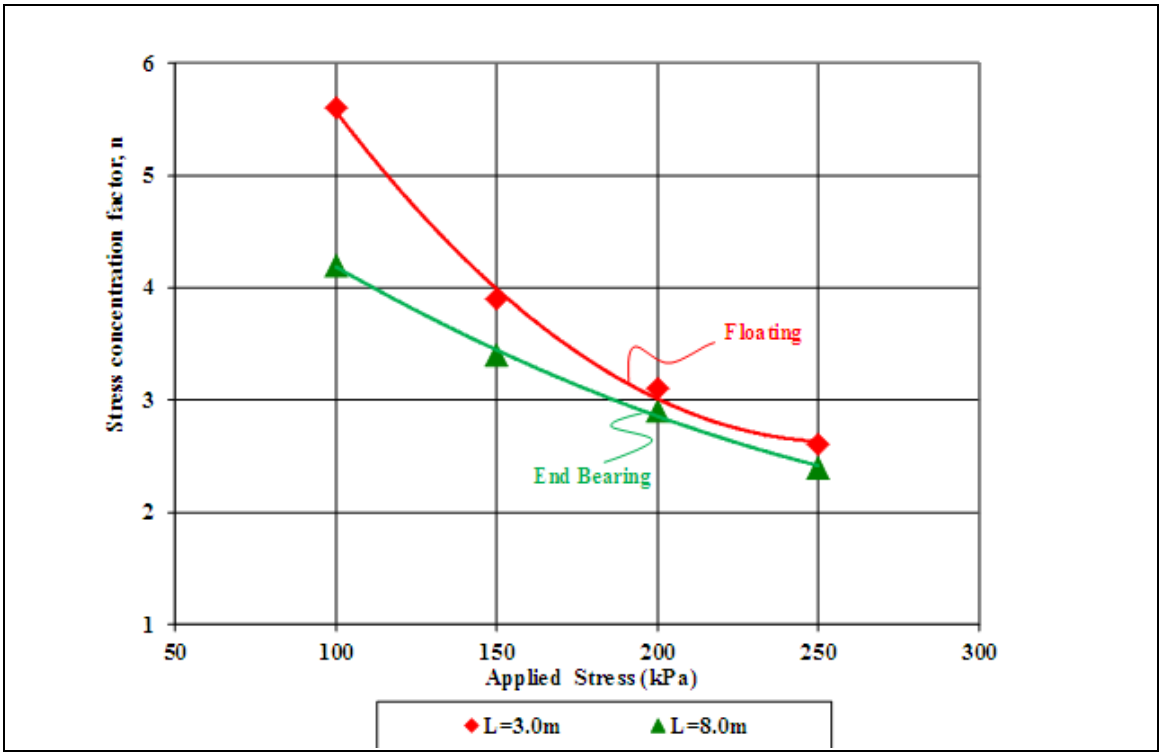

Figure 7: Variation of n value with applied surface pressure

6. CONCLUSIONS

A full-scale field study was performed to investigate the floating aggregate pier behavior in a soft clayey soil.

The settlement improvement ratio calculated from the surface settlements shows a decreasing trend with increasing vertical stress. The magnitude of the improvement ratio is at the order of 0.5 at 50 kPa and is reduced to an average value of 0.3 at 200 kPa of vertical stress. This means that the efficiency of the piers in reducing the settlements becomes more effective at relatively higher vertical stress range.

Increasing the column length from 3 m to 8 m, settlements are improved by an additional thirty percent. Floating columns appear to be effective in reducing the settlements.

The results clearly indicate that, there is a net reduction in settlements in the untreated zone of the reinforced soil as compared to untreated soil profile. This reduction is due to the smaller magnitude of vertical stress is transmitted to the untreated zone since the treated upper zone is stiffer as compared to lower untreated zone.

As a general trend the n factor has a tendency to decrease with increasing vertical stress. In this study, values of stress concentration factor, n, varied over a range 2.4 and 5.6, which is comparable with the previously reported values of n.

REFERENCES

Greenwood D.A., 1991, "Load Tests on Stone Column" Deep Foundation Improvements: Design, Construction and Testing, ASTM Publication

Kitazume M.,2005, The Sand Compaction Pile Method, Taylor and Francis Group, London, UK

Mitchell, J.K., 1982, "Soil Improvement, State-of –the Art Report" Proceedings of the 10th Int. Conf. on SMFE, Stockholm, Vol.4, pp.509-565.

White et al., 2007, "Support Mechanisms of Rammed Aggregate Piers. I: Experimental Results" Journal of Geotechnical and Geoenvironmental Engineering, Vol. 133, No. 12, December 2007, pp. 1503-1511.

Behavior of a Pile-Supported Embankment using rigid piles with variable inertia

Daniel Dias, Joseph Fourier University, LTHE, Grenoble, France, daniel.dias@ujf-grenoble.fr
Jérôme Grippon, Franki Fondation, France, jgrippon.franki@wanadoo.fr
Miguel Nunez, Insa de Lyon, garmike@yahoo.com

ABSTRACT

The increasing lack of good quality foundation soils allowing the development of roadway, motorway, or railway networks, as well as large scale industrial facilities, necessitates the use of reinforcement techniques aimed at improving the global performance of such soils, both in terms of settlement reduction and increasing load bearing capacity. Among the various available techniques, the improvement of foundation soils by incorporating vertical stiff piles appears to be a particularly appropriate solution, since it is easy to implement and does not require any substitution of significant volumes of soft soil.
The technique consists in driving a group of regularly spaced piles through the soft soil layer down to an underlying competent substratum, the surface load being thus transferred to this substratum by means of those reinforcing piles, which illustrates the case of a piled embankment. The differential settlements at the base of the embankment between the soft soil and the stiff piles lead to an "arching effect" in the embankment due to shearing mechanisms in the fill. This effect, which can be accentuated by the use of large pile caps, allows partial load transfer onto the pile, as well as surface settlement reduction, thus ensuring that the surface structure works properly.
A technique for producing rigid piles has been developed to achieve in a single operation a rigid circular pile associated with a cone shaped head reversed on the place of a rigid circular pile with a distribution armed slab. This technique has been used with success in a pile-supported road near Bourgoin-Jallieu (France).
In this article, a numerical study based on this real case is proposed to highlight the functioning mode of this new technique in the case of industrial slabs.

1. INTRODUCTION

The achievement of pile-supported embankments using rigid piles to support distributed loads (road, bridge abutment backfill, industrial floors, sewage treatment plants, ...) has strongly grown in France.
The traditional process involves the completion of a regular grid of rigid piles, combined with a mattress which allows the load transfer by shearing and arching effect. It will permit to limit absolute settlement and minimize differential settlement.
In order to have at the lower part of the earth transfer platform a larger contact area to allow better distribution of efforts to the piles, while maintaining an identical pile shaft, an increase of the pile head section is possible.
This system exists in the form of squared concrete slabs placed on the head of the pile. The major drawback of this device is the fact that it necessitates two separate interventions (completion of the pile and installing the precast slab) and is difficult to set up.
The concept of rigid piles with variable inertia permits therefore to produce a circular pile associated with a conical head. It can be realized in one time and ensure the continuity of the inclusion.

2. PROJECT DESCRIPTION

2.1. General information

As part of the creation of a hospital complex in the town of Bourgoin Jallieu (France), the French government has decided to create a 2x2 road by extending the existing road and creating a roundabout by setting up embankments on compressible grounds.
The improvement work by rigid piles has been done over a length of about 400m. The initial solution consisted of the creation of rigid piles associated with precast concrete slabs. Another innovative solution has been proposed : the creation of circular rigid piles of 0.35m diameter with an extended head diameter (rigid piles with Variable Inertia) in a regular grid to deal with highly compressible soils.
The rigid piles with variable inertia have been associated with horizontal geosynthetic reinforcement before the embankments realization and the creation of the pavement. The choice of the rigid piles with variable inertia has

been done for several reasons as its easy completion (no necessary to handle precast concrete slabs), the time reduction, the increase of efficiency and the significant savings in concrete and steel.

2.2. GEOTECHNICAL CONTEXT

The work site (Figure 1) is an ancient swamp more or less dry with a water table at shallow depth. The various geotechnical investigations have highlighted the following lithological succession:
- A cover of silty clay brown to blackish,
- Recent alluvium consisting of three fairly heterogeneous main assemblies:
  - Predominantly alluvial clay, plastic, gray to beige, soft to very soft,
  - Peat brown to black with its base of small decomposed plants,
  - Alluvial clay-loam wet and very soft,
- A compacted sandy gravel layer.

The stiffer layer is located at about 5 meters above the ground surface.

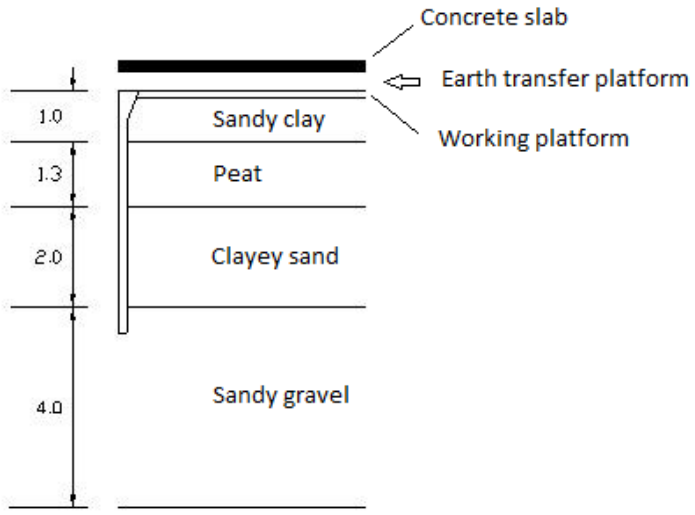

Figure 1: Geological profile

3. NUMERICAL MODELLING

The numerical study presented in this paper aims to better understand the behaviour of piled earth platforms using rigid piles with variable inertia. This academic study uses the real geometry and properties for the constitutive materials of the Bourgoin Jallieu site.
A unit cell of a regular square grid pattern of 2.5m is considered. Figure 2b shows the top view of the pile grid part and indicates the unit cell simulated in the numerical model. The 3D geometry is simplified to a two dimensional axisymmetric one with an equivalent radius of 1.41m. A finite element model was defined using Plaxis. This type of modelling gives results with a good accuracy compared to a 3D modelling. The error between axisymetric and 3D models is less than 9% (Nunez, 2007).

3.1. Properties of numerical models

The introduced geometry (Figure 2b) has 4.3 m high of homogeneous compressible horizontal soil layers (Sandy clay, peat and clayey sand) supported by 0.35 m of diameter piles. The piles are 4.8 m of depth with a spacing of 2.5 m. On the sandy clay, a working platform of 0.3m high has been created. The earth platform of 0.5 m height was placed over the piles. Figure 2a shows the detail of the variable inertia pile head. The reference case of this study is developed to take into account the presence of a structure at the surface. A concrete slab of 0.22m thickness is placed over the earth platform. A surcharge of 25 kPa is then setup on this structure.

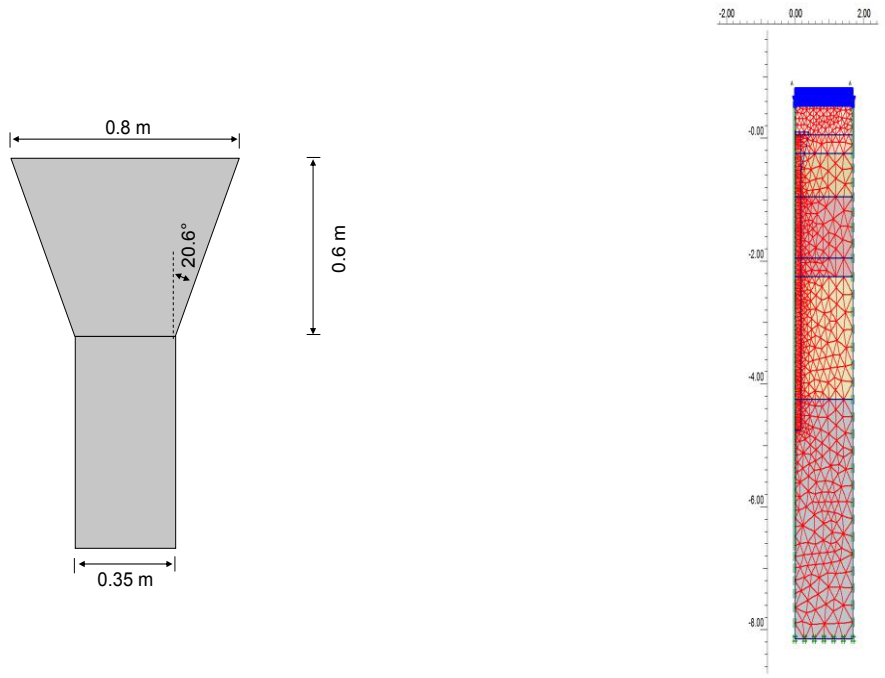

(a) Detail of the rigid pile head (b) Numerical model

Figure 2: Simulated zone

Geotechnical tests (oedometer, triaxial, a loading test and penetrometers) have permitted to obtain the geomechanical characteristics of the soil layers. 10 kPa of over-consolidation was initially applied to the sandy clay layer. The constitutive model adopted for the compressible layers is the Soft Soil Model implemented in Plaxis. Table 1 presents the geomechanical parameters for these layers.
For the other soil layers (earth transfer platform, working platform and sandy gravel), a linear elastic perfectly plastic with a Mohr Coulomb criterion has been adopted (table 2). For the structural elements, linear elasticity has been used.
All the numerical calculations have been done in drained conditions.

Table 1: Geomechanical parameters for the soils simulated using the Soft Soil model

Soil layer	**Cc**	**Cs**	**e0**	**ϕ' (°)**	**γ (kN/m^3)**
Sandy clay	0.45	0.04	1.17	29.4	18
Peat	1.31	0.13	2.46	19.3	15
Clayey sand	0.45	0.04	1.17	23.2	18

Table 2: Geomechanical parameters for the other soil layers and for the structural elements

Soil layer	**E (MPa)**	**ν**	**ϕ' (°)**	**C' (kPa)**	**ψ (°)**	**γ (kN/m^3)**
Earth transfer platform	50	0.3	35	0	5	20
Working platform	30	0.3	30	0	0	19
Sandy gravel	90	0.3	41	10	5	19
Concrete slab	11000	0.2				25
Vertical pile	8000	0.2				25

Frictional interfaces were placed between the pile and compressible soil layers. An ultimate skin friction parameter q_s=30kPa was used.

The numerical calculations were analysed in terms of stress efficacy. Authors propose the term of efficacy in order to determine the effectiveness of reinforcement. (Terzaghi, 1943; Hewlett and Randolph, 1988; British Standard BS8006, 1995; Guido et al., 1987; Russell and Pierpoint, 1997, Rogbeck et al., 1998). Stress efficacy is the ratio between the load transmitted to the head of the pile and the total load on the unit grid.
Another parameter has been defined the settlement efficacy which represents the settlement reduction given by the pile reinforcement compared to a free field. The definition of this ratio is

$$E_{Settl} = 1 - \frac{S_{reinf}}{S_{unreinf}} \quad (1)$$

Where S_{reinf} is the settlement of the soil mass with pile reinforcement and $S_{unreinf}$ without pile reinforcement.

4. RESULTS

4.1. Reference case

Figure 3 shows the vertical displacement field in the soil mass, the maximum is located at the interface between the working platform and the mat between the two piles. Figure 4 permits to clearly identify the neutral point where foundation soil and piles settlements are equal and where the pile is vertically loaded at its maximum. At this point the maximum vertical stress on the rigid pile is equal to 2490 kN/m^2.

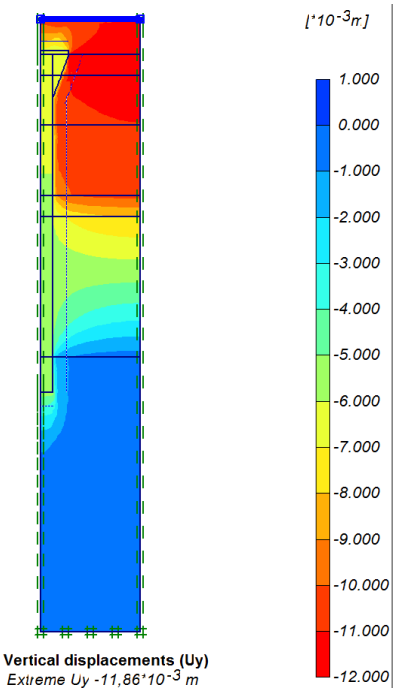

Figure 3. Vertical displacement

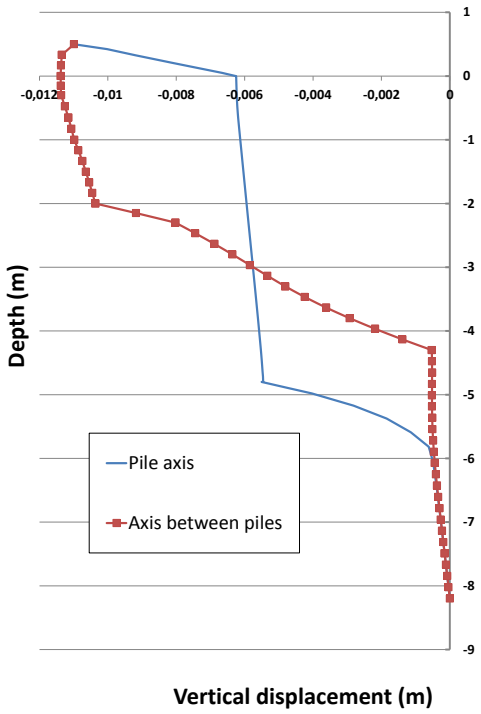

Figure 4. Vertical displacement on the pile and between two piles

In the reference case the bending moment reaches the value of 14.08 kN.m/m.

An interesting point is the distribution of the skin friction along the pile. In the case of INIV reinforcement, the friction is only saturated at the pile toe (i.e. ultimate skin friction reached). This is due to the inclination of the pile head which do not permit to increase the friction in the first 0.6m. In this zone, the negative friction cannot be developed and is then transferred to the layers above. In the case of this type of pile, care on the friction conditions at the bottom of the pile must be taken. In terms of loading in the reinforced area, due to the small height between the pile head and the slab complete arching cannot occur and a stress concentration occurs on the zone at the top of the pile.

Due to the inclination of the pile head, a tension concentration of 0.5 MPa appears at its corner. The concrete of the vertical pile can therefore sustain a tensile stress of 1.2 MPa.

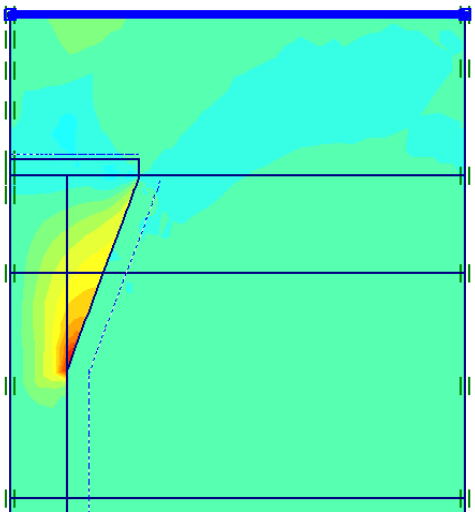

Figure 5: Shear stress distribution

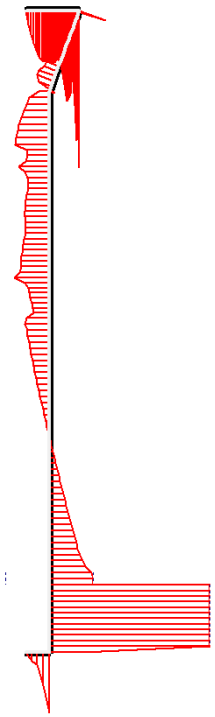

Figure 6. Friction along the pile (maximum 110 kPa)

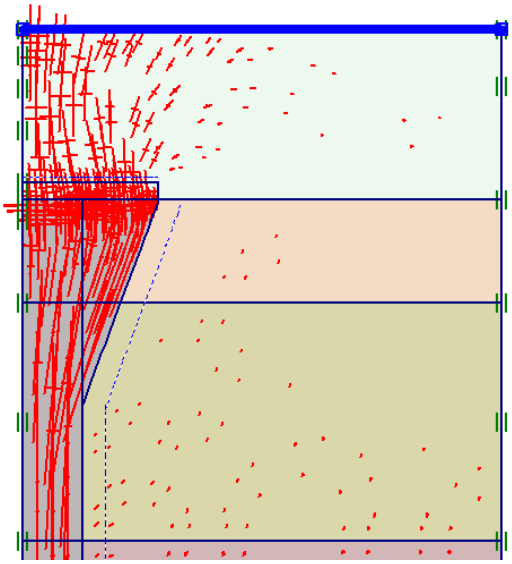

Figure 7. Principal stresses distribution (Extreme total principal stress -2,21MPa)

4.2. Influence of the mattress thickness

The study of the mattress thickness influence highlight the required thickness necessary to develop complete arching. It can be seen that with a value higher than 0.70m for the mattress thickness (reference case), a decrease of the bending moment is observed. This effort reaches a negligible value for a mattress thickness equivalent to the distance between vertical piles. It is therefore not necessary to increase the thickness of the mattress to the value of the mesh to allow the development of the arching effect.

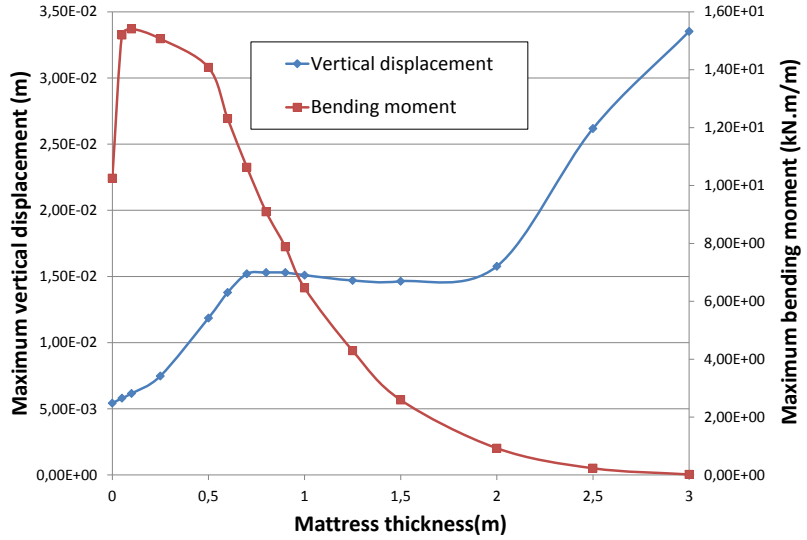

Figure 8: Maximum vertical displacement and maximum bending moment vs mattress thickness

4.3. Influence of the rigid pile diameter

To better show the influence of a variable inertia head, a preliminar study considering a circular conventional pile has been done. The influence of the pile diameter has been investigated by a parametric study based on the reference case. The pile diameter has been modified on a range between 0,35m to 2m.

Figure 9 shows the evolution of the maximum displacement with the increase of the pile diameter. The decrease of this parameter is important till a diameter of 0.50m, after this value the vertical displacement reaches a threshold. In terms of bending moment in the slab, this value of the pile diameter is an interesting zone where the evolution of bending moment changes. Before this value, an increase is observed till a maximum of 13. kN.m, after we can observe a decrease.
In this reference case, a pile diameter of 0.7m corresponds to the case where the slab is the more loaded and then its contribution to the displacement limitation is the highest. For higher values of the pile diameter, the curvature of the slab is lower due to the pile diameter and then the bending moment decrease. These results depend on the height of the matress (which was a constant for the parametric study) .

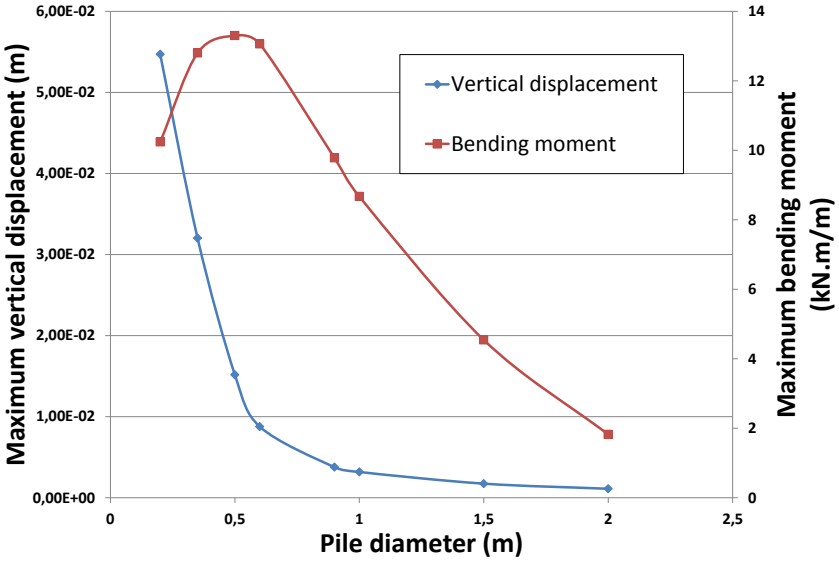

Figure 9: Maximum vertical displacement on the soil and bending moment on the slab versus the upper head diameter

Considering the efficacies, the stress and the settlement efficacies have the same tendency. They increase with the increase of the pile diameter.

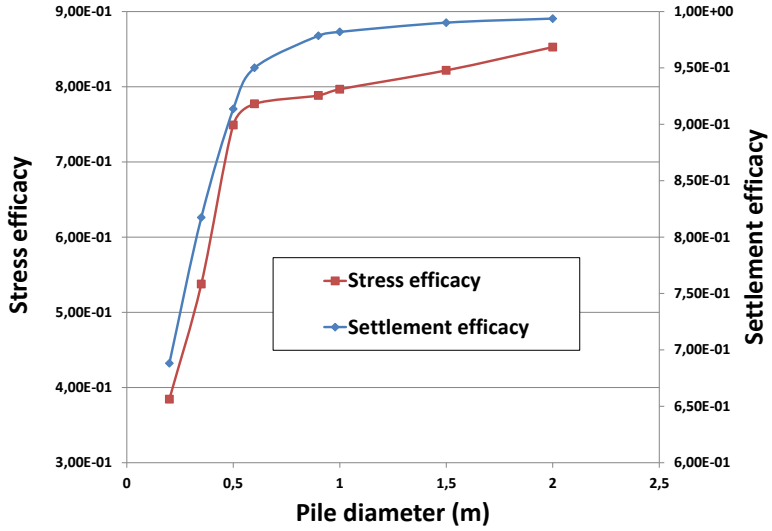

Figure 10: Stress and settlement efficacy

4.4. Comparison with a variable head diameter (INIV piles)

To compare the behaviour of the circular piles with the ones which have a variable inertia at the head, a parametric study on the pile head diameter has been done. The diameter of the lower part of the pile was fixed to 0.35m, then the head diameter has been modified in the range 0.35m to 2m.

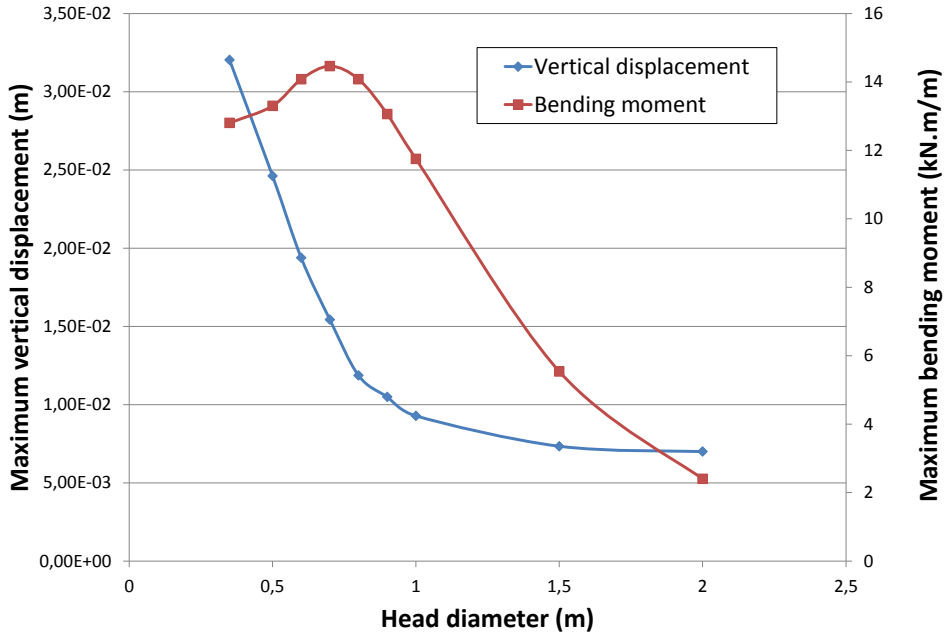

Figure 11: Maximum vertical displacement on the soil and bending moment on the slab versus the upper head diameter

The behavior of the rigid pile with variable inertia is quite close to the behavior of the circular pile. The first curve shows a decrease of the vertical settlements till a plateau and at the same time for the bending moment a increase and then a decrease of the bending moment with a passage by a peak for a value of the pile diameter head of 0.7m (Figure 11).

The comparisons between these two types of piles will be always done considering the pile head diameter.

Figure 12 shows the comparison between the two type of piles in terms of vertical displacements. One can see that for the same pile head diameter, the circular piles are more efficient and permit to better reduce the settlements at the interface between the working platform and of the mat.

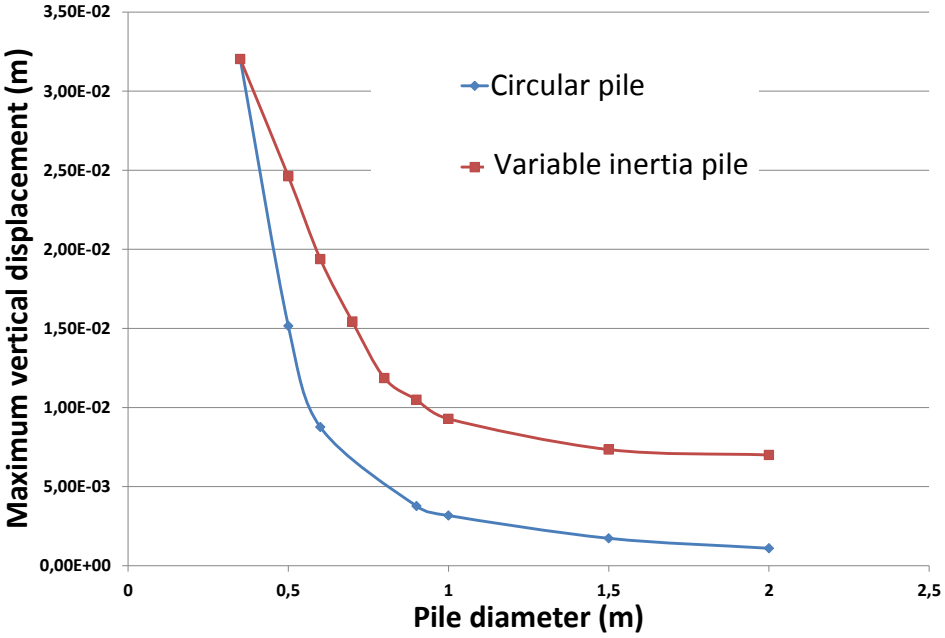

Figure 12: Comparison in terms of maximum vertical displacement between circular piles and variable inertia piles

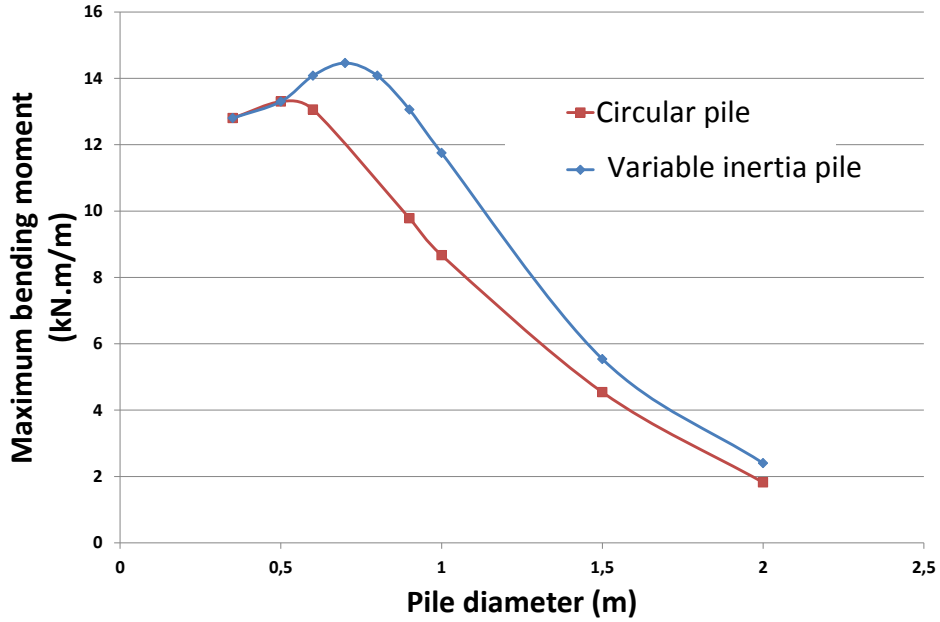

Figure 13: Comparison in terms of bending moment between circular piles and variable inertia piles

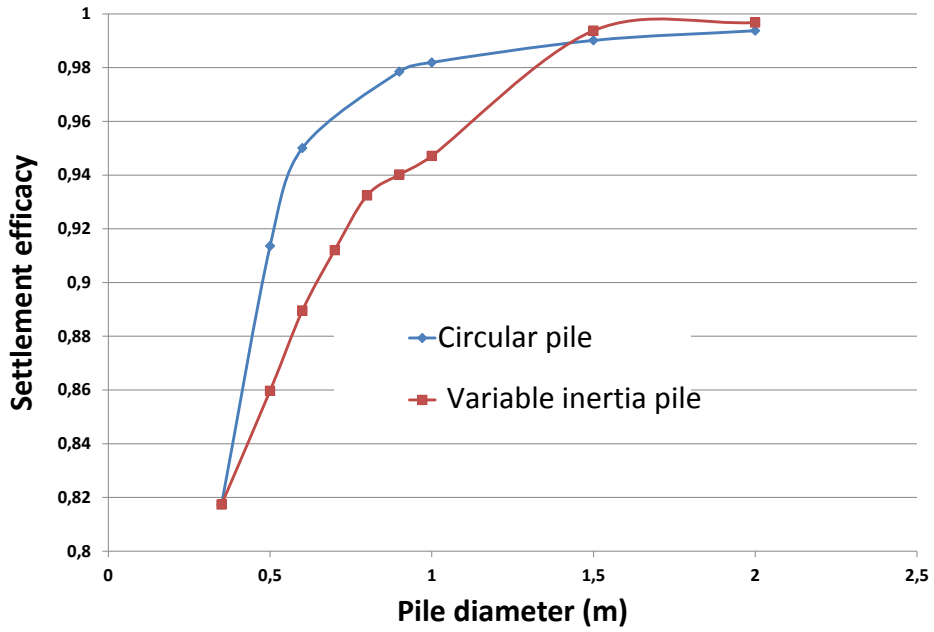

Figure 14: Comparison in terms of bending moment between circular piles and variable inertia piles

The same tendency is observed for the bending moments. The circular piles are more efficient. It is due to the relative displacement between the soil at the pile head corner which is higher in the case of the variable inertia pile. However, the volume of incorporated material is significantly lower in the case of a rigid pile with variable inertia compared to a circular pile of same head diameter (76% less for a head of 0.8m diameter).

Pile head diameter (m)	0.35	0.50	0.60	0.70	0.80	0.90	1.00	1.50
Volume of the circular pile (m^3)	0.46	0.94	1.36	1.85	2.41	3.05	3.77	8.48
Volume of the pile with variable inertia (m^3)	0.46	0.49	0.51	0.54	0.57	0.60	0.64	0.86

Comparing piles with variable inertia (head diameter of 0.80m and shaft diameter of 0.35m) and a circular pile of 0.35m diameter, the reduction of the vertical settlement is much larger (decrease of 63.2%) in the first case. However, the induced bending moment in the pavement is more important in the case of variable inertia piles (increase of 7.4%).

5. CONCLUSION

The functioning mode of the variable inertia piles is different from classical circular piles. The negative friction cannot be totally developed at the pile head and then the efforts are redistributed along the pile shaft. A higher attention of the friction conditions at the pile toe must then be paid.

The comparison of the variable inertia piles with the circular ones has shown that the two type of piles have the same behaviour if we consider the bending moments in the slab or the stress and settlement reduction.

With the same head diameter, the circular pile permit a higher reduction of the vertical settlement and of the induced bending moment in the pavement that the pile with variable inertia. However, the necessary volume of the material to be included is much larger for the circular pile.

By comparing the pile of variable inertia of the reference case and the circular inclusion with the same shaft diameter, the decrease of the vertical settlement is more important in the case of variable inertia piles. However, the moment induced in the pavement by including variable inertia piles remains larger.

The enlargement of the head diameter to 1.00m for the variable inertia pile of 0.35m diameter shaft in the reference configuration permits to variable inertia piles to be more effective than circular piles of the same shaft diameter in terms of vertical settlement reduction and also in terms of the bending moment in the pavement.

REFERENCES

BS8006, British Standards 1995. Code of Practice for Strengthened/Reinforced Soils and Other Fills. Section 8: Design of Embankments with Reinforced Soil Foundation on Poor Ground. British Standard Institution, London, pp. 80–121.

Guido V.A., Kneuppel J.D., Sweeny M.A., 1987. Plate loading tests on geogridreinforced earth slabs. In: Proceedings of the Geosynthetics '87, New Orleans, USA. IFAI, pp. 216–22.

Hewlett, W.J., Randolph, M.F., 1988. Analysis of piled embankments. Ground Engineering 21 (3), 12–18.

Nunez, M.A., Dias, D., Poilpré, C., Kastner, R., 2007. Influence of vertical rigid piles as ground improvement technique over a roadway embankment. 2D and 3D numerical modelling. 5th International Workshop on Application of Computational Methods in Geotechnical Engineering, Guimaraes, Portugal.

Russell D., Pierpoint N., 1997. An assessment of design methods for piled embankments. Ground Engineering 30 (11), 39-44.

Rogbeck, Y., Gustavson, S., Södergren, I., Lindquist, D., 1998. Reinforced pile embankments in Sweden - design aspects. Proceedings 6th Int. Conf. on Geosynthetics, Atlanta, vol. II, pp. 755–762. 25–29 March.

Terzaghi K., 1943.Theoretical soil mechanics. J Wiley and Sons, New York.

Spread foundations on rigid inclusions subjected to complex loading: Comparison of 3D numerical and simplified analytical modelling

Daniel Dias, Joseph Fourier University, LTHE, Grenoble, France, daniel.dias@ujf-grenoble.fr
Bruno Simon, TERRASOL, Paris, France, b.simon@terrasol.com

ABSTRACT

This paper relates results of a large number of 3D numerical models of a single spread footing over a soil reinforced by four rigid inclusions and submitted to a large set of complex loading. This numerical study using the FLAC 3D software was done under funding of the ASIRI research project in an aim to support appropriate guidelines for design of such foundations. From these models a database of displacements and stresses in any 4 piles was built. An alternate simplified approach is also described using tools commonly used for pile foundation design. All results are found to be in fair agreement. This gives credit to the use of the simplified approach for design of this kind of foundation.

1. INTRODUCTION

Soil reinforcement by rigid inclusions has proved to be an efficient foundation solution for ground slabs of industrial facilities. Slabs submitted to uniform loading can be designed from the results of an axisymmetric numerical model of the elementary reinforcement cell including the tributary slab, the granular layer, the inclusions and the soil volume around (Cuira and Simon, 2009). Data gathered by the French ASIRI national research project have demonstrated that such simple models are reliable and easy to use providing that some basic requirements are fulfilled (ASIRI, 2012).
Industrial or commercial facilities often have locally concentrated loads, from their columns or inner bearing walls. They are usually founded using a compound foundation system comprising a concrete spread footing, a granular layer acting as a load transfer platform and a limited number of rigid inclusions below. Such conditions preclude use of axisymmetric models and require truly 3D models. Since loading of these individual foundations involves vertical as well as horizontal loading, with some possible eccentricity, such 3D models cannot be reduced by symmetry considerations. They remain a difficult engineering task and require strong computational effort. Some simplified numerical models are therefore required so that design of this appealing foundation solution remain a task within reach of these quite common projects.
An extensive numerical study of a single spread footing over a soil reinforced by four rigid inclusions and submitted to a large set of complex loading has been carried out within the framework at the ASIRI research project. The FLAC 3D finite difference software was used to run these models and establish a database of displacements and stresses in any 4 inclusions. An alternate simplified approach was also developed using tools commonly used for pile foundation design.
This paper describes both the numerical Flac 3D study and the simplified approach and compares both results.

2. INVESTIGATED CASE AND ASSOCIATED NUMERICAL MODEL

The study was led for one usual case of a spread footing lying over soft soil which is reinforced by four rigid inclusions arranged in a square grid, as illustrated by Figure 1.
The concrete square spread footing is 2m long and 0.5m thick; it lies on a 0.5m thick granular layer (granular pad). The soft soil layer has a total thickness 6.5m below the granular pad base; it rests on top of a rigid stratum.
The inclusion diameter is 0.34m and the pile spacing is 2m.
Due to symmetry condition, only half of the problem is modelled when combined loadings are used (inclined) and a quarter if only vertical loadings are applied. The calculations are performed using the finite difference software Flac3D (Itasca, 2002). The numerical model for the half model includes about 75,000 zones and 90,000 grid points.

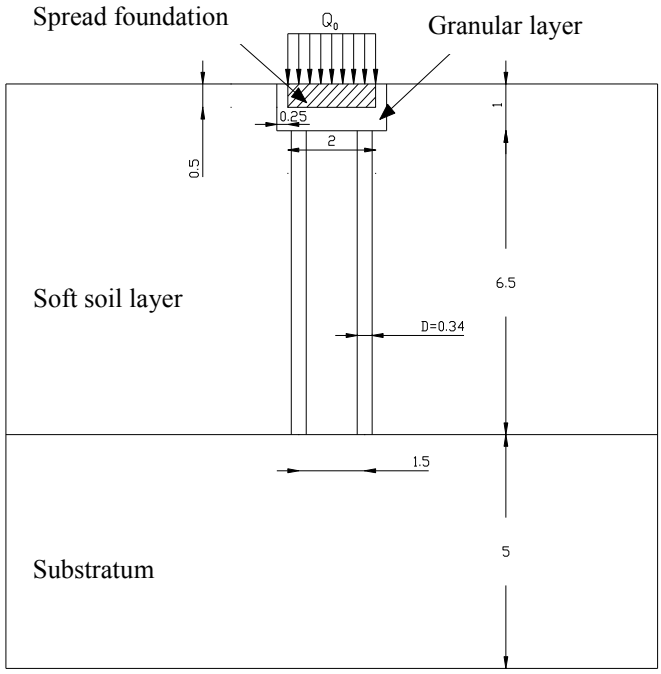

Figure 1: Geometrical configuration studied

Figure 2 is a top view of the numerical model. The model length in the horizontal direction is seven times the pile spacing (14m). The piles are stopped at the bearing stratum upper face. Interfaces are considered in this model: relative displacement is possible between the piles and the soft soil as well as between the granular mat and the footing.

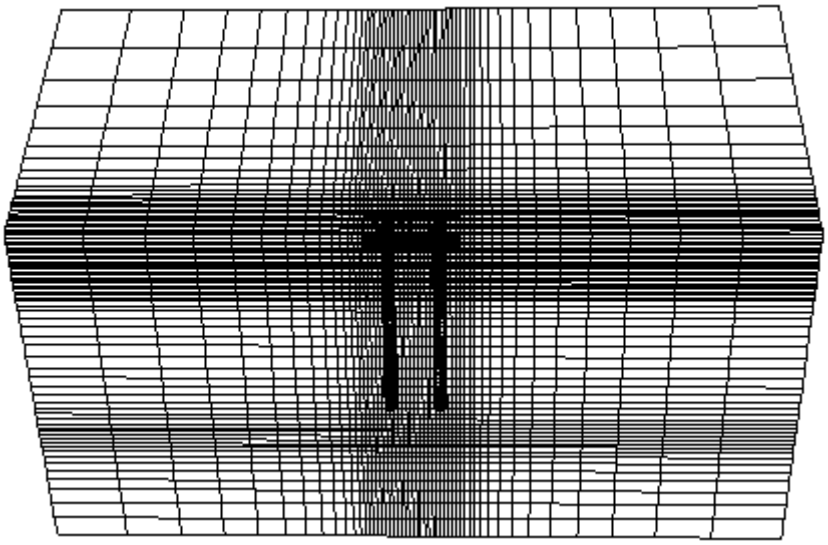

Figure 2: View of the three dimensional numerical model of soft ground improved by piles

The foundation pad was constructed in several phases:
- Excavate the zone for the granular mat and for the footing,
- Setup of the piles in one phase: the pile installation is not taken into account,
- Installation of the granular mat,
- Setup of the footing,
- Initialization of the displacements.

The model equilibrium is reached at each step. The time dependant behaviour of the system is not investigated here, the calculations are performed in drained conditions.

3. GROUND CHARACTERISTICS AND BEHAVIOUR MODELLING

This part presents the geotechnical properties assigned for each part of the system (soft ground, granular mat, footing and piles) and the constitutive models used for the calculations.

3.1. Soft soil

Soft soil layers which are reinforced by a grid of piles are typically clay and/or silt deposits. The Modified Cam Clay model (Roscoe and Burland, 1968) is widely used to simulate the behaviour of such deposits (Mestat et al. 2004): this model is used here.
The marine soft deposit of Muar in Malaysia was simulated using this constitutive model (Indraratna et al. 1992). The soft soil is lightly over consolidated, which is represented by an over-consolidation pressure equal to σ_v' + 10kPa, where σ_v' is the effective vertical stress. The parameters used in the modelling are given in Table 1.

Table 1: Cam-Clay model parameters for the soft soil layer

Parameter	**λ**	**κ**	**M**	**e_λ**	**ν**	**γ (kN/m^3)**	**K_0**
Value	0.13	0.048	1.2	Variable 3.4 to 3.8	0.35	17	0.8

Note: λ = slope of the normal consolidation line; κ = slope of the swelling line; *M* = frictional constant; e_λ =void ratio at normal consolidation for p=1 kPa; ν=Poisson's ratio; γ=unit weight and K_0=horizontal earth pressure coefficient at rest.

3.2. Granular material

The embankment material is generally gravel or coarse soils. Its behaviour is highly nonlinear (Paute et al. 1994). A two mechanism isotropic hardening elastoplastic model CJS2 has been used to simulate the granular material behaviour. The CJS2 model derives from the CJS model developed by Cambou and Jafari (1988) for cohesionless soils. The original model has two mechanisms, the compression mechanism having isotropic hardening and the deviatoric mechanism having two hardening mechanisms, one is isotropic and the other is deviatoric. The elastic part is nonlinear. The granular material described and tested by Fragaszy et al. (1992) is used in these calculations. The corresponding friction angle for this granular material is equal to 35°.

Table 2: CJS2 Model Material Parameters for Granular material

Material parameter	G_0 (MPa)	K^0_e (MPa)	**n**	**β**	R_c	A (Pa^{-1})	**R_m**	γ	K_{0p} (MPa)
Value	5	13	0.6	0.27	0.001	0.35	0.35	0.9	50

3.3. Inclusions and footing

The inclusions are reinforced concrete piles. They behave elastically and the elastic parameters are E = 20GPa and ν = 0.2. Same parameters apply to the concrete spread footing.

4. PARAMETRIC STUDY

Several loading cases have been studied. An uniform distributed load q is applied incrementally to the footing by 50 kPa steps; load inclination θ to the vertical axis is taken 0, 5°, 10°, 20°, 30° and 40° in turn.
In a preliminary stage, the same numerical model serves to simulate a few specific simple loading cases to help the calibration of some of the distinctive geotechnical parameters used by the simplified method, i. e. the Menard pressuremeter modulus and the limiting values of shaft friction and point pressure. This included:

- loading at the head of a single inclusion either axially or transversely, to get the corresponding load-pile displacement curves at head and tip;
- loading of the footing either vertically or horizontally with inclusions replaced by soil elements to get the corresponding load-displacement curve of the non reinforced case.

5. NUMERICAL RESULTS

Figure 3 shows the displacement field for a pad foundation surcharge of 150 kPa inclined at a 20° angle. One can see that the pile at the left hand displaces more than the other one. Soil displacement is significant down to 1.5m from the pile heads.

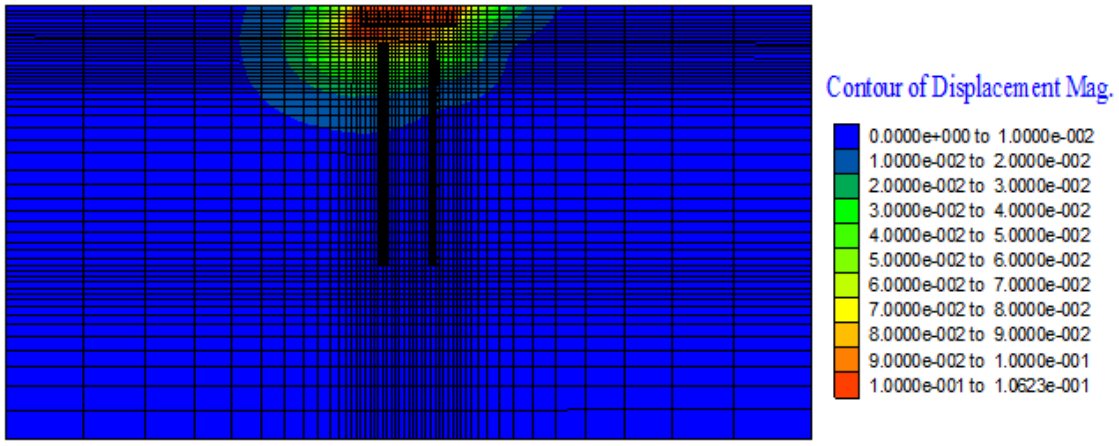

Figure 3: Displacement field - loading q=150 kPa inclined at $\theta = 20°$

Even when the loading is purely vertical, the inclusions are submitted to a bending moment. For a loading of 150 kPa, this bending moment can reach 2.3 kNm (Figure 4).
The bending moment increases with the load inclination and reaches 16.5 kNm in the front (left) inclusion when inclination is 20°. The rear (right) inclusion always bears a moment less than the front inclusion. Difference between front and rear pile moments also increases with load inclination and reaches 7kNm in the last case.
For more inclined loading, failure can be observed in the numerical calculations. A loading of 100 kPa is the maximum for 30° and 75 kPa for 40°.

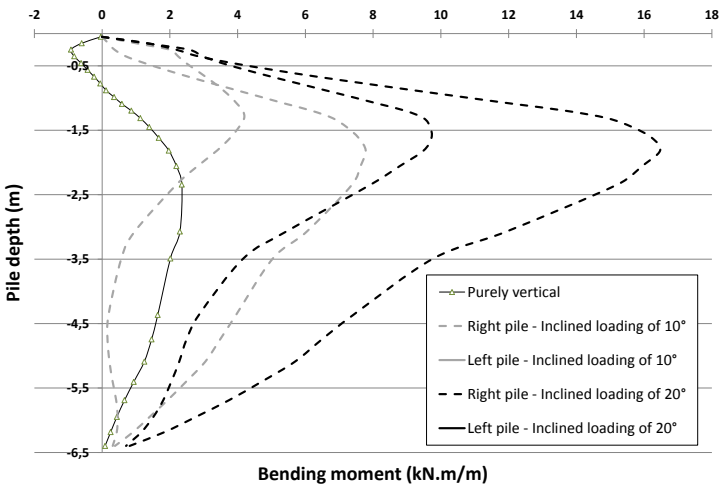

Figure 4: Bending moment for different load inclinations - q=150kPa

6. SIMPLIFIED ANALYTICAL METHOD

6.1. Presentation

The simplified analytical method for designing spread foundations over inclusion reinforced soils was described by Simon (2010). It consists of assimilating the reinforced soil volume with inclusions aligned along the footing at an equivalent homogeneous monolith, leading to a consecutive analysis of the following:

- the interaction between inclusions inside the reinforced volume, for the purpose of establishing the properties of this equivalent homogeneous monolith;

- then the interaction of this monolith with the exterior, unreinforced soil block.

The monolith studied herein is the vertical axis prism circumscribed at the footing which includes the granular mat, the soft soil layer reinforced by inclusions and the upper part of the bearing layer.

6.2. Under vertical loading

This approach entails 3 successive steps which are carried out using ordinary tools for deep foundation design, i.e. study of an isolated pile or of a pile located at the centre of a reinforcement element mesh, under vertical loading, through use of transfer functions characterizing shaft friction and point pressure mobilization around the pile (Cuira and Simon, 2010). In the reinforcement mesh case, the analytical model is of a biphasic type (i. e. associating a pile domain and a soil domain) where interaction forces between both domains are expressed by the same transfer functions as an isolated pile, just replacing the absolute pile-displacement by the relative soil-pile displacement. The transfer functions given by Frank et Zhao (1982) are used; they depend solely on the Menard pressuremeter modulus E_M, the limiting shaft friction value q_s (resp. point pressure q_p) for any given pile diameter and type (Bustamante et Frank, 1999).

Beforehand calculations considering the case of an axially loaded isolated inclusion demonstrated that values of Table 3 led to load-displacement curves at head and tip that agreed well with the numerically derived ones, using Flac 3D. Settlement of the soft soil is calculated using oedometric parameters derived from the values in Table 1.

Table 3: Complementary soil parameters for the simplified method

	E_M (MPa)	q_s (kPa)	q_p (MPa)
Soft soil	2.5	30	-
Bearing stratum	8.0	-	7.2

6.2.1. Step 1

A study of the behaviour, under distributed vertical load, of a basic cell without any interaction with the external domain (i.e. case of a cell placed in the middle of a multiple network of identical cells) serves to establish the horizontal plane position underneath the inclusion tip where soil settlement is uniform (lower neutral plane). The average settlement derived between the upper cell face (below the footing) and this lower plane allows evaluating the apparent modulus of deformation E* of the cell under vertical loading (Figure 5).

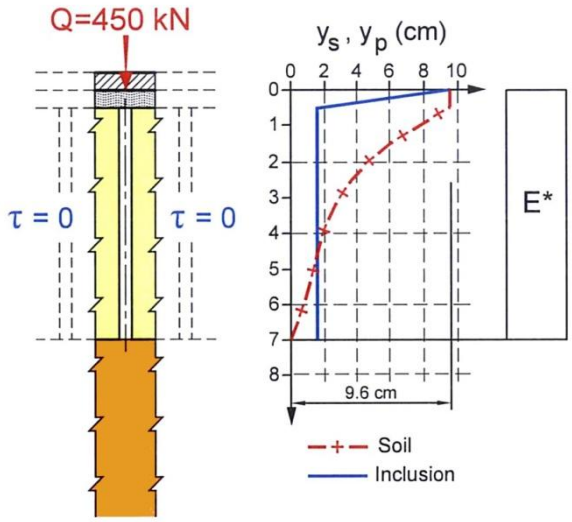

Figure 5: Step 1 of the calculation according to the simplified method - Cell mesh area 1,5 m^2, vertical load case q = 200 kPa

6.2.2. Step 2

A study of the vertical monolith with modulus E* assimilated to an isolated pile interacting with the exterior (non-reinforced) soil domain, exposed to vertical force Q, determines the profile $y_s(z)$ of the average monolith settlement, in accounting for shaft friction mobilization on the monolith perimeter. The

settlement recorded at the head y_s remains less than the settlement of the cell studied during Step 1, as a result of the load diffusion by means of shaft friction towards the surrounding soil block (Figure 6).

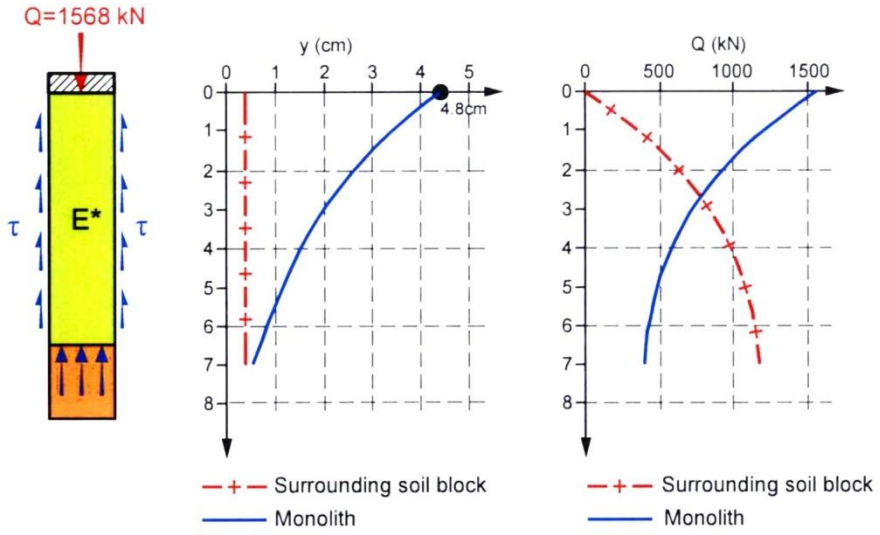

Figure 6: Step 2 of the calculation according to the simplified method - Monolith cross-section area 2.8 m^2, vertical load case q = 200 kPa

The friction taken into account at the monolith edge is soil-soil friction; its limiting value may be assimilated with the undrained cohesion c_u of the soft soil (estimated around 60 kPa in this specific case). This monolith calculation also proved to be able to predict with sufficient accuracy the settlement of the footing lying on an unreinforced soil, as derived numerically using Flac 3D.

6.2.3. Step 3

The load-displacement curve of an inclusion assumed to be isolated (including the granular pad prism displaying the same cross-section as inclusion) in a soil block subjected to an imposed settlement profile as calculated in step 2 makes it possible to establish the load value to apply at the head of this column in order to obtain the same settlement as previously calculated at top of the model. This load value then determines the distribution of axial forces $Q_p(z)$ in the actual inclusion.
The simplified method incorporates neither the Mohr Coulomb failure criterion of the granular layer material nor a full constitutive law for negative skin friction. Therefore to validate the simplified model consistency, it is necessary to verify that the stress found at the inclusion head is compatible with the granular layer shear strength characteristics and also that the friction mobilized above the neutral plane is compatible with the limiting value of negative skin friction Ktanδ σ_v' (ASIRI, 2012).

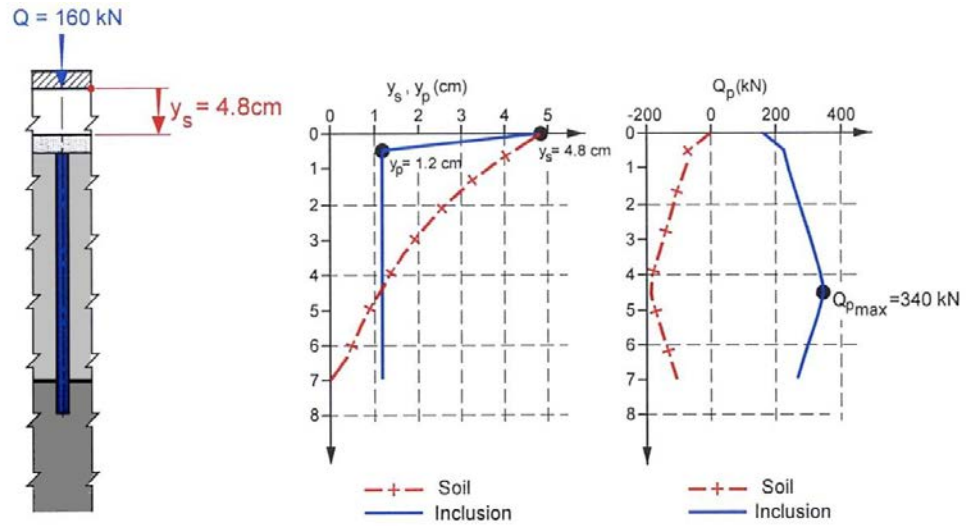

Figure 7: Step 3 of the calculation according to the simplified method - Inclusion diameter 0.34 m, vertical load case q = 200 kPa

6.2.4. Comparison between the simplified method and the Flac 3D numerical study

The comparison of results concerning the inclusion axial load or the pile and average soil settlement has shown fair agreement between the numerical Flac 3D calculation and the simplified method. This is illustrated by Figure 8 for the vertical load case q = 200 kPa.

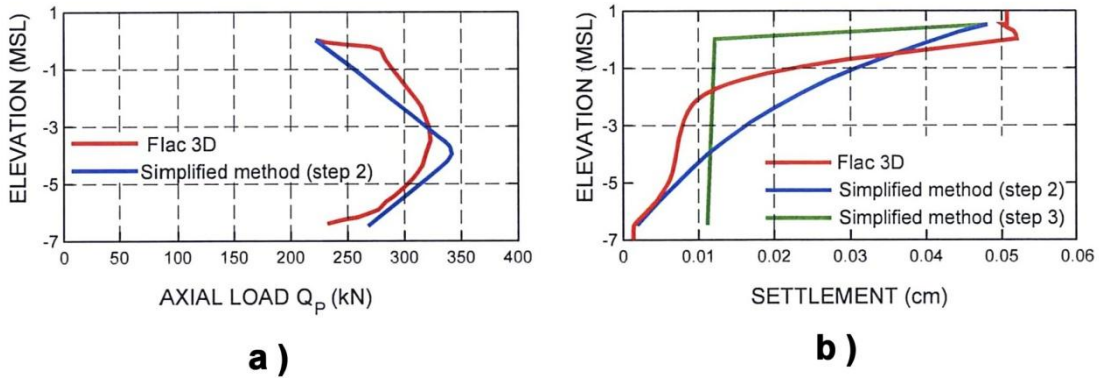

Figure 8: Comparison between simplified analytical method and numerical Flac 3D – Vertical load case q = 200 kPa. (a) Axial load in inclusions (b) Soil and pile settlement

6.3. Under transverse loading

The simplified method is composed of two successive additional steps (Simon, 2010). Both make use of an ordinary tool for pile foundation design, i. e. study of an isolated pile bearing on elastic-plastic springs ($p = p(y) < p_{lim}$).and subjected to transverse loading, as depicted by force T and bending moment M applied at the head and/or a displacement imposed on the surrounding soil g(z).
The p-y curve is calculated from the assumed E_M Menard pressuremeter modulus, following standard expressions for sustained loading (Frank, 1999).
Beforehand calculations by this approach of a horizontal loading at the head of a single inclusion establish that E_M value for soft soil given in Table 3 (together with a limit pressure value p_l = 0.25 MPa) leads to a load-displacement curve that agreed well with the numerically derived ones, using Flac 3D.

6.3.1. Step 4

The monolith with an equivalent modulus of E* (as established during step 1) is assimilated with a transversely-loaded pile interacting with the external unreinforced soil block via elastic-plastic springs The calculation establishes a lateral displacement profile g(z) for the monolith under action of the horizontal force T and bending moment M loading applied to the footing (Figure 9).
The limited monolith length-to-width ratio and its orthotropic nature however necessitate taking shear deformations of the pile into account, in addition to bending deformations. The simple model of a slender beam, commonly used for piles, tends to be inappropriate. These shear deformations are controlled by the G*A' factor (with G* being the equivalent shear modulus of the monolith and A' the reduced shear cross-section).The equivalent shear modulus G* may be assimilated with the shear modulus G_{sol} of the soil on its own (since the contribution of inclusions to shear strength in effect remains negligible compared to that of the soil). Bending deformations depend from the factor E*I (where E* is the monolith's apparent equivalent modulus -established during step 1- and I the monolith flexural rigidity).
A monolith calculation of the same kind also enabled to predict with sufficient accuracy the horizontal displacement of the footing lying on an unreinforced soil, as derived numerically using Flac 3D. In that case, G* and E* of the monolith were assimilated to G_{sol} and E_{sol}.

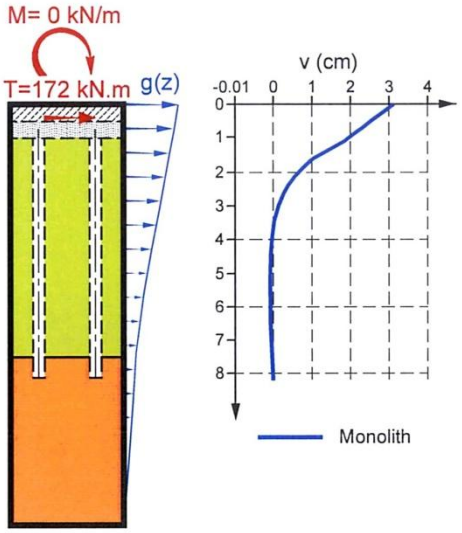

Figure 9: Step 4 of the calculation, according to the simplified method - Monolith cross-section area 2.8 m^2, inclined load case q = 200 kPa, $\theta = 10°$

6.3.2. Step 5

A subgrade reaction pile model, limited to the inclusion alone and assumed subjected to the previous displacement field g(z), enables to calculate the shear force and bending moment distributions in the inclusion for any given set of boundary conditions at the inclusion head and tip.
A horizontal force can develop at any inclusion head by friction exerted by the granular pad. A limiting value of this force can thus be found by considering the concomitant axial load in the same case. One can nevertheless observe that this force cannot induce a displacement of the inclusion head that exceeds displacement of the surrounding soil. Therefore a quite conservative assumption consists of selecting for the boundary condition $T_p(0)$ a value that "reduces" inclusion head displacement to that of the surrounding soil. This is illustrated in Figure 10 for the same example as already introduced.

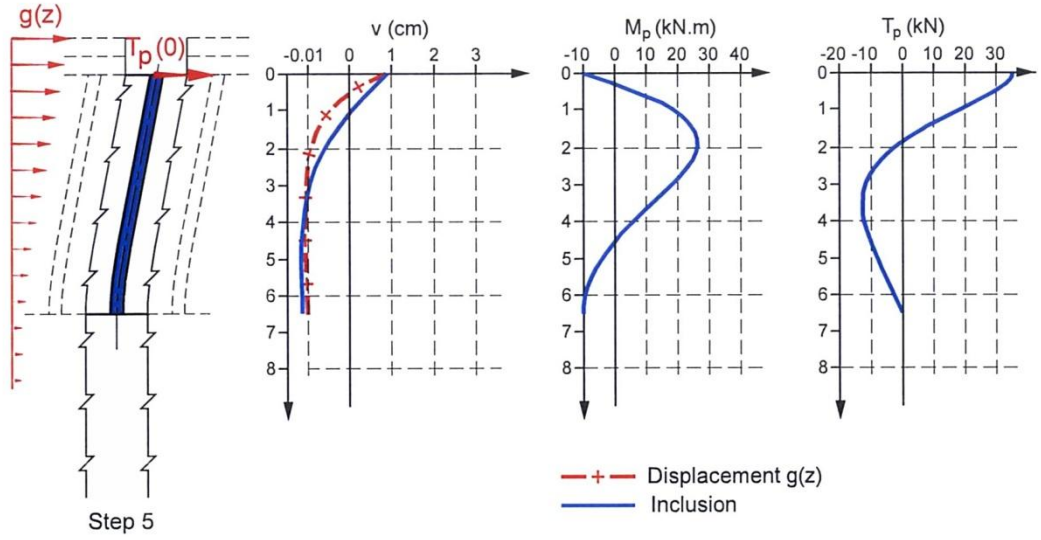

Figure 10: Step 5 of the calculation, according to the simplified method

Axial forces in the inclusions depend on the cell position with respect to the axis of rotation. The footing rotation ω (as calculated during Step 4) actually determines settlement along the axis of the cell placed a distance d from the axis of rotation, as follows: $y_p = \omega.d$.
The associated axial forces in the inclusion placed at the centre of this cell can then be estimated by assimilating them with the axial forces found under a uniform vertical loading of the cell that yields the same settlement. This step is performed by means of a specific calculation linking Steps 2 and 3.

The values of the corresponding axial force, shear force and bending moment obtained according to the vertical and transverse load cases must be combined in order to verify stresses in the inclusions.

6.3.3. Comparison between the simplified method and the Flac 3D numerical study

Figure 11 plots the different inclusion displacement fields which are obtained when the shear force boundary condition $T_p(0)$ value is varied between 0 and the one giving equal soil and inclusion displacements at head. They can also be compared to the front inclusion displacement field as calculated by Flac 3D. This latter one reveals a strong similarity with the simplified method curve for $T_p(0) = 0$.
The same holds true for the bending moment (or the shear force) profiles shown on Figure 12(a) (or Figure 12(b)).
For this particular case, best agreement is found assuming in step 5 of the simplified method that no friction develops at the inclusion head thus giving T(0) = 0. This suggests that the granular pad shear strength was fully mobilized under the vertical load component, leaving no residual friction capacity in reaction to any soil-pile horizontal displacement; this could also be stated: "*the vertical axis remains a principal stress direction in the vicinity of the inclusion head during transverse loading*".
Further evaluation of the simplified method is planned using the results of an on-going dedicated centrifuge testing program also funded by the ASIRI project.

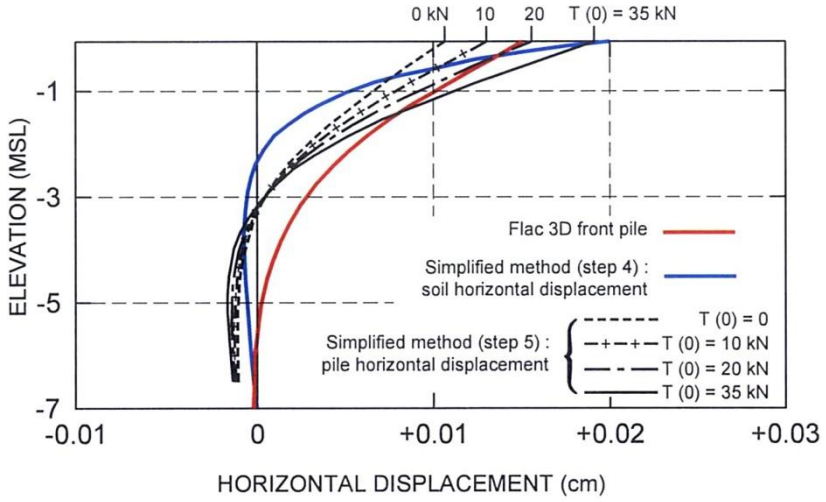

Figure 11: Comparison of the horizontal displacement profile calculated by Flac 3D model and the simplified method for a range of shear force boundary conditions T(0) at the inclusion head– Inclined load case q = 200 kPa θ = 10°

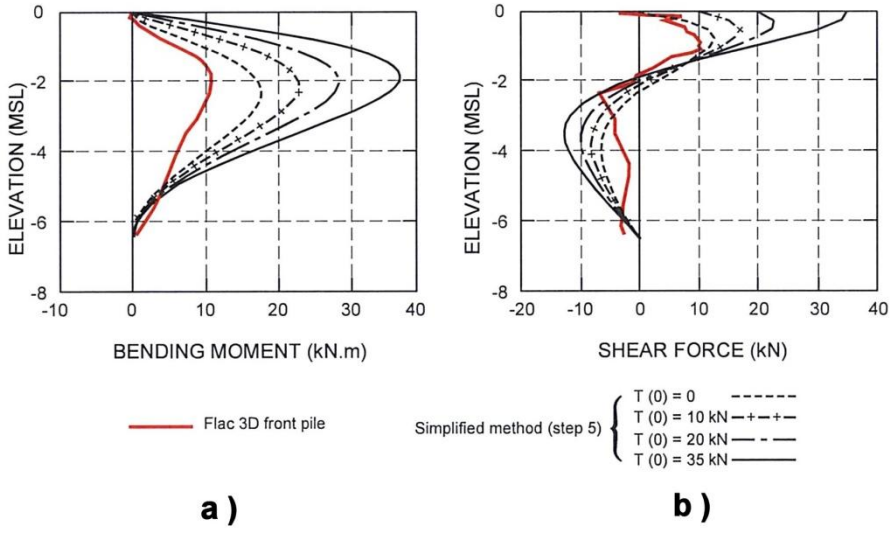

Figure 12: Comparison between Flac 3D results and simplified method results obtained with a range of shear force boundary conditions T(0) at inclusion head– Inclined load case q = 200 kPa θ = 10° (a) Bending moment (b) Shear force.

7. CONCLUSION

Flac 3D numerical modelling of a single spread footing on soft soil which is reinforced by four rigid inclusions has been carried out for a comprehensive range of loading conditions as for load intensity or inclination. Despite its simplicity, this foundation solution proves a heavy modelling task in order to maintain a proper balance between calculation practicability and solution accuracy. Results of these calculations were intended to serve as a reference case to elaborate guidelines for the design of foundations of this kind.

In that goal the Flac numerical model was also used to establish the load-displacement curves of the different structural elements (footing, inclusions) which are combined in this foundation solution, when vertical or horizontal loading is applied directly at the head of this element, left isolated in the same soil body.

This proved useful to calibrate in a step by step approach, a simplified method of designing the compound foundation obtained by associating a spread footing, a granular pad and a few inclusions. The simplified method which was evaluated in this way makes use of tools commonly used for pile foundation design under vertical or transverse loading. The comparison between the Flac 3D numerical results and those of the simplified method has so far shown quite fair agreement in all the investigated cases. Further evaluation is planned using the results of an on-going dedicated centrifuge testing program which was also started under the funding of the ASIRI project.

8. ACKNOWLEDGEMENT

The authors wish to acknowledge the French national project (ASIRI) for funding this research. This work was made possible thanks to the financial support of DRAST and RGCU.

REFERENCES

ASIRI, 2012, Recommendations for design, construction and control of foundation over soils reinforced by inclusions, Presses des Ponts, Paris.

Bustamante M., Frank R., 1999, Current French design practice for axially loaded piles, Ground Engineering, March 1999, 38 – 44.

Cambou B., Jafari K., 1988, Modèle de comportement des sols non cohérents. Revue Française de Géotechnique, vol. 44, pp 43-55.

Cuira F., Simon B., 2009, Deux outils simples pour traiter des interactions complexes d'un massif renforcé par inclusions rigides, Proc. 17th ICSMFE vol. 2, 1163 – 1166, Alexandria.

Fragaszy R.J., Su J., Siddigi H., Ho C.J., 1992, Modelling strength of sandy gravel. Journal of Geotechnical and Geoenvironmental Engineering, vol. 118, n° 6, pp 920-935.

Frank. R, Zhao SR., 1982, Estimation par les paramètres pressiométriques de l'enfoncement sous charge axiale des pieux forés dans les sols fins, Bull. Liaison P. et Ch.,119, 17 – 24 (in french)

Frank R., 1999, Calcul des fondations superficielles et profondes, Presses des Ponts, Paris (in french).
et Author, Year, Title, Journal/ Place of issue/Editor

Indraratna B., Balasubramaniam A.S., Balachandran S., 1992, Performance of test embankment constructed to failure on soft marine clay. Journal of Geotechnical Engineering, vol. 118, n° 1, pp 12-33.
Itasca, Flac3D - User's Guide. 2002

Mestat P., Dhouib A., Magnan J.P., Canepa Y. , 2004, Résultats de l'exercice de prévision des tassements d'un remblai construit sur des colonnes ballastées. ***In:*** *MAGNAN J.-P. Ed. Proc. of Symp. Int. sur l'Amélioration des Sols en Place (ASEP-GI), Paris : Presses de l'Ecole Nationale des Ponts et Chaussées, vol. 2, pp 1-13.*

Paute J.-L., Hornych P., Benaben J.-P., 1994, Comportement mécanique des graves non-traitées. Bulletin de Liaison des Ponts et Chaussées, 1994, vol. 190, pp 27-38.

Roscoe, K.H. and J.B. Burland. 1968. On the generalized stress strain behaviour of wet clay. In Engineering Plasticity, eds. J. Heyman and F.A. Leckie, 535-609. Cambridge, England: Cambridge University Press.

Simon B., 2010, Une méthode simplifiée pour le calcul des semelles sur sol renforcé par inclusions rigides, JNGG 2010, vol.1, 529-536, Grenoble-INP.

Improvement of soft soils using reinforced sand over stone columns

Nagy Abdel Hamid El Mahallawy, Lecturer of Geotechniques, El Shorouk Academy, cedc_eng@yahoo.com

ABSTRACT

In the present study, a series of laboratory model tests have been developed to study the behavior of unreinforced and geogrid-reinforced sand bed resting on stone columns. It has been observed that the soft clay is improved with stone columns. The diameter of stone columns has been taken as 50 mm, three stone columns have been used in the study with spacing of 75mm, while the footing is represented by a plate of 350x250x10mm for all the model tests carried out. Load was applied to the soil bed through the footing until the total settlement reached at least 5% of footing length.The influence of the thickness of unreinforced as well as geogrid-reinforced sand bed and the number of geogrid reinforcement on the performance of stone columns have also been investigated. The inclusion of geogrid layer within sand bed also increases the load carrying capacity and decreases the settlement of the soil. However multilayer reinforcement system is effective to transfer the stress from soil to stone columns. Significant improvement in load-carrying capacity of soft soil is observed due to the placement of sand bed over stone columns. Single layer reinforcement with stone columns is very effective to reduce the total settlement as there is considerable reduction in the total settlement due to stone column itself. The inclusion of reinforcement in the sand bed decreases significantly the depth of sand layer.

1. INTRODUCTION

One of the techniques extensively used in soft soils is the use of stone columns.The use of stone columns can accelerate consolidation of the soft ground and consequently accelerate the strength gain of the surrounding soft soil. It has been used to increase the bearing capacity of soft soils and reduce the settlement of superstructures constructed upon.

In recent years, many studies have been carried out to understand the behavior of foundation reinforced by stone columns without considering the inclusion of geosynthetic reinforcement[1-5].Many researches have studied the load-settlement behavior of single or multilayer geosynthetic-reinforced granular beds resting on soft soil without stone columns inclusions [6-15] .Most of the works reported in the literature are developed for foundations either reinforced by stone columns or geosynthetic layers. Limited studies have been done on the combined use of geosynthetic reinforcement and stone columns [16]. Han and Gabr [17] presented a numerical analysis of single layer geosynthetic-reinforced pile-supported earth platform over soft soil. Deb et al. [18] developed a lumped parameter model for single layer geosynthetic-reinforced granular fill-soft soil with stone columns. However, in the field multilayer geosynthetic reinforcements can be used along with stone columns. Thus, it is necessary to study the multilayer geosynthetic-reinforced granular fill resting over soft soil improved with stone columns.One of the techniques extensively used in soft soils is vibroreplacement, which consists of replacing some of the soft soil with crushed rock or gravel to form an array of stone columns beneath the foundation. Although the use of conventional stone columns in soft soil deposits was found to benefit foundations in many respects, Madhav and Miura, 1994 (19).The degree of improvement of a soft soil by stone columns is due to two factors. The first one is inclusion of a stiffer column material (such as crushed stones, gravel, sand) in the soft soil. This is largely reported in the literature [20- 25]. The second factor is the densification of the surrounding soft soil during the installation of the vibrocompacted stone column itself and the subsequent consolidation process occurring in the soft soil before the final loading of improved soil. The experimental work performed by Wattes et al. [26], and Vautrain [27] verifies that the installation of vibrocompacted stone columns leads to an improvement of the in situ soft soil characteristics and consequently, enhances the load displacement response of reinforced soil ,Guetif ,et al,2008, [28]. However, Greenwood [29] proposed an empirical method for estimating the reduction of settlement of reinforced soil taking into account the installation process of stone columns. In the present study, laboratory model tests have been conducted on three stone columns to study the effect of reinforcement and number of reinforced layers as well as unreinforced sand bed on settlement response. The maximum number of the reinforced layers and unreinforced sand bed has also been determined.

2. MATERIALS

2. Clayey soils

The properties of clay have been presented in table 1. Unconfined compressive strength (UCS) tests were carried out on clay samples. Water content of the clay was maintained at 25% throughout the series of tests. The bulk unit weight of the clay at 25% water content was determined to maintain identical unit weight in all the tests.

2.2. Sand

A commercially available graded sand were used to prepare the sand bed placed below the clay bed and over the stone column- improved soft clay.The average particle size of sand was ranging between 1-4mm. Crushed stone materials of size 2—8 mm were chosen to prepare the stone column, the particles were generally sub-angular.Sand &stone properties are represented in table2.
To maintain same unit weight of sand in each test, the required weight of sand in each layer was calculated based on bulk unit weight. The sand was poured in two layers. Each layer was compacted with steel hammer to achieve the required thickness .The same procedure was used for stone columns, but the stone was poured in five layers.

2.3. Geogrid

Biaxial geogrid was used as a reinforcement layer. The properties of geogrid reinforcement have been presented in Table 3.

Table 1: Engineering properties of clayey soil

Property	Soil
Classification	CL
Colour	Brown
Liquid limit%	45
Plastic limit%	20
Plasticity index%	25
Optimum moisture content%	18.0
Maximum dry unit weight	17 KN/m^3
Specific gravity	2.63
Bulk unit weight at 25%water content	19.2KN/m^3

Table 2: Properties of sand &stone

Parameters	Values	
	Sand	stone
Specific gravity	2,7	2.67
Maximum dry unit weight	19.2 KN/m^3	17.5KN/m^3
Bulk unit weight at 65% relative density	17.9 KN/m^3	16.1KN/m^3

Table 3: Properties of grogrid

Parameter	Value
Aperture size	135x135mm
Thickness	1.omm
Weight	285gm/m^2
Strain at failure	3.5%
Elastic axial stiffness at 1% strain	300 KN/m
Maximum tensile strength	8.5 K N/m

3. TESTING PROGRAMME

3.1. Experimental setup

To prepare the soil bed, a rectangular tank of 1000 mm x 250 mm size and 500 mm high was used in all the tests. , a thin-walled aluminium tube measuring 50 mm in outside diameter was pushed slowly through the clay sample to a depth of 35cm. Centrality was achieved by using a guide attached to the top of the cylinder. The sample within the tube was retrieved, creating a cylindrical cavity of 50 mm diameter at the centre of the clay.Three cylindrical cavities were achieved representing the stone columns with 50mm diameter &spacing 75mm. The stone column was installed up to 35cm depth in clay bed. Compaction were used to the clay, stones and sand to achieve the required density of the materials. Steel plate of 350 x 100 mm and thickness 10 mm was used as footing to apply the load. Dial gauges were used for measuring the settlement of footing during the application of load. The diameter of stone columns was chosen to be 50 mm each, in all the tests and the depth of clay bed was maintained at 350 mm; below the clay bed, a 50mm sand bed was at the bottom of the container. The first test was carried out on clay bed without any improvement techniques and the load-settlement behaviour was investigated. Other tests were carried out on soft soil improved by stone column alone and on soft soil improved by stone column along with unreinforced and geogrid-reinforced sand bed. Plate 1. shows the schematic diagram of the test setup.Summary of the tests conducted has been presented in fig 2,3,4,5&6.

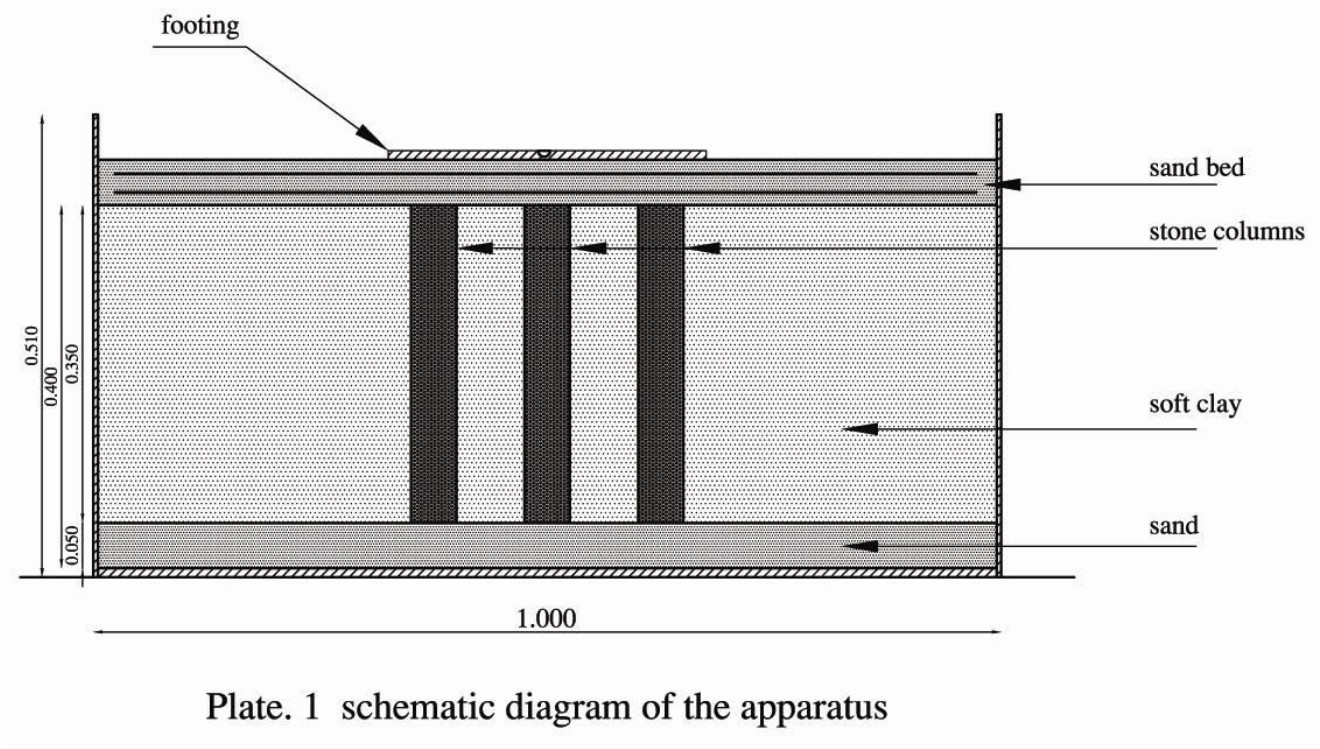

Plate. 1 schematic diagram of the apparatus

3.2. Preparation of clay bed

In all the tests, identical technique was to prepare the clay bed. To maintain similar properties throughout the tests, clay bed was prepared at 25% water content in all the cases. The bulk unit weight at 25% water content was found as 19.2 kN/m3. To maintain same unit weight of clay in each test, the container was filled in five equal layers of 70 mm thickness and the required weight of clay in each layer was calculated. Each layer was compacted with steel hammer to achieve the required thickness.

3.3. Column construction

A replacement technique was considered the most easily repeated method for column installation in very soft soils. After preparing the clay bed of 350 mm over a sand bed 50mm thickness at the bottom of the container, three cylindrical holes of diameter 50 mm &spacing of 75mm were dug at the centre of the clay bed by steel pipe of 50 mm diameter and a depth of 350mm. The unit weight of stones was determined and using the known volume of the hole, the total weight of stone required to fill up the hole was determined. Total weight of stone material was divided into five equal layers to fill up the hole. Each

layer of stone was poured and compacted with steel bar in such a manner that the finished height of each layer of stone column was 70 mm.

3.4. Preparation of sand bed

The weight of sand required to form a certain thickness of the bed for the lower and upper bed was determined by knowning unit weight of sand . For different thicknesses of sand, the required weight of sand was calculated and preparation of bed was carried out in layers. Each layer was compacted with a hammer with equal efforts of compaction to achieve the required depth of sand bed.

3.5. Test procedure

Loading was applied through a footing resting on the prepared soil bed and resistance offered by test bed with or without stone column was measured with the help of proving ring. Load was applied in equal increments and each increment of the load was maintained until negligible change in the settlement was observed. The settlement due to increment of each equal interval of loading step was observed through three mechanical dial gauges having least count of 0.02 mm fixed on the footing. Loading was applied until the total settlement of the footing attained was at least 5% of footing length.

4. RESULTS AND DISCUSSION

4.1. Thickness of sand bed

To determine the optimum thickness of unreinforced sand bed, the thickness of sand bed was varied from 20mm to 80mm.The load carrying capacity at 175mm settlement has been calculated. From Fig. 1, it has been observed that the placement of sand bed over stone column-improved soft clay increases the load-carrying capacity of the improved soil . As compared to unimproved clay bed, an improvement of 75% in load- carrying capacity has been observed when the clay bed is improved with stone column only. As compared to unimproved clay bed, 100,126,140,167&180% improvement in load-carrying capacity has been observed when unreinforced sand bed of 20, 40, 50, 60 & 80mm is placed over stone column-improved soft clay respectively. Fig. 1 shows the load settlement characteristics of the unreinforced sand bed of different thicknesses placed over stone column-improved clay.For 20,40,50,60&80 mm sand bed thickness, a loading intensity of 0.6 kN, as compared to unimproved soil, the settlement has been reduced by 63%, 69.2%,80%,87% and 90.7% respectively. For 1.0KN the settlement has been reduced by 60%, 74.8%, 80 %, 85.6 % and 88% respectively. The increase of sand bed thickness increases the load-carrying capacity also the settlement reduction increases up to a thickness of 60mm whereas beyond this value the reduction of settlement decreases and the increase of thikness is insignificant.

4.2. Number of geogrid-reinforced sand bed

The thickness of sand bed was taken 60mm in the study .The reinforced geogrids was taken 1, 2, 3 &4 layers.

Fig. 2 shows the load-settlement characteristics of the geogrid reinforced sand bed of 1, 2, 3 & 4 reinforced layers placed over stone column-improved clay. The improvement in load-carrying capacity at 175 mm settlement is 180%&200% when unreinforced and geogrid reinforced sand bed with optimum number of layers has been placed over stone column improved soft clay respectively.

It has been observed that as the number reinforcement layer increase, the reduction in settlement increase. To determine the optimum number of the geogrid-reinforced sand bed 1, 2, 3&4 layers of geogrids were used.Results obtained when using three layers of reinforcement are nearly close to those obtained with four layers.

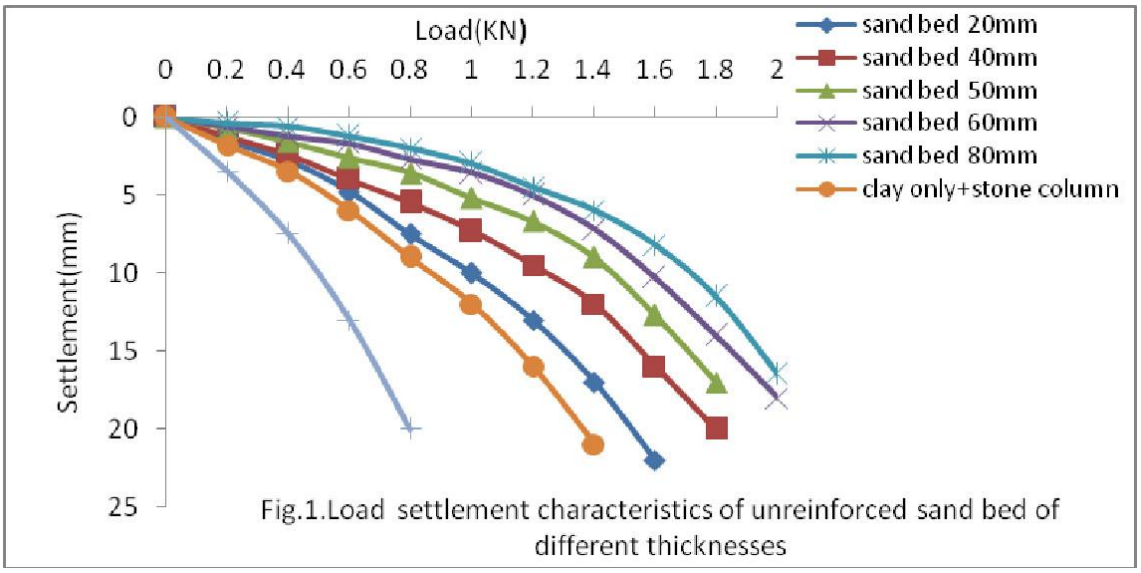

Fig.1.Load settlement characteristics of unreinforced sand bed of different thicknesses

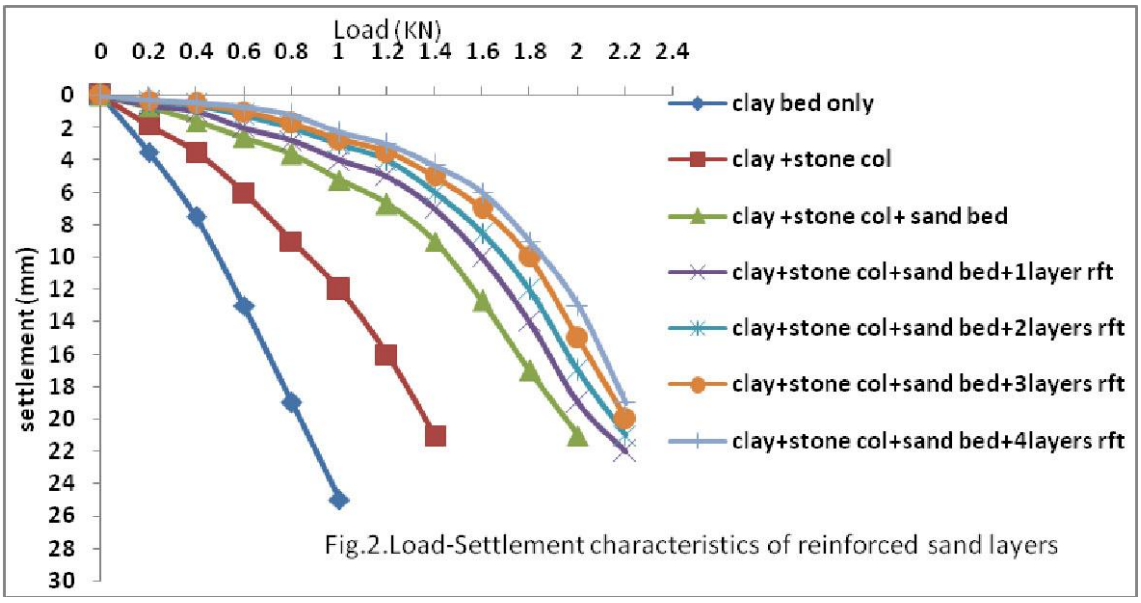

Fig.2.Load-Settlement characteristics of reinforced sand layers

A loading intensity of 0.2 kN, as compared to unimproved sand bed, the settlement has been reduced by 15.3%, 43.2%, 57% respectively .For 0.6 kN, as compared to unimproved sand bed, the settlement has been reduced by 23%, 53.8%, 61.5% respectively. For 1.0KN the settlement has been reduced by 31%, 43%,47% respectively.

The presence of reinforcement layers in sand bed increases the load-carrying capacity also the settlement reduction increases with the increase of number of geogrid layers up to a value of 3 layers, whereas beyond this value the reduction of settlement is insignificant. At low sand bed thickness, large deflection has occurred in the geogrid reinforcement directly underneath the footing.The large deflection of the geogrid reinforcement would mobilize the membrane action and induce more mobilized tension in the geogrid layer.The vertical component of the tensile force acting in the geogrid reinforcement partially counterbalances the superimposed load exerted by the overlying soil. As a result, the vertical stress is reduced in the zone below the reinforcement due to combined action of mobilized tension in the reinforcement and membrane action in its curvature [31-33] (Burd, 1995; Lee et al., 1999; Basudhar et al., 2008),[34] Deb et al,2011). However, when the sand bed reinforcement layers increases, a major portion of the shear failure zone of the soil is developed above the reinforcement layer and the deflection of the reinforcement also decreases. This led to reduction in the utilization of membrane action and less mobilized tension in the geogrid has been induced [32](Lee et al., 1999). This phenomenon reduces the effectiveness of the geogrid layer causing reduction in bearing capacity. Thus, the stone column under geogrid-reinforced sand bed produces less bearing capacity than that under geogrid-reinforced sand bed. Studies show that as the thickness of the reinforced sand bed is equal to or greater

than the optimum thickness of the unreinforced sand bed, the bearing capacity of unreinforced and reinforced sand bed is almost same [32](Lee et al., 1999). This is due to the fact that as the thickness of the reinforced sand bed increases, the deflection of the reinforcement decreases and the effectiveness of the reinforcement also decreases. When the thickness of the reinforced sand bed is equal to or greater than the optimum thickness of the unreinforced sand bed the effectiveness of the reinforcement is almost insignificant. Thus, the geogrid-reinforced sand bed with 60 mm thickness will almost same bearing capacity as compared to that under an unreinforced sand bed with 80mm thickness. The improvement in load-carrying capacity, as compared to unimproved soft clay, at 175 mm settlement is 180% and 200% when unreinforced and geogrid-reinforced sand beds with optimum thickness have been placed over stone column-improved soft clay, respectively.[32] Lee et al. (1999) reported similar observation based on numerical and model studies of strip footing resting on reinforced- granular fill-soft soil system without stone column inclusions. Due to presence of stiffer stone column in the soft clay, lower optimum thickness of the sand bed has been required as compared to the optimum thickness under without stone column condition to get the maximum improvement in load-carrying capacity of improved ground. However, from the present study and the results reported by [32]Lee et al. (1999), it has been observed that the ratio of optimum thickness of the unreinforced to geogrid- reinforced sand bed is almost similar for both the cases under with and without stone columns [34](Deb et al,2011).

4.3. Thickness of reinforced sand bed

Figure 3.shows the load-settlement characteristics of the geogrid reinforced sand bed of different thicknesses placed over stone column-improved clay. To determine the optimum thickness of the geogrid-reinforced sand bed, 3 layers of geogrid reinforcement was chosen with 20,40, 50, 60, 80 mm of sand bed. It has been observed that as the thicknes of reinforced sand bed increases the load-carrying capacity increases up to a depth of 60mm whereas beyond this value ,the increase of the thickness of the sand bed is insignificant. When the thickness of the reinforced sand bed is equal to or greater than the optimum thickness of the unreinforced sand bed the effectiveness of the reinforcement is almost insignificant (Lee et al., 1999).The improvement in load-carrying capacity, as compared to unimproved soft clay over stone column and geogrid-reinforced sand beds which have been placed over stone column-improved soft clay at 17.5 mm settlement with thickness of sand bed 20mm is 35.7% and 138% respectively,for 40mm thickness,50%,163% respectively ,for 50mm thickness,57.5%,175% respectively,for 60mm thickness, 64.5%,188% respectively, for 80mm thickness,71.4%,200% respectively.

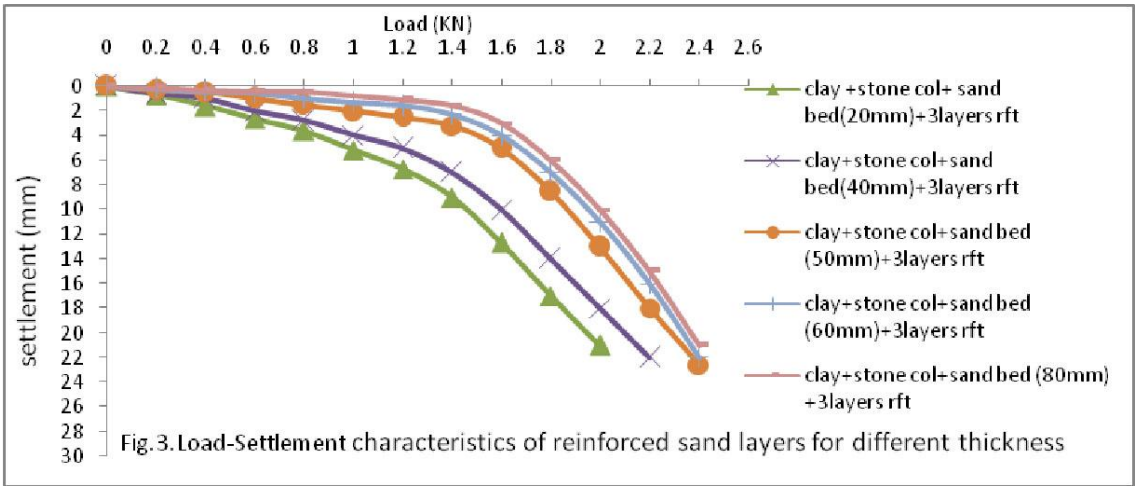

Fig.3. Load-Settlement characteristics of reinforced sand layers for different thickness

4.4. Length of geogrid

Figure 4.shows the load-settlement characteristics of sand bed reinforced by geogrid reinforcement of various lengths. From the load- settlement characteristics, it has been observed that for a particular settlement, the load-carrying capacity increases as the length of the geogrid increases upto twice the length of the footing, whereas beyond this value the increase of length is insignificant.The length of geogrid used was 1L,1.5 L,2 L,2.5 Lwhile the sand bed was 60mm.Thus, the optimal extent of the reinforcement is twice the length of the footing; and, beyond this length any additional reinforcement is ineffective.

However, in the present study, the model container has been taken as sufficiently large to reduce the boundary effects. To reduce the scaling effects, the dimensions of the various components have been chosen proportionally with the prototype dimensions. In the present experimental study, small aperture

size and thin model geogrid with relatively low stiffness has been used to avoid the size effect in the model experimental results. However, in case of field application comparatively large aperture size and thicker geogrids with higher stiffness are usually used. Thus, the chosen model geogrid properties used in the present experiments are suitable to achieve the same performance results as compared to full-scale geogrid. Thus, the results of the present laboratory model study are useful to investigate the behaviour of the unreinforced and geogrid-reinforced sand bed resting over stone column-improved soft clay.

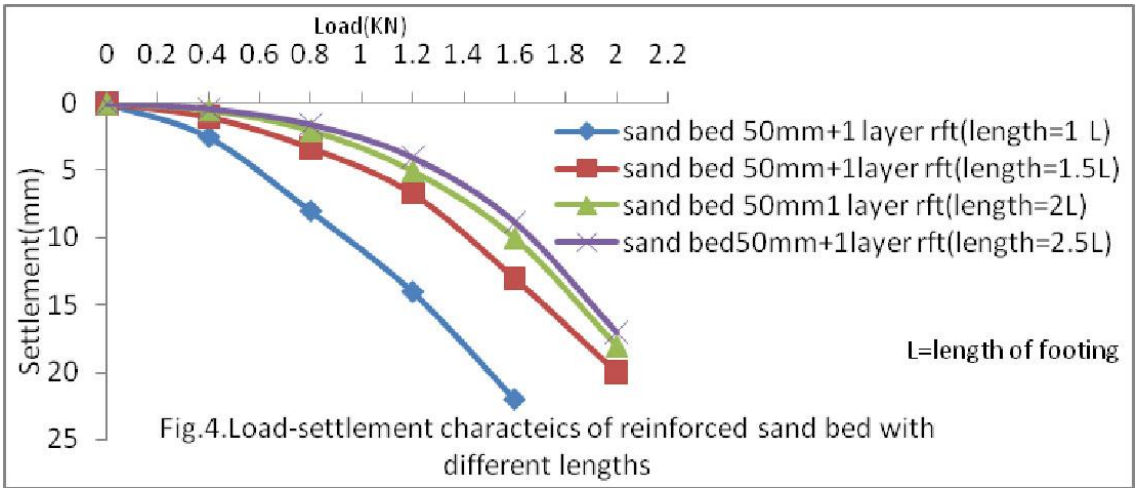

Fig.4.Load-settlement characteics of reinforced sand bed with different lengths

4.5. Load-settlement characteristics

Fig. 5. shows the load-settlement characteristics of the unimproved clay bed, clay bed improved by stone column alone and clay bed improved by stone column along with 60 mm thick unreinforced and geogrid-reinforced sand bed. The
number of the geogrid layer has been taken as 1,2, & 3layers. The improvement in load-carrying capacities under different conditions has been computed at 175 mm settlement,5% of the footing length. From Fig. 5, it has been observed that the placement of sand bed over stone column-improved soft clay increases the load - carrying capacity of
the improved soil and the use of geogrid layer within the sand bed is effective in further increment of the same. As compared to unimproved clay bed, an improvement of 75% in load- carrying capacity has been observed when the clay bed is improved with stone column only. As compared to unimproved clay bed, 140% improvement in load-carrying
capacity has been observed when unreinforced sand bed is placed over stone column-improved soft clay and for reinforced sand bed the improvement is 150,175,200% for 1,2, & 3 reinforcement layers respectively. For a loading
intensity of 0.5 kN, as compared to unimproved soil, the settlement has been reduced by 41.6%, 67%,83.3%,86.2% and 91.6% when the soil is improved by only stone column, by stone column along with unreinforced and geogrid-reinforced sand bed1,2,3 layers respectively. For a loading intensity of 1.0 kN, as compared to the presence of stone columns, unreinforced sand bed,reinforced sand bed with 1,2,3 layers,the reduction is 35.7%,57.1%,71.4%,78.5&85.7% respectively in settlement has been observed ; whereas for a loading intensity of 1.5 kN, the reduction in settlement is 29.1%,50%,62.5%,67% &79.2% respectively. Thus, it can be said that the geogrid reinforcement is more effective for higher loading intensity than for lower loading intensity. Similar behaviour has been
observed by Deb et al. (2008)[30] in the developed model for geosynthetic-reinforced granular fill-soft soil system with stone columns.

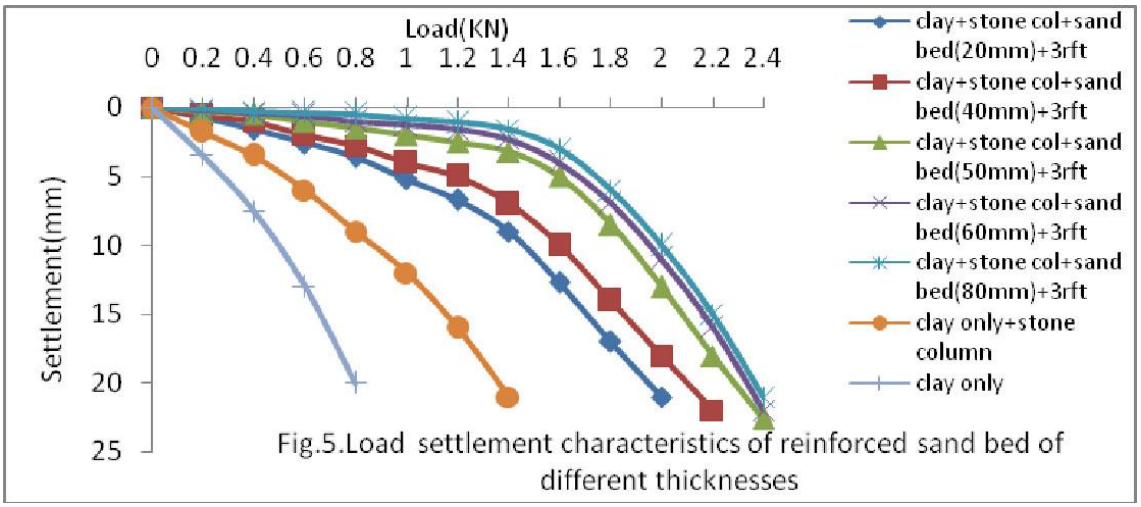

Fig.5.Load settlement characteristics of reinforced sand bed of different thicknesses

5. CONCLUSIONS

Based on the experimental results the following conclusions can be drawn:

I. The presence of stone columns in soft clay improves the load- carrying capacity and decreases the settlement of the soft soil. The placement of sand bed further increases the load-carrying capacity and decreases the settlement of the stone column- improved soil. The inclusion of geogrid as reinforcing element in the sand bed significantly improves the load-carrying capacity and reduces the settlement of the soil. As compared to unimproved soft clay, 75%, 140 % and 200% improvement in load- carrying capacity have been observed (at settlement equal to 5% of the footing length) when soft clay is improved by stone column alone, by placing of unreinforced and geogrid-reinforced sand bed of optimum thickness over stone column, respectively.

2. The optimum thickness of unreinforced sand bed placed over the stone column- improved soft clay is 1.6 times the optimum thickness of the geogrid-reinforced sand bed. The optimum thickness of unreinforced and geogrid-reinforced sand bed is 0.23 and 0.143 times the length of the footing, respectively.

3- It has been observed from the load- settlement characteristics that for a particular settlement, the load-carrying capacity increases as the length of the geogrid increases upto twice the length of the footing, whereas beyond this value the increase of length is insignificant.

4- The presence of reinforcement layers in sand bed increases the load-carrying capacity also the settlement reduction increases with the increase of number of geogrid layers up to a value of 3 layers, whereas beyond this value the reduction of settlement decreases.

5-, It has been observed that the placement of sand bed over stone columns-improved soft clay increases the load- carrying capacity of the improved soil and the use of geogrid layer within the sand bed is effective.

6-The sand bed layer below stone columns is effective to prevent any deformation to the stone columns due to loading of footing. The chosen model of the stone column properties used in the present experiments are suitable to achieve the same performance results as compared to full-scale stone columns.

REFERENCES

[1] Balaam N. P., Booker, J.R..,1981. Analysis of rigid raft supported by granular piles. Tnt J for Numer & Anal Methods Geomech 5,379-403.

[2] Alamgir, M.,Miura N,Poorooshasb,R..B., Madhav, M.R.,1996. Deformation analysis of soft ground reinforced by columnar inclusions. Comput Geotech; 18(4): 26790

[3] Poorooshasb RB.Meyerhof 1997, Analysis of behavior of stone columns and lime columns. Comput Geotech,20(1),47- 70.

[4] Lee JS. Pande 1998, Analysis of stone-column reinforced foundations. Tnt J NumerAnal Methods Geomec, 12(12):1001 20.

[5] Shahu, J.T., Madhav, M.R.., Hayashi .S. ,2000. Analysis of soft ground- granular pile - Granular mat system. Comput Geotech 27(1), 45- 62.

[6] Madhav, M.R.., Poorooshasb ,H.B. 1988.A new model for geosyntheticreinforced soil.Comput Geotech 6(4),277-290

[7] Poorooshasb, R.B. 1989.Analysis of geosynthetic reinforced soil using a simple transform function. Comput Geotech 8(4,289 -309).

[8] Ghosh , C., Madhav, M.R..,1994. Settlement response of a reinforced shallow earth bed. Geotext Geomembranes13(9),643 -656.

[9] Shukla, S.K., Chandra , S.,1994.The effect of prestressing on the settlement characteristics of geosynthetic-reinforced soil. Geotext Geomembranes13(8),531- 43.

[l0] Shukla ,5.K. ,Chandra ,S.,1995. Modeling of geosynthetic-reinforced engineered granular fill on soft soil. Geosynth Tnt 2(3), 603- 17.

[11] Yin ,J.R., 1997.Modeling geosynthetic-reinforced granular fills over soft soil.Geosynth Tnt 4(2), 165-1 85.

[12] Nogami, T., Yong, T.Y., 2003.Load- settlement analysis of geosynthetic reinforced soil &with a simplified model. Soils Found 43(3), 33-42.

[13] Maheshwari , P., Basudhar, .K.., Chandra, S., 2004. Analysis of beams on reinforced granular beds. Geosynth Tnt ll(6),470-4 80.

[14] Deb, K.., Chandra, S., Basudhar, P.K., 2005. Settlement response of a multilayer geosynthetic-reinforced granular fill-soft soil system. Geosynth Tnt 12(6), 288-298.

[15] Deb, K. Chandra, S., Basudhar, P .K.,2007.Nonlinear analysis of multilayer extensible geosynthetic-reinforced granular bed on soft soil. Geotech Geol Eng. Tnt J; 25(1),11- 23.

[16]Gniel .J, Bouazza, 2003. A Improvement of soft soils using geogrid encased stone columns. Geotextiles &Geomembranes27,(208),p167-175.

[l7] Han J. Gabr, M.A, 2002, Numerical analysis of geosynthetic- reinforced and pile-supported earth platform over soft soil. J Geotech Environ Eng, ASCE 128(1), 44- 53.

[18] Deb, K., Basudhar, P.K., Chandra ,S.,2007. Generalized model for geosynthetic reinforced granular fill-soft soil with stone columns. mt J Geomech ASCE z7(4),266-2 76.

[19] Madhav, M.R., and Miura, N., 1994.Improvement granular column capacity by geogrid reinforcement. Int.Proceedings of the 5th International conference on Geotextiles, Geomembranes and Related Products, Singapore, pp351-356.

[20] Balaam, N.P., Booker, J.R.., 1981.Analysis of rigid rafts supported by granular piles.Tnt J Numer anal Moth Geomech,5(4),379- 403.

[21] DTU 13.2 (Documents Techniques Unifies). Colonnes ballastCes; 1992, Chapitre VIII.

[22] Priebe, H., 1995. The design of vibro replacement. Ground Eng, 31 7

[23] Poorooshasb, H.R., Meyerhof, G.G. 199., Analysis of behaviour of stone columns and lime columns. Comput Geotech 20(1),47 70.
[24] Bouassida, M., Guetif., de Buhan, P. Dormieux, L. 2003.Estimation par une approche Variationnelle du tassement d'un sol renforcé par colonnes. Rexue Française de GCotech, 102-21 9.

[25] Dhouib, A., Blondeau, F. Colonnes ballastées. 2005. Edition Presses de l'Ccole nationale des ponts et chausses, Paris.

[26] Wattes, K.S., Johnson, D., Wood, L.A, Saadi, A.,2000. An instrumented trial of vibro ground treatment supporting strip foundations in a variable fill. Geotechnique 50(6), 699-708.

[27] Vautrain J.Comportementetdimensionnement des colonnes ballast Ces.1980Revue Française de GCotech11, 59-73
[28]Guetif, Z., Bouassida, M., Debats, J.M, 2007. Improved soft clay characteristics due to stone column installation. Computers & Geotechnics, 34, p104-111.

[29] Greenwood, D.A. 1970.Mechanical improvement of soils below ground surface. In: Proceedings of the conference on ground engineering. Institution of Civil Engineers, London. paper II. p. 11-22.

[30]Deb. K., Chandra., S., Basudhar, P.K. ,2008 .Response of multilayer geosynthetic- reinforced bed resting on soft soil with stone column..Computers &Geotechnics 35,p323-330.

[31]Burd, H.J., 1995. Analysis of membrane in reinforced unpaved roads. Canadian Geotechnical Journal 32,946-956.

[32]Lee, 1CM., Manjunath, V.R., Dewaikar, D.M., 1999. Numerical and model studies of strip footing supported by a reinforced granular fill-soft soil system. Canadian Geotechnical Journal36, 793-806.

[33]Basudhar, RIC, Dixit, RM., Gharpure, A., Deb, IC, 2008. Finite element analysis of geotextile-reinforced sand-bed subjected to strip loading. Geotextiles and Geomembranes 26, 91-99.

[34]Deb. K, Kumar. N , Babasaheb.J., 2011, Laboratory model studies on unreinforced and geogrid-reinforced sand bed over stone column-improved soft clay, Geotextiles & Geomembranes, p190-196.

Determination of pore size distribution to identify plastic zones around stone columns

Jean N.F. Gautray, Institute for Geotechnical Engineering, ETH Zürich, Switzerland, jean.gautray@igt.baug.ethz.ch
Jan Laue & Sarah M. Springman, Institute for Geotechnical Engineering, ETH Zürich, Switzerland,
jean.gautray@igt.baug.ethz.ch

ABSTRACT

Stone columns have proven to be an efficient ground improvement technique in soft soils. They stiffen the ground and provide drainage while changing the preferred drainage path from vertical to horizontal. However, smear and plastic annuli appear around these columns during installation. While plastic hardening supports an inclusion and promotes settlement control, the smear and plastic zones can also have a negative influence on the efficiency of the accelerated drainage and the bearing capacity.

The distribution and extent of the disturbed and plastic zones is still unclear. In an effort to gain a better comprehension of this, stone columns were installed in a clay model in the Institute for Geotechnical Engineering (IGT) geotechnical centrifuge at the ETH Zürich. Samples were then taken at different depths and different distances from a stone column. These samples have been tested in the clay mineralogy laboratory of the ETH Zürich using the mercury intrusion porosimetry (MIP) technique. The results provide further insight into the pore distribution around a stone column and the variations with depth. Different scenarios tested in the centrifuge show that the pore volume indeed decreases with increasing depth and that the stone column, as well as loading histories, do have an influence on it.

The pore volume determinations will be linked to other measurements available from the centrifuge model tests so that mechanical models of the distribution of the annular zones around stone columns can be evaluated.

1. INTRODUCTION

Soft soils may have been considered less suitable for construction in the past. However, due to demographic inflation, the need for construction land has sharpened, which has triggered the requirement for engineers to find solutions to overcome the challenges encountered.
One of the solutions, which has been implemented successfully for some years, is the construction of granular inclusions (sand or stone columns) in the soft soil. Such inclusions present two advantages for the construction: on the one hand, they stiffen the host soil and on the other hand, they influence the time-dependent effects (which rigid inclusions cannot do) as long as the main drainage path for excess pore pressures caused by loading changes from vertical to horizontal. This allows the consolidation time to be reduced. These two effects make it possible to build in areas that were previously thought to be unsuitable for construction.
However, this solution is not perfect, as long as installation effects occur due to the construction procedure. Weber (2008) conducted series of centrifuge tests in order to investigate the behaviour of ground improvement with stone columns under embankment loading. He built patterns of stone columns using an installation tool with an inner diameter of 8mm (and a wall thickness t = 1mm), which, under 50 times earth gravity, corresponds to 60cm and identified three disturbed zones around stone columns (Figure 1):

- a first zone in which stones and clay are mixed (zone 1), with a thickness of approximately 2mm, corresponding on the one hand to the cavity produced by the installation tool and on the other hand to the expansion of the stone column into the host soil,
- a second zone in which the clay particles are reoriented in a semi-vertical direction (zone 2), with a thickness of approximately 2mm
- a third zone in which the host soil is compacted radially (zone 3), with a thickness of about 6mm.
- a fourth zone in which the horizontal stresses are moderately increased while no compaction can be measured (zone 4).

The pore size distribution of these three zones has been investigated over the depth of the column and will be reported in this paper. A centrifuge test was conducted to construct stone columns in remoulded clay inflight in the centrifuge. Sampling at different depths and distances from the inclusions made it possible

to investigate the influence of these two parameters on the development of the installation effects with depth.

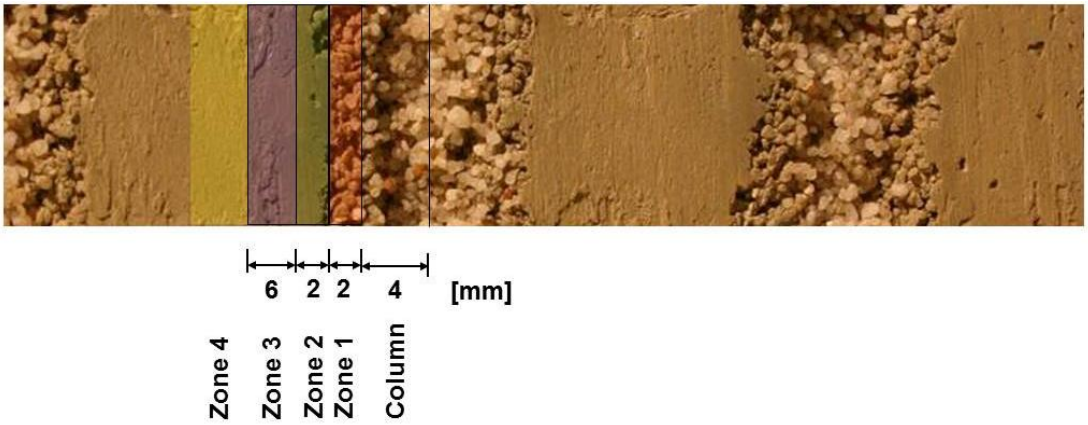

Figure 1: Spatial distribution of the installation effects around stone columns (Weber, 2008)

2. CENTRIFUGE TESTING

2.1. Basic principles

The increase of the centripetal acceleration due to the rotational movement of the model resting in the drum of the ETH Zürich geotechnical centrifuge (Springman et al., 2001) causes a modification of the stress distribution (Figure 2; Laue, 1996). Thus a similar stress distribution is provided in a small scale model (scaled with n, n being the number of times that the earth gravity is increased in the model) as at prototype scale. As a result of this process, the dissipation of excess pore pressure is accelerated by n^2 (Schofield, 1980).
Another advantage of physical modelling under increased gravity is the possibility to modify key parameters in rapid sequence in a specific boundary value problem.

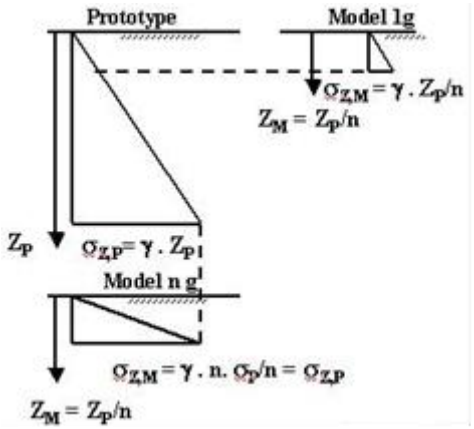

Figure 2: Comparison of the stress distributions in the centrifuge under ng and under 1g (Laue, 1996)

2.2. Host material

Natural silty clay from Birmensdorf, Switzerland, was used for the centrifuge test. This material was originally deposited postglacially under lacustrine conditions, while it was extracted from an excavation pit and reconstituted as a slurry using a vacuum mixer.
Several studies on the reconstituted Birmensdorf clay were conducted (e.g. Messerklinger et al, 2003; Trausch-Giudici, 2004; Messerklinger, 2006; Nater, 2007; Weber, 2008). Some key properties are recorded in table 1.

Table 1: Properties of the reconstituted Birmensdorf clay (after Panduri, 2000; Küng, 2003)

USCS classification	CH
Clay particle content from sedimentation analysis < 2µm [%]*	42
Liquid limit w_l [%]*	45-62 (av. 60)
Plastic limit w_p [%]*	18-26 (av. 21)
Plasticity index I_p [%]*	27-36 (av. 30)
Effective angle of friction φ'_{cv} [°]	24.5
Effective cohesion c' [kN/m^2]	0
Grain specific gravity G_s	2.75
Grain size d_{50} [µm]	4

* by weight

The soil was prepared in a slurry (Figure 3) at a water content of about 90% and then consolidated under a press (Figure 4). The load was gradually increased after consolidation of the previous step was completed, until a vertical stress of $\sigma'_v = 100\ kPa$ was reached.

Figure 3: Pouring slurry into the container

Figure 4: Consolidation of the slurry in a container

2.3. Stone column material

Quartz sand (fraction 0.5 – 1 mm) is used for constructing the sand columns. This material was tested by Weber (2008) and selected properties can be found in Table 2.

Table 2: Selected properties of the column material (Weber, 2008)

USCS classification	SP
Density ρ_s [g/cm^3]	2.65
Angle of repose φ' [°]	37.0
d_{50} [mm]	0.75
Coefficient of uniformity [-]	1.4
Coefficient of gradation [-]	1.0
Shape of the grains	Semi-angular to slightly rounded

2.4. Test layout and programme

The container dimensions were 40cm in diameter (inner diameter) and 20cm in height, which, under a gravity level of 50g, correspond to 20m and 10m, respectively. The soil sample was 16cm in height while the columns had a length of 12cm, which corresponds, in prototype dimensions, to 8m and 6m respectively. Four columns were to be installed in the soil sample (the layout of the test can be seen in Figure 5 and Figure 6):

- the column OR with a compaction regime of 15/10[1], which was not loaded after construction,
- the column OL with a compaction regime of 15/10 and loaded up to 75kPa with a circular footing with a diameter D = 56mm,
- the column UL without compaction and not loaded after construction, in order to investigate the influence of the shear path on the development of the installation effects,
- the column UR consisted of the intrusion of the stone column installation tool (cf. next paragraph) without either loading or pouring in granular material, in order to determine the part of the installation effects appearing during driving the tool in.

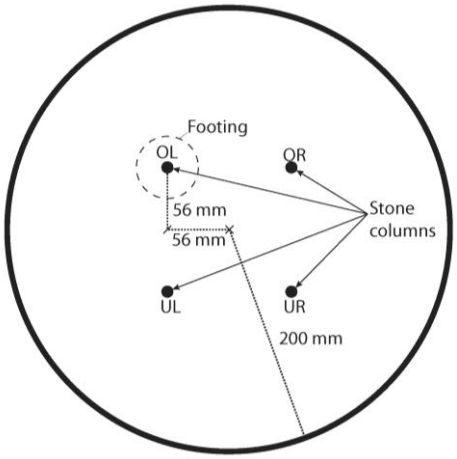

Figure 5: Layout of the stone columns

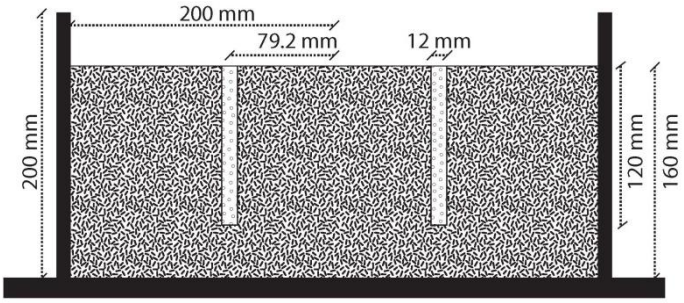

Figure 6: Cross-section of the model

2.5. Test conduction and sample extraction

The centrifuge was started after installing the container in the drum, and the gravity level was increased to 50g, while the pore pressures and the change in the surface level were recorded with PPTs and a laser, respectively. The installation of the stone columns was begun once the consolidation process was complete.

The columns were built using the installation tool developed by Weber (2008, Figure 7), which reproduces a dry bottom-feed installation process but without vibration. The tool consists of a hollow cylinder with an external diameter of 10mm (t = 1mm), which is driven into the soil sample by means of a screw-driven actuator. Drawing pins are installed on the surface of the clay in order to localise where the columns are to be built and to prevent the filling tube from being blocked with clay.

Different mechanisms are present within the clay during the insertion of the tool into the model. On the one hand, spherical cavity expansion occurs around the tip and on the other hand, the clay surrounding the tool experiences local cyclic shearing as well as cylindrical cavity expansion as part of the compaction process during the reinsertion regime, as sand is compressed radially into the surrounding clay. It is to be noted that the sand grains penetrate into the host soil.

The construction of the columns was achieved without difficulty for the first two elements (OL, OR, Figure 5). However, the drawing pin locating the 3rd column to be built (UL, Figure 5) could not be met perfectly due to an unexpected slight change in the coordinate setup, which led to an obstruction of the installation tool. However, the last "column" (UR, Figure 5) could be constructed safely, since no material had to be poured in.

[1] The compaction regime is defined by a length of withdrawal and of reinsertion of the filling tube; in this case, the compaction regime was 15/10, that is 15mm withdrawal followed by 10mm reinsertion, until the tube was extracted from the soil sample.

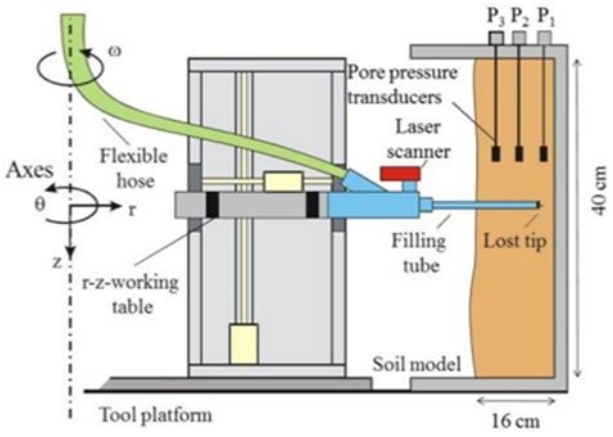

Figure 7: Stone column installation tool (Weber, 2008)

3. MERCURY INTRUSION POROSIMETRY (MIP) TESTING

3.1. Introduction

Winslow & Shapiro (1959) proposed to determine the pore size distribution of samples using MIP. The measurements done with this technique are based on the intrusion of mercury into the pores of a sample under an applied pressure. The diameter of the pores filled is inversely proportional to the pressure applied, according to Washburn's equation (Washburn, 1921):

$$d = \frac{-4\sigma\cos\theta}{p} \quad (1)$$

where d is the pore diameter, p the mercury pressure, σ the surface tension and θ the wetting angle for mercury.

The surface tension of mercury is 480 mN/m at 20°C, while it is assumed that the wetting angle of contact for purified mercury is 130° for clay minerals at room temperature (Diamond, 1970). The surface tension and wetting angle are the given parameters in this case, while the mercury pressure varies. A variation of the mercury pressure of 10N triggers a change in the order of 0.015mm in the calculated pore diameter.

3.2. Sample preparation

The 4 columns were extracted after the completion of the centrifuge test using cylindrical steel tubes with an outer diameter of D = 70mm (and wall thickness t = 2mm), as can be seen in Figure 8. The samples were then removed from the steel tubes using a steel cylinder with a diameter of D = 65mm in order to obtain an even distribution of the necessary load to extract the samples on the cross-section.
The clay cylinders were then divided in half before slices were cut out in order to produce usable MIP samples, an example of which is given in Figure 9. Smaller samples were then cut out of the cylindrical clay samples, derived from the first two columns (OR and OL, Figure 5) at different depths in order to be investigated with the MIP technique, before being dried in an oven.

3.3. Results of the investigations

Tests were conducted on samples extracted from 2cm, 4cm, 6cm, 8cm and 10cm depth for the loaded column (OL, Figure 5) and from 4cm, 8cm and 11cm depth for the unloaded column (OR, Figure 5). Two samples were investigated for each depth, the scope being to investigate zones 2 and 3 (Figure 1) in order to determine the variation of their extent with depth and loading. However, cutting the samples was not trivial, due to the solid consistency of the dried samples and to the small distances at stake. The zones investigated here are defined as "inner" and "outer". The "inner" zone is located within 0.7cm and 1.2cm from the column centre, while the "outer" zone is located within 1.2cm and 2.0cm from the column centre. Although this does not correspond exactly to the spatial distribution proposed by Weber (2008, Figure 1), it allows the influence of the installation effects on the pore size distribution to be determined.

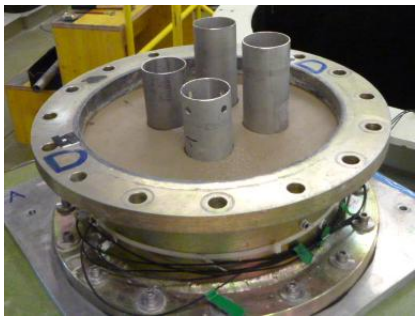

Figure 8: Steel pipes inserted into the model

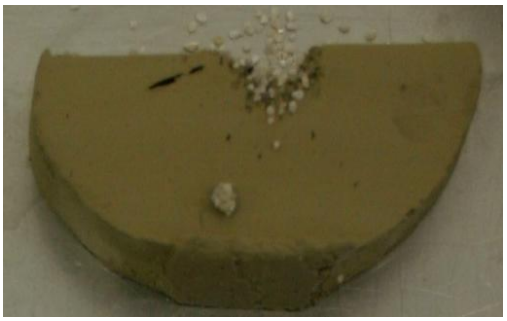

Figure 9: Typical MIP sample

The results of the tests conducted can be found in Figure 10 and Figure 11. They are consistent with the results published by Weber et al. (2010), although the radial influence of the column is not seen quite as clearly, due to the coarser distribution of the zones investigated. Cumulative pore volume (Figure 10 (a)) and porosity of the sample (Figure 10 (b)) are presented as a function of the depth for the upper loaded column (OL, Figure 5). Figure 11 (a) and (b) shows the same parameters for the upper unloaded column (OR, Figure 5).

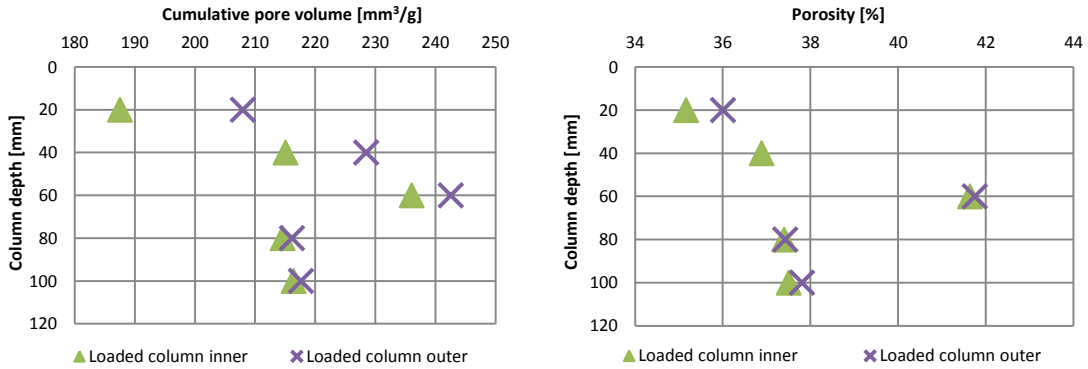

Figure 10: Cumulative pore volume and porosity distributions for upper the loaded column (OL)

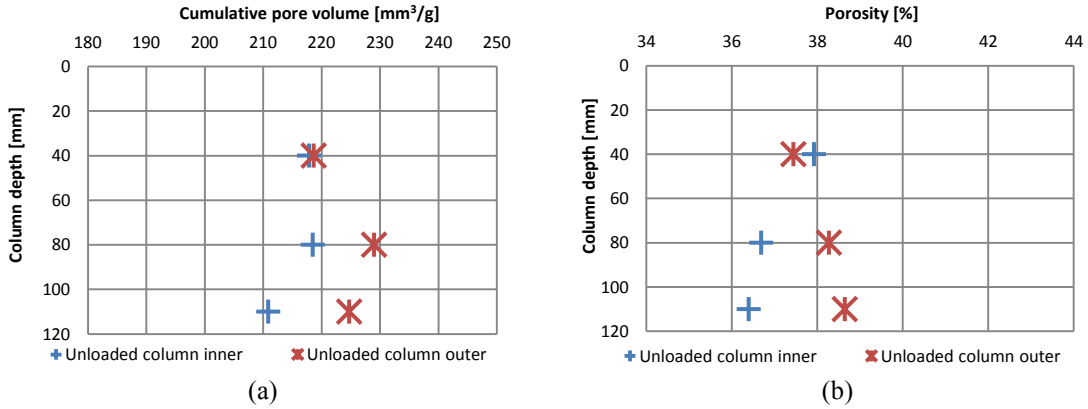

Figure 11: Cumulative pore volume and porosity distributions for the upper unloaded column (OR)

The cumulative pore volume and the porosity measurements from the loaded column (Figure 10 (a) and (b)) are correlated, which makes sense. This correlation is also present, although this is slightly less clear, in the case of the unloaded column (Figure 11 (a) and (b)).

The cumulative pore volume as well as the porosity distributions of the loaded column (Figure 10 (a) and (b)) shows the influence of the bulging of the top end of the column, which in turn exhibits the combined influence of the undrained shear strength (Figure 12) of the host soil and of depth on the behaviour of the stone column. The pore volume and the porosity increase significantly over the top 60mm of the column, which shows the diminishing effect of the radial expansion with increasing undrained shear strength in the soft silty clay (Figure 12). The cumulative pore volume and porosity values at a depth of 60mm are

rather unexpected though (these were expected to increase with depth initially and then remain roughly constant) and remain to be checked. This could be due to a loosening of the host soil caused by a change of the curvature of the expanded column from convex to concave or this could link to the effects of the footing load. This remains to be checked in subsequent investigations.
The influence of depth is not clear for the unloaded sample in this case (Figure 11 (a) and (b)). The increase of porosity with depth for the outer zone unloaded sample (Figure 11 (b)) might be considered questionable and should also be checked in further investigations.

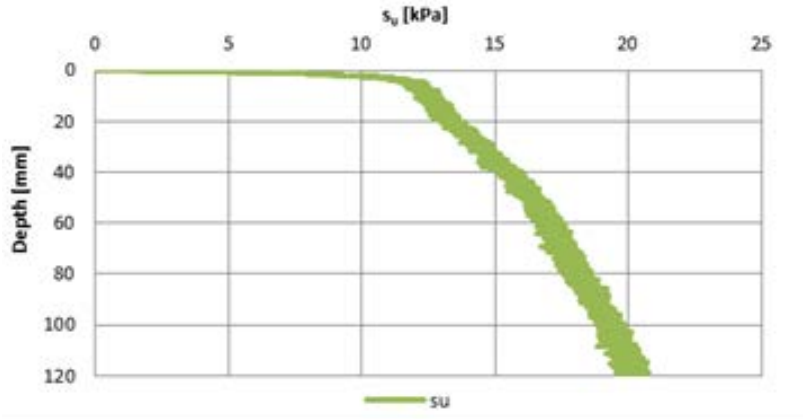

Figure 12: Evolution of the undrained shear strength with depth

The amount of stress effectively transferred into the soil was estimated after Adam (2011) in order to quantify the influence of the loading. It is assumed that the stress σ_0 is evenly distributed on the footing. The stress repartition between soil and column can then be estimated with the following equation

$$\sigma_0 = \frac{\sigma_1^S \cdot A^S + \sigma_1^B \cdot A^B}{A^S + A^B} \tag{2}$$

with

$$\sigma_1^S = \frac{1+\sin\varphi^S}{1-\sin\varphi^S} \cdot \left(\sigma_1^B + 2 \cdot c^B\right) \tag{3}$$

Knowing that σ_0 = 75kPa and inserting (3) into (2) allows for σ_1^B to be determined. In this case, the following stresses were calculated:

- $\sigma_1^B = 65.9\ kPa$,
- $\sigma_1^S = 265\ kPa$.

A calculation to determine, according to Boussinesq (1885), how the vertical stresses (σ_1^B, Figure 13) are reduced with depth under a circular footing delivers the distribution shows in Figure 14.

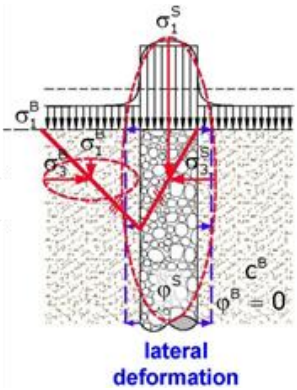

Figure 13: Stress repartition between soil and stone column (Adam, 2011)

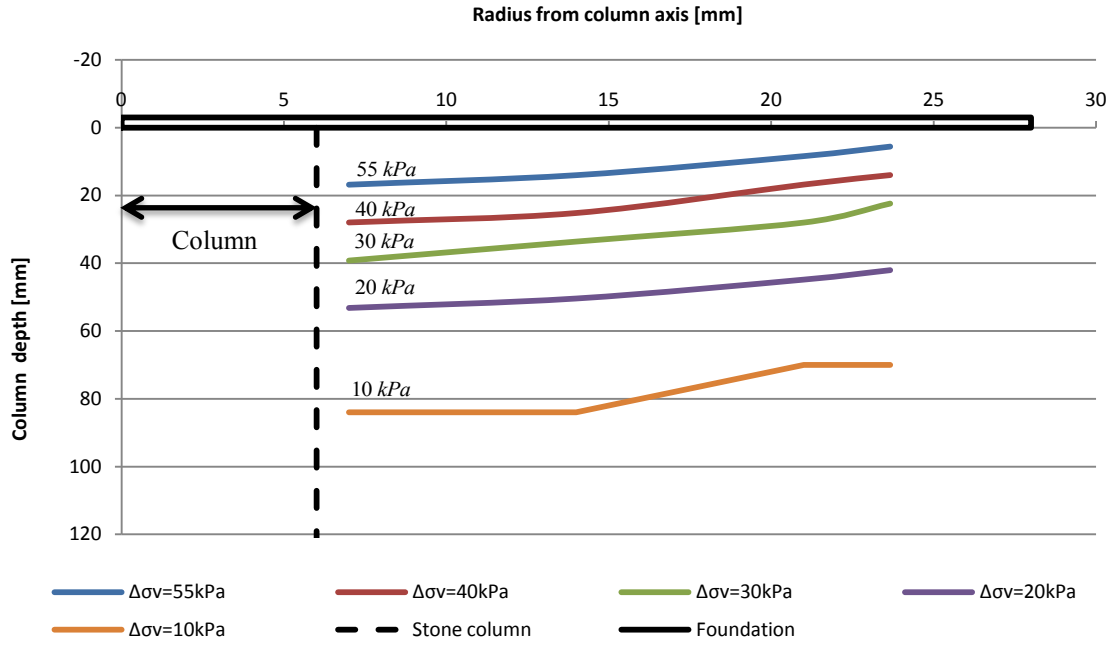

Figure 14: Vertical stress increment contours under the 56mm diameter circular footing derived from Boussinesq (1885) theory

The preconsolidation stress (σ_1' = 100kPa) was not exceeded during the test, which explains why the influence of loading on the cumulative pore volume (Figure 10 and Figure 11) is not very marked. This was exacerbated by the small stress increases over depth and due to the lack of measurements between the surface and 40mm depth.

The installation process of the stone columns triggers radial expansion, marked by an increase in the radial principal stress in the soft ground σ_3^B (Figure 13). Subsequent loading of the column does in turn increase the lateral loading of the host soil as well, due to radial expansion of the column which is caused by the Poisson's ratio effect.
The displacement at the top of the column due to distributed loading can be estimated to be $\varepsilon_a \Delta L$ where ε_a is the axial deformation and ΔL the considered incremental length (Figure 15). The lateral displacement can then be calculated with the Poisson's ratio as being $-\nu\varepsilon_a\Delta L$, which, as mentioned above, will trigger lateral loading of the host soil. These effects will be investigated in the future.

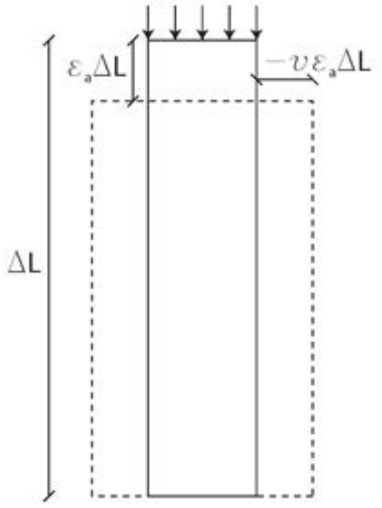

Figure 15: Illustration of the Poisson's ratio effect

4. CONCLUSIONS AND OUTLOOK

These investigations showed the influence of the installation effects on the pore size distribution around stone columns, and are in agreement with the results published by Weber et al. (2010). The influence of depth (i.e. of the undrained shear strength) can be seen relatively clearly while the effect of loading is harder to determine, due, on the one hand, to the applied load being smaller than the preconsolidation load and, on the other hand, to the lack of measurement near the surface for the unloaded column. This makes it impossible to achieve a direct comparison.

However, this study is part of on-going research, which foresees other centrifuge tests with varying loading on stone columns and investigations on samples from these centrifuge tests. These investigations will include MIP, laboratory (triaxial and ring shear) tests as well as X-Ray tomography. The lessons learned from the first investigations presented here will be incorporated in order to obtain a better insight into the effects taking place around stone columns during installation and loading.

REFERENCES

Adam, D., 2011, Bodenverbesserung versus Hybridgründung und Tieffundierung – Vergleich der Gründungskonzepte von drei Projekten mit Tragweite für Europa, Institut für Geotechnik, ETH Zürich, Kolloquium, 17.11.2011, www.igt.ethz.ch.

Boussinesq, J., 1885, Applications des potentiels à l'étude de l'équilibre et du mouvement des solides élastiques, Gauthier-Villars.

Diamond, S., 1970, Pore size distribution in clays, Clays Clay Miner., 18(1), 7-23.

Küng, H., 2003, Undrainierte Scherfestigkeit an aufbereitetem Seebodenlehm, Diplomarbeit, Institut für Geotechnik, ETH Zürich.

Laue, J., 1996, Zur Setzung von Flachfundamenten auf Sand unter wiederholten Lastereignissen, Schriftenreiche des Lehrstuhls für Grundbau und Bodenmechanik der Ruhr-Universität Bochum, Heft 15, Bochum.

Messerklinger, S., Kahr, G., Plötze, M., Trausch-Giudici, J.L., Springman, S.M. & Lojander, M., 2003, Mineralogical and mechanical behaviour of soft Finnish and Swiss clays, Int. Workshop on geotechnics of soft soils (eds. P.A. Vermeer, H.F. Schweiger, M. Karstunen & M. Cudny – Essen: Verlag Glückhauf GmbH), 467-472.

Messerklinger, S., 2006, Non-linearity and small strain behaviour in lacustrine clay, Veröffentlichungen des Instituts für Geotechnik, ETH Zürich, Band 225, VDF-Verlag, ETH Zürich.

Nater, P., 2007, Belastungs- und Verformungsverhalten von geschichteten Bodensystemen unter starren Kreisfundamenten, Veröffentlichungen des Instituts für Geotechnik, ETH Zürich, Band 226, VDF-Verlag, ETH Zürich.

Panduri, R, 2000, Versuchsschüttung Nordwestumfahrung Zürich: CPT, Laborversuche & numerische Modellierung, Institut für Geotechnik, ETH Zürich.

Schofield, A.N., 1980, Cambridge Geotechnical Centrifuge Operations, Géotechnique, 30(3), 227-268.

Springman, S.M., Laue, J., Boyle, R., White, J. & Zweidler, A., 2001, The ETH Zürich geotechnical drum centrifuge, Int. J. Phys. Modelling Geotech. 1(1), 59-70.

Trausch-Giudici, J.L., 2004, Stress-strain characterisation of Seebodenlehm, Veröffentlichungen des Instituts für Geotechnik, ETH Zürich, Band 223, VDF-Verlag, ETH Zürich.

Washburn, E.W., 1921, The dynamics of capillary flow. Phys. Rev. 17(3), 273-283.

Weber, T., 2008, Modellierung der Baugrundverbesserung mit Schottersäulen, Veröffentlichungen des Instituts für Geotechnik, ETH Zürich, Band 232, VDF-Verlag, ETH Zürich.

Weber, T., Plötze, M., Laue, J., Peschke, G., Springman, S.M., 2010, Smear zone identification and soil properties around stone columns constructed in-flight in centrifuge model tests, Géotechnique, 60(3), 197-206.

Winslow, N.M., Shapiro, J.J., 1959, An instrument for measurement of pore size distribution by mercury penetration, ASTM Bulletin, 236, 39-54.

Optimisation of Stone Column Design Using Transparent Soil and Particle Image Velocimetry (PIV)

Peter Kelly and Jonathan A. Black; Department of Civil Engineering, University of Sheffield, UK

ABSTRACT

The development of transparent synthetic soil has enabled non-intrusive measurement of internal soil displacement and detection of pre-failure strains using laser aided imaging and Particle Image Velocimetry. The work described in this paper, applies this novel methodology to evaluate the deformation and failure behaviour of stone column foundations in reduced scale physical models. End bearing and bulge failure have previously been reported in literature based on post examination of failed samples, however, the prodominant mode reported is often contradictory and key parameters such as (i) column length to diameter ratio (L/d), (ii) area replacement ratio (A_s) and (iii) as well as column-column and column-footing interactions are believed to govern the failure behaviour. Three tests have been conducted on an 18mm diameter isolated columns of L/d ratios equal to 4, 6 and 8 installated in a 220mm test bed. Visualisation of real-time internal displacement has indicated that an isolated stone column fails through a combination of compression, bulging and end bearing failure each occurring at various levels of foundation displacement. Increasing the column length beyond L/d = 4 at constant replacement ratio provided a negligible increase in load capacity and the predominant failure mode observed was bulge failure. In addition, some base penetration was observed in the shorter column (L/d=4) at smaller foundation displacements of 5 to 10mm, however the effect of this punching diminished with increasing foundation displacement up to 20mm, due to the prevalence of the bulging mechanism, thus bearing capacity was not badly affected. Longer columns exhibited virtually no end penetration and the internal column compression extended to a depth of approximately L/d=6.

1. INTRODUCTION

The vibrated stone column technique is a ground treatment process used to improve the load bearing capacity and settlement characteristics of soft compressible soils. The traditional application of stone columns is to support widespread loading using a large infinite column group; however, in recent years the technique has been extended to stabilise isolated pad and strip footings using smaller group configurations. Current design practice is based on the unit cell concept whereby it is proposed that each column in the group acts independently (Priebe, 1995). Previous investigations (Hu, 1995; McKelvey, 2002, Black, 2007 and Black et al. 2010) have shown that group columns exhibit complex behavior and the overall stability is dependent on soil, column and foundation interactions.

Many fundamental concepts associated with stone column behaviour have originated from understanding gained through reduced scale physical model experiments. Pioneering work by Hughes and Withers (1974) on isolated stone columns determined that bulge and end bearing failure modes occurred dependant on column length to diameter (L/d). The authors also reported that for increasing column length beyond the L/d = 4 no improvement in load capacity was observed. Recent investigations by Hu (1995) and McKelvey (2002) evaluated the bearing capacity behaviour of large and small group configurations respectively. In both studies L/d = 6 was stated as the optimium bearing capacity based on post failure observations obtained by exhuming the columns after failure. Furthermore, Hu (1995) also revealed that in addition to axisymmetric bulging, columns in close proximity within group configurations were susceptible to 'buckling and bending' which instigated shear failure.

Black (2007) investigated the aspect of settlement performance of isolated and group columns using a large triaxial cell equipped with dual load functionality to test samples 300mm in diameter. An L/d ratio of 8 was reported to be optimal for settlement serviceability criteria. This work also identified the presence of a "block failure mechanism" in small column groups whereby the columns and confined central clay region acted as a single entity punching into the weaker soil below.

Column behavior is highly dependant on design criteria such as column spacing (S), area replacement ratio (A_s); column geometry (L/d) and group configuration (i.e. strip, pad etc.). The uncertainty

surrounding how these factors influence column performance further exacerbate limitations of the current design protocol and make confident predictions of group performance problematic. Prior to evaluating the column groups there is a clear need for improved understanding of isolated column behaviour as this will be critical in examining and quantifying effects that govern the behaviour of multi-column configurations. The work presented in this paper focuses on this aspect and evaluates the behaviour of an isolated column at a range of L/d ratio for a constant area replacement area. The column is installed in a bed of transparent soil and internal displacements are captured using laser aided imaging and Particle Image Velocimetry (PIV).

1.1 Transparent Soil Development

Recent developments in transparent synthetic soil (Iskander et al., 1994, 2002, Gill, 1999, Sadek et al. , 2002 and McKelvey, 2002) has enabled the development of non-intrusive geotechnical modelling techniques. Transparent soil consists of silica aggregate mixed with mineral oils of matched refractive indice to produce a transparent medium. Early work utilised amorphous silica as aggregate for transparent soil due to its hygroscopic properties, whereby it absorbs pore pressure and displaces air, leading to excellent transparency (Iskander et al. 1994). Magued et al. (2002) conducted a series of triaxial compression, consolidation and permeability classification tests on a range of amorphous silica mixes, where it was observed that the properties measured were consistent with those of naturally occurring clay.

A key aspect of transparent soils is their visual clarity. Optical properties of amorphous silica based soil degrade significantly with increasing soil depth which restricts the size of physical models that can be produced. Gill (1999) developed a mixture based on fumed silica aggregate blended with 70:30 crystal light liquid paraffin and mineral spirits. This material has increased optical clarity over its amorphous silica predecessors, which has enabled greater viewing depths and consequently larger soil models to be achieved.

1.2 Internal Displacement Measurement

Hughes and Withers (1974) used a radiographic technique where lead shot markers were inserted into the soil during mixing and installation. On loading, X-rays were fired at the sample, locating the positions of the markers at regular intervals. This enabled the tracking of the markers and therefore general soil deformations to be determined in the vicinity of the deforming column. Despite its general success this technique has not been repeated in subsequent studies due to its reliance on expensive radiography equipment and health risks associated with using X-rays. Another drawback of this method is the reliance on lead shot embedded within the soil. This can produce compliance errors in soil stresses and may even produce a reinforcing effect in the soil. Gill (1999) utilsed a similar methodology of visually tracking the position of discrete plastic target beads suspended within transparent soil to determine soil disturbance during pile and penetrometer installation (Figure 1a). Although this method mitigated the need for expensive X-ray facilities, the measurement resolution was low and detailed strain information around the pile was limited due to the small number of target beads.

Ongoing work at the University of Sheffield has focused on enhancing the optical quality of transparent soil and also increasing the measurement density. This has been achieved by incorporating reflective seeding particles into the soil. A laser light sheet is used to illuminate the seeding particles on a plane of interest within the soil which produces a dense texture pattern that yields high measurment resolution capacity (Figure 1b). An image sequence of the loading event is captured using a digitial camera and soil displacement information is determined using Particle Image Velocimetry (PIV) techniques. This methodology has been successfully applied to investigate continuous flight auger piles (Hird et al. 2008) and helical screw piles (Stanier, 2011).

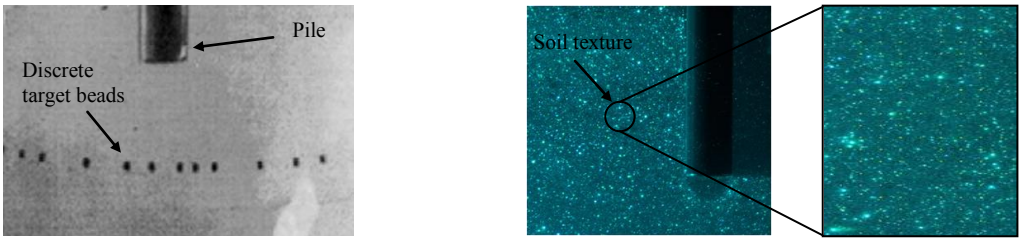

Figure 1: Transparent soil (a) with target beads (after Gill, 1999), (b) internal texture illuminated by laser sheet.

2. RESEARCH METHODOLGY

2.1 Experimental Configuration

A laser is used to produce a coherent beam of light which is then scattered using an optical lens to produce a vertical sheet of light. This light sheet enters the transparent soil model through a side window in the test chamber and illuminates a vertical plane of soil within the model. As loading occurs, soil deformation on the illuminated plane is captured through the front viewing window by a digital SLR camera. These images are analysed using the image processing PIV algorithm, GeoPIV (White et al. 2003) to determine the soil displacements. Photogrammetric processing algorithms based on the pin-hole camera projection model are used to correct and minimise errors caused by lens distortion during the analysis process. A further advantage of the transparent soil methodology is that chamber boundary effects when viewing displacements against a rigid viewing window associated with plane strain modelling protocol are significanlty reduced. A summary of this experimental setup is shown in Figure 2.

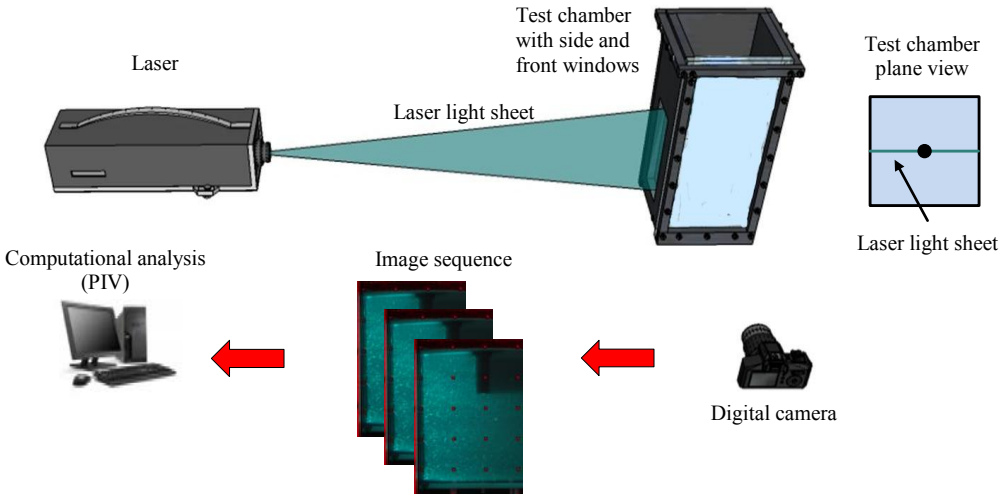

Figure 2: Experimental configuration summary (after Ballacchino (2011))

2.2 Test Chamber

Two test chambers (200mm[L] x 200mm[W] x 560mm[H]) were fabricated in which repeatable soft clay beds are formed from slurry. The main chamber is constructed of 20mm thick aluminium plates that are sealed using silicone and bolted with M6 bolts. The chamber incorporates side and front Perspex windows (20mm thick) to allow laser penetration at a plane of interest and digital images to be captured (Figure 3a). The base of the chamber is also made from Perspex to enable a laser sheet to enter the model in the vertical orientation. An extension collar is provided to accomodate the height of soil slurry required to achieve a test bed depth of 220mm. This is removed prior to column installation and loading to aid model preparation. The test box is anodised black to absorb the laser light sheet once inside the chamber and to minimise reflections.

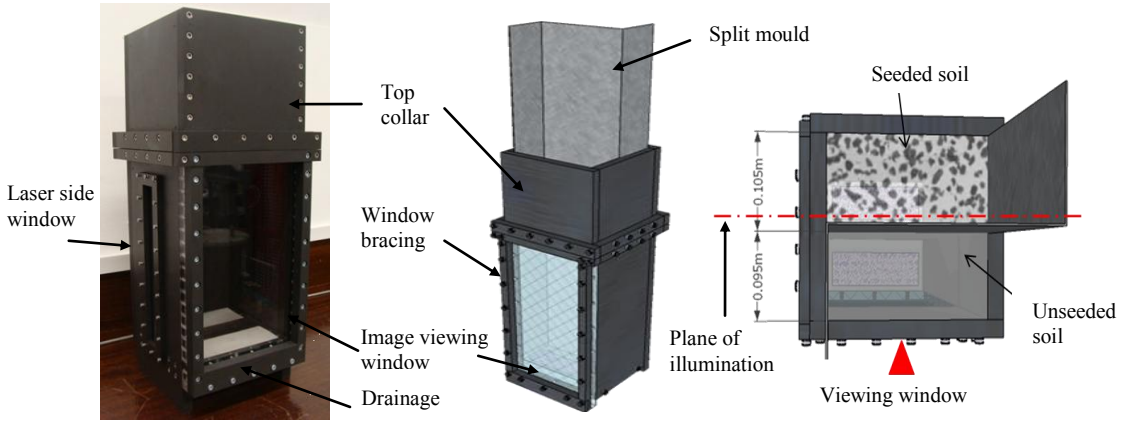

Figure 3: Experimental setup (a) test chamber (b) sample prepartion (after Ballacchino (2011))

2.3 Soil Model Preparation

Fumed silica powder, 6% by mass of the pore fluid is mixed to form a consistent soil slurry. The pore fluid consists of crystal light liquid paraffin and mineral spirits mixed at a ratio of 23:77, this ratio has been determined from previous investigations to provide composite slurry of matched refractive index. Timiron seeding particles of size d_{50} = 18-25µm are added to half the slurry mixture, 0.03% by mass of the silica powder. This quantity was determined as giving the best soil texture for PIV analysis which is described in Section 2.3.1. The mixture is mixed thoroughly using a hand held Kenwood food mixer and it is then placed inside a large vacuum chamber to de-air. The removal of air to form a two phase material is a vital step, as entrained air in the mixture leads to a loss of transparency and over exposure in terms of brightness in the images. The soil slurry is poured into the chamber with the aid of a split-mould. The split mould is used to enable seeded particles to be located only in the rear portion of the model; the front section contains no timiron particles to provide optimal transparency to the plane of interest (Figure 3b). This variation does not adversely affect sample behaviour as the particle size and mass of the seeding particles is very small. The split mould is removed to produce a vertical seeded-unseeded soil interface; any adhered slurry is scrapped off back into the chamber. The split mould produces a seeded and unseeded region of 105mm and 95mm depths respectively; this off-centre interface provides sufficient overlap to produce high quality seeding texture when the laser sheet is passed along the centreline of the chamber. The slurry is then consolidated in stages of 0, 6, 12, 25, 50 and 100kPa to produce a final bed height of 220mm with an undrained shear strength of approximately 15kPa. At the final pressure increment, the coefficient of consolidation (c_v) and the coefficient of volume compressibility (m_v) were 1.5 m^2/year and 4.2 kN/m^2 respectively which is consistent with other results quoted in literature (Stanier, 2011, McKelvey, 2002 and Gill, 1999).

2.3.1 Soil Tracking Assessment

The ability of the transparent soil to track displacements has been evaluated in relation to the quantity of timiron seeding particles and patch size used in the GeoPIV process. This was conducted using the same methodology proposed by White et al. (2003) whereby an image containing soil texture was translated manually by a known displacement of 10 pixels in the horizontal direction using Matlab™. The GeoPIV algorithm then was used to track the translated displacement for each timiron concentration at patch sizes of between 10 and 50 pixels. The standard error was determined and this is plotted in Figure 4. It is known that the precision of soil tracking decreases with increasing patch size, according to the following equation (White et al. 2003):

$$\rho_{pixel} = \frac{0.6}{L} + \frac{150000}{L^8} \quad (1)$$

Where L is the patch size in pixels and ρ_{pixel} is the standard error in pixels. The standard error in both the horizontal and vertical directions are plotted against patch size. The most accurate tracking was achieved using a larger patch sizes of 50 pixels as these patches contained a greater degree of unique intensity gradient. The average error ranges from an optimum value of 0.0052 pixels at a patch size 50 to 0.057 at patch size 10. It is evident from the graph that the measured precision is sensitive to timiron concentration. The best results occured when the mass of timiron was 0.03%, which is comfortably within

the upper bound limit of the GeoPIV alogorithm suggested by White et al. (2003), and for this reason it has been used in the present study.

2.4 Column Installation

The most frequently adopted column installation method in practice is the dry bottom feed due to its ease of installation and suitability for a wide range of soil conditions. Furthermore, it also reduces potential risk associated of ground contamination being washed to the ground surface as can be the case for wet installation methods. Replicating the exact vibration installation method at reduced scale is highly difficult and a range of methodologies have been adopted to conduct column installations in small scale physical modelling. In an effort to produce a densely compacted column representative of the prototype, columns were formed using a replacement technique. Excess oil was drained off the top of the model before column drilling to ensure that the column was augured in a dry state. A 16mm auger was used to bore into the soil to achieve the required column depth at drive rate of 0.2 mm/s and a rotation rate of 0.4rps controlled automatically using a two degree of freedom actuator. These settings were selected to provide a neutral drive velocity as this minimised disturbance in the soil bed (Hird et al. 2008). The auger was removed and reintroduced into the hole in a number of stages during drilling so that the spoil could be cleared from the auger flight; this prevented the auger from clogging and generating suction forces. The cavity was then backfilled with aggregate (0.8-1.2mm grain size) and compacted in 20mm stages until the model surface was reached. The columns were constructed using stress control methodology using a compaction bar and integrated load cell. A pre-stress of 100kPa was achieved at each compaction stage which produced columns having typical densities of 2650kg/m^3. Trial installations indicated this value was the maximum stress to prevent causing excessive bulging or punching of the column during the installation process. The final installed column diameter was approximately 18mm which is slightly larger than the initial bored hole due to the compaction process. Internal displacements during the boring and compaction stages were recorded as part of this investigation; however this is beyond the remit of the present paper.

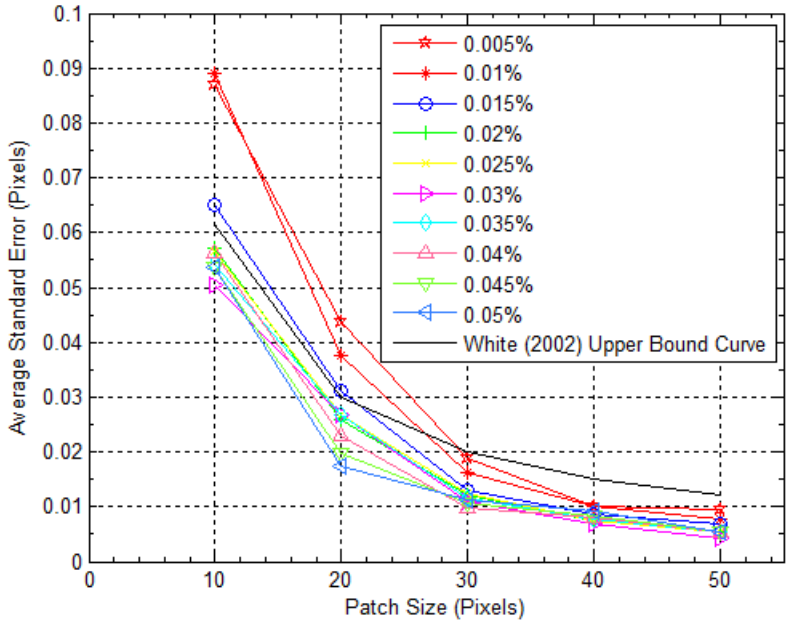

Figure 4: Investigation of optimum timiron content

2.5 Foundation loading

After installation the sample was allowed to rest for a period of 24 hours, to ensure disapation of any excess pore pressures generated during the installation process. A circular foundation 32.85 mm in diameter, representing an area replacement ratio of 3.3 was used in the results reported in this paper. The foundation was aligned centrally over the column location and a load cell and displacement transducer were positioned. At this point the digital camera was located on a tripod in front of and perpendicular to the viewing window ensuring that the full area of interest could be observed. The camera was set to a focal length of 55mm, with f-stop of 8 and an apparature of 1/13, as determined in a previous

investigation to provide the optimum image resolution. The camera was focused manually to provide the greatest claity of texture illuminated by the laser sheet. A grid of control target markers were located in front of the perspex viewing window to provide a reference frame of known coordinates in the field of view which enabled camera distorsions to be corrected and scaling of the images. The camera was set to rapid bust mode to record images at the rate of 3fps, once stable strain controlled loading was applied to the foundation at the rate of 0.2mm/s using the vertical drive function of the actuator system. Loading was terminated at a foundation displacement of 20mm which produced an image sequence in the region of 300 for analysis.

3. ISOLATED COLUMN TEST RESULTS AND DISCUSSION

Three tests conducted on isolated columns are presented as part of this paper to demonstrate the potential new insight that can be achieved using this test methodology. All columns had a final installed diameter of 18mm and are of length of 72mm, 108mm and 144mm, representing L/d ratios of 4, 6 and 8 respectively. The image sequences captured during the tests were processed using GeoPIV to produce velocity trajectories of soil displacements. Further post processing enables horizontal and vertical displacement contours and total shear strain contours to be plotted. Horizontal displacement away from the column (to the left in the figures) is signified by a +ve notation and downward vertical movement contours are highlighted as –ve notation. In addition, due to the visibility of the granular column texture within the images, soil tracking in this region was also possible. This is significant as it enables the compression of the column relative to the surrounding soil to also be visualised and determined.

3.1 Development of Displacement Behaviour

Images recorded during the foundation loading are used to provide an overview of the generation of soil and column displacement, this is particularly beneficial as it allows the development of the failure mode to be evaluated. Figure 5 shows the development of internal displacements at 5mm, 10mm and 20mm foundation penetration. It can be seen that that the column fails by compressing and bulging into the surrounding soil. At 5mm footing displacement, there is some vertical displacement at the column base, and the column has compressed over its entire length. The overhang of the foundation beyond the column diameter provides increased stress in the soil to prevent lateral deformation (bulging) at this footing displacement level, only 1mm is observed at a depth of 20mm below original column level. As the loading continues to 10mm and 20mm displacement, the column continues to compress internally with some small increased penetration of 0.3mm and 0.8mm respectively being observed. At these greater displacements there is significant increased levels of dilation in the upper region of the column reaching a maximum of 4mm at the end of loading. This is due to the fact that the lateral resistance of the soil is not sufficient to restrain the column from bulging in a cylindrical cavity expansion. Inclusion of similar plots for L/d = 6 and 8 cannot be included due to space limitations; however, similar bulge failure was observed in each of these tests although virtually no base penetration occurred. It must be highlighted however that these observations are based solely for the soil strength used in this investigation. Increased soil strength will naturally provide greater resistance to bulging thus increased base penetration may occur.

3.2 Impact of column L/d geometry

The overall impact of L/d on column behaviour can be observed for Test 2 (L/d=6) and Test 3 (L/d=8) in Figure 6 and 7 respectively at the foundation displacement of 20mm. It is clear from all the plots, that lateral deformation of the soil and column (bulging) is significant in the upper 30-40mm of the column, reasons for which were highlighted in Section 3.1. The maximum displacement occurs at the soil-column interface and reduces in magnitude with increasing radial distance from the column. The largest soil displacements and resulting shear strains are confined within approximately 1 column diameter; however, the zone of influence extends to around 2 column diameters where the magnitude of shear strain is 25%. Further investigations into this aspect will be significant in refining the optimum column spacing for multi-column installations.

Vertical displacements in the soil are largest immediately beneath the foundation, however it is interesting to note that the magnitude determined is lower than the applied foundation displacement. This is attributed to the fact that the soil displacement presented is separated into both the vertical and horizontal components, as the column compresses and bulges. The soil surrounding the column can easily deform in the lateral direction as the column dilates. The reduction of internal compression along the depth of the column indictes the point at which the column length could be optimised for bearing capacity. As discussed previously, 0.8mm of punching into the underlying soil was observed for L/d =4 (Figure 5). In

Figure 6 and 7 when the column length is extended to L/d=6 and 8 (108mm and 144mm), punching is significantly reduced to below 0.3mm in both tests. The corresponding increase in bearing capacity observed between the columns of L/d=4 and L/d=8 is low at only 5% (Figure 8), thus it could be argued that extending the column to greater depth is unnecessary and an inefficient design.

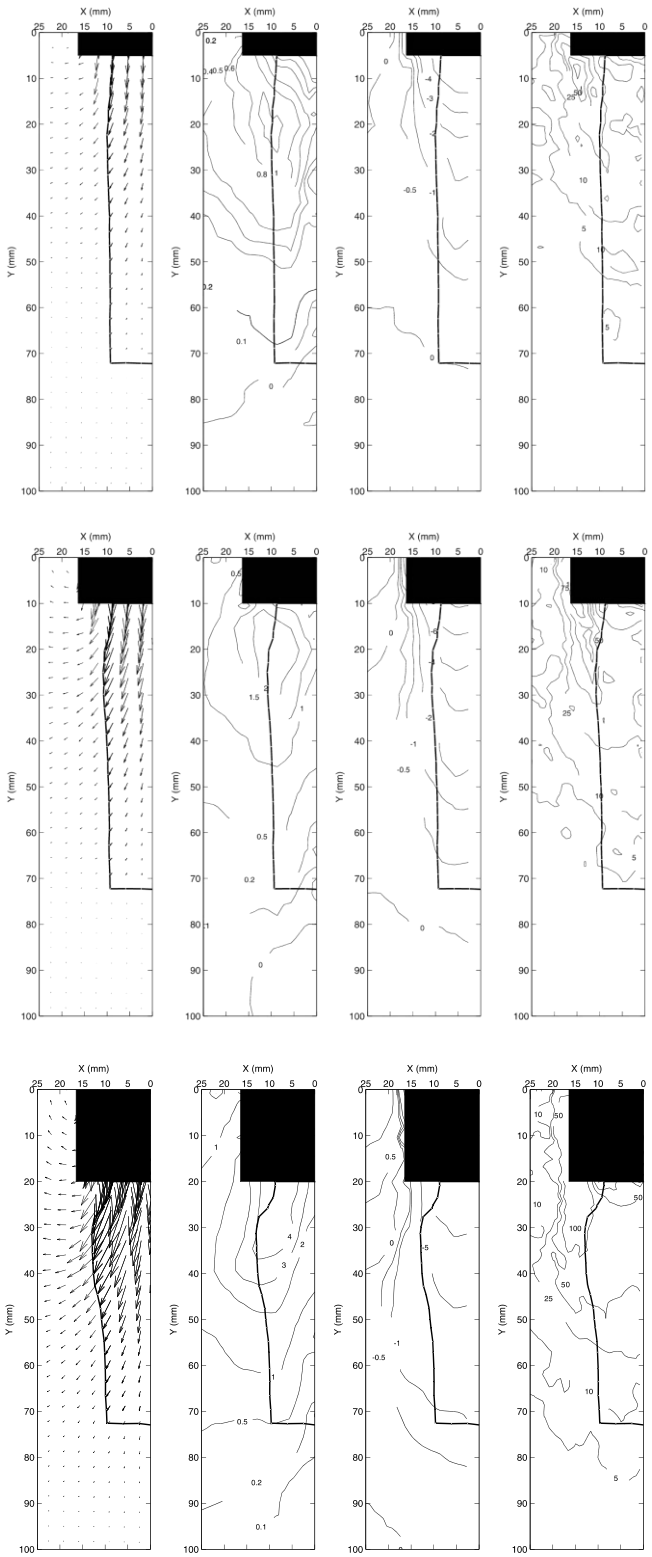

Figure 5: Test 1: L/d = 4. Velocity vector fields, displacement contours in the x and y directions (mm) and total shear strains (%), respectively at 5mm, 10mm and 20mm footing displacement.

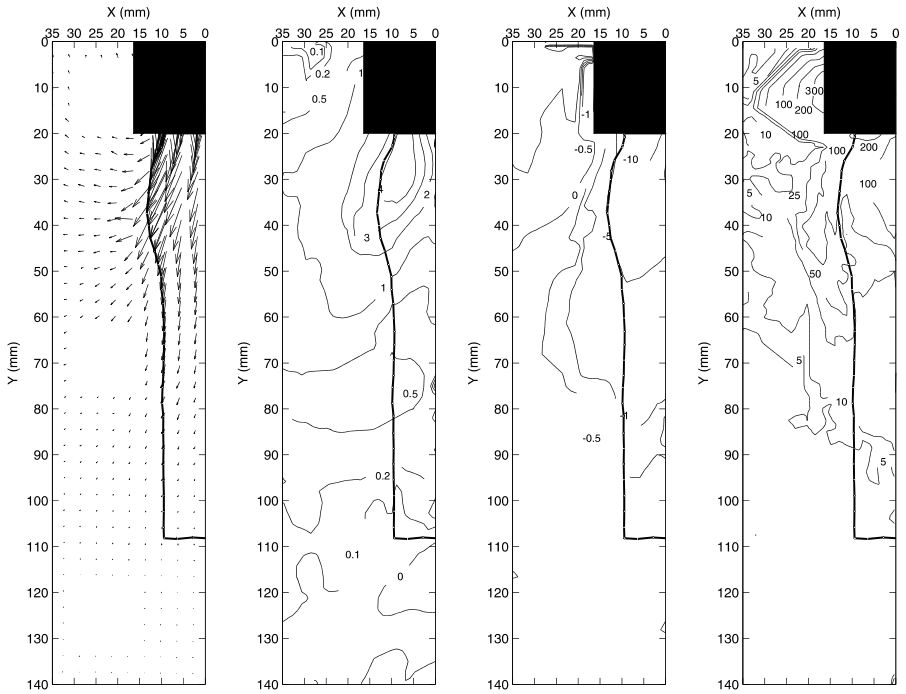

Figure 6: Test 2: L/d = 6. Velocity vector fields, displacement contours in the x and y directions (mm) and total shear strains (%), respectively at 5mm, 10mm and 20mm footing displacement.

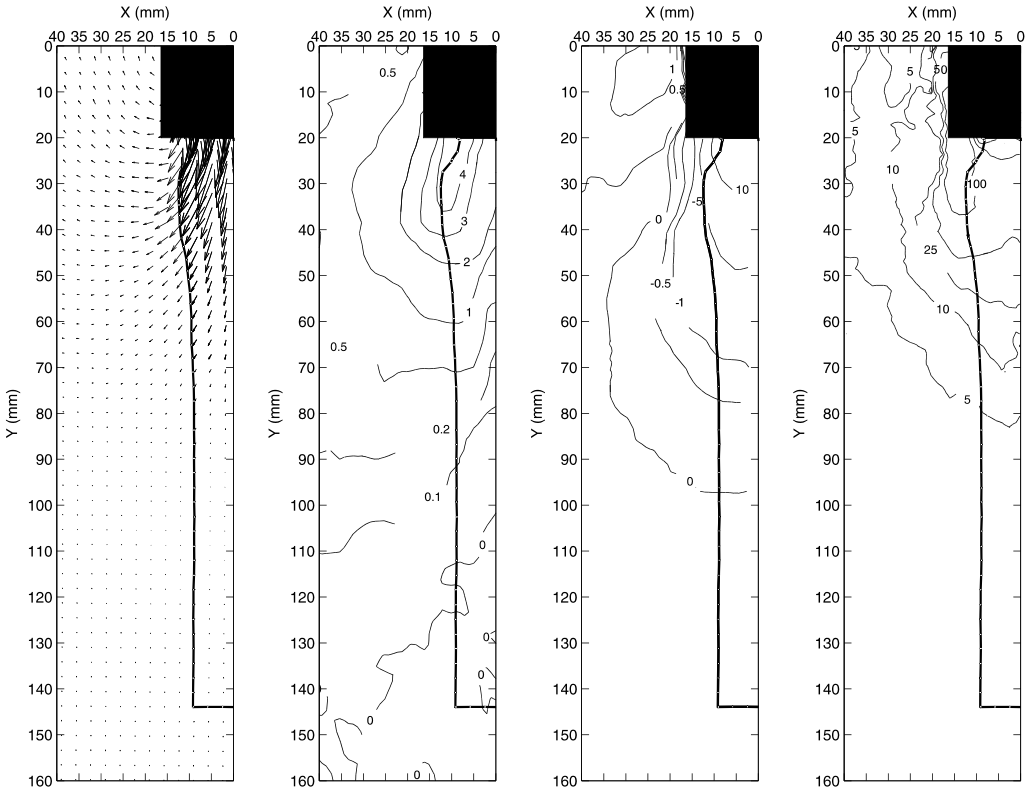

Figure 7: Test 3: L/d = 8. Velocity vector fields, displacement contours in the x and y directions (mm) and total shear strains (%), respectively at 5mm, 10mm and 20mm footing displacement.

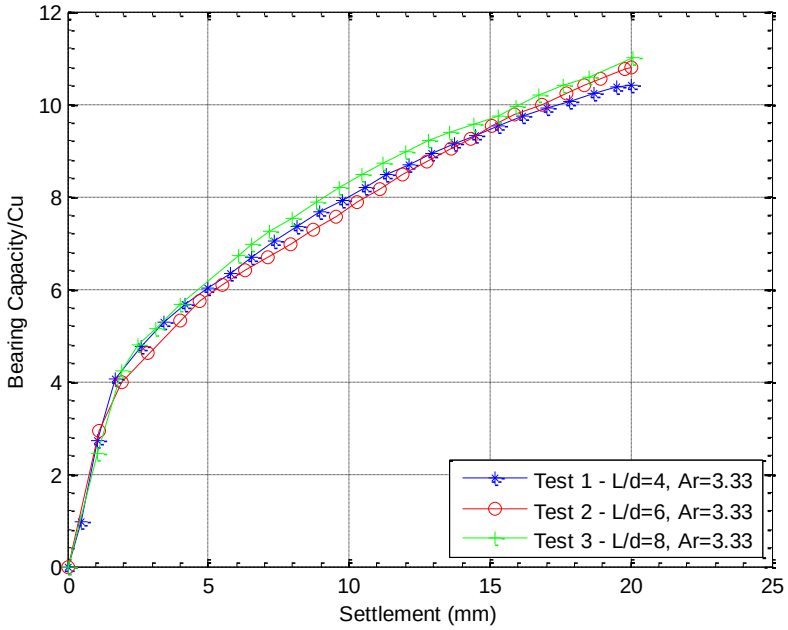

Figure 8: Load bearing characteristics of isolated stone columns

4. CONCLUSIONS AND FUTURE WORK

The work describes the use of a novel test methodology of transparent soil and laser aided imaging to visualise the generation of internal soil and column displacements. Post processing yields the magnitude of soil displacement and shear strain experienced. The potential of this technique to provide increased measurement resolution and thus greater understanding of stone column behaviour is clearly evident through the results presented in this paper. In this respect, the results show that increasing the length of an isolated column beyond L/d = 4 at a constant replacement ratio of 3.33, provides no additional increase in load capacity. In all cases the predominant failure mode observed was bulge failure. In addition, base penetration was observed in the shorter column (L/d=4) at smaller foundation displacements of 5 – 10mm, however the effect of this punching diminished with increasing foundation displacement up to 20mm, due to the prevalence of the bulging mechanism, thus bearing capacity was not badly affected. Longer columns exhibited virtually no end penetration and the internal column compression extended to a depth of approximately L/d=6. These findings are in agreement with the previously published work by Hughes and Withers (1974). Isolated columns are rarely employed in practice though, with columns usually deployed in group configurations. Further group tests are planned on both pad and strip footings and observations relating to the column zone of influence will be fundamental in understanding the complex group behaviour.

Funding for this research is gratefully acknowledged from the Engineering and Physical Sciences Research Council (EPSRC) Grant Reference: EP/G067260/1. Additional support from Aztec Oils in providing the oil material for this investigation and the Geotechncial technical staff in the Deperamant of Cicil and Structural Engineering, University of Sheffield is also acknowledged.

REFERENCES

Ballacchino,G. (2011). Evaluation of Ground Displacements During Press-Piling. Masters Thesis. The University of Sheffield.

Black, J.A. (2007). The settlement performance of a footing supported on soft clay reinforced with vibrated stone columns. PhD Thesis. The Queens University of Belfast.

Black, J.A., Sivakumar, V and Bell, A.L. (2011). The settlement performance of stone column foundations. Geotechnique, Vol. 61, No. 11: p 909 –922

Gill, D. (1999) Experimental and theoretical investigations of pile and penetrometer installation in clay. PhD Thesis, Trinity College Dublin.

Hird, C., Ni Q. And Guymer, I. (2008). Physical modelling of displacements around continuous augers in clay, Proc. 2nd British Geotechnical Association International Conference on Foundations 1:565-574.

Hu, W. (1995). Physical modelling of group behaviour of stone column foundations. PhD Thesis, University of Glasgow.

Hughes, J.M.O. and Withers, N.J. (1974). Reinforcing of soft cohesive soils with stone columns. Ground Engineering, Vol. 2, p42-49.

Iskander, M., Lai, J., Oswald, C.J., and Mannheimer, R.J.(1994). "Development of a transparent material to model the geotechnical properties of soils." Geotechnical Testing Journal, GTJODJ, Vol. 17, No. 4, December 1994, p425-433.

Iskander, M., Liu, J. & Sadek, S. (2002). Transparent amorphous silica to model clay, Journal of Geotechnical and Geoenvironmental Engineering 128, No. 3: p262–273.

McKelvey, D. (2002). The performance of vibrated stone column reinforced foundations in deep soft ground. PhD Thesis. The Queens University of Belfast.

Magued G., Iskander, P. E., Jinyuan, L., and Sadek, S. (2002). Journal of Geotechnical and Geoenvironmental Engineering, 128(3): 262-273.

Sadek, S., Iskander, M., and Liu, J. (2002) "Geotechnical properties of transparent silica." Canadian Geotechnical Journal, Vol. 39, p111-124.

Stanier, S. (2008).Modelling the behaviour of helical screw piles. PhD Thesis. University of Sheffield.

Priebe, H.J. (1995) The design of vibro replacement. Ground Engineering, Vol.28, No. 10, pp 31-37.

White, D.J., Take, W.A. and Bolton, M.D. (2003) "Soil deformation measurement using Particle Image Velocimetry (PIV) and Photogrammetry" Geotechnique 53, No.7, 619-631.

Ground improvement methods for establishment of the federal road B 176 on a new elevated dump in the brown coal area of MIBRAG

Dipl.-Ing. Johannes F. Kirstein, BVT DYNIV GmbH; Germany, jkirstein@dyniv.com
Dr.-Ing. Carsten Ahner, Landesamt für Straßenbau und Verkehr; Germany, Carsten.Ahner@lasuv.sachsen.de
Dr.-Ing. Stephan Uhlemann, MIBRAG; Germany, Stephan.uhlemann@mibrag.de
Dipl.-Ing. Peter Uhlich, CDM Consult GmbH; Germany, Peter.Uhlich@cdmsmith.com

ABSTRACT

The MIBRAG Company explores large new brown coal areas south of Leipzig in Germany. Large machines separate coal and soil directly at the surface up to 60 m deep. This is the reason to shift the existing B176 road up to 1 km in position on more than 5 km length.
The new road is built from the existing road on natural soil conditions over a large dump with up to 60 m deep mixed sand, silt and coarse clay. This fine soil will be in loose condition when the large machines are gone.
The new road on this dump is expected to settle in different ways at about 1 m in total due to the different age and thickness of the dump, the load of up to 15 m high dams and finally the rising ground water level within the next hundred years.
Controlled Modulus Columns CMC are used as rigid inclusions at the border to the natural soil and as bridge foundations in different conditions in order to guarantee small settlements. The vibration free drilling technique is necessary to work in only 1m distance to the MIBRAG production technique.
Considerable parts of the dump were treated by dynamic consolidation and dynamic replacement. This soil improvement method was used for dams up to 4 m height, partially in combination with a 3 m thick fly ash stabilized load transfer layer.
The higher dams are up to 70 m wide and 15 m high. Because of significant stability problems, 15 m deep stone columns are installed floatingly in the 60 m deep dump below the 15 m high dam with slopes of 1 : 2.
The design and the settlements were significantly optimized by the combination of the different soil improvement techniques. The calculations were additionally based and optimized on DIN EN 4094-5 Ménard pressuremeter results gained before and after the execution. Long-time measurement systems like horizontal and vertical inclinometers will control the success during the next years. First results are published in this article.

1. INTRODUCTION: RELOCATION OF THE B 176 THROUGH MIBRAG

The area south of Leipzig is characterized by brown coal mining, and with an area of 500 km^2 it is one of the largest landscape construction sites in Europe along with the Lusatian Lakeland. The natural area contains various stages of daylight mining; there are stages of exposure, of full operation and of re-integration into nature. The existing federal road B 176 between Pödelwitz and Neukieritzsch will be relocated by the MIBRAG for brown coal mining in the coming years until 2013. The first construction section has an overall length of 8.3 km. The federal road B 176 will be rebuilt by MIBRAG 5.5 kilometers on the young elevated dump of the Vereinigtes Schleenhain mine and will be handed over to the State Agency for Road and Transport.

The young mixed dump with large areas of at least 60 m and partially up to 105 m depth down to the natural soil can only be founded afloat to remain cost-effective. The connection to the existing B176 takes place on the so-called mainland area. Accordingly, the transition from the dump body that has been stratified over years to natural soil are geotechnically challenging. Another problem of the different settlement behavior results from the varying altitude of the road which goes from ground equal to 15 m above ground level. Without using ground improvement methods, different settlements of up to one meter would have to be expected.

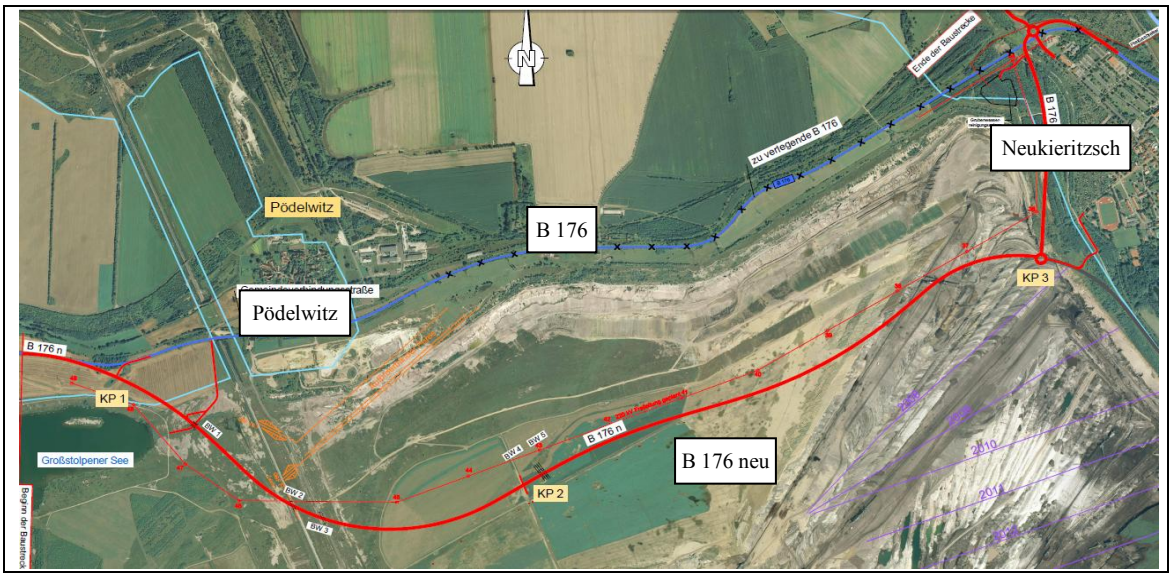

Photo 1 : old existing B176 and planned route of the new B176 [3]

For ground improvement in dam layers of up to 3 m height, mainly the intensive dynamic compaction (Dyniv) was used, while for the dams up to 15 m in height and 70 m in width, stone columns were used. In the transition zones between Dyniv and stone columns, Dyniv columns were executed as dynamic replacement. Like the bridge buildings, the transition to the natural soil was founded with the Controlled Modulus Columns - Procedure (CMC), full-displacement-columns in which the displaced soil will be replaced by non-reinforced concrete.
Soil characteristics of the young dump recorded before ground improvement are compared to those taken after ground improvement. With the help of various ground improvement methods, the reduction and stability verification were provided by using the Ménard pressuremeter with additional securities. By adjusting the ground improvement methods for the various sections, a technical and economical optimization has been achieved, thanks to the Ménard pressuremeter. The proven soil characteristics as well as the latest results of settlement measurements in the course of the embankment are remarkable.

2. SITE INVESTIGATION, GEOLOGICAL FEATURES

In central Germany, there are mainly dumps with mixed soils of different silt contents. Due to the filling technology from a great height, poorly compacted inhomogeneous rib structures were created.
The dump of Schleenhain was filled in two horizontal sections in the 1st underlying and 2nd overhead dump (see Figure 2). The 1st underlying dump has a thickness of 15 to 35 m and was built with the stacker by dumping below and above the working level by direct casting. The second dump was realized with a belt stacker by dumping below and above working level till ground level. The final eastern section has been implemented by dumping below and above working level until 2009.

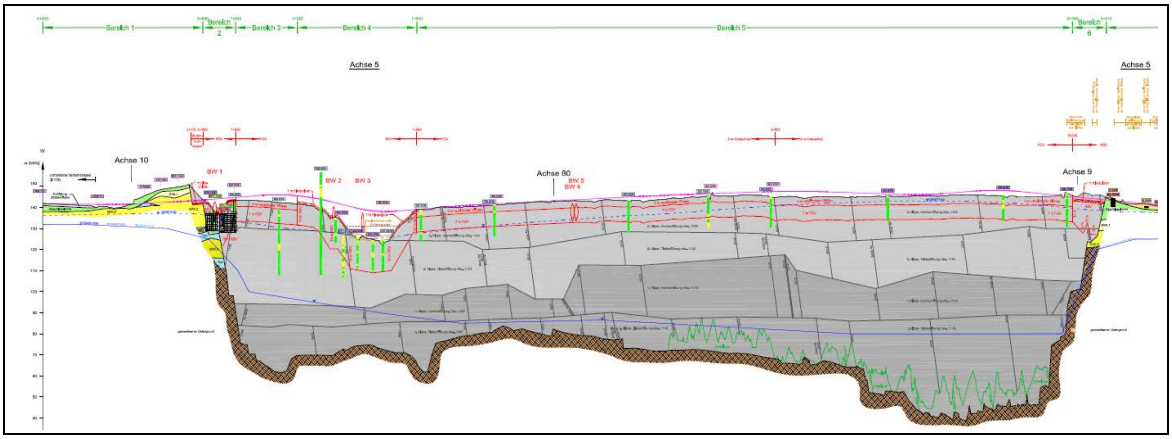

Figure 1 : Longitudinal tilt in the path field of new B176 [3]

These mixed soil dumps are much more settlement sensitive than natural soil. Especially in the upper soil layers down to a depth of 10 m, the soils are often grained loosely. A reliable assessment of the interaction between structure and subsoil is very difficult on mixed dump soil.

Photo 2 : Development of the dump Schleenhain where the B176 is built on

As a result of loose graining, or rather the inhomogeneity of material and density, the soil is different from natural formations. Even good experiences with the development of soft natural soil are not transferable to mixed ground dump [3]. The process of conveying, transporting and tipping is the reason that the dump is locally marked by extreme material and density inhomogeneities in a very confined space. The defining characteristic of the mixed soil dump is the distinctive material inhomogeneity and chaotic material structure with a fine particle fraction of 0 to 50%. Due to the cohesive fines and loose grain, there is a very strong consistency sensitivity and the risk of loss of strength due to plasticization by water ingress.

The most striking feature of a group of materials is the grain-size distribution. Due to the degradation process, characteristic groups of materials are found over large areas of mixed soil dump. The reason for this is because the natural ground is truncated, transported and tilted under constant technology. "The spatial arrangement of different groups of materials can change very quickly in the dump. Often, only areas like clusters of a particular material or group determine density [3]." In addition, strong variations of the state variables, voltage and number of pores, occur that are much stronger than those in the natural soil. Especially, the upper area of the dump is problematic. Only by overwhelming, the inhomogeneities are suppressed and the grain-structure is homogenized.

For planning the construction of the B176, a variety of soil investigations in situ and laboratory tests were realized:

Field investigation:
- old wells / ram core drilling samples
- cone penetration test CPT according to DIN 4094-1
- trenching

Laboratory tests:
- grading curves
- water content
- consistency limits
- proctor density / opt. water content

The exploration results from the dump ground show a large variation in grain size.

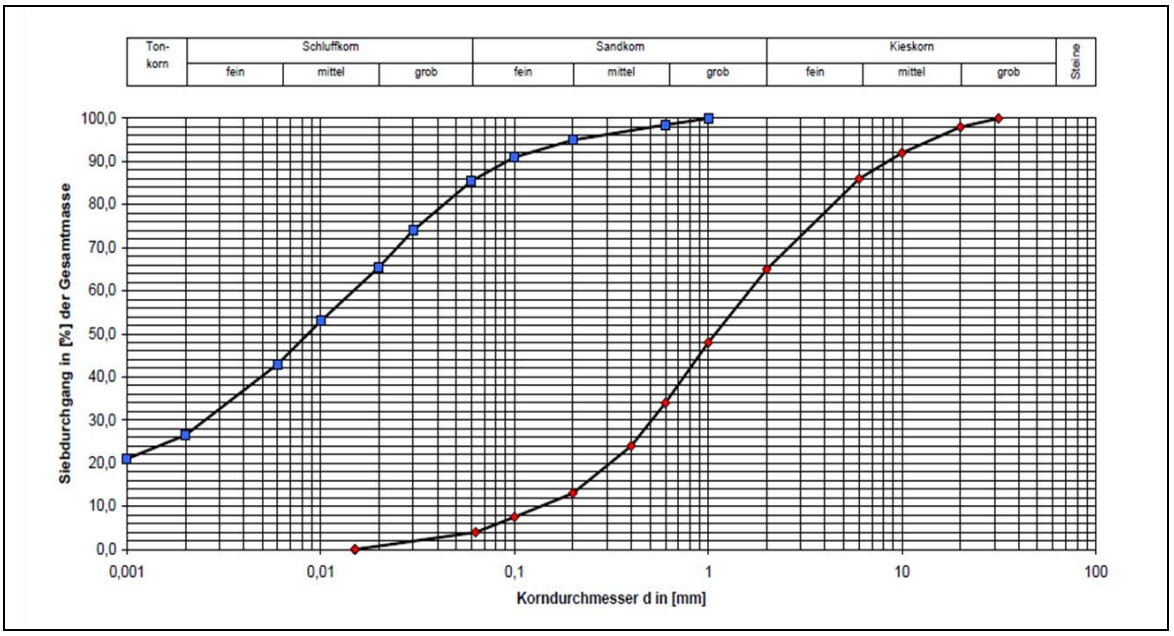

Figure 2 : Spread of grading curves of the dump soil [3]

The following fractions have been used for the assessment of ground improvement for road bases on the second, upper dump, according to geotechnical report [3] :

- 20% boulder clay
- 20% sands and gravels
- 25% tertiary clay
- 30% fine and medium sand
- 5% brown coal

Table 1: Soil properties according to the geotechnical report[3]developed by cone penetration tests CPT

	Mixed grained dump material			Non – cohesive dump material	
Depth [m]	**Stiffness E_s [kN/m^2]**	**friction ϕ [°]**	**cohesion c` [kN/m^2]**	**ϕ [°]**	**c` [kN/m^2]**
0 – 2.5	5500	11	6		
2.5 - 5		12.6	6.8		
5 – 7.5		13.7	7.5		
7.5 – 10		15.3	8.4		
10 – 12.5		16.4	9		
12.5 - 15		17.4	9.6		
15 – 17.5		18.9	10.5		
17.5 - 20		20.4	11.4		
20	5500	22	12	30	5
30	9000				
60	30000	25	12		

The outcome of this is a ratio of the geological parental material "non-cohesive: cohesive" of ~ 55 : 45. This mixed-grain dump represents almost the entire soil at the immediate mining area.
Details on the growing surface with loess and boulder-clay and silt layers of the Quaternary will not be presented here.

Currently, the groundwater level has been decreased to at least 35 - 40 m below ground-level by the ongoing drainage of the daylight mining, whereupon the relatively steeply running saturation lines of the depression cone have all developed in tilted, grown border slopes. By the year 2100, a static groundwater level should be reached after turning off the pumps at an altitude of 125 m of about 15 m significantly below the gradient and at least slightly below the lowest foundation of new dams, more than 20 m higher than now.
With wn = 10% ... 14%, the calculated current water content under the influence of dewatering is in the normal range of natural humidity. Laboratory tests showed a proctor density about $\rho Pr = 1.846$ g/cm^3, and a proctor humidity ratio about wPr = 9.9% and thus good compression options.

Cone penetration tests from the dump at up to ca. 20 m depth vary mainly in the range qc ~ 1.0 MN / m^2 ... 3.5 MN / m^2, which lead to the derivation of stiffness modules Es ~ 2 MN / m ... 9 MN / m, average = 5.5 MN, in the geotechnical report.

It is a mixed-grain dump (fine particle fraction> 20% ... 25%) in the earth-moist state because of the fine particle fraction and the storage of loose grains of mixed pseudo-cohesive soil tilting plasticized with water access. In the event of plasticization, the shear strength drops to about 50% of the baseline values.

3. METHODS OF SOIL IMPROVEMENT

The young mixed dump with at least 60 m depth to the natural soil in most areas is only to be grown economically afloat. Hugh settlement and differential settlement of the open dump will be induced because of the inhomogeneous composition and will further be increased by changing loads. The gradient is partly the same without no new off-load and in other areas dams dumped up to 15 m tall with correspondingly large loads. On-site tender for large stone columns in construction section 2 and 4 [3] has been submitted to the MIBRAG by BVT DYNIV GmbH and finally commissioned as a secondary offer based on the optimal sequence of Ménard Pressiometry subsoil improvement in the CMC, and stone column and DYNIV-process.

3.1. RSV (stone columns)

Photo 3: Leader-guided and free-riding-on-the-device technology for stone columns B176

The known method of stone columns was uniformly provided in the tender for the difficult transition from the growing areas at the dump edge to the dump. Similarly, stone columns were executed at the high dams to improve the stability of the installation of material with a correspondingly high friction angle required. In addition of demonstrating the stability of the improvement by the required friction angle a mean modulus was 15 MN/m over 15 m execution depth has been demanded [3].

3.2. PMT - pressuremeter tests (Ménard pressuremeter)

The soundings developed by Louis Ménard, and named after him, are known worldwide as the "Ménard pressuremeter", and are considered a valuable procedure in the European Standards EN anchored by 4094-5 [3] and, as in the ISO / FDIS 22476-4:2009 [10][3] explained in detail.

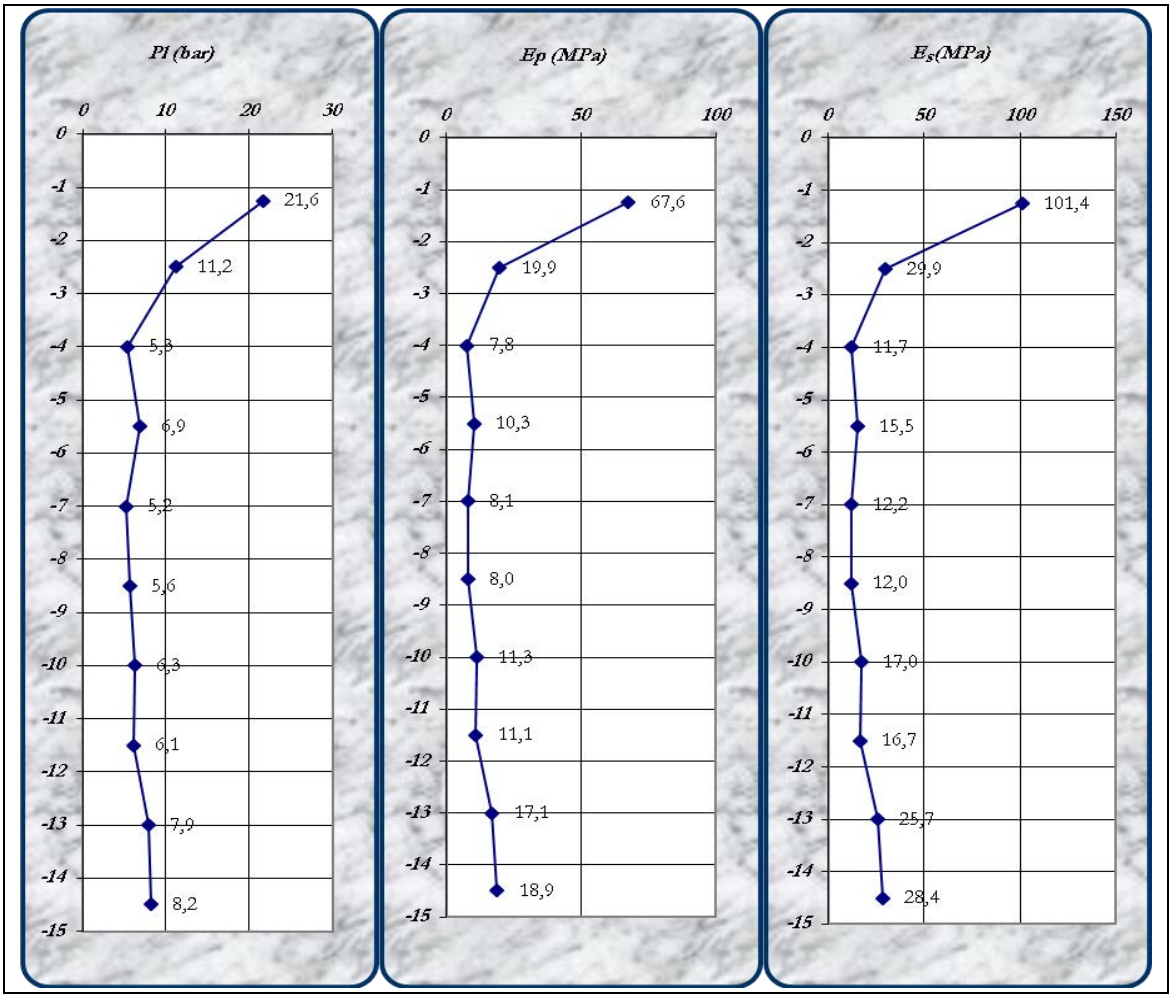

Figure 3: Pressuremeter test results of section 15, before soil improvement with representation boundary pressure Pl, Ménard modulus Ep and stiffness modulus Es on the depth

The Ménard pressuremeter method, which is unfortunately quite costly, offered the following advantages in the dump Schleenhain when compared to the cone penetration tests CPTs:

- Directly opposed to the CPT destructive sensing pressure probes at the tip of small
- Cross-sections, the pressuremeter sensor uses the total volume of soil around the measuring cell of a much larger probe.
- Unlike the CPTs, the PMT method shows reliable correlations between measured values and stiffness modules not only in cohesionless but also in cohesive formations.
- For artificial and unconsolidated fillings, the limit pressure and Ménard module are reliable characteristics of their relationship and the stiffness modulus is determined.
- The protracted consolidation-process after the production of vibro-techniques like stone columns must not necessarily be waited for.

Due to these advantages of the Ménard pressuremeter, a comprehensive addition supplement of preliminary exploration was commissioned by the building owner Mibrag.

With the help of Ménard pressuremeter tests, the design of the stone columns has been optimized and more than twice the initial modulus between the columns has been taken into account. The improvement between the stone columns was also performed with the pressuremeter and is explained in detail along with the results.

3.3. CMC - Controlled Modulus Columns

The CMC method is well known but sometimes confused with reinforced concrete piles. The CMC are a ground improvement method. CMC are accomplished non-reinforced and are arranged in a two to three times denser grid than reinforced concrete piles and never are they directly linked by steel to the structure. A major advantage of this method is the vibration-free production of these columns. So, this method can be executed for example within a city close to adjacent buildings or on vibration-sensitive structures [7]. The CMC are manufactured as a full-displacement method under high torque and high activation energy. They ensure a very high degree of soil improvement. This is due to the pre-compaction of the soil, which results from the full displacement without material conveying. Along the special concrete C 35/45 XA3, which has been injected with high pressures and is surrounded by compacted soil, there exists a significant additional skin friction composite. With the Controlled Modulus Column (CMC) process, a particularly low level of incorporation into the soil is workable because reliable for the detection of the external load by means of load test results, particularly high values for peak pressure and skin friction are shown. The usual length of a CMC column is between 3 and 18 m. In exceptional cases, lengths of up to 25 m are possible.

Because of its controlled modulus, the CMC column can be used in very different soils, including very soft plastic and organic soils with Cu values significantly less than 15 kN / m². This variability allows for a very large spectrum of the CMC method. The method has extensively been described in publications by University of Freiberg (2005 [5]), University of Braunschweig (2007 [6][8]) and Technical University of Munich (2009 [8]), and was applied to the foundation of bridges BW 1 and BW 2 on the B176 due to convincing results from load tests executed in advance in addition to the dam foundation. The publication by CMC – Bauen im Bestand [7]with the references in rail and road use was the basis for the use of this method directly on the running belt conveyors.

3.4. FWC falling weight compaction and DYNIV - Intensive Dynamic Compaction

By drop weights (m = 10 – 30 t) the ground is compressed at the drop weight compression FWC. The grid spacing depends on soil type and desired compression. In general, this distance is between 3 to 15 m.
The drop weights are dropped repeatedly to the ground which has to be compacted. The impact of the falling weight produces a compaction of the soil. Here, the impact rate acts in accordance with the same parameters as the grid spacing. The number of blows per compaction point at the falling weight compaction is also pretended. In the Intensive Dynamic Compaction DYNIV the masses of the drop weights are increased up to 200 t and the desired compressions are calibrated on large test fields including the pressuremeter. Also a real free fall is possible with the DYNIV process. This, for example, is described in the publication [11][3].
Partially saturated and saturated soils can be compacted by this method. The effectiveness decreases in cohesive soils with high water content. So the applicability of the method is largely determined by the existing soil.
In construction sections 3 and 5 with flat dams, the FWC was accomplished at a depth of 3 to 5 m below ground level. It was intended that two passes be made with four strokes of a 20 tons of weight from a height of 20 meters. The third pass should generate a harmonization of the surface after the distribution of masses. After some discussion, the third FWC-pass should be replaced by a double drum roller in six production steps. Because the cohesive shares were higher than predicted in the geotechnical report [3] at last the loose upper layer of 1 m minimum, thickness was prepared with ash on hit cone level and fitted in a thickness of 30 cm. So an E_{V2} of 45 N / m² could be ensured at the working level of the ash stabilization. The overlying layers were also fitted with improved ash. This created a stable floating bar. Differential settlement cannot be beaten, so the new road can be built upon risklessly. The executed economic process suites particularly in areas with low load growth and may well be used in line construction.

3.5. Dynamic Replacement (DR)

The Dynamic Replacement is a further development of intensive dynamic compaction. It is suitable for soft, cohesive and organic soil formations. The resulting blow-piles of the intensive dynamic compaction are filled with gravel or coarse material and are afterwards compacted by further blows. The result is comparable to the stone columns, for which the grid and especially the diameter of the is substantially larger. Accordingly, Dynamic Replacement was used as high transition between the stone columns and FCW.

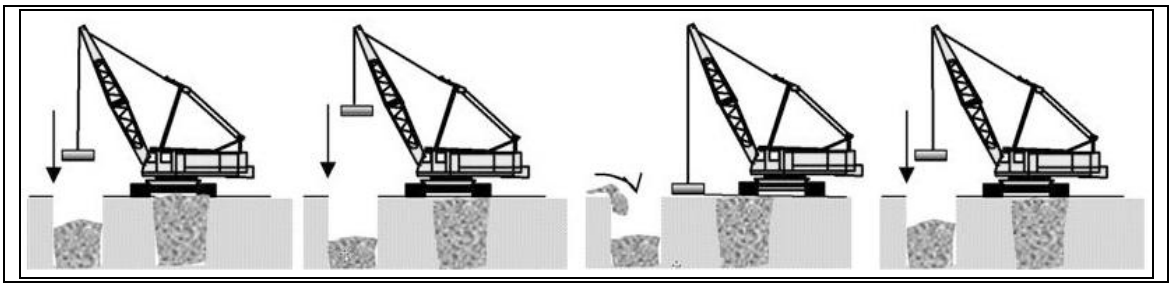

Photo 4: Dynamic Replacement

4. PLANNING

The connection of the new B176 to the old B176 takes place on the so-called mainland area. This is characterized by the transition from natural soil towards the central part of the route on dump area. From this point of view it will become a geotechnical challenging transitions in the route. Other settlement issues are arising from the different altitudes of the main road and the associated bridging of deep terrain by a causeway. Without the use of specially adapted ground improvement methods reductions of up to one meter would be expected. Under the assumption of three buildings to be established, so that different levels of power and possible tilting of large differential settlements a special sequence of ground improvement methods was necessary.

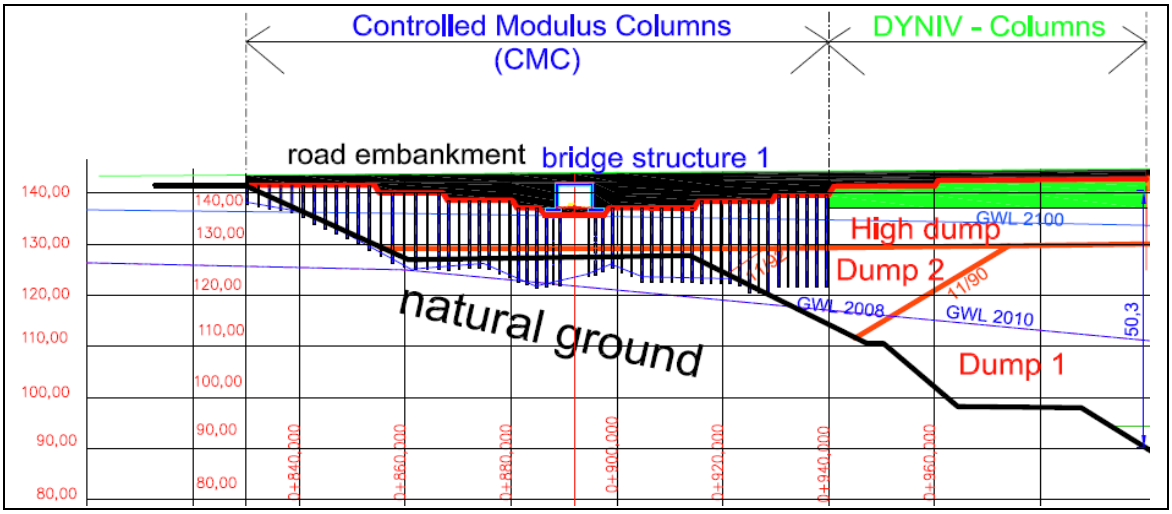

Figure 4: Principle section along the line in the transition from the natural ground to the dump

The following detailed building phase 2 includes the floating chartered buildings structure 2 and 3. The tunnel structure 2 above the belt conveyor is founded by the vibration-free CMC method. For the rising to an about 15 m tall dam with a 70 m wide bottom the stone columns were used.

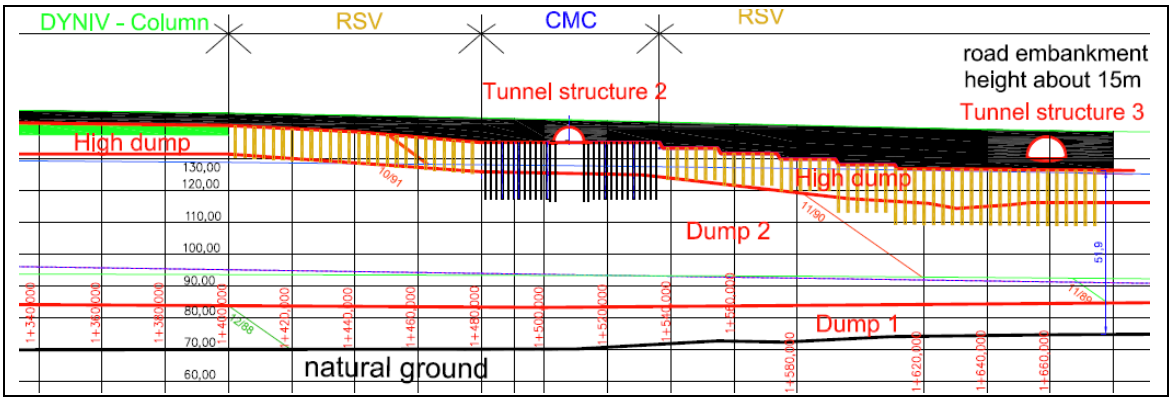

Figure 5: Principle section along the line in the transition from the natural ground to the dump

The following picture gives an overview of the different improvement techniques carried out in the area on the belt conveyors BW 2. The apparent from the longitudinal section levels showed a height difference of 1.75 m respectively between the different working platforms.

Photo 5 : Ripping holes for the two devices RSV, CMC directly on BW2 and PMT in front

The stone columns reach 10 m to 15 m deep. The improved soil characteristics were determined in relation to the stresses according to the next figure: by the load below the maximum height of the dam a larger improvement in the characteristic values can be achieved than on the parts with lower stresses, where a less optimal angle of friction by installed gravel was taken into account. The friction angle of the gravel was used to check with a large scale shear tests.

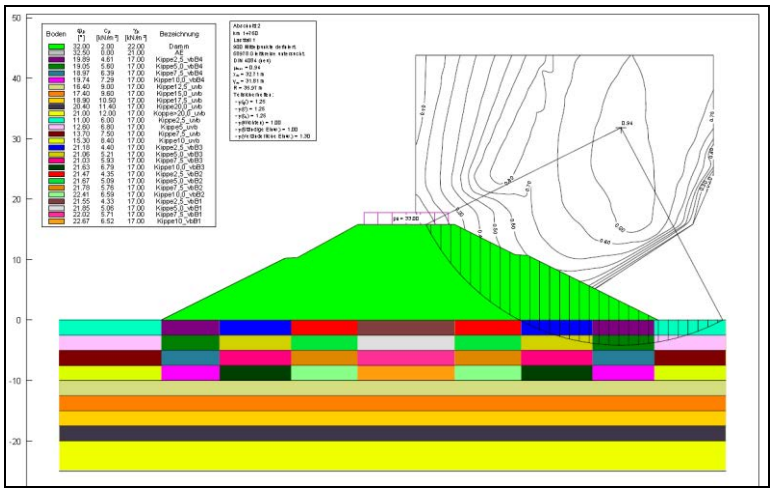

Figure 6: Stability analysis taking stress-dependent soil parameters into account

5. RESULTS OF THE SOIL IMPROVEMENT

Here we show some exemplary results for the stone columns, determined in experimental fields and explorations before and after near the highest dam-cross-section for the derivation of the following calculation model.
The Menard pressuremeter explorations (DIN 4094-5) were performed centrally in the columns and exactly between, according to the following photographs.

Photo 6 : Execution of the Ménard pressuremeter

Due to the compaction at optimum proctor water content, most often an improvement between the columns with the factor of 2 was measured. Together with the mean stiffness modulus of Ec = 100 MN/m^2 in the columns with at least 70 cm diameter, this results in a design relevant modulus of Es =30 MN/m^2 for the improved ground.

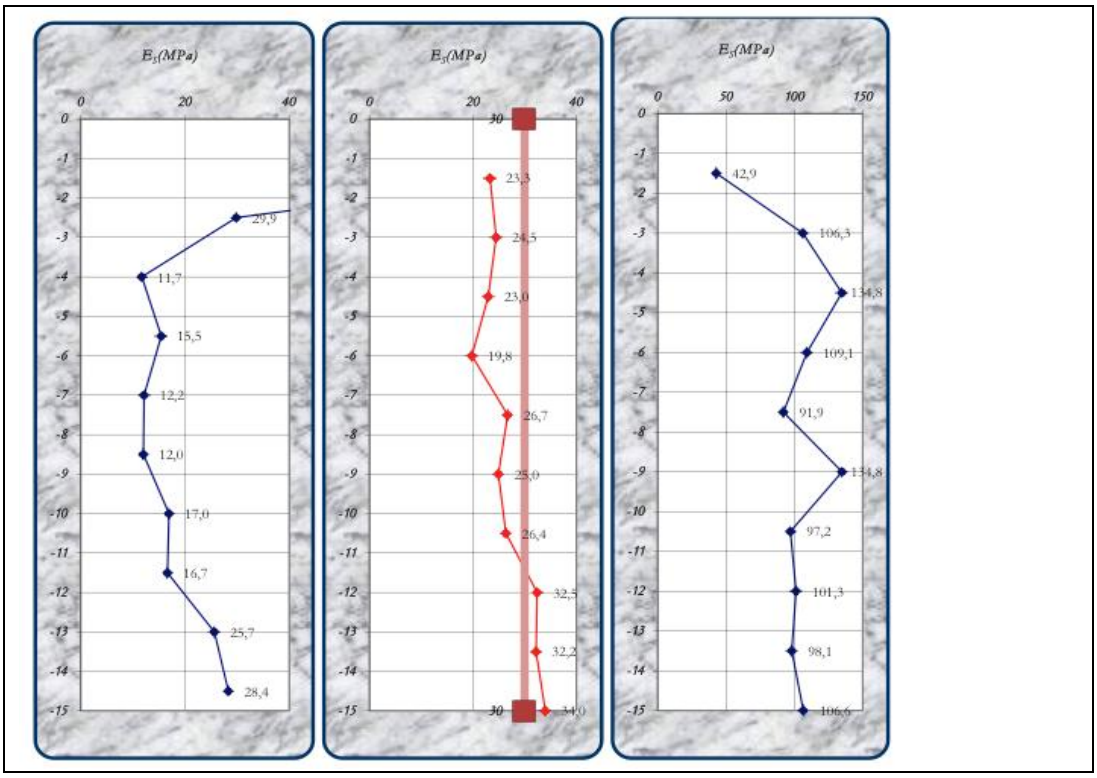

Figure 7 : Results from the preliminary measurements (left panel), from in between the columns (right panel), and within the columns plus the derivation for the determined design relevant rigid module Es = 30 MN/m2 (central panel)

The remarkable doubling of the stiffness modulus in the grid centred between the columns was made possible by the optimum Proctor water content of the deposits of the mining ground, and also by the powerful V23 vibrator. A transfer of these high values to other constructions projects without these optimal conditions is not possible and it is highly recommended to use a project-specific calibration with test fields and the Ménard pressuremeter.
Even the following penetration tests between the columns show a doubling of the values. It should be noted that the starting values were derived too low. In relation the tendency of improvement of the CPT`s is corresponding to the Ménard pressuremeter. Absolute values of the stiffness modulus in cohesive soils can be measured only with help of additional calibrations like pressuremeter and oedometer tests on undisturbed soil samples.

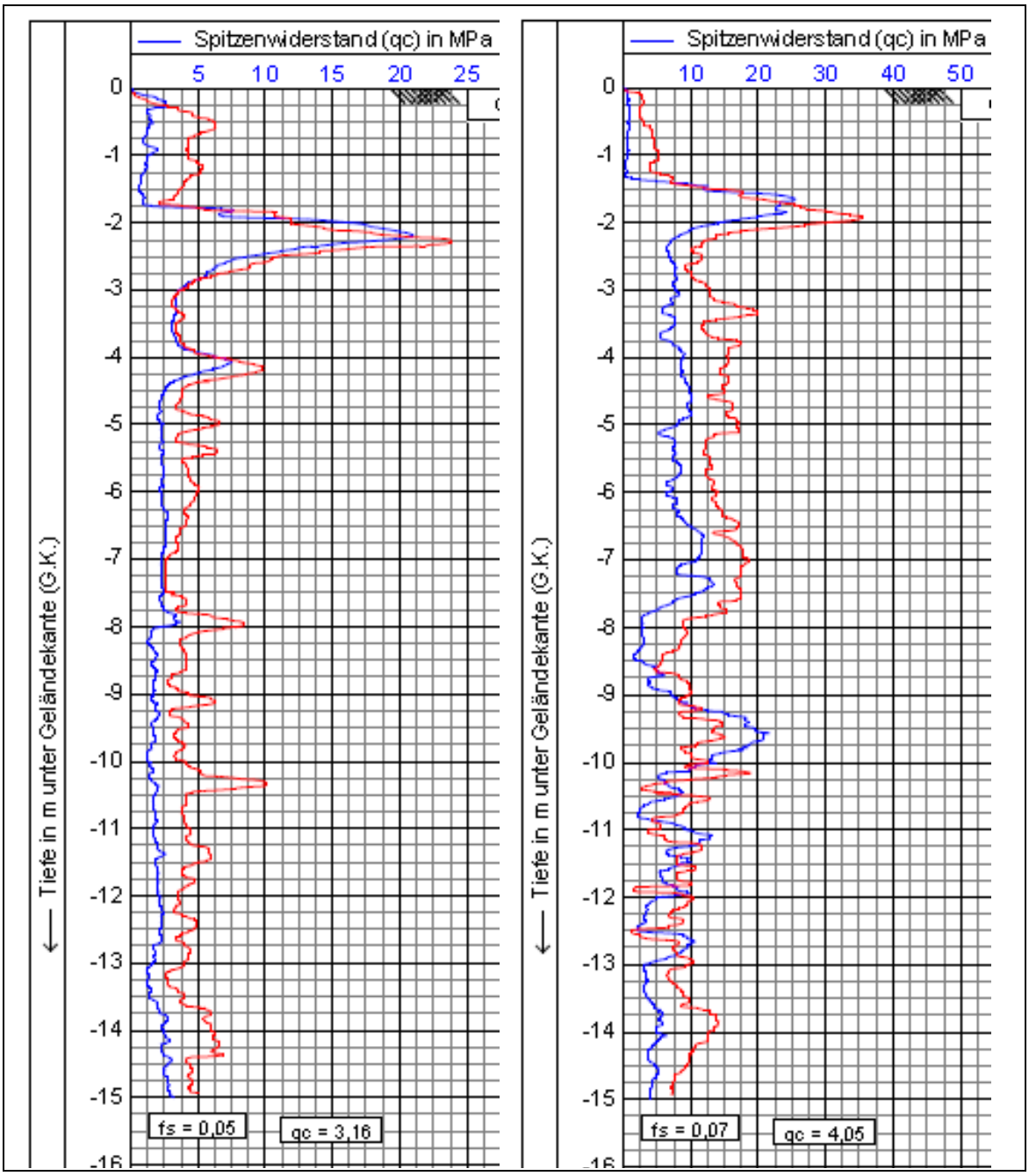

Figure 8: Pressure probe by comparison before and afterwards the vibro between the columns

6. NUMERICAL SETTLEMENT FORECAST

The settlement analysis and stability calculation is based on the creation of a geotechnical calculation model. Based on the geological conditions, the hydrological data, and mechanical parameters of the soil which have been determined by the numerous field trails and laboratory tests, this model was developed in the course of a Diploma thesis.[9]
According to the planning documents, the settlement forecast was created with the PLAXIS software.

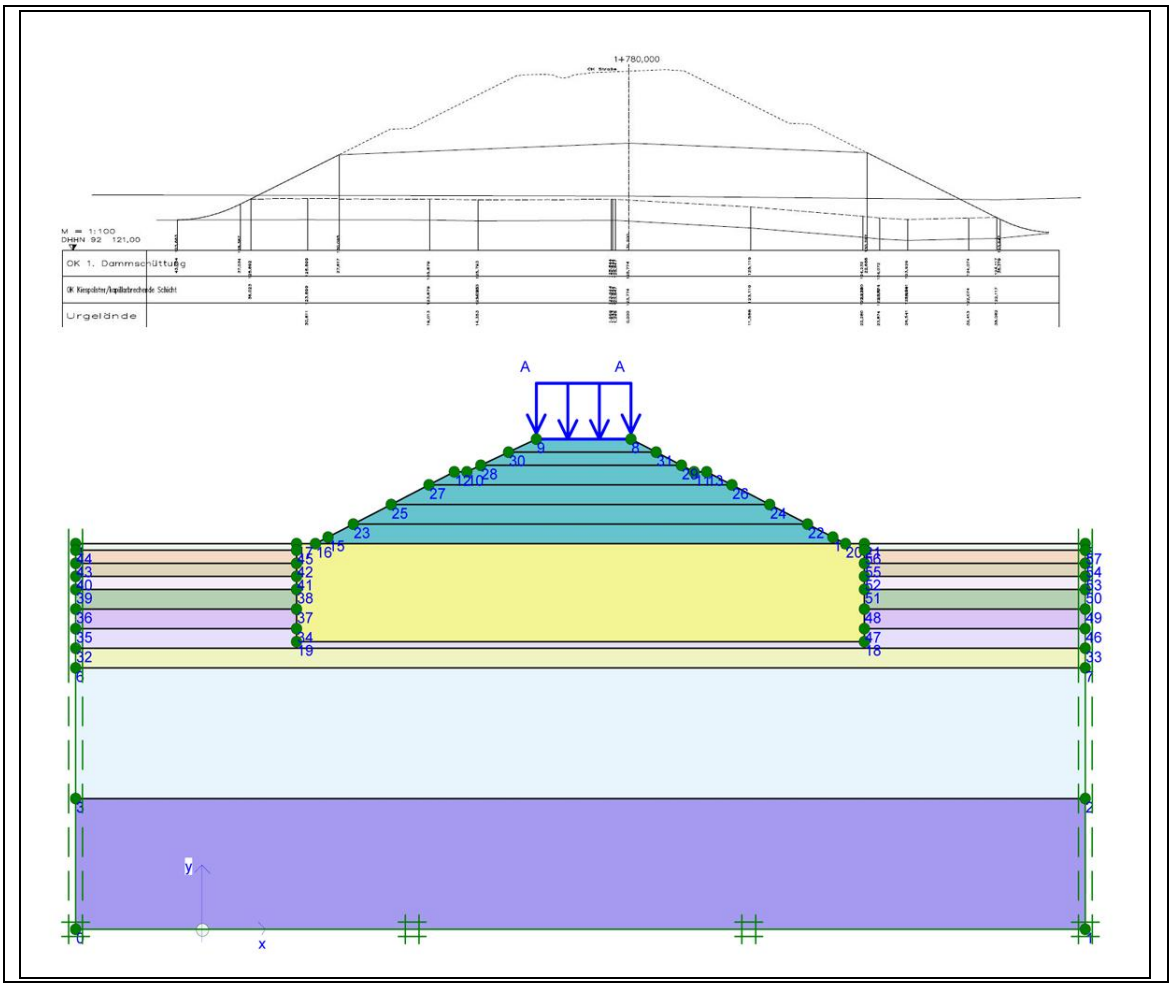

Figure 9: CAD model and PLAXIS model

The layers of the dump from ground level up are divided into three 20 m thick layers. The first 20 meters from the side of the dam at ground surface contain the layer structure of the graded soil characteristics of the dump, shown in Table 1.
The improvement depth by stone columns below the dam holds a depth of 15 m. This improved ground beneath the dam is grouped with the averaged factor of the measured ground improvement E_s = 30 MN/m^2.

The natural soil begins after two further dump floor layers with a depth of 20 m at the lower model domain.

As part of the thesis [9], the highly variable results of the finite element calculation from the linear-elastic, perfectly plastic "Mohr Coulomb model" and the elasto-plastic "Hardening Soil model" of PLAXIS have been compared regarding the applicable constitutive equations.

Here we present the results of the Hardening Soil model, where the stiffness modules for the settlement forecast for the next load level are sequentially increased after each load level according to oedometer test results from the dump bottom.

Each of the following six beds corresponds to a dam height increase of nearly 3 m with corresponding settlements. On the one hand, these settlements decrease with each dumping due to a smaller width and with it decrease the loads. On the other hand, not inconsiderable settlements of the dam itself are added (see Figure 11).

Station	1+780 HS 30
Steps of the Deposit	Ground Settlement [cm]
1	10
2	10
3	10
4	10
5	5
6	5
Traffic	6
Total Ground Settlement	56

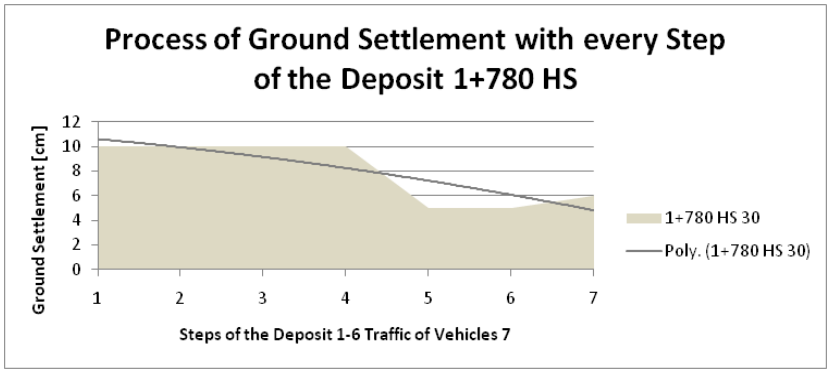

Figure 10: Representation of the predicted total settlements with Plaxis calculation section of the maximum embankment height

Based on the calculation with PLAXIS and experience with sand interlayers in mixed soil dump, it is hoped that the settlements occur mostly after a short period during the construction of the dam and will quickly subside.
The expected results of the Hardening Soil model at the highest altitude of the dam at about 15 m, with some 50 cm settlement, need to be compared to the double ratio of approximately 1 m in the forecast of Mohr Coulomb.

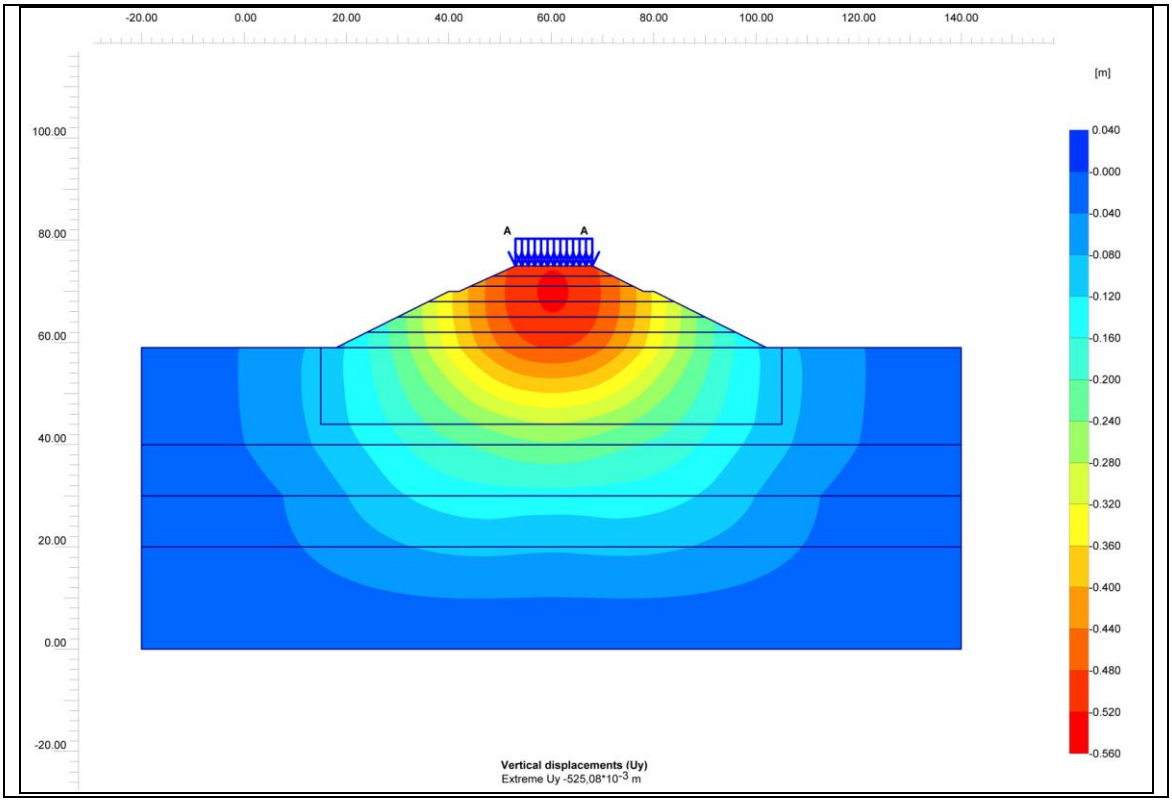

Figure 11: Total reduction in the forecast with PLAXIS HS cross section maximum dam height

7. OBSERVATION METHOD: FIRST RESULTS OF THE MONITORING

Seven cross-border horizontal inclinometers were installed below the dam and three vertical inclinometers were installed at the dump bottom with highest altitudes along the construction route. The measurements are performed during the earth work phase of constructions for producing of the nearly 15 m tall dam according to the following definition: Every 3 m of height growth of the dam and immediately after reaching the final height and then every 3 month.

The following presented cross-section measurement with first results is located on the cross-section of the proposed settlement forecast.

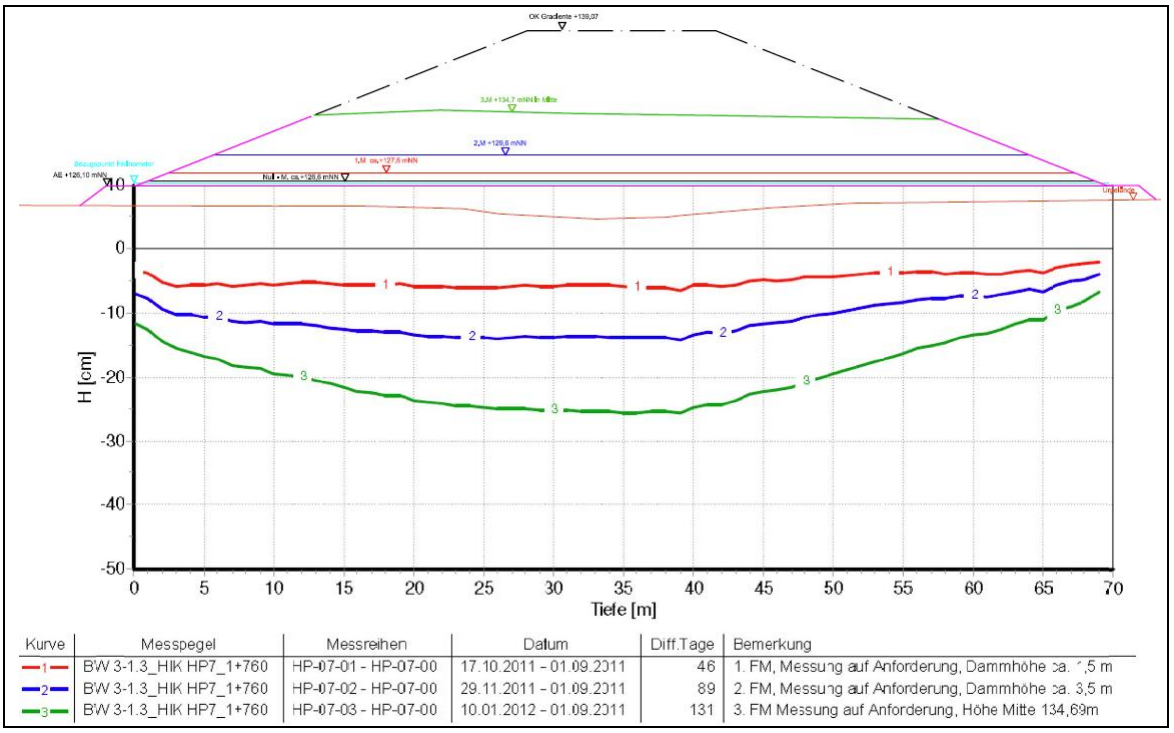

Kurve	Messpegel	Messreihen	Datum	Diff.Tage	Bemerkung
1	BW 3-1.3_HIK HP7_1+760	HP-07-01 - HP-07-00	17.10.2011 - 01.09.2011	46	1. FM, Messung auf Anforderung, Dammhöhe ca. 1,5 m
2	BW 3-1.3_HIK HP7_1+760	HP-07-02 - HP-07-00	29.11.2011 - 01.09.2011	89	2. FM, Messung auf Anforderung, Dammhöhe ca. 3,5 m
3	BW 3-1.3_HIK HP7_1+760	HP-07-03 - HP-07-00	10.01.2012 - 01.09.2011	131	3. FM Messung auf Anforderung, Höhe Mitte 134,69m

Figure 12: first measurement results: bulk layers and color coded settlement events

The actual measured values of the monitoring in all cross sections correspond in order of magnitude to the predicted settlement and underline the accuracy of the Ménard pressuremeter and their determent soil parameters, which were used for the finite element model.

8. SUMMARY

The construction of roads on mining areas requires close cooperation between miners, engineers, geotechnical engineers and contractors, as the mining technical characteristics, requirements in road construction and geotechnical characteristics must always be brought into line and finished with high-end quality.

A very comprehensive site of investigation is essential in dealing with dump soil. The Ménard pressuremeter brought significant findings throughout the additional preliminary survey and also an experience for cost optimization in the interests of the client MIBRAG. Based on the findings and an optimized pre-planning process, the BVT DYNIV GmbH was contracted with the alternative solution, which also received the consent of the client MIBRAG and the later acquiring department of highways.

A technical and economic optimization was achieved by additional soil Ménard pressuremeter investigation and adjusting the ground improvement methods to the respective sections. With the help of various ground improvement methods, higher than contractual standards concerning settlement reduction and stability, were performed successfully with additional securities.

The high quality of the construction with stone columns, dynamic replacement and CMC-columns was documented not only in foundation with the usual protocols of the manufacturer, but also tested regularly during the construction phase by the Ménard pressuremeter.

The settlement calculations were based on the Ménard modulus and demonstrate a significant increase of quality. Later observation methods confirm the predictions with first measurement during the growing dam.

REFERENCES

[1] *Lausitzer und Mitteldeutsche Bergbau – Verwaltungsgesellschaft mbH, 1999, Schlussbericht – Bauen auf Mischbodenkippen des Braunkohletagebaus im Mitteldeutschen Revier. Senftenberg.*

[2] *Buja, H.-O., 2009, Handbuch der Baugrunderkennung – Geräte und Verfahren. Wiesbaden.*

[3] *G.U.B Ingenieur AG, 2010, Ersatz der Bundesstraße B176 zwischen Pödelwitz und Neukieritzsch, Baugrundgutachte, Dresden.*

[4] *DIN Deutsches Institut für Normung, 2001, DIN EN 4094-5: Bohrlochaufweitungsversuche.*

[5] *Kirstein, J.F.; Chaumeny J.L., 2005, Ein neues Verfahren zur Bodenverbesserung: CMC (Controlled Modulus Columns) aus Frankreich. Veröffentlichungen des Instituts für Geotechnik TU Bergakademie Freiberg, Heft 2005-2, Freiberg.*

[6] *Meyer, N.; Emersleben, A.; Kirstein J.F., 2007, Probebelastungen von CMC-Säulengruppen – Einfluss der Lastverteilungsschichtauf die Beanspruchung des Untergrundes und der Säulen. Pfahl – Symposium 2007, Institut für Grundbau und Bodenmechanik, TU Braunschweig.*

[7] *Bank, M. von; Kirstein, J. F., 2010, CMC-Gründungen im Bestand - Ein innovatives System zur Bodenverbesserung für höchste Anforderungen. TU Graz, Gruppe Geotechnik, Gratz.*

[8] *Meyer, M.; Emersleben, A.; Tietjen K.; Kristein J.F., 2009, Lastverteilungsschichten aus Geozellen über CMC-Säulen. 11. Informations- und Vortragsveranstaltung der Fachsektion Geokunststoffe der Deutschen Gesellschaft für Geotechnik e.V. (FSK-GEO), München.*

[9] *Vogel, S., 2011, Setzungsprognosen und Monitoring beim Neubau einer mit unterschiedlichen Bodenverbesserungstechniken auf einer jungen Kippe gegründeten Bundesstraße. Diplomarbeit, Dresden.*

[10] *ISO/FDIS 22476-4:2009, 2009, Geotechnical investigation and testing – Field testing – Part 4: Ménard pressuremeter.*

[11] *Chaumeny, J.L.; Hecht, T.; Kirstein, J.F.; Krings, M.; Lutz, B., 2008, Dynamische Intensivverdichtung (DYNIV®) für die Kreuzung eines aktiven Erdfallgebietes im Zuge der Bundesautobahn BAB A 71. VERÖFFENTLICHUNGEN des Grundbauinstitutes der Technischen Universität Berlin, Heft 42, Berlin.*

[12] *EIBS GmbH, 2010, Planfeststellungsunterlage zum Ersatz der Bundesstraße B 176 zwischen Pödelwitz und Neukieritzsch, Bauabschnitt 1 (unpublished).*

[13] *EIBS GmbH, 2010, Ersatz der Bundesstraße B 176 zwischen Pödelwitz und Neukieritzsch, Ausschreibung RSV im Bereich 2 bis 4.*

Rigid inclusions in combination with fast wick drain consolidation as soil improvement method in very soft and fat northern German clay

Dipl.-Ing. Johannes Kirstein, BVT DYNIV GmbH, Germany, jkirstein@dyniv.com
Dipl.-Ing. Niels Wittorf, Ingenieurbüro Dr. Lehners und Wittorf, Germany, wittorf@geo-technik.com

ABSTRACT

Large areas nearby the northern sea are nearly flat and in their elevation shortly above or under the sea level. Soft soil of silt, clay, mud and peat reach between five and twenty meters from the surface, before glacial sands are following.
In the German example of an new road crossing with 1.5 to 7.0 m high dams nearby the Danish border especially soft clays were found 13 to 20 m deep below sea level. The undrained shear strength of the clay varies between 7 and 20 kN/m². The water content was almost 100 % and the organic matter below 6 %. The consolidation coefficient Cv < 0.3 m²/year demonstrates a significant fat clay which requires long time or small grid of vertical drains for consolidation. Due to stability calculations the smallest grid of vertical drains with only 0,5 m distance were installed in the part of the highest dam, which were built in three load steps, each time waiting for 60 to 80 % consolidation degree before loading the next step. Even using 600 kN/m geogrids totally around 150 cm vertical settlements and around 20 cm horizontal deformations in each direction were measured throughout one year of monitoring.
These deformations were too much for the existing and running highway in the middle of the new projects. So CMC as rigid inclusions were installed up to 22 m deep with different load transfer platforms on top. In order to secure the installation process of the rigid inclusions additional vertical drains were installed in the soft soil before. During the full displacing CMC drilling process an equivalent amount of pore water flew through the drains within the next hours in the areas of unconsolidated clays. Within the first half year the rigid inclusion construction had less than 2 cm deformation, nearly nothing compared to the wick drain consolidated parts of the project.

1. INTRODUCTION AND DESCRIPTION OF THE PROJECT

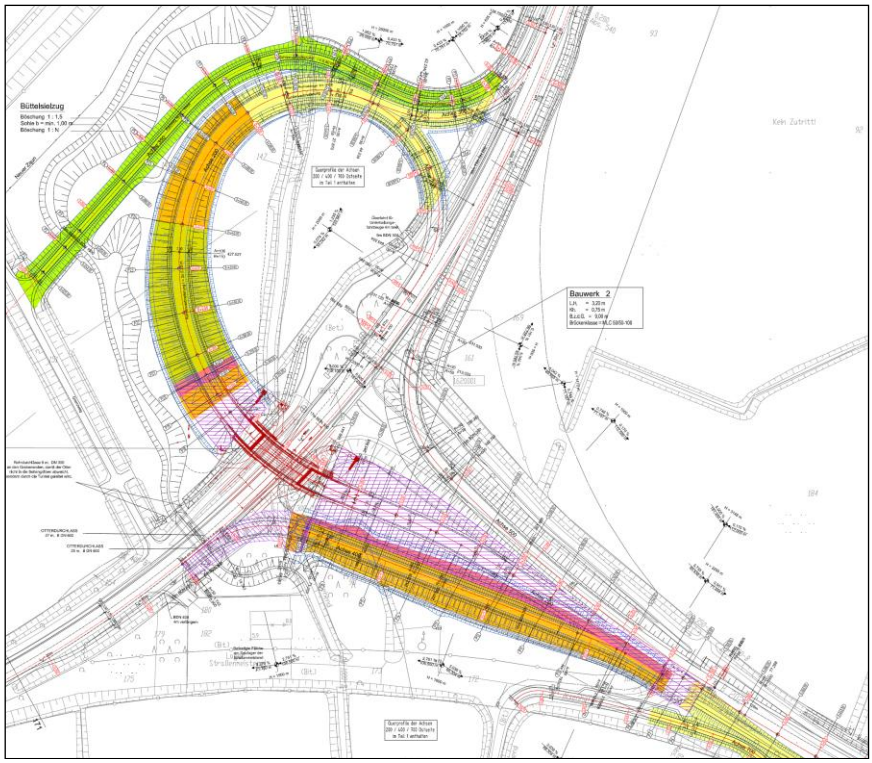

Figure 1: project overview: crossing highways B5 and B202 (CMC close to bridge and coloured areas with vertical drains and preloading)

The existing westcoast highway B5 near the German city of Husum will be extended from two to three lines in the future in order to take more traffic fluently. The crossing between B5 and B202 was prepared by the following bridge project with high dams on the unconsolidated soft soils, typical at the flat costal region near the north sea.
All traffic constructions bring new loads in form of dead- and live-loads to these soft soils. Without soil improvement methods large long-time settlements are following, which cause often damages to the road construction.
The traffic on the highways B5 and B202 in the site had to continue during the construction period without additional stability risks or settlements, especially when the 1.5 to 7 m high dams are built directly besides the traffic. There are different stages to look at, but we will focus only on the western part with the highest dam nearby the bridge.

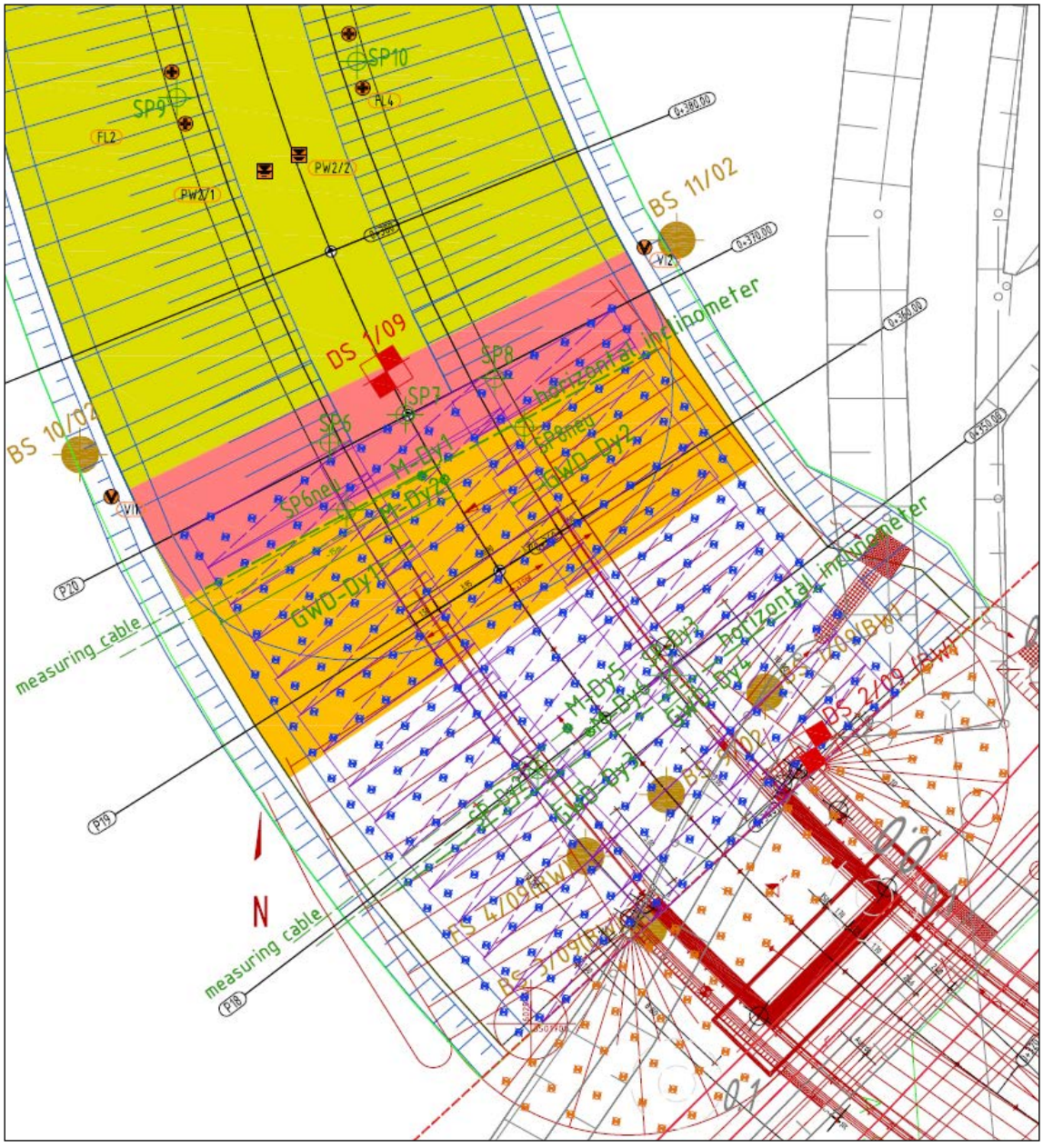

Figure 2: detail of the highest dam west with the bridge abutment over the highway B5 (CMC close to bridge and coloured areas with vertical drains and preloading)

Due to stability and settlement calculations the foundation took place with the following steps in the workflow according to the figure 3 below:

1. Installation of vertical drains in different grids from a one meter thick sand working platform.
2. Preloading with three load steps with a distance of 30 m security and working space from the bridge and existing highway B5. (A)

3. The measured settlements of the consolidation process in figure 8 fit to the given predictions according to figure 5. An additional strong geotextile layer of 600 kN/m short live strength between dam and vertical drains had not much influence on the vertical inclinometer results with 27 cm of deformation in figure 9.
4. After waiting for 1.3 m settlement according to figure 8 a part of the dam and preload was temporarily rebuilt in order to install the controlled modulus Columns CMC. (B)
5. The preload was brought back to the border of the foundation systems between CMC and vertical drains in order to optimize the settlement behaviour.(C)
6. Deep foundation of the bridge took place on rammed concrete piles with additional surrounding sockets in the soft soils.
7. The CMC were installed between the rammed piles afterwards free of vibrations. [1]

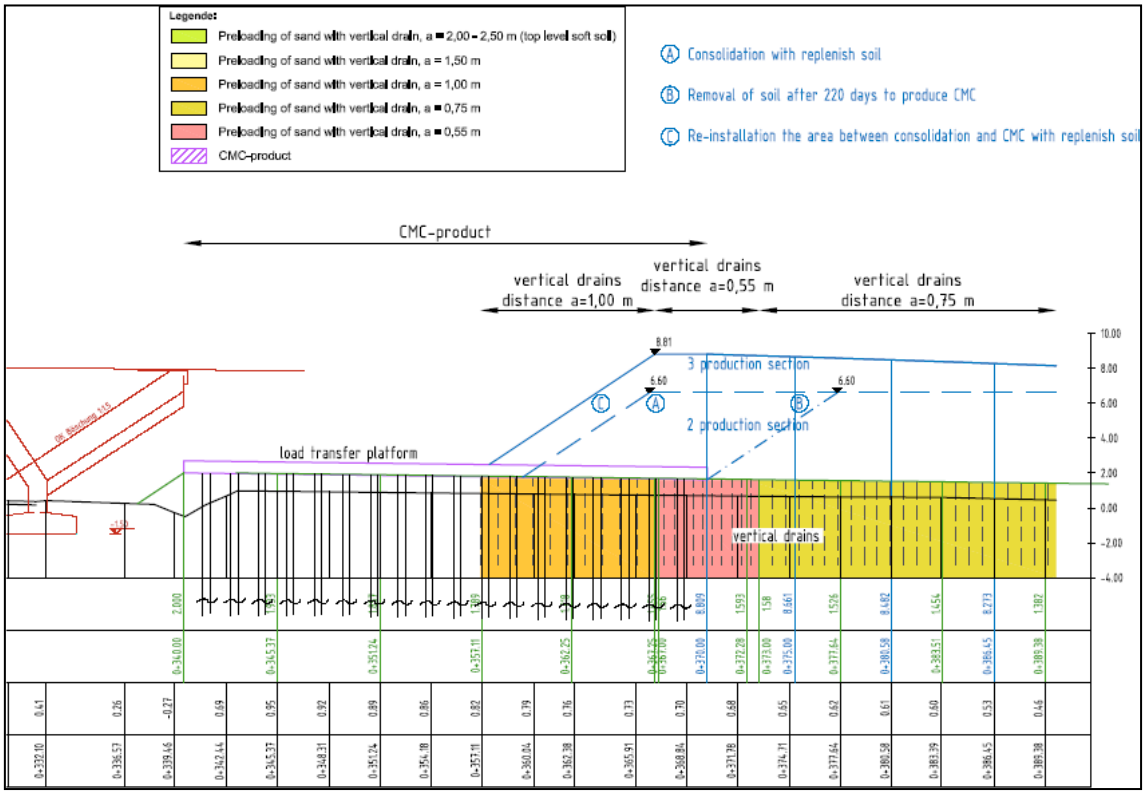

Figure 3 : steps of consolidation and construction

The workflow with different steps was necessary because of stability calculations and the wide influence of the settlements during the consolidation. The CMC brought the following advantages:

- short time of execution just in time
- the vibration free technique allows to work close to the piles of the bridge
- The settlements of the dam foundation on CMC with a stiff load transfer layer corresponds to the bridge abutment

2. SOIL-PARAMETERS

After the first part of soil investigations with several borings (BS) and cone penetration tests (CPT) it was clear that there was a problem of stability and consolidation time due to the almost fat clay in the upper soft soil layer. The project can be described with two layers of soft soils divided by a loose sand layer in between. This package reaches 13m up to 22m in the deepest parts from the surface.
The vane tests in the soft soil are the results of shear vane tests multiplied with factors of 0.5 to 0.65 linked to the plasticity according to Bjerum standard DIN 4094-4, Part 4[2]. Additional to the standard test of water contend, organic matter and plasticity index several load-settlement tests were executed.

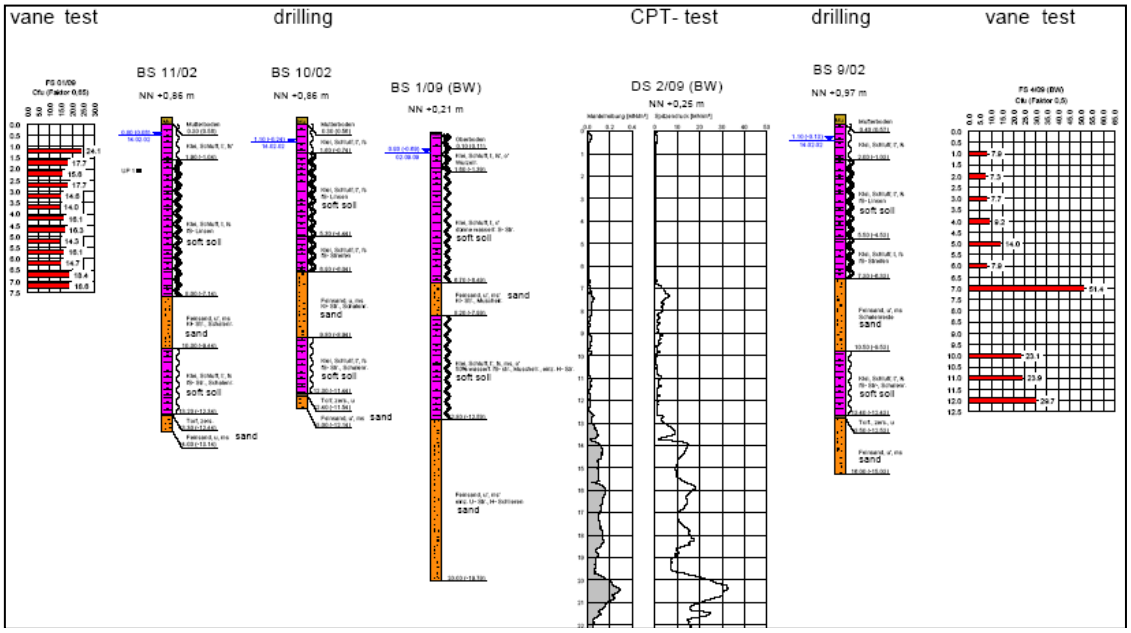

Figure 4 : boring, cone penetration test and shear vane test in the detail area bridge west

The vane tests show an undrained shear strength of Cu = 6 to 8 kN/m² near the bridge and an undrained shear strength of Cu = 12 to 20 kN/m² in other parts of the project. This was one more reason to take a CMC foundation nearby the bridge in the area of the lowest undrained shear strength. According to this decision and the results of soil investigation and laboratory the geotechnical engineers could assume an undrained shear trength of Cu = 12 kN/m² in the coloured vertical drain areas. The representative soil parameters for the calculation of consolidation and stability in the project are given in the following table.

Table 1: soil parameters for the calculation of consolidation and stability in the coloured drain areas

soil properties soil	Soil - group DIN 18196	density γ_k / γ_k' [kN/m³]	shear strength φ'_k [Grad]	cohesion c'_k	$c_{u,k}$ [kN/m²]	modulus $E_{s,k}$ [MN/m²] 10 - 50 kN / m²	50 - 100 kN / m²	100 - 150 kN / m²	consolidation coeffi-cient c_v [m²/s]	water perme-ability k_f [m/s]	peak pressure q_c [MN/m²]	skin friction f_s [MN/m²]
replenish soil sand	SE - SW	18 / 10	30,0	---		60			$6{,}0 \cdot 10^{-1}$	$1{,}0 \cdot 10^{-4}$	---	---
soft soil, clay [top level]	OT	14 / 4	17,5	15	12	0,6	0,8	1,2	$8{,}0 \cdot 10^{-9}$	$1{,}0 \cdot 10^{-10}$	0,2	0,01
soft soil, silt [top level]	UA - OT	15 / 5	20,0	10	12	0,6	0,8	1,2	$2{,}0 \cdot 10^{-8}$	$2{,}5 \cdot 10^{-10}$	0,2	0,01
sand	SE – SU*	18 / 10	27,5	---		25			$2{,}5 \cdot 10^{-3}$	$1{,}0 \cdot 10^{-6}$	4,0	0,03
soft soil, silt [down level]	UA - OU	16 / 6	20,0	10	20	1,8	2,0	2,2	$1{,}0 \cdot 10^{-7}$	$5{,}0 \cdot 10^{-10}$	1,5	0,03
sand	SE - SU	18 / 10	30,0	---		80			$8{,}0 \cdot 10^{-1}$	$1{,}0 \cdot 10^{-4}$	10,0	0,1

3. SOIL IMPROVEMENT TECHNIQUES

3.1. Vertical drains

It was a typical installation with flat vertical drains in different grids with lengths between 15 m (corresponding to the conditions in Figure 4) and 22 m in other parts of the project. It was necessary to pass the intermediate sandlayer in order to place the vertical drains in the glacial sand below the second layer of soft soil.
The small grids in this project were generated by the stepwise loading and the fat clay in the upper layer of soft soil with special low permeability and the corresponding primary consolidation coefficient.

Photo 1: installation of vertical drains on a dry one meter thick sandplatform

3.2. Controlled Modulus Columns CMC

The controlled modulus columns CMC are developed for execution in soft soils. The full displacement auger retains the right borehole diameter over more than two meter length. The controlled module secures the right concrete pressure and volume throughout the concreting, which is sensible in very soft soils.
The typical piling standards give a minimum limit of 15 kN/m² undrained shear strength to use cast-in-place-concrete. By the standard DIN EN 12699 [3] above Cu = 15 kN/m² the minimal distance of full displacing elements is linked to the undrained shear strength. Critical distance is only relevant during a certain time of concrete hardening.
Compared to vibrating techniques the fast CMC can be performed in softer soils with lower undrained shear strength. There are several references with CMC-installation directly nearby fresh CMC under Cu < 15 kN/m² conditions.
In this project the CMC have been first successfully checked under conditions with the lowest Cu-values by integrity tests and dynamic pile tests. Loads larger than 500 kN could be tested with a additionally factor of security larger than 2 FOS on the CMC, driven in the glacial sand layer.
A part of the further CMC production fresh directly nearby fresh CMC was improved through a vertical drain intermediate between the CMC. Immediately the CMC installation the water starts after of the vertical drain even on the top of the sandy working platform. A continuous flow during several hours up to one day and the amount of water show an efficient fast additional consolidation. The CMC force

during short time more water than the classical preloading with drains, where no water was seen on the one meter thick sand platform.
Compared with other CMC areas the heave of working platform and the concrete excessively consumption, normally increasing with the thickness of softsoil, could be reduced by the additional intermediate vertical drains.

Photo 2: installation of CMC combined with vertical drains with water on the platform

4. CALCULATIONS AND PREDICTIONS

4.1. Consolidation and stability calculations in the parts with vertical drains

First 1,29 m of total settlements were calculated in the area west of the bridge with the following timeline of primary and secondary consolidation according to figure 5.

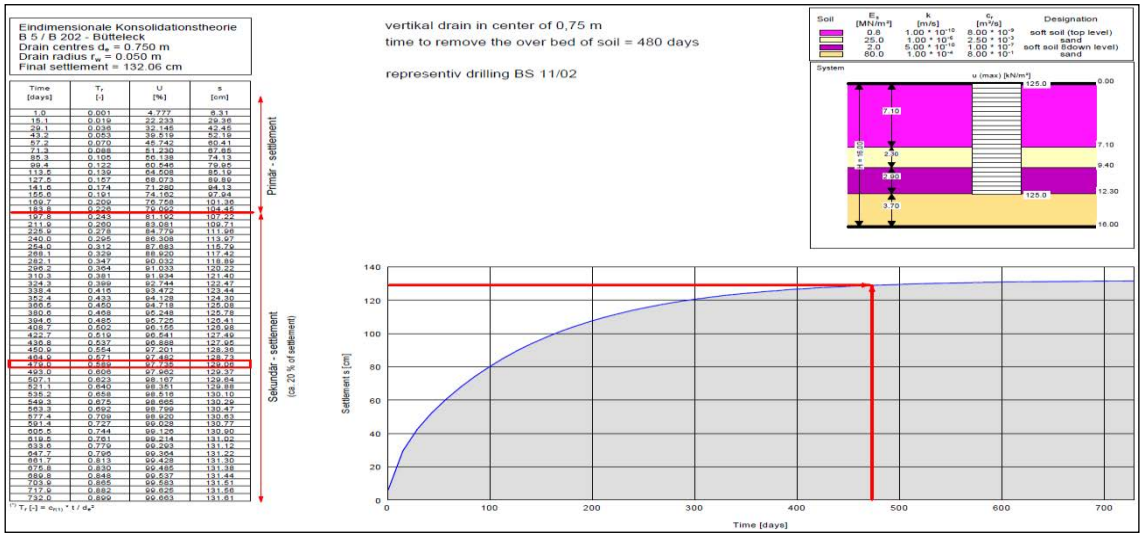

Figure 5 : ½ year of primary consolidation even with vertical drains in a grid of 0.75 m

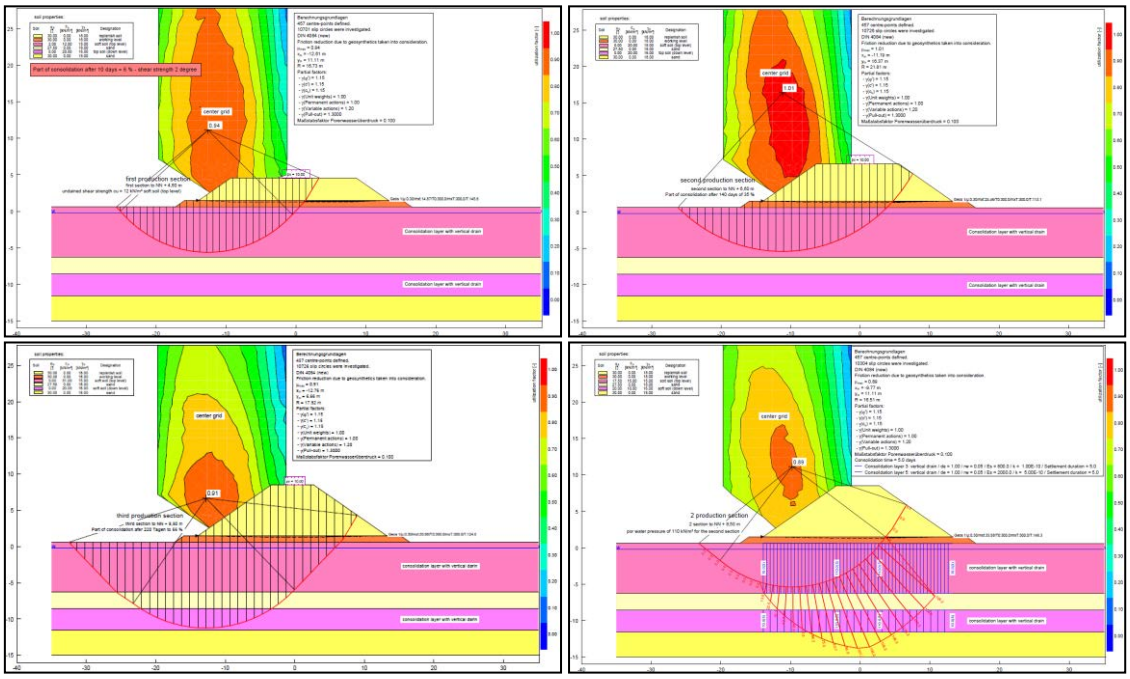

Figure 6 : stability calculation of three loading steps and control calculation of the final situation

The stability calculations are based on Cu and made three steps of loading with berms and twice waiting for the sufficient degree of consolidation necessary.
The following improvement of the Cu-values in each load step are added to the basic Cu value: [4]

$$\Delta c_u = \sigma \tan \varphi'_k \, U \qquad (1)$$

with

Δc_u : improvement of undrained shear strength Cu
σ: stress in the step of calculation
φ'_k : degree of friction
U: degree of consolidation

The control results of the final situation stability analysis based on phi´, C´ and porewater pressure show that the calculations based on undrained shear strength Cu are on the safe side.

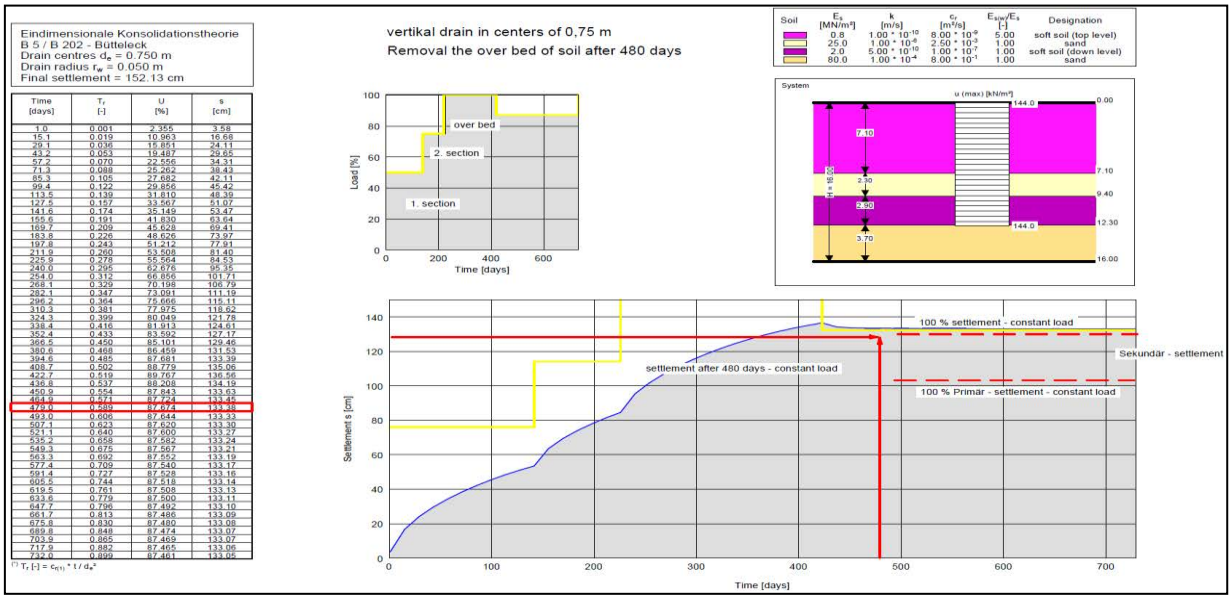

Time [days]	T_r [-]	U [%]	s [cm]
1.0	0.001	2.355	3.58
15.1	0.019	10.963	16.68
29.1	0.036	15.851	24.11
43.2	0.053	19.487	29.65
57.2	0.070	22.556	34.31
71.3	0.088	25.262	38.43
85.3	0.105	27.682	42.11
99.4	0.122	29.856	45.42
113.5	0.139	31.810	48.39
127.5	0.157	33.567	51.07
141.6	0.174	35.149	53.47
155.6	0.191	41.830	63.64
169.7	0.209	45.628	69.41
183.8	0.226	48.626	73.97
197.8	0.243	51.212	77.91
211.9	0.260	53.508	81.40
225.9	0.278	55.564	84.53
240.0	0.295	62.676	95.35
254.0	0.312	66.856	101.71
268.1	0.329	70.198	106.79
282.1	0.347	73.091	111.19
296.2	0.364	75.666	115.11
310.3	0.381	77.975	118.62
324.3	0.399	80.049	121.78
338.4	0.416	81.913	124.61
352.4	0.433	83.592	127.17
366.5	0.450	85.101	129.46
380.6	0.468	86.459	131.53
394.6	0.485	87.681	133.39
408.7	0.502	88.779	135.06
422.7	0.519	89.767	136.56
436.8	0.537	88.208	134.19
450.9	0.554	87.843	133.63
464.9	0.571	87.724	133.45
479.0	0.589	87.674	133.38
493.0	0.606	87.644	133.33
507.1	0.623	87.620	133.30
521.1	0.640	87.600	133.27
535.2	0.658	87.582	133.24
549.3	0.675	87.567	133.21
563.3	0.692	87.552	133.19
577.4	0.709	87.540	133.17
591.4	0.727	87.528	133.16
605.5	0.744	87.518	133.14
619.5	0.761	87.508	133.13
633.6	0.779	87.500	133.11
647.7	0.796	87.492	133.10
661.7	0.813	87.486	133.09
675.8	0.830	87.480	133.08
689.8	0.848	87.474	133.07
703.9	0.865	87.469	133.07
717.9	0.882	87.465	133.06
732.0	0.899	87.461	133.05

Figure 7 : settlement calculation with consolidation time and degree of the three loading steps

The settlement calculation had to be repeated according to the stability analysis with the fitting consolidation process in each of the three load steps.
The results of the settlement and stability calculations are summed up in the following tables. The drain grids correspond to the number of load steps.

Table 2: Results: calculation of consolidation

axis	station	load		sections			drilling number	grid	permanent load		overload	remaining settlement
		permanent load	overload	number	stress	time for next section		drains	whole settlement	settlement after 480 d	settlement after 480 d	
		kN/m²	kN/m²	piece	kN/m²	Tage		m	cm	cm	cm	cm
200	0+500	43	60	1	60	0	BS 14/02	1,50	45	37	52	0
200	0+440	90	106	2	53	0	BS 13/02	1,25	108	100	95	13
					43	140		1,00	108	106	104	3
200	0+380	122	144	3	72	0	BS 11/02	1,00	132	111	115	17
					36	140		0,75	132	129	133	1
					36	220		0,55	transition construction to CMC			

Table 3 : Results: Stability calculation

Achse	Station	section	level of section	time of section	center	calculation approach	part of consolidation	approch of water pressure	utilization factor	traffic load
			NN + m	days	[m]		[%]	[kN/m²]	[-]	
200	0+500	1	3,8	0	1,50	water pressure	0	60	0,67	
						undrain shear strength	0	0	**0,96**	
									1,03	X
200	0+440	1	3,7	0	1,00	water pressure	0	60	0,62	
		2	5,9	140				72	0,83	
200	0+440	1	3,7	0	1,00	undrain shear strength	0	0	**0,96**	
									1,01	X
		2	5,9	140	1,00		36	0	**0,94**	
									0,97	X
200	0+380	1	4,6	0	1,00	water pressure	0	72	0,55	
		2	8,5	140	1,00		0	110	0,89	
200	0+380	1	4,6	0	0,75	undrain shear strength	0	0	**0,94**	X
		2	6,6	140			35	0	**0,98**	
									1,01	X
		3	8,5	220			56	0	**0,88**	
									0,91	X

4.2. Controlled Modulus Columns CMC

Due to really very soft soils the CMC are designed to take full load, neglecting the small load bearing capaticity of the soil inbetween. With 500 kN characteristic load per CMC the settlement corresponds to the piles of the bridge, but only for the CMC itself. Below the dam is no concrete slab like the foundation of the bridge.
Reinforced earth with galvanized steel was designed to hold the large forces of active earth pressure. Because of the large geotextile deformations during the consolidationperiod, described in the following monitoring results, it was the decision to take a stronger construction with nearly no deformation. First compared with plastic geotextile and –grid steel material has only very small elastic deformations, which are relevant to the horizontal deformations of a wide dam. Additional gravel parts in the sandy load transfer platform LTP secure nearly deformation-free friction.

5. MONITORING RESULTS

5.1. Wick drains

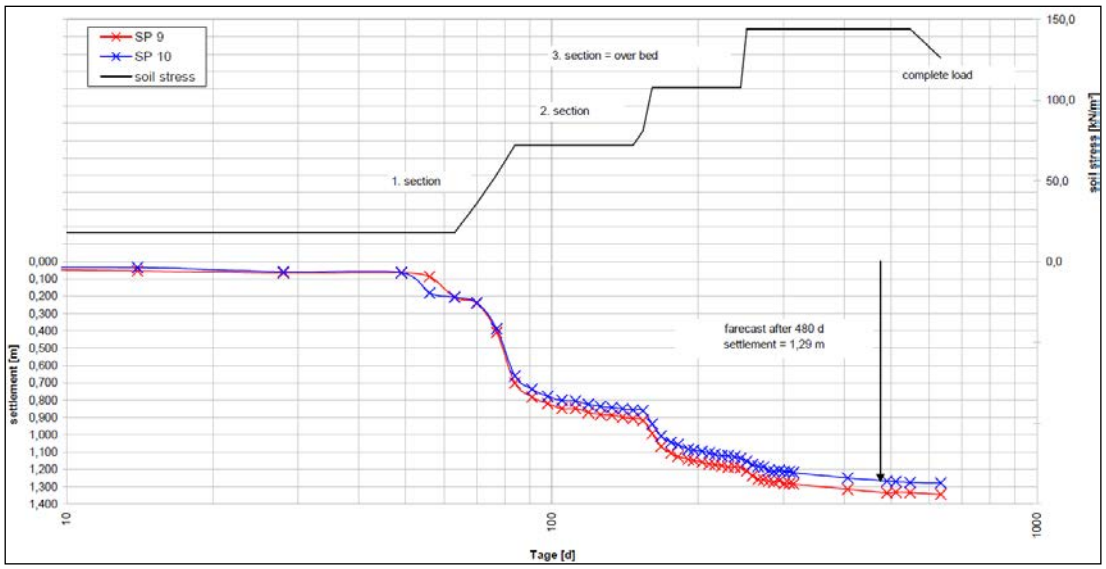

Figure 8 : measurment at the settlement plates SP 9 und SP10.

The measured settlements of the consolidation process in figure 7 fit to the given predictions of figure 5. An additional strong geotextile layer of 600 kN/m short live strength between dam and vertical drains had not much influence on the vertical inclinometer results with 27 cm of deformation.

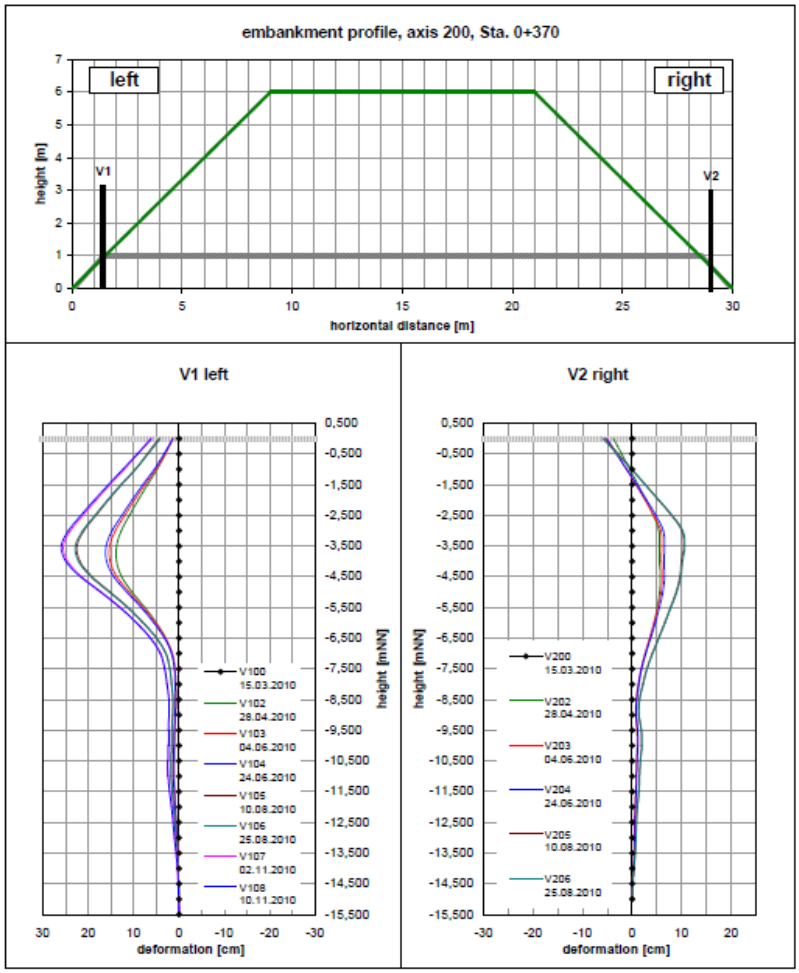

Figure 9 : vertical inclinometer results at the 7 m high damm with drains and 600 kN/m geotextile

5.2. Controlled Modulus Columns CMC

According on the following figure several measurement systems were installed between CMC and reinforced earth in the load transfer platform. Electrical signals show nearly full stress concentration on the CMC and less than one centimetre of horizontal deformation.
We will concentrate on the vertical deformations measured five times during the last year. The horizontal inclinometer crosses only six marked CMC-columns according to figure 2 and figure 9. We find around one centimetre CMC settlement and two centimetre due to reinforced earth steel construction on the soil in between. The small settlements correspond to the predicted and measured stresses.

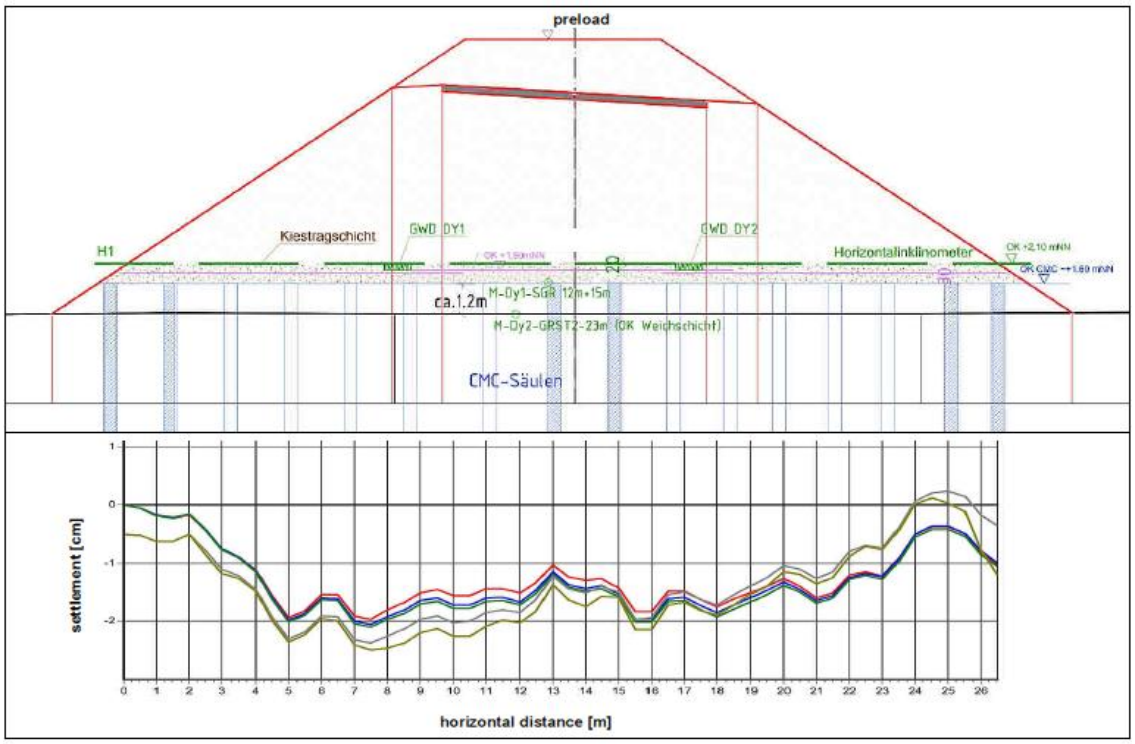

Figure 10 : horizontal inclinometer results with arround 1 cm of CMC settlements and 2 cm of reinforced earth settlements

6. SUMMARY AND CONCLUSIONS

In the difficult road crossing and soil conditions additional for soil investigations and laboratory tests are the basis of a proper design. Long time oedometer test allow precise predictions of consolidation processes forced by different grids of vertical drains. Large deformations of up to 150 cm of settlements and 27 cm of horizontal displacement fit to the calculation and show that it was the right decision not to consolidate the highest dams on the softest soil directly beside the bridge over the running traffic on the highway B5.
Vibration free CMC in combination with reinforced earth ensure the required quality of less than two centimetre differential settlements to the piled bridge.
With a detailed planning of the steps in the workflow, right predictions and a fitting monitoring system economic soil improvement techniques can be combined with deep foundations in one project and even very soft soil can be treated successfully.

REFERENCES

[1] *J.F. Kirstein, M.v. Bank, 2010, CMC-Gründungen im Bestand – Ein innovatives System zur Bodenverbesserung für höchste Anforderungen, Graz (AT).*

[2] *DIN Deutsches Institut für Normung, 2002, DIN 4094-4: Subsoil – field testing – part 4 : Field vane test.*

[3] *DIN Deutsches Institut für Normung, 2001, DIN EN 12699: Execution of special geotechnical work - Displacement piles; German version EN 12699:2000.*

[4] *J-L Chaumeny, J.F.Kirstein, S. Varaksin, 2008, An experience of consolidation of extremly soft mud for one of Europe's largest projects "The AIRBUS A-380" asembly factory in Hamburg-Germany, Glasgow.*

Critical Height of Column-Supported Embankments from Bench-Scale and Field-Scale Tests

Michael McGuire, Virginia Tech, U.S.A., mcguirem@vt.edu
Joel Sloan, U.S. Air Force, Republic of Korea, sloanja@vt.edu
Jim Collin, The Collin Group Ltd., U.S.A., jim@thecollingroup.com
George Filz, Virginia Tech, U.S.A., filz@vt.edu

ABSTRACT

Bench-scale and field-scale tests of column-supported embankments were performed to determine the critical height above which the embankment surface does not exhibit differential settlement due to the deformations that occur at the base of the embankment. The bench-scale tests show that the critical height increases as the clear spacing between columns increases for a fixed column diameter, which was an expected result; however, an unexpected result was that the critical height decreases as the column diameter decreases for a fixed center-to-center spacing of the columns. One hypothesis for this outcome is that increased compliance at the top of smaller diameter columns increases the settlement of the ground surface directly above the column, thereby decreasing the difference between the ground surface settlement at the column location and the ground surface settlement at the location farthest from columns within a unit cell, with an accompanying decrease in the critical height. One column configuration was investigated in the field-scale tests, and the critical height was consistent with the results from the bench-scale tests. This paper summarizes the test programs and the key findings.

1. INTRODUCTION

This paper provides a summary of the bench-scale experiments performed by McGuire (2011) and the field-scale experiments performed by Sloan (2011). The equipment and testing procedures are described and the key results related to differential settlement at the surface of a column-supported embankment are presented and compared to conventional design recommendations in which the minimum embankment height is related to clear spacing between adjacent columns.

1.1. Overview of CSE technology

Column-supported embankments (CSEs) with or without basal geosynthetic reinforcement can be used in soft ground conditions to reduce settlement by transferring the embankment load to the columns through stress redistribution above and below the foundation subgrade level. Column-supported embankments are typically used to accelerate construction and/or protect adjacent facilities from additional settlement. The column elements consist of driven piles or formed-in-place columns that are installed in an array to support a bridging layer or load transfer platform. The bridging layer is constructed to enhance load transfer using several feet of compacted sand or sand and gravel that may include one or more layers of high-strength geotextile or geogrid reinforcement.

Mobilization of the mechanisms of load transfer to the columns in a column-supported embankment requires some amount of differential settlement at the base of the embankment. When the embankment height is low relative to the clear spacing between columns, poor ride quality can occur due to surface expression of differential settlements at the base of the embankment. Examples of this type of failure are reported by Coghlin (2005), Camp and Siegel (2006), and Ting et al. (1994).

1.2. Definitions and existing guidance for critical height

In this paper, the term "critical height", H_{crit}, is defined as the embankment height above which differential settlements at the base of the CSE do not produce measurable differential settlement at the embankment surface. This definition is similar to Naughton's (2007) use of critical height to refer to the vertical distance from the top of the pile caps to the plane of equal settlement in the embankment. Other authors use critical height in other ways, e.g., Horgan and Sarsby (2002) and Chen et al. (2008) use critical height to refer to the height above which all additional loads due to fill and surcharge are distributed completely to the pile caps. As shown in Table 1, the conventional approach is to determine the critical height, as defined here, as a proportionality factor times the clear span between adjacent

columns; however, consensus has not been established on what proportionality factor to use or whether a single proportionality factor is applicable to all column arrangements.

Table 1: Abridged summary of existing recommendations for minimum embankment height to avoid differential surface settlement (which is defined herein as the critical height) from McGuire (2011)

Reference	**Minimum embankment height(1)**
British Standard, BS8006 (1995)	0.7 (s – a)
Carlson (1987)	1.0 (s – a)
Nordic Handbook (2002)	1.2 (s – a)
Chen et al. (2008)	1.6 (s – a)
Demerdash (1996)	1.7 (s – a)
Hewlett and Randolph (1988)	2.0 (s – a)

Note (1): s = center-to-center spacing of columns or pile caps
a = width of square pile caps

1.3. Introduction to the CSE tests

The bench-scale and field-scale experiments discussed herein are also described by McGuire (2011), Sloan (2011), and Filz et al. (2012). McGuire (2011) and Filz et al. (2012) compare the results related to critical height from both sets of experiments to other experiments and case histories found in the literature.

The dashed lines in Figure 1 show definitions of unit cells for rectangular and triangular column arrangements with column spacings equal to s_1 and s_2 and column diameter equal to d. Special cases of these configurations are square and equilateral triangular arrays where s_1 equals s_2. When square columns or pile caps are used, an equivalent round column can be defined using the equal area conversion recommended by Smith (2005), McGuire (2011), and Sloan (2011). To describe deformation at the embankment surface, McGuire (2011) defined the dimension s' as the greatest distance a location within the unit cell can be from the edge of the closest round column. Below the critical height, locations at the embankment surface a distance s' from the nearest column receive the least support from the column and experience the largest settlement, whereas locations directly over the column axis experience the smallest settlement. The difference in settlement at these locations is the maximum differential surface settlement, dS_{max}. McGuire (2011) found that dS_{max} increases approximately in proportion with the magnitude of the maximum differential base settlement, dS_b. McGuire (2011) and Sloan (2011) also found that the ratio dS_{max}/dS_b decreases in an approximately linear fashion as embankment height increases until reaching a value of zero at and beyond the critical height.

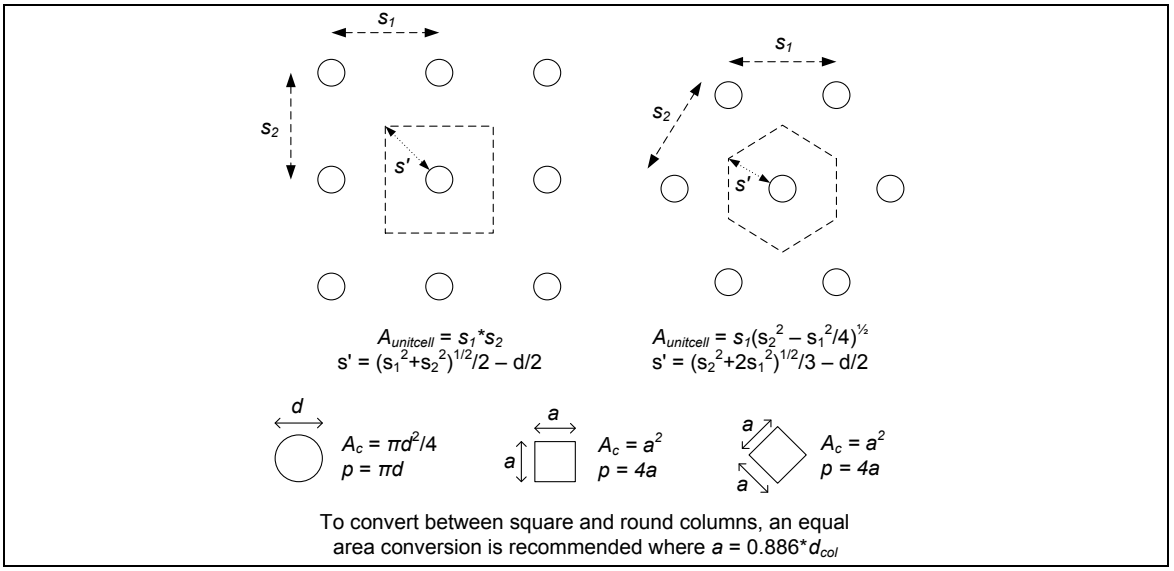

Figure 1: Definition sketch for interpretation of test results and critical height determination

2. BENCH-SCALE TESTS

The primary objective of the bench-scale tests was to investigate the influences of embankment height, differential base settlement, column diameter, column spacing, the presence and stiffness of reinforcement, and surcharge pressure on surface deformation. Performing the tests at the bench scale afforded the ability to conduct a large number of tests and evaluate a wide range of parameter values. A total of 183 bench-scale tests were performed using single and multi-column arrangements over the course of the testing program. The test equipment, materials, procedures, data acquisition, data reduction, parameter variations, and test results are described in detail by McGuire (2011).

2.1. Description of equipment and procedures

The apparatus consisted of a circular open tank with an inside diameter of just under 23 inches. A photo and schematic of the test equipment is provided in Figure 2. The test equipment could be configured to test the single and multi-column configurations shown in Table 2. Differential movement between the columns and the base of the sample was displacement-controlled using a motorized jack. To simplify the equipment, the base and lateral boundaries of the sample were held fixed, and the columns were displaced upwards into the sample. This differential movement is exactly equivalent to fixing the columns and having the base and lateral boundaries of the sample settle uniformly. Surface deformations resulting from the differential movement at the base were measured using a non-contact laser distance transducer mounted to a linear motion carriage outfitted with a draw wire sensor. This arrangement provided the ability to obtain a profile of surface deformation without disturbing the sample surface. Influences of the lateral model boundary were mitigated by keeping the area of interest (unit cell or single column) away from the walls of the sample tank and, when possible, including extra rows of columns around the unit cell. The left portion of Figure 3 shows the laser profiler and the columns inside the empty sample tank. The right portion of Figure 3 provides an example of the measurements of surface settlement obtained using the laser profiler at increasing magnitudes of differential base settlement.

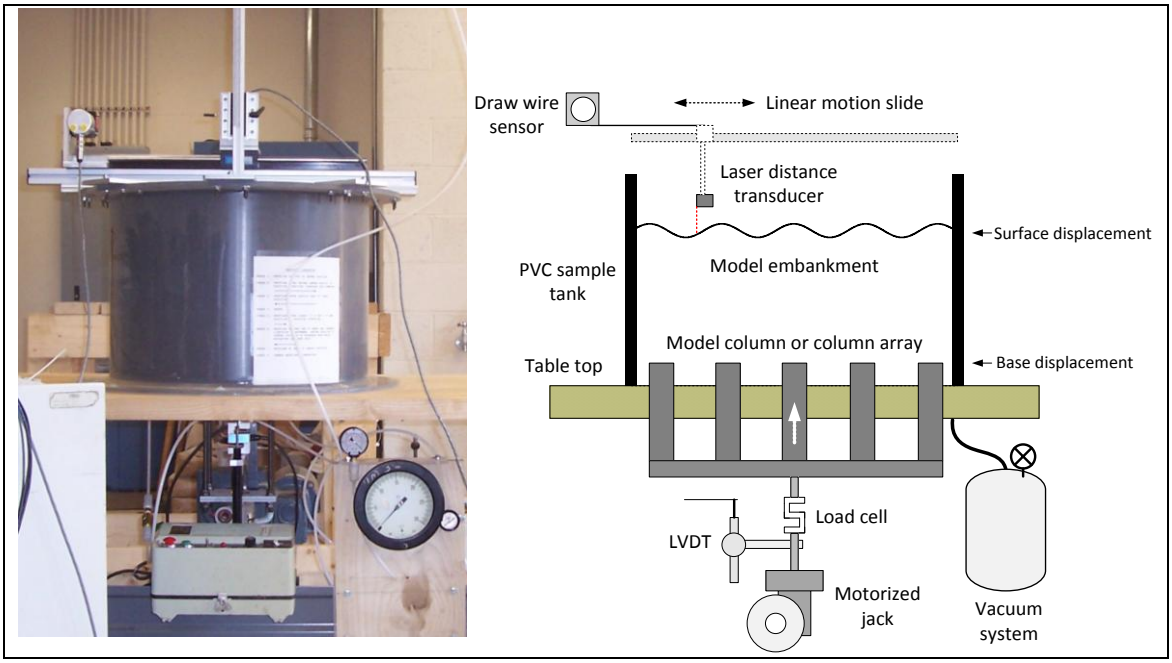

Figure 2: Photo and schematic of bench-scale test apparatus

Table 2: Column configurations evaluated in bench-scale experiments

Apparatus Configuration	Single Column 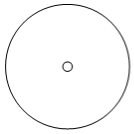	2x2 Array 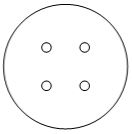	5x5 Array 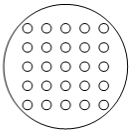
Column Spacing (*s*), inches	Not applicable	7.00	3.50
Column Diameter (*d*), inches	0.75 1.25 2.00 3.00	0.75 - 2.00 -	0.75 1.25 2.00 -
Area Replacement Ratio (a_s), %	Not applicable	1 - 6 -	4 10 26 -

A clean, poorly-graded, medium-grained, sub-angular sand was used as the bench-scale embankment material, and samples up to about 11 inches high were prepared dry at one of three relative densities ranging from about 70 to 100 percent using the technique of air pluviation. The apparatus also included a vacuum system that provided the ability to conduct tests under sub-atmospheric conditions. The vacuum system was capable of applying up to 3 psi of equivalent overburden pressure on the surface of the sample.

Three types of biaxial polypropylene netting with different tensile stiffnesses were selected for use as the geosynthetic reinforcement. The influence of reinforcement stiffness on surface deformation was investigated by changing either the stiffness or number of the reinforcement layers.

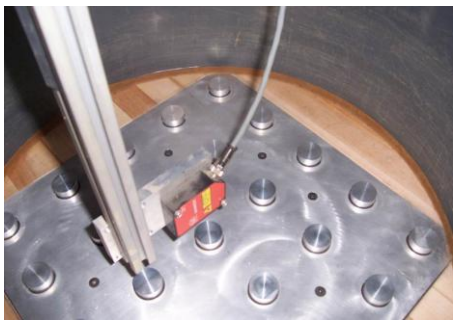

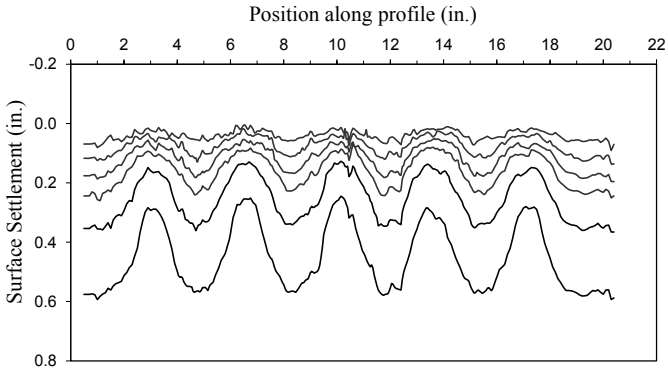

Figure 3: (Left) View inside soil tank of bench-scale test apparatus showing columns and laser profiler. (Right) Sample measurements of surface settlement at six magnitudes of differential base settlement.

2.2. Results for critical height

The results from the bench-scale tests indicate that critical height depends primarily on the spacing and diameter of the columns. This dependency is illustrated in Figure 4 which shows the ratio dS_{max}/dS_b versus sample height normalized by column diameter for the five unit cell geometries evaluated. As indicated by the tick marks and labels, the value of H_{crit}/d for each unit cell geometry was evaluated as the intercept of the trend of the data with dS_{max}/dS_b equal to zero. Over the range of relative densities investigated from about 70% to 100%, the relative density of the sand did not measurably affect the critical height. The inclusion of one or two layers of reinforcement with one of three different tensile stiffnesses reduced the magnitude of differential surface settlements for the sand below the critical height, but also did not measurably affect the critical height. Demerdash (1996) also reached the conclusion that the stiffness of reinforcement does not significantly affect the critical height.

The significance of scale effects on the results were investigated by applying surcharge pressure to the sample surface and by performing a three-dimensional modelling study using FLAC^{3D}. The application of vacuum pressure up to 3 psi did not measurably affect the deformed shape of the soil surface. The results

of three-dimensional numerical modelling described by McGuire (2011) found that critical heights calculated at the model scale and at ten times the model scale were the same. The critical heights from the numerical analyses were also in very good agreement with the critical heights from the bench-scale tests.

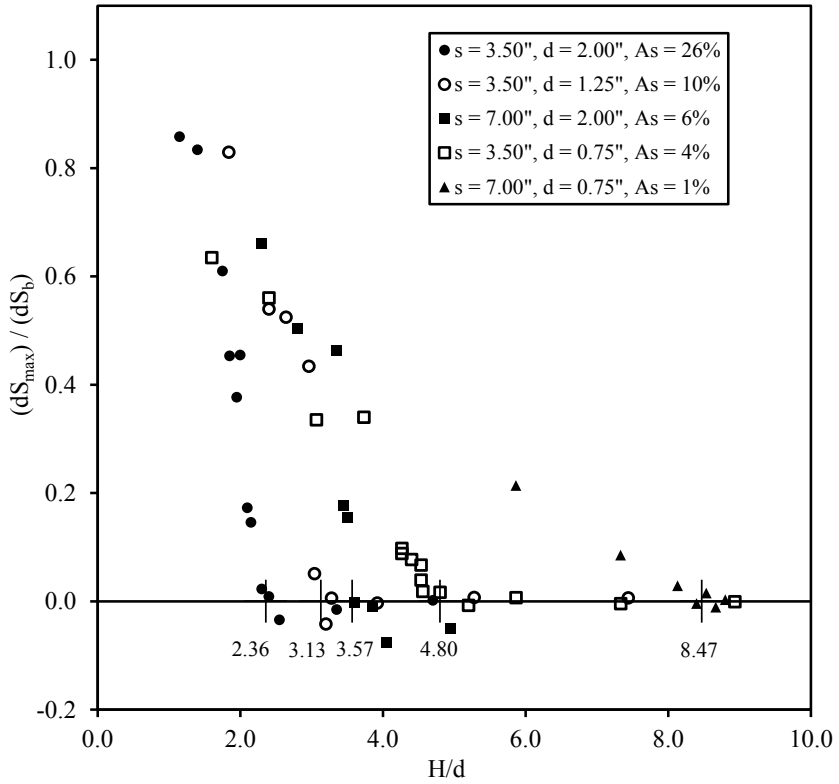

Figure 4: Ratio of maximum differential surface settlement to maximum differential base settlement versus sample height divided by column diameter for samples without reinforcement prepared dry at D_r = 87%. Labels indicate H_{crit}/d for each of the unit cell geometries evaluated.

3. FIELD-SCALE TESTS

The primary objective of the field-scale tests was to determine the critical height for a specific column arrangement and geogrid configuration using relatively well-graded gravel for the fill material. Although more costly and time-consuming than the bench-scale tests, field-scale tests offered the ability to use typical CSE construction materials and apply traffic loading at a scale approaching that of typical CSEs used in geotechnical practice.

A total of four field-scale tests were performed with an array of nine, 2 ft diameter columns. The test equipment, materials, procedures, data acquisition, data reduction, parameter variations, and test results are described in detail by Sloan (2011).

3.1. Description of equipment and procedures

The CSE test facility is located at Virginia Tech and consists of a 30 ft by 30 ft concrete mat foundation. A 1 ft wide, 16 in. high, CMU wall is located at the perimeter of the mat foundation (see Figure5a). For the tests described in this paper, a 22 ft by 22 ft test area was used. Precast concrete columns with a 2-ft diameter and height equal to the perimeter wall (16 in.), were placed on the surface of the slab in a square array with 6 ft center-to-center spacing (see Figure 5b). A layer of geonet was placed at the base of the slab as shown in Figure 5c. Expanded polystyrene (EPS) geofoam was used to fill the spaces between the perimeter wall and the columns. The result was a level working platform for embankment construction as shown in Figure 5d.

Three of the four tests used three layers of Tensar BX1500 biaxial geogrid placed within the first six inches of fill, one layer immediately on top of the columns and two layers with strong axes placed perpendicular to one another at an elevation of 6 inches above the columns. The fourth test used five

layers of Tensar BX1500 geogrid, each spaced 6 inches apart, beginning with the layer immediately on top of the columns. The fill was a relatively well-graded crushed gravel meeting the specifications of West Virginia Division of Highways (2000) Class 1, and was placed and compacted in lifts to a relative compaction of approximately 93% of modified Proctor. Figure 6 shows the details of instrumentation, geogrid placement, fill placement, and fill compaction.

Load cells were placed within the central column of the 9-column array (see Figure 6a), earth pressure cells were placed within the embankment fill, strain gages were placed on the geogrid, and tubes for determining the settlement profiles were placed at various embankment elevations and cross sections. Embankment elevations were measured using a total station.

Upon completion of the embankment, an environmentally friendly solvent derived from the peels of citrus fruit, d-Limonene, was introduced through a PVC pipe network and spread across the base of the mat foundation by the geonet. d-Limonene dissolves EPS on contact and may be used on EPS to minimize the volume of EPS in landfills (Noguchi et al. 1998).

The presence of the d-Limonene dissolved the geofoam so that the weight of the embankment was supported completely by the columns and perimeter wall. The instrumentation was used to measure the response of the embankment, and surface settlements were measured by surveying with a total station.

The embankment surface was surveyed before dissolving the geofoam to establish the initial embankment elevation. At a minimum, the embankment surface was resurveyed at 1 day, 3 days, and 7 days after dissolving the geofoam in order to calculate the settlements at those time intervals. Seven days after dissolving the geofoam, the embankment was trafficked with a small, rubber-tired, skid-steer loader and any additional settlement was measured. The settlements at 7 days, prior to trafficking with the skid-steer loader, are termed the "before traffic" settlements. The measurements recorded after trafficking with the skid-steer loader are termed the "after traffic" settlements. Figure 7 provides an example plot showing differential surface settlement from total station measurements.

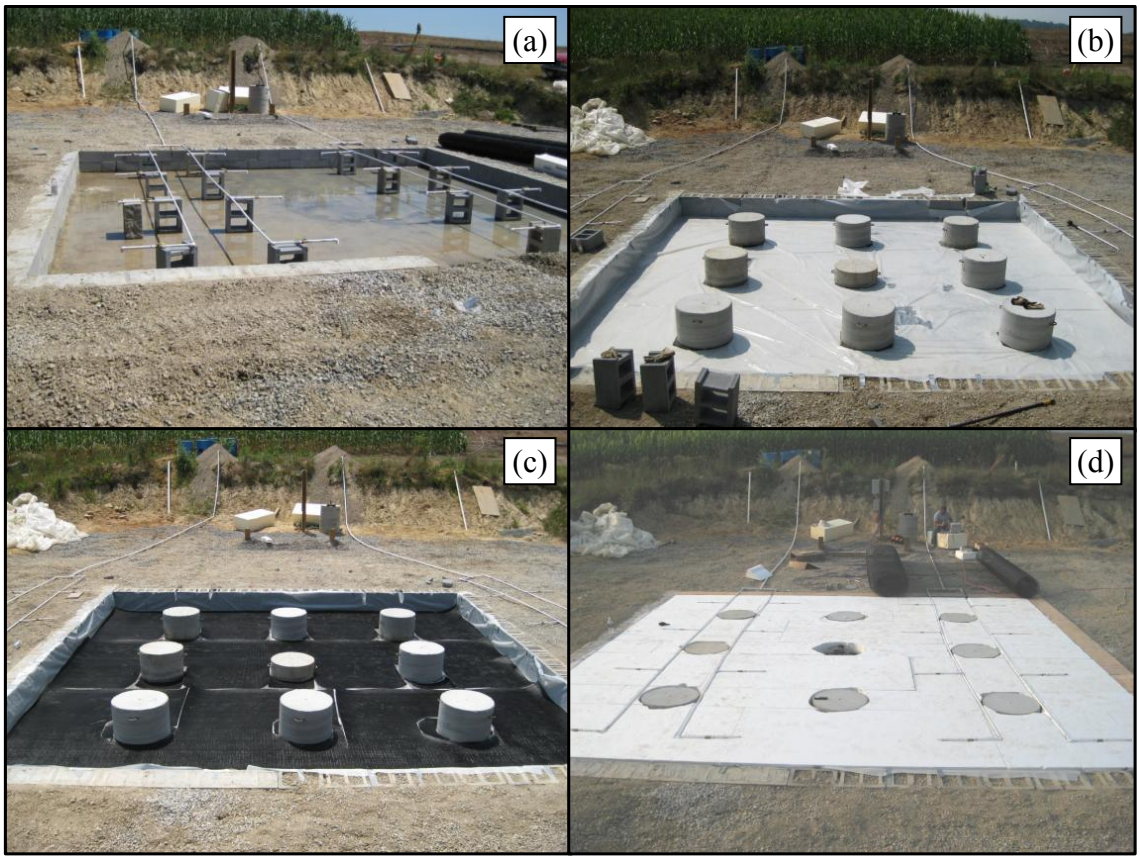

Figure 5: a) calibration of the geofoam dissolver distribution system, b) column placement, c) columns with geonet placed at the base of the mat foundation, and d) working platform for embankment construction after placement of geofoam.

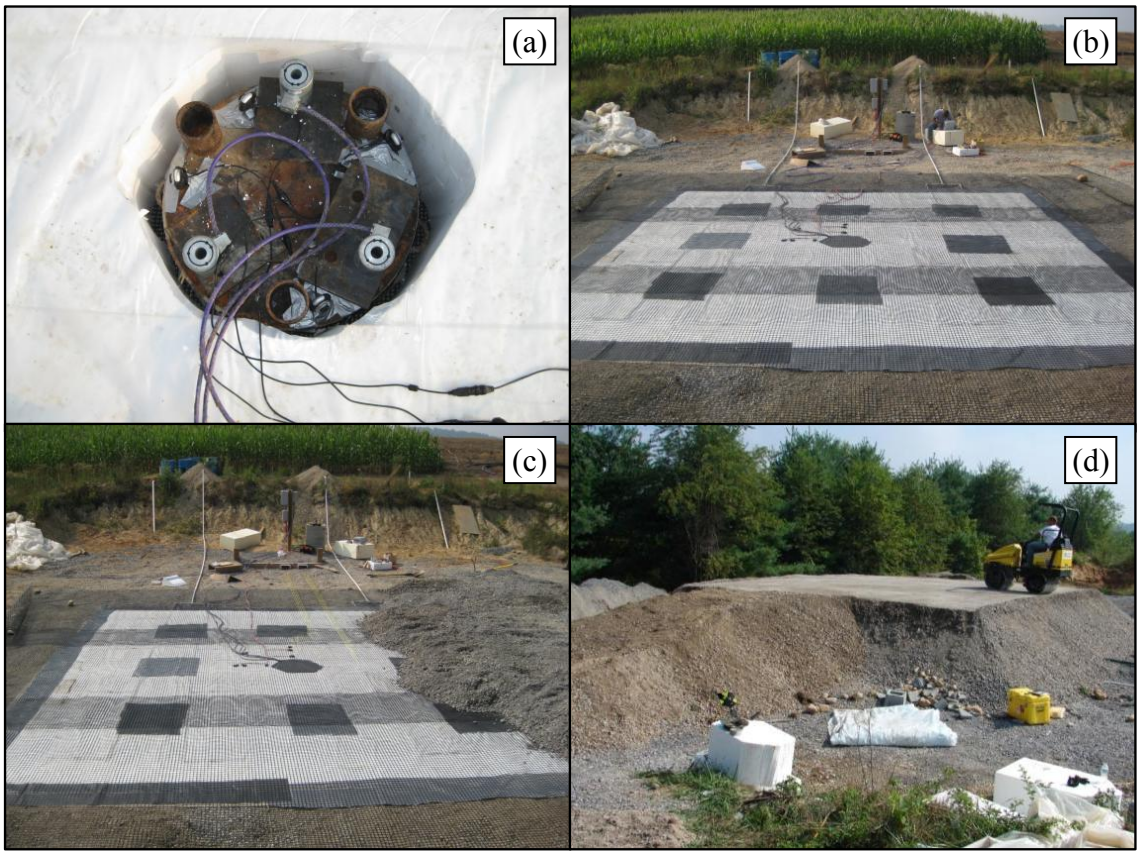

Figure 6: a) load cells and webcams in central column, b) first layer of geogrid over the geofoam and columns, c) placement of the first fill layer, d) compaction of fill on an embankment nearing completion.

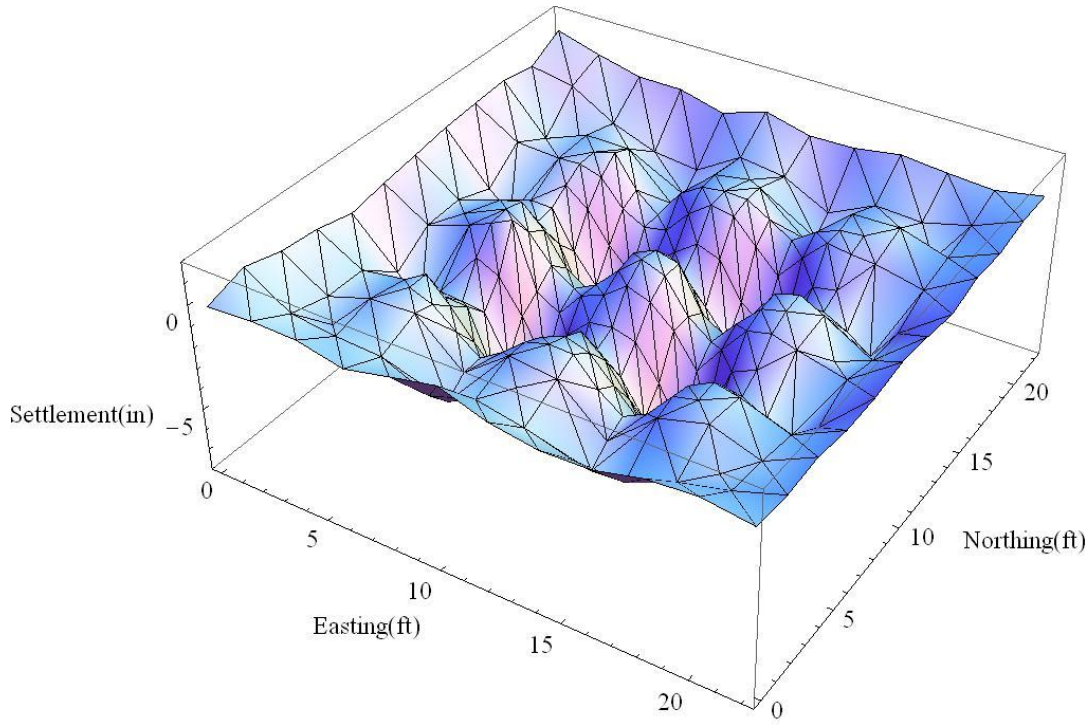

Figure 7: Plot of surface settlement for an embankment below the critical height with a 9-column array.

3.2. Results for critical height

A total of four CSE tests were conducted with 2.0 ft diameter columns in a square array with a center-to-center column spacing of 6.0 ft. Embankment heights ranged from 4.0 ft to 7.5 ft. Figure 8 shows the

dS_{max}/dS_b versus H/d results for all four embankments in the before traffic and after traffic cases. Key results from Figure 8 are:

- The trafficking process induced additional settlements for embankments below the critical height.
- dS_{max}/dS_b is approximately linear for embankments below the critical height in both the before and after traffic cases.

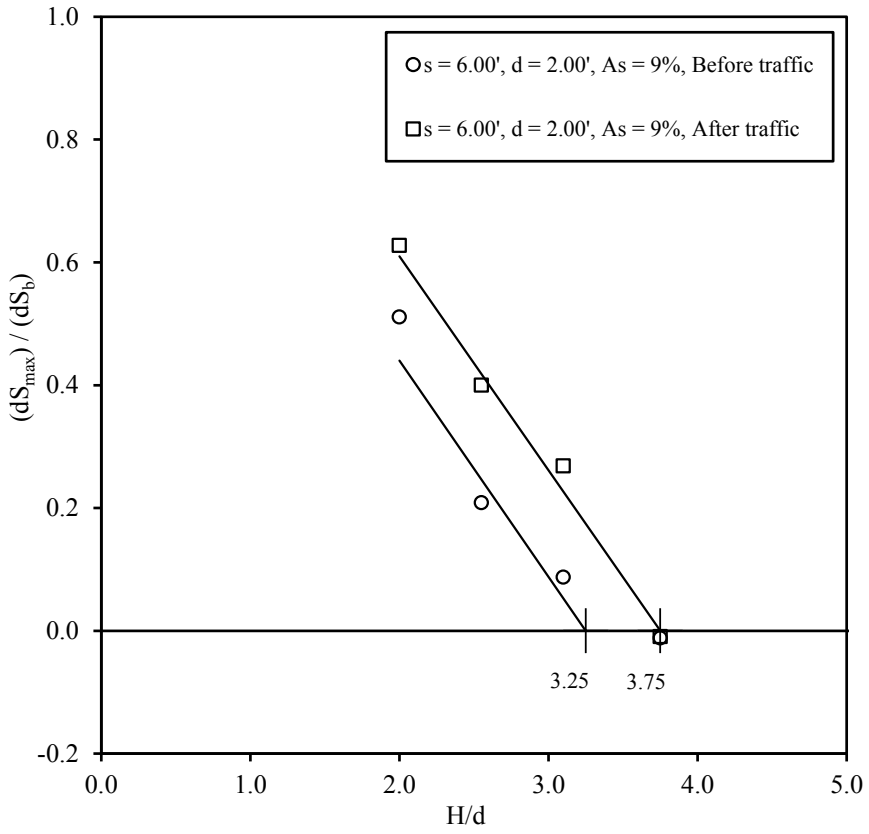

Figure 8: Ratio of maximum differential surface settlement to maximum differential base settlement versus sample height divided by column diameter. Labels indicate H_{crit}/d evaluated before and after trafficking.

4. INTEGRATED FINDINGS AND CONCLUSIONS

Using the results from the bench-scale tests, 3-D numerical analyses, experiments by others, and published case histories, McGuire (2011) proposed the relationship between unit cell geometry and critical height in Equation 1.

$$H_{crit} = 1.15s' + 1.44d \quad (1)$$

Figure 9 shows that the critical height measured from the field-scale tests by Sloan (2011) is in good agreement with the results of the bench-scale tests by McGuire (2011). Substituting the relationships shown in Figure 1, the conventional approach for pile caps in a square array with a proportionality factor of 1.5 can be expressed as $H_{crit} = 2.12s' - 0.27d$. Figure 9 shows that the conventional approach is unconservative for low values of s'/d and conservative for high values of s'/d, according to the results of the bench-scale experiments. Furthermore, no single ratio of H_{crit} to the clear span reproduces the trend given by Equation 1.

The results of the bench-scale tests show that the critical height increases as the clear spacing between columns increases for a fixed column diameter. This result is consistent with the conventional approach of estimating critical height in proportion to the clear span between columns. However, when column diameter decreases for a fixed center-to-center spacing of the columns, thus increasing the clear span, the bench-scale tests show that the critical height decreases rather than increases as predicted by the conventional approach. One hypothesis for this outcome is that increased compliance at the top of smaller diameter columns increases the settlement of the ground surface directly above the column axis,

S_c, thereby decreasing the difference between the minimum surface settlement over the column axis and the maximum surface settlement at the location farthest from columns within a unit cell, with an accompanying decrease in the critical height. Figure 10 shows measurements from the bench-scale tests of the ratio of the surface settlement over the column axis to the maximum differential base settlement, S_c/dS_b, for samples below the critical height. The results show that compliance over the column increases as the normalized sample height increases. When column diameter is small relative to the sample height, corresponding to high values of H/d, the settlement over the column approaches the magnitude of the differential base settlement. Similar results were obtained from laboratory-scale multi-column tests by Demerdash (1996) and anchor pull-out tests performed by Fadl (1981).

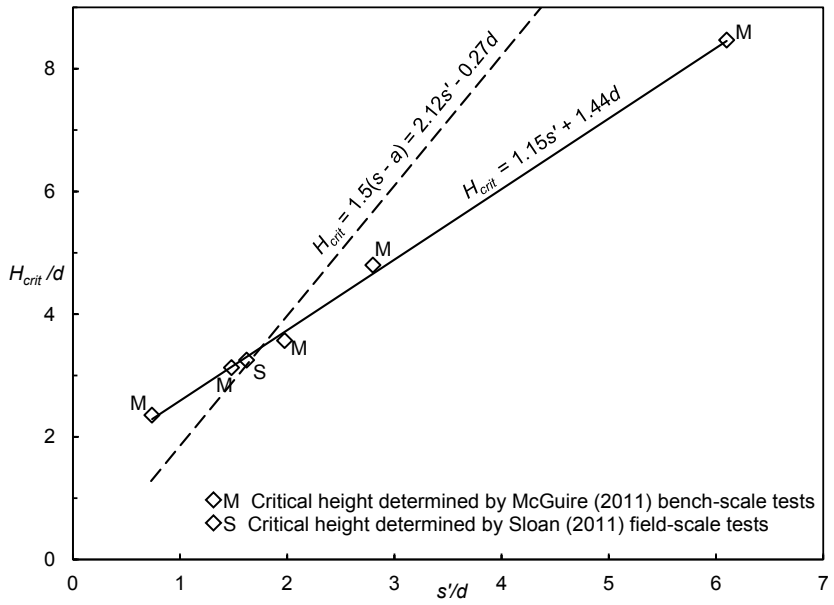

Figure 9: Critical height from tests by McGuire (2011) and Sloan (2011)

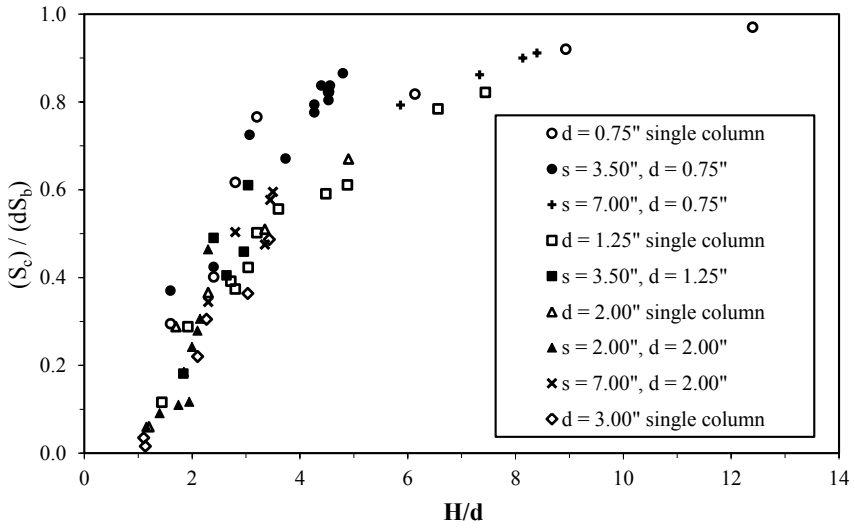

Figure 10: Measurements of the ratio of surface settlement over the column axis to maximum differential base settlement versus sample height divided by column diameter for unreinforced bench-scale tests performed using dry sand prepared at Dr = 87%.

REFERENCES

British Standards Institution (1995). BS8006 Code of Practice for Strengthened/Reinforced Soils and Other Fills, BSI, London, U.K.

Camp, W. M., and Siegel, T. C. (2006). "Failure of a column-supported embankment over soft ground." Proceedings of the 4th International Conference on Soft Soils Engineering, Vancouver, Canada.

Carlson, B. (1987). "Reinforced soil, principles for calculation." Terratema AB, Linköping, Sweden.

Chen, Y. M., Cao, W. P., and Chen, R. P. (2008). "An experimental investigation of soil arching within basal reinforced and unreinforced piled embankments." Geotextiles and Geomembranes, 26, 164-174.

Coghlin, J. (2005). "Brian Blair and Joan Blair (and other individuals identified in the schedule attached to the writ summons dates 17 April 2003) v AWG Residential Limited and Brendan Loughran, Edna Loughran, Dermot Loughran and Eunin Loughran Trading as Brendan Loughran and Sons and Rosorry Development and TPA Taylor, GI Black, RG Kerr and N Magill Practising as Taylor and Boyd (a firm) and Tensar International Limited." Neutral Citation, No. 2005 NIQB 68. , N. I. C. Service, ed.

Demerdash, M. A. (1996). "An experimental study of piled embankments incorporating geosynthetic basal reinforcement." Doctoral Disseration, University of Newcastle-Upon-Tyne, Department of Civil Engineering.

Fadl, M. O. (1981). "The behavior of plate anchors in sand." PhD Dissertation, University of Glasgow, Glasgow.

Filz, G.M., Sloan, J.A., McGuire, M.P., Collin, J.G., and Smith, M.E. (2012). "Column-supported embankments: settlement and load transfer." GeoCongress2012, Oakland, California, in press.

Hewlett, W. J., and Randolph, M. F. (1988). "Analysis of piled embankments." Ground Engineering, 21(3), 12-18.

Horgan, G. J., and Sarsby, R. W. (2002). "The arching effect of soils over voids and piles incorporating geosynthetic reinforcement." Geosynthetics – 7th ICG, 373-378.

McGuire, M.P. (2011). "Critical height and surface deformation of column-supported embankments." PhD Dissertation, Virginia Polytechnic Institute and State University, Blacksburg.

NGG (2002). "Nordic Handbook - Reinforced soils and fills." Nordic Geotechnical Society, Stockholm, Sweden.

Noguchi, T., Miyashita, M., Inagaki, Y., and Watanabe, H. (1998). "A new recycling system for expanded polystyrene using a natural solvent. Part 1. A new recycling technique." Paching Technology and Science, 11:19-27.

Sloan, J. A. (2011). "Column-supported embankments: Full-scale tests and design recommendations." PhD Dissertation, Virginia Polytechnic Institute and State University, Blacksburg.

Smith, M. E. (2005). "Design of bridging layers in geosynthetic-reinforced column-supported embankments." PhD Dissertation, Virginia Polytechnic Institute and State University, Blacksburg.

Ting, W. H., Chan, S. F., and Ooi, T. A. (1994). "Design methodology and experiences with pile supported embankments." Developments in Geotechnical Engineeering, Balkema, Rotterdam, 419-432.

West Virginia Division of Highways. (2000). Standard Specifications: Roads and Bridges. Division 300, Section 307: Crushed Aggregate Base Course.

Load-settlement responses of columnar foundation reinforcements

Giuseppe Modoni, Università degli Studi di Cassino, Italy, modoni@unicas.it
Joanna Bzówka, Silesian University of Technology, Gliwice, Poland, Joanna.Bzowka@polsl.pl
Anna Juzwa, Silesian University of Technology, Gliwice, Poland, Anna.Juzwa@polsl.pl
Alessandro Mandolini, Seconda Università degli Studi di Napoli, Italy, alessandro.mandolini@unina2.it
Francesca Valentino, Seconda Università degli Studi di Napoli, Italy, Francesca.valentino@unina2.it

ABSTRACT

Reinforcement of soil with stiff columnar inclusions is by far the most traditional and frequently adopted solution to face bearing failure and intolerable settlements of foundations. The equipments and construction procedures adopted to conjugate effective load transfer to the surrounding soil with faster and economical execution are among the most remarkable examples of inventiveness in geotechnical engineering. Nowadays a variety of technological developments is available to build new structures on difficult subsoil conditions, including innovative methods for the installation of piles and ground improvement techniques based on mixing of natural soil with cementing agents. However a rational approach for the choice of the most suitable foundation system should require careful analyses to be performed on the load settlement response of the single columnar elements. While these analyses are available in the literature for traditional pile types as a basis for empirical or sound theoretical design rules, only limited spotlike results can be found for new pile types and moreover for cemented soil columns. The present paper aims to fill this gap by performing a comparative analysis of the load settlement responses of different columnar inclusions. To this aim a large number of case studies has been collected, partly from the literature partly from original files of the authors, and classified based on the execution technology. Selected examples are analysed in the paper where axial loading tests conducted up to relatively large settlements are combined with geotechnical investigation of the subsoil. Hyperbolic interpolation of each load settlement curve is performed and a unifying scaling criterion is applied to the fitting parameters to account for the different dimensions of columns. Scaled parameters obtained from different tests are finally related to the subsoil properties in order to perform a comparative analysis of the trends derived for the different reinforcements. Interpretation of the differences observed on the bearing capacity and on the initial stiffness of the various columnar inclusions is given in the light of the different disturbance produced on the surrounding soil by the installation systems.

1. INTRODUCTION

Reinforcement of soils with stiff columnar inclusions represents the most traditional and frequently adopted solution to build structures on different subsoil without the risk of intolerable settlements or even failure. For long time timber, steel and, subsequently, reinforced concrete piles have been driven into soil by hammering machines (e.g. Tomlinson, 1994) to transfer loads to deeper and more competent strata. In the first half of the past century, progressively more powerful and effective drilling machines were built (e.g. Benoto – Mac Donald, 1953) to reach deeper subsoil levels with larger diameter piles. In the past decades big effort has been spent to develop new technologies aimed to improve the performance of piles and/or reduce the time and cost of installation. Among them, great success has been gained by the continuous flight auger technique (CFA, see Neate, 1988), conceived to combine large dimensions and ease of execution typical of bored piles with larger bearing capacities approaching, under some circumstances, those of driven ones.
At the same time, increasingly refined technologies like jet grouting (Yahiro and Yoshida, 1973), deep soil mixing (FHWA, 1999) and lime stabilisation (Ho, 1996) have been extensively adopted to create columns of natural soil mixed with bonding agents. Several application of jet grouting can be found now in the literature aimed to the foundation of new buildings (e.g. Perelli Cippo and Tornaghi, 1985) or to the underpinning of pre-existing ones (e.g. Shibazaki and Ohta S., 1982). Deep soil mixing method is applied to the reinforcement of foundation for different structures (e.g. Topolnicki, 2003).
Among all possibilities, the choice of the most convenient reinforcement system should be derived from a balance of various considerations regarding the suitability of the technique to the present subsoil conditions and to the surrounding environment, accessibility of equipments to the construction site, expertise of contractors, time and cost of installation and, last but not least, expected mechanical performance of the reinforcements.

Independently on the specific purpose of the reinforcement, whether it consists in an increase of the bearing capacity or in a reduction of settlements under working loads, a comparative analysis on the response of columns created with different techniques would be advantageous for design considerations. The experience so far cumulated has widely demonstrated that the bearing capacity of single columns subjected to axial loading is strongly dependent on the modification induced on the surrounding subsoil by the installation procedures.

Piles constructed by drilling holes and replacing soil with concrete, named replacement or preferably non-displacement piles (NDP), determine an overall relief of stresses leading to a partial loosening of the soil both along the shaft and at the bottom of the hole.

Piles constructed by inducing displacement, named driven or preferably displacement piles (DP), generally produces an increase of radial and vertical stresses and a compaction of the surrounding soil, with obvious beneficial effects on the response to axial loading.

Depending on the specific procedure adopted during their installation, CFA piles show an intermediate behaviour compared with the two above mentioned categories: the displacement of the soil during the auger insertion can be in fact partially or totally compensated by the removal of soil entrapped within the turns of the auger during its retrieval. Several experimental results are available in literature where identical CFA piles installed in the same subsoil exhibited different load-settlement behaviour (approaching DP or NDP) as a function of the combination of installation parameters (Mandolini et al., 2002).

Jet grouting technique is based on high speed injection of fluids (cement-water mix, sometimes supplied by air and/or water) within previously drilled boreholes. The result of treatment is a partial removal of soil and a cementation of the remaining part in order to form a pseudo-cylindrical body (column). In principle, the diameter of jet grouting columns is given by the interaction between the erosive action of jets and the resistance of soils to cutting. Therefore, the desired diameter is obtained by properly selecting the injection technique (single, double or triple fluid) and by tuning the operational parameters (number and diameter of nozzles, injection pressure and/or flow rate, lifting speed of the monitor and grout mix composition). This type of foundation reinforcement can be broadly categorised in the class of ND piles. However, a peculiar aspect of jet grouting is represented by the irregular shape of columns, dictated contemporarily by the increase of soil resistance with depth and by random variations of the soil composition (Modoni & Bzówka, 2011). The resulting jagged profile is recognised to play a beneficial role on the response of columns since it promotes a better transfer of loads to the surrounding soil. Few experimental results available in literature (e.g. Bustamante, 2002; Modoni, 2011) seem to confirm that larger axial loads can be supported by jet grouting columns compared with NDP piles of similar dimensions. However, in the authors' knowledge, a comprehensive evaluation of the load-settlement response of jet grouting columns, based on a systematic comparison with piles formed with other techniques, has not been attempted yet.

The purpose of the present paper is to experimentally detect the influence of the installation technique on the load-settlement responses for different types of columnar reinforcements. Bearing in mind this goal, the results of several full scale axial loading tests carried out on columns of different dimensions (diameter, length) and installed with different techniques have been collected. The examined columns have been classified as displacement, non displacement, CFA piles and jet grouting columns. The results obtained for each group, expressed in terms of bearing capacity and mobilisation of load with settlement, are related to the properties of soil directly obtained from in situ investigations. Finally a comparison among all results is made, pointing out on the role of the installation technology, to support the selection among the different techniques and address preliminary design of columns for which not well established rules exist.

2. INTERPRETATION OF LOAD SETTLEMENT CURVES

The factors governing the response of axially loaded columns can be identified in the characteristics of columns (primarily diameter and length, with a minor role played by the column material stiffness), the properties of the undisturbed soil as measured before the installation of piles and the modifications induced on the surrounding soil by the installation of columns. To focus on this latter aspect, the results of axial loading tests on columns created with different systems in rather similar soil conditions are examined. Attention has been paid separately to the failure conditions and to the development of settlements at the beginning of tests. In particular, a failure load Q_{lim} has been conventionally defined as the one corresponding to a movement of the column's head equal to 10% of the nominal diameter. In most tests, since the maximum recorded movement was less than this limit, the load-movement curves have been extrapolated using the method proposed by Chin and Vail (1973). This method assumes a hyperbolic relation between applied load Q and settlement w is as described by the following expression:

$$Q = w / (m + n \cdot w) \quad (1)$$

A typical example of results is reported in Fig. 1 for a test on a jet grouting column having a diameter of 0.92 m (Bzówka & Pieczyrak, 2008). It shows that uncertainty of extrapolation can be minimized provided that the final linear trend in the w/Q-w plot is sufficiently developed, i.e. relatively high maximum settlements are reached during the test. For this reason, a selection has been necessary among all results and tests reaching particularly low settlements have been discarded.

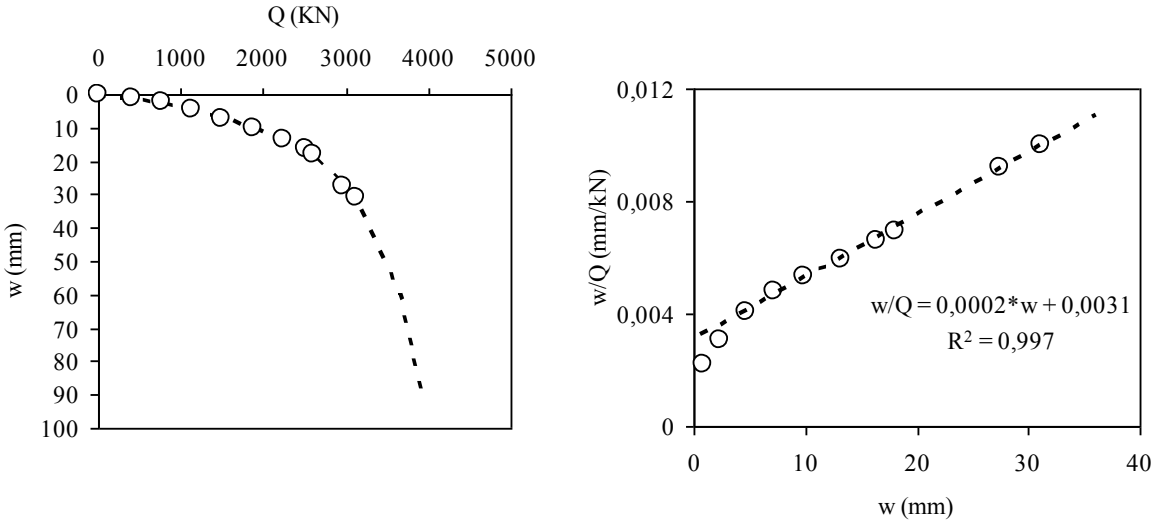

Figure 1: Extrapolation of the load settlement curve for the estimate of Q_{lim}.

All the available load test results have been subdivided into four different groups: non-displacement (NDP), displacement (DP) and CFA piles (CFAP) and Jet-Grouting columns (JGC).
In order to compare the load-settlement curves coming from tests on columns of the same group but different size (diameter and length), loads have been scaled with respect to the measured, or extrapolated, values of Q_{lim} and settlement have been scaled with respect to w_{lim} (=0.1*D).
Moreover, to take into account the amount of area over which unit resistance are mobilized, the available values of Q_{lim} have been scaled with respects to the nominal contact area of the column ($A = \pi \cdot D^2/4 + \pi \cdot D \cdot L$) that, in some way, is representative of the column costs. It follows that the ratio Q_{lim}/A could represent a bearing capacity indicator, which gives the amount of failure load per unit area of column available for resistance development. Similar scrutiny of data can be found in the literature (e.g. Mandolini et al., 2005) for NDP, DP and CFA piles installed in similar soil conditions. Finally, the undisturbed properties of the surrounding soil have been introduced in the analysis by relating the Q_{lim}/A ratios to the average cone resistance q_c measured with CPT tests along with the column length.

3. LOADING TEST RESULTS

3.1. Non-Displacement piles

In Fig. 2 the experimental data related to all ND piles (whose main data are listed in the Table) are reported. Looking at the non-dimensional curves $Q/Q_{lim} - w/w_{lim}$ (Fig. 2a), data are scattered as a consequence of a number of factors including: different slenderness ratio L/D playing a role in the ratio between the shaft and the base load; specific construction procedures (i.e. dry excavation, bentonite mud, steel temporary casing, etc.). Among all results, the two piles NDP6 and NDP7 deserve a particular attention because, in spite of significantly lower dimensions, present comparatively higher values of the ratio Q_{lim}/A (Fig. 2b). This effect can be ascribed to the particular technique adopted during their installation. Both piles were in fact constructed with the Wolfsholtz patented method (1926) based on the ejection of concrete supplied by pressurized air.

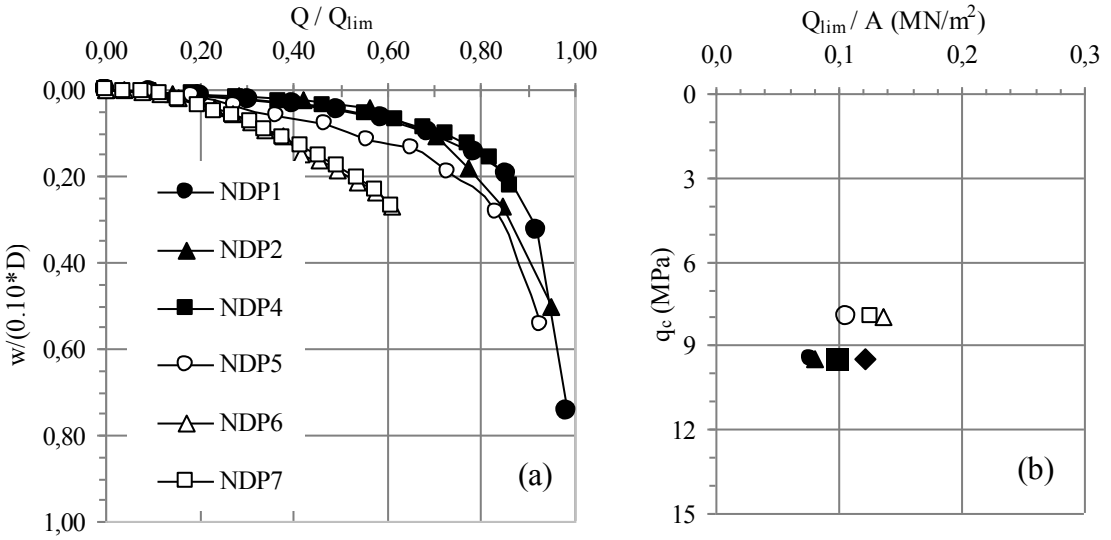

N° [-]	q_c [MPa]	L [m]	D [m]	Q_{max} [MN]	w_{max} [mm]	w_{max}/D [-]	Q_{lim} [MN]	$(\Delta Q/\Delta w)_o$ [MN/m]	Reference [-]
NDP1	9.44	42.0	1.50	15.0	111.5	0.074	15.3	1540.0	Mandolini (1994)
NDP2	9.44	42.0	2.00	20.3	100.0	0.050	21.3	2000.0	
NDP3	9.44	42.0	1.50	16.7	123.2	0.082	22.3	1763.6	
NDP4	9.44	42.0	2.00	28.0	45.00	0.023	32.4	2608.7	
NDP5	8.00	10.7	1.18	4.05	64.00	0.054	4.38	444.4	Tejchman (2001)
NDP6	8.00	6.60	0.40	0.70	10.80	0.027	1.15	900.0	
NDP7	8.00	6.60	0.40	0.70	10.70	0.027	1.07	600.0	

Figure 2: Experimental data for NDP: (a) non-dimensional curves; bearing capacity indicator (b).

3.2. Displacement piles

In Figure 3 the experimental data related to all D piles (whose main data are listed in the Table) are reported. It can be clearly seen from Fig. 3a that data are less scattered if compared to ND piles, even though this group includes piles installed with very different techniques (Pressodrill, Bauer Screw Pile, Multiton, Vibrotrevi, Franki).

This result can be explained considering that, independently on the adopted installation procedure, the increase of stress and the compaction produced on the surrounding soil give similar effects on the axial loading response. It is also particularly interesting to note (Figure 3b) that an almost linear relation exists between the bearing capacity indicator Q_{lim}/A and the q_c values.

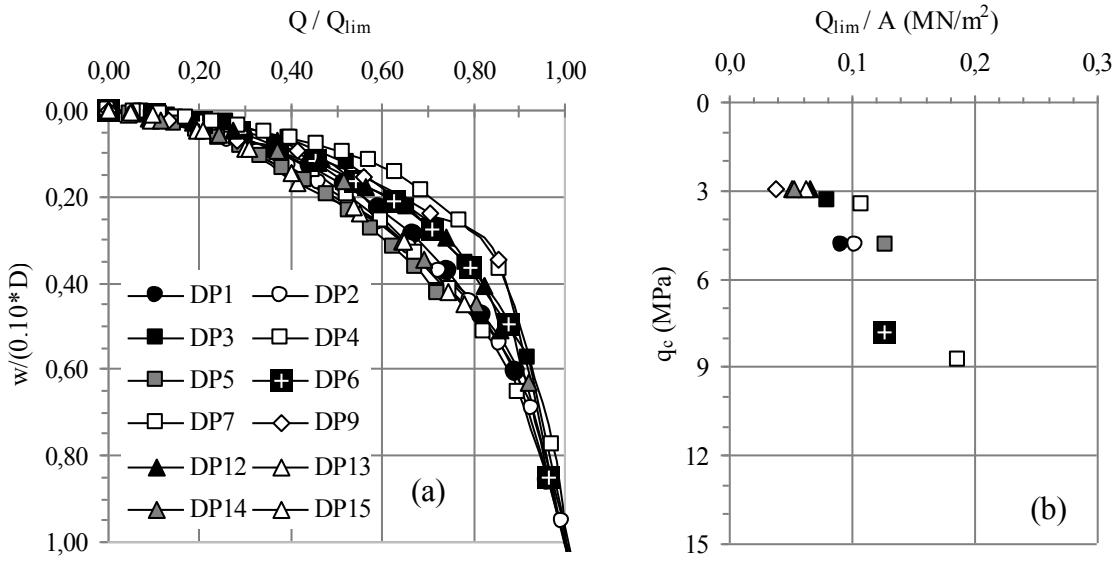

N° [-]	Pile type [-]	q_c [MPa]	L [m]	D [m]	Q_{max} [MN]	w_{max} [mm]	w_{max}/D [-]	Q_{lim} [MN]	$(\Delta Q/\Delta w)_o$ [MN/m]	Reference [-]
DP1	Pressodrill	4,84	23,1	0,60	4,20	70,62	0,118	4,03	422,54	Mandolini (1994)
DP2	Pressodrill	4,84	23,1	0,60	4,80	84,87	0,141	4,53	350,88	
DP3	Bauer	3,39	17,0	0,62	2,80	74,89	0,121	2,67	370,85	Mandolini (2011)
DP4	Bauer	3,51	22,0	0,62	4,80	66,64	0,107	4,67	634,44	
DP5	Bauer	4,83	29,0	0,62	5,27	26,24	0,042	7,27	560,30	
DP6	Bauer	7,80	14,6	0,51	3,00	53,73	0,105	2,96	437,34	
DP7	Bauer	8,79	14,3	0,62	5,27	64,18	0,104	5,25	837,21	
DP8	Multiton	2,96	30,0	0,46	2,90	19,93	0,043	3,96	291,67	Massaro et al. (2006)
DP9	Multiton	2,96	31,0	0,41	1,50	41,12	0,100	1,50	150,54	
DP10	Multiton	4,31	42,0	0,41	2,70	20,90	0,051	3,44	355,93	
DP11	Multiton	4,31	42,0	0,46	3,00	17,51	0,038	3,49	244,19	
DP12	Vibrotrevi	2,97	22,0	0,50	1,95	25,50	0,051	2,27	300,00	
DP13	Vibrotrevi	2,97	22,0	0,50	1,62	21,00	0,042	2,17	166,67	
DP14	Vibrotrevi	2,97	22,0	0,50	1,60	31,50	0,063	1,79	166,67	
DP15	Vibrotrevi	2,94	24,8	0,50	1,60	22,40	0,045	2,05	500,00	

Figure 3: Experimental data for DP: (a) non-dimensional curves; bearing capacity indicator (b).

3.3. CFA piles

As discussed in the previous paragraphs, the behaviour of this pile type is strongly affected by the installation parameters specifically adopted in each case (penetration and revolution rates during the insertion of the auger; retrieval rate and concrete supply pressure during the retrieval of the auger). Depending on how these parameters are combined, different effects on the surrounding soil are expected (net effect of compaction or loosening), giving rise to behaviours similar in some cases to ND piles, in other cases to D piles. It follows that some scattering (even if lesser than that of ND piles) must be expected as shown in Fig. 4a, mainly due to different selection in the installation parameters as rationally explained by Mandolini et al. (2002) on the basis of the simple screw theory. It is worthwhile to note that an increase of more than 50% of the bearing capacity indicator Q_{lim}/A has been measured for identical piles (CFAP1 and CFAP3) in the same subsoil conditions (q_c = 4.42 MPa) installed with same equipment at few metres each other but with different installation parameters.

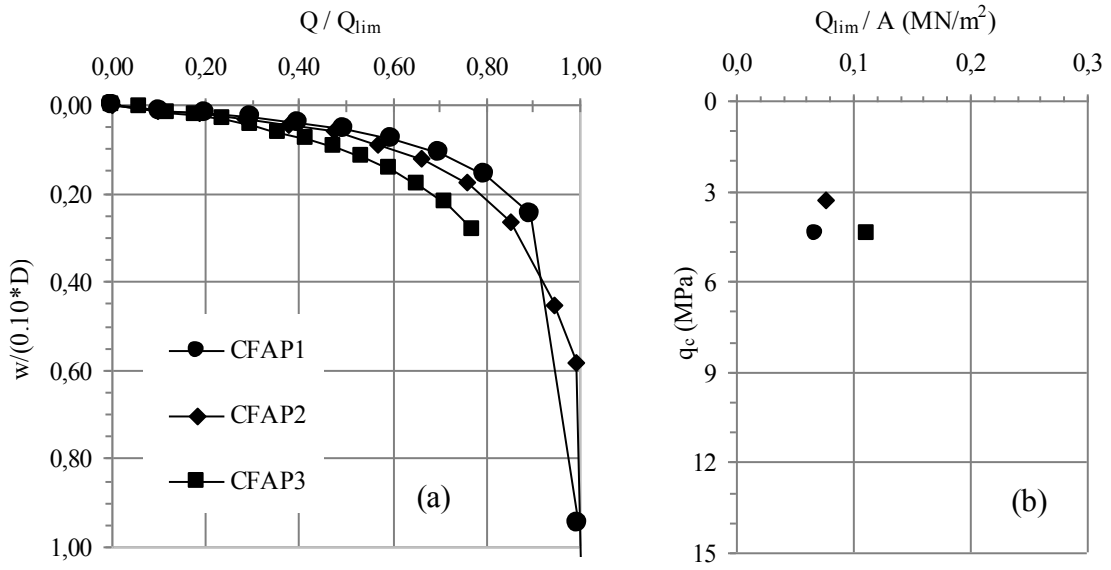

n° [-]	q_c [MPa]	L [m]	D [m]	Q_{max} [MN]	w_{max} [mm]	w_{max}/D [-]	Q_{lim} [MN]	$(\Delta Q/\Delta w)_o$ [MN/m]	Reference [-]
CFAP1	4.42	24.0	0.80	4.08	75.62	0.095	4.10	539.47	Mandolini et al. (2002)
CFAP2	3.30	22.5	0.60	3.26	81.94	0.137	3.24	314.43	
CFAP3	4.42	24.1	0.80	5.03	22.78	0.028	6.86	645.67	

Figure 4: Experimental data for CFA piles: (a) non-dimensional curves; bearing capacity indicator (b).

3.4. Jet grouting columns

Previous axial loading tests (Maertens and Maekelberg, 2001) have shown that the performance of jet grouting columns may be significantly inhibited by the collapse of the cemented soil. When this aspect is introduced in the load settlement analyses of single or grouped columns and typical strengths of cemented soil are considered, it is easily demonstrated that increases of column length beyond certain limits become ineffective (Modoni, 2011). For this reasons jet grouting is typically performed up to relatively limited depths (the columns studied examined in the present case are 7-8 metres long). The examined results show a similar trend of the dimensionless load settlement curves (Fig.5a) but significantly different values of Q_{lim}/A (Fig.5.b). A possible explanation for the latter evidence could consist in the random variations of the geometrical profiles, different from case to case depending on the heterogeneity of subsoil composition.

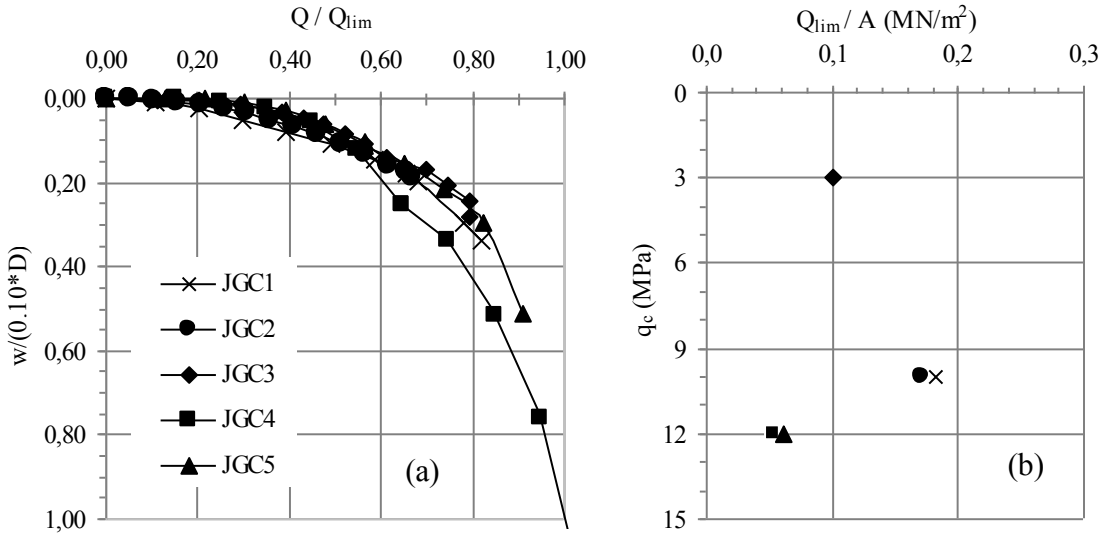

N° [-]	q_c [MPa]	L [m]	D [m]	Q_{max} [MN]	w_{max} [mm]	w_{max}/D [-]	Q_{lim} [MN]	$(\Delta Q/\Delta w)_o$ [MN/m]	Reference [-]
JG1	10.0	7.0	0.92	3.11	31.14	0.034	3.81	246.39	Bzówka & Pieczyrak (2008)
JG2	10.0	7.0	0.92	2.38	17.28	0.019	3.57	723.16	
JG3	3.00	4.0	0.80	0.84	22.68	0.028	1.06	259.17	Pieczyrak (2010)
JG4	12.0	8.0	0.35	0.50	42.33	0.121	0.48	206.17	Pieczyrak (2009)
JG5	12.0	8.0	0.35	0.50	17.92	0.051	0.55	668.00	

Figure 5: Experimental data for JG: (a) non-dimensional curves; bearing capacity indicator (b).

4. COMPARATIVE ANALYSIS OF RESULTS

In general, the loads applied at the column head are transferred to the surrounding soil along the lateral surface and at the base. Results of load tests on fully instrumented piles are of particular importance to understand how the applied load is shared among these two components. It is widely acknowledged that, for piles installed in homogenous soils, the relative importance of the two components at failure (respectively S_{lim} and P_{lim} at the side and the base) is strongly governed by the piles shape (namely length and diameter). In particular, for short and/or large diameter piles a predominance of the load transferred from the base is normally expected ($S_{lim}/P_{lim} < 1$), while for long and/or slender piles shaft resistance prevails ($S_{lim}/P_{lim} > 1$). The geometrical characteristics of piles are also of particular relevance in determining the shape of the load-settlement curves, as a consequence of the different growth of S and P with settlements. In fact, while S involves a sliding mechanism on the pile's shaft, resulting in a stiff response with S_{lim} attained at relatively small settlements (about 1-3% of D), mobilisation of P involves a punching mechanism at the pile's base where relatively large settlements are required to reach P_{lim} (10% of D or more). Keeping in mind these differences, it was decided to relate the load test results to the pile slenderness ratio (L/D), focusing particularly on the resistance (Q_{lim}) and on the initial stiffness $(\Delta Q/\Delta w)_o$. With regard to the former, the previously introduced bearing capacity indicator (Q_{lim}/A) has been divided by the unit cone resistance q_c to give an overall bearing capacity index. This latter has been then plotted versus L/D taking care to distinguish with symbols and shaded areas the data pertaining to each pile category (Fig. 6). As expected, for the range of comparable values of L/D (20-40), displacement piles (DP) exhibit larger values of $Q_{lim}/(A \cdot q_c)$ than non-displacement piles (NDP) and jet-grouting columns (JGC). Continuous flight auger piles (CFAP) give resistances comparable with those of DP piles, confirming that accuracy on the installation may lead to very satisfactory results. It is finally worth noting that dots representative of NDP and JGC are located in the same (lower) region of the plot, hence confirming the substantial equivalence among the two categories in terms of resistance. Some differences seem more related to the different L/D values typically used for piles and jet-grouting columns. In

particular, the low slenderness ratios currently adopted of jet grouting, dictated by the inherent weakness of the constituent materials, produce relatively high efficiencies.

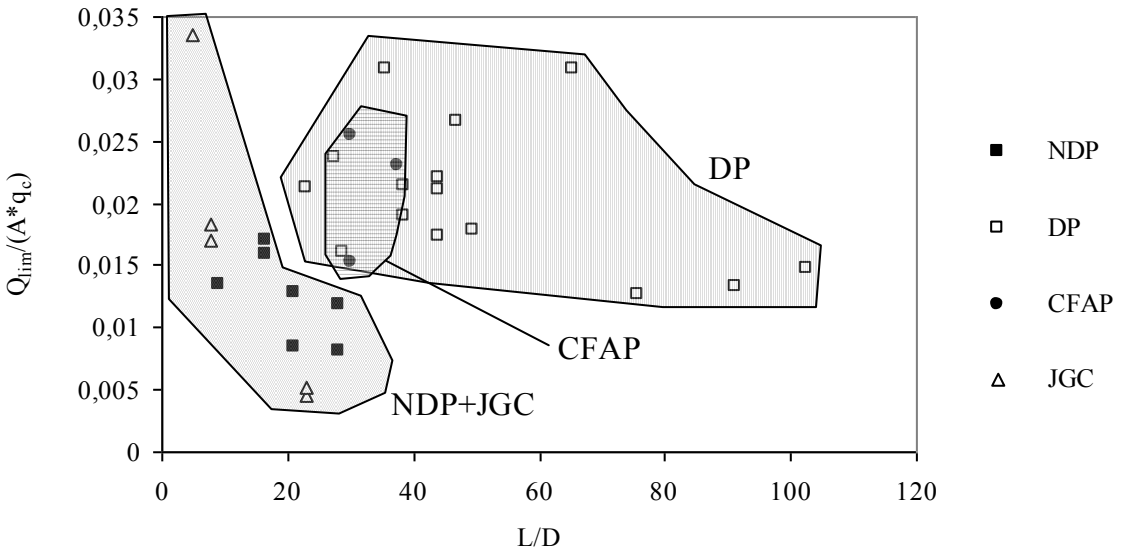

Figure 6: Bearing capacity ratio of columns installed with different techniques.

With regard to the initial stiffness of the pile-soil complex, data has been interpreted adopting the analytical solution given by Randolph & Wroth (1978), i.e. assuming that the loads applied during the initial part of tests are mainly transferred to the soil from the pile shaft (Q ≈ S). When introducing this assumption in the simple scheme of rigid pile embedded in a homogeneous elastic half-space, the axial pile-soil stiffness can be expressed as:

$$Q / w \approx S / w_s = 2 \cdot \pi \cdot L \cdot G / \zeta \quad (2)$$

ws represents the pile settlement measured at the shaft, equal to w if the pile is perfectly rigid, and ζ is equal to ln[5·(1-ν)·L/D]. For a given Poisson's coefficient (ν), the shaft flexibility coefficient ζ depends on the slenderness ratio L/D. If the "undisturbed" soil shear stiffness G is related to qc, as in typical empirical formula (G = k·qc with k dependent on the grain size distribution and relative density), the following non-dimensional parameters can be finally derived:

$$Q / (w \cdot L \cdot q_c) = 2 \cdot \pi \cdot k / \zeta \quad (3)$$

In similar subsoil conditions (as in the case examined in the present study), the "undisturbed" values of k should be similar before the pile installation, potentially different after pile installation due to changes in soil stiffness induced by the specifically adopted technology. It follows that the ratio k/ζ should depend on the "disturbance" (improvement or reduction) of soil stiffness and on the slenderness ratio L/D.

In Fig. 7 the initial soil-column stiffness $(\Delta Q/\Delta w)_o$, obtained by interpolating the first three points of the load-settlement curve (in order to eliminate experimental errors potentially occurring at very small settlements) has been divided by $(L \cdot q_c)$ and plotted versus the slenderness ratio L/D. Again data of each category have been distinguished in the plot by adopting specific symbols and shaded areas.

In the range of comparable values for L/D (20-40), the same conclusions drawn before in terms of resistance seems to appear: the response of displacement piles (DP) if stiffer than non-displacement piles (NDP) and jet-grouting columns (JGC), with continuous flight auger piles (CFA) exhibiting an intermediate behaviour. Again the relatively low slenderness of jet grouting columns promotes a good performance of the reinforcement in terms of settlement reduction.

In general, however, data appears to be less clustered than those concerning resistance, accordingly with other previous theoretical and experimental studies (e.g., Randolph, 2003; Mandolini et al., 2005). Such a difference can be explained considering that the resistance depends primarily on the properties of soil positioned near the interfaces (shaft and base of the pile), i.e. a very thin cylinder of soil whose properties can be strongly modified by the pile installation. On the contrary, the initial stiffness depends on the deformation of a larger mass of soil extending well far from the pile axis (several or tens of metres depending on L/D). Hence a reduced influence of the modification induced in the thin cylinder mentioned before must be expected. In conclusion, the installation technology plays a more significant role on the resistance of reinforcing columns, than on their initial stiffness.

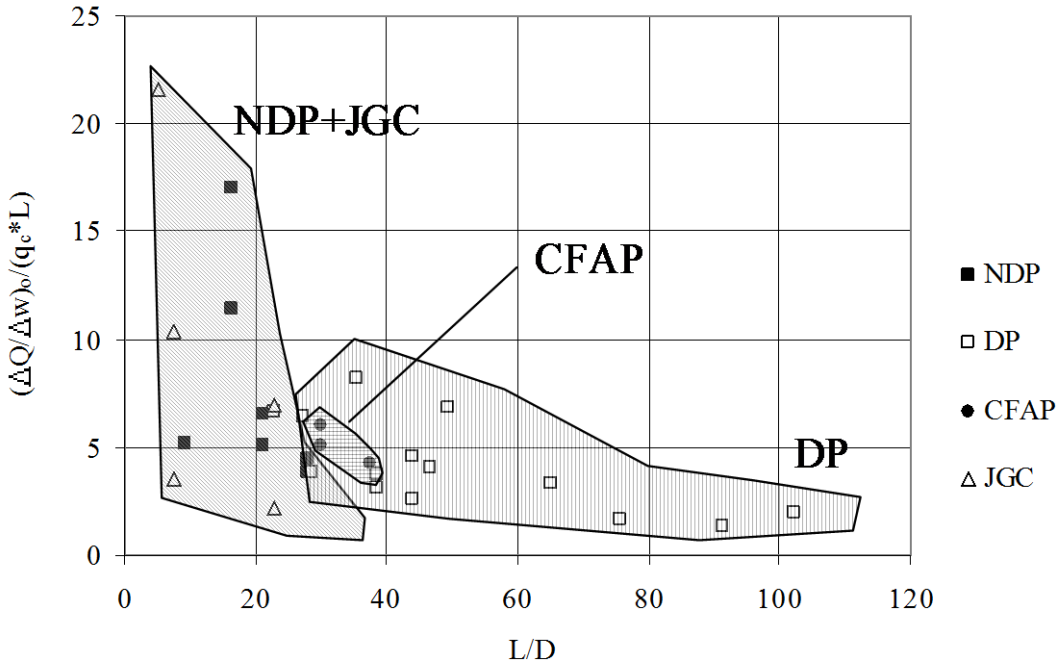

Figure 7: Dimensionless initial stiffness of the pile-soil complex.

5. CONCLUDING REMARKS

Different types of columnar reinforcements can be nowadays adopted to face bearing failure and intolerable settlements of foundations. Together with the traditional driven or drilled solutions, innovative reinforcing columns have been conceived to conjugate ease and fastness of installation with good performances. Advantages and limitations of each technique should be measured in terms of suitability (costs and feasibility) to the present conditions, but also performing preliminary mechanical analyses. The results of axial loading tests performed on different types of columnar reinforcements, grouped as Displacement, Non-Displacement, CFA piles and Jet Grouting columns, have been comparatively analysed in the paper to detect the influence of the installation technology on the load-settlement response. In spite of simplification introduced to compare all results, some effects of the technology could be highlighted. The summary of results has in fact shown that displacement piles (Pressodrill, Bauer Screw Pile, Multiton, Vibrotrevi and Franki) give higher failure loads compared with other categories, as a consequence of the increase of stresses and compaction produced near the interface between soil and pile. On the contrary, non displacement piles exhibit smaller failure loads due to soil loosening and stress reduction. If accuracy is placed in their installation, CFA piles show failure loads similar to DP. Jet-grouting columns behave similarly as NDP but, due to a combination of factors (i.e.: jagged column profile, which increases the shaft friction, limited slenderness) they are particularly effective reinforcements. With regard to the initial stiffness, the scattering of data seems mostly connected with the largely different ranges of L/D allowed by the different technologies (lower than 20 for JGC, more than 100 for DP). However, a similar conclusion as drawn for resistance can be derived among the different pile types, but with lesser extent due to the completely different soil masses involved in the interaction with piles near and far from failure.

REFERENCES

Bustamante M. (2002) "Les colonnes de jet grouting". Report of the Seminar: Pathologies des sols et des foundations, Hammamet (Tunisia) (French).

Bzówka J., Pieczyrak J. (2008): Pull out and load tests for jet grouting columns, Proceedings of the 11th Baltic Sea Geotechnical Conference, 15-18 September 2008, Gdańsk, Vol. 2, pp. 929-933.

Chin, F. K., and Vail, A. J. (1973). "Behavior of piles in alluvium." Proc. Eighth Int. Conf. on Soil Mech. and Found. Engrg., Moscow, Soviet Union, 2.1, 47-52.

Federal Highway Administration (1999), An introduction to the deep mixing methods as used in geotechnical applications, prepared by the ECO Geo systems, L.P. FHWA-RD-99-138 and FHWA-RD-99-144.

Ho, C. (1996) Treatment of soft clays with high organic content using lime piles" Proceedings of the 2nd Int. Conf. on Soft Soil Engineering, Nanjing, pp. 986-991.

Mac Donald, J. (1953), Foundations for Ringsend Power Station, Dublin, ,Geotechnique, Vol. 3, N°4, pp.143-153.

Maertens J., Maekelberg W. (2001). "Special applications of the jet-grouting technique for underpinning works". Proc. of the XV ICSMFE, Istanbul (Turkey), 1795-1798.

Mandolini, A., (1994), Cedimenti di fondazioni su pali, PhD Thesis, Dept. of Geotech. Eng., University of Napoli "Federico II"(Italian).

Mandolini, A., Russo G. and Viggiani C.(2002), Full scale loading testson instrumented CFA piles, Deep Foundation Congress, GeoInstitute of the ASCE, Orlando, Florida, pp.1088-1096.

Mandolini, A., Russo G. and Viggiani C. (2005). "Pile foundations: experimental investigations, analysis and design", State of the art report XVI ICSMGE, Osaka, 177-216.

Mandolini A., (2011), Full scale tests on piles, private communication.

Massaro I., Cotecchia F., Mandolini A. (2006), Comportamento di pali di diversa tecnologia in sabbie piroclastiche: analisi e progettazione, Proc. of V Nat. Conf. of Geotechnical Engineering, Bari (Italian).

Modoni, G., Bzówka, J., (2011), Analysis of foundations reinforced with jet grouting, Journal of Geotechnical and Geoenvironmental Engineering, ASCE, submitted for publication.

Modoni, G., (2011), Analisi e progettazione di fondazioni rinforzate con jet grouting, Atti del XXVI Convegno Nazionale di Geotecnica, Associazione Geotecnica Italiana, Napoli, 22-24 June, pp.199-215 (Italian).

Neate, J. J. (1988). "Augered cast-in-place piles." 13th Annual Meeting, Deep Foundations Institute, Atlanta, Ga., 167-175.

Perelli Cippo A. and Tornaghi R. (1985). "Soil improvement by jet grouting". Underpinning, Surrey University Press, S. Thorburn and J.F. Hutchison Eds., 276-292

Pieczyrak J. (2009.b). "Load tests of jet grouting columns in building, Kielce, Poland". GEOREM, private communication.

Pieczyrak J. (2010). "Load tests of jet grouting columns under swimming pool, Trzebnica, Poland". GEOREM. private communication.

Randolph, M.F. (2003). "43rd Rankine Lecture: Science and empiricism in pile foundation design." Géotechnique, 53(10), 847-875

Randolph, M.F., Wroth, C.P. (1978). "Analysis of deformations of vertically loaded piles." Journal of Geotechnical Engineering, ASCE, 104(GT12), 1465-1488

Shibazaki M., Ohta S. (1982). "A unique underpinning of soil solidification utilizing super-high pressure liquid jet", Proc. of the Conference of Grouting in Geotechnical Engineering, New Orleans, 680-693.

Tejchman A. Gwizdała K., Dyka I., Świniański J., Krasiński A. (2001). "Load capacity and settlement of foundation piles", Gdansk University, Poland.

Tomlinson, M.J., (1994), Pile Design and Construction Practice, Taylor & Francis eds., Fourth Editions.

Topolnicki M. (2003): Ground improvement, Charter 10: In-situ soil mixing, Ed. M.P. Moseley and K. Kirsch, Blackie Academic & Professional, an imprint of Chapman &Hall, CRC Press, Inc..

Yahiro T. and Yoshida H. (1973). "Induction grouting method utilizing high speed water jet", Proc. of the VIII Int. Conf on Soil Mechanics and Foundation Engineering, Moscow (Russia), 402-404.

Wolfsholtz, A., (1926), Method of and apparatus for making compressed concrete piles - United Kingdom Patent GB265861.

Axial Capacity of Vibro-Concrete Columns

Alexander B. Reeb, Virginia Tech, USA, reeba@vt.edu;
James G. Collin, The Collin Group, Ltd., USA, jim@thecollingroup.com

ABSTRACT

This study considers the axial capacity of Vibro-Concrete Columns (VCCs). VCCs are constructed similar to bottom-feed stone columns but use concrete instead of stone to form the column. They are typically installed in soft or compressible soils, which do not provide adequate lateral support for stone columns, and generate most of their capacity from end-bearing resistance on stiffer underlying strata. In current practice, there does not exist a standard design methodology specifically developed for VCCs. Instead, VCCs are designed using modified drilled shaft or driven pile design methods. In this study, the authors have analyzed 17 VCC case histories with load test information to determine the accuracy of drilled shaft and driven pile design methods for predicting VCC axial capacity. Based on these analyses, it has been found that drilled shaft methods generally predict a lower bound of VCC capacity while driven pile methods generally predict an upper bound. This paper discusses the study approach and collection of case histories, interpretation of load test results, application of design methods, and the study results and conclusions.

1. INTRODUCTION

This paper describes the authors' efforts to evaluate current design procedures for Vibro-Concrete Columns (VCCs) and to provide recommendations for a standard design methodology which more accurately predicts axial capacity.

1.1. Background

VCCs are a type of ground improvement used to increase the bearing capacity of soft soils overlying stiffer strata. A vibroflot, sometimes in combination with pre-augering, is used to form the initial column cavity. The column is constructed by pumping concrete to fill the void at the vibroflot tip during withdraw. Repenetration stokes are often used near the bottom and top of the column in order to form bulbs of densified concrete. The bottom bulb serves to improve bearing capacity while the top bulb ensures adequate load transfer at the surface and helps minimize the clear span between adjacent columns. Figure 1 shows a typical VCC construction.

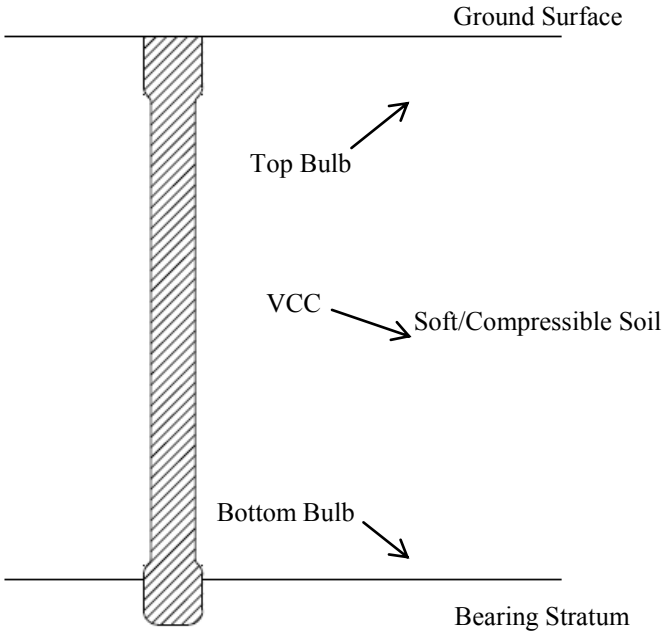

Figure 1: Typical VCC construction.

In current practice, there does not exist a standard design methodology specifically developed for VCCs. Instead, VCCs are designed using modified drilled shaft or driven pile design methods. Unfortunately, these methods do not accurately model the effects of the limited densification of soils during VCC construction. Drilled shaft design methods tend to underpredict capacity, while driven pile methods tend to overpredict capacity. In this paper, the authors have considered available case histories in order to assess the current state of practice and provide recommendations for determining the axial capacity of VCCs.

1.2. Approach

A straightforward and simple approach was used in this study. The approach is summarized by the following steps:

1. VCC case history and load test information was collected.
2. Load test results were analyzed to determine "actual" VCC axial capacities based on different interpretation methods.
3. Soil conditions and VCC geometry were used to determine design axial capacities based on different design procedures.
4. "Actual" and design capacities were compared and recommendations provided based on the results.

2. ANALYSIS

Over the course of this study, data from 17 VCC load tests have been collected representing seven different projects. All of the case histories were provided by private industry, one of which is also described in the literature. Although significantly more case histories exist in the literature, many of these did not contain the level of detail required for this study.

For each of the case histories the following information was collected:

- Column load test results – load-settlement curve preferred
- Column geometry – detailed column installation records preferred
    - Depth of column embedment
    - Bottom column bulb diameter
    - Shaft diameter (average value)
- Soil profile in vicinity of column – adjacent boring preferred
    - Depth to GWT
    - Soil descriptions and layering
- Soil parameters in vicinity of column – adjacent boring with SPT data preferred
    - Friction angles and cohesion ideal, but not generally determined in practice
    - Soil unit weight

2.1. Determination of "Actual" Capacities

Of the 17 collected VCC load tests, nine were static load tests and eight were statnamic load tests. The static load tests were analyzed using three different standard load test interpretation methods: Davisson (1972), Kyfor et al. (1992), and Kulhawy (2004). Each of these methods can be used to graphically interpret failure load. A failure line is drawn with an initial displacement offset based on VCC geometry and a slope based on either elastic compression or a modified interpretation thereof. In this study, the column bottom bulb diameter was used in place of the pile or drilled shaft diameter in the offset calculations. This is justifiable since the offset is representative of the toe movement required to mobilize end-bearing resistance. The intersection of the failure line with the load-displacement curve from the load test is interpreted as failure. These methods are described in more detail in the literature. Because some of the VCC load tests were not loaded sufficiently, it was only possible to interpret failure loads for four of the nine load tests based on these methods. The statnamic load tests were not analyzed using these methods because their applicability is unknown.

For all of the load tests, a subjective analysis was performed and it was noted if the test appeared to indicate an ultimate failure load, after which a small increase in load resulted in a large increase in displacement. Based on this subjective analysis, it appeared that four of the load tests clearly failed, two of which were static and two of which were statnamic load tests.

In order to be consistent in this study, it was decided to use the maximum load from each load test as the "actual" capacity of the VCC. For load tests that appear to indicate an ultimate failure load, the maximum

load test load should be approximately equal to the ultimate failure load. For load tests that do not appear to indicate an ultimate failure load, the maximum load test load can be taken as a lower bound for the ultimate failure load. Readers should keep this in mind when viewing the results of this study.

2.2. Determination of Design Capacities

Most of the VCCs analyzed in this study were installed through loose cohesionless or soft clay soils to a denser cohesionless bearing stratum below. In addition, typically only SPT N-values were provided. As a result, soil properties for the cohesionless soils could be estimate based on correlations but it was not possible to estimate soil properties for the clay soils with reasonable accuracy. However, the clay soils were typically soft, so they should not contribute significantly to VCC capacity, and most of the VCC soil profiles were dominated by cohesionless soils. Therefore, it was acceptable to neglect the contributions of clay soils to design capacity in these cases. Of the 17 collected VCC load tests, it was not possible to determine design capacities for five of the VCCs. Three VCCs contained too much clay in the subsurface profile, and, in the other two cases, the VCC geometry was not clearly specified. Two more of the VCCs had significant clay in the profile but design capacities were still calculated. In addition, not enough information was available regarding the subsurface profile for two other VCCs and it was only possible to calculate base resistance for these VCCs. Therefore, for these last four cases (which correspond to numbers 1, 2, 14, and 15 in Figure 2), the calculated design capacities would be greater if more complete information was available.

For the 12 cases where design capacities were calculated, the following design methods were used:

- O'Neill and Reese (1999) method from the *1999 FHWA Drilled Shafts Manual*
- Meyerhof (1976) for drilled shafts and driven piles
- Modified version of the U.S. Army Corps of Engineers (ACE 1991) method from *EM 1110-2-2906 Design of Pile Foundations*
- Neely (1990) method for expanded-base piles

A short summary of each design method is provided below.

2.2.1. O'Neill and Reese (1999)

This design method is based on the *1999 FHWA Drilled Shafts Manual* (O'Neill and Reese) and is sometimes referred to as the depth-dependent β method. A β value is calculated for each soil layer based on the soil description, depth to the middle of the layer, and average N_{60} blow counts for the layer. Unit shaft resistance is calculated for each soil layer by multiplying the β value by the vertical effective stress at the middle of the layer. Base resistance is calculated based on the average N_{60} value (not corrected for overburden) of the base layer. O'Neill and Reese recommend that average N_{60} values to a distance of two base diameters below the base be used.

2.2.2. Meyerhof (1976)

The Meyerhof methods are based on *Bearing Capacity and Settlement of Pile Foundations* (Meyerhof 1976). Unit shaft resistance is calculated for each soil layer based on the average corrected N_{60} values. Unit shaft resistance is limited to a maximum value of 2,000 psf as recommended in the *1998 FHWA manual Design and Construction of Driven Pile Foundations* (Hannigan). Unit base resistance is calculated by first determining the limiting value of unit base resistance for the base layer from the corrected N_{60} value. Next, the limiting values of unit base resistance for the layers immediately above and below the base layer are calculated. If one of the bounding layers has a lower value of unit base resistance and the pile tip is within 10 base diameters of that layer, the unit base resistance is reduced by the weighted average of the two values. For example, if a pile terminates at the interface of a loose layer overlaying a dense layer, the limiting value of unit base resistance for the loose layer is used. For a pile that terminates 10 base diameters or more from either bounding layer, the limiting value of unit base resistance for the base layer is used.

Separate equations are provided for "bored piles" (drilled shafts) and driven piles in Meyerhof (1976). The equations for drilled shafts predict smaller values of shaft and base resistance than the driven pile equations.

2.2.3. *Modified ACE (1991)*

This design method is a modified version of the ACE method from *EM 1110-2-2906 Design of Pile Foundations*. For this method, shaft resistance and end-bearing resistance are assumed to increase linearly with increased vertical effective stress. Unlike the ACE method, a critical depth, below which shaft resistance and end-bearing resistance remain constant, is not used. Unit shaft resistance is calculated for each layer based on the lateral earth pressure coefficient (K), the vertical effective stress at the middle of the layer, and the friction angle between the soil and column. Guidance on K values can be found on pages 4-12 and 4-13 of the ACE manual. Unit base resistance is determined using the vertical effective stress at the base of the column and the bearing capacity factor Nq.

2.2.4. *Neely (1990)*

From *Bearing Capacity of Expanded-Base Piles in Sand* (Neely 1990), this design method was empirically developed for expanded-base piles (i.e., pressure injected footings or Franki Piles). Expanded-base piles are installed by driving a steel pipe with concrete plug into the ground. After the desired depth is reached, the steel pipe is held in place as the concrete plug is driven outward through the base, resulting in a bottom bulb or expanded-base. Additional charges of concrete are driven though the pipe to form the column. The pipe can either be removed during installation or left in place. The bearing capacity of expanded-base piles tends to be greater than that of ordinary piles due to the greater densification achieved at the base during installation. Based on his analysis of load test results, Neely (1990) recommends that the bearing capacity of expanded-base piles be estimated by correlations between N_{60} values (corrected for overburden) of the bearing layer and base resistance, similar to the Meyerhof methods. Unlike the Meyerhof methods, the based resistance is calculated based on the total embedment of the pile, and is not dependent on soil layering.

2.3. "Actual" vs. Design Capacities

Figure 2 shows the arithmetic difference between "actual" and design axial capacities for individual VCCs. As discussed in Section 2.1, the "actual" capacity was taken as the maximum load from the load test. Therefore, if a VCC load test was not taken to failure, it would be expected that design methods would "overpredict" capacity as shown in the figures below. The only load tests that appeared to fail based on a subjective review were numbers 1, 4, 11, and 14 as indicated in Figure 2. (Load test 13 also appeared to fail but it was not possible to calculate design capacities for this VCC.) Of the load tests that failed, 4 and 11 had the most complete information regarding soil conditions and VCC geometry. As mentioned above, the calculated design capacities for VCCs 1, 2, 14, and 15 would be greater if more complete information was available.

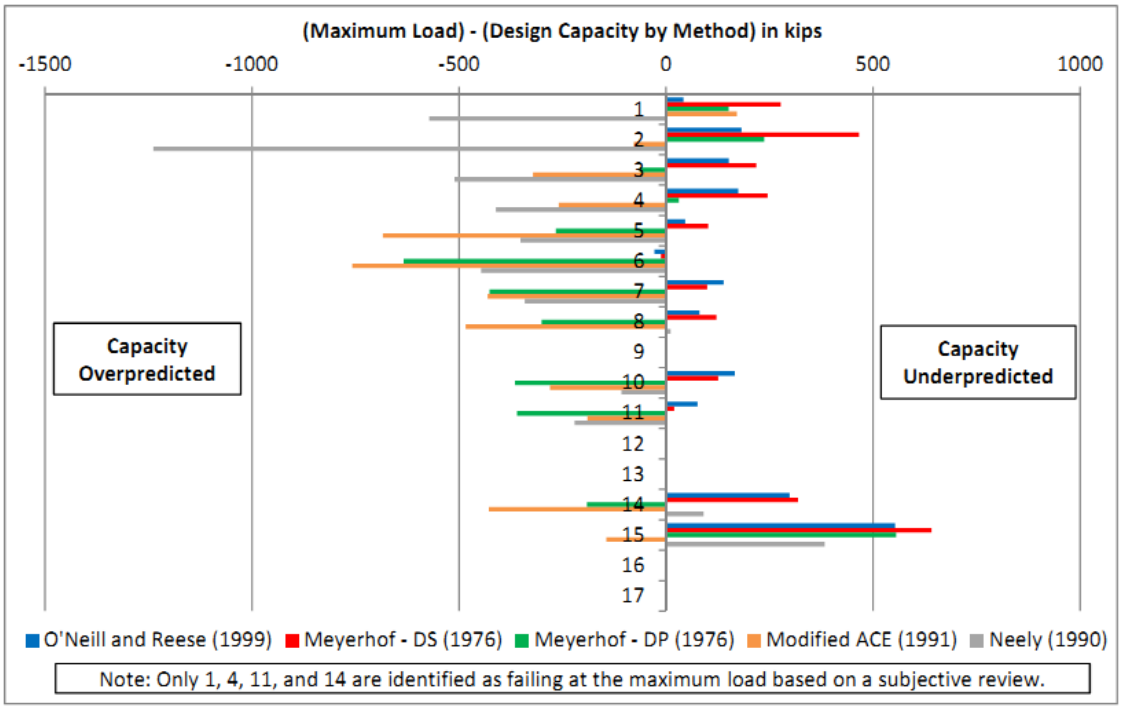

Figure 2: Comparison of "actual" and design capacities.

3. RESULTS

Obviously, the available data is very limited and it is difficult to provide recommendations for a standard VCC design procedure. Based on the limited data that has been analyzed, it seems apparent that current design procedures fall significantly short of accurately determining VCC axial capacities. As suggested in Section 1.1, the drilled shaft methods generally tended to underpredict capacity and the driven pile procedures generally tended to overpredict capacity.

The Meyerhof method for drilled shafts and the O'Neill and Reese method seemed to predict a lower bound for VCC axial capacity. Both methods predicted capacities for nearly every case (11 out of 12) that were less than the VCC "actual" axial capacity. In the one case where the predicted capacity was not exceeded, the predicted capacities were less than 10% greater than the "actual" axial capacity, and the "actual" axial capacity was equal to the maximum load test load and not the true axial capacity for this VCC (i.e., the load test did not appear to fail at this load). The Meyerhof method for driven piles, Modified ACE method, and Neely method all generally predicted capacities that were greater than the VCC "actual" axial capacity. However, these results were not as consistent.

4. CONCLUSION

In conclusion, it is the finding of this paper that the O'Neill and Reese method and Meyerhof method for drilled shafts can be used as lower bounds for estimating ultimate axial capacity of VCCs, and the Meyerhof method for driven piles, Modified ACE method, and Neely method can often be taken as upper bounds. However, these recommendations should be validated and refined by analyses on additional case histories.

REFERENCES

ACE (1991). Design of Pile Foundations. EM 1110-2-2906.

Davisson, M. T., (1972). High Capacity Piles, Proceedings of Lecture Series on Innovations in Foundation Construction, ASCE, Illinois Section, Chicago, March 22, pp. 81-112.

Hannigan, P.J., et al. (1998). Design and Construction of Driven Pile Foundations, Volume I. Publication No. FHWA-HI-97-013.

Kulhawy, F. H., (2004). On the Axial Behavior of Drilled Foundations, GeoSupport 2004: Drilled Shafts, Micropiling, Deep Mixing, Remedial Methods, & Specialty Foundation Systems (GSP 124), Ed. J. P. Turner and P.W. Mayne, ASCE, Reston, VA, February, pp. 34-51.

Kyfor, Z. G., Schnore, A. R., Carlo, T. A., Baily, P. F., (1992). Static Testing of Deep Foundations, U.S. Department of Transportation, Federal Highway Administration, Washington DC, Report No. FHWA-SA-91-042, 174 p.

Meyerhof, G. G. (1976). Bearing Capacity and Settlement of Pile Foundations. Journal of the Geotechnical Engineering Division of the ASCE, Vol. 102, No. GT3. March 1976.

Neely, William J. (1990). Bearing Capacity of Expanded-Base Piles in Sand. Journal of Geotechnical Engineering, ASCE, Vol. 116, No. 1, pp. 73-87.

O'Neill, W. M., Reese, C. L. (1999). Drilled Shafts: Construction Procedures and Design Methods. Publication No. FHWA-IF-99-025.

A Study on the Use of Drilled Shafts to Reinforce Stiff Clay with Very Weak Sliding Planes

Rodolfo Sancio, MMI Engineering, USA, rsancio@mmiengineering.com)
Osama Safaqah, Imperial Oil Resources, Canada)
Patrick Wong, ExxonMobil Development Company, USA,
Chunling Li, Geosyntec Consultants, USA, cli@geosyntec.com
Paul Sabatini, Geosyntec Consultants, USA, psabatini@geosyntec.com)
Billy Villet, MMI Engineering, USA, bvillet@mmiengineering.com)

ABSTRACT

The use of driven piles, drilled shafts, soil mixed columns, and aggregate piers to support reinforced and unreinforced embankments in soft soil profiles has become a reliable foundation and ground improvement method. Their use under storage tanks with soft foundation soils has also been widely documented. The purpose of the vertical elements (or columns) is to reduce the load on the soft ground by transferring these loads to deeper and more competent strata, and to increase the shear resistance of the soil.
The literature on the use of vertical elements to support embankments typically refers to their use in soft soils because stiff soils seldom require improvement.
This paper describes a feasibility study conducted using finite element analyses to evaluate the use of drilled shafts to support a 20-m high mechanically stabilized earth (MSE) wall. The MSE wall was to be founded over stiff heavily overconsolidated clay that exhibits presheared subhorizontal planes that have been mobilized to their residual shear strength. The analyses showed that drilled shafts can be used to support the MSE wall and effectively mitigate sliding through the weak planes.

1. INTRODUCTION

The operator of a large oil sand extraction facility in the Athabasca region of Canada required a 20-m high and approximately 450-m long mechanically stabilized earth (MSE) wall to be built over a site with a subsurface profile comprising stiff, overconsolidated, and slickensided montmorillonitic clay shales and silts of the cretaceous Clearwater formation. Typically, MSE walls can be built over this profile without major concerns regarding global stability. However, previous experience for this formation in the Athabasca region site indicated that the clay shale profile exhibits presheared subhorizontal layers that are characterized by having shear strength at residual values (e.g., Alencar et al. 1994, Moore et al. 2006). Construction of the MSE wall over this subsurface profile could potentially lead to global instability due to sliding surfaces that develop through the weak layers.

Given the extensive experience with the construction of reinforced and unreinforced embankments and walls over piles and columns, the project team evaluated the feasibility for the construction of the 20-m high MSE over a grid of reinforced (or unreinforced) concrete drilled shafts. The term “column” is used in this paper to describe a ground improvement technique that creates vertical elements that are stiffer than the surrounding soil and therefore have the ability to “attract” loads imposed by the overlying embankments. Such technologies include, among others, Rammed Aggregate Piers (RAP) and Deep Soil Mixing (DSM) piers, as well as the drilled shafts referred to throughout this paper.

This paper presents the analyses that were conducted to evaluate the feasibility of a 20-m high MSE wall over a grid of reinforced concrete drilled shafts to mitigate the potential for global instability due to sliding along weak layers.

2. ANALYSIS OVERVIEW

Placement of MSE walls and embankments over columns rely on relieving the ground from the embankment stresses that are caused by the self weight of the embankment and other live loads. Embankment stresses are distributed or shed onto the columns due to the higher stiffness of the columns compared to the ground and the combination of the effect of soil arching and the tensile strength of the soil reinforcement (geosynthetics, steel strips, etc.) The stresses on the columns are transmitted to lower strata through side friction and/or end bearing. The use of columns also has the effect of increasing the

overall shear strength of the soil under the MSE wall or embankment. The concept works in situations where weak sliding planes are present because piles provide shear and bending resistance along weak layers.

The British Standard BS 8006:1995 "Code of practice for strengthened/reinforced soils and other fills" includes recommendations and guidelines for analysis and design of pile supported embankments. According to BS 8006:1995, "The technique of piling enables embankments to be constructed to unrestricted heights at any construction rate (assuming the fill is suitably stable) with subsequent controlled post-construction settlements." Figure 1 shows the ultimate limit states recommended in BS 8006:1995 that should be considered in the design of these structures, namely:

a) Pile group capacity, where the structural capacity of the piles is checked.
b) Pile group extent, which refers to the verification of the stability of the embankment at the edges.
c) Vertical load shedding, where the effect of load shedding on the localized settlement of the surface of the embankment is checked.
d) Lateral sliding stability of the embankment fill, where the reinforcement should be designed to resist the horizontal force due to lateral sliding.
e) Overall stability, where verification of the stability of the system is checked.

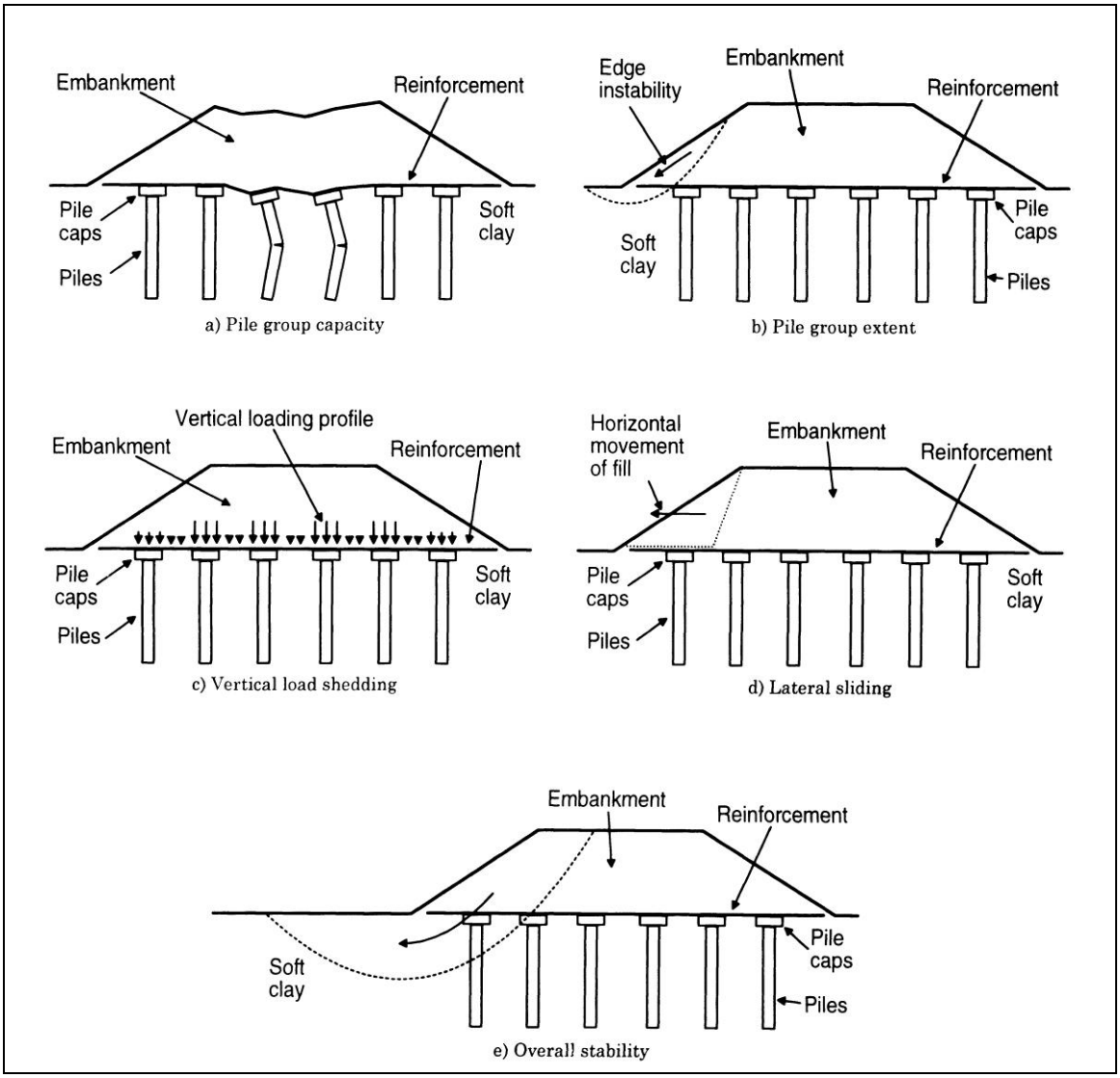

Figure 1: Ultimate Limit States for Basal Reinforced Piled Embankments (from BS 8006:1995)

The five limit states described above can be studied by conducting two dimensional (2D) or three dimensional (3D) finite element analyses of the MSE wall system. The analyses can be used to satisfy Factor of Safety for global stability and serviceability limit states. The stresses in the piles that are calculated in the analyses can be compared with the structural capacity of the piles (compressive, shear,

and bending), and sliding and global stability can be studied by interpreting the strains and displacements in the soil and piles. Although not shown in Figure 1, the stresses in the internal reinforcement calculated from the finite element analyses can be checked against their capacity.

3. SUBSURFACE CONDITIONS

3.1. Stratigraphy

For this project, the subsurface conditions consist of approximately 26 m of grey-black shales interbedded with clayey silt and glauconitic fine-grained sand of the cretaceous Clearwater formation (Kc). The materials in this unit typically classify as fat clay (CH), lean clay (CL), and silt (ML) according to the Unified Soil Classification System (USCS). The Clearwater facies present at this site unit are Kcc, Kcb, and Kca, and Kcw. The symbol Kc will be used for brevity. The Kc unit occasionally exhibits sub horizontal presheared layers that can be as thin as a few decimeters or as thick as a few meters. These layers are significantly weaker than the cross bedded shale.

The location of these weak layers within the profile is difficult to assess using common geotechnical site investigation tools because the index properties and penetration resistance are not very different than that of the overlying and underlying materials. These units, however, are known to exhibit slightly lower densities when surveyed using downhole gamma loggers and can sometimes be visually detected in cores due to combined presence of slickensides and very high PI.

The Kc unit is underlain by 3 m of interbedded glauconitic fine to medium grained sandy silt, silt and clayey silt. The geologic symbol of this unit, also of the Clearwater formation, is Kcw.

Oil-bearing sand, silty sand, silty clay and clay of marine and estuarine origin underlie the Kcw to the extent of interest. The geologic symbol of this unit is Ukm. The materials of this unit typically classify as SM, SW, SC. SP according to the USCS.

3.2. Material Parameters

The Clearwater formation has been extensively tested and studied by others such as described by Alencar et al. (1994) and Wedage et al. (1998), Moore et al. (2006) and shear strength parameters appropriate for slope stability analyses have been developed. Also, numerous embankments and dykes have been built and monitored at this facility providing information for shear strength assessment. The response of the soils at the site is best predicted by using effective stress parameters in combination with the use of appropriate characterization of the pore water pressure, as will be described in a subsequent section.

Table 1 lists the effective stress shear strength and elastic parameters for the materials for input in the elasto-plastic Mohr Coulomb constitutive model, which we considered appropriate to represent the response of the materials for this evaluation. The Mohr-Coulomb shear strength envelope parameters, friction angle (φ), and cohesion intercept (c) were chosen based on site specific soil data obtained for this study, which was at times consistent with values used by others to characterize similar the soil units (e.g., Moore et al., 2006, Alencar et al, 1994, and Wedage et al., 1998). The magnitude of the elastic modulus (E) for the Kc and Ukm was initially chosen to be similar to the values previously used by Alencar et al. (1994) and Wedage et al. (1998), respectively. However, greater values were justified and implemented as is described in the next section.

Table 1: Material elastic and shear strength parameters used in the analysis

Material	E (MPa)	μ	γ (kN/m^3)	φ (degrees)	c (kPa)	K_0
MSE Wall Backfill	50	0.2	19.1	33	1	-
Cross bedded shale (Kc)	45 to 90	0.35	20	20	25 to 50	2
Weak layers (Kc)	45 to 90	0.35	20	8	1	2
Kcw	200	0.2	20	33	20	2
Ukm	250	0.2	21	54	20	2

3.2.1. *Shear Wave Velocity Measurements*

The magnitude of the shear wave velocity (V_s) was measured during a site-specific geotechnical investigation conducted by others at several borings throughout the site of the MSE wall using the downhole technique. The plot on Figure 2 presents the measurements of V_s as a function of depth below the ground surface. The best-fit line, calculated using the least square method, and the standard deviation of the residuals are also shown. The plot shows that the best-fit line of V_s increases with depth from a value of approximately 340 m/s at ground surface to 600 m/s at 26 m below ground surface.

The magnitude of the elastic modulus was calculated using elastic theory following the equation below, where G_{max} is the small strain shear modulus, D is a correction factor that accounts for strain degradation of the modulus, and ρ is the mass density. The values of E plotted on the right side of Figure 2 were developed using the elastic theory based procedure with a relatively low correction factor of D = 0.1, which is founded on strain-based modulus degradation. The plot shows that representative values of E increase with depth from 70 MPa at ground surface to 150 MPa at 26 m, and are significantly greater than the value of 45 MPa used by Wedage et al (1998). Moreover, a magnitude of D = 0.3 may be more appropriate considering that the material is subjected to significant strains only along the weak layers.

$$E = D \cdot E_{max} = D \cdot 2 \cdot (1 + \mu) \cdot G_{max} = D \cdot 2 \cdot (1 + \mu) \cdot \rho \cdot V_s^2$$

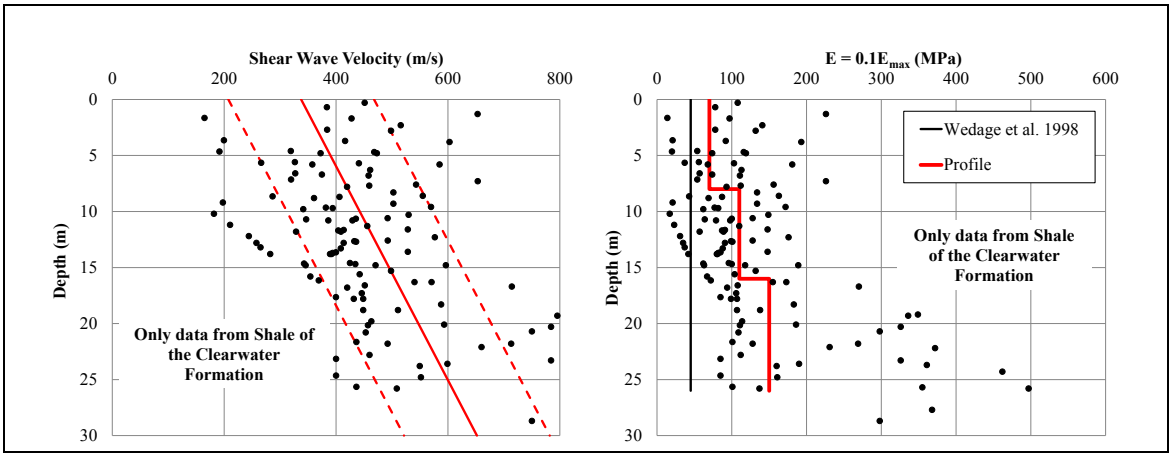

Figure 2: Plot of shear wave velocity and derived elastic modulus

As listed on Table 1, a range of 45 to 90 MPa was used to characterize the modulus of the clay shale. The lower value of the range was used to maintain consistency with values used in the literature, whereas the higher value of the range was considered to be better justified because it was conservatively estimated from in situ measurements of V_s.

3.3. Excess Pore Water Pressures

The site has been extensively instrumented with vibrating wire piezometers over the last 20 years. This has allowed the operators of the facility to develop an understanding of the excess pore water pressures that develop upon loading and unloading of the clay shale. The pore water pressures for our calculations were prescribed by the site operators for this analysis using the R_u parameter, which is defined as the ratio of the pore water pressure, u, and the total vertical stress (σ_t). For these analyses, R_u = 0.45 was used to describe initial conditions and R_u = 0.65 was assumed to be representative of the pore water pressure conditions immediately after the placement of fill (i.e., applicable to the areas loaded by the construction of the MSE wall).

4. METHODOLOGY USED FOR ANALYSIS

4.1. 2D Finite Element Analyses

Finite element analyses were carried out to model the construction of the MSE wall over concrete columns using PLAXIS 2D v.8.6 developed by PLAXIS of Delft, The Netherlands. PLAXIS 2D uses 15-node triangular elements. The finite element mesh was generated by first selecting a global coarseness and then allowing PLAXIS to generate the finite element mesh automatically. The mesh was then inspected and remeshed in areas where stress concentrations or relatively large shear strains would be

expected to be computed, like, for example, at the toe of the MSE wall and within weak layers. Individual elements typically had a dimension between 1 and 10 m.

The concrete columns were modeled using solid, linear elastic elements, rather than structural elements. The interface between the concrete columns and the surrounding shale was modeled using interface elements. In PLAXIS, the shear strength at an interface is computed as the product of a reduction factor and the strength parameters (tangent of the friction angle and cohesion) of the adjacent material. Therefore, an interface adjacent to a phi-c material will unavoidably have phi-c strength characteristics.

The elastic modulus of unreinforced concrete columns was assumed to be 24.8 GPa. This value was reduced to represent the separation between columns in the out-of-plane direction, such that the ratio of 24.8 GPa and the modulus that was used in the analysis is equal to the assumed separation distance between adjacent columns.

The reinforcement of the MSE wall was modeled using geosynthetic elements in PLAXIS to which an elastic axial stiffness and strength was assigned that was representative of Reinforced Earth Company (RECO) metal strips separated 0.75 m horizontally and 0.5 m vertically. The interface strength with the soil was assigned as equal to the friction angle of the soil based on testing conducted by Brockbank et al. (1992).

4.2. Parametric Analysis

Parametric analyses were conducted to assess the effect of: (a) the number, depth, and thickness of the weak layers within the shale; (b) the magnitude of the elastic modulus of the shale; and (c) the number, spacing, and depth of the drilled shafts.

Available case histories show that displacements occur over a maximum of two weak layers with most movement concentrated over one of the weak layers, however, analyses were conducted assuming the existence of one, two, three, four, or six weak layers. The thickness of these weak layers was assumed to be 0.5-m or 2-m, and the separation between weak layers was assumed to be 6 m or 8 m between the center of the layers. The depth from the ground surface to the top of the first weak layer was assumed to be either 2 m, 6 m, or 24 m below ground surface.

An initial geometry consisting of five rows of 29-m long and 1-m diameter drilled shafts (Geometry 1) was used. However, this system would collapse after placement of only 14 m of fill, when six 2-m thick weak layers were assumed within the profile.

Subsequently, the following drilled shaft geometries were considered in the parametric analyses:

- A configuration of nine rows of 1-m diameter and 29-m long columns with a separation of 4 m between columns (Geometry 2).
- A configuration of five rows of 1-m diameter and 29-m long columns with a separation of 8 m between columns (Geometry 3).
- A configuration of seven rows of 1-m diameter and 29-m long columns with a separation of 4 m between the first five rows and 8 m between the subsequent rows (Geometry 4, which is shown schematically on Figure 3).
- A configuration of seven rows of 1-m diameter and 30-m long columns with a separation of 4 m between the first five rows and 8 m between the subsequent rows (Geometry 5).
- A configuration of five rows of 1-m diameter and 30-m long columns with a separation of 4 m between columns (Geometry 6).

The results of the other parametric analysis are described in the next section.

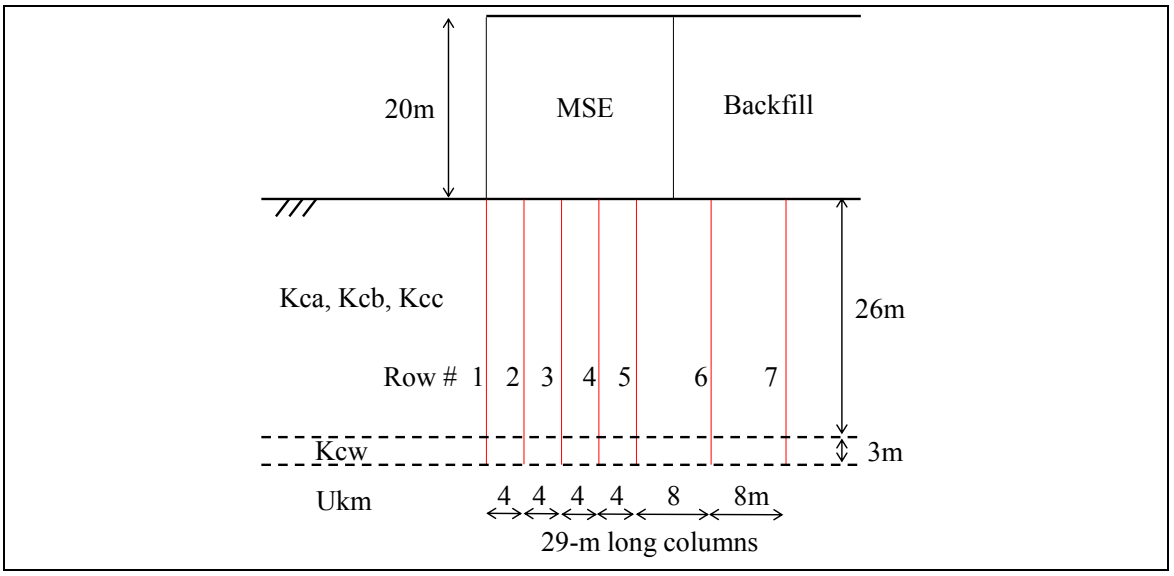

Figure 3: Schematic cross section layout of Geometry 4

4.3. Results of the Analysis

4.3.1. Factor of Safety and Displacements

Based upon the results of numerous preliminary analyses, it was concluded that the factor of safety (*FS*) and the horizontal displacement of the toe of the wall (δ_{xA}) were computed output values that could be used to judge the acceptability of a particular geometry and subsurface layering. PLAXIS allows the calculation of the factor of safety (*FS*) by progressively decreasing the magnitude of the shear strength of the materials until very large deformations develop. The factor of safety is the ratio of the initial strength and the strength that leads to significant deformation. The results of the parametric analysis are summarized in Table 2.

Table 2: Summary of parametric 2D FE analysis for the MSE wall over drilled shafts

Case	Geometry	Description of Weak Layers	*FS*	δ_{xA} (m)
1	2	One 2-m thick layer. Top of layer at 2 m below ground surface.	1.50	0.31
2	3	One 2-m thick layer. Top of layer at 2 m below ground surface.	1.02	0.72
3	4	One 2-m thick layer. Top of layer at 2 m below ground surface.	1.46	0.42
4	5	Six 0.5-m thick layers every 6 m. Top of first layer is at 2 m below ground surface.	1.42	0.67
5	5	Three 0.5-m thick layers every 8 m. Top of first layer is at 2 m bgs.	1.49	0.44
6	5	One 0.5-m thick layer. Top of layer is at 6 m below ground surface. A 2-m thick layer of soil cement (E = 150 MPa, φ = 42 deg, c = 100 kPa) was added under ground surface.	1.56	0.28
7	5	One 0.5-m thick layer. Top of layer is at 6 m below ground surface.	1.59	0.30
7b	5	As Case 14, but K_0 = 0.8 in Clearwater formation and U_{km}	1.22	0.70
8	5	One 0.5-m thick layer. Top of layer is at 6 m below ground surface. $E_{cross\ bedded\ shale}$ = 90 MPa, $E_{weak\ layer}$ = 45 MPa.	1.59	0.22
9	6	One 0.5-m thick layer. Top of layer is at 6 m below ground surface. $E_{cross\ bedded\ shale}$ = 90 MPa, $E_{weak\ layer}$ = 45 MPa.	1.36	0.56
10	6	One 0.5-m thick layer. Top of layer is at 6 m below	1.34	0.74

Case	Geometry	Description of Weak Layers	*FS*	δ_{xA} (m)
		ground surface. Columns are modeled with beam elements with same EA and EI as soil element columns		
11	5	One 0.5-m thick layer. Top of layer is at 6 m below ground surface. $E_{cross\ bedded\ shale}$ = 90 MPa, $E_{weak\ layer}$ = 10 MPa.	1.58	0.21
12	6	One 0.5-m thick layer. Top of layer is at 6 m below ground surface. $E_{cross\ bedded\ shale}$ = 90 MPa, $E_{weak\ layer}$ = 10 MPa.	1.36	0.56
13	6	Four 0.5-m thick weak layers. Top of layers at 6 m, 12 m, 18 m, and 24 m below ground surface. $E_{weak\ layer}$ = 10 MPa.	1.27	1.16
14	6	Four 0.5-m thick weak layers. Top of layers at 6 m, 12 m, 18 m, and 24 m below ground surface. $E_{cross\ bedded\ shale}$ = 90 MPa, $E_{weak\ layer}$ = 10 MPa.	1.27	0.94
15	6	One 0.5-m thick weak layer. Top of layer at 24 m below ground surface. $E_{weak\ layer}$ = 10 MPa.	1.37	0.52
16	6	One 0.5-m thick weak layer. Top of layer at 24 m below ground surface. $E_{cross\ bedded\ shale}$ = 90 MPa, $E_{weak\ layer}$ = 10 MPa.	1.37	0.39
17	5	Four 0.5-m thick weak layers. Top of layers at 6 m, 12 m, 18 m, and 24 m below ground surface. $E_{weak\ layer}$ = 10 MPa.	1.48	0.43
18	5	Four 0.5-m thick weak layers. Top of layers at 6 m, 12 m, 18 m, and 24 m below ground surface. $E_{cross\ bedded\ shale}$ = 90 MPa, $E_{weak\ layer}$ = 10 MPa.	1.48	0.31
19	5	One 0.5-m thick weak layer. Top of layer at 24 m below ground surface. $E_{weak\ layer}$ = 10 MPa.	1.58	0.26
20	5	One 0.5-m thick weak layer. Top of layer at 24 m below ground surface. $E_{cross\ bedded\ shale}$ = 90 MPa, $E_{weak\ layer}$ = 10 MPa.	1.58	0.19
21	5	Four 0.5-m thick weak layers. Top of layers at 6 m, 12 m, 18 m, and 24 m below ground surface. Cohesion of cross bedded Kc = 50 kPa. $E_{cross\ bedded\ shale}$ = 90 MPa, $E_{weak\ layer}$ = 10 MPa.	1.74	0.13

The deformed finite element mesh for Case 21 is shown on Figure 4, where the MSE wall exhibits near uniform horizontal displacement over the piles that exhibit free head type deformation along their length. Figure 5 shows the shear strains that develop in Case 21, where strain concentrations are shown to develop in the weak layers.

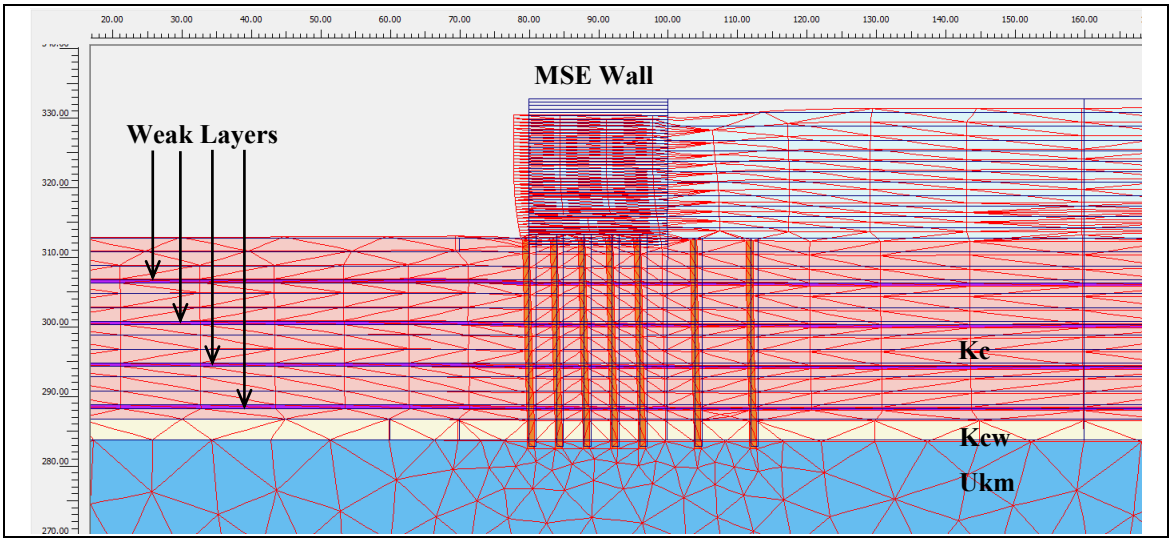

Figure 4: Deformed mesh of Case 21

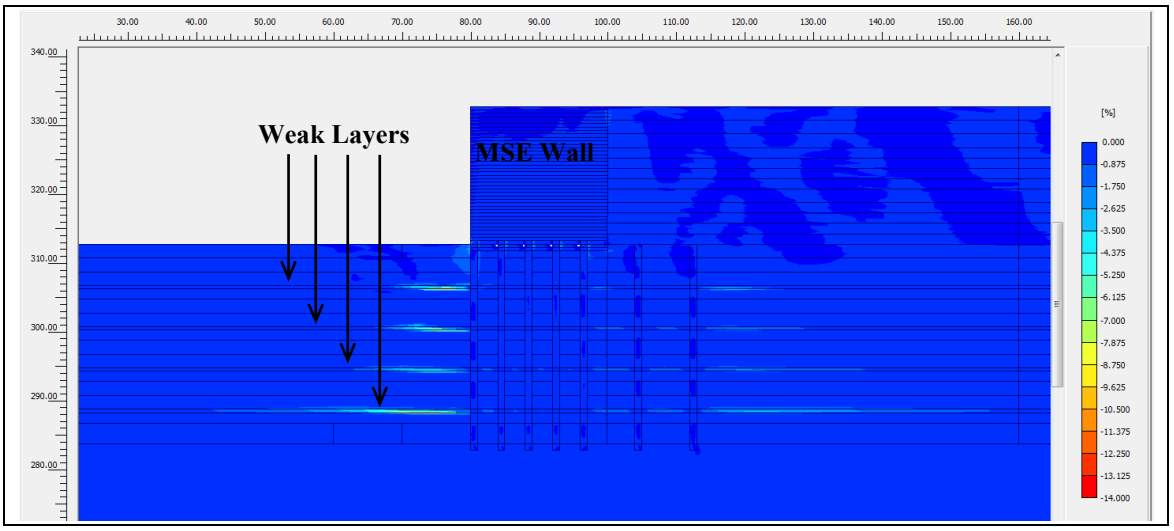

Figure 5: Shear strains in Case 21

The results of the parametric analysis showed that:

1) An increase in the number of rows of drilled shafts (with a corresponding reduction in drilled shaft spacing) resulted in an increase in the factor of safety and a decrease in the displacement of the toe of the wall.
2) The addition of a layer of soil cement at the top of the drilled shafts had a minor reduction of the displacement at the toe of the wall (e.g., Cases 6 and 7).
3) The choice of K_0 has a significant effect on the computed factor of safety and displacement. A higher initial value of K_0 causes the system to exhibit less displacement (e.g., Cases 7 and 7b).
4) The displacement of the MSE wall was detrimentally affected by:
   a. An increase in the number of assumed weak layers within the profile (e.g., Cases 4, 5, and 6, and Cases 12 and 14). As described above, the number, depth, and thickness of the weak layers were ultimately estimated for design based on low density zones and high PI values.
   b. An increase in the assumed thickness of the weak layers.
   c. The proximity of the weak layer to the top of the soil profile.
5) A decrease in the modulus of the weak layer had a negligible effect on the computed factor of safety and displacement of the wall (e.g., Cases 9 and 12).
6) An increase in the modulus of the shale from 50 MPa to 90 MPa caused a reduction of the computed displacement of the wall in the range of 20% to 73% (e.g., Cases 7 and 8, Cases 13 and 14, Cases 17 and 18, and Cases 19 and 20) without any noticeable effect on the computed factor of safety.
7) The use of structural elements with equivalent moment of inertia and area instead of soil elements to characterize the columns causes the wall to exhibit deformations that were 32% larger (e.g., Cases 9 and 10). The project team considered that the use of structural elements was inappropriate because it did not properly model the replacement of soil with stronger and stiffer material (i.e., reinforced concrete).
8) The use of a higher value of the cohesion has a significant effect on the factor of safety and displacement of the wall as can be noted by comparing the results of Cases 17 and 21.

4.3.2. Stresses in the Reinforcement

The plot on Figure 6 shows the tensile force in the reinforcement per meter of wall length at 3, 8, 13, and 18 m measured from the top of the wall in analysis Case 21 (Table 2), which is considered representative of a condition with high factor of safety and relatively low displacements. For comparison, the tensile strength of one strip is approximately 79 kN when considering 12% area reduction due to corrosion, thus the tensile strength per meter for a separation of 0.5 m is 158 kN, and the tensile strength per meter for a separation of 0.75 m is 105 kN/m.

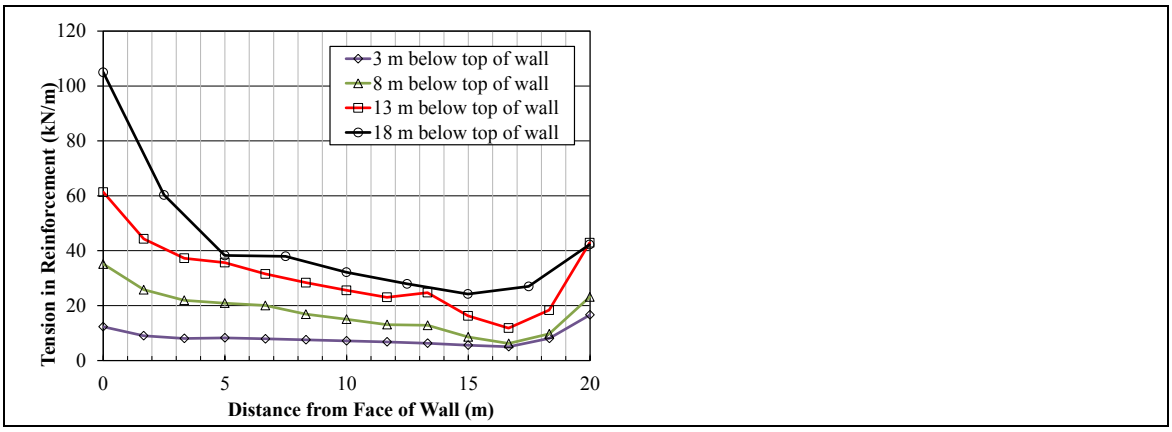

Figure 6: Plot of tension in the MSE reinforcement as a function of the distance from the face of the wall

The values in the plot indicate that the tension in the reinforcement is near constant at a given elevation, and that, as expected, the tensile force increases as the elevation decreases, i.e., is greater in the reinforcement that is closest to the base of the wall than the reinforcement that is near the top of the wall because of the effect of higher vertical stresses at depth.

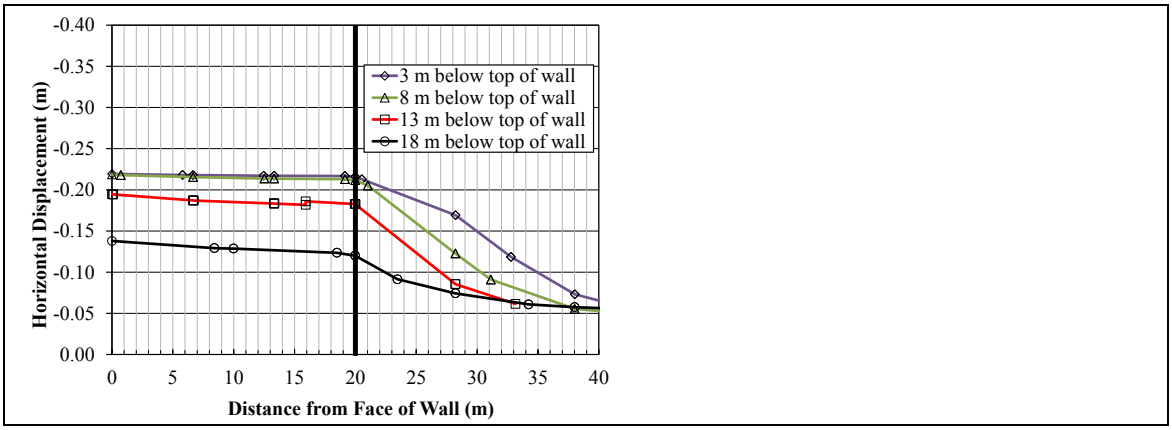

Figure 7 :Plot of horizontal displacement of the soil adjacent to the reinforcement as a function of the distance from the face of the wall

The plot in Figure 7 shows the horizontal displacement of the soil slightly above the reinforcement at the same elevation as for the tensile forces shown in Figure 6. The displacements in Figure 7 are near constant within the MSE wall (first 20 m) and then decrease beyond the reinforced area. The near constant tensile force is thus consistent with the near constant horizontal displacement as it takes differential displacements to develop tension in the reinforcement. The displacement between reinforcements is similar at 7, 12, and 17 m above ground surface, which indicates a near translational response of the wall.

4.3.3. Steel Reinforcement

The steel reinforcement (A_s) required for each row of drilled shafts was calculated by extracting the axial force and bending moment form the finite element analysis, applying a load factor of 1.5 consistent with CSA 23.3-04, and plotting on an interaction diagram. The bending moments calculated for Case 21 are shown on Figure 8. For this case, the drilled shafts would need between 1% and 2% steel reinforcement.

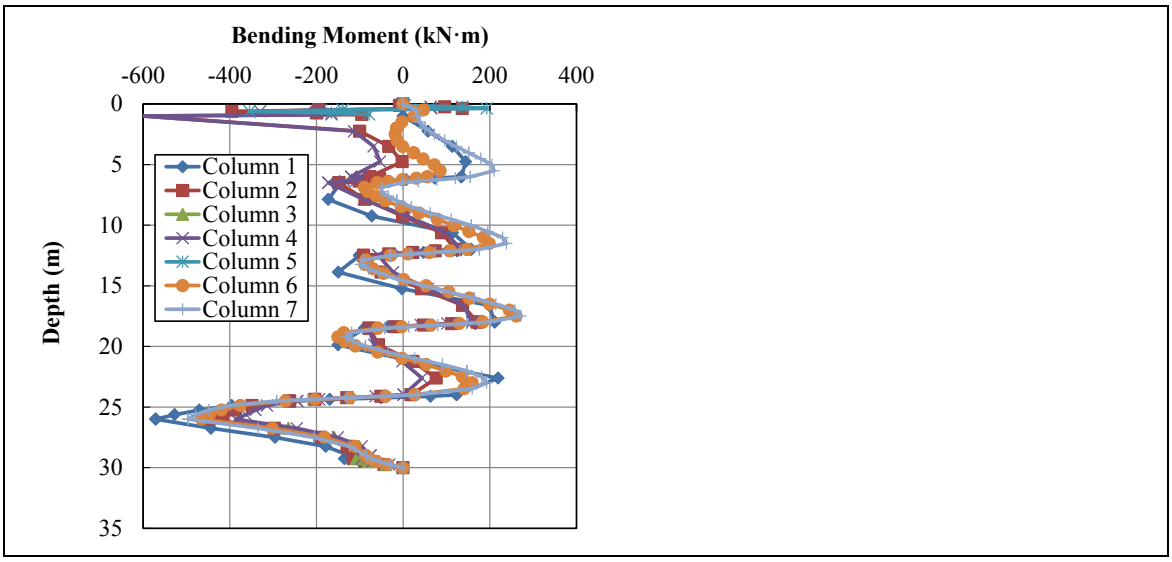

Figure 8: Bending moment diagram of the seven rows of drilled shafts (columns) for Case 21

5. SUMMARY

This paper describes the steps followed to verify the feasibility of the use of drilled shafts to support an MSE wall by showing that the wall could be built with a calculated factor of safety of 1.5 or greater and displacements at the toe of 0.3 m or less. For this, the MSE wall would be placed over seven rows of 1-m diameter and 30-m long drilled shafts distributed in a rectangular pattern. The first five rows of columns would have a center-to-center separation of 4 m, and the subsequent rows would be separated 8 m apart. The first row of columns would be aligned with the face of the wall. The separation between columns measured in the direction parallel to the face of the wall (i.e., out of plane) would be approximately 3.5 m. The analyses indicated that the drilled shafts would require between 1 and 2% percent steel reinforcement.

The study presented in this paper also found that the magnitude of the computed displacements is highly sensitive to the strength and compressibility parameters selected to characterize the shale and other subsurface materials.

REFERENCES

Alencar, J., Morgenstern, N.R., and Chan, D.H. (1994) Analysis of Foundation Deformations beneath the Syncrude Tailings Dyke. Canadian Geotechnical Journal, Vol. 31, No. 6, pp. 868-884.

Brockbank, W.J., Kalynchuk, G., and Scherger, B. (1992) Use of Oil Sand for Construction of a Reinforced Earth Dump Wall. Proceedings of the Annual Conference of the Canadian Geotechnical Society.

Moore, T., Sobkowicz, J., Workman, C., and Sission, R. (2006). Simulation of Large Tank Loading Using a Test Fill. 59th Canadian Geotechnical Conference, Sea to Sky, Edmonton, Alberta, pp. 977-984.

Wedage, A.M.P., Morgenstern, N.R., and Chan, D.H. (1998) Simulation of time-dependent movements in Syncrude tailings dyke foundation. Canadian Geotechnical Journal, Vol. 35, 284-298.

Behaviour of a shallow foundation on soil reinforced by Mixed Module Columns® – Experimental study

Hana Santruckova, *Grenoble-INP, UJF-CNRS, 3SR, Grenoble, France, hana@geo.hmg.inpg.fr*
Pierre Foray, *Grenoble-INP, CNRS, 3SR, Grenoble, France, Pierre.Foray@grenoble-inpg.fr*
Stéphane Grange, *UJF-CNRS-INPG, 3SR, Grenoble, France, Stephane.Grange@ujf-grenoble.fr*
Alberto Cofone, *Grenoble-INP, UJF-CNRS, 3SR, Grenoble, France*
Serge Lambert, *Keller Fondations Spéciales, Duttlenheim, France, serge.lambert@keller-france.com*
Philippe Gotteland, *UJF-CNRS-INPG, 3SR, Grenoble, France, Philippe.Gotteland@ujf-grenoble.fr*
Jimmy Wher, *Keller Holding GmbH, Offenbach, Germany J.Wehr@kellerholding.com*

ABSTRACT

Mixed Module Columns (CMMs) are a ground reinforcement technique, which combines two soil improvement methods widely used in current practice. They are composed of a soft upper part (Stone Column) which offers shear and moment capacity, and a rigid lower part (Rigid Inclusion) which gives bearing capacity. In order to design CMMs, the response of this combined system to different static and dynamic loads must be understood. This paper presents results from an experimental study performed in Laboratoire 3S-R (Grenoble). A reduced (1/10) physical model consisting of a group of four CMMs, supporting a shallow foundation, is studied in clay. A special emphasis is given to the study of the inertial effects of seismic type loading. Since the rigid inclusion is an unreinforced concrete pile, it has a reduced moment and shear capacity. Consequently, these forces are monitored in the rigid inclusion to verify the safety of current design practice. For this purpose, one of the rigid inclusions is instrumented with 20 levels strain gauges measuring flexural strain, used to calculate the bending moment along the pile. This gives pile deflection (y) by double integration and soil reaction (p) by double derivation. P-y curves are thus obtained. Combined vertical and horizontal static and dynamic loading is applied to the shallow foundation model. A parametric study is presented, varying the stone column height, to define its effect on the settlements of the foundation and lateral pile performance. It is shown, that on one hand, the CMMs with shorter stone columns allow less settlement but on the other hand, the shorter stone columns tend to transfer higher shear force to the head of the rigid inclusion. Since the Mixed Module Column technology is an alternative to the soil improvement by rigid inclusions (RI), the two soil reinforcement methods are compared. It is shown, that the CMM tend to dissipate more energy than the RI technique. As a consequence, head of the rigid inclusion of the CMM undergoes less deformation than the head of the rigid inclusion within the RI soil reinforcement.

1. INTRODUCTION

Mixed Module Columns (CMM®) is an alternative solution for the widely used soil reinforcement techniques, such as stone columns and rigid inclusions. It combines the features of these two techniques and seems to present an interest for foundation projects in seismic areas. A CMM® is composed of two parts: an upper part in compacted gravel (short stone column) overlaying a rigid inclusion in its lower part. A transition zone links the two parts (Bustamante et al., 2006). When using rigid inclusions as reinforcement of soft soil, the inclusions need often to be reinforced by steel elements or to be associated with a granular mattress in order to sustain horizontal loadings related to wind or earthquakes. These shortcomings can be avoided by introducing the upper part of the CMM® in expanded gravel. This upper part, more flexible in its interaction with the surrounding soft soil, acts as a dissipative rotulated zone which transmits less energy towards the superstructure by kinematic effect and less energy downwards to the rigid part of the CMM® by inertial effect. Many studies have been carried out on vertically loaded shallow foundations lying on soft soil reinforced by stone columns, or vertical rigid inclusions, or vertically and laterally loaded pile foundations (Chenaf 2006, Georgiadis et al. 1992, Li & Byrne 1992, Rosquoët et al. 2007, Thorel et al. 2010, among others). However, less work has been found on reinforcement by CMM® in seismic areas (Hatem et al. 2009). This paper presents the study of the response of a square footing embedded in clay reinforced by four CMM® and submitted to cyclic horizontal loading. In a previous work, 2D models were used in order to visualize the movements of the column and rigid part and to compare it with numerical modelling (Zang et al 2010, Zang 2011). In our case, physical models in 3D are tested at a scale 1/10 in the large tank "VisuCuve" of Laboratoire 3S-R in order to analyse the interaction mechanisms. Dynamic loadings are applied to the foundation model in order to evaluate the inertial effects. The response of a CMM® system is compared to the one of a similar system combining rigid inclusions and a complete gravel mattress. A parametric study is performed,

varying the height of the upper part in compacted gravel in order to determine its influence on the response of the rigid lower part.

2. PHYSICAL MODELLING

2.1. Presentation of the physical models

The reduced model presented in this work is submitted to a normal gravity "g*=1" and the conditions for a rigorous similitude with respect to the stress level "σ*=1" are not fulfilled. Even though the scaling laws are not strictly respected, the main objective of the physical modelling is to perform a qualitative study of the CMM® soil reinforcement, studying its behaviour under combined loading and comparing its performance to RI technology. In a further step, the results of the physical model will be used to calibrate a numerical model which should then be able to reproduce the field conditions.

A reduced model with a scale of 1/10 of a square footing with a width of 24 cm and a thickness of 2cm is realized. It is installed on clay reinforced either by the CMM® or the RI. The dimensions of the system and the mechanical parameters of the soil are summarized on Figure 1. The rigid part of the CMM® and RI is modelled in 3D by a hollow aluminium pile (16mm in external diameter and 8mm in internal diameter). The transition zone is represented by an aluminium funnel, which is firmly fixed to the head of the pile and is filled with gravel. This transition zone is followed by a gravel column for the case of CMM® or by a gravel mattress for the case of RI. The height of the upper flexible part is 5 cm, 8 cm or 10 cm and the effect of this height on lateral performance of the rigid inclusion is studied. The length of the lower rigid part is 50 cm where the toe of the rigid inclusion is embedded into a metal plate, avoiding any movement. The axial distance between the two CMM® models is 12cm. The foundation model is embedded into the soil of its whole thickness.

In order to study lateral performance of the rigid inclusion, one pile is instrumented with twenty levels of strain gages. The strain gages are in such configuration that flexural deformation of the rigid inclusion can be measured. Having deformation monitoring at twenty positions on the 50 cm long pile, a well detailed deformation profile can be obtained.

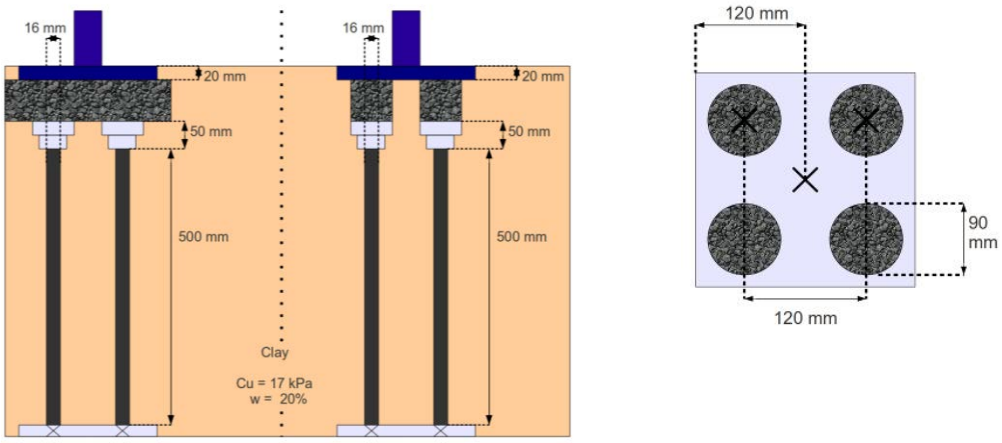

Figure 1: Physical models in scale 1/10

2.2. Experimental Methodology

The used experimental device is a modification of "VisuCuve", a device developed in Lab 3SR and previously used for studying soil-pipeline interaction (Orozco et al., 2007). The "VisuCuve" setup is adjusted to meet the required loading conditions, i.e. combined vertical and horizontal loading of shallow foundation with resulting settlement and horizontal movement of this foundation, while preventing it from rotation in any possible sense. Further modifications are done in order to make the system sufficiently resistant to vibrations caused by dynamic loading. The "Visucuve" is filled with saturated clay and a physical model of soil reinforced by CMM and RI technology is installed.

2.2.1. Experimental Device description

The experimental setup "VisuCuve", shown in Figure 2, consists of a large rigid and impervious tank of 2m long, 1m wide and 1m deep, where one half of the tank is filled with saturated clay and the physical model is placed in the centre of the soil mass. Two rails which are fixed on top of the tank enable a metal trolley to slide horizontally on top of the tank. The trolley is connected to a dynamic horizontal loading system, a fast electro-mechanical actuator with a maximum velocity of 700mm per second. It is a roller screw type linear actuator EXLAR FT35-2410-FIA-EX4-L2 mounted with a high performance brushless motor, allowing a variable-frequency drive. This horizontal guidance system allows a dynamic horizontal loading of a foundation model, which is fixed to the trolley by an anti-rotation ball bearing. A vertical load is applied to the foundation by an actuator, which is fixed to the metal trolley and the ball bearing is the linking element between the actuator and the foundation. The introduced system allows controlled foundation loading and displacement in vertical direction as well as in horizontal direction. The horizontal and vertical forces are measured by two load cells fixed on the loading system. The horizontal and vertical displacements of the foundation model are measured by two LVDTs.

The physical models used are introduced in section 2.1. One of the four tubes representing the rigid inclusion (Figure 3) is equipped with twenty levels of strain gauges, measuring flexion of the tube under applied horizontal loading. The pile surface has a system of grooves wide enough for the strain gages to be stuck in them. This protects the strain gauges against possible mechanical damage. In addition to the strain gages, pile is equipped with a small size accelerometer, which is fixed at a very bottom part of the transition zone. This accelerometer does not register a clear signal during the dynamic experiments, which is assumed to be due to the wave reflection within the VisuCuve. Wires connecting gauges and accelerometer with acquisition system are lead through the hollow pile centre.

Figure 2: The experimental device "Visucuve"

Figure 3: Rigid part and transition zone of the physical model

2.2.2. The soil mass preparation

The clay mass is created by a careful assembly of clay bricks (Photo1) where an effort is made to create a soil mass as homogeneous as possible and to ensure good contacts between the rigid inclusions and the soil. The clay used has a cohesion *c* of 18 kPa and its water content *w* is 0.2. For the case of CMM®, four gravel columns were installed on top of the transition zone within the clay mass (Photo2) and the gravel was compacted to a final unit weight of 1.6g/cm^3 in average. The procedure of stone column installation in the small scale model approaches the procedures applied on construction sites. In the case of RI, the gravel mattress is compacted in a way to obtain a gravel unit weight of the same order as for the stone columns.


Photos 1, 2: Soil preparation procedure

2.2.3. The loading procedure

Once the foundation model is in contact with the reinforced soil, the vertical force is applied in five steps, arriving to a final vertical load of 5000N. This load is kept constant for two hours in minimum to enable soil mass consolidation. The vertical load of 5000N represents a weight of a superstructure and is approximately 1/3 of the vertical bearing capacity of shallow foundation on soil reinforced by CMM®. After the stage of soil consolidation, the vertical load is kept constant while thirty cycles of horizontal cyclic loading are applied with constant displacement amplitude of +/- 2mm and a frequency of 2.7Hz.

2.3. The data treatment

A correct treatment of the obtained experimental data is essential and can eventually enable a proper understating of the problem concerned. The instrumented pile monitored a flexural strain at twenty vertical levels. Taking the Hook's law as a constitutive relation and applying the equation for static lateral performance of Euler-Bernoulli beam, the bending moment along the pile is obtained. The main difficulty in such an analysis is a correct and time effective interpolation of moment data along
the pile length. This is done with a polynomial function of sixth degree, which is found to fit best
the data concerned. Applying boundary conditions by setting the displacement and rotation at the pile toe to zero, lateral pressure *p* and deflection *y* are obtained:

$$p = \frac{d^2M}{dz^2} \tag{1}$$

$$y = \iint \frac{M}{EI} dz^2 \tag{2}$$

These physical values and their derivatives are used in the presented work to study the lateral pile behaviour.

3. RESULTS

3.1. Combined static loading – Swipe Test

Experiments under combined static load are presented in the following section. The aim is to find the ultimate combination of vertical load V and horizontal load H that will cause a bearing capacity failure of a shallow foundation. A failure envelope, defining a critical combination of H and V load is analytically described by the following equation presented by Butterfield & Gottardi (1994):

$$\frac{H}{t_h} = \frac{V.(V_{max} - V)}{V_{max}} \tag{3}$$

where V_{max} is vertical bearing capacity and t_h is a footing-soil friction coefficient. This failure envelope can be found experimentally by vertical loading of a shallow foundation up to its ultimate bearing capacity, blocking the foundation at its vertical position and then applying horizontal displacement. This procedure is commonly referred as a "swipe test". The measured vertical and horizontal forces applied by the foundation on the soil provide the failure envelope.

A swipe test was carried out for a case of a foundation embedded in pure clay and a foundation on soil improved by CMM®. A comparison of these two tests is shown in Figure 3. It can be seen that the failure envelope of a foundation on soil reinforced by CMM® is much larger than the failure envelope of a foundation in pure clay. The shape of the two envelopes is homothetic with a size ratio of approximately 4 between the swipe test envelope for soil reinforced by CMM® and the swipe test envelope for pure clay.

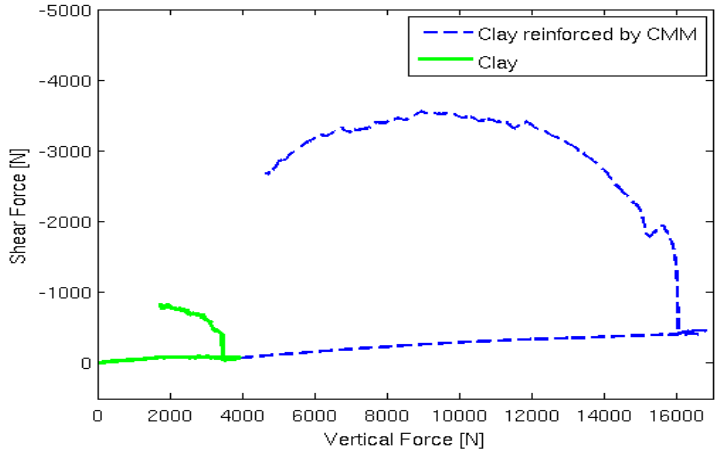

Figure 3: Swipe test for clay and soil reinforced by CMM®

The performed swipe test is also used to verify the position of the imposed dynamic loading (presented in the next section) within the failure surface. Figure 4 shows that the cyclic loading path is situated inside the rupture surface, although bearing capacity loss by foundation sliding is the most probable failure mechanism.

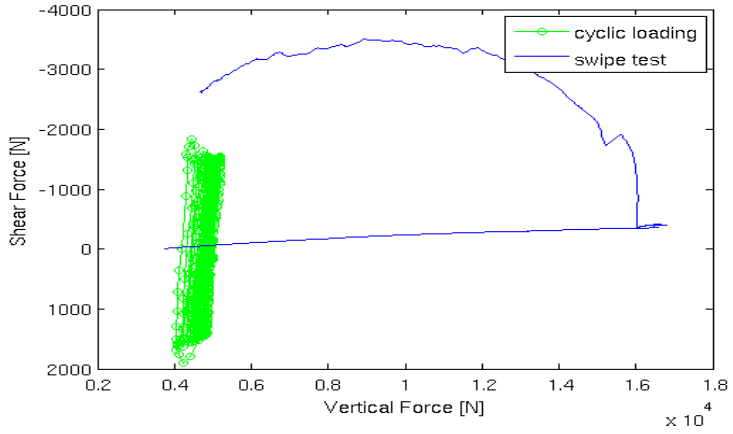

Figure 4: Position of the imposed cyclic loading within the failure envelope

3.2. Vertical static and horizontal dynamic loading of a shallow foundation on soil reinforced by CMM

The behaviour of shallow foundation under dynamic loading on soil reinforced by CMM® is studied. The height of the stone columns is varied in order to study the effect its height on not only the foundation performance but also the behaviour of the rigid inclusion, which is supporting the stone column from underneath.

3.2.1. Foundation settlement

Shallow foundation settlement under vertical constant and horizontal dynamic loading is studied. Stone columns, making part of the CMM system, are varied in their height in order to evaluate their height influence on the lateral pile performance. The results obtained are shown in Figure 5, where it can be seen that the amount of settlement under the dynamically loaded foundation increases with increasing stone column height. This phenomenon can be explained by an assumption that shorter stone columns tend to transfer more of the imposed vertical load to the rigid inclusions and therefore the upper, flexible part of the CMM system is less compacted under the combined load.

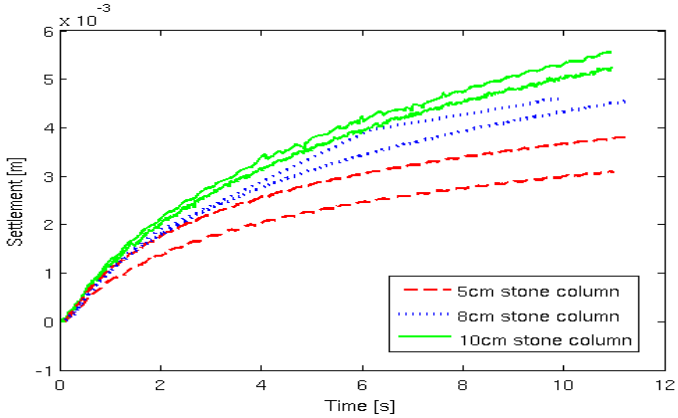

Figure 5: Foundation settlement under dynamic loading - soil reinforced by CMM®

3.2.2. Lateral pile performance

In the current practice, the rigid part of the CMM, meaning the concrete pile, doesn't contain any steel reinforcement. For this reason, lateral pile performance is studied on the physical model presented. Stone columns height is varied (5, 8 and 10 cm) in order to study its effect on behaviour of the rigid inclusion, which is supporting the stone column from underneath.

As the foundation model applies cyclic loading to the soil improved by CMM, the instrumented pile undergoes a deformation. This deformation is monitored and treated in order to obtain pile deflection, bending moment, shear force and lateral soil reaction along with the cyclic loading. Conclusions are then made on the lateral pile performance in relation to number of cycles and the stone column height. A simplified graphical representation of such data evaluation is shown in Figures 6 and 7. It can be seen that the pile head deflection has a form of a sinusoid, where local maxima and minima can be defined. Time instants t1 to t6 define the deflection maxima and minima for first, fifteenth and thirtieth cycle of the loading. Bending moment, deflection and shear force at time instants t1 to t6 are then plotted. Figures 6 and 7 show an example of such experimental results for a test, where the stone column is 5 cm high. It can be seen, that the bending moment at the pile head doesn't reach a zero value. This is due to a rotation of the funnel, which is fixed to the pile head. Figures 6 and 7 show, that the pile performs a reversible behaviour at the beginning of the cyclic loading. As the number of cycles increases, the pile doesn't enter the zone of negative deflection and shows a very important deflection accumulation with the dynamic loading. This accumulated lateral displacement develops in direction towards unreinforced soil, i.e. out of the pile group and has a tendency to stabilize towards the end of the cyclic loading. It can be noticed, that the pile undergoes lateral movement up to a depth of approximately 25cm out of its 50cm length. This corresponds to once to twice foundation width.

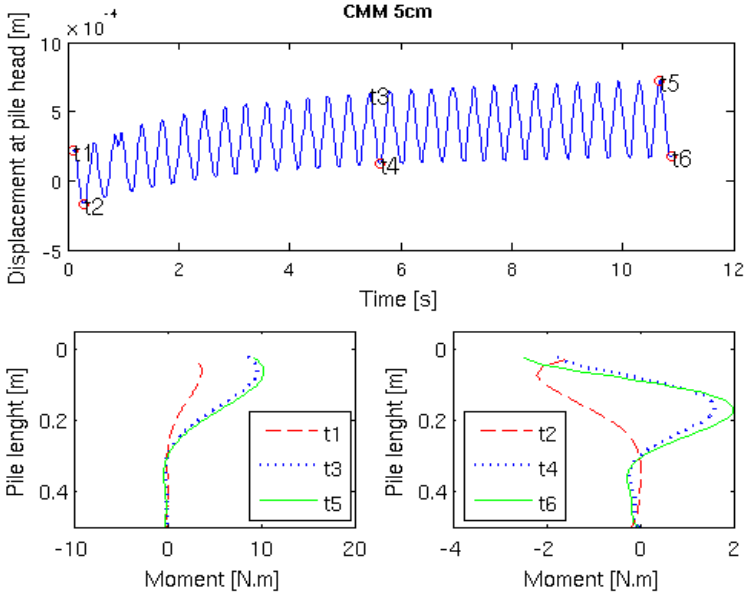

Figure 6: Moment along the instrumented pile at times t1 to t6

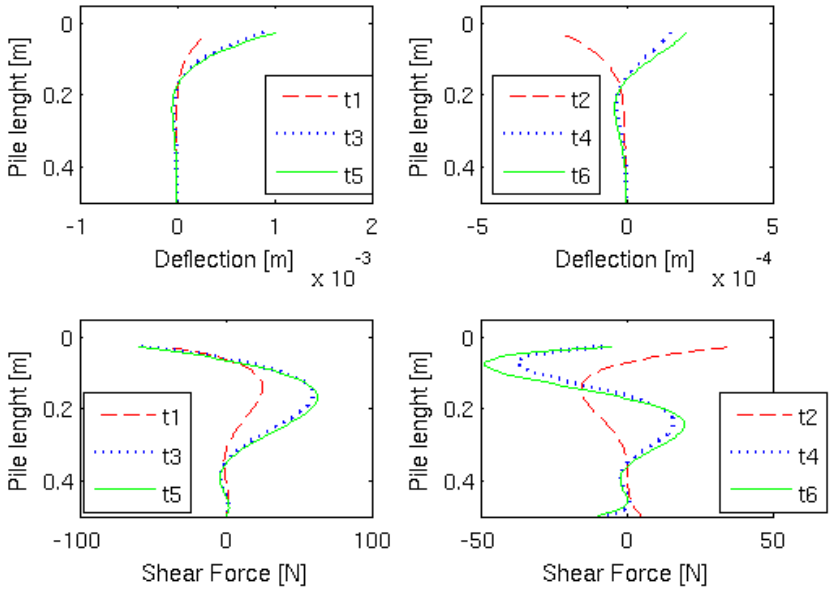

Figure 7: Deflection and shear force along the instrumented pile at times t1 to t6

Relation between the pile lateral performance and the stone column height is studied. Figure 8 shows pile head behaviour plotted in the p-y space. Each subfigure contains p-y loops obtained during the cyclic loading for different stone columns heights (5, 8 and 10 cm). It can be seen, that for experiments with 8cm and 5cm stone columns, there if found no apparent influence of stone column height on the deflection, nor lateral soil reaction monitored along the pile during the cyclic loading. On the contrary, lateral performance of a pile supporting a 10 cm high stone column seems to vary from lateral performance of a pile supporting a stone column of 5cm or 8cm.

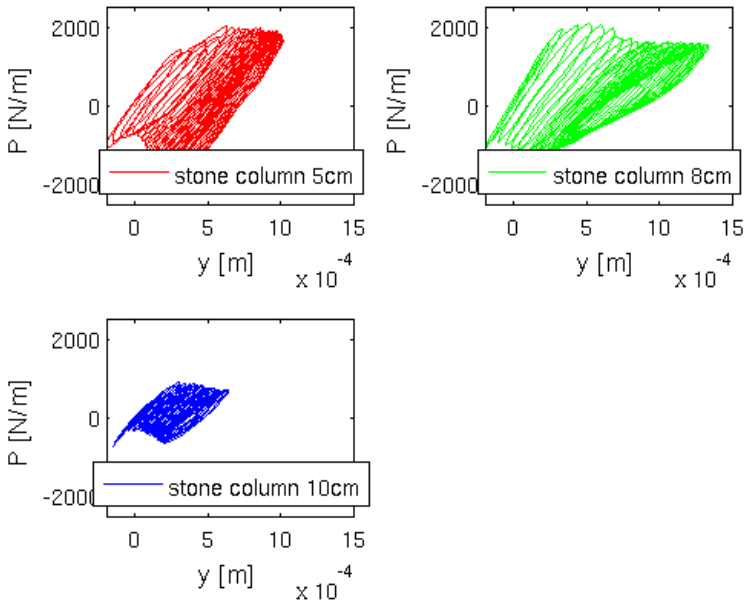

Figure 8: p-y curves obtained at pile head for experiments with 5cm, 8cm and 10 high stone column

3.3. Comparison between CMM and RI techniques

Experiment with the two soil reinforcement technologies, the Mixed Module Columns and the Rigid Inclusions, were performed. Energy dissipated is evaluated by calculating the loop area and the results are compared for the two technologies. It is observed that the clay reinforced by the stone columns has an

ability to dissipate more energy than the gravel mattress, although the amount of dissipated energy stays in the same order. As a consequence, a rigid inclusion supporting a stone column (CMM) undergoes less cyclic loading than a rigid inclusion supporting a gravel mattress (RI). This is confirmed by plotting the P-Y curves at the head of the instrumented rigid inclusion for the case of CMM and RI reinforcement. It is shown in Figure 9 that the P-Y loops are bigger for the rigid inclusion making part of the RI technology.

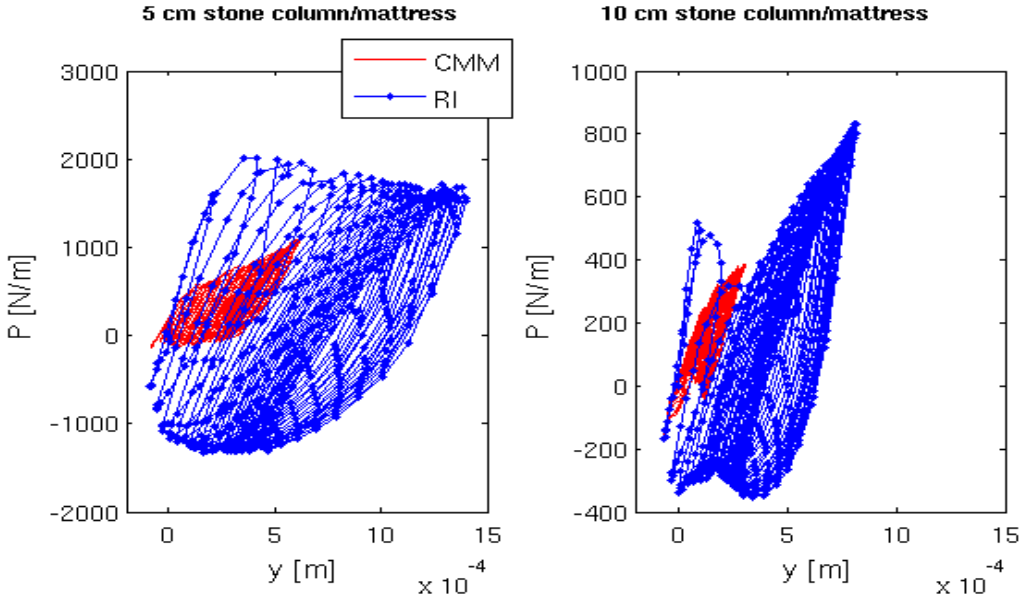

Figure 9: P-Y loops at the top of the rigid inclusion for the two soil improvement technologies

4. CONCLUSION

The presented experimental study concerns shallow foundation behaviour on soil reinforced by Mixed Module Colums® (CMMs®). A comparison between failure envelopes (Butterfield&Gottardi ,1994) for clay and for clay reinforced by CMMs is made. It is shown, that the clay reinforced by CMMs allow four times higher horizontal and vertical loading before reaching its bearing capacity. A special emphasis is given to the study of the inertial effect of seismic type of loading. A parametric study is done, varying the stone column height, to define its effect on the foundation settlement and lateral pile performance. It is shown, that CMMs, having shorter stone columns, allow less foundation settlement under dynamic loading. On the other hand, it is also found that by decreasing the stone column height, the bending moment and therefore deflection transformed to the pile head increases. It is therefore essential for the CMM design to make a good compromise between the allowed foundation settlements and the allowed shear force transferred to the rigid part of the CMM. Comparing the performance of CMM and RI reinforcement technology, it is found that the clay reinforced by the stone columns has an ability to dissipate more energy than the gravel mattress.

The experimental results presented are used for a calibration of a numerical model. This allows an extension to real field conditions.

REFERENCES

Bustamante M., Blondeau F., Aguado P., 2006, Cahier des charges Colonnes à Module Mixte. KELLER Fondations Spéciales.

Butterfield R., Gottardi G., 1994, A complete three-dimensional failure envelope for shallow footings on sand., Géotechnique 44, No. 1, 181-184

Chenaf N. ,2006, Interaction inertielle et interaction cinématique. PhD Dissertation, Ecole Centrale de Nantes.

Hatem A., Shahrour I., Lambert S., Alsaleh H., 2009, Analyse du comportement sismique des sols renforcés par des inclusions rigides et par des colonnes à module mixte. AUGC.

Li Y., Byrne P.M., 1992, Lateral pile response to monotonic head loading. Canadian Geotechnical Journal, No. 29, pp. 955-970.

Orozco M., Foray P., Nauroy J.F., 2007, Pipe-soil horizontal dynamic stiffness in soft soils. Proceedings of the Sixteenth International Offshore and Polar Engineering Conference, Lisbon, Portugal: 1193-1198.

Remaud D., 1999, Pieux sous charges laterales: étude expérimentale de l'effet de group. PhD Dissertation, Ecole Centrale de Nantes.

Rosquoët F., Thorel L., Garnier J., Canepa Y., 2007, Lateral cyclic loading of sand-installed piles. Soils&Foundations, Vol. 47, no. 5, pp. 821-832.

Thorel, L.Dupla, J.C., Rault, G., Canou, J., Baudoin, G., Dinh Q.A., Simon, B., 2010, Pile-supported earth platforms: Two approaches with physical models. In "Physical Modelling in Geotechnics" Proc. of the7th Int. Conf. on Physical Modelling in Geot., ICPMG 2010, Zurich, Swizerland, pp.1363-1369.
Zang X., 2011, Modélisation physique et numérique des interactions sol-structure sous solicitations dynamiques transverses. PhD Dissertation, Université de Grenoble

Zhang X., Foray P., Gotteland Ph., Lambert S., Alsaleh H., 2010, Seismic performance of mixed module columns and rigid inclusions. 7th International Conference on Physical Modelling in Geotechnics, july, Zurich, Swizerland, 6pp.

A model study on settlement behaviour of granular columns in clay under compression loading

Maral Tekin, GEOMED Geotech. Cons., Inves. Co, Turkey, mtekin@geomed.com.tr
M.Ufuk Ergun, Civil Engineering Department, Middle East Technical University, Turkey, eruf@metu.edu.tr

ABSTRACT

A model study was performed in order to examine the factors that affect the settlement behaviour of floating and end bearing type of granular columns, like replacement ratio, number of columns, column length, loading area, loading level, settlement reduction factors, ß, achieved under 3D footings and 1-D (unit cell) type of loadings. Settlement reduction factors for B=100 mm and B=200 mm plates (footings) for end-bearing columns have been compared with the settlement reduction factors obtained from 1-D (unit cell) tests and design charts prepared based on unit cell concept. It is also aimed to find effective length in floating type columns that provides significant settlement improvement under footings. Subsurface displacements and strains were measured by miniature borehole settlement gages along columns and in untreated soil below columns under loading plates.

1. INTRODUCTION

Granular column construction involves the partial replacement of unsuitable subsurface soils with a compacted vertical column of stone and sand. Displacement type of placement is also possible. This application is suited to improve soft silts and clays and loose silty sands with a replacement ratio of 10 to 35 percentages. Usually there is a common tendency to make the columns rest on competent layers in end bearing. Floating type of columns are not well studied.

Granular column application is very successful in improving slope stability of both embankments and natural slopes, increasing bearing capacity, reducing total and differential settlements and increasing the time rate of settlements.

In literature, settlement improvement factor of column groups for different area replacement ratio is based on unit cell concept for end bearing columns.

In this experimental study, it was desired to work on floating type of columns and to compare their settlement behaviour with that of end bearing columns.

2. EXPERIMENTAL WORKS

2.1. Properties of Kaolin Clay and Sand Used in Model Tests

The model tests were carried out in loading tanks with a diameter of 410 mm in which commercially available remoulded kaolinite type clay was consolidated from paste (moisture content w=42%) with a pressure of σ_v=50 kPa. Kaolin clay is classified as CH according to Unified Classification System. However, it is slightly above A-line just at the border of MH. The liquid and plastic limit values are 51% and 29% respectively. The plasticity of the kaolin (PI=22%) is not so high to lead swelling or shrinkage.

The clay 'foundation' soil had average undrained shear strength of 25 kPa at the completion of the consolidation in the tank. The coefficient of volume compressibility m_v values obtained by laboratory consolidation tests in the pressure intervals that correspond to those in the model tests are given in Table 1.

Table 1: m_v values determined from laboratory consolidation test for/in pressure intervals in model tests

Test No	**Pressure 50-75 kPa m_v (m^2/kN) ($x10^{-2}$)**		**Pressure 75-100 kPa m_v (m^2/kN) ($x10^{-2}$)**	
Test No:1 Test No:2 Test No:3	0.0409 0.0442	0.0426 (average)	0.0324 0.0345 0.0363	0.0344 (average)

Grain size distribution of the sand used in granular column formation was obtained based on Dc/D (column diameter/typical particle size) ratio applied in site stone column applications. The grain size distribution and physical properties of sand are shown in Table-2 and Table-3 respectively.

Table 2: Grain size distribution of sand used as granular column

Sieve #	**D (mm)**	**Percent finer than D (%)**
50	0.315	100
70	0.210	70
100	0.149	38
200	0.074	6
325	0.035	0

Table 3: Physical properties of sand used as granular column

USCS	**D_{10} (mm)**	**D_{30} (mm)**	**D_{60} (mm)**	**C_u**	**C_c**	**e_{max}**	**e_{max}**	**G_s**	**ϕ^0**
SP	0.083	0.120	0.195	2.34	0.89	0.961	0.581	2.683	42

2.2. Experiment Set-Up

Loading tanks were designed as huge oedometers (d=410 mm, h=390 mm) to be used for both in clay foundation preparation and in the main loading test. Pressure was applied on the clay reinforced with granular columns with the aid of loading plates by means of an air-jack which is mounted on a frame and connected to a compressor (Figure-1). The loading plate diameters of B=100 mm, B=200 mm and B= 410 mm simulate footing and 1-D (unit cell) conditions respectively.

Settlement of loading plate was recorded automatically by two displacement transducers, LVDT connected to a data acquisition instrument.

Miniature magnetic switch apparatus is developed based on the measurement principle of magnetic extensometer to determine subsurface settlements occurring throughout the length of granular columns and untreated area under columns. The apparatus consists of an antenna rod, ring type magnets (inner part is magnet), a measurement probe with a magnetic switch and a worm gear device designed to move the probe inside the antenna rod slowly. The base of the antenna rod was placed at the bottom of the tank to avoid uncontrolled displacements. In each case, clay was bored and antenna rod (d=6mm) was inserted into this hole. Then the hole was filled with sand or clay till to the desired level at which settlement measurement would be taken. At this point, ring type magnet with a diameter of 13 mm was passed through the antenna rod (Photo-1). This process continued until the surface was reached. At least eight magnets were placed around each antenna rod. A hollow ramming device was used to compact sand and get the required 80% relative density and compression of clay. Reference readings were taken throughout antenna rod to specify the locations of the magnets before starting the test. Subsurface settlements due to loading are determined by relative movements of the magnets with respect to their initial locations.

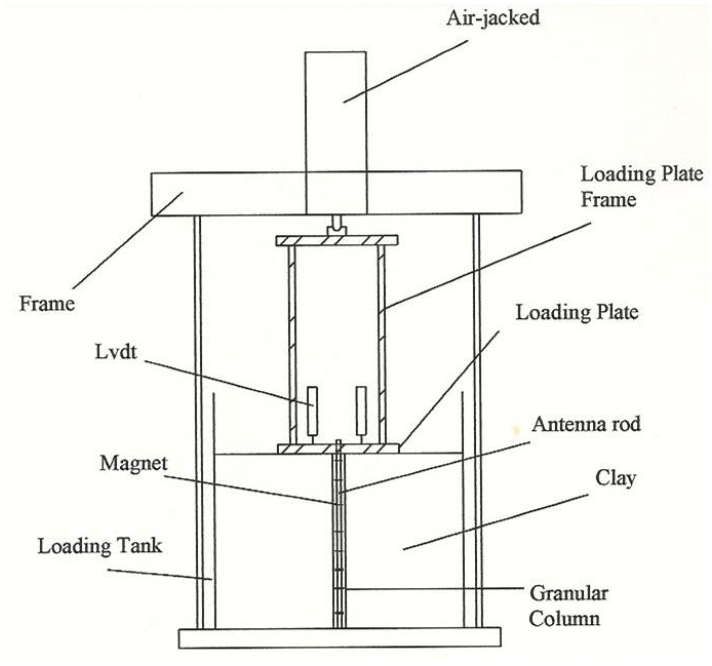

Figure 1: Sketch of the experiment setup

Photo 1: Placement of ring type magnet to the antenna rod

The test procedure is as follows;

1. When consolidation of clay foundation was ended jack, loading frame and 410 mm diameter loading plate were demounted.

2. The clay on the top was removed until a clay foundation with a height of 290 mm was achieved. After flattening the surface, pre-bored steel plate with specific area replacement ratio was put on the surface to prepare the columns in the desired pattern (Photo-2). An auger with a diameter of 20 mm was used to drill the clay till the desired depth was reached (granular column length)

3. The bored hole was filled with sand and rammed in a controlled manner to have a relative density of about 80% throughout the column length. This procedure was continued up to the surface.

4. In each test, two granular columns were instrumented, the middle column and one of the closest columns to the middle to examine subsurface settlements.

5. After column preparation, the surface was flattened again, and loading plate was put on the clay, and loading mechanism was mounted.

6. Two displacement transducers were located on the loading plate and connected to the ADU unit to record the plate settlement automatically. Before starting the test, reference readings were taken throughout the antenna rods to determine the initial locations of the magnets, and read-out unit was initialized to have initial readings of the displacement transducers.

7. 75 kPa was applied to the loading plate. For the first 30 minutes of the test, displacement transducer readings were taken automatically with 5 sec periods then after 30 minutes till the end of consolidation, this period was increased to 30 minutes.

8. At the end of consolidation (test), final readings were taken throughout the antenna rods

9. In the two test series, test was repeated with 100 kPa loading and then with 125 kPa (after 75 kPa). In these cases, steps 7 and 8 were repeated at each loading pressure.

Photo 2: Clay is drilled with aid of prebored steel plate and auger

Tests without granular column installation (untreated soils) but with the same loading levels and instrumentation were performed for each loading plate diameter to find out the contribution of granular column groups to settlement reduction.

3. TEST RESULTS

In this study, model tests have been performed to examine both the effects of L/B (column length/loading plate diameter), L/D (column length/column diameter), as (area replacement ratio) on settlement behaviour of floating type granular column groups and the difference in settlement reduction between footings and 1-D type of wider loading. Column length, loading plate diameter, area replacement ratio and loading level were the variables, but thickness of the clay (290 mm) and diameter of granular columns (20 mm) were kept constant in all tests. The summary of all details of the model test study is given in Table- 4. The findings are as follows;

Table 4: Summary of test series

Series No	Loading Plate Diameter, B (mm)	Pressure Applied (kPa)	Area Replacement Ratio, a_s	Number of Columns	L (mm)	L/D	L/B
I	100	75	Untreated (without column)				
II	100	75	0.40	7	140 210 290 (end b.)	7.0 10.5 14.5	1.4 2.1 2.9
III	100	75	0.22	7	60 100 140 210 290 (end b.)	3.0 5.0 7.0 10.5 14.5	0.6 1.0 1.4 2.1 2.9
IV	200	75,100,125	Untreated (without column)				
V	200	75,100,125	0.22	19	100 140 200 275	5.0 7.0 10.0 13.75	0.5 0.7 1.0 1.375
VI	200	75,100	0.12	13	100 140	5.0 7.0	0.5 0.7
VII	410	75,100	Untreated (without column)				
VIII	410	75,100	0.22	85	200 290 (end b.)	10.0 14.5	0.490 0.707

3.1. Number of Columns

In series II and III, the number of columns under the loading plate is the same, but the location of the columns i.e., spacing between the columns are different. There is almost no difference (only 1%) between the settlements for the same column length. On the other hand, in series V and VI there is a settlement decrease of 10% between the footings (B=200 mm, 75 kPa) supported by floating 19 columns compared to 13 columns having the same length (L=100 mm). A similar difference of 11% is observed in series of 140 mm long columns. It is seen that number of columns under footings is an influencing factor for the settlements but not the pattern of them.

3.2. Settlement Reduction Factor, β in Footing and Unit Cell Concept

Settlement reduction factor β is the ratio of the settlement without columns S_{unt}, i.e. untreated case, to the settlement S_t occurring in the presence of granular columns. This factor is very commonly used to grade the improvement works with granular columns.

It is intended to simulate unit cell criteria by means of 1-D loading condition. In literature most design charts are based on the assumption that unlimited column grid under unlimited area is loaded. Within this grid a "unit cell" is described as a single column and the surrounding tributary soil area (a_s, area replacement ratio; area of column/tributary area). Not only the lateral deformation but also shear stresses cannot occur at the outside boundaries of the unit cell because of symmetry and geometry. Therefore, 1-D loading case does not seem to conflict with the unit cell concept.

Settlement reduction factors determined in footing type of loading (B=10cm and B=20cm) are considerably lower compared to those measured in 1-D condition (B=41cm). The β values obtained in the tests and the ones obtained by design charts proposed by different authors are given in Figure-2. All the values are for end bearing columns. The internal friction angle of the sand column with a relative density

of 80% is 42^0 based on triaxial test results. The ratio of sand elastic deformation modulus to clay elastic deformation modulus, E_s/E_c is around 20-26.

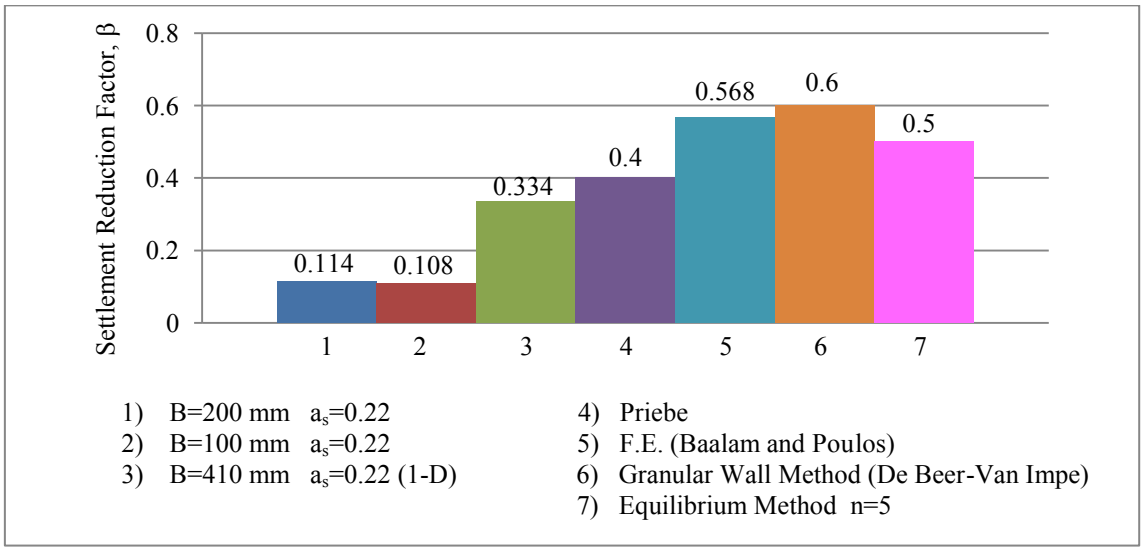

Figure 2: Comparison of test results with literature

3.3. Effective Column Length in Floating Type against Settlement Reduction

H=290 mm thick clay foundation corresponds to H/B=2.9 and H/B=1.45 for plates B=100 mm and B=200 mm.

As seen in Figure-3, settlement reduction factor β is nearly the same under plates B=100 mm and B=200 mm when column length is longer than L/D=10.

Settlement reduction factors start increasing more rapidly for column lengths smaller than L/D=10 under B=200 mm footing. There is nearly a linear increase in settlement reduction factors as the length of the columns decrease till L/D=7 under B=100 mm footing. For columns shorter than L/D=5 decrease in the improvement is observed. It seems that minimum column lengths under the both loading plates correspond to L/B=1 ratio under which improvement is not much effective.

In Figure 4, β – L/B graphs of B=100 mm (H/B=2.9) and B=200 mm (H/B=1.45) footings are nearly parallel. In both of them, settlement improvement decreases considerably in columns shorter than L/B=1.

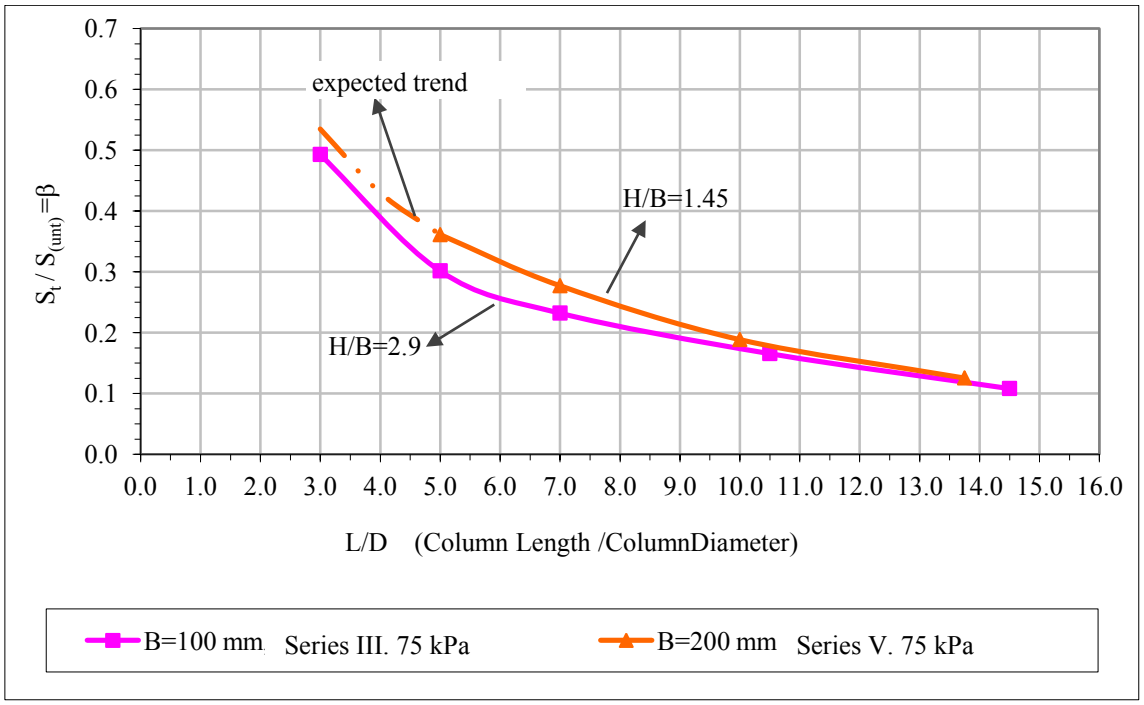

Figure 3: β – L/D relation for series III and V for 75 kPa loading

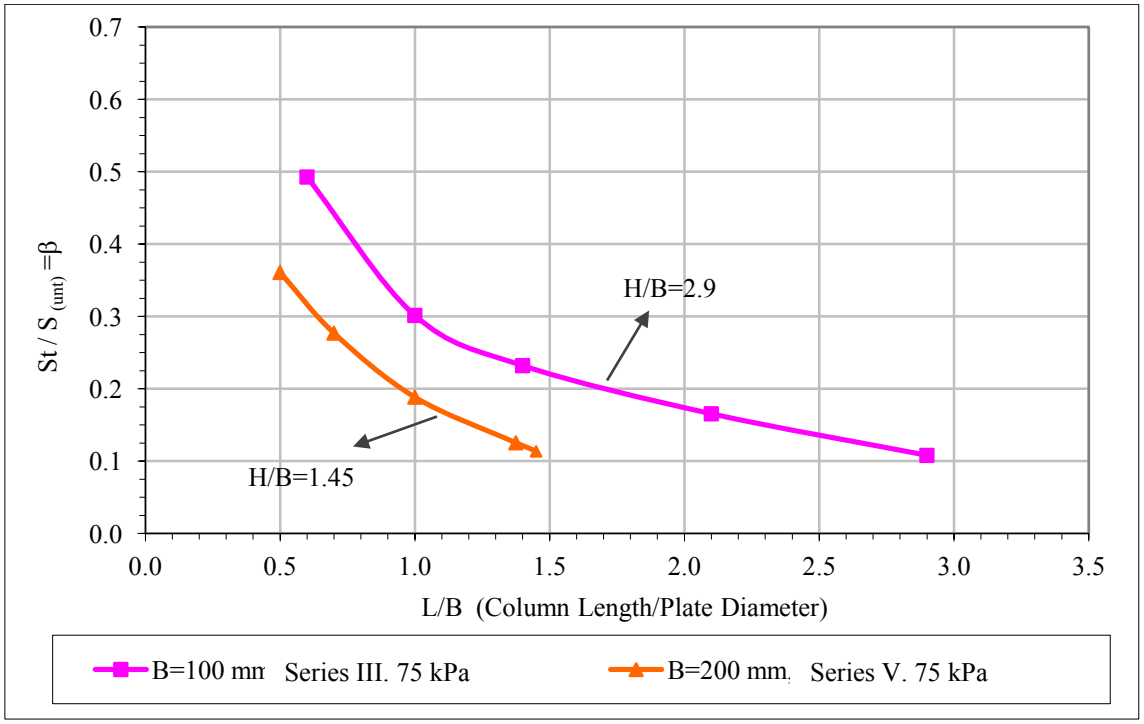

Figure 4: β – L/B relation for series III and V for 75 kPa loading

3.4. Strain Mechanism along Depth of Floating Columns

In the model study subsurface settlements have been measured in the specific locations by means of magnetic switch instrumentation system (miniature "borehole" settlement gauge). The strains that occur along the floating type of columns, the untreated soil beneath them have been examined. It is aimed to study the changes in the strain mechanisms.

A detailed presentation of strains under various footings is to be the subject of another research paper. Here the results under 100mm plate only will be presented.

The distribution strains under 100mm diameter plate supported by 60 mm, 100 mm, 140 mm, 210 mm long columns are presented in Figure-5. It is interesting to note that use of columns longer than roughly 120 mm (L/B=1.2) does not contribute to settlement reduction significantly. The strains along the columns are not uniform, more at the central zones. Highly strained zones are noticeable under short columns down to depths three times the length of columns.

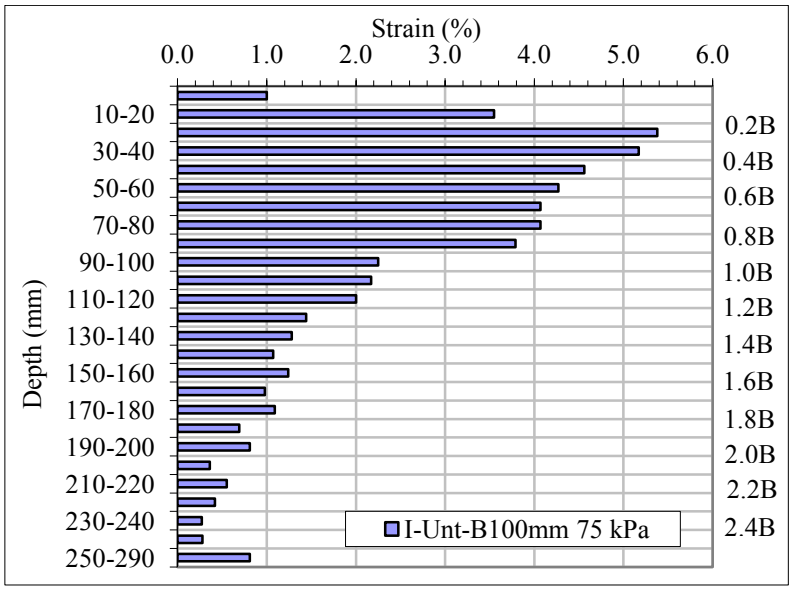

Figure 5a: Untreated test

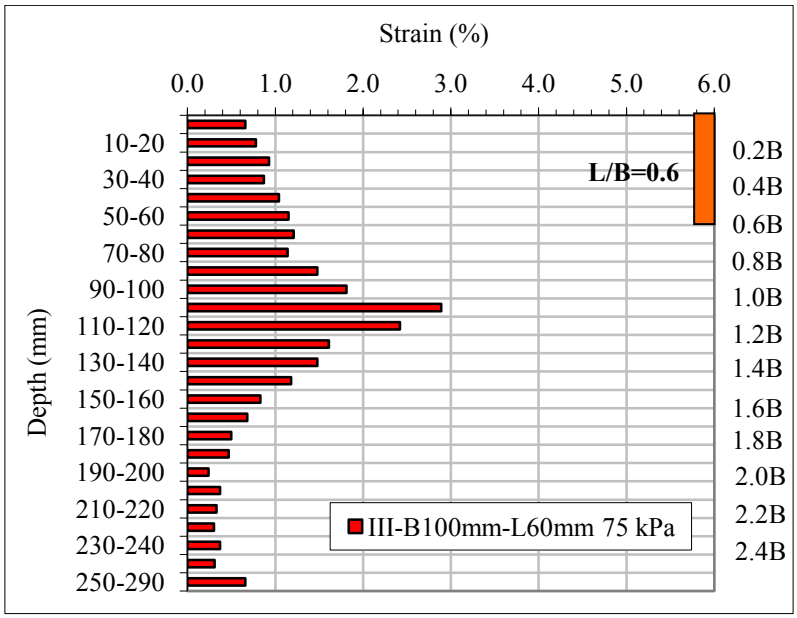

Figure 5b: L=60 mm (L/B=0.6)

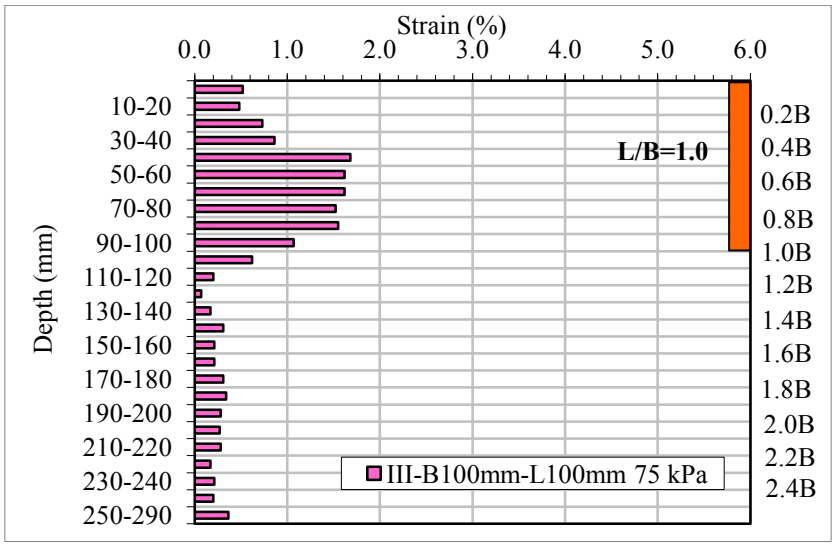

Figure 5c: L=100 mm (L/B=1.0)

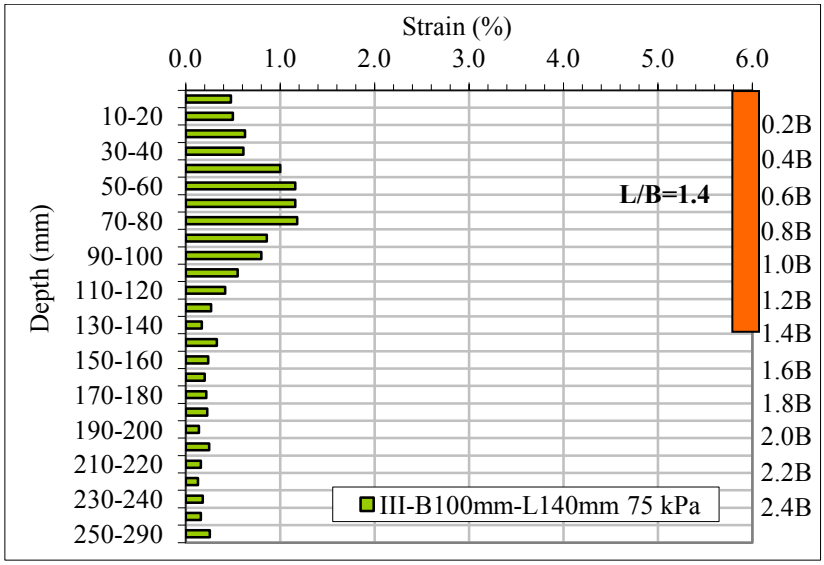

Figure 5d: L=140 mm (L/B=1.4)

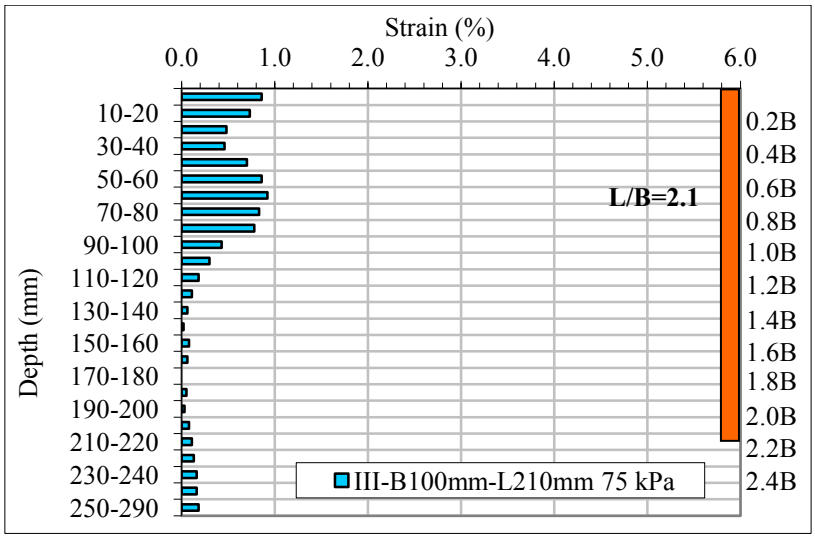

Figure 5e: L=210 mm (L/B=2.1)

4. CONCLUSION

In the design of floating columns under footings number of columns rather than pattern is significant in reducing the settlements. In this respect the use of a_s and unit cell concept may not be relevant.

In footings treated with granular column groups, settlement reduction factor β is significantly smaller than obtained from common design charts based on (unit cell) area replacement ratio a_s. In case of designing footings by using those charts, settlement improvement is underestimated.

In floating type of granular columns, column length of L/B=1.2 is sufficient to reduce strains occuring in underlying soil but strains along column is still high.

REFERENCES

R.D. Barksdale, R.C. Bachus, 1983, Design and Construction of Stone Columns-I/ FHWA-/RD-83/026

V. Baumann, G.E.A.Bauer, 1974,The Performance of Foundations on Various Soils Stabilized by Vibro-Compaction Method/Canadian Geotechnical Journal

N.P. Balaam, H.G. Poulos, 1978,Methods of Analysis of Single Stone Columns /Symposium on Soil Reinforcing and Stabilizing Techniques/Sydney Australia

Basal reinforced piled embankments in the Netherlands, Field studies and laboratory tests

Van Eekelen[1,2], S.J.M. and Bezuijen[1,3], A.
Deltares[1], Delft University of Technology[2] and Ghent University[3]
Suzanne.vanEekelen@Deltares.nl

ABSTRACT

In 2010, several European countries (Germany, Britain and the Netherlands), published a new or a revised design guideline for the design of piled embankments. France will follow in 2012. Both the Dutch (CUR226) and the German design guideline (EBGEO chapter 9) based their design calculations (for the vertical load) for the geosynthetic reinforcement on Zaeske's model (2001). This model consists of two calculation steps: (1) the load distribution (arching) and (2) the load-deflection behaviour of the membrane. In the Netherlands, a research program is carried out for further optimizing the Dutch design guideline.
This research program consists of several long-term field studies, an extensive laboratory test series and finite element analysis. The test set up of the laboratory makes it possible to evaluate specifically calculation steps 1 and 2 separately and develop modifications of the model. This paper describes the field studies and the laboratory experiments briefly and gives an overview of the main results.

1. INTRODUCTION

During the last eight centuries, the Dutch had to protect the low parts of their country against sea level rise by the construction of polders. Regularly, the weak and compressible soil in these polders gives major problems while constructing roads or railroads. The subsoil typically consists of 6 to 18 meters of soft and compressible organic clay and peat deposits (undrained strength of 10 kPa or less is no exception), and below that a firm stratum of sand. The ground water table is just below ground surface. During many centuries, the Dutch in these areas therefore mainly chose to travel by boat.
However, cars and trains were developed and the need for road and railroads grew. The usual solution of raising sand embankments appeared not to be possible in areas with very soft layers. Solutions with the 'rijzen bed' (fascine mattress) below groundwater or concrete slaps on piles were constructed.

Since the beginning of the twenty-first century, the Dutch have been constructing more and more piled embankments. Because of the very soft soils, only piled embankments with a basal reinforcement are built. Between 2002 and 2012, the Dutch constructed around 30 piled embankments.
A basal piled embankment consists of a field of piles with (or sometimes without) pile caps with an embankment (fill), that is reinforced with a geosynthetic reinforcement (GR). This paper considers the design of the geosynthetic reinforcement (GR). The Netherlands, Germany and Britain published a new or updated design guideline for geosynthetic reinforced piled embankments. These guidelines (respectively CUR 226 (2010), EBGEO (2010) and BS8006 (2010)) consider the influence of the vertical load (traffic load, soil weight) and the horizontal load (breaking forces, spreading forces, centrifugal forces etcetera) separately. This paper only considers the consequences of the vertical load.

First, the paper summarizes the basic idea of GR design, considering vertical load only. Then, the paper presents two field studies and summarizes the results of these measurements. This leads to the purpose of a model experiments series. After describing the tests, the most important conclusions of the experiments and the field studies lead to suggestions for the modification of the CUR 226 calculation model.

2. SUMMARY DESIGN GUIDELINES

The calculation of the GR strains from the vertical load is usually carried out in two steps, as shown in Figure 1. In the first step, the vertical load is divided into two parts. The first part is transferred to the piles directly, and called 'A' (kN/pile). The second part is the 'rest'. In Figure 1 this 'rest' is called 'B+C'. Part A is relatively large due to arching. Therefore, this step 1 is called the 'arching step'. Both EBGEO and CUR226 adopted Zaeske's model (Zaeske, 2001) for this calculation step. BS8006 adopted Marston's (1913) model, and modified this model to get a 3D model (as described in Van Eekelen, 2011a and Lawson, 2012).

In step 2, it is assumed that the GR strip between two piles is normative for the GR design. In other words, it is assumed that the strains occur mainly in this strip. Assuming a load distribution on this GR strip, and support from the subsoil (if allowed), the GR strain ε can be calculated. CUR and EBGEO calculate with a triangular distribution of the load on the GR strip, while BS8006 chose for an equally distributed load, and never allows calculating with subsoil support. Lawson (2012) suggests interpreting the BS8006 differently: namely to consider the net load on the GR.

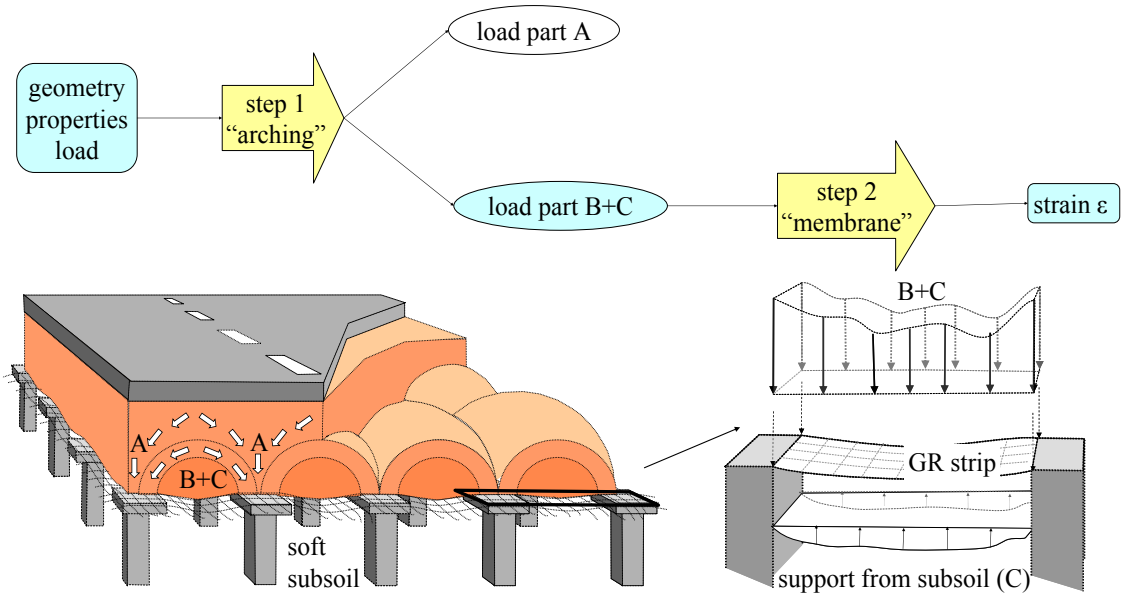

Figure 1: The calculation of the GR strain due to vertical load is carried out in two steps.

Step 2 implicitly results in a further division of the vertical load, as shown in Figure 2; load A goes directly to the piles (arching), load B is transferred through the GR to the piles and load C is carried by the subsoil. It should be noted that load A, B and C are expressed in kN/pile and that A, B and C are vertical loads.

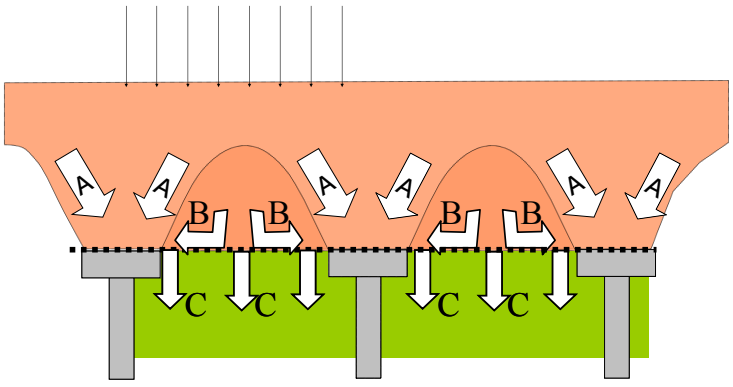

Figure 2: Load distribution in a piled embankment.

3. FIELD TESTS

Table 1 presents two recent Dutch field studies: a railway in Houten (*a*) and a highway's exit near Woerden (*b*). Figure 3 and Figure 4 compare the resulting measurements of the load distribution with EBGEO/CUR predictions. The figures show that the measured load part A is higher than the predicted load part A. Thus, calculation step 1 underestimates the arching in comparison with the measurements.
Load part B is related directly to the GR strain ε and thus the tensile force in the GR and is therefore an important parameter. The figures show that the measured B is (much) lower than the EBGEO/CUR prediction, which is therefore on the safe side.

Table 1: Overview of three Dutch field tests

		Houten Railway		**Woerden Highway's exit**
	in use since	November 2008		June 2009
		location 1	location 2	
Geometry and properties	soil conditions	1 m sand, 3 m soft clay, 20 m sand		17 m soft clay
	pile foundation	High Speed Piles (HSP), pile shafts ø0.22 m, cast in situ pile heads ø0.40 m.		prefab piles 0.29x0.29 m^2, smooth square prefab pile caps 0.75x0.75 m^2
	centre-to-centre distance piles	1.25x1.40 m^2	1.45x1.90 m^2	2.25x2.22 m^2
	height embankment[a]	2.60 m	2.60 m	1.53-1.89 m
	reinforcement across (bottom layer)	Fortrac M 450/50 (PVA)	Fortrac R 600/50 T (PET)	Stabilenka 600/50 (PET)
	reinforcement along (top layer)	Fortrac M 450/50 (PVA)		Fortrac R 600/50 T (PET)
Monitoring	load distribution	A, A+B		traffic weight, A, A+B, locally C
	settlements	settlement tubes and surface scanning		settlement tubes and surface scanning
	GR strains	Glötzl transducers		strain gables, and optic fibres
	pile moments	no		yes; optic fibres
	references	Van Duijnen et al., 2010		Van Eekelen et al., 2012b

[a] at monitoring location (road surface or top of rail - pile cap head)

As the measured B is lower than the calculated B, it is expected that the measured GR strain is smaller than the calculated GR strain. This is confirmed in Figure 5. This figure presents the measured (temporary) increase in GR strain that occurs during passages of trucks. The GR strains were measured with optic fibres. The shape of the two trucks can be recognized in the measurements, especially ε01 shows clearly the difference between the three set of wheels axles of truck 1 (the centre wheel is lifted) and the four wheel axles of truck 2. These measurements are presented more in detail in Van Eekelen and Bezuijen, 2012.

The extra GR strain around piles 692-680 is predicted with EBGEO/CUR and a modified version of EBGEO/CUR (with an inverse triangular load distribution as described in Van Eekelen et al., 2011d). To determine the temporary extra strain due to a truck, the difference between two situations is determined. The first situation is the one without traffic, with a GR stiffness determined from the isochronous curves for 1 year loading time and 1.5% estimated strain, resulting in a GR stiffness J = 5180 kN/m^2. The second situation with a truck of 32 ton and a GR stiffness determined for 1 month loading time and 1.5% estimated strain, resulting in GR stiffness J = 5319 kN/m^2. EBGEO/CUR predicts 0.5% extra GR strain, the modified version with the inverse triangle predicts 0.22%. The increase in GR strain ε09 and ε03 lies around 0.1%.

It is concluded that the design model of EBGEO and CUR underestimate the arching (A), and overestimate the GR strains in comparison with the field measurements. In the next sections, this will be further analysed.

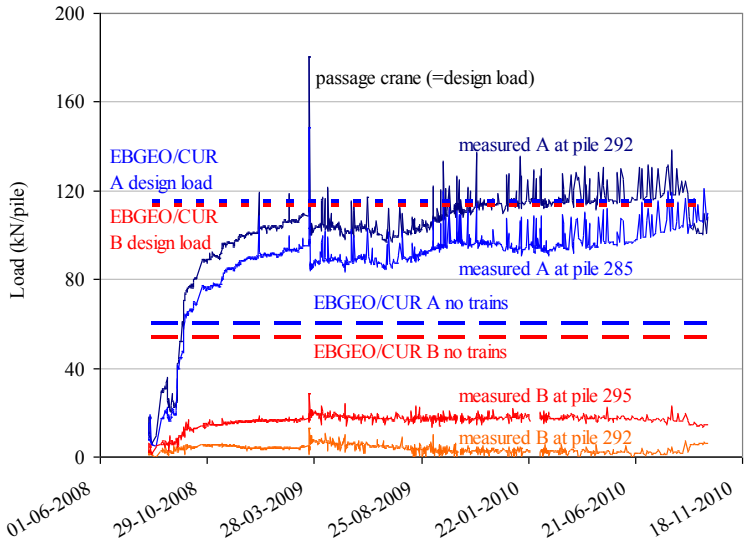

Figure 3: Results of field measurements at the Houten railway (Van Duijnen, 2010). Subgrade reaction k in predictions: k = 100 kN/m³

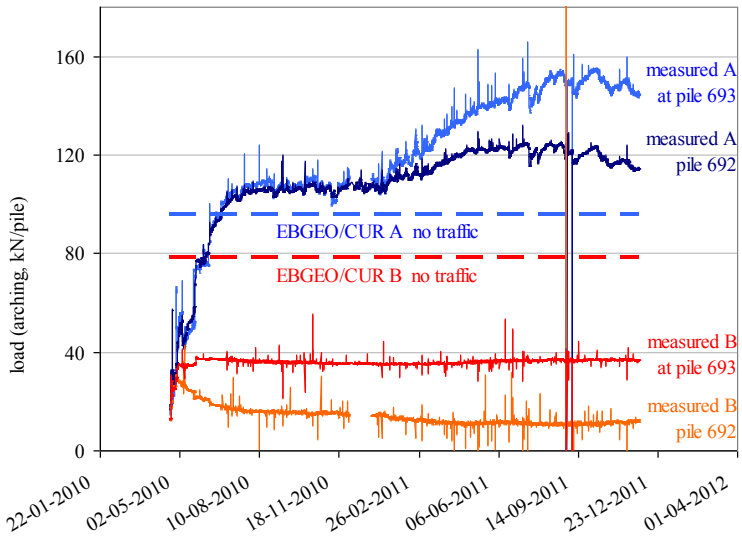

Figure 4: Results of field measurements near Woerden, see also Figure 5. Subgrade reaction k in predictions: k = 0 kN/m3 (no subsoil).

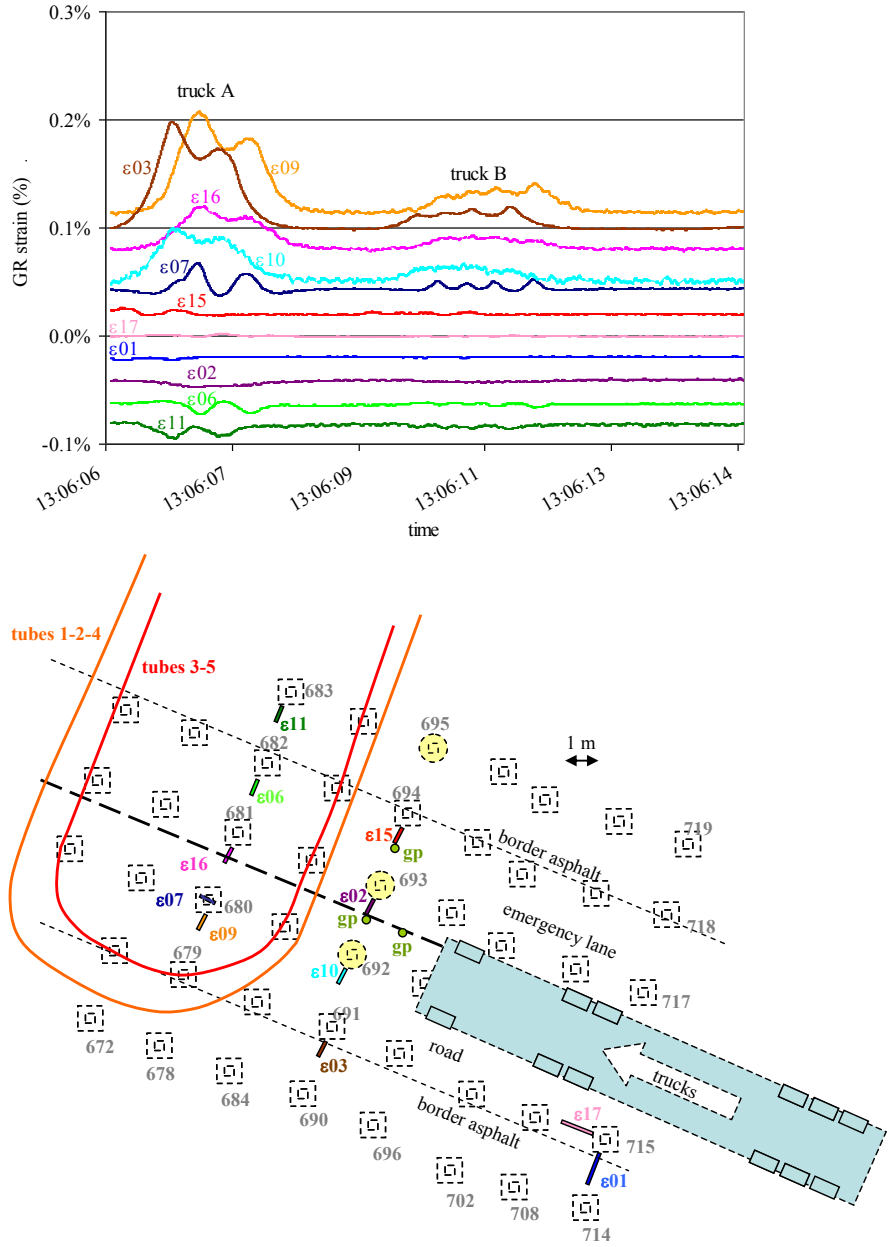

Figure 5: Measurements of the GR strains during the passage of two trucks on 6 September 2011.

4. LABORATORY EXPERIMENTS

A series of nineteen piled embankment model experiments was carried out in the Deltares laboratory. The main purpose of the experiments was to understand why the predicted GR strains are larger than the GR strains that were measured in the field.
Starting point was that it had to be possible to validate calculation steps 1 and 2 separately (Figure 1). Therefore, it was necessary to be able to measure load parts A, B, C (Figure 2) and the GR strain separately. Furthermore, GR was to be included, and the fill had to be as realistic as possible, that means that most tests were carried out with a granular fill of crushed recycled construction material.

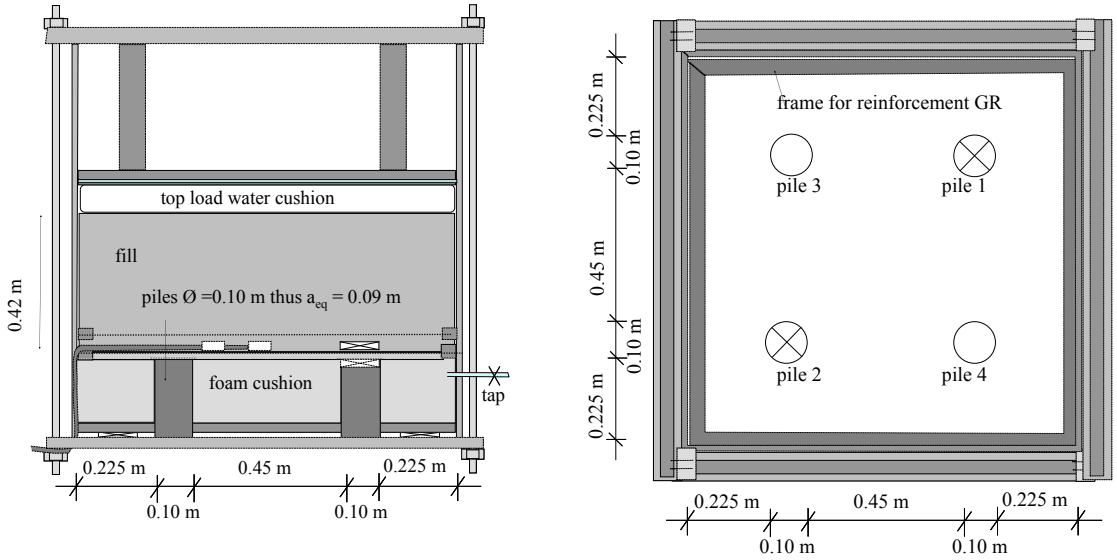

Figure 6: Side view and top view of the test set-up

Photo 1: Test set-up

The nineteen tests were conducted by using the test set-up given in Figure 6. A foam cushion modelled the soft soil around the 4 piles. This cushion was a watertight wrapped soaked foam rubber cushion. A tap allowed drainage of the cushion during the test, which modelled the consolidation process of the soft soil.
A 1.5 to 2 cm layer of sand was applied on top of the foam cushion and the piles. On top of this, a stiff steel frame was placed on which the GR was attached. The GR was a geotextile or a geogrid. The stiffness of the GR varied per test, and the number of reinforcement layers varied between one and two.
The embankment was fine sand (Itterbeck sand (125-250 μm) or granular fill (crushed granular rubble 1-16 mm) of varying height, although in most tests 0.42 m. The top load was applied with a water cushion that applied stresses comparable with field stresses.

After the installation of the fill, each test was carried out as follows: (1) one drainage step foam cushion (modelling subsoil consolidation), (2) installation of the water cushion and first top load increase, (3) one

or more drainage steps (4) second top load increase, (5) one or more drainage steps and so on, up to the maximal top load (varying between 50 and 100 kPa) and the subsequent drainage steps.
The test set-up is similar to the test set-up of Zaeske (2001). In the series reported here, however, the fill in most tests was granular material instead of sand, the subsoil support was controlled with the foam cushion and the load distribution was measured differently.

The following features were measured: pressures on the piles, both on top of and below the GR. The pressure in the foam cushion and the water cushion, the total load on the foam cushion, strains of the GR and settlements of the GR at 3 to 5 locations.

The results of the first twelve tests are described, analysed and compared with CUR/EBGEO calculations extensively in Van Eekelen et al., 2011c and 2011d. The next section gives the most important conclusions of the nineteen tests.

5. SUGGESTIONS FOR MODIFICATIONS ANALYTICAL MODEL

5.1. Calculation step 1

As shown in section 2, calculation step 1 divides the vertical load into two parts: A and B+C. Figure 7 compares the measured and calculated results of step 1 (load part A). The figure shows that the measured A follows a smoothly ascending curve when plotted against net load. The figure also shows that consolidation of the subsoil results in increased measured arching (A) in the fill. Consolidation (subsoil deformation) is obviously necessary for the development of arching.
According to EBGEO/CUR, the arching is independent from the deformation due to consolidation of the subsoil. This results in a calculated value for arching load part A that is lower than measured in the model tests, and in turn gives a calculation for load part B+C (and thus GR strain) that is higher than measured in the model tests. The improvement of step 1 is subject for further study, and will be published at a later date.

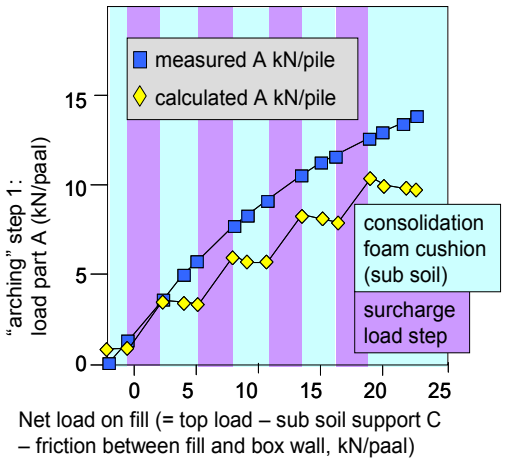

Figure 7: Measured and calculated (CUR/EBGEO) result of step 1 (arching)

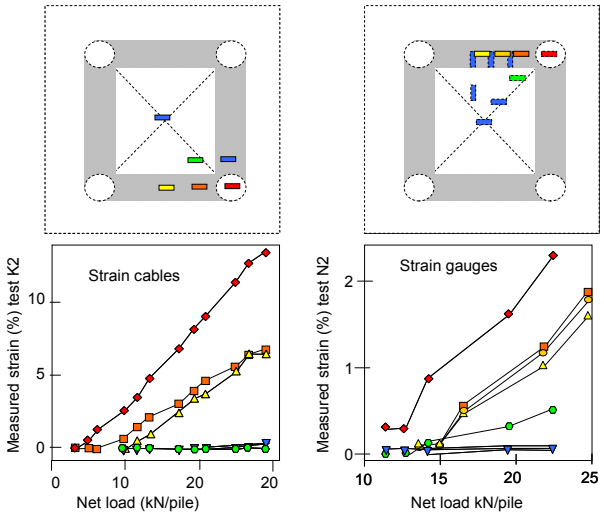

Figure 8: Measured strains occur mainly in the tensile strips that lie on the GR strip between adjacent piles, in accordance with the calculation models (see Figure 1).,

5.2. Calculation step 2

Calculation step 2 (membrane step), consists of two parts. Firstly, the assumption is made that the GR strains occur mainly in the GR strips as shown in Figure 1. Figure 8 confirms this first assumption: all tests show that the GR strains occur mainly in the tensile strips that lie on top of and between adjacent piles.
EBGEO/CUR226 calculations do not take GR strains on the pile caps into account, although these can be the largest GR strains under specific conditions, such as for the smooth, small-diameter pile caps in the test set-up. As this has not been confirmed in most field tests, it is decided not to modify the step 2 calculations on the basis of this conclusion, which is a decision on the 'safe side'.

The loading and supporting of the GR strip is considered in the second part of step 2, as shown in Figure 1. The load distribution on the strip is directly related to the deformed shape of the GR, as shown in Figure 9. EBGEO/CUR226 uses the (blue) triangular load distribution, while the British BS8006 uses the (red) equally distributed load.

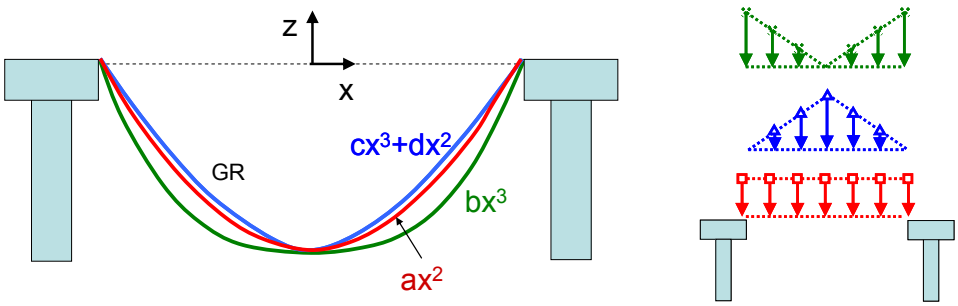

Figure 9: Relation between shape deformed GR (left) and load distribution (right).

The shape of the deformed GR is measured both with a liquid levelling system, and by scanning the surface of the sand layer below the GR, before and after the test. The results of both measurements, of several tests, are presented in Figure 10. From this, it should be concluded that the load distribution on the GR strip agrees best (at least) with the (green) inverse triangle of Figure 9. This is also confirmed by the direct measurements of the vertical load with extra force transducers on the GR strips between the piles, as shown in Figure 11 and by numerical calculations as shown by Den Boogert et al., 2012.

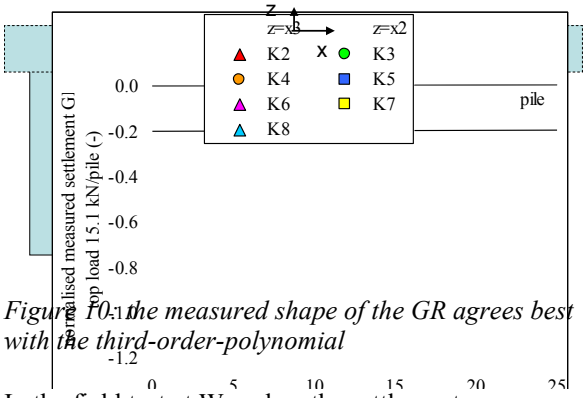

Figure 10: the measured shape of the GR agrees best with the third-order-polynomial

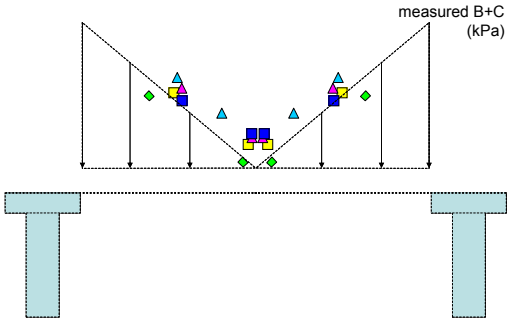

Figure 11: measured load distribution on the GR strip

In the field test at Woerden, the settlements were measured by measuring the water pressure within tubes. It was necessary to measure the settlements each 0.10 m (normally, this is 0.50 m), to be able to determine the shape of the deformed GR. Figure 12 gives the measured GR deformations for tube 3 (Figure 5), that lies directly upon the GR, across piles. The second derivative of these measurements corresponds directly with the load distribution on the GR strips. Taking the second derivative introduces quite some scatter, even after some averaging, but the shape of the (red) lines approaches more the inversed triangle than a triangular or constant load distribution.

It is concluded that the distribution of the line load on the reinforcement strip between two piles tends to have the distribution of an inverse triangle. However, EBGEO/CUR calculations are based on a triangular-shaped line load.
Considering the subsoil support (Figure 1) of the GR strip, EBGEO/CUR mobilises only part of the subsoil, namely the area below the GR strips between the piles. Van Eekelen et al., (2011d) suggest how the supporting subsoil area can be increased to the entire available area below the GR, as described more in detail in Lodder et al., (2012).
Figure 13 shows the results of modifying EBGEO/CUR-step 2 by improving both the subsoil support and the load distribution. The figure shows that this gives a much better agreement with the measurements, and 19-26% less GR strain than the EBGEO/CUR assumptions. Changing these features can thus give a reduction of 19-26% of necessary GR strength.

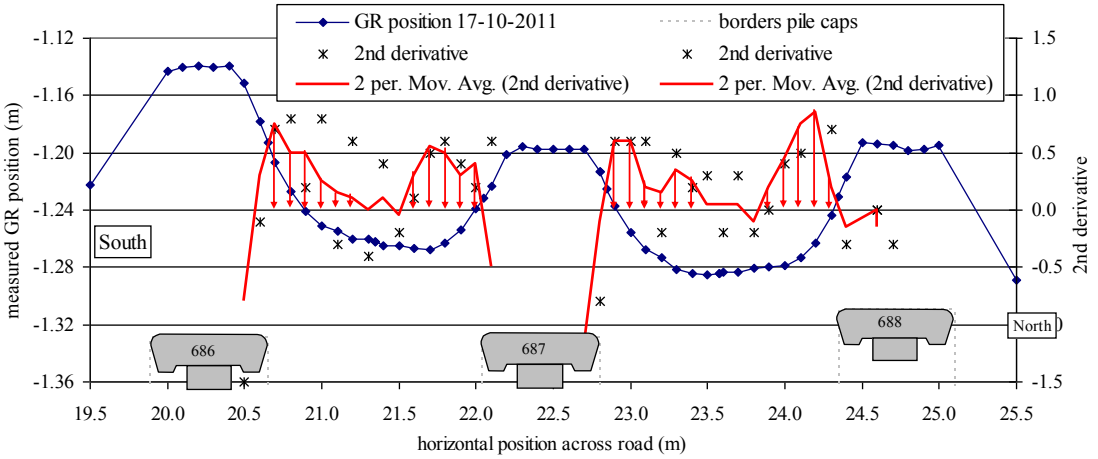

Figure 12: Measured settlements in Woerden, October 2011, road had been in use for ca. 16 months

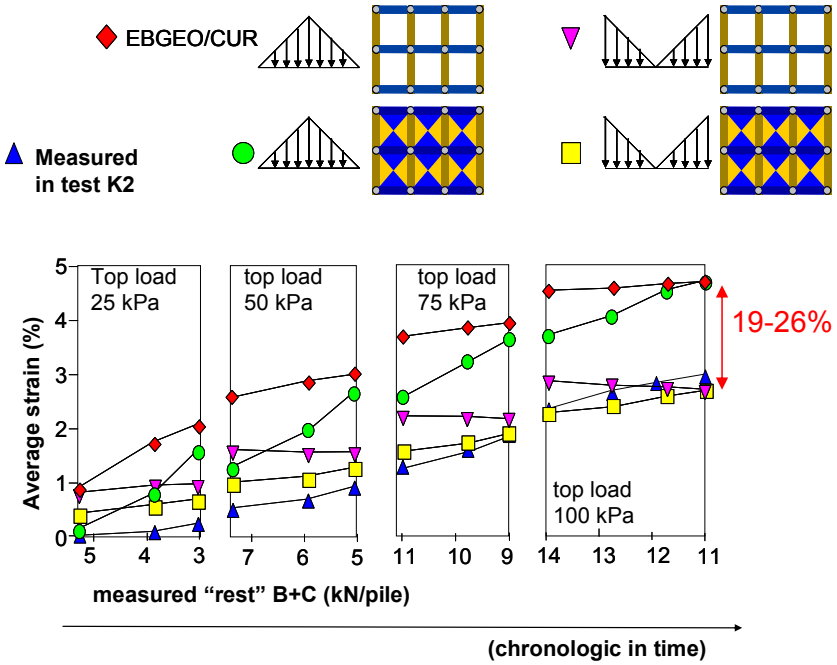

Figure 13: Comparison measurements and calculations step 2; effect of modifications CUR/EBGEO calculation model: a. modification load distribution (from triangular shape to inverse triangular shape) and b. modification subsoil support (from below GR strip only to below entire, diamond shaped GR area)

6. CONCLUSIONS

Both the Dutch CUR 226 (2010) and the German EBGEO (2010) adopted their basic calculation model for the GR design of Zaeske (2001). This model consists of two steps: the arching step that distributes the load in a part that is transferred directly to the piles and a 'rest load' and the membrane step, calculation the GR strain from the 'rest load'.

An ongoing Dutch research program must lead to more understanding of the arching mechanism and membrane mechanisms, and in time lead to a new version of the Dutch guideline. Several field tests show that the measured GR strains in the field are considerably smaller than the strains predicted with the calculation model of Zaeske. The purpose of model experiments was therefore to understand the difference between calculated and measured GR strains.

The model tests show that consolidation of the subsoil results in an increase of arching (an increasing A). This behaviour is not described in the arching models of Zaeske (or the BS8006) yet and is subject of further study. The measured strains in the experiments confirm the assumption of calculation step 2, that the GR strain occur mainly in the GR strips between two adjacent piles. Finally, it is shown that two

modifications of the calculation model improve the agreement between calculations and measurement for step 2 considerably for both static loading and dynamic loading by trucks:

- The load distribution on the GR strip should have the shape of an inverse triangle, rather than the triangular shape of the EBGEO/CUR or the equally distributed load of the BS8006.
- The subsoil support should be taken into account for the entire area below the GR, not only for the area between the adjacent piles.

Adopting these two modifications leads to 19-26% less GR strain, and therefore to 19-26% less required GR strength.

REFERENCES

BS8006-1: 2010. Code of practice for strengthened/reinforced soils and other fills. British Standards Institution, ISBN 978-0-580-53842-1

CUR 226, 2010, Ontwerprichtlijn paalmatrassystemen (Design guideline piled embankments). ISBN 978-90-376-0518-1 (in Dutch)

EBGEO, 2010. Empfehlungen für den Entwurf und die Berechnung von Erdkörpern mit Bewehrungen aus

Geokunststoffen – EBGEO, 2. Auflage, German Geotechnical Society, ISBN 978-3-433-02950-3 (in German).

Den Boogert, T.J.M., Van Duijnen, P.G., Peter, M.G.J.M. and Van Eekelen, S.J.M., 2012, Paalmatrasproeven II, Eindige elementenberekeningen, GeoKunst, GeoTechniek January 2012, pp. 52-57, in Dutch

Lawson, C.R., 2012, Role of Modelling in the Development of Design Methods for Basal Reinforced Piled Embankments, to be published in the Proceedings of EuroFuge 2012, Delft, the Netherlands.

Lodder, H.J., Van Eekelen, S.J.M. and Bezuijen, A., 2012, The influence of subsoil reaction on the geosynthetic reinforcement in piled embankments., to be published in the Proceedings of EuroGeo 2012, Valencia in Spain.

Van Eekelen, S.J.M., Jansen, H.L., Van Duijnen, P.G., De Kant, M., Van Dalen, J.H., Brugman, M.H.A., Van der Stoel, A.E.C., Peters, M.G.J.M., 2010a. The Dutch Design Guideline for Piled Embankments. In: Proceedings of 9 ICG, Brazil, pp. 1911-1916.

Van Eekelen, S.J.M., Bezuijen, A. and Alexiew, D., 2010b, The Kyoto Road, monitoring a piled embankment, comparing 31/2 years of measurements with design calculations, published in the Proceedings of 9ICG, Brazil, 2010, pp. 1941-1944.

Van Eekelen, S.J.M.; Bezuijen, A. and Van Tol, A.F., 2011a. Analysis and modification of the British Standard BS8006 for the design of piled embankments. Geotextiles and Geomembranes 29 (2011) pp.345-359.

Van Eekelen, S.J.M., Lodder, H.J., Bezuijen, A., 2011b. Load distribution on the geosynthetic reinforcement within a piled embankment, in: Proceedings of ICSMGE 2011, Athens, 1137-1142.

Van Eekelen, S.J.M., Bezuijen, A., Lodder, H.J., van Tol, A.F., 2011c. Model experiments on piled embankments. Part I, Geotextiles and Geomembranes. doi:10.1016/j.geotexmem.2011.11.002, published on line at http://dx.doi.org/10.1016/j.geotexmem.2011.11.002.

Van Eekelen, S.J.M., Bezuijen, A., Lodder, H.J., van Tol, A.F., 2011d. Model experiments on piled embankments. Part II, Geotextiles and Geomembranes. doi:10.1016/j.geotexmem.2011.11.003., published on line at http://dx.doi.org/10.1016/j.geotexmem.2011.11.002.

Van Eekelen, S.J.M., Bezuijen, A., 2012a. Model experiments on piled embankments, 3D test series, to be published in the Proceedings of EuroFuge 2012, Delft, the Netherlands.

Van Eekelen, S.J.M., Bezuijen, A., 2012b. Does a piled embankment 'feel' the passage of a heavy truck? High frequency field measurements., to be published in the Proceedings of EuroGeo 2012, Valencia, Spain.

Zaeske, D., 2001. Zur Wirkungsweise von unbewehrten und bewehrten mineralischen Tragschichten über pfahlartigen Gründungselementen. Schriftenreihe Geotechnik, Uni Kassel, Heft 10, February 2001 (in German).

Design risks of ground improvement methods including rigid inclusions

J. Wehr, Keller Holding GmbH, Offenbach, Germany, j.wehr@kellerholding.com
M. Topolnicki, Keller Polska Sp. z o.o., Gdynia, Poland, mtopolnicki@keller.com.pl
W. Sondermann, Keller Grundbau GmbH, Offenbach, Germany, w.sondermann@kellergrundbau.com

ABSTRACT

After an introductory presentation of design approaches the risks involved are investigated. Considered are different ground improvement methods, like soil mixing, vibro compaction and vibro stone columns, as well as pile-like supporting elements, including vibro concrete columns and full displacement columns named rigid inclusions.
The difference in stiffness of the inserted material and the soil determines the design and the risks involved. Three categories with increasing risk are proposed. Ground improvement methods, ductile in compliance with EN 1997-1 and DIN 1054, proved to be extraordinary robust and present only a small risk with regard to a possible variation of soil and material parameters and loads. The design is usually determined by the serviceability limit state.
Risks increase with the application of non-ductile methods with small column diameter, like rigid inclusions, because the ultimate limit state is controlling the behaviour. Namely, in order to mobilize high skin friction, the lower and upper end of the column have to fail during punching in the soil below and the load transfer platform above. Even a small variation in material parameters, system geometry or loads may lead to a complete loss of bearing capacity and progressive failure, resulting in expensive damages of civil engineering structures and time consuming repair works.

1. INTRODUCTION

Since the 40's of the 20th century ground improvement methods have been successfully applied to improve the bearing capacity and/or stability and/or deformation characteristics of soft soils for a variety of applications. The involved technologies of ground improvement have won a substantial market share in relation to competitive procedures, such as traditional piling or heavy foundation solutions.

Present requirements for well-positioned ground improvement methods, which represent established professional practice and also reflect respective regulations included in standards and codes, comprise:

- The involved procedure is based on a well-defined execution process, manageable and controllable in each stage,
- The procedure is calculable and repeatable,
- The process involved should allow for optimisation of the solution applied in relation to expected functional performance,
- The success of performance of the procedure is verifiable by measurements and/or field tests,
- The execution time is relatively short (in comparison to the total construction period),
- An immediate use of the improved ground is possible,
- Cost of application is competitive.

Traditionally, piling or direct exchange of soft soil has been used to bridge or replace layers with insufficient bearing capacity. The aim of modern ground improvement methods is to in-crease the bearing capacity of the ground in order to bear the loads with compatible deformations. Consequently, not the entire action is taken by the supporting elements, but only the difference between the required and existing bearing capacity without ground improvement, what contributes to the attractiveness and customer's use of ground improvement. The degree to which the existing ground can be intentionally

used to support acting loads, which may vary from zero up to allowable limit, depends on the characteristic of the ground improvement method involved and the design solution adopted.

A systematic overview with classification of the different methods can be found in figure 1, excluding surcharge, Sondermann and Kirsch [1].

Compaction	
Static methods	Dynamic methods
Pre-loading Pre-loading with consolidation aid Compaction grouting Influencing the ground water	Compaction by vibrations - using depth vibrator - using vibratory hammer Impact compaction - drop weight - explosion - air pulse method

Reinforcement		
Displacing effect	Without displacing effect	
	Mechanical introduction	Hydraulic introduction
Vibro stone columns Vibro concrete columns Sand compaction piles Lime/cement-stabilising columns Compaction grouting	DSM-method FMI-method Injections Freezing	Jet grouting

Figure 1: Ground improvement methods

Due to constantly increasing competition and pressure to shorten execution times the application limits of existing ground improvement methods had to be extended. This resulted in a rapid development and use of alternative procedures in the last years.

2. STANDARDS AND RECOMMENDATIONS

The growing importance of ground improvement methods in Europe and world-wide is also reflected by the recent development of normative documents. Standardization committees as well as national and international working groups have compiled and even still work on various recommendations and codes. The most important sets of rules and recommendations, which define current standards for ground improvement measures, include (but are not limited to):

- European standard for Deep Soil Mixing, EN 14679,
- European standard for Ground Treatment by Deep Vibration, EN 14731,
- European standard for Vertical Drains, EN 15235,
- Recommendation 6.9 by EBGEO „Rein-forced embankments on pile-like elements", Working Group 5.2 of the German Geotechnical Society DGGT,
- Bulletin for the installation, calculation and quality control of stabilization columns for ground improvement, Working Group 2.8 of the German Geotechnical Society DGGT, Part 2 „Mortar columns" (in German),
- Amélioration des Sols par Inclusions Rigides, ASIRI, (2011), Ground improvement with stabilising columns, Draft (in French) [2].

3. LIMITATIONS AND RISKS OF GROUND IMPROVEMENT METHODS

There is still a research need for a more comprehensive investigation of the limits between different soil improvement methods, pile-like elements and piles. Generally there are the following risks of geotechnical methods:

Servicibility limit states (DIN EN 1997-1):
- larger settlements
- tilting or sliding of a footing

Ultimate limit states (DIN EN 1997-1):
- larger settlements
- tilting due to excentric load
- punching failure of column head and toe
- bearing capacity failure
- slope stability failure
- sliding failure

The risk level of various ground improvement methods can indeed be different! The following three categories with increasing risk level can be identified. In each category the typical risks are:

Category A:
- Larger settlements

Category B:
- Larger settlements
- Structural failure (internal failure due to vertical loads)
- Overall bearing capacity failure (external punching failure of column toe or head)

Category C:
- Larger settlements
- Structural failure (internal failure due to vertical and horizontal loads, buckling)
- Bearing capacity failure (external punching failure of column toe or head)
- Overall bearing capacity failure, slope stability failure

3.1. Category A (low risk)

In definitely true ground improvement methods the columns have to be supported by the surrounding soil in order to keep their shape. Therefore the columns themselves do not have an own failure load. Usually the serviceability limit state (deformations) is decisive in the geotechnical design. All these methods pose a low risk because they are sufficiently ductile as specified in DIN 1054 “Supplementary rules to DIN EN 1997-1” of the Eurocode 7 and robust. Robustness is here defined as the ability of a system to maintain its function during soil parameter and load variation. It is important to note that the bearing capacity is not exceeded even if the columns are overloaded. Vibro compaction and vibro stone columns, executed with depth vibrators as well as band, sand and gravel drains and sand compaction piles are included herein. The design is done, e. g., with the Priebe method [3] or the Balaam/Booker method [5].

3.2. Category B (medium risk)

The next, medium risk category includes all methods that involve columns with a diameter equal to or greater than 30 cm, in which plastic deformations are considered with sufficient safety factors against failure load. These are, e. g.,: lime/cement columns installed with the dry method, deep soil mixing with the wet method, vibro mortar columns and vibro concrete columns, and combined concrete/gravel columns like columns with mixed modulus (CMM). The design is conducted, e. g., with DIN 4017, using the Brinch-Hansen approach for the bearing capacity of the column base, and additionally with DIN 1045 for the structural bearing capacity.

3.3. Category C (high risk)

This category includes all pile-like elements with a small diameter (i.e., generally below 30 cm) and material to soil stiffness ratio well above the limit identified in section 4.

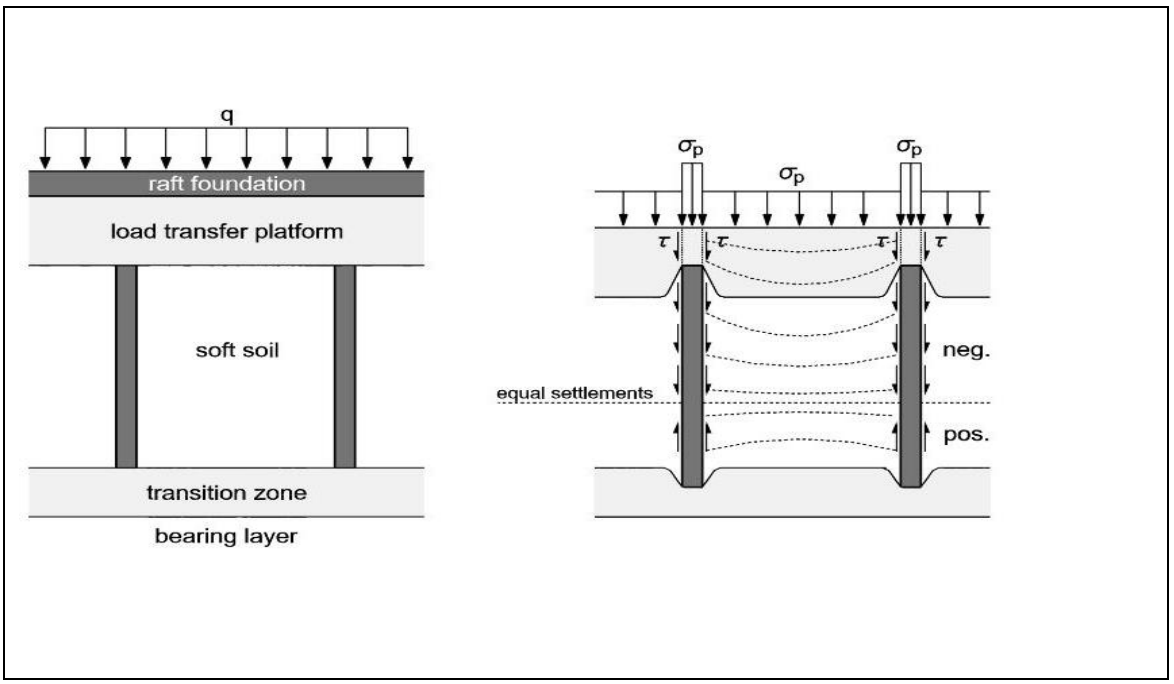

Figure 2: System of category C with stresses and settlements

Due to the adopted design negative and positive skin friction will develop along such elements (figure 2), while the design load is close to the failure load. Even small variations of soil parameters and/or acting loads may easily cause sudden loss of the bearing capacity of the column material or the ground, with all related consequences for the super structure. Care should be taken especially in soft soils and with weak load distribution layers. Consequently, the risk involved in application of such methods of ground improvement is much higher, compared to category A, in particular, and also to B. Therefore the methods ascribed to category C require more attention.

In category C there are stabilizing columns installed using dry granular binders, which harden upon contact with the ground water (Combined Soil stabilisation with Vertical columns), columns made of ready mixed wet materials, as well as rigid inclusions like Controlled Modulus Columns (Wong and Muttuvel [9]), made of regular concrete or specific mortar.

All columns are usually unreinforced. Column diameter may vary between the lower limit of 12 to 15 cm, as in the German recommendation [8], through frequently used up to 40 cm. Steel reinforcements in form of single bars or profiles can also be installed in columns with a diameter above 25 cm, but this is usually limited to restricted areas due to cost increase (Wong and Muttuvel [9]).

As outlined in the recommendations for „the installation, calculation and quality control of stabilizing columns for ground improvement“ (DGGT 2002 [8] in Germany, and ASIRI 2011 [2] in France), the loads are gradually transferred from the soil to much stiffer stabilizing columns. Generally, the supporting system shows a similarity to a “floating foundation” or a “pile-raft” design, the difference being the embedment of the supporting elements, which only slightly penetrate into the underlying bearing layer. This kind of system has significant influence on the load distribution pattern between the columns and the soil.

As specified in DIN EN 1997-1, many calculation methods are based on the assumption of a sufficiently ductile behaviour of the supporting soil-structure interaction system. In DIN 1054 a sufficiently ductile behaviour is assumed if the ultimate limit state is preceded by large displacements. If this ductility is missing, an ultimate limit state with sudden and progressive failure may easily appear. Particularly this risk exists for controlled modulus columns, because the design takes into account that some columns are already partially broken (Wong and Muttuvel [9]). Therefore standard geotechnical calculation methods,

well suitable for ground improvement categories A and B, should not be directly applied in category C because of much lower safety level of such systems, which does not comply with DIN 1054 or DIN EN 1997-1 recommendations. Further dedicated research is needed to find out how much the existing partial safety factors of DIN 1054 have to be increased for category C.

Special attention is also required in case of unreinforced slender elements subjected to tensile loads, which can easily break. Such failures have been often observed, although not documented, e.g. during column execution, when influenced by ground heave, as well as after column completion due to associated earth works or heavy vehicles passes. Quite often there is also a danger of column buckling, especially for diameters less than 30 cm, which has to be assessed [2].
Due to the complicated interaction between soil and structure all these methods have to be classified as GK3 according to DIN 1054. The observational method must not be applied due to missing ductility of the system (DIN 1054).

There are certain similarities to the combined piled raft foundation. However, the piles are directly connected to the raft and therefore a punching failure of the column head is not possible. Furthermore the diameter of the piles is much larger than 30 cm resulting in lower risks of the piled raft foundation.

4. INFLUENCE OF THE SUPPORTING ELEMENT TO SOIL STIFFNESS RATIO

Crucial for the risk assessment of all ground improvement methods considered in this paper and evaluated in the following chapter is the stiffness ratio between a supporting member, i.e. column or pile-like element, and the soil, which – unfortunately – is often not rigorously taken into account or even entirely ignored.

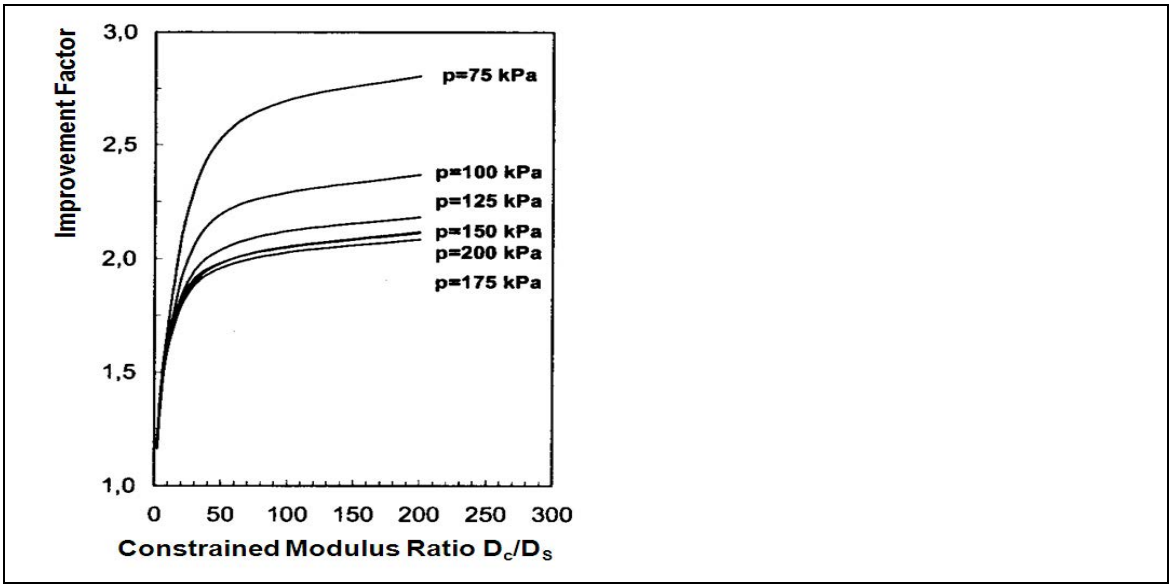

Figure 3: Settlement improvement factor [4]

There are, however, the following exceptions:

- In his thesis Kirsch [4] examines the influence of the variation of the constrained modulus ratio between 2 and 200 on the settlement improvement factor which is denoted as the settlement ratio of the unimproved soil to the improved soil. As shown in figure 3, the settlement improvement factor increases less and less with increasing stiffness ratio and loading stress level. Only below a ratio of ca. 40 to 50 a relevant increase of the settlement improvement factor can be expected. Thus larger stiffness factors are not efficient in terms of soil improvement.

- In the EBGEO recommendation [10] for geotextile coated columns there are certain design rules for the horizontal geogrid design above the columns. Below a stiffness ratio (column/soil) of 50 a geogrid is not necessary because of the self regulating system. For an intermediate stiffness ratio between 50 and 75 a geogrid design is recommended in special cases. However, if the ratio is higher than 75 a

geogrid must be foreseen. The core of geotextile coated columns is granular but due to the relatively stiff "sock" they may be regarded as transition to cement and concrete columns.

- For lime/cement deep mixing columns there are similar approaches. The undrained shear strength of the column c_{US} should not exceed 150 kPa [6]. Based on the empirical relationship M = 50 to 150 x c_{US} a compression modulus of M = 7.5 MPa to 22.5 MPa can be calculated. Considering the very soft soils in Scandinavia, with compression moduli around 0.3 MPa, average stiffness ratios of 50 can be back calculated.

Summarizing the above findings it can be stated that the stiffness ratio of approx. 40 to 50 between the supporting element and the soil can be regarded as an upper limit for efficient ground improvement methods. This is because any further increase of stiffness of the supporting element is ineffective and does not contribute to acceleration of the settlement and to the increase of settlement improvement factor. It is therefore recommended to decrease the columns stiffness in soft soils in order to remain below a stiffness ratio column/soil of 50.

The influence of large horizontal forces or earthquake loading has been neglected at this stage of consideration. Also special rigid inclusions, formed with a weak mortar UCS < 5 MPa, should be investigated in more detail.

Moreover, it should be also noted that stiffer supporting elements usually require increased cement consumption. Consequently, the use of less stiffer columns will have a positive effect on the equivalent CO2 emission, as shown by Zöhrer et al. [7].

It would be appreciated if future research could focus on the column to soil stiffness ratio of currently relevant ground improvement methods.

5. CONCLUSION AND OUTLOOK

Three ground improvement categories with increasing risks are proposed. True ground improvement methods in category A, e.g., vibro compaction and vibro stone columns, are ductile according to DIN 1054 and Eurocode 7. Moreover, they maintain their stability even when variations in soil and material parameters occur, and therefore incorporate only small risks. For the geotechnical design the serviceability limit state is usually a determining factor.
The methods in category B, that utilizes columns with a diameter of more than 30 cm, involve an average risk. And the risk of an increased stiffness ratio is here compensated with an increased column diameter.
Methods with non-ductile behaviour in category C, that use columns with a small diameter of less than 30 cm, e.g., rigid inclusions, represent a much higher risk because the geotechnical design is usually governed by ultimate limits states. To enable the full development of high skin friction along the columns such supporting systems allow significant punching of the column foot and column head into the soil layers. Thus at least for single and strip footings even a small variation in the mechanical parameters, system geometry or loads may lead to a complete failure with related consequences.

The difference in stiffness between the columns and the soil plays a fundamental role in ground improvement supporting systems. The stiffness ratio of approximately 40 to 50 is regarded as an upper limit for true ground improvement solutions, which account for ground interaction. A further increase in column stiffness is ineffective.

The goal of further research should be the establishment of a reliable limit classification of various ground improvement methods including granular and stiff elements with focus on the column to soil stiffness ratio. In any case, the term 'Ground Improvement' should not be used to undermine the safety level of existing piling standards, nor to countervail certification documents issued by, e.g., the Institute for Bautechnik in Germany and to design full displacement piles (EN 12699) with ground improvement methods.

It is very much appreciated by the authors that the French ASIRI recommendation finally has been changed fundamentally to increase the safety level at least to a certain extent. Generally two cases are distinguished:

- If stiff columns like rigid inclusion are necessary for bearing capacity of shallow foundations (global factor of safety without rigid inclusions < 2.4) or slope stability (global factor of safety approx. < 1.4)

they have to be designed according to the local piling standard. Reinforcement has to be used where the columns are not entirely compressed which means that no tensile stresses are allowed.

- If stiff columns like rigid inclusion are not necessary for bearing capacity of shallow foundations (global factor of safety without rigid inclusions approx. > 2.4) or slope stability (global factor of safety > 1.4) they are designed as ground improvement. Reinforcement is not necessary where the maximum tensile stress according to EC2 is not exceeded.

REFERENCES

[1] W. Sondermann, K. Kirsch, 2009 Grundbautaschenbuch, „Baugrundverbesserung“, Teil 2, Kapitel 2.2, Ernst & Sohn Verlag, Berlin

[2] ASIRI, 2011, Amélioration des Sols par Inclusions Rigides, Bodenverbesserung mit Stabilisierungssäulen, Draft, www.irex-asiri.fr

[3] H. Priebe, 1995, Die Bemessung von Rüttelstopfverdichtungen, Die Bautechnik 72 (1995), Heft 3, 183-191.

[4] F. Kirsch, 2004, Experimentelle und numerische Untersuchungen zum Tragverhalten von Rüttelstopfsäulen, Dissertation am Institut für Grundbau und Bodenmechanik, Heft 75, Braunschweig

[5] N. P. Balaam, J. R. Booker, 1981, Analysis of rigid rafts sup-ported by granular piles, International Journal for Numerical and Analytical Methods in Geomechanics (1981), Vol. 5, 379-403.

[6] B. Broms, 2004, Lime and lime/cement columns, Ground improvement, Eds. M.P. Moseley and K. Kirsch, Spon Press, London and New York

[7] A. Zöhrer., W. Wehr, M. Stelte, 2010, Is ground engineering environmentally friendly?, 11th International EFFC-DFI conference, Session 3: sustainability in the foundation industry, London, on DVD

[8] DGGT, 2002, Deutsche Gesellschaft für Geotechnik e.V., Merkblatt für die Herstellung, Bemessung und Qualitätssicherung von Stabilisierungssäulen zur Untergrundverbesserung, Teil 1- CSV-Verfahren

[9] Wong, P., Muttuvel, T., 2011, Support of Road Embankments on Soft Ground using Controlled Modulus Columns, International Conference on Advances in Geotechnical Engineering, Nov. 2011, Perth, Australia

[10] EBGEO, 2011, Recommendation for design and analysis of earth structures using geosynthetic reinforcement, section 6.10, Ernst&Sohn

PLATINUM SPONSORS

GOLD SPONSORS

SILVER SPONSORS

ORGANIZING SECRETARIAT

Belgian Building Research Institute

With the support of TIS-SFT